Editor Tim Storr

Ligand Design in Medicinal Inorganic Chemistry

WILEY

Ligand Design in Medicinal Inorganic Chemistry

Ligand Design in Medicinal Inorganic Chemistry

Edited by

TIM STORR

Department of Chemistry, Simon Fraser University, Burnaby, BC V5A-1S6, Canada

WILEY

This edition first published 2014

Registered office
John Wiley & Sons Ltd, The Atrium, Southern Gate, Chichester, West Sussex, PO19 8SQ, United Kingdom

Library of Congress Cataloging-in-Publication Data

Ligand design in medicinal inorganic chemistry / editor, Tim Storr.
pages cm
Includes bibliographical references and index.
ISBN 978-1-118-48852-2 (cloth)
1. DNA-drug interactions. 2. Ligand binding (Biochemistry) 3. Drugs–Design. 4. Pharmaceutical chemistry. I. Storr, Tim, editor of compilation.
QP624.75.D77L54 2014
612′.01524 – dc23

2013049102

A catalogue record for this book is available from the British Library.

ISBN: 9781118488522

Typeset in 10/12pt TimesLTStd by Laserwords Private Limited, Chennai, India

1 2014

Contents

About the Editor

Tim Storr obtained his B.Sc. from the University of Victoria, Canada, and his Ph.D. in Medicinal Inorganic Chemistry from the University of British Columbia, Canada, in 2005 working with Professor Chris Orvig. He then pursued postdoctoral studies with Professor T. Daniel P. Stack at Stanford University studying metalloenzyme mimics. In 2008 he joined the faculty at Simon Fraser University, Canada, as an assistant professor where his bioinorganic chemistry research programme targets the development of new chemical tools to diagnose and treat disease. His research is funded by the Natural Sciences and Engineering Research Council and the Michael Smith Foundation for Health Research. Current research interests include metal overload disorders, Alzheimer's disease, cancer, diagnostic imaging, site-selective therapies, and catalysis.

List of Contributors

Peter J. Barnard
Department of Chemistry, La Trobe Institute for Molecular Science, La Trobe University, Melbourne Victoria, 3086, Australia

Michael W. Beck
Department of Chemistry, University of Michigan, 930 North University Avenue, Ann Arbor, Michigan 48109, USA

Heloisa Beraldo
Departamento de Química, Universidade Federal de Minas Gerais, Av. Presidente Antonio Carlos 6627, Belo Horizonte, MG, 31270-901, Brazil

Susan J. Berners-Price
Institute for Glycomics, Griffith University, Gold Coast Campus, Gold Coast Queensland, 4222, Australia

Christophe Biot
UMR CNRS 8576, Unité de Glycobiologie Structurale et Fonctionnelle, Université Lille 1, 59650 Villeneuve d'Ascq, France

Célia S. Bonnet
Centre de Biophysique Moléculaire, UPR 4301 CNRS, Rue Charles Sadron, Université d'Orléans, Orléans, 45071, France

Eszter Boros
A.A. Martinos Center for Biomedical Imaging, Massachusetts General Hospital, Harvard Medical School, 149 13th St, Charlestown, MA, USA, 02129

Seth M. Cohen
Department of Chemistry and Biochemistry, 9500 Gilman Drive, University of California, San Diego, CA, 92093, USA

Mike Coogan
Department of Chemistry, Faraday Building, Lancaster University, Bailrigg, Lancaster, LA1 4YB, UK

Tara R. deBoer-Maggard
Department of Chemistry and Biochemistry, University of California, 1156, High Street, Santa Cruz, CA, 95064, USA

Pascale Delangle
UMR-E3, Laboratoire Reconnaissance ionique et Chimie de Coordination, Université Joseph Fourier – Grenoble 1/CEA/Institut Nanoscience et Cryogénie/SCIB, 17 rue des martyrs, 38054, Grenoble, France

Alaina S. DeToma
Department of Chemistry, University of Michigan, 930 North University Avenue, Ann Arbor, Michigan, 48109, USA

Dustin Duncan
Department of Chemistry, Simon Fraser University, 8888 University Drive, Burnaby, BC, V5A-1S6, Canada

Cara L. Ferreira
Nordion, 4004 Wesbrook Mall, Vancouver, BC, Canada, V6T 2A3

Christelle Gateau
UMR-E3, Laboratoire Reconnaissance ionique et Chimie de Coordination, Université Joseph Fourier – Grenoble 1/CEA/Institut Nanoscience et Cryogénie/SCIB, 17 rue des martyrs, 38054, Grenoble, France

Michael Gottschaldt
Laboratory for Organic and Macromolecular Chemistry, Friedrich-Schiller-University Jena, Humboldtstrasse 10, 07743, Jena, Germany
Jena Center for Soft Matter (JCSM), Friedrich-Schiller-University Jena, Philosophenweg 7, 07743, Jena, Germany

Trevor W. Hambley
School of Chemistry, University of Sydney, City Road, Darlington, NSW 2008, Australia

Oluwatayo F. Ikotun
Department of Radiology, Washington University, 510 S. Kingshighway Blvd, St Louis, MO, USA, 63110

Michael R. Jones
Department of Chemistry, Simon Fraser University, 8888 University Drive, Burnaby, BC, V5A-1S6, Canada

Alice V. Klein
School of Chemistry, University of Sydney, NSW 2006, Australia

Kyle J. Korshavn
Department of Chemistry, University of Michigan, 930 North University Avenue, Ann Arbor, Michigan, 48109, USA

Suzanne E. Lapi
Department of Radiology, Washington University, 510 S. Kingshighway Blvd, St Louis, MO, USA, 63110

Mi Hee Lim
Department of Chemistry, University of Michigan, 930 North University Avenue, Ann Arbor, Michigan, 48109, USA
Life Sciences Institute, University of Michigan, 210 Washtenaw Ave., Ann Arbor, Michigan, 48109, USA
Department of Chemistry, Ulsan National Institute of Science and Technology (UNIST), 50 UNIST-gil, Eonyan-eup, Ulju-gun, Ulsan, 698-798, Korea

Bernadette V. Marquez
Department of Radiology, Washington University, 510 S. Kingshighway Blvd, St Louis, MO, USA, 63110

David P. Martin
Department of Chemistry and Biochemistry, 9500 Gilman Drive, University of California, San Diego, CA, 92093, USA

Pradip K. Mascharak
Department of Chemistry and Biochemistry, University of California, 1156, High Street, Santa Cruz, CA, 95064, USA

Yuji Mikata
KYOUSEI Science Center, Nara Women's University, Kitauoya-Higashi-machi, Nara 630-8506, Japan

Elisabeth Mintz
UMR 5249, Laboratoire Chimie et Biologie des Méteaux, Université Joseph Fourier – Grenoble 1/CNRS/CEA/Institut de Recherches en Sciences et Technologies pour le Vivant/LCBM, 17 rue des martyrs, 38054, Grenoble, France

Changhua Mu
Department of Chemistry, Simon Fraser University, 8888 University Drive, Burnaby, British Columbia V5A 1S6, Canada

Maribel Navarro
Chemistry and Analytical Sciences, School of Veterinary and Life Sciences, Murdoch University, Perth, Western Australia 6150, Australia

Elizabeth J. New
School of Chemistry, The University of Sydney, Sydney, NSW, 2006, Australia

Edward S. O'Neill
School of Chemistry, The University of Sydney, Sydney, NSW, 2006, Australia

Amit S. Pithadia
Department of Chemistry, University of Michigan, 930 North. University Avenue, Ann Arbor, Michigan, 48109, USA

David T. Puerta
Department of Chemistry and Biochemistry, 9500 Gilman Drive, University of California, San Diego, CA, 92093, USA

Tim Storr
Department of Chemistry, Simon Fraser University, 8888 University Drive, Burnaby, BC, V5A-1S6, Canada

Éva Tóth
Centre de Biophysique Moléculaire, UPR 4301 CNRS, Rue Charles Sadron, Université d'Orléans, Orléans, 45071, France

Rafael Pinto Vieira
Department of Chemistry, Simon Fraser University, 8888 University Drive, Burnaby, BC, V5A-1S6, Canada
Departamento de Química, Universidade Federal de Minas Gerais, Av. Presidente Antonio Carlos 6627, Belo Horizonte, MG, 31270-901, Brazil

Charles J. Walsby
Department of Chemistry, Simon Fraser University, 8888 University Drive, Burnaby, British Columbia V5A 1S6, Canada

1

Introduction to Ligand Design in Medicinal Inorganic Chemistry

Michael R. Jones, Dustin Duncan, and Tim Storr

Department of Chemistry, Simon Fraser University, 8888 University Drive, Burnaby, BC, V5A-1S6, Canada

Medicinal inorganic chemistry continues to provide significant innovation in both diagnostic and therapeutic medicine. The field can be divided into two main categories: drugs that target metal ions in some form, and metal-based drugs in which the central metal ion is essential for the clinical application. Although the field of medicinal inorganic chemistry is not new, a better understanding of metal ion interactions in the body has enabled the development of many effective disease treatment strategies involving metal ions. The development of Cisplatin (*cis*-$[Pt(NH_3)_2Cl_2]$) has played an instrumental role in bringing the field of medicinal inorganic chemistry into the mainstream [1]. Cisplatin and the second generation analog Carboplatin, shown in Figure 1.1, are the most commonly prescribed anticancer agents which greatly improve survival rates in ovarian, bladder, cervical, and testicular cancers [2].

However, as recently written by Norman and Hambley, "with the notable exception of platinum anticancer drugs, metal-based therapeutics occupy a relatively minor place in the organic dominated history of drug development [3]." Therefore, there is a broad scope for innovation in the field of medicinal inorganic chemistry! An inherent advantage of metal complexes lies in the accessibility of multiple oxidation states, overall charge, and geometries. However, these properties can become a disadvantage if not controlled in the biological application. Predicting the behavior of metal-based medicinal agents *in vivo* is a major challenge facing medicinal inorganic chemists today. The history and basic concepts of medicinal inorganic chemistry have been comprehensively reviewed [4–11]. The main goal of this book is to highlight the role of ligand design in the rapidly expanding field of medicinal inorganic chemistry [12–14]. Through a series of 14 chapters, expert researchers describe the importance of ligand design in medicinal inorganic chemistry.

Ligand Design in Medicinal Inorganic Chemistry, First Edition. Edited by Tim Storr.

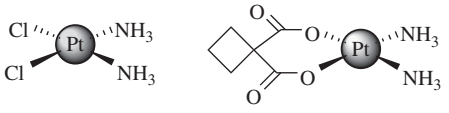

(a) (b)

Figure 1.1 *Platinum-containing chemotherapeutic drug molecules ((a) Cisplatin and (b) the second generation analog Carboplatin). See Chapter 2 for more details*

Metal ions have an essential role in the human body by providing charge balance, facilitating electron transport, and catalyzing enzymatic transformations. For each application, the metal cation and the atoms immediately surrounding the metal cation (i.e., coordination sphere) can be tuned specifically. The type, number, and geometry of the ligands, commonly in the form of amino acid side-chains, ensure that the active site is maintained (Table 1.1).

Continued research into the uptake, transport, and utilization of metal ions in the body has enabled the development of many disease treatment strategies targeting metals. For example, the role of ligand design in essential metal overload disorders such as Wilson's disease (Cu) and Hemochromatosis (Fe) is discussed by Delangle and co-workers in Chapter 11. In addition, the role of dysregulated metal ions in protein misfolding diseases of the brain, and the design of molecules targeting these processes, are discussed by Lim and co-workers in Chapter 10. Finally, the design of metal-binding molecules that inhibit the biological function of metalloproteins is discussed by Cohen and co-workers in Chapter 14 [16].

Table 1.1 *A brief introduction to essential metal ions in the body and their functions [15]*

Metal ions	Coordination number, geometry, ligand preferences	Function
Na^{+}	6, octahedral, carboxylate/ether/hydroxyl	Charge balance, osmotic pressure, and nerve activity
Mg^{2+}	6, octahedral, carboxylate/phosphate	Structural role in hydrolases, isomerases, and phosphate transfer
K^{+}	6–8, flexible, carboxylate/ether/hydroxyl	Charge balance, osmotic pressure, and nerve activity
Ca^{2+}	6–8, flexible, carbonyl/carboxylate/phosphate	Structural, charge balance, reaction initiator, and phosphate transfer
Cr^{3+}	6, octahedral, oxygen-donors	Essential to carbohydrate/lipid metabolism
$Mn^{2+/3+}$	6, tetragonal/octahedral, carboxylate/hydroxide/imidazole/phosphate	Structural role in oxidases
$Fe^{2+/3+}$	4 or 6, tetrahedral or octahedral, carboxylate/oxide/phenolate/thiolate/imidazole/pyrrole	Electron transfer in oxidases and oxygen binding/transport
$Co^{+/2+/3+}$	4 or 6, tetrahedral or octahedral, carboxylate/imidazole/thioether/thiolate	Alkyl group transfer (B_{12}), oxidases
$Cu^{+/2+}$	3–5, trigonal planar, tetrahedral, square planar, square pyramid, carboxylate/imidazole/thioether/thiolate	Electron transfer, oxidases, and hydroxylases
Zn^{2+}	4 or 5, tetrahedral or square pyramid, carbonyl/carboxylate/imidazole/thiolate	Structure in zinc fingers, gene regulation, anhydrases, dehydrogenases, and peptidases

Natural systems provide much of the inspiration for the strategies employed by medicinal inorganic chemistry researchers. Thus, the design of active agents uses many of the same features present in biological systems to stabilize metal ions. The ligand(s) play a key role in determining the pharmacokinetic parameters of the metal-containing drug molecule allowing for tuning of a compound for the specific application. Basic inorganic chemistry concepts such as Hard Soft Acid Base (HSAB) Theory, kinetic inertness, and thermodynamic stability, can be used in the design process [17, 18]. Ligands can be purposefully chosen to limit complex dissociation and metal-associated toxicity *in vivo* in the presence of endogenous metal-binding molecules such as citrate, phosphate, bicarbonate, and biomolecules such as glutathione, transferrin, and albumin. Additional factors that must be considered include: matching the oxidation state and coordination preferences of the metal ion, kinetics of complex formation, water solubility, overall charge, and the pathway of excretion from the body. Depending on the application, a larger degree of importance may be placed on specific design features of the medicinal agent. For magnetic resonance imaging (MRI) contrast agents discussed by Bonnet and Tóth in Chapter 12, the Gd^{III} ion offers the best response and is incorporated into all but one of the commercially-approved agents. However, the high concentration used and known toxicity of the Gd^{III} ion in the body necessitates the use of ligands that confer kinetic inertness and high thermodynamic stability to the complex. High thermodynamic stability of Gd^{III} complexes, along with other lanthanides, is achieved with multidentate poly(amino)polycarboxylate ligands which form strong electrostatic interactions with the hard cation. Example ligands include the linear diethylenetriaminepentaacetic acid (DTPA) and macrocyclic 1,4,7,10-tetraazacyclododecane-1,4,7,10-tetraacetic acid (DOTA). The Gd^{III} complexes of both of these ligands have been approved for clinical use and are shown in Figure 1.2.

Many of the same important design features for MRI contrast agents are applicable to metal-based radiopharmaceutical research as described by Ferreira and co-workers in Chapter 3. For metal-based radiopharmaceuticals, the low concentration of the radionuclide available in the ligand complexation step, as well as the short half-life of many radionuclides (e.g., $^{68}Ga = 68$ minutes), require careful consideration of the kinetics of complex formation. For the binding of metal ions *in vivo*, as described in Chapter 11 for metal overload disorders of Cu and Fe, ligand design needs to take into account the binding preferences of a specific oxidation state of the metal ion. As an example, in the Fe-overload disorder Hemochromatosis, the development of binding agents that stabilize the more kinetically-inert Fe^{III} oxidation state are of interest. A high affinity for Fe^{III} is necessary in order to compete with the iron transport protein, transferrin. An additional important design consideration is the Fe^{III}/Fe^{II} redox potential of the resulting complex. A value below −300 mV (vs. the Normal Hydrogen Electrode (NHE)) is hypothesized to prevent redox-cycling in the presence of biological reducing agents, such as ascorbate and glutathione, and the possibility of generating reactive oxygen species (ROS) *in vivo* [19, 20]. However, the design of metal complexes that undergo redox processes under controlled conditions in the body has proven to be an effective targeting method in cancer diagnosis and therapy. Under certain conditions, the reducing environment of hypoxic tumor tissues [21] can be exploited for the

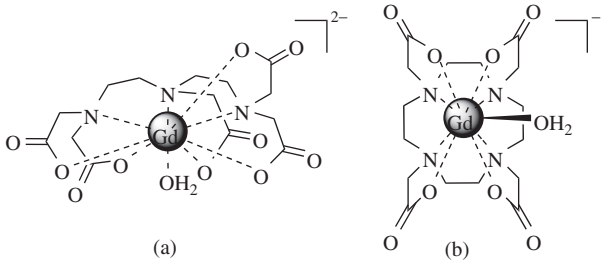

Figure 1.2 *Examples of gadolinium complexes used in MRI imaging (a) Gd-DTPA and (b) Gd-DOTA. See Chapter 12 for further details*

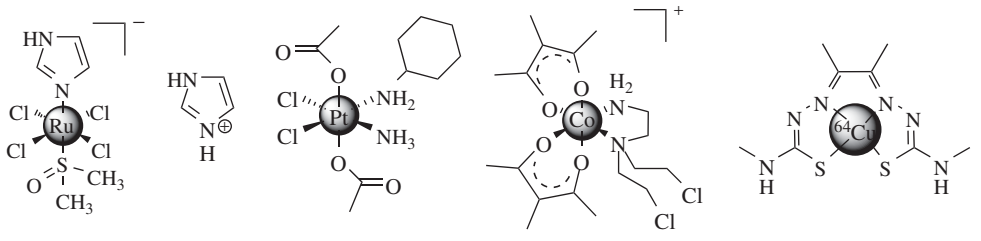

Figure 1.3 *Redox-activated metal complexes. Reduction* in vivo *results in a more kinetically-labile metal center: (a) Ru^{III} complex NAMI-A [19, 27]. One hypothesized mechanism of action involves reduction to Ru^{II}. (b) Pt^{IV} complex Satraplatin [28]. Activation occurs upon reduction to Pt^{II}. (c) A Co^{III} complex containing a nitrogen mustard [24]. Reduction to Co^{II} leads to ligand exchange and activation of the nitrogen mustard. (d) $^{64}Cu^{II}$ATSM [29]. Reduction to $^{64}Cu^{I}$ leads to ligand exchange and intracellular trapping of the metal ion*

selective activation of metal-based diagnostics and therapeutics [22]. Examples include Ru-based anticancer agents (Chapter 15), Pt^{IV} complexes (Chapter 2), Co^{III} compounds [23, 24], and the radiopharmaceutical ^{64}Cu-diacetyl-bis-N^4-methylthiosemicarbazone (^{64}CuATSM) (Chapters 3 and 7). The anticancer activity of the ferrocene-containing ferrocifens [25], and antimalarial activity of ferrocene-containing agents discussed in Chapter 8 [26], may in part be due to redox activation of the ferrocene unit and generation of ROS.

In addition to providing a stable complex, ligands can impart additional properties to metal ions. For example, ligand photosensitization of metal complexes can provide an emissive response useful for imaging and/or drug activation. Ligands are essential to the development of emissive metal complexes for biological applications. There has been significant interest in the development of both transition metal- (Chapter 4) and lanthanide- (Chapter 5) containing optical probes. In Chapters 4 and 5, the important design features of metal-based optical probes are described in detail. Optical probes, in general, permit the *in vitro* visualization of biological processes at the subcellular level, and have recently been reported for *in vivo* diagnostic applications [30, 31]. Properties such as biological stability, large Stokes shift (difference in energy between excitation and emission wavelengths), and long luminescence lifetimes of metal-based probes provide an improvement over organic fluorophores. In almost all cases, metal-containing optical probes depend on photophysical processes involving the ligand, and the majority of ligands used are conjugated heterocycles including bipyridine, phenanthroline, and phenylpyridines. These same planar aromatic heterocyclic ligands can also display DNA-intercalating ability, thereby providing a targeting feature to certain optical probes [32]. As discussed by Coogan in Chapter 4, transition metal optical probes containing d^6 complexes (Re^{I}, Ru^{II}, and Ir^{III}) are the most commonly studied (Figure 1.4), and more recently d^8 and d^{10} platinum and gold complexes have been reported. The combination of optical imaging and cytotoxicity in one agent is briefly described for both Pt (Chapter 2) and Au (Chapter 9) complexes. Lanthanide probes employ much of the same design features as MRI agents (thermodynamic stability and kinetic inertness), and in contrast to the transition metal optical probes, the emission is primarily metal-based (4*f* electrons), thus leading to sharp line-like emission spectra. The low extinction coefficients of lanthanide ions (*f-f* transitions are Laporte forbidden) necessitates the use of a sensitizing moiety, an organic absorber which can transfer energy to the lanthanide excited state. In the majority of cases, the sensitizer is either directly bound to the lanthanide ion, or attached to a chelating ligand that is bound to the lanthanide ion (Figure 1.4). As described by O'Neill and New in Chapter 5, the long luminescence lifetimes, and information rich spectra of lanthanide complexes, provide many opportunities in optical imaging research. Ligand photosensitization of metal complexes can be used in a number of pharmaceutical applications, where following excitation, the energy transfer can initiate ligand

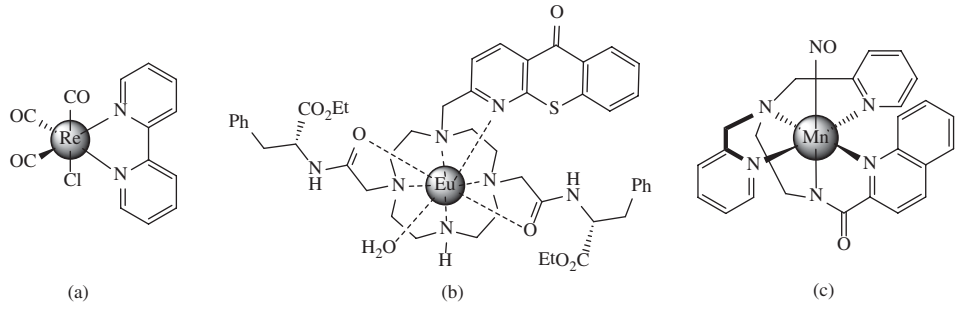

Figure 1.4 *Examples of photoactivated metal complexes: (a) An emissive Re^{I} tricarbonyl complex [33]. (b) An emissive Eu^{III} complex containing a sensitizer (in bold) for* in vitro *imaging [34]. (c) A Mn complex that releases NO under photoexcitation [35]*

dissociation leading to the release of bioactive agents. Energy transfer can also occur to exogenous molecules such as O_2 which is the mechanism of activation in photodynamic therapy. In Chapter 13, Mascharak and co-workers describe the design features of metal complexes that are activated by light. Through ligand design, they show that photoactivation is controlled by the power, wavelength, and exposure time of the light. Specific examples include photoactivated toxicity and the release of small-molecule signaling agents such as NO and CO (Figure 1.4).

The targeting of a diagnostic and/or therapeutic agent in the body is essential to an accurate diagnosis as well as for limiting the off-target toxicity of the administered drug in therapeutic applications. In the case of Cisplatin, uptake is not specific to cancer cells and thus off-target toxicity is a major limiting factor, with less than 1% of the injected drug reaching its tumor DNA target [36]. Despite this drawback, Cisplatin is still an effective front-line treatment. A major research focus for medicinal chemists today is to improve the targeting of the medicinal agent and a large number of innovative ideas are presented in this book. We will only highlight a few specific examples here. Information on the uptake, transport, localization, and eventual excretion of a drug molecule is instrumental in the design of more effective agents. An interesting example is the longstanding (several thousand years!) application of Au in medicine. The emergence of specific thiol and selenol protein drug targets such as thioredoxin reductase, and the use of ligands to control cellular uptake and reactivity of the Au metal center, are excellently described by Berners-Price and Barnard in Chapter 9. In Chapter 7, Vieira and Beraldo detail the design of Schiff base-derived ligands in a number of disease applications. Many of the chapters describe the attachment of a biological targeting vector to a metal complex. Biological targeting vectors include, but are not limited to: carbohydrates, amino acids, peptides, antibodies, and active drug molecules. The distance between the targeting vector and the metal complex is an important design consideration. Mikata and Gottschaldt review the use of carbohydrate targeting ligands in Chapter 6. Appending a carbohydrate moiety to a metal complex has the ability to reduce toxicity, and improve solubility and molecular targeting of the metal-based drug via use of carbohydrate active transport pathways. In Chapter 8, Navarro and Biot describe the attachment of the known antimalarial Chloroquine (CQ), either pendent or directly bound to a metal complex, which affords a series of new leads that overcome the CQ-resistance of the malaria parasite (Figure 1.5). A major mechanism of drug transport in the blood is via binding to the hydrophobic pockets of the protein human serum albumin (HSA). Targeted HSA binding greatly enhances contrast for the commercially available blood pool imaging agent MS-325 (Chapter 12); a pendent lipophilic phosphine moiety is attached to the Gd^{III} complex which interacts with HSA and slows the rotational correlation time (τ_R) of the complex (Figure 1.5). The development of a series of Ru anticancer agents that employ ligands designed to interact with HSA and improve targeting are described by Mu and Walsby in Chapter 15.

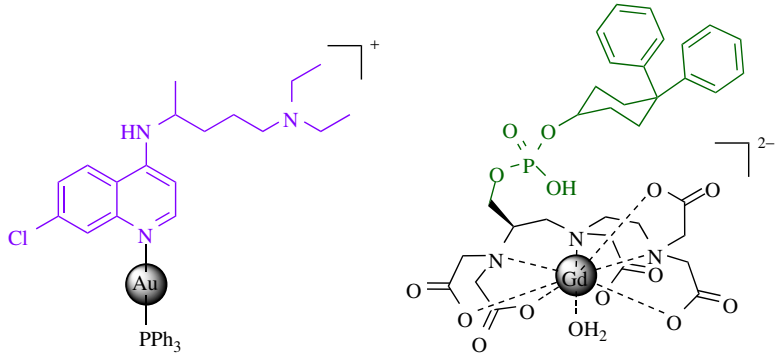

Figure 1.5 *Metal-based agents with attached targeting molecules: (a) A Au complex [37] connected to the malaria drug chloroquine (in bold). (b) The MRI agent MS-325 with attached HSA targeting unit (in bold) [38]*

Metal complexes attached to peptide targeting vectors are of great interest in medicinal inorganic chemistry and the identification of new disease targets will lead to continual development in this area. A number of radiodiagnostic agents containing tumor-specific peptides attached to radiometal chelates are discussed by Ferreira and co-workers in Chapter 3. High target to background ratios provide non-invasive images of tumors and metastatic tissue, and also present the possibility of attaching therapeutic isotopes (e.g., ^{90}Y and ^{153}Sm) for treatment. Similar peptide targeting strategies are discussed for Pt (Chapter 2) and Au (Chapter 9) anticancer agents to take advantage of specific active transport pathways. The use of radiolabeled antibodies for tumor imaging and therapy is of significant interest. The extended plasma half-life of antibodies requires a long-lived isotope to obtain useful diagnostic images. The application of ^{89}Zr (Chapter 3), and the use of desferrioxamine (DFO) as the metal chelate (a biological siderophore shown in Figure 1.6), in combination with antibodies such as Bevacizumab demonstrates the influence of medicinal inorganic chemistry in modern diagnostic imaging. Finally, the recent development of a Cu^{I} pro-ligand that is selectively activated in liver hepatocytes shows considerable promise as a Wilson's disease treatment (Chapter 11) [39]. These compounds are decorated with carbohydrate residues that are recognized by the asialoglycoprotein receptor (ASGP-R), and once internalized, cleavage of disulfide bonds in the reducing intracellular medium releases the active chelator. Pro-chelator molecules also show considerable promise in binding dysregulated metals in neurodegenerative disease (Chapter 10) [40, 41].

The field of medicinal inorganic chemistry offers an important opportunity to expand our ability to diagnose and treat disease. Throughout this book, the authors have described the importance of ligand design in tailoring the properties of drug candidates to the specific application. Each individual chapter shares significant

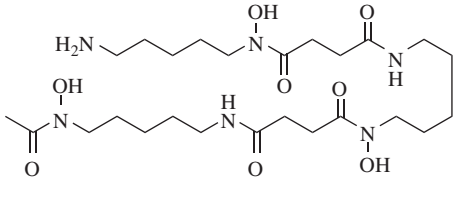

Figure 1.6 *Desferrioxamine (DFO) is a bacterial siderophore produced by the actinobacteria* Streptomyces pilosus. *DFO is used to treat acute iron poisoning (Chapter 11), and is also used as a radiometal chelate (Chapter 3)*

insight into how ligand design is increasing our understanding of pathophysiology of disease, and providing a mechanism to increase the efficacy of drug molecules. We hope you enjoy each chapter as much as we have, and apply the concepts and insights within to your own research in medicinal inorganic chemistry.

References

1. Rosenberg, B., Vancamp, L., Trosko, J.E. and Mansour, V.H. (1969) Platinum compounds – a new class of potent antitumor agents. *Nature*, **222**, 385–386.
2. Harper, B.W., Krause-Heuer, A.M., Grant, M.P. *et al*. (2010) Advances in platinum chemotherapeutics. *Chem. Eur. J.*, **16** (24), 7064–7077.
3. Norman, J.F. and Hambley, T.W. (2011) Targeting strategies for metal-based therapeutics, in *Bioinorganic Medicinal Chemistry* (ed E. Alessio), Wiley-VCH Verlag GmbH, Weinheim, pp. 58–87.
4. Metzler-Nolte, N. and Alberto, R. (2010) *Medicinal Inorganic Chemistry: Concepts, Applications, and Perspectives*, Wiley-VCH Verlag GmbH, Weinheim.
5. Alessio, E. (2011) *Bioinorganic Medicinal Chemistry*, Wiley-VCH Verlag GmbH & Co KGaA, Weinheim.
6. Dabrowiak, J.C. (2009) *Metals in Medicine*, John Wiley & Sons, Ltd, Chichester.
7. Farrer, N.J. and Sadler, P.J. (2011) Medicinal inorganic chemistry: state of the art, new trends, and a vision of the future, in *Bioinorganic Medicinal Chemistry* (ed E. Alessio), Wiley-VCH Verlag GmbH, Weinheim, pp. 11–57.
8. Sessler, J.L., Doctrow, S.R., McMurry, T.J. and Lippard, S.J. (eds) (2005) *Medicinal Inorganic Chemistry*, American Chemical Society, Washington, DC.
9. Thompson, K.H. (2011) Medicinal inorganic chemistry: an introduction, in *Encyclopedia of Inorganic and Bioinorganic Chemistry*, John Wiley & Sons, Ltd, Chichester, DOI: 10.1002/9781119951438.eibc0362.
10. Thompson, K.H. and Orvig, C. (2003) Boon and bane of metal ions in medicine. *Science*, **300** (5621), 936–939.
11. Jaouen, G.M.N. (2010) *Medicinal Organometallic Chemistry*, Springer, Heidelberg.
12. Chiang, L., Jones, M.R., Ferreira, C.L. and Storr, T. (2012) Multifunctional ligands in medicinal inorganic chemistry-current trends and future directions. *Curr. Top. Med. Chem.*, **12** (3), 122–144.
13. Storr, T., Thompson, K.H. and Orvig, C. (2006) Design of targeting ligands in medicinal inorganic chemistry. *Chem. Soc. Rev.*, **35** (6), 534–544.
14. Thompson, K.H. (2011) Medicinal inorganic chemistry: ligand design objectives and principles, in *Encyclopedia of Inorganic and Bioinorganic Chemistry*, John Wiley & Sons, Ltd, Chichester, DOI: 10.1002/9781119951438.eibc0365.
15. Roat-Malone, R. (2007) *Bioinorganic Chemistry: A Short Course*, Wiley-Interscience.
16. Meggers, E. (2011) From conventional to unusual enzyme inhibitor scaffolds: the quest for target specificity. *Angew. Chem. Int. Ed.*, **50** (11), 2442–2448.
17. Wolfgang, K. and Schwederski, B. (2013) *Bioinorganic Chemistry – Inorganic Elements in the Chemistry of Life: An Introduction and Guide*, John Wiley & Sons, Ltd, Chichester.
18. Housecrofte, C.S. and Sharpe, A.G. (2012) *Inorganic Chemistry*, 4th edn, Prentice Hall.
19. Mestroni, G., Alessio, E., Sava, G. *et al*. (1994) Water-soluble ruthenium(III)-dimethyl sulfoxide complexes: chemical behaviour and pharmaceutical properties. *Metal-Based Drugs*, **1** (1), 41–63.
20. Pierre, J.L. and Fontecave, M. (1999) Iron and activated oxygen species in biology: the basic chemistry. *Biometals*, **12** (3), 195–199.
21. Hanahan, D. and Weinberg, R.A. (2011) Hallmarks of cancer: the next generation. *Cell*, **144** (5), 646–674.
22. Graf, N. and Lippard, S.J. (2012) Redox activation of metal-based prodrugs as a strategy for drug delivery. *Adv. Drug Delivery Rev.*, **64** (11), 993–1004.
23. Chang, J.Y.C., Lu, G.L., Stevenson, R.J. *et al*. (2013) Cross-bridged cyclen or cyclam Co(III) complexes containing cytotoxic ligands as hypoxia-activated prodrugs. *Inorg. Chem.*, **52** (13), 7688–7698.
24. Craig, P.R., Brothers, P.J., Clark, G.R. *et al*. (2004) Anionic carbonato and oxalato cobalt(III) nitrogen mustard complexes. *Dalton Trans.*, **4**, 611–618.
25. Hillard, E., Vessieres, A., Thouin, L. *et al*. (2006) Ferrocene-mediated proton-coupled electron transfer in a series of ferrocifen-type breast-cancer drug candidates. *Angew. Chem. Int. Ed.*, **45** (2), 285–290.

26. Dubar, F., Slomianny, C., Khalife, J. *et al*. (2013) The ferroquine antimalarial conundrum: redox activation and reinvasion inhibition. *Angew. Chem. Int. Ed.*, **52** (30), 7690–7693.
27. Sava, G., Capozzi, I., Clerici, K. *et al*. (1998) Pharmacological control of lung metastases of solid tumours by a novel ruthenium complex. *Clin. Exp. Metastasis*, **16** (4), 371–379.
28. Mellish, K.J. and Kelland, L.R. (1994) Mechanisms of acquired-resistance to the orally-active platinum-based anti-cancer drug bis-acetato-amine-dichloro-cyclohexamine platinum(IV) (JM216) in 2 human ovarian-carcinoma cell lines. *Cancer Res.*, **54** (23), 6194–6200.
29. Obata, A., Yoshimi, E., Waki, A. *et al*. (2001) Retention mechanism of hypoxia selective nuclear imaging/radiotherapeutic agent Cu-diacetyl-bis(N-4-methylthiosemicarbazone) (Cu-ATSM) in tumor cells. *Ann. Nucl. Med.*, **15** (6), 499–504.
30. Rao, J.H., Dragulescu-Andrasi, A., Yao, H.Q. and Yao, H.Q. (2007) Fluorescence imaging in vivo: recent advances. *Curr. Opin. Biotechnol.*, **18** (1), 17–25.
31. Ntziachristos, V., Ripoll, J., Wang, L.H.V. and Weissleder, R. (2005) Looking and listening to light: the evolution of whole-body photonic imaging. *Nat. Biotechnol.*, **23** (3), 313–320.
32. Zeglis, B.M., Pierre, V.C. and Barton, J.K. (2007) Metallo-intercalators and metallo-insertors. *Chem. Commun.*, **44**, 4565–4579.
33. Fernandez-Moreira, V., Thorp-Greenwood, F.L. and Coogan, M.P. (2010) Application of d(6) transition metal complexes in fluorescence cell imaging. *Chem. Commun.*, **46** (2), 186–202.
34. Pal, R., Parker, D. and Costello, L.C. (2009) A europium luminescence assay of lactate and citrate in biological fluids. *Org. Biomol. Chem.*, **7** (8), 1525–1528.
35. Heilman, B. and Mascharak, P.K. (2013) Light-triggered nitric oxide delivery to malignant sites and infection. *Philos. Trans. R. Soc. A*, (371).
36. Galanski, M., Jakupec, M.A. and Keppler, B.K. (2005) Update of the preclinical situation of anticancer platinum complexes: novel design strategies and innovative analytical approaches. *Curr. Med. Chem.*, **12** (18), 2075–2094.
37. Navarro, M., Perez, H. and SanchezDelgado, R.A. (1997) Toward a novel metal-based chemotherapy against tropical diseases. 3. Synthesis and antimalarial activity in vitro and in vivo of the new gold-chloroquine complex Au(PPh3)(CQ) PF6. *J. Med. Chem.*, **40** (12), 1937–1939.
38. Caravan, P., Cloutier, N.J., Greenfield, M.T. *et al*. (2002) The interaction of MS-325 with human serum albumin and its effect on proton relaxation rates. *J. Am. Chem. Soc.*, **124** (12), 3152–3162.
39. Pujol, A.M., Cuillel, M., Jullien, A.S. *et al*. (2012) A sulfur tripod glycoconjugate that releases a high-affinity copper chelator in hepatocytes. *Angew. Chem. Int. Ed.*, **51** (30), 7445–7448.
40. Schugar, H., Green, D.E., Bowen, M.L. *et al*. (2007) Combating Alzheimer's disease with multifunctional molecules designed for metal passivation. *Angew. Chem. Int. Ed.*, **46** (10), 1716–1718.
41. Charkoudian, L.K., Pham, D.M. and Franz, K.J. (2006) A pro-chelator triggered by hydrogen peroxide inhibits iron-promoted hydroxyl radical formation. *J. Am. Chem. Soc.*, **128** (38), 12424–12425.

2

Platinum-Based Anticancer Agents

Alice V. Klein and Trevor W. Hambley

School of Chemistry, University of Sydney, NSW 2006, Australia

2.1 Introduction

The ligands of platinum anticancer complexes influence everything from the type of pharmaceutical formulation required, to the pharmacokinetics and the mode of cytotoxicity. The ligands determine the aqueous solubility of platinum complexes, which in turn determines the route of drug administration; for instance, oral *versus* intravenous. Once the platinum complex enters the circulation, its reactivity dictates the number of unwanted side-reactions with blood proteins, while the size, charge, lipophilicity and shape of the ligands influence the distribution of the complex throughout the body and the rate at which it is excreted. High molecular weight ligands are useful for trapping platinum complexes in tumour tissue; a phenomenon known as the enhanced permeability and retention (EPR) effect [1, 2], while charged ligands can be employed to enhance tumour penetration [3, 4]. Lipophilic ligands are useful for increasing cellular uptake [5, 6], while the shape of the ligands can be tailored to improve DNA affinity, facilitate binding with receptors on the surface of tumour cells, and inhibit enzymes involved in cancer progression. The ligands also determine the type of DNA-adduct that is formed, as well as the mode of cell-death that ensues. As a result, careful consideration must be exercised in the choice of ligands, in order to optimise the anticancer properties of novel platinum complexes.

2.2 The advent of platinum-based anticancer agents

The era of platinum-based chemotherapy dawned in the 1960s, following Barnett Rosenberg's serendipitous discovery of the antiproliferative effects of cisplatin (**1**) [7]. Cisplatin was granted FDA approval in 1978, with its success paving the way for the regulatory approval of the second- and third-generation platinum

Ligand Design in Medicinal Inorganic Chemistry, First Edition. Edited by Tim Storr.

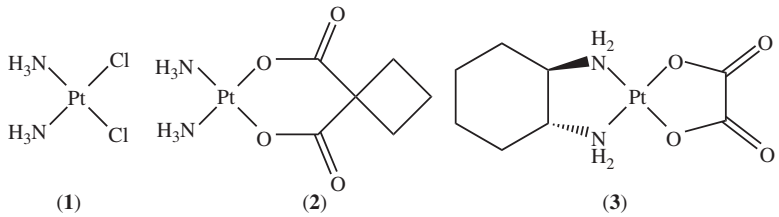

Figure 2.1 *Platinum anticancer complexes that have been granted FDA approval. Cisplatin (**1**), carboplatin (**2**) and oxaliplatin (**3**)*

anticancer agents, carboplatin (**2**) and oxaliplatin (**3**) [8, 9] (Figure 2.1). Platinum drugs play a central role in cancer treatment and are used today in almost half of all chemotherapeutic regimes, often in combination with other anticancer agents [8, 10]

Since the discovery of the anticancer properties of cisplatin, a vast amount of research has been directed towards understanding its mode of action. To reach its biological target, DNA, cisplatin must travel through the bloodstream, in which the relatively high chloride concentration (~100 mM) largely prevents aquation of the chlorido ligands [8, 9, 11, 12], although binding to blood proteins including human serum albumin and haemoglobin is known to occur [13–15]. Upon arrival at the tumour site, cellular uptake of cisplatin is achieved either by passive diffusion down a concentration gradient [11, 12], or by facilitated transport mechanisms, for instance, *via* the copper transporter-1 (CTR1) [16–19] or the organic cation transporters (OCTs) [20–22]. Once the drug enters cells, the lowered chloride ion concentration (3–20 mM) allows activation of the platinum complex by aquation of one or both of the chlorido ligands [11, 12]. In its activated form, cisplatin can bind to DNA, usually by forming crosslinks with adjacent purines on the same DNA strand, though crosslinks can also form between guanines separated by another base or between opposite strands [9, 23, 24]. These platinum-DNA adducts cause distortions in the DNA structure, including unwinding and bending, which can trigger apoptotic cell death [9, 24, 25]. Alternatively, the drug may react with intracellular components including glutathione, metallothionein, membrane phospholipids and cytoskeletal microfilaments [9, 11, 26]. Cisplatin can also be removed from tumour cells by the copper efflux transporters ATP7A and ATP7B and the GS-X efflux pumps, a family of organic anion transporters which are able to export platinum-glutathione adducts out of cells [17, 27–30]. The extracellular and intracellular promiscuity of cisplatin results in less than 1% of intravenously administered drug reaching its tumour DNA target [10].

Cisplatin has been used to treat many tumour types, including ovarian, bladder, head and neck, cervical and non-small-cell lung cancer, and is particularly useful for treating testicular cancer, for which it boasts an overall cure rate exceeding 90% [10, 25, 31]. There are, however, several limitations related to its clinical use. The leading drawback of the drug is its severe dose-limiting side-effects, which arise from its indiscriminate uptake by all rapidly dividing cells (including tumour cells but also, for instance, bone marrow cells), and the pressure on the kidneys to excrete the drug from the body [8]. Side-effects include nephrotoxicity, emetogenesis, neurotoxicity, myelosuppression and otoxicity [8, 10, 25]. Furthermore, numerous cancer types are able to develop resistance to cisplatin, by means of enhanced DNA adduct repair and tolerance, reduced cellular uptake and increased efflux, downregulation of cell-death pathways, and inactivation by proteins and thiols [8, 9, 11, 25]. Finally, cisplatin has been found to suffer from poor tumour penetration, with evidence suggesting that clinically effective doses of the drug are only delivered to tumour cells situated closest to blood vessels [32, 33].

2.3 Strategies for overcoming the limitations of cisplatin

In response to the limitations of cisplatin, a vast number of analogues have been devised, with the majority being based on the structure-activity relationships elucidated by Cleare and Hoeschele in 1973 [34]. Their work suggests that neutral, square-planar platinum(II) complexes containing a pair of non-leaving amine ligands (monodentate or bidentate) in a *cis*-configuration, opposing a pair of *cis*-configured monodentate or bidentate anionic leaving ligands (often chlorido, carboxylato or hydroxido groups) are likely to exhibit anticancer activity (Figure 2.2). The non-leaving ligands dictate the structure of the DNA adducts formed, thereby influencing the anticancer activity of the drug, while the leaving ligands affect rate of reaction, biodistribution and toxicity [10, 35].

Carboplatin and oxaliplatin are successful anticancer drugs that emerged using this strategy, thereby validating Cleare and Hoeschele's model. Carboplatin is less toxic than cisplatin, while oxaliplatin is able to circumvent cisplatin resistance [8, 36–38]. Despite these modest improvements, however, neither drug exhibits a high level of tumour selectivity. Myelosuppression is a dose-limiting side-effect of carboplatin, while oxaliplatin is limited by its neurotoxicity [8]. Additionally, both drugs have been found to penetrate tumours poorly [39, 40]. As a result of these limitations, there has been an increased focus in recent years on developing agents which violate classic structure-activity rules, in the hope of circumventing resistance mechanisms, improving tumour selectivity and penetration and reducing side-effects. Some examples of novel platinum anticancer candidates include platinum(IV) complexes [41], *trans*-complexes [42], charged complexes [43], complexes with unusual DNA-binding modes (Section 2.5.1), as well as complexes that target enzymes (Section 2.5.2), transporters (Section 2.6.1), receptors (Section 2.6.2) and/or the EPR effect (Section 2.6.3).

2.4 The influence of ligands on the physicochemical properties of platinum anticancer complexes

Ligand modification in platinum complexes can be used to fine-tune physicochemical properties such as solubility, lipophilicity and reactivity, and in the case of platinum(IV) complexes, the rate of reduction.

2.4.1 Lipophilicity

The lipophilicity of platinum complexes impacts their ability to passively diffuse across the lipid bilayers of cellular membranes, and is determined by their relative solubility in lipid-like (e.g. cellular membranes) *versus* aqueous (e.g. intra- and extracellular fluid) environments [44]. Broadly speaking, cellular accumulation can be enhanced by increasing the lipophilicity of the constituent ligands, for example, by incorporating aromatic substituents or by increasing the length of hydrocarbon chains within the ligands [44–48]. Platts *et al*. have identified an exponential relationship between lipophilicity and cellular accumulation for five platinum

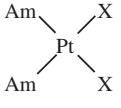

Figure 2.2 *General structure of classical platinum(II) anticancer complexes. Am = non-leaving amine ligand and X = anionic leaving ligand*

complexes synthesised by Loh *et al*. [5] in 41M human ovarian carcinoma cells [45], and the same relationship for eight complexes prepared by Ang *et al*. [6] in both HT29 colon carcinoma and A549 lung carcinoma cells. Importantly, higher cellular accumulation was found to correlate with higher cytotoxicity [5, 6], suggesting that lipophilic ligands can be used to enhance anticancer activity. In addition, the more lipophilic complexes were shown to accumulate more readily in cisplatin-resistant cells, possibly due to their greater capacity for passive diffusion, which allows them to bypass the active transport mechanisms that are partially relied on by cisplatin to enter cells [5, 44]. In the 1990s, Kelland *et al*. investigated a set of platinum(IV) complexes of the general formula *cis,trans,cis*-[$PtCl_2(OCOR_1)_2NH_3(RNH_2)$], finding that cytotoxicity increased as the lipophilicity of the *R* and R_1 substituents increased [49]. As the *R* group increased stepwise from cyclobutane through to cycloheptane, anticancer activity increased in parallel. Similarly, as the number of carbons in the R_1 substituent increased from $R_1 = -CH_3$ through to $-C_5H_{11}$, cytotoxicity also increased in a linear fashion. One of the lead compounds that emerged from this study, satraplatin (**4**), is the platinum(IV) complex to have progressed furthest in clinical trials to date (Figure 2.3). Satraplatin is a lipophilic analogue of cisplatin which is able to overcome cisplatin resistance by accumulating more readily in cells [50].

While lipophilic ligands have been shown to be useful for improving anticancer activity and attenuating resistance, the downside of more lipophilic complexes is that their ability to penetrate tumours may be compromised. Since tumour cells proliferate at a faster rate than the growth of new blood vessels, isolated regions of cells develop which are located more than 100 μm from the vasculature [51]. This is in contrast with regular tissue, in which all cells exist within a few cell diameters (~70 μm) from blood vessels to allow efficient delivery of oxygen and nutrients [51]. As a result, platinum complexes may be required to diffuse up to 200 μm from the vasculature in order to destroy all viable cells in a tumour [51, 52]. The high cellular uptake of lipophilic complexes is likely to lead to sequestration in tumour cells closest to the blood supply, leaving more isolated regions of tumours untouched. Bryce *et al*. have investigated this phenomenon by comparing the tumour penetration of Pt1C3 (**5**), a cisplatin analogue in which one of the ammine ligands has

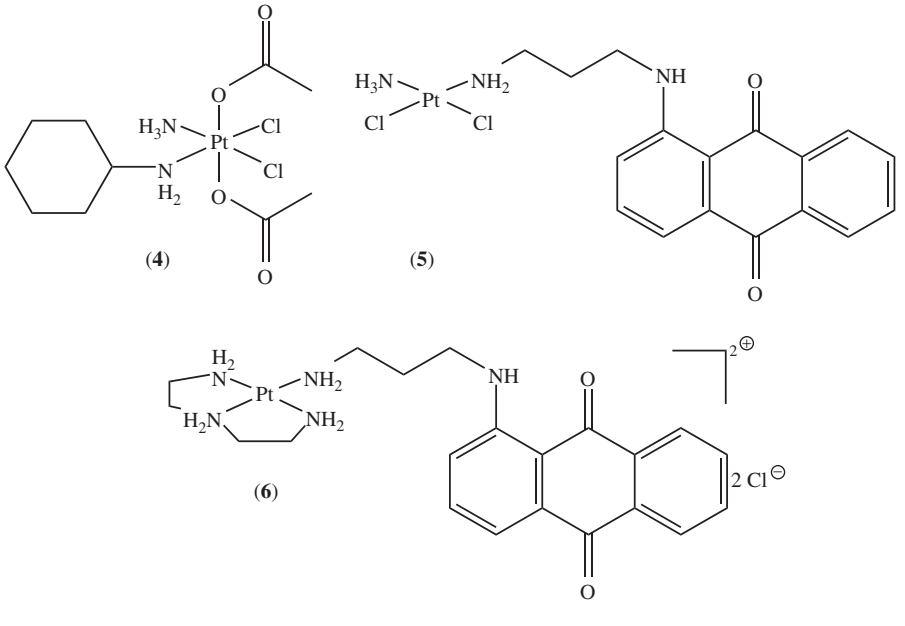

Figure 2.3 *Satraplatin (**4**), Pt1C3 (**5**) and Ptdien1C3^{2+} (**6**)*

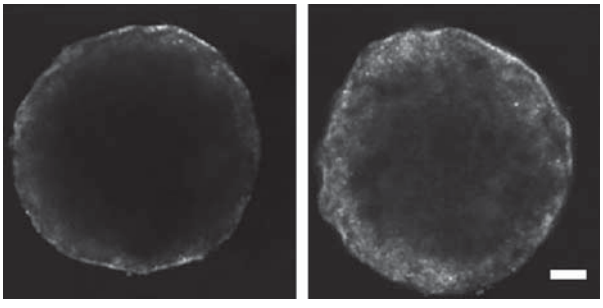

(a) (b)

Figure 2.4 *Fluorescence images of DLD-1 spheroids treated with (a) Pt1C3 (**5**) and (b) Ptdien1C3^{2+} (**6**). Scale bar represents 100* μm. *With kind permission from Dr J. Zhang © J. Zhang, 2013*

been modified to incorporate a lipophilic anthraquinone group, with that of its doubly-charged hydrophilic counterpart, Ptdien1C3^{2+} (**6**) (Figure 2.3) [3]. The fluorescent anthraquinone component was used to map the diffusion profiles of the complexes in spheroid tumour models using confocal microscopy. After a 24 hour incubation period, the more hydrophilic complex, Ptdien1C3^{2+}, was found to effectively diffuse into the spheroids, while the more lipophilic Pt1C3 was restricted to the outer cell layers (Figure 2.4). Synchrotron radiation-induced X-Ray fluorescence (SR-XRF) platinum mapping was used as a complementary method to confirm the superior spheroid penetration of Ptdien1C3^{2+} [4]. This discrepancy presumably reflects the differences in cellular accumulation of the two complexes. The cellular accumulation of Pt1C3 is almost 10 times higher than Ptdien1C3^{2+} after a 24 hour treatment period [3], and this favourable cellular uptake is believed to lead to rapid sequestration in the peripheral cell layers of spheroids, preventing the complex from penetrating further into central regions. These results highlight the need to choose ligands whose lipophilicity strikes a balance between optimal anticancer activity/reduced resistance and effective tumour penetration.

2.4.2 Reactivity

The design of leaving and non-leaving ligands can also influence the reactivity of platinum complexes. The lability of leaving ligands determines how quickly the complex is aquated to its activated form *in vivo*, thereby affecting how many side-reactions take place en route to the tumour site [35, 46, 53]. This is exemplified by carboplatin, in which the two chlorido leaving ligands of cisplatin have been replaced with a less labile bidentate cyclobutane-1,1-dicarboxylato ligand. The slower aquation kinetics of carboplatin reduce the toxicity of the drug relative to cisplatin, and as such, higher doses can be administered [8, 10, 36]. Similarly, oxaliplatin is significantly less toxic than cisplatin due to the lower lability of the bidentate oxalato leaving group [8, 54].

The non-leaving ligands of platinum complexes influence the reactivity of platinum complexes with deactivating biomolecules including thiols and DNA mismatch repair proteins, and can be selected to reduce drug resistance. Oxaliplatin circumvents cisplatin resistance by forming platinum-DNA adducts which are able to escape detection by DNA repair proteins [37, 38, 55]. The drug contains a bulky bidentate *R,R*-cyclohexane-1,2-diamine non-leaving ligand in place of the two ammine ligands of cisplatin, which is able to block repair proteins from making contact with damaged DNA [55]. Oxaliplatin is approved for the treatment of colorectal cancer, which is intrinsically resistant to cisplatin and carboplatin [8, 38]. Picoplatin (**7**) is an analogue of cisplatin in which one of the non-leaving ammine ligands has been replaced with a 2-methylpyridine ring (Figure 2.5). The pyridine ring sits at an almost perpendicular angle to the plane defined by the platinum and donor atoms, thereby positioning the methyl substituent directly over the platinum centre [56]. The platinum atom is thus shielded from nucleophilic attack by thiols, allowing

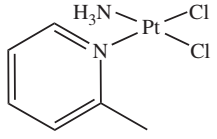

(**7**)

Figure 2.5 *Picoplatin*

the complex to overcome glutathione-mediated resistance. Accordingly, picoplatin has been shown to be significantly more effective than cisplatin and carboplatin in cisplatin-resistant cell lines [8, 57, 58]. Due to its slower aquation kinetics and reduced reactivity with nucleophiles, picoplatin binds to DNA at a slower rate than cisplatin; however, the platinum-DNA adducts formed are repaired to a lesser extent than those produced by cisplatin [57].

2.4.3 Rate of reduction

Platinum(IV) complexes contain two extra axial ligands to give an octahedral structure, and can be considered prodrug forms of platinum(II) complexes, since their activity relies on reduction *in vivo* to the cytotoxic platinum(II) species (Figure 2.6) [41, 59]. The slower rates of ligand exchange characteristic of platinum(IV) complexes have brought them into the spotlight in recent years, as they offer the opportunity to reduce the toxic side-effects associated with their platinum(II) counterparts [41, 59].

The reduction rate of platinum(IV) prodrugs dictates the rate at which the active platinum(II) cytotoxin is released, and represents a key feature in their design. Until recently, the conventional wisdom was that the reduction rate of platinum(IV) complexes was primarily determined by the identity of the axial ligands [59]. More recent work suggests, however, that ease of reduction is determined by the propensity of all constituent ligands, both axial and equatorial, to form electron-transfer bridges with reducing agents [60]. Chlorido and hydroxido ligands have been shown to be effective bridging ligands, leading to relatively rapid reduction, while carboxylato and amine ligands are poor bridging ligands and can be employed to stabilise platinum(IV) complexes [60]. Chen *et al*. have investigated the rate of reduction of a platinum(IV) complex containing only carboxylato and amine ligands, *trans*-[Pt(OAc)$_2$(ox)(en)] (**8**) (Figure 2.7), finding the half-life of the complex to be 2.5 and 27 days in the presence of excess ascorbate and cysteine respectively [61]. Ascorbate is a common biological reductant, while cysteine mimics the reducing action of glutathione, albumin and other endogenous thiols on platinum(IV) complexes.

While it is desirable for platinum(IV) prodrugs to be kinetically inert in the circulation, they must be able to release the active platinum(II) cytotoxin upon entry into tumour cells. Despite having been shown to be exceptionally stable in the presence of small molecule reductants (ascorbate and cysteine), *trans*-[Pt(OAc)$_2$(ox)(en)] exhibits a half-life between 2 and 6 hours in DLD-1 human colon cancer cells, most likely due to reduction by high molecular weight biomolecules such as reductases [61]. This observation

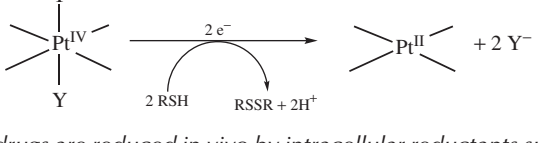

Figure 2.6 *Platinum(IV) prodrugs are reduced in vivo by intracellular reductants such as thiols. The two-electron process generally involves loss of the axial ligands (Y) to give the active platinum(II) cytotoxin*

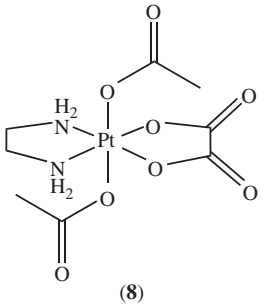

(**8**)

Figure 2.7 *trans-[Pt(OAc)$_2$(ox)(en)]*

suggests that platinum(IV) prodrug design should focus on employing ligands which endow the highest possible stability in the bloodstream, since the strongly reducing nature of the intracellular environment can be relied on to reduce all platinum(IV) complexes once inside target tumour cells.

2.5 Ligands for enhancing the anticancer activity of platinum complexes

To enhance the antiproliferative effects of platinum complexes, one strategy is to incorporate ligands that increase binding affinity for DNA. Alternatively, enzyme-inhibiting ligands can be used to overcome cisplatin resistance or increase apoptosis.

2.5.1 Ligands for improving DNA affinity

Intercalators are a class of planar, aromatic and polycyclic compounds that can slide between adjacent DNA base pairs [62, 63]. They are useful ligands for platinum anticancer complexes due to their high affinity for DNA, which acts to localise the platinum complex in the vicinity of DNA, increasing the rate of platination [64–68]. In addition, platinum-intercalator conjugates can generate novel DNA lesions that are able to evade repair mechanisms [67, 68]. The lipophilicity of intercalators facilitates cell penetration, while their innate fluorescence allows mapping of their distributions in cells and tumour models using fluorescence microscopy [3, 69, 70]. Finally, intercalators are known to exhibit anticancer activity of their own, due to (i) their tendency to lengthen and unwind the double-helical structure of DNA and (ii) their ability to disable topoisomerase activity *via* the formation of ternary DNA-intercalator-topoisomerase complexes [63, 71, 72]. It has been shown that when co-administered with cisplatin, intercalators generate a synergistic effect [73, 74], and in many cases, platinum-intercalator conjugates are more cytotoxic than their individual components [65, 66, 68, 75].

Several different types of intercalator have been investigated to improve the anticancer activity of platinum complexes, including phenanthridiniums [64], phenazines [65], anthracenes [66, 76], acridines [67, 68, 75] and anthraquinones [3, 70, 77–79] (Figure 2.8). A family of cationic platinum(II)-phenanthridinium species (**9**) has been shown to damage DNA at a markedly faster rate than cisplatin, with one analogue inflicting the same level of DNA damage in 30 minutes as cisplatin produced in 18 hours [64]. Similarly, a set of platinum(II) complexes linked to phenazine-1-carboxamides (**10**) has been found to exhibit enhanced DNA-binding compared to the parent platinum analogue, with complete DNA-unwinding taking place within 3 hours [65]. Moreover, the conjugates were reported to be significantly more cytotoxic than their platinum and intercalator subunits. The platinum(II)-anthracene complexes, [Pt(A9opy)Cl$_2$] (**11**) and *cis*-[Pt(A9pyp)(dmso)Cl$_2$] (**12**),

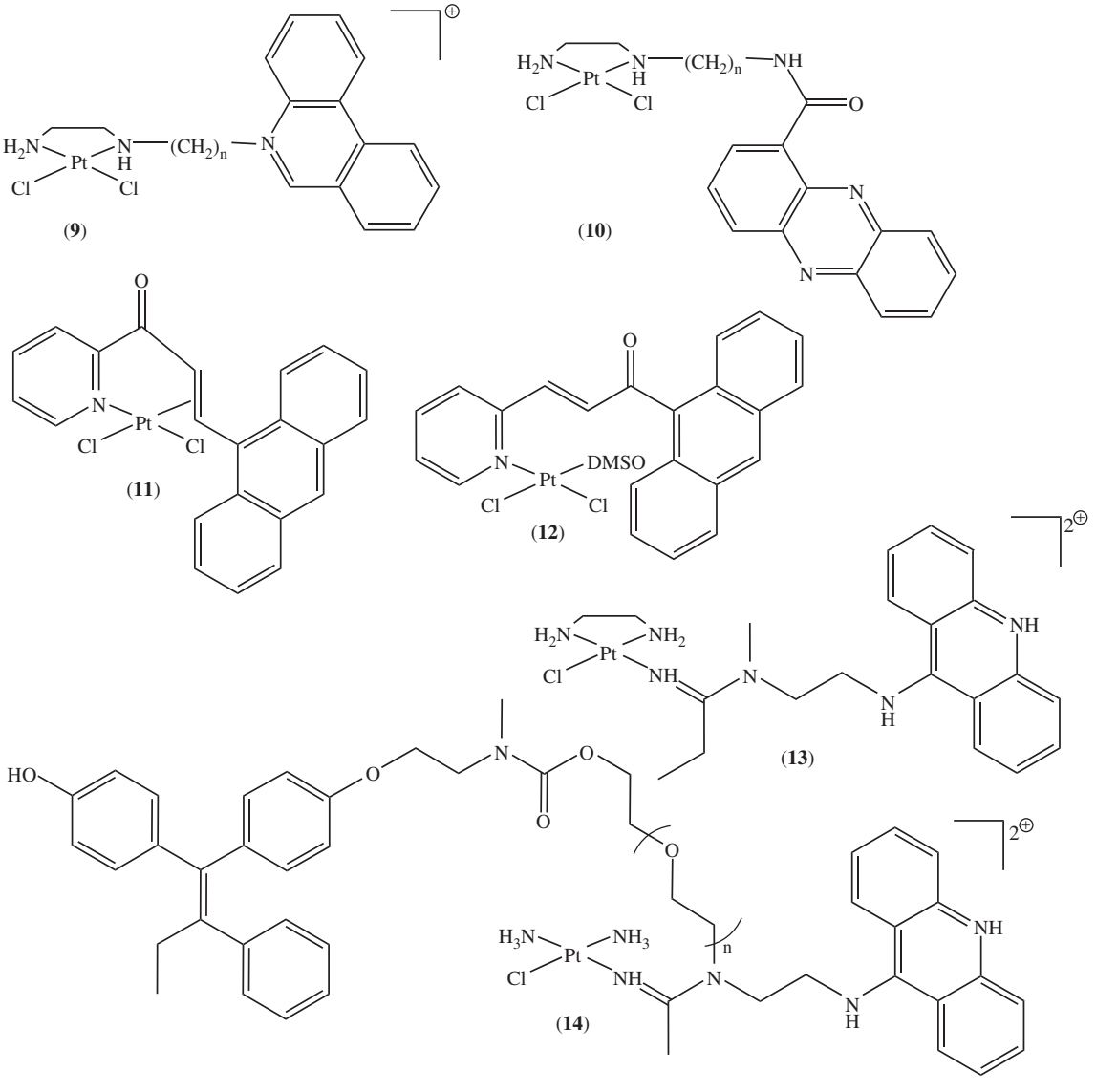

Figure 2.8 *Platinum complexes containing DNA-targeting ligands*

also rapidly bind to DNA and exhibit high activity in both cisplatin-resistant and -sensitive human ovarian carcinoma cells [66].

The most potent platinum-intercalator complex developed to date is a platinum(II)-acridine complex (**13**) developed by Bierbach *et al*., which is approximately 500 times more cytotoxic than cisplatin in non-small-cell lung cancer cells [68, 80, 81]. The monofunctional–intercalative DNA-binding mode of the platinum(II)-acridine conjugate has been shown to be inherently more damaging than the cross-links formed by cisplatin [68]. Unfortunately, the complex is poorly tolerated in mice [68, 81], and the prototype is now undergoing structural modifications in an effort to moderate its systemic toxicity. Most recently, the

platinum(II)-acridine complex has been coupled to tamoxifen, with the view to enhancing selectivity for breast cancer and reducing interactions with healthy tissue [82]. At this stage, no *in vivo* evaluations of the platinum(II)-acridine-tamoxifen conjugate (**14**) have been reported.

2.5.2 Ligands for inhibiting enzymes

Another approach for enhancing the anticancer activity of platinum complexes is to incorporate ligands that inhibit particular enzymes. Enzyme inhibitors have been attached to platinum complexes containing either (i) one or more leaving ligand(s) (Figure 2.9) or (ii) only non-leaving ligands (Figure 2.10). In the former case, a dual mode of cytotoxicity is provided, whereby the complex can target the enzyme of interest *and* DNA. In the latter case, the main role of the platinum is to provide a central framework for organising an organic enzyme inhibitor in three-dimensional space, in order to optimise its binding properties.

2.5.2.1 Complexes with one or more leaving ligand(s)

Marmion *et al*. have incorporated a histone deacetylase inhibitor, in the form of a suberoylanilide hydroxamic acid (SAHA) group, into the bidentate malonato leaving ligand of a cisplatin analogue [83]. By inhibiting

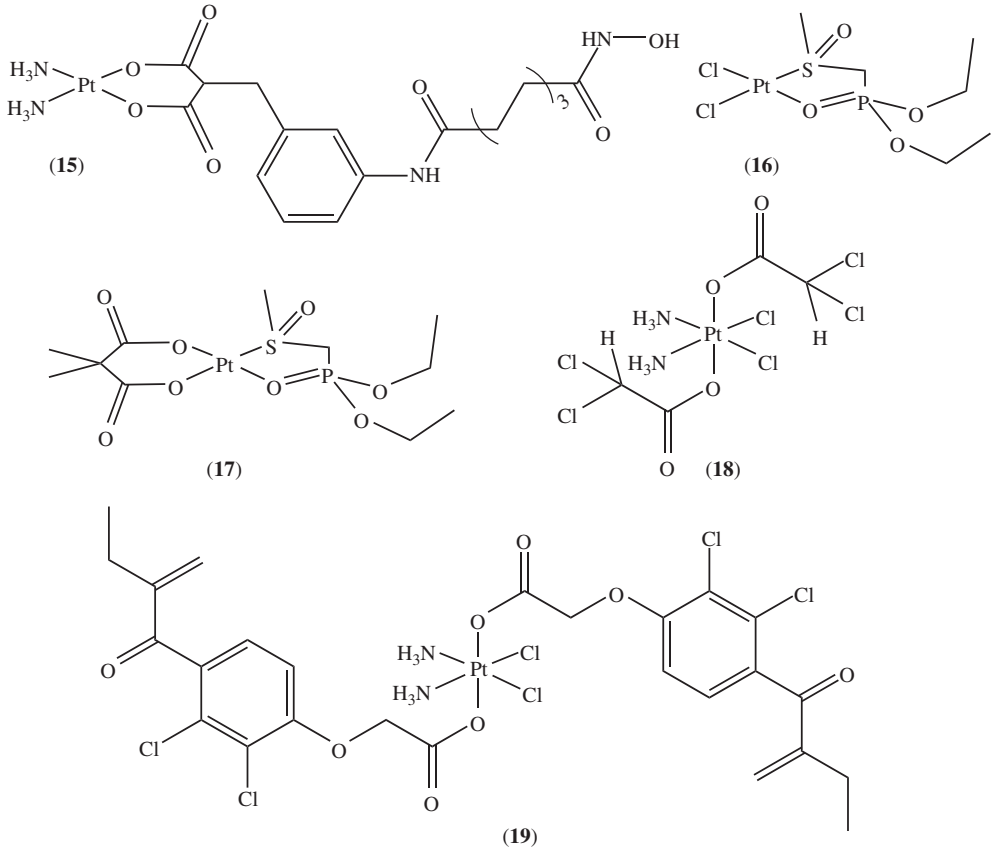

Figure 2.9 *Platinum complexes containing enzyme-targeting ligands and one or more leaving ligand(s)*

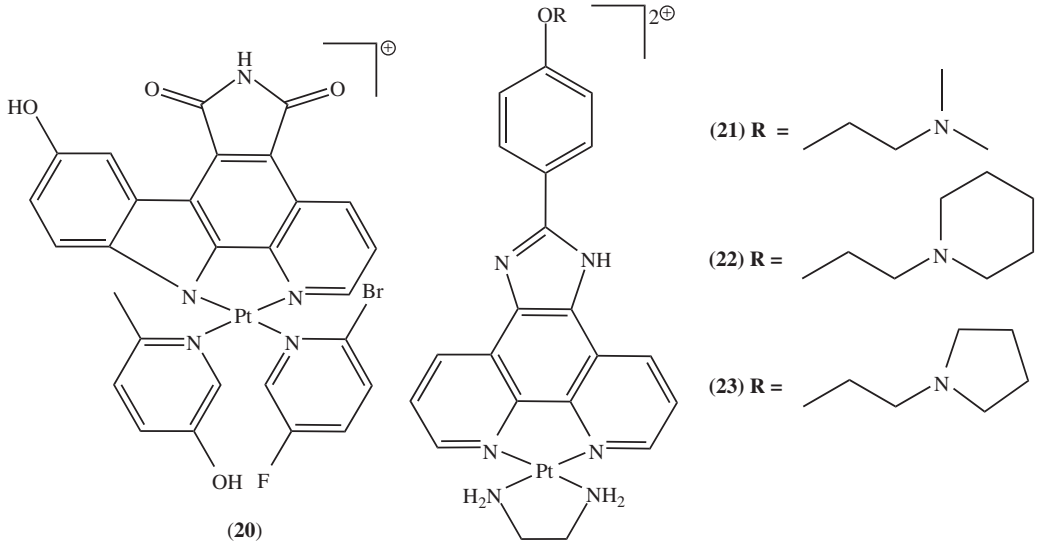

Figure 2.10 *Platinum complexes containing enzyme-targeting ligands and no leaving ligands*

histone deacetylase function, SAHA has been shown to induce growth arrest and apoptosis in a range of different tumour types, both *in vitro* and *in vivo* [84, 85]. SAHA is well tolerated in humans and is approved for the treatment of cutaneous T-cell lymphoma [86]. The antiproliferative properties of SAHA were envisaged to complement the activity of the DNA-binding platinum component; however, the platinum(II)-SAHA complex (**15**) exhibited slightly lower activity than cisplatin in a range of different tumour cell lines. This was consistent with the observation that the rate of DNA platination of the conjugate was significantly lower than that of cisplatin. The platinum(II)-SAHA complex also failed to exhibit any histone deactylase inhibitory activity, most likely due to interference from the malonato component with the SAHA-enzyme binding interactions. A positive finding was that the platinum(II)-SAHA conjugate demonstrated significantly less toxicity than cisplatin in normal human dermal fibroblast cells, hinting that SAHA may confer some degree of tumour cell selectivity.

Matrix metalloproteinases (MMPs) are a family of zinc-dependent endopeptidases that mediate homeostasis of the extracellular environment [87]. There is a strong link between MMP overexpression and tumour progression, rendering them a useful drug target [87]. Bisphosphonates are known to inhibit MMP activity [88], providing a rationale for tethering them to platinum(II) complexes. They also show a high affinity for bones, and have been investigated for their potential to target platinum complexes to bone cancer (Section 2.6.4) [89–91]. Coluccia *et al*. have synthesised two platinum(II) complexes bound to a bisphosphonate analogue, SMP (diethyl [(methylsulfinyl)methyl]phosphonate) [92]. The two complexes, [$PtCl_2$(SMP)] (**16**) and [Pt(dimethylmalonato)(SMP)] (**17**), were shown to strongly inhibit MMP-3, MMP-9 and MMP-12 through a non-competitive mechanism, though their anticancer activities were markedly lower than that of cisplatin. The authors speculated that the reduced activity of [$PtCl_2$(SMP)] may reflect rapid aquation and inactivation by thiols and other platinophiles en route to the DNA target. Reinforcing this theory was the observation that [$PtCl_2$(SMP)] undergoes rapid aquation, most likely due to the *trans* effect exerted by the sulfur atom. In contrast, the relatively slow aquation kinetics of [Pt(dimethylmalonato)(SMP)] may slow its adduct formation with DNA, thereby limiting its cytotoxic potential.

Tumour cells are characterised by their excess reliance on glycolysis for energy production; a phenomenon known as the Warburg effect [93–95]. A useful agent for exploiting this feature of cancer cells is dichloroacetate, a mitochondrial pyruvate dehydrogenase kinase inhibitor which downregulates glycolysis, ultimately leading to cell death [96]. Dhar and Lippard have installed dichloroacetate ligands in the axial positions of a platinum(IV) cisplatin derivative to improve its potency in tumour cells [97]. Upon entry into cells, the platinum(IV)-dichloroacetate (**18**) conjugate was envisaged to undergo intracellular reduction to produce cisplatin and two equivalents of dichloroacetate, allowing simultaneous attack of nuclear DNA and mitochondrial pyruvate dehydrogenase kinase. The conjugate was reported to be more cytotoxic than dichloroacetate in a range of tumour cells, but exhibited slightly poorer activity than cisplatin. An encouraging finding was that when MRC-5 normal lung fibroblasts and A549 human lung carcinoma cells were co-cultured and treated with the platinum(II)-dichloroacetate complex, a viability assay revealed selective killing of the A549 cancer cells. Furthermore, it was confirmed that the conjugate was able to inflict mitochondrial damage in addition to DNA damage. Finally, the conjugate was reported to accumulate more readily than cisplatin in cisplatin-resistant human epidermoid adenocarcinoma KB-CP 20 and hepatoma BEL 7404-CP 20 cancer cells, most likely due to its higher lipophilicity [98]. Higher lipophilicity is useful for enhancing activity, though this may be at the expense of tumour penetration (Section 2.4.1).

Another enzyme-targeting ligand that has been explored for enhancing the anticancer activity of platinum complexes is ethacrynic acid [99]. Ethacrynic acid is an inhibitor of glutathione-S-transferases (GSTs), a family of enzymes which is overexpressed in cisplatin-resistant cell lines [99, 100]. GST can catalyse the reaction between cisplatin and glutathione, promoting drug resistance [101]. By tethering two ethacrynic acid molecules to a platinum(IV) cisplatin derivative, the cytotoxicity of the resulting compound (**19**) was found to be more than double that of cisplatin after a 24 hour incubation period, though no major difference was evident after 72 hours [99]. It may be the case that the lipophilic platinum(IV)-ethacrynic acid complex accumulates more rapidly than cisplatin in cells over the first 24 hours, but both complexes reach the same steady state of platinum accumulation over a longer timeframe. Indeed, the conjugate was found to accumulate in A549 lung carcinoma cells approximately 10 times more than cisplatin over a 90 minute incubation period. Alternatively, the initially higher activity of the conjugate may reflect GST inhibition. It was shown that the GST levels of A549 lung carcinoma cells exposed to the platinum(IV)-ethacrynic acid complex decreased to 22.6% of the control level, while those treated with ethacrynic acid and cisplatin decreased to 78.5 and 63.6% of the control level respectively. Moreover, when the conjugate was tested directly against specific GST isozymes, it was found to inhibit GSTP1-1 and GSTA1-1 to less than 10% of their original activity.

2.5.2.2 Complexes with no leaving ligands

Protein kinases, a family of enzymes responsible for mediating signal transduction and cell signalling pathways, represent another potential target for anticancer drugs [102]. Genetic mutations in protein kinase-mediated signalling processes have been implicated in cancer proliferation and motility [102]. Protein kinase inhibitors can induce cell cycle arrest and apoptosis, usually by binding at the adenosine triphosphate (ATP) binding site [103, 104]. Meggers *et al*. have synthesised a series of platinum complexes designed to mimic the shape of staurosporine, a natural product whose kinase-inhibiting properties have been well documented [103, 105, 106]. The most potent of the series (**20**) exhibited nanomolar inhibitory activity against the protein kinase GSK-3α. Similarly, Child *et al*. have reported a series of platinum(II) complexes containing substituted phenanthroline ligands which inhibit two protein kinases, MAPK and Cdk2, at micromolar concentrations [104]. In both studies, the platinum centres functioned solely as scaffolds for the enzyme inhibitors, rather than conferring any cytotoxicity themselves through DNA-binding. Though no *in vivo* evaluations of the complexes were reported, they are likely to induce toxic side-effects, since

many protein kinase types share structurally similar binding sites [104]. For this reason, staurosporine and its derivatives are known to produce a number of different side-effects including hyperglycemia and hypotension, limiting their clinical utility [107, 108].

Platinum complexes can also be used to inhibit telomerase, an enzyme which is upregulated in more than 85% of cancers, while only being expressed at low levels in normal tissue [109]. G-quadruplexes formed from G-rich DNA sequences are believed to exist in the telomeres, multifunctional nucleoprotein complexes that protect the ends of chromosomes from degradation and fusion with neighbouring chromosomes [110, 111]. The life span of normal cells is limited by the shortening of the telomeres with each replication cycle; however, in tumour cells, upregulation of telomerase elongates the telomeres, resulting in cell immortality [110, 112]. G-quadruplexes in telomere regions are believed to inhibit the activity of telomerase, providing the impetus for using G-quadruplex stabilisers as antiproliferative agents [113]. Effective G-quadruplex stabilisers are believed to consist of (i) an extended π-surface, (ii) positively-charged substituents that can interact with the grooves and loops of the G-quadruplex and (iii) a positively-charged centre that can reside near the centre of the G-quartet [113, 114]. Platinum complexes containing non-leaving aromatic ligands are thus attractive candidates for G-quadruplex stabilisers. Wei *et al*. have developed three platinum(II)-phenanthroline derivatives ((**21**–**23**)) which are excellent stabilisers of *h*-telo, *c*-kit2 and *c*-myc G-quadruplexes [113]. Moderate selectivity for quadruplex *versus* duplex DNA was also reported. Encouragingly, (**21**) and (**23**) were shown to be strong *in vitro* inhibitors of telomerase, exhibiting higher activity than the free phenanthroline-based ligands. Curiously, (**22**) produced relatively little inhibitory activity and emerged as the weakest G-quadruplex stabiliser of the series, but displayed the most potent antitumour activity. The reasons for this unexpected result are yet to be resolved.

Recent work by Balasubramanian *et al*. has shown that G-quadruplex DNA can be visualised in cell nuclei and chromosomes, helping to resolve the existing controversy of whether G-quadruplexes do in fact exist in mammalian cells [115]. They developed an antibody known as BG4, which exhibits low nanomolar affinity for G-quadruplex DNA and no detectable binding to an RNA hairpin, single-stranded DNA or double-stranded DNA [115]. Using immunofluorescence to visualise the distribution of BG4 in chromosomes, it was shown that G-quadruplexes represent a very small component of the chromosomes, and that in actual fact, G-quadruplex structures mostly exist outside the telomeres. These results hint that (i) to be effective, G-quadruplex stabilisers must display excellent selectivity for quadruplex *versus* duplex DNA and (ii) that it may be difficult to selectively target G-quadruplexes in telomere regions.

2.6 Ligands for enhancing the tumour selectivity of platinum complexes

Efforts to reduce the side-effects of platinum anticancer agents, prevent drug loss *via* side-reactions, and treat specific tumour types, have increasingly shifted attention towards targeted delivery strategies; with no new small-molecule platinum drug entering clinical trials since 1999 [8]. Targeted delivery, often described as the ‘magic bullet’ or ‘guided missile’ approach, employs ligands that are able to selectively deliver platinum drugs to tumour sites while circumventing normal, healthy tissue. Targeting ligands are designed to exploit unique characteristics of tumour cells, such as higher consumption of particular nutrients or overexpression of certain enzymes or receptors, or they may target features of the tumour microenvironment, including the EPR effect. Finally, targeting ligands may not only provide a means of docking platinum drugs at tumour sites, but may also perform anticancer functions themselves upon release from the platinum centre.

Targeting ligands have been used to improve the tumour selectivity of both platinum(II) and platinum(IV) complexes. The advantage of platinum(IV) complexes is that targeting groups can be attached to the axial sites without modifying the structure of the cytotoxic platinum(II) component. Once inside tumour cells, reduction of the complex releases the targeting ligand(s), allowing the platinum(II) cytotoxin to bind to DNA.

The disadvantage of this strategy is that the axial targeting ligands may be lost upon reduction of the complex in the circulation, preventing delivery of the platinum(II) cytotoxin to its intended destination. Targeting groups attached to the equatorial non-leaving ligands of platinum(IV) complexes or the non-leaving ligands of platinum(II) complexes are less likely to be lost from the platinum centre before reaching the tumour site; however, because they do not undergo intracellular release from the platinum centre, they may interfere with DNA-binding. As a result, targeting ligands should be attached to either (i) the axial ligands of highly stable platinum(IV) complexes or (ii) the leaving ligands of platinum(II) complexes with relatively slow aquation kinetics. Alternatively, targeting ligands which do not impede DNA-binding can be conjugated to the equatorial non-leaving ligands of platinum(IV) complexes or the non-leaving ligands of platinum(II) complexes.

2.6.1 Ligands for targeting transporters

The rapid growth and proliferation of tumour cells increases their consumption of nutrients such as glucose, amino acids and fatty acids, which are used for energy production or as building blocks for the production of DNA, RNA, proteins and lipids [117]. To satisfy their increased appetite, tumour cells upregulate certain nutrient transporters, including the glucose transporters GLUT1 and SGLT1 and the amino acid transporters xCT/4F2hc, LAT1/4F2hc, ASCT2 and $ATB^{0,+}$ [117–119]. By incorporating nutrients that facilitate tumour cell uptake, it is believed that the tumour selectivity of platinum complexes can be improved (Figure 2.11) [118, 120–126].

Liu *et al*. have prepared a series of oxaliplatin analogues functionalised with glucose molecules (**24–26**) [121]. The oxalato ligand of oxaliplatin was replaced with a malonato ligand to provide an extra carbon as an attachment point for the glucose molecule. Similarly to oxalato complexes, malonato complexes are characterised by relatively slow aquation kinetics [127]. In view of this, the glucose targeting group was envisaged to remain bound to the platinum centre in the bloodstream, and only released once inside target cells. The platinum(II)-glucose conjugates were found to be up to 10 times more cytotoxic than oxaliplatin in tumour cells. To determine whether the higher potency of the complexes was related to increased uptake by

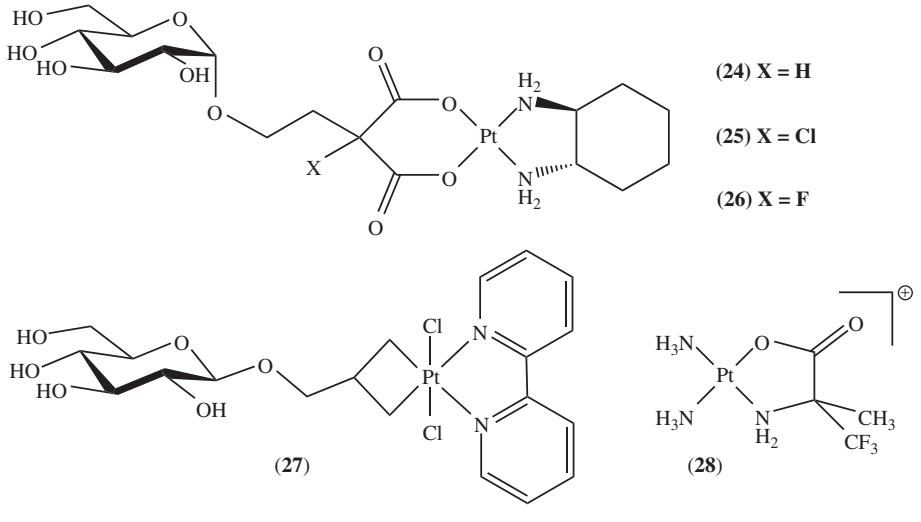

Figure 2.11 *Platinum complexes containing transporter-targeting ligands*

glucose transporters, the cytotoxicity of (**26**) was measured when co-administered with phlorizin, an inhibitor of SGLT. It was revealed that the activity of the complex was greatly reduced in the presence of phlorizin, while the inhibitor had little effect on the cytotoxicity of oxaliplatin, suggesting that the anticancer activity of the platinum(II)-glucose conjugates is largely dependent on uptake by glucose transporters. Finally, the conjugates were reported to be approximately five times less toxic to mice than oxaliplatin.

Hoberg and Stocker have used a novel synthetic route to incorporate a glucose molecule into a platinum(IV) complex [123]. The platinacyclobutane complex (**27**) was synthesised by coupling glucose to cyclopropylmethanol, before reacting with Zeise's dimer ($[Pt(C_2H_4)Cl_2]_2$). The resulting complex was designed to be carried into tumour cells by glucose transporters, at which point intracellular reduction would remove the glucose targeting group from the platinum centre, releasing cisplatin. No biological evaluations of the complex have been reported at this stage, though it is a strategy worthy of further investigation.

At this point in time, only a handful of studies have investigated the use of amino acids as targeting ligands for platinum complexes, without a great degree of success [125, 126, 128]. Zunino *et al*. have tethered a wide range of amino acids to a cisplatin analogue, finding the resulting complexes to be significantly less active than cisplatin in both *in vitro* and *in vivo* models [125, 126]. Similarly, Jin *et al*. have reported that platinum(II) complexes containing 1,10-phenanthroline and a variety of amino acid ligands are also significantly less cytotoxic than cisplatin [129]. It may be the case that natural amino acid ligands are too susceptible to degradation in biological environments to function as useful targeting groups. Synthetic amino acids may represent more effective biocarriers, since they often exhibit greater metabolic stability, and in some instances, enhanced biological activity [130, 131]. Margiotta *et al*. have investigated the use of α-trifluoromethylalanine as a non-natural amino acid targeting ligand for platinum(II) complexes [124]. $[Pt(NH_3)_2(R\text{-Tfm-Ala})]^+$ (**28**), where *R*-Tfm-Ala is the *(R)*-enantiomer of trifluoromethylalanine, is one of the most cytotoxic platinum-amino acid conjugates reported to date, though it is still less active than cisplatin (Figure 2.11).

2.6.2 Ligands for targeting receptors

Targeting ligands can also be used to convey platinum complexes to particular receptors that are overexpressed on the surface of tumour cells, including folate [132], $\alpha_v\beta_3$ [133], transcobalamin II (TCII) [134], neurotensin (NT) [135], SSTR [135], oestrogen [136, 137], translocator protein (TSPO) [138], CD13 [139] and Her2/neu receptors [140] (Figures 2.12 and 2.13). Upon binding to these receptors, the complexes are internalised by cells *via* endocytosis. Once inside cells, an appropriate cleavage mechanism is generally required to release the active platinum cytotoxin from the targeting ligand, such that optimal DNA-binding can take place. In addition to boosting tumour selectivity, receptor-targeting can also be used to improve the cellular uptake and/or cytotoxicity of platinum complexes.

2.6.2.1 Platinum(II) receptor-targeted complexes

Vitamin B_{12} is a type of receptor-targeting ligand whose potential for enhancing the tumour selectivity of platinum(II) complexes has been explored [118, 134]. B_{12} readily binds to apo-TCII, a carrier protein in the plasma, allowing subsequent binding to TCII, a vitamin B_{12} receptor that is overexpressed in cancers of the ovary, kidney, uterus, testis, brain, colon, lung and myelocytic blood cells [118, 134]. Ruiz-Sánchez *et al*. have developed a number of platinum(II)-vitamin B_{12} conjugates, *cis*-$[PtCl(NH_3)_2B_{12}]^+$ (**29**), *trans*-$[PtCl(NH_3)_2B_{12}]^+$ (**30**) and *cis*-$[PtCl_2(NH_3)B_{12}]$ (**31**), in which B_{12} is coordinated to the platinum through its cyanide group [118]. Importantly, it was shown that the B_{12} ligand remains stably bound to the platinum in human blood serum. The platinum(II)-B_{12} conjugates can be deemed prodrugs, since release of the active platinum(II) components requires intracellular reduction of the Co^{III} metal centre of B_{12}

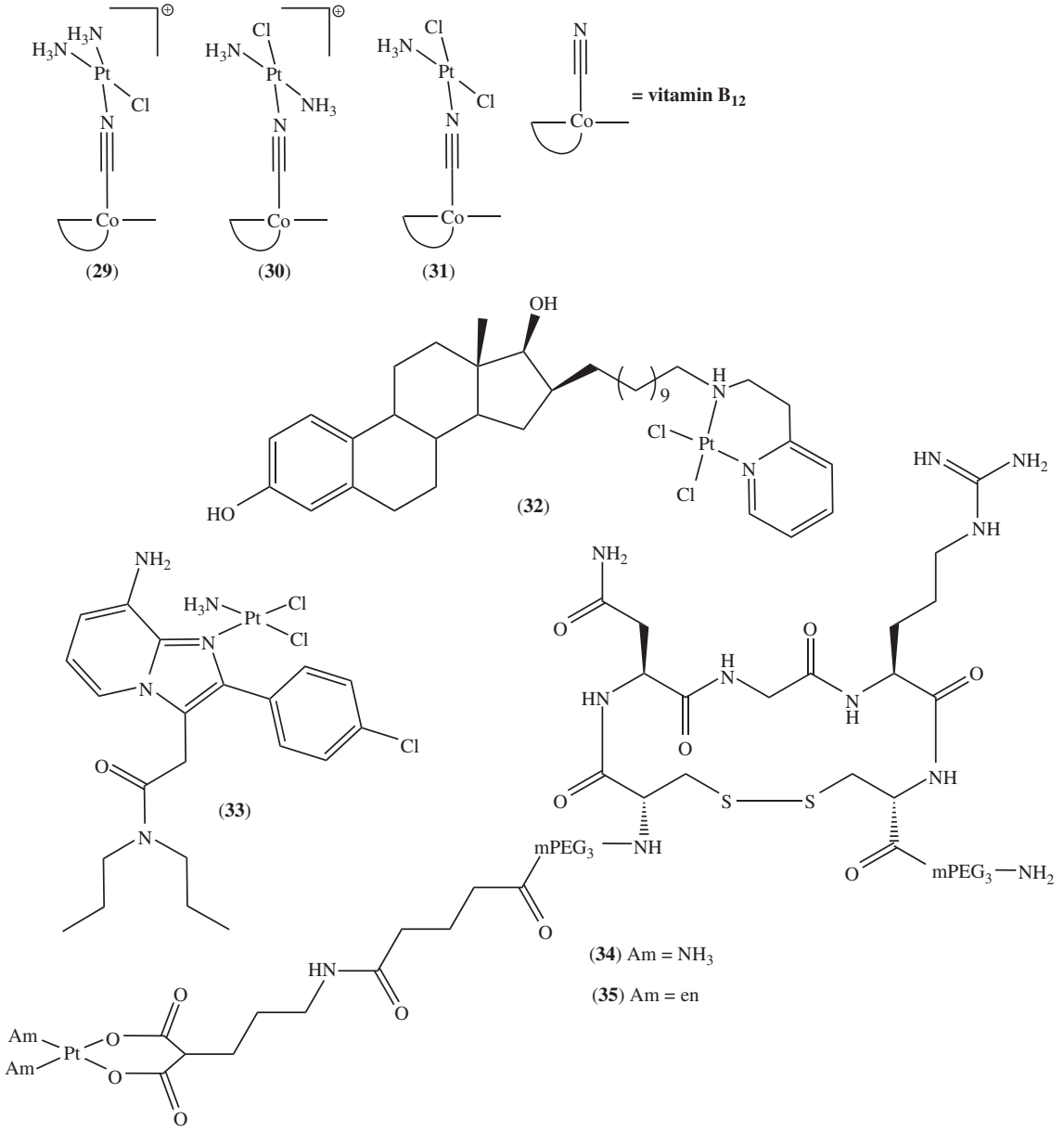

Figure 2.12 *Platinum(II) complexes containing receptor-targeting ligands*

to Co^{II} and Co^{I} and subsequent adenosylation by adenosyltransferase [141]. Cytotoxicity assays found the platinum(II)-vitamin B_{12} conjugates to be significantly less active in monolayer cells than cisplatin, though this is not a meaningful comparison, since the conjugates are believed to rely on receptor-mediated endocytosis to enter cells. Cisplatin, which readily undergoes passive diffusion into cells, presumably exhibits higher activity due to its enhanced cellular accumulation. Notably, the platinum(II) complexes cleaved from

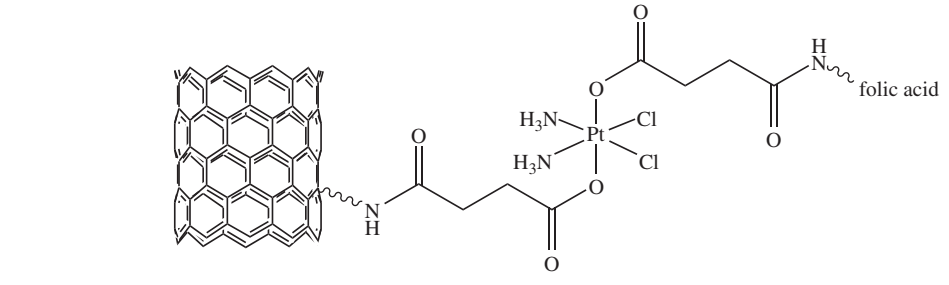

(**36**)

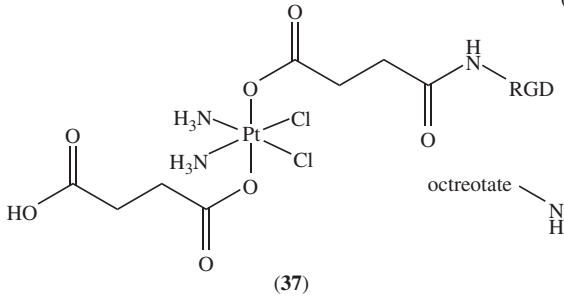

(**37**)

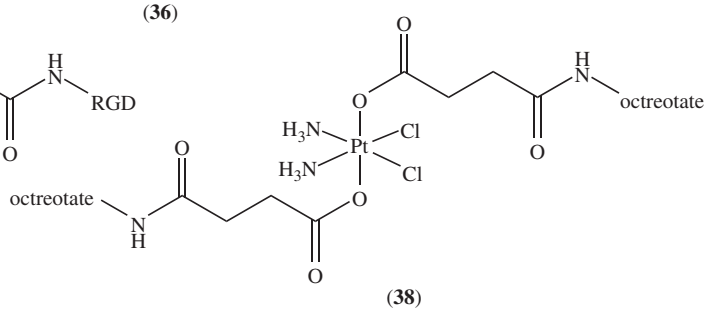

(**38**)

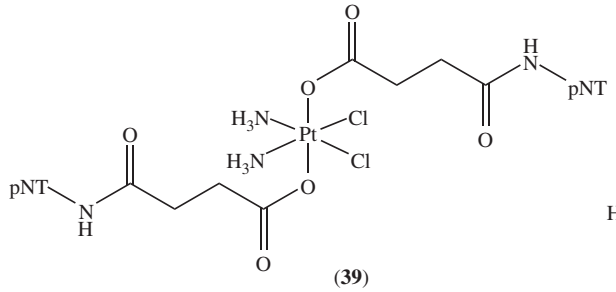

(**39**)

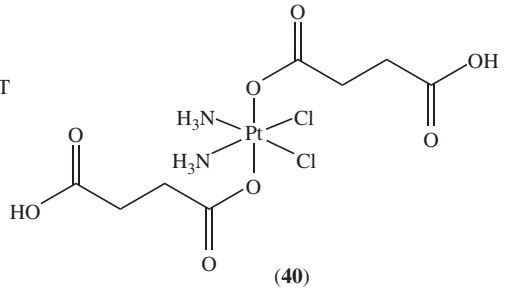

(**40**)

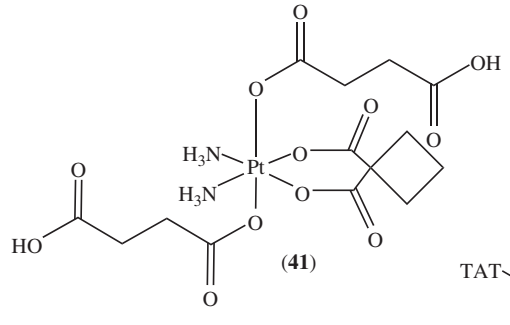

(**41**)

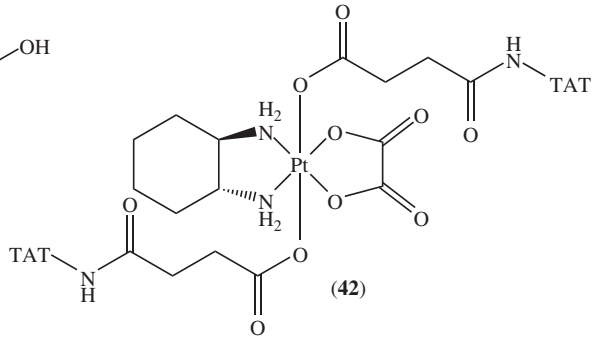

(**42**)

Figure 2.13 *Platinum(IV) complexes containing receptor-targeting ligands. RGD = Arg-Gly-Asp, octreotate = cyclic peptide D-Phe-Cys-Phe-D-Trp-Lys-Thr-Cys-Thr-OH (disulfide bridge between Cys2 and Cys7), pNT = Lys-Lys-Pro-Tyr-Ile-Leu and TAT = Tyr-Gly-Arg-Lys-Lys-Arg-Arg-Gln-Arg-Arg-Arg*

B_{12} exhibited similar activity to cisplatin in A2780 and MCF7 cancer cells, hinting that the platinum(II)-B_{12} prodrugs should be as effective as cisplatin once activated inside target cells. Finally, cytotoxicity assays performed in apo-TCII and B_{12} free media revealed that the activity of the conjugates was dependent on the addition of apo-TCII. This indicates that binding to apo-TCII and subsequent internalisation by the TCII receptor is the main pathway by which the platinum(II)-B_{12} complexes enter cells, suggestive of a high level of selectivity.

Oestradiol, the most active endogenous oestrogen, is another type of targeting ligand that has been employed for enhancing the tumour selectivity of platinum(II) complexes. The initiation and progression of oestrogen receptor-α (ERα)-positive breast cancers is largely driven by the upregulation of ERα, which is present in nearly two-thirds of all breast cancers [142]. Oestradiol binds to ERα, whereupon it is internalised by cells *via* endocytosis [143]. Bérubé *et al*. have designed three oestradiol-linked cisplatin analogues which display high ERα affinity and better activity than cisplatin in breast cancer cell lines [136]. The most promising of the series (**32**) also produced more significant tumour regression than cisplatin in a xenograft mouse model of human ERα-positive breast cancer [137]. Importantly, in the ERα-negative xenograft model, there was no difference between cisplatin and (**32**) in terms of tumour regression. More recently, the same authors devised analogous carboplatin- and oxaliplatin-oestradiol conjugates [136]. These were less cytotoxic than their cisplatin-oestradiol counterparts; however, two of the oxaliplatin derivatives exhibited low nanomolar affinities for ERα, representing a slight improvement on the cisplatin analogues. An interesting point to note is that although the oestradiol components were tethered to non-leaving ligands of the platinum(II) complexes, the long aliphatic or polyethylene glycol (PEG) spacers that were used to separate the platinum and oestradiol components appeared to minimise interference from the bulky targeting group with DNA-binding. The most active platinum(II)-oestradiol conjugates had the longest spacers between the two subunits (11 carbon chains).

TSPO 18 kDa receptors are also potential targets for tumour-selective anticancer drugs, as they are upregulated in several cancer types, including brain, breast, prostate and colorectal, and their expression increases in parallel with tumour malignancy [144, 145]. Although they are also present on cell surface membranes, they primarily reside on the mitochondrial membranes, where they form part of the mitochondrial permeability transition pores (MPTs) [146]. MPT pores are multiproteic complexes that play a key role in regulating cell survival or death [146]. Binding ligands are believed to be able to stimulate opening of the pores, triggering a cascade of events leading to apoptosis [138]. A cisplatin analogue containing a non-leaving TSPO-targeting ligand (**33**) has been investigated for its TSPO-binding affinity, cellular accumulation and anticancer activity [138]. The targeted platinum complex displayed nanomolar affinity towards TSPO receptors, while showing no affinity for central benzodiazepine receptors, indicative of a high level of receptor selectivity. The cytotoxicity of the complex in a range of tumour cell lines was comparable to that of cisplatin, and its activity did not diminish in cisplatin-resistant cells. As a result, it appears that the inclusion of the TSPO-targeting group in the non-leaving ligands of cisplatin does not impede DNA-binding. The complex was observed to accumulate in C6 glioma cells almost 60 times more than cisplatin after a 24-hour incubation period, consistent with the extra lipophilicity endowed by the TSPO-targeting ligand. It should be noted that the lipophilicity of the targeted complex is likely to reduce its tumour penetration, while also facilitating passive diffusion into non-target cells, which would lead to side-effects. *In vivo* studies will be required to assess the tumour selectivity of the novel platinum complex.

CD13 receptors are useful for drug targeting as they are expressed on the surface of endothelial cells in the vasculature and angiogenic tissue of prostate, lung, pancreas, kidney, breast, ovarian and colon cancer, while being absent from the normal vasculature [139, 147–152]. Based on the knowledge that NGR (Asn-Gly-Arg) peptides selectively bind to CD13 receptors, Hammer *et al*. have coupled the cyclic peptide CNGRC to cisplatin and [$PtCl_2$(en)] *via* a malonato leaving ligand [139]. MiniPEG groups were also incorporated into the structures to improve solubility. Because the malonato group conferred structural similarity with carboplatin,

the anticancer activities of the two platinum(II)-CNGRC conjugates (**34**) and (**35**) were compared with that of carboplatin. In CD13(+) PC-3 prostate cancer cells, the conjugates were more potent than carboplatin, while the free peptide exhibited negligible cytotoxicity. Interestingly, when (**35**) was incubated with increasing concentrations of the free peptide, the activity of the conjugate declined, presumably due to competition with the peptide for CD13 receptor-mediated endocytosis into cells. In contrast, increasing concentrations of the free peptide did not affect the cytotoxicity of carboplatin, as it does not bind to CD13 receptors. Cellular accumulation studies revealed that 12-fold and 3-fold more platinum accumulated in CD13(+) PC-3 cells treated with conjugates (**34**) and (**35**) respectively than those treated with carboplatin, which the authors speculate may reflect enhanced cellular uptake due to receptor-mediated endocytosis; though the experiment would need to be repeated in CD13(−) cells to test this hypothesis. Since the targeting group is attached to the platinum centre *via* a leaving ligand, aquation of the complex inside cells was envisaged to release the active platinum cytotoxin. A possible drawback of these conjugates *in vivo* may be the peptide-malonato ligand being removed by aquation in the bloodstream, before being able to deliver the platinum complexes to CD13-expressing cells.

In another approach, Gao *et al*. have developed platinum(II)-herceptin conjugates for targeting Her2/neu receptors, which are overexpressed in 20–30% of breast cancers [140, 153]. Herceptin is a humanised monoclonal antibody that is one of the most effective biological treatments for breast cancer [140]. A number of different mechanisms are believed to contribute to its anticancer properties, one of which involves stimulation of Her2 endocytosis [153, 154]. A cisplatin analogue containing a functionalised cyclohexane-1,2-diamine non-leaving ligand was bound to the backbone of herceptin through an unknown coordination mode. When 10 platinum units were attached to the herceptin backbone, the activity of the resulting conjugate was 16 times higher in Her2/neu-overexpressing SK-BR-3 cancer cells than in normal fibroblasts, suggestive of a high degree of selectivity. Interestingly, the platinum(II)-herceptin conjugate is stable at normal extracellular pH (7.4), but the platinum and antibody components begin to dissociate as pH is lowered, with complete dissociation taking place at pH 4.8. As a result, the authors speculate that the conjugate remains intact outside target cells, with the platinum(II) cytotoxin only being released upon exposure to the mildly acidic conditions found in lysosomes (pH 5.5) following endocytosis [140].

2.6.2.2 Platinum(IV) receptor-targeted complexes

Folate receptors (FRs) are attractive drug targets, since they are highly expressed in epithelial, ovarian, cervical, breast, lung, kidney, colorectal and brain tumours, while being expressed at significantly lower levels in normal tissue [155, 156]. Folic acid has a high affinity for FRs, rendering it a useful tumour-targeting ligand. Lippard *et al*. have synthesised a platinum(IV) analogue of cisplatin with a folic acid molecule positioned in one axial site and a carbon nanotube in the other [132]. The folic acid component was designed to increase tumour selectivity, while the carbon nanotube was incorporated to exploit the EPR effect (Section 2.6.3). It was envisaged that the conjugate (**36**) would selectively bind to FRs, at which point it would be actively transported into tumour cells. Intracellular reduction would then release cisplatin from the bulky axial groups, allowing the free drug to bind to DNA. The platinum(IV)-nanotube-folic acid conjugate was found to be more active than cisplatin in FR(+) KB cells, with an IC_{50} value of 0.010 μM, compared with 0.086 μM for cisplatin. In addition, the conjugate was shown to be approximately five times more active in FR(+) KB cells than in FR(−) NTera-2 cells. This may reflect differences in the KB and NTera-2 cell lines, or it may be indicative of higher accumulation in KB cells due to FR-mediated endocytosis.

Targeting of integrin receptors is another strategy that has been investigated for improving the tumour selectivity of platinum anticancer complexes. The $\alpha_v\beta_3$ receptor is of particular interest, as it has been implicated in the initiation, progression and metastasis of many solid tumour types [157, 158]. $\alpha_v\beta_3$ integrins are expressed on the surface of normal endothelial cells, but they are expressed to a significantly higher extent on the surface

of proliferating endothelial cells during tumour angiogenesis and metastasis [157, 158]. A useful targeting group for delivering anticancer drugs to $\alpha_v\beta_3$ is the RGD (Arg-Gly-Asp) peptide motif, which strongly binds to the integrin receptor [159]. Lippard *et al*. have coupled RGD to the axial ligand of a platinum(IV) cisplatin analogue, anticipating that the resulting complex (**37**) would bind to $\alpha_v\beta_3$ on the surface of tumour cells, undergo endocytosis, and subsequently be reduced by intracellular reductants to yield cisplatin [133]. It was revealed that the cytotoxicity of the platinum(IV)-RGD conjugate was comparable to that of cisplatin in both BCE and HMVEC endothelial cells. When an $\alpha_v\beta_3$-binder, in the form of the cyclic pentapeptide (RGDfK)c, was co-administered with the conjugate, the activity of the conjugate was partially diminished, suggesting that it was competing to some extent with (RGDfK)c for $\alpha_v\beta_3$ receptor-mediated endocytosis. Reinforcing this notion was the finding that the conjugate was approximately three times less potent in β_3 knockdown HMVEC cells than in regular HMVEC cells.

In a similar approach, Ravera and co-workers have coupled a NT-like peptide, pNT (Lys-Lys-Pro-Tyr-Ile-Leu), and a somatostatin analogue, octreotate ($_D$-Phe-Cys-Phe-$_D$-Trp-Lys-Thr-Cys-Thr-OH), to a platinum(IV) cisplatin derivative, in order to target NT receptors and somatostatin receptors (SSTRs). Both NT and SSTR receptors are known to be overexpressed in several types of cancer [135]. The activities of the platinum(IV)-octreotate and -pNT conjugates ((**38**) and (**39**) respectively) were shown to be markedly higher than that of their *cis,cis,trans*-diamminedichloridodisuccinatoplatinum(IV) precursor (**40**) in a range of tumour cell lines, though this is not a meaningful comparison. At biological pH, the two axial succinato ligands of (**40**) are deprotonated at the terminal carboxylic acid positions, conferring a two minus charge upon the complex. Anionic platinum complexes are known to exhibit very poor cellular uptake and weak anticancer activity; Gui has shown, for example, that the disuccinato platinum(IV) analogue of carboplatin (**41**) exhibits negligible cellular uptake and cytotoxicity in A2780 cells [160]. A more informative comparison would be with cisplatin or a disuccinato platinum(IV) analogue in which the carboxylates have been functionalised to give a neutral compound. Finally, the IC_{50} values of the two platinum(IV)-peptide complexes were discovered to have little correlation with NT and SSTR expression, indicating that receptor-mediated endocytosis does not play a major role in their cellular uptake.

At this point, it should be noted that all receptor-targeted platinum(IV) complexes described thus far are based on a cisplatin structural motif, with receptor-targeting ligands positioned in the axial sites. Since they have been designed to be primarily taken up by cells *via* receptor-mediated endocytosis, their activities in monolayer cells should be lower than that of cisplatin. This is because cisplatin readily undergoes passive diffusion into cells, which is a more efficient uptake mechanism than active transport. In actual fact, the FR-targeted complex was found to be moderately more cytotoxic than cisplatin, while the $\alpha_v\beta_3$-targeted complex was comparable in activity (no data is available for the NT- and SSTR-targeted complexes). Moreover, only a partial dependence on receptor-mediated cellular uptake was observed for the FR- and $\alpha_v\beta_3$-targeted complexes, while no receptor selectivity was apparent for the NT- and SSTR-targeted complexes.

A possible explanation for these findings is that the receptor-targeted platinum(IV) agents detailed thus far undergo passive diffusion into cells, in addition to active transport. This property would be unfavourable, since it would allow the conjugates to passively diffuse into normal, healthy cells, in addition to target tumour cells. Alternatively, the platinum(IV) conjugates may undergo reduction in the cell growth medium, releasing cisplatin, which is then able to passively diffuse into cells. This would not be unexpected, as each of the complexes contains two equatorial chlorido ligands. As discussed in Section 2.4.3, chlorido ligands coordinated to platinum(IV) complexes give rise to relatively fast reduction rates. Rapid reduction of these complexes would be unfavourable in a clinical setting, since the receptor-targeting groups would be lost in the circulation, releasing the active platinum(II) cytotoxins prematurely and generating unwanted side-reactions.

Keppler *et al*. have used a more stable platinum(IV) framework in their synthesis of a receptor-targeted anticancer agent [161]. A TAT peptide fragment (Tyr-Gly-Arg-Lys-Lys-Arg-Arg-Gln-Arg-Arg-Arg) was coupled to a platinum(IV) oxaliplatin derivative incorporating only amine and carboxylato ligands, which are less able

to form electron-transfer bridges with reductants than chlorido ligands (Section 2.4.3). The TAT peptide is able to chaperone drugs with poor permeating abilities across cell membranes, and there is also evidence that it is able to cross the blood-brain barrier [161–165]. While the mechanisms by which the TAT peptide crosses cell membranes remain contentious, a significant portion of TAT peptide uptake is believed to involve binding to heparan sulfate receptors and subsequent endocytosis into cells [166]. Since oxaliplatin exhibits relatively low accumulation in cancer cells, it was anticipated that the incorporation of a TAT peptide fragment may improve its cellular uptake and hence its anticancer activity. The oxaliplatin-based platinum(IV)-TAT conjugate (**42**) displayed an antiproliferative effect across a number of different cancer cell lines, though its cytotoxicity was not compared with that of cisplatin or oxaliplatin [161]. It should be noted that, since heparan sulfate receptors are not limited to cancer cells, the TAT group does not confer any tumour selectivity. The platinum(IV)-TAT conjugate represents the first example of a receptor-targeted platinum(IV) complex constructed from a relatively inert coordination sphere, representing a design strategy that should be employed to maximise the stability of future receptor-targeted platinum(IV) complexes

2.6.3 Ligands for targeting the EPR effect

Another feature of tumours that can be exploited to improve the tumour selectivity of platinum complexes is the unusual architecture of the vasculature. Blood vessels in tumours are irregular in shape, leaky and dilated, and the endothelial cells are poorly aligned and characterised by large fenestrations [1, 2]. As a result, large molecules such as polymers and nanoparticles present in the blood plasma are able to leak into tumour tissue, while being largely restricted from entering normal, healthy tissue [1, 2]. In addition, these large molecules tend to be retained by the tumour mass due to poor lymphatic drainage [1, 2]. This phenomenon, dubbed the EPR effect, provides the rationale for employing high molecular weight ligands to selectively deliver platinum complexes to tumour regions. A possible drawback of high molecular weight ligands is that their size may restrict the penetration of platinum complexes into solid tumours, though this is yet to be investigated. Several different types of high molecular weight ligands have been employed in the context of platinum drug design, including polymers, nanoparticles and nanotubes. Furthermore, receptor-targeting groups can be attached to high molecular weight ligands to endow them with additional tumour selectivity.

2.6.3.1 Polymer ligands

Polymers for exploiting the EPR effect should be biodegradable and non-toxic, and must contain functional groups that allow simple conjugation to platinum complexes (Figure 2.14). Upon tumour uptake, it is important for polymer ligands to release their platinum cargo, allowing DNA-binding to take place. In view of this, cleavable spacers that undergo selective degradation in tumour regions are necessary to link the platinum and polymer components. Platinum-polymer linkers can be designed to be cleaved by enzymes upregulated in cancer, or by pH-sensitive hydrolytic reactions [141].

Currently, the most successful platinum-polymer conjugate to have been developed is AP5346 (ProLindac™) (**43**), which consists of a 25 kDa hydrophilic hydroxypropylmethacrylamide (HPMA) polymer linked to multiple units of an oxaliplatin analogue *via* pH-sensitive polyglycine side chains [167]. The pH-sensitive spacers were designed to be cleaved in the characteristically acidic microenvironment of tumours [52], and the rate of release of the oxaliplatin analogue from the polymer backbone was found to be 6.7 times greater at pH 5.4 than at pH 7.4 after 24 hours [167]. Biologically relevant thiols such as cysteine, glutathione and methionine were also shown to cleave the platinum complex from the polymer in saline solution, suggesting that AP5346 is likely to undergo some degradation in the circulation. An encouraging finding was that an equitoxic dose of the conjugate delivers 16 times more platinum to tumours than oxaliplatin and 14 times more platinum to tumour DNA [167]. Moreover, AP5346 has been reported to inhibit tumour growth in mouse

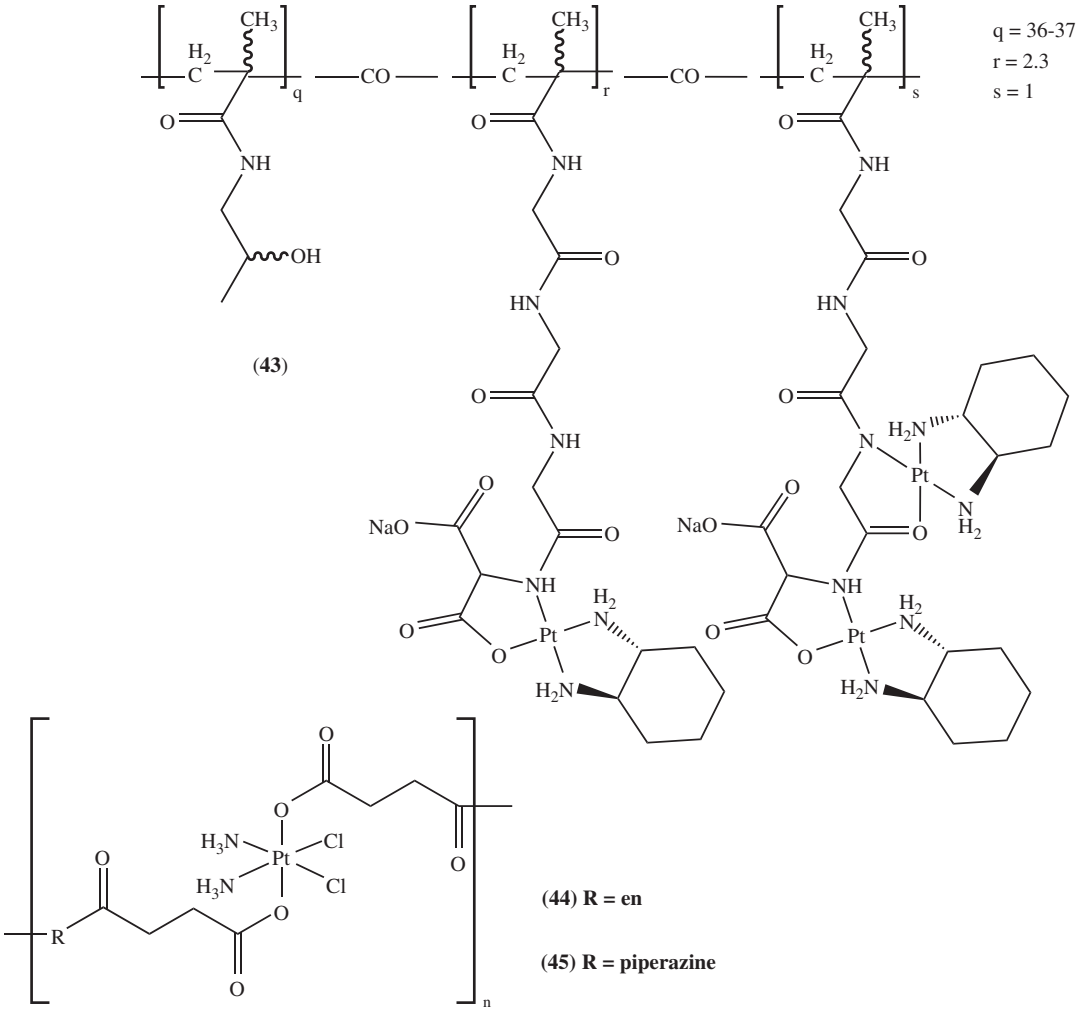

Figure 2.14 *Platinum complexes containing polymer ligands for exploiting the EPR effect. en = ethane-1,2-diamine*

models of B16 melanoma, cisplatin-resistant M5076, and 2008 human ovarian cancer to a significantly greater extent than equitoxic doses of oxaliplatin and carboplatin [167]. A Phase I/II study of the conjugate in ovarian cancer patients revealed that it was able to achieve clinically effective stabilisation of the disease and did not induce acute neurotoxicity, which is a common side-effect of oxaliplatin [8]. There were no treatment-related deaths, though mild to moderate side-effects were reported, including nausea, vomiting and paresthesia [167]. ProLindac™ is now in Phase II clinical development.

In an alternative approach to targeting the EPR effect, Shen *et al*. have developed polymers of *cis,cis,trans*-diamminedichloridodisuccinatoplatinum(IV) (**40**) [168]. The axial succinato ligands were coupled *via* ethane-1,2-diamine or piperazine linkers to yield the polymers (**44**) and (**45**) respectively. The platinum(IV) polymers were designed to be selectively taken up by tumours, at which point intracellular reduction would reduce each of the platinum(IV) units, degrading the polymer and releasing a large payload

of cisplatin. The two polymers were found to have high platinum contents (27.7% for (**44**) and 29.6% for (**45**)) and exhibited high stability in water. The activities of the platinum(IV) polymers in MDA-MB-468, SKOV-3 and MCF-7 tumour cell lines were compared with the activity of the platinum(IV) monomer. In each cell line, the platinum(IV) polymers displayed two to three times higher cytotoxicity than the disuccinato platinum(IV) monomer. *In vivo* evaluations in tumour-bearing mice revealed that treatment with (**44**) resulted in almost three-fold higher platinum accumulation in tumour tissue than the corresponding treatment with the disuccinato platinum(IV) monomer. Caution must be exercised when interpreting these results, however, since disuccinato platinum(IV) complexes do not provide a meaningful benchmark for assessing anticancer efficacy (Section 2.6.2.2). No comparisons with cisplatin were reported.

2.6.3.2 Carbon nanotube ligands

Carbon nanotubes are nanometre-sized tubular allotropes of carbon which have been tethered to platinum complexes to improve their tumour uptake through the EPR effect (Figure 2.15) [169]. Carbon nanotubes possess a number of advantages as drug delivery agents, including excellent cell membrane permeability, long circulating times and intrinsic near-infrared fluorescent properties, which allow their distribution in biological systems to be mapped [169, 170]. Their large surface area allows loading with multiple drug molecules, such that large payloads of cytotoxin can be delivered to tumour sites [169, 170]. Though there are some reports of carbon nanotube-related toxicity, the evidence is inconclusive and attention to factors such as length and purity may allow toxicity to be minimised [169, 171].

Rusling *et al*. have loaded cisplatin molecules onto a single-walled carbon nanotube (SWNT) by coordinating carboxylic acid groups on the surface of the nanotube to each platinum centre [172]. To specifically target head and neck squamous cell carcinoma (HNSCC) cancer, in which epidermal growth factor (EGF) receptors are overexpressed, the nanotube was also functionalised with EGF. In addition, an analogous conjugate was prepared in which cisplatin was replaced with a quantum dot (Qdot), in order to examine the distribution of this type of targeted conjugate in tumour cells and tumour-bearing mice. It was found that cellular internalisation of the Qdot-SWNT-EGF conjugate primarily relied on binding to EGF receptors and subsequent endocytosis, suggesting that the cisplatin-SWNT-EGF conjugate (**46**) should be selective for cells in which EGF is upregulated. Once taken up by cells, aquation of the cisplatin molecules was anticipated to release them from the carrier, since the SWNT-EGF component was conjugated to the leaving ligands. The biodistribution of the Qdot-SWNT-EGF conjugate was also examined in real time in mice bearing HNSCC tumour xenografts. The conjugate was observed to diffuse out of the vasculature within 20 minutes post-injection and rapidly accumulate in the tumour mass. Importantly, Qdot-SWNT alone was not taken up by tumours, reinforcing the key role of the EGF targeting group in mediating uptake by squamous cells. In the same xenograft model, the cisplatin-SWNT-EGF conjugate markedly slowed tumour growth, while no tumour regression was produced by the untargeted cisplatin-SWNT conjugate.

Lippard *et al*. have derivatised a single-walled carbon nanotube with 65 units of a platinum(IV) complex, each of which were tethered to the nanotube *via* an axial succinato ligand [173]. In NTera-2 testicular carcinoma cells, the IC_{50} of the platinum(IV)-SWNT conjugate (**47**) was shown to be 20 nM, making it slightly more cytotoxic than cisplatin ($IC_{50} = 50$ nM). Moreover, twice the amount of platinum was measured in cells treated with the conjugate than those dosed with cisplatin after a 1.5 hour incubation period. The conjugate is believed to enter cells *via* endocytosis, whereupon reduction of the complex releases free cisplatin from the SWNT. When folic acid was attached to the other axial ligand of the platinum(IV) complex, a dual targeting mode was introduced, whereby the resulting conjugate could target both the EPR effect *and* FRs [132]. The anticancer activity of the folic acid-platinum(IV)-SWNT conjugate was discussed in Section *2.6.2.2*

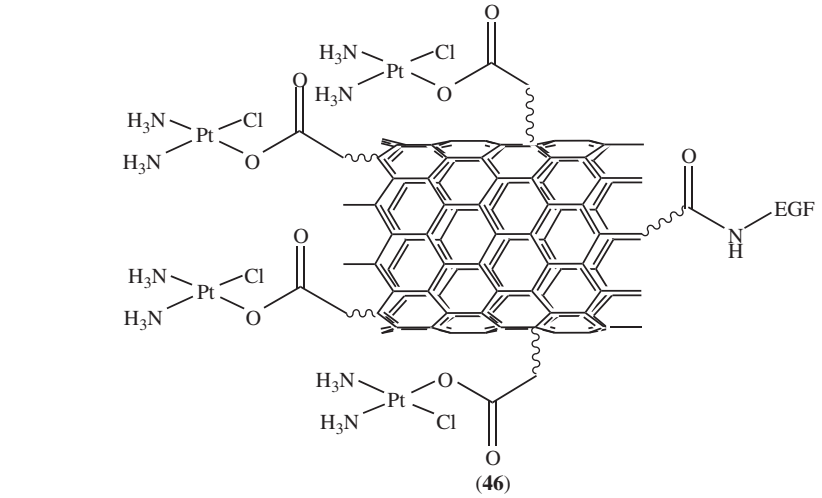

(**46**)

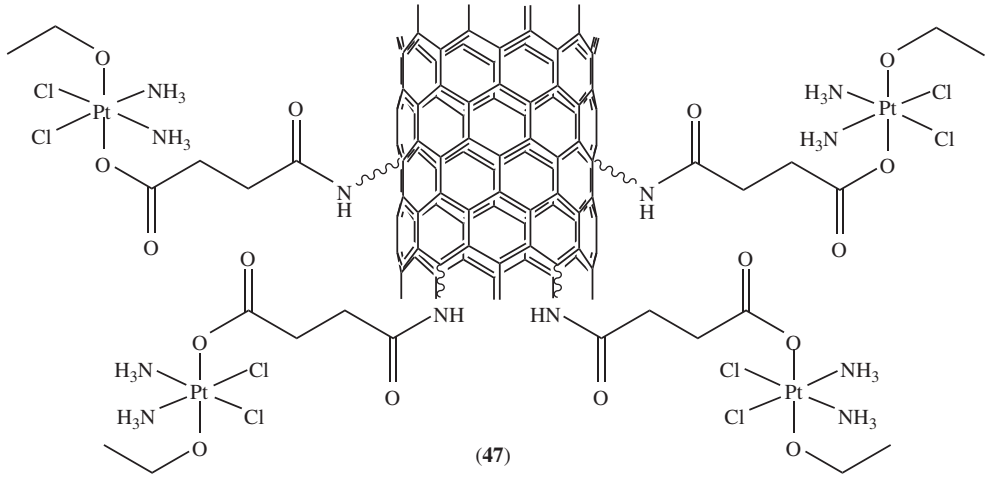

(**47**)

Figure 2.15 *Platinum complexes containing single-walled carbon nanotube ligands for exploiting the EPR effect. EGF = epidermal growth factor*

2.6.3.3 Gold nanoparticle ligands

Gold nanoparticles are useful carriers for exploiting the EPR effect as they are inert, non-toxic and easy to both synthesise and derivatise [174]. Gold nanoparticle-drug conjugates are taken up by cells *via* endocytosis [175], at which point a mechanism is required to release the drug from its carrier.

Wheate *et al*. have tethered oxaliplatin to gold nanoparticles as a means of delivering the drug selectively to tumours (Figure 2.16) [176]. Approximately 280 oxaliplatin units were loaded onto each gold nanoparticle by coordinating the terminal carboxylate groups of surface-bound thiolated PEG linkers to each platinum unit. Upon endocytosis into tumour cells, aquation of the platinum(II) complexes was envisaged to release them from the nanoparticle surface, allowing DNA binding to take place. After incubating A549 lung cancer cells for 4 hours with either oxaliplatin or the oxaliplatin-nanoparticle conjugate (**48**), twice the amount of platinum was found in cells treated with the conjugate. Moreover, the oxaliplatin-loaded nanoparticles were almost six times more cytotoxic than the orphan drug in the same cell line.

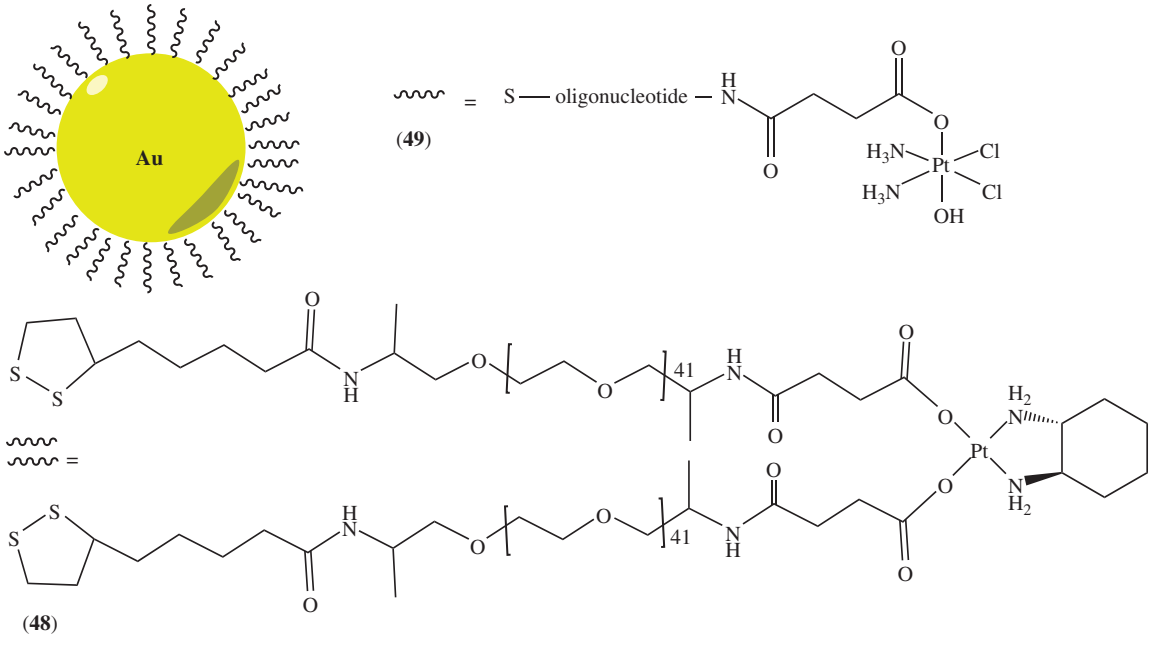

Figure 2.16 *Platinum complexes containing gold nanoparticle ligands for exploiting the EPR effect*

A platinum(IV) analogue of cisplatin containing a single axial succinato ligand has also been tethered to gold nanoparticles, by forming amide bonds between the carboxylate groups of each platinum(IV) unit and amine-functionalised oligonucleotides bound to the surface of the nanoparticles [177]. Following endocytosis into cells, it was expected that intracellular reduction of each platinum(IV) unit would release free cisplatin. Encouragingly, it was found that the platinum(IV)-nanoparticle conjugate (**49**) was up to 12 times more potent than cisplatin in a range of tumour cells.

2.6.3.4 Gold nanorod ligands

Gold nanorods exhibit longer circulation times than gold nanoparticles, allowing them to accumulate in tumours to a greater extent [178]. They possess unique optical properties and can be irradiated with near-infrared wavelengths, either to visualise tumours or for photothermal therapy [178, 179]. Liu *et al*. have loaded cisplatin onto PEGylated gold nanorods to improve the tumour selectivity of the drug *via* passive targeting (Figure 2.17) [180]. PEGylated gold nanorods have been shown to be highly stable and relatively non-toxic *in vivo* [181]. The amine-functionalised ends of the PEG groups were coupled to a platinum(IV) prodrug form of cisplatin, and the cytotoxicity of the resulting platinum-loaded nanorod (**50**) was assessed in a range of tumour cell lines. The platinum(IV)-nanorod conjugate was revealed to be most active in MCF-7 breast cancer cells, with an IC_{50} value of 0.18 μM, compared with 11.8 μM for cisplatin. In addition, it was shown that four times the amount of platinum accumulated in MCF-7 cells treated with the platinum-loaded nanorods than those treated with cisplatin. Work is now underway to investigate whether photothermal irradiation can enhance the antitumour activity of the platinum(IV)-nanorod conjugate in tumour cells [180].

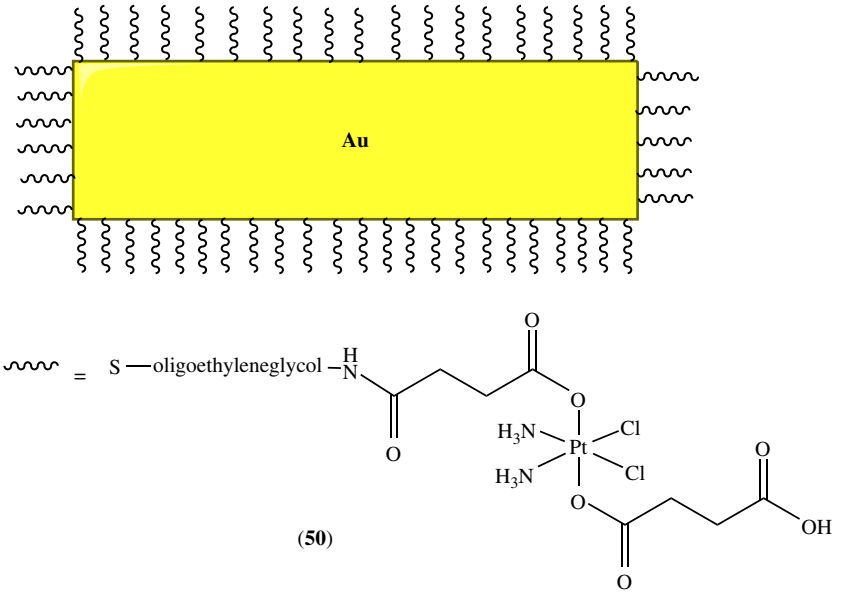

(**50**)

Figure 2.17 *Platinum complex tethered to a gold nanorod to exploit the EPR effect*

2.6.4 Ligands for targeting bone cancer

Bone cancer can be divided into two categories: (i) tumours that originate in the bones (mainly osteosarcoma) and (ii) bone metastases that are derived from other cancers, such as breast, prostate and kidney [182]. Despite the extensive side-effects of cisplatin, it remains one of the most commonly used chemotherapies to treat osteosarcoma [183]. To improve the selectivity of cisplatin for bone cancer and reduce its systemic toxicity, bone-targeting ligands may be employed (Figure 2.18).

Bisphosphonates exhibit a high affinity for bone hydroxyapatite crystals, making them attractive candidates for treating a number of different bone diseases [182, 184]. A major advantage of bisphosphonates is that they are able to inhibit osteoclast-mediated bone resorption, the primary mechanism by which bone destruction occurs in osteoporosis and cancer patients [182, 184–186]. Klenner *et al*. have examined the antitumour effects of two platinum(II)-bisphosphonato complexes ((**51**) and (**52**)) in transplantable osteosarcomas in rats [89]. The bisphosphonates were incorporated as leaving ligands to allow release of the active platinum component following binding to the calcium of the hydroxyapatite bone matrix. Treatment with the two complexes significantly inhibited tumour growth and increased survival time from 6 weeks in control animals to 12–15 weeks in treated animals. Cisplatin displayed comparable reduction in tumour growth to the platinum(II)-bisphosphonato complexes, but survival time was reduced and the treated animals died as a result of toxic side-effects.

Natile *et al*. have developed dinuclear platinum(II)- and platinum(IV)-bisphosphonato complexes ((**53**) and (**54**) respectively) and a trinuclear platinum(II)-bisphosphonato analogue (**55**) for targeting bone cancer [90]. The platinum(IV) analogue was designed to be a more water soluble version with greater resistance towards reducing agents in the blood. It was found that the platinum(IV)-bisphosphonato conjugate displayed a half-life of approximately 2 hours when incubated with 4 equiv. of the biological

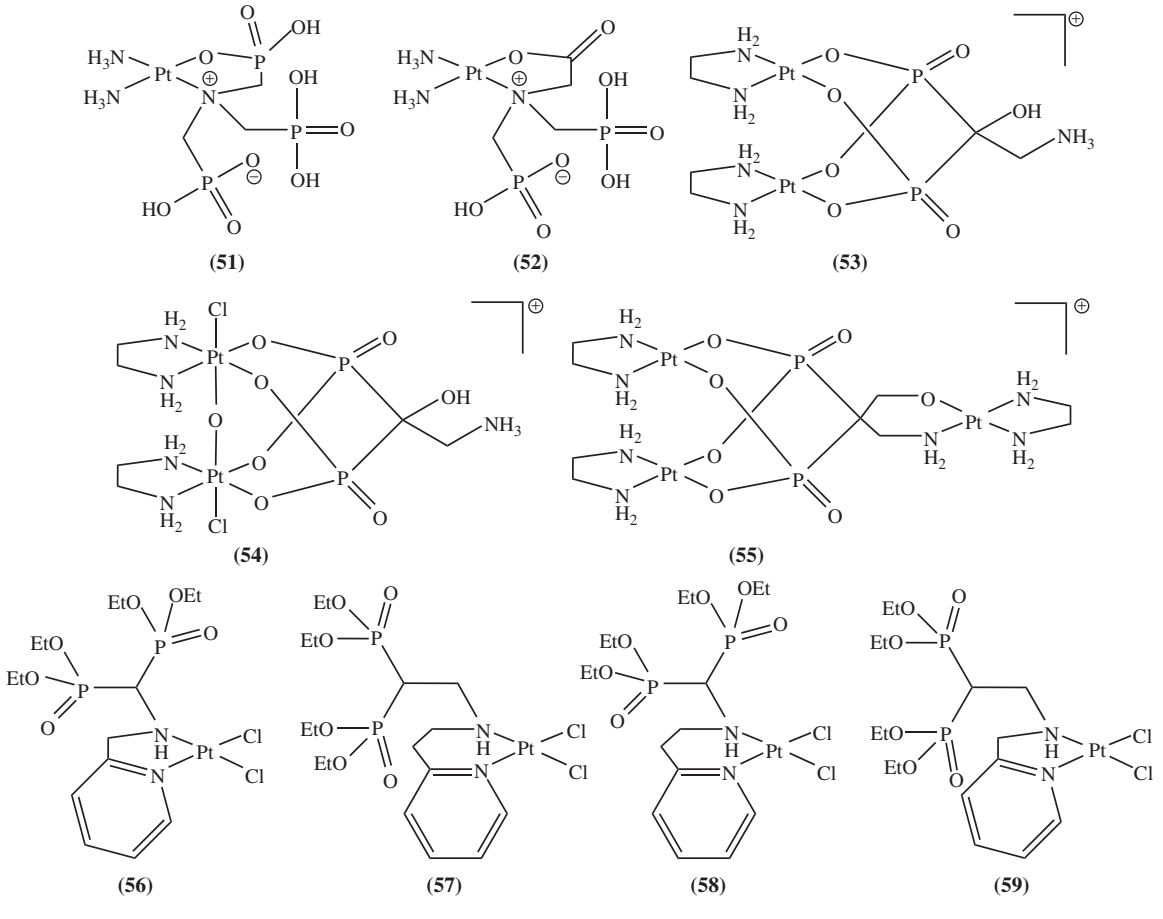

Figure 2.18 *Platinum complexes containing bone-targeting ligands*

reducing agent glutathione at 22 °C. Based on the work of Chen *et al*., this complex is likely to be reduced more rapidly *in vivo*, as complexes with high stability towards simple reducing agents have been shown to undergo reduction at a markedly faster rate in biological systems (Section 2.4.3) [61]. An important observation was that after glutathione reduced the platinum(IV)-bisphosphonato complex, it then deactivated the resulting platinum(II) complex by displacing the bisphosphonato leaving ligands. The susceptibility of the platinum(II)-bisphosphonato complex to deactivation by thiols highlights the main disadvantage of incorporating tumour-targeting groups into the leaving ligands of platinum complexes. The cytotoxicities of the three complexes were investigated in C6 rat glioma, HeLa human cervix carcinoma and HepG2 human hepatocellular carcinoma cells. The least active of the series was the platinum(IV) complex, possibly due to its higher kinetic stability. The trinuclear platinum(II) complex was more potent than the dinuclear complex, presumably because it delivers a higher payload of platinum into cells. Despite being the most cytotoxic of the series, the trinuclear species was still approximately two to seven times less active than cisplatin in the cell lines tested. The authors speculated that the platinum-bisphosphonato complexes would be more active in hydroxyapatite matrices, since binding to calcium would favour displacement of the bisphosphonato ligands and release of the active platinum cytotoxins.

In an alternative approach, Guo *et al*. incorporated bisphosponate groups into the non-leaving ligands of a series of picoplatin analogues [91]. The positioning of the bone-targeting groups in the non-leaving ligand sites was designed to prevent their loss in the circulation, though a drawback of this strategy is that they may hinder DNA-binding. Indeed, circular dichroism and electrophoretic mobility studies revealed that the four complexes exhibit negligible binding to DNA. In MG-63 human osteosarcoma and COC1 ovarian cancer cells, complexes (**57**) and (**59**) displayed some antiproliferative activity, though less than cisplatin. Complexes (**56**) and (**58**) displayed negligible activity, most likely due to the shorter distance between the platinum centre and bisphosphonato group. The observation that complexes (**57**) and (**59**) produced anticancer activity in spite of minimal DNA binding is suggestive of a novel mode of cytotoxicity. An apoptotic assay of (**59**), the complex with the highest activity, demonstrated that the mechanism by which it inflicts cell death is different to that of cisplatin. As yet it has not been established whether these complexes are active against bone cancer.

2.7 Ligands for photoactivatable platinum complexes

Another strategy for killing cancer cells, while leaving healthy tissue intact, is to develop platinum prodrugs that can be activated by light at specific tumour sites. Sadler *et al*. have reported a number of platinum(IV) complexes containing azide ligands which are relatively stable and non-toxic in the dark, and importantly, are not readily reduced by glutathione (Figure 2.19) [187–190]. These complexes contain azide-to-Pt^{IV} charge-transfer bands that are suitable for photoactivation, and oxygen is not required for the activation process [187]. This may provide an advantage over photodynamic therapy, which requires oxygen, visible light and a photosensitising chemical to produce antitumour effects, reducing its effectiveness in hypoxic tumour regions [189]. UVA light was required to photoactivate the first generation of diazido platinum(IV) complexes ((**60**) and (**61**)), which is not an ideal wavelength range for clinical applications, since it is less able to penetrate tissue than visible wavelengths [190]. More recently, *trans,trans,trans*-$[Pt(N_3)_2(OH)_2(pyridine)_2]$ (**63**), has been revealed to be cytotoxic to a range of tumour cells at micromolar doses when activated with UVA, blue or green light, while showing no antiproliferative activity in the dark [188]. Moreover, the complex was shown to be cytotoxic to cisplatin-resistant A2780 human ovarian carcinoma cells [188]. The pyridine ligands were positioned *trans* to one another based on previous findings that *trans,trans,trans*-$[Pt(N_3)_2(OH)_2(NH_3)_2]$ (**61**) is a more effective photoactivatable agent than *cis,trans,cis*-$[Pt(N_3)_2(OH)_2(NH_3)_2]$ (**60**), though the reasons for this are unclear [190].

The mode of action of (**63**) appears to be distinct from that of classical platinum complexes. One route of photodecomposition of the diazido platinum(IV) complex to the active platinum(II) cytotoxin involves two one-electron transfers from the azido ligands, generating N_2 and platinum(II), the latter of which can bind to DNA [191]. Sixteen times more DNA-bound platinum is found in cells treated with the diazido platinum(IV) complex under irradiation than an equivalent dose of cisplatin in the dark [192]. Of particular note

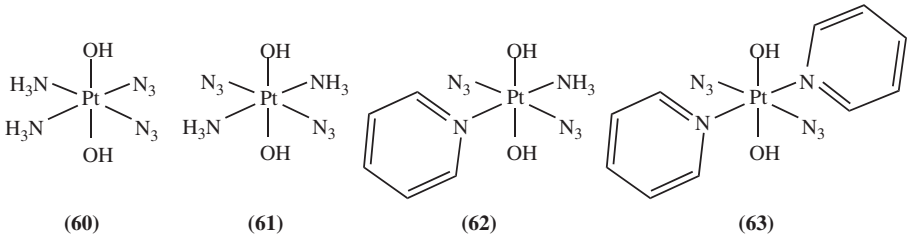

(60) **(61)** **(62)** **(63)**

Figure 2.19 *Platinum complexes containing photoactivatable ligands*

was the observation that DNA-platination does not occur in cells treated with (**63**) in the dark [192]. It was also discovered that the platinum-DNA adducts formed upon treatment with the diazido platinum(IV) complex under irradiation are different to those formed by cisplatin and transplatin, and that these novel adducts can inhibit DNA transcription by stalling RNA polymerase II [192]. Finally, recent work suggests that the generation of azidyl radicals is an important contributor to the anticancer activity of the diazido platinum(IV) complex. Interestingly, it has been discovered that tryptophan, an efficient mediator of electron transfer, is able to quench these azidyl radicals, suppressing the anticancer activity of the photoactivatable complex [193]. This is of clinical significance, as it suggests that tryptophan could be administered to patients following treatment with the photoactivatable complex to prevent possible side-effects from sunlight exposure.

The antitumour activity of a related photoactivatable complex, *trans,trans*-[$Pt(N_3)_2(OH)_2(NH_3)$(pyridine)] (**62**) has been examined in mice bearing OE19 oesophageal xenografts [187]. When tumour-bearing mice were treated with (**62**) and irradiated with blue light (420 nm), the rate of tumour growth was found to be slightly slower than for non-irradiated mice treated with the same complex. Tumour growth was slower in both the irradiated and non-irradiated treatment groups than in the irradiated and non-irradiated control groups. Encouragingly, the photoactivatable platinum(IV) complex did not appear to be toxic in mice, even when administered at a dose 10-fold higher than the maximum tolerated dose of cisplatin.

2.8 Conclusions

Over the last half century, great inroads have been made towards understanding the effects of ligand modifications on the biological behaviour of platinum anticancer complexes. Early on, small modifications were made to cisplatin ligands to manipulate simple physicochemical properties such as solubility and lipophilicity, while more recently, the field has advanced to using sophisticated ligands which can bind to specific enzymes, transporters and receptors.

In spite of these advances, there are still many hurdles to overcome in terms of designing optimal platinum anticancer complexes. One of the major challenges is determining where to strike the balance between cytotoxicity and tumour penetration, since the high cellular accumulation required for high activity is usually a barrier to tumour penetration. A possible strategy to overcome this problem may be to introduce ligands which prevent cellular uptake under normal conditions, but can be cleaved from the platinum cytotoxin in tumour tissue (perhaps by upregulated enzymes or by the characteristic acidic/hypoxic conditions), allowing entry into target cells.

From the studies detailed in this chapter, it can be seen that 2D monolayer cells are the most commonly used model to evaluate the effectiveness of novel platinum complexes, with IC_{50} values often being treated as the best indicator of anticancer efficacy. However, the nature of monolayer cells, in which cells are spread out within a uniform environment and exposed to a uniform drug concentration, fails to reflect the complexity of the tumour microenvironment and the cell-cell and cell-extracellular matrix (ECM) interactions which are known to influence drug response [51, 194–196]. Importantly, cytotoxic assays in monolayer cells do not give any information on the tumour penetration of anticancer compounds, and it is common for high activity in monolayer cells to be a poor predictor of activity in 3D models and success in the clinic [194]. For example, paclitaxel has been reported to be approximately 100 times less potent in MCF-7 human breast carcinoma and DLD-1 human colon carcinoma spheroids than in monolayer cells [197]. As a result, it is believed that the field of platinum drug design can benefit greatly from employing 3D tumour models to complement 2D studies.

Platinum(IV) complexes offer a number of advantages over traditional platinum(II) anticancer agents, in terms of greater synthetic flexibility and higher kinetic stability. In this chapter, it has been shown that a multitude of different targeting groups can be tethered to the axial ligands of platinum(IV) complexes, from peptides

and enzyme inhibitors to carbon nanotubes and gold nanoparticles. Despite the hypothesised advantages of platinum(IV) complexes, they have so far failed to show any major advantages over their platinum(II) counterparts, and no platinum(IV) complex has managed to gain regulatory approval to date. This may be the fault of the design strategies used, since all three platinum(IV) complexes that have entered clinical trials thus far have contained chlorido ligands, which are known to destabilise platinum(IV) complexes by forming electron-transfer bridges with biological reductants. Similarly, most of the platinum(IV) complexes described in this chapter have been based on a cisplatin framework, and have therefore contained two chlorido ligands. It would be useful for future platinum(IV) drug design to focus on employing ligands which are more resistant towards reduction, such that premature release of the active platinum(II) cytotoxin does not occur.

In conclusion, existing platinum complexes are highly effective antiproliferative agents, whose clinical usefulness is limited by issues of toxic side-effects, poor tumour penetration and drug resistance. The more we understand about how different types of ligands influence biological behaviour, the closer we will come to selectively delivering platinum complexes to target tumour cells, optimising resistance to extracellular reducing agents and deactivating biomolecules, and enhancing diffusion into hard-to-reach tumour regions.

References

1. Iyer, A.K., Khaled, G., Fang, J. and Maeda, H. (2006) Exploiting the enhanced permeability and retention effect for tumor targeting. *Drug Discov. Today*, **11** (17-18), 812–818.
2. Maeda, H. (2001) The enhanced permeability and retention (EPR) effect in tumor vasculature: the key role of tumor-selective macromolecular drug targeting. *Adv. Enzyme Regul.*, **41**, 189–207.
3. Bryce, N.S., Zhang, J.Z., Whan, R.M. *et al*. (2009) Accumulation of an anthraquinone and its platinum complexes in cancer cell spheroids: the effect of charge on drug distribution in solid tumour models. *Chem. Commun. (Camb.)*, (19), 2673–2675.
4. Zhang, J.Z., Bryce, N.S., Lanzirotti, A. *et al*. (2012) Getting to the core of platinum drug bio-distributions: the penetration of anti-cancer platinum complexes into spheroid tumour models. *Metallomics*, **4** (11), 1209–1217.
5. Loh, S.Y., Mistry, P., Kelland, L.R. *et al*. (1992) Reduced drug accumulation as a major mechanism of acquired resistance to cisplatin in a human ovarian carcinoma cell line: circumvention studies using novel platinum (II) and (IV) ammine/amine complexes. *Br. J. Cancer*, **66** (6), 1109–1115.
6. Ang, W.H., Pilet, S., R.S. *et al*. (2005) Synthesis and characterization of platinum(IV) anticancer drugs with functionalized aromatic carboxylate ligands: influence of the ligands on drug efficacies and uptake. *J. Med. Chem.*, **48** (25), 8060–8069.
7. Rosenberg, B., VanCamp, L., Trosko, J.E. and Mansour, V.H. (1969) Platinum compounds: a new class of potent antitumor agents. *Nature*, **222** (5191), 385–386.
8. Wheate, N.J., Walker, S., Craig, G.E. and Oun, R. (2010) The status of platinum anticancer drugs in the clinic and in clinical trials. *Dalton Trans.*, **39** (35), 8113–8127.
9. Kelland, L. (2007) The resurgence of platinum-based cancer chemotherapy. *Nat. Rev. Cancer*, **7** (8), 573–584.
10. Galanski, M., Jakupec, M.A. and Keppler, B.K. (2005) Update of the preclinical situation of anticancer platinum complexes: novel design strategies and innovative analytical approaches. *Curr. Med. Chem.*, **12** (18), 2075–2094.
11. Hall, M.D., Okabe, M., Shen, D.-W. *et al*. (2008) The role of cellular accumulation in determining sensitivity to platinum-based chemotherapy. *Annu. Rev. Pharmacol. Toxicol.*, **48**, 495–535.
12. Klein, A.V. and Hambley, T.W. (2009) Platinum drug distribution in cancer cells and tumors. *Chem. Rev. (Washington)*, **109** (10), 4911–4920.
13. Timerbaev, A.R., Aleksenko, S.S., Polec-Pawlak, K. *et al*. (2004) Platinum metallodrug-protein binding studies by capillary electrophoresis-inductively coupled plasma-mass spectrometry: characterization of interactions between Pt(II) complexes and human serum albumin. *Electrophoresis*, **25** (13), 1988–1995.
14. Ivanov, A.I., Christodoulou, J., Parkinson, J.A. *et al*. (1998) Cisplatin binding sites on human albumin. *J. Biol. Chem.*, **273** (24), 14721–14730.
15. Mandal, R., Kalke, R. and Li, X.-F. (2004) Interaction of oxaliplatin, cisplatin, and carboplatin with hemoglobin and the resulting release of a heme group. *Chem. Res. Toxicol.*, **17** (10), 1391–1397.

16. M.T. Kuo, H.H.W. Chen, I.S. Song, *et al*., The roles of copper transporters in cisplatin resistance, *Cancer Metastasis Rev.*, **26**(1), 71–83 (2007).
17. Safaei, R. (2006) Role of copper transporters in the uptake and efflux of platinum containing drugs. *Cancer Lett.*, **234** (1), 34–39.
18. Ishida, S., Lee, J., Thiele, D.J. and Herskowitz, I. (2002) Uptake of the anticancer drug cisplatin mediated by the copper transporter Ctr1 in yeast and mammals. *Proc. Natl. Acad. Sci. U.S.A.*, **99** (22), 14298–14302.
19. Howell, S.B., Safaei, R., Larson, C.A. and Sailor, M.J. (2010) Copper transporters and the cellular pharmacology of the platinum-containing cancer drugs. *Mol. Pharmacol.*, **77** (6), 887–894.
20. Burger, H., Zoumaro-Djayoon, A., Boersma, A.W.M. *et al*. (2010) Differential transport of platinum compounds by the human organic cation transporter hOCT2 (hSLC22A2). *Br. J. Pharmacol.*, **159** (4), 898–908.
21. Ciarimboli, G., Deuster, D., Knief, A. *et al*. (2010) Organic cation transporter 2 mediates cisplatin-induced oto- and nephrotoxicity and is a target for protective interventions. *Am. J. Pathol.*, **176** (3), 1169–1180.
22. K.K. Filipski, R.H. Mathijssen,T.S. Mikkelsen, *et al*., Contribution of organic cation transporter 2 (OCT2) to cisplatin-induced nephrotoxicity, *Clin. Pharmacol. Ther. (New York)*, **86**(4), 396–402 (2009).
23. Fichtinger-Schepman, A.M.J., Van der Veer, J.L., Den Hartog, J.H.J. *et al*. (1985) Adducts of the antitumor drug cis-diamminedichloroplatinum(II) with DNA: formation, identification, and quantitation. *Biochemistry*, **24** (3), 707–713.
24. Siddik, Z.H. (2003) Cisplatin: mode of cytotoxic action and molecular basis of resistance. *Oncogene*, **22** (47), 7265–7279.
25. Wang, D. and Lippard, S.J. (2005) Cellular processing of platinum anticancer drugs. *Nat. Rev. Drug Discov.*, **4** (4), 307–320.
26. Gonzalez, V.M., Fuertes, M.A., Alonso, C. and Perez, J.M. (2001) Is cisplatin-induced cell death always produced by apoptosis? *Mol. Pharmacol.*, **59** (4), 657–663.
27. Samimi, G., Safaei, R., Katano, K. *et al*. (2004) Increased expression of the copper efflux transporter ATP7A mediates resistance to cisplatin, carboplatin, and oxaliplatin in ovarian cancer cells. *Clin. Cancer Res.*, **10** (14), 4661–4669.
28. Rabik, C.A., Maryon, E.B., Kasza, K. *et al*. (2009) Role of copper transporters in resistance to platinating agents. *Cancer Chemother. Pharmacol.*, **64** (1), 133–142.
29. Ishikawa, T., Wright, C.D. and Ishizuka, H. (1994) GS-X pump is functionally overexpressed in cis-diammine-dichloroplatinum(II)-resistant human leukemia HL-60 cells and down-regulated by cell differentiation. *J. Biol. Chem.*, **269** (46), 29085–29093.
30. Suzuki, T., Nishio, K. and Tanabe, S. (2001) The MRP family and anticancer drug metabolism. *Curr. Drug Metab.*, **2** (4), 367–377.
31. Einhorn, L.H. (2002) Curing metastatic testicular cancer. *Proc. Natl. Acad. Sci. U.S.A.*, **99** (7), 4592–4595.
32. Los, G., Mutsaers, P.H.A., Lenglet, W.J.M. *et al*. (1990) Platinum distribution in intraperitoneal tumors after intraperitoneal cisplatin treatment. *Cancer Chemother. Pharmacol.*, **25** (6), 389–394.
33. Alderden, R.A., Mellor, H.R., Modok, S. *et al*. (2007) Elemental tomography of cancer-cell spheroids reveals incomplete uptake of both platinum(II) and platinum(IV) complexes. *J. Am. Chem. Soc.*, **129** (44), 13400–13401.
34. Cleare, M.J. and Hoeschele, J.D. (1973) Antitumor activity of group VIII transition metal complexes. I. Platinum(II) complexes. *Bioinorg. Chem.*, **2** (3), 187–210.
35. Khokhar, A.R., Xu, Q., Newman, R.A. *et al*. (1992) Synthesis, characterization, and antitumor activity of new chloroethylamine platinum complexes. *J. Inorg. Biochem.*, **45** (3), 211–219.
36. Knox, R.J., Friedlos, F., Lydall, D.A. and Roberts, J.J. (1986) Mechanism of cytotoxicity of anticancer platinum drugs: evidence that cis-diamminedichloroplatinum(II) and cis-diammine(1,1-cyclobutanedicarboxylato)platinum-(II) differ only in the kinetics of their interaction with DNA. *Cancer Res.*, **46** (4, Pt. 2), 1972–1979.
37. Nehme, A., Baskaran, R., Nebel, S. *et al*. (1999) Induction of JNK and c-Abl signalling by cisplatin and oxaliplatin in mismatch repair-proficient and -deficient cells. *Br. J. Cancer*, **79** (7/8), 1104–1110.
38. Raymond, E., Faivre, S., Chaney, S. *et al*. (2002) Cellular and molecular pharmacology of oxaliplatin. *Mol. Cancer Ther.*, **1** (3), 227–235.
39. Los, G., Verdegaal, E.M.E., Mutsaers, P.H.A. and McVie, J.G. (1991) Penetration of carboplatin and cisplatin into rat peritoneal tumor nodules after intraperitoneal chemotherapy. *Cancer Chemother. Pharmacol.*, **28** (3), 159–165.

40. Gholap, D., Verhulst, J., Ceelen, W. and Vanhaecke, F. (2012) Use of pneumatic nebulization and laser ablation-inductively coupled plasma-mass spectrometry to study the distribution and bioavailability of an intraperitoneally administered Pt-containing chemotherapeutic drug. *Anal. Bioanal. Chem.*, **402** (6), 2121–2129.
41. Hall, M.D., Mellor, H.R., Callaghan, R. and Hambley, T.W. (2007) Basis for design and development of platinum(IV) anticancer complexes. *J. Med. Chem.*, **50** (15), 3403–3411.
42. Kalinowska-Lis, U., Ochocki, J. and Matlawska-Wasowska, K. (2008) Trans geometry in platinum antitumor complexes. *Coord. Chem. Rev.*, **252** (12-14), 1328–1345.
43. Lovejoy, K.S. and Lippard, S.J. (2009) Non-traditional platinum compounds for improved accumulation, oral bioavailability, and tumor targeting. *Dalton Trans.*, (48), 10651–10659.
44. Oldfield, S.P., Hall, M.D. and Platts, J.A. (2007) Calculation of lipophilicity of a large, diverse dataset of anticancer platinum complexes and the relation to cellular uptake. *J. Med. Chem.*, **50** (21), 5227–5237.
45. Platts, J.A., Hibbs, D.E., Hambley, T.W. and Hall, M.D. (2001) Calculation of the hydrophobicity of platinum drugs. *J. Med. Chem.*, **44** (3), 472–474.
46. Montana, A.M. and Batalla, C. (2009) The rational design of anticancer platinum complexes: the importance of the structure-activity relationship. *Curr. Med. Chem.*, **16** (18), 2235–2260.
47. Mistry, P., Kelland, L.R., Loh, S.Y. *et al*. (1992) Comparison of cellular accumulation and cytotoxicity of cisplatin with that of tetraplatin and amminedibutyratodichloro(cyclohexylamine)platinum(IV) (JM221) in human ovarian carcinoma cell lines. *Cancer Res.*, **52** (22), 6188–6193.
48. Kvardova, V., Hrstka, R., Walerych, D. *et al*. (2010) The new platinum(IV) derivative LA-12 shows stronger inhibitory effect on Hsp90 function compared to cisplatin. *Mol. Cancer*, **9**, 147.
49. Kelland, L.R., Murrer, B.A., Abel, G. *et al*. (1992) Ammine/amine platinum(IV) dicarboxylates: a novel class of platinum complex exhibiting selective cytotoxicity to intrinsically cisplatin-resistant human ovarian carcinoma cell lines. *Cancer Res.*, **52** (4), 822–828.
50. Mellish, K.J. and Kelland, L.R. (1994) Mechanisms of acquired resistance to the orally active platinum-based anticancer drug bis-acetato-ammine-dichloro-cyclohexylamine platinum (IV) (JM216) in two human ovarian carcinoma cell lines. *Cancer Res.*, **54** (23), 6194–6200.
51. Minchinton, A.I. and Tannock, I.F. (2006) Drug penetration in solid tumours. *Nat. Rev. Cancer*, **6** (8), 583–592.
52. Tredan, O., Galmarini, C.M., Patel, K. and Tannock, I.F. (2007) Drug resistance and the solid tumor microenvironment. *J. Natl. Cancer Inst.*, **99** (19), 1441–1454.
53. Shamsuddin, S., Takahashi, I., Siddik, Z.H. and Khokhar, A.R. (1996) Synthesis, characterization, and antitumor activity of a series of novel cisplatin analogs with cis-1,4-diaminocyclohexane as nonleaving amine group. *J. Inorg. Biochem.*, **61** (4), 291–301.
54. Boulikas, T. and Vougiouka, M. (2003) Cisplatin and platinum drugs at the molecular level (review). *Oncol. Rep.*, **10** (6), 1663–1682.
55. Kasparkova, J., Vojtiskova, M., Natile, G. and Brabec, V. (2008) Unique properties of DNA interstrand cross-links of antitumor oxaliplatin and the effect of chirality of the carrier ligand. *Chem. Eur. J.*, **14** (4), 1330–1341.
56. Chen, Y., Guo, Z., Parsons, S. and Sadler, P.J. (1998) Stereospecific and kinetic control over the hydrolysis of a sterically hindered platinum picoline anticancer complex. *Chem. Eur. J.*, **4** (4), 672–676.
57. Holford, J., Sharp, S.Y., Murrer, B.A. *et al*. (1998) In vitro circumvention of cisplatin resistance by the novel sterically hindered platinum complex AMD473. *Br. J. Cancer*, **77** (3), 366–373.
58. Beale, P., Judson, I., O'Donnell, A. *et al*. (2003) A phase I clinical and pharmacological study of cis-diammine-dichloro(2-methylpyridine) platinum II (AMD473). *Br. J. Cancer*, **88** (7), 1128–1134.
59. Hall, M.D. and Hambley, T.W. (2002) Platinum(IV) antitumour compounds: their bioinorganic chemistry. *Coord. Chem. Rev.*, **232** (1-2), 49–67.
60. Zhang, J.Z., Wexselblatt, E., Hambley, T.W. and Gibson, D. (2012) Pt(IV) analogs of oxaliplatin that do not follow the expected correlation between electrochemical reduction potential and rate of reduction by ascorbate. *Chem. Commun. (Cambridge, UK)*, **48** (6), 847–849.
61. Chen, C.K.J., Zhang, J.Z., Aitken, J.B. and Hambley, T.W. (2013) The influence of equatorial and axial carboxylato ligands on the kinetic inertness of platinum(IV) complexes in the presence of ascorbate and cysteine, and within DLD-1 cancer cells. *J. Med. Chem.*, **56**, 8757–8764.

62. Rehn, C. and Pindur, U. (1996) Molecular modeling of intercalation complexes of antitumor active 9-aminoacridine and a [d,e]-anellated isoquinoline derivatives with base paired deoxytetranucleotides. *Monatsh. Chem.*, **127** (6/7), 645–658.
63. Martinez, R. and Chacon-Garcia, L. (2005) The search of DNA-intercalators as antitumoral drugs: what it worked and what did not work. *Curr. Med. Chem.*, **12** (2), 127–151.
64. Whittaker, J., McFadyen, W.D., Wickham, G. *et al*. (1998) The interaction of DNA-targeted platinum phenanthridinium complexes with DNA. *Nucleic Acids Res.*, **26** (17), 3933–3939.
65. Perrin, L.C., Prenzler, P.D., Cullinane, C. *et al*. (2000) DNA targeted platinum complexes: synthesis, cytotoxicity and DNA interactions of cis-dichloroplatinum(II) complexes tethered to phenazine-1-carboxamides. *J. Inorg. Biochem.*, **81** (1–2), 111–117.
66. Marques-Gallego, P., Kalayda, G.V., Jaehde, U. *et al*. (2009) Cellular accumulation and DNA platination of two new platinum(II) anticancer compounds based on anthracene derivatives as carrier ligands. *J. Inorg. Biochem.*, **103** (5), 791–796.
67. Temple, M.D., McFadyen, W.D., Holmes, R.J. *et al*. (2000) Interaction of cisplatin and DNA-targeted 9-aminoacridine platinum complexes with DNA. *Biochemistry*, **39** (18), 5593–5599.
68. Ma, Z., Choudhury, J.R., Wright, M.W. *et al*. (2008) A non-cross-linking platinum-acridine agent with potent activity in non-small-cell lung cancer. *J. Med. Chem.*, **51** (23), 7574–7580.
69. Alderden, R.A., Mellor, H.R., Modok, S. *et al*. (2006) Cytotoxic efficacy of an anthraquinone linked platinum anticancer drug. *Biochem. Pharmacol.*, **71** (8), 1136–1145.
70. Jansen, B.A.J., Wielaard, P., Kalayda, G.V. *et al*. (2004) Dinuclear platinum complexes with N,N′-bis(aminoalkyl)-1,4-diaminoanthraquinones as linking ligands. Part I. Synthesis, cytotoxicity, and cellular studies in gA2780 human ovarian carcinoma cells. *J. Biol. Inorg. Chem.*, **9** (4), 403–413.
71. Lee, C.-H., Hsieh, M.-Y., Hsin, L.-W. *et al*. (2012) Anthracenedione-methionine conjugates are novel topoisomerase II-targeting anticancer agents with favorable drug resistance profiles. *Biochem. Pharmacol.*, **83** (9), 1208–1216.
72. Hayashi, M. and Harada, Y. (2007) Direct observation of the reversible unwinding of a single DNA molecule caused by the intercalation of ethidium bromide. *Nucleic Acids Res.*, **35** (19), e125/1–e125/7.
73. Malinge, J.M. and Leng, M. (1986) Reaction of nucleic acids and cis-diamminedichloroplatinum(II) in the presence of intercalating agents. *Proc. Natl. Acad. Sci. U.S.A.*, **83** (17), 6317–6321.
74. Gibson, D., Gean, K.F., Katzhendler, J. *et al*. (1991) Preparation, characterization, and anticancer activity of a series of cis-$PtCl_2$ complexes linked to anthraquinone intercalators. *J. Med. Chem.*, **34** (1), 414–420.
75. Carland, M., Grannas, M.J., Cairns, M.J. *et al*. (2010) Substituted 9-aminoacridine-4-carboxamides tethered to platinum(II)diamine complexes: chemistry, cytotoxicity and DNA sequence selectivity. *J. Inorg. Biochem.*, **104** (8), 815–819.
76. Gude, L., Fernandez, M.-J., Grant, K.B. and Lorente, A. (2002) Anthracene and naphthalene (2,2′-bipyridine)-platinum(II) conjugates: synthesis and DNA photocleavage. *Tetrahedron Lett.*, **43** (27), 4723–4727.
77. Gibson, D., Mansur, N. and Gean, K.F. (1995) Preparation, characterization, and antitumor properties of cis-dichlorodiammineplatinum complexes linked to anthraquinones through position number 2. *J. Inorg. Biochem.*, **58** (2), 79–88.
78. Hall, M.D., Alderden, R.A., Zhang, M. *et al*. (2006) The fate of platinum(II) and platinum(IV) anti-cancer agents in cancer cells and tumors. *J. Struct. Biol.*, **155** (1), 38–44.
79. D. Gibson, I. Binyamin, M. Haj, , *et al*., Anthraquinone intercalators as carrier molecules for second-generation platinum anticancer drugs, *Eur. J. Med. Chem.*, **32**(10), 823–831 (1997).
80. Graham, L.A., Wilson, G.M., West, T.K. *et al*. (2011) Unusual reactivity of a potent platinum-acridine hybrid antitumor agent. *ACS Med. Chem. Lett.*, **2** (9), 687–691.
81. Suryadi, J. and Bierbach, U. (2012) DNA metalating-intercalating hybrid agents for the treatment of chemoresistant cancers. *Chem. Eur. J.*, **18** (41), 12926–12934.
82. Ding, S., Qiao, X., Kucera, G.L. and Bierbach, U. (2013) Design of a platinum-acridine-endoxifen conjugate targeted at hormone-dependent breast cancer. *Chem. Commun. (Cambridge, UK)*, **49** (24), 2415–2417.
83. Brabec, V., Griffith, D.M., Kisova, A. *et al*. (2012) Valuable insight into the anticancer activity of the platinum-histone deacetylase inhibitor conjugate, cis-[$Pt(NH_3)_2$malSAHA$_{-2H}$)]. *Mol. Pharm.*, **9** (7), 1990–1999.

84. Butler, L.M., Zhou, X., Xu, W.-S. *et al*. (2002) The histone deacetylase inhibitor SAHA arrests cancer cell growth, up-regulates thioredoxin-binding protein-2, and down-regulates thioredoxin. *Proc. Natl. Acad. Sci. U.S.A.*, **99** (18), 11700–11705.
85. Sangeetha, S.R., Singh, N., Vender, J.R. and Dhandapani, K.M. (2009) Suberoylanilide hydroxamic acid (SAHA) induces growth arrest and apoptosis in pituitary adenoma cells. *Endocrine*, **35** (3), 389–396.
86. Jain, S., Zain, J. and O'Connor, O. (2012) Novel therapeutic agents for cutaneous T-cell lymphoma. *J. Hematol. Oncol.*, **5**, 24.
87. Overall, C.M. and Kleifeld, O. (2006) Tumour microenvironment – opinion: validating matrix metalloproteinases as drug targets and anti-targets for cancer therapy. *Nat. Rev. Cancer*, **6** (3), 227–239.
88. Green, J.R. (2004) Bisphosphonates: preclinical review. *Oncologist*, **9** (Suppl. 4), 3–13.
89. Klenner, T., Wingen, F., Keppler, B.K. *et al*. (1990) Anticancer-agent-linked phosphonates with antiosteolytic and antineoplastic properties: a promising perspective in the treatment of bone-related malignancies? *J. Cancer Res. Clin. Oncol.*, **116** (4), 341–350.
90. Piccinonna, S., Margiotta, N., Pacifico, C. *et al*. (2012) Dinuclear Pt(II)-bisphosphonate complexes: a scaffold for multinuclear or different oxidation state platinum drugs. *Dalton Trans.*, **41** (32), 9689–9699.
91. Xue, Z., Lin, M., Zhu, J. *et al*. (2010) Platinum(II) compounds bearing bone-targeting group: synthesis, crystal structure and antitumor activity. *Chem. Commun. (Cambridge, UK)*, **46** (8), 1212–1214.
92. Sasanelli, R., Boccarelli, A., Giordano, D. *et al*. (2007) Platinum complexes can inhibit matrix metalloproteinase activity: platinum-diethyl[(methylsulfinyl)methyl]phosphonate complexes as inhibitors of matrix metalloproteinases 2, 3, 9, and 12. *J. Med. Chem.*, **50** (15), 3434–3441.
93. Dang, C.V. and Semenza, G.L. (1999) Oncogenic alterations of metabolism. *Trends Biochem. Sci.*, **24** (2), 68–72.
94. Vander Heiden, M.G., Cantley, L.C. and Thompson, C.B. (2009) Understanding the warburg effect: the metabolic requirements of cell proliferation. *Science (Washington)*, **324** (5930), 1029–1033.
95. Warburg, O. (1956) On the origin of cancer cells. *Science*, **123** (3191), 309–314.
96. Michelakis, E.D., Webster, L. and Mackey, J.R. (2008) Dichloroacetate (DCA) as a potential metabolic-targeting therapy for cancer. *Br. J. Cancer*, **99** (7), 989–994.
97. Dhar, S. and Lippard, S.J. (2009) Mitaplatin, a potent fusion of cisplatin and the orphan drug dichloroacetate. *Proc. Natl. Acad. Sci. U.S.A.*, **106** (52), 22199–22204, S/1–S/11.
98. Xue, X., You, S., Zhang, Q. *et al*. (2012) Mitaplatin increases sensitivity of tumor cells to cisplatin by inducing mitochondrial dysfunction. *Mol. Pharm.*, **9** (3), 634–644.
99. Ang, W.H., Khalaila, I., Allardyce, C.S. *et al*. (2005) Rational design of platinum(IV) compounds to overcome glutathione-S-transferase mediated drug resistance. *J. Am. Chem. Soc.*, **127** (5), 1382–1383.
100. Saburi, Y., Nakagawa, M., Ono, M. *et al*. (1989) Increased expression of glutathione S-transferase gene in cis-diamminedichloroplatinum(II)-resistant variants of a Chinese hamster ovary cell line. *Cancer Res.*, **49** (24Pt. 1), 7020–7025.
101. Goto, S., Iida, T., Cho, S. *et al*. (1999) Overexpression of glutathione S-transferase π enhances the adduct formation of cisplatin with glutathione in human cancer cells. *Free Radic. Res.*, **31** (6), 549–558.
102. Olive, D.M. (2004) Quantitative methods for the analysis of protein phosphorylation in drug development. *Expert Rev. Proteomics*, **1** (3), 327–341.
103. Lawrie, A.M., Noble, M.E.M., Tunnah, P. *et al*. (1997) Protein kinase inhibition by staurosporine revealed in details of the molecular interaction with CDK2. *Nat. Struct. Biol.*, **4** (10), 796–801.
104. Child, E.S., Georgiades, S.N., Rose, K.N. *et al*. (2011) Inhibition of mitogen-activated protein kinase (MAPK) and cyclin-dependent kinase 2 (Cdk2) by platinum(II) phenanthroline complexes. *J. Chem. Biol.*, **4** (4), 159–165.
105. Liu, J., Hu, Y., Waller, D.L. *et al*. (2012) Natural products as kinase inhibitors. *Nat. Prod. Rep.*, **29** (3), 392–403.
106. Williams, D.S., Carroll, P.J. and Meggers, E. (2007) Platinum complex as a nanomolar protein kinase inhibitor. *Inorg. Chem.*, **46** (8), 2944–2946.
107. Sausville, E.A., Arbuck, S.G., Messmann, R. *et al*. (2001) Phase I trial of 72-hour continuous infusion UCN-01 in patients with refractory neoplasms. *J. Clin. Oncol.*, **19** (8), 2319–2333.
108. Manns, J., Daubrawa, M., Driessen, S. *et al*. (2011) Triggering of a novel intrinsic apoptosis pathway by the kinase inhibitor staurosporine: activation of caspase-9 in the absence of Apaf-1. *FASEB J.*, **25** (9), 3250–3261. doi: 10 1096/fj 10-177527

109. Vonderheide, R.H. (2002) Telomerase as a universal tumor-associated antigen for cancer immunotherapy. *Oncogene*, **21** (4), 674–679.
110. Rao, L., Dworkin, J.D., Nell, W.E. and Bierbach, U. (2011) Interactions of a platinum-modified perylene derivative with the human telomeric G-quadruplex. *J. Phys. Chem. B*, **115** (46), 13701–13712.
111. Blackburn, E.H., Greider, C.W. and Szostak, J.W. (2006) Telomeres and telomerase: the path from maize, Tetrahymena and yeast to human cancer and aging. *Nat. Med. (New York)*, **12** (10), 1133–1138.
112. Harley, C.B. (2008) Telomerase and cancer therapeutics. *Nat. Rev. Cancer*, **8** (3), 167–179.
113. Wei, C., Wen, Y. and Wang, J. (2013) Novel platinum complexes as efficient G-quadruplex DNA binders and telomerase inhibitors. *Int. J. Biol. Macromol.*, **55**, 185–192.
114. Musetti, C., Krapcho, A.., Palumbo, M. and Sissi, C. (2013) Effect of G-quadruplex polymorphism on the recognition of telomeric DNA by a metal complex. *PLoS One*, **8** (3), e58529.
115. Biffi, G., Tannahill, D., McCafferty, J. and Balasubramanian, S. (2013) Quantitative visualization of DNA G-quadruplex structures in human cells. *Nat. Chem.*, **5** (3), 182–186.
116. Yuan, L., Tian, T., Chen, Y. *et al*. (2013) Existence of G-quadruplex structures in promoter region of oncogenes confirmed by G-quadruplex DNA cross-linking strategy. *Sci. Rep.*, **3**, 1811, 9 pp..
117. Ganapathy, V., Thangaraju, M. and Prasad, P.D. (2009) Nutrient transporters in cancer: relevance to Warburg hypothesis and beyond. *Pharmacol. Ther.*, **121** (1), 29–40.
118. Ruiz-Sanchez, P., Koenig, C., Ferrari, S. and Alberto, R. (2011) Vitamin B12 as a carrier for targeted platinum delivery: in vitro cytotoxicity and mechanistic studies. *J. Biol. Inorg. Chem.*, **16** (1), 33–44.
119. Russell-Jones, G.J. and Alpers, D.H. (1999) Vitamin B12 transporters. *Pharm. Biotechnol.*, **12** (Membrane Transporters as Drug Targets), 493–520.
120. Berger, I., Nazarov, A.A., Hartinger, C.G. *et al*. (2007) A glucose derivative as natural alternative to the cyclohexane-1,2-diamine ligand in the anticancer drug oxaliplatin? *ChemMedChem*, **2** (4), 505–514.
121. Liu, P., Lu, Y., Gao, X. *et al*. (2013) Highly water-soluble platinum(II) complexes as GLUT substrates for targeted therapy: improved anticancer efficacy and transporter-mediated cytotoxic properties. *Chem. Commun. (Cambridge, UK)*, **49** (24), 2421–2423.
122. Moeker, J., Salge-Bartels, U. and Thiem, J. (2012) Formation of glyco-functionalized platinum complexes by cross-metathesis and evaluation of their efficacy in inhibition of lung tumor cell lines. *J. Carbohydr. Chem.*, **31** (9), 702–710.
123. Stocker, B.L. and Hoberg, J.O. (2006) Synthesis of platinacyclobutanes bearing biological components for targeted, cisplatin prodrugs. *Organometallics*, **25** (19), 4537–4541.
124. Margiotta, N., Papadia, P., Lazzaro, F. *et al*. (2005) Platinum-based antitumor drugs containing enantiomerically pure α-trifluoromethyl alanine as ligand. *J. Med. Chem.*, **48** (24), 7821–7828.
125. Colombo, A., Di Gioia, R., Pasini, A. *et al*. (1986) Antitumor complexes of platinum with carrier molecules. 3. Cytotoxicity of some platinum amino acid complexes against cisplatin-sensitive and resistant L1210 leukemia cells. *Inorg. Chim. Acta*, **125** (1), L1–L3.
126. Bersanetti, E., Pasini, A., Pezzoni, G. *et al*. (1984) Antitumor complexes of platinum with carrier molecules. 2. Mixed complexes of amino acids and tert-butylamine. *Inorg. Chim. Acta*, **93** (4), 167–172.
127. Pavelka, M., Lucas, M.F.A. and Russo, N. (2007) On the hydrolysis mechanism of the second-generation anticancer drug carboplatin. *Chem. Eur. J.*, **13** (36), 10108–10116.
128. Iakovidis, A. and Hadjiliadis, N. (1994) Complex compounds of platinum(II) and (IV) with amino acids, peptides and their derivatives. *Coord. Chem. Rev.*, **135/136**, 17–63.
129. Jin, V.X. and Ranford, J.D. (2000) Complexes of platinum(II) or palladium(II) with 1,10-phenanthroline and amino acids. *Inorg. Chim. Acta*, **304** (1), 38–44.
130. Asensio, A., Bravo, P., Crucianelli, M. *et al*. (2001) Synthesis of nonracemic α-trifluoromethyl α-amino acids from sulfinimines of trifluoropyruvate. *Eur. J. Org. Chem.*, **8**, 1449–1458.
131. Bravo, P., Crucianelli, M., Vergani, B. and Zanda, M. (1998) Sulfinimines of trifluoropyruvate: novel intermediates for chiral non racemic α-trifluoromethyl α-amino acids. *Tetrahedron Lett.*, **39** (42), 7771–7774.
132. Dhar, S., Liu, Z., Thomale, J. *et al*. (2008) Targeted single-wall carbon nanotube-mediated Pt(IV) prodrug delivery using folate as a homing device. *J. Am. Chem. Soc.*, **130** (34), 11467–11476.

133. Mukhopadhyay, S., Barnes, C.M., Haskel, A. *et al*. (2008) Conjugated platinum(IV)-peptide complexes for targeting angiogenic tumor vasculature. *Bioconjug. Chem.*, **19** (1), 39–49.
134. Gupta, Y., Kohli, D.V. and Jain, S.K. (2008) Vitamin B12-mediated transport: a potential tool for tumor targeting of antineoplastic drugs and imaging agents. *Crit. Rev. Ther. Drug Carrier Syst.*, **25** (4), 347–379.
135. Gaviglio, L., Gross, A., Metzler-Nolte, N. and Ravera, M. (2012) Synthesis and in vitro cytotoxicity of cis,cis,trans-diamminedichloridodisuccinatoplatinum(IV)-peptide bioconjugates. *Metallomics*, **4** (3), 260–266.
136. Saha, P., Descoteaux, C., Brasseur, K. *et al*. (2012) Synthesis, antiproliferative activity and estrogen receptor α affinity of novel estradiol-linked platinum(II) complex analogs to carboplatin and oxaliplatin. Potential vector complexes to target estrogen-dependent tissues. *Eur. J. Med. Chem.*, **48**, 385–390.
137. Van Themsche, C., Parent, S., Leblanc, V. *et al*. (2009) VP-128, a novel oestradiol-platinum(II) hybrid with selective anti-tumour activity towards hormone-dependent breast cancer cells in vivo. *Endocr.-Relat. Cancer*, **16** (4), 1185–1195.
138. Margiotta, N., Denora, N., Ostuni, R. *et al*. (2010) Platinum(II) complexes with bioactive carrier ligands having high affinity for the translocator protein. *J. Med. Chem.*, **53** (14), 5144–5154.
139. Ndinguri, M.W., Solipuram, R., Gambrell, R.P. *et al*. (2009) Peptide targeting of platinum anti-cancer drugs. *Bioconjug. Chem.*, **20** (10), 1869–1878.
140. Gao, J., Liu, Y.G., Liu, R. and Zingaro, R.A. (2008) Herceptin-platinum(II) binding complexes: novel cancer-cell-specific agents. *ChemMedChem*, **3** (6), 954–962.
141. Wang, X. and Guo, Z. (2013) Targeting and delivery of platinum-based anticancer drugs. *Chem. Soc. Rev.*, **42** (1), 202–224.
142. Miyoshi, Y., Murase, K., Saito, M. *et al*. (2010) Mechanisms of estrogen receptor-α upregulation in breast cancers. *Med. Mol. Morphol.*, **43** (4), 193–196.
143. Bondar, G., Kuo, J., Hamid, N. and Micevych, P. (2009) Estradiol-induced estrogen receptor-α trafficking. *J. Neurosci.*, **29** (48), 15323–15330.
144. Pretner, E., Amri, H., Li, W. *et al*. (2006) Cancer-related overexpression of the peripheral-type benzodiazepine receptor and cytostatic anticancer effects of Ginkgo biloba extract (EGb 761). *Anticancer Res.*, **26** (1A), 9–22.
145. Han, Z., Slack, R.S., Li, W. and Papadopoulos, V. (2003) Expression of peripheral benzodiazepine receptor (PBR) in human tumors: relationship to breast, colorectal, and prostate tumor progression. *J. Recept. Signal Transduction*, **23** (2-3), 225–238.
146. Gendelman, H.E. and Ikezu, T. (eds) (2008) *Neuroimmune Pharmacology*, Springer, New York.
147. Stange, T., Kettmann, U. and Holzhausen, H.J. (2000) Immunoelectron microscopic demonstration of the membrane proteases aminopeptidase N/CD13 and dipeptidyl peptidase IV/CD26 in normal and neoplastic renal parenchymal tissues and cells. *Eur. J. Histochem.*, **44** (2), 157–164.
148. Ikeda, N., Nakajima, Y., Tokuhara, T. *et al*. (2003) Clinical significance of aminopeptidase N/CD13 expression in human pancreatic carcinoma. *Clin. Cancer Res.*, **9** (4), 1503–1508.
149. Guzman-Rojas, L., Rangel, R., Salameh, A. *et al*. (2012) Cooperative effects of aminopeptidase N (CD13) expressed by nonmalignant and cancer cells within the tumor microenvironment. *Proc. Natl. Acad. Sci. U.S.A.*, **109** (5), 1637–1642, S/1–S/13.
150. Hashida, H., Takabayashi, A., Kanai, M. *et al*. (2002) Aminopeptidase N is involved in cell motility and angiogenesis: its clinical significance in human colon cancer. *Gastroenterology*, **122** (2), 376–386.
151. Ichimura, E., Yamada, M., Nishikawa, K. *et al*. (2006) Immunohistochemical expression of aminopeptidase N (CD13) in human lung squamous cell carcinomas, with special reference to bestatin adjuvant therapy. *Pathol. Int.*, **56** (6), 296–300.
152. Bhagwat, S.V., Petrovic, N., Okamoto, Y. and Shapiro, L.H. (2003) The angiogenic regulator CD13/APN is a transcriptional target of Ras signaling pathways in endothelial morphogenesis. *Blood*, **101** (5), 1818–1826.
153. Cho, H.-S., Mason, K., Ramyar, K.X. *et al*. (2003) Structure of the extracellular region of HER2 alone and in complex with the Herceptin Fab. *Nature (London)*, **421** (6924), 756–760.
154. Harari, D. and Yarden, Y. (2000) Molecular mechanisms underlying ErbB2/HER2 action in breast cancer. *Oncogene*, **19** (53), 6102–6114.
155. Zwicke, G.L., Ali Mansoori, G. and Jeffery, C.J. (2012) Utilizing the folate receptor for active targeting of cancer nanotherapeutics. *Nano Rev.*, **3**, 18496.

156. Vlahov, I.R. and Leamon, C.P. (2012) Engineering folate-drug conjugates to target cancer: from chemistry to clinic. *Bioconjug. Chem.*, **23** (7), 1357–1369.
157. Shin, S., Wolgamott, L. and Yoon, S.-O. (2012) Integrin trafficking and tumor progression. *Int. J. Cell Biol.*, **2012**, 516789, 7 pp..
158. Desgrosellier, J.S. and Cheresh, D.A. (2010) Integrins in cancer: biological implications and therapeutic opportunities. *Nat. Rev. Cancer*, **10** (1), 9–22.
159. Lee, S., Xie, J. and Chen, X. (2010) Peptides and peptide hormones for molecular imaging and disease diagnosis. *Chem. Rev. (Washington)*, **110** (5), 3087–3111.
160. X.Gui (2007) The design and in vitro testing of a potentially tumour selective platinum(IV) complex. Honours, University of Sydney.
161. Abramkin, S., Valiahdi, S.M., Jakupec, M.A. *et al*. (2012) Solid-phase synthesis of oxaliplatin-TAT peptide bioconjugates. *Dalton Trans.*, **41** (10), 3001–3005.
162. Munyendo, W.L.L., Lv, H., Benza-Ingoula, H. *et al*. (2012) Cell penetrating peptides in the delivery of biopharmaceuticals. *Biomolecules*, **2** (2), 187–202.
163. Torchilin, V.P. (2008) TAT peptide-mediated intracellular delivery of pharmaceutical nanocarriers. *Adv. Drug Deliv. Rev.*, **60** (4-5), 548–558.
164. Schwarze, S.R., Ho, A., Vocero-Akbani, A. and Dowdy, S.F. (1999) In vivo protein transduction: delivery of a biologically active protein into the mouse. *Science (Washington, DC)*, **285** (5433), 1569–1572.
165. Liu, L., Guo, K., Lu, J. *et al*. (2008) Biologically active core/shell nanoparticles self-assembled from cholesterol-terminated PEG-TAT for drug delivery across the blood-brain barrier. *Biomaterials*, **29** (10), 1509–1517.
166. Richard, J.P., Melikov, K., Brooks, H. *et al*. (2005) Cellular uptake of unconjugated TAT peptide involves clathrin-dependent endocytosis and heparan sulfate receptors. *J. Biol. Chem.*, **280** (15), 15300–15306.
167. Nowotnik, D.P. and Cvitkovic, E. (2009) ProLindac (AP5346): a review of the development of an HPMA DACH platinum polymer therapeutic. *Adv. Drug Deliv. Rev.*, **61** (13), 1214–1219.
168. Yang, J., Liu, W., Sui, M. *et al*. (2011) Platinum (IV)-coordinate polymers as intracellular reduction-responsive backbone-type conjugates for cancer drug delivery. *Biomaterials*, **32** (34), 9136–9143.
169. Meng, L., Zhang, X., Lu, Q. *et al*. (2012) Single walled carbon nanotubes as drug delivery vehicles: targeting doxorubicin to tumors. *Biomaterials*, **33** (6), 1689–1698.
170. Liu, Z., Chen, K., Davis, C. *et al*. (2008) Drug delivery with carbon nanotubes for in vivo cancer treatment. *Cancer Res.*, **68** (16), 6652–6660.
171. Lacerda, L., Bianco, A., Prato, M. and Kostarelos, K. (2006) Carbon nanotubes as nanomedicines: from toxicology to pharmacology. *Adv. Drug Deliv. Rev.*, **58** (14), 1460–1470.
172. Bhirde, A.A., Patel, V., Gavard, J. *et al*. (2009) Targeted killing of cancer cells in vivo and in vitro with EGF-directed carbon nanotube-based drug delivery. *ACS Nano*, **3** (2), 307–316.
173. Feazell, R.P., Nakayama-Ratchford, N., Dai, H. and Lippard, S.J. (2007) Soluble single-walled carbon nanotubes as longboat delivery systems for platinum(IV) anticancer drug design. *J. Am. Chem. Soc.*, **129** (27), 8438–8439.
174. Ghosh, P., Han, G., De, M. *et al*. (2008) Gold nanoparticles in delivery applications. *Adv. Drug Deliv. Rev.*, **60** (11), 1307–1315.
175. Verma, A. and Stellacci, F. (2010) Effect of surface properties on nanoparticle-cell interactions. *Small*, **6** (1), 12–21.
176. Brown, S.D., Nativo, P., Smith, J.-A. *et al*. (2010) Gold nanoparticles for the improved anticancer drug delivery of the active component of oxaliplatin. *J. Am. Chem. Soc.*, **132** (13), 4678–4684.
177. Dhar, S., Daniel, W.L., Giljohann, D.A. *et al*. (2009) Polyvalent oligonucleotide gold nanoparticle conjugates as delivery vehicles for platinum(IV) warheads. *J. Am. Chem. Soc.*, **131** (41), 14652–14653.
178. von Maltzahn, G., Park, J.-H., Agrawal, A. *et al*. (2009) Computationally guided photothermal tumor therapy using long-circulating gold nanorod antennas. *Cancer Res.*, **69** (9), 3892–3900.
179. Huang, X., El-Sayed, I.H. and El-Sayed, M.A. (2010) Applications of gold nanorods for cancer imaging and photothermal therapy. *Methods Mol. Biol. (Totowa)*, **624**(Cancer Nanotechnology), 343–357.
180. Min, Y., Mao, C., Xu, D. *et al*. (2010) Gold nanorods for platinum based prodrug delivery. *Chem. Commun. (Cambridge, UK)*, **46** (44), 8424–8426.

181. Niidome, T., Yamagata, M., Okamoto, Y. *et al*. (2006) PEG-modified gold nanorods with a stealth character for in vivo applications. *J. Control. Release*, **114** (3), 343–347.
182. Moriceau, G., Ory, B., Gobin, B. *et al*. (2010) Therapeutic approach of primary bone tumours by bisphosphonates. *Curr. Pharm. Des.*, **16** (27), 2981–2987.
183. Pasello, M., Michelacci, F., Scionti, I. *et al*. (2008) Overcoming glutathione S-transferase P1-related cisplatin resistance in osteosarcoma. *Cancer Res.*, **68** (16), 6661–6668.
184. Papapoulos, S.E. (2006) Bisphosphonate actions: physical chemistry revisited. *Bone*, **38** (5), 613–616.
185. Cremers, S.C.L.M., Pillai, G. and Papapoulos, S.E. (2005) Pharmacokinetics/pharmacodynamics of bisphosphonates. Use for optimisation of intermittent therapy for osteoporosis. *Clin. Pharmacokinet.*, **44** (6), 551–570.
186. Roodman, G.D. (2001) Biology of osteoclast activation in cancer. *J. Clin. Oncol.*, **19** (15), 3562–3571.
187. Westendorf, A.F., Woods, J.A., Korpis, K. *et al*. (2012) Trans,trans,trans-[$Pt^{IV}(N_3)_2(OH)_2(py)(NH_3)$]: a light-activated antitumor platinum complex that kills human cancer cells by an apoptosis-independent mechanism. *Mol. Cancer Ther.*, **11** (9), 1894–1904.
188. Farrer, N.J., Woods, J.A., Salassa, L. *et al*. (2010) A potent trans-diimine platinum anticancer complex photoactivated by visible light. *Angew. Chem. Int. Ed.*, **49** (47), 8905–8908, S/1–S/40.
189. Bednarski, P.J., Mackay, F.S. and Sadler, P.J. (2007) Photoactivatable platinum complexes. *Anticancer Agents Med Chem.*, **7** (1), 75–93.
190. Mackay, F.S., Woods, J.A., Moseley, H. *et al*. (2006) A photoactivated trans-diammine platinum complex as cytotoxic as cisplatin. *Chem. Eur. J.*, **12** (11), 3155–3161.
191. Ronconi, L. and Sadler, P.J. (2008) Unprecedented carbon-carbon bond formation induced by photoactivation of a platinum(IV)-diazido complex. *Chem. Commun. (Cambridge, UK)*, (2), 235–237.
192. Pracharova, J., Zerzankova, L., Stepankova, J. *et al*. (2012) Interactions of DNA with a new platinum(IV) azide dipyridine complex activated by UVA and visible light: relationship to toxicity in tumor cells. *Chem. Res. Toxicol.*, **25** (5), 1099–1111.
193. Butler, J.S., Woods, J.A., Farrer, N.J. *et al*. (2012) Tryptophan switch for a photoactivated platinum anticancer complex. *J. Am. Chem. Soc.*, **134** (40), 16508–16511.
194. Elliott, N.T. and Yuan, F. (2011) A review of three-dimensional in vitro tissue models for drug discovery and transport studies. *J. Pharm. Sci.*, **100** (1), 59–74.
195. May, J.E., Xu, J., Morse, H.R. *et al*. (2009) Toxicity testing: the search for an in vitro alternative to animal testing. *Br. J. Biomed. Sci.*, **66** (3), 160–165.
196. Lin, R.-Z. and Chang, H.-Y. (2008) Recent advances in three-dimensional multicellular spheroid culture for biomedical research. *Biotechnol. J.*, **3** (9-10), 1172–1184.
197. Nicholson, K.M., Bibby, M.C. and Phillips, R.M. (1997) Influence of drug exposure parameters on the activity of paclitaxel in multicellular spheroids. *Eur. J. Cancer*, **33** (8), 1291–1298.

3

Coordination Chemistry and Ligand Design in the Development of Metal Based Radiopharmaceuticals

Eszter Boros[1], Bernadette V. Marquez[2], Oluwatayo F. Ikotun[2], Suzanne E. Lapi[2], and Cara L. Ferreira[3]

[1]*A.A. Martinos Center for Biomedical Imaging, Massachusetts General Hospital, Harvard Medical School, 149 13th St, Charlestown, MA, USA, 02129*
[2]*Department of Radiology, Washington University, 510 S. Kingshighway Blvd, St. Louis, MO, USA, 63110*
[3]*Nordion, 4004 Wesbrook Mall, Vancouver, BC, Canada, V6T 2A3*

3.1 Introduction

Metals play a dominate role in the field of nuclear medicine. Metals make up the majority of the periodic table and the majority of the chart of nuclides. So, there is a vast array of metal radionuclides or "radiometals" with properties valuable for nuclear imaging and radiotherapy. The majority of nuclear medicine procedures, diagnostic, and therapeutic, rely on radioactive metal isotopes. Not surprisingly the coordination chemistry of metals continues to be widely investigated as part of efforts to develop new and improved radiopharmaceuticals. Many of the characteristics of coordination complexes sought for other metal based drugs, such as magnetic resonance imaging (MRI) contrast agents, are also relevant for metal based radiopharmaceuticals. But due to numerous unique aspects of radiochemistry, other factors in coordination chemistry and other attributes of the resulting coordination complexes are of specific importance in developing radiometal based drugs for nuclear medicine.

Ligand Design in Medicinal Inorganic Chemistry, First Edition. Edited by Tim Storr.

3.1.1 Metals in nuclear medicine

Current clinical nuclear imaging uses radionuclides with either single photon emissions or positron emissions for SPECT (single photon emission computed tomography) or PET (positron emission tomography), respectively. In both types of imaging, the patient is injected with the radiopharmaceutical and the emission of the radionuclide is detected by "cameras" outside the patient. SPECT imaging is the most widely used nuclear imaging technique, and the most widely used radionuclide used in SPECT radiopharmaceuticals is the second row transition metal ^{99m}Tc. For example, the ^{99m}Tc complex sestamibi is used in millions of nuclear imaging scans per year, and is a principal diagnostic technique for evaluating cardiac patients. Coordination complexes of numerous other metal radionuclides are also used in clinical practice. Table 3.1 lists radiometals applicable to SPECT imaging and examples of radiopharmaceuticals. PET currently provides higher resolution due to the detection of coincident gamma photons created by the annihilation of the emitted positron. PET is a relatively newer technique in clinical nuclear medicine, and to date no radiopharmaceuticals containing metal radionuclides are approved for clinical use. But, researchers are looking to exploit the attractive selection of positron emitting metal radioisotopes (Table 3.1), and numerous PET imaging agents that contain radiometals are in development.

Therapeutic internal source radiopharmaceuticals have been a notable addition to the treatment options for several types of cancer [7]. In radiotherapy, patients are injected with a radiopharmaceutical which localizes at the disease site and emits less penetrating radiation that deposits its energy within a short distance thereby damaging proximal cells. Beta particle emitting radionuclides can effectively kill tumor cells through direct interaction and via the cross-fire effect. To date, several metal radionuclides that produce beta emissions are in clinical use in different parts of the world and other beta emitting radionuclides are being investigated for the development of the next generation of therapeutic radiopharmaceuticals. Two other types of emissions may also have potential for radiotherapy, alpha particles, and auger electrons. In both cases the particles are even

Table 3.1 *Radiometals and associated radiopharmaceuticals applicable for nuclear imaging*

SPECT Radiometal	Emission properties	Example radiopharmaceuticals
^{99m}Tc	$t_{1/2} = 6.01$ h, $\gamma = 140$ keV	^{99m}Tc-sestamibi, ^{99m}Tc-medronate
^{67}Ga	$t_{1/2} = 3.26$ d, $\gamma = 93$, 185, and 300 keV	^{67}Ga citrate
^{111}In	$t_{1/2} = 2.80$ d, $\gamma = 171$ keV	111In-DTPA-octreotide
PET Radiometals	Emission properties	Example radiopharmaceuticals
^{68}Ga	$t_{1/2} = 14.7$ h, $\beta^+ = 89\%$	^{68}Ga-DOTATOC
^{64}Cu	$t_{1/2} = 12.7$ h, $\beta^+ = 18\%$	^{64}Cu-ATSM
^{86}Y	$t_{1/2} = 14.7$ h, $\beta^+ = 33\%$	^{86}Y-DOTA-Phe^1-Tyr^3-octreotide (phase I) [1]
^{89}Zr	$t_{1/2} = 78.4$ h, $\beta^+ = 22\%$, $E_{ave}(\beta^+) = 396.9$ keV	^{89}Zr-DFO-huJ591 (phase I/II) – metastatic prostate cancer [2, 3] ^{89}Zr-bevacizumab – breast cancer [4] ^{89}Zr-nanocolloidal albumin – oral cancer [5] ^{89}Zr-trastuzumab – breast cancer [6]
^{55}Co	$t_{1/2} = 17.53$ h, $\beta^+ = 76\%$	–
^{44}Sc	$t_{1/2} = 3.97$ h, $\beta^+ = 94.3\%$	–

Table 3.2 *Radiometals and associated radiopharmaceuticals applicable for radiotherapy*

Radiometal	Emission properties	Example radiopharmaceuticals
^{186}Re	$t_{1/2} = 3.72$ d, β^-	^{186}Re
^{188}Re	$t_{1/2} = 17$ h, β^-	^{188}Re
^{67}Cu	$t_{1/2} = 61.8$ h, β^-	^{67}Cu antibodies
^{90}Y	$t_{1/2} = 64$ h, β^-	^{90}Y-DOTATOC
^{177}Lu	$t_{1/2} = 6.65$ d, β^-	^{177}Lu–DOTATOC
^{153}Sm	$t_{1/2} = 46.5$ h, β^-	^{153}Sm-EDTMP (trade name Quadramet)
^{166}Ho	$t_{1/2} = 26.8$ h, β^-	^{166}Ho-DOTMP

less penetrating and deposit their energy only a short distance from where they decay. Metal radionuclides with emissions relevant to radiotherapy and radiotherapeutic agents are listed in Table 3.2.

Because of the wide variation of metal radionuclides, they also play a significant role in the emerging area of theranostic nuclear medicine [8]. Generally, theranostics are single agents that can be used for both diagnostic and therapeutic purposes. Several metal radioisotopes have both detectable emissions for diagnostic nuclear imaging procedures and therapeutic emission for radiotherapy and are well suited to the development of a single theranostic agent. Alternatively, a single metal can have different radioisotopes that can be interchanged to make a theranostic pair. For example, a radiopharmaceutical that incorporates a Cu atom can be prepared with positron emitting radioisotope ^{64}Cu for diagnostic PET imaging or the beta particle emitting ^{67}Cu for radiotherapy. Finally, metals with similar coordination properties can be used to prepare similar agents that can be paired for diagnostic and therapeutic procedures. For example, ^{111}In and ^{68}Ga somatostatin agents are used for diagnosis and staging of neuroendocrine tumors, then analogous or similar ^{90}Y somatostatin agents can be used for radiotherapy [9]. Thoughtful coordination chemistry is crucial to ensuring that the *in vivo* properties are near equivalent for any "theranostic" pair prepared from two different metal radionuclides.

3.1.2 The importance of coordination chemistry

Only a few metal radionuclides can be injected directly into a patient and be effectively used as an imaging or radiotherapy agent. Hence, the coordination of a chelate or ligand(s) around the metal radionuclide is instrumental in the development of radiopharmaceuticals. Like other metal based drugs, coordination chemistry in radiopharmaceutical development is central to creating a stable, non-toxic compound as a safe and effective agent. As well, coordination chemistry impacts the "medicinal" properties of the agent. Radiopharmaceutical coordination complexes can be separated into two types, metal-essential and metal-non-essential. Metal-essential radiopharmaceuticals depend on the physical properties of the complex itself to direct the agent to the biological target. ^{99m}Tc-sestamibi is an example of a metal-essential radiopharmaceutical, because it relies on the lipophilic and cationic properties of the overall complex to localize in viable cardiac muscle. Metal-non-essential radiopharmaceuticals do not require the presence of the coordinated metal to direct them to their biological target. Typically these types of agents have a targeting moiety that is tethered to the metal using a bifunctional chelate. Bifunctional chelates, as the name implies, serve two functions:

1. To covalently bond to the targeting moiety
2. To stably coordinate to the metal.

Since the coordinated metal is an addition to the targeting moiety, it is not only non-essential, it can often negatively impact the properties of the agent. For both metal-essential and metal-non-essential types of radiopharmaceutical, coordination chemistry plays an important role in transforming the metal radionuclide into a drug that can be used to safely and effectively diagnose or treat disease.

3.1.3 Overview

In this chapter the numerous factors of coordination chemistry specific to metal radionuclides relevant for radiopharmaceutical development will be discussed. First, the ideal properties of radionuclides for different applications will be examined to illustrate how the metal radionuclide is chosen, and the numerous attributes of the ideal coordination reactions and final coordination environment will be examined. Finally, the coordination chemistry of specific metal radionuclides will be given a closer look for several of the most common radiometals currently used in or with significant potential for use in radiopharmaceuticals.

3.2 General metal based radiopharmaceutical design

3.2.1 Choice of radionuclide

The choice of radionuclide is dependent on the specific application. Selection of radionuclide can be based on two main criteria:

1. The nuclear emission properties; the types of emissions and the energy of the emissions.
2. The half-life of the radionuclide.

So, the radionuclide is first chosen based on the appropriateness of the emission types and the emission energies for the application. Emission types useful for imaging must be penetrating, so that they can pass through the patient and be detected, such as gamma photons and positron emissions. The energy of the emissions can impact the resolution of the images and the radiation dose given to the patient [10]. For therapeutic purposes the ideal emissions, such as beta particles, should be less penetrating and deliver localized energy to damage and destroy the disease target. Both the type and the energy of therapeutic emissions can impact the effectiveness of the treatment and the range or treatment area. For example, the higher the average or maximum beta particle emission energy the further the average distance that the particles will travel in tissue and the greater area that will be treated [11]. But, if the application is to treat small areas such as microtumors, lower energy particles would be preferred to minimize radiation exposure of surrounding healthy tissue [12]. Most radionuclides have more than one type or energy of emission. So, a maximum number of useful emissions (emission that can be used for detection or for therapy) and a minimum number of non-useful emissions are desired to limit the amount of unnecessary radiation exposure to patients and medical staff.

The half-life of the radionuclide is chosen to best match the application. The half-life must be long enough to facilitate all steps from preparation of the radiopharmaceutical through to the final nuclear medicine diagnostic procedure or effective radiotherapy treatment. With respect to preparation of the radiopharmaceutical the half-life must be long enough to allow the required synthetic chemistry and purification, as well as delivery of the radiopharmaceutical to the hospital or clinic where it will be used. Once injected the half-life must also be long enough to allow localization of the radiopharmaceutical to the disease state of interest and clearance of the radiopharmaceutical from non-target background tissue. The time required for localization and clearance is dependent on the agent. Small molecule radiopharmaceuticals typically localize and clear in minutes or hours while larger molecules, such as radiolabeled proteins or antibodies, can take days [13]. For therapy, a longer half-life means that the agent will irradiate the target disease state and potentially be more

effective, assuming the agent or at least the radionuclide remains localized at the target. But for imaging, an unnecessarily long half-life could result in excess radiation exposure to the patient. In short, the half-life of the chosen radionuclide needs to be long enough to be effective for the radiopharmaceutical's intended use, but no longer.

3.2.2 Production of the radiometal starting materials

The production method of the radionuclide determines the form of the starting material, and hence has implications for the subsequent coordination chemistry. There are three methods by which radiometals of interest to nuclear medicine are produced; from a parent/daughter generator, using a cyclotron, or in a reactor. Radionuclides that can be acquired from a generator have a practical advantage in nuclear medicine. Several isotopes are available via decay of a long lived parent isotope. In these cases the parent can be placed on a column and the daughter can be periodically eluted off. The ability to elute the isotope as needed and on-site is advantageous with respect to time and cost. The availability of ^{99m}Tc from a generator is one of the reasons that this radioisotope has dominated nuclear imaging. Many radionuclides are yielded from solid metal targets that are dissolved in acid and separated from the target material and other impurities. The resulting starting material is typically an acidic aqueous solution of the metal in a particular oxidation state. Other radiometals are acquired from generators or processed to provide the radionuclide in different aqueous solutions. The oxidation state of the radiometal, as well as the matrix (typically a solution) that the radiometal is in must be taken in to account when designing the coordination chemistry. For example, chelates and ligands must be both stable and soluble in the matrix, as do reducing agents if required.

3.2.3 Ligand and chelate design consideration

3.2.3.1 Stability

One of the most important goals in design of the coordinating ligands or chelates for metal based radiopharmaceuticals is to yield a complex that will be stable. As a drug, the complex must be stable under the physiological conditions that it will be used in. Radiopharmaceuticals are typically injected, so the complex must be stable in aqueous environments at neutral pH and in the presence of blood proteins. Furthermore, the complex must be stable to any other biological process, such as metabolic processes that it can be expected to be exposed to.

Coordinating groups that produce strong bonds can be chosen to produce a thermodynamically stable complex. The matching of the relative hardness of donor groups to the relative hardness of the radiometal to be complexed is ideal. Thermodynamic stability can also be enhanced by using multivalent ligands and taking advantage of the chelate effect.

For metal based radiopharmaceuticals kinetic stability often has a greater importance than thermodynamic stability. Radiopharmaceuticals are injected in extremely small quantities; they are at a low concentration in preparation and are further diluted once they are administered into the blood stream. As such, the radiopharmaceutical is exposed to many magnitude higher concentrations of potentially competing ligands. Trace levels of competing metals, either different metals or non-radioactive isotopes of the radionuclide being used, are also in much greater concentration and can easily displace the metal radionuclide if the coordination complex is not kinetically inert. The oxidation state of the radiometal in the complex can be one design factor, opting for the most inert electronic states. The ligands or chelates can also be designed to promote the ideal geometry for the appropriate inert electronic state, whether high spin or low spin. Finally, multivalent chelates, especially more rigid macrocyclic chelates, can help compensate for kinetic lability. If one coordinating group dissociates, it remains in close proximity to the metal center, making it more probable it will re-coordinate to the metal.

3.2.3.2 Coordination reaction kinetics

Radiopharmaceutical synthesis is typically very time sensitive. The longer a reaction takes the more of the radionuclide is lost to decay. Since the radionuclide is the limiting starting material, loss in decay means a lower yield of radiopharmaceutical. Obviously, the shorter the half-life of the radionuclide, the more time sensitive the coordination reaction. As such the coordination reaction itself must have appropriately fast kinetics. If the reaction is quantitative, if all of the radionuclide is consumed, the need for a final purification step may not be required further saving time. If purification is necessary, it also must be a relatively fast process to be useful in radiopharmaceutical preparation.

Designing ligands and chelates that facilitate fast and complete coordination of radiometals is of specific importance to metal based radiopharmaceuticals. While simple small ligands with strong donor groups can provide fast reactions, they can produce a mixture of species, they may be more labile, and they may limit the ability to incorporate targeting moieties. Multivalent acyclic and macrocyclic chelates can provide greater stability and allow for more simple incorporation of target moieties or properties, but with increasing rigidity the reaction kinetics are often slower. Furthermore, multivalent chelates can also result in a mixture of species with differing physical properties. In the development of chelates that facilitate incorporation of radiometals into radiopharmaceuticals, designing ligands that balance the need for fast reaction kinetics, function, and stability is a priority.

Two further methods commonly used to increase the reaction rates for radiometal coordination are to increase the chelate concentration or to increase the reaction temperature. Since the radiometal is in low concentration, the chelate concentration remains relatively unchanged throughout the reaction. So assuming first order kinetics, the chelate concentration is proportional to the reaction rate. But, large excesses of chelate may require the addition of time-consuming purification steps. Without purification the excess chelate can lower the effective specific activity of the radiopharmaceutical. Lower specific activity means the excess chelate can compete with the radiopharmaceutical for the disease state target *in vivo*, resulting in poorer diagnostic images or lower efficacy therapeutics. Increase in temperature can also increase the reaction rate of metal coordination, especially for macrocyclic chelates that can have higher reaction threshold energies. But, using elevated temperature is not feasible when the system includes sensitive targeting vectors such as peptides or antibodies. One solution is to conjugate the sensitive targeting vector after metal coordination, but this second step again adds time to the preparation of the radiopharmaceutical and may also require additional purification step(s) [14].

3.2.3.3 Pharmacokinetics

Pharmacokinetic properties are particularly important for radiopharmaceuticals, and can be modified using chelate design. Radiopharmaceuticals and their metabolites in non-target background tissue are indistinguishable from the radiopharmaceutical at the target site. For imaging, background radioactivity can diminish image contrast significantly. For radiotherapy, background activity increases patient radiation exposure and limits dosing and thereby efficacy. So, for all applications target site retention and background clearance are crucial. The chelate can be designed to optimize pharmacokinetics [15, 16]. The charge of donor groups can be designed to generate a certain charge for the resulting radiometal complex. Neutral charged species are particularly important for radiopharmaceuticals that must pass the blood-brain barrier. Negatively charged complexes have been shown to have relatively faster blood and renal clearance [17]. Lipophilic chelates can also be used to facilitate longer circulation times or cellular uptake to enhance target retention [18], while the incorporation of hydrophilic groups into the chelate can increase renal over hepatic clearance. More innovative chelate development for pharmacokinetic modulation includes increasing the number of targeting moieties on the chelate to increase retention [19] and adding cleavable linkages to facilitate metabolism and clearance [20].

The use of chelates to form coordination complexes provides an adaptable scaffold to optimize the *in vivo* properties of the radiopharmaceutical.

3.3 Survey of the coordination chemistry of radiometals applicable to nuclear medicine

3.3.1 Technetium

^{99m}Tc, the metastable decay product of ^{99}Mo, has been a radionuclide of interest in radiopharmaceutical chemistry and nuclear medicine for the past four decades [21]. ^{99m}Tc has ideal physical properties ($t_{1/2} = 6$ hours, 99% decay through $\gamma = 141$ keV) for imaging with SPECT [22]. Additionally, the mother nuclide ^{99}Mo can be immobilized on solid alumina sorbent material and used for multiple days as a portable source for highly pure ^{99m}Tc isotope, as the so-called ^{99m}Tc generator. As a result, the chemistry of ^{99m}Tc has been extensively researched. Today, nearly 85% of all diagnostic scans are done with ^{99m}Tc and hence nuclear medicine has become highly dependent on the (reactor-) production of large quantities of ^{99}Mo. The aging reactor facilities in Chalk River (Canada) and Petten (Netherlands) are currently struggling to meet the high demand of the radionuclide, leading to the recent isotope shortage, as both reactors had to be shut down for extensive repairs between the years of 2008 and 2010. This has rekindled interest in direct production of ^{99m}Tc using cyclotrons, but also in the short-lived, cyclotron-produced PET radionuclide ^{94m}Tc and other alternative radiometals [23].

A variety of Tc oxidation states can be stabilized in aqueous media, and can be relevant for nuclear medicine applications, as long as they are easily attainable from TcO_4^-, which is the form of Tc present in generator or cyclotron target eluate [24]. TcO_4^-, with Tc in oxidation state +7, is chemically inert and generally requires strongly reductive conditions to transition into lower oxidation states. Figure 3.1 summarizes oxidation states and preferred donor atom combinations, which constitute specific Tc-coordination cores. The most commonly used core is provided through the reduction of TcO_4^- with $SnCl_2$ to afford the "coordinatively more cooperative" oxo-species Tc(V) with a weak, placeholder ligand such as glucoheptonate or gluconate which then subsequently is exchanged with a strongly coordinating tetradentate chelate. The final product then constitutes either a small, technetium essential coordination complex, or a technetium tagged complex, which bears the targeting moiety attached through a linker to the chelate (Figure 3.1) [21].

The first generation of Tc imaging agents developed and used clinically was compromised exclusively of technetium essential small molecule complexes, which were able to localize in the tissue of interest due to charge, polarity, and size of the corresponding complex. After the advent of TcO_4^- as a thyroid imaging agent (due to its similarity to I^-) [25], other small molecular, Tc essential coordination complexes were developed as imaging agents for kidney, liver, brain, and heart and continue to be used successfully for this purpose until today. Among some of the most prominent ones are Tc-sestamibi for myocardial perfusion [26] and Tc-mertiatide for imaging of the renal tract [27], both developed by Davison and Jones. Figure 3.2 summarizes the most relevant examples, including the tissue/organ they target [28, 29].

Following the development of organ-specific Tc-based imaging agents, bifunctional chelates with the capability of introducing a Tc label onto target-specific biomolecules had gained greater interest and

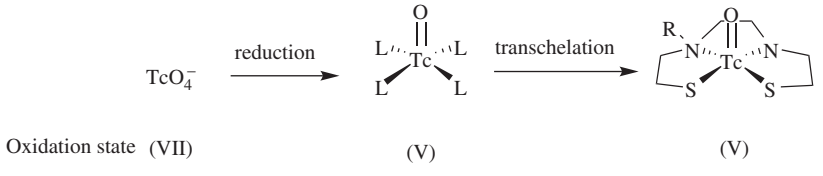

Figure 3.1 *Typical reaction sequence for the synthesis of Tc-oxo complexes*

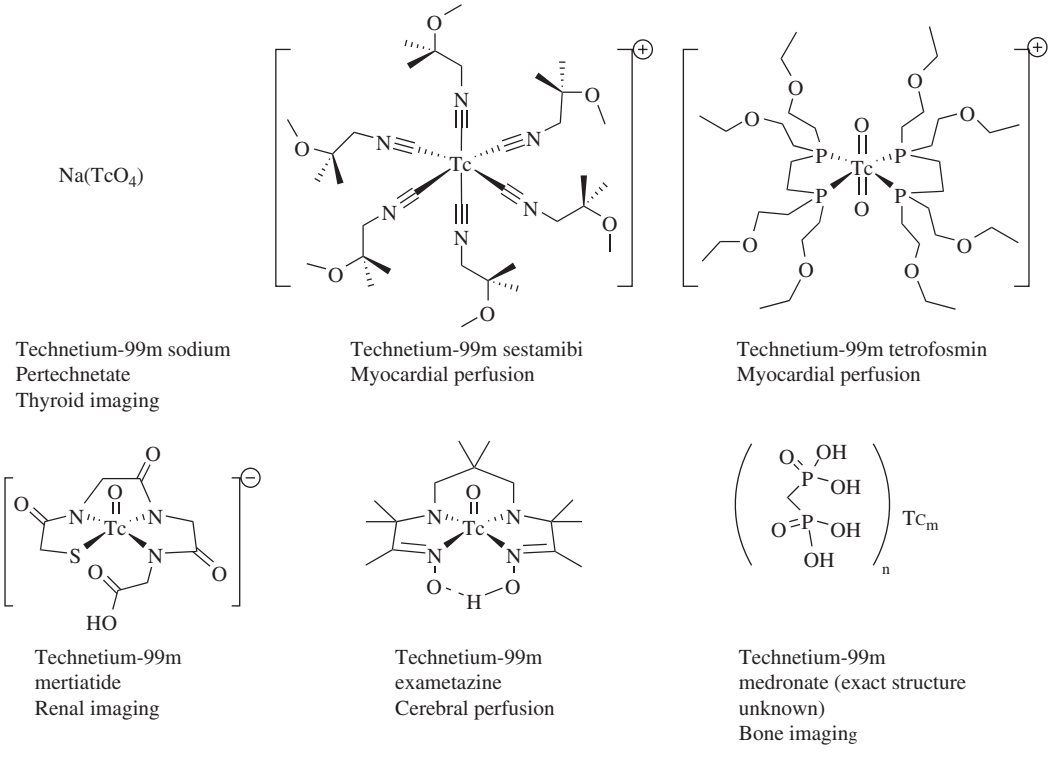

Figure 3.2 *Representative examples of Tc-based imaging agents in clinical use*

relevance. Continued efforts of Katzenellenbogen and coworkers to incorporate the Tc complex into steroid-like structures were successful in terms of over-all structural mimicry, but only showed moderate binding efficiency to the protein target [30, 31]. It was found that for receptor specific targeting, a technetium tagged approach is more suitable, where the Tc complex is not part of the structure binding to the receptor.

Some of the initially most frequently used coordinating ligands for this purpose are of the $N_{4-x}S_x$ type, first developed by Davison and coworkers (Figure 3.3, structure **A**), being versatile in terms of structure of the tetradentate ligand scaffold [32–34]. Some drawbacks of this system include, besides the stringent reductive conditions, rapid re-oxidation or the formation of *syn* and *anti* isomers, which can exhibit different *in vivo* behavior [35]. The deep understanding of the Tc(V)-oxo chemistry due to research done over the course of multiple decades continues to produce new versions and applications of this core; but extensive investigation of ^{99}Tc coordination and redox chemistry over multiple decades has led to the development of a great number of alternative, successfully used coordination environments.

Two subsequently developed cores are the nitrido $[TcN]^{2+}$-core (Figure 3.3, structure **B**, Marchi and coworkers) [36, 37] and the $Tc(HYNIC)^{-}$ core (Figure 3.3, structure **C**, by Abrams and coworkers) [38]. While both systems exhibit interesting coordination chemistry and can produce stable complexes, the multi-step labeling procedure and difficulties in characterizing the chemical structure of the complexes formed render these systems less compatible with kit formulations. Only one nitrido complex (nitridotechnetium(V)) [39] has become clinically used as a myocardial perfusion agent. Lack of stability of some of the less coordinatively saturated HYNIC species bearing Cl^{-} as one or two co-ligands has also been reported

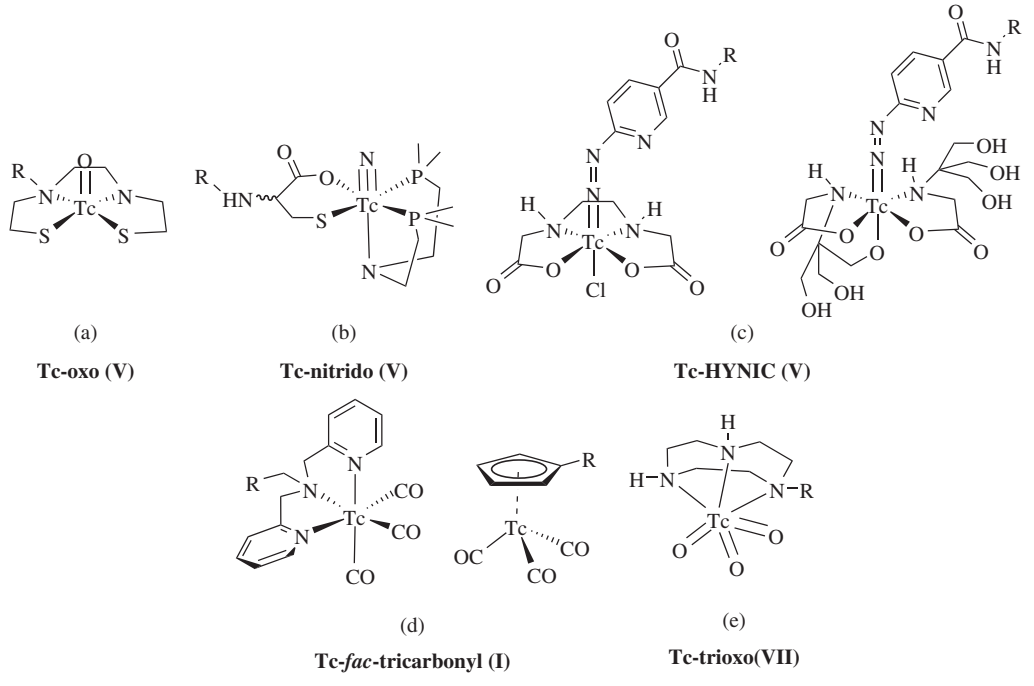

Figure 3.3 *Common Tc core structures utilized for bifunctional, Tc-tagged conjugates. R indicates the point of derivatization*

and was tackled by substitution of stronger sigma donating ligands and has provided more stable derivatives which have led to successful synthesis of stable conjugates with peptides and antibodies [40, 41].

Abandoning the high oxidation state Tc(V)-cores constituted a different approach; Alberto and coworkers pioneered a corresponding kit formulation, which produces the *fac*-$[^{99m}Tc(CO)_3]^+$ core with three labile aquo ligands [42]. The compound $[^{99m}Tc(CO)_3(H_2O)_3]^+$ is stable and soluble in aqueous solution and the water ligands can be readily exchanged using a range of multidentate ligand systems (Figure 3.3, structure **D**) [43, 44].

The low-spin, d^6 system exhibits increased inertness compared to the Tc^V oxo-core (d^2), slowing ligand exchange rates and providing a highly versatile, stable coordination environment, even with ligand systems such as the cyclopentadienyl moiety [43] and truncated, nido-carboranes [45]. This facilitates simple modification of the pharmacokinetic behavior by adaptation of the coordinating ligand system and has led to a wide variety of applications for small molecule imaging agents [46, 47], bioconjugates of small molecules [48, 49], and a plethora of peptide conjugates [50–52].

Most recent developments include the Tc trioxo-core bearing a Tc with the oxidation state +7, which is isolobal, having similar valence electrons and structure, to the *fac*-$[^{99m}Tc(CO)_3]^+$, but cannot be destabilized through re-oxidation, but only through ligand hydrolysis (Figure 3.3, structure **E**) [53] It is also found to be considerably less lipophilic compared to the *fac*-$[^{99m}Tc(CO)_3]^+$ core. Furthermore, the potential of [3+2] cycloaddition of two of the oxo ligands with alkenes may pave the way for the successful construction of trifunctional Tc complexes [54].

The complex redox chemistry, paired with alternative ways to produce this isotope essential to nuclear medicine, provides the basis for continued interest in ^{99m}Tc. Table 3.3 summarizes the most relevant Tc cores in order of decreasing oxidation state and lists properties such as reducing agent and conditions required for their synthesis, as well as their key properties.

Table 3.3 *Summary of most commonly used Tc cores and their key features*

Core	Oxidation state	Oxidizing agent used	Common ligand systems	Other features
TcO_3^+	(VII)	SSP-PR_3, re-oxidation	N_3	[3+2] cycloaddition possible with two oxo ligands to form trifunctional system
$Tc{=}O^{3+}$	(V)	$SnCl_2{\bullet}2H_2O$ glucoheptonate	$N_{4-x}S_x$	[3+1], [2+2] donor sets are also stable
$O{=}Tc{=}O^+$	(V)	$SnCl_2{\bullet}2H_2O$ glucoheptonate	$N_{4-x}P_x$	[2+2] system used commercially
$Tc{\equiv}N^{2+}$	(V)	$SnCl_2{\bullet}2H_2O$, succinic dihydrazide	N, O, S, and P	[2+2] preferred
$Tc{=}N{=}N\text{-}R^{3+}$	(V)	$SnCl_2{\bullet}2H_2O$ glucoheptonate	HYNIC combined with $N_{5-x}O$(or $P)_x$	Charge and polarity can be influenced by choice of N, O, or P donor ligands
$Tc(CO)_3$	(I)	$K_2[H_3BCO_2]$	$N_{3-x}O_x$	[2+1] possible but tridentate is preferred

3.3.2 Rhenium

There are two radioisotopes of rhenium with potential application to nuclear medicine. Both ^{186}Re ($t_{1/2} = 3.68$ days and $\beta^- = 1.07$ MeV) and ^{188}Re ($t_{1/2} = 17$ h d and $\beta^- = 2.12$ MeV) are beta particle emitters with energies relevant to radiotherapy. Re is the third row transition metal congener of Tc, and therefore has similar chemistry to Tc and could be used as a therapeutic partner to ^{99m}Tc based imaging agents [8]. ^{186}Re is produced by neutron capture on stable, natural Re or enriched ^{185}Re targets leading to a relatively low specific activity product [55]. Recent studies have also been conducted producing this isotope via proton irradiation of enriched ^{186}W [56]. ^{188}Re can be acquired from a ^{188}W generator to give a high specific activity radionuclide. In all cases the Re radionuclide starting material is an inert perrhenate salt (ReO_4^-), similar to the ^{99m}Tc pertechnetate starting material.

Similar to Tc, Re radionuclides must be first reduced from the chemical inert ReO_4^- species to a lower oxidation state in order to facilitate the coordination of ligands or chelates. Common oxidation states for Re radiopharmaceuticals are V, IV, and I. Compared to pertechnetate, it has been found that perrhenate requires a stronger reducing environment or a greater concentration of reducing agents to ensure reduction [57]. This is partially due to the difference in reduction potential but it is further complicated by the generation of oxidizing free radicals from the interaction of beta particles with water molecules in the reaction solution. The predilection of Re radionuclides to re-oxidize more readily than Tc analogs has been cited as the reason for differences in the biodistribution of Tc and Re complexes of hydroxyethylene diphosphonate (HEDP), bone imaging and radiotherapy agents, respectively [57, 58].

Because of the general parallels between Tc and Re chemistry, similar metal cores and chelate systems with similar types of donor groups discussed for Tc have been pursued for Re based radiopharmaceuticals. Early development of Re based potential radiopharmaceuticals was focused on the Re^V oxo-core. Numerous small molecules and larger biomolecules, such as peptides, have been radiolabeled with the Re^V oxo-core using two $N_{4-x}S_x$ tetradentate chelates for complexation; [14, 59–62] tetradentate systems containing phosphine donor groups have also been investigated [63]. Examples of these systems are illustrated Figure 3.4. The close similarity of the Re and Tc analogs of these systems has been demonstrated through comparison of

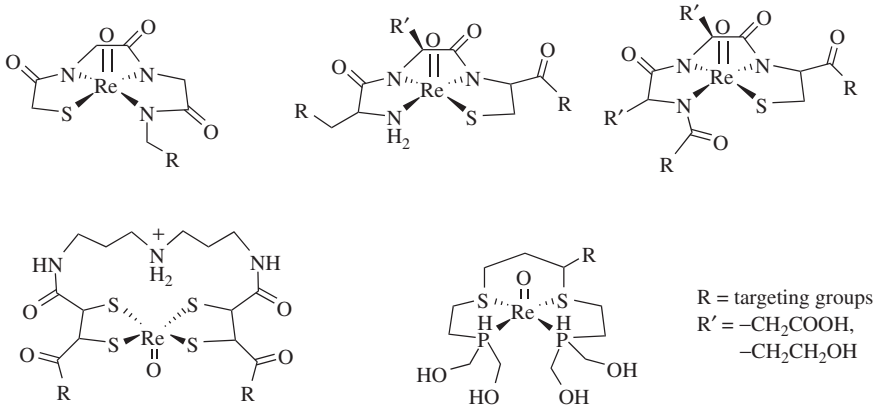

Figure 3.4 *Examples of tetradentate chelates investigated for coordination of the Re^{V}oxo core*

X-ray crystallography structures [64] and *in vivo* biodistribution [59, 61]. More recently, the $Re^{I}(CO)_3$ core has been the focus of Re based radiopharmaceutical development due to the inert electronic configuration. The preparation of the $[Re(H_2O)_3(CO)_3]^+$ precursor for subsequent complexation requires different reaction conditions than the Tc analog, using an amine borane reducing agent in the presence of CO [65, 66]. Numerous bidentate and tridentate chelates with hard and or soft donors have been subsequently coordinated to this versatile Re core including radiolabeling with either ^{188}Re or ^{186}Re [65–69].

The adaptation of the extensive research on Tc chemistry to Re analogs continues to facilitate the development of Re based radiotherapeutics to complement Tc based diagnostic agents. Further development of Re coordination complexes applicable to radiotherapy could be improved by increased availability of either ^{186}Re or the ^{188}W/^{188}Re generator, which will likely coincide with the clinical approval and wide adoption of Re based radiopharmaceuticals.

3.3.3 Gallium

Gallium is a main group metal, but has many similarities to transition metals with respect to its coordination chemistry. Because of its low redox potential, Ga^{III} is the only relevant oxidation state in aqueous media, with its valence electrons in a d^{10} configuration. Besides being present in bauxite and zinc ores, Ga does not occur in nature [70]. Ga has two stable isotopes, ^{69}Ga and ^{71}Ga (60.1 and 39.9% natural abundance respectively). Ga also provides a variety of radionuclides of interest for nuclear medicine. ^{66}Ga ($t_{1/2} = 9.5$ hours, β^+ 56% and $E_{max} = 4.3$ MeV) relies on cyclotron production and decays with a half-life comparable to ^{64}Cu, but ^{66}Ga emits a much higher energy β^+. ^{67}Ga ($t_{1/2} = 78$ hours, EC with γ emissions of 92 keV (38%), 184 keV (23%), and 300 keV (16%)) has been used successfully as a SPECT agent for a few decades [71]. ^{68}Ga ($t_{1/2} = 68$ minutes, β^+ 89% and $E_{max} = 1.9$ MeV) has received the greatest amount of attention in recent years due to the availability of the ^{68}Ge generator, which, similar to the ^{99}Mo generator for ^{99m}Tc, can serve as a mobile source of isotope [21]. The ^{68}Ge/^{68}Ga generator system has the potential to be eluted for up to one year due to the long half-life ($t_{1/2} = 271$ days) of the parent radionuclide ^{68}Ge [72]. The ^{68}Ga generator has been used to prepare ^{68}Ga radiopharmaceuticals for clinical imaging in Europe for several years, but the development of a generator with regulatory approval for human use will further facilitate the transition of ^{68}Ga based agents into the clinic in North America [73]. One of the most sophisticated commercially available and most frequently used generator systems is based on titanium dioxide (Cyclotron Co., Ltd., Obninsk, Russia). The elution of

free, cationic ^{68}Ga with low acid concentration of 0.1 M HCl, makes this generator suitable for universal application for radiopharmaceutical preparations [74].

Ga^{III} forms stable complexes with many multidentate ligands. While Ga^{I} is only stable in non-aqueous media, under physiological conditions Ga^{III} is the only stable and relevant oxidation state.

Tetradentate to hexadentate coordination has been reported; however, many Ga coordination complexes tend to be rather labile. In order to be suitable for applications as a radiopharmaceutical, the Ga^{III} ion must be inert toward *in vivo* hydrolysis to form soluble $[Ga(OH)_4]^-$ (the predominant species at physiological conditions) or transchelation by the iron scavenging protein transferrin [75].

Gallium(III) is only present as the aqua ion at pH < 3, so coordination must happen under acidic conditions. The free hydrated Ga^{III} cation is only stable under acidic conditions, while above pH 4 formation of hydroxide species $Ga(OH)_3$ (pH 4–7) and $[Ga(OH)_4]^-$ (>pH 7) occurs [76]. To make the metal ion available for ligand systems that coordinate preferentially at pH < 5, a pre-labeling strategy uses a weakly coordinating ligand such as citrate, which is then easily replaced by a stronger ligand system [77]. Considering the short half-life of ^{68}Ga, a direct labeling strategy is preferred, which can be executed at a pH compatible with biomolecules. An additional non-negligible factor includes kinetic stability of the formed complex toward the iron sequestering protein transferrin, which is capable of transchelating weakly bound Ga^{III} due to the similarity between the charge to size ratio of Ga^{III} and Fe^{III} [78].

^{67}Ga(citrate) has been in use for several decades as a SPECT imaging agent for inflammation and lymphoma; however, its mode of action relies on the rapid in vivo transchelation to ^{67}Ga-transferrin. No small molecule Ga complexes are approved for imaging but have become a heavily investigated target in recent years. Considering the great commercial success of small molecule SPECT agents based on ^{99m}Tc, this area of research remains an interesting and potentially lucrative avenue.

Currently the only ^{68}Ga-based radiopharmaceutical in clinical studies is the bioconjugate ^{68}Ga-DOTANOC [79]. It relies on a complex pre- and post-labeling purification system, because the macrocyclic chelate used for this conjugate is 1,4,7,10-tetraazacyclododecane–N,N′,N″,N‴-tetraacetic acid (DOTA), a chelate with less than favorable labeling properties.

Considering the short half-life of this radionuclide, a kit formulation, where the generator is directly eluted into a vial containing the ligand system and biomolecule, forming a ready-to-inject radiopharmaceutical would be a major advantage for a compound with potential for clinical applications [21].

The efficient and strong chelation of radiometals of gallium(III) has been investigated since the first advent of ^{68}Ga with high hopes for potentially useful complexes in radiopharmacy. Bifunctional versions, introduced by Maecke and coworkers of the tri-aza-based aminocarboxylate macrocyclic chelate 1,4,7-triazacyclononane-1,4,7-triacetic acid (NOTA) continue to deliver highly promising results for the rapid and stable chelation of ^{68}Ga [80].

The commercial supply of the ^{68}Ge generator has recently fueled the development of an array of chelates for Ga^{III} (structures summarized in Figure 3.5 and their corresponding thermodynamic stability constant and labeling properties are given in Table 3.4).

In order to furnish the ideal bifunctional chelate for ^{68}Ga, rapid coordination under mild conditions (pH > 4, room temperature, labeling within 15 minutes), high kinetic stability (stable versus *apo*-transferrin challenge and *in vivo* conditions) and simple synthesis and functionalization (for applications for peptide labeling) are key. Sufficient kinetic inertness in vivo to prevent transchelation and loss of the radiometal is strongly desired. A thermodynamic stability constant log K_{ML} above the value found for the main *in vivo* competitor, transferrin (log $K_{ML} = 20.3$) is preferred; however, it is the ligand exchange kinetics that will ultimately govern the fate of the radionuclide [78].

Among the poly-aza macrocyclic structures, the multi-functional 3,6,9,15-tetraazabicyclo[9.3.1]pentadeca-1(15),11,13-triene-3,6,9,-triacetic acid (PCTA) has also been explored recently for the purpose of ^{68}Ga radiolabeling. Ferreira and coworkers were able to show that chelation occurs rapidly and in a kinetically inert

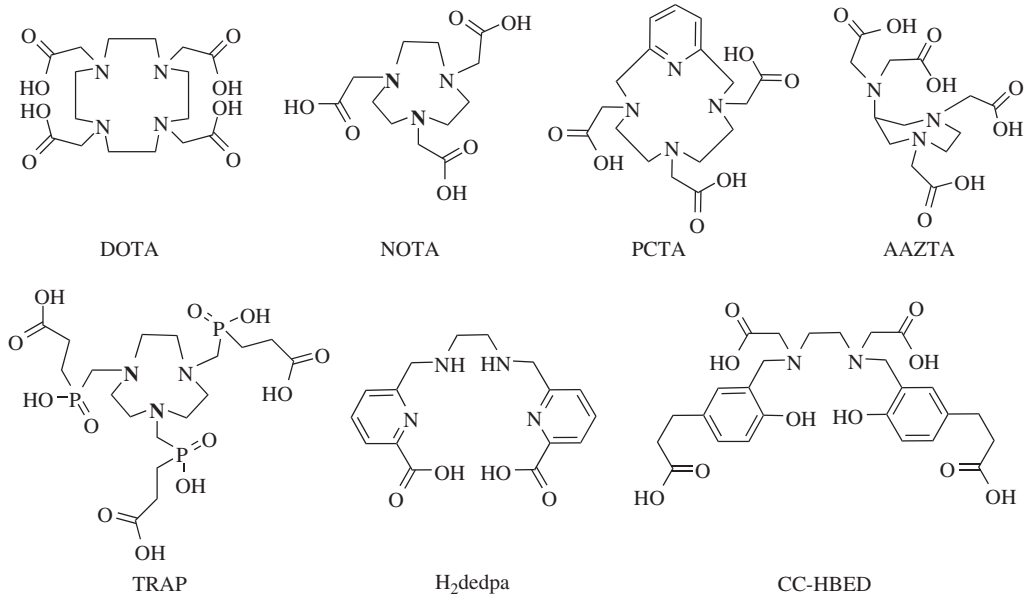

Figure 3.5 *Structures of chelates for gallium(III)*

Table 3.4 *Thermodynamic stability constants and labeling conditions for chelates for gallium(III)*

Ligand	Labeling conditions (yield)	Log K_{ML}
DOTA	5 min, 80 °C (95%)	21.33
NOTA	10 min, room temperature (>98%)	30.98
PCTA	10 min, room temperature (>98%)	19.37
AAZTA	10 min, room temperature (>98%)	22.2
TRAP	5 min, 95 °C (>98%)	26.2
H_2dedpa	10 min, room temperature (>98%)	28.1

fashion with the non-derivatized complex [81]. The corresponding RGD derivative was also formed and shown to have the same characteristics in terms of radiolabeling and kinetic inertness. Additionally, utility for biofunctional tumor imaging was also demonstrated [82].

Another multifunctional chelate, 6-amino-6-methylperhydro-1,4-diazepine tetraacetic acid, AAZTA, has also been found to be suitable for rapid and kinetically stable complexation by Parker and coworkers [83]. The determination of thermodynamic stability constants by Aime and coworkers provides additional support [84] for the utility of AAZTA for the labeling with ^{68}Ga.

Taking into consideration the low pH of the ^{68}Ge generator eluate, Notni *et al*. have investigated NOTA type derivatives with pendant phosphonates. These ligand systems are capable of efficient chelation of ^{68}Ga at as low as pH 2 [85]. Labeling occurs rapidly under heat, forming highly inert systems regardless of the pendant biomolecule or functional group. Subsequently, Notni and coworkers have successfully explored peptide conjugates such as RGD derivatives as well as small molecule agents targeting bone [86, 87].

As rapid and mild chelation conditions are of great relevance for ^{68}Ga, acyclic chelates have also been subject of continued investigation. With choice of the right donor set, the kinetic lability of Ga^{III} can be considerably decreased, while maintaining rapid and efficient chelation of the radionuclide. A derivative of N,N-bis(2-hyroxybenzyl)ethylenediamine-N,N,-diacetic acid (HBED), which is a well-established acyclic chelate, is experiencing a recent rekindled interest: CC-HBED. Eisenhut and coworkers have successfully used this chelate conjugated to the prostate specific membrane antigen (PSMA) inhibitor Glu-NH-CO-NH-Lys(Ahx) and labeled the corresponding conjugate rapidly and efficiently at room temperature within 1 minute. In a subsequent biodistribution study, the HBED-CC conjugate clearly outperformed the DOTA-conjugate in tumor uptake, despite very similar in vitro affinity measured [88].

Orvig and coworkers reported the application of the pyridyl derivative 1,2-[{6-(carboxylato)-pyridine-2-yl} methylamino]ethane (dedpa) for the stable and efficient labeling of Ga radioisotopes [89]. This acyclic scaffold is found to be rather versatile in terms of derivatization and has found applications for bioconjugate chemistry as well as in development of potential myocardial perfusion agents, while maintaining the favorable labeling characteristics of rapid and mild complexation within 10 minutes at room temperature [90, 91].

Two closely related acyclic systems and a bifunctional version YM103, part of the HPO (3-hydroxy-4-pyridinone) ligand family were also recently reported to label quantitatively at room temperature within 5 minutes at pH 6.5 by Blower and coworkers. A corresponding first bioconjugate was also successfully labeled and provides an additional potential avenue for labeling of Ga isotopes [92].

3.3.4 Indium

The indium radioisotope ^{111}In is currently used clinically for SPECT imaging ($t_{1/2} = 2.8$ days, $\gamma = 245$, 172 keV). ^{111}In based radiopharmaceuticals include ProstaScint and ^{111}In-ibritumomab which are both radiolabeled monoclonal antibodies for cancer imaging [93]. ^{111}In-ibritumomab provides biodistribution data to allow dosimetry estimation for the analogous ^{90}Y radiotherapeutic, Zevalin [94]. ^{111}In also has potential as a novel radiotherapeutic due to the emission of auger electrons, which can effectively kill cells if the radionuclide is localized in the cell [95]. ^{111}In is relatively widely available and is produced by several commercial companies via the cyclotron irradiation of Cd targets. The radionuclide is processed to provide HCl solutions of the trichloride species.

Although the radiochemistry of ^{111}In has many parallels with the Ga radionuclides, it also has important and substantial differences. Like Ga, the low redox potential of In in aqueous solutions means only one oxidation state, indium(III), is relevant to radiopharmaceutical chemistry. As well, indium(III) like gallium(III) is prone to hydrolysis under basic conditions, so coordination chemistry must be done in a slightly acidic environment, typically pH 4–5. Using buffers that contain weakly coordinating ligands, such as citrate and acetate buffers, are also conducive to inhibiting the formation of often insoluble In hydroxide species. But, indium(III) has a larger ionic radius than gallium(III). As a result, it prefers higher coordination numbers, and often accommodates 7–8 donor groups. As well, indium(III) is less analogous to Fe, and so ^{111}In based complexes are less susceptible to transchelation by iron transport proteins, such as transferrin.

Indium(III) is a hard metal ion and prefers hard donor groups, such as oxygen and nitrogen donors. The majority of chelates that have been investigated for ^{111}In complexation are acyclic or cyclic poly-aza carboxylate systems. Acyclic systems such as diethylenetriaminepentaacetic acid (DTPA) have been widely used to coordinate ^{111}In [96–99], and is the chelate used in some clinical ^{111}In based radiopharmaceuticals [9]. Despite high thermodynamic stability of In(DTPA), the *in vivo* stability of these systems leaves room for improvement. Analogs of DTPA that incorporate cyclic groups into the chelate background have provided In complexes with improved stability [100] and more recently an acyclic system with pyridyl groups (Octapa) that forms stable In^{III} complexes has also been introduced [101]. The structures of acyclic systems used for In^{III} are given in Figure 3.6. While Ga^{III} is a fit for small poly-aza macrocycles like NOTA, ^{111}In is more stable

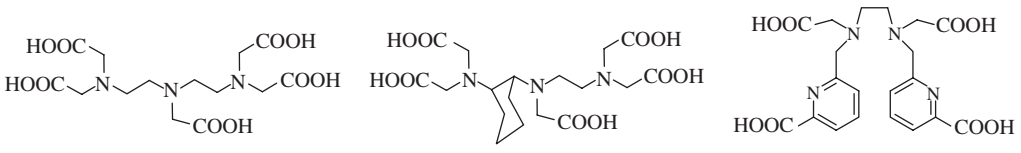

Figure 3.6 *Acyclic chelates commonly used to coordinate In^{III}, Y^{III}, and lanthanides*

with larger poly-aza macrocycles like DOTA [15, 16], which can accommodate both the larger ionic size and demand for higher coordination numbers of In^{III}. Numerous ^{111}In based potential radiopharmaceutical agents have been developed using DOTA or a DOTA derivative [16, 18, 99, 102]. While the macrocyclic systems provide greater thermodynamic and *in vivo* stability for In^{III} complexes, they often require heating to facilitate coordination of ^{111}In. For this reason acyclic systems are still used for ^{111}In radiolabeling of sensitive biomolecules such as monoclonal antibodies. It should be noted that many of the chelates used to coordinate ^{111}In have more donor groups than indium(III) can accommodate. While the excess of donor groups promoted coordination sphere saturation, it also results in numerous coordination isomers [103]. As well, metal complexes of macrocycles like DOTA have been shown to form stereoisomers [104]. The different isomers and the stereoisomers are not equivalent, as they can differ in stability, charge, and other physical properties. Notably the biodistributions of these isomers has been shown to differ [105], which could lead to regulatory difficulties for promising radiopharmaceuticals. An exception is the octapa system; the coordination complex In(octapa) has been fully characterized as single non-fluxional species [101].

^{111}In continues to be an important radiometal for clinical nuclear imaging, applicable to the most widely available imaging method, SPECT. Future radiopharmaceutical development with ^{111}In will be stimulated by the need for a relevant imaging surrogate for trivalent therapeutic radioisotopes such as ^{90}Y, including the related need for robust chelate systems that can be used to form equivalent complexes with both ^{111}In and therapeutic radioisotopes.

3.3.5 Yttrium and lanthanides

^{90}Y and several of the lanthanides (^{153}Sm, ^{166}Ho, and ^{177}Lu) all have emission applicable to radiotherapy. The radionuclides have a range of half-lives and useful therapeutic emissions of various energies, which can be matched to specific radiotherapeutic applications; Table 3.2 lists their emission properties. While most are only therapeutic, ^{177}Lu also has emissions applicable to SPECT imaging. Each of these radioisotopes can be produced by neutron irradiation in a nuclear reactor, except ^{90}Y which is acquired in high specific activity from a $^{90}Sr/^{90}Y$ generator. The radionuclides are available as weak HCl solutions or as the dried trichloride species.

The coordination chemistry of ^{90}Y and the lanthanide radionuclides is similar. Each is in a trivalent oxidation state in aqueous solution, and they all have similar ionic radii. In comparison to the other trivalent radionuclides discussed, gallium(III) and indium(III), Y and the lanthanides prefer even greater coordination numbers [7–9]. Although ^{111}In is used as a imaging surrogate for ^{90}Y based therapeutics, the differences in the coordination chemistry results in complexes with different stability, charge, and polarity, producing different *in vivo* properties [98, 103, 106]. While the $^{111}In/^{90}Y$ imaging/therapy pair is considered adequate [9, 99], the use of a single radionuclide, such as ^{177}Lu would eliminate issues related to coordination differences.

Octadentate and higher denticity chelates are preferred for Y and lanthanide radionuclides. Acyclic systems, such as DTPA [98] and CHX-DTPA have been widely investigated and used for ^{90}Y based radiotherapy [94]. Quadramet, a radiotherapeutic for bone palliation and myeloablation, is a ^{153}Sm complex of the acyclic chelate EDTMP (ethylenediaminetetramethylenephosphonate). Several other

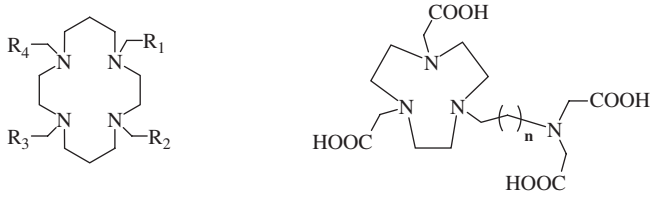

Figure 3.7 *TETA and pendant arm structures*

radiotherapeutic lanthanides and ^{90}Y have also been complexed with EDTMP and investigated [106]. Typically, these metals are more kinetically inert than In^{III} or Ga^{III}, but kinetic stability issues with acyclic systems *in vivo* have been noted [107]. Macrocyclic chelates with eight or more donors offer improved complex stability for Y and lanthanide radionuclides. DOTA and numerous derivatives of DOTA are considered to be more stable chelates *in vivo* for ^{90}Y and ^{177}Lu [12, 103, 105]. Studies with a peptide conjugated DO3A chelate showed better stability for the radionuclides with smaller ionic radii, ^{90}Y and ^{177}Lu, compared to radionuclides with larger ionic radii, ^{153}Sm and ^{166}Ho [108]. Larger macrocyclic chelates, such as derivatives of TETA (1,4,8,11-tetraazacyclotetradecane-N,N′,N″,N‴-tetraacetic acid), have shown promising *in vivo* properties with the larger ionic radii lanthanide radionuclides.(Figure 3.7) [109] One limitation of the macrocyclic systems is the need to heat the coordination reaction, which is not applicable to many biomolecule targeting vectors. Several groups have investigated increasing the length and number of pendant donor groups on the macrocycle, and shown that these chelates have improved coordination kinetics with Y and equivalent stability to the Y(DOTA) complex [110]. These are derivatives of NOTA, [2-(4,7-biscarboxymethyl[1, 4, 7]triazacyclononan-1-yl)ethyl(carboxymethyl)amino] acetic acid tetrahydrochloride (**1**) and [3-(4,7-biscarboxymethyl[1, 4, 7]triazacyclononan-1-yl)propyl-(carboxymethyl)amino]acetic acid tetrahydrochloride (**2**) (Figure 3.7).

As the need for novel treatments for diseases like cancer continues, the potential of radiotherapy will promote innovation in the coordination chemistry of ^{90}Y and lanthanides such as ^{177}Lu. Further modification to macrocyclic chelates for Y and lanthanide radionuclides will seek to balance the need for stability and the need for fast coordination under mild conditions that are appropriate for sensitive biomolecules.

3.3.6 Copper

Copper is a transition metal highly abundant in nature and essential to living organisms, as it is part of the catalytically active center of cytochrome c oxidase [111]. Copper has multiple stable isotopes, ^{63}Cu and ^{65}Cu (69.1 and 30.9% natural abundance respectively), which serve as a convenient tool for the investigation and characterization of the coordination complexes formed, both micro- and macroscopically. Multiple non-stable isotopes of Cu are of interest for PET. Besides the high energy β^+ emitting nuclides ^{60}Cu and ^{61}Cu, two other nuclides have received considerably more attention: ^{62}Cu ($t_{1/2} = 9.8$ minutes, β^+ 98% and $E_{max} = 2.910$ MeV), especially due to the availability of a generator with the mother nuclide ^{62}Zn ($t_{1/2} = 9.1$ hours), and ^{64}Cu ($t_{1/2} = 12.7$ hours, β^+ 17.4%, $E_{max} = 0.656$ MeV, β^- 39%, and $E_{max} = 0.573$ MeV). Great improvements were made to the $^{62}Zn/^{62}Cu$ generator around the time of first clinical studies with Cu(PTSM), PTSM = pyruvaldehyde bis(N4-methylthiosemicarbazone), for hypoxic tissue imaging [112], however in recent years the more long lived isotope ^{64}Cu has received much greater attention.

Several Cu radionuclides are produced by accelerator-based methods. Currently, the most common production method utilizes a medical cyclotron, where the radionuclide is made via the (p,n) reaction from highly enriched ^{64}Ni (or ^{61}Ni to produce ^{61}Cu) [113–115]. This method has the advantage of being economical and allows for production of ^{64}Cu at high purity, high yield (up to 185 GBq (5 Ci)) and high specific activity. After processing the radionuclides are in the +2 oxidation state in an HCl solution, thus the chemistry typically begins with a buffering step and $CuCl_2$ starting material.

^{67}Cu typically requires a higher energy accelerator and has been produced via proton irradiation of ^{68}Zn [116]. Various separation methods have been reported including solvent extraction and ion exchange [117].

The longer half-life is more applicable to developing PET agents with larger biomolecules, such as monoclonal antibodies that may require longer circulation times before imaging to achieve optimal target uptake. While not available as a generator produced isotope, the longer half-life allows for shipment of the isotope to remote areas where no cyclotron is available. Additionally, the emitted β^+ is low energy and hence will produce higher resolution images [71]. ^{64}Cu also decays through β^- decay and internal conversion, which provides potential for use in therapy; however it is the longer-lived, exclusively β^- emitting ^{67}Cu ($t_{1/2} = 61$ hours and β^- 100%, with energies of 0.577, 0.484, and 0.395 MeV), which is considered the more suitable Cu radioisotope relevant for therapeutic applications [71].

Three oxidation states (+1, +2, and +3) are accessible for copper in aqueous solution. As Cu^I, the metal ion has a d^{10} configuration with a preference for rather soft ligands, forming a variety of fairly labile complexes. Under normal, oxidative conditions the predominant oxidation state is Cu^{II}, with the metal ion in d^9 configuration [118].

If dissociated from the coordinating ligand *in vivo*, ^{64}Cu rapidly associates with Cu-transport proteins in the serum and is subsequently taken up in the liver, giving rise to a characteristic biodistributional pattern and pharmacokinetics, which allow the study of diseases related to impaired Cu-metabolism, such as Wilson's disease [119]. Opposed to the great variety in Tc-based small molecule agents, only few Cu-based agents have been explored for this purpose. One of the only agents of this type is the thiosemicarbazone "pair" Cu(ATSM) and Cu(PTSM) (Figure 3.8). $^{62/64}$Cu(ATSM), ATSM = diacetyl-bis(N4-methylthiosemicarbazone), has been shown to be selective for hypoxic cancers and ischemic myocardial tissue, while Cu(PTSM) lacks this ability and serves as a perfusion-only analog. Mechanistic studies examining the hypoxia-selectivity of Cu(ATSM) have presented a number of mechanisms that explain the activity of this agent. Copper(ATSM) readily diffuses into cells, where it is selectively bioreduced and trapped within viable cells under hypoxic conditions.

While Cu(PTSM), like Cu(ATSM), freely diffuses into cells, it does not provide the selectivity for hypoxic cells; therefore, Cu(PTSM) is a surrogate marker of perfusion. Currently, Cu(ATSM) is undergoing phase II clinical trials. Another thiosemicarbazone derivative, Cu(ETS), ETS = ethylglyoxal bisthiosemicarbazone, has also generated considerable interest due to great potential as a perfusion agent with similar, but somewhat improved, biodistribution compared to Cu(PTSM) [120].

In recent years, ^{64}Cu has generated great interest as one of the radiometals of choice for peptide and antibody labeling. A variety of complex geometries with tetra- to hexadentate environments have been reported

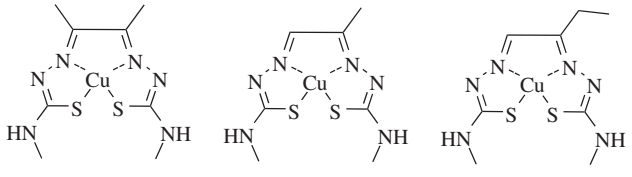

Figure 3.8 *Structures of semicarbazone copper complexes of interest for hypoxia and perfusion imaging*

and include square planar, trigonal bipyramidal, square pyramidal, and distorted octahedral [71]. The ligand exchange kinetics of Cu^{II} are very rapid, therefore only ligands which can provide kinetically inert coordination with strong crystal field stabilization for complexation are suitable for incorporation into radiopharmaceuticals.

Macrocyclic and cage-like hexadentate ligand systems are among the current front runners for stable coordination with minimal metal ion loss even after multiple days of incubation under physiologically relevant conditions. Acyclic chelates often fall victim to rapid decomplexation kinetics, resulting in the loss of the radiometal. It was found that Cu^{II} complexes formed with cyclam-derivatives (1,4,8,11-tetraazacyclotetradecane) are generally more kinetically inert than the ones formed with cyclen (1,4,7,10-tetraazacyclododecane) due to the preference of Cu^{II} to form coordination complexes containing a mixture of five- and six-membered metallacycles [121]. DOTA, often considered the workhorse ligand for radiometal based nuclear medicine, has been well documented to lack kinetic inertness for use as a ligand for copper(II) [122]. A number of research groups have invested considerable time and effort to evaluate alternative, highly kinetically inert ligand systems. The most successful concepts include the poly-aza cage SarAr, developed by Sargeson and coworkers [123] and its corresponding bifunctional derivatives and bioconjugates developed by Smith [124], Conti [125] and Donnelly [126]. While representing a challenge in orthogonal protection group chemistry, this scaffold has the advantage of chelating ^{64}Cu at room temperature and physiological conditions – a key feature for the labeling of antibodies and other, more sensitive biomolecules. Cross-bridged derivatives of cyclam have also provided ligands for the kinetically inert complexation of Cu, investigated by Weisman, Anderson and coworkers [127, 128]. While the initially developed di-carboxylate ligand CB-TE2A only achieved high radiochemical yields at pH 8 and 95 °C, the more recently reported CB-TE1A1P is capable of chelating ^{64}Cu at room temperature and has been successfully used for the labeling of Somatostatin. Another, recently evaluated ligand with labeling characteristics comparable to SarAr is PCTA [129]. The bifunctional version of this chelate has successfully been used for labeling of gastrin-releasing peptide receptor specific peptide sequence bombesin [130].

Besides these bifunctional chelates exclusively used for ^{64}Cu, NOTA has been also evaluated for this purpose, and was found to be yet another viable alternative bifunctional chelator. Maecke and coworkers found that the ^{64}Cu-complexes of NOTA and CB-TE2A RGD conjugates showed very similar in vivo behavior [131].

In Figure 3.9 and Table 3.5, a selection of important chelate structures and some of their relevant characteristics such as labeling conditions and thermodynamic stability constant of the corresponding Cu complex are given. It is important to note that thermodynamic stability is virtually irrelevant for the application of radiometals. Instead, the evaluation of kinetic inertness in vitro is crucial for the validation of bifunctional chelate systems. As loss of Cu in vivo can be facilitated through a variety of processes, a number of corresponding experiments approximating this decomplexation process have been designed. This includes indirect measurements such as serum stability, liver uptake, or physiologically irrelevant experimental conditions such as heating the complex in 5N HCl [132]. More recently, Packard and coworkers have developed and successfully employed competition with excess cold Cu at a variety of concentrations and pH values for this purpose [133, 134].

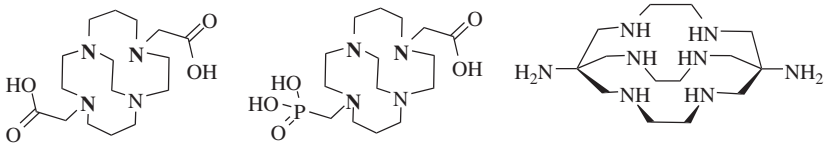

Figure 3.9 *Structures of the most relevant bifunctional chelates for labeling of ^{64}Cu*

Table 3.5 *Summary of key properties of the most relevant chelates for labeling of ^{64}Cu*

Ligand system	Labeling conditions	log K_{ML}
NOTA	30 min, room temperature	19.8, 21.6
DOTA	5 min, room temperature	22.7
DiSarAr	5 min to 1 h, room temperature	n.d.
CB-TE2A	1 h, 95 °C	n.d.
CB-TE1A1P	30 min, room temperature	n.d.
PCTA	10 min, room temperature	18.8

n.d. = not determined

In conclusion, there is no universal chelate solution which can be applied to the ^{64}Cu radiolabeling of every biomolecule. The suitable choice depends on labeling properties, polarity and charge in combination of the target tissue and the intrinsic properties of the biomolecule used.

3.3.7 Zirconium

Zirconium-89 (^{89}Zr) is a PET radionuclide that has emerged in the last 10 years as the preferred isotope for antibody-based imaging or immunoPET [135]. The rise of ^{89}Zr has been spurred in part by the relative ease of production and its favorable physical characteristics [136, 137]. ^{89}Zr has a half-life of 78.4 hours, which is compatible with the pharmacokinetic half-life of antibodies ($t_{1/2} = 2-7$ days), and a relatively low average positron energy of 395.5 keV resulting in high image resolution. The positron decay of ^{89}Zr is accompanied by a high energy 909 keV gamma ray; however, the energy disparity with the PET detected 511 keV photons prevents interference with detected coincident photons [137]. The cornerstone of radiometal utility for *in vivo* applications lies in the formation of stable chelate complexes; thus, various chelates have been explored for ^{89}Zr complexation [135, 137]. As a +4 metal ion, in aqueous solutions zirconium typically forms complexes with 6–8 coordination numbers, with 8-coordination modes resulting in optimal stabilization of the metal center [138].

^{89}Zr is made via the (p,n) reaction on naturally abundant ^{89}Y using a biomedical cyclotron [139, 140]. Several separation methods have been investigated, particularly by researchers at VU Amsterdam [141], including solvent extraction [142, 143], cation and anion chromatography [142–144], and solid-phase hydroxamate resins to achieve high radionuclide purity [141, 145]. Currently, ^{89}Zr production is relatively standardized and can be isolated at high purity (radiochemical purity of 99.9%) and at high specific activity (5.28–13.43 mCi/μg) [139]. Zirconium is typically provided as zirconium oxalate; however straightforward methods exist to convert this to zirconium chloride which is more applicable to coordination chemistry.

Zirconium is a hard Lewis acid and thus prefers hard Lewis bases as donor groups, thus it is not surprising that the hydroxamate rich desferrioxamine B (DFO) is the most successful and most utilized ligand for ^{89}Zr chelation [135–137]. The DFO ligand appeal is further fueled by the fact that it is a FDA approved drug, Desferal, and is considered safe in its bare and metal-complexed form [136]. Currently, there are no crystal structures of the Zr-DFO complex; however, Holland and coworkers utilized density functional theory (DFT) to characterize the coordination environment of zirconium [2]. This work revealed DFO complexes zirconium in a hexadentate manner with the metal coordination sphere occupied by oxygen atoms of DFO, with the seventh and eighth coordination sites of zirconium occupied by water molecules [2]. To date, physical structure studies and thermodynamic stability constants for Zr-DFO have yet to be reported. However, the work of Baroncelli and others determined the stability of Zr^{IV} complexation to a hydroxamate group as

10^{12}, increasing to 10^{24} when bound to two hydroxamate group [136, 146]. It can thus be postulated that the binding of Zr^{IV} by three hydroxamate groups as observed in DFO would result in stability of $\sim 10^{36}$; a value comparable to $>10^{31}$ reported for iron(III)-DFO [136, 147].

Radiolabeling of DFO with ^{89}Zr occurs rapidly and efficiently at a 1 : 1 metal to ligand ratio under ambient conditions. Works by Meijs *et al*. and others have shown the high stability of ^{89}Zr-DFO complexes, experiments conducted in serum show minimal demetallation of ^{89}Zr. In serum metal loss of 0.2 and 2% was reported for 24 hours and 7 day incubation [2, 148]. While *ex vivo* studies have indicated the high stability of ^{89}Zr-DFO complex, *in vivo* studies using ^{89}Zr-DFO-antibodies however indicate ^{89}Zr is released from the DFO chelate characterized by non-specific and persistent accumulation to the bone matrix of ∼6–10% ID/g in animal models [149, 150]. Abou *et al*. hypothesized that the observed bone accumulation may either be a result of detachment of ^{89}Zr-DFO from the antibody carrier or the transmetallation of ^{89}Zr from the DFO chelate [151]. The authors demonstrated the rapid biological clearance of ^{89}Zr-DFO complex with no sign of bone uptake, essentially negating the hypothesis of ^{89}Zr-DFO dissociation [151]. The authors also administered ^{89}Zr salts like ^{89}Zrchloride and ^{89}Zroxalate, which resulted in bone matrix associated activity of ∼16% ID/g, supporting the latter hypothesis where ^{89}Zr is transmetallated from the chelate. This work further supports the early findings of Sastry *et al*. and Backstrom *et al*. who determined zirconium has a high affinity for the bone matrix [2, 151–153]. The preferential localization of decomplexed ^{89}Zr to the bone is a profile of particular concern in nuclear medicine as bone accumulation limits the clinically administered dose of ^{89}Zr-PET tracers. This phenomenon has been restricted to preclinical rodent models; in clinical investigations bone localization of ^{89}Zr has been negligible [6]. However, as clinical dosimetry is determined from preclinical biodistribution studies, thus it is important to address this physiological profile.

Presently, DFO remains the only available chelator for stable complexation of ^{89}Zr. However, acyclic ligands including ethylenediaminetetraacetic acid (EDTA) and DTPA have been investigated to understand the coordination of chemistry of non-radioactive zirconium [154]. EDTA complexes with zirconium in a similar manner as DFO, where the ligand acts as a hexadentate ligand bound to zirconium via two nitrogen atoms of ethylenediamine and four oxygen atoms of the carboxyl groups. To complete the eight coordination modes of zirconium two water molecules are bound [154]. DTPA however, complexes zirconium in an octadentate manner and the ligand solely satisfies the metal's coordination number binding via three nitrogen and five oxygen atoms [155]. Attempts to radiolabel DTPA functionalized antibody constructs, however, have been unsuccessful with labeling success of less than 0.1% reported, suggesting nitrogen rich donor chelates may not be ideal for ^{89}Zr complexation [156]. With DFO as the only available ligand for ^{89}Zr, further research is necessary to identify novel zirconium specific ligands with high *in vivo* stability (Figure 3.10).

3.3.8 Scandium

Scandium radioisotopes ^{44}Sc (β^+-emitter, $t_{1/2} = 3.92$ hours) and ^{47}Sc (β^--emitter, $t_{1/2} = 3.35$ days) have applications in PET imaging and radiotherapy, respectively. Due to the relatively short half-life of ^{44}Sc and the limited availability of ^{47}Sc in the past, ^{46}Sc (γ-emitter, $t_{1/2} = 83.79$ days) has been used as a substitute to evaluate the stability of various ligands complexed with scandium *in vitro* [157, 158] and *in vivo* [159, 160]. ^{44}Sc has been produced via irradiation of natural calcium targets followed by dissolution in water and filtration of the desired product [161]. ^{44}Sc is recovered in the chloride form. This isotope has also been produced via a long lived generator parent ^{44}Ti, yielding ^{44}Sc in weak HCl solution.

Examples of macrocyclic ligands that chelate the trivalent scandium in a 1 : 1 metal:ligand stoichiometric ratio include TETA, DOTA, 1,4,7-Triazacyclodecane-N,N′,N″-triacetic acid (10-ane), and NOTA, while acyclic ligands include DTPA and EDTA (Figures 3.5, 3.6, and 3.10). Note that these ligands are not specific for scandium complexation, but are also used to chelate other metals (e.g., Rare earths and transition metals). For molecular targeting applications, these ligands are available as bifunctional chelates; they serve as both

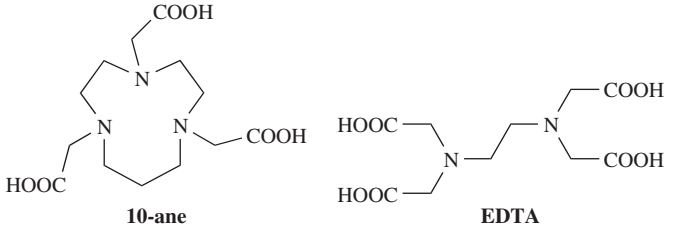

Figure 3.10 *Structures of 10-ane and EDTA*

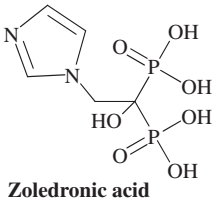

Figure 3.11 *Structure of zoledronic acid for ^{47}Sc bone radiotherapy*

a metal chelate and contain reactive groups for conjugation to various probes such as peptides, antibodies, and nanoparticles. Other molecules including zoledronic acid and indazolebisphosphonates have been used to chelate ^{47}Sc for bone radiotherapy because of their high affinity for the bone matrix (Figure 3.11) [159, 162].

Radiolabeling ligands with scandium and the stability of the scandium-ligand complex are important to reduce the retention of free Sc radioisotope in non-target organs such as liver, muscle, and intestine over 24 hours, whereas DTPA-chelated ^{46}Sc rapidly clears from these organs within 1 hour post-injection into normal mice [160]. Thus, it is important to select ligands which form stable complexes with scandium. Thermodynamic equilibrium (stability) constants (log K) measure the strength of interaction between the metal and its ligand in equilibrium and may be used as a criterion for ligand selection using the same metal. Huclier-Markai *et al*. have determined stability constants of ^{46}Sc complexes with DOTA, NOTA, TETA, DTPA, and EDTA using a free ion selective radiotracer extraction method [157]. They have found that DOTA exhibited the highest stability with log K of 22.5, followed by DTPA (log K 22.0) > EDTA (log K 21.0) > NOTA (log K 18.5) > TETA (log K 18.0) [157]. Majkowska-Pilip and Bilewicz also measured stability constants of ^{46}Sc complexes with DOTA, NOTA, and other macrocyclic ligands using radio-HPLC and concur that DOTA was thermodynamically most stable with log K of 27, followed by NOTA (log K 16.5) and 10-ane (log K 10.3) [158].

Mouse serum stability studies have shown that decomplexation of ^{46}Sc from DTPA-antibody conjugate results in 25% transchelation to transferrin, a metal-binding protein present in serum, while 75% remained with the DTPA-antibody conjugate after 24 hours [160]. Despite decomplexation of ^{46}Sc, the radiolabeled antibody conjugate yielded significant uptake in the target organ of interest. Transchelation of ^{46}Sc is in agreement with [157], which compares the stability of ^{46}Sc-labeled DTPA and DOTA in the presence of rat serum and shows that ^{46}Sc decomplexes from DTPA after two days. Here, $^{46}Sc(DOTA)^{-}$ proved superior to $^{46}Sc(DTPA)^{2-}$ with practically no decomplexation in the presence of serum over seven days [157]. A DOTA-containing radiopharmaceutical peptide probe, DOTA-TOC, has been investigated to optimize radiolabeling conditions of ^{44}Sc and to determine its stability [163]. This molecule has been challenged with a gross excess of other DOTA-binding metals including Fe^{3+} and Cu^{2+}, which resulted in greater than 98%

intact ^{44}Sc-DOTA-TOC. Additionally, challenging with a 100-fold stoichiometric excess of other ligands, EDTA and DTPA, yields greater than 97% intact ^{44}Sc-DOTA-TOC and shows that ^{44}Sc cannot be displaced from DOTA once the complex is formed.

While DOTA has proven to be the most thermodynamically stable ligand over other macrocyclic and acyclic ligands mentioned above, radiolabeling conditions require ambient temperature for 24 hours or high temperatures (70–95 °C) for several minutes in acetate buffer (pH 4–6) [157, 158, 164]. Peptide probes as exemplified by DOTA-TOC do not present challenges with radiolabeling with $^{44/46}$Sc at high temperatures because peptides in general do not have defined tertiary (three-dimensional) structures like proteins. Additionally, improvements with radiolabeling DOTA-TOC using ^{44}Sc have been achieved using microwave-assisted heating as fast as 3 minutes to maximize the use of this relatively short-lived isotope [163]. In contrast, protein probes denature at high temperatures because their tertiary and quaternary structures are disrupted, presenting a challenge with radiolabeling DOTA-protein conjugates. Milder methods have yet to be optimized.

Historically, DTPA has been the ligand of choice for conjugation to antibodies and subsequent radiolabeling with scandium radioisotopes [160, 164]. DTPA-antibody conjugates can be radiolabeled with ^{46}Sc under mild and relatively fast conditions of 37 °C for 15 minutes in citrate buffer, pH 6 [160]. ^{47}Sc-labeled DTPA-antibody conjugate has also been compared to other radiometals ^{111}In and ^{90}Y [165]. Vaughan *et al*. have shown that ^{47}Sc-DTPA-antibody has the highest accumulation in the liver compared to ^{111}In and ^{90}Y-labeled DTPA-antibody conjugates [165]. Here, kinetic stability may dominate over thermodynamic stability *in vivo* due to transmetallation reactions with metal-binding proteins like transferrin.

Recently, more acyclic ligands have been investigated for radiolabeling with ^{47}Sc, including DFO and ethylene glycol-bis(2-aminoethylether)-N,N,N′,N′-tetraacetic acid (EGTA) [164]. Phosphate buffered-saline stability studies have found that EGTA is comparable to DTPA. Interestingly, the amount of EGTA needed to achieve >97% radiolabeling yield is about seven times less than that required for DTPA with reaction times of about 10 minutes at 37 °C. In this study, DFO achieved 96% radiolabeling yield using 1 : 1 Sc:DFO molar ratio. These ligands have yet to be investigated for their stability *in vitro* in the presence of serum as well as *in vivo*.

In conclusion, properties of scandium radioisotopes may advance imaging and therapy but finding the best ligands and optimizing radiolabeling conditions for each type of probe conjugated to that ligand are still in progress. To date, DOTA is the ligand of choice for small molecule and peptide probes. The DTPA ligand for antibody probes has its challenges with *in vivo* stability, but the selectivity of antibodies for their antigens allow for the delivery of scandium radioisotopes to their target. More investigations are needed to improve radiolabeling with the more stable DOTA ligand.

3.3.9 Cobalt

Cobalt-55 (^{55}Co), a positron-emitting isotope, has been investigated as a free metal tracer for brain imaging *in vivo* using PET. Cobalt has the ability to mimic calcium influx, making it an excellent tracer to localize brain injury [166]. ^{55}Co has a relatively long half-life of 17.53 hours compared to the standard PET isotope, fluorine-18 ($t_{1/2} = 1.83$ hours), making ^{55}Co useful for radiolabeling of protein and peptide probes for molecular imaging of various disease processes. For this purpose, metal chelates conjugated to such probes are necessary to bind ^{55}Co stably and reduce transmetallation reactions with serum proteins *in vivo*. ^{57}Co ($t_{1/2} = 270.9$ days), a gamma-emitting isotope, has commonly been used as a surrogate to investigate new probes, and has been applied toward SPECT imaging or gamma camera imaging, rather than PET [167, 168].

Serum stability studies by Meares *et al*. using human serum have determined that a DOTA analog, *p*-nitrobenzyl-DOTA, formed a more stable complex with ^{57}Co than an EDTA analog, *p*-nitrobenzyl-EDTA [169] (Figure 3.12). After several days, ^{57}Co remained chelated to the DOTA molecule, whereas ^{57}Co

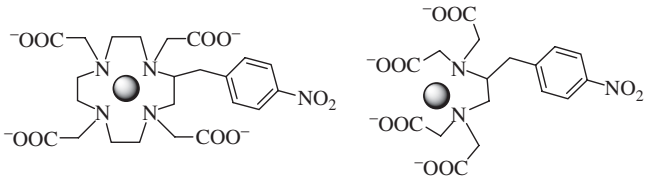

***p*-nitrobenzyl-DOTA** ***p*-nitrobenzyl-EDTA**

Figure 3.12 *Structures of* p*-nitrobenzyl-DOTA and* p*-nitrobenzyl-EDTA in complex with a metal (sphere). The nitrobenzyl side chain from these chelates serves as a site for modification to electrophilic groups for conjugation to proteins or other biomolecules [169, 170]*

decomplexed from EDTA and bound to several serum proteins. The p-nitrobenzyl moiety in these metal chelates is designed for modification to electrophilic groups for conjugation to antibody probes [170].

A method of producing ^{55}Co has been reported via deuteron bombardment of iron using a cyclotron [171]. During purification of cobalt radioisotopes, as with many other radiometals, iron contaminants have been removed so that it does not interfere with cobalt radiolabeling of a DOTA-containing peptide, for example, DOTA-TOC. ^{55}Co-DOTA-TOC has applications in PET imaging of somatostatin receptor subtype 2 (SSTR2). Radiolabeling the peptide with ^{58m}Co ($t_{1/2} = 9.04$ hours), an Auger-emitting isotope, has applications in therapy of tumors that overexpress this receptor. Optimal radiolabeling has been achieved using acetate buffer pH ~ 5 at 80 °C for 30 minutes, with radiochemical yield and purity greater than 99%. Specific activity of this reaction has been determined as 4 MBq/nmol ^{58m}Co-DOTA-TOC and 0.21 MBq/nmol ^{55}Co-DOTA-TOC with maximum theoretical yields of 12.8 and 6.6 GBq/nmol, respectively. The authors have noted that specific activity may be improved by improving the isotope yield during production with longer irradiation time, higher beam current or more simply, avoiding long delays between cyclotron bombardment and the radiolabeling reaction.

Another study by Heppeler *et al*. compared the binding affinities and biological properties of $^{57}Co^{2+}$- and $^{68}Ga^{3+}$-labeled DOTA-TOC [167]. Higher tumor uptake and faster normal organ clearance have been observed with ^{57}Co-DOTA-TOC than ^{68}Ga-analog. *In vitro* cell studies have also determined that ^{57}Co-DOTA-TOC has higher affinity and higher rate of internalization. These findings suggest that the overall charge of the radiotracer may affect the pharmacokinetic properties and receptor binding affinity.

A DOTA-containing affibody has been radiolabeled with ^{57}Co [168]. DOTA-Z_{2395}-C affibody (referred to as DOTA-affibody hereafter) is a 7 kDa protein with picomolar affinity for human epidermal receptor 2 (HER2), an overexpressed receptor in some cancers, notably breast cancer. For this small protein, radiolabeling has been achieved at 60 °C in acetate buffer (pH 5.5) for 10 minutes with 99.5% yield and a specific activity of about 0.17 MBq/nmol, which is comparable to the yield and specific activity of the peptide probe, ^{55}Co-DOTA-TOC, as discussed above. ^{57}Co-DOTA-affibody is stable to challenging with 100-fold excess EDTA with 98% of ^{57}Co associated with the DOTA-affibody molecule. Incubation in phosphate buffered saline (PBS) has resulted in minimal decomplexation of ^{57}Co with 97 and 94% still associated with DOTA-affibody after 4 and 24 hours, respectively. Furthermore, the ^{57}Co-DOTA-affibody has been shown to retain antigen-binding capability, despite the 60 °C radiolabeling temperature. Interestingly, Wållberg *et al*. have compared ^{57}Co- and ^{111}In-labeled affibody using gamma camera imaging and SPECT imaging, respectively [174]. The co-injection of the two probes has determined that ^{57}Co-labeled affibody achieved better tumor-to-normal organ ratios than its ^{111}In counterpart. Significant kidney uptake was also observed but is attributed to the clearance of the affibody rather than decomplexation of the radioisotopes.

Other ligands for cobalt radioisotopes have been developed. Carbohydrate-modified 3-hydroxy-4-pyridinone ligands have been synthesized and radiolabeled with ^{55}Co as 2 : 1 ligand:metal ratio (Figure 3.13) [172]. Ferreira *et al*. have designed these bifunctional ligands serving as a metabolic tracer using the carbohydrate moiety, similar to the standard ^{18}F-fluorodeoxyglucose (FDG) radiotracer, and also as a chelating agent using the pyridinone moiety. High radiolabeling yield of 95% has been achieved in as little as 5 minutes at ambient temperature under neutral pH conditions. More investigations are necessary to evaluate the *in vivo* properties of these radiotracers.

Cyclen analogs, Cpy2 and CRpy2, are ligands that have only been explored with non-radioactive Co^{2+} [173]. Bernier *et al*. have also compared chelation with Cu^{2+} and Zn^{2+}. Based on stability constants, Cu^{2+} forms the most stable complex, while Co^{2+} and Zn^{2+} complexes are equivalent. The stability of cobalt-complexes has been determined in order of decreasing stability with stability constants in parentheses: CRpy2 (18.18) > Cpy2 (17.57) > DO2A (16.9) > and cyclen (13.79). Structures of these macrocycles are depicted in Figure 3.14. In these cyclen analogs, the nitrogen atoms from the pyridine moiety are involved in the cobalt complex. Radiolabeling conditions for these new chelates and their *in vivo* stability remain to be investigated.

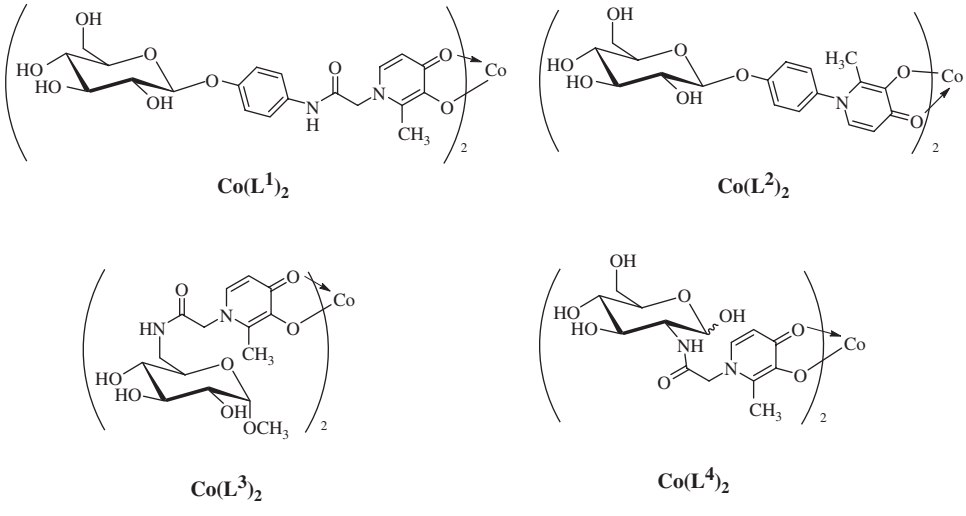

Figure 3.13 *Cobalt complexes of 3-hydroxy-4-pyridinone ligands modified with carbohydrates [168]*

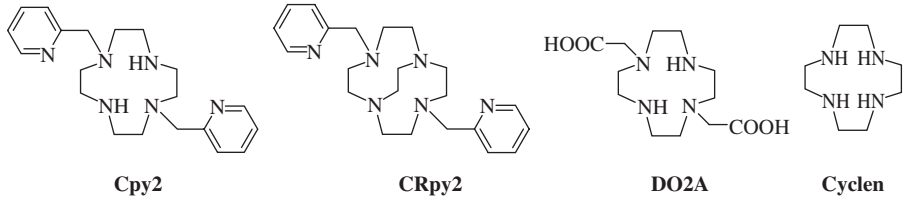

Figure 3.14 *Structures of cyclen analogs*

3.4 Conclusions

Radiometals are at the core of nuclear medicine. They provide countless options for radiochemists developing new diagnostic and therapeutic agents to customize the agents for their intended application. The flexibility of radiometals will be beneficial considering the increasing focus on personalized medicine with highly specific disease targets and the advent of theranostics.

Coordination chemistry will continue to play a central role in the development of metal based radiopharmaceuticals. For radionuclides that are just beginning to be brought into the clinic, such as ^{68}Ga, ^{44}Sc, and ^{89}Zr, basic coordination chemistry and the design of new optimal chelate systems will be beneficial. Chelates will need to be designed that meet the requirements of low toxicity and physiological stability, but will also need to be designed for the unique requirements of radiochemistry; for example, fast, quantitative coordination reactions, and the formation of kinetically inert complexes. Even for radiometals conventionally used in nuclear medicine, such as ^{111}In and ^{90}Y, new chelates that can balance the need for stability and fast reactions under mild conditions applicable to sensitive targeting vectors, such as antibodies, will be advantageous. There is also great opportunity to utilize chelate design to add further value to potential radiopharmaceuticals.

References

1. Nayak, T.K. and Brechbiel, M.W. (2011) 86Y based PET radiopharmaceuticals: radiochemistry and biological applications. *Med. Chem.*, **7** (5), 380–388.
2. Holland, J.P., Divilov, V., Bander, N.H. *et al*. (2010) ^{89}Zr-DFO-J591 for immunoPET of prostate-specific membrane antigen expression in vivo. *J. Nucl. Med.*, **51** (8), 1293–1300.
3. ClinicalTrials.gov A Phase I/II Study of Clinical and Molecular Correlates of Positron Emission Tomography (PET) With 89Zr-DFO-huJ591 in Metastatic Prostate Cancer. ClinicalTrials.org2013 [updated July 5, 2013, July 8, 2013], http://clinicaltrials.gov/ct2/show/record/NCT01543659 (accessed 25 October 2013).
4. Gaykema, S.B., Brouwers, A.H., Lub-de Hooge, M.N. *et al*. (2013) ^{89}Zr-Bevacizumab PET imaging in primary breast cancer. *J. Nucl. Med.*, **54** (7), 1014–1018.
5. Heuveling, D.A., van Schie, A., Vugts, D.J. *et al*. (2013) Pilot study on the feasibility of PET/CT lymphoscintigraphy with ^{89}Zr-nanocolloidal albumin for sentinel node identification in oral cancer patients. *J. Nucl. Med.*, **54** (4), 585–589.
6. Dijkers, E.C., Oude Munnink, T.H., Kosterink, J.G. *et al*. (2010) Biodistribution of ^{89}Zr-trastuzumab and PET imaging of HER2-positive lesions in patients with metastatic breast cancer. *Clin. Pharmacol. Ther.*, **87** (5), 586–592.
7. Tomblyn, M. (2012) Radioimmunotherapy for B-cell non-hodgkin lymphomas. *Cancer Control*, **19** (3), 196–203.
8. Cutler, C.S., Hennkens, H.M., Sisay, N. *et al*. (2013) Radiometals for combined imaging and therapy. *Chem. Rev.*, **113** (2), 858–883.
9. de Jong, M., Breeman, W.A., Kwekkeboom, D.J. *et al*. (2009) Tumor imaging and therapy using radiolabeled somatostatin analogues. *Acc. Chem. Res.*, **42** (7), 873–880.
10. Lubberink, M. and Herzog, H. (2011) Quantitative imaging of 124I and 86Y with PET. *Eur. J. Nucl. Med. Mol. Imaging*, **38** (Suppl. 1), S10–S18.
11. Lee, E.J. and Weinhous, M.S. (1997) Physics and basic parameters of brachytherapy. *J. Surg. Oncol.*, **65** (2), 143–150.
12. Kwekkeboom, D.J., Bakker, W.H., Kooji, P.P. *et al*. (2001) [177Lu-DOTAOTyr3)octreotate: comparison with [111In-DTPAo]octreotide in patients. *Eur. J. Nucl. Med.*, **28** (9), 1319–1325.
13. Olafsen, T., Betting, D., Kenanova, V.E. *et al*. (2009) Recombinant Anti-CD20 antibody fragments for small-animal PET imaging of B-cell lymphomas. *J. Nucl. Med.*, **50** (9), 1500–1508.
14. Giblin, M.F., Jurisson, S. and Quinn, T.P. (1997) Synthesis and characterization of rhenium-complexed α-melanotropin analogs. *Bioconjugate Chem*, **8** (3), 347–353.

15. Ferreira, C.L., Holley, I., Bensimon, C. *et al*. (2012) Pharmacokinetic modulation of radiolabeled chelates facilitated by phosphonate ester coordinating groups. *Mol. Pharmaceutics*, **9** (8), 2180–2196.
16. Giblin, M.F., Gali, H., Sieckman, G.L. *et al*. (2004) In Vitro and in Vivo comparison of human escherichia coli heat-stable peptide analogues incorporating the 111In-DOTA group and distinct linker moieties. *Bioconjugate Chem.*, **15** (4), 872–880.
17. Rajagopalan, R., Grummon, G.D., Bugaj, J. *et al*. (1997) Preparation, characterization, and biological evaluation of technetium(V) and rhenium(V) complexes of novel heterocyclic tetradentate N_3S ligands. *Bioconjugate Chem.*, **8** (3), 407–415.
18. Garrison J.C., Rold T.L., Sieckman G.L. *et al*. Evaluation of the pharmacokinetic effects of various linking groups using the 111In-DOTA-X-BBN(7-14)NH2 structural paradigm in a prostate cancer model. *Bioconjugate Chem.* 2008; **19**(9): 1803-1812.
19. Borbas, K.E., Ferreira, C.S.M., Perkins, A. *et al*. (2007) Design and synthesis of mono- and multimeric targeted radiopharmaceuticals based on novel cyclen ligands coupled to anti-MUC1 aptamers for the diagnostic imaging and targeted radiotherapy of cancer. *Bioconjugate Chem.*, **18** (4), 1205–1212.
20. Akizawa, H., Imajima, M., Hanaoka, H. *et al*. (2013) Renal brush border enzyme-cleavable linkages for low renal radioactivity levels of radiolabeled antibody fragments. *Bioconjugate Chem.*, **24** (2), 291–299.
21. Bartholomä, M.D., Louie, A.S., Valliant, J.F. and Zubieta, J. (2010) Technetium and gallium derived radiopharmaceuticals: comparing and contrasting the chemistry of two important radiometals for the molecular imaging era. *Chem. Rev.*, **110**, 2903–2920.
22. Dilworth, J.R. and Parrott, S.J. (1998) The biomedical chemistry of technetium and rhenium. *Chem. Soc. Rev.*, **27**, 43–55.
23. Pillai, M.R.A., Dash, A. and Knapp, F.F.R. (2013) Sustained availability of 99mTc: possible paths forward. *J. Nucl. Med.*, **54** (2), 313–323.
24. Abram, U. and Alberto, R. (2006) Technetium and rhenium: coordination chemistry and nuclear medical applications. *J. Braz. Chem. Soc.*, **17** (8), 1486–1500.
25. Abdel Razzak, M., Naguib, M. and el-Garhy, M. (1967) Fate of sodium pertechnetate-technetium-99m. *J. Nucl. Med.*, **8** (1), 50–59.
26. Jones, A.G., Abrams, M.J., Davison, A. *et al*. (1984) Biological studies of a new class of technetium complexes - the Hexakis(Alkylisonitrile)Technetium(I) Cations. *Int. J. Nucl. Med. Biol.*, **11** (3-4), 225–234.
27. Davison, A., Depamphilis, B.V., Faggiani, R. *et al*. (1985) The preparation, characterization, and crystal and molecular-structure of oxobis(Ethan-1,2-Dithiolato-S, Mu-S′)technetium(V)Oxo(Ethan-1,2-Dithiolato-S,S′)-technetium(V) $[(TcO)_2(SCH_2CH_2S)_3]$ – a Tc(V) compound containing metal sulfur metal bridges. *Can. J. Chem.*, **63** (2), 319–323.
28. Nosco, D.L. and Beaty-Nosco, J.A. (1999) Chemistry of technetium radiopharmaceuticals 1: chemistry behind the development of technetium-99m compounds to determine kidney function. *Coord. Chem. Rev.*, **184**, 91–123.
29. Schwochau, K. (1994) Technetium radiopharmaceuticals – fundamentals, synthesis, structure, and development. *Angew. Chem., Int. Ed. Engl.*, **33** (22), 2258–2267.
30. Hom, R.K., Chi, D.Y. and Katzenellenbogen, J.A. (1996) Heterodimeric bis(amino thiol) complexes of oxorhenium(V) that mimic the structure of steroid hormones. Synthesis and stereochemical issues. *J. Org. Chem.*, **61** (8), 2624–2631.
31. Hom, R.K. and Katzenellenbogen, J.A. (1997) Technetium-99m-labeled receptor-specific small-molecule radiopharmaceuticals: recent developments and encouraging results. *Nucl. Med. Biol.*, **24**, 485–498.
32. Shi J., Kim Y.-S., Chakraborty S. *et al*. 2-Mercaptoacetylglycylglycyl (MAG_2) as a bifunctional chelator for ^{99m}Tc-labeling of cyclic RGD dimers: effect of technetium chelate on tumor uptake and pharmacokinetics. *Bioconjugate Chem.* 2009;**20**(8):1559-1568.
33. Riddoch, R.W., Schaffer, P. and Valliant, J.F. (2006) A solid-phase labeling strategy for the preparation of technetium and rhenium bifunctional chelate complexes and associated peptide conjugates. *Bioconjugate Chem.*, **17**, 226–235.
34. Baidoo, K.E., Lin, K.-S., Zhan, Y. *et al*. (1998) Design, synthesis, and initial evaluation of high-affinity technetium bombesin analogues. *Bioconjugate Chem.*, **9**, 218–225.
35. Francesconi, L.C., Graczyk, G., Wehrli, S. *et al*. (1993) Synthesis and characterization of neutral M(V)O (M = Tc, Re) amine-thiol complexes containing a pendant phenylpiperidine group. *Inorg. Chem.*, **32** (14), 3114–3124.

36. Marchi, A., Rossi, R., Magon, L. *et al*. (1990) Complexes of Tc-V and Tc-III with tridentate schiff-bases derived from S-methyl dithiocarbazate - crystal-structures of chloro[S-Methyl 3-(2′-Hydroxy-1-naphthylmethylene)-dithiocarbazato(2-)]oxotechnetium(V) and dichloro[S-methyl 3-(2-hydroxybenzylidene)dithiocarbazato(1-)]-bis(triphenylphosphine)-technetium(III). *J. Chem. Soc. Dalton.*, **4**, 1411–1416.
37. Marchi, A., Rossi, R. and Marvelli, L. (1993) Nitrido technetium(V) complexes with amino-acids – preparation and x-ray crystal-structure of the L-cysteinate ethyl-ester technetium(V) complex. *Inorg. Chem.*, **32** (22), 4673–4674.
38. Abrams, M.J., Larsen, S.K. and Zubieta, J. (1991) Investigations of the technetium-hydrazido core. Synthesis and structural characterization of $[(n\text{-}C_4H_9)_4N][Tc_2(NNPh_2)_2(C_6Cl_4O_2)_2]*CH_2Cl_2*2CH_3OH$, a Tc(V)/Tc(VI) catecholate complex with the hydrazido ligands adopting the unusual n1 bridging mode. *Inorg. Chem.*, **30**, 2031–2035.
39. Ghezzi, C., Fagret, D., Arvieux, C.C. *et al*. (1995) Myocardial kinetics of Tcn-noet – a neutral lipophilic complex tracer of regional myocardial blood-flow. *J. Nucl. Med.*, **36** (6), 1069–1077.
40. Liu, S., Edwards, D.S. and Harris, A.R. (1998) A novel ternary ligand system for Tc-99m-labeling of hydrazino nicotinamide-modified biologically active molecules using imine-N-containing heterocycles as coligands. *Bioconjugate Chem.*, **9** (5), 583–595.
41. Liu, S., Edwards, D.S., Looby, R.J. *et al*. (1996) Labeling a hydrazino nicotinamide-modified cyclic IIb/IIIa receptor antagonist with Tc-99m using aminocarboxylates as coligands. *Bioconjugate Chem.*, **7** (1), 63–71.
42. Alberto, R., Schibli, R., Egli, A. *et al*. (1998) A novel organometallic aqua complex of Technetium for the labeling of biomolecules: Synthesis of $[^{99m}Tc(OH_2)_3(CO)_3]^+$ from $[^{99m}TcO_4]^-$ in aqueous solution and its reaction with a bifunctional ligand. *J. Am. Chem. Soc.*, **120** (31), 7987–7988.
43. Bernard, J., Ortner, K., Spingler, B. *et al*. (2003) Aqueous synthesis of derivatized cyclopentadienyl complexes of technetium and rhenium directed toward radiopharmaceutical application. *Inorg. Chem.*, **42** (4), 1014–1022.
44. Alberto, R., Schibli, R., Waibel, R. *et al*. (1999) Basic aqueous chemistry of $[M(OH_2)_3(CO)_3]^+$ (M = Re, Tc) directed towards radiopharmaceutical application. *Coord. Chem. Rev.*, **192**, 901–919.
45. Green, A.E.C., Causey, P.W., Louie, A.S. *et al*. (2006) Microwave-assisted synthesis of 3,1,2-and 2,1,8-Re(I) and Tc-99m(I)-metallocarborane complexes. *Inorg. Chem.*, **45** (15), 5727–5729.
46. Maria, L., Susana, C., Videira, M. *et al*. (2007) Rhenium and technetium tricarbonyl complexes anchored by pyrazole-based tripods: novel lead structures for the design of myocardial imaging agents. *Dalton Trans.*, 3010–3019.
47. Storr, T., Obata, M., Fisher, C.L. *et al*. (2004) Novel carbohydrate-appended metal complexes for potential use in molecular imaging. *Chem. Eur. J.*, **11** (1), 195–203.
48. James, S., Maresca, K.P., Allis, D.G. *et al*. (2006) Extension of the single amino acid chelate concept (SAAC) to bifunctional biotin analogues for complexation of the $M(CO)_3^{+1}$ core (M = Tc and Re): synthesis, characterization, biotinidase stability, and avidin binding. *Bioconjugate Chem.*, **17**, 579–589.
49. Müller, C., Hohn, A., Schubiger, P.A. and Schibli, R. (2006) Preclinical evaluation of novel organometallic Tc-99m-folate and Tc-99m-pteroate radiotracers for folate receptor-positive tumour targeting. *Eur. J. Nucl. Med. Mol. Imaging*, **33** (9), 1007–1016.
50. Staveren, D.R.V., Mundwiler, S., Hoffmanns, U. *et al*. (2004) Conjugation of a novel histidine derivative to biomolecules and labelling with $[^{99m}Tc(OH_2)_3(CO)_3]^+$. *Org. Biomol. Chem.*, **2**, 2593–2603.
51. Alves, S., Correia, J.D.G., Gano, L. *et al*. (2007) In vitro and in vivo evaluation of a novel $^{99m}Tc(CO)_3$-pyrazolyl conjugate of cyclo-(Arg-Gly-Asp-d-Tyr-Lys). *Bioconjugate Chem.*, **18**, 530–537.
52. Stephenson, K.A., Banerjee, S.R., Besanger, T. *et al*. (2004) Bridging the gap between in vitro and in vivo imaging: isostructural Re and Tc-99m complexes for correlating fluorescence and radioimaging studies. *J. Am. Chem. Soc.*, **126** (28), 8598–8599.
53. Braband, H., Tooyama, Y., Fox, T. and Alberto, R. (2009) Syntheses of high-valent fac-[99mTcO3]+ complexes and [3+2] cycloadditions with alkenes in water as a direct labelling strategy. *Chem. Eur. J.*, **15** (3), 633–638.
54. Braband, H., Imstepf, S., Benz, M. *et al*. (2012) Combining bifunctional chelator with (3+2)-cycloaddition approaches: synthesis of dual-function technetium complexes. *Inorg. Chem.*, **51** (7), 4051–4057.
55. Ehrhardt, G.J., Ketring, A.R. and Ayers, L.M. (1998) Reactor-produced radionuclides at the University of Missouri Research Reactor. *Appl. Radiat. Isot.*, **49** (4), 295–297 (Epub 1998/03/31).

56. Moustapha M.E., Ehrhardt G.J., Smith C.J., *et al*. Preparation of cyclotron-produced 186Re and comparison with reactor-produced 186Re and generator-produced 188Re for the labeling of bombesin. *Nucl. Med. Biol.* 2006;**33**(1):81-89. (Epub 2006/02/07).
57. Deustch, E., Lisbon, K., Vanderheyden, J.L. *et al*. (1986) The chemistry of rhenium and technetium as related to the use of isotopes of these elements in therapeutic and diagnostic nuclear medicine. *Nucl. Med. Biol.*, **13**, 465.
58. Ketring, A.R. (1987) 153Sm-EDTMP and 186Re-HEDP as bone therapeutic radiopharmaceuticals. *Nucl. Med. Biol.*, **14**, 223.
59. Seifert, S., Heinrich, T., Jentschel, C. *et al*. (2006) Preparation and biological characterization of isomeric 188Re(V) Oxocomplexes with tetradentate S4 ligands derived from meso-dimercaptosuccinic acid for labeling of biomolecules. *Bioconjugate Chem.*, **17** (6), 1601–1606.
60. Costopoulos, B., Benaki, D., Pelecanou, M. *et al*. (2004) Structural study by NMR of oxorhenium-RGD decapeptide complex for application in radiotherapy. *Inorg. Chem.*, **43** (18), 5598–5602.
61. Cyr, J.E., Pearson, D.A., Wilson, D.M. *et al*. (2007) Somatostatin receptor-binding peptides suitable for tumor radiotherapy with Re-188 and Re-186. Chemistry and initial biological studies. *J. Med. Chem.*, **50** (6), 1354–1364.
62. Ogawa, K., Takhiro, M., Arano, Y. *et al*. (2005) Development of rhenium-186-labeled MAG3-conjugated biphosphonate for the palliation of metastatic bone pain based on the concept bifunctional radiopharmaceuticals. *Bioconjugate Chem.*, **16** (4), 751–757.
63. Gali, H., Hoffman, T.J., Sieckman, G.L. *et al*. (2001) Synthesis, characterization, and labeling with 99mTc/188Re of peptide conjugates containing a dithia-biphosphine chelating agent. *Bioconjugate Chem.*, **12** (3), 354–363.
64. Kurti, L., Papgiannopoulou, D., Padaopoulos, M. *et al*. (2003) Synthesis and characterization of novel 99gTc(V) and Re(V) complexes with water-soluble tetraza diamid dipyridino ligands: single x-ray structural investigation of mono- and dinuclear complexes. *Inorg. Chem.*, **42** (9), 2960–2967.
65. Ferreira, C.L., Bayly, S.R., Green, D.E. *et al*. (2006) Carbohydrate-appended 3-hydroxy-4-pyridinone complexes of the $[M(CO)_3]^+$ core (M = Re, ^{99m}Tc, ^{186}Re). *Bioconjugate Chem.*, **17** (5), 1321–1329.
66. Schibli, R., Schwarzbach, R., Alberto, R. *et al*. (2002) Steps toward high specific activity labeling of biomolecules for therapeutic application: preparation of precursor [188Re(H2O)3(CO)3] + and synthesis of tailor-made bifunctional ligand systems. *Bioconjugate Chem.*, **13** (4), 750–756.
67. Rosales, R., Finucane, C., Foster, J. *et al*. (2010) 188Re(CO)3-Dipicolylamine-alendronate: a new bisphosphonate conjugate for the radiotherapy of bone metastases. *Bioconjugate Chem.*, **21** (5), 811–815.
68. Bayly, S.R., Fisher, C.L., Storr, T. *et al*. (2004) Carbohydrate conjugates for molecular imaging and radiotherapy. *Bioconjugate Chem.*, **15** (4), 923–926.
69. Causey, P.W., Besanger, T.R., Schaffer, P. and Valliant, J.F. (2008) Expedient multi-step synthesis of organometallic complexes of Tc and Re in high effective specific activity. A new platform for the production of molecular imaging and therapy agents. *Inorg. Chem.*, **47** (18), 8213–8221.
70. Wagner, G.H. and Gitzen, W.H. (1952) Gallium. *J. Chem. Educ.*, **29** (4), 162.
71. Wadas, T.J., Wong, E.H., Weisman, G.R. and Anderson, C.J. (2010) Coordinating radiometals of copper, gallium, indium, yttrium, and zirconium for PET and SPECT imaging of disease. *Chem. Rev.*, **110** (5), 2858–2902.
72. Gleason, G.I. (1960) A positron cow. *Int. J. Appl. Radiat. Isot.*, **8**, 90–94.
73. Rufini, V., Calcagni, M.L. and Baum, R.P. (2006) Imaging of neuroendocrine tumors. *Semin. Nucl. Med.*, **36**, 228–247.
74. Velikyan, I., Maecke, H. and Langstrom, B. (2008) Convenient preparation of 68Ga-based PET-radiopharmaceuticals at room temperature. *Bioconjugate Chem.*, **19** (2), 569–573.
75. Emery, T. (1986) Exchange of iron by gallium in siderophores. *Biochemistry*, **25** (16), 4629–4633.
76. Bandoli, G., Dolmella, A., Tisato, F. *et al*. (2009) Mononuclear six-coordinated Ga(III) complexes: a comprehensive survey. *Coord. Chem. Rev.*, **253**, 56–77.
77. Sun, Y., Anderson, C.J., Pajeau, T.S. *et al*. (1996) Indium(III) and gallium(III) complexes of bis(aminoethanethiol) ligands with different denticities: stabilities, molecular modeling, and in vivo behavior. *J. Med. Chem.*, **39**, 458–470.
78. Harris, W.R. and Pecoraro, V.L. (1983) Thermodynamic binding constants for gallium transferrin. *Biochemistry*, **22**, 292–299.

79. Ambrosini, V., Tomassetti, P., Castellucci, P. *et al*. (2008) Comparison between ^{68}Ga-DOTA-NOC and ^{18}F-DOPA PET for the detection of gastro-entero-pancreatic and lung neuro-endocrine tumours, **35**, 1431–1438.
80. André, J.P., Maecke, H.R., Zehnder, M. *et al*. (1998) 1,4,7-Triazacyclononane-1-succinic acid-4,7-diacetic acid (NODASA): a new bifunctional chelator for radio gallium-labelling of biomolecules. *Chem. Commun.*, 1301–1302.
81. Ferreira, C.L., Lamsa, E., Woods, M. *et al*. (2010) Evaluation of bifunctional chelates for the development of gallium-based radiopharmaceuticals. *Bioconjugate Chem.*, **21** (3), 531–536.
82. Ferreira, C.L., Yapp, D.T.T., Mandel, D. *et al*. (2012) 68Ga small peptide imaging: comparison of NOTA and PCTA. *Bioconjugate Chem.*, **23** (11), 2239–2246.
83. Waldron, B.P., Parker, D., Burchardt, C. *et al*. (2013) Structure and stability of hexadentate complexes of ligands based on AAZTA for efficient PET labelling with gallium-68. *Chem. Commun.*, **49**, 579–581.
84. Baranyai, Z., Uggeri, F., Maiocchi, A. *et al*. (2013) Equilibrium, kinetic and structural studies of AAZTA complexes with Ga3+, In3+ and Cu2+. *Eur. J. Inorg. Chem.*, **2013** (1), 147–162.
85. Notni, J., Hermann, P., Havlíckova, J. *et al*. (2010) A triazacyclononane-based bifunctional phosphinate ligand for the preparation of multimeric ^{68}Ga tracers for positron emission tomography. *Chem. Eur. J.*, **16**, 7174–7185.
86. Notni, J., Pohle, K. and Wester, H.-J. (2013) Be spoilt for choice with radiolabelled RGD peptides: preclinical evaluation of ^{68}Ga-TRAP(RGD)$_3$. *Nucl. Med. Biol.*, **40**, 33–41.
87. Notni, J., Plutnar, J. and Wester, H.-J. (2012) Bone seeking TRAP conjugates: surprising observations and implications on development of gallium-68-labeled bisphosphonates. *EJNMMI Res.*, **2**, 13.
88. Eder, M., Schäfer, M., Bauder-Wüst, U. *et al*. (2012) 68Ga-complex lipophilicity and the targeting property of a urea-based PSMA inhibitor for PET imaging. *Bioconjugate Chem.*, **23** (4), 688–697.
89. Boros, E., Ferreira, C.L., Cawthray, J.F. *et al*. (2010) Acyclic chelate with ideal properties for ^{68}Ga PET imaging agent elaboration. *J. Am. Chem. Soc.*, **132** (44), 15726–15733.
90. Boros, E., Ferreira, C.L., Patrick, B.O. *et al*. (2011) New Ga derivatives of the H_2dedpa scaffold with improved clearance and persistent heart uptake. *Nucl. Med. Biol.*, **38** (8), 1165–1174.
91. Boros, E., Ferreira, C.L., Cawthray, J.F. *et al*. (2012) RGD conjugates of the H2dedpa scaffold: synthesis, labelling and Imaging with ^{68}Ga nuclear medicine and biology. *Nucl. Med. Biol.*, **39** (6), 785–794.
92. Berry, D.J., Ma, Y., Ballinger, J.R. *et al*. (2011) Efficient bifunctional gallium-68 chelators for positron emission tomography: tris(hydroxypyridinone) ligands. *Chem. Commun.*, **47** (25), 7068–7070.
93. Biersack, H.J., Briele, B., Hotze, A.L. *et al*. (1992) The role of nuclear medicine in oncology. *Ann. Nucl. Med.*, **5** (3), 131–136.
94. Ferrer, L., Malek, E., Bodet-Milin, C. *et al*. (2012) Comparison of dosimetric approaches for fractionated radioimmuno radiotherapy for non-Hodgkin lymphoma. *Q. J. Nucl. Med. Mol. Imaging*, **56** (6), 529–537.
95. Fasih, A., Fonge, H., Cai, Z. *et al*. (2012) 111In-DTPA-nimotuzumab with/without modification with nuclear translocation sequence (NLS) peptides: an Auger electron emitting radioimmunotherapeutic agent for EGFR-positive and trastuzumab (Herceptin)-resistant breast cancer. *Breast Cancer Res. Treat.*, **135** (1), 189–200.
96. Jasanada, F., Urizzi, P., Souchard, J.-P. *et al*. (1996) Indium-111 labeling of low density lipoproteins with DTPA-bis(stearylamide): evaluation of potential radiopharmaceutical for tumor localization. *Bioconjugate Chem.*, **7** (1), 72–81.
97. Kurihara, A. and Pardridge, W.M. (2000) AB1-40 peptide radiopharmaceuticals for brain amyloid imaging: 111In chelation, conjugation to poly(ethylene glycol)-biotin linkers and autoradiography with alzheimer's disease brain sections. *Bioconjugate Chem.*, **11** (3), 380–386.
98. Hsieh, W.Y. and Liu, S. (2004) Synthesis, characterization, and structures of indium In(DTPA-BA_2) and yttrium Y(DTPA-BA_2)(CH_3OH) complexes (BA = benzylamine): models for 111In- and 90Y-labeled DTPA biomolecule conjugates. *Inorg. Chem.*, **43** (19), 6006–6014.
99. Kwekkeboom, D.J., Kooji, P.P., Bakker, W.H. *et al*. (1999) Comparison of 111In_DOTA-Tyr3-octreotide and 111In-DTPA-octreotide in the same patients: biodistribution, kinetics, organ and tumor uptake. *J. Nucl. Med.*, **40** (5), 762–767.

100. Wei, L., Zhang, X., Gallazzi, F. *et al*. (2009) Melanoma imaging using (111)In-, (86)Y- and (68)Ga-labeled CHX-A″-Re(Arg11)CCMSH. *Nucl. Med. Biol.*, **36** (4), 345–354.
101. Price, E.W., Cawthray, J.F., Bailey, G.A. *et al*. (2012) H4octapa: an acyclic chelator for 111In radiopharmaceuticals. *J. Am. Chem. Soc.*, **134** (20), 8670–8683.
102. Yang, C.T., Li, Y. and Liu, S. (2007) Synthesis and structural characterization of complexes of a DO3A-conjugated triphenylphosphonium cation with diagnostically important metals ions. *Inorg. Chem.*, **46** (21), 8988–8997.
103. Liu, S., Pietryka, J., Ellars, C.E. and Edwards, D.S. (2002) Comparison of yttrium and indium complexes of DOTA-BA and DOTA-MBA: models for 90Y and 111In-labeled DOTA-biomolecule conjugates. *Bioconjugate Chem.*, **13** (4), 902–913.
104. Corneillie, T.M., Fisher, A.J. and Meares, C.F. (2003) Crystal structures of two complexes of the rare-earth-DOTA-binding antibody 2D12.5: ligand generality from a chiral system. *J. Am. Chem. Soc.*, **125** (49), 15039–15048.
105. Schlesinger, J., Koezle, I., Bergmann, R. *et al*. (2008) An 86Y-labeled mirror-image oligonucleotide: influence of Y-DOTA isomers on the biodistribution in rats. *Bioconjugate Chem.*, **19** (4), 928–939.
106. Sohalb, M., Ahmad, M., Jehangir, M. and Perveen, A. (2011) Ethylene diamine tetramethylene phosphonic acid labeled with various B(-)-emitting radiometals: labeling optimization and animal biodistribution. *Cancer Biother. Radiopharm.*, **26** (2), 159–164.
107. Camera, L., Kinuya, S., Garmestani, K. *et al*. (1994) Evaluation of the serum stability and in vivo distribution of CHX-DTPA and other ligands for yttrium labeling of monoclonal antibodies. *J. Nucl. Med.*, **35** (5), 882–889.
108. Ballard, B., Jiang, Z., Soll, C.E. *et al*. (2011) In vitro and in vivo evaluation of melanin-binding decapeptide 4B4 radiolabeled with 177Lu, 166Ho, and 153Sm radiolanthanides for the purpose of targeted radionuclide therapy melanoma. *Cancer Biother. Radiopharm.*, **26** (5), 547–556.
109. Lima, L.M., Delgado, R., Marques, F. *et al*. (2010) TETA analogue containing one methylenephosphonate pendant arm: lanthanide complexes and biological evaluation of its 153Sm and 166Ho complexes. *Eur. J. Med. Chem.*, **45** (12), 5621–5627.
110. Chong, H.S., Garmestani, K., Ma, D. *et al*. (2002) Synthesis and biological evaluation of novel macrocyclic ligands with pendent donor groups as potential yttrium chelators for radioimmunothrapy with improved complex formation kinetics. *J. Med. Chem.*, **45** (16), 3458–3464.
111. Tsukihara, T., Aoyama, H., Yamashita, E. *et al*. (1995) Structures of metal sites of oxidized bovine heart cytochrome c oxidase at 2.8 A. *Science*, **269** (5227), 1069–1074.
112. Haynes, N., Lacy, J., Nayak, N. *et al*. (2000) Performance of a 62Zn/62Cu generator in clinical trials of PET perfusion agent 62Cu-PTSM. *J. Nucl. Med.*, **41** (2), 309–314.
113. McCarthy, D.W., Shefer, R.E., Klinkowstein, R.E. *et al*. (1997) Efficient production of high specific activity 64Cu using a biomedical cyclotron. *Nucl. Med. Biol.*, **24** (1), 35–43.
114. Szelecsenyi, F., Blessing, G. and Qaim, S.M. (1993) Excitation function of proton induced nuclear reactions on enriched ^{61}Ni and ^{64}Ni: possibility of production of no-carrier-added ^{61}Cu and ^{64}Cu at a small cyclotron. *Appl. Radiat. Isot.*, **44**, 575–580.
115. Smith, S.V., Waters, D. and DiBartolo, N. (1996) Carrier-free copper-64 isolated from GA-67 waste for use in PET and therapy. *J. Nucl. Med.*, **37** (5), 894.
116. Medvedev, D.G., Mausner, L.F., Meinken, G.E. *et al*. (2012) Development of a large scale production of 67Cu from 68Zn at the high energy proton accelerator: closing the 68Zn cycle. *Appl. Radiat. Isot.*, **70** (3), 423–429 (Epub 2011/12/07).
117. Smith, N.A., Bowers, D.L. and Ehst, D.A. (2012) The production, separation, and use of 67Cu for radioimmunotherapy: a review. *Appl. Radiat. Isot.*, **70** (10), 2377–2383 (Epub 2012/08/09).
118. Martell, A.E. and Welch, M.J. (1995) Gallium and indium complexes as radiopharmaceuticals. Handbook of metal-ligand interactions in biological fluids. *Bioinorg. Chem.*, **2**, 1067–1078.
119. Scheinberg, I.H. and Morell, A.G. (1957) Exchange of ceruloplasmin copper with ionic CU64 with reference to Wilson's disease. *J. Clin. Invest.*, **36** (8), 1193–1201.
120. Wallhaus, T., Lacy, J., Whang, J. *et al*. (1998) Human biodistribution and dosimetry of the PET perfusion agent copper-62-PTSM. *J. Nucl. Med.*, **39** (11), 1958–1964.
121. Boswell, C.A., Sun, X., Niu, W. *et al*. (2004) Comparative in vivo stability of copper-64-labeled cross-bridged and conventional tetraazamacrocyclic complexes. *J. Med. Chem.*, **47** (6), 1465–1474.

122. Sibbons, K.F., Shastri, K. and Watkinson, M. (2006) The application of manganese complexes of ligands derived from 1,4,7-triazacyclononane in oxidative catalysis. *Dalton Trans.*, **5**, 645–661.
123. Bernhardt, P.V., Harrowfield, J.M., Hockless, D.C.R. and Sargeson, A.M. (1994) N-methylated macrobicyclic hexaamines of copper(II) and nickel(II): large steric effects. *Inorg. Chem.*, **33** (25), 5659–5670.
124. Huang, S., Joso, R., Fuchs, A. *et al*. (2008) Probing solid – liquid interfaces using radiotracer technology: characterization of functionalized microspheres. *Chem. Mater.*, **20** (16), 5375–5380.
125. Cai, H., Li, Z., Huang, C.-W. *et al*. (2010) Evaluation of copper-64 labeled AmBaSar conjugated cyclic RGD peptide for improved MicroPET imaging of integrin αvβ3 expression. *Bioconjugate Chem.*, **21** (8), 1417–1424.
126. Ma, M.T., Cooper, M.S., Paul, R.L. *et al*. (2011) Macrobicyclic cage amine ligands for copper radiopharmaceuticals: a single bivalent cage amine containing two Lys3-bombesin targeting peptides. *Inorg. Chem.*, **50** (14), 6701–6710.
127. Wong E.H., Weisman G.R., Hill D.C., *et al*. Synthesis and characterization of cross-bridged cyclams and pendant arm derivatives, and structural studies of their copper(II) complexes. *J. Am. Chem. Soc.* 2000;**122**:10561-10572.
128. Wei, L., Ye, Y., Wadas, T.J. *et al*. (2009) ^{64}Cu-Labeled CB-TE2A and diamsar-conjugated RGD peptide analogs for targeting angiogenesis: comparison of their biological activity. *Nucl. Med. Biol.*, **36**, 277–285.
129. Tircsó, G., Benyó, E.T., Suh, E.H. *et al*. (2009) S)-5-(p-Nitrobenzyl)-PCTA, a promising bifunctional ligand with advantageous metal ion complexation kinetics. *Bioconjugate Chem.*, **20** (3), 565–575.
130. Ait-Mohand, S., Fournier, P., Dumulon-Perreault, V. *et al*. (2011) Evaluation of 64Cu-labeled bifunctional chelate–bombesin conjugates. *Bioconjugate Chem.*, **22** (8), 1729–1735.
131. Dumont, R.A., Deininger, F., Haubner, R. *et al*. (2011) Novel 64Cu- and 68Ga-labeled RGD conjugates show improved pet imaging of $\alpha_v\beta_3$ integrin expression and facile radiosynthesis. *J. Nucl. Med.*, **52** (8), 1276–1284.
132. Woodin, K.S., Heroux, K.J., Boswell, C.A. *et al*. (2005) Kinetic inertness and electrochemical behavior of copper(II) tetraazamacrocyclic complexes: possible implications for in vivo stability. *Eur. J. Inorg. Chem.*, **25**, 4829–4833.
133. Dearling, J.L.J., Voss, S.D., Dunning, P. *et al*. (2011) Imaging cancer using PET – the effect of the bifunctional chelator on the biodistribution of a 64Cu-labeled antibody. *Nucl. Med. Biol.*, **38** (1), 29–38.
134. Maheshwari, V., Dearling, J.L.J., Treves, S.T. and Packard, A.B. (2012) Measurement of the rate of copper(II) exchange for 64Cu complexes of bifunctional chelators. *Inorg. Chim. Acta*, **393**, 318–323.
135. Ikotun, O.F. and Lapi, S.E. (2011) The rise of metal radionuclides in medical imaging: copper-64, zirconium-89 and yttrium-86. *Future Med. Chem.*, **3** (5), 599–621. (Epub 2011/04/30).
136. Severin, G.W., Engle, J.W., Barnhart, T.E. and Nickles, R.J. (2011) 89Zr radiochemistry for positron emission tomography. *Med. Chem.*, **7** (5), 389–394 (Epub 2011/06/30).
137. Deri, M.A., Zeglis, B.M., Francesconi, L.C. and Lewis, J.S. (2013) PET imaging with 89Zr: from radiochemistry to the clinic. *Nucl. Med. Biol.*, **40** (1), 3–14. (Epub 2012/09/25).
138. Greenwood, N.N. and Earnshaw, A. (1998) *Chemistry of the Elements*, 2nd edn, Elsevier.
139. Holland J.P., Sheh Y., Lewis J.S. Standardized methods for the production of high specific-activity zirconium-89. *Nucl. Med. Biol.* 2009;**36**(7):729-739. (Epub 2009/09/02).
140. Zweit, J., Downey, S. and Sharma, H.L. (1991) Production of no-carrier-added zirconium-89 for positron emission tomography. *Appl. Radiat. Isot.*, **42** (2), 199–201.
141. Meijs, W.E., Herscheid, J.D.M., Haisma, H.J. *et al*. (1994) Production of highly pure no-carrier added 89Zr for the labelling of antibodies and a positron emitter. *Appl. Radiat. Isot.*, **45**, 1143–1147.
142. Link, J.M., Krohn, K.A. and Eary, J.F. (1986) ^{89}Zr for antibody labelling and positron tomography. *J. Labeled Compd. Radiopharm.*, **23**, 1297–1298.
143. Dejesus, O.T. and Nickles, R.J. (1990) Production and Purification of Zr-89, a Potential Pet Antibody Label. *Appl. Radiat. Isot.*, **41** (8), 789–790.
144. Kandil, S.A., Scholten, B., Saleh, A.M. *et al*. (2007) A comparative study on the separation of radiozirconium via ion-exchange and solvent extraction techniques, with particular reference to the production of ^{88}Zr and ^{89}Zr in proton induced reactions on yttrium. *J. Radioanal. Nucl. Chem.*, **274**, 45–52.
145. Verel, I., Visser, G.W., Boellaard, R. *et al*. (2003) 89Zr immuno-PET: comprehensive procedures for the production of 89Zr-labeled monoclonal antibodies. *J. Nucl. Med.*, **44** (8), 1271–1281. (Epub 2003/08/07).
146. Baroncelli, F. and Grossi, G. (1965) The complexing power of hydroxamic acids and its effect on the behaviour of organic extractants in the reprocessing of irradiated fuels – I the complexes between benzohydroxamic acid and zirconium, iron (III) and uranium (VI). *J. Inorg. Nucl. Chem.*, **27** (5), 1085–1092.

147. Keberle, H. (1964) The biochemistry of desferrioxamine and its relation to iron metabolism. *Ann. N. Y. Acad. Sci.*, **119**, 758–768. (Epub 1964/10/07).
148. Meijs, W.E., Herscheid, J.D., Haisma, H.J. and Pinedo, H.M. (1992) Evaluation of desferal as a bifunctional chelating agent for labeling antibodies with Zr-89. *Int. J. Rad. Appl. Instrum. A*, **43** (12), 1443–1447. (Epub 1992/12/01).
149. Evans, M.J., Holland, J.P., Rice, S.L. *et al*. (2013) Imaging tumor burden in the brain with 89Zr-transferrin. *J. Nucl. Med.*, **54** (1), 90–95. (Epub 2012/12/14).
150. Aerts, H.J., Dubois, L., Perk, L. *et al*. (2009) Disparity between in vivo EGFR expression and 89Zr-labeled cetuximab uptake assessed with PET. *J. Nucl. Med.*, **50** (1), 123–131. (Epub 2008/12/19).
151. Abou, D.S., Ku, T. and Smith-Jones, P.M. (2011) In vivo biodistribution and accumulation of 89Zr in mice. *Nucl. Med. Biol.*, **38** (5), 675–681. (Epub 2011/07/02).
152. Sastry, B.V., Owens, L.K. and Ball, C.O. (1964) Differences in the distribution of zirconium-95 and niobium-95 in the rat. *Nature*, **201**, 410–411. (Epub 1964/01/25).
153. Backstrom, J., Hammarstrom, L. and Nelson, A. (1967) Distribution of zirconium and niobium in mice. Autoradiographic study. *Acta Radiol. Ther. Phys. Biol.*, **6** (2), 122–128. (Epub 1967/04/01).
154. Pozhidaev, A.I., Porai-Koshits, M.A. and Polynova, T.N. (1974) Crystal structure of zirconium ethylenediaminetetraacetate tetrahydrate. *J. Struct. Chem.*, **15** (4), 548–553.
155. Ilyukhin, A.B., Davidovich, R.L., Samsonova, I.N. and Teplukhina, L.V. (2000) Eightfold-coordinated diethylenetriaminepentaacetate: crystal structures of K[M(Dtpa)] 3H2O (M = Zr or Hf) and NH4[Sn(Dtpa)] H2O. *Crystallogr. Rep.*, **45** (1), 39–43.
156. Perk, L.R., Visser, O.J., Stigter-van Walsum, M. *et al*. (2006) Preparation and evaluation of (89)Zr-Zevalin for monitoring of (90)Y-Zevalin biodistribution with positron emission tomography. *Eur. J. Nucl. Med. Mol. Imaging*, **33** (11), 1337–1345 (Epub 2006/07/13).
157. Huclier-Markai, S., Sabatie, A., Ribet, S. *et al*. (2011) Chemical and biological evaluation of scandium(III)-polyaminopolycarboxylate complexes as potential PET agents and radiopharmaceuticals. *Radiochim. Acta*, **99** (10), 653–662.
158. Majkowska-Pilip, A. and Bilewicz, A. (2011) Macrocyclic complexes of scandium radionuclides as precursors for diagnostic and therapeutic radiopharmaceuticals. *J. Inorg. Biochem.*, **105** (2), 313–320.
159. Neves, M., Teixeira, F.C., Antunes, I. *et al*. (2011) Chemical and biological evaluation of 153 Sm and 46/47 Sc complexes of indazolebisphosphonates for targeted radiotherapy. *Appl. Radiat. Isot.*, **69** (1), 80–84.
160. Anderson, W.T. and Strand, M. (1985) Stability, targeting, and biodistribution of scandium-46- and gallium-67-labeled monoclonal antibody in erythroleukemic mice. *Cancer Res.*, **45** (5), 2154–2158.
161. Severin, G.W., Engle, J.W., Valdovinos, H.F. *et al*. (2012) Cyclotron produced 44gSc from natural calcium. *Appl. Radiat. Isot.*, **70** (8), 1526–1530. (Epub 2012/06/26).
162. Majkowska, A., Neves, M., Antunes, I. and Bilewicz, A. (2009) Complexes of low energy beta emitters 47Sc and 177Lu with zoledronic acid for bone pain therapy. *Appl. Radiat. Isot.*, **67** (1), 11–13.
163. Pruszynski, M., Majkowska-Pilip, A., Loktionova, N.S. *et al*. (2012) Radiolabeling of DOTATOC with the long-lived positron emitter 44Sc. *Appl. Radiat. Isot.*, **70** (6), 974–979.
164. Połosak, M., Piotrowska, A., Krajewski, S. and Bilewicz, A. (2012) Stability of 47Sc-complexes with acyclic polyamino-polycarboxylate ligands. *J. Radioanal. Nucl. Chem.*, **100**, 1–6.
165. Vaughan, A.T., Yankuba, S.C. and Anderson, P. (1987) Antibodies labeled with metallic radionuclides: influence of nuclide chemistry on dose distribution. *NCI Monogr.*, **3**, 141–144.
166. De Reuck, J., Santens, P., Strijckmans, K. and Lemahieu, I. (2001) Cobalt-55 positron emission tomography in vascular dementia: significance of white matter changes. *J. Neurol. Sci.*, **193** (1), 1–6.
167. Heppeler, A., André, J.P., Buschmann, I. *et al*. (2008) Metal-Ion-dependent biological properties of a chelator-derived somatostatin analogue for tumour targeting. Chemistry – A. *Eur. J.*, **14** (10), 3026–3034.
168. Wållberg, H., Ahlgren, S., Widström, C. and Orlova, A. (2010) Evaluation of the radiocobalt-labeled [MMA-DOTA-Cys61]-ZHER2:2395-Cys affibody molecule for targeting of HER2-expressing tumors. *Mol. Imaging Biol.*, **12** (1), 54–62.
169. Meares, C.F., Moi, M.K., Diril, H. *et al*. (1990) Macrocyclic chelates of radiometals for diagnosis and therapy. *Br. J. Cancer Suppl.*, **10**, 21–6.

170. Meares, C.F., McCall, M.J., Reardan, D.T. *et al*. (1984) Conjugation of antibodies with bifunctional chelating agents: isothiocyanate and bromoacetamide reagents, methods of analysis, and subsequent addition of metal ions. *Anal. Biochem.*, **142** (1), 68–78.
171. Thisgaard H., Olesen M.L., Dam J.H. Radiosynthesis of 55Co- and 58mCo-labelled DOTATOC for positron emission tomography imaging and targeted radionuclide therapy. *J. Label. Compd. Radiopharm.* 2011;**54**(12):758–762.
172. Ferreira, C.L., Lapi, S., Steele, J. *et al*. (2007) 55Cobalt complexes with pendant carbohydrates as potential PET imaging agents. *Appl. Radiat. Isot.*, **65** (12), 1303–8.
173. Bernier, N., Costa, J., Delgado, R. *et al*. (2011) trans-Methylpyridine cyclen versus cross-bridged trans-methylpyridine cyclen. Synthesis, acid-base and metal complexation studies (metal = Co2+, Cu2+, and Zn2+). *Dalton Trans.*, **40** (17), 4514–26.
174. Wållberg, H, Ahlgren, S, Widström, C, Orlova, A. (2010) Evaluation of the radiocobalt-labeled [MMA-DOTA-Cys61]-Z HER2:2395(-Cys) affibody molecule for targeting of HER2-expressing tumors. *Mol Imaging Biol*. **12** (1): 54–62.

4

Ligand Design in *d*-Block Optical Imaging Agents and Sensors

Mike Coogan

Department of Chemistry, Faraday Building, Lancaster University, Bailrigg, Lancaster, LA1 4YB, UK

4.1 Summary and scope

Ligand design is crucial to transition metal optical imaging agents and sensors in biomedical applications, from tailoring the optical properties of the probe to controlling its toxicity for *in vivo* applications. This chapter attempts to show how it is possible to develop appropriate ligand systems for particular applications by considering the separate factors which control all of the important properties in the context of traditional issues of coordination chemistry. There are many examples of *d*-block optical probes applied in the detection, or quantitative analysis of biorelevant materials *in vitro* after isolation, but this chapter will focus on those which are applied to cells, tissue samples or samples of crude biological material rather than purified analytes. The reason for this distinction is that while some of the ligand design criteria are common to both applications, there are additional considerations which must be met working with samples which retain, for example lipid membranes. As the other design features for probes in terms of a detectable response to analyte, and so on are common to both sets of agents all the important criteria for both sets will be considered and discussed, but most of the detailed discussion will be chosen from the more biological, as opposed to analytical, examples. The area will be introduced, and the important criteria in probe design, and the important families of probes already existing, will be discussed. The important concepts behind using ligands to control photophysical and biological behaviour will be discussed in detail, and an overview of important examples given. Finally, a brief summary of the prospects for bimodal probes incorporating *d*-block optical probes into agents capable of simultaneously imaging in other modalities will be presented.

Ligand Design in Medicinal Inorganic Chemistry, First Edition. Edited by Tim Storr.

4.2 Introduction

Optical imaging agents and sensors fall into two main categories, those which sense or image by colour contrast (i.e. transmitted or reflected light) and those which use emitted light, fluorescent or phosphorescent probes to create an image or indicate the presence of an analyte. While these involve contrasting photophysical processes in the detection step, the coordination chemistry involved is in most cases similar, and these aspects of ligand design will be considered together. The main attractions of transition metal imaging agents and sensors are due to the particular characteristics of their emission and so most work focuses on luminescent complexes, often studied in cellular systems by confocal fluorescence microscopy. Whatever the nature of the detection step, the aspects of ligand design involved in controlling the other important properties of a probe such as solubility, toxicity, and so on are identical, and in discussion of these no distinction between probe types need be made. A set of criteria for an effective optical probe have previously been defined for cell imaging work [1], but as advances in optical imaging agents and sensors allow extensions into whole body studies (see below) these must be extended to the more general case; so, for instance, the ability to permeate a cell membrane has to be considered along with the ability to pass, for example the blood–brain barrier along with blood clearance times and gut wall permeation for oral administration.

4.2.1 Criteria for biological imaging optical probes

- Photophysical properties: the probe must absorb/emit at wavelengths which pass though the tissue/sample concerned. In general biological material absorbs more at the shorter wavelength, high energy, region of the visible spectrum and so long wavelength excitation and emission are desirable. Near infrared (NIR) has better tissue penetration than visible light and whole body studies are possible with NIR emitters, at least in small animals. It should be noted, however, that the relationship between resolution and wavelength of radiation means that NIR imaging can never achieve the same resolution as vis/uv microscopy. Background noise from fluorescence from biological material itself (autofluorescence) can make detection of the signal from artificial imaging agents and sensors difficult, and thus it is desirable that probes have photophysical properties (luminescence lifetime, emission wavelengths, and so on) which are different to autofluorescence. Autofluorescence tends to have a short luminescence lifetime, and a small 'Stokes shift' – that is the difference in wavelength between the excitation and emission wavelengths.
- Solubility: the probe must remain in solution in the medium (usually aqueous in physiological studies) at least on the timescale of the experiment. Ligands which are highly lipophilic can cause precipitation of imaging agents and aggregate formation.
- Toxicity: the probe must be non-toxic for *in-vivo* work and non-cytotoxic for *in vitro* cellular work, at least for the timescale of the experiment. As many metal ions are notoriously toxic the ligand framework must tame them for *in vivo* applications.
- Stability: the probe must be stable in the environment it is applied. For many transition metal complexes their reactivity towards water and oxygen are the main issues, but biomolecules such as thiols can be problematical with specific imaging agents and sensors.
- Transport properties: the probe must be able to cross barriers (usually lipophilic in nature) in order to reach the desired site of action. Transition metal complexes of highly polar ligands (amines and carboxylates), or which are highly charged, may be too polar to permeate lipid membranes, and may require active transport mechanisms, or complicated delivery systems for *in vivo* use.
- Distribution: the probe must localise in the site of interest, and this is almost entirely controlled by ligand features rather than metal ion.
- Detectable response to environment: while many probes are useful simply as contrast agents allowing high-resolution imaging, other applications require a response to an analyte. One of the strengths of optical

probes over many other modalities is that both the absorption and emission properties of probes can often be tailored to change as a function of the local environment. The electronic transitions involved in the absorption/emission of light reflect orbital energy gaps which are sensitive to the environment of the molecule (e.g. solvation, protonation state, and so on). Additionally, reaction or interaction with another molecule can modulate these transitions in a characteristic manner allowing specific detection responses.

4.3 Overview of transition-metal optical probes in biomedicinal applications

Owing to the problems of tissue penetration of visible light and related wavelengths most transition metal optical probes which have found applications in biomedical fields are used in tissue or cell imaging studies in microscopy or related applications rather than in whole body imaging. Even in cases where there is sufficient tissue penetration of the relevant wavelength to allow detection of a probe within a body it can be difficult to accurately determine the probe's distribution within the specimen due to 'surface weighting'. As the signal passes through tissue its intensity is rapidly reduced, meaning that areas of probe location near the surface lead to disproportionally intense signal compared with areas of even much higher probe concentration deeper within the sample. Although advanced tomographic computing techniques can compensate for these effects and allow 3D images to be reconstructed the fact that different tissue types reduce signal intensities to different levels makes this challenging at all but the smallest depths. Given these limitations most applications of transition metal optical probes have been in cell microscopy, in which the sample depth is very small, tissue penetration of visible wavelengths is good, and there is usually no problem encountered with differential signal attenuation with depth of the area being imaged.

4.3.1 Common families of transition metal probes

The transition metal optical imaging agents and sensors which have been most widely applied in biomedical studies to date are based around mid- to late-transition metals in low oxidation states. Rhenium, ruthenium and iridium are the most studied systems, with a wide range of d^6 complexes of these metals having been applied in different biological systems [1]. More recently d^8 and d^{10} platinum and gold species have also attracted attention [2] with combined imaging and therapeutic applications of cytotoxic gold(I) complexes being particularly interesting. Typical structures are illustrated in Figure 4.1.

4.3.1.1 Group VII: Rhenium and technetium-based imaging agents and probes

The most common rhenium(I)-based lumophores which have been developed as imaging and sensing agents are based on the *fac*-$[Re(CO)_3(bpy)]^+$ core (where bpy (bipyridine) represents any chelating diimine ligand containing the structural features of bpy, phenanthroline, etc.) [3]. The Tc (see Chapter 3 for further details) analogues are similar and more detail is given in the sections below on SAAC (Single Amino Acid Conjugate) chemistry and bimodal imaging (Section 4.9.2). The *fac*-$[Re(CO)_3(bpy)]^+$ unit shows the attractive photophysical properties and stability which are essential for imaging agents and are discussed below, and is easily accessed with flexibility in the choice of the sixth ligand which allows tuning of properties for particular applications [4]. These complexes are usually synthesised from parent pentacarbonyl halides, $[Re(CO)_5X]$ (X = Cl/Br) in three steps. Initially the pentacarbonyl halide is treated with the diimine to form the neutral tricarbonyl diimine halides, *fac*-$[Re(CO)_3(bpy)X]$. These are isolated exclusively as the *fac*-isomers as a result of the *trans*-influence, and this geometry is maintained through all subsequent steps. Usually the complexes are then converted into activated intermediates by substitution of the halide with either acetonitrile or THF (by abstraction of halide with a silver salt in the relevant solvent) or triflate by simple reaction with triflic

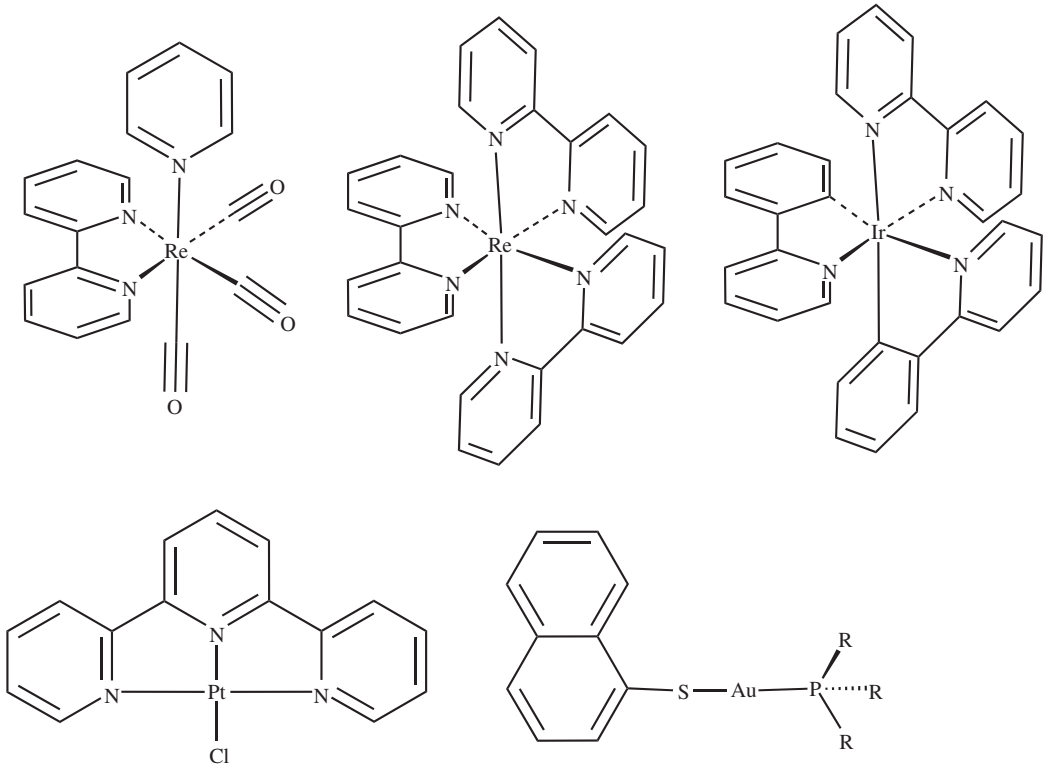

Figure 4.1 *Typical structures of Re, Ru, Ir, Pt and Au optical probes*

acid. These intermediates are then treated with the required ligand (usually a substituted pyridine) to give the final, stable, cationic complexes, typically in good overall yields. Typical reagents and reaction conditions are shown in Scheme 4.1. Rhenium(I) and technetium(I) have a d^6 electronic configuration, and are usually only stable in this oxidation state with high field ligands, and thus they have low spin arrangements. The complexes are typically approximately octahedral with distortions induced by the geometrical restraints of the bpy unit.

4.3.1.2 Group VIII: Ruthenium and osmium-based imaging agents and probes

Ruthenium(II) imaging and sensing agents are typically based around derivatives of the well-known lumophores $[Ru(bpy)_3]^{2+}$ in which one of the bpy units has been replaced with a more complex ligand, usually still a chelating diimine of the bpy type, but bearing substitution appropriate for the desired application [5]. There are a very small number of analogous osmium complexes which have also been used in imaging experiments [6]. These complexes are usually synthesised from the reaction of the neutral dichloride $[Ru(bpy)_2Cl_2]$ with the substituted bpy N^N, followed by salt metathesis to give the dicationic products, $[Ru(bpy)_2(N^N)]^{2+}$. $[Ru(bpy)_2Cl_2]$ itself is commercially available but can be prepared from ruthenium(III) chloride by reaction with bpy, but in the presence of excess of chloride to suppress the thermodynamically favoured production of the homoleptic tris-bypyridine complex $[Ru(bpy)_3]^{2+}$. The solvent for this step is usually a sacrificial alcohol which acts as the electron donor for the reduction of Ru^{III} to Ru^{II}, itself being

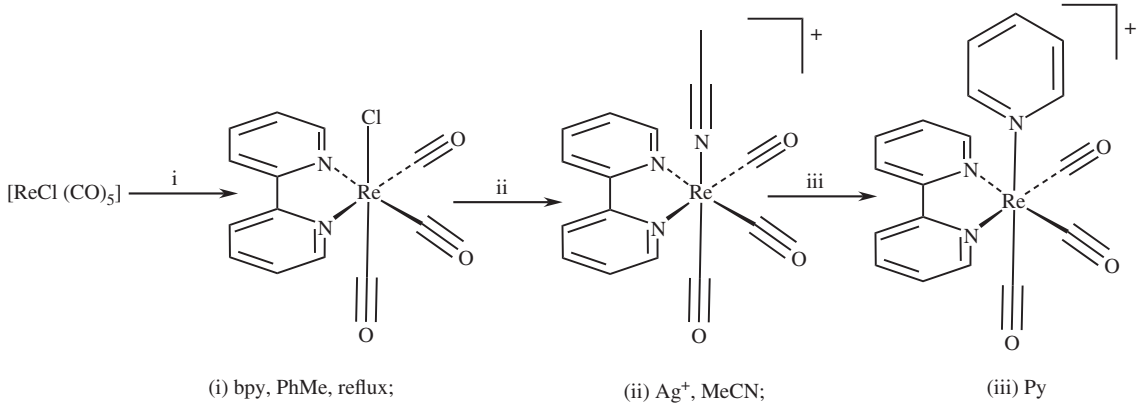

Scheme 4.1 *Synthesis of rhenium-based imaging agents*

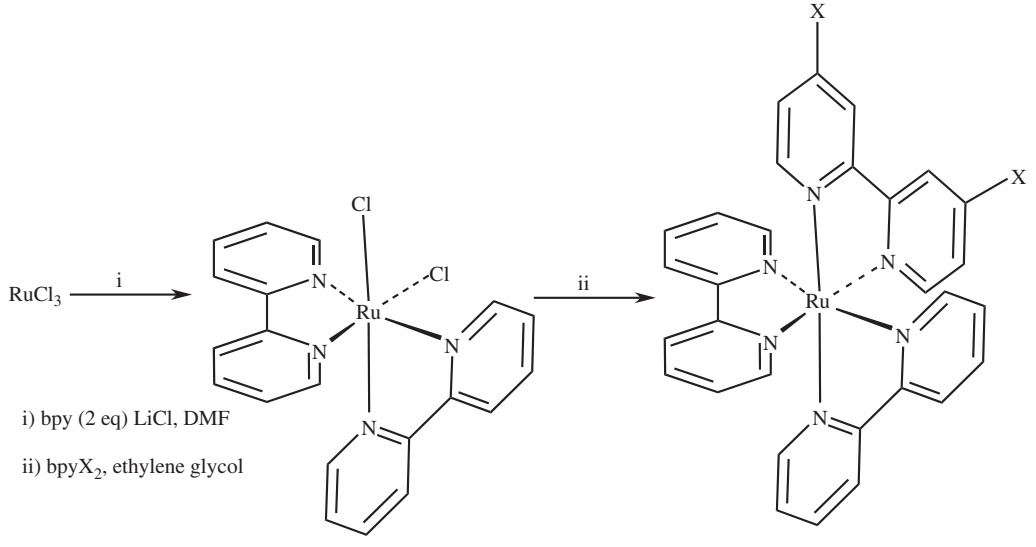

Scheme 4.2 *Synthesis of ruthenium-based imaging agents*

oxidised to the derived carboxylic acid. Typical reagents and reaction conditions are shown in Scheme 4.2. It should be noted that these complexes exist as a mixture of Λ and Δ isomers, and that these typical conditions yield a racemic mixture of the products. As all biological material is itself chiral and thus experiences different interactions with these isomers they should really be considered as a pair of distinct complexes which will have different *in vivo* properties unless the isomers are separated. Ruthenium(II) and osmium(II) have a d^6 electronic configuration, and they are almost always observed in low spin arrangements. The complexes are typically approximately octahedral with distortions induced by the geometrical restraints of the bpy units, and deviations from local C_3 symmetry in cases where the three chelating ligands are significantly different from each other.

4.3.1.3 Group IX: Iridium and rhodium-based imaging agents and probes

Iridium(III) lumophores used in sensing and imaging (and the very few examples of rhodium(III)-based analogues) are usually based on a core of a bis-cyclometallated ligand such as 2-phenylpyridine (2-ppy) with a third neutral, bidentate chelating ligand such as bpy, giving a monocationic complex of the general formula $[Ir(ppy)_2(N\text{^}N)]^+$ [7, 8]. Typically these complexes are synthesised in two steps from the reaction of iridium(III) chloride with the protonated form of the cyclometallating ligand, to give the neutral bis-cyclometallated, chloride-bridged dimer, which is then cleaved by reaction with a chelating di-imine such as bpy to give the monocationic product. Both the intermediate chloride-bridged dimer and the final species are normally formed as single isomers in which the two cyclometallating ligands are arranged with mutually *cis*-carbon donors, which are themselves *trans*-to the two donors derived from the non-cyclometallating units (Cl or bpy), which can be explained by the *trans*-influences of these ligands. Again, as for ruthenium, optical isomers are formed, and must be separated if the complexes are to be considered as single species in a biological environment. Ir^{III} and Rh^{III} have a d^6 electronic configuration and are almost exclusively low spin, with approximately octahedral geometry, but with occasionally significant distortions. Typical reagents and conditions for the synthesis of iridium-based agents are shown in Scheme 4.3.

4.3.1.4 Group X: Platinum-based imaging agents and probes

Most of the leading platinum-based lumophores are based around Pt^{II} complexes of tridentate chelating systems such as terpyridine, or analogous cyclometallating ligands like the pincer systems in which the central terpyridine nitrogen is replaced with a carbon [2, 7]. Pd cyclometallates are often emissive but have not been used as probes in biomedical applications. The complexes based on neutral N^N^N ligands are synthesised by simple ligand exchange reactions of platinum salts, and the cyclometallates under conditions analogous to those used in the first step of Scheme 4. Simple treatment of platinum(II) halido species (usually the tetrachloroplatinate salts $Na_2/K_2/(NH_4)_2[PtCl_4]$ are used as they are more soluble than the neutral halides) with cyclometallating ligands (ppy, Phbpy, etc.) under neutral or mildly basic conditions leads to the luminescent cyclometallated complexes. These Pt^{II} complexes with a d^8 electronic configuration are usually square planar and can suffer from low solubility.

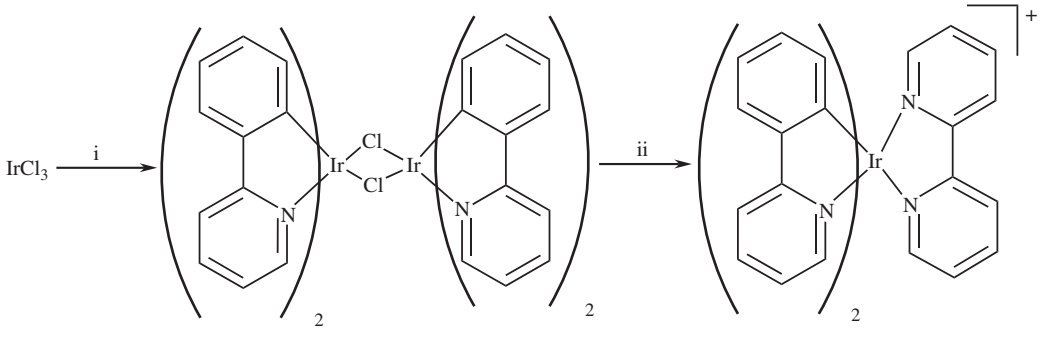

(i) ppy, methoxyethanol; (ii) bpy, methoxyethanol

Scheme 4.3 *Synthesis of typical Ir probe*

4.3.1.5 Group XI: Gold-based imaging agents and probes

There are a variety of gold(I) complexes which have so far been applied in imaging and none has yet emerged as the favoured system, as the application of gold complexes in imaging is in its infancy [2, 7]. Copper(I) and silver(I) lumophores with interesting phosphorescence are known but not as biomedical probes. Most of the systems used in imaging are gold(I) phosphine derivatives containing a linear P-Au-L unit in which L is a soft heteroatom or organometallic donor. Usually these are prepared by the reactions of gold(I) phosphine halides R_3PAuX (X = Cl/Br) with anions or with organometallic units which are subsequently deprotonated. The gold(I) phosphine precursors are generated by the reduction of Au^{III} species with excess of phosphine. The more labile thioether species R_2SAuX (typically $R_2S = Me_2S$, THT) are generated analogously from the reduction of the Au^{III} halide with excess of thioether, but these often react with good donors by loss of both the THT and halide to give the homoleptic species. Heteroleptic neutral gold phosphine thiolates are usually formed by the reaction of thiols with gold(I) phosphine halides under basic conditions. Neutral gold(I) alkynyl phosphine complexes can be formed under analogous conditions to the thiolates, but are also available from the base-free reactions of gold(I) phosphine halides with terminal alkynes in the presence of silver(I) salts, or from the reaction of gold(I) halides with copper alkynyls in catalytic processes. Homoleptic cationic or anionic species are available by displacement of both ligands from the thioether-substituted gold(I) halides with neutral (phosphine and carbine) or anionic (thiolate and alkynyl) ligands respectively. Gold(I) complexes have a d^{10} electronic configuration and are typically of linear geometry. Some of the most interesting examples of gold lumophoric probes involve complex macromolecular ligands or aggregates and are described later.

4.4 Ligand design for controlling photophysics

4.4.1 Photophysical processes in transition metal optical imaging agents and sensors

The majority of transition metal optical probes rely on photophysical processes which directly involve the ligand electronic states. In many cases charge transfer between metal and ligand occurs upon absorption of light, and in others ligand-based electronic transitions are involved (or a mixture of the two), but it is very rare for purely metal-based transitions to be important, hence ligand properties are intimately involved in the light-absorbing or -emitting processes [1–3, 5].

4.4.2 Photophysically active ligand families – tuning electronic levels

The majority of ligands used as the photophysically active unit in TM optical imaging agents and sensors are conjugated aromatic heterocycles which can either accept electrons in metal-to-ligand charge transfer (MLCT) processes or which can undergo intra- (or inter-) ligand (IL) electron transfer transitions upon absorption of light. Typical examples include bpy and related ligands (typically with Re and Ru) and cyclometallating ligands such as phenylpyridines (usually with Ir/Rh). Alkynyl and thiolate ligands are also important in the later d^8 and d^{10} systems, which can be photophysically active in some cases. MLCT processes typically involve transfer of electrons from metal-based *d*-orbitals to vacant ligand-based π^* orbitals, and the IL transitions important in imaging processes transfer from occupied π, σ or non-bonding orbitals to vacant π^* orbitals. The archetypal process, and that which dominates Re and Ru systems, involves an excited triplet electronic state, (^{3}MLCT) emission, generated by spin-orbit-coupling-mediated intersystem crossing from the initial singlet state, as summarised in the simplified Jablonski diagram in Figure 4.2. The final emission of a photon

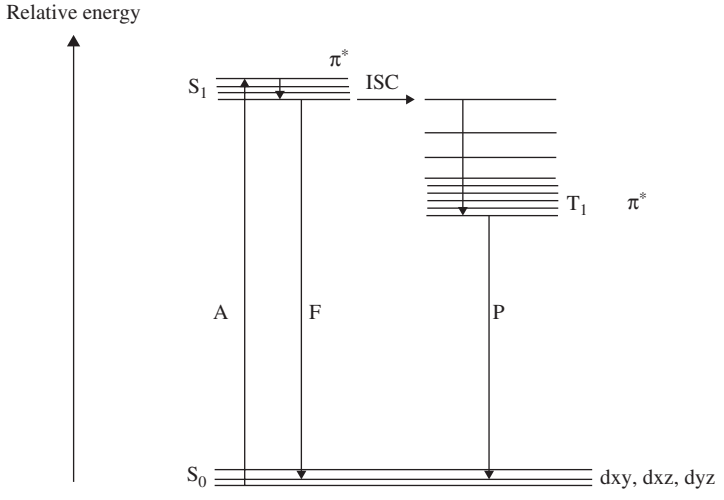

Figure 4.2 *Simplified Jablonski diagram for a ^{3}MLCT emissive complex. A = absorption; F = fluorescence; P = phosphorescence; S = singlet; T = triplet; ISC = inter system crossing; small line separations = vibrational energy levels; Right hand labels = orbital character*

from the ^{3}MLCT state is formally forbidden, and thus slow, leading to a long luminescence lifetime, and the energy lost in the intersystem crossing to the triplet state is responsible for the large Stokes shift associated with these complexes. Thus, with large Stokes shifts and long lifetimes making emission from transition metal probes easy to distinguish from autofluorescence (see Section 4.2.1) these complexes have ideal properties or imaging applications [9, 10].

Generally, whether the transition is of MLCT or IL nature, increased conjugation in the ligand leads to a red-shift of the transition, as the acceptor orbital which is usually of π* character is lowered in energy, and this outweighs any other changes in energy levels due to, for example ligand field effects. Substituent effects in purely MLCT processes are generally predictable in direction, in that electron-donating groups blue-shift the transitions, while electron-withdrawing substituents red-shift transitions. In luminescent complexes however, the relative degrees of blue- or red- shift which will be induced in the absorption and emission transitions of a complex by a given change in substituent are harder to predict. For instance, in the series of complexes $ReCl(CO)_3$(4,4′di-X-bpy) as the substituent X changes from electron donating (NH_2) to electron withdrawing (NO_2), while both absorption and emission red-shift (λ_{max} abs X = NH_2 350 nm, X = NO_2 448 nm; λ_{max} emit X = NH_2 573 nm and X = NO_2 780 nm), the change in absorption wavelength (98 nm) is much smaller than the change in emission wavelength (207 nm) (Figure 4.3) [11].

This difference illustrates that while it is possible to tune the photophysical properties of complexes by ligand design, even in simple cases the magnitude of changes induced by ligand substitution is difficult to predict. In cases which involve more transitions, or more complex transitions than pure MLCT, such as those involved in luminescence from cyclometallated iridium complexes of the general type $[Ir(C\hat{}N)_2(N\hat{}N)]^+$ where (C^N) is a cyclometallating ligand such as ppy and (N^N) is a chelating diamine such as bpy, the effects of changes to a simple ligand are even harder to predict. As these complexes may emit from MLCT, IL or even other states, and many of the orbitals involved are close in energy, changing ligand substitution to alter the orbital energies of one state may lead to a switch of emission from that state to one of a different nature completely [12]. Even in the apparently simplest of cases changes to ligand structure can sometimes have dramatic and unpredictable effects on the emission profile of the complex: Re complexes of tripodal ligands such as those

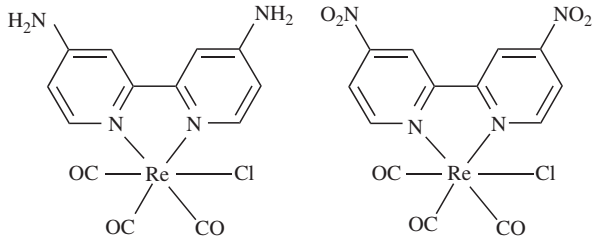

Figure 4.3 *Tuning MLCT emission with ligand substitution*

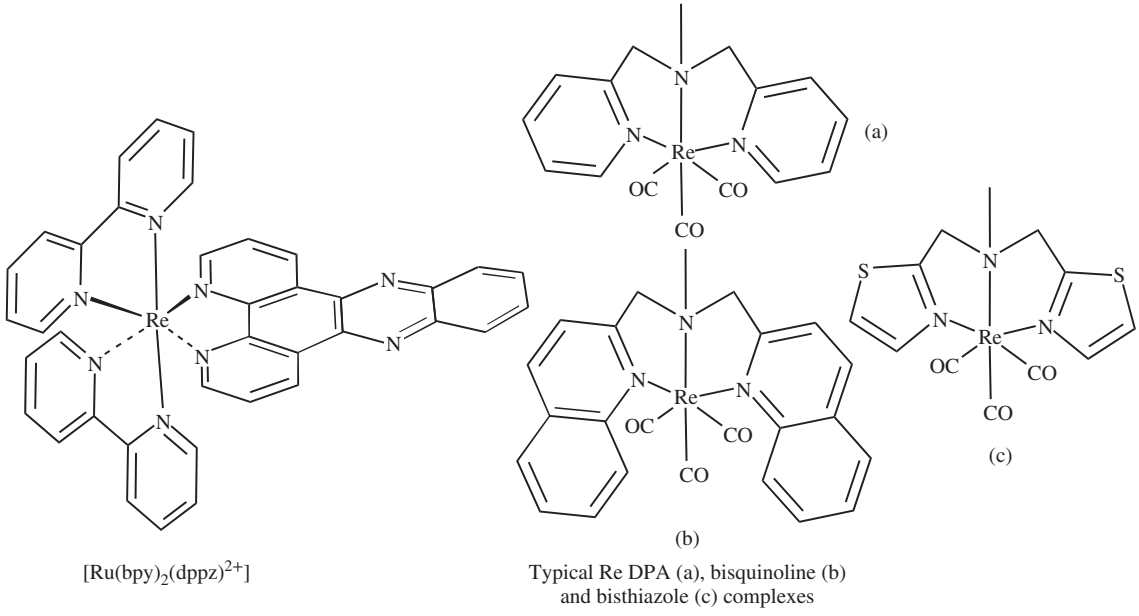

Figure 4.4 *(a–c) Molecular structure of DNA sensor [Ru(bpy)$_2$(dppz)$^{2+}$ and Re-complexes related to the DPA ligand*

related to dipicolylamine (dpa, Figure 4.4) have been shown to be emissive if the terminal pyridines are substituted for more highly conjugated systems such as quinolones, and so on. The [M(CO)$_3$(dpa)] unit has been used as the core of a bio-targeting system in the SAAC strategy (see Section 4.7.3.3) to provide a series of analogous complexes in which the M = ^{99m}Tc analogue provides radioimaging capability, and the M = Re analogue provides a 'cold' model complex. In the more conjugated systems such as the bisquinolines, the M = Re analogues are used as fluorescent analogues of the radioimaging agents for cell microscopy, but the emission characteristics of the complexes are easily explained by MLCT processes analogous to the better explored [Re(CO)$_3$(bpy)] lumophores. However, when the terminal heterocycle was changed from quinolone (Figure 4.4) to thiazole (Figure 4.4), in order to improve water-solubility for biological application, a dramatic change in the photophysics was noted. The wavelength of emission of the complex now changed as a function of the wavelength of excitation which was used to irradiate the sample [13]. Samples which can emit at more

than one wavelength are extremely rare, as one of the principles of photophysics is that emission is observed from the lowest energy state of a given spin multiplicity, that is singlet fluorescence/triplet phosphorescence (see Figure 4.2). While complexes are known which show, two emission bands this phenomenon is rare itself and more complex behaviour is highly unusual. Dual emission is known in iridium, rhenium and ruthenium complexes [14–17], and while it is usually little more than an oddity, in the bisthiazole complex dual emission was utilised as a method of enhancing output intensity. In this case it was possible to independently excite a pair of transitions and collect the emissions associated with each, summing the emission intensities in a merged image to dramatically increase signal-to-noise ratio [18].

4.4.3 Ligands which control photophysics through indirect effects

In certain cases the photophysical properties of a complex can be controlled by the use of large ligand architectures which have the effect of altering the local environment of the complex (rather than using the coordination sphere to directly change energy levels of electronic states) and this can have surprisingly large effects on the emission characteristics of the imaging agents and sensors. Other interactions such as excited-state reactions with specific analytes can change emission properties and be used to detect the reactant's presence. The commonest effect here is simple quenching of the excited states, often by collisional quenching with triplet oxygen ($^3O_2$) which is an effective quencher of the triplet excited states usually found in transition metal lumophores, particularly $[Ru(bpy)_3]^{2+}$ and related complexes. The mechanism of quenching of the triplet excited state is thought to be a very efficient triplet-triplet annihilation in which an initial excited-state complex of the triplet metal complex and triplet oxygen decomposes to the ground state of the complex, and the excited (singlet) state of oxygen ($^1O_2$) (Equation (4.1)). The high toxicity of singlet oxygen should therefore be noted when live-organism studies are undertaken with complexes which show efficient oxygen quenching [19].

$$^3[Ru(bpy)_3] + {}^3O_2 \rightarrow \{^3[Ru(bpy)_3] \ldots {}^3O_2\} \rightarrow {}^1[Ru(bpy)_3] + {}^1O_2 \tag{4.1}$$

Probes can be designed to indicate the presence of oxygen or measure its concentration by the loss of emission intensity if the concentration of probe can be easily assessed. In live biological systems where it is hard to know the concentration of probe the local concentration of oxygen can be assessed instead by the decrease in luminescence lifetime induced by oxygen. As lifetime-based methods are independent of probe concentration these are ideal for *in vivo* studies [20]. Another example of a pronounced effect of the environment on the photophysical properties of imaging agents and sensors is the 'turn on' switch of properties induced by an interaction of certain complexes with DNA [21]. Complexes of a variety of transition metals containing the dppz ligand (dppz = dipyrido[3,2-*a*;2′,3′-*c*]phenazine) (Figure 4.4) show a strong interaction with DNA in which the large planar dppz unit intercalates into one of the grooves of DNA. The effect of this intercalation is to protect the surface of the dppz ligand from interaction with water, and this leads to an enhancement of luminescence. The details of the electronic origin of this enhancement vary between the dppz complexes of different metals, as does the size of the increase in emission, but in most cases it is effectively a 'turn on' effect in which the free complex is only very weakly emissive, if at all, while the intercalated complex is highly emissive.

4.4.4 Transition metal optical probes with carbonyl ligands

One class of ligand which holds a special place in transition metal chemistry, and which has two useful roles in optical imaging agents and sensors, is CO, which can be used directly as a probe for imaging in vibrational microscopy, and also exerts a pronounced ligand field effect on the electronics of complexes thus influencing their photophysical properties indirectly. While the orbitals involved in absorption or emission may have some CO character in MLCT and related processes, the influence of CO ligands is more usually related

to the lowering of the energy of filled *d*-orbitals due to their π-acceptor nature. In addition to this indirect involvement in electronic transitions, the vibrational spectra of metal carbonyls often show bands at around 2000 cm^{-1}, a region of the spectrum which is clear of any background signals from biological material. Thus a family of optical probes exists which exploits the metal carbonyl IR band as a high signal-to-noise ratio probe for IR/vibrational microscopy. Where the carbonyls are combined with other (photophysically active) ligands, probes which can be used in more than one imaging mode can result (see Section 4.9).

4.5 Ligand design for controlling stability

The issue of stability is crucial for transition metal agents in biomedical work for a number of reasons, the most important of which relates to heavy metal toxicity. Most of the heavy metals which show the efficient spin-orbit coupling required for triplet excited states (see Section 4.4.2) are moderately to highly toxic as the free metal ions and so ligand systems must be carefully designed to control this toxicity. Generally, heavy metal ions are toxic as a result of their interactions with biomolecules containing S, N or O donor atoms which act as ligands for the metal ions, forming complexes in which the natural role of the biomolecule is disrupted. While the best known examples of this involve the nitrogen atoms from DNA bases, softer donors such as sulfur and selenium from the active sites of enzymes can also interact with soft metals such as gold, inhibiting the enzymes and leading to cell death. The most successful strategies for controlling metal ion toxicity in imaging probes therefore rely upon formation of kinetically inert complexes in which all, or the majority, of the coordination sites are occupied, preventing such interactions with DNA, enzymes, and so on. The low rates of ligand substitution associated with ligand field effects in the d^6 low-spin electronic configuration have led to the popularity of Re^{I}, Ru^{II} and Ir^{III} agents with high field ligands which force the low-spin configuration [1]. Additionally, chelating ligands such as bpy and phenylpyridine endow the complexes with additional stability.

4.6 Ligand design for controlling transport and localisation

Transport of exogenous imaging agents and sensors through biological barriers, usually lipophilic membranes, can be achieved by either passive diffusion or active transport, and different ligand-design strategies are required to encourage each mechanism. Other methods for introducing probes into cells which disrupt the natural function or organisation such as microinjection, or electroporation (in which membrane penetration is induced by application of an electrical field) can be undesirable if they cause too much change to the system under study.

4.6.1 Passive diffusion

Passive diffusion requires that the probe is sufficiently lipophilic to be miscible with the membrane, which usually requires ligands with a high ratio of hydrocarbon to polar groups, and that the charge-to-size ratio is low. For instance, monocationic complexes of the type $[Ir(ppy)_2(byp)]^+$ tend to enter cells well regardless of additional substitution, whereas the dicationic complex $[Ru(bpy)_3]^{2+}$ which has an almost identical external surface profile is generally less able to cross membranes and is often only able to enter cells in endosomes from which it is unable to escape easily [2]. While too great a charge can lower lipophilicity and thus hinder permeation through membranes, the ligand set should be selected to reduce the complexes' charge, not to cancel it, as an overall cationic charge is desirable due to membrane potential. The inside of healthy cells is kept at a negative potential compared with the outside by the action of ion pumps which transport ions asymmetrically across the membrane, leading to a higher concentration of anions inside and cations outside,

which generates an electrical potential across the membrane. Thus, any positively charged species which is capable of permeating the membrane will tend to accumulate on the inside of the cell, whereas anions will be expelled. Thus to be taken up by ***passive transport*** ligands should be chosen which are of the appropriate charge and hydrocarbon-to-polar-unit ratio to give complexes which are both ***cationic*** and ***lipophilic***.

4.6.2 Active transport

Active transport is the general term for energy-dependent uptake in which the probe is transported into the cell by one of the many mechanisms cells use to acquire their nutrients and other vital materials. Some of these mechanisms are responsible for the uptake of particular chemicals such as glucose, or B_{12} and are highly specific to these substrates, others are more general and involve 'scooping' in some of the surrounding medium. Targeting specific mechanisms of uptake involves substituting ligands with the natural substrate for the uptake mechanism, or a close mimic. For instance, a rhenium complex appended with a B_{12} unit was used to demonstrate the presence of the cubilin receptor in lung cancer cells [18]. This study exploited an extremely complex uptake mechanism for B_{12} which requires that the B_{12} appended probe is previously bound to intrinsic factor (IF), as cubilin recognised the IF-B_{12} conjugate, and then acts in concert with other transmembrane proteins to transport the IF-B_{12} conjugate into the cell. Other less specific forms of uptake involve, for example macropinocytosis which simply involves engulfing some of the extracellular fluid into pockets of membrane which pinch-off inside the cell. It is difficult to specifically target this mechanism with ligand design, but it can allow the internalisation of highly polar anionic complexes which are not taken up by other means. Occasionally active transport through mechanisms which involve the formation of endosomes may itself be problematical in that while the agent is carried into the interior of the cell, if it is unable to easily and rapidly escape the endosome then it may not reach the target of the study.

4.7 Ligand design for controlling distribution

Once probes have been transported into cells, in order to be useful in providing contrast in images they must not distribute evenly but target the entity under investigation, whether this is a particular organelle, a receptor protein or any other target. Some of the organelles within cells can be targeted by charge as they have their own membranes and membrane potentials associated with them, for instance the interior of mitochondria are negatively charged with respect to the cytoplasm in general, so cationic complexes have a tendency to accumulate within them. Highly specific targeting of organelles can be achieved by reaction and supramolecular chemistry. For instance, imaging agents and sensors can be designed which react to form irreversible covalent bonds to biochemicals which are themselves localised in specific organelles.

4.7.1 Mitochondrial-targeting probes

One particularly attractive organelle for such targeting are the mitochondria. Mitochondria are the cell's powerhouse, generating most of the ATP (energy source) in eukaryotic cells, but also have important roles in differentiation, signalling and cell death. As mitochondrial malfunction is important to many diseases, and as mitochondria may play a role in aging, they are an important target of study in biology and medicine, and imaging agents and sensors which target the mitochondria are of great interest. Mitochondria are separated from the cytoplasm by an outer membrane, and there is a mitochondrial membrane potential (MMP) which makes the inside of mitochondria at a negative potential compared with the surrounding cytoplasm. Thus, cationic complexes will tend to accumulate within mitochondria by charge attraction forces. However, most probes which are simply attracted to mitochondria by charge show low levels of specificity – that is, while there is a good level of probe in mitochondria, there are also high levels in other organelles which

makes image interpretation complex. A more successful design of mitochondrial probe has involved taking advantage of another feature of the mitochondria, which is that they have high concentrations of the reduced form of thiols, particularly reduced glutathione (GSH). As thiols in the reduced form are powerful nucleophiles, probes have been designed to tag thiols in biomolecules with fluorophores using this reactivity with maleimides and iodoacetamides [22] both having been used as the electrophilic partner in the conjugation reaction. Targeting of mitochondria through thiol-reactivity has formed the basis of one of the Mitotracker™ family of fluorophores, in which a xanthene-based probe is substituted with a chloromethyl unit, which acts as the electrophile reacting with GSH, and so on immobilising the probe in the mitochondria. While the commercially available probes are highly selective for mitochondria they have short lifetimes and small Stokes shifts by comparison with transition metal-based systems which emit from triplet states. Thus, a probe has been designed which combines the biochemical properties of the Mitotracker™ dyes [23], incorporating a chloromethyl unit for thiol-reactivity in a rhenium *fac*-tricarbonyl unit as the basic lumophore, which gives large Stokes shift and a long luminescence lifetime [24]. In fact this probe illustrates some of the complications in ligand design for this type of system, as the ligand responsible for the thiol reactivity, a chloromethylpyridine unit, had to be constructed by post-coordination modification of an hydroxymethylpyridine ligand, as, while the chloromethylpyridine unit is commercially available, direct coordination of this to the rhenium *fac*-tricarbonyl core simply resulted in halide abstraction to give the rhenium chloride, rather than coordination of the pyridine nitrogen. However, once formed the chloromethylpyridine complex showed the desired thiol reactivity, and in live cell imaging experiments showed good selectivity for mitochondrial localisation. Interestingly the hydroxymethyl precursor itself shows very good mitochondrial accumulation, significantly higher than would be expected for a simple cationic species [25]. This may indicate that *in vivo* the hydroxy group itself becomes reactive and immobilises the probe in the mitochondria. One possible mechanism for this is phosphorylation to an electrophilic methylene phosphate unit which itself could react with thiols, not unreasonable given the important role of phosphorylation in the biochemistry of mitochondria (Scheme 4.4).

Other transition metal probes which target the mitochondria have been developed based on the isothiocyanate technology discussed below. These cyclometallated iridium complexes react with mitochondrial proteins having accumulated there by charge/lipophilicity attraction. As for the chloromethyl probes it is likely that the mitochondrial accumulation is initially reversible, but that the reaction immobilises the conjugated system in the mitochondria [26].

4.7.2 Nuclear-targeting probes

The nucleus and in particular the nucleoli are important organelles as they harbour the genetic material involved in replication. In order to target the nucleus or nucleoli probes must be able to cross internal membranes, although nuclear pores allow some transport across the nuclear membranes, both by diffusion and by active mechanisms. Typically probes which target the nucleus are of particular interest in that they bind to genetic material, and the majority contain large planar aromatic or heteroaromatic ligands which intercalate or otherwise weakly bind to DNA or RNA. A variety of nuclear targeting probes based around rhenium complexes appended with acridine units have been reported [27, 28] taking advantage of this interaction between planar heterocycles and nucleic acids. A platinum probe which localised in the nucleus has been devised [29] which appears to work by a different mechanism to the planar heterocycles which intercalate with nucleobases. Although targeting nucleoli, and being a planar aromatic structure, it appears not to bind to RNA or DNA, but instead to nuclear proteins or peptides. Gold complexes which show nuclear localisation are known [30]. These incorporate a thionapthalimide ligand, and it is this planar aromatic system which is thought to bind to DNA, along with the lipophilicity of a phosphine unit which is thought to be responsible for their ability to cross the nuclear membrane. In some cases such as in complexes containing the DPPZ ligand (see Section 4.4.3) the interaction of the ligand with the genetic material is detectable as a result of changes to the optical response triggered by this interaction. While ruthenium DNA targeting probes are well developed [1]

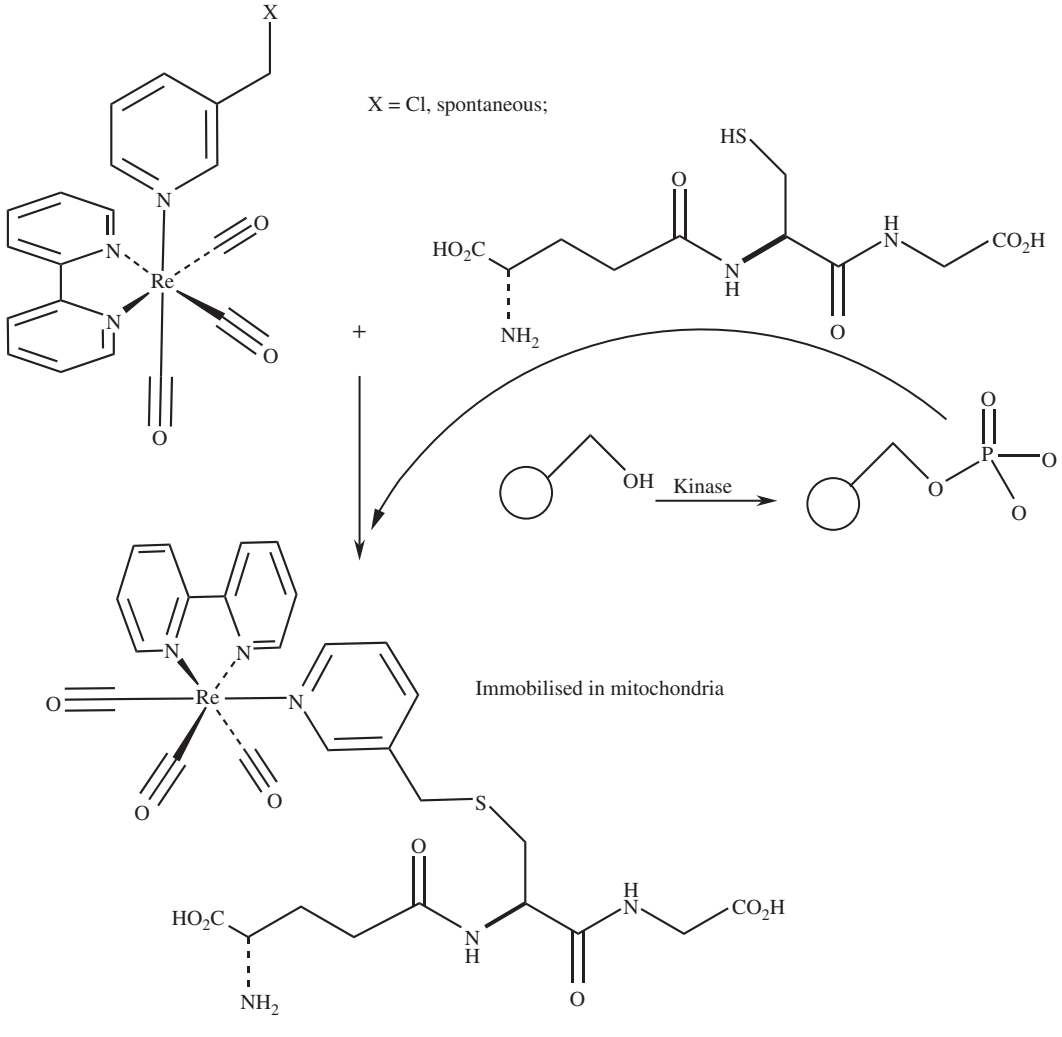

Scheme 4.4 *Mitochondrial selective rhenium probe*

there are other DNA and RNA targeting complexes, and the selectivity of complexes for DNA vs RNA may be sensitive to small changes in ligand structure [2].

4.7.3 Bioconjugation

Bioconjugation – that is, the conjoining of a probe (or other cargo) to a biomolecule – is a powerful technique for controlling uptake and localisation, and there are many examples of the bioconjugation of transition metal imaging agents to biological vectors. The choice of vector is dependent upon the target, and it is rare for the biomolecule to be involved in the coordination chemistry, so in ligand design terms the issue is to design probes which are simple to conjugate to a variety of biomolecules. In many cases this is as simple as to have a reactive handle on an otherwise inert ligand, so the monocarboxylic acid derivatives of bpy, phenanthroline, and so on are used for coupling to amine- or alcohol-appended biomolecules, or the corresponding

amino-ligands act as the nucleophilic components in couplings with biomolecules with a free carboxylate. There is usually an alkyl chain spacer unit included between the ligand/complex and the biomolecule, and the choice of the length of this linker can be unexpectedly important. A short linker may lead to the bulk of the complex compromising the expected biological behaviour of the vector by interfering with its natural interactions with receptors; however, too long a chain can also cause problems as in some cases, when the probe is acting as a sensor, the interaction of the probe with the target of the vector is important for detection of the binding event. The practicalities and approaches for bioconjugation differ with the vector in question but there are certain general considerations and approaches, and a small number of important examples of strategies and vectors will be described.

4.7.3.1 Avidin-biotin conjugation

A popular target for bioconjugation is to append a probe with biotin, a small molecule which has a free carboxylic acid unit allowing easy connection to a ligand, and which binds to the tetrameric protein avidin with one of the strongest natural binding constants known, about 10^{15} [31]. This figure means that at normal concentrations, at equilibrium, it can be assumed that, in effect, all of a biotinylated substrate is bound to avidin. The combination of ease of conjugating biotin to a substrate, plus this strong binding, has led to many applications of the biotin-avidin system in biomedical studies. The binding constants of modified biotins to avidin are easily determined by displacement of the weakly binding (2-(4-hydroxyphenylazo)benzoic acid) (HABA), which when bound to avidin shows a characteristic band at 500 nm. Avidin is an interesting binding protein as it is tetrameric, so can bind up to four of the biotinylated substrates. It has been noted that when certain organic fluorophores are bound to biotin, then exposed to avidin while they show strong binding (determined by HABA assay) the observed fluorescence intensity decreases markedly. This has been attributed to self-quenching, due to the presence of more than one biotinylated fluorophore bound to the same avidin, bringing them within the Förster radius for energy transfer. When two or more fluorophores which have a small Stokes shift are in close special proximity self-quenching can occur via FRET, whereby energy is transferred from a fluorophore in its exited state to one in the ground state, effectively passing the excitation energy forwards and backwards between them [32]. For this to occur they must be both within the Förster radius, and show spectral overlap between the excitation and emission bands, although it should be noted that the process by which energy is transferred between molecules is non-radiative and thus does not represent the emission of a photon from one followed by absorption by another. As a certain proportion of fluorophores relax from the excited state by non-radiative decay, any process which successively transfers the excitation between different molecules leads to a loss of emission intensity as the amount of non-radiative decay is increased. Many *d*-block lumophores have been conjugated to biotin and the results of their exposure to avidin studied, and it has been found that, in general, the effect of avidin binding on these lumophores is the opposite, that is, the intensity of emission increases upon the binding of the biotin unit [1]. The reason why the emission is not lost due to self-quenching is easily explained by the larger Stokes shifts associated with *d*-block lumophores than organic fluorophores; however, the explanation for the increases in intensity is more complex. It is generally accepted that the insertion of a complex in a small binding pocket will protect it from collisional quenching by solvent molecules, particularly water, and thus as less energy is lost to non-radiative mechanisms the intensity of emission will increase. In addition to the increase in intensity, there is generally also an increase in the luminescence lifetime associated with binding, for the same reasons. However, while the increases in both intensity and lifetime strongly indicate protection from quenching, there is some evidence that protection from quenching by $^3O_2$ rather than water is important, at least in some cases [33]. Regardless of the mechanistic detail behind the enhancement of both intensity and lifetime of luminescence upon binding of biotin-appended transition metal lumophores to avidin, it is undoubtedly related to some protection from the environment which is endowed by encapsulation, or semi-encapsulation, upon insertion of the biotin-probe

conjugate into the binding pocket of avidin. The binding pocket of avidin is a channel of coiled peptide ribbon which presents a hydrophobic tube, one end of which emerges from the peptide into the exterior, the other end of which closes with a series of more polar amino acid residues arranged to provide a series of hydrogen bond donors and acceptors to maximise the attractive interactions with biotin. In particular the urea unit of biotin is responsible for a large proportion of the energy driving the binding as its NH and C=O bonds all participate in strong H-bonding with the avidin host. Although less important there are other contributors to the strength of binding, including hydrophobic effects leading to an enthalpic and entropic driving force for the alkyl side chain of biotin to replace water molecules interacting with the hydrophobic channel which leads to the H-bonding domain. In particular, though, it is the combination of a relatively long channel leading to a highly specific strong binding interaction which leads to some of the most important features which must be considered when designing biotinylated *d*-block probes for avidin binding. As mentioned previously, it is essential to include a linker between the complex and the biotin unit but the length of this linker has important consequences for both binding and the observed modulation of photophysical properties which is used to report on the binding event. The HABA assay can be used to independently confirm binding constants in order to quantify the binding-to-modulation effect. It is observed, for instance, in a series of analogous biotinylated iridium complexes in which the length of the linker between the biotin unit and the complex itself has an effect on both the binding constant and the photophysics, but the effect on each is in the opposite sense. It is found that a short linker chain leads to the maximum change in the photophysics, with the maximum increase in emission intensity and lifetime, but also has the lowest binding constant. Conversely, a long linker chain gives the strongest binding but the binding is associated with the smallest change in photophysical properties. These results can be explained by considering which factors are important for strong binding and which are important for a large change in photophysics. Strong binding, as already mentioned, is associated with the ability of the biotin urea unit to hydrogen bond with amino acid residues at the inner terminus of the binding pocket. If the linker chain is too short to allow the biotin unit to reach deep into the binding pocket then the octahedral metal complex, being a large roughly spherical appendage at the other end of the alkyl chain, acts as a stopper preventing the biotin from reaching the optimal position for hydrogen bonding, leading to low binding constants. On the other hand, this case also has the metal complex being pulled into the mouth of the binding pocket as the biotin feels attraction to the hydrogen bonding sites, leading to the maximum level of protection of the excited state from quenching interactions with the environment (be this solvent or dioxygen), and hence the maximum enhancement of photophysical properties. A long linker, however, allows the biotin unit to easily penetrate the binding pocket and achieve the optimal arrangement for strong hydrogen bonding to the host, which leads to the strongest binding constants. However, as the alkyl chain is long compared with the distance from the hydrogen bonding site to the mouth of the binding pocket, the complex is not pulled into the mouth of the pocket, and so only experiences a relatively weak interaction with the surface of the avidin. As much of the surface of the lumophoric complex is thus still able to experience quenching interactions with the environment there is less enhancement of emission lifetime and intensity than is the case with shorter chains (Scheme 4.5) [34–36]. While there are many examples of bioconjugation of Re, Ru and Ir probes with biotin, and there have been intensive studies of binding and luminescence changes in the presence of avidin/streptavidin (the bacterial analogue of avidin), imaging experiments with biotinylated *d*-block probes have not shown a general pattern of uptake and localisation which can be confidently assigned to this bioconjugation [34–36]. While it is clear that probes incorporating a biotin unit are generally taken up well by a range of cell types, it is not easy to determine whether this is due to their triggering a specific response to the biotin or whether general considerations of balancing lipophilicity and polarity are responsible for the uptake. Regardless of this, bioconjugation of *d*-block probes with biotin and the studies of their behaviour upon binding to avidin were an important step in establishing the relative behaviour of metallo-lumophores and traditional organic fluorophores in the biological environment.

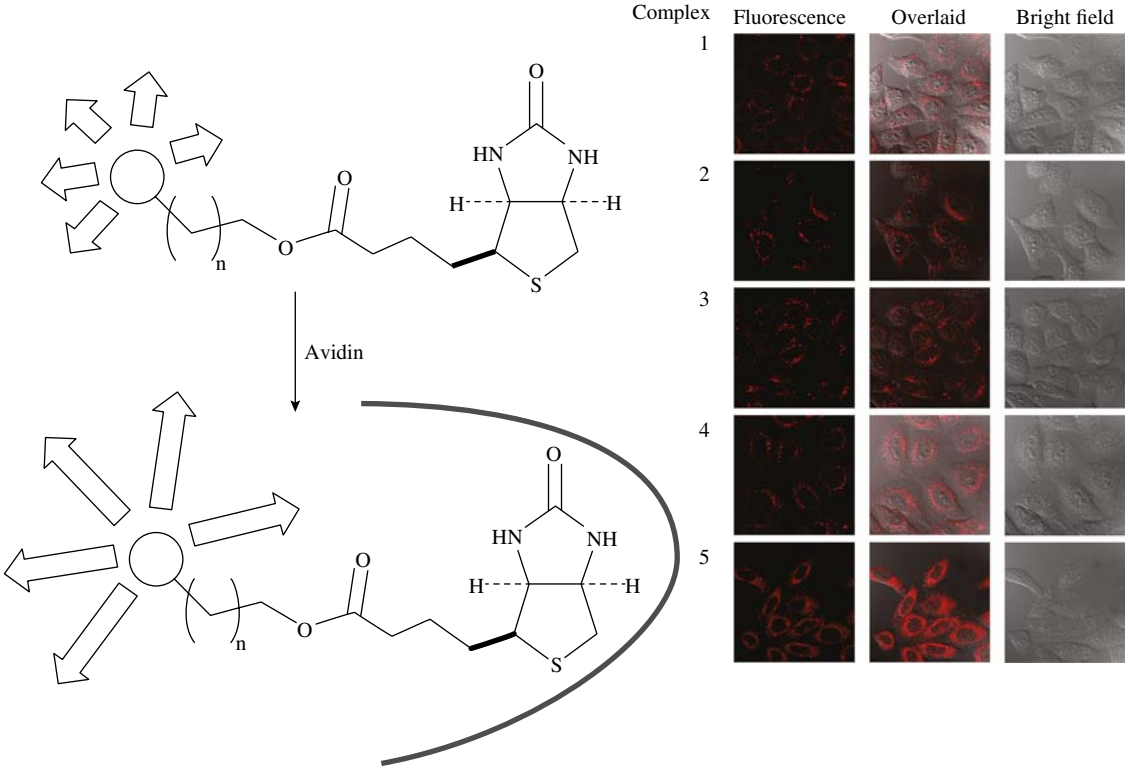

Scheme 4.5 *Luminescence enhancement on avidin binding of biotin-appended lumophores, and cell imaging with biotinylated iridium complexes. Reprinted with permission from Ref. [36]. Copyright © (2009) American Chemical Society. (See plate section for the colour version of the scheme)*

4.7.3.2 Bioconjugation to estradiol and indoles

As well as biotin, a number of transition metal probes have been conjugated to other small-molecule biomarkers known to bind to receptors or trigger uptake pathways. For instance, estradiol binds to the oestrogen receptor (ER) triggering changes including translocation into the nucleus and DNA binding to regulate gene activity. A variety of *d*-block complexes have been conjugated to estradiol and their uptake and localisation studied in imaging experiments. Typically they show excellent cellular uptake, although whether this is due to triggering specific ER-mediated processes or as a result of the lipophilicity of the steroidal unit is less clear [35]. Indole-appended *d*-block probes have also been prepared and their interactions with indole-binding protein BSA studied. Good uptake was observed in imaging experiments of certain examples, apparently by an energy-dependent mechanism [36].

4.7.3.3 The Single Amino Acid Conjugate (SAAC) concept

Although the archetypal rhenium lumophores are based around the $Re(CO)_3$ core with a bpy or related ligand, there is another class of complex in which a tridentate unit consisting of an amine and two heterocycles linked through methylene bridges, such as the dpa ligand, forms the face-capping unit. There has been a large body of work devoted to the development of bioprobes based around this system in which the central amine

is derived from the amine-side chain-substituted amino-acid lysine (Scheme 4.6) [37–39]. In this work the α-amino and acid groups of the lysine are incorporated into a peptide while the ε-amino group forms the central amine of the dpa (or similar ligand). As the metal complex formed is separated from the peptide backbone by a five-carbon chain, the biological function is usually not disrupted by incorporation of this unit, and the chelate effect ensures that a metal fragment can be securely bound by the tridentate dpa-type ligand. This strategy has been applied in particular to the tagging of biomolecules with the $Tc(CO)_3$ fragment which is useful in radioimaging applications, and which requires ligand systems which give complexes with appropriate properties for radiopharmaceuticals: kinetic stability, fast and simple aqueous chemistry, specific activity and control of *in vivo* behaviour. This topic is covered in more detail in Chapter 3 and only a brief background of the properties and use of Tc will be included here with a focus on optical properties of SAAC complexes and approaches to bimodal radio/optical agents using this system. The SAAC system was designed for radioimaging applications, and the parent complexes in which the primary coordination sphere is essentially an N-substituted dpa are non-emissive (or have no metal-based emission). SAAC-Re complexes have been studied as 'cold' models of the Tc analogues to allow the coordination chemistry, aqueous stability, and so on to be studied without the drawbacks of using radioactive material. It should be noted that in addition to the isotope used in radioimaging ^{99m}Tc ($t_{1/2} = 6$ hours) there is also a much longer lived isotope ^{99}Tc ($t\,1/2 = 2 \times 10^5$ years) which has a well-established coordination chemistry which in fact shows some significant differences from that of Re. However, ^{99}Tc is itself a β-emitter and so many groups prefer to use 'cold' Re as the model for ^{99m}Tc as in many cases it provides a safe and reasonably accurate model. As groups were interested in whether appending a SAAC-appended metal core to a peptide would interfere with the peptide's natural function it was important to study these systems with high-resolution imaging methods. SPECT, the radioimaging technique which uses ^{99m}Tc, is ideal for whole-body deep-penetration studies, but suffers from limited resolution, typically in the mm range. While mm resolution is suitable for whole-body scanning and detection of, for example tumours, it is not sufficient to determine whether a modified peptide is still showing the same cellular level behaviour as the parent. Thus, in order to confirm that SAAC-modified peptides retained the expected behaviour in terms of, for example, binding to receptors a luminescent analogue suitable for fluorescence microscopy was required. Therefore an analogue of the dpa SAAC system was devised which would show the same properties with respect to suitability for radioimaging applications, but also show luminescence. The parent SAAC systems in which the heterocyclic ligands are pyridine do not show useful luminescence such as that associated with bpy complexes as the lower conjugation of a single monodentate pyridine unit does not stabilise the electron-transfer process of MLCT as well as in the chelating bpy and so MLCT energy levels are not in the useful part of the spectrum. However, it is possible to lower the MLCT energy level not by linking the pyridines into a bpy, but by retaining the SAAC structure while increasing conjugation by extending the π-system of the individual heterocycles by replacing the pyridines with quinolones. The bisquinolinylamine rhenium complex thus obtained shows long lived (μs) luminescence in the visible region typical of triplet emission with some MLCT character (although mixed with IL states) [40]. The core bisquinolinylamine SAAC unit, SAACQ, was then conjugated to a small peptide sequence fMLF known to target the formyl receptor protein and it was demonstrated that the cellular behaviour of the luminescent rhenium complex was essentially identical with that of a model fluorescent fMLF fragment. To validate the bisquinoline system SAACQ for radioimaging applications the ^{99m}Tc complex was formed and shown to be stable in buffer containing competitive ligands, indicating its suitability for *in vivo* use. While this first example of a luminescent imaging agent based on emissive variations of the SAAC unit required excitation with uv which causes tissue damage, later examples were capable of excitation in the visible region, and indeed showed remarkably variable luminescence [18]. Further discussion of SAAC and related luminescence is included in the bimodal imaging Section 4.9; however, in terms of ease and power of bioconjugation, incorporating a rapid binding unit which forms stable complexes into the side-arm of an amino acid fragment is a supremely attractive approach.

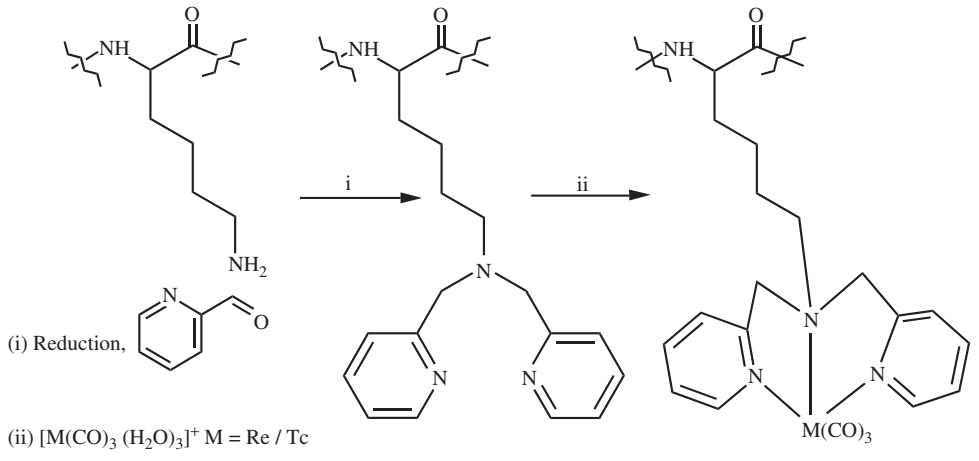

Scheme 4.6 *The SAAC system*

4.7.3.4 Conjugation to PNA

PNA, Peptide Nucleic Acid is a synthetic mimic of DNA/RNA in which the classic sugar-phosphate backbone is replaced with an artificial peptide, each subunit of which bears one of the natural nucleobases [41]. These entities bind well to the complementary strands of the natural oligonucleotides, showing the classic Watson-Crick hydrogen bonding to the complimentary bases, but with enhanced binding as in particular they are neutral and thus do not suffer Coulombic repulsions between strands, and also as they are somewhat hydrophobic [42]. PNAs have been used in many genomic applications due to this strong binding, and to their high (peptide-like) stability in aqueous environments [43]. Bioconjugation of tracers to PNAs is well developed and there are examples of the bioconjugation of PNA with transition metal lumophores based on Re and Ru, usually conjugated to the bpy-type-ligand-derived unit via an amide derivative of a bpy or phen (phen = 1,10-phenanthroline)carboxylate [44]. A rhenium complex in which PNA is conjugated to a SAACQ-ligand has been applied in bioimaging, and good accumulation in the cytoplasm was observed, although the system required electroporation to penetrate the cells, and uv excitation, suggesting limitations for *in vivo* use (Figure 4.5) [45].

A more unusual class of Re-PNA conjugates, in which the emissive unit is neither a bisquinolone of the SAAC type nor a bisimine such as phen/bpy, is the dinuclear Re diazine (pyridazine) complex

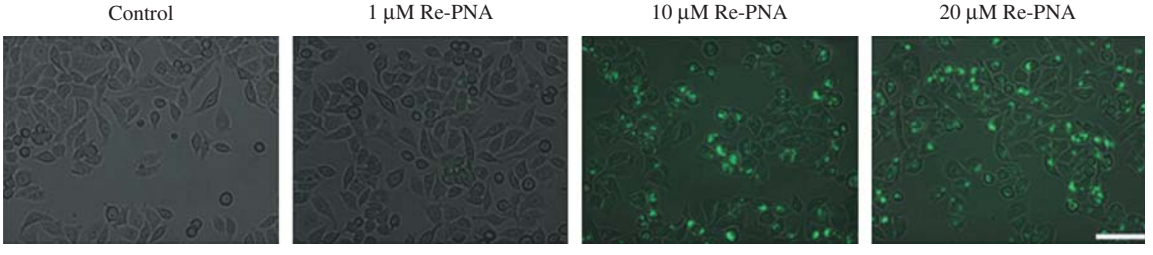

Figure 4.5 *Imaging with Re-PNA SAAQ conjugate. Reproduced from Ref. [45] with permission of The Royal Society of Chemistry. (See plate section for the colour version of this figure)*

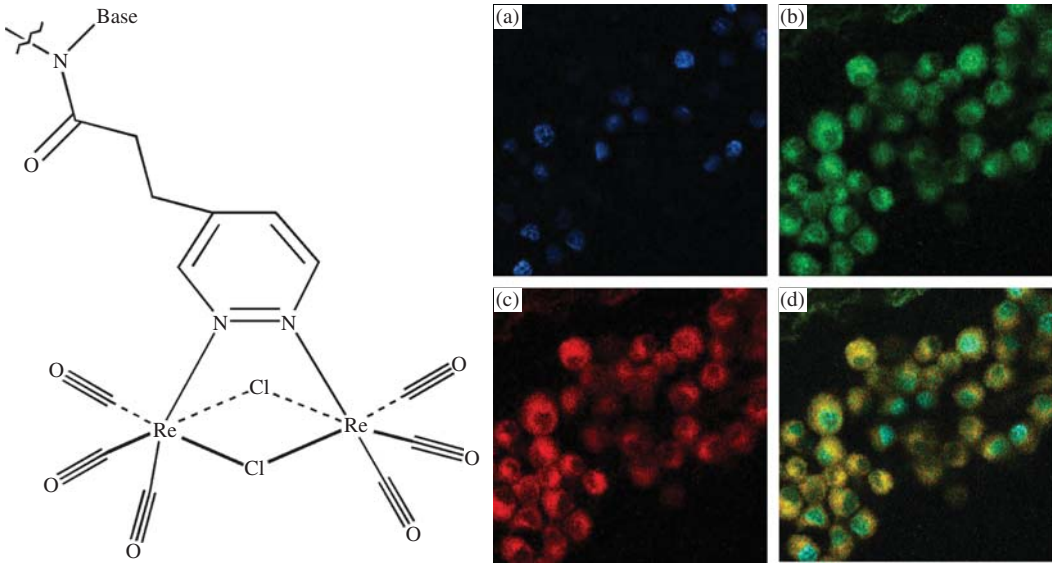

Figure 4.6 *Molecular structure of $[Re_2(\mu\text{-}Cl)_2(CO)_6(\mu\text{-}1,2\text{-diazine})]$ PNA conjugates and luminescence images in macrophages through 485/30 (a), 535/50 (b) and 600/40 (c) bandpass filters and their superposition (d) to show the differential emission. Reprinted with permission from Ref. [46]. Copyright © (2012) American Chemical Society. (See plate section for the colour version of this figure)*

$[Re_2(\mu\text{-}Cl)_2(CO)_6(\mu\text{-}1,2\text{-diazine})])_2$ [46]. These are members of a family of dinuclear halide bridged complexes which has recently been reported [47, 48]. These are remarkable for showing visible wavelength emission from $d\pi(Re)-\pi^*$(diazine) triplet metal-ligand-to-ligand charge transfer excited states (^{3}MLLCT), even though the heterocyclic ligand involved is much smaller than the typical highly conjugated systems involved in MLCT [48, 49]. The complexes prepared from 1,2-diazines bearing alkyl-appended carboxylic acid derivatives also show good luminescence and the carboxylate is attractive for bioconjugation. Interestingly, dimeric complexes of this sort bioconjugated to PNA units showed good cell uptake, with the cellular localisation determined by the nature of the PNA units chosen. Possibly the most remarkable feature of this system is that the observed emission wavelength differs quite substantially depending upon environment. The emission from the nucleus differed markedly from that from the cytoplasm in all cases, indicating a pronounced photophysical effect upon interaction of the complex with DNA (Figure 4.6). While it is to be expected that the PNA appendages would strongly interact with DNA, the effect on the emission characteristics was less expected as the emission emanates from the complex itself, which is rather insulated from the PNA strand, and thus it was not expected to strongly interact with DNA. In fact this effect is even evident in the simple parent complex which has not been PNA appended (although its localisation behaviour is different), which bears an alkyl chain and acid but no nucleobases, suggesting that this behaviour is intrinsic to these dimeric species rather than a function of the PNA unit.

4.7.3.5 Bioconjugation with isothiocyanates

Isothiocyanates are molecules containing the –N=C=S functional group which react with amines to form thioureas, which are robust units, so they have become a popular method for attaching fluorescent tags or other units to the N-terminus of peptides/proteins, or other biomolecules with a reactive primary amine [50]. As

isothiocyanates are themselves synthesised from the reaction of primary amines with thiophosgene, it is possible to convert a complex bearing an aminopyridine or related ligand into an isothiocyanate-functionalised luminescent probe. A number of transition metal lumophores bearing isothiocyanates are known which react with amines to give the thiourea linked conjugates, and the amines used include the important biomolecule BSA. This approach has even been used to link BSA to biotin through a rhenium *fac*-tricarbonyl bpy lumophore [51].

4.8 Selected examples of ligand design for important individual probes

4.8.1 A pH-sensitive ligand to control Ir luminescence

An iridium(III) complex which is based on the usual phenylpyridine bis-cyclometallated core, but using a pyridylbenzimidazole in place of the more typical bpy or phen, shows how changes in one ligand can give particularly useful properties to an otherwise standard probe [52]. The pyridylbenzimidazole unit incorporates an additional nitrogen which is not coordinated to the metal and is free to be protonated, with its pKa (6.6) being in the region which is useful in biological analysis as while it would be unprotonated in most normal healthy tissue types, it lies well within the range of physiological pHs, with the more acidic end of the range often being associated with disease or damage (Scheme 4.7). There is an easily detectable difference in luminescence between the unprotonated and protonated forms ($\lambda_{max\ em}$: 521, 590 nm and τ: 5.8, 5.6 μs respectively) so application is possible not only in imaging, but using the ability of luminescence to be modulated by the chemical environment and simultaneously act as a sensor. This probe showed good uptake in CHO cells and was able to report that the local pH in the organelles was well above 6.6 as most of the complex is unprotonated, with the centre of the emission showing only a slight red-shift from the unprotonated form. This was the first study to demonstrate that co-localisation experiments could be achieved using temporal rather than wavelength methods. Co-localisation is a technique for determining the site of localisation of a new agent by comparison with the localisation of a well established fluorophore. A cell sample is incubated with the two agents simultaneously then imaged to determine the localisation of each agent. Traditionally the emission from the two agents with different emission maxima is distinguished by using filters or monochromation to

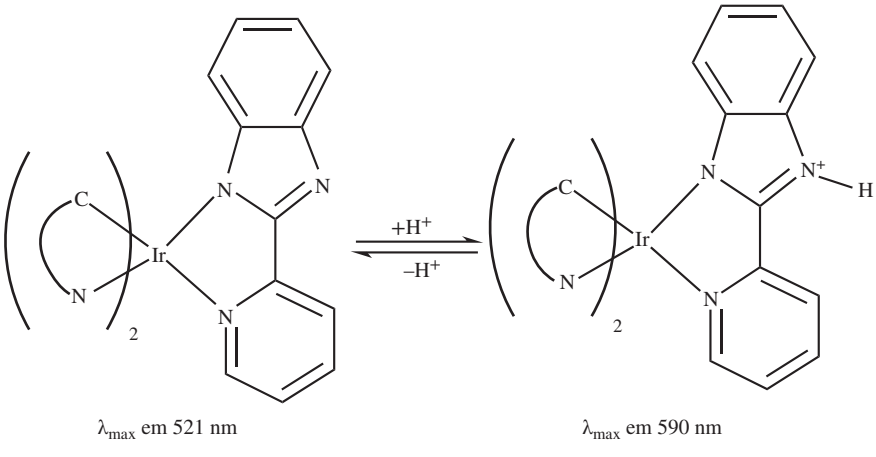

Scheme 4.7 *pH sensitivity of pyridyl benzimidazole Ir probe*

separate the two signals, which are used to generate intensity map images in different colours. Overlap of the signal from each agent is known as co-localisation and illustrated with a merged image showing colour mixing. This Ir complex was used to demonstrate a new technique whereby a co-stain with a much shorter lifetime (Hoescht 33342, 3.6 ns) was co-incubated with the Ir complex, and images derived from the (much brighter) Hoescht agent were acquired with no time delay, and then images showing only the Ir complex were acquired after a 10 ns delay. In this case (also the first example of time-resolved imaging with an Ir probe) the two agents were demonstrated not to co-localise but to separately occupy the nucleus (Hoescht) and cycloplasmic organelles (Ir probe).

4.8.2 Dimeric NHC ligands for gold cyclophanes

One example of an imaging agent based on a phenomenon which is mechanistically distinct from the MLCT and ligand-based transitions which characterise most of the *d*-block lumophores involves the application of dimeric gold complexes. There is another chapter devoted to the biological action of gold complexes, but it is obvious that an ability to image the site of localisation of any drug on a subcellular level is very useful in attempting to understand the mode of action. In this context, when a family of dimeric gold complexes emerged as promising leads an interesting possibility to combine imaging and therapy was identified. The gold centres in these complexes were held in a well defined special relationship by a linear arrangement of NHC donors, themselves defining a cyclophane (Figure 4.7). Complexes or materials in which two or more Au^I centres are close to each other [53] display emission from bands which cannot be assigned to ligand- or metal-based transitions, or conventional MLCT/LMCT, and which are assigned as involving a metal-metal orbital and MMLCT or LMMCT states are invoked. These states arise from relativistic effects in which the heavy Au ion causes an acceleration of the valence electrons, increasing effective nuclear charge [54, 55]. The effect is to mean that the less diffuse s and p orbitals contract and are stabilised whereas the more diffuse d and f orbitals expand due to the s and p orbitals more effectively shielding the nuclear charge. In this state, Au-Au interactions are possible even in a d^{10} Au^I complex as the filled $5d_z^2$ orbital is now expanded and destabilised, and mixes with the empty 6s and $6p_z$ to form new orbitals, of lower energy. Thus the LUMO is reduced in energy and the LMMCT/MMLCT bands red-shifted [56], although a raising of HOMO levels can also be involved [57]. The original complexes had rather long linkers between the NHC-Au-NHC units, which precluded efficient Au-Au orbital overlap, but reducing the linker length led to a red-shift of both excitation

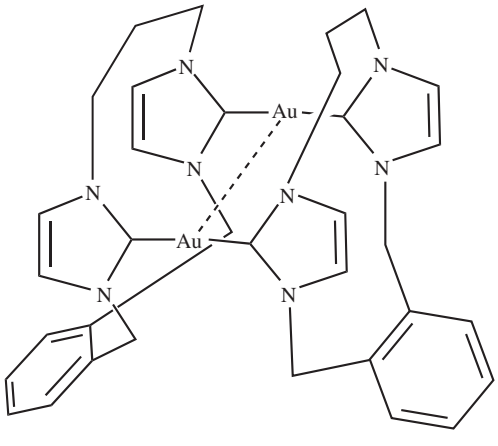

Figure 4.7 *Au-Au probe*

and emission, making them suitable for cell imaging [58]. This system exemplifies how ligand design can be used to tune the photophysical properties of an otherwise unsuitable system to allow cell imaging to reveal otherwise obscure information about the behaviour of pharmaceuticals. There are very few other examples of gold(I) imaging agents [59], and it is less clear that these involve Au-Au-based transitions.

4.9 Transition metal probes incorporating or capable of more than one imaging mode

Most transition metal optical probes have been applied in fluorescence microscopy, which is an important and powerful technique in diagnostics and medical imaging due to the level of detail which it can reveal. However, while a very high degree of resolution is available in optical imaging, allowing imaging of sub-cellular structures on the low micron scale, as the tissue penetration of visible wavelengths limits the general applicability of optical techniques in whole-body studies, in clinical applications this technique is limited to examining cells grown or isolated from a blood or other fluid sample, or tissue samples removed for biopsy, and other techniques such as must be used to provide different levels of penetration and detail [60–62]. In many cases this means that a patient undergoes a different scanning or imaging technique (e.g. PET, MRI and X-ray) which is capable of deep penetration of tissue for the whole body scan to pinpoint the site of, for example a tumour, and then an excised sample must be stained with a fluorophore for the high resolution microscopy technique to allow investigation of the disease at sub-cellular level. The ideal scenario would be one in which a single scan could identify the site of the disease in the whole body scan, then focus in to reveal the microscopic detail of the disease and allow accurate diagnosis including biochemical and subcellular detail. There are technical reasons to do with the basic physics behind MRI, PET, and so on which means that this is not only currently unrealised, but actually impossible with direct application of the methods now available. In principle, tissue-penetrating NIR fluorescence imaging has the potential to realise this combination of macro- and microscopic imaging (with some loss of resolution compared with visible light due to the longer wavelengths), but the closest currently practical approach is to accept that two imaging modalities will be required, and to design a probe which is capable of providing contrast in each of them. The field of bimodal imaging has been reviewed before [63, 64] and the principle advantages and concerns spelled out in great detail, so only those points relevant to ligand design with *d*-block probes will be included in this discussion. The advantages of a bimodal imaging agent to the patient are obvious in that if a single chemical species can assist in the whole body probe and then the microscopy then this limits the number of injections and exposure to potentially toxic chemical species which the patient must undergo. In terms of the accuracy of the diagnosis, injection of a single agent which is used to identify the site for removal of a biopsy sample, followed by microscopic imaging of the sample using the same agent removes the possibility for many false positive and false negative results. For instance, if a mono-modal whole-body technique identifies a growth, and a biopsy sample is removed which is not representative of the area, then staining of this sample with a second agent followed by microscopy could indicate that the tissue is normal, leading to an inaccurate diagnosis. If the agent that had identified the growth by the whole-body technique were also fluorescent, then as no second staining would be undertaken a sample removed from the wrong area of the body would not contain the fluorophore and the error would be obvious. Thus *d*-block imaging agents that are also capable of application in PET, SPECT or MRI are of great interest as potential bimodal imaging agents.

4.9.1 Bimodal MRI/optical probes

While bimodal MRI/fluorescent agents are attractive there are technical issues which make the design of ligands and complexes which could provide such agents challenging concerning both retaining the efficacy in each mode in a combined agent, and the relative doses required for each modality. MRI contrast agents usually

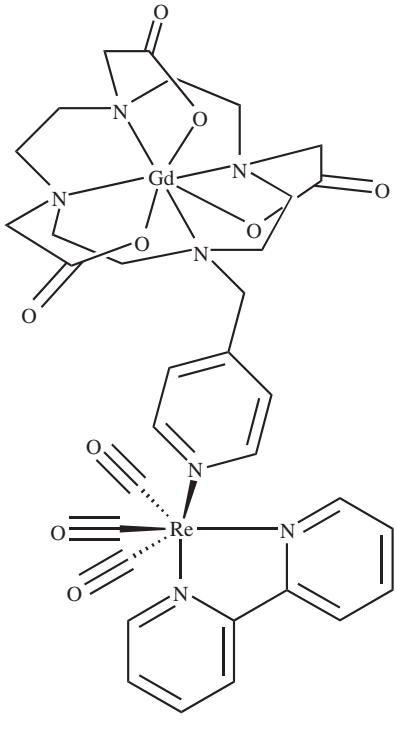

Figure 4.8 *Re-Gd conjugate for MRI/optical imaging*

rely upon paramagnetic metal complexes to enhance relaxivity in surrounding water molecules in the patient and so provide information about the area in which the agent is localised [65]. There have been attempts to develop agents based on nanomaterials, especially lanthanide-based units which can be both highly paramagnetic and luminescent [66]. Unfortunately, many paramagnetic complexes are efficient quenchers of *d*-block luminescence, making combined MRI/luminescent agents based on these examples challenging targets. However, the dominant agents currently used for enhancing contrast in MRI are based around gadolinium which due to its electronic configuration usually does not quench *d*-block luminescence, although the relative doses used in MRI contrast are orders of magnitude higher than for fluorescence microscopy. Mixed *d*- and *f*-block multinuclear complexes are known which show intense metal-centered emission, combined with high relaxivity, which have the potential to be applied as bimodal MRI/fluorescence imaging agents. A combination of a gadolinium complex appended with a pyridine side-chain, with a rhenium bpy fragment, gives a potential bimodal agent (Figure 4.8) with a luminescence lifetime of 240 ns, which is long enough to allow differentiation from autofluorescence, and a relaxivity of 8.6 mM^{-1} s^{-1} at 500 MHz (although this figure is sensitive to the presence of phosphate which competes for Gd binding with the water necessary for high relaxivity) [67].

4.9.2 Bimodal radio/optical probes

Potentially more promising as the two modalities are better suited to combination are combined fluorescence- and radio-imaging agents [68]. Not only is there no mechanistic interference between the fundamental basis of radiation and fluorescence, as there is from the common quenching of fluorescence excited states by unpaired electrons, but in fact the two techniques are (in the final steps) detected by the

same technology so can share a common platform. A typical radioimaging arrangement involves emitted γ-rays striking a scintillation crystal, which itself then emits photons of visible light, which are then enhanced with a photomultiplier and detected by conversion to an electrical signal *via* a camera. While this is a very different approach to confocal microscopy the common point of photon detection has been used to develop combined radio- and fluorescence-detection [69]. Additionally the dosage required for radioimaging is very low (typically pm). While fluorescence microscopy usually operates at somewhat higher concentrations, time-resolved techniques which remove background autofluorescence can allow detection at similar concentrations, and even single-molecule detection is possible with fluorescence. There are a number of reports of bimodal radio-fluorescence imaging agents which have been developed by the simple conjugation of an organic fluorophore with a binding site for a radioactive metal isotope [70–72], but there is a drawback to this approach. There is an intrinsic advantage to systems which are bimodal as a result of dual properties of a single chemical species (single entity agents) as oppose to those which simply ligate two imaging agents of different structures, each of which is an imaging agent for a different modality. If the bimodality results from combining separate whole-body and fluorescent probes, then there is a risk that *in vivo* metabolic processes may cleave the tether which binds the two entities and they may accumulate in different parts of the body. If this occurs quickly then the mistake is obvious, as a tissue sample from the area highlighted by the whole-body agent will show no luminescence; however, more subtle problems can occur if breakdown happens slowly. If the combined agents remain attached until they reach the general site of interest, but then slowly are cleaved then they may show different local concentrations related to their own change and lipophilicity which could have serious consequences for diagnosis. Even in the case of rapid breakdown in which the cells excised show no luminescence, this makes the use of sensor on/off probes impossible, as the result of the other imaging modality can no longer be taken to indicate the presence of the luminescent agent. The ideal system would be one in which the agents stopped working in their respective modalities, or dramatically altered their responses if they became separated, and as radioisotopes continue to emit whatever their chemical environment it is likely that detection of the breakdown must be achieved through a change in luminescence. In this respect probes which rely upon a radioisotope of a metal for PET/SPECT imaging and MLCT for the luminescence mode could be the ideal bimodal imaging agents. The biodistribution of the radioisotope would be controlled by the lipophilicity, and so on of the ligand system, targeting the organ or disease of interest, and in the event of breakdown (which would otherwise give misleading results as the free metal ion would have unexpected distribution) it would be obvious that the metal ion was no longer associated with ligand as luminescence would cease.

The analogy between Tc and Re has already been discussed and many probes of the SAACQ type have been proposed as potential bimodal imaging agents, following the first example 'bridging the gap' between radio- and optical detection [40]. In most cases the luminescence is demonstrated in a 'cold' Re model and radio-detection with Tc, and in some cases there have been rigorous studies to show the accuracy of the Re/Tc analogy in terms of the solubility, charge, lipophilicity and stability of each agent, which should ensure that in any real-world application it could be guaranteed that the Tc and Re species would accumulate in the same areas. Whether mixed Tc and Re agents should be considered truly bimodal is a moot point, as in terms of licensing and testing two chemical species are involved, but the luminescence of Tc SAAC species themselves is not known. There is in fact little known of the luminescence of Tc-based MLCT systems at all, and no potentially bimodal examples of Tc-bpy complexes analogous to the well-known fluorophores are known [73]. One system has been reported which combines Re-bpy luminescence with the ability to bind other metals, including Cu which has a useful long lived PET isotope ^{64}Cu. This system is in fact a trimeric cage based around terpy (terpy = 2,2′;6′,2″-terpyridine), which coordinates in a bidentate mode, with each of the potentially tridentate ligands having a pendant vacant pyridine donor which together form a macrocylic Cu binding site [74]. This system is interesting in that the neutral, empty form is not able to penetrate cells, but the cationic 'loaded' form incorporating metal salts does, making it a potential bimodal uptake system

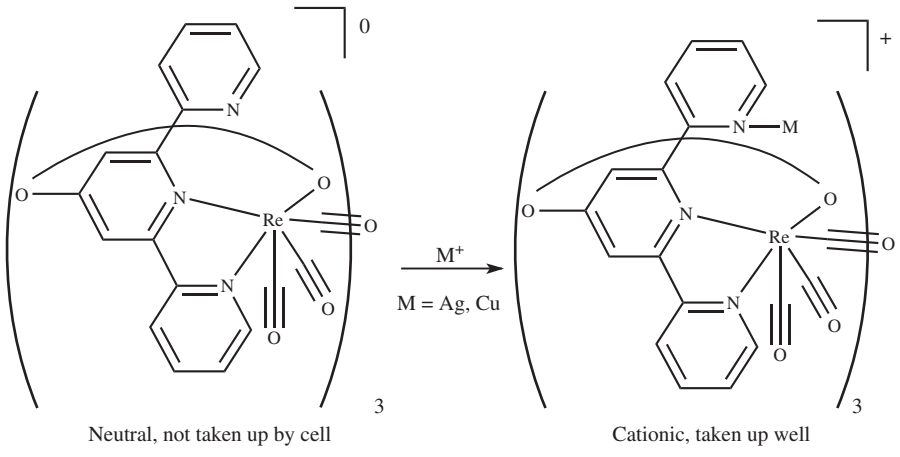

Scheme 4.8 *Re/Cu conjugate for PET/Fluorescence imaging*

for PET active metal ions (Scheme 4.8) [75]. However, as the luminescence originates from the cage and the PET activity would come from a ligated metal, decomplexation would give a free PET-active metal and an empty cage unit which would still be emissive, leading to possible complications.

4.9.3 Bimodal IR/optical probes

One example of a truly single entity bimodal imaging agent uses the C-O stretching band of a $Re(CO)_3$ fragment in IR microscopy while simultaneously using the MLCT emission which arises from its coordination to a heterocyclic ligand. IR microscopy of living cells is an established technique [76] but often relies upon the IR active bands in the biological material for contrast. This approach allows for the combination of microscopy and IR spectroscopy to be used to probe the biology of the system in question [77] but has now been combined with an agent based on a rhenium complex which is IR active and luminescent in a bimodal imaging experiment. The ligand in this case is a triazole-substituted pyridine, prepared by a copper-mediated cyclisation of a diazide and ethynylpyridine. This unusual ligand gives a rhenium *fac*-tricarbonyl complex which gives similar luminescent properties to the better known bpy analogues with a large Stokes shift and emitting at 510 nm. This probe has been termed a Single Core Multimodal Probe for Imaging (SCoMPI) and in breast cancer cells fluorescence microscopy using the MLCT bands and Synchrotron FTIR SpectroMicroscopy (SR-FTIR-SM) with the Re-CO were both used to visualise localisation in the Golgi apparatus. In this case the N_3 stretch of the azide unit was also able to be used as an IR probe, as N_3 also gives a band in the transparent window of biological material between about 1800–2300 cm^{-1} [78]. The lower resolution of IR microscopy compared with visible wavelength fluorescence can be observed in Figure 4.9.

4.10 Conclusions and prospects

Transition metal complexes have already found a niche in bioimaging, not replacing the traditional organic fluorophores, but complementing them with attractive properties such as large Stokes shifts and long lifetimes

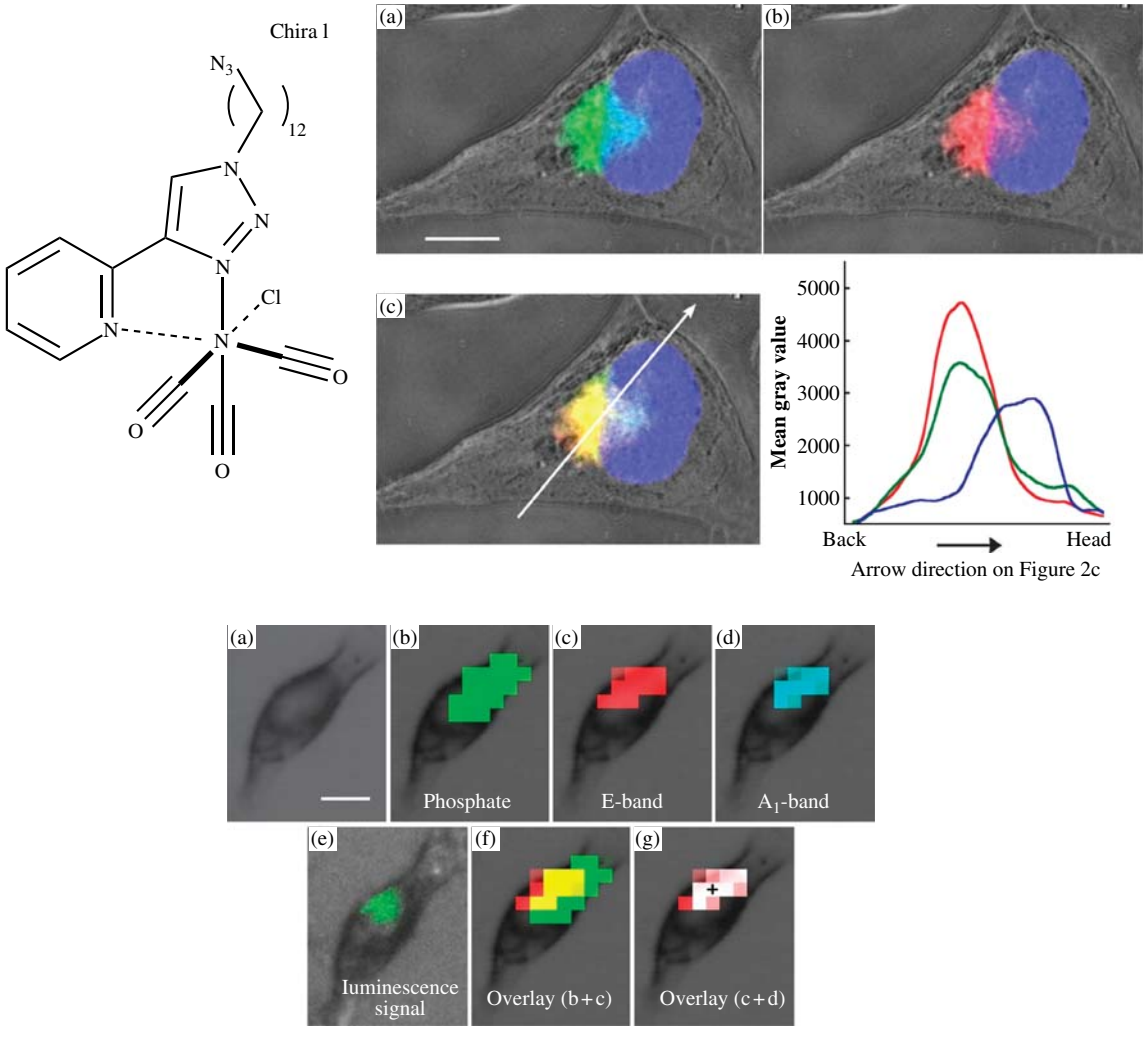

Figure 4.9 *SCoMPI Re-CO probe for IR/fluorescence imaging (a) fluorescence microscopy showing co-localisation with Golgi stain (b) and IR microscopy (c). Reproduced from Ref. [78] with permission of The Royal Society of Chemistry. (See plate section for the colour version of this figure)*

allowing new techniques such as differential excitation and time-resolved methods to be developed. The different mechanisms of excitation and emission found in each complex render them suitable to particular sensing or imaging roles, such as triplet extinction being useful in oxygen sensing, and it is the diverse range of charge transfer and other mechanisms, and electronic states available with *d*-block complexes, which will ensure their role in the design of advanced biological probes. As these more specialist applications become more advanced and touch on real-world issues such as diagnosis, ligand design will be crucial in developing truly useful agents.

Abbreviations

THF	Tetrahydrofuran
THT	Tetrahydrothiphene
ATP	Adenosine triphosphate
FRET	Förster Resonance Energy Transfer
BSA	Bovine Serum Albumin
SPECT	Single Photon Emission Computerised Tomography
SAACQ	Single Amino Acid Chelate Quinoline
fMLF	N-Formyl-Met-Leu-Phe
CHO	Chinese Hamster Ovarian
NHC	N-Heterocyclic Carbene
PET	Positron Emission Tomography
LUMO	Lowest Unoccupied Molecular Orbital
HOMO	Highest Occupied Molecular Orbital
LMCT	Ligand To Metal Charge Transfer
MMLCT	Metal-Metal to Ligand Charge Transfer
LMMCT	Ligand To Metal-Metal Charge Transfer
MRI	Magnetic Resonance Imaging
SAAC	Single Amino Acid Chelate
SAAQ	Single Amino Acid Quinoline
FTIR	Fourier Transform Infra Red
DPA	Dipicolylamine
Phbpy	Phenylbipyridine

References

1. Fernández-Moreira, V., Thorp-Greenwood, F.L. and Coogan, M.P. (2010) Application of d6 transition metal complexes in fluorescence cell imaging. *Chem. Commun.*, **46**, 186–202.
2. Balasingham, R.G., Coogan, M.P. and Thorp-Greenwood, F.L. (2011) Complexes in context: attempting to control the cellular uptake and localisation of rhenium fac-tricarbonyl polypyridyl complexes. *Dalton Trans.*, **40**, 11663–11674.
3. Coleman, A., Brennan, C., Vos, J.G. and Pryce, M.T. (2008) Photophysical properties and applications of Re(I) and Re(I)–Ru(II) carbonyl polypyridyl complexes. *Coord. Chem. Rev.*, **252**, 2585–2595.
4. Amoroso, A.J., Coogan, M.P., Dunne, J.E. *et al*. (2007) Rhenium fac tricarbonyl bisimine complexes: biologically useful fluorochromes for cell imaging applications. *Chem. Commun.*, 3066–3068.
5. Juris, A., Balzani, V., Barigellatti, F. *et al*. (1988) Ruthenium(II) polypyridine complexes: photophysics, photochemistry, electrochemistry, and chemiluminescence. *Coord. Chem. Rev.*, **84**, 85–277.
6. Yang, T.S., Xia, A., Liu, Q. *et al*. (2011) Polymer nanoparticles with an embedded phosphorescent osmium(II) complex for cell imaging. *J. Mater. Chem.*, **21**, 5360–5367.
7. Thorp-Greenwood, F.L. (2012) An introduction to organometallic complexes in fluorescence cell imaging: current applications and future prospects. *Organometallics*, **31**, 5686–5692.
8. Lo, K.K.-W., Li, S.P.-Y. and Zhang, K.Y. (2011) Development of luminescent iridium(III) polypyridine complexes as chemical and biological probes. *New J. Chem.*, **35**, 265–287.
9. Evans, R.C., Douglas, P. and Winscom, C.J. (2006) Coordination complexes exhibiting room-temperature phosphorescence: evaluation of their suitability as triplet emitters for light-emitting diodes. *Coord. Chem. Rev.*, **250**, 2093–2126.
10. Zhao, Q., Huang, C.H. and Li, F.Y. (2011) Phosphorescent heavy-metal complexes for bioimaging. *Chem. Soc. Rev.*, **40**, 2508–2524.

11. Worl, L.A., Duesing, R., Chen, P. *et al*. (1991) Photophysical properties of polypyridyl carbonyl complexes of rhenium(I). *Dalton Trans.*, 849–858.
12. Lowry, M.S., Hudson, W.R., Pascal, R.A. and Bernhard, S. (2004) Accelerated luminophore discovery through combinatorial synthesis. *J. Am. Chem. Soc.*, **126**, 14129–14135.
13. Henry, K.E., Balasingham, R.G., Vortherms, A.R. *et al*. (2013) Emission wavelength variation with changes in excitation in a Re(I)–bisthiazole ligand complex that breaks the Kasha–Vavilov rule. *Chem. Sci.*, **4**, 2490–2495.
14. Keyes, T.E. (1998) Evidence for the presence of dual emission in a ruthenium(II) polypyridyl mixed-ligand complex. *Chem. Commun.*, 889–894.
15. Glazer, E.C., Magde, C. and Tor, Y. (2005) Ru(II) complexes that break the rules: structural features regulating dual emission. *J. Am. Chem. Soc.*, **127**, 4190–4192.
16. Lo, K.K.-W., Zhang, K.Y., Leung, S.-K. and Tang, M.–.C. (2008) Exploitation of the dual-emissive properties of cyclometalated iridium(III)–polypyridine complexes in the development of luminescent biological probes. *Angew. Chem. Int. Ed.*, **7**, 2213–2216.
17. Morimoto, T., Ito, M., Koike, K. *et al*. (2012) Dual emission from rhenium(I) complexes induced by an interligand aromatic interaction. *Chem. Eur. J.*, **18**, 3292–3304.
18. Vortherms, A.R., Kahkoska, A.R., Rabideau, A.E. *et al*. (2011) A water soluble vitamin B12-Re(I) fluorescent conjugate for cell uptake screens: use in the detection of cubilin in the lung cancer line A549. *Chem. Commun.*, **47**, 9792–9794.
19. Bacon, J.R. and Demas, J.N. (1987) Determination of oxygen concentrations by luminescence quenching of a polymerimmobilized transition-metal complex. *Anal. Chem.*, **59**, 2780–2785.
20. Rosenzweig, Z. and Kopelman, R. (1995) Development of a submicrometer optical fiber oxygen sensor. *Anal. Chem.*, **67**, 2650–2654.
21. A.E. Friedman, J.-C. Chambron, J.-P. Sauvage, *et al*., Molecular 'Light Switch' for DNA: Ru(bpy)2(dppz)2+, *J. Am. Chem. Soc.*, **112**, 4960–4962 (1990).
22. Castellano, F.N., Dattelbaum, J.D. and Lakowicz, J.R. (1998) Long-lifetime Ru(II) complexes as labeling reagents for sulfhydryl groups. *Anal. Biochem.*, **255**, 165–170.
23. Minamikawa, T., Sriratana, A., Williams, D.A. *et al*. (1999) Chloromethyl-X-rosamine (MitoTracker Red) photosensitises mitochondria and induces apoptosis in intact human cells. *J. Cell Sci.*, **112**, 2419–2430.
24. Amoroso, A.J., Coogan, M.P., Dunne, J.E. *et al*. (2008) 3-Chloromethylpyridyl bipyridine fac-tricarbon rhenium: a thiol-reactive luminophore for fluorescence microscopy accumulates in mitochondria. *New J. Chem.*, **32**, 1097–1102.
25. Fernández-Moreira, V., Thorp-Greenwood, F.L., Amoroso, A.J. *et al*. (2010) Uptake and localisation of rhenium fac-tricarbonyl polypyridyls in fluorescent cell imaging experiments. *Org. Biomol. Chem.*, **8**, 3888–3901.
26. Wang, B., Liang, Y., Dong, H. *et al*. (2012) A luminescent cyclometalated iridium(III) complex accumulates in mitochondria and induces mitochondrial shortening by conjugation to specific protein targets. *ChemBioChem*, **13**, 2729–2737.
27. N. Agorastos, L. Borsig, A., Renard *et al*., Cell-specific and nuclear targeting with [M(CO)3]+ (M = ^{99m}Tc, Re)-based complexes conjugated to acridine orange and bombesin, *Chem. Eur. J.*, **13**, 3842–3852 (2007).
28. Esteves, T., Xavier, C., Gama, S. *et al*. (2010) Tricarbonyl M(I) (M = Re, ^{99m}Tc) complexes bearing acridine fluorophores: synthesis, characterization, DNA interaction studies and nuclear targeting. *Org. Biomol. Chem.*, **8**, 4104–4116.
29. Koo, C.K., Leo, K.Y., Wong, K.L. *et al*. (2010) A Triphenylphosphonium-Functionalised Cyclometalated Platinum(II) Complex as a Nucleolus-Specific Two-Photon Molecular Dye. *Chem. Eur. J.*, **16**, 3942–3950.
30. Bagowski, C.P., You, Y., Scheffler, H. *et al*. (2009) Naphthalimide gold(I) phosphine complexes as anticancer metallodrugs. *Dalton Trans.*, 10799–10805.
31. Diamandis, E.P. and Christopoulos, T.K. (1991) The biotin-(strept)avidin system: principles and applications in biotechnology. *Clin. Chem.*, **37**, 625–636.
32. Lakowicz, J.R. (ed) (2006) *Principles of Fluorescence Spectroscopy*, Springer, New York.
33. Soller, T., Ringler, M., Wunderlich, M. *et al*. (2008) Streptavidin reduces oxygen quenching of biotinylated ruthenium(II) and palladium(II) complexes. *J. Phys. Chem. B*, **112**, 12824–12826.
34. Lo, K.K.-W. and Lau, J.S.-Y. (2007) Cyclometalated iridium(III) diimine bis(biotin) complexes as the first luminescent biotin-based cross-linkers for avidin. *Inorg. Chem.*, **46**, 700–709.

35. Lo, K.K.W., Lee, T.K.M., Lau, J.S.Y. *et al*. (2008) Luminescent biological probes derived from ruthenium(II) estradiol polypyridine complexes. *Inorg. Chem.*, **47**, 200–208.
36. Zhang, K.Y. and Lo, K.K.-W. (2009) Synthesis, properties, and live-cell imaging studies of luminescent cyclometalated iridium(III) polypyridine complexes containing two or three biotin pendants. *Inorg. Chem.*, **48**, 6011–6025.
37. Levadala, M.K., Taggart, L., Ryan, L. *et al*. (2004) A new strategy for the preparation of peptide-targeted radiopharmaceuticals based on an Fmoc-lysine-derived single amino acid chelate (SAAC). Automated solid-phase synthesis, NMR characterization, and in vitro screening of fMLF(SAAC)G and fMLF[(SAAC-Re(CO)3)+]G. *Bioconjugate Chem.*, **15**, 128–136.
38. Banerjee, S.R., Babich, J.W. and Zubieta, J. (2005) Site directed maleimide bifunctional chelators for the M(CO)3+ core (M =(99m)Tc, Re). *Chem. Commun.*, 1784–1786.
39. Bartoloma, M., Valliant, J., Maresca, K. *et al*., (2009) Single amino acid chelates (SAAC): a strategy for the design of technetium and rhenium radiopharmaceuticals. *Chem. Commun.*, 493–512.
40. Stephenson, K.A., Banerjee, S.R., Besenger, T. *et al*. (2004) Bridging the gap between in vitro and in vivo imaging: isostructural Re and 99mTc complexes for correlating fluorescence and radioimaging studies. *J. Am. Chem. Soc.*, **126**, 8598–8599.
41. Nielsen, P.E., Egholm, M., Berg, R.H. and Buchardt, O. (1991) Sequence-selective recognition of DNA by strand displacement with a thymine-substituted polyamide. *Science*, **254**, 1497–1500.
42. Egholm, M., Buchardt, O., Christensen, L. *et al*., (1993) PNA hybridizes to complementary oligonucleotides obeying the Watson-Crick hydrogen-bonding rules. *Nature*, **365**, 566–568.
43. Nielsen, P.E. (2001) Peptide nucleic acid: a versatile tool in genetic diagnostics and molecular biology. *Curr. Opin. Biotechnol.*, **12**, 16–20.
44. Joshi, T., Barbante, G.J., Francis, P.S. *et al*. (2011) Electrochemiluminescent peptide nucleic acid-like monomers containing Ru(II)-dipyridoquinoxaline and Ru(II)-dipyridophenazine complexes. *Inorg. Chem.*, **50**, 12172–12183.
45. Gasser, G., Pinto, A., Neumann, S. *et al*. (2012) Synthesis, characterisation and bioimaging of a fluorescent rhenium-containing PNA bioconjugate. *Dalton Trans.*, **41**, 2304–2313.
46. Mari, C., Panigati, M., Alfonso, L.D. *et al*. (2012) NMR spectroscopy in bioinorganic chemistry. *Organometallics*, **31**, 5918–5928.
47. Panigati, M., Mauro, M., Donghi, D. *et al*., (2012) Luminescent dinuclear rhenium(I) complexes containing bridging 1,2-diazine ligands: photophysical properties and application. *Coord. Chem. Rev.*, **256**, 1621–1643.
48. Donghi, D., D'Alfonso, G., Mauro, M. *et al*., (2008) A new class of luminescent tricarbonyl rhenium(I) complexes containing bridging 1,2–diazine ligands: electrochemical, photophysical and computational characterization. *Inorg. Chem.*, **47**, 4243–4255.
49. Ferri, E., Donghi, D., Panigati, M. *et al*., (2010) Luminescent conjugates between dinuclear rhenium(I) complexes and peptide nucleic acids (PNA) for cell imaging and DNA targeting. *Chem. Commun.*, **46**, 6255–6257.
50. The, T.H. and Feltkamp, T.E.W. (1970) Conjugation of fluorescein isothiocyanate to antibodies. I. Experiments on the conditions of conjugation. *Immunology*, **18**, 865–873.
51. Lo, K.K.-W., Louie, M.-W., Sze, K.-S. and Lau, J.S.-Y. (2008) Rhenium(I) polypyridine biotin isothiocyanate complexes as the first luminescent biotinylation reagents: synthesis, photophysical properties, biological labeling, cytotoxicity, and imaging studies. *Inorg. Chem.*, **47**, 602–611.
52. Murphy, L., Congreve, A., Palsson, L.-O. and Williams, J.A.G. (2010) The time domain in co-stained cell imaging: time-resolved emission imaging microscopy using a protonatable luminescent iridium complex. *Chem. Commun.*, **46**, 8743–8745.
53. Lagunas, M.C., Fierro, C.M., Pintado-Alba, A. *et al*. (2007) Factors affecting luminescence and aurophilicity on digold(I) complexes and their potential as cation probes. *Gold Bull.*, **40**, 135–141.
54. Yam, V.W.W. and Cheng, E.C.C. (2008) Highlights on the recent advances in gold chemistry – a photophysical perspective. *Chem. Soc. Rev.*, **37**, 1806–1813.
55. Shaw, C.F. (1999) Gold-based therapeutic agents. *Chem. Rev.*, **99**, 2589–2600.
56. Yam, V.W.W., Chan, C.L., Li, C.K. and Wong, K.M.C. (2001) Molecular design of luminescent dinuclear gold(I) thiolate complexes: from fundamentals to chemosensing. *Coord. Chem. Rev.*, **216**, 173–194.

57. Assefa, Z., McBurnett, B.G., Staples, R.J. and Fackler, J.P. (1995) Structures and spectroscopic properties of gold(I) complexes of 1,3,5-triaza-7-phosphaadamantane (TPA). Part 2. Multiple-state emission from (TPA)AuX (X = Cl, Br, I) complexes. *Inorg. Chem.*, **34**, 4965–4972.
58. Barnard, P.J., Wedlock, L.E., Baker, M.V. *et al*., (2006) Luminescence studies of the intracellular distribution of a dinuclear gold(I) N-heterocyclic carbene complex. *Angew. Chem. Int. Ed.*, **45**, 5966–5970.
59. Vergara, E., Cerrada, E., Casini, A. *et al*., (2010) Antiproliferative activity of gold(I) alkyne complexes containing water-soluble phosphane ligands. *Organometallics*, **29**, 2596–2602.
60. Kherlopian, A.R., Song, T., Duan, Q. *et al*. (2008) A review of imaging techniques for systems biology. *BMC Syst. Biol.*, **2**, 74.
61. Pysz, M.A., Gambhir, S.S. and Willmann, J.K. (2010) Molecular imaging: current status and emerging strategies. *Clin. Radiol.*, **65**, 500–516.
62. Baker, M. (2010) Whole-animal imaging: the whole picture. *Nature*, **463**, 977–980.
63. Jennings, L.E. and Long, N.J. (2009) 'Two is better than one'–probes for dual-modality molecular imaging. *Chem. Commun.*, 3511.
64. Manning, H.C., Goebel, T., Thompson, R.C. *et al*., (2004) Targeted molecular imaging agents for cellular-scale bimodal imaging. *Bioconjugate Chem*, **15**, 1488–1495.
65. Lauffer, R.B. (1987) Paramagnetic metal complexes as water proton relaxation agents for NMR imaging: theory and design. *Chem. Rev.*, **87**, 901–927.
66. W. Ting Ren, L. Bo Liang, and F. Qi, Bimodal fluorescence and magnetic resonance imaging using water-soluble hexagonal NaYF4:Ce,Tb,Gd nanocrystals, *J. Nanomater.*, **2011**, 531217 (2011).
67. Koullourou, T., Natrajan, L.S., Bhavsar, H. *et al*. (2008) Synthesis and spectroscopic properties of a prototype single molecule dual imaging agent comprising a heterobimetallic rhenium-gadolinium complex. *J. Am. Chem. Soc.*, **130**, 2178–2179.
68. Thorp-Greenwood, F.L. and Coogan, M.P. (2011) Multimodal radio- (PET/SPECT) and fluorescence imaging agents based on metallo-radioisotopes: current applications and prospects for development of new agents. *Dalton Trans.*, **40**, 6129–6143.
69. Boschi, F., Spinelli, A.E., Ambrosio, D. *et al*. (2009) Combined optical and single photon emission imaging: preliminary results. *Phys. Med. Biol.*, **54**, L57-L62.
70. Bhushan, K.R., Misra, P., Liu, F. *et al*. (2008) Detection of breast cancer microcalcifications using a dual-modality SPECT/NIR fluorescent probe. *J. Am. Chem. Soc.*, **130**, 17648–17649.
71. Sampath, L., Wang, W. and Sevick-Muraca, E.M. (2008) Near infrared fluorescent optical imaging for nodal staging. *J. Biomed. Opt.*, **13**, 041312.
72. Lia, C., Wang, W., Wu, Q. *et al*. (2006) Dual optical and nuclear imaging in human melanoma xenografts using a single targeted imaging probe. *Nucl. Med. Biol.*, **33**, 349–358.
73. Kurz, P., Probst, B., Spingler, B. and Alberto, R. (2006) Ligand variations in [ReX(diimine)$(CO)_3$] complexes: effects on photocatalytic CO_2 reduction. *Eur. J. Inorg. Chem.*, **2006**, 2966–2974.
74. Coogan, M.P., Fernández-Moreira, V., Kariuki, B.M. *et al*., (2009) A rhenium tricarbonyl 4′-oxo-terpy trimer as a luminescent molecular vessel with a removable silver stopper. *Angew. Chem. Int. Ed.*, **48**, 4965–4968.
75. Thorp-Greenwood, F.L., Fernández-Moreira, V., Millet, C.O. *et al*. (2011) A 'Sleeping Trojan Horse' which transports metal ions into cells, localises in nucleoli, and has potential for bimodal fluorescence/PET imaging. *Chem. Commun.*, **47**, 3096–3098.
76. Kodali, D.R., Small, D.M., Powell, J. and Krishnan, K. (1991) Infrared micro-imaging of atherosclerotic arteries. *Appl. Spectrosc*, **45**, 1310–1317.
77. Trevisan, J., Angelov, P.P., Carmichael, P.L. *et al*. (2012) Extracting biological information with computational analysis of Fourier Transform Infrared (FTIR) biospectroscopy datasets: current practices to future perspectives. *Analyst*, **137**, 3202–3215.
78. Clede, S., Lambert, F., Sandt, C. *et al*. (2012) A rhenium tris-carbonyl derivative as a single core multimodal probe for imaging combining infrared and luminescent properties. *Chem. Commun.*, **48**, 7729–7731.

5

Luminescent Lanthanoid Probes

Edward S. O'Neill and Elizabeth J. New

School of Chemistry, The University of Sydney, Sydney, NSW, 2006, Australia

5.1 Introduction

The study of biological processes in living cells requires techniques which allow for the observation of changes within cells in real time. As a result, a number of different imaging techniques have been developed over the course of the last century, enabling us to gain sophisticated information about tissue and cells within living systems. These techniques span the electromagnetic spectrum, from high energy gamma and X-ray imaging, to long wavelength magnetic resonance imaging (Figure 5.1).

The quality of information that can be gained from an imaging set-up is measured in terms of its sensitivity and resolution. The *sensitivity* is the minimum signal that can be distinguished from background noise, and is often reported as the minimum concentration required for detection. The terms *spatial* and *temporal resolution* refer to the precision of the measurement with respect to location and time, respectively. In addition to these two parameters, whole animal imaging also requires good tissue penetration.

Amongst imaging techniques, optical (visible) imaging, with its intermediate location on the electromagnetic spectrum, represents a good compromise for both sensitivity and resolution [1]. The intermediate wavelengths and energies utilised also require the simplest equipment, which generally translates to cost efficiency. Optical imaging may involve the use of a range of instruments, from the simple light microscope, to the more advanced flow cytometer or confocal microscope.

The primary disadvantage of optical imaging is its poor depth penetration, which is generally limited to a few millimetres. This can be addressed by imaging near-infrared (IR) emission, which can penetrate up to 10 cm [2], or by using bioluminescent systems, in which there is a lack of any background signal [3]. Because of this poor tissue penetration, optical imaging finds its greatest utility in the study of tissue or cells, where it has the potential to provide very powerful information about intracellular mechanisms and interactions.

Ligand Design in Medicinal Inorganic Chemistry, First Edition. Edited by Tim Storr.

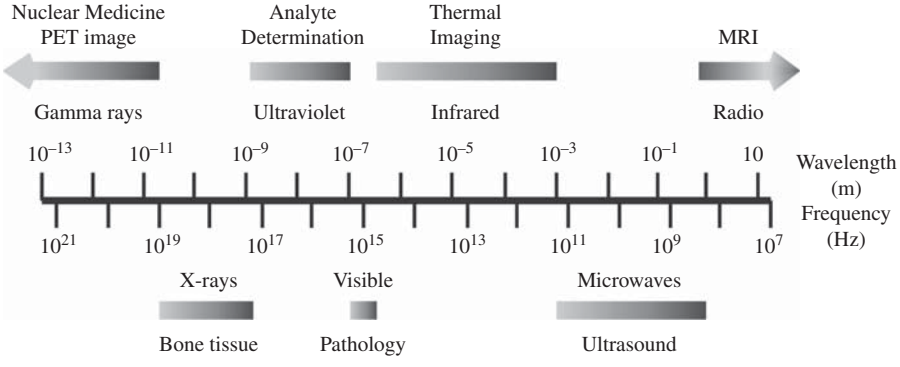

Figure 5.1 *Imaging techniques lie at different locations on the electromagnetic spectrum*

A more specific form of optical imaging is luminescence imaging, in which information is gained from the emission output of luminescent molecules. There are a number of naturally-occurring luminescent molecules within a cell, such as chlorophyll, reduced nicotinamide adenine dinucleotide (NADH) and oxidised flavin adenine dinucleotide (FAD), but luminescence imaging more commonly requires the use of extrinsic luminophores, which are referred to as luminescent probes.

It is important, at this point, to draw distinctions between the terms *luminescence*, *fluorescence* and *phosphorescence*. The term luminescence refers to the emission of light from an electronically excited state of a substance [4], and encompasses both fluorescence and phosphorescence, according to the nature of the excited state. Fluorescence arises from the relaxation of an electron from an excited singlet state to the ground state. This is a rapid, spin-allowed process, and fluorescence lifetimes are therefore very short, typically nanoseconds. Phosphorescence is the emission of light from a triplet excited state. As such transitions are forbidden, phosphorescence lifetimes are of the order of milliseconds to seconds. Here, we use the term luminescence to encompass both processes, as it allows the greatest generality.

In general, luminescent probes can be divided into two classes:

1. Those that act as markers of regions within the cell. For example, probes may selectively localise to the nucleus or mitochondria and therefore highlight those regions of the cell. The luminescence output of these stains can give information about the physical lay-out of the cell.
2. Those that give information about the chemical environment of the cell, whether the local chemical environment (pH or redox state), the presence of molecules (such as metal ions or anions) or enzyme reactions within the cell. These are often referred to as molecular imaging probes.

5.2 Luminescent probes

A number of probes have been developed for use in luminescence imaging, based on a number of scaffolds including organic fluorophores, recombinant proteins, quantum dots and emissive metal complexes (Figure 5.2). Small molecule organic dyes, such as those derived from fluorescein and rhodamine, are extremely versatile, with simple modifications yielding vastly different fluorescence properties [5, 6]. The pH-sensitivity and photobleaching tendency of these dyes has seen development of newer generation dyes such as boron dipyrromethanes (BODIPY) and AlexaFluor [7]. The use of fluorescent proteins as cellular probes gained momentum with the discovery [8] and molecular cloning [9] of the green fluorescent

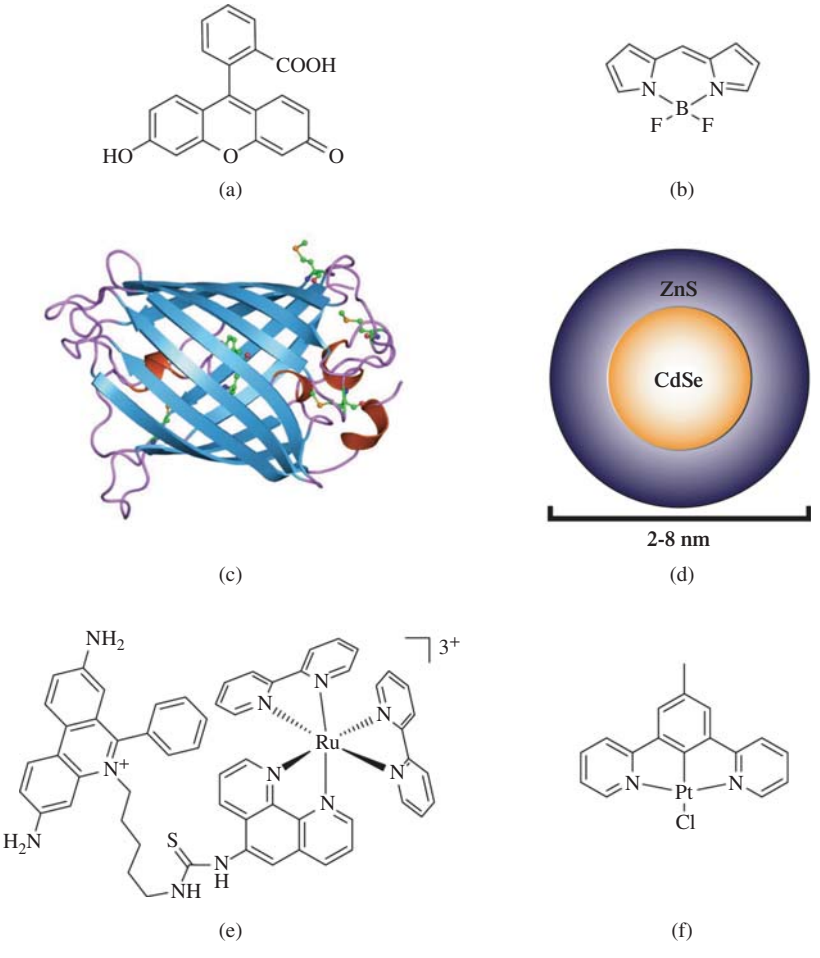

Figure 5.2 *Examples of luminescent probes: organic dyes (a) fluorescein and (b) BODIPY, (c) fluorescent protein GFP [11] (d) quantum dot, and transition metal complexes based on (e) ruthenium and (f) platinum. (See plate section for the colour version of this figure)*

protein (GFP) and subsequent protein engineering [10]. The utility of these two classes of fluorescent probes is compromised by their broad and featureless emission profiles, small Stokes shifts (separation between excitation and emission wavelengths) and the poor signal-to-noise ratios achieved due to overlap of fluorescence with cellular autofluorescence.

More recent work has seen the use of quantum dots, which are based on fluorescent semiconducting nanocrystals and generally contain elements from groups II and VI or from groups III and V. Quantum dots are bright and photostable, have large absorption coefficients, and their emission can be readily tuned over a broad spectrum [12]. While intracellular delivery of quantum dots has been reported [13], their use is limited by their relatively large size (2–8 nm).

In parallel to the development of quantum dots, luminescent transition metal complexes have arisen in the past 20 years as another alternative to small organic dyes and fluorescent proteins [14]. These complexes are primarily based on the d^6 and d^8 metal ions of the platinum group elements, and are explored

in Chapter 10. Another class of luminescent metal complexes comprises the lanthanoids, which will be the focus of this chapter.

Over the past decade, a wide array of luminescent lanthanoid complexes have been designed as cellular probes, in parallel with extensive development of complexes for use in immunoassays [15–17]. The range of luminescent lanthanoid cellular probes has been extensively reviewed elsewhere [18–21]. In this chapter, we briefly consider the properties of luminescent lanthanoid complexes, and explore aspects of ligand design that are of greatest importance in dictating probe behaviour.

5.3 The lanthanoids – an overview

The term lanthanoid refers to the 14 elements that follow lanthanum in atomic number. Traditionally referred to as *lanthanides*, the term lanthanoid is gaining preference in deference to IUPAC nomenclature, in which the -ide suffix refers to anions. The lanthanoids have also traditionally been termed the *rare earths*, but this is also a misleading description – even the rarest lanthanoid, thulium, is more abundant than mercury, cadmium or selenium. Lanthanoids are extracted primarily from the ores bastnäsite and monazite, and deposits of these ores are distributed throughout the world.

The lanthanoids are characterised by sequential filling of the 4*f* subshell. They are highly electropositive metals, and exist primarily as the M^{3+} ions, for which they have $4f^n5d^06s^0$ configurations. In addition to the M^{3+} forms, Eu, Yb and Sm can be prepared as M^{2+} ions (with Eu^{2+} being the most stable). Ce^{4+}, Pr^{4+} and Tb^{4+} are also observed, with only Ce^{4+} exhibiting kinetic stability in water.

The poor shielding of 4*f* electrons results in a decrease in size with increasing atomic number – a phenomenon termed the *lanthanoid contraction*. Nevertheless, there is a notable similarity in size between members of the lanthanoid series, which confounded efforts to separate elements in ores in the early years of extraction. Today, we can use this similarity to our advantage, by drawing conclusions about the structure of complexes through studying different lanthanoids by different techniques. For example, the magnetic properties of a Ln^{3+} complex can be studied using the Gd^{3+} form in NMR studies, and combined with electronic information gained from luminescence studies of the Eu^{3+} or Tb^{3+} forms.

Lanthanoids behave as hard acids, binding preferentially to F and O donors. The stability of lanthanoid complexes can be increased by means of the chelate effect – suitable chelating groups will be discussed in Section 5.6.1. Complexes commonly have coordination numbers of 6, 7, 8 or 9. A range of geometries are observed, including trigonal prismatic, square antiprismatic and dodecahedral.

Consideration of these general characteristics of lanthanoids is essential in the rational design of ligands for luminescent lanthanoid probes. More specifically, understanding the photophysical properties of the lanthanoids enables the selection of appropriate chromophore groups. This is therefore the focus of the following section.

5.4 Photophysical properties of luminescent lanthanoid complexes

The electronic configurations of the trivalent lanthanoids ($[Xe]4f^n$, $n = 0–14$) gives these ions distinctive photophysical properties which have been helpfully explained elsewhere [16, 22–25]. These configurations give rise to a large number of electronic levels, which can be quantified by Equation 5.1. For Gd^{3+}, with its seven unpaired electrons, this gives 3432 levels.

$$\frac{14!}{n!(14-n)!} \tag{5.1}$$

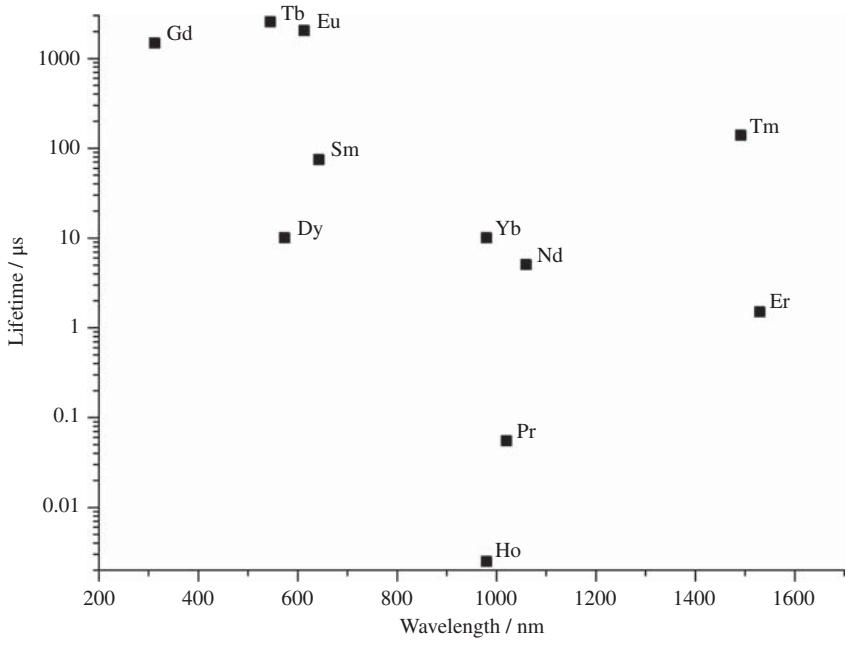

Figure 5.3 *Lanthanoid ions have varying maximal emission wavelengths and luminescence lifetimes*

These electronic levels are described by the Russell-Saunders coupling, a model which can be applied in this case of strong coupling, although normally considered most appropriate for weak spin-orbit coupling [26]. Levels are therefore given three quantum numbers *S, L* and *J*, which give rise to term symbols of $^{(2S+1)}L_J$.

There are two key characteristics of *f* orbitals which are crucial to the optical behaviour of lanthanoids. First, the 4*f* electrons are shielded by the 5*p* and 6*s* orbitals and are therefore not involved in chemical bonding. As a result, luminescence is primarily metal-centred, and spectra are line-like, characteristic of each metal and largely independent of coordination environment. Emission of different lanthanoids ranges from near-IR to UV (Figure 5.3), which strongly dictates the ions with greatest utility in luminescent probes: studies tend to focus on the visible (blue Tm, green Tb, orange Sm and red Eu) and near-IR emitters (e.g. Pr, Nd, Er and Yb).

The second characteristic is that *f-f* transitions are Laporte-forbidden, becoming only partially allowed by weak coupling with asymmetric ligand vibrations, resulting in very low extinction coefficients (of less than $1\,M^{-1}\,cm^{-1}$). This gives rise to long luminescence lifetimes, which can be as long as 2 ms for Tb^{3+} (Figure 5.3). The visible emission, good quantum yields (greater than 10%) and long luminescence lifetimes (of the order of ms) for Eu^{3+} and Tb^{3+} have resulted in their dominance of the field, and subsequent discussion will therefore focus on complexes of these two lanthanoids. There is much current interest, however, in complexes which emit in the near-IR region, as the greater tissue penetration lends itself to *in vivo* imaging. The comments made throughout this chapter in terms of ligand design, while being based on examples of Eu^{3+} and Tb^{3+}, are certainly applicable to systems bearing other lanthanoids.

5.4.1 The need for a sensitiser

The low molar extinction coefficients of the lanthanoid ions mean that optical irradiation will not be sufficient to populate excited energy states. These states can be populated efficiently by using a high intensity laser, but

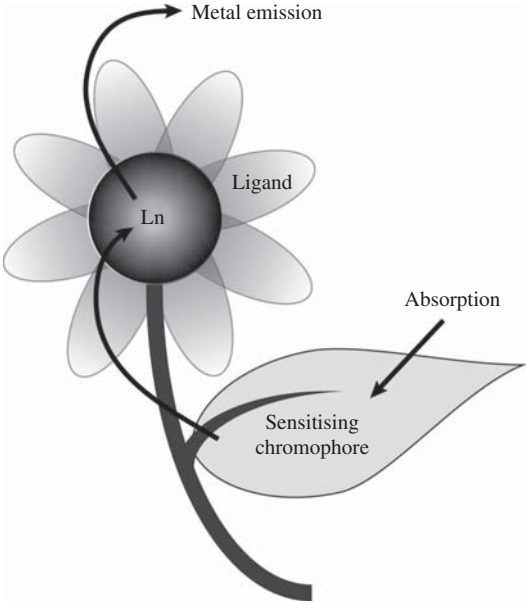

Figure 5.4 *Lanthanoid complexes can harvest energy from light using an organic chromophore as a sensitiser*

this method is not practical for cellular studies, where such a laser would be harmful to cells. The more preferable method is the use of an 'antenna' to capture the energy of excitation light and transfer it to the lanthanoid ion. This is usually achieved by using an organic chromophore, which is also called a sensitiser (Figure 5.4) [27].

The energy processes involved in sensitisation can be explained by using a Jablonski diagram, such as the one shown in Figure 5.5. The sensitiser is first excited to a vibrationally excited level of the S_1 (or S_n) band by absorption of a photon. This excited state then relaxes, either by non-radiative vibrational relaxation followed by fluorescence, or by intersystem crossing (ISC) to the triplet, T_1 manifold. There are then three possible pathways from the T_1 state: back–ISC to S_1, phosphorescence and energy transfer to the lanthanoid excited state [23]. The most efficient sensitisers will primarily undergo this latter process.

For a system in which the chromophore has a high molar extinction coefficient and efficient ISC and energy transfer processes, the effective molar absorption coefficient of the metal will be greatly enhanced, allowing for significant emission following excitation by conventional light sources. In the case of sensitised lanthanoid emission, we define the luminescence quantum yield as the ratio of the number of photons emitted through lanthanoid luminescence to the number absorbed by the sample, as shown in Equation 5.2. This value is the product of the efficiencies (η) of each of the individual energy transfer steps involved in reaching the lanthanoid emissive state, and the quantum yield of the directly excited lanthanoid (Q_{Ln}; Equation 5.3). Hypothesised mechanisms of energy transfer have been helpfully reviewed elsewhere [23, 28].

$$Q = \frac{\text{number of emitted photons}}{\text{number of absorbed photons}} \tag{5.2}$$

$$Q = \eta_{ISC} \cdot \eta_{ET} \cdot Q_{Ln} \tag{5.3}$$

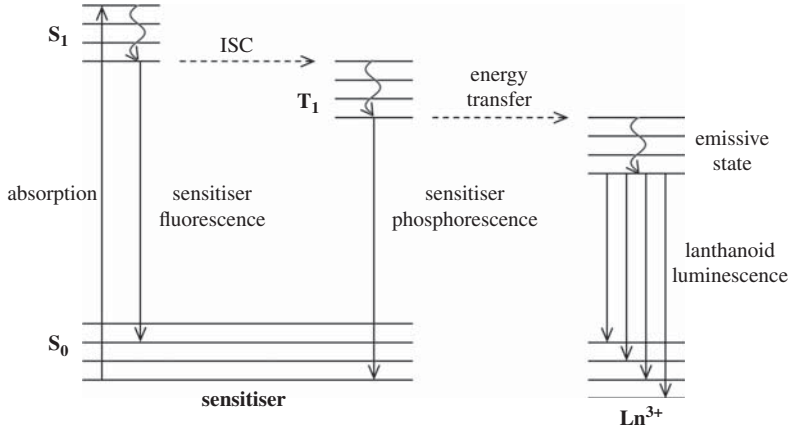

Figure 5.5 *Simplified Jablonski diagram showing the main energy transitions involved in sensitisation of lanthanoids. Wavy lines signify vibrational relaxation processes*

5.5 The suitability of lanthanoid complexes as luminescent probes

From this discussion of the photophysical properties of lanthanoid complexes, it is apparent that they are suitable for use as luminescent probes, offering a number of advantages over the other classes of optical probes outlined in Section 5.2. Principal advantages are found in the large apparent Stokes shift, information-rich spectra and long luminescence lifetimes.

The Stokes shift is the difference in energy (and therefore wavelength) between excitation and emission maxima. For fluorescent molecules, this is typically very small, and results from the loss of thermal energy prior to the fluorescence transition. When the Stokes shift is small, there is significant overlap between excitation and emission spectra, and excitation light can therefore interfere with emitted light. The large apparent Stokes shift for luminescent lanthanoids arises from the energy separation between excitation of the sensitising chromophore and emission from the lanthanoid excited state. Indeed, for many systems there is negligible overlap between excitation and emission spectra (Figure 5.6a), ensuring that all emitted light can be measured without any interference from exciting light.

As discussed in Section 5.4, luminescent lanthanoids exhibit numerous electronic levels. The most populated of these excited and ground state levels give rise to well-defined bands in emission spectra (Figure 5.6a). For example, Eu^{3+} complexes exhibit five bands (corresponding to $\Delta J = 0-4$), each of which contains hyperfine structure. Analysis of these bands can give detailed information about the system, particularly about the coordination sphere of the lanthanoid [22, 29, 30].

Another challenge in fluorescence microscopy is the inherent fluorescence of many subcellular species, which contribute to a significant background in images. This can be overcome by the use of time-gated imaging, in which this short-lived (nanosecond lifetime) background fluorescence is disregarded, and only the longer-lived luminescence from reporter molecules is collected (Figure 5.6b). Luminescent lanthanoid complexes, with their millisecond lifetimes, are ideal for such an application.

Luminescent lanthanoid complexes, therefore, are ideal candidates for use as luminescent probes. To ensure their applicability and suitability, however, ligands must be judiciously designed to ensure that they satisfy a number of key criteria for a probe of the cellular environment. An extensive, but not comprehensive, list of criteria includes chemical properties (complex stability, photophysical properties and analyte response) and

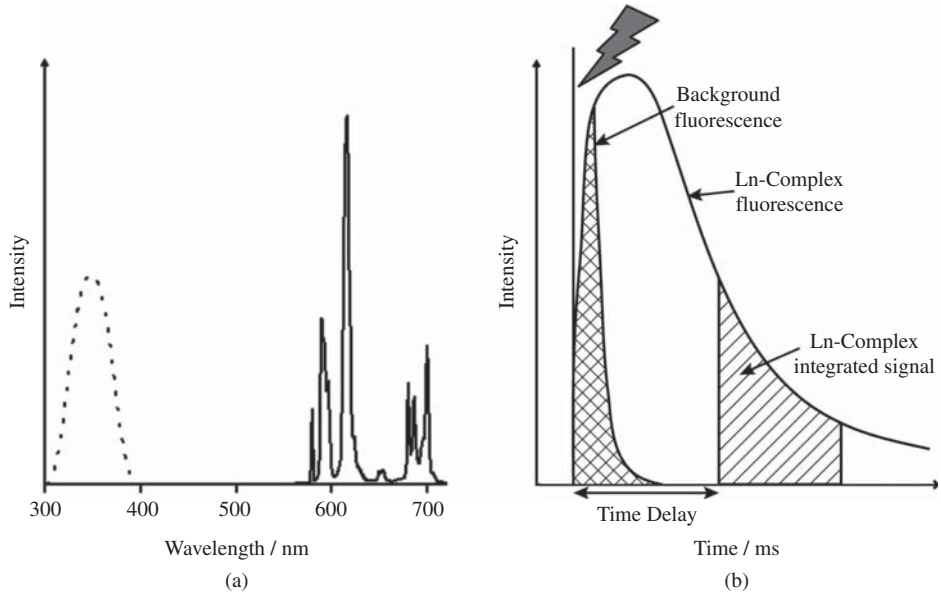

Figure 5.6 *Characteristic features of lanthanoids are (a) large apparent Stokes shifts between excitation (dotted) and emission (solid), information-rich emission spectra and (b) capacity for use in time-gated imaging, where short-lived background fluorescence can be gated out*

biological behaviour (cellular uptake, localisation to the desired region of the cell and minimal perturbation of cellular homeostasis). Each of these factors must be considered in ligand design, and we will address each in turn in the following sections.

5.6 Modulating chemical properties by ligand design

5.6.1 Chemical stability

The choice of the ligand scaffold for a luminescent lanthanoid complex is essential – it enables appendage of the sensitising chromophore, and can be tuned to achieve selectivity, and to control biological properties. Since the behaviour of the luminescent lanthanoid relies on its encapsulation within a ligand, it is important that the resulting complex is highly stable. If the complex does not have sufficient stability, it can easily degrade in the cell, losing its sensing ability. Stability is also essential in ensuring non-toxicity, as will be discussed in Section 5.7.3.

In order to function as a cellular probe, the lanthanoid complex must be stable across a range of pH values, in solutions which contain other competing metal ions, and the hydrophilicity/lipophilicity of the complex must be appropriately balanced not only to shield the lanthanoid from quenching water molecules but also to ensure desired interaction with subcellular species [31].

Selection of an appropriate ligand set for a luminescent lanthanoid complex requires careful consideration of the coordination chemistry of the lanthanoids. Coordination numbers of 7, 8 or 9 are most commonly-observed for lanthanoid complexes [32]. The lanthanoids, as hard donors, form complexes

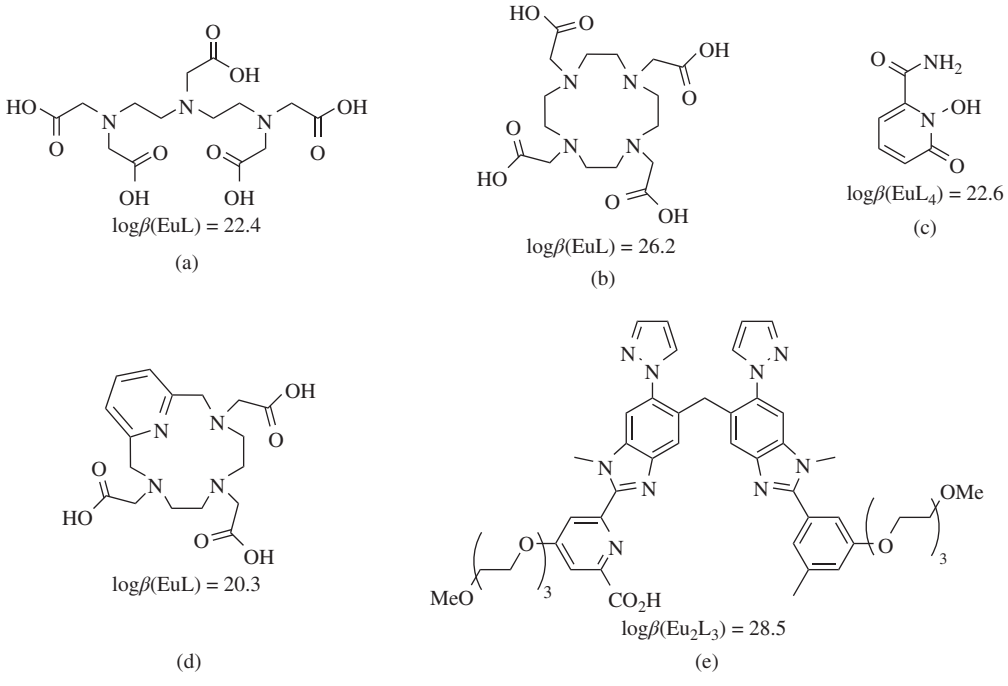

Figure 5.7 *Examples of suitable ligand systems for luminescent lanthanoid complexes and their approximate stability constants in Eu complexes. (a) diethylenetriaminepentaacetic acid (DTPA) [37], (b) 1,4,7,10-tetraazacyclododecane-1,4,7,10-tetraacetic acid (DOTA) [38], (c) 6-carbamoyl-1-hydroxypyridin-2-one (1,2-HOPO) [16], (d) 3,6,9,15-tetraazabicyclo[9.3.1]pentadeca-1(15),11,13-triene-3,6,9-triacetic acid (PCTA) [39] and (e) a helicate ligand [40]*

containing N- and O-donor ligands [33]. In order to prevent displacement of the ion by competing biological molecules, the lanthanoid-ligand complex must exhibit high kinetic and thermodynamic stability with respect to metal loss. Many of the early studies of suitable ligands for lanthanoid complexes arose from the investigation of gadolinium complexes for use as contrast agents, for which there is a similar requirement for high stability [34].

A number of different ligand systems, both linear and macrocyclic, have demonstrated utility for luminescent lanthanoid complexes (Figure 5.7). These include linear polyamino carboxylates such as DTPA (diethylene triamine pentaacetic acid) [34] and their macrocyclic analogues, derivatives of DOTA (1,4,7,10-tetraazacyclododecane-1,4,7,10-tetraacetic acid) [35]. The latter, highly-stable cyclen-based ligands have found widespread use in numerous classes of lanthanoid complexes [27]. Other ligand systems include calixarenes [36] and Schiff-base ligands, formed from the self-condensation of formyl and amine precursors.

Ligands for luminescent lanthanoid complexes therefore contain a number of essential components (Figure 5.8). The basic ligand set, whether linear or macrocyclic, will also contain a number of pendant arms to ensure that the required coordination number is achieved. These are commonly based on carboxylates or amides. In addition, the ligand must include one or more sensitising chromophores, as will be discussed in the next section. The rest of the discussion will focus on these essential components of ligand design.

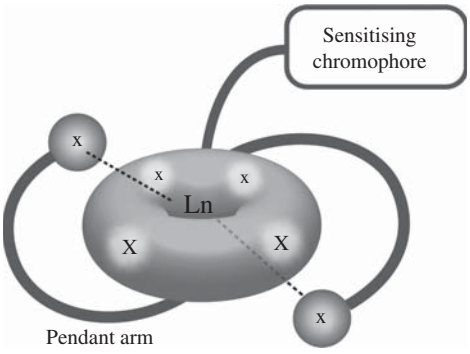

Figure 5.8 *The generic structure of a luminescent lanthanoid complex includes a ligand (often macrocyclic), a number of pendant arms and one or more sensitising chromophores (X = N or O)*

5.6.2 Photophysical properties

The nature of sensitisation dictates that the photophysical properties of the probe are primarily controlled by the choice of chromophore. The requirement for a sensitising chromophore is a high molar absorption coefficient at an appropriate excitation wavelength. For single photon microscopy, such excitation should be in the range 337–420 nm; higher energy excitation could cause radiation damage to cells, whereas lower energy excitation does not allow intramolecular energy transfer to occur. In order for effective activation of the lanthanoid excited state, the chromophore should have a triplet energy which is at least 1500 cm^{-1} higher than the emissive state of the lanthanoid (17 240 and 20 400 cm^{-1} for Eu and Tb respectively). A smaller energy difference will favour thermally accessible back energy transfer, in which energy transfer occurs to the triplet state of the sensitiser, leading to a decreased lifetime and emission intensity [41].

Selection of a chromophore must take into consideration the efficacy of energy transfer to the lanthanoid ion. For efficient transfer, the triplet state of the chromophore should be readily populated; that is, the rate of ISC must be more rapid than the rates of the fluorescence and non-radiative decay processes. Finally, the quantum efficiency of energy transfer will be maximised when the sensitiser-lanthanoid distance is minimised. This can be achieved through direct coordination of the chromophore to the metal centre. Recent work has centred on chromophores such as *m*-terphenyls [42], phenanthrolines [43], tetraazatriphenylenes [44, 45], azaxanthones and azathiaxanthones [46, 47] (Figure 5.9).

As well as selecting a suitable sensitising chromophore, it is important to determine the number of chromophores to be included in the ligand. The overwhelming majority of complexes incorporate a single chromophore, but some recent reports of complexes with multiple sensitisers give very distinctive photophysical and biological behaviour [48–51].

Another important aspect of ligand design regarding photophysical behaviour is in the regulation of luminescence quenching. The quantum yield of sensitised lanthanoid emission can be decreased by a number of different deactivation pathways, which can occur at any stage of the electron transfer process (Figure 5.10). The singlet and triplet states of the sensitiser may be quenched by electron, energy or vibrational energy transfer processes [22, 52, 53]. The quantum yield can also be decreased by quenching of the excited state of the lanthanoid(III) ion, which is susceptible to deactivation by transfer of vibrational energy to N–H, C–H or O–H oscillators [54–56]. In addition, the lanthanoid excited state can be quenched by energy transfer to a proximal acceptor group of similar energy [57]. The extent of excited state quenching is therefore an important consideration in the design of luminescent lanthanoid complexes for use as cellular probes, and it is particularly important that luminescent lanthanoids are resistant to quenching by biological reductant molecules and proteins.

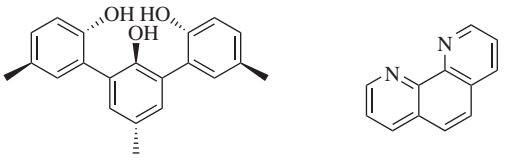

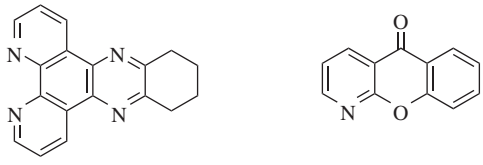

Figure 5.9 *Examples of suitable chromophores for luminescent lanthanoid complexes, and their triplet energies. (a) m-terphenyl, (b) phenanthroline, (c) 10,11,12,13-tetrahydrodipyrido[3,2-a:2′,3′-c]phenazine (dpqC) and (d) azaxanthone*

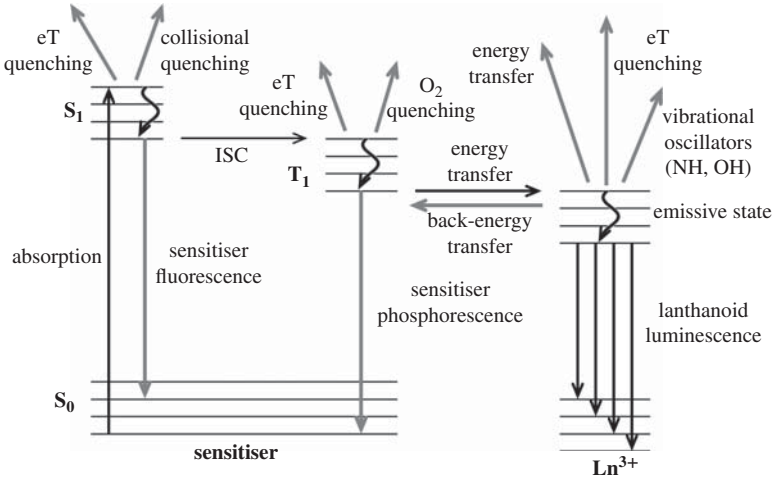

Figure 5.10 *At each step of the energy pathway there are processes that could lead to quenching of luminescence. Energy flow from sensitiser to lanthanoid luminescence is shown in black; quenching pathways are shown in grey*

5.6.3 Analyte response

Reporting on different chemical states requires a different luminescence response in the presence or absence of the signal. This means that the probe must not only bind to or interact with the signal, but this event must also change the photophysical properties of the system. A number of different approaches have been adopted to achieve responsive lanthanoid probes, which have been thoroughly reviewed in recent years [16, 18–20, 25]. The following discussion uses the term analyte response to encompass not only the sensing of chemical

species, but also chemical conditions, such as pH or redox state (for which the analytes are protons, or oxidising or reducing species).

In considering ligand design for responsive systems, three important design features can be modulated to signal the presence of an analyte: change in the chromophore, change in the pendant arm structure or variation in the lanthanoid ion. Specific examples of each class of responsive complex are discussed in more detail below.

The discussion that follows will focus on design of ligands to elicit an analyte response. It is also essential to ensure that this response is specific to the analyte of interest, another important aspect of ligand design that will also be addressed.

Another significant aspect in the design of a responsive probe is the reversibility of the sensing process. An irreversible process is one in which the probe cannot be regenerated by a subsequent lowering of analyte concentration. In general, reversible probes are preferable, as they are useful for measurement of fluctuating levels of analyte over time. There are some cases where an irreversible probe might be favoured, such as a very low analyte concentration, for which an accumulation of reacted probe over time can enhance the signal. Reversibility of probes will also be considered below.

When the chromophore structure is changed, there will be a variation in the sensitisation efficiency of the system, which can produce a dramatic change. In general, this emission change involves a turn-on or turn-off of luminescence, rather than a variation in relative peak intensities. Variation of chromophore structure in response to an analyte can be achieved by a number of different mechanisms, illustrated in Figure 5.11, which involve both changes in the structure of the chromophore and in its electronics.

There are a number of examples of responsive complexes in which the analyte reacts with the chromophore, changing its structure and hence its sensitising ability (Figure 5.11a). In such a case, ligand design requires the use of a chromophore which can undergo a selective reaction with the analyte. For example, Tb.**1** contains a boronate group, which reacts selectively with H_2O_2 over other reactive oxygen species [58]. This reaction causes unmasking of aniline, which can sensitise Tb. In an interesting second example, H_2O_2 can again react with a boronate in Eu.**2** to unmask a reactive intermediate that rearranges to form a coumarin, a good sensitiser of lanthanoids [59]. Such sensors involve an irreversible reaction, and as a result, the sensors themselves are not reversible.

A second mechanism for sensing involves displacement of the chromophore from the complex (Figure 5.11b). This mechanism has been utilised in Eu.**3**, where the naphthyl β-diketonate sensitiser is displaced by the analyte−bicarbonate. The loss of sensitisation results in a loss of luminescence [60]. This process is likely to be irreversible in complex systems, as the sensitiser, once decomplexed, will not be present in high enough local concentrations to recombine with the complex.

The third sensing mechanism relates to the cases in which the analyte of interest can itself act as a sensitiser (Figure 5.11c). When present in high enough concentrations, this analyte can replace the coordinated water molecules, resulting in sensitisation of the lanthanoid, and hence luminescence. For example, Tb.**4** can utilise this process to detect dipicolinic acid, a characteristic component of bacterial spores [61]. This process can only be utilised for analytes that can act as good sensitisers of lanthanoid ions, and is therefore not very generalisable.

Analyte sensing can also be achieved by electronic modulation of the chromophore, to alter its sensitising ability (Figure 5.11d). This may be reversible, such as in the alleviation of photoinduced electron transfer (PET) quenching by metal ion binding [62], or may involve irreversible reaction [63]. For example, Eu.**5** contains an anthracene group which deactivates the excited state of the terpyridyl sensitiser. This quenching is hindered in the endoperoxide which is formed upon selective reaction with singlet oxygen [64].

A final sensing strategy which involves the chromophore is variation of the distance between the chromophore and the sensitising group (Figure 5.11e). This is most commonly achieved in systems for which analyte binding causes a conformational change that brings together the two groups, therefore affecting the

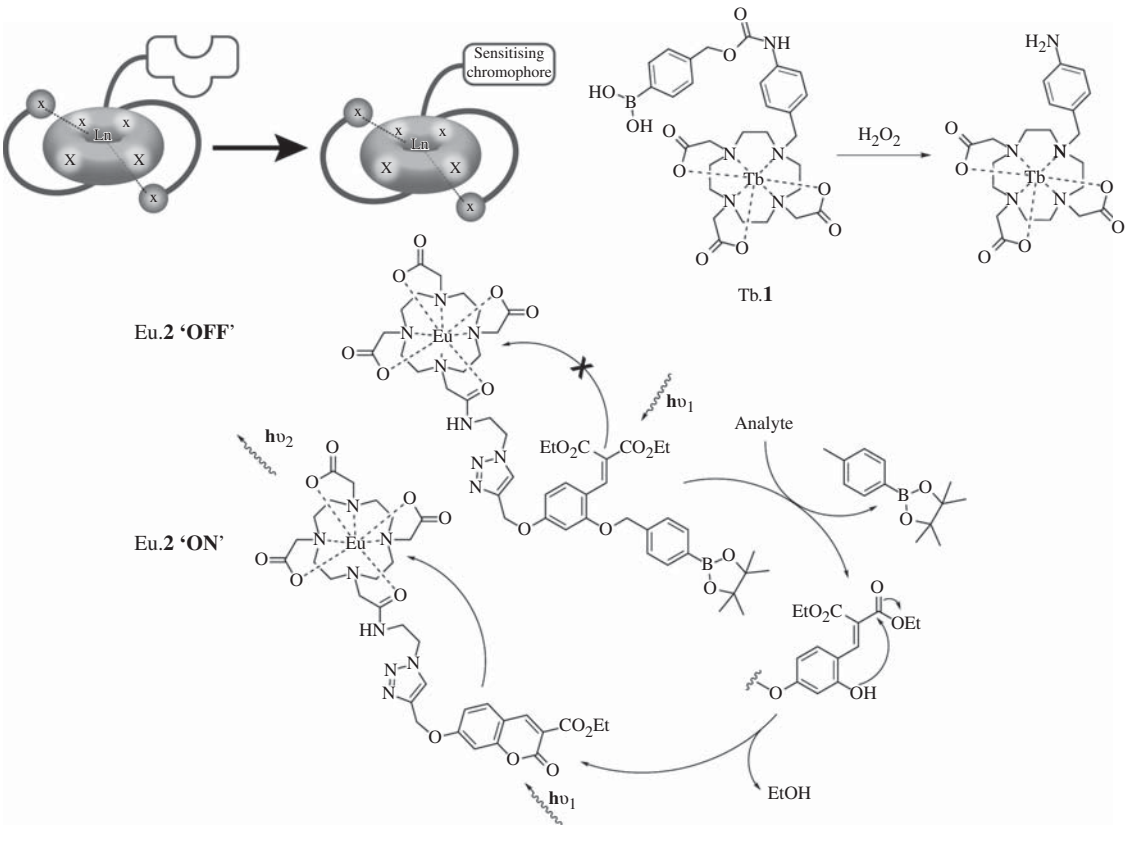

Figure 5.11 *Responsive lanthanoid complexes that sense analytes through modulation of the chromophore can do so by various mechanisms: (a) variation of the chromophore structure, (b) decomplexation of the chromophore*

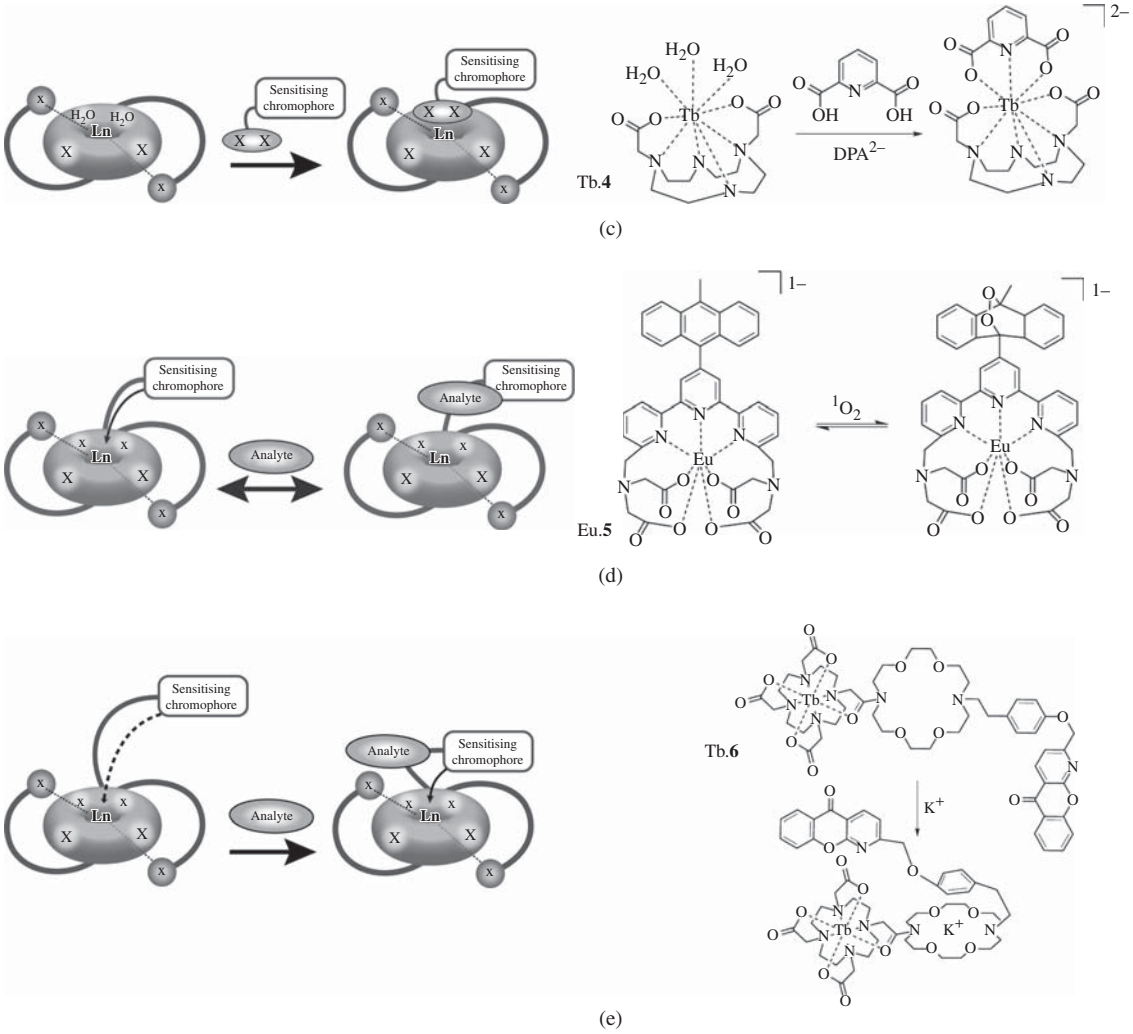

Figure 5.11 *(c) addition of the analyte as an antenna (d) electronic modulation of the chromophore and (e) changing the distance between the chromophore and the lanthanoid*

efficiency of sensitisation. For example, Tb.**6** contains a long, flexible linker between the sensitiser and the chromophore which includes a diazacrown ether. K^+ can bind to this group, and to the aryl ether group close to the sensitiser, thus locking the complex into a conformation in which the chromophore is close to the terbium centre [65]. This process is highly reversible and selective for K^+ over other alkali earth metals.

In addition to these sensing strategies, which involve variation about the chromophore, the pendant arms can also be involved in responsive probes (Figure 5.12). There are two main mechanisms by which analyte binding can be achieved utilising the pendant arms. First, the ligand can be designed such that it contains one or more bound water molecules. Analyte binds to displace the water, thereby decreasing the luminescence quenching by O-H oscillations, and increasing the overall luminescence (Figure 5.12a). The design of pendant arms in the molecule is crucial in these cases, to control the sterics and electronics of the complex, and thus

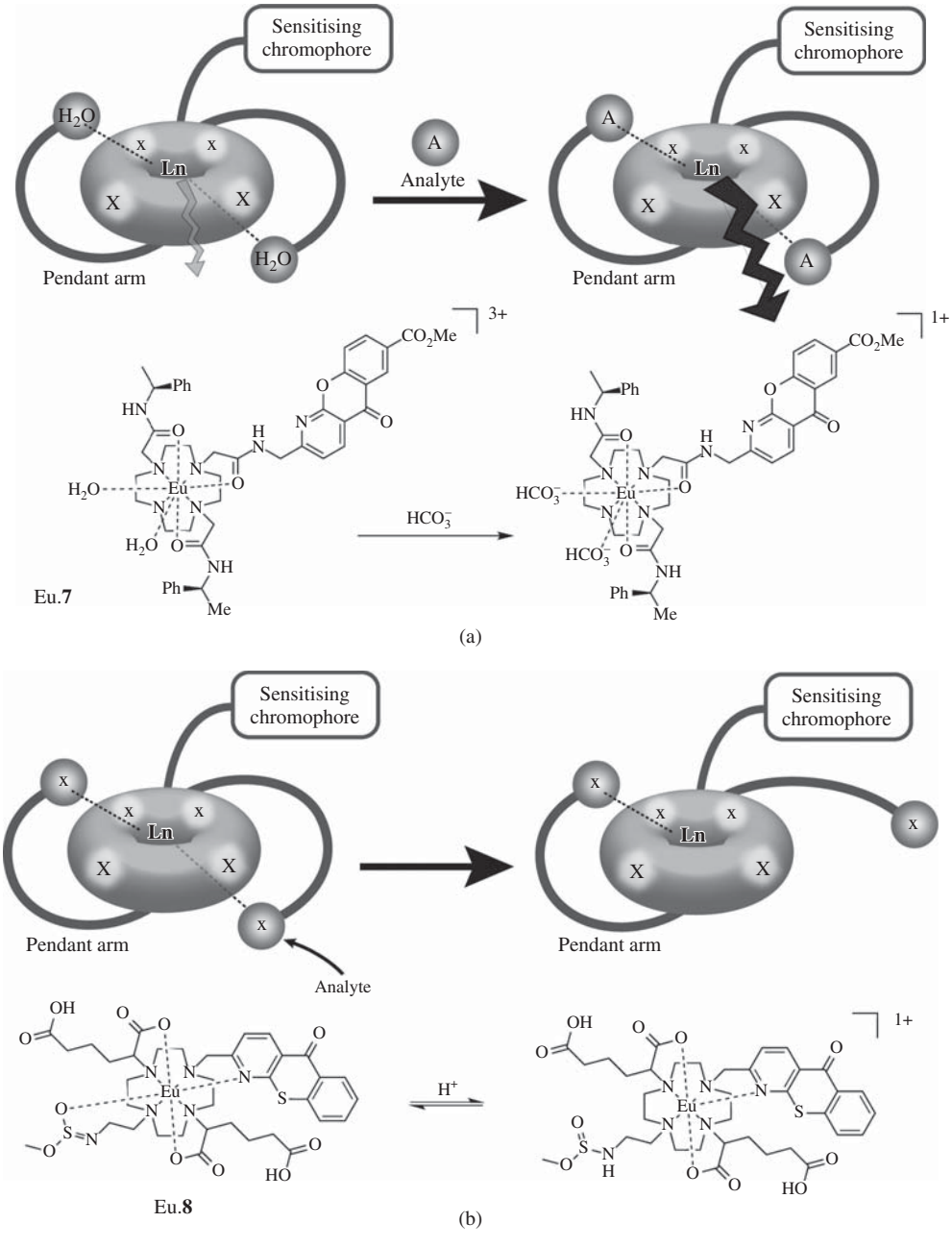

Figure 5.12 *Responsive lanthanoid complexes can sense analytes through modulation of the pendant arms, by: (a) changing the hydration state of the complex or (b) perturbation of the electronic environment*

ensure selectivity for the analyte of interest. For example, Eu.**7** contains two bound water molecules which can be selectively displaced by bicarbonate, resulting in a 250% increase in fluorescence, and a variation in the shape of the Eu luminescence spectrum [66].

Secondly, analytes can trigger modification of the pendant arms themselves, leading to variation of the electronic environment of the lanthanoid and hence its luminescence spectrum (Figure 5.12b). Eu complexes, in particular, can give valuable information about analytes by this mechanism, as their emission spectra reflect the coordination sphere around the metal. For Eu complexes, the $\Delta J = 2$ ($^5D_0 \rightarrow {}^7F_2$) and $\Delta J = 4$ ($^5D_0 \rightarrow {}^7F_4$) transitions are especially sensitive to the nature and symmetry of the coordination sphere, as it represents an electric-dipole allowed transition [41]. In general, the luminescence changes elicited by this mechanism are more subtle than following perturbation of the chromophore, but they can be more information-rich as they elicit ratiometric changes to the lanthanoid emission. An example of such a complex is Eu.**8**, which contains an N-linked methylsulfonamide pendant arm [67]. Under acidic conditions, protonation of the nitrogen results in a change in the coordination number from 8 to 7, with a resulting change to the form of the Eu spectrum. The ratiometric change of the $\Delta J = 4$ peak relative to $\Delta J = 1$ can be utilised to determine pH.

A final sensing mechanism which has proved to be successful involves modulation of the lanthanoid ion itself, rather than the chromophore or ligand structure. In particular, a number of cases have been identified where Eu and Tb complexes have disparate responses to analyte, and therefore the simultaneous use of both complexes enables measurement of a ratiometric response (Figure 5.13). This is possible as Eu and Tb complexes with the same ligand generally have identical physical and biological behaviour, and vary only in photophysical properties. For example, at basic pH, both Eu.**9** and Tb.**9** are luminescent, but at acidic pH, the

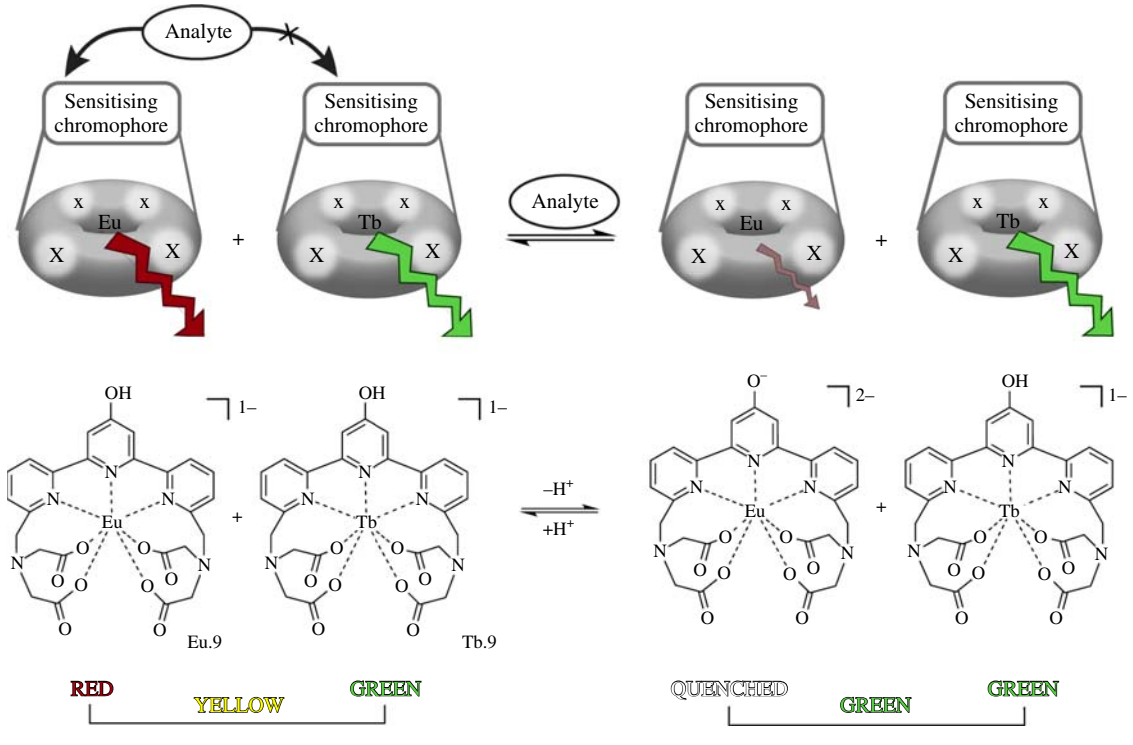

Figure 5.13 *Mixtures of Eu and Tb complexes of the same ligand can be used to give information about analytes. (See plate section for the colour version of this figure)*

Eu form is quenched by intramolecular charge transfer, while the Tb complex retains its luminescence [68]. The mixture of complexes therefore changes from green to yellow luminescence upon acidification.

5.7 Modulating biological properties by ligand design

5.7.1 Cellular uptake

Since the role of lanthanoid-based sensors is to probe the intracellular environment, it is essential that complexes are able to readily cross the cell membrane. Ideally, this cellular uptake should be rapid, and the accompanying egress slow, so that the probe accumulates within the cell. Uptake of exogenous molecules into a cell may occur by one of two main mechanisms [69]:

1. Passive transport, which describes the movement of molecules down their concentration gradient, for which no energy input is required. For example, osmosis is the passive transport of water.
2. Active transport, which requires the input of energy, and can involve the use of specific membrane-bound carriers or channels such as the N^+/K^+-ATPase, or can occur by vesicular transport, in which extracellular particles are encapsulated into membrane-bound vesicles which are subsequently internalised.

Ligand design can therefore incorporate strategies to enhance cellular uptake. For lanthanoid complexes, these have found extensive application in Gd-containing magnetic resonance imaging (MRI) contrast agents, for which intracellular concentrations must be on the order of millimolar [70]. Strategies include electroporation [71] and encapsulation into liposomes [72, 73]. In addition, complexes can be conjugated to macromolecules such as peptides [74–77], dendrimers [78], dextrans [79] and TiO_2 [80] or gold [81] nanoparticles. A final strategy involves the appendage of cell-penetrating peptides such as the TAT peptide sequence from the HIV virus [82–84] and the positively-charged octaarginine moiety [77, 85–88].

Compared with MRI, luminescence has much greater sensitivity, and therefore far lower intracellular concentrations are required: concentrations of 10 μM give readily-measured signals for microscope studies [21]. As a result, it is not common to employ any of the plethora of strategies used to enhance Gd-complex uptake for MRI; one isolated example of a polyarginine-tagged terbium complex did not report appreciable differences in cellular uptake compared with the control complex [89]. Instead, it appears that luminescent lanthanoid complexes are taken into cells in sufficient concentrations for microscopy, without the need for specific ligand design. The following sections summarise the reasons why this has proven to be generic for a broad spectrum of lanthanoid complexes [18]. First, however, it is important to consider how best to observe cellular uptake.

Early studies of the uptake of luminescent lanthanoid complexes into cells correlated cellular luminescence with uptake. It has since become evident, however, that intracellular quenching of fluorescence can interfere with such analysis. Susceptibility to quenching varies greatly with ligand design, and a poor visibility in cells tends to indicate a high degree of quenching rather than minimal cellular uptake. It is therefore necessary to find an alternative means of determining levels of cellular uptake. Quantification of lanthanoid concentration within cells has typically employed inductively-coupled plasma-mass spectrometry (ICP-MS), which can detect concentrations as low as ppt for most elements [90]. This must be calibrated against cell number, to enable approximate calculation of intracellular lanthanoid concentration, whether by sorting and counting cells by flow cytometry, or quantifying protein content using a biochemical assay.

The most comprehensive study of the cellular uptake of luminescent lanthanoid complexes sampled a range of complexes with varying charge, counterion, lipophilicity, sensitising chromophore and lanthanoid ion [91]. Uptake was quantified using ICP-MS and calibrated against protein content determined by the bicinchoninic acid (BCA) method. Results revealed very similar rates of cellular uptake for all complexes, regardless of their

structure. Furthermore, cellular uptake was dramatically decreased when incubation was carried out at 4 °C rather than 37 °C, suggesting an active, energy dependent mode of uptake. In order to identify the mode of active uptake responsible in this case, further uptake studies were performed in the presence of inhibitors of the various endocytic uptake pathways. For all complexes studied, it was found that cellular uptake was decreased in the presence of wortmannin and amiloride, which inhibit the process of macropinocytosis. Inhibitors of all other pathways had no significant effect on cellular uptake. This finding was confirmed by using two activators of macropinocytosis – phorbol 12-myristate 13-acetate (PMA) and 1,2-dipalmitoyl-*rac*-diacylglycerol (DAG) – both of which increased cellular uptake (Figure 5.14). Subsequent studies have corroborated these findings for more structurally-diverse complexes [92].

Unlike other common active uptake pathways such as caveolae- and clathrin-mediated endocytosis, macropinocytosis is a non-specific mechanism, for which ligand-binding is not required [93]. Instead, vesicles are formed by ruffling of the membrane in response to some form of stimulation. This ruffling results in the formation of large, irregular vesicles called macropinosomes. The process is driven by actin, and is similar to phagocytosis in immune cells. Further confirmation of a macropinocytotic pathway of cellular uptake was gained by observing the complexes in the early macropinosome, which exists within the first few minutes of cellular uptake. At early time-points, lanthanoid complexes were found to colocalise with fluorescein-labelled dextran beads, which accumulate in the macropinosomes (Figure 5.15) [94].

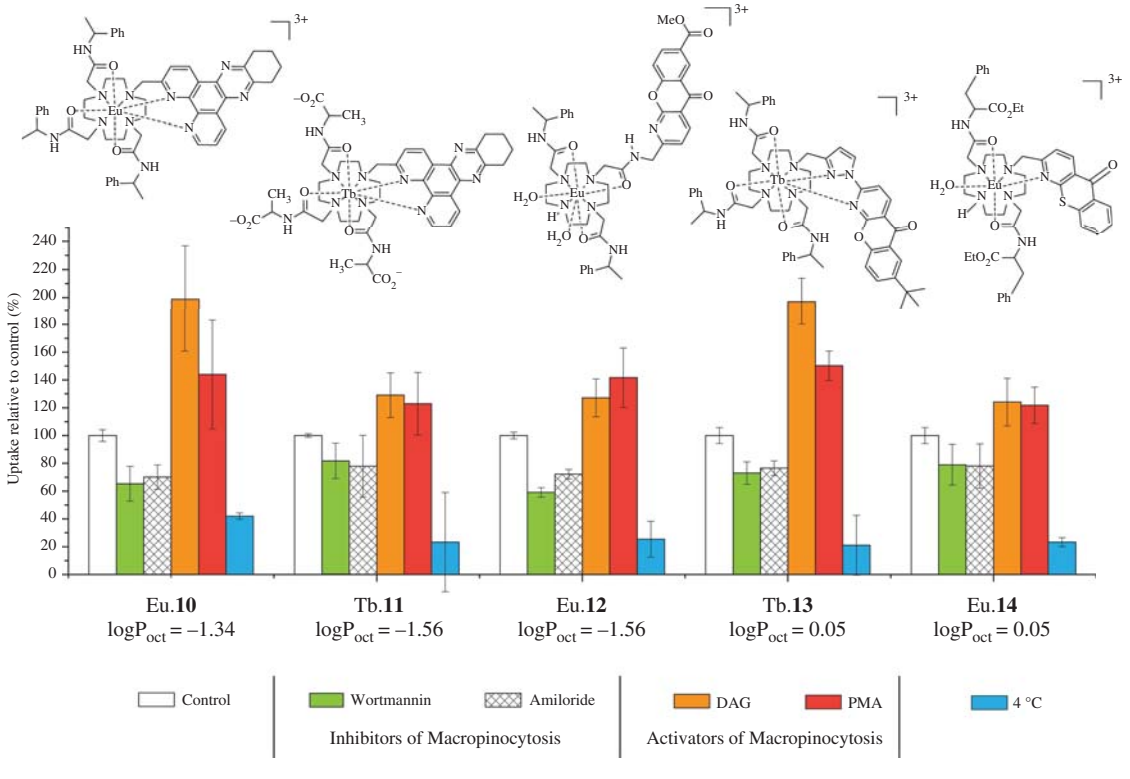

Figure 5.14 *A series of lanthanoid complexes with widely-diverging structures and lipophilicities all show comparable levels of cellular uptake. This uptake was decreased at low temperatures and in the presence of inhibitors of macropinocytosis, and was increased in the presence of activators of macropinocytosis. (See plate section for the colour version of this figure)*

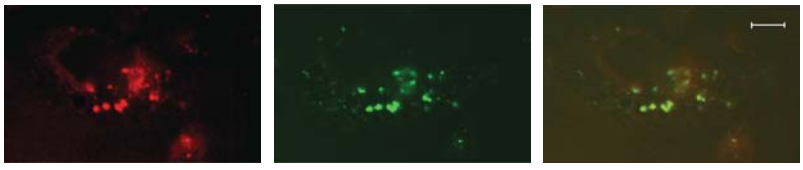

(a) (b) (c)

Figure 5.15 *Fluorescence microscopy images of Chinese Hamster Ovary (CHO) cells treated with [Eu.12]Cl_3 (100 μM) and FITC-dextran (70 kDa, 2.5 mg/ml) for 15 minute. (a) Eu luminescence, (b) fluorescein fluorescence and (c) overlay of Eu and fluorescein channels showing that the Eu complex is in the macropinosomes after 15 minute. Scale bar represents 20 μm [94]. Reproduced from [94] with permission of The Royal Society of Chemistry. (See plate section for the colour version of this figure)*

It appears, based on these findings, that for cyclen-based lanthanoid complexes, it is not necessary to incorporate strategies for cellular uptake into the ligand design. This is a consequence of the particular mode of cellular uptake involved; while other endocytotic pathways require receptor binding which would presumably be very structure-specific, and passive membrane diffusion is highly-lipophilicity dependent, macropinocytosis is a non-specific process [95]. This is consistent with the observation that all complexes studied, regardless of structure, are internalised by this mechanism. No study has so far addressed the question of what stimulates ruffling of the membrane, and the formation of macropinosomes, and this remains an area for further investigation. It is important to note that these cellular uptake studies were performed at concentrations below 100 μM. It is likely that at much higher concentrations (in the millimolar range) there is also some passive diffusion of complex across the cell membrane.

5.7.2 Localisation to desired region of the cell

An essential feature of an intracellular probe is that it must localise to the region of the cell on which it is intended to report. The conditions within a specific organelle can often give the most useful information about cellular function and dysfunction. For example, a number of lysosomal storage diseases are characterised by an elevation in lysosomal pH but only minimally perturbed cytoplasmic pH [96], while variation in mitochondrial redox state is often an early indicator of apoptosis [97].

A number of strategies have been developed to assist the delivery of exogenous molecules to specific sub-cellular locations, and a small number of these strategies have been incorporated into the ligand design for luminescent lanthanoid complexes. Appendage of an oligoguanidinium group to Tb (Figure 5.16a) directed the complex to the mitochondria, but this was accompanied by cell death *via* apoptosis [89]. An alternative mitochondrial-targeting group, the tetraphenylphosphonium cation, was used to deliver dysprosium thiocyanate complexes to the mitochondria, with remarkably low toxicity (Figure 5.16b) [98]. Finally, terbium complexes were targeted to the folate receptor by incorporation of the substrate folate molecule (Figure 5.16c) [99].

These results show that it is possible to design ligands that incorporate targeting groups to control sub-cellular distribution. The scarcity of reported complexes of such strategies, however, reflects the ease with which localisation can be controlled by much simpler aspects of ligand design. The primary evidence for this has been obtained from a comprehensive study of over seventy luminescent lanthanoid complexes, for which the relationships between structure and localisation could be determined [18, 21, 91]. Complexes were all based on a cyclen macrocycle, with a single sensitising chromophore and two or three pendant arms. These complexes could be divided into four groups according to their sub-cellular localisation, with each class

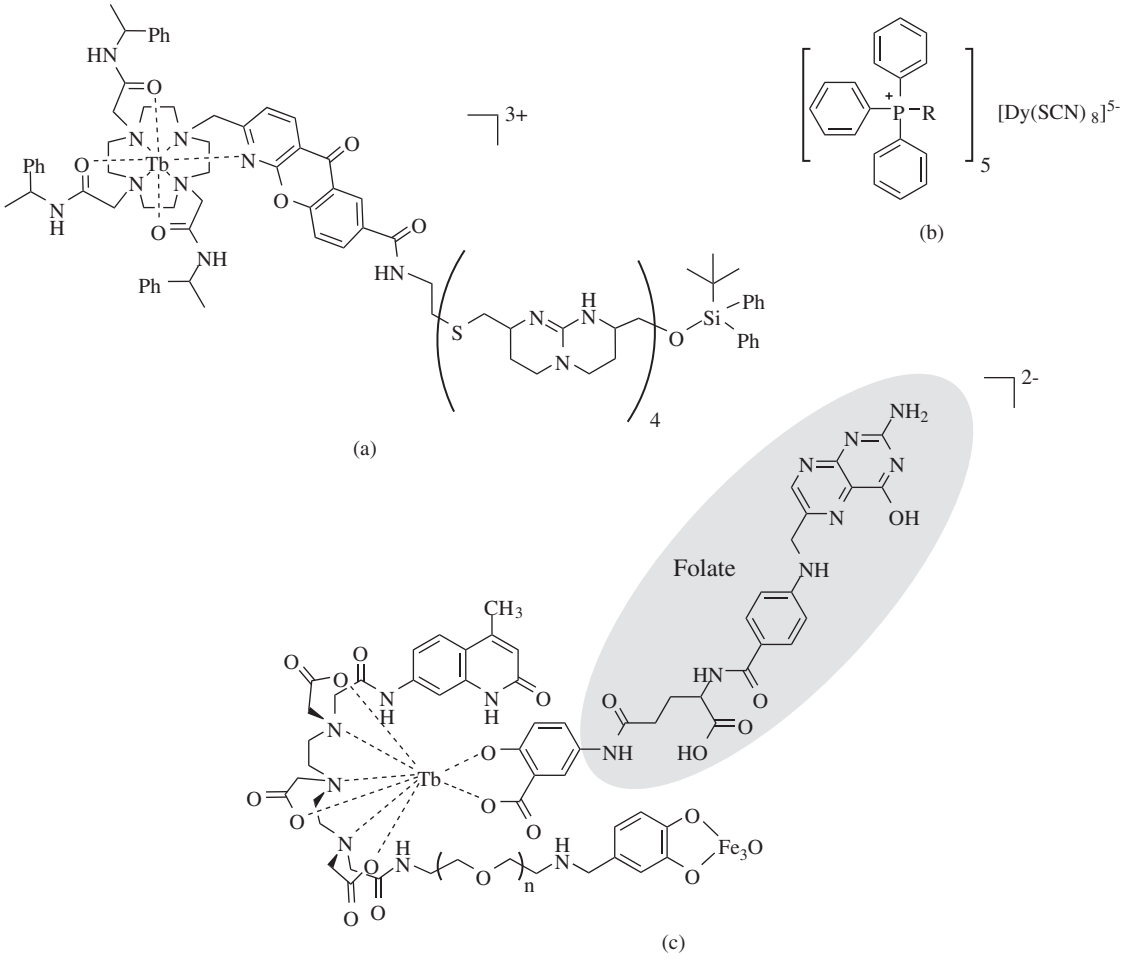

Figure 5.16 *Luminescent lanthanoid complexes can be directed to subcellular locations by using targeting groups such as (a) tetraguanidinium, (b) tetraphenylphosphonium to target mitochondria and (c) folate to target the folate receptor*

exhibiting distinct behaviour. The following discussion summarises these classes of complexes and presents the structure-activity relationships that control localisation.

The largest group of complexes comprises those which localise to the lysosomes (Figure 5.17a). This localisation persists over periods from 5 minutes to 24 hours. A much smaller group was observed to localise to the mitochondria (Figure 5.17b). These complexes did not perturb mitochondrial membrane potential (MMP), but were observed to move from the mitochondria to the lysosomes after longer periods of time (greater than 12 hours) [100]. An additional class of complexes appeared to localise simultaneously in both the lysosomes and mitochondria (Figure 5.17c). These complexes did cause some changes to MMP, and as a result were

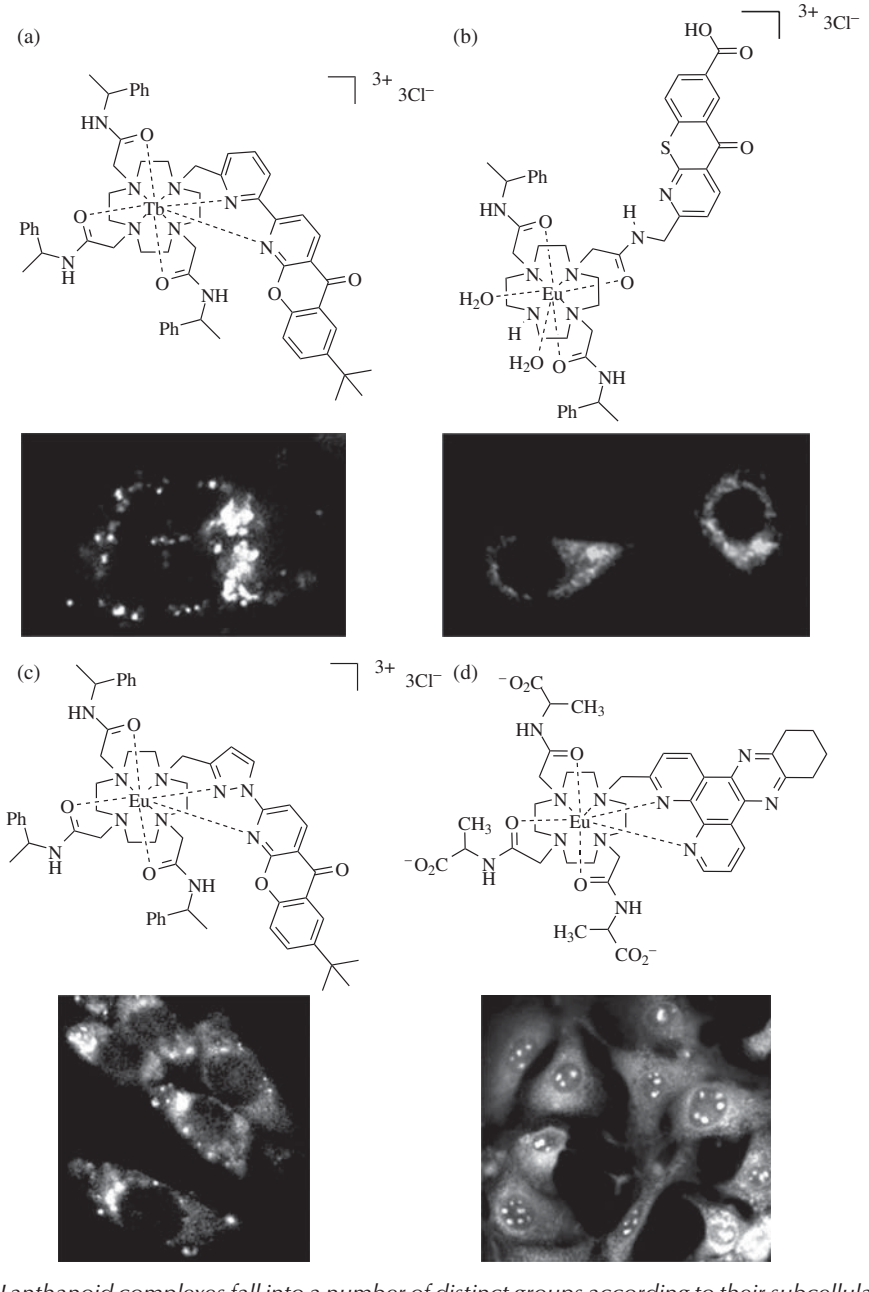

Figure 5.17 *Lanthanoid complexes fall into a number of distinct groups according to their subcellular localisation, with examples shown here. (a) Lysosomal, (b) mitochondrial, (c) lysosomal and mitochondrial and (d) nucleolar*

slightly more toxic to cells. Finally, a class of complexes could be observed in the nucleoli, the protein-rich regions of the nucleus (Figure 5.17d).

More detailed studies of the nucleolar-localising complexes revealed that this subcellular distribution was most pronounced in cells which were under stress. It appears that these complexes cause some permeabilisation of the cell membrane, which therefore promotes transport across the nuclear membrane. Indeed, the localisation of other, mitochondrially- and lysosomally-localising complexes could be shifted towards the nucleolus by permeabilisation of the cell membrane with a surfactant [94]. Complexes which localise to the nucleoli appear to be those which cause some cytotoxicity. For this class, the counterion to the positively-charged lanthanoid complex has some effect – triflate appears to promote cellular permeability, and therefore nuclear uptake.

For all four classes of complexes, some clear relationships between structure and localisation can be determined. The nature of the lanthanoid ion and pendant arms, and the charge on the complex, has no effect on localisation. Nor do dramatic changes in geometry, whether configurational or conformational. The two factors that do appear to have an effect are the number of pendant arms (the ligand denticity), and the nature of the chromophore and its point of attachment to the macrocycle. For example, alteration of the methylene linkage in Eu.**15** to an amide group in Eu.**12** shifts the localisation from lysosomes to mitochondria, while subsequent addition of a pendant arm to give Eu.**16** results in the lysosomal/mitochondrial localisation (Figure 5.18). Complexes of this general structure which have subsequently been reported are also in agreement with these general trends [66, 101, 102], but new scaffolds have also been observed with characteristic localisation profiles, such as a nuclearly-localising cyclen-based complex with two sensitising chromophores [50] and a mitochondrially-localised complex of the smaller triazacyclononane macrocycle with three appended sensitising groups [92]. The general trends observed are only applicable for a small subset of all conceivable luminescent lanthanoid probes, of one generic structure type, and it is likely that future research will yield much more comprehensive structure-activity relationships.

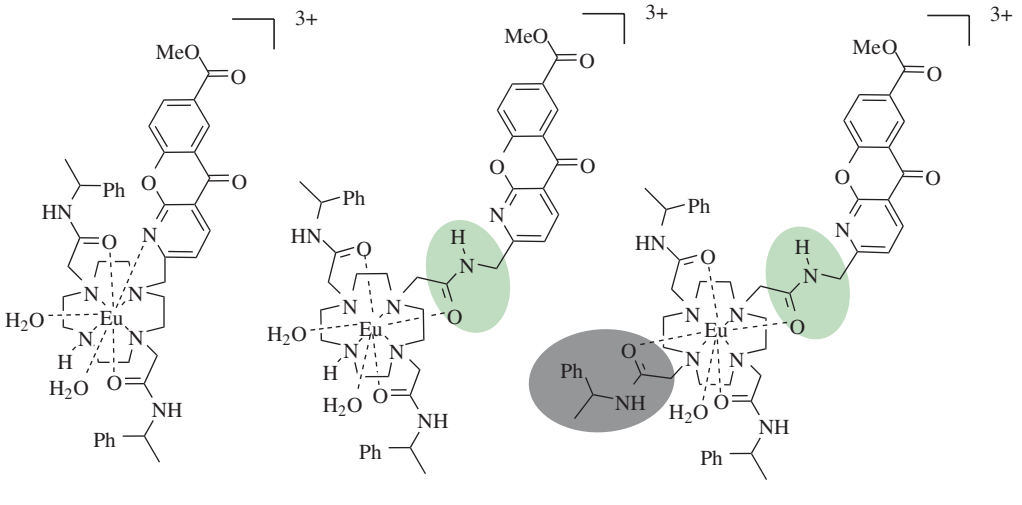

Eu.**15** Lysosomal

Eu.**12** Mitochondrial

Eu.**16** Mitochondrial / Lysosomal

Figure 5.18 *Changes in the sensitising chromophore and the number of pendant arms results in variation of subcellular localisation*

The observation that a range of sub-cellular locations could be accessed by lanthanoid complexes is consistent with the mode of uptake, discussed in Section 5.7.1. It is believed that macropinosomes, compared with other vesicles, are large and leaky, which means that they readily release their contents into the cytoplasm [103], from where they can be sequestered by organelles or other cellular processing pathways. This can account for the fact that complexes which are internalised by the same mechanism can subsequently be observed in divergent locations of the cell.

It is clear, therefore, that for certain regions of the cell – namely the lysosomes, mitochondria and, to a lesser extent the nucleolus – simple ligand design can achieve desired localisation. Where other localisations are desired, it is likely that more concerted efforts are required, such as the incorporation of small targeting groups to the ligand, or the use of a different basic ligand structure.

5.7.3 Maintenance of cellular homeostasis

The toxicity of free lanthanoid ions is a widely-discussed area, primarily with respect to the use of gadolinium complexes in magnetic resonance imaging. A small subset of patients, comprising those who suffer from renal dysfunction, experience severe nephrotoxicity effects from Gd treatment [104], and this has led to the issuing of increased safety warnings for all U.S. Federal Drug administration (FDA)-approved contrast agents [105]. Lanthanoids have also long been known to contribute to severe liver damage [106].

As with many toxic metals, the lanthanoids are able to mimic Ca^{2+} in the body, due to their similar ionic radii. Lanthanoid ions have a number of diverse effects on biological systems which contribute to their toxicity. They can bind irreversibly to calcium channels, inhibiting the Ca^{2+}-ATPase that regulates muscular contraction [107]. Lanthanoid ions can cause both necrosis, by perforating cell membranes [108], and apoptosis, by a variety of mechanisms [109]. The lanthanoids can replace Ca^{2+} in enzymes, therefore inhibiting activity, but can also mimic Mg^{2+}, Fe^{3+} and Mn^{2+} [110], and by this similarity can also affect the stability of microtubules [111, 112].

It appears that lanthanoid toxicity is largely systemic – affecting organ function – rather than acting on the level of individual cells. It is therefore of far greater concern for Gd-based MRI contrast agents, which are administered to the whole body on much higher concentrations, than for luminescent lanthanoids intended for use as cellular probes. Regardless, one of the primary requirements for any cellular probe is that it minimally perturbs cellular homeostasis, and non-toxicity of the probe is therefore an important concern.

The solution – for Gd contrast agents and luminescent lanthanoids alike – is to encapsulate the ion in a highly stable ligand in which it will remain for the duration of its time in the biological system. This has proved to be very effective – one study found that when chelated gadolinium was injected into rats at a dose 50 times higher than the lethal dose of free Gd^{3+}, no toxicity was observed [113]. This study also demonstrated that the toxicity of a Gd complex is inversely proportional to the stability of the complex. Indeed, the fact that MRI contrast agents can be used in such high doses is testament to the success of this strategy, with the few examples of nephrotoxicity resulting from far greater retention in the kidney in the cases of renal dysfunction. For other lanthanoids, this principle also applies. The achievement of chemical stability is therefore an important feature in ligand design.

Since luminescent lanthanoid complexes are most useful in cellular rather than whole body studies, it is cytotoxicity rather than systemic toxicity with which we are concerned. Cytotoxicity is most readily measured by assays which enable calculation of an inhibitory concentration (IC_{50}) at which 50% of the cells are no longer viable, and incubation times are typically 24 hours. These results must be interpreted in the context of routine dosing concentrations, which for luminescent lanthanoid complexes are below 100 μM for incubation times under 1 hour.

IC_{50} values for a range of luminescent lanthanoid complexes have been measured using the MTT or WST-1 assays, both of which measure the conversion of tetrazolium into an insoluble formazan product by

mitochondrial reductase in viable cells. These various studies overwhelmingly found very high IC_{50} values, of greater than 200 μM for 24 hours [18, 50, 89, 92, 100, 101, 114–120]. It seems, therefore, that lanthanoid complexes which are encapsulated by a macrocycle are generally non-toxic, but it is important to carefully consider dosage concentrations. Early studies with luminescent lanthanoid complexes used concentrations as high as 1 mM, which exceeds the 24 hours IC_{50} for most complexes [121, 122]. At near-toxic concentrations, even if the cell remains viable, it can be compromised, and permeabilisation of the cell membrane at such high dosing concentrations can perturb aspects such as sub-cellular localisation [94, 123].

Analysis of cytotoxicity results reveals some general trends in relating ligand design to cell viability, but these conclusions are made on a relatively small sample size, and therefore have not been very thoroughly investigated. The nature of the lanthanoid ion itself does not appear to influence toxicity. Neutral complexes are generally less cytotoxic than cationic complexes, with triflate salts more toxic than chloride salts. There is no clear trend between choromophore or pendant arms and cytotoxicity, but these various studies identified a small class of complexes which did show appreciable toxicity, and it is valuable to examine these complexes to understand mechanisms by which they kill cells.

The more toxic lanthanoid complexes (with IC_{50} values less than 50 μM) are shown in Figure 5.19. Complex Eu.**17**, bearing an azathioxanthone chromophore, exhibits appreciable toxicity, far higher than the analogous azaxanthone. Importantly, however, other complexes incorporating the identical azathioxanthone chromophore were non-toxic. Instead, it appears that cytotoxicity accompanies dissociation of the complex, releasing the free chromophore which can be oxidised to the toxic sulfone form [100]. This emphasises the importance of a stable complex in ensuring cellular viability.

Complexes Eu.**18** and Eu.**19** were synthesised as part of a series bearing azaxanthone chromophores appended to various groups intended to influence cellular behaviour [89]. These two complexes are considerably more cytotoxic than the parent azaxanthone complex that bears no appendage. Mechanisms of toxicity were evaluated using an apoptosis-necrosis flow-cytometry assay, which can differentiate between programmed cell death (apoptosis) and unregulated death from trauma (necrosis) [124]. The flow cytometric analysis clearly showed that Eu.**18** causes cell death by necrosis, which is consistent with the explanation that the long hydrophobic chain lodges in the lipid bilayer, disrupting the cell membrane. This acts as a caution for future probe design, for which such moieties should be avoided. Eu.**19**, on the other hand, caused cell death by apoptosis, with a population of cells observed in apoptosis, but the majority of cells being late apoptotic. This complex bears a polyguanidinium vector intended to transport the conjugate to the mitochondria. It is likely that the complex caused damage to the mitochondria, which play a key role in the induction of apoptosis.

Eu.**20**, while less toxic than the previous three complexes, still shows appreciable toxicity compared with the majority of complexes. Since this complex was found to partition in the mitochondria and lysosomes, disruption of MMP was measured as a possible cause of toxicity [91]. MMP was measured using a flow cytometry assay with two fluorescent mitochondrial dyes [125]. The analysis found that Eu.**20** did cause some uncoupling of the MMP, which could be responsible for cell death, probably by apoptosis.

In addition to minimise toxicity of probes, it is also important to ensure that probes will have minimal interaction with normal cellular processes: if they disrupt these processes, they will not be suitable to report on homeostatic functions. For a mitochondrially-targeted probe, therefore, the complex should have minimal effect on MMP. To this end, MMP was assessed for a range of complexes, in addition to Eu.**20**. It was found that the probes which partitioned to both the mitochondrial and lysosomes, of which Eu.**20** is an example, all disrupted MMP. In contrast, the purely mitochondrial probes discussed in Section 5.7.2 did not disrupt MMP, even after 24 hours. These probes therefore have more promise as sensors for the mitochondria.

It seems, therefore, that for luminescent lanthanoid complexes, toxicity is the exception rather than the rule. If a complex is sufficiently stable, it can be reasonably assumed to be non-toxic. Most exceptions to this arise from the appendage of bulky groups onto the ligand, which are incompatible with the cell. This means that

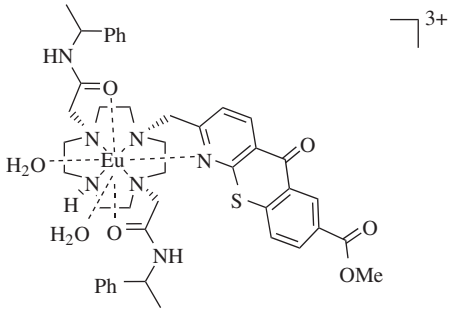

[Eu.**17**]$^{3+}$

IC_{50} = 5.6 μM

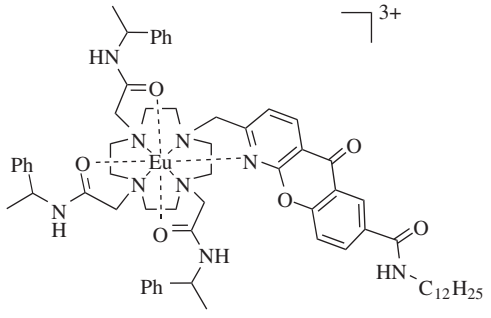

[Eu.**18**]$^{3+}$

IC_{50} = 7.2 μM

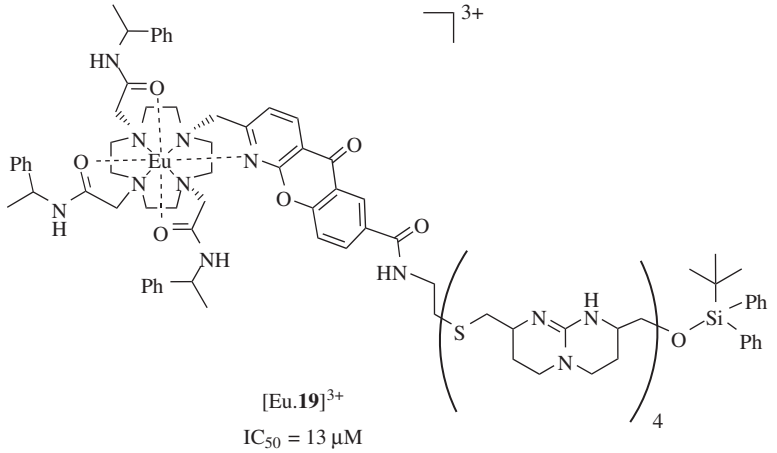

[Eu.**19**]$^{3+}$

IC_{50} = 13 μM

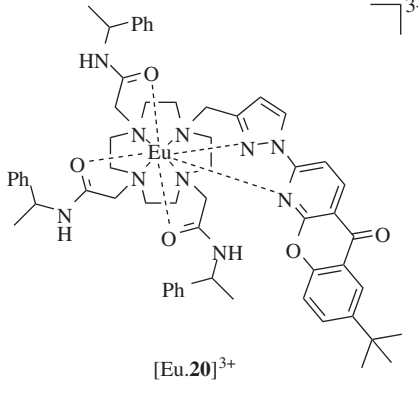

[Eu.**20**]$^{3+}$

IC_{50} = 41 μM

Figure 5.19 *Luminescent lanthanoid complexes are generally not toxic to cells. Some isolated examples, shown here, exhibit appreciable toxicity (IC_{50} values are for 24 hour incubation)*

ligand design does not need to focus on the achievement of a non-toxic complex, but rather can be directed towards other biological and chemical properties of interest.

5.8 Concluding remarks

This chapter has highlighted a number of aspects of chemical and biological behaviour which should be screened at an early stage in the design process to assess for potential use as a cellular probe. Importantly, cellular behaviour of putative probes should be screened before incorporation of complex strategies to elicit uptake or controlled cellular localisation.

Luminescent lanthanoid complexes certainly show great promise for probes of cellular structure and function. With careful selection of ligand features, the behaviour of the probes can be finely controlled, and these complexes stand to play an important role in biological studies in the future.

Acknowledgement

We gratefully acknowledge Professor David Parker at Durham University for his leading research in this field, and for his invaluable mentorship.

References

1. Massoud, T.F. and Gambhir, S.S. (2003) Molecular imaging in living subjects: seeing fundamental processes in a new light. *Genes Dev.*, **17**, 545–580.
2. Sutton, E.J., Henning, T.D., Pichler, B.J. *et al*. (2008) Cell tracking with optical imaging. *Eur. Radiol.*, **18**, 2021–2032.
3. Welsh, D.K. and Noguchi, T. (2012) Cellular bioluminescence imaging. *Cold Spring Harbor Protoc.*, **2012** (8). doi: 10.1101/pdb.top070607
4. Lakowicz, J.R. (1999) *Principles of Fluorescence Spectroscopy*, Springer, New York.
5. Ueno, T., Urano, Y., Setsukinai, K. *et al*. (2004) Rational principles for modulating fluorescence properties of fluorescein. *J. Am. Chem. Soc.*, **126** (43), 14079–14085.
6. Urano, Y., Kamiya, M., Kanda, K. *et al*. (2005) Evolution of fluorescein as a platform for finely tunable fluorescence probes. *J. Am. Chem. Soc*, **127** (13), 4888–4894.
7. Yogo, T., Urano, Y., Ishitsuka, Y. *et al*. (2005) Highly efficient and photostable photosensitizer based on BODIPY chromophore. *J. Am. Chem. Soc*, **127** (35), 12162–12163.
8. Shimomura, O., Johnson, F.H. and Saiga, Y. (1962) Extraction, purification and properties of aequorin, a bioluminescent protein from the luminous hydromedusan, *Aequorea*. *J. Cell. Comp. Physiol*, **59**, 223–239.
9. Prasher, D.C., Eckenrode, V.K., Ward, W.W. *et al*. (1992) Primary structure of the Aequorea victoria green-fluorescent protein. *Gene*, **111**, 229–233.
10. Tsien, R.Y. (1998) The green fluorescent protein. *Annu. Rev. Biochem*, **67**, 509–544.
11. Ormö, M., Cubitt, A.B., Kallio, K. *et al*. (1996) Crystal structure of the Aequorea victoria green fluorescent protein. *Science*, **273** (5280), 1392–1395 Image from the RCSB PDB (www.pdb.org) of PDB ID 1ema.
12. Chen, W.C.W., Maxwell, D.J., Gao, X.H. *et al*. (2002) Luminescent quantum dots for multiplexes biological detection and imaging. *Curr. Opin. Biotechnol*, **12**, 40–46.
13. Wu, X.Y., Liu, H.J., Liu, J.Q. *et al*. (2003) Immunofluorescent labeling of cancer marker Her2 and other cellular targets with semiconductor quantum dots. *Nat. Biotechnol.*, **21**, 41–46.
14. Keefe, M.H., Benkstein, K.D. and Hupp, J.T. (2000) Luminescent sensor molecules based on coordinated metals: a review of recent developments. *Coord. Chem. Rev*, **205**, 201–228.

15. Handl, H.L. and Gillies, R.J. (2005) Lanthanide-based luminescent assays for ligand-receptor interactions. *Life Sci*, **77** (4), 361–371.
16. Moore, E.G., Samuel, A.P.S. and Raymond, K.N. (2009) From antenna to assay: lessons learned in lanthanide luminescence. *Acc. Chem. Res*, **42** (4), 542–552.
17. Hagan, A.K. and Zuchner, T. (2011) Lanthanide-based time-resolved luminescence immunoassays. *Anal. Bioanal. Chem*, **400** (9), 2847–2864.
18. Montgomery, C.P., Murray, B.S., New, E.J. *et al*. (2009) Cell-penetrating metal complex optical probes: targeted and responsive systems based on lanthanide luminescence. *Acc. Chem. Res*, **42**, 925–937.
19. Bunzli, J.-C.G. (2009) Lanthanide luminescent bioprobes (LLBs). *Chem. Lett*, **38**, 104–109.
20. Thibon, A. and Pierre, V.C. (2009) Principles of responsive lanthanide-based luminescent probes. *Anal. Bioanal. Chem*, **394**, 107–120.
21. New, E.J., Parker, D., Smith, D.G. and Walton, J.W. (2010) Development of responsive lanthanide probes for cellular applications. *Curr. Opin. Chem. Biol*, **14**, 238–246.
22. Parker, D. (2004) Excitement in f block: structure, dynamics and function of nine-coordinate chiral lanthanide complexes in aqueous media. *Chem. Soc. Rev*, **3**, 156–165.
23. Døssing, A. (2005) Luminescence from lanthanide(3+) ions in solution. *Eur. J. Inorg. Chem*, **2005**, 1425–1434.
24. Bünzli, J.-C.G., Comby, S., Chauvin, A.-S. and Vandevyver, C.D.B. (2007) New opportunities for lanthanide luminescence. *J. Rare Earths*, **25** (3), 257–274.
25. Bünzli, J.-C.G. (2010) Lanthanide luminescence for biomedical analyses and imaging. *Chem. Rev.*, **110** (5), 2729–2755.
26. Atkins, P. and de Paula, J. (2002) *Atkins' Physical Chemistry*, Oxford University Press, Oxford.
27. Bünzli, J.-C.G. and Piguet, C. (2005) Taking advantage of luminescent lanthanide ions. *Chem. Soc. Rev*, **34**, 1048–1077.
28. Beeby, A., Faulkner, S., Parker, D. and Williams, J.A.G. (2001) Sensitised luminescence from phenanthridine appended lanthanide complexes: analysis of triplet mediated energy transfer processes in terbium, europium and neodymium complexes. *J. Chem. Soc., Perkin Trans. 2*, **2001**, 1268–1273.
29. Mironov, V.S., Galyametdinov, Y.G., Ceulemans, A. *et al*. (2002) Room-temperature magnetic anisotropy of lanthanide complexes: a model study for various coordination polyhedra. *J. Chem. Phys*, **116** (11), 4673–4685.
30. Dickins, R.S., Parker, D., Bruce, J.I. and Tozer, D.J. (2003) Correlation of optical and NMR spectral information with coordination variation for axially symmetric macrocyclic Eu(III) and Yb(III) complexes: axial donor polarisability determines ligand field and cation donor preference. *J. Chem. Soc. Dalton Trans*, 1264–1271.
31. Mathis, G. and Bazin, H. (2011) Stable luminescent chelates and macrocyclic compounds. *Springer Ser. Fluoresc*, **7**, 47–88.
32. Greenwood, N.N. and Earnshaw, A. (1997) *Chemistry of the Elements*, Butterworth-Heinemann, Oxford.
33. Aspinall, H.C. (2001) *Chemistry of the f-Block Elements*, CRC Press, Boca Raton, FL.
34. Reichert, D.E., Lewis, J.S. and Anderson, C.J. (1999) Metal complexes as diagnostic tools. *Coord. Chem. Rev*, **184**, 3–66.
35. Lukeš, I., Kotek, J., Vojtíšek, P. and Herman, P. (2001) Complexes of tetraazacycles bearing methylphosphinic/phosphonic acid pendant arms with copper(II), zinc(II) and lanthanides(III). A comparison with their acetic acid analogues. *Coord. Chem. Rev*, **216–217**, 287–312.
36. Sabbatini, N., Guardigli, M., Mecati, A. *et al*. (1990) Encapsulation of lanthanide ions in calixarene receptors. A strongly luminescent terbium(3+) complex. *J. Chem. Soc., Chem. Commun*, 878–879.
37. Wu, S.L. and Horrocks, W.D. (1996) General method for the determination of stability constants of lanthanide ion chelates by ligand − ligand competition: laser-excited Eu3+ luminescence excitation spectroscopy. *Anal. Chem*, **68** (2), 394–401.
38. Wu, S.L. and Horrocks, W.D. (1997) Direct determination of stability constants of lanthanide ion chelates by laser-excited europium(III) luminescence spectroscopy: application to cyclic and acyclic aminocarboxylate complexes. *J. Chem. Soc., Dalton Trans*, (9), 1497–1502.
39. Tircsó, G., Kovács, Z. and Sherry, A.D. (2006) Equilibrium and formation/dissociation kinetics of some LnIIIPCTA complexes. *Inorg. Chem*, **45** (23), 9269–9280.

40. Deiters, E., Song, B., Chauvin, A.S. *et al*. (2009) Luminescent bimetallic lanthanide bioprobes for cellular imaging with excitation in the visible-light range. *Chemistry*, **15** (4), 885–900.
41. D. Parker, J.A.G. Williams. Responsive luminescent lanthanide complexes. In: Sigel A., Sigel H. (eds) *Metal Ions in Biological Systems – The Lanthanides and Their Interrelations with Biosystems*. Marcel Dekker, New York p. 233–280 (2003).
42. Wolbers, M.P.O., van Veggel, F.C.J.M., Snellink-Ruël, B.H.M. *et al*. (1998) Photophysical studies of *m*-terphenyl-sensitized visible and near-infrared emission from organic 1: 1 lanthanide ion complexes in methanol solutions. *J. Chem. Soc., Perkin Trans. 2*, 2141–2150.
43. Quici, S., Marzanni, G., Cavazzini, M. *et al*. (2002) Highly luminescent Eu^{3+} and Tb^{3+} macrocyclic complexes bearing an appended phenanthroline chromophore. *Inorg. Chem*, **41**, 2777–2784.
44. Bobba, G., Frias, J.-C. and Parker, D. (2002) Highly emissive, nine-coordinate enantiopure lanthanide complexes incorporating tetraazatriphenylenes as probes for DNA. *Chem. Commun*, 890–891.
45. Poole, R.A., Bobba, G., Cann, M.J. *et al*. (2005) Synthesis and characterisation of highly emissive and kinetically stable lanthanide complexes suitable for usage '*in cellulo*'. *Org. Biomol. Chem*, **3**, 1013–1024.
46. Parker, D. and Yu, J. (2005) A pH-insensitive, ratiometric chemosensor for citrate using europium luminescence. *Chem. Commun*, 3141–3143.
47. Atkinson, P., Findlay, K.S., Kielar, F. *et al*. (2006) Azaxanthones and azathioxanthones are effective sensitisers for europium and terbium luminescence. *Org. Biomol. Chem*, **4**, 1707–1722.
48. Imperio, D., Giovenzana, G.B., Law, G.L. *et al*. (2010) Synthesis and comparative anion binding profiles of two di-aqua Eu(III) complexes. *Dalton Trans*, **39** (41), 9897–9903.
49. Parker, D., Walton, J.W., Lamarque, L. and Zwier, J.M. (2010) Comparative study of the luminescence properties and relative stability of a series of europium(III) complexes bearing one to four coordinated azaxanthone groups. *Eur. J. Inorg. Chem*, **25**, 3961–3966.
50. Law, G.-L., Man, C., Parker, D. and Walton, J.W. (2010) Observation of the selective staining of chromosomal DNA in dividing cells using a luminescent terbium(III) complex. *Chem. Commun*, **46** (14), 2391–2393.
51. Walton, J.W., Carr, R., Evans, N.H. *et al*. (2012) Isostructural series of nine-coordinate chiral lanthanide complexes based on triazacyclononane. *Inorg. Chem.*, **51** (15), 8042–8056.
52. Parker, D. (2000) Luminescent lanthanide sensors for pH, pO_2 and selected anions. *Coord. Chem. Rev*, **205**, 109–130.
53. Parker, D., Dickins, R.S., Puschmann, H. *et al*. (2002) Being excited by lanthanide coordination complexes: aqua species, chirality, excited-state chemistry, and exchange dynamics. *Chem. Rev*, **102** (6), 1977–2010.
54. Beeby, A., Clarkson, I.M., Dickins, R.S. *et al*. (1999) Non-radiative deactivation of the excited states of europium, terbium and ytterbium complexes by proximate energy-matched OH, NH and CH oscillators: an improved luminescence method for establishing solution hydration states. *J. Chem. Soc., Perkin Trans. 2*, **1999**, 493–503.
55. Dickins, R.S., Parker, D., de Sousa, A.S. and Williams, J.A.G. (1996) Closely diffusing O-H, amide N-H and methylene C-H oscillators quench the excited state of europium complexes in solution. *Chem. Commun*, 697–698.
56. Hebbink, G.A., Reinhoudt, D.N. and van Veggel, F.C.J.M. (2001) Increased luminescent lifetimes of Ln3+ complexes emitting in the near-infrared as a result of deuteration. *Eur. J. Org. Chem*, **2001**, 4101–4106.
57. Faulkner, S., Pope, S.J.A. and Burton-Pye, B.P. (2005) Lanthanide complexes for luminescence imaging applications. *Appl. Spectrosc. Rev*, **40** (1), 1–31.
58. Lippert, A.R., Gschneidtner, T. and Chang, C.J. (2010) Lanthanide-based luminescent probes for selective time-gated detection of hydrogen peroxide in water and in living cells. *Chem. Commun. (Cambridge, UK)*, **46**, 7510–7512.
59. Pershagen, E., Nordholm, J. and Borbas, K.E. (2012) Luminescent lanthanide complexes with analyte-triggered antenna formation. *J. Am. Chem. Soc*, **134** (24), 9832–9835.
60. Leonard, J.P., dos Santos, C.M.G., Plush, S.E. *et al*. (2007) pH driven self-assembly of a ternary lanthanide luminescence complex: the sensing of anions using a [small beta]-diketonate-Eu(III) displacement assay. *Chem. Commun*, (2), 129–131.
61. Cable, M.L., Kirby, J.P., Sorasaenee, K. *et al*. (2007) Bacterial spore detection by [Tb3 + (macrocycle)(dipicolinate)] luminescence. *J. Am. Chem. Soc*, **129** (6), 1474–1475.

62. Ye, Z.Q., Wang, G.L., Chen, J.X. *et al*. (2010) Development of a novel terbium chelate-based luminescent chemosensor for time-resolved luminescence detection of intracellular Zn2+ ions. *Biosens. Bioelectron*, **26** (3), 1043–1048.
63. Terai, T., Kikuchi, K., Urano, Y. *et al*. (2012) A long-lived luminescent probe to sensitively detect arylamine N-acetyltransferase (NAT) activity of cells. *Chem. Commun. (Cambridge, UK)*, **48**, 2234–2236.
64. Song, B., Wang, G., Tan, M. and Yuan, J. (2006) A europium(III) complex as an efficient singlet oxygen luminescence probe. *J. Am. Chem. Soc*, **128** (41), 13442–13450.
65. Thibon, A. and Pierre, V.C. (2009) A highly selective luminescent sensor for the time-gated detection of potassium. *J. Am. Chem. Soc*, **131**, 434–435.
66. Smith, D.G., Law, G.-L., Murray, B.S. *et al*. (2011) Evidence for the optical signalling of changes in bicarbonate concentration within the mitochondrial region of living cells. *Chem. Commun*, **47** (26), 7347–7349.
67. Pal, R. and Parker, D. (2007) A single component ratiometric pH probe with long wavelength excitation of europium emission. *Chem. Commun*, 474–476.
68. Liu, M.J., Ye, Z.Q., Xin, C.L. and Yuan, J.L. (2013) Development of a ratiometric time-resolved luminescence sensor for pH based on lanthanide complexes. *Anal. Chim. Acta*, **761**, 149–156.
69. Sherwood, L. (2001) *Human Physiology: from Cells to Systems*, 4th edn, Brooks/Cole, Pacific Grove, CA.
70. Ahrens, E.T., Rothbacher, U., Jacobs, R.E. and Fraser, S.E. (1998) A model for MRI contrast enhancement using T_1 agents. *Proc. Natl. Acad. Sci. U.S.A*, **95** (15), 8443–8448.
71. Terreno, E., Crich, S.G., Belfiore, S. *et al*. (2006) Effect of the intracellular localization of a Gd-based imaging probe on the relaxation enhancement of water protons. *Magn. Reson. Med.*, **55** (3), 491–497.
72. Kabalka, G.W., Davis, M.A., Moss, T.H. *et al*. (1991) Gadolinium-labeled liposomes containing various amphiphilic Gd-DTPA derivatives: targeted MRI contrast enhancement agents for the liver. *Magn. Reson. Med*, **19**, 406–415.
73. Hak, S., Sanders, H.M.H.F., Agrawal, P. *et al*. (2009) A high relaxivity Gd(III)DOTA-DSPE-based liposomal contrast agent for magnetic resonance imaging. *Eur. J. Pharm. Biopharm*, **72**, 397–404.
74. Curtet, C., Maton, F. and Havet, T. (1998) Polylysine-Gd-DTPA(n) and polylysine-Gd-DOTA(n) coupled to anti-CEA F(ab′)(2) fragments as potential immunocontrast agents – relaxometry, biodistribution, and magnetic resonance imaging in nude mice grafted with human colorectal carcinoma. *Invest. Radiol*, **33**, 752–761.
75. Bhorade, R., Weissleder, R., Nakakoshi, T. *et al*. (2000) Macrocylic chelators with paramagnetic cations are internalized into mammalian cells via an HIV-Tat derived membrane translocation peptide. *Bioconjugate Chem*, **11**, 301–305.
76. Heckl, S., Debus, J., Jenne, J. *et al*. (2002) CNN-Gd^{3+} enables cell nucleus molecular imaging of prostate cancer cells: the last 600 nm. *Cancer Res*, **62**, 7018–7024.
77. Allen, M. and Meade, T.J. (2003) Synthesis and visualization of a membrane-permeable MRI contrast agent. *J. Biol. Inorg. Chem*, **8** (7), 746–750.
78. Wiener, E.C., Konda, S., Shadron, A. *et al*. (1997) Targeting dendrimer-chelates to tumors and tumor cells expressing the high-affinity folate receptor. *Invest. Radiol*, **32**, 748–754.
79. Casali, C., Janier, M. and Canet, E. (1998) Evaluation of Gd-DOTA-labeled dextran polymer as an intravascular MR contrast agent for myocardial perfusion. *Acad. Radiol*, **5**, 214–218.
80. Endres, P.J., Paunesku, T., Vogt, S. *et al*. (2007) DNA – TiO2 nanoconjugates labeled with magnetic resonance contrast agents. *J. Am. Chem. Soc*, **129**, 15760–15761.
81. Song, Y., Xu, X., MacRenaris, K.W. *et al*. (2009) Multimodal gadolinium-enriched DNA-gold nanoparticle conjugates for cellular imaging. *Angew. Chem. Int. Ed*, **48**, 9143–9147.
82. Lewin, M., Carlesso, N., Tung, C.H. *et al*. (2000) Tat peptide-derivatized magnetic nanoparticles allow in vivo tracking and recovery of progenitor cells. *Nat. Biotechnol*, **18** (4), 410–414.
83. Wunderbaldinger, P., Josephson, L. and Weissleder, R. (2002) Tat peptide directs enhanced clearance and hepatic permeability of magnetic nanoparticles. *Bioconjugate Chem*, **13** (2), 264–268.
84. Zhao, M., Kircher, M.F., Josephson, L. and Weissleder, R. (2002) Differential conjugation of tat peptide to superparamagnetic nanoparticles and its effect on cellular uptake. *Bioconjugate Chem*, **13** (4), 840–844.
85. Allen, M.J., MacRenaris, K.W., Venkatasubramanian, P.N. and Meade, T.J. (2004) Cellular delivery of MRI contrast agents. *Chem. Biol*, **11** (3), 301–307.
86. Endres, P.J., MacRenaris, K.W., Vogt, S. *et al*. (2006) Quantitative imaging of cell-permeable magnetic resonance contrast agents using x-ray fluorescence. *Mol. Imaging*, **5** (4), 485–497.

87. Endres, P.J., MacRenaris, K.W., Vogt, S. and Meade, T.J. (2008) Cell-permeable MR contrast agents with increased intracellular retention. *Bioconjugate Chem*, **19** (10), 2049–2059.
88. Que, E.L., New, E.J. and Chang, C.J. (2012) A cell-permeable gadolinium contrast agent for magnetic resonance imaging of copper in a Menkes disease model. *Chem. Sci*, **3** (6), 1829–1834.
89. Kielar, F., Congreve, A., Law, G.-L. *et al*. (2008) Two-photon microscopy study of the intracellular compartmentalisation of emissive terbium complexes and their oligo-arginine and oligo-guanidinium conjugates. *Chem. Commun*, 2435–2437.
90. Ha, Y., Tsay, O.G. and Churchill, D.G. (2011) A tutorial and mini-review of the ICP-MS technique for determinations of transition metal ion and main group element concentration in the neurodegenerative and brain sciences. *Monatsh. Chem*, **142** (4), 385–398.
91. New, E.J., Congreve, A. and Parker, D. (2010) Definition of the uptake mechanism and sub-cellular localisation profile of emissive lanthanide complexes as cellular optical probes. *Chem. Sci*, **1**, 111–118.
92. Walton, J.W., Bourdolle, A., Butler, S.J. *et al*. (2013) Very bright europium complexes that stain cellular mitochondria. *Chem. Commun*, **49** (16), 1600–1602.
93. Sieczkarski, S.B. and Whittaker, G.R. (2002) Dissecting virus entry via endocytosis. *J. Gen. Virol*, **83**, 1535–1545.
94. New, E.J. and Parker, D. (2009) The mechanism of cell uptake for luminescent lanthanide optical probes: the role of macropinocytosis and the effect of enhanced membrane permeability on compartmentalisation. *Org. Biomol. Chem*, **7**, 851–855.
95. Watts, C. and Marsh, M. (1992) Endocytosis: what goes in and how? *J. Cell Sci*, **103**, 1–8.
96. Fukuda, T., Ewan, L., Bauer, M. *et al*. (2006) Dysfunction of endocytic and autophagic pathways in a lysosomal storage disease. *Ann. Neurol*, **59** (4), 700–708.
97. Cai, J. and Jones, D. (1999) Mitochondrial redox signaling during apoptosis. *J. Bioenerg. Biomembr*, **31** (4), 327–334.
98. Li, M., Ganea, G.M., Lu, C. *et al*. (2012) Lipophilic phosphonium-lanthanide compounds with magnetic, luminescent, and tumor targeting properties. *J. Inorg. Biochem*, **107**, 40–46.
99. Wang, B., Hai, J., Wang, Q. *et al*. (2011) Coupling of luminescent terbium complexes to Fe_3O_4 nanoparticles for imaging applications. *Angew. Chem. Int. Ed*, **50**, 3063–3066, S/1–S/16.
100. Murray, B.S., New, E.J., Pal, R. and Parker, D. (2008) Critical evaluation of five emissive europium(III) complexes as optical probes: correlation of cytotoxicity, anion and protein affinity with complex structure, stability and intracellular localisation profile. *Org. Biomol. Chem*, **6**, 2085–2094.
101. Smith, D.G., McMahon, B.K., Pal, R. and Parker, D. (2012) Live cell imaging of lysosomal pH changes with pH responsive ratiometric lanthanide probes. *Chem. Commun*, **48** (68), 8520–8522.
102. Smith, D.G., Pal, R. and Parker, D. (2012) Measuring equilibrium bicarbonate concentrations directly in cellular mitochondria and in human serum using europium/terbium emission intensity ratios. *Chem. Eur. J*, **18** (37), 11604–11613.
103. Racoosin, E.L. and Swanson, J.A. (1992) M-CSF-induced macropinocytosis increases solute endocytosis but not receptor-mediated endocytosis in mouse macrophages. *J. Cell Sci*, **102** (4), 867–880.
104. Rofsky, N.M., Sherry, A.D. and Lenkinski, R.E. (2008) Nephrogenic systemic fibrosis: a chemical perspective1. *Radiology*, **247** (3), 608–612.
105. FDA (2010) FDA Drug Safety Communication: New Warnings for Using Gadolinium-Based Contrast Agents in Patients with Kidney Dysfunction. FDA Alert: US FDA.
106. Sarkander, H.I. and Brade, W.P. (1976) On the mechanism of lanthanide-induced liver toxicity. *Arch. Toxicol*, **36** (1), 1–17.
107. Cuthbert, A.W. (1988) The multiple physiological roles of calcium: possible sites for pharmacological intervention, in *Calcium in Drug Actions* (ed P. Baker), Springer, Berlin, Heidelberg, pp. 1–6.
108. Cheng, Y., Liu, M., Li, R. *et al*. (1999) Gadolinium induces domain and pore formation of human erythrocyte membrane: an atomic force microscopic study. *Biochim. Biophys. Acta, Biomembr*, **1421** (2), 249–260.
109. Wang, K., Li, R., Cheng, Y. and Zhu, B. (1999) Lanthanides – the future drugs? *Coord. Chem. Rev*, **190–192**, 297–308.
110. Fricker, S.P. (2006) The therapeutic application of lanthanides. *Chem. Soc. Rev*, **35** (6), 524–533.

111. Monasterio, O., Acoria, M., Diaz, M.A. and Lagos, R. (1993) The binding of terbium ions to tubulin induces ring formation. *Arch. Biochem. Biophys*, **300** (2), 582–587.
112. Soto, C., Rodríguez, P.H. and Monasterio, O. (1996) Calcium and gadolinium ions stimulate the GTPase activity of purified chicken brain tubulin through a conformational change. *Biochemistry*, **35** (20), 6337–6344.
113. Cacheris, W.P., Quay, S.C. and Rocklage, S.M. (1990) The relationship between thermodynamics and the toxicity of gadolinium complexes. *Magn. Reson. Imaging*, **8** (4), 467–481.
114. Vandevyver, C.D., Chauvin, A.S., Comby, S. and Bünzli, J.-C.G. (2007) Luminescent lanthanide bimetallic triple-stranded helicates as potential cellular imaging probes. *Chem. Commun*, (17), 1716–1718.
115. Song, B., Vandevyver, C.D.B., Chauvin, A.S. and Bunzli, J.-C.G. (2008) Time-resolved luminescence microscopy of bimetallic lanthanide helicates in living cells. *Org. Biomol. Chem*, **6** (22), 4125–4133.
116. Kielar, F., Law, G.-L., New, E.J. and Parker, D. (2008) The nature of the sensitiser substituent determines quenching sensitivity and protein affinity and influences the design of emissive lanthanide complexes as optical probes for intracellular use. *Org. Biomol. Chem*, **6**, 2256–2258.
117. Montgomery, C.P., New, E.J., Palsson, L.O. *et al*. (2009) Emissive and cell permeable pyridyl and pyrazolyl-1-azaxanthone lanthanide complexes and their behaviour *in cellulo*. *Helv. Chim. Acta*, **92** (11), 2186–2213.
118. New, E.J., Parker, D. and Peacock, R.D. (2009) Comparative study of the constitution and chiroptical properties of emissive lanthanide complexes with a common tetraazatriphenylene sensitiser: the nature of the sensitiser determines quenching sensitivity and cellular uptake. *Dalton Trans*, 672–679.
119. Law, G.L., Wong, K.L., Man, C.W.Y. *et al*. (2009) A two-photon europium complex as specific endoplasmic reticulum probe. *J. Biophotonics*, **2** (12), 718–724.
120. Law, G.-L., Pal, R., Palsson, L.O. *et al*. (2009) Responsive and reactive terbium complexes with an azaxanthone sensitiser and one naphthyl group: applications in ratiometric oxygen sensing in vitro and in regioselective cell killing. *Chem. Commun*, (47), 7321–7323.
121. Bretonniere, Y., Cann, M.J., Parker, D. and Slater, R. (2004) Design, synthesis and evaluation of ratiometric probes for hydrogencarbonate based on europium emission. *Org. Biomol. Chem*, **2**, 1624–1632.
122. Pandya, S., Yu, J. and Parker, D. (2006) Engineering emissive europium and terbium complexes for molecular imaging and sensing. *Dalton Trans*, 2757–2766.
123. Yu, J., Parker, D., Pal, R. *et al*. (2006) A europium complex that selectively stains nucleoli of cells. *J. Am. Chem. Soc*, **128**, 2294–2299.
124. Ormerod, M.G. (2000) Flow cytometry in the study of apoptosis, in *Flow Cytometry: A Practical Approach* (ed M.G. Ormerod), Oxford University Press, Oxford, pp. 235–248.
125. Prendergrass, W., Wolf, N. and Poot, M. (2004) Efficacy of MitoTracker GreenTM and CMXRosamine to measure changes in mitochondrial membrane potentials in living cells and tissues. *Cytometry*, **61A**, 162–169.

6

Metal Complexes of Carbohydrate-targeted Ligands in Medicinal Inorganic Chemistry

Yuji Mikata[1] and Michael Gottschaldt[2,3]

[1]*KYOUSEI Science Center, Nara Women's University, Kitauoya-Higashi-machi, Nara, 630-8506, Japan*
[2]*Laboratory for Organic and Macromolecular Chemistry, Friedrich Schiller University Jena, Humboldtstrasse 10, 07743, Jena, Germany*
[3]*Jena Center for Soft Matter (JCSM), Friedrich Schiller University Jena, Philosophenweg 7, 07743, Jena, Germany*

6.1 Introduction

Carbohydrates play many important roles in living systems. Respiration produces energy from carbohydrates, and many molecules or tissues of significant biological importance, including nucleic acids, glycoprotein, glycolipids and cell walls contain a wide variety of carbohydrates in many forms as essential components. Oligomeric carbohydrates displayed on the surface of cell walls control cell recognition and immunologic response; they are accountable for the identity of individual cells.

As an energy source, monosaccharides have to be taken up by cells. Since this process cannot occur by the penetration of the hydrophilic carbohydrates through the lipophilic cell membrane, certain mechanisms to absorb specific carbohydrates into cell cytoplasm are necessary. A genome-wide similarity search identified 13 passive facilitative transporters (GLUT1-12 and H(+)-myo-inositol transporter (HMIT)) as well as 6 sodium-dependent sugar transporters (SGLTs) [1]. The proteins belonging to the GLUT-family all consist of 12 membrane spanning connected helices forming specific 'channels' to allow the hexoses to pass through the cell membranes (in both directions) [2]. Beyond dispute is that different cell types express different transporters to a different extent in their cell membranes (also depending on cell stage, hormones, etc.) and that in cancerous cells with a high energy consumption level these activities are heavily upregulated in order to assuage their need for nutrients. The transporters GLUT1-4 are mainly responsible for D-glucose uptake. Among them, GLUT1 is the best explored (very much selective for D-glucose, no larger substituent

Ligand Design in Medicinal Inorganic Chemistry, First Edition. Edited by Tim Storr.

on the sugar tolerated) which is ubiquitous in human cells. Its upregulation in tumour and inflammatory tissue is used for visualization by positron emission tomography (PET) applying 2-^{18}F-fluoro-2-deoxy-D-glucose (FDG) as the radiotracer. Other unidentified saccharide transporter proteins may exist and studies to explore such proteins are ongoing. Therefore, many drug candidates bearing carbohydrate targeting groups have been studied in order to enhance cancer-selective uptake.

Carbohydrates regulate cell-cell communications due to carbohydrates on the cell surface, which induce specific recognition, binding and immunologic response. Cell-specific uptake of sugar-substituted oligomers, dendrimers, polymers or nanoobjects through such recognition events and subsequent, for example endocytotic uptake also promotes the importance of carbohydrate-bearing materials as potential devices to deliver anticancer drugs and as imaging tools for diagnostic purposes.

Another important biological function of carbohydrates is their ability to pass through the blood brain barrier (BBB) because glucose is the primary energy source for the brain. Thus, there is a possibility that functionalized glucose and other related compounds may permeate through the BBB, acting as effective pharmaceutical and/or diagnostic reagents in the brain.

Essential metal ions in trace amounts exhibit significant biological importance; many transition metal ions are found in prosthetic groups of different enzymes. There are a lot of enzymes that require iron, zinc, magnesium, manganese or other metal ions for their catalytic activity. A deficiency of such metal ions inhibits necessary molecular transformations and disrupts homeostasis. However, an excess of metal ions above the necessary concentration range in living organisms can be harmful and induce many health problems. Toxic metal ions are considered to have a very small acceptable concentration limit in the body. Regulation of both essential and toxic metal ions by appropriate control of their concentration in specific tissues and/or the whole body can be aided by clinical treatment. Simple metal salts can also be administrated as supplemental drugs.

Ligands effectively modulate the uptake rate, uptake amount, uptake specificity for certain cells/tissues, residence time in the body, and toxicity of coordinated metal ions. Such modulation of the properties of metal complexes can be achieved by variation of lipophilicity/hydrophilicity balance, specific recognition by receptors, charge cancellation and toxicity masked by coordination. Considering the biological importance of carbohydrates discussed above, carbohydrate-based ligand design for metal complexes can be an effective strategy for the development of potential drug molecules. The hydrophilicity of carbohydrates enhances the water-solubility of sugar-connected metal complexes, and the structural diversity of carbohydrates allows the synthesis of versatile libraries of complexes. As connecting segments between chelating moieties and carbohydrates in carbohydrate-conjugated ligands, *O*-, *N*-, *S*- and *C*-glycoside linkages can be designed. Among them, *C*-glycosides are carbon analogs of naturally existing *O*-glycosides and exhibit extremely high stability toward chemical and enzymatic degradation. Since naturally-occurring antibiotics include *C*-glycosidic compounds, *C*-glycoside-containing ligands are attractive for medicinal molecular design.

From a green chemistry perspective, carbohydrates are natural products, reproducible and sustainable resources, with complex structures including pre-arranged asymmetric carbon atoms and functional groups. Thus, most synthetic routes to obtain carbohydrate-functionalized molecules are completed bio-synthetically, and the resulting molecules are inexpensive. During enzymatic digestion of carbohydrate-pendant metal complexes, it is likely that the carbohydrate moiety would be metabolized as a natural product, so it would exhibit extremely high biocompatibility.

Evaluating the above criteria, a carbohydrate-targeted approach for medicinal inorganic chemistry is a very attractive molecular design strategy for functional metal complexes. In this chapter, recent progress for carbohydrate-based metal complexes [3–6] is summarized briefly and future prospects for the effective molecular design of carbohydrate-functionalized ligands and metal complexes is proposed.

6.2 Radioactive metal complexes bearing a carbohydrate moiety

Radiopharmaceutical imaging is a rapidly growing field. For PET 2-^{18}F-2-deoxy-D-glucose (FDG) is the most frequently applied radio tracer. The over-expression of the GLUT1 transporter in cancer or similar rapidly growing cells enhances the uptake of FDG, which can therefore be used to identify the location of cancerous cells in the human body. Because the half-life of ^{18}F is considerably short ($t_{1/2} = 110$ minutes), clinical facility for PET diagnosis requires large cyclotron equipment and radiochemical laboratories nearby in order to generate radiotracers of this fast-decaying isotope. ^{68}Ga is a metallic positron emitter with a half-life of 68 minutes but in contrast to ^{18}F it is produced from a germanium-based generator that can be located on-site [7]. In this context, single photon emission computed tomography (SPECT) is also a widely used imaging process. SPECT can employ group VII metals such as ^{99m}Tc ($t_{1/2} = 110$ minutes and $\gamma = 142.7$ keV) and ^{186}Re ($t_{1/2} = 3.68$ days, $\beta = 1.07$ MeV and $\gamma = 137$ keV)/^{188}Re ($t_{1/2} = 16.98$ hours, $\beta = 2.12$ MeV and $\gamma = 155$ keV), which have ideal properties for radiopharmaceutical imaging as well as therapeutic nuclear medicine, respectively. In addition, $^{99m}TcO_4^-$ and the more convenient $[^{99m}Tc(CO)_3(H_2O)_3]^+$ are obtained easily from a small ^{99}Mo generator kit [8]. Versatile ligand design can be used to stabilize the complexes and influence uptake rate, accumulation and localization. Introduction of carbohydrate radionuclide complexes to nuclear medicine is therefore of particular interest [9, 10].

At an early-stage, comprehensive studies using ^{99m}Tc tricarbonyl complexes with several different tridentate chelating moieties including iminodiacetate (IDA), *N*-(2-pyridylmethyl)glycine (NPG) and $N_{aliphatic}$-tethered histidine at the C-1, C-2, C-3 and C-6 position of glucose have been reported by Shibli *et al*. (Figure 6.1) [11]. The experimental results indicate that uptake of these complexes was relatively low and not mediated by a GLUT1-dependent process. Among the complexes tested, only complexes carrying C-2 substituted glucose exhibited competitive yeast hexokinase (HK) inhibition activity, which would result in steady internalization of the tracers by phosphorylation of the substrates to negatively charged products. A docking study utilizing X-ray crystallographic analysis data of the carbohydrate binding site of HK suggests that the C-2 position of glucose is the most tolerated position for synthetic functionalization to connect a metal binding unit to the monosaccharide.

Considering the above results that C-2 functionalization is the most suitable for connecting a metal binding moiety to glucose, Orvig and co-workers extensively investigated glucosamine (2-amino-2-deoxyglucose) ligands with extended carboxamide or amine linkages that can be effectively introduced via acylation or reductive alkylation, respectively. Dipicolylamine [12], *N*-(2-hydroxybenzyl)glycine [13], 3-hydroxy-4-pyridinone [14] and cyclopentadienylato [15] groups were utilized as metal binding moieties in addition to the above mentioned functionalities (Figure 6.2). Even for the derivatives containing a long linker chain ($\sim C_{10}$) in which

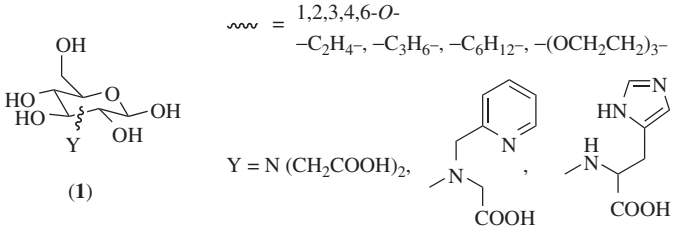

Figure 6.1 *Glucose-functionalized ligands for ^{99m}Tc and Re*

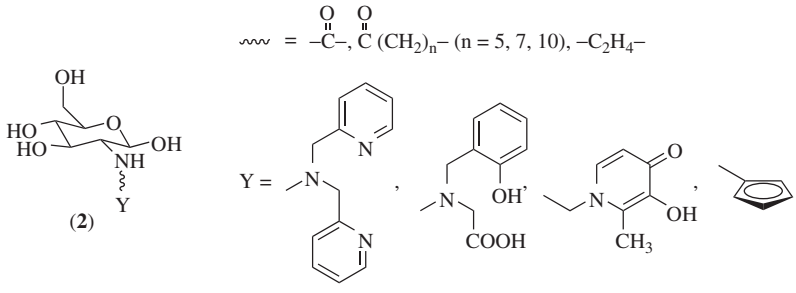

Figure 6.2 *Glucosamine-functionalized ligands for ^{99m}Tc and Re*

the carbohydrate moieties and the metal chelating centres were well separated, the glucosamine-based ^{99m}Tc complexes exhibited neither GLUT1 transportation nor HK inhibition activity on a satisfactory level [16].

Other selected examples for carbohydrate-conjugated ligands suitable for chelation of ^{99m}Tc and $^{186/188}$Re tricarbonyl metal centres are shown in Figure 6.3. Bidentate (**3, 4**) [17, 18], tridentate (**5, 6**) [19, 20] and tetradentate (**7, 8**) [21, 22] binding motifs have been most prominently studied. The tetradentate ligands can also form stable complexes with $[Tc=O]^{3+}$ and $[Re=O]^{3+}$ metal centres. Considering the charge compensation of the metal centre by the ligand, neutral bidentate ligands complexed to $Tc(CO)_3X$ (X = halogen), monoanionic tridentate ligands complexed to $[Tc(CO)_3]^+$ and trianionic tetradentate ligands bound to $[Tc=O]^{3+}$ will lead to uncharged complexes which may exhibit superior cell membrane permeability. In order to assess the stability of the metal-ligand interaction in these complexes, ~100 equivalents of histidine or cysteine were incubated with these metal complexes for 24 hours at 37 °C and then the percentage of degradation was investigated. Such histidine/cysteine challenge experiments reveal that tridentate chelation to the $[Tc(CO)_3]^+$ core is generally more stable than bidentate ligand binding. Utilizing the metal binding moieties shown in Figure 6.3, a large variety of different carbohydrates have been applied. In the bidentate ligand series, steric bulk of the carbohydrate moiety tends to enhance the stability of chelate binding, due to the prevention of the close approach of competing ligands. Carbohydrates have been attached to these ligands as *O*-, *N*-, *S*- and *C*-glycosides. Yang *et al*. synthesized the ^{99m}Tc-complex of ethylenedicysteine-deoxyglucose (^{99m}Tc-ECDG, **7**) and studied its biodistribution in lung tumour-bearing mice [21]. They observed higher tumour-to-brain and tumour-to-muscle tissue ratios for ^{99m}Tc-ECDG compared with ^{18}F-FDG, but a lower tumour-to-blood ratio. Connection of the monoamino-monoamide dithiol (MAMA) or the mercaptoacetylglycylglycylglycine (MAG_3, **8**) to 2-deoxy-2-aminoglucose (DG), galactose (Gal) or glucose with different linking units and radiolabelling with ^{99m}Tc afforded radiotracers with a sugar-dependent biodistribution *in vivo* possessing promising tumour-to-muscle ratios (^{99m}Tc-MAG_3-DG in MA891 breast tumour bearing mice [22]; ^{99m}Tc-MAG_3-Glc in Ehrlich tumour bearing mice [23, 24]) or enrichment in the liver as a potential imaging agent for hepatic function (^{99m}Tc-MAG_3-Gal in healthy Swiss mice [25]). In addition to these studies, at the moment no further evidence concerning the carbohydrate-promoted enhancement of cellular uptake of radioactive sugar metal complexes via the GLUT pathway has been reported.

Implementing 'Click Chemistry' proposed by Sharpless and Meldal [26, 27], carbohydrate moieties and metal binding sites are easily combined via copper-catalyzed 1,3-dipolar addition of azides and alkynes. Additionally, the formed 1,2,3-triazoles are able to contribute to metal cation chelation. Click chemistry therefore not only enables convenient coupling of two components but also provides in some cases a strong metal binding group in the proper position by a careful reaction design. This 'Click-to-Chelate' strategy has been widely applied to the synthesis of carbohydrate-pendant tridentate (**9**) and bidentate (**10**) ligands for ^{99m}Tc and Re ions (Figure 6.4) [28, 29]. In most of the cases, sugar-connected azides were coupled with alkynes

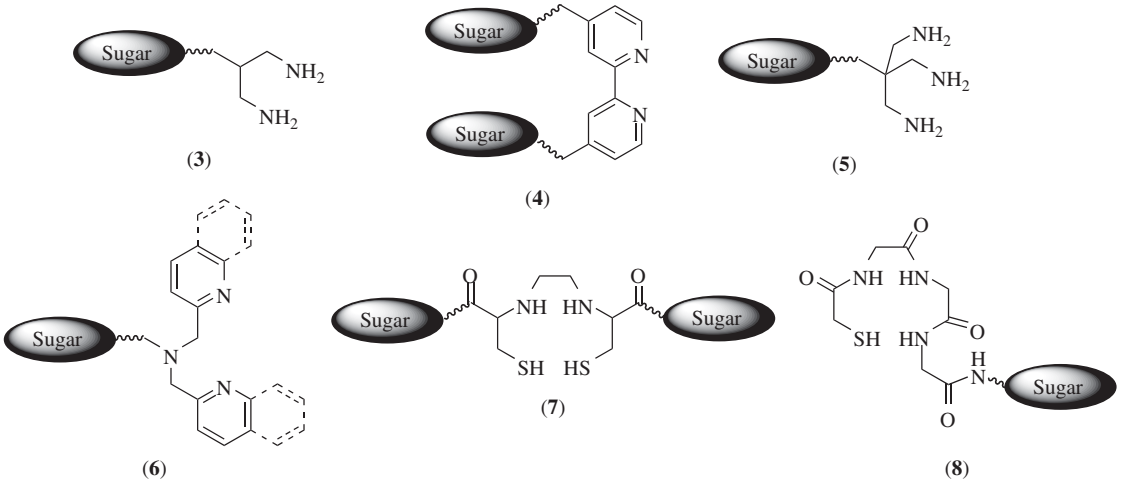

Figure 6.3 *Selected examples for carbohydrate-functionalized coordination motifs for ^{99m}Tc and Re*

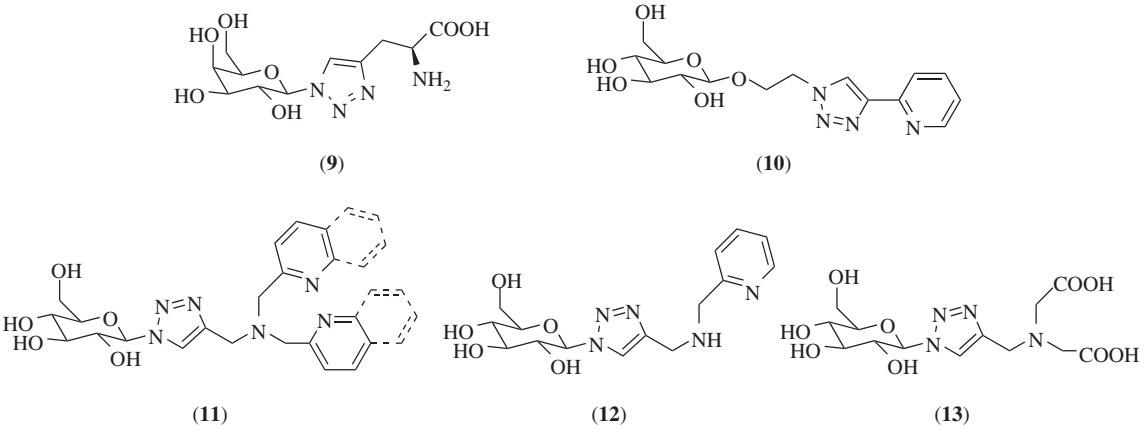

Figure 6.4 *Carbohydrate-functionalized 1,2,3-triazoles as ligands for ^{99m}Tc and Re*

containing additional metal binding sites such as primary amines, carboxylates and pyridines. The spacers between the carbohydrate and the metal centre can be modulated by a selection of sugar-azide substrates. To circumvent the formation of copper complexes with the resulting or preformed chelating units, Gouin and co-workers applied the heterogeneous copper-catalyzed cycloaddition (using copper- impregnated charcoal as the catalyst under microwave irradiation) to produce glucosylated ligands for $^{99m}Tc^{I}$ and Re^{I} or even to couple preformed Re-carbonyl complexes to the monosaccharide [30]. The obtained ligands **11–13** (all of them carrying a glucose unit) were radiolabelled with $^{99m}Tc^{I}$ and injected into healthy Wistar rats. Excellent *in vitro* stability, and fast *in vivo* blood clearance, together with low specific organ uptake has been observed for these glycoconjugates.

For the development of metal-based tracers for PET imaging, positron-emitting radionuclides have to be used, most appropriately ^{68}Ga ($t_{1/2} = 68$ minutes and $\beta^{+} = 1.9$ MeV), ^{64}Cu ($t_{1/2} = 12.7$ hours and

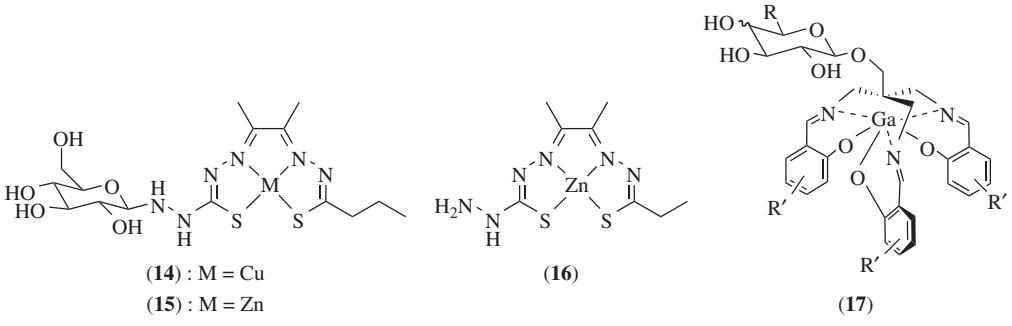

Figure 6.5 *^{64}Cu and Zn complexes for hypoxic cell imaging and a ^{68}Ga-complex*

$\beta^+ = 656$ keV) or ^{55}Co ($t_{1/2} = 17.6$ hours, $\beta^+ = 1513$ and 1037 keV). Only a very limited number of publications have appeared utilizing these radionuclides connected to a carbohydrate-based ligand. Dilworth and co-workers synthesized intermediate complexes of copper and zinc supported by two types of asymmetrical bis(thiosemicarbazonato) ligands, and further functionalized via introduction of a glucose moiety via a short hydrazide linker at the C-1 position of D-glucose (Figure 6.5) [31]. These ligands possess a 2N2S tetradentate dianionic environment, affording neutral complexes with divalent transition metals. Copper-64 labelling of these bis(thiosemicarbazonato) ligands has been carried out in order to test them as tracers for radiopharmaceutical imaging of hypoxic tissues. Cell uptake and washout studies using neutrophil cells indicate that under normoxic conditions the uptake of the ^{64}Cu-labelled complex (**14**) is rapid but reversible (less than 1% after triple washouts) and the complex was not trapped inside the cells. Confocal fluorescence microscopy utilizing fluorescent zinc complexes (**15**) and (**16**) incorporated into human IGROV-1 ovarian cancer cells showed internalization of the complexes, with a slower incorporation rate for the lipophilic complex (**16**) in comparison with the water-soluble glucose conjugate (**15**). Although routinely used for the labelling, for example of peptides, ^{68}Ga complexes of sugar-containing ligands are rarely found in the literature. Solely Orvig and co-workers described ('cold') gallium(III) and indium(III) complexes of 3-hydroxy-4-pyridinonato-monosaccharides [32]. Tripodal tris-salicylidene imines have been connected to different monosaccharides and complexed to Ga^{III} and In^{III} metal ions [33]. The glucose-bearing ligand was radiolabelled with $^{68}Ga^{III}$ to obtain the first saccharide-derived radioactive gallium complex (**17**), which additionally showed high stability against apo-transferrin as well as blood plasma.

6.3 MRI contrast agents utilizing metal complexes bearing carbohydrate moieties

Magnetic resonance imaging (MRI) is one of the most rapidly growing molecular imaging methodologies in clinical applications. Acceleration of the spin relaxation rate of the nucleus of interest, in most cases hydrogen nuclei of metal-bound water molecules, affords a signal which can be recorded with high spatial resolution. Lanthanide metals, most prominently represented by Gd, have been reported as effective MRI contrast agents possessing enough chemical stability with appropriate nitrogen-containing polycarboxylate ligands such as 1,4,7,10-tetrakis(carboxymethyl)-1,4,7,10-tetraazacyclododecane (DOTA) for *in vivo* applications [34, 35].

One possibility for the use of a carbohydrate in this area is as a multifunctional central scaffold for the attachment of a number of Gd^{III}-DOTA complexes, as has been recently applied by Martinez and co-workers [36]. They functionalized all eight free OH-groups of sucrose via 'click'-chemistry with Gd^{III}-DOTA complexes and used the materials for MRI of the gastrointestinal tract of C3H mice after oral administration.

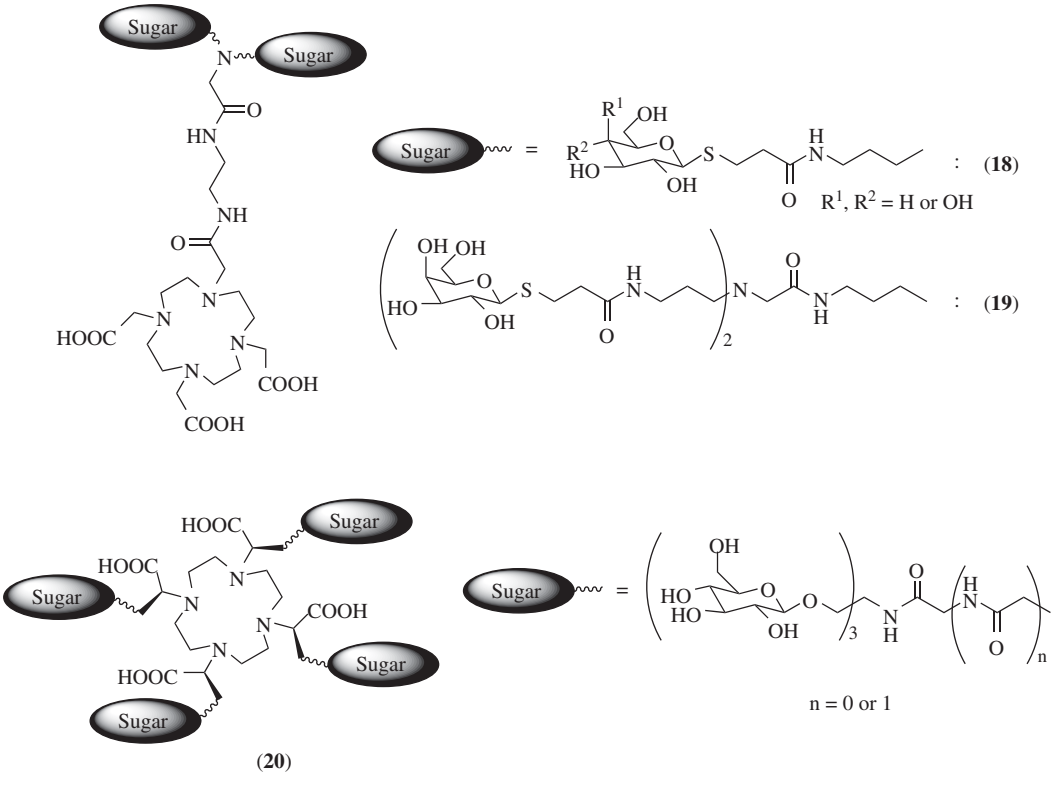

Figure 6.6 *Carbohydrate-functionalized DOTA ligands for Gd coordination*

In contrast to this, Figure 6.6 shows several examples for carbohydrate-conjugated ligands for MRI probes. Examples of central metals include Sm^{3+}, Eu^{3+} and Gd^{3+}. Most of them utilize a DOTA-lanthanide core as the centre and one or two carbohydrate functions which are tethered via amide linkages. In some cases, *S*-glycosides were used in order to prevent enzymatic cleavage. Enhanced water solubility and specific *in vivo* distribution of these complexes directed by attached carbohydrates are of primary interest.

André *et al*. have envisaged that the interaction of lectin and glycoconjugate (**18**) and (**19**) could considerably restrict the tumbling movement and therefore increase the relaxation rate of protons of Gd-bound water molecules [37]. However, they observed a slight increase (~5%) in proton relaxivity in a solution of 0.5% RCA_{120} (*Ricinus communis* agglutinin, Mw = 120 000) probably due to insufficient proportion (~8%) of lectin-bound Gd probes even for those with multivalent carbohydrate display. A combined NMR (nuclear magnetic resonace) and modelling study on lanthanum(III) complexes revealed, that besides the multivalent binding of the carbohydrate units to the lectin, also the structure of the linker units (length, flexibility and chemical nature) contributes to the overall affinity of the glycoconjugates to their biological target [38].

Parker and co-workers designed Gd-glycoconjugates with dendric structure (**20**) approaching to a spherical shape [39]. An enhanced contribution from water molecules in the second coordination sphere to the Gd-centre to promote a rapid water exchange with effective coupling between the Gd-water vector and the tumbling motion of the whole molecule was carefully considered. These C_4 symmetric, homochiral complexes exhibited increased relaxivity.

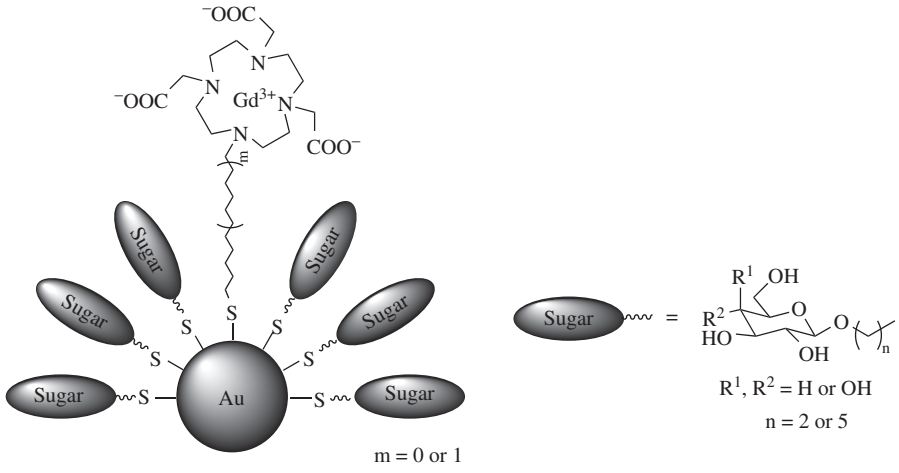

(**21**)

Figure 6.7 *Glyconanoparticle-functionalized Gd complexes*

Penadés and co-workers functionalized gold glyconanoparticles (GNPs) with Gd complexes to evaluate the carbohydrate effect in water relaxivity and demonstrated the possibility for a multimodal application (Figure 6.7) [40]. They indicated that increase in molecular size by introduction of a nanocluster to a Gd complex is not sufficient to increase the relaxivity. On the other hand, galactose- and lactose-coated GNPs showed significantly higher relaxivity than the glucose-bearing derivative, indicating that the selection of carbohydrate has a significant effect on the relaxation of the water protons. In addition to the stereochemistry of sugar configuration, the location of the carbohydrate relative to the Gd centre also affects the relaxivity. Carbohydrates may create specific interactions with water molecules in its solvation shell, aligning the water molecules in the proximity of the metal ions promoting the water exchange with the bulk solvent. Such interactions work more effectively for attached galactose and lactose moieties than the glucose residues and result in enhanced signal sensitivity in these systems. More recent studies on the usage of Gd-GNPs functionalized with different sugar moieties for cellular labelling clearly show a sugar-dependent uptake or interaction of the coated GNPs into/with different cell lines [41]. On fixed Raji, Raji DC-SIGN, HepG2 or GL261 cells different changes of relaxation time have been observed.

Meade and co-workers demonstrated the successful use of carbohydrates as a cleavage reagent to report a specific enzymatic activity [42]. As shown in Figure 6.8, the galactose moiety in the Gd-DOTA complex (**22**) blocks the remaining inner sphere site of Gd for water-coordination. Exposure of this complex to β-galactosidase (β-gal) cleaves the galactose blocking group from the chelator and the relaxation time of nearby water molecules increases, resulting in an enhancement of the magnetic resonance signal. For the other examples containing a chiral centre at the β-position of the macrocycle (nearest to carbohydrate) and a methyl substituent (**23**), the pendant galactose moiety no longer acts as a blocking group but as a bidentate anion. The carbohydrate occupies two available coordination sites of the Gd-ion in the pre-cleavage state, lowering the background signal [43]. Since the α-isomer (**24**) with its chirality at the distal side from the saccharide exhibits galactose blocking behaviour on the Gd centre, the linker design in these carbohydrate conjugates should be done under careful consideration. A strategy using so called 'self-immolative' linkers – which undergo a 'self-destructive' cascade reaction after enzymatic cleavage of a substituent was applied to β-glucuronidase-responsive Gd complexes (**25a**) [44] and PARACEST (paramagnetic chemical

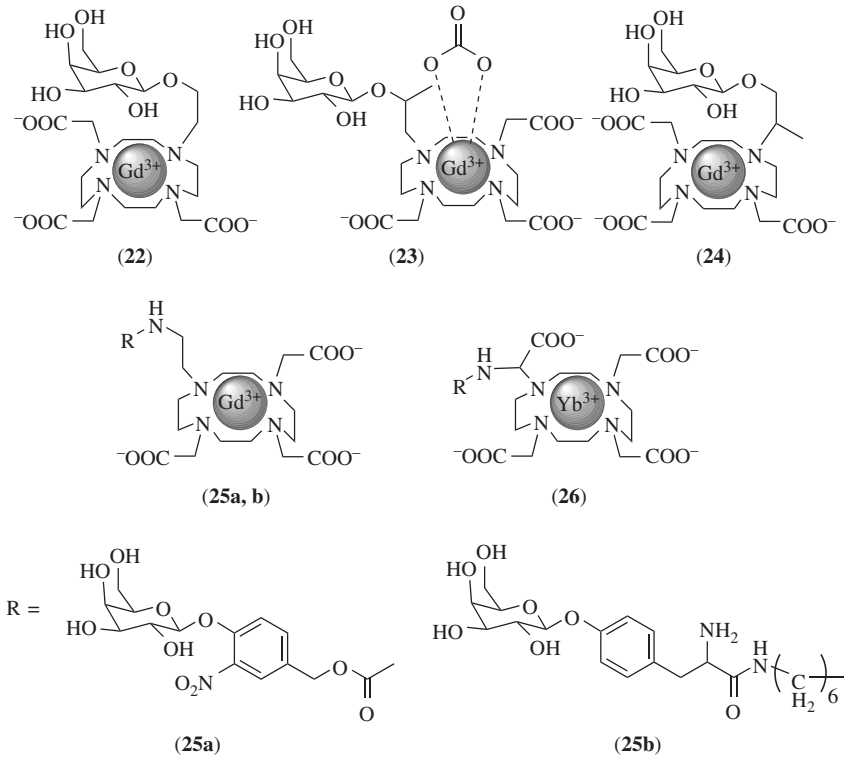

Figure 6.8 *Galactose-attached Gd complexes for β-galactosidase responsible MRI probes*

exchange saturation transfer) MRI probes possessing Ln centres (**26**), both having an extended linker chain with a *p*-hydroxybenzyl alcohol spacer [45]. A series of further 'self-immolative' Gd^{III} and Yb^{III} DOTA complexes with different β-D-galactose substitution patterns resulting in aminal derivatives of the lanthanoid(III) complexes after enzymatic action has been described more recently and the PARACEST effect under different pH has been studied [46].

Arena and co-workers expanded the approach of β-gal-sensing MRI reporter molecules toward a Gd-DOTA-complex connected to β-D-galactopyranose through a tyrosine-containing linker (**25b**) [47]. After uptake into melanoma tumour cells, the complex undergoes enzymatic transformations (first cleavage of the galactose residue by β-gal, second oxidation of the remaining tyrosine-bearing complex by tyrosinase) leading to a melanin oligomeric/polymeric mixture with a marked increase of water proton relaxation rate. A good MRI contrast was observed in murine melanoma tumour bearing mice 5 hours post injection of the complex in B16-F10*LacZ* tumours (with β-gal expression), but not in B16-F10 tumours (not expressing the enzyme).

6.4 Fluorescent complexes with carbohydrate-conjugated functions

Fluorescence detection or imaging of target molecules is a common methodology with high sensitivity and wide applicability. Recent developments in fluorescent molecular imaging enable the visualization of many

biologically important molecules even in transient and low concentrations in real-time analysis in living cells or even small animals. In comparison to other diagnostic modalities such as PET/SPECT and MRI, already discussed above, possible weakness of optical imaging lies in its low sensitivity in deeper regions of tissues. However, there are a wide variety of possibilities to use fluorescent markers in life sciences where optical molecular imaging can be applied as a tool for visualizing the target on the tissue surface. Since light of longer wavelength is known to penetrate deeper into tissue, chromophores that absorb lower energy light for excitation have been extensively investigated. In this respect, the two-photon excitation strategy is effective to improve the shallow depth of optical imaging. In any case, careful probe design by synthetic chemistry plays a central role in future development of fluorescent molecular imaging.

Selected examples for ligands functionalized with carbohydrate(s) that emit luminescence upon metal binding are shown in Figure 6.9. Compounds (**27–30**) are non-fluorescent ligands and used as fluorescent probes for metal ions. The galactose-naphthol conjugate (**27**) responds to copper with a OFF-ON-OFF fluorescence signal depending on the copper(II) concentration in HEPES buffer solution [48]. The glucosamine-based naphthol compound (**28**) acts as a fluorescent zinc sensor. The resulting zinc complex can be used as a relatively non-specific phosphate probe, because phosphate anions remove zinc from the complex, yielding non-fluorescent free ligand (**28**) [49]. Quinoline derivatives have been extensively studied as zinc-sensing devices, named as TSQ (6-methoxy-8-*p*-toluenesulfonamidoquinoline), Zinquin and TQEN [50]. The bisquinoline-derived compound (**29**) bearing two glucose moieties was prepared and its zinc-specific fluorescent enhancement was reported by Mikata *et al*. [51]. (**29**) exhibited higher fluorescent response than the *N,N*-isomer (**30**), probably due to an intramolecular quenching mechanism. Additionally, in living cells, (**29**) exhibited a 1.8-fold higher fluorescence signal in comparison with the analog ligand not bearing the glucose residues, due to its enhanced uptake into cell by the targeting ability of the attached carbohydrates.

The click-to-chelate reaction employing glucose-azide and 2-ethynylpyridine affords 4-(2-pyridyl)-1,2,3-triazole (Figure 6.4) which is structurally related to the well-known chelator 2,2′-bipyridine. Obata *et al*. used the bidentate, glucoconjugated ligand (**10**) to complex the $Re(CO)_3$ core and investigated the photophysical properties of the obtained $Re(CO)_3X$ complexes [29]. Gottschaldt *et al*. have prepared bipyridine ligands (**4**) with two carbohydrate residues in the 4,4′-position (Figure 6.3) [18]. The thioglycoside linkage was adopted to prevent undesired endogenous hydrolysis catalyzed by glycosidases. Besides the radioactive

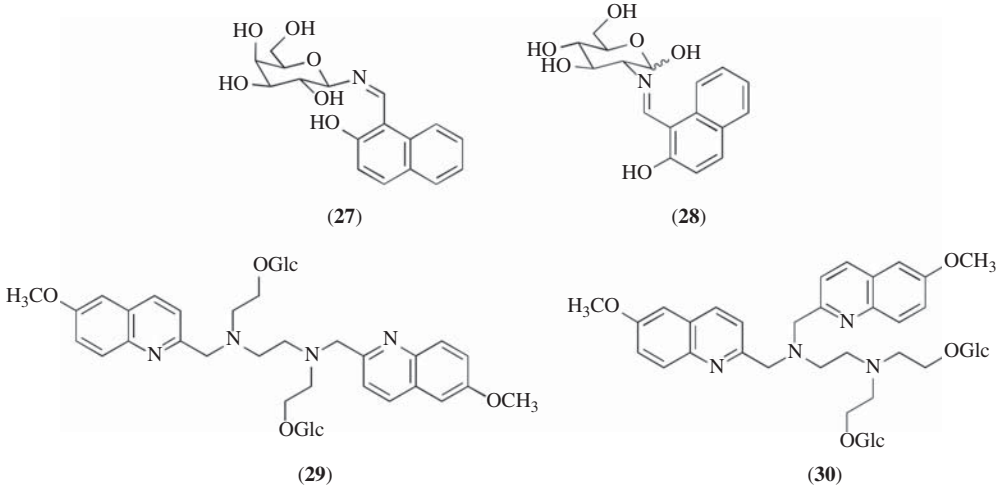

Figure 6.9 *Carbohydrate-attached fluorescent metal ion probes*

$^{99m}Tc(CO)_3(H_2O)$ complexes, $Re(CO)_3Cl$ complexes of these bidentate ligands emit 600–640-nm phosphorescence upon excitation with 350 nm light in aqueous solution. Their stability seemed to be not high enough for usage in *in vitro* applications since decomposition was observed during incubation of the complexes with excess of histidine. Kobayashi and co-workers reported that analogous Fe^{2+} and more stable Ru^{2+} complexes of the general formula ML_3 show significantly enhanced lectin binding [52]. In this case, glucose and mannose with *O*- and *N*-glycosidic linkages were chosen. Their flexible and densely packed saccharide shells play a critical role in the high lectin-affinity. The Ru^{II} complexes emit with strong luminescence at about 600 nm, possibly due to a shielding effect of the sugar residues. The respective unsubstituted $[Ru(bpy)_3]^{2+}$ or $[Ru(bpy\text{-}OH)_3]^{2+}$ complexes exhibited significantly smaller luminescence quantum yields than the carbohydrate-coated ones. Similar results for the photophysical behaviour of the ruthenium(II) complexes from the thioglycosides ligands (**4**) have been observed [53]. Additionally, a sugar-dependent uptake into HepG2 cells was reported. Only the glucose-bearing complex was able to enter the cells in an efficient manner.

Zubieta and co-workers utilized the DQA (di(2-quinolymethyl)amine) chelating moiety as a tridentate metal-binding ligand analogous to DPA (di(2-pyridylmethyl)amine) for the coordination of the rhenium tricarbonyl core (**31**, Figure 6.10) [54]. Mikata *et al*. synthesized twelve $Re(CO)_3$ complexes with *O*- and *C*-glycosides bound to tridentate NPG, DPA and DQA chelating moieties (**32**) [55]. They evaluated cellular uptake of these complexes by means of MIP-MS (microwave-induced plasma mass spectrometry). As a result, attached carbohydrate units reduced the uptake into HeLa cells in comparison with structurally smaller Re complexes without carbohydrates. However, the DQA derivatives exhibited better uptake among the carbohydrate-pendant complexes due to the enhanced lipophilicity. Analysis by fluorescent microscopy of PC-12 cells incubated with methoxyquinoline Re^{I}-complex revealed that the complex stays in the cytosol.

Lo and co-workers reported glucose-pendant polypyridyl Re^{I} complexes (**33**) with long linker chains (Figure 6.11) [56]. These complexes exhibit a ^{3}MLCT emission at about 550 nm. Importantly, ICP-MS investigations indicate that the uptake of these complexes into HeLa cells was inhibited by D-glucose in a concentration-dependent manner. Interestingly, 2-deoxyglucose also showed inhibition similar to D-glucose but L-glucose did not. These results clearly show that the uptake of these glucose-pendant Re complexes includes a GLUT-mediated pathway. Fluorescent microscopic analysis further revealed the localization of these complexes mainly in mitochondria.

Kobayashi, Urano and co-workers reported an exciting fluorescent β-gal probe to be used for targeted tumour imaging (Figure 6.12) [57]. Although this work does not contain any metal complex, it provides some great aspects for future design of fluorescent molecules in the field of medicinal inorganic chemistry. They have developed fluorescein-based TG (Tokyo Green) probes TG-βGal (**34**) with β-galactose moieties as specific enzymatic cleavage sites. Thereby, the β-galactose residues also act as triggers of fluorescence.

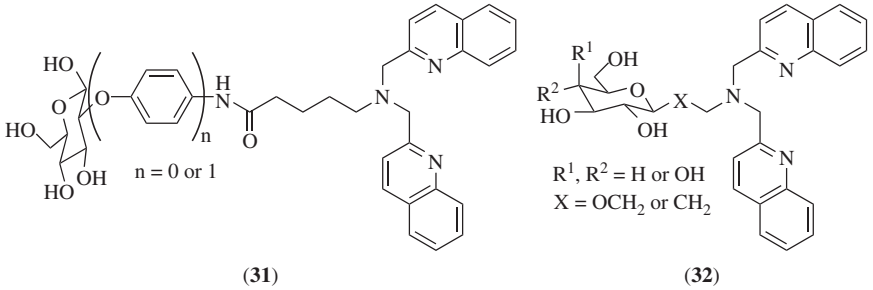

(**31**) (**32**)

Figure 6.10 *Carbohydrate-attached fluorescent ligands*

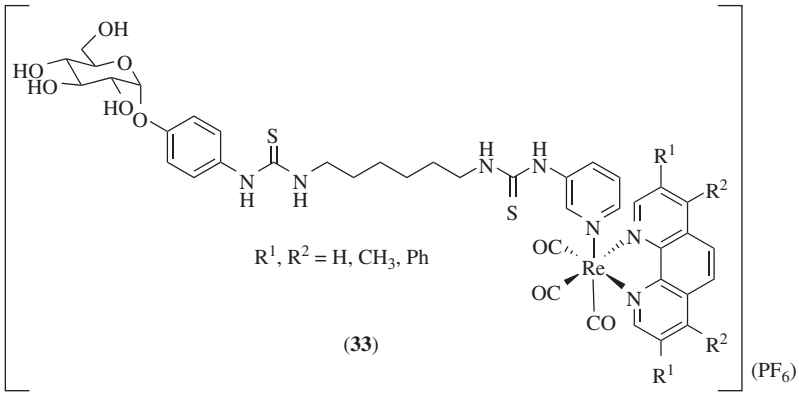

Figure 6.11 *Glucose-pendant fluorescent Re^{I} complexes*

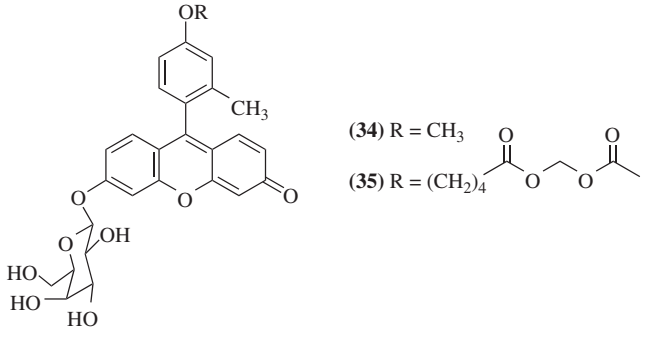

Figure 6.12 *Fluorescent probes for β-galactosidase imaging in cancer cells*

Removal of β-galactose units affords highly fluorescent anionic xanthene molecules. They applied a two-step strategy in which a tumour-targeting avidin-β-gal conjugate was administrated first to localize β-gal to tumour cells and in a second step AM-TG-βGal (**35**), which has an acetoxymethyl (AM) ester moiety, was applied to light up the cancer cells. The high affinity of avidin with lectins on the surface of cancer cells promotes the uptake. The presence of β-gal in the cancer cells led to target-specific fluorescence by accumulation of fluorescent species at the target site with a high signal to noise ratio. Using this method, they were able to visualize cancer cells as small as 200 μm

The epimeric pair of the two glycoligands (**36**) and (**37**) prepared by Policar and co-workers having xylo- and ribo-1,2-*O*-isopropylidenefuranose scaffolds, respectively, exhibited preorganized intramolecular excimer formation of the aforementioned 4-(2-pyridyl)-1,2,3-triazole chromophores in aqueous solution by a hydrophobic π-π stacking interaction (Figure 6.13) [58]. These ligands bind to copper as evidenced by the quenching of fluorescence, and the resulting copper complexes exhibited a mirror image Cotton effect in the circular dichroism (CD) spectra in water. X-ray crystallography revealed that these complexes form 2 : 2 complexes (ligand:metal ion). The opposite pseudoenantiomeric character at the metal centre was induced by a slightly coiled structure originating from each sugar configuration and the rigidity of the metal binding site.

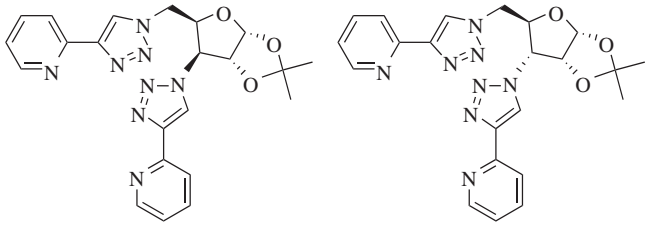

(**36**) (**37**)

Figure 6.13 *Epimeric pair of glycoligands derived from xylo- and ribofuranose*

6.5 Carbohydrate-attached photosensitizers for photodynamic therapy (PDT)

As mentioned in previous sections, optical imaging of cancer cells contributes to fundamental research in the laboratory, diagnosis in clinics and physical surgery in hospitals. Instead of emitting fluorescence or phosphorescence, some photoactivated species are able to damage cells by energy transfer to biologically important molecules directly in cells or activation of small molecules, such as molecular oxygen, generating reactive oxygen species including singlet oxygen ($^1O_2$), hydroxyl radicals ($^{\bullet}OH$), hydrogen peroxide (H_2O_2) and superoxide (O_2^-). This photoactivation-induced chemotherapy called PDT (photodynamic therapy) has developed during the last 30 years. Mainly porphyrin derivatives have been widely used as photosensitizers based on their intrinsic property for selective accumulation in cancer cells. Other reagents including photoactivatable metal complexes have been extensively studied. Requisites for such photoactive metal complexes include high efficiency of energy transfer (higher quantum yield), high photochemical stability (decreased or no photo-bleaching), long-wavelength activation light to reduce undesired cell damage and expand the light-penetrating depth in tissues, and high cancer-accumulation efficiency. Carbohydrates are able to enhance water-solubility, biocompatibility and targeting properties to many types of photosensitizers [59–61].

Mikata *et al*. prepared tetra- and octa-glycoconjugated tetraphenylporphyrins (**38**) and reported that the photocytotoxicity of these compounds are sugar-dependent (Figure 6.14) [62]. In particular, the acetyl-protected glucose derivative exhibited significant photocytotoxicity. The octa-glycosylated derivative with free OH-groups showed no photocytotoxicity after irradiation, most probable due to the high hydrophilicity and the large globular shape of the molecule. Because $^1O_2$ production activity was found to be almost the same for all compounds, the sugar-dependence of phototoxicity has to be due to the differences in the amount of compounds taken up by the cells. They extended this work to corresponding sugar-appended chlorins [63] and more highly-water soluble, maltohexaose-attached porphyrins [64]. Superior cytotoxicity was observed for chlorin derivatives bearing carbohydrates with free OH-groups, and photodynamic activity was sugar-dependent. Among mono-, *cis/trans*-bis-, tris- and tetrakis-maltohexaosylated tetraphenylporphyrins, the mono-maltohexaosylated derivative (**39**) was the most effective photosensitizer for PDT against HeLa cells.

Krausz and co-workers synthesized mono-thioglycosylated tetraphenylporphyrins (**40**) and bis-thioglycosylated Protoporphyrin IX derivatives (**42**) with glucose, galactose and mannose [65]. The *S*-glycosidic bonds were chosen to prevent endogenous hydrolysis catalyzed by glycosidases. The applied photocytotoxicity assay revealed that all ortho-isomers as well as the para-glucosylated isomer were photoactive. The activities of these compounds are similar to Protoporphyrin IX. The glycosylated Protoporphyrin IX derivatives with methyl ester groups were much more active than Protophophyrin IX. However, hydrolysis

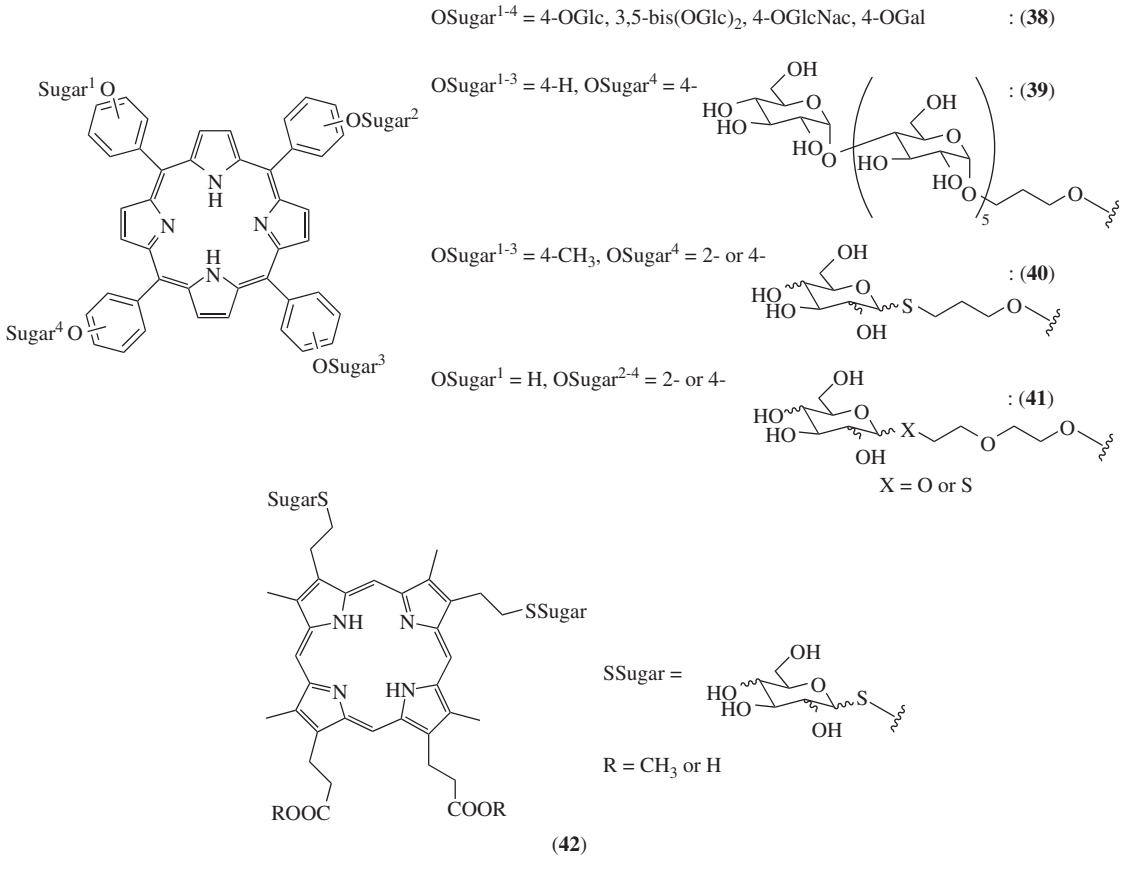

Figure 6.14 *Carbohydrate-attached porphyrins as photosensitizers for PDT*

of methyl esters led to inactivation of the photosensitizers, probably because of prevention of cell uptake. Later, a more efficient route for the synthesis of porphyrin-carbohydrate conjugates was reported by Drain and co-workers [66]. They treated OH-protected thiosugars with tetrakis(pentafluorophenyl)porphyrin to afford a derivative with four *S*-glycosidic bonds at the para-positions of all perfluorophenyl rings. Fluorescence microscopy revealed that the glucose-attached derivatives were extensively incorporated into human breast cancer MDA-MB-231 breast cancer cells and the transformed $3Y1^{v\text{-}Src}$ (3Y1 rat fibroblasts over-expressing activated v-Src kinase) cells in contrast to the galactose-bearing derivative. These results correspond to the observed differences in necrosis and apoptosis induced by photoirradiation. Blais and co-workers synthesized triglycosylated porphyrins (**41**) connected to α-/β-mannose and α-/β-galactose with diethylene glycol spacer with terminal *O*- or *S*-glycosidic linkage [67]. On first glance, the substitution with carbohydrates enhances both cell internalization and phototoxicity. However, the correlation of both results is not straightforward. Interestingly, absence of glucose in the growth media resulted in decreased uptake of the carbohydrate-porphyrin conjugates of ~50% while the uptake of non-carbohydrate porphyrin was unaffected, suggesting that the internalization occurs partly via an active transport pathway that requires energy.

As metal-containing photosensitizers with carbohydrate functionality, Tomé, Cavaleiro and co-workers synthesized zinc phthalocyanines (**43** and **44**) bearing galactose moieties attached via a C-6 linkage

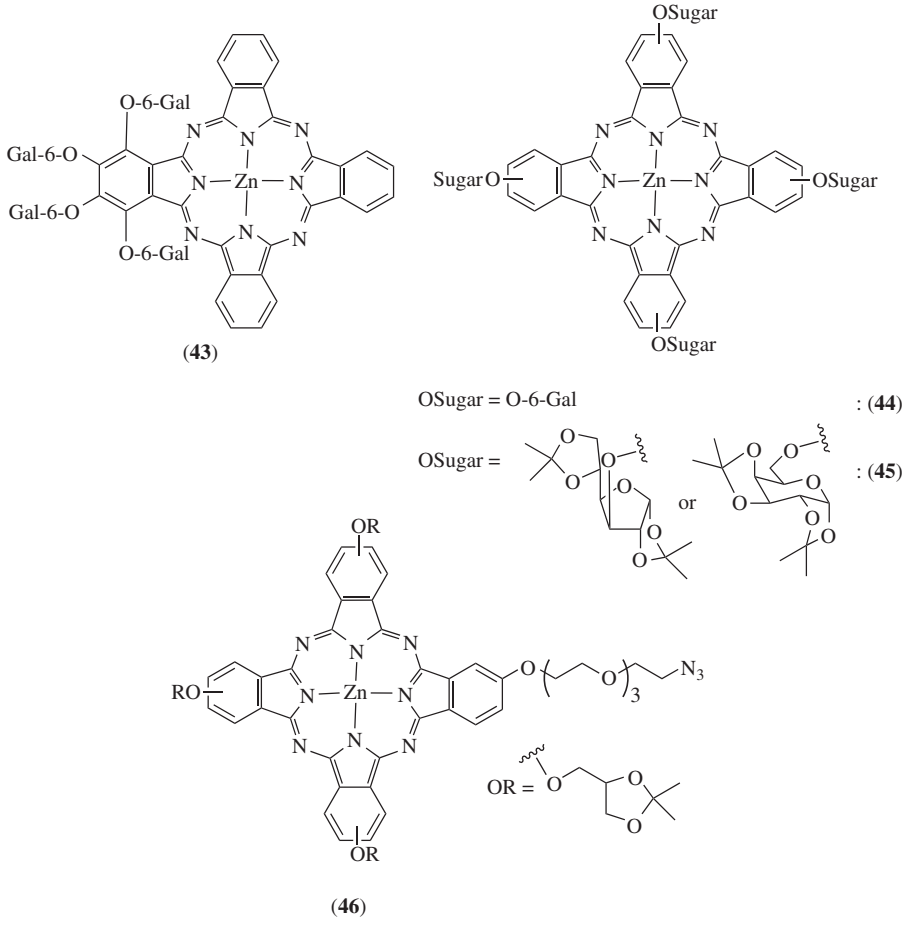

Figure 6.15 *Carbohydrate-functionalized zinc phthalocyanines and azido precursor*

(Figure 6.15) [68, 69]. Recent results show that the asymmetric glycophthalocyanine (**43**) had the most promising results in *in vitro* experiments (in comparison to the derivatives **44**) with a higher phototoxicity toward cancerous cells (HeLa) compared with nonmalignant cells [70]. Lafont and co-workers clicked glucosyl, galactosyl, mannosyl and lactosyl alkynes with the phthalocyanine azide (**46**) [71]. A similar approach for the synthesis of a whole library of glycoconjugated porphyrin compounds, including the histo-blood-group antigen trisaccharide Lewis^X and *N*-acetyl-lactosamine, was applied by Daly *et al*. [72]. A first screening of the compounds for their PDT activity against human oesophageal cancer cell lines shows at least that the variation in the carbohydrate group appeared to modulate the biological behaviour of the glycoporphyrins. But the $^1O_2$ production under irradiation was less effective than for commercial photosensitizers and a change of the tetrapyrrole core to chlorin was suggested. *Vice versa*, alkyne-substituted porphyrins were treated with sugar azides to obtain compounds with three glycosyl units applying microwave irradiation but up to now no *in vitro* data for their activity has been reported [73]. Ng and co-workers investigated photodynamic activity using mono- and tetra-glycosylated zinc phthalocyanines (**45**) (Figure 6.15) [74]. The mono-glycosylated analogues exhibited higher phototoxicity against HT29

human colon adenocarcinoma and HepG2 human hepatocarcinoma cells. Additionally, zinc complexes are less toxic than the corresponding silicon(IV) analogs, probably due to increased stacking tendency caused from the lack of axial substituents. Fluorescence microscopy revealed that all mono-substituted analogs have a better cellular uptake compared with the pure porphyrins.

In order to shift the absorption wavelength to lower energy (for deeper tissue penetration of the light) another approach is to use simultaneous two-photon absorption (TPA) to excite the photosensitizer. Recently the synthesis of conjugated zinc porphyrin oligomers (**47–50**) bearing α-mannose residues (Figure 6.16) has been reported [75, 76]. So far only the complexes substituted with acetyl-protected carbohydrates were studied in detail for their photophysical properties in organic solvents. Most favourable conjugation of the porphyrin systems was achieved for the dimers (**47**) and (**49**) connected by ethynyl and butadiyne linkers. With the observed TPA cross-section values of 8000 and 4200 GM at excitation wavelength between 790 and 950 nm as well as the measured high $^1O_2$ quantum yields these compounds are promising candidates for the further development of targeted TPA photosensitizers.

Besides fullerenes and porphyrins, also the carbohydrate-substituted ruthenium bipyridyl complexes (discussed as fluorescent probes earlier) could be used as photosensitizers, since they are able to produce $^1O_2$ under irradiation [53]. In order to selectively target the GLUT5 transporter (which is suggested to be expressed by certain cancer cells and responsible for the uptake of fructose into the cells), Lo and co-workers most recently synthesized cyclometallated iridium(III) bipyridine D-fructose complexes (**51** and **52**, Figure 6.17) [77]. They could prove their preliminary assumption that the uptake of the complexes was mediated by GLUT5 of the breast cancer cells, as the complexes were located in the mitochondria and possessed photoinduced cytotoxic activity.

Recent rapid progress in the development of metal complexes which can be activated by irradiation is of significant interest because the resulting compounds have potential to be light-activated agents

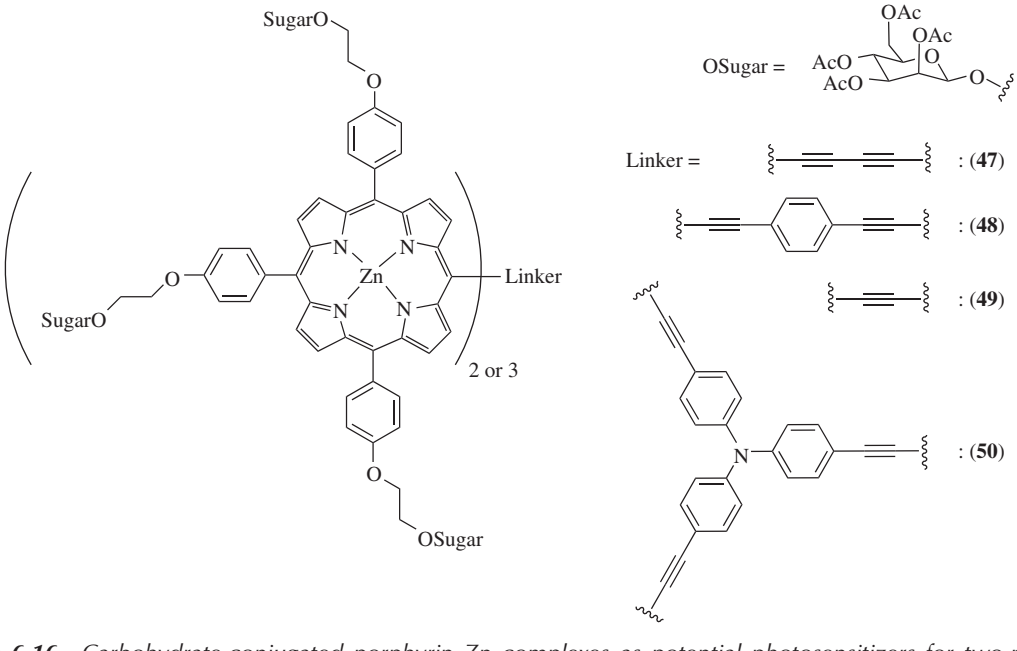

Figure 6.16 *Carbohydrate-conjugated porphyrin Zn complexes as potential photosensitizers for two-photon absorption PDT*

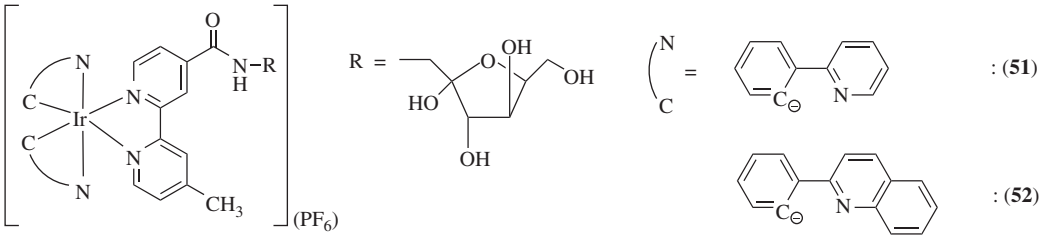

Figure 6.17 *Fructose-functionalized cyclometallated Ir^{III} complexes with GLUT5 selective uptake*

[78–80]. This class of complexes includes compounds that form photoadducts with DNA, photonucleases (photo-triggered DNA cleavage inducer), and NO- or CO-releasing complexes. Various kinds of metals, including Cr, Co, Ru, Rh, Re, Os, Ir, Pt and Au, as well as Cu, Fe and Mn with ligand absorption, have been studied. To the best of our knowledge, however, none of these complexes utilized a carbohydrate-targeting moiety. As described in the last section of this chapter, there are a lot of possible approaches remaining for the design of such carbohydrate-targeted metal complexes.

6.6 Carbohydrate-based metal complexes exhibiting anticancer activity

Undoubtedly, the most important drug in medicinal inorganic chemistry is the anticancer agent cisplatin (**53**, *cis*-diamminedichloroplatinum(II), *cis*-DDP) (Figure 6.18). Rosenberg observed the proliferation inhibition of *E. coli* around a platinum electrode in his research [81], which led to the discovery of cisplatin in 1969 [82]. Even 40 years later, cisplatin is the most widely used anticancer drug, and total sales including the second and third generation drugs (i.e. carboplatin **54** and oxaliplatin **55**) has reached to 3.4 billion dollars per year worldwide. Cisplatin is intravenously administrated to patients, and the neutral, small molecule is taken up into cells via passive diffusion through cell membranes. Inside the cells, cisplatin is hydrolyzed to *cis*-$[Pt(NH_3)_2(H_2O)_2]^{2+}$, due to the low concentration of chloride ions, and then, this cationic species interacts with negatively-charged DNA and other biological molecules. The mechanism of the anticancer activity of cisplatin is still not fully understood, but covalent bond formation with N7 of guanine (G) bases in DNA strands and subsequent specific protein recognition of the bent structure of platinated duplexes at their guanine-guanine (GG) site with a bifunctional 1,2-intrastrand crosslink is believed to play a key role for the activity [83]. Other new platinum compounds including Pt^{IV} complexes, multinuclear platinum complexes, and monofunctional and *trans*-derivatives are extensively investigated [84–86].

To introduce a targeting function to platinum complexes, attachment of carbohydrates has been tested (Figure 6.19) [87]. Tsubomura, Yano and co-workers prepared dichloro platinum complexes ligated by 2,3-dideoxy-2,3-diamino sugars (**57**) [88]. Although the ligand synthesis requires multistep reactions, the antitumour activity of (**57**) against sarcoma S180 and L1210 cells implanted in mice was promising. A *T*/*C* value (ratio in mean survival time between treated group (*T*) over control group (*C*)) of 410% was obtained for the glucose complex at 50 mg/kg dose. Positive control using cisplatin was comparable (*T*/*C* = 237% at 8 mg/kg dose) with that for the glucose complex at the similar dose (*T*/*C* = 220% at 10 mg/kg dose). Compared with cisplatin which has a high toxicity (LD_{50} = 13 mg/kg), the diamino sugar moiety significantly reduces the toxicity of the platinum drug, allowing for a high dosage of the complex to result in higher anticancer activity than cisplatin. Recently, Keppler and co-workers examined the *in vitro* anticancer activity of glucose complex (**57**) and its analogs with different leaving groups including diiodide, oxalate and malonate [89]. Comparison of the cytotoxicities of these complexes against four different cancer cell lines

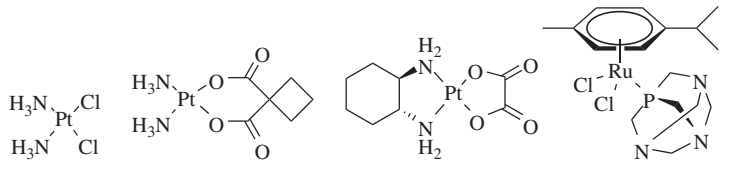

(**53**) (**54**) (**55**) (**56**)

Figure 6.18 *Selected platinum- and ruthenium-based anticancer drugs*

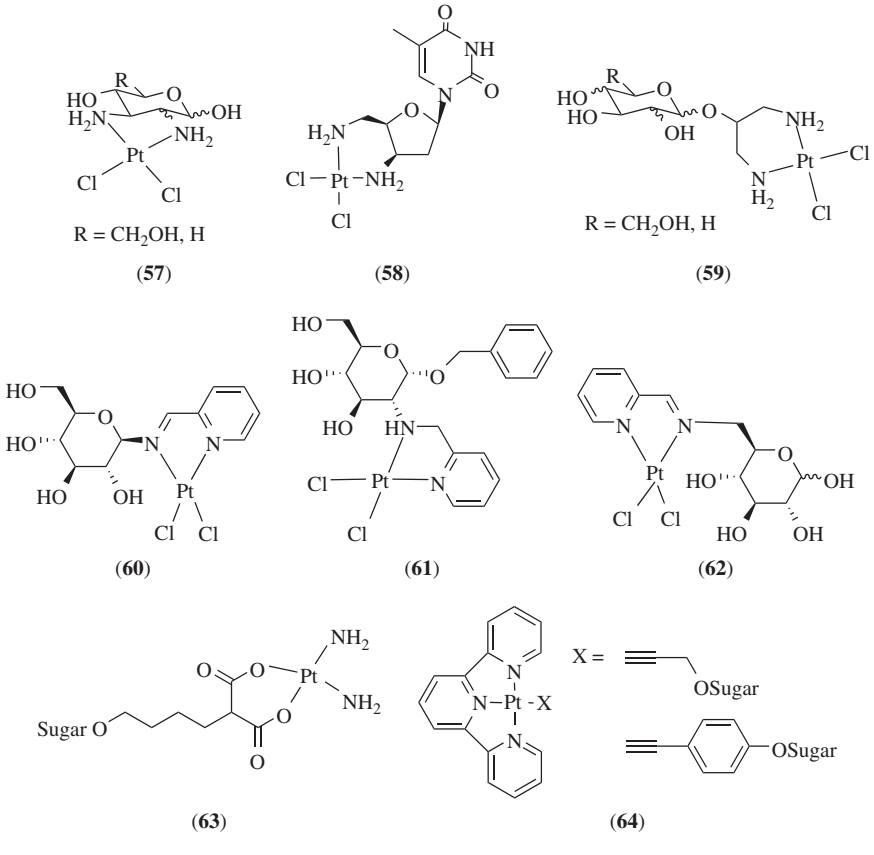

(**57**) (**58**) (**59**)

(**60**) (**61**) (**62**)

(**63**) (**64**)

Figure 6.19 *Selected carbohydrate-functionalized platinum complexes*

(HeLa, CH1, SW480 and U2OS) according to their covalent bond formation ability to deoxyguanosine monophosphate (dGMP) in solution suggested that the DNA binding is not the only determinant for the elucidation of the complexes' activity. Hanessian and Wang prepared platinum complexes bearing analogous 2,3-dideoxy-2,3-diaminopyranoxyloses (**57**, R = H) [90]. The *in vivo* antitumour activity against P338 leukemia ($T/C = 227\%$ at 25 mg/kg dose) and L1210 cells ($T/C = 323\%$ at 50 mg/kg dose) were similar to cisplatin at lower doses (4 mg/kg for P338 and 25 mg/kg for L1210). Analog complexes with a methyl

glycoside ligand and a carboplatin analog, which has cyclobutane-1,1-dicarboxylate as leaving group, were found to be less active. A mitochondrial mode of action has been proposed by Onambele *et al*. for a platinum complex derived from thymidine (**58**) [91]. Apoptosis was also induced in cisplatin-resistant cell lines and the platinum(II) complex with the amino group in an axial orientation at the C-3 position showed the most promising results due to the different mode of action compared with cisplatin.

In order to attach diamine functions to carbohydrates in a more convenient way, two groups employed 1,3-diamino-2-propyl glycosides (**59**) [92, 93]. The three- or four-step procedures allow versatile synthesis of carbohydrate-pendant *cis*-dichloroplatinum(II) complexes. Wang and co-workers reported that *in vitro* antitumour activity of glucose complex is similar to cisplatin against human ovarian cancer cell A2780S and human melanoma MeWo, but less active against cisplatin-resistant A2780cP [93]. Mikata *et al*. prepared eight carbohydrate-cisplatin conjugates which utilized glucose, mannose, galactose, xylose and L-glucose with six- or five-membered chelates, and tested their *in vivo* antitumour activity against P388 cells implanted in mice [94]. Although a *T*/*C* value of 194% at 400 mg/kg dose was obtained for the α-galactose complex, generally carbohydrate reduced both activity and toxicity of these platinum complexes. The differential effects of the carbohydrate moieties on the antitumour activity could be understood by selective uptake of complexes or selective processing (e.g. hydrolysis or phosphorylation) of the carbohydrate residue before/after entering into cells to afford the active compound. Corresponding palladium(II) complexes were also examined but showed almost no *in vivo* cytotoxicity against P388 cells implanted in mice [95]. A similar strategy for the introduction of two coordinating nitrogen atoms to obtain carbohydrate-based ligands was applied by Cucciolito *et al*., treating 2-pyridinecarboxaldehyde with different deoxyaminosugars to obtain the corresponding imines (or after reduction with $NaBH_4$ the resulting amines) [96]. The obtained Pt^{II} complexes (e.g. **60–62**) have been shown to be much less cytotoxic *in vitro* against HeLa and MCF-7 cells than cisplatin.

Another strategy to obtain sugar-containing Pt-complexes is the introduction of the carbohydrate units to the 'leaving ligand' of the coordination sphere of the platinum (not substituting the nitrogens). Recently Möker and Thiem synthesized a library of ligands derived from 2-substituted malonic acid containing a variety of differently bound saccharides (**63**) [97]. So far they only studied the stability of the complexes in phosphate buffered saline (PBS)-buffer, but data for their *in vitro* activity in particular in comparison with carboplatin are supposed to be published soon. Che and co-workers synthesized organometallic terpyridine-platinum complexes (**64**) with glycosylated acetylides or arylacetylides [98]. They confirmed intercalative DNA-binding ability of these complexes by spectral changes and gel mobility shift assays. The *in vitro* cytotoxicities against several cell lines for some compounds were about 100-times higher than that of cisplatin.

Non-platinum anticancer metal complexes have been reported for Ru, Ir, Os, Co, Au, Pd, and so on and are of growing importance [99, 100]. However, in comparison with the large number of studied complexes only a very few complexes with an attached carbohydrate moiety have been reported. Driven by the results obtained for RAPTA-C (**56**), Berger *et al*. synthesized glycofuranosidic phosphite ligands and coordinated them to Ru^{II} arenes [101]. The resulting complexes (Figure 6.20, general structure **65**) were tested for their *in vitro* action against different human cancer and nontumourigenic cell lines. Although with relatively high IC_{50} values (less activity), the carbohydrate based Ru complexes showed selectivity for the cancer cell lines. Additionally, the authors proposed a different mode of action compared with cisplatin based on the results for the cisplatin-resistant cells. More recently, they expanded the scope and synthesized the analogous Os^{II} complexes [102]. The osmium(II) compounds were shown to possess an even smaller *in vitro* anticancer activity then the aforementioned ruthenium(II) complexes. Exchange of the halogen ligands at the ruthenium or osmium centres (with oxalate or malonate residues) dramatically increased the stability of the complexes and decreased their ability to bind to their biological targets, resulting in even lower cytotoxic activity [103]. Using the alkyne-azide 'click' reaction, Deepthi *et al*. connected ferrocene to different monosaccharides (**66**) [104]. They showed that the linker between the sugar and the ferrocene has a less pronounced influence on

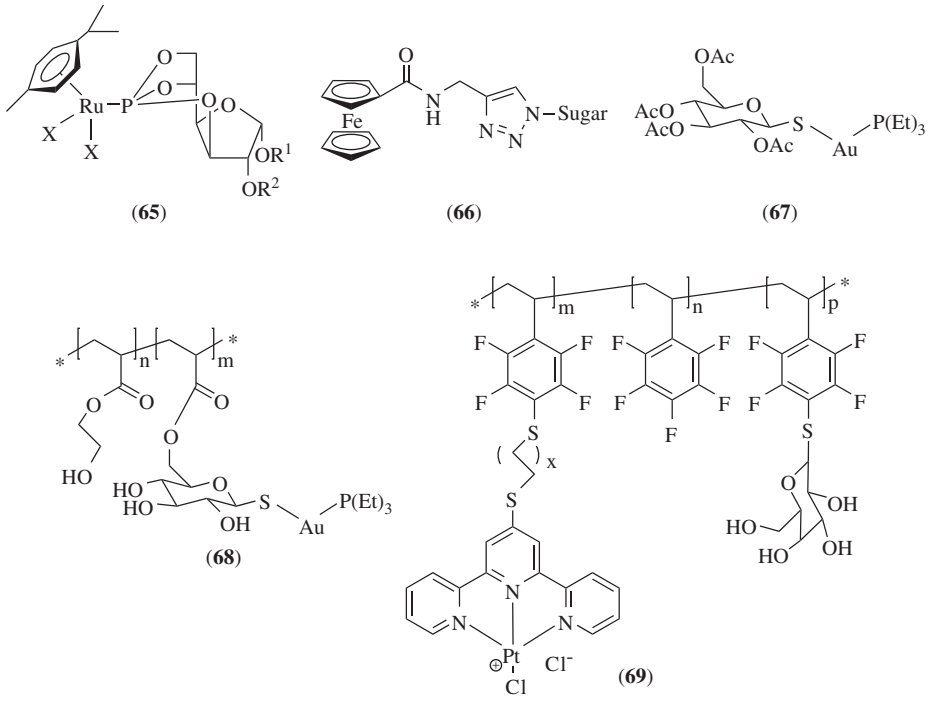

Figure 6.20 *Selected examples for ruthenium, ferrocene and gold complexes currently under investigation as anticancer agents and metallo-glycopolymers*

the cytotoxic activity of the complexes and that the more hydrophilic compounds are less toxic. Solely the hydrophobic derivatives still carrying protective groups (e.g. benzyl and isopropylidene) are cytotoxic even possessing some cell selectivity. The reasons for this so far remain unexplored.

A carbohydrate-appended metal complex recently also under investigation again as an anticancer drug is the gold complex with carbohydrate functionality, auranofin (**67**) (see Chapter 9 for further details) [105]. Metalloglycopolymers are a newly emerged class of substances which combine all the advantages of sugar-metal complexes, metallopolymers and glycopolymers. Within the current literature, solely two examples exist, which significantly outperform the respective low molar mass metal complexes in *in vitro* studies. The first example – a glycopolymer carrying multiple units of auranofin (**68**), in which auranofin was bound to a polymer and self-assembled into spherical micelles, inhibited the proliferation of ovarian cancer cells (OVCAR-3s) [106]. The metalloglycopolymer revealed higher activity than the low molar mass drug presumably due to different cellular uptake mechanism of the micellar structures, that is, endocytosis. Wild *et al*. could show that the galactosylated metalloglycopolymer carrying Pt^{II} terpyridine complexes (**69**) revealed much greater apoptotic activity towards acute leukemia cells (Nalm-6) than cisplatin [107]. The nano-sized, self-assembled agglomerates of this polymer were also able to overcome the resistance in both daunorubicin and vincristine-resistant cells. Additional reasons for the increased activity of these compounds, such as internalization by other mechanisms (like receptor-mediated endocytosis), remained unexplored in these first studies.

6.7 Carbohydrate-appended metallic nanoparticles, quantum dots, electrodes and surfaces

Analogous to mono- or multinuclear metal complexes with a distinct metal centre discussed in previous sections, aggregated or bulk metal materials including metal oxide and gold nanoparticles (NPs), semiconductor nanoparticles or quantum dots (QDs), electrodes and other metal surfaces can also be functionalized with carbohydrates [108, 109]. The change in size to the nanometer scale results in different properties of the nanoparticles. For instance, in semiconductors the restriction of electronic motion to a limited nanometer scale results in a new very strong absorption [110]. Biocompatibility, water-solubility and the targeting potential of carbohydrates can introduce beneficial properties to these materials for biological or biomedical applications, creating new methodologies and significant advances in glycobiology itself [109].

Kataoka and co-workers prepared gold nanoparticles (1–10 nm size range) in the presence of PEG (poly(ethylene glycol)) possessing thiol and acetal groups [111]. After converting the obtained acetals to aldehydes, lactose or mannose derivatives with an amine function were attached by reductive amination. The lactose-conjugated gold nanoparticles exhibited aggregation in the presence of a lectin (RCA_{120}) that recognizes galactose, changing the absorption spectra in the visible range from pinkish-red to purple. This colour change is reversible and selective to the attached carbohydrates. With this method the lectin concentration can be quantified with high sensitivity. Recent improvements for the preparation of carbohydrate-functionalized nanoparticles include silica-coated Ag, Fe_3O_4 and ZnS-CdS nanoparticles with attached dextran (*via* carbamate bonds at C-2 positions) [112]. The resulting 10–40 nm particles are robust, water-soluble and stable. Addition of concanavalin A (Con A) to the dextran-functionalized Ag nanoparticles developed aggregation or precipitation associated with a red-shift in the plasmon absorption band and a reduced peak absorbance.

Superparamagnetic nanoparticles are very prominent in imaging and therapeutic applications and their *in vivo* distribution can be widely altered by suitable surface functionalization [113]. Besides dextran coatings, also synthetic glycopolymers can be applied [114]. Huang and co-workers reported the preparation of magnetic glyconanoparticles (MGNPs) with Fe_3O_4 as the central core coated by silica-functionalized with alkyl chains [115]. The carbohydrate connection was achieved either by amide or click coupling. In addition to the *O*-glycosidic linkages utilizing mannose, galactose, fucose and sialic acid, an *N*-glycoside with *N*-acetylglucosamine was employed. Magnetic separation of fluorescently labelled Con A by mannose-coated MGNP was successful (89%), whereas weakly bound galactose-coated MGNP removed only 8% of Con A. Binding of these carbohydrate-MGNP conjugates with Con A can also be monitored by MRI because MGNP aggregation led to a reduction of the *T*2-relaxation time, resulting in a negative contrast. Using an array of MGNPs, they suggested ‘MRI signatures’ that distinguish closely related isogenic tumour cells based on specific carbohydrate-protein interaction occurring on the tumour cell surface.

Sangregorio and co-workers prepared other MGNPs specifically designed as magnetic fluid hyperthermia heat mediators and negative contrast agents for MRI [116]. Magnetic hyperthermia is based on the exothermic properties of magnetic materials under the influence of an alternating current magnetic field, and regarded as promising cancer thermotherapy agents. Using rhamnose, mannose and ribose, iron oxide NPs were coated via phosphonate functions. Attached carbohydrates afforded water solubility leading to improved dispersion properties, reduced cytotoxicity and enhanced cell-targeting abilities of the MGNPs.

QDs are versatile tools utilizing small metal particles that exhibit size-dependent fluorescence intensity or colour changes. Carbohydrate-coated QDs have been reported and PEGylated QDs provide an efficient alternative to previous approaches in preventing cytotoxicity. In this context Seeberger and co-workers reported

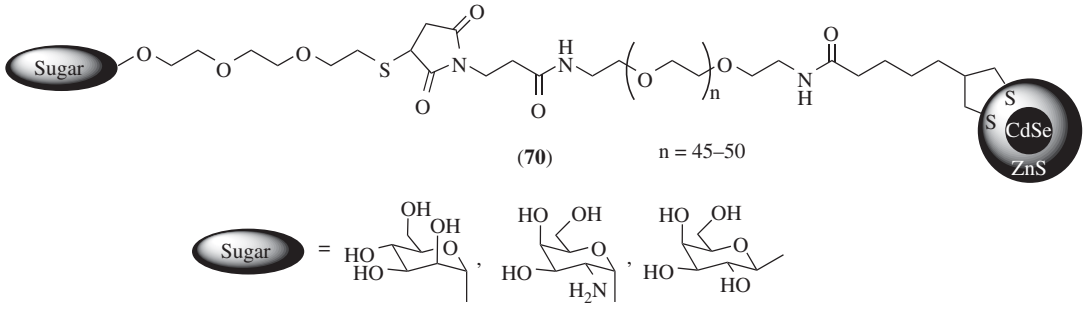

Figure 6.21 *Carbohydrate-capped quantum dots*

the preparation of carbohydrate-capped QDs with a PEG_{2000} linker (**70**) that can be used for *in vitro* and *in vivo* applications (Figure 6.21) [117, 118]. Using flow cytometry, they showed that D-galactose-capped QDs (Gal-QDs) are preferably taken up by HepG2 cells via the asialoglycoprotein receptor (ASGP-R) mediated pathway because ASGP-R knockdown HepG2 cells exhibited diminished uptake of Gal-QDs. *In vivo* applications using D-mannose- and D-galactosamine-capped QDs resulted in a high number of QDs sequestered in the liver, revealed by fluorescence microscopic analysis of livers of sacrificed mice. In a similar synthetic approach multivalent *N*-acetyllactosamine modified QDs have been obtained and their interaction with galectin-3 modified surfaces has been shown using surface plasmon resonance (SPR) [119]. Such protein carbohydrate interactions can be used to, for example detect bacteria in cell suspensions containing as few as 10^4 *E. coli* per millilitre (by binding of the FimH mannose-specific lectin on the bacteria cell surface). Mannose modified 15 nm diameter nanoparticles produced an intense, broad luminescence emission at 550 nm of induced luminescent aggregates of *Escherichia coli* [120].

Vice versa carbohydrate arrays fabricated on gold films (**71**) were prepared by Corn, Kiessling and co-workers to study carbohydrate-protein interactions with SPR (Figure 6.22) [121]. The terminal amine tethered to the gold surface via thiolate assembly was connected to mannose and galactose via disulfide formation. The SPR imaging distinguished the specific carbohydrate-protein interactions, namely, favourable Con A-mannose and Jacalin-galactose pairs. Array-based sensors with immobilized carbohydrates on a sensing surface have several advantages including low consumption of analytes, the ability to perform parallel screening of multiple interactions, and efficient response readout. Van Duyne and co-workers prepared mannose-displayed SAMs (self-assembled monolayers) on gold surfaces or silver nanosensors fabricated by nanosphere lithography (NSL), for SPR and localized surface plasmon resonance (LSPR) analyses, respectively [122]. To achieve high affinity binding and specificity, a novel clustered immobilization strategy was designed which uses colloidal gold nanoparticles attached to a substrate and coated with poly(amido amine) dendrimer succinamic acid G5 (PAMAM-G5) dendrimers which are in a second step coupled with lactose or *N*-acetylglucosamine (GlcNAc) conjugates [123]. In a quantitative test using the obtained GlcNAc-immobilized LSPR sensor, the $\Delta\lambda$ max value for the WGA lectin was concentration-dependent, with a lower detection limit of 78 nM. Wang and co-workers used click chemistry to construct carbohydrate-functionalized SAMs [124]. Azido sugars displaying glycosylated mannose, lactose and α-Gal were fabricated to a gold surface coated with alkynethiols. Specific mono-, di- and trisaccharide carbohydrate-protein interactions (mannose-Con A, lactose-ECL (*Erythrina cristagalli* lectin), and α-Gal-anti-Gal anitibody) were evaluated by QCM (quartz crystal microbalance), SPR, AFM (atomic force microscopy) and electrochemical analyses. Iyer, Heineman and co-workers developed electrochemical impedance spectroscopy (EIS) to detect bacteria after they were captured with synthetic glycans immobilized

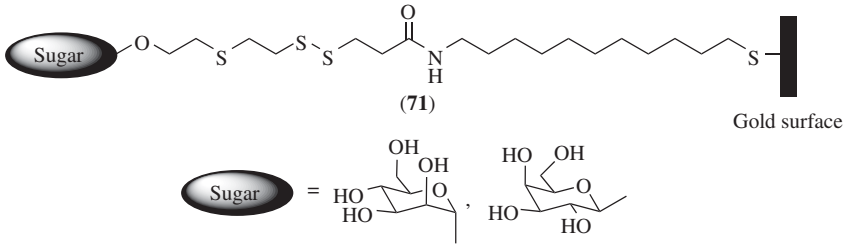

(**71**)

Figure 6.22 *Surface modification with carbohydrate probes*

on a gold disk electrode as SAMs [125]. Impedance measurements (Nyquist plot) showed shifts due to the binding of *E. coli* ORN 178, which binds specifically to α-mannosides.

6.8 Concluding remarks

In this chapter, a few limited examples from a wide variety of potential applications of carbohydrate-metal conjugates for inorganic pharmacology have been shown. In most cases the appropriate ligand design based on BFC (bifunctional chelate) theory, in which the carbohydrate function is coupled to the metal-complex as a targeting function, was shown to be the key element. Specific noncovalent binding events with proteins, including specific enzymatic cleavage, delivery/activation of carbohydrate-functionalized metal complexes to/at specific cells, tissues and organs dominate the biological activity of the compounds.

Recent examples reported by Schugar, Orvig and co-workers demonstrate an intelligent application of carbohydrate-appended ligands in their free form (Figure 6.23) [126, 127]. Compound (**72**) bears a glucose unit that masks the OH group of the hydroxypyridinone and facilitates the crossing of the compound through the BBB. Enzymes in the brain such as glycosidase are expected to cleave off the glucose protecting unit to trigger metal binding and antioxidant activity of the hydoxypyridinone as a treatment for Alzheimer's disease. Permeation into the brains of rats was confirmed by imaging of a respective ^{125}I-radiolabelled compound. The ligand comprising two carbohydrate units (**73**) exhibited antioxidant activity and reduces Zn^{2+}- and Cu^{2+}-induced $A\beta_{1-40}$ aggregation *in vitro*. Gottschaldt *et al*. have prepared *S*-glycoside-based tripodal ligands [128]. The *in vitro* antimicrobial activity of the corresponding silver complexes (**74**) revealed activity to a broad range of different pathogens along with a decreased cytotoxicity to mammalian cells (compared with

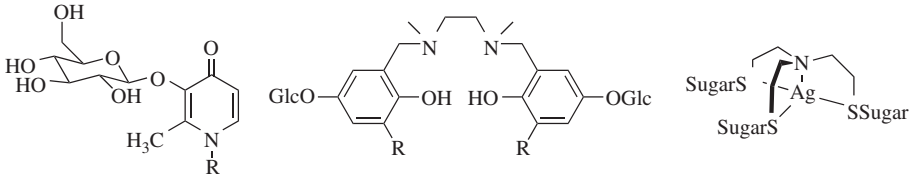

(**72**) (**73**) (**74**)

Figure 6.23 *Carbohydrate-functionalized metal ion chelators for AD treatment and tripodal silver complexes as antimicrobial agents*

the free silver(I) salts), independent of the type of sugar used. These approaches are examples for possible additional applications and further directions for the investigation of carbohydrate-based ligands and metal complexes in medicinal inorganic chemistry.

Another possibility to use carbohydrate-based ligand design for medicinal inorganic chemistry will be the introduction of multimodality functions. Several imaging modalities like PET, SPECT, MRI and fluorescence, and so on can be combined into one molecular probe using metal complexes. Carbohydrate-functionalized analogs of such compounds are applicable not only for diagnosis but also for therapeutic application and will enter the field of clinical treatment called theranostics. As mentioned in the above sections, switchable systems triggered by light and/or specific enzymatic digestion, as well as pH, temperature, and so on, are of significant interest. Carbohydrate-functionalized metal complexes with a sophisticated design to be activated by an external trigger will appear in the near future.

References

1. Joost, H.G. and Thorens, B. (2001) The extended GLUT-family of sugar/polyol transport facilitators: nomenclature, sequence characteristics, and potential function of its novel members. *Mol. Membr. Biol.*, **18** (4), 247–256.
2. Sun, L., Zeng, X., Yan, C. *et al*. (2012) Crystal structure of a bacterial homologue of glucose transporters GLUT1-4. *Nature*, **490** (7420), 361–366.
3. Gyurcsik, B. and Nagy, L. (2000) Carbohydrates as ligands: coordination equilibria and structure of the metal complexes. *Coord. Chem. Rev.*, **203**, 81–149.
4. Storr, T., Thompson, K.H. and Orvig, C. (2006) Design of targeting ligands in medicinal inorganic chemistry. *Chem. Soc. Rev.*, **35**, 534–544.
5. Gottschaldt, M. and Schubert, U.S. (2009) Prospects of metal complexes peripherally substituted with sugars in biomedical applications. *Chem. Eur. J.*, **15**, 1548–1557.
6. Mikata, Y. and Yano, S. (2012) Development of sugar-based materials for biological devices. *Curr. Top. Med. Chem.*, **12**, 145–157.
7. Mueller, D., Klette, I., Baum, R.P. *et al*. (2012) Simplified NaCl based Ga-68 concentration and labeling procedure for rapid synthesis of Ga-68 radiopharmaceuticals in high radiochemical purity. *Bioconjugate Chem.*, **23** (8), 1712–1717.
8. Alberto, R., Schibli, R., Egli, A. and Schubiger, P.A. (1998) A novel organometallic aqua complex of technetium for the labeling of biomolecules: aqueous solution and its reaction with a bifunctional ligand. *J. Am. Chem. Soc.*, **120**, 7987–7988.
9. Bowen, M.L. and Orvig, C. (2008) 99m-Technetium carbohydrate conjugates as potential agents in molecular imaging. *Chem. Commun.*, 5077–5091.
10. Morais, G.R., Falconer, R.A. and Santos, I. (2013) Carbohydrate-based molecules for molecular imaging in nuclear medicine. *Eur. J. Org. Chem.*, **2013** (8), 1401–1414.
11. Schibli, R., Dumas, C., Petrig, J. *et al*. (2005) Synthesis and in vitro characterization of organometallic rhenium and technetium glucose complexes against Glut 1 and hexokinase. *Bioconjugate Chem.*, **16**, 105–112.
12. Storr, T., Fisher, C.L., Mikata, Y. *et al*. (2005) A glucosamine–dipicolylamine conjugate of 99mTc(I) and 186Re(I) for use in imaging and therapy. *Dalton Trans.*, 654–655.
13. Bowen, M.L., Lim, N.C., Ewart, C.B. *et al*. (2009) Glucosamine conjugates bearing N,N,O-donors: potential imaging agents utilizing the $[M(CO)_3]^+$ core (M = Re, Tc). *Dalton Trans.*, 9216–9227.
14. Ferreira, C.L., Bayly, S.R., Green, D.E. *et al*. (2006) Carbohydrate-appended 3-hydroxy-4-pyridinone complexes of the $[M(CO)_3]^+$ core (M = Re, ^{99m}Tc, ^{186}Re). *Bioconjugate Chem.*, **17**, 1321–1329.
15. Ferreira, C.L., Ewart, C.B., Bayly, S.R. *et al*. (2006) Glucosamine conjugates of tricarbonylcyclopentadienyl rhenium(I) and technetium(I) cores. *Inorg. Chem.*, **45**, 6979–6987.
16. Bowen, M.L., Chen, Z.-F., Roos, A.M. *et al*. (2009) Long-chain rhenium and technetium glucosamine conjugates. *Dalton Trans.*, 9228–9236.
17. Storr, T., Obata, M., Fisher, C.L. *et al*. (2005) Novel carbohydrate-appended metal complexes for potential use in molecular imaging. *Chem. Eur. J.*, **11**, 195–203.

18. Gottschaldt, M., Koth, D., Müller, D. *et al*. (2007) Synthesis and structure of novel sugar-substituted bipyridine complexes of rhenium and 99m-technetium. *Chem. Eur. J.*, **13**, 10273–10280.
19. Storr, T., Sugai, Y., Barta, C.A. *et al*. (2005) Carbohydrate-appended 2,2'-dipicolylamine metal complexes as potential imaging agents. *Inorg. Chem.*, **44**, 2698–2705.
20. Gottschaldt, M., Bohlender, C., Muller, D. *et al*. (2009) Rhenium and 99m-technetium complexes of monosaccharide based tripodal triamines as potential radio imaging agents. *Dalton Trans.*, **26**, 5148–5154.
21. Yang, D.J., Kim, C.G., Schechter, N.R. *et al*. (2003) Imaging with Tc-99m ECDG targeted at the multifunctional glucose transport system: feasibility study with rodents. *Radiology*, **226** (2), 465–473.
22. Chen, X.J., Li, L., Liu, F. and Liu, B.L. (2006) Synthesis and biological evaluation of technetium-99m-labeled deoxyglucose derivatives as imaging agents for tumor. *Bioorg. Med. Chem. Lett.*, **16** (21), 5503–5506.
23. de Barros, A.L.B., Cardoso, V.N., Mota, L.D. *et al*. (2009) Synthesis and biological evaluation of technetium-labeled D-glucose-MAG(3) derivative as agent for tumor diagnosis. *Bioorg. Med. Chem. Lett.*, **19** (9), 2497–2499.
24. de Barros, A.L.B., Cardoso, V.N., Mota, L.D. *et al*. (2010) A novel D-glucose derivative radiolabeled with technetium-99m: synthesis, biodistribution studies and scintigraphic images in an experimental model of Ehrlich tumor. *Bioorg. Med. Chem. Lett.*, **20** (8), 2478–2480.
25. de Barros, A.L.B., Cardoso, V.N., Mota, L.D. and Alves, R.J. (2010) Synthesis and biodistribution studies of carbohydrate derivatives radiolabeled with technetium-99m. *Bioorg. Med. Chem. Lett.*, **20** (1), 315–317.
26. Kolb, H.C., Finn, M.G. and Sharpless, K.B. (2001) Click chemistry: diverse chemical function from a few good reactions. *Angew. Chem. Int. Ed.*, **40**, 2004–2021.
27. Meldal, M. and Tomøe, C.W. (2008) Cu-catalyzed azide-alkyne cycloaddition. *Chem. Rev.*, **108**, 2952–3015.
28. Mindt, T.L., Struthers, H., Brans, L. *et al*. (2006) "Click to chelate": synthesis and installation of metal chelates into biomolecules in a single step. *J. Am. Chem. Soc.*, **128**, 15096–15097.
29. Obata, M., Kitamura, A., Mori, A. *et al*. (2008) Syntheses, structural characterization and photophysical properties of 4-(2-pyridyl)-1,2,3-triazole rhenium(I) complexes. *Dalton Trans.*, 3292–3300.
30. Benoist, E., Coulais, Y., Almant, M. *et al*. (2011) A Click procedure with heterogeneous copper to tether technetium-99m chelating agents and rhenium complexes. Evaluation of the chelating properties and biodistribution of the new radiolabelled glucose conjugates. *Carbohydr. Res.*, **346** (1), 26–34.
31. Holland, J.P., Aigbirhio, F.I., Betts, H.M. *et al*. (2007) Functionalized bis(thiosemicarbazonato) complexes of zinc and copper: synthetic platforms toward site-specific radiopharmaceuticals. *Inorg. Chem.*, **46**, 465–485.
32. Green, D.E., Ferreira, C.L., Stick, R.V. *et al*. (2005) Carbohydrate-bearing 3-hydroxy-4-pyridinonato complexes of gallium(III) and indium(III). *Bioconjugate Chem.*, **16** (6), 1597–1609.
33. Gottschaldt, M., Bohlender, C., Pospiech, A. *et al*. (2009) In-III and Ga-III complexes of sugar-substituted tripodal trisalicylidene imines: the first Ga-68-labelled sugar derivative. *Eur. J. Inorg. Chem.*, **2009** (28), 4298–4307.
34. Hermann, P., Kotek, J., Kubícek, V. and Lukes, I. (2008) Gadolinium(III) complexes as MRI contrast agents: Ligand design and properties of the complexes. *Dalton Trans.*, 3027–3047.
35. Terreno, E., Castelli, D.D., Viale, A. and Aime, S. (2010) Challenges for molecular magnetic resonance imaging. *Chem. Rev.*, **110**, 3019–3042.
36. Martinez, G.V., Navath, S., Sewda, K. *et al*. (2013) Demonstration of a sucrose-derived contrast agent for magnetic resonance imaging of the GI tract. *Bioorg. Med. Chem. Lett.*, **23** (7), 2061–2064.
37. André, J.P., Geraldes, C.F.G.C., Martins, J.A. *et al*. (2004) Lanthanide(III) complexes of DOTA–glycoconjugates: a potential new class of lectin-mediated medical imaging agents. *Chem. Eur. J.*, **10**, 5804–5816.
38. Teixeira, J.M.C., Dias, D.M., Canada, F.J. *et al*. (2011) The interaction of La3+ complexes of DOTA/DTPA glycoconjugates with the RCA(120) lectin: a saturation transfer difference NMR spectroscopic study. *J. Biol. Inorg. Chem.*, **16** (5), 725–734.
39. Fulton, D.A., Elemento, E.M., Aime, S. *et al*. (2006) Glycoconjugates of gadolinium complexes for MRI applications. *Chem. Commun.*, 1064–1066.
40. Marradi, M., Alcántara, D., de la Fuente, J.M. *et al*. (2009) Paramagnetic Gd-based gold glyconanoparticles as probes for MRI: tuning relaxivities with sugars. *Chem. Commun.*, 3922–3924.
41. Irure, A., Marradi, M., Arnáiz, B. *et al*. (2013) Sugar/gadolinium-loaded gold nanoparticles for labelling and imaging cells by magnetic resonance imaging. *Biomater. Sci.*, **1**, 658–668.

42. Moats, R.A., Fraser, S.E. and Meade, T.J. (1997) A "smart" magnetic resonance imaging agent that reports on specific enzymatic activity. *Angew. Chem., Int. Ed. Engl.*, **36**, 726–728.
43. Urbanczyk-Pearson, L.M., Femia, F.J., Smith, J. *et al*. (2008) Mechanistic investigation of beta-galactosidase-activated MR contrast agents. *Inorg. Chem.*, **47**, 56–68.
44. Duimstra, J.A., Femia, F.J. and Meade, T.J. (2005) A gadolinium chelate for detection of beta-glucuronidase: a self-immolative approach. *J. Am. Chem. Soc.*, **127**, 12847–12855.
45. Chauvin, T., Durand, P., Bernier, M. *et al*. (2008) Detection of enzymatic activity by PARACEST MRI: a general approach to target a large variety of enzymes. *Angew. Chem. Int. Ed.*, **47**, 4370–4372.
46. Chauvin, T., Torres, S., Rosseto, R. *et al*. (2012) Lanthanide(III) complexes that contain a self-immolative arm: potential enzyme responsive contrast agents for magnetic resonance imaging. *Chem. Eur. J.*, **18** (5), 1408–1418.
47. Arena, F., Singh, J.B., Gianolio, E. *et al*. (2011) beta-Gal gene expression MRI reporter in melanoma tumor cells. Design, synthesis, and in vitro and in vivo testing of a Gd(III) containing probe forming a high relaxivity, melanin-like structure upon beta-Gal enzymatic activation. *Bioconjugate Chem.*, **22** (12), 2625–2635.
48. Singhal, N.K., Ramanujam, B., Mariappanadar, V. and Rao, C.P. (2006) Carbohydrate-based switch-on molecular sensor for Cu(II) in buffer: absorption and fluorescence study of the selective recognition of Cu(II) ions by galactosyl derivatives in HEPES buffer. *Org. Lett.*, **8**, 3525–3528.
49. Mitra, A., Hinge, V.K., Mittal, A. *et al*. (2011) A zinc-sensing glucose-based naphthyl imino conjugate as a detecting agent for inorganic and organic phosphates, including DNA. *Chem. Eur. J.*, **17**, 8044–8047.
50. Mikata, Y., Wakamatsu, M. and Yano, S. (2005) Tetrakis(2-quinolinylmethyl)ethylenediamine (TQEN) as a new fluorescent sensor for zinc. *Dalton Trans.*, 545–550.
51. Mikata, Y., Ugai, A., Yasuda, K. *et al*. (2012) Quinoline-based, glucose-pendant fluorescent zinc probes. *Chem. Biodivers.*, **9**, 2064–2075.
52. Hasegawa, T., Yonemura, T., Matsuura, K. and Kobayashi, K. (2003) Artificial metalloglycoclusters: compact saccharide shell to induce high lectin affinity as well as strong luminescence. *Bioconjugate Chem.*, **14**, 728–737.
53. Gottschaldt, M., Schubert, U.S., Rau, S. *et al*. (2010) Sugar-selective enrichment of D-glucose substituted ruthenium bipyridyl complex inside HepG2 cancer cells. *ChemBioChem*, **11**, 649–652.
54. Banerjee, S.R., Babich, J.W. and Zubieta, J. (2006) A new bifunctional amino acid chelator targeting the glucose transporter. *Inorg. Chim. Acta*, **359**, 1603–1612.
55. Mikata, Y., Takahashi, K., Noguchi, Y. *et al*. (2012) Synthesis of rhenium(I) tricarbonyl complexes with carbohydrate-pendant tridentate ligands and their cellular uptake. *Eur. J. Inorg. Chem.*, **2012** (2), 217–225.
56. Louie, M.-W., Liu, H.-W., Lam, M.H.-C. *et al*. (2011) Luminescent rhenium(I) polypyridine complexes appended with an alpha-D-glucose moiety as novel biomolecular and cellular probes. *Chem. Eur. J.*, **17**, 8304–8308.
57. Kamiya, M., Kobayashi, H., Hama, Y. *et al*. (2007) An enzymatically activated fluorescence probe for targeted tumor imaging. *J. Am. Chem. Soc.*, **129**, 3918–3929.
58. Garcia, L., Maisonneuve, S., Xie, J. *et al*. (2010) Sugars to control ligand shape in metal complexes: conformationally constrained glycoligands with a predetermination of stereochemistry and a structural control. *Inorg. Chem.*, **49**, 7282–7288.
59. Taquet, J.-P., Frochot, C., Manneville, V. and Barberi-Heyob, M. (2007) Phthalocyanines covalently bound to biomolecules for a targeted photodynamic therapy. *Curr. Med. Chem.*, **14**, 1673–1687.
60. Ballut, S., Makky, A., Chauvin, B. *et al*. (2012) Tumor targeting in photodynamic therapy. From glycoconjugated photosensitizers to glycodendrimeric one. Concept, design and properties. *Org. Biomol. Chem.*, **10**, 4485–4495.
61. Zheng, X. and Pandey, R.K. (2008) Porphyrin-carbohydrate conjugates: impact of carbohydrate moieties in photodynamic therapy (PDT). *Anti-Cancer Agents Med. Chem.*, **8**, 241–268.
62. Mikata, Y., Onchi, Y., Tabata, K. *et al*. (1998) Sugar-dependent phototoxic property of tetra- and octa-glycoconjugated tetraphenylporphyrins. *Tetrahedron Lett.*, **39**, 4505–4508.
63. Mikata, Y., Onchi, Y., Shibata, M. *et al*. (1998) Synthesis and phtotoxic property of tetra- and octa-glycoconjugated tetraphenylchlorins. *Bioorg. Med. Chem. Lett.*, **8**, 3543–3548.
64. Mikata, Y., Shibata, M., Baba, Y. *et al*. (2012) Synthesis and photodynamic properties of maltohexaose-conjugated porphyrins. *J. Porphyrins Phthalocyanines*, **16**, 1177–1185.
65. Sylvain, I., Zerrouki, R., Granet, R. *et al*. (2002) Synthesis and biological evaluation of thioglycosylated porphyrins for an application in photodynamic therapy. *Bioorg. Med. Chem.*, **10**, 57–69.

66. Chen, X., Hui, L., Foster, D.A. and Drain, C.M. (2004) Efficient synthesis and photodynamic activity of porphyrin-saccharide conjugates: targeting and incapacitating cancer cells. *Biochemistry*, **43**, 10918–10929.
67. Laville, I., Pigaglio, S., Blais, J.-C. *et al*. (2006) Photodynamic efficiency of diethylene glycol-linked glycoconjugated porphyrins in human retinoblastoma cells. *J. Med. Chem.*, **49**, 2558–2567.
68. Ribeiro, A.O., Tomé, J.P.C., Neves, G.P.M.S. *et al*. (2006) [1,2,3,4-Tetrakis(alpha/beta-D-galactopyranos-6-yl)-phthalocyaninato]zinc(II): a water-soluble phthalocyanine. *Tetrahedron Lett.*, **47**, 9177–9180.
69. Soares, A.R.M., Tomé, J.P.C., Neves, G.P.M.S. *et al*. (2009) Synthesis of water-soluble phthalocyanines bearing four or eight D-galactose units. *Carbohydr. Res.*, **344**, 507–510.
70. Soares, A.R.M., Neves, M.G.P.M.S., Tomé, A.C. *et al*. (2012) Glycophthalocyanines as photosensitizers for triggering mitotic catastrophe and apoptosis in cancer cells. *Chem. Res. Toxicol.*, **25** (4), 940–951.
71. Zorlu, Y., Dumoulin, F., Bouchu, D. *et al*. (2010) Monoglycoconjugated water-soluble phthalocyanines. Design and synthesis of potential selectively targeting PDT photosensitisers. *Tetrahedron Lett.*, **51**, 6615–6618.
72. Daly, R., Vaz, G., Davies, A.M. *et al*. (2012) Synthesis and biological evaluation of a library of glycoporphyrin compounds. *Chem. Eur. J.*, **18** (46), 14671–14679.
73. Garcia, G., Naud-Martin, D., Carrez, D. *et al*. (2011) Microwave-mediated "click-chemistry" synthesis of glycoporphyrin derivatives and in vitro photocytotoxicity for application in photodynamic therapy. *Tetrahedron*, **67** (26), 4924–4932.
74. Choi, C.-F., Huang, J.-D., Lo, P.-C. *et al*. (2008) Glycosylated zinc(II) phthalocyanines as efficient photosensitisers for photodynamic therapy. Synthesis, photophysical properties and in vitro photodynamic activity. *Org. Biomol. Chem.*, **6**, 2173–2181.
75. Achelle, S., Couleaud, P., Baldeck, P. *et al*. (2011) Carbohydrate-porphyrin conjugates with two-photon absorption properties as potential photosensitizing agents for photodynamic therapy. *Eur. J. Org. Chem.*, **2011** (7), 1271–1279.
76. Hammerer, F., Achelle, S., Baldeck, P. *et al*. (2011) Influence of carbohydrate biological vectors on the two-photon resonance of porphyrin oligomers. *J. Phys. Chem. A*, **115** (24), 6503–6508.
77. Lo, K.K.-W., Law, W.H.-T., Chan, J.C.-Y. *et al*. (2013) Photophysical and cellular uptake properties of novel phosphorescent cyclometalated iridium(III) bipyridine d-fructose complexes. *Metallomics*, **5** (7), 808–812.
78. Crespy, D., Landfester, K., Schubert, U.S. and Schiller, A. (2010) Potential photoactivated metallopharmaceuticals: from active molecules to supported drugs. *Chem. Commun.*, **46**, 6651–6662.
79. Schatzschneider, U. (2010) Photoactivated biological activity of transition-metal complexes. *Eur. J. Inorg. Chem.*, **2010** (10), 1451–1467.
80. Farrer, N.J., Salassa, L. and Sadler, P.J. (2009) Photoactivated chemotherapy (PACT): the potential of excited-state d-block metals in medicine. *Dalton Trans.*, 10690–10701.
81. Rosenberg, B., van Camp, L. and Krias, T. (1965) Inhibition of cell division in Escherichia coli by electrolysis products from a platinum electrode. *Nature*, **205**, 698–699.
82. Rosenberg, B., VanCamp, L., Trosko, J.E. and Mansour, V.H. (1969) Platinum compounds; a new class of potent antitumour agents. *Nature*, **222**, 385–386.
83. Jamieson, E.R. and Lippard, S.J. (1999) Structure, recognition, and processing of cisplatin-DNA adducts. *Chem. Rev.*, **99**, 2467–2498.
84. Lovejoy, K.S. and Lippard, S.J. (2009) Non-traditional platinum compounds for improved accumulation, oral bioavailability, and tumor targeting. *Dalton Trans.*, 10651–10659.
85. Harper, B.W., Krause-Heuer, A.M., Grant, M.P. *et al*. (2010) Advances in platinum chemotherapeutics. *Chem. Eur. J.*, **16**, 7064–7077.
86. Kelland, L. (2007) The resurgence of platinum-based cancer chemotherapy. *Nat. Rev. Cancer*, **7** (8), 573–584.
87. Hartinger, C.G., Nazarov, A.A., Ashraf, S.M. *et al*. (2008) Carbohydrate-metal complexes and their potential as anticancer agents. *Curr. Med. Chem.*, **15**, 2574–2591.
88. Tsubomura, T., Ogawa, M., Yano, S. *et al*. (1990) Highly active antitumor platinum(II) complexes of amino sugars. *Inorg. Chem.*, **29**, 2622–2626.
89. Berger, I., Nazarov, A.A., Gartinger, C.G. *et al*. (2007) A glucose derivative as natural alternative to the cyclohexane-1,2-diamine ligand in the anticancer drug oxaliplatin? *ChemMedChem*, **2**, 505–514.
90. Hanessian, S. and Wang, J. (1993) Synthesis and biological evaluation of novel chiral non-racemic diaminoplatinum analogs based on a tetrahydropyran motif. *Can. J. Chem.*, **71**, 886–895.

91. Onambele, L.A., Koth, D., Czaplewska, J.A. *et al*. (2010) Mitochondrial mode of action of a thymidine-based cisplatin analog breaks resistance in cancer cells. *Chem. Eur. J.*, **16**, 14498–14505.
92. Yano, S., Shinohara, Y., Mogami, K. *et al*. (1999) Synthesis of useful chelating reagents having a sugar unit, 1,3-diamino-2-propyl beta-D-glucopyranoside and 1,3-diamino-2-propyl alpha-D-mannopyranoside. *Chem. Lett.*, 255–256.
93. Chen, Y., Heeg, M.J., Braunshweiger, P.G. *et al*. (1999) A carbohydrate-linked cisplatin analogue having antitumor activity. *Angew. Chem. Int. Ed.*, **38**, 1768–1769.
94. Mikata, Y., Shinohara, Y., Yoneda, K. *et al*. (2001) Unprecedented sugar-dependent in vivo antitumor activity of carbohydrate-pendant cis-diamminedichloroplatinum(II) complexes. *Bioorg. Med. Chem. Lett.*, **11**, 3045–3047.
95. Brudziñska, I., Mikata, Y., Obata, M. *et al*. (2004) Synthesis, structural characterization, and antitumor activity of palladium(II) complexes containing a sugar unit. *Bioorg. Med. Chem. Lett.*, **14**, 2533–2536.
96. Cucciolito, M.E., Litto, R.D., Fanizzi, F.P. *et al*. (2010) Hydrophilic ligands derived from glucose: synthesis, characterization and in vitro cytotoxic activity on cancer cells of Pt(II) complexes. *Inorg. Chim. Acta*, **363** (4), 741–747.
97. Möker, J. and Thiem, J. (2012) Synthesis and hydrolysis studies of novel glyco-functionalized platinum complexes. *Carbohydr. Res.*, **348**, 14–26.
98. Ma, D.-L., Shum, T.Y.-T., Zhang, F. *et al*. (2005) Water soluble luminescent platinum terpyridine complexes with glycosylated acetylide and arylacetylide ligands: photoluminescent properties and cytotoxicities. *Chem. Commun.*, 4675–4677.
99. Ott, I. (2009) On the medicinal chemistry of gold complexes as anticancer drugs. *Coord. Chem. Rev.*, **253**, 1670–1681.
100. Reisner, E., Arion, V.B., Keppler, B.K. and Pombeiro, A.J.L. (2008) Electron-transfer activated metal-based anticancer drugs. *Inorg. Chim. Acta*, **361**, 1569–1583.
101. Berger, I., Hanif, M., Nazarov, A.A. *et al*. (2008) In vitro anticancer activity and biologically relevant metabolization of organometallic ruthenium complexes with carbohydrate-based ligands. *Chem. Eur. J.*, **14** (29), 9046–9057.
102. Hanif, M., Nazarov, A.A., Hartinger, C.G. *et al*. (2010) Osmium(II)- versus ruthenium(II)-arene carbohydrate-based anticancer compounds: similarities and differences. *Dalton Trans.*, **39** (31), 7345–7352.
103. Hanif, M., Meier, S.M., Kandioller, W. *et al*. (2011) From hydrolytically labile to hydrolytically stable RuII–arene anticancer complexes with carbohydrate-derived co-ligands. *J. Inorg. Biochem.*, **105** (2), 224–231.
104. Deepthi, S.B., Trivedi, R., Giribabu, L. *et al*. (2013) Effect of amide-triazole linkers on the electrochemical and biological properties of ferrocene-carbohydrate conjugates. *Dalton Trans.*, **42** (4), 1180–1190.
105. Lima, J.C. and Rodriguez, L. (2011) Phosphine-gold(I) compounds as anticancer agents: general description and mechanisms of action. *Anticancer Agents Med. Chem.*, **11** (10), 921–928.
106. Pearson, S., Scarano, W. and Stenzel, M.H. (2012) Micelles based on gold-glycopolymer complexes as new chemotherapy drug delivery agents. *Chem. Commun.*, **48** (39), 4695–4697.
107. Wild, A., Babiuch, K., Konig, M. *et al*. (2012) Synthesis of a glycopolymeric Pt-II carrier and its induction of apoptosis in resistant cancer cells. *Chem. Commun.*, **48** (51), 6357–6359.
108. Reichardt, N.C., Martin-Lomas, M. and Penades, S. (2013) Glyconanotechnology. *Chem. Soc. Rev.*, **42** (10), 4358–4376.
109. Huang, G.L., Cheng, F., Chen, X. *et al*. (2013) Recent progress on the applications of multifunctional glyconanoparticles. *Curr. Pharm. Des.*, **19** (13), 2454–2458.
110. Burda, C., Chem, X., Narayanan, R. and El-Sayed, M.A. (2005) Chemistry and properties of nanocrystals of different shapes. *Chem. Rev.*, **105**, 1025–1102.
111. Otsuka, H., Akiyama, Y., Nagasaki, Y. and Kataoka, K. (2001) Quantitative and reversible lectin-induced association of gold nanoparticles modified with alpha-lactosyl-omega-mercapto-poly(ethylene glycol). *J. Am. Chem. Soc.*, **123**, 8226–8230.
112. Earhart, C., Jana, N.R., Erathodiyil, N. and Ying, J.Y. (2008) Synthesis of carbohydrate-conjugated nanoparticles and quantum dots. *Langmuir*, **24**, 6215–6219.
113. Hilger, I. and Kaiser, W.A. (2012) Iron oxide-based nanostructures for MRI and magnetic hyperthermia. *Nanomedicine*, **7** (9), 1443–1459.
114. Babiuch, K., Wyrwa, R., Wagner, K. *et al*. (2011) Functionalized, biocompatible coating for superparamagnetic nanoparticles by controlled polymerization of a thioglycosides monomer. *Biomacromolecules*, **12** (3), 681–691.

115. El-Boubbou, K., Zhu, D.C., Vasileiou, C. *et al*. (2010) Magnetic glyco-nanoparticles: a tool to detect, differentiate, and unlock the glyco-codes of cancer via magnetic resonance imaging. *J. Am. Chem. Soc.*, **132**, 4490–4499.
116. L. Lartigue, C. Innocenti, T. Kalaivani, *et al*., Water-dispersible sugar-coated iron oxide nanoparticles. An evaluation of their relaxometric and magnetic hyperthermia properties, *J. Am. Chem. Soc.*, **133**, 10459-10472 (2011).
117. Kikkeri, R., Lepenies, B., Adibekian, A. *et al*. (2009) In vitro imaging and in vivo liver targeting with carbohydrate capped quantum dots. *J. Am. Chem. Soc.*, **131**, 2110–2112.
118. Bellapadrona, G., Tesler, A.B., Grünstein, D. *et al*. (2012) Optimization of localized surface plasmon resonance transducers for studying carbohydrate-protein interactions. *Anal. Chem.*, **84**, 232–240.
119. Yang, Y., Xue, X.-C., Jin, X.-F. *et al*. (2012) Synthesis of multivalent N-acetyl lactosamine modified quantum dots for the study of carbohydrate and galectin-3 interactions. *Tetrahedron*, **68** (35), 7148–7154.
120. Mukhopadhyay, B., Martins, M.B., Karamanska, R. *et al*. (2009) Bacterial detection using carbohydrate-functionalised CdS quantum dots: a model study exploiting E. coli recognition of mannosides. *Tetrahedron Lett.*, **50** (8), 886–889.
121. Smith, E.A., Thomas, W.D., Kiessling, L.L. and Corn, R.M. (2003) Surface plasmon resonance imaging studies of protein-carbohydrate interactions. *J. Am. Chem. Soc.*, **125**, 6140–6148.
122. Yonzon, C.R., Jeoung, E., Zou, S. *et al*. (2004) A comparative analysis of localized and propagating surface plasmon resonance sensors: the binding of concanavalin A to a monosaccharide functionalized self-assembled monolayer. *J. Am. Chem. Soc.*, **126**, 12669–12676.
123. Ogiso, M., Kobayashi, J., Imai, T. *et al*. (2013) Carbohydrate immobilized on a dendrimer-coated colloidal gold surface for fabrication of a lectin-sensing device based on localized surface plasmon resonance spectroscopy. *Biosens. Bioelectron.*, **41**, 465–470.
124. Zhang, Y., Luo, S., Tang, Y. *et al*. (2006) Carbohydrate-protein interactions by "clicked" carbohydrate self-assembled monolayers. *Anal. Chem.*, **78**, 2001–2008.
125. Guo, X., Kulkarni, A., Doepke, A. *et al*. (2012) Carbohydrate-based label-free detection of Escherichia coli ORN 178 using electrochemical impedance spectroscopy. *Anal. Chem.*, **84**, 241–246.
126. Schugar, H., Green, D.E., Bowen, M.L. *et al*. (2007) Combating Alzheimer's disease with multifunctional molecules designed for metal passivation. *Angew. Chem. Int. Ed.*, **46**, 1716–1718.
127. Storr, T., Merkel, M., Song-Zhao, G.X. *et al*. (2007) Synthesis, characterization, and metal coordinating ability of multifunctional carbohydrate-containing compounds for Alzheimer's therapy. *J. Am. Chem. Soc.*, **129**, 7453–7463.
128. Gottschaldt, M., Pfeifer, A., Koth, D. *et al*. (2006) Silver(I) complexes based on novel tripodal thioglycosides: synthesis, structure and antimicrobial activity. *Tetrahedron*, **62**, 11073–11080.

7

Design of Schiff Base-derived Ligands: Applications in Therapeutics and Medical Diagnosis

Rafael Pinto Vieira[1,2] and Heloisa Beraldo[2]

[1]*Department of Chemistry, Simon Fraser University, 8888 University Drive, Burnaby, BC, V5A-1S6, Canada*
[2]*Departamento de Química, Universidade Federal de Minas Gerais, Av. Presidente Antonio Carlos 6627, Belo Horizonte, MG, 31270-901, Brazil*

7.1 Introduction

Hydrazones, semicarbazones, and thiosemicarbazones (Figure 7.1) are Schiff base-derived compounds that have been extensively investigated due to their wide range of pharmacological applications.

Structure-activity relationship (SAR) studies involving these compounds, together with investigations on their biological targets, have provided valuable information for the design of new potentially active scaffolds. Since these compounds are strong chelators their pharmacological properties are modulated by the presence of metals and in some cases metal coordination is part of their mechanism of action.

In the present work a brief review on the pharmacological profile of these compounds will be presented as well as some strategies for the use of the azomethine function in the design of new bioactive ligands and metal complexes. Three cases will be considered: (i) the design of thiosemicarbazones and hydrazones as drug candidates for cancer chemotherapy; (ii) the design of bis(thiosemicarbazones) as ligands for copper(II) complexes with potential applications in medical diagnosis; and (iii) the design of Schiff base-derived ligands as anti-parasitic drug candidates: applications in the therapeutics of Chagas disease.

Ligand Design in Medicinal Inorganic Chemistry, First Edition. Edited by Tim Storr.

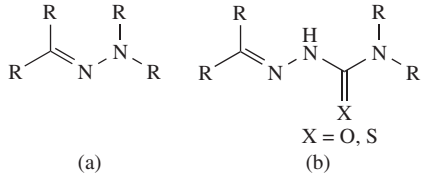

Figure 7.1 *Generic chemical structure of hydrazones ((a) R = H, alkyl, aryl, acyl, or aryl groups) thiosemicarbazones and semicarbazones ((b) X = S, O; R = H, alkyl, and/or aryl groups)*

7.2 Design of thiosemicarbazones and hydrazones as drug candidates for cancer chemotherapy

According to the World Health Organization (WHO) cancer is a generic term for a large group of diseases. It is characterized by an uncontrolled growth and spread of cells that can affect almost any part of the body. The growths frequently invade surrounding tissues and can metastasize to distant sites, causing physical and functional damage to invaded areas. Cancer is the leading cause of death worldwide. In spite of the high mortality rates depending on the types of cancer, a significant proportion of cancers can be cured through surgery, radiotherapy, and/or chemotherapy [1].

Surgery and radiotherapy dominated cancer treatment until the 1960s. Later, it became clear that survival rates increased by the use of combination chemotherapy, which opened up the opportunity to apply drugs in conjunction with surgery and/or radiation treatments [2].

After the identification of numerous molecular targets chemotherapy is now considered to be in the age of "targeted therapy" and random screening is being replaced by assays against specific targets [2]. Although the development of cancer therapy has been notable, drug resistance and treatment failure still pose great challenges to health systems.

Thiosemicarbazones have shown significant antineoplastic activity against a large number of human tumor cell lines under *in vitro* conditions [3, 4]. α(N)-heterocyclic thiosemicarbazones present the N-N-S donor structure that favors metal coordination. After complexation, two five-membered chelate rings are formed, displaying a conjugated structure, and a potential π-π interaction surface that seems to be essential for their pharmacological activity (Figure 7.2) [4, 5].

The first evidence of the antineoplastic activity of α(N)-heterocyclic thiosemicarbazones was reported in 1956 for 2-formylpyridine thiosemicarbazone (**PT**, Figure 7.3), which demonstrated anti-leukemia activity [3, 4, 6]. It has been suggested that α(N)-heterocyclic thiosemicarbazones act as tridentate chelating systems and that modifications in the ring system while retaining the ligand pattern could alter the bioactivity and toxicity of the compounds. Electron densities, substituents, and geometry proved to have strong effects on the pharmacological activity [7]. A number of thiosemicarbazones were assayed against transplanted rodent tumors. 1-formylisoquinoline thiosemicarbazone (**IQ-1**, Figure 7.3) was predicted and found active, while the

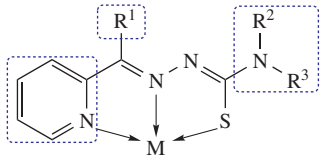

Figure 7.2 *Zones of structural modification and coordination positions in the basic skeleton of α(N)-heterocyclic thiosemicarbazones. M = metal; R^1, R^2, and R^3 = H, alkyl, and/or aryl groups*

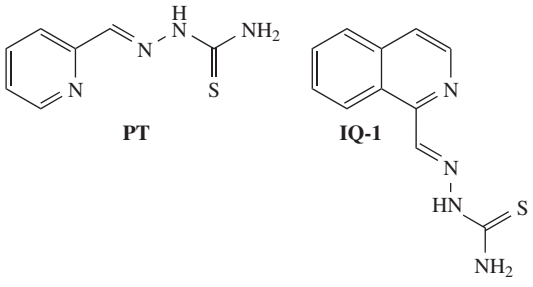

Figure 7.3 *Chemical structures of 2-formylpyridine thiosemicarbazone (**PT**) and 1-formylisoquinoline thiosemicarbazone (**IQ-1**)*

3-formylisoquinoline congener was predicted and found inactive in the tested tumors. All effective compounds presented the N-N-S tridentate chelating system. Antineoplastic activity was only verified when the side chain was located at a position α to the heteroaromatic nitrogen atom [8].

PT and **IQ-1** caused marked inhibition of the incorporation of ^{3}Hthymidine into the DNA of several tumor cell lineages. The syntheses of RNA and proteins were considerably less sensitive to the compounds. The site of metabolic lesion on DNA biosynthesis was located in the conversion of ribonucleotides into deoxyribonucleotides, a rate-limiting step in DNA synthesis, catalyzed by the iron-containing enzyme ribonucleoside diphosphate reductase (RDR) [9].

Studies on the mode of action indicated that **PT** and **IQ-1** caused inhibition of RDR which was noncompetitive with respect to the ribonucleotide substrate. The mechanism of action of α(N)-heterocyclic carboxaldehyde thiosemicarbazones was investigated by taking **IQ-1**, a potent inhibitor of DNA biosynthesis, as a prototype of the class [10]. The compound proved to be a powerful inhibitor of DNA replication in Sarcoma 180 cells *in vitro*. It was demonstrated that **IQ-1** induces a decrease in intracellular pools of deoxyribonucleotides and that the site of action is RDR [10, 11]. The data suggested that it is unlikely that the inhibitor interacts with the site on the enzyme that binds the nucleotides. However, a correlation was found between RDR blockage and the concentration of the substrate dithiothreitol, used as a model for the thioredoxin–thioredoxin reductase–NADPH system (NADPH = nicotinamide adenine dinucleotide diphosphate). The partially competitive relationship between **IQ-1** and the dithiol indicated binding of the inhibitor at or near the site on RDR normally occupied by this substrate [3, 10, 11].

Mammalian RDR consists of two non-identical homodimers R1 and R2. The active site is located in the R1 subunit. The R2 subunit contains two Fe^{III} ions connected by a μ-oxo-bridge and a free stable tyrosine radical essential for enzymatic activity [12].

The original hypothesis suggested that **IQ-1** acted to inhibit RDR by coordinating iron required for the enzyme catalytic activity. However, binding of free iron by **IQ-1** revealed that it was not responsible for inhibition. The possibility that the inhibitor might have interacted with an enzyme-iron complex was considered, but subsequently discarded. It seemed probable that the active form of the drug was an iron complex. The complex might have bound to a site normally occupied by iron and the dithiol substrate, blocking electron transfer. Studies indicated that the active form of the drug was its Fe^{II} complex [3, 11].

Heterocyclic thiosemicarbazones have the ability to remove iron from ferritin [13] and from transferrin, suggesting that this type of reaction is a plausible mechanism by which the compounds can bind iron in organisms [14].

The cytotoxicity of metal complexes of 5-substituted-**PT**s has been investigated [15]. The iron complexes with 5-methyl-, 5-Cl-, 5-CF_3-substituted derivatives completely prevented Ehrlich ascites tumor growth. The iron complexes of **IQ-1, PT**, and 4-methyl-5-amino-1-formylisoquinoline thiosemicarbazone (**MAIQ-1**) were shown to be three- to sixfold more active than their free ligands as inhibitors of RDR to which no iron had been added [16].

Studies on the mechanism of inhibition of mammalian RDR by **IQ-1** suggested that the tyrosine free radical present in the structure of the enzyme was the target of the drug and that the thiosemicarbazone exerted its inhibitory activity by inactivating the radical. It was suggested that the Fe^{II} complex of bound **IQ-1** reacts with oxygen leading to the reversible destruction of the radical. The effects of thiols on inhibition were attributed to their ability to reduce Fe^{III} to Fe^{II}, which was necessary for drug action [17, 18].

Our group demonstrated that Fe^{III} complexes of **PT** and 2-acetylpyridine thiosemicarbazone are reduced by the cellular thiol-like reducing agents dithiothreitol (a model for thioredoxin) and *N*-acetyl-L-cysteine (a model for glutathione), suggesting a similar mode of action. The pathway could have involved oxidation of the Fe^{II} complex of the drug, with the release of one electron and the consequent inactivation of the tyrosine free radical, followed by reduction of the Fe^{III} complex by a cellular thiol [19, 20].

5-Hydroxy-2-formylpyridine thiosemicarbazone (**5-HP**) was the first member of the α(N)-heterocyclic thiosemicarbazone series to be clinically evaluated [21]. However, conjugation to form glucuronides was the major metabolic fate of **5-HP**, which showed rapid clearance. In addition, **5-HP** exhibited low affinity with RDR. The iron chelation efficacy of **5-HP** was apparent from the characteristic dark-green urine observed after administration to patients, which was likely to have been due to the excretion of the **5-HP**-Fe^{II} complex. Although transient decreases in blast counts were observed in patients with acute leukemia, no remission, or antitumor activity was noted in patients with solid tumors [22]. This lack of activity was attributed to the low RDR inhibitory potency of the compound, its rapid biotransformation to an O-glucuronide derivative and the rapid excretion of the metabolite [21]. These drawbacks resulted in the development of a second generation of α(N)-heterocyclic thiosemicarbazones which had greater affinity with the target.

Distinct α-N-heterocyclic thiosemicarbazones can be obtained from modifications in essentially three different points of their basic skeleton: (i) the heterocyclic ring; (ii) the N^4-substituents on the thiosemicarbazone moiety; and (iii) the N-N-S chelating system (see Figure 7.2). These modifications can change the physicochemical properties of the resulting compounds, modulating their interactions with biological targets [4].

Information for the design of more effective inhibitors of RDR has been provided by SAR studies which determined the structural requirements for optimum enzyme-inhibitor interaction [9]. The 3-, 4-, and 5-methyl substituted **PT** derivatives proved to be slightly more active than the parent compound. **IQ-1** was the most powerful inhibitor within the isoquinoline family. The fact that **IQ-1** was considerably more potent than **PT** as an RDR inhibitor suggested the occurrence of a hydrophobic interaction between the benzenoid portion of the molecule and the enzyme, which explained the fact that 3-, 4-, and 5-methyl-substituted **PT** derivatives presented increased activity. The decreased inhibitory potencies of the 6-methyl **PT** derivative and of the 3-methyl **IQ-1** derivative suggested that the enzyme had low bulk tolerance [9]. The hydrophobic phenyl ring was introduced at various positions in the **PT** molecule to enhance affinity for the target, and the effect of these variations on RDR activity was tested. The data suggested that 2-formyl-4-(*m*-aminophenyl)pyridine thiosemicarbazone possessed the optimum combination of structural features and was the most active of the *m*-aminophenyl derivatives as an inhibitor of both tumor growth and RDR [23, 24].

5-Amino-**IQ-1** appeared to be a candidate as a second-generation compound with clinical potential in cancer chemotherapy since it exhibited similar RDR inhibition potency as **IQ-1** but could be rendered soluble as an acidic salt [25]. In **MAIQ-1**, steric hindrance to enzymatic substitution of the 5-amino function was achieved by insertion of a methyl group. **MAIQ-1** was found to be a powerful antineoplastic agent, and a very effective inhibitor of RDR [26].

Alkylation of the amino group on the pyridine ring leads to steric hindrance to enzymatic acetylation of the amino function, and in addition increased lipophilicity. The 5-methylamino, 5-ethylamino, and 5-allylamino **PT** derivatives proved to be good inhibitors of RDR activity, with significant antitumor activity *in vivo* and tolerable toxicity [27].

α(N)-Heterocyclic thiosemicarbazones are the strongest known RDR inhibitors and were found to be much more potent than hydroxyurea (Figure 7.4), an RDR inhibitor in clinical use. New heterocyclic thiosemicarbazones have been prepared and evaluated, which by virtue of their structures were resistant to O-glucuronidation [27]. Among them, 3- and 5-aminopyridine-2-carboxaldehyde thiosemicarbazone showed

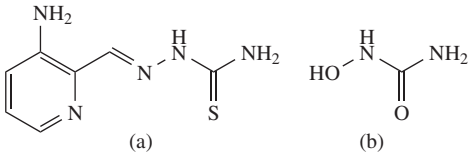

Figure 7.4 *Chemical structures of 3-aminopyridine-2-carboxaldehyde thiosemicarbazone (triapine, (a)) and hydroxyurea (b)*

significant antitumor activity in mice carrying L1210 leukemia [28]. 3-Aminopyridine-2-carboxaldehyde thiosemicarbazone ("triapine," Figure 7.4) demonstrated potent inhibition of L1210 leukemia cells *in vitro*, curative capacity for mice carrying L1210 leukemia, marked RDR inhibition, and effectiveness against hydroxyurea-resistant cells. In addition, triapine strongly inhibited the growth of murine M109 lung carcinoma and A2780 human ovarian carcinoma xenografts in mice. Furthermore, tumor cells were more sensitive to the DNA-synthesis inhibitory action of triapine than normal cells. The compound was able to cross the blood-brain barrier and to inhibit the growth of L1210 cells in the brain. Finally, a combination of triapine with cisplatin or doxorubicin caused a synergistic cytotoxic effect on L1210 cells in mice, due to the fact that the drug prevented the repair of DNA damage induced by these antineoplastic agents [29, 30]. Triapine has also shown the best results in biotransformation assays, and it is now being tested as an antitumor agent in Phase II clinical trials (Triapine®; Vion Pharmaceuticals Inc, New Haven, CT) [4 and references therein].

Thiosemicarbazones with different ring systems such as benzene, furan, and thiophene have been prepared and evaluated for their cytotoxic activities [4]. Replacement of the six-membered heterocyclic ring by five-membered rings can reduce or even extinguish the activity of these compounds [5]. Changes in structural features, lipophilicity, and reactivity can be easily performed by modifications on the thiosemicarbazone moiety. Substitution of the hydrogen attached to N2 can decrease or cancel out the antiproliferative activity, since the absence of the ionizable proton hinders electron delocalization and metal binding [4, 31].

N^4-substituted thiosemicarbazones show higher cytotoxic activity in comparison to non-substituted analogs. In general, this effect is attributed to modifications in the partition coefficient of the compounds and increased lipophilicity, facilitating the access to intracellular targets [4]. Substituent groups at N^4 include hydrogen, alkyl and aryl groups, and heterocyclic rings, where N^4 is at least one of the heteroatoms.

Our research group demonstrated that N^4-phenyl-2-acetylpyridine thiosemicarbazone (**H2Ac4Ph**) and its N^4-*ortho*-, -*meta*-, and -*para*-chlorophenyl, and N^4-*ortho*-, -*meta*-, and -*para*-tolyl derivatives show cytotoxicity at nanomolar concentrations against malignant gliomas [32]. More recently the cytotoxic activities of **H2Ac4Ph** and its N^4-*ortho*-, -*meta*-, and -*para*-fluorophenyl- (**H2Ac4oFPh**, **H2Ac4mFPh, H2Ac4pFPh**), N^4-*ortho*-, -*meta*-, and -*para*-chlorophenyl- (**H2Ac4oClPh**, **H2Ac4mClPh, H2Ac4pClPh**), N^4-*ortho*-, -*meta*-, and -*para*-iodophenyl- (**H2Ac4oIPh**, **H2Ac4mIPh, H2Ac4pIPh**), and N^4-*ortho*-, -*meta*-, and -*para*-nitrophenyl- (**H2Ac4oNO_2Ph**, **H2Ac4mNO_2Ph, H2Ac4pNO_2Ph**) derivatives (Figure 7.5) were assayed against MCF-7 (breast adenocarcinoma), U87 (glioblastoma multiforme expressing wild-type p53 protein), and T98G (glioblastoma multiforme expressing mutant p53) malignant human tumor cells

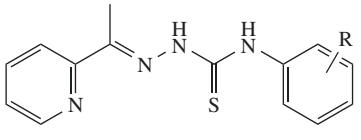

Figure 7.5 *Chemical structure of N^4-phenyl-2-acetylpyridine thiosemicarbazone (H2Ac4Ph) derivatives, where R = H, CH_3, F, Cl, I, or NO_2 (ortho, meta, and para)*

[33]. The compounds were cytotoxic at nanomolar doses against the studied tumor cell lineages. SAR data indicated similar correlations between the chemical descriptors and cytotoxicity against MCF-7 and U87 cells but different correlations between descriptors and cytotoxicity against T98G and U87 cells. The direct correlation between the HOMO (highest occupied molecular orbital) energies and activities against MCF-7 and U87 cells was an important finding since the HOMO energy is related to the molecule reactivity. In addition, the results indicated that the more negatively charged the sulfur atom, the higher the antiproliferative effect against MCF-7 and U87 cells. The sulfur atom may play an important role in the thiosemicarbazone reactivity and, therefore, in its cytotoxic activity. HOMO density plots revealed distinct electronic delocalization among the thiosemicarbazones, which may partially account for the differences in activity of these compounds, although other parameters may not be excluded [33].

Treatment with the 2-acetylpyridine-derived thiosemicarbazones induced irregularities in cellular shape, cell shrinkage, and membrane blebbing characteristics of programmed cell death for U87, T98G, and MCF-7 cells. Chromatin condensation and DNA fragmentation were also found in all treated cells when stained with 4′,6-diamidine-2-phenylindole dihydrochloride (DAPI) (Figure 7.6). Hence, apoptosis induction could have been at least in part responsible for the reduction of cell survival. Under acridine orange/ethidium bromide (AO/EB) staining control cells showed cytoplasm and nucleus with homogeneous green and minimal orange fluorescence. Treated cells presented chromatin condensation (bright green fragments) and absence of EB fluorescence, indicating preserved membrane. These features are typical of early apoptosis. Moreover, treated cells showed large acidic compartments in the cytoplasm, and visible red fluorescence, indicating the presence of autophagolysosomes, characteristic of cells engaged in autophagy (Figure 7.6). Our results suggested that the thiosemicarbazones under study were able to induce two types of programmed cell death [33].

The first evidence for the increase in cytotoxic activity of thiosemicarbazones upon coordination was reported for iron and copper complexes [15]. Later results have shown the same tendency for complexes with other metals [34–36].

We demonstrated that when 2-acetylpyridine- and 2-benzoylpyridine-derived thiosemicarbazones coordinated with Au^{I}, the cytotoxic effect of the thiosemicarbazones increased against human leukemia cells [37]. Similarly, coordination of 2-benzoylpyridine-derived thiosemicarbazones with Sb^{III} strongly enhanced

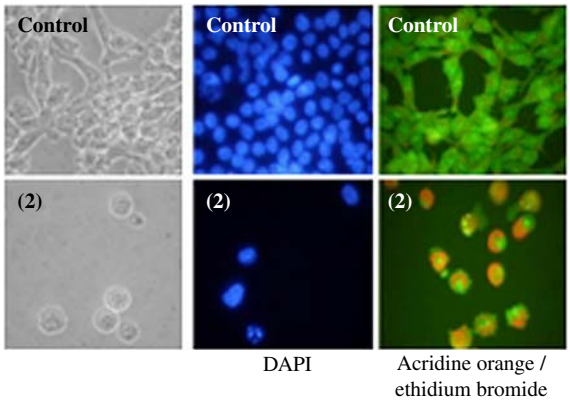

Figure 7.6 *Apoptosis (DAPI staining) and autophagy (AO/EB staining) in T98 cells induced by N^4-o-fluorophenyl-2-acetylpyridine thiosemicarbazone (compound 2). (See plate section for the colour version of this figure)*

their cytotoxicity against leukemia cell lineages [38]. Complexation to Ga^{III} also resulted in higher cytotoxic activity of 2-pyridineformamide-derived thiosemicarbazones against malignant glioblastoma cells [39].

Owing to the strong affinity of hydrazones and thiosemicarbazones for iron, these compounds could function as potential iron chelators and thus be employed in the treatment of cancer. Iron is crucial for cellular growth as it is required in the RDR active site. Iron is the most abundant trace metal in the human organism [40] and it is essential in many biological processes, being involved in electron transport, nucleotide synthesis, and erythropoiesis [41]. The broad range of biological functions of iron can be attributed to an evolutionary process of organisms that selected this metal due to the capacity that it has for conversion from Fe^{II} to Fe^{III} oxidation states [42].

In neoplastic cells alterations in iron metabolism have been correlated with the pathogenesis of cancer [43]. Tumor cells require much greater amounts of iron than normal cells, to facilitate their rapid proliferation. Hence, processes that regulate iron metabolism are modified in cancer cells [44]. The importance of iron in cellular proliferation is demonstrated by the occurrence of reduced DNA synthesis under conditions of iron-deficiency. Cellular iron uptake from transferrin (Tf) is determined by the number of transferrin receptors (TfRs) on the cell surface. Transferrin receptor 1 (TfR1) is a glycoprotein ubiquitously expressed in nucleated cells [45–47]. The main role of TfR1 is related to the uptake of iron [48] and its high expression on the tumor cell surface could be due to the high requirement for iron by RDR. In neoplastic cells an increase in expression of TfR results in a greater rate of Fe uptake and its incorporation in RDR.

RDR catalyzes the reduction of ribonucleotides to deoxyribonucleotides, and provides the precursors needed for both DNA synthesis and repair. Eukaryotic RDR consists of two non-identical homodimers, R1 and R2. The R2 subunit contains two Fe^{III} ions and a free stable tyrosine radical essential for enzymatic activity. Reactions of the di-iron center involving radicals from the R1 and R2 units are required to start catalytic activity. Human RDR presents a subunit known as p53R2. The p53R2 subunit also contains an Fe-binding site. Thus, the activity of RDR is susceptible to inactivation by iron chelators [12]. The tyrosine free radical is stabilized by Fe. Under Fe deprivation, enzyme inactivation results in cell cycle arrest [44]. RDR is often over-expressed in cancer cells, which makes this enzyme an attractive target for chemotherapy.

Iron chelators were initially investigated as therapeutic agents for the treatment of iron overload diseases. Desferrioxamine (**DFO**), the first chelator to be approved for the treatment of β-thalassemia [44], revealed *in vitro* anti leukemia effects. It has been demonstrated that iron depletion was the main mechanism of the antiproliferative effects of **DFO**. The antitumor activity of **DFO** was also demonstrated in clinical trials [22 and references therein].

Interest in the antineoplastic potential of iron chelators led to the investigation of orally active aroylhydrazones. The archetype of aroylhydrazone-based iron chelators is pyridoxal isonicotinoyl hydrazone (**PIH**, Figure 7.7) [49]. Comparison of the affinities of **DFO** and **PIH** for iron can be made by analyses of the *p*[M] values ($p[M] = -\log$ [uncomplexed ion]), which are derived from the complex formation constant. The *p*[M] value is the amount of metal ion not bound to the chelator under given *p*H and at specified metal and ligand concentration. At *p*H 7.4, $[Fe^{III}] = 1$ g/mol and [ligand] = 1 mmol/l the *p*[M] values for **PIH** and **DFO** are 27.7 and 28.6, respectively, indicating that displacement of PIH by **DFO** is thermodynamically favored. This effect has been shown *in vitro* [49].

However, it has been demonstrated that **PIH** mobilizes mitochondrial iron from reticulocytes and is far more effective than **DFO** at inhibiting ^{59}Fe uptake from transferrin. This effect was attributed to the greater lipophilicity of **PIH** and its ability to permeate membranes [50 and references therein].

Although **PIH** has greater iron chelation efficacy under biological conditions than **DFO**, little difference was verified in the ability of the two ligands to inhibit DNA synthesis in SK-N-MC neuroepithelioma cells, indicating a lack of correlation between Fe coordination ability and inhibition of DNA synthesis.

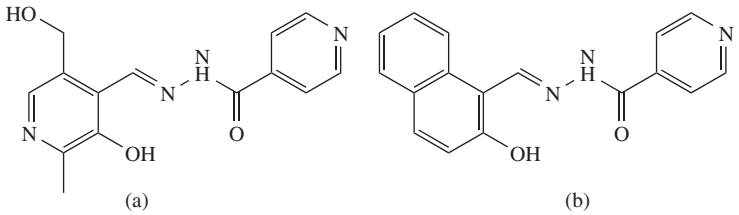

Figure 7.7 *Chemical structures of pyridoxal isonicotinoyl hydrazone (PIH, (a)) and 2-hydroxy-1-naphthylaldehyde isonicotinoyl hydrazone (b)*

Hence different chelators target distinct intracellular iron pools to induce their antineoplastic effects [50 and references therein].

SAR studies of aroylhydrazones were performed based on the development of **PIH** analogs. These compounds were classified in three main groups: pyridoxal benzoyl hydrazone derivatives, salicylaldehyde benzoyl hydrazone derivatives, and 2-hydroxy-1-naphthylaldehyde benzoyl hydrazone derivatives [50].

The pyridoxal benzoyl hydrazone derivatives were the least active as antiproliferative agents *in vitro* in spite of showing high Fe chelation ability both *in vitro* and *in vivo*. Hence they could be suitable for the treatment of Fe overload [50]. Results have shown that the naphthylaldehyde derivatives presented the greatest efficacy as antiproliferative agents. 2-Hydroxy-1-naphthylaldehyde isonicotinoyl hydrazone (Figure 7.7) proved to be one of the most active chelators among the compounds under study [51, 52].

The hydrazones mechanism of action was related to complexation of iron from pools required for RDR enzymatic activity [53]. Additional investigation on 2-hydroxy-1-naphthylaldehyde isonicotinoyl hydrazone suggested that it induced a decrease in the expression of cyclins responsible for the progression of the cell cycle. Studies have also shown that iron chelation up-regulates the expression of metastasis suppressor factors [54–56]. Coordination of this compound with iron prevented its antiproliferative activity, demonstrating that its ability to chelate iron plays an essential role in the cytotoxic activity [22].

PIH analogs known as di-2-pyridyl ketone isonicotinoyl hydrazone (**PKIH**) derivatives have also been developed. **PKIH** derivatives proved to be highly cytotoxic and selective against certain cancer cells. Interestingly, cytotoxicity of the **PKIH** analogs is maintained even after complexation with iron [57]. The **PKIH** derivatives were considered to be more specific in regards to inhibition of RDR activity. However, since iron complexes of **PKIH** analogs were redox active and exerted an antiproliferative effect similar to that of their uncomplexed ligands, the activity of these compounds might not be related to iron chelation. Further studies have shown that the compounds could act by redox mechanisms leading to DNA damage [57–59].

It is well known that the antineoplastic effects of Ga^{III} are due to its ability to mimic iron, resulting in disruption of normal iron metabolism and inhibition of iron-dependent processes. The **PIH** Ga^{III} complex proved to be a better antiproliferative agent than the free ligand, suggesting that the complex might dissociate after entering the cell, with the release of free Ga^{III} ions to affect intracellular iron metabolism [51].

α(N)-Heterocyclic thiosemicarbazones are one of the most important classes of iron chelators already characterized as potential antineoplastic agents [9, 13, 60, 61]. Their antiproliferative activity is due to several processes related to RDR inhibition. In the investigation of these processes triapine was taken as a prototype. Some studies have suggested the reduction of Fe^{III}-triapine to Fe^{II}-triapine with ROS (reactive oxygen species) formation which in turn inactivates the enzyme by quenching the tyrosine free radical on RDR [62–64]. Other studies have suggested that the thiosemicarbazone might deplete the intracellular iron pools, also causing RDR inactivation [65, 66]. However, the compound itself proved to be less effective as an RDR inhibitor than its Fe^{II} complex [64], indicating that an Fe^{II}-triapine complex mediates the ROS formation.

It has been suggested that inhibition of mouse RDR by triapine occurs through perturbation of the diiron center. Unlike hydroxyurea, the major effect of triapine is not to directly reduce the tyrosine radical, but may involve specific binding of the drug to the R2 surface, resulting in labilization of the iron center. In the absence of external reductants, triapine coordinates Fe^{III}. In the presence of reductants, protein-bound Fe^{III} may be reduced to Fe^{II} before coordination. Loss of iron from R2 protein immediately leads to destruction of the tyrosine radical. The Fe^{II}-triapine complex may further react with oxygen, which gives rise to the generated ROS provoking enzyme damage [12].

The low cytotoxicity exhibited by the stable Fe^{III}-triapine complex was explained by the fact that it does not coordinate RDR-bound iron, and possibly allows for enzyme reactivation. The protective effect that the Fe^{III} complex has on RDR *in vivo* confirms that the mechanism of RDR inhibition by triapine should involve iron chelation. The Ga^{III}-triapine complex shows a low stability constant at physiological pH resulting in higher cytotoxicity, similar to that of the free ligand. Hence, once in the cell it is likely that the complex releases gallium and the ligand binds iron. In addition, free Ga^{III} interferes with iron metabolism [12].

Our group demonstrated that 2-pyridineformamide-derived thiosemicarbazones exhibited cytotoxicity against RT2 (expressing p53 protein) and T98 (expressing mutant p53 protein) malignant glioblastoma cells. Coordination to Ga^{III} strongly increased the cytotoxic potential in some complexes against both RT2 and T98 cells. All thiosemicarbazones and Ga^{III} complexes were able to induce cell death by apoptosis [39]. Since the thiosemicarbazones proved to strongly coordinate Fe^{II} and Fe^{III} [67], a mode of action similar to that of triapine could have taken place. Furthermore, we also showed that Ga^{III} complexes with a family of 2-acetylpyridine-derived thiosemicarbazones were more active as cytotoxic agents against T98G glioma cells and against MCF-7 breast cancer cells in comparison with the free thiosemicarbazones [68].

Based on previous results from the **PKIH** series and on thiosemicarbazones, SAR studies led to the development of other thiosemicarbazone derivatives presenting iron chelating ability and antiproliferative activities [31]. Compounds of the di-2-pyridyl ketone thiosemicarbazone (**DpT**) series are hybrids of the **PKIH** and 2-hydroxy-1-naphthylaldehyde thiosemicarbazone series, which proved to present structural features suitable for antineoplastic activity [50].

DpT derivatives (Figure 7.8) exhibited antiproliferative activity and increased ability to modulate intracellular iron [69, 70]. Derivatives with a methyl group at N2 presented low antiproliferative activity, since substitution hinders electron delocalization on the thiosemicarbazone moiety, which in turn prevents iron binding, demonstrating how crucial the iron chelating properties are for the antineoplastic activity of these compounds [70].

The **DpT** derivatives have been tested on *in vivo* models, in order to confirm the suitable results obtained *in vitro*. **Dp44mT** (Figure 7.8) demonstrated significant antiproliferative activity in different tumor cell lineages, such as lung carcinoma M109, and in a variety of solid human tumor xenografts in nude mice [69, 70]. In addition, the compound was less toxic than triapine, proved to be effective in vinblastine-resistant cell lines, and acted via a p53-independent mechanism to inhibit cell proliferation [69–73]. This finding is very important

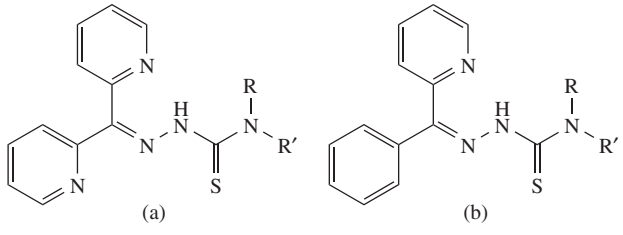

Figure 7.8 *Di-2-pyridyl ketone thiosemicarbazone derivatives (DpT, (a)) and 2-benzoylpyridine-derived thiosemicarbazone (BpT, (b)) derivatives (R, R′ = H, alkyl, or aryl). In Dp44mT R = R′ = methyl*

since 50% of tumors have mutant p53 and the latter mutations are responsible for chemotherapeutic resistance. The high efficacy of **DpT** derivatives was mainly attributed to their considerable lipophilicity and dominant neutral charge at physiological pH. This thus provided the compounds with access to the intracellular milieu with subsequent iron mobilization to form redox-active complexes which are able to generate ROS [69].

Considering the strategy of increasing log *P* values to improve access to the intracellular environment, studies have been performed involving the replacement of the 2-pyridyl ring of the **DpT** derivatives with a phenyl group, resulting in the 2-benzoylpyridine-derived thiosemicarbazone (**BpT**) series (Figure 7.8). It was predicted that this replacement would cause an extra effect, by decreasing the electron-withdrawal property of the pyridyl group and increasing the iron-chelating ability of the compounds. The **BpT** series had greater and selective antiproliferative effect in a neuroepithelioma tumor cell line in comparison with the **DpT** series. Since compounds of the **DpT** series were more effective in increasing iron efflux and inhibiting cellular iron uptake in comparison with **BpT** chelators, other factors non-related to iron coordination might have been responsible for the **BpT** activities. It has been suggested that redox cycling could play an important role in their antiproliferative effect [74].

First row transition metal (M^{II}) complexes with **DpT** undergo transmetallation in the presence of Fe^{II}, evidencing the high affinity of the **DpT** ligands for Fe^{II}. Hence, the binding of intracellular iron, rather than other metals, is most significant in terms of the bioactivities of these compounds. In addition, the M^{II} complexes of **DpT** analogs were found to be as potent as antiproliferative agents as the free thiosemicarbazones, suggesting that the complexes could act as lipophilic carriers, entering cells to deliver the metal and free ligand. Upon entering the cell, the complexes probably dissociate and bind intracellular iron, promoting iron depletion, and redox cycling. Since the iron complexes of the **DpT** series demonstrated reduced antineoplastic effects, pre-saturation with iron probably prevents chelation of intracellular iron. Hence, intracellular binding of iron and redox cycling are possibly essential processes in the mode of antiproliferative activity of **DpT** compounds [44].

PKIH ligands are N-N-O chelating systems with moderate antiproliferative effects while **DpT** ligands are N-N-S chelating systems presenting significant antiproliferative activity. A series of thiohydrazone ligands was generated in which the aroylhydrazone carbonyl oxygen was replaced by a sulfur atom, with the formation of O-N-S or N-N-S chelating agents [58, 59, 69, 75]. The O-N-S ligands exhibited lower antiproliferative effects in comparison with the parent aroylhydrazones, whereas the N-N-S ligands showed higher antiproliferative activity in comparison with the parent aroylhydrazones. The antiproliferative effects of the thiohydrazones proved to be similar to those of the **DpT** and **BpT** series [75].

7.3 Design of bis(thiosemicarbazone) ligands

7.3.1 Bis(thiosemicarbazones) and their metal complexes as anticancer agents

Synthesis of bis(thiosemicarbazones) was first reported in 1902 [76]. The characterization of their bioactivities afforded the driving force for the exploration of the chemistry of these compounds [77].

Research on the antitumor activity of bis(thiosemicarbazones) dates from the 1950s, when it was shown that glyoxaldehyde bis(thiosemicarbazone) (**H_2gts**, Figure 7.9) inhibited the growth of sarcoma 180 tumors in Swiss mice when orally administered [78]. The proposed mode of action of the compound involved coordination of essential metals with the consequent inhibition of metal-dependent cellular processes [79]. Treatment with glyoxal bis(N^4-methyl-3-thiosemicarbazone) (**H_2gtsm**, Figure 7.9) resulted in a 45% reduction in tumor weight in comparison with the control group. Interestingly 2,3-butanedione-derived bis(thiosemicarbazones) (Figure 7.9) were inactive in this model [78].

2-Oxo-3-ethoxybutyraldehyde bis(thiosemicarbazone) (**H_2kts**, Figure 7.9) demonstrated antineoplastic activity against transplanted sarcoma 180 tumors in Swiss mice [80, 81] and several transplanted rodent

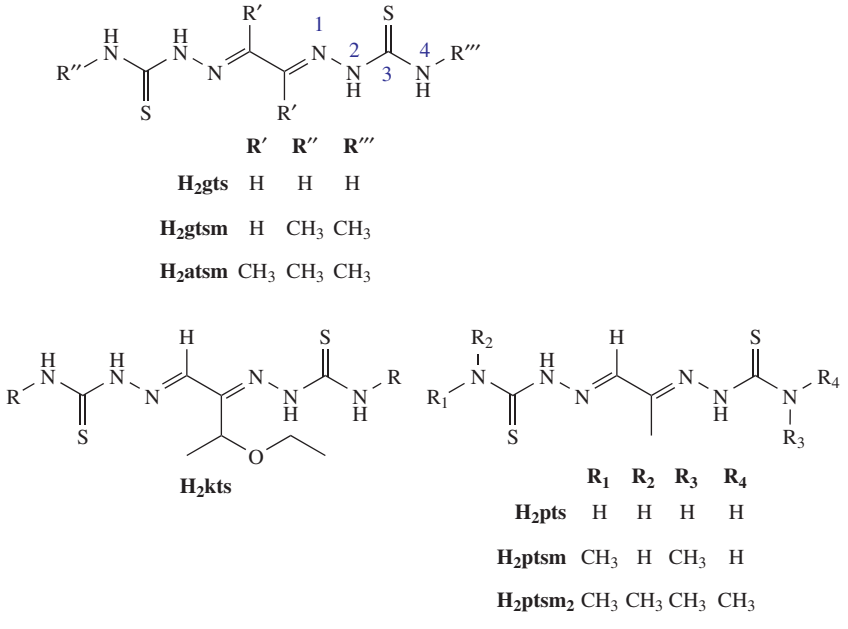

Figure 7.9 *Chemical structures of bis(thiosemicarbazones)*

tumors [82]. Elimination of copper from the diet of rats bearing Walker 256 carcinoma resulted in a loss of the **H_2kts** antitumor activity [35], indicating that the antineoplastic activity of **H_2kts** could probably be attributed to [Cu^{II}(kts)].

Upon coordination to Cu^{II} double deprotonation of bis(thiosemicarbazone) ligands occurs yielding neutral bis(thiosemicarbazonato)copper(II) complexes which are very lipophilic and membrane permeable [79, 83]. It has been suggested that [Cu^{II}(kts)] crosses the cell membrane into the cytosol where Cu^{II} was thought to be reduced to Cu^{I}. This results in consequent ligand dissociation, in which the bis(thiosemicarbazone) is believed to be released from the cell, while the metal remains retained within [84, 85].

A study on the interactions of bis(thiosemicarbazonato)copper(II) complexes with tumor cells and mitochondria was carried out. Reduction of Cu^{II} to Cu^{I} by cellular thiols with subsequent release of the ligand leading to an increase in copper concentration inside the cell was thought to occur, along with general poisoning, inhibition of DNA synthesis, and extensive oxidation of thiols to disulfides [84–86].

Metal dissociation from [Cu^{II}(kts)] has been suggested since no EPR (electron paramagnetic resonance) signals attributed to Cu^{II} species were identified in Ehrlich ascite cells treated with the complex, whereas Cu^{I} was spectroscopically detected by addition of a Cu^{I} chelator. The short half-life of this process indicated that [Cu^{II}(kts)] was rapidly metabolized inside the cell or on the cell surface, with release of free bis(thiosemicarbazone) and cell-bound copper. In addition, it was shown that the metabolism of the complex decreased in the presence of thiol-inhibiting reagents [79]. Correlations between reactivity toward sulfhydryl groups and cytotoxicity were observed for a family of bis(thiosemicarbazonato)copper(II) complexes, suggesting that cytotoxic activity was probably dependent on the intracellular release of the metal following reduction of Cu^{II} to Cu^{I} [87]. The reactivity of the complexes was directly related to their ability to inhibit DNA synthesis and cellular respiration [79, 83, 87].

Changes to the bis(thiosemicarbazone) backbone considerably modify the biological properties of their copper complexes [88]. It has been suggested that diacetyl bis(N^4-methylthiosemicarbazonato)copper(II)

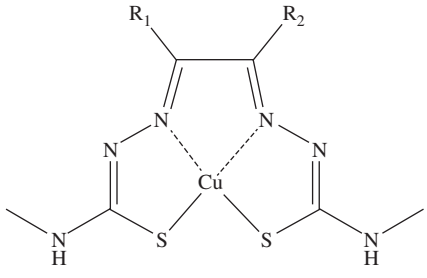

	R_1	R_2
[Cu(II)(gtsm)]	H	H
[Cu(II)(atsm)]	CH_3	CH_3
[Cu(II)(ptsm)]	H	CH_3

Figure 7.10 *Chemical structures of [Cu^{II}(gtsm)], [Cu^{II}(atsm)], and [Cu^{II}(ptsm)]*

[Cu^{II}(atsm)] (Figure 7.10) enters cells and that copper is retained only in hypoxic cells. In contrast, when glyoxal bis(N^4-methylthiosemicarbazonato)copper(II), [Cu^{II}(gtsm)] (Figure 7.10) enters the cell the metal is released and trapped regardless of the oxygen concentration [89–95]. Differences in reduction potential and the consequent metal release properties of [Cu^{II}(atsm)] and [Cu^{II}(gtsm)] were thought to account for the inactivity of the 2,3-butanedione-derived bis(thiosemicarbazones) in early studies of Swiss mice carrying Sarcoma 180 [79].

Hence, it has been suggested that bis(thiosemicarbazonato)copper(II) complexes with lower redox potential exhibited less tendency to undergo intracellular reduction. Substitution of hydrogen with methyl groups on the bis(thiosemicarbazone) backbone, it was contended, resulted in less electron transfer to the metal. Larger substituents were also supposed to provide steric hindrance around the metal center and could disfavor reaction with sulfhydryl reductants. Substituents at the terminal nitrogen proved to affect the lipophilicity of the compounds. EPR data indicated that the more lipophilic complexes could be trapped in the lipid bilayer, keeping the metal as Cu^{II} [96]. For [Cu^{II}(kts)] log $P \approx 1.7$, while for [Cu^{II}($ktsm_2$)] log $P \approx 3.4$ (**H2ktsm$_2$** = 2-oxo-3-ethoxybutyraldehydebis(N^4-dimethylthiosemicarbazone)) [97].

7.3.2 Design of bis(thiosemicarbazones) as ligands for copper(II) complexes with potential applications in medical diagnosis

Taking into account the numerous advantages of imaging with copper radionuclides, several research groups developed copper complexes with bis(thiosemicarbazones) as potential imaging agents (see Chapter 3 for further details on ligand design in radiochemistry). Hence, a number of bis(thiosemicarbazone) ligands have been investigated as delivery vehicles for copper radioisotopes due to the high stability of their neutral, lipophilic, and membrane-permeable Cu^{II} complexes. The ability of bis(thiosemicarbazonato)copper(II) complexes to cross cell membranes was soon identified as valuable for perfusion imaging, particularly in the brain and heart. The antineoplastic activity of these complexes was considered irrelevant at the low concentrations required for PET (positron emission tomography) imaging [96].

A study of ^{64}Cu-labeled **H_2kts** tissue distribution in mice was performed. A 15.4% injected dose per gram was detected in fibrosarcoma xenografts after 48 hours but the tumor-to-blood ratio proved to be low. In other tested tumors there was no accumulation, while high initial uptake in lung, heart, kidney, and liver was observed [98].

^{67}Copper(II) complexes with pyruvaldehyde bis(thiosemicarbazone) [Cu^{II}(pts)], pyruvaldehyde bis(N^4-methylthiosemicarbazone) [Cu^{II}(ptsm)], and pyruvaldehyde bis(N^4-dimethylthiosemicarbazone) [Cu^{II}($ptsm_2$)] (see Figure 7.9 for ligand structures) were examined as potential tracers for evaluation of cerebral and myocardial blood flow. A high yield was obtained for all complexes. In both [$^{67}Cu^{II}$(ptsm)] and [$^{67}Cu^{II}$($ptsm_2$)] a maximum of 3.2% of the injected dose reached the brain at 1 minute after injection while [$^{67}Cu^{II}$(pts)] showed noticeably less blood-brain barrier permeability. For [$^{67}Cu^{II}$(ptsm)] radioactivity in the brain remained constant over a period of 1 minute to 2 hours whereas [$^{67}Cu^{II}$($ptsm_2$)] cleared rapidly after an initial high level of uptake [99].

Blood-brain barrier permeability and the level of retention were associated with lipophilicity and alkylation at the terminal nitrogen in the bis(thiosemicarbazone) chain [97]. The clearance of [$^{67}Cu^{II}$($ptsm_2$)] was attributed to its lower redox potential, which was thought to have resulted in resistance to significant dissociation and retention. Although the more lipophilic complexes apparently showed high initial brain uptake, they should also have been susceptible to entrapment in the lipid bilayer of the membranes where they were not subject to the effect of reductants [97, 100]. Since the complexes must first be able to cross the blood–brain barrier and other cell membranes, suitable lipophilicity should be taken into consideration for the design of bis(thiosemicarbazone) ligands. [Cu^{II}(ptsm)] was chosen as the most promising derivative for cerebral and myocardial imaging studies [96].

The PET images of [$^{64}Cu^{II}$(ptsm)] and [$^{62}Cu^{II}$(ptsm)] in animals and humans were shown to be comparable to those obtained using ^{15}O-labeled water. The ready availability of ^{62}Cu from the ^{62}Zn/^{62}Cu generator suggested that this could be a suitable clinical imaging technique [77].

Tumor hypoxia is closely related to the resistance of solid tumors to radiotherapy and chemotherapy, and with initiation of angiogenesis and metastasis leading to malignant evolution. Owing to the high impact of hypoxia on patient survival, methods for its detection and quantification have been extensively investigated. Different radio-labeled markers have been developed for hypoxia PET imaging, including [Cu^{II}(atsm)], where the radionuclide is ^{60}Cu, ^{62}Cu, or ^{64}Cu. The utilization of [$^{60}Cu^{II}$(atsm)] proved to be useful in predicting the outcome of radiotherapy treatment in small-scale clinical studies, and [$^{64}Cu^{II}$(atsm)] recently entered clinical trials in the United States. However, its blood clearance and excretion kinetics are not ideal, and high levels of liver and kidney uptake were verified. Hence structural changes to modify the bio-distribution properties of this compound, in particular, its excretion pathway, without decreasing its ability to discriminate tumor hypoxia are highly desirable [101].

A comparison between [$^{64}Cu^{II}$(atsm)] and [$^{60}Cu^{II}$(atsm)] in cervical cancer patients indicated that ^{64}Cu produced better images with less noise. Toxicology studies in animals and patient monitoring showed that the doses used for both isotopes were safe to be clinically employed [102].

Fujibayashi and his colleagues first reported the hypoxic selectivity of [$^{62}Cu^{II}$(atsm)] in an ischemic isolated heart model. [$^{62}Cu^{II}$(atsm)] but not [$^{62}Cu^{II}$(ptsm)] shows rapid uptake and washout in normal mitochondria, in accordance with its lower redox potential, which is similar to that of NADH in the mitochondrial electron transport chain. Retention of [Cu^{II}(atsm)] in perfused rat hearts at high oxygen concentrations was ~23% after 15 minutes, whereas under hypoxia conditions a four-fold increase in retention (81%) was observed [92].

[$^{62}Cu^{II}$(ptsm)] was promoted as a blood flow agent [103]. When another methyl substituent was added to the diimine backbone of [$^{62}Cu^{II}$(atsm)], the complex was found to accumulate in hypoxic myocardium. The additional methyl group had a minor effect on partition coefficient but a more substantial effect on $Cu^{II} \rightarrow Cu^{I}$ reduction potential [92]. It was shown that uptake of [Cu^{II}(atsm)] in a number of tumor cells increased with decreasing the oxygen concentration. Unfortunately, this hypoxic effect was not verified in all cell lineages, and some cell lines showed no hypoxic selectivity at all [92, 97].

^{64}Cu complexes with different glyoxaldehyde-, pyruvaldehyde-, and 2,3-butanedione-derived ligands were incubated with Chinese hamster ovary cells (CHO320) under normoxic and hypoxic conditions. Although some members of the series did not show hypoxia selectivity, several complexes demonstrated significant

selectivity, indicating that these compounds could offer a basis for development of hypoxia-targeting radiopharmaceuticals for positron emission tomography (^{60}Cu, ^{61}Cu, ^{62}Cu, and ^{64}Cu) and targeted radiotherapy (^{64}Cu and ^{67}Cu) [90].

Studies were also performed with EMT6 mouse carcinoma cells and hypoxic selectivity for [Cu^{II}(atsm)] was demonstrated. Uptake of [$^{64}Cu^{II}$(atsm)] increased with decreasing oxygen concentration while uptake of [$^{64}Cu^{II}$(ptsm)] was independent of oxygen concentration. *Ex vivo* imaging experiments showed uniform distribution of [$^{60}Cu^{II}$(ptsm)] throughout the tumor, while heterogeneous uptake of [$^{64}Cu^{II}$(atsm)] was verified, indicative of selective trapping of [$^{64}Cu^{II}$(atsm)] into the hypoxic tumor cells [93].

An investigation on the mechanism of [Cu^{II}(atsm)] retention in some hypoxic cell lines involved an SAR study of a family of $^{64}Cu^{II}$ bis(thiosemicarbazone) complexes that differed only in number and location of alkyl or aryl substituents. Log *P* values in the series were in the 0.45–2.69 range and the $Cu^{II} \rightarrow Cu^{I}$ redox potential ranged from −0.31 to −0.59 V with respect to a standard Ag electrode. Copper(II) reduction was followed with a combination of electrochemistry, optical spectrometry, and density functional theory (DFT) calculation techniques [104].

The metabolism of bis(thiosemicarbazonato)copper(II) complexes is thought to be remarkably sensitive to the substituents on the diimine backbone of the ligand. It has been suggested that [Cu^{II}(atsm)] is sufficiently resistant except in hypoxic cells where it is believed to undergo reduction. [Cu^{II}(atsm)] is able to cross the blood–brain barrier, an important prerequisite for neuroimaging applications. Unlike [$^{64}Cu^{II}$(ptsm)], which shows no selectivity, [$^{64}Cu^{II}$(atsm)] seems to exhibit hypoxia selectivity. Changes to the ligand skeleton, such as the presence of electron-donating alkyl groups, decreases the $Cu^{II} \rightarrow Cu^{I}$ redox potential of the complex, which in general is thought to result in enhanced hypoxia selectivity. Complexes with glyoxal-derived bis(thiosemicarbazones), such as [Cu^{II}(gtsm)], those with one alkyl group of pyruvaldehyde-derived bis(thiosemicarbazones), such as [Cu^{II}(ptsm)] and those with two alkyl groups of 2,3-butanedione-derived bis(thiosemicarbazones), such as [Cu^{II}(atsm)] have a redox potential in the −0.42 to −0.44 V, −0.50 to −0.53 V, and −0.57 to −0.59 V ranges, respectively [89]. Substitution with alkyl groups at the terminal nitrogen apparently does not appreciably affect the redox potential or hypoxia selectivity [96].

DFT calculations indicated that the nature of the LUMO (lowest unoccupied molecular orbital) orbitals depends on the substituents in the bis(thiosemicarbazone) backbone, which in turn have influence on hypoxia selectivity [94]. It has been suggested that hypoxia-selective complexes possess metal-based LUMO orbitals, while non-selective complexes present predominantly ligand-based LUMO orbitals. Redox processes in the complexes can occur at the ligand or the metal depending on the type of substituents [105].

The first studies on the mechanism of hypoxia selectivity of [Cu^{II}(atsm)] indicated simple redox sequestration of the Cu^{I} complex at low oxygen concentrations. Further investigation suggested that the anionic Cu^{I} complex was not stable in a protic environment and protonation of the ligand could have occurred before dissociation [106].

It has been proposed that reduction of [Cu^{II}(atsm)] to [Cu^{I}(atsm)]$^{-}$ takes place continuously in both normoxic and hypoxic cells, but in the presence of oxygen [Cu^{I}(atsm)]$^{-}$ is rapidly reoxidized to [Cu^{II}(atsm)] which could freely diffuse in and out of cells. [Cu^{I}(atsm)]$^{-}$ is believed to be trapped and could dissociate and transfer the radionuclide to other macromolecules inside the cell. However, this mechanism does not account for the variability with tumor cell lineage. In addition, it does not explain the paradoxical increase in [Cu^{II}(atsm)] uptake as pO_2 increases after an episode of hypoxia [104].

Identification of intact copper(II) complex within cells under aerobic uptake indicated that intracellular reduction is at least not complete in the presence of air. It has been suggested that cytoplasm NADPH cytochrome P450 reductase and NADPH cytochrome b5 reductase were the reducing agents [107]. The reductive potential of these enzymes is enhanced under hypoxic conditions possibly allowing reduction of [Cu^{II}(atsm)] and subsequent dissociation [77].

One potential difficulty with the use of [Cu^{II}(atsm)] as a hypoxia imaging agent is related to the variable *in vitro* uptake of the compound among different tumor cell lineages at the same oxygen concentration. Therefore, the high uptake in tumors may only partially be a direct consequence of hypoxia. However, extremely high-contrast images of [Cu^{II}(atsm)] were obtained in a diversity of tumors, suggestive of significant tumor hypoxia [108]. Studies on the applicability of [Cu^{II}(atsm)] as a biomarker of treatment outcome in cervical carcinoma are currently underway. Whether hot spots within PET images of [Cu^{II}(atsm)] actually represent hypoxia is uncertain. It is possible that oxygen concentration is only one of the different processes affecting [Cu^{II}(atsm)] distribution and that uptake of this complex might better represent a general prognosticator of poor treatment response than of tumor hypoxia *per se* [109].

A preclinical investigation with [$^{62}Cu^{II}$(atsm)] suggested that it was reduced and retained in hypoxic tissues, but it rapidly washed out of normoxic tissues. The partition coefficients of [Cu^{II}(atsm)] and [Cu^{II}(ptsm)] are essentially the same. However, because of its lipophilicity, the early uptake and washout of [Cu^{II}(atsm)] could probably be influenced by regional blood flow, which is a major confounder with hypoxia [92].

An initial study of 14 patients with non-small cell lung cancer revealed that [$^{60}Cu^{II}$(atsm)] uptake was able to predict response to therapy with radiation or chemotherapy. In addition, 15 patients with cancer of the uterine cervix were imaged with [$^{60}Cu^{II}$(atsm)]. Four-year overall survival estimates were 75% for patients when the [$^{60}Cu^{II}$(atsm)] PET study was negative and 33% when it was positive, suggesting the importance of further clinical evaluation of [$^{60}Cu^{II}$(atsm)] [104 and references therein].

7.3.3 Design of functionalized bis(thiosemicarbazone) ligands to target selected biological processes

Unsymmetrical bis(thiosemicarbazone) pro-ligands can be designed in order to synthesize novel bis(thiosemicarbazone)-based compounds. When one substituent at the terminal nitrogen is a reactive amino group (Figure 7.11), the bis(thiosemicarbazone) scaffold may be conjugated to a biologically active molecule [101].

Preparation of unsymmetrical bis(thiosemicarbazones) containing a reactive amino group at the terminal nitrogen is achieved by the addition of 4-methyl-3-thiosemicarbazide to 2,3-butanedione. This process yields a mono(thiosemicarbazone) which reacts with thiocarbohydrazide and produces the **atsm/a-H_2** ligand.

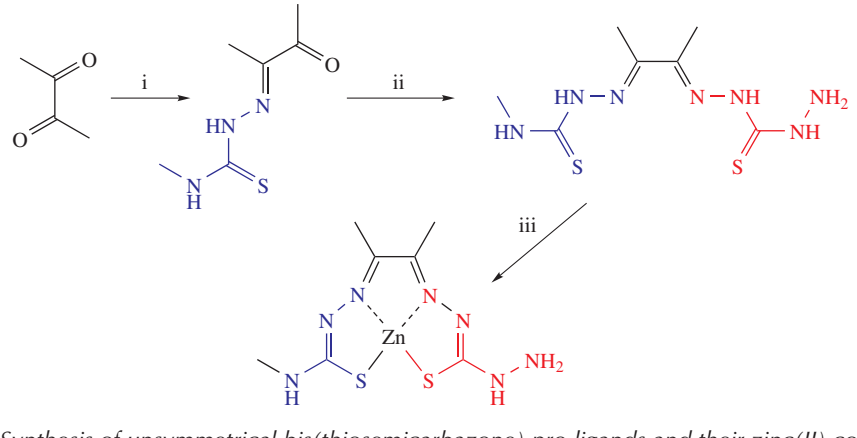

Figure 7.11 *Synthesis of unsymmetrical bis(thiosemicarbazone) pro-ligands and their zinc(II) complexes. (i) 4-methyl-3-thiosemicarbazide; (ii) thiocarbohydrazide; and (iii) zinc acetate*

Atsm/a-H_2 may be converted into [Zn(atsm/a)], which is useful in the syntheses of numerous functionalized bis(thiosemicarbazones) [109] (see Figure 7.11).

These bifunctional ligands coordinate metal ions and provide pendant amino groups that can be functionalized with targeting molecules such as glucose. Glucose shows a hydrophilic character and the ability to be metabolized by many types of tumors. Hence, a [Cu^{II}(atsm-glucose)] (Figure 7.12) derivative could also present these properties and therefore be useful as an improved hypoxic tumor-imaging agent [101].

Glucose conjugates of bis(thiosemicarbazonato)zinc(II) complexes were synthesized. Their copper(II) counterparts were prepared via transmetallation, which was revealed to be a feasible method for radio-labeling these compounds with copper radionuclides. Preliminary cell washout studies were carried out under normoxic conditions, and the uptake and intracellular distribution were investigated using confocal fluorescence microscopy on IGROV human ovarian cancer cells [110].

In addition, bifunctional bis(thiosemicarbazone) chelating ligands containing aliphatic carboxylate groups for conjugation to targeting molecules were prepared by a selective transamination reaction of diacetyl 4,4,4′-trimethylbis(thiosemicarbazone) with 6-aminohexanoic acid and 4-aminobutyric acid [111].

Bombesin (BBN) is a neuropeptide first isolated from the skin of the frog *Bombina bombina* [112]. New bis(thiosemicarbazone) bifunctional chelators were conjugated to a BBN-derived peptide which is responsible for high binding affinity to gastrin releasing peptide (GRP) receptors [113] which are over-expressed in several human tumor cells.

Incorporation of an aromatic dicarboxylate functional group in a bis(thiosemicarbazone) containing a terminal hydrazine functional group gave as product a derivative which was conjugated to a modified bombesin sequence (BBS). Preliminary biodistribution measurements showed good tumor uptake in nude mice with PC-3 tumor xenografts [113].

Further examples of bis(thiosemicarbazone) ligand design are found in the development of fluorescent compounds by incorporation of a fluorophore moiety into the bis(thiosemicarbazone) molecule. From fluorescence studies it has been suggested that uptake of [Zn^{II}(atsm)] in cells is differentially compartmentalized, distribution within the cytoplasm varying with the cell type. Since the copper(II) analogs are not fluorescent, fluorescent-tagged ligands were designed by covalently linking a pyrene fluorophore to

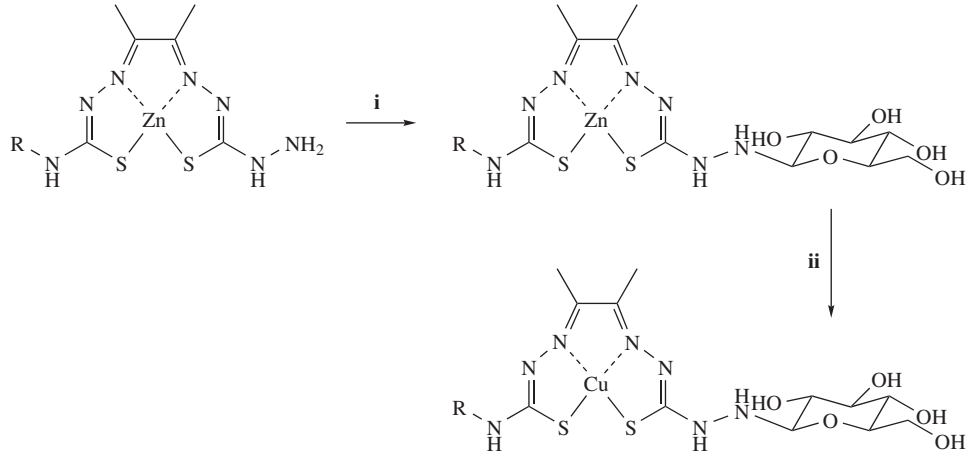

Figure 7.12 *Synthesis of glucose-functionalized bis(thiosemicarbazonato) zinc(II) and copper(II) complexes. (i) α,β-D-glucose, HCl(aq), methanol, reflux and (ii) transmetallation: aqueous solutions of the corresponding zinc(II) complex mixed with an aqueous solution of copper acetate*

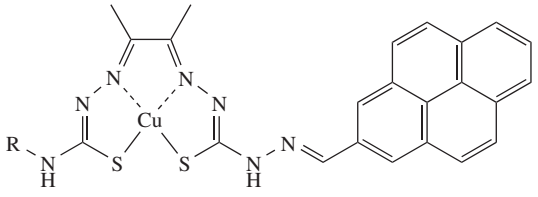

Figure 7.13 *Bis(thiosemicarbazonato)copper(II) complexes containing a pyrene fluorophore*

bis(thiosemicarbazone) ligands containing a primary amine at the terminal nitrogen (Figure 7.13). Confocal fluorescence microscopy of the copper(II) complexes indicated that [Cu^{II}(atsm)] might be localized in vesicles of lysosomal and autophagic origin in M17 and possibly HeLa cell lines [114].

Although [Zn^{II}(atsm)] is weakly fluorescent [Cu^{II}(atsm)] quenches emission. However, if the 4,4-difluoro -4-bora-3a,4a-diaza-*s*-indacene (BODIPY) fluorescent scaffold is appended to the ligand forming **atsmbodipy**, strong fluorescence can be observed. The lifetime profiles for cells exposed to [Cu^{II}(atsmbodipy)] and **atsmbodipy** are distinctly different. In addition, decay curves for the complex show a very rapid initial process absent for the free ligand. Analysis of the decay curves for individual points within the cell showed the signature short decay time of the complex. The results indicated stability of the [Cu^{II}(atsm)] core under aerobic conditions [77 and references therein].

Since [Cu^{II}(atsm)] has sufficient stability for diagnostic imaging applications and is known to cross the blood–brain barrier, bifunctional chelates based on this scaffold have in principle the potential to be employed as neuroimaging agents. Hence these systems could be useful in the early detection of neurodegenerative diseases such as Alzheimer's disease (AD) [115].

The amyloid cascade hypothesis proposes that the aggregation and deposition of the β-amyloid (Aβ) peptide is a causal factor in the progression of AD [116]. However, the presence of Aβ plaques does not reliably correlate with cognitive impairment. Thus, one explanation for the evolution of the disease is that it is not the amyloid deposits themselves but soluble oligomeric forms of amyloid in proximity with metal ions that are the toxic species [117]. However, oligomers and plaques are believed to be in equilibrium and although the exact role of Aβ plaques in the onset of dementia is controversial, extensive cortical Aβ deposition is evident in post-mortem analysis of AD patients [115].

Aβ is released into the synapse, where the peptide and metal ions such as Cu and Zn are present in sufficiently high quantities to promote an interaction. In fact amyloid plaques can be described as "metallic sinks" due to the extremely high concentrations of Cu (~400 mM), Zn, and Fe (~1 mM) that are found in senile plaques isolated from AD patients [118]. It has been proposed that the natural roles of Aβ and the amyloid precursor protein are as copper binding and regulating proteins [119 and references therein].

A bis(thiosemicarbazone) with an appended fluorescent plaque-targeting *trans*-stilbene group was prepared by treating *trans*-stilbene aldehyde with **atsm/a**-H_2. The resulting complex [Cu^{II}(atsm-stilbene)] retains fluorescence from stilbene, since the metal is probably sufficiently distant from stilbene not to quench fluorescence. Interaction of the complex with synthetic $A\beta_{1-42}$ was suggested based on its ability to compete with thioflavin-T (2-[*p*-(dimethylamino)phenyl]-3,6-dimethylbenzothiazolium chloride) for binding to $A\beta_{1-42}$ as shown by a fluorescence assay. Upon addition of [Cu^{II}(atsm-stilbene)] to a solution containing $A\beta_{1-42}$ and thioflavin-T an intense decrease in fluorescence of thioflavin was observed, indicating displacement of thioflavin-T. In contrast, addition of [Cu^{II}(atsm)], which does not contain the appended plaque-targeting stilbene group, only results in a 10% drop in fluorescence intensity. Furthermore, significant changes of fibrils upon addition of [Cu^{II}(atsm-stilbene)] were shown by transmission electron microscopy (TEM). In addition, the complex proved to bind selectively to Aβ plaques in post-mortem human brains from AD patients. The compound was radio-labeled with ^{64}Cu and the brain uptake determined in a transgenic

animal model of AD. It has been observed that it crosses the blood–brain barrier and displays increased uptake in the brain of the transgenic animals in comparison with controls. Thus, this compound could present the potential to be employed as a ^{64}Cu radiopharmaceutical to assist in the diagnosis of AD by positron emission tomography [115 and references therein].

The mechanism of bis(thiosemicarbazonato)copper(II) complexes uptake into cells has not been extensively investigated. In the earlier models the complex was thought to move into the cells by passive diffusion. A recent study on the uptake of cold [Cu^{II}(atsm)] and [Cu^{II}(gts)] in human U87MG glioblastoma and BE(2)-M17 neuroblastoma cells suggested that a combination of uptake and efflux processes took place. The data indicated that [Cu(gts)] and [Cu(atsm)] were taken into cells by combined passive and facilitated mechanisms. No evidence was found to support a role for a copper transporter in accumulation of the compounds. It was suggested that the metal from both [Cu(gts)] and [Cu(atsm)] underwent a process of cellular efflux by activated transport [120].

A study in aqueous media of [Cu^{II}(gtsm)] and [Cu^{II}(atsm)] in the presence of reducing agents was carried out. While both ligands have high affinities with copper(I) they cannot compete with Cu^{I}-binding proteins. In fact, in the presence of these proteins, reduction of the bis(thiosemicarbazonato)copper(II) complexes was thought to occur, leading to irreversible transfer of the metal to the proteins. It has been shown that ascorbate and glutathione were able to reduce [Cu^{II}(gtsm)] but not [Cu^{II}(atsm)] in the presence these proteins. Hence a correlation was established between the distinct cellular retention properties of the complexes and their reduction potential. Endogenous reducing agents in normal cells were thought to reduce [Cu^{II}(gtsm)] but not [Cu^{II}(atsm)], which was considered to have been washed out. In the more reducing environment of hypoxic cells reduction of [Cu^{II}(atsm)] with retention of copper was also thought to occur [121]. However, the experimental conditions employed in these experiments are far from what the conditions could be inside the cells.

In a recent work the mechanism of intracellular accumulation of copper(II) complexes with glyoxaldehyde-derived bis(thiosemicarbazones) (“g” series) and 2,3-butanedione-derived bis(thiosemicarbazones) (“a” series) having different substituents at the thiosemicarbazone terminal nitrogen was investigated. Leukemia K562 cells and K562 cells over-expressing P-glycoprotein (K562/ADR) (where ADR means the adriamycin-resistant form) were used as models. In all cases the rate of uptake was high and no difference in rate of uptake and intracellular concentration was detected between the two series. It was suggested that both types of complexes can be released by the cells. At the steady state the concentration gradient between intracellular and extracellular media was the same and did not depend on whether accumulation or washout was considered. None of the compounds acted as a substrate of P-glycoprotein, a key element of the molecular machinery responsible for the permeability properties of the blood brain barrier. The data showed that copper does not accumulate in mitochondria or in lysosomes, and that accumulation does not depend on energy. However, when cells were incubated with micromolar concentrations of the complexes the intracellular concentration of copper was in the millimolar range [122].

The copper(II) complexes were added to a suspension of K562 cells and the EPR spectrum was recorded as a function of time. EPR data together with TEM images strongly supported the hypothesis for the mode of action of these compounds: the complexes in the extracellular medium can diffuse passively through the membrane driven by the concentration gradient between extracellular and intracellular compartments, in accordance with the trans-membrane equilibrium. As the complexes undergo aggregation inside the cell, more and more compounds enter the cell to ensure equilibrium (in the extracellular medium, due to the release of a small amount of lipids by the cells no aggregation of the complexes was observed). Therefore, aggregation is the driving force for the intracellular accumulation of the complexes [122].

Inside the cells most of the complexes are insoluble. The choice of a solvent that does not correctly mimic the intracellular medium probably explains why to our knowledge aggregation has not so far been reported. The so called selective release of copper by [Cu^{II}(gtsm)] versus [Cu^{II}(atsm)] has been explained by the fact

that complexes of the "a" series are more difficult to reduce than those of the "g" series [95]. However, the reduction potential of these complexes has been measured in DMSO or at least in a solvent in which they are soluble.

We observed very high accumulation of complexes inside the cells, the driving force being aggregation. No intracellular reduction of the "g" series compounds was noticed, whereas those of the "a" series undergo intracellular thiyl radical formation. In fact, oxidation of thiols by copper with formation of radicals is well known [123]. To our knowledge this is the first report on the formation of a thiyl radical upon treatment of cells with bis(thiosemicarbazonato)copper(II) complexes. These observations should result in a different interpretation for the molecular basis of the therapeutic effects of these complexes [122].

7.4 Design of Schiff base-derived ligands as anti-parasitic drug candidates: Applications in the therapeutics of chagas disease

The anti-parasitic properties of Schiff base-derived compounds are well known. In the present section strategies for the design of azomethine-containing drug candidates for the treatment of Chagas disease will be presented.

Chagas disease or American trypanosomiasis is a major health problem which affects around 20 million people in Central and South America, being the leading cause of heart diseases in Latin America. The epidemiology of Chagas disease remains a challenge, since the sylvatic transmission cycle of the parasite occurs in a complex network including several mammalian species [124]. The disease is caused by the protozoan *Trypanosoma cruzi*, which is transmitted to humans and other mammals by blood-sucking insect vectors [125 and references therein]. The parasite replicates in the vectors as the epimastigote form, and it is released in excrement as the highly infective trypomastigotes that invade mammalian tissues via wounds provoked by blood-sucking action. The parasite multiplies inside the cells as the amastigote form, which is released as the trypomastigote form that invades other tissues [125]. Parasitic protozoa share many common characteristics with their mammalian hosts, making the development of effective and selective drugs a hard task. So far treatment of Chagas disease is based on the non-specific nitro-heterocyclic drugs Nifurtimox (4-[(5-nitrofurfurylidene)amino]-3-methylthiomorpholine-1,1-dioxide, Nfx) and benznidazole (*N*-benzyl-2-nitro-1-imidazoleacetamide, Bnz) (Figure 7.14). These compounds present severe undesirable effects and show limited efficacy in the chronic form of the disease. In addition, their antiparasitic activity is linked to mammalian host toxicity [126]. Both Nfx and Bnz act via reduction of the nitro group. In the case of Nfx, reduction generates an unstable nitro anion radical ($R-NO_2^{\bullet -}$), which produces highly toxic ROS. The mode of action of Bnz involves covalent modification of macromolecules by nitro reduction intermediates [125].

Rational approaches for the design of new antitrypanosomal drug candidates are being considered as a consequence of the increased understanding of the biochemistry and physiology of *T. cruzi*. Different strategies in

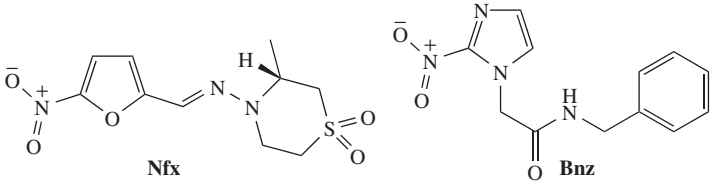

Figure 7.14 *Chemical structures of nifurtimox (Nfx) and benznidazole (Bnz)*

drug discovery for Chagas disease are currently in progress based on the validation of several targets. The most relevant targets include sterol biosynthesis, cysteine proteases, pyrophosphate metabolism, and purine salvage pathway. Other strategies for antitrypanosomal drug design include thiol-dependent redox metabolism, lysophospholipid analogs, and DNA binders [127].

Numerous enzymes which are essential for the parasite survival but are absent in the host have been identified as potential targets for new antitrypanosomal drug candidates. Cruzipain is a cysteine protease responsible for the major proteolytic activity in all stages of the parasite life cycle. Cruzain is a cruzipain recombinant form. Inhibitors of cruzipain can selectively block proliferation of *T. cruzi*, both *in vitro* and *in vivo* and have curative activity in murine models of Chagas disease.

Enzymes involved in the synthesis and metabolism of trypanothione have also been identified as potential targets [126]. Trypanothione, N^1,N^8-bis(glutathionyl)spermidine, is a conjugate between glutathione and spermidine which does not occur in mammals, and is critical for the parasite survival, where it mimics the function of glutathione in other cells. Trypanosomatids do not contain glutathione reductase and instead glutathione disulfide is reduced by thiol-disulfide exchange with trypanothione. Trypanothione disulfide formed in this process is further reduced by trypanothione reductase. Trypanothione is involved in the maintenance of intracellular thiol concentration, in peroxide removal, and in free radical trapping [128].

5-Nitrofurfural and 5-nitrothiophene-2-carboxaldehyde semicarbazide derivatives proved to generate nitro anion radicals and to show *in vitro* antitrypanosomal activity [129]. Since the nitrofuran and nitrothiophene groups presented a good profile of activity, a family of compounds containing the nitroheterocyclic group and a spermidine-mimetic moiety was designed. Hence 5-nitro-2-furaldehyde semicarbazone and 5-nitrothiophene-2-carboxaldehyde semicarbazone were obtained (Figure 7.15), in which the N4-semicarbazone moiety was replaced by aliphatic, aryl, and heterocyclic amines that were spermidine mimics. Only nitrofurfurylidene derivatives showed interesting *in vitro* trypanocidal activity. It was shown that lipophilicity was not important for the antitrypanosomal activity. All nitrofurfurylidene semicarbazones having an acyclic aminic residue exhibited good effect. For this set of compounds, activity was more dependent on the chain length than on the electronic effects due to the presence of heteroatoms [128].

Although incorporation of the spermidine-mimetic group was intended to increase the selectivity of these compounds, *in vitro* and *in vivo* antitrypanosomal assays of a series of 5-nitro-2-furaldehyde- and 5-nitrothiophene-2-carboxaldehyde-derived semicarbazones (Figure 7.15) showed that they were not effective. SAR studies indicated that the lipophilic–hydrophilic balance might play an important role in the *in vivo* activity [130].

Ruthenium(II) complexes of the 5-nitrofuryl-containing semicarbazones were obtained but proved to lack antitrypanosomal activity probably due to their high protein binding capacity and their high hydrophilicity [131].

As previously mentioned cruzipain is expressed in all life cycle stages of *T. cruzi*, being essential for replication of the intracellular form. Cruzipain inhibition is currently one of the most widely studied strategies in the design of new antitrypanosomal drug candidates. Cruzipain inhibitors include a series of vinyl sulfones, α-hydroxy ketones, thiosemicarbazones, and 2-hydroxyaryl-*N*-acylhydrazone derivatives [132].

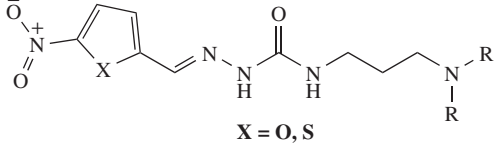

Figure 7.15 *Chemical structure 5-nitro-2-furaldehyde and 5-nitrothiophene-2-carboxaldehyde-derived semicarbazones containing a spermidine-mimic group*

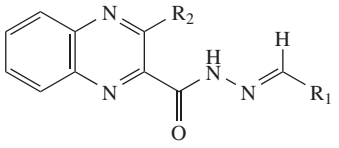

Figure 7.16 *Quinoxaline-N-acylhydrazone (NAH) derivatives designed as cruzain inhibitors*

The *N*-acylhydrazone moiety (NAH, RCONHN=CHR) has been largely used in the design of new bioactive compounds including antitrypanosomal drug candidates. A series of quinoxaline *N*-acylhydrazone (NAH) derivatives was planned as cruzain inhibitors (Figure 7.16). The design was conducted by applying the bioisosterism strategy and taking into consideration the role of the quinoxaline nucleus as an important scaffold, since some quinoxaline derivatives demonstrated trypanocidal effect. In addition, the NAH subunit shows an aza-vinyl relationship with the amide group of peptides, as the primary site of hydrolysis catalyzed by proteases. Furthermore, the iminic double bond can act as a hydrophobic anchor. Some of the compounds were as active as Nfx, when assayed *in vitro* against epimastigote forms of *T. cruzi* with good selectivity indexes [132].

Thiosemicarbazones have been tested against the growth of *Trypanosoma cruzi, Trypanosoma brucei, Plasmodium falciparum*, and other parasites. The effectiveness of thiosemicarbazones against these parasites has been related to their capacity to act as inhibitors of cysteine proteases including cruzipain [133].

Cohen and co-workers first introduced the thiosemicarbazone functionality into compounds designed to inhibit cruzipain. Some thiosemicarbazone derivatives are potent inhibitors of cruzipain and show *in vitro* trypanocidal activity. Hence this class of compounds has been identified as lead scaffolds of cruzipain inhibitors [134]. 3′-Bromopropiophenone thiosemicarbazone proved to act as an inhibitor of cruzipain and cured mammalian cell cultures infected with *T. cruzi*. The compound showed no toxicity for mammalian cells at concentrations that were trypanocidal. Following this lead, more than one hundred compounds were designed. An SAR study was carried out and many potent analogs with IC_{50} values in the nanomolar range were identified. The results indicated that aryl thiosemicarbazone is an effective scaffold for killing the parasites [134].

Docking studies of one of the most active derivatives into the active site of cruzipain suggested covalent attack of Cys25 toward the thiocarbonyl carbon assisted by the transfer of the His159 proton to the thiocarbonyl sulfur (Figure 7.17). The non-peptide nature of thiosemicarbazones, their small size, and extremely low cost of syntheses indicated that these compounds are promising prototypes of antitrypanosomal drug candidates [134].

A library of thiosemicarbazones was screened against cruzain, falcipain-2, and rhodesain, and against the respective parasite sources of these cysteine proteases, *T. cruzi, Plasmodium falciparum*, and *Trypanosoma brucei*. Compounds that were effective against the enzymes and the parasites were identified but also some which were parasiticidal but inactive against the proteases. Several derivatives were effective in killing all tested parasites. Most of the promising lead compounds proved to be non-toxic in mice. The results indicated that thiosemicarbazones represent validated drug leads that kill several species of protozoan parasites through the inhibition of cysteine proteases as well as other targets [135].

5-Nitrofuryl-derived thiosemicarbazones were designed as compounds containing the thiosemicarbazone function, a potent cruzipain-inhibitor moiety, and the 5-nitrofuryl group, an oxidative stress promoter. Some of the derivatives exhibited high anti-*T. cruzi* activity *in vitro* and *in vivo* [125, 128, 130, 136, 137]. The compounds induced oxidative stress into the parasite as the main mechanism of action [125].

Palladium(II) complexes with nitrofuryl-containing thiosemicarbazones proved to be more active than Nfx *in vitro* against the epimastigote form of *T. cruzi*. In most cases, the activity of the thiosemicarbazone was maintained or slightly increased upon coordination. Although the complexes bind DNA, their toxic effect

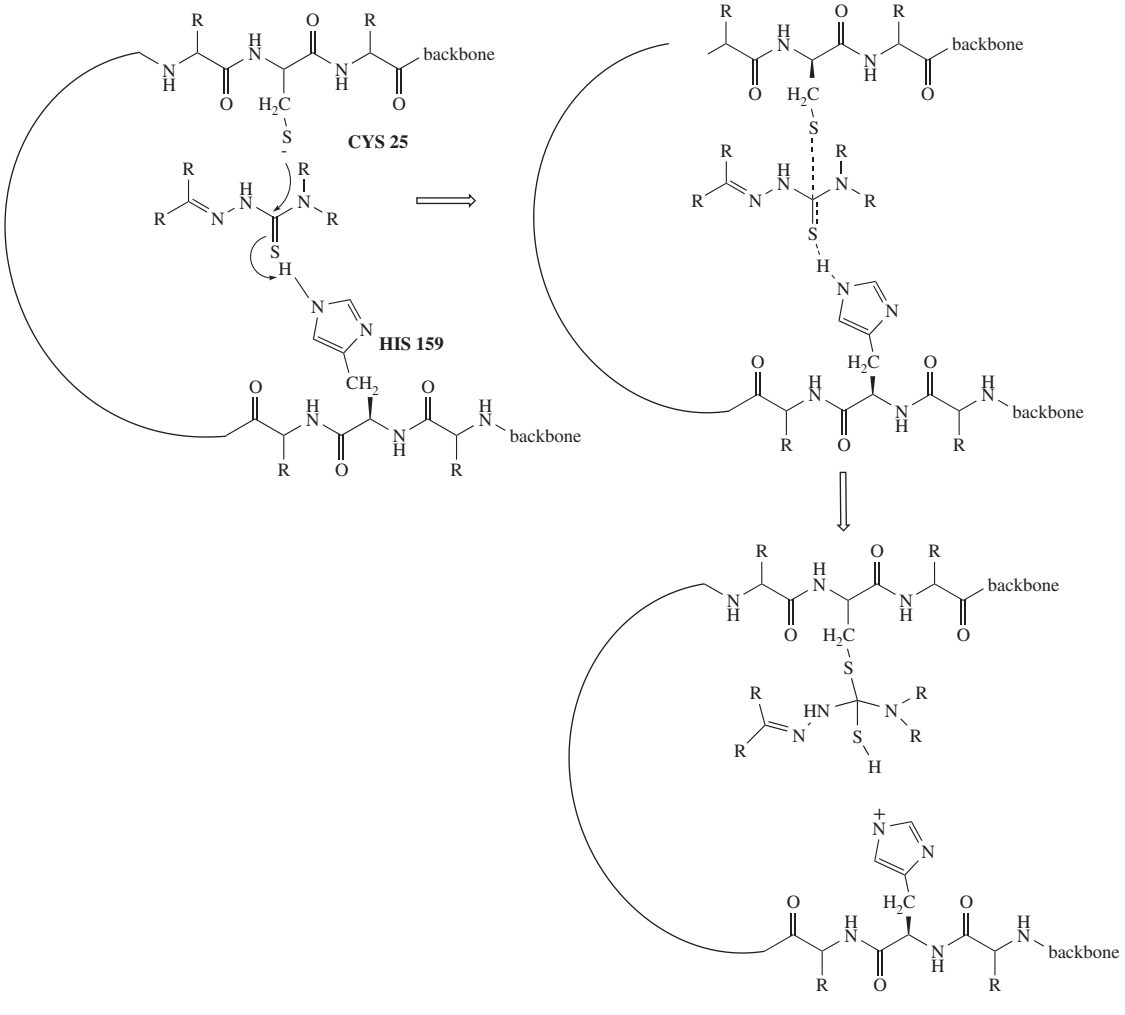

Figure 7.17 *Proposed mode of interaction of thiosemicarbazones with cruzipain*

seems to be related to redox metabolism. The proposed main mechanism of trypanocidal activity of the complexes was oxidative stress as a result of their bio-reduction and extensive redox cycling. Irreversible inhibition of trypanothione reductase by these compounds should enhance oxidative stress in the parasite [138].

1-Indanone-derived thiosemicarbazones with different patterns of substitution in the aromatic ring and N^4-phenyl-substituted derivatives were obtained. Most of the compounds displayed high trypanosomicidal activity. All compounds under study showed nonspecific cytotoxicity to human erythrocytes. Some of the thiosemicarbazones presented high therapeutic indexes. Selected derivatives proved to be moderate inhibitors of cruzipain [139].

Palladium(II) and platinum(II) complexes with 1-indanone thiosemicarbazones were evaluated for their activity against the epimastigote form of *T. cruzi*. Some complexes showed significantly higher activity than the corresponding ligands and Nfx. Antitrypanosomal activity and selectivity toward the parasite were both

higher for the Pd^{II} compounds. However, metal coordination improved bioactivity but resulted in increased mammalian cytotoxicity [140].

A family of nitroacetophenone thiosemicarbazones and their copper(II) complexes were assayed for their ability to inhibit *in vitro* the growth of *T. cruzi* epimastigote forms. Upon coordination the activity of the thiosemicarbazones significantly increased. One of the complexes was active with an IC_{50} in the nanomolar range and a good selectivity index. However, the corresponding ligand, although being less potent, showed higher selectivity. Electrochemistry studies suggested the formation of the $Ar-NO_2^{\bullet -}$ nitro anion radical in the thiosemicarbazones, which was not observed separately in the complexes, indicating that in this case, once formed the radical reacts immediately [141].

The significant enhancement of activity upon coordination to copper(II) could be due either to changes in lipophilicity, to a greater stability of the thiosemicarbazone in the complex or to redox effects involving both thiosemicarbazone and copper. A mode of action comprising intracellular reduction of the nitro group has been proposed [141].

$[RuCl(HL1)(L2)(dppb)]PF_6$ complexes were obtained from $[RuCl_2(bipy)(dppb)]$, $[RuCl_2(Mebipy)(dppb)]$, and $[RuCl_2(phen)(dppb)]$ in which HL1 = N^4-methyl-4-nitrobenzaldehyde thiosemicarbazone or N^4-methyl-4-nitroacetophenone thiosemicarbazone, L2 = 2,2-bipyridine (bipy), 4,4-dimethyl-2,2-bipyridine (Mebipy) or 1,10-phenanthroline (phen), and dppb = 1,4-bis(diphenylphospino)butane. In all cases the thiosemicarbazone binds to the metal through the sulfur atom. All complexes were more active *in vitro* as inhibitors of the growth of *T. cruzi* in comparison with their corresponding ligands and the ruthenium precursors, suggesting the occurrence of a synergistic effect involving the thiosemicarbazone and ruthenium. One of the complexes, which showed the lowest IC_{50} against *T. cruzi*, proved to be non-toxic to red blood cells, presenting a high selectivity index [142].

The ruthenium complexes were able to form the $Ar-NO_2^{\bullet -}$ nitro anion radical in a potential range similar to that of nitro-containing antitrypanosomal drugs. Hence, intracellular nitro-moiety reduction followed by redox cycling yielding ROS could be one of their modes of action. However, since the ruthenium precursors also presented antitrypanosomal activity other mechanisms could take place as well [142].

7.5 Concluding remarks

Schiff base derivatives comprise several classes of compounds with interesting properties and a wide pharmacological profile. In the present chapter some strategies for the design of Schiff base-derived ligands with potential applications in therapeutics and medical diagnosis were discussed. Schiff base derivatives make up a valuable platform for the design of ligands that are planned to interact with specific biological targets in the discovery of novel lead scaffolds. Hence, the Schiff base group can be considered as a privileged structure, which is actively being employed in the design of new bioactive compounds.

References

1. WHO World Health Organization. http://www.who.int/topics/cancer/en/ (accessed 12 May 2103).
2. DeVita, V.T. and Chu, E. (2008) A history of cancer chemotherapy. *Cancer Res.*, **68** (21), 8643–8653.
3. Beraldo, H. and Gambino, D. (2004) The wide pharmacological versatility of semicarbazones, thiosemicarbazones and their metal complexes. *Mini Rev. Med. Chem.*, **4** (1), 31–39.
4. Matesanz, A.I. and Souza, P. (2009) Alpha-N-heterocyclic thiosemicarbazone derivatives as potential antitumor agents: a structure-activity relationships approach. *Mini Rev. Med. Chem.*, **9** (12), 1389–1396.
5. Liu, M., Lin, T. and Sartorelli, A.C. (1995) Chemical and biological properties of cytotoxic alpha-(N)-heterocyclic carboxaldehyde thiosemicarbazone. *Prog. Med. Chem.*, **32**, 1–35.

6. Brockman, R.W., Thomson, J.R., Bell, M.J. and Skipper, H.E. (1956) Observations on the antileukemic activity of pyridine-2-carboxaldehyde thiosemicarbazone and thiocarbohydrazone. *Cancer Res.*, **16** (2), 167–170.
7. French, F.A. and Blanz, E.J. (1965) The carcinostatic activity of α-(N) heterocyclic carboxaldehyde thiosemicarbazones. I. Isoquinoline-1-carboxaldehyde thiosemicarbazone. *Cancer Res.*, **25** (9), 1454–1458.
8. French, F.A. and Blanz, E.J. (1966) The carcinostatic activity of thiosemicarbazones of formyl heteroaromatic compounds. 3. Primary correlation. *J. Med. Chem.*, **9** (4), 585–589.
9. Sartorelli, A.C., Agrawal, K.C. and Moore, E.C. (1971) Mechanism of inhibition of ribonucleoside diphosphate reductase by a-(N)-heterocyclic aldehyde thiosemicarbazones. *Biochem. Pharmacol.*, **20** (11), 3119–3123.
10. Sartorelli, A.C., Agrawal, K.C., Tsiftsoglou, A.S. and Moore, E.C. (1977) Characterization of the biochemical mechanism of action of α-(N)-heterocyclic carboxaldehyde thiosemicarbazones. *Adv. Enzyme Regul.*, **15**, 117–139.
11. Brockman, R.W., Sidwell, R.W., Arnett, G. and Shaddix, S.M. (1970) Heterocyclic thiosemicarbazones: correlation between structure, inhibition of ribonucleotide reductase, and inhibition of DNA viruses. *Proc. Soc. Exp.*, **133** (2), 609–614.
12. Popović-Bijelić, A., Kowol, C.R., Lind, M.E. *et al*. (2011) Ribonucleotide reductase inhibition by metal complexes of Triapine (3-aminopyridine-2-carboxaldehyde thiosemicarbazone): a combined experimental and theoretical study. *J. Inorg. Biochem.*, **105** (11), 1422–1431.
13. Antholine, W., Knight, J., Whelan, H. and Petering, D.H. (1977) Studies of the reaction of 2-formylpyridine thiosemicarbazone and its iron and copper complexes with biological systems. *Mol. Pharmacol.*, **13** (1), 89–98.
14. Ankel, E. and Petering, D.H. (1980) Iron-chelating agents and the reductive removal of iron from transferrin. *Biochem. Pharmacol.*, **29** (12), 1833–1837.
15. Antholine, W.E., Knight, J.M. and Petering, D.H. (1976) Inhibition of tumor cell transplantability by iron and copper complexes of 5-substituted 2-formylpyridine thiosemicarbazones. *J. Med. Chem.*, **19** (2), 339–341.
16. Saryan, L.A., Ankel, E., Krishnamurti, C. *et al*. (1979) Comparative cytotoxic and biochemical effects of ligands and metal complexes of alpha-N-heterocyclic carboxaldehyde thiosemicarbazones. *J. Med. Chem.*, **22** (10), 1218–1221.
17. Thelander, L., Gräslund, A. and Thelander, M. (1983) Continual presence of oxygen and iron required for mammalian ribonucleotide reduction: possible regulation mechanism. *Biochem. Biophys. Res. Commun.*, **110** (3), 859–865.
18. Thelander, L. and Gräslund, A. (1983) Mechanism of inhibition of mammalian ribonucleotide reductase by the iron chelate of 1-formylisoquinoline thiosemicarbazone. Destruction of the tyrosine free radical of the enzyme in an oxygen-requiring reaction. *J. Biol. Chem.*, **286** (7), 4063–4066.
19. Beraldo, H., Fantini, E., Borges, R.H.U. *et al*. (1990) Spectroscopic studies of metal-complexes containing pi-delocalized sulfur ligands - Mossbauer and kinetic studies of iron(II) and iron(III) complexes of the antitumor agent 2- formylpyridine thiosemicarbazone. *Inorg. Chim. Acta*, **172** (1), 113–117.
20. Borges, R.H., Paniago, E. and Beraldo, H. (1997) Equilibrium and kinetic studies of iron(II) and iron(III) complexes of some alpha (N)-heterocyclic thiosemicarbazones. Reduction of the iron(III) complexes of 2-formylpyridine thiosemicarbazone and 2-acetylpyridine thiosemicarbazone by cellular thiol-like reducing agents. *J. Inorg. Biochem.*, **65** (4), 267–275.
21. DeConti, R.C., Toftness, B.R., Agrawal, K.C. *et al*. (1972) Clinical and pharmacological studies with 5-hydroxy-2-formylpyridine thiosemicarbazone. *Cancer Res.*, **32** (7), 1455–1462.
22. Yu, Y., Gutierrez, E., Kovacevic, Z. *et al*. (2012) Iron chelators for the treatment of cancer. *Curr. Med. Chem.*, **19** (17), 2689–2702.
23. Agrawal, K.C., Lin, A.J., Booth, B.A. *et al*. (1974) Potential antitumor agents. 9. 2-Formyl(m-amino)phenylpyridine thiosemicarbazones. *J. Med. Chem.*, **17** (6), 631–635.
24. Agrawal, K.C., Lin, A.J., Booth, B.A. *et al*. (1975) Potential antitumor agents. 12. 2-Formyl-4-aminophenylpyridine thiosemicarbazones. *J. Med. Chem.*, **18** (4), 368–371.
25. Agrawal, K.C., Lin, A.J., Booth, B.A. and Sartorelli, A.C. (1968) Potential antitumor agents. I. A series of 5-substituted 1-formylisoquinoline thiosemicarbazones. *J. Med. Chem.*, **11** (4), 700–703.
26. Agrawal, K.C., Mooney, P.D. and Sartorelli, A.C. (1976) Potential antitumor agents. 13. 4-Methyl-5-amino-1-formylisoquinoline thiosemicarbazone. *J. Med. Chem.*, **19** (7), 970–972.
27. Liu, M.C., Lin, T.S., Cory, J.G. *et al*. (1996) Synthesis and biological activity of 3- and 5-amino derivatives of pyridine-2-carboxaldehyde thiosemicarbazone. *J. Med. Chem.*, **39** (13), 2586–2593.

28. Liu, M.C., Lin, T.S., Cory, J.G. and Sartorelli, A.C. (1992) Synthesis and antitumor activity of amino derivatives of pyridine-2-carboxaldehyde thiosemicarbazone. *J. Med. Chem.*, **35** (20), 3672–3677.
29. Finch, R.A., Liu, M.C., Cory, A.H. *et al*. (1999) Triapine (3-aminopyridine-2-carboxaldehyde thiosemicarbazone; 3-AP): an inhibitor of ribonucleotide reductase with antineoplastic activity. *Adv. Enzyme Regul.*, **39** (1), 3–12.
30. Richardson, D.R. (2002) Iron chelators as therapeutic agents for the treatment of cancer. *Crit. Rev. Oncol. Hematol.*, **42** (3), 267–281.
31. Lovejoy, D.B. and Richardson, D.R. (2002) Novel "hybrid" iron chelators derived from aroylhydrazones and thiosemicarbazones demonstrate selective antiproliferative activity against tumor cells. *Blood*, **100** (2), 666–676.
32. Lessa, J.A., Mendes, I.C., da Silva, P.R. *et al*. (2010) 2-Acetylpyridine thiosemicarbazones: cytotoxic activity in nanomolar doses against malignant gliomas. *Eur. J. Med. Chem.*, **45** (12), 5671–5677.
33. Soares, M.A., Lessa, J.A., Mendes, I.C. *et al*. (2012) N4-Phenyl-substituted 2-acetylpyridine thiosemicarbazones: cytotoxicity against human tumor cells, structure-activity relationship studies and investigation on the mechanism of action. *Bioorg. Med. Chem.*, **20** (11), 3396–3409.
34. Pérez, J.M., Matesanz, A.I., Martín-Ambite, A. *et al*. (1999) Synthesis and characterization of complexes of p-isopropyl benzaldehyde and methyl 2-pyridyl ketone thiosemicarbazones with Zn(II) and Cd(II) metallic centers. Cytotoxic activity and induction of apoptosis in Pam-ras cells. *J. Inorg. Biochem.*, **75** (4), 255–261.
35. Petering, H.G., Buskirk, H.H. and Crim, J.A. (1967) Effect of dietary mineral supplements of the rat on the antitumor activity of 3-ethoxy-2-oxobutyraldehyde bis(thiosemicarbazone). *Cancer Res.*, **27** (6), 1115–1121.
36. Rodriguez-Argüelles, M.C., Ferrari, M.B., Fava, G.G. *et al*. (1995) 2,6-Diacetylpyridine bis(thiosemicarbazone) zinc complexes: synthesis, structure, and biological activity. *J. Inorg. Biochem.*, **58** (3), 157–175.
37. Lessa, J.A., Guerra, J.C., de Miranda, L.F. *et al*. (2011) Gold(I) complexes with thiosemicarbazones: cytotoxicity against human tumor cell lines and inhibition of thioredoxin reductase activity. *J. Inorg. Biochem.*, **105** (12), 1729–1739.
38. Reis, D.C., Pinto, M.C., Souza-Fagundes, E.M. *et al*. (2010) Antimony(III) complexes with 2-benzoylpyridine-derived thiosemicarbazones: cytotoxicity against human leukemia cell lines. *Eur. J. Med. Chem.*, **45** (9), 3904–3910.
39. Mendes, I.C., Soares, M.A., Dos Santos, R.G. *et al*. (2008) Gallium(III) complexes of 2-pyridineformamide thiosemicarbazones: cytotoxic activity against malignant glioblastoma. *Eur. J. Med. Chem.*, **44** (5), 1870–1877.
40. Baran, E.J. (2004) Trace elements supplementation: recent advances and perspectives. *Mini Rev. Med. Chem.*, **4** (1), 1–9.
41. Eisenstein, R.S. (2000) Iron regulatory proteins and the molecular control of mammalian iron metabolism. *Annu. Rev. Nutr.*, **20**, 627–662.
42. Crichton, R.R. and Pierre, J.L. (2001) Old iron, young copper: from Mars to Venus. *Biometals*, **14** (2), 99–112.
43. Hoffbrand, A.V., Ganeshaguru, K., Hooton, J.W. and Tattersall, M.H. (1976) Effect of iron deficiency and desferrioxamine on DNA synthesis in human cells. *Br. J. Haematol.*, **33** (4), 517–526.
44. Kovacevic, Z., Kalinowski, D.S., Lovejoy, D.B. *et al*. (2011) The medicinal chemistry of novel iron chelators for the treatment of cancer. *Curr. Top. Med. Chem.*, **11** (5), 483–499.
45. Larrick, J.W. and Cresswell, P. (1979) Modulation of cell surface iron transferrin receptors by cellular density and state of activation. *J. Supramolecular Struct.*, **11** (4), 579–586.
46. Syed, B.A., Sargent, P.J., Farnaud, S. and Evans, R.W. (2006) An overview of molecular aspects of iron metabolism. *Hemoglobin*, **30** (1), 69–80.
47. Daniels, T.R., Delgado, T., Rodriguez, J.A. *et al*. (2006) The transferrin receptor part I: biology and targeting with cytotoxic antibodies for the treatment of cancer. *Clin. Immunol.*, **121** (2), 144–158.
48. Levy, J.E., Jin, O., Fujiwara, Y. *et al*. (1999) Transferrin receptor is necessary for development of erythrocytes and the nervous system. *Nat. Genet.*, **21** (4), 396–399.
49. Richardson, D.R. and Ponka, P. (1998) Orally effective iron chelators for the treatment of iron overload disease: the case for a further look at pyridoxal isonicotinoyl hydrazone (PIH) and its analogs. *J. Lab. Clin. Med.*, **132** (4), 351–352.
50. Richardson, D.R., Kalinowski, D.S., Lau, S. *et al*. (2009) Cancer cell iron metabolism and the development of potent iron chelators as anti-tumour agents. *Biochim. Biophys. Acta*, **1790** (7), 702–717.
51. Richardson, D.R., Tran, E.H. and Ponka, P. (1995) The potential of iron chelators of the pyridoxal isonicotinoyl hydrazone class as effective antiproliferative agents. *Blood*, **86** (11), 4295–4306.

52. Chaston, T.B. and Richardson, D.R. (2003) Interactions of the pyridine-2-carboxaldehyde isonicotinoyl hydrazone class of chelators with iron and DNA: implications for toxicity in the treatment of iron overload disease. *J. Biol. Inorg. Chem.*, **8** (4), 427–438.
53. Green, D.A., Antholine, W.E., Wong, S.J. *et al*. (2001) Inhibition of malignant cell growth by 311, a novel iron chelator of the pyridoxal isonicotinoyl hydrazone class: effect on the R2 subunit of ribonucleotide reductase. *Clin. Cancer Res.*, **7** (11), 3574–3579.
54. Darnell, G. and Richardson, D.R. (1999) The potential of iron chelators of the pyridoxal isonicotinoyl hydrazone class as effective antiproliferative agents III: the effect of the ligands on molecular targets involved in proliferation. *Blood*, **94** (2), 781–792.
55. Gao, J. and Richardson, D.R. (2001) The potential of iron chelators of the pyridoxal isonicotinoyl hydrazone class as effective antiproliferative agents, IV: the mechanisms involved in inhibiting cell-cycle progression. *Blood*, **98** (3), 842–850.
56. Le, N.T. and Richardson, D.R. (2004) Iron chelators with high antiproliferative activity pregulate the expression of a growth inhibitory and metastasis suppressor gene: a link between iron metabolism and proliferation. *Blood*, **104** (9), 2967–2975.
57. Bernhardt, P.V., Caldwell, L.M., Chaston, T.B. *et al*. (2003) Cytotoxic iron chelators: characterization of the structure, solution chemistry and redox activity of ligands and iron complexes of the di-2-pyridyl ketone isonicotinoyl hydrazone (HPKIH) analogues. *J. Biol. Inorg. Chem.*, **8** (8), 866–880.
58. Becker, E.M., Lovejoy, D.B., Greer, J.M. *et al*. (2003) Identification of the di-pyridyl ketone isonicotinoyl hydrazone (PKIH) analogues as potent iron chelators and anti-tumour agents. *Br. J. Pharmacol.*, **138** (5), 819–830.
59. Chaston, T.B., Yuan, J., Watts, R.N. *et al*. (2004) The potent anti-tumor activity of novel iron chelators derived from di-2-pyridylketone isonicotinoyl hydrazone involves Fenton-derived free radical generation. *Clin. Cancer Res.*, **10** (21), 7365–7374.
60. Agrawal, K.C. and Sartorelli, A.C. (1978) The chemistry and biological activity of alpha-(N)-heterocyclic carboxaldehyde thiosemicarbazones. *Prog. Med. Chem.*, **15**, 321–356.
61. Sartorelli, A.C. and Booth, B.A. (1967) Inhibition of the growth of sarcoma 180 ascites cells by combinations of inhibitors of nucleic acid biosynthesis and the cupric chelate of kethoxal bis-(thiosemicarbazone). *Cancer Res.*, **27** (9), 1614–1619.
62. Yu, Y., Wong, J., Lovejoy, D.B. *et al*. (2006) Chelators at the cancer coalface: desferrioxamine to triapine and beyond. *Clin. Cancer Res.*, **12** (23), 6876–6883.
63. Chaston, T.B., Lovejoy, D.B., Watts, R.N. and Richardson, D.R. (2003) Examination of the antiproliferative activity of iron chelators: multiple cellular targets and the different mechanism of action of triapine compared with desferrioxamine and the potent pyridoxal isonicotinoyl hydrazone analogue 311. *Clin. Cancer Res.*, **9** (1), 402–414.
64. Shao, J., Zhou, B., Di Bilio, A.J. *et al*. (2006) A ferrous-triapine complex mediates formation of reactive oxygen species that inactivate human ribonucleotide reductase. *Mol. Cancer Ther.*, **5** (3), 586–592.
65. Cooper, C.E., Lynagh, G.R., Hoyes, K.P. *et al*. (1996) The relationship of intracellular iron chelation to the inhibition and regeneration of human ribonucleotide reductase. *J. Biol. Chem.*, **271** (34), 20291–20299.
66. Nyholm, S., Mann, G.J., Johansson, A.G. *et al*. (1993) Role of ribonucleotide reductase in inhibition of mammalian cell growth by potent iron chelators. *J. Biol. Chem.*, **268** (35), 26200–26205.
67. Vilhena, F.S., Teixeira, L.R., Alves, O.C. *et al*. (2013) Study in aqueous solutions of bioactive 2-pyridineformamide-derived thiosemicarbazones and their iron(II) and iron(III) complexes. *J. Solution Chem.*, **42** (3), 555–565.
68. Lessa, J.A., Soares, M.A., dos Santos, R.G. *et al*. (2013) Gallium(III) complexes with 2-acetylpyridine-derived thiosemicarbazones: antimicrobial and cytotoxic effects and investigation on the interactions with tubulin. *Biometals*, **26** (1), 151–165.
69. Richardson, D.R., Sharpe, P.C., Lovejoy, D.B. *et al*. (2006) Dipyridyl thiosemicarbazone chelators with potent and selective antitumor activity form iron complexes with redox activity. *J. Med. Chem.*, **49** (22), 6510–6521.
70. Yuan, J., Lovejoy, D.B. and Richardson, D.R. (2004) Novel di-2-pyridyl-derived iron chelators with marked and selective antitumor activity: in vitro and in vivo assessment. *Blood*, **104** (5), 1450–1458.
71. Guimaraes, D.P. and Hainaut, P. (2002) TP53: a key gene in human cancer. *Biochimie*, **84** (1), 83–93.
72. Lowe, S.W. (1995) Cancer therapy and p53. *Curr. Opin. Oncol.*, **7** (6), 547–553.

73. O'Connor, P.M., Jackman, J., Bae, I. *et al*. (1997) Characterization of the p53 tumor suppressor pathway in cell lines of the National Cancer Institute anticancer drug screen and correlations with the growth-inhibitory potency of 123 anticancer agents. *Cancer Res.*, **57** (19), 4285–4300.
74. Kalinowski, D.S., Yu, Y., Sharpe, P.C. *et al*. (2007) Design, synthesis, and characterization of novel iron chelators: structure–activity relationships of the 2-benzoylpyridine thiosemicarbazone series and their 3-nitrobenzoyl analogues as potent antitumor agents. *J. Med. Chem.*, **50** (15), 3716–3729.
75. Kalinowski, D.S., Sharpe, P.C., Bernhardt, P.V. and Richardson, D.R. (2007) Design, synthesis, and characterization of new iron chelators with anti-proliferative activity: structure–activity relationships of novel thiohydrazone analogues. *J. Med. Chem.*, **50** (24), 6212–6225.
76. Neuberg, C. and Neimann, W. (1902) Eine methode zur isolirung von aldehyden und ketonen. *Chem. Ber.*, **35**, 2054–2056.
77. Dilworth, J.R. and Hueting, R. (2012) Metal complexes of thiossemicarbazones for imaging and therapy. *Inorg. Chim. Acta*, **389**, 3–15, and references therein.
78. French, F.A. and Freelander, B.L. (1958) Carcinostatic action of polycarbonyl compounds and their derivatives. IV. Glyoxal bis(thiosemicarbazone) and derivatives. *Cancer Res.*, **18**, 1290–1300.
79. Minkel, D.T. and Petering, D.H. (1978) Initial reaction of 3-ethoxy-2-oxobutyraldehyde bis(thiosemicarbazonato) Cu(II) with Ehrlich ascites tumour cells. *Cancer Res.*, **38**, 117–123.
80. French, F.A. and Freelander, B.L. (1958) Carcinostatic action of polycarbonyl compounds and their derivatives I. 3-ethoxy-2-ketobutyraldehyde and related compounds. *Cancer Res.*, **18**, 172–175.
81. Mihich, E. and Nichol, C.A. (1965) Kethoxal bis(thiosemicarbazone): I. Effects against experimental tumors. *Cancer Res.*, **25**, 1410–1416.
82. Petering, H.G., Buskirk, H.H. and Underwood, G.E. (1964) Antitumor action of 2-oxo-3-ethoxybutyraldehyde bis(thiosemicarbazone) and similar compounds. *Cancer Res.*, **24**, 367–372.
83. Bica, L., Meyerowitz, J., Parker, S.J. *et al*. (2011) Cell cycle arrest in cultured neuroblastoma cells exposed to a bis(thiosemicarbazonato) metal complex. *Biometals*, **24** (1), 117–133.
84. Booth, B.A. and Sartorelli, A.C. (1967) Metabolic effects of copper in intact cells; comparative activity of cupric chloride and the cupric chelate of kethoxal bis(thiosemicarbazone). *Mol. Pharmacol.*, **3** (3), 290–302.
85. Crim, J.A. and Petering, H.G. (1967) Antitumor activity of Cu(II) KTS, the copper(II) chelate of 3-ethoxy-2-oxobutyraldehyde bis(thiosemicarbazone). *Cancer Res.*, **27A**, 1278–1285.
86. Chan-Stier, C.H., Minkel, D. and Petering, D.H. (1976) Reactions of bis(thiosemicarbazonato) copper(II) complexes with tumor cells and mitochondria. *Bioinorg. Chem.*, **6**, 203–217.
87. Minkel, D.T., Saryan, L.A. and Petering, D.H. (1978) Structure-function correlations in the reaction of bis(thiosemicarbazonato) copper(II) complexes with Ehrlich ascites tumor cells. *Cancer Res.*, **38**, 124–129.
88. Blower, P.J., Castle, T.C., Cowley, A.R. *et al*. (2003) Structural trends in copper(II) bis(thiosemicarbazone) radiopharmaceuticals. *Dalton Trans.*, **7**, 4416–4425.
89. Dearling, J.L.J., Lewis, J.S., McCarthy, D.W. *et al*. (1998) Redox-active metal complexes for imaging hypoxic tissues: structure-activity relationships in Cu(II) bis(thiosemicarbazone) complexes. *J. Chem. Soc., Chem. Commun.*, **21**, 2531–2533.
90. Dearling, J.L., Lewis, J.S., Mullen, G.E. *et al*. (1998) Design of hypoxia-targeting radiopharmaceuticals: selective uptake of copper-64 complexes in hypoxic cells in vitro. *Eur. J. Nucl. Med.*, **25**, 788–792.
91. Dearling, J.L., Lewis, J.S., Mullen, G.E. *et al*. (2002) Copper bis(thiosemicarbazone) complexes as hypoxia imaging agents: structure-activity relationships. *J. Biol. Inorg. Chem.*, **7**, 249–259.
92. Fujibayashi, Y., Taniuchi, H., Yonekura, Y. *et al*. (1997) Copper-62-ATSM: a new hypoxia imaging agent with high membrane permeability and low redox potential. *J. Nucl. Med.*, **38**, 1155–1160.
93. Lewis, J.S., McCarthy, D.W., McCarthy, T.J. *et al*. (1999) Evaluation of 64Cu-ATSM in vitro and in vivo in a hypoxic tumor model. *J. Nucl. Med.*, **40**, 177–183.
94. Maurer, R.I., Blower, P.J., Dilworth, J.R. *et al*. (2002) Studies on the mechanism of hypoxic selectivity in copper bis(thiosemicarbazone) radiopharmaceuticals. *J. Med. Chem.*, **45**, 1420–1431.
95. Vavere, A.L. and Lewis, J.S. (2007) A radiopharmaceutical for the PET imaging of hypoxia. *Dalton Trans.*, **43**, 4893–4902.

96. Paterson, B.M. and Donnelly, P.S. (2011) Copper complexes of bis(thiosemicarbazones): from chemotherapeutics to diagnostic and therapeutic radiopharmaceuticals. *Chem. Soc. Rev.*, **40**, 3005–3018.
97. John, E.K. and Green, M.A. (1990) Structure-activity relationships for metal-labeled blood flow tracers: comparison of keto aldehyde bis(thiosemicarbazonato)copper(II) derivatives. *J. Med. Chem.*, **33** (6), 1764–1770.
98. Pastakia, B., Lieberman, L.M., Gatley, S.J. *et al*. (1980) Tissue distribution of copper-labeled 3-ethoxy-2-oxobutyraldehyde bis (thiosemicarbazone) (Cu-64 KTS) in mice and rats: concise communication. *J. Nucl. Med.*, **21** (1), 67–70.
99. Green, M.A., Klippenstein, D.L. and Tennison, J.R. (1988) Copper(II) bis(thiosemicarbazone) complexes as potential tracers for evaluation of cerebral and myocardial blood flow with PET. *J. Med. Chem.*, **29** (9), 1549–1557.
100. Subczynski, W.K., Antholine, W.E., Hyde, J.S. and Petering, D.H. (1987) Orientation and mobility of a copper square-planar complex in lipid bilayer. *J. Am. Chem. Soc.*, **109**, 46–52.
101. Bayly, S.R., King, R.C., Honess, D.J. *et al*. (2008) In vitro and in vivo evaluations of a hydrophilic 64Cu-Bis(Thiosemicarbazonato)-glucose conjugate for hypoxia imaging. *J. Nucl. Med.*, **49** (11), 1862–1868.
102. Lewis, J.S., Laforest, R., Dehdashti, F. *et al*. (2008) An imaging comparison of 64Cu-ATSM and 60Cu-ATSM in cancer of the uterine cervix. *J. Nucl. Med.*, **49** (7), 1177–1182.
103. Green, M.A., Mathias, C.J., Welch, M.J. *et al*. (1990) Copper-62-labeled pyruvaldehyde bis(*N*4-methylthiosemicarbazonato)copper(II): synthesis and evaluation as a positron emission tomography tracer for cerebral and myocardial perfusion. *J. Nucl. Med.*, **31** (12), 1989–1996.
104. Krohn, K.A., Link, J.M. and Mason, R.P. (2008) Molecular imaging of hypoxia. *J. Nucl. Med*, **49** (Suppl 2), 129S–148S.
105. Holland, J.P., Barnard, P.J., Collison, D. *et al*. (2008) Synthesis, X-ray crystallography, spectroelectrochemistry and computational studies on potential copper-based radiopharmaceuticals. *Eur. J. Inorg. Chem.*, **2008** (22), 3549–3560.
106. Holland, J.P., Barnard, P.J., Collison, D. *et al*. (2008) Spectroelectrochemical and computational studies on the mechanism of hypoxia selectivity of copper radiopharmaceuticals. *Chemistry*, **14** (19), 5890–5907.
107. Obata, A., Yoshimi, E., Waki, A. *et al*. (2001) Retention mechanism of hypoxia selective nuclear imaging/radiotherapeutic agent Cu-diacetyl-bis(N4-methylthiosemicarbazone) (Cu-ATSM) in tumor cells. *Ann. Nucl. Med.*, **15** (6), 499–504.
108. Carlin, S. and Humm, J.L. (2012) PET of hypoxia: current and future perspectives. *J. Nucl. Med.*, **53** (8), 1171–1174.
109. Christlieb, M., Cowley, A.R., Dilworth, J.R. *et al*. (2007) New bimetallic compounds based on the bis(thiosemicarbazonato) motif. *Dalton Trans.*, 327–331.
110. Holland, J.P., Aigbirhio, F.I., Betts, H.M. *et al*. (2007) Functionalized bis(thiosemicarbazonato) complexes of zinc and copper: synthetic platforms toward site-specific radiopharmaceuticals. *Inorg. Chem.*, **46** (2), 465–485.
111. Paterson, B.M., Karas, J.A., Scanlon, D.B. *et al*. (2010) Versatile new bis(thiosemicarbazone) bifunctional chelators: synthesis, conjugation to bombesin(7-14)-NH(2), and copper-64 radiolabeling. *Inorg. Chem.*, **49** (4), 1884–1893.
112. Erspamer, V., Erpamer, G.F. and Inselvini, M. (1970) Some pharmacological actions of alytesin and bombesin. *J. Pharm. Pharmacol.*, **22** (11), 875–876.
113. Hueting, R., Christlieb, M., Dilworth, J.R. *et al*. (2010) Bis(thiosemicarbazones) as bifunctional chelators for the room temperature 64-copper labeling of peptides. *Dalton Trans.*, **39**, 3620–3632.
114. Price, K.A., Crouch, P.J., Lim, S. *et al*. (2011) Subcellular localization of a fluorescent derivative of CuII(atsm) offers insight into the neuroprotective action of CuII(atsm). *Metallomics*, **3** (12), 1280–1290.
115. Hickey, J.L. and Donnelly, P.S. (2012) Diagnostic imaging of Alzheimer's disease with copper and technetium complexes. *Coord. Chem. Rev.*, **256**, 2367–2380.
116. Hardy, J.A. and Higgins, G.A. (1992) Alzheimer's disease: the amyloid cascade hypothesis. *Science*, **256** (5054), 184–185.
117. Gong, Y.S., Chang, L., Viola, K.L. *et al*. (2003) Alzheimer's disease-affected brain: presence of oligomeric A beta ligands (ADDLs) suggests a molecular basis for reversible memory loss. *Proc. Natl. Acad. Sci. U.S.A.*, **100** (18), 10417–10422.
118. Kenche, V.B. and Barnham, K.J. (2011) Alzheimer's disease and metals: therapeutic opportunities. *Br. J. Pharmacol.*, **163**, 211–219.

119. Green, D.E., Bowen, M.L., Scott, L.E. *et al*. (2010) In vitro studies of 3-hydroxy-4-pyridinones and their glycosylated derivatives as potential agents for Alzheimer's disease. *Dalton Trans.*, **39**, 1604–1615, and references therein.
120. Price, K.A., Crouch, P.J., Volitakis, I. *et al*. (2011) Mechanisms controlling the cellular accumulation of copper bis(thiosemicarbazonato) complexes. *Inorg. Chem.*, **50** (19), 9594–9605.
121. Xiao, Z., Donnelly, P.S., Zimmermann, M. and Wedd, A.G. (2008) Transfer of copper between bis(thiosemicarbazone) ligands and intracellular copper-binding proteins. Insights into mechanisms of copper uptake and hypoxia selectivity. *Inorg. Chem.*, **47** (10), 4338–4347.
122. Lambert, C., Beraldo, H., Lievre, N. *et al*. (2013) Bis(thiosemicarbazone) copper complexes: mechanism of intracellular accumulation. *J. Biol. Inorg. Chem.*, **18** (1), 59–69.
123. Smith, R.C., Reed, V.D. and Hill, W.E. (1994) Oxidation of thiols by copper(II). *Phosphorus, Sulfur Silicon Relat. Elem.*, **90**, 147–154.
124. Briones, M.R., Souto, R.P., Stolf, B.S. and Zingales, B. (1999) The evolution of two Trypanosoma cruzi subgroups inferred from rRNA genes can be correlated with the interchange of American mammalian faunas in the Cenozoic and has implications to pathogenicity and host specificity. *Mol. Biochem. Parasitol.*, **104** (2), 219–232.
125. Aguirre, G., Boiani, L., Cerecetto, H. *et al*. (2004) In vitro activity and mechanism of action against the protozoan parasite Trypanosoma cruzi of 5-nitrofuryl containing thiosemicarbazones. *Bioorg. Med. Chem.*, **12** (18), 4885–4893.
126. Urbina, J.A. (2002) Chemotherapy of Chagas disease. *Curr. Pharm. Des.*, **8** (4), 287–295.
127. Sánchez-Sancho, F., Campillo, N.E. and Paez, J.A. (2010) Chagas disease: progress and new perspectives. *Curr. Med. Chem.*, **17** (5), 423–452.
128. Cerecetto, H., Di Maio, R., Ibarruri, G. *et al*. (1998) Synthesis and anti-trypanosomal activity of novel 5-nitro-2-furaldehyde and 5-nitrothiophene-2-carboxaldehyde semicarbazone derivatives. *Farmaco*, **53** (2), 89–94.
129. Olea-Azar, C., Atria, A.M., Di Maio, R. *et al*. (1998) Electron spin resonance and cyclic voltammetry studies of nitrofurane and nitrothiophene analogues of nifurtimox. *Spectrosc. Lett.*, **31** (4), 849–857.
130. Cerecetto, H., Di Maio, R., González, M. *et al*. (2000) Synthesis and antitrypanosomal evaluation of E-isomers of 5-nitro-2-furaldehyde and 5-nitrothiophene-2-carboxaldehyde semicarbazone derivatives. Structure-activity relationships. *Eur. J. Med. Chem.*, **35** (3), 343–350.
131. Pagano, M., Demoro, B., Toloza, J. *et al*. (2009) Effect of ruthenium complexation on trypanocidal activity of 5-nitrofuryl containing thiosemicarbazones. *Eur. J. Med. Chem.*, **44** (12), 4937–4943.
132. Romeiro, N.C., Aguirre, G., Hernández, P. *et al*. (2009) Synthesis, trypanocidal activity and docking studies of novel quinoxaline-N-acylhydrazones, designed as cruzain inhibitors candidates. *Bioorg. Med. Chem.*, **17** (2), 641–652.
133. Lozano, N.B., Maltarollo, V.G., Weber, K.C. *et al*. (2012) Molecular features for antitrypanosomal activity of thiosemicarbazones revealed by OPS-PLS QSAR studies. *Med. Chem.*, **8** (6), 1045–1056.
134. Du, X., Guo, C., Hansell, E. *et al*. (2002) Synthesis and structure-activity relationship study of potent trypanocidal thio semicarbazone inhibitors of the trypanosomal cysteine protease cruzain. *J. Med. Chem.*, **45** (13), 2695–2707.
135. Greenbaum, D.C., Mackey, Z., Hansell, E. *et al*. (2004) Synthesis and structure-activity relationships of parasiticidal thiosemicarbazone cysteine protease inhibitors against plasmodium falciparum, trypanosoma brucei, and trypanosoma cruzi. *J. Med. Chem.*, **47** (12), 3212–3219.
136. Martinez-Merino, V. and Cerecetto, H. (2001) CoMFA-SIMCA model for antichagasic nitrofurazone derivatives. *Bioorg. Med. Chem.*, **9** (4), 1025–1030.
137. Paulino, M., Iribarne, F., Hansz, M. *et al*. (2002) Computer assisted design of potentially active anti-trypanosomal compounds. *J. Mol. Struct. THEOCHEM*, **584** (1-3), 95–105.
138. Otero, L., Vieites, M., Boiani, L. *et al*. (2006) Novel antitrypanosomal agents based on palladium nitrofurylthiosemicarbazone complexes: DNA and redox metabolism as potential therapeutic targets. *J. Med. Chem.*, **49** (11), 3322–3331.
139. Caputto, M.E., Fabian, L.E., Benítez, D. *et al*. (2011) Thiosemicarbazones derived from 1-indanones as new anti-Trypanosoma cruzi agents. *Bioorg. Med. Chem.*, **19** (22), 6818–6826.

140. Santos, D., Parajón-Costa, B., Rossi, M. *et al*. (2012) Activity on Trypanosoma cruzi, erythrocytes lysis and biologically relevant physicochemical properties of Pd(II) and Pt(II) complexes of thiosemicarbazones derived from 1-indanones. *J. Inorg. Biochem.*, **117**, 270–276.
141. Pérez-Rebolledo, A., Teixeira, L.R., Batista, A.A. *et al*. (2008) 4-Nitroacetophenone-derived thiosemicarbazones and their copper(II) complexes with significant in vitro anti-trypanosomal activity. *Eur. J. Med. Chem.*, **43** (5), 939–948.
142. Rodrigues, C., Batista, A.A., Ellena, J. *et al*. (2010) Coordination of nitro-thiosemicarbazones to ruthenium(II) as a strategy for anti-trypanosomal activity improvement. *Eur. J. Med. Chem.*, **45** (7), 2847–2853.

8

Metal-based Antimalarial Agents

Maribel Navarro[1] and Christophe Biot[2]

[1] *Chemistry and Analytical Sciences, School of Veterinary and Life Sciences, Murdoch University, Perth, Western Australia 6150, Australia*
[2] *UMR CNRS 8576, Unité de Glycobiologie Structurale et Fonctionnelle, Université Lille 1, 59650 Villeneuve d'Ascq, France*

8.1 Background

Malaria is one of the world's most ancient diseases; it originated in West and Central Africa, which accompanied human migrations to the shores of the Mediterranean, the Indian peninsula, Southeast Asia, Northern Europe and the Americas. In the past, malaria was common in marshes and swampy areas of ancient Rome, and people blamed the unhealthiness in these areas on rot and decay that wafted out on the foul air. Hence, the name is derived from the Italian, '*mal aria*', or bad air. At present, the most endemic areas of malaria are Africa, India, Southeast Asia and South America (Figure 8.1)

Despite the important effort made in research and investment in its control, prevention and treatment, malaria remains as one of the main causes of mortality and morbidity in the world. This disease is one of the most devastating human parasitic infections. According to the World Health Organization (WHO), an estimated 3.3 billion people were at risk of malaria in 2010. During that year, an estimated, 216 million episodes of malaria occurred, of which ∼174 million cases were in the African Region. There were an estimated 655 000 malaria deaths, of which 91% were in Africa, with children under five years of age and pregnant women being most severely affected. The *World Malaria Report 2011* also reported there is a significant and durable progress in battling this major public health problem. Reductions in reported malaria cases of more than 50% have been recorded between 2000 and 2010 in 43 of the 99 countries with ongoing transmission, while downward trends of 25–50% were seen in eight other countries. The estimated incidence of malaria globally has decreased by 17% since 2000 and malaria-specific mortality rates by 26% [1]. However, these data are in

Ligand Design in Medicinal Inorganic Chemistry, First Edition. Edited by Tim Storr.

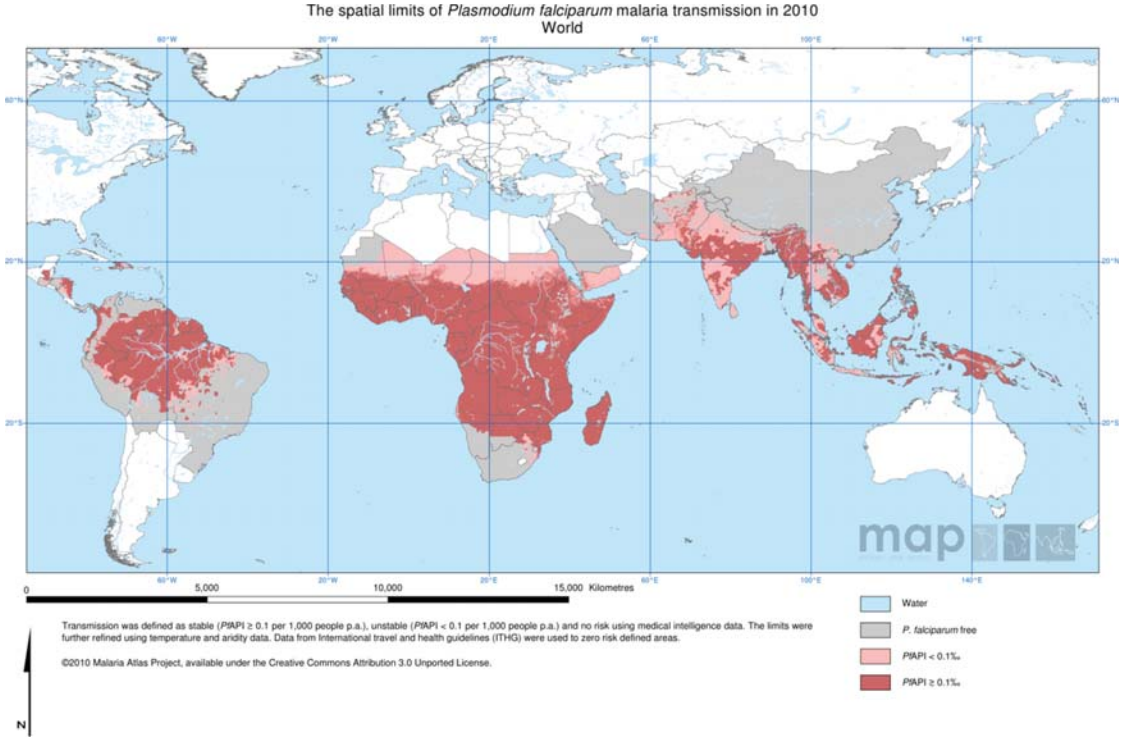

Figure 8.1 *Geographical distribution of malaria worldwide*

contrast with the results of Murray *et al.* who announced nearly 1.24 million deaths per year. These alarming data have been refuted by the WHO in an official statement. Such differences may be explained by the difference in methods used. The WHO study is based on reports provided by governments whereas Murray *et al.* used numbers provided by the communities [2].

Malaria is transmitted to humans by the bite of infected female mosquitoes of more than 30 anopheline species. Five species of parasites of the genus *Plasmodium* are infectious to humans: *P. falciparum, P. vivax, P. ovale, P. malariae* and *P. knowlesi.* Malaria due to *P. falciparum* is the most deadly, and it predominates in Africa. *P. vivax* is less dangerous but more widespread, and the other three species are found much less frequently.

The life cycle of the causative agent of malaria is quite complicated and represented in Figure 8.2. Humans are infected with *P. falciparum* haploid sporozoites by the bite of an infected female mosquito. The sporozoites, present in the infected mosquito's salivary glands, are injected into the skin as the mosquito probes the skin preparing to take a blood meal (i). Only a small number of sporozoites are injected, and these enter the blood stream (ii) and travel to the liver where they invade hepatocytes (iii). Sporozoites also enter the draining lymphatics and travel to the draining lymph node (iv) where T cell priming has been reported to occur. In a hepatocyte, the parasite replicates and differentiates, giving rise to many thousands of merozoites that are released into the blood (v). Merozoites infect red blood cell (RBC) and, within 12 hours, remodel the RBC and its membrane, thereby facilitating the growth of the parasites and allowing the infected RBC to bind to

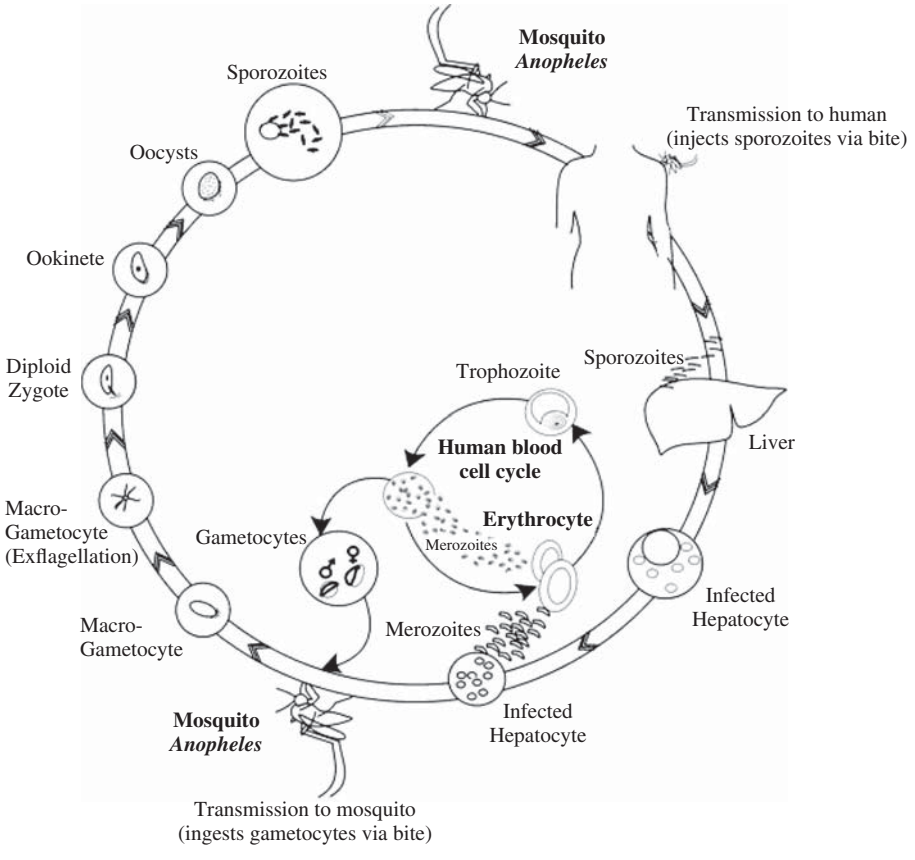

Figure 8.2 *Plasmodium falciparum life cycle*

the endothelium in different tissues, avoiding clearance in the spleen. Merozoites then replicate in the RBC, giving rise to up to 24 new merozoites per RBC (vi). The released merozoites infect new RBCs, and the cycle of RBC invasion, replication, rupture and reinvasion continues until treatment with antimalarials or control by an immune response. At some point in a poorly understood process, a subset of merozoites differentiates into male and female gametocytes (vii). These gametocytes, taken up in the blood meal by the mosquito, develop into gametes that fuse in the midgut of the mosquito to form a motile zygote, the ookinete, where meiosis occurs (viii). The ookinete crosses the midgut wall and forms an oocyst that develops into sporozoites that enter the mosquito salivary gland, thereby completing the cycle [3].

At least three different approaches have been taken to attack this public health problem: first, insecticides, where the indiscriminate use of insecticides, in addition to insects' resistance to these chemicals, resulted in this practice being discarded. However, nowadays there is renewed interest in the use of indoor residual spraying (IRS) as one of the primary vector control interventions for reducing and interrupting malaria transmission in African countries. Secondly, vaccination is one of the most effective modes of treatment available, but despite these efforts there are no available vaccines that effectively target this parasitic infection. The last one would be chemotherapy [4], which will be deeply discussed in the present chapter.

8.2 Standard antimalarial chemotherapy

Malaria control has relied heavily on a restricted number of chemically related drugs belonging to either the quinoline or the antifolate groups. Drug discovery and development is a long, risky and expensive venture, and very few new antimalarial drugs were developed in the last quarter of the twentieth century (only four of the almost 1400 registered drugs worldwide during 1975–1999) [5].

8.2.1 Quinoline-based antimalarials

Quinoline-based antimalarials have been widely used for the treatment of malaria. Drugs belonging to this group are shown in Figure 8.3. Quinine (**8.3a**) a natural product extracted from the Cinchona tree, was the first antimalarial drug used for two centuries, and still is widely used in the treatment of multidrug-resistant malaria. Chloroquine (CQ, **8.3b**), a synthetic drug used widely after the second World War, was the most successful drug ever used in the treatment of malaria. CQ showed high effectiveness against all parasite

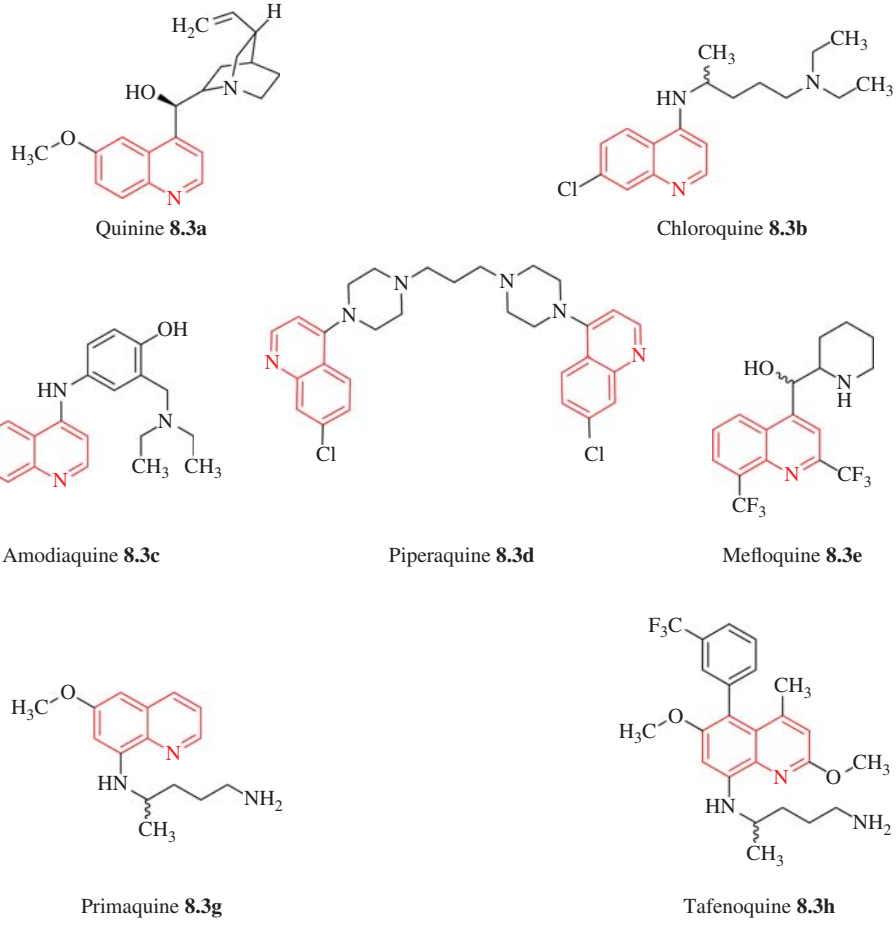

Figure 8.3 *Quinoline-based compounds commonly used as antimalarial agents*

strains, and low cost of production, good tolerance in the patient, less toxicity compared with quinine, but unfortunately a CQ-resistant strain appeared and it efficacy disappeared. Amodiaquine (**8**.**3c**), piperaquine (**8**.**3d**) and mefloquine (**8**.**3e**) were synthesized as a replacement for CQ in the first line treatment of malaria. However, owing to different reasons they are not used as a mono-therapy, nowadays they are used in combination with artesunate. Primaquine (**8**.**3f**) and tafenoquine (**8**.**3g**) belong to the family of 8-aminoquinolines. Both drugs are very effective against *P. vivax.* They are ideal as prophylactics and can be used alone in the treatment of malaria caused by *P. vivax* or in combination with other antimalarial drugs.

8.2.2 Quinoline-based antimalarials target

It is generally accepted that quinoline-based antimalarials target the catabolism of the host's haemoglogin by the parasite, which takes place in the acidic 'digestive vacuole' (DV) [6, 7], specifically inhibiting haemozoin formation [8]. The hypothesis that haematin is the target of some antimalarials originated from early studies conducted in the 1960s showing that CQ forms a complex with haematin [9]. Since then haem, haematin and haemozoin have been drug targets for a number of 4-aminquinoline antimalarials, CQ and amodiaquine (**8**.**3c**), as well as the quinolinemethanols, quinine (**8**.**3a**) and mefloquine (**8**.**3e**), and there is evidence suggesting that these drugs act by preventing the detoxification of haematin. The mechanism of action by which these drugs are able to avoid the formation of the haemozoin has been the subject of various debates and hypotheses in the scientific world, among which (i) spectroscopic and computational evidence led to suggestions that the interaction of CQ with haematin was responsible for antimalarial activity by preventing its incorporation into β-haematin [10, 11] (Figure 8.4). Another theory (ii) involves haemozoin crystals and proposes that the drug's interaction with the surface of the crystal prevents growth and thus the parasite's detoxification process. In another hypothesis (iii), Sullivan suggests that the drugs act by incorporation of a drug-haem complex into the haemozoin growth and the drug does not associate significantly with haemozoin in the absence of dimer elongation [12]. By using cell fractionation and measurement of Fe^{III}haem-pyridine, Egan *et al.* showed that CQ causes a dose-dependent decrease in haemozoin and a simultaneous increase in toxic free haem in cultured *P. falciparum* that is directly correlated with parasite survival [13]. This study provides direct evidence in support of the haemozoin inhibition hypothesis as the mechanism of action of CQ.

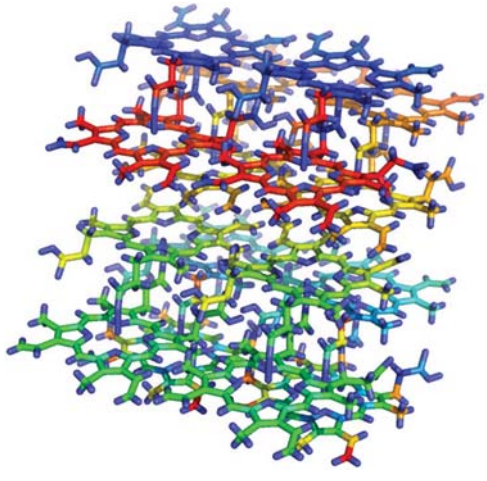

Figure 8.4 X-ray structure of malaria pigment β-haematin

Given that haemozoin formation is unaltered in drug resistance, it remains an excellent target for new drugs. Considerable recent advances in the understanding of these drugs' interactions with both haematin and haemozoin have been made [14, 15]. Together with advances in computational methods and development of new assay methods, this suggests that significant progress in the design and discovery of compounds of this type is likely in the next few years.

Malaria parasites degrade haemoglogin in an acidic compartment within the parasite called a food vacuole (FV) that has a pH in the range 5.2–5.6 [16]. This process involves aspartic proteinase enzymes called plasmepsins I [17] and II [18] and a cysteine proteinase enzyme called falcipain [19]. Haem is derived from haemoglogin; the iron centre is oxidized, probably through spontaneous auto oxidation by O_2, to produce haematin (aquaferriprotoporphyrin IX or H_2O-Fe^{III}PPIX). Haem is toxic to *Plasmodium* in high concentrations due to the generation of reactive oxygen species which are yielded by the oxidation of the iron. These, amongst other things, cause lipid peroxidation in the parasite [20]. The parasite has generated a detoxification mechanism, in which the haematin forms a highly insoluble, microcrystalline substance present in the FV called haemozoin (malaria pigment) [21].

Several mechanisms have been proposed for the production of haemozoin in *Plasmodium* and the area is highly controversial. Membrane lipids [22] and/or histidine-rich protein-2 (HRP-2) [23] are also reported to initiate or catalyze haemozoin formation, and have been suggested to play a role *in vivo* [24].

Other authors have described a haem detoxification protein which is claimed to be more potent than either lipids or HRP [21]. Another hypothesis suggests, however, that the process might occur in acidic vesicles that transport RBC cytoplasm to the FV. This hypothesis has some appeal, because it proposes that haemozoin formation occurs on the surface of an inner membrane within the vesicle derived from the parasitophorous vacuole membrane. This membrane is suggested to both catalyze haemozoin formation and act as a sacrificial sink for the hydrogen peroxide formed as a result of haem auto oxidation, accounting for the preservation of the porphyrin from degradation and protection of the FV. It is also possible that many processes contribute to the formation of haemozoin.

The chemical nature of haemozoin has been the subject of study and speculation since Brown [25] first remarked on the similarity between haemozoin and haematin (ferriprotoporphyrin IX hydroxide), which other hypotheses had considered a linear polymer of haem [26]. Now, from the evidence obtained, it is postulated that haemozoin is a cyclic dimer of haem [27] in which haem units are dimerized through reciprocal iron–carboxylate bonds; dimers are then also linked with each other through hydrogen bonds between remaining carboxylate groups, leading to chain extensions. This structure of haemozoin differentiates it from monomeric haem, haem aggregates and μ-oxo-dimers and provides it with distinct solubility, X-ray diffraction and FT-IR characteristics. In the same study it was demonstrated that β-haematin (Fe^{III}-protoporphyrin-IX)$_2$ is chemically, spectroscopically and crystallographically identical to haemozoin. These molecules are linked into dimers through reciprocal iron–carboxylate bonds to one of the propionic side chains of each porphyrin, and the dimers form chains linked by hydrogen bonds in the crystal. These results have implications in our understanding of the action of current antimalarial drugs and possibly for the design of new therapeutic agents.

8.2.3 Other standard antimalarial therapies

In search of new and more effective organic drugs that can prevent the parasite resistance, a significant contribution of the active component (Figure 8.5), artemisinin (**8.5a**), in the field of malarial chemotherapy has been identified. Difficulties in the formulation of artemisinin led to discovery of its water-soluble counterparts, dihydroartemisinin (**8.5b**) and artesunate (**8.5c**) [28]. These compounds are believed to be activated by the iron-rich environment inside the parasite [29]. Generation of such a reactive chemical entity produces

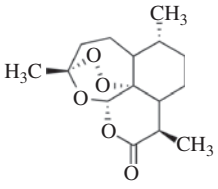

Artemisinin **8.5a**

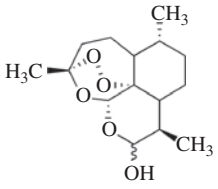

Dihydroartemisinin **8.5b**

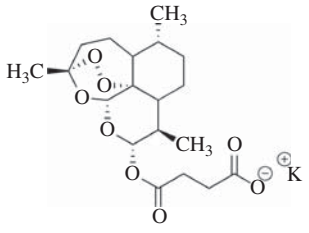

Artesunate **8.5c**

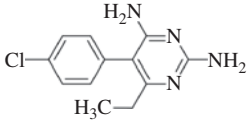

Pyrimethamine **8.5d**

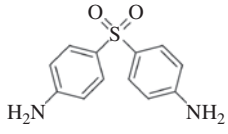

Dapsone **8.5e**

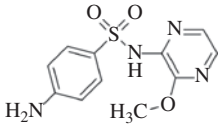

Sulfalene **8.5f**

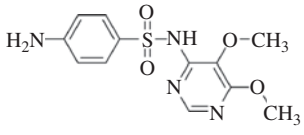

Sulfadoxine **8.5g**

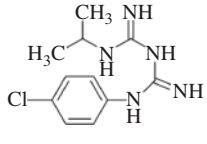

Proguanil **8.5h**

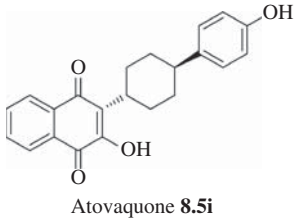

Atovaquone **8.5i**

Figure 8.5 *Other standard antimalarial drugs*

several chemical transformations [30–32]. Haem has been implicated in the mode of action of artemisinin, which has been proposed to form radical adducts with haem that act against the parasite [33].

Other types of antimalarial drugs are the antifolates, which interfere with folate metabolism, a pathway essential to malaria parasite survival. This class of drugs includes effective causal prophylactic and therapeutic agents, some of which act synergistically when used in combination with one another. The most commonly used antifolate combinations are pyrimethamine (**8.5d**), dapsone (**8.5e**) as a DHFR (dihydrofolate reductase) inhibitor combined with sulfalene (**8.5f**) or sulfadoxine (**8.5g**), as a DHPS (dihydropteroate synthase) inhibitor [34]. Unfortunately, the antifolates have been proven to be susceptible to resistance by the malaria parasite. Resistance is caused by point mutations in DHFR and DHPS, the two key enzymes in the folate biosynthetic pathway that are targeted by the antifolates [35]. There are numerous marketed monotherapies from this class such as proguanil (**8.5h**) and mefloquine (**8.3e**). Drug combinations of proguanil and atovaquone (**8.5i**) are also available [36].

8.3 Metal complexes in malaria

8.3.1 Chloroquine as an inter-ligand in the design of metal-based antimalarial agents

The emergence and spread of CQ-resistant malaria parasites is the major threat to effective malaria control. So far, malaria can be defined as a severe worldwide health problem, which makes it mandatory for scientists to broaden the domain of available therapies well beyond the conventional purview of medicinal chemistry within the context of pharmaceutical research.

Advances in the rational design of metal-based therapeutic agents have increased after the important discovery of cisplatin, a successful Pt-based anticancer drug [37, 38] which has been the main impetus for the expansion of metal complexes in cancer and other pathologies. Metal complexes in medicine provide many advantages to give more effective syntheses of metallopharmaceuticals. First, reliable preparations of stable transition metal complexes with variable and predictable structures; secondly, the possibility to select and fine-tune ligand affinities according to electron transfer, substitution rates, reduction potentials, and so on. The last advantage is an increasing knowledge of the biological effects of metals in the organism and efficient biological targeting. These parameters have helped in the development of new drugs for medical problems such as cancer and bacterial, viral and parasitic infections such as malaria [39].

In 1996, a series of metal-CQ complexes were designed in order to increase the antimalarial activity and avoid the resistance of malaria parasites. Sánchez-Delgado and Navarro groups proposed the modification of CQ through the incorporation of a transition metal into the molecular structure. Figure 8.6 shows the metal complexes synthesized, characterized and evaluated; the first ones were RhCl(COD)CQ (**8.6a**) and $[RuCl_2(CQ)]_2$ (**8.6c**) (COD: 1,5-Cyclooctadiene). The *in vitro* activities showed a 4.5-times enhancement when complex **8.6c** was compared with the standard drug chloroquine diphosphate (CQDP), demonstrating that coordination to ruthenium is effective in circumventing the resistance of two CQ-resistant strains of *P. falciparum* (FcB1 and FcB2). *In vivo* experiments displayed that complex **8.6a** caused a reduction of the parasitemia by 73% and complex **8.6c** reduced parasitemia by 94% at a concentration equivalent to 1 ED_{50} (50% effective levels) of CQDP [40]. In other efforts to obtain metal complexes of greater efficacy, these investigators isolated a gold complex of CQ, $[Au(PPh_3)(CQ)]PF_6$ (**8.6g**), which caused marked inhibition of the *in vitro* growth of *P. berghei.* It was also very effective against two CQ-resistant FcB1 and FcB2 strains of *P. falciparum,* displaying an activity 5–10-fold greater than the corresponding CQDP [41]. Encouraged by this higher activity, a series of new gold-CQ complexes (**8.6h–8.6j**) were developed by the coordination of gold to CQ with different changes in the structure of the $[Au(PPh_3)(CQ)]PF_6$ complex. These changes included variations of the phosphine ligand with the purpose of inducing changes in the electronic and steric properties, variations of the counter anion (e.g. nitrate in **8.6j**), variations of the gold oxidation state, such as Au^{I} (**8.6g–8.6j**) and Au^{III} (**8.6k**) or using biologically important ligands such as 1-thio-β-D-glucose 2,3,4,6-tetraacetate [42]. The highest activity in FcB1 and W2 strains was obtained for $[Au(PEt_3)(CQ)]PF_6$, (**8.6i**) which is 5 and 1.4 times more active than CQDP respectively, while gold(III) complexes such as $[Au(Cl)_2(CQ)_2]Cl$ (**8.6k**) showed excellent activity in strains K1 (around two times more effective than CQDP). However, no clear structure–activity relationships could be established for this series of compounds.

With these encouraging results, the Sánchez-Delgado group adopted a new molecular design in their research to further explore biological activity of first-generation compounds of Ru, varying the ancillary ligands and the overall charge of the complexes. The new Ru^{II} CQ complexes $[Ru(\eta^6\text{-arene})(CQ)]^{2+}$ (such as **8.6b**) showed activity *in vitro* against four CQ-susceptible strains (FcB1, 3D7, PFB and F32) and three CQ-resistant strains (W2, Dd2 and K1) of *P. falciparum.* These results have special importance for the susceptible strains, with the potency of all complexes consistently higher than that of CQDP. From these results, the authors propose that the combination of Ru^{II} and CQ in a single molecule produces an enhanced activity against resistant strains of the parasite [43].

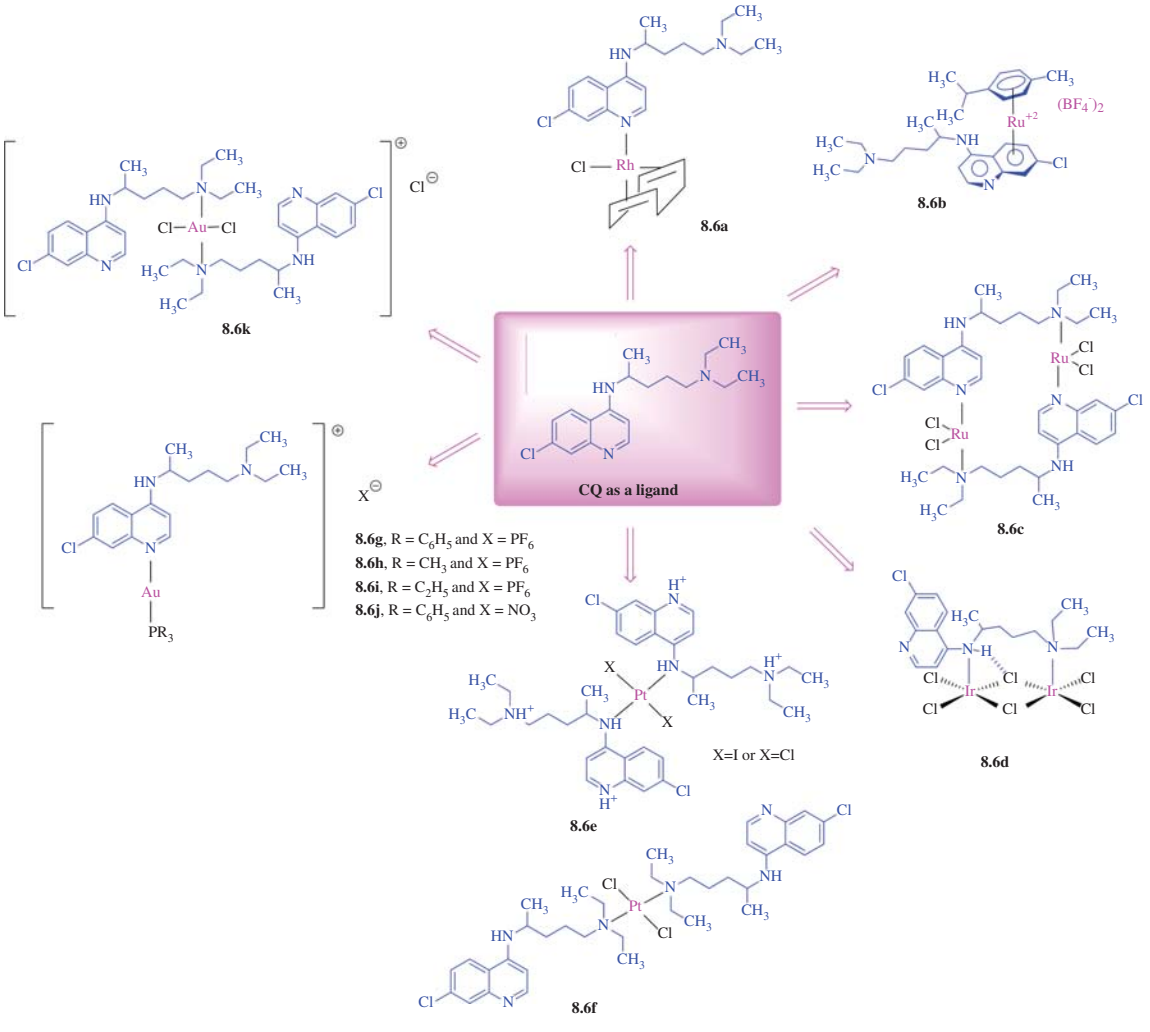

Figure 8.6 *Proposed structures of selected metal-CQ complexes*

CQ has been coordinated to other metals such as iridium (**8.6d**), and evaluated against *P. berghei in vitro,* displaying moderate activities [44]. Platinum-CQ derivatives (**8.6e** and **8.6f**) showed higher antimalarial activity than free ligands (M. Navarro and W. Castro, unpublished result) [45–47].

All these results combined show the potential of coordinating transition metals to CQ in order to improve the antimalarial activity of this drug, and demonstrate the validity of this concept in the search for novel CQ-derived antimalarial drugs capable of overcoming resistance.

Knowledge of a compound's mechanism of action can help us to understand the function and effect that a complex can have within the body, and is a tool to help redesign syntheses and strategies in order to increase biological activity and avoid parasite resistance. To this effect, research has been conducted into finding the possible mechanism of action of the metal-CQ derivatives, specifically two potential targets of action based on the accepted mechanisms of action for the CQ: the inhibition of haemozoin (malarial pigment) formation and DNA interaction.

The mechanism of action of quinoline-based antimalarials has been extensively investigated. CQ is believed to act by concentrating in the parasite DV and preventing the crystallization of toxic haem into haemozoin, leading to membrane damage and parasite death [48]. It is uncertain how this drug's mechanism operates, but it is well established that CQ forms complexes with haematin in solution and is an inhibitor of β-haematin formation [11, 49]. Interaction studies of some metal-CQ complexes with haematin by spectrophotometric titration showed the values for the association constants of the complexes to be only slightly lower than the value for CQDP under the experimental conditions used. The values were also very similar to each other, indicating that the metal-CQ derivatives evaluated interact with haematin in a similar way and to a comparable extent as CQDP [50–52]. An exception to this is the $[Au(CQ)(PPh_3)]PF_6$ complex, which showed a higher log *K,* indicating that the complex interacts with haematin more strongly than CQDP. A number of haem aggregation inhibition activity (HAIA) assays have been proposed and discussed in the literature [53–55]. Sánchez-Delgado proposed a variation of the β-haematin inhibition activity method reported by Egan [56] to measure the abilities of CQDP and complexes to inhibit the formation of β-haematin in interfacing, specifically for metal-CQ derivatives. All complexes evaluated are significantly more potent than CQDP for inhibiting haem aggregation near the interface. For example, the $[Au(CQ)(PPh_3)]PF_6$ was approximately five times more potent than CQ, a result which is in excellent agreement with the *in vitro* antimalarial results obtained against the CQ-resistant FcB1 and FcB2 strains of *P. falciparum.* These results lead to the conclusion that: (i) the main mechanism of the action of the complex metal-CQ is the inhibition of formation of β-haematin and so trials in these targets (specifically in interfacing) are excellent predictors of the *in vitro* biological activity and (ii) the metal-CQ derivatives are potential drugs for the development of chemotherapies against malaria.

8.3.2 Chloroquine as an intra-ligand in the design of metal-based antimalarial agents

Great success was found with impressive biological results in the introduction of the ferrocenyl moiety into the lateral side chain of CQ, specifically 7-chloro-4-[[[2-[(*N*,*N*-dimethylamino)methyl]-*N*-ferrocenyl]methyl]-amino]quinoline, well known as ferroquine (FQ, SSR97193, Figure 8.7) [57]. In comparison with CQ, the *in vitro* antimalarial activity of FQ was assessed in 11 studies including 19 laboratory *P. falciparum* clones. FQ is more active than CQ on CQ-susceptible and CQ-resistant parasites [58]. No differences were observed between the different formulations of FQ: base, ditartrate or dihydrochloride salts. The location of the ferrocene moiety inside the lateral chain was one of the key determinants of the antimalarial activity of these compounds towards CQ-resistant parasites [59].

FQ possesses planar chirality due to its 1,2-unsymmetrically substituted ferrocene moiety. Activity of pure enantiomers was compared with the racemate *in vitro* and *in vivo. In vitro,* the FQ enantiomers and the racemate were found to be equally active against the CQ-susceptible and CQ-resistant *P. falciparum* strains HB3 and Dd2. *In vivo,* both enantiomers were slightly less active than the racemic mixture against CQ-sensitive and CQ-resistant *P. vinckei,* suggesting an additive or synergetic effect between the two. Moreover, (1′*R*)-FQ displayed a slightly improved curative effect than (1′*S*)-FQ, suggesting minor differences in pharmacokinetics properties. Actually, the *in vitro* cytotoxicities of (1′*R*)-FQ and (1′*S*)-FQ and the racemate appeared similar in the L5178Y cell proliferative assay. Critical adverse effects were not observed during Phase I and IIa of clinical trials with the racemate [60].

The efficacy of FQ was monitored in several rodent malarial strains that are widely used for *in vivo* tests (e.g. *P. berghei N, P. yoelii NS* and *P. vinckei).* Each of these strains showed a very wide range of curative doses for CQ, ranging from 50 mg kg^{-1} per day to more than 100 mg kg^{-1} per day in the standard four day test. Subsequently, *P. yoelii NS* was tested in the absence and presence of CQ pressure (CQ ED_{90}: 2.78 and 8.33 mg kg^{-1} per day, respectively). The CQ *P. vinckei* had a CQ curative dose of 70 mg kg^{-1} per day, while the curative dose for the CQ-resistant clone was up to 400 mg kg^{-1} per day. For all strains tested, ED_{90}-values were

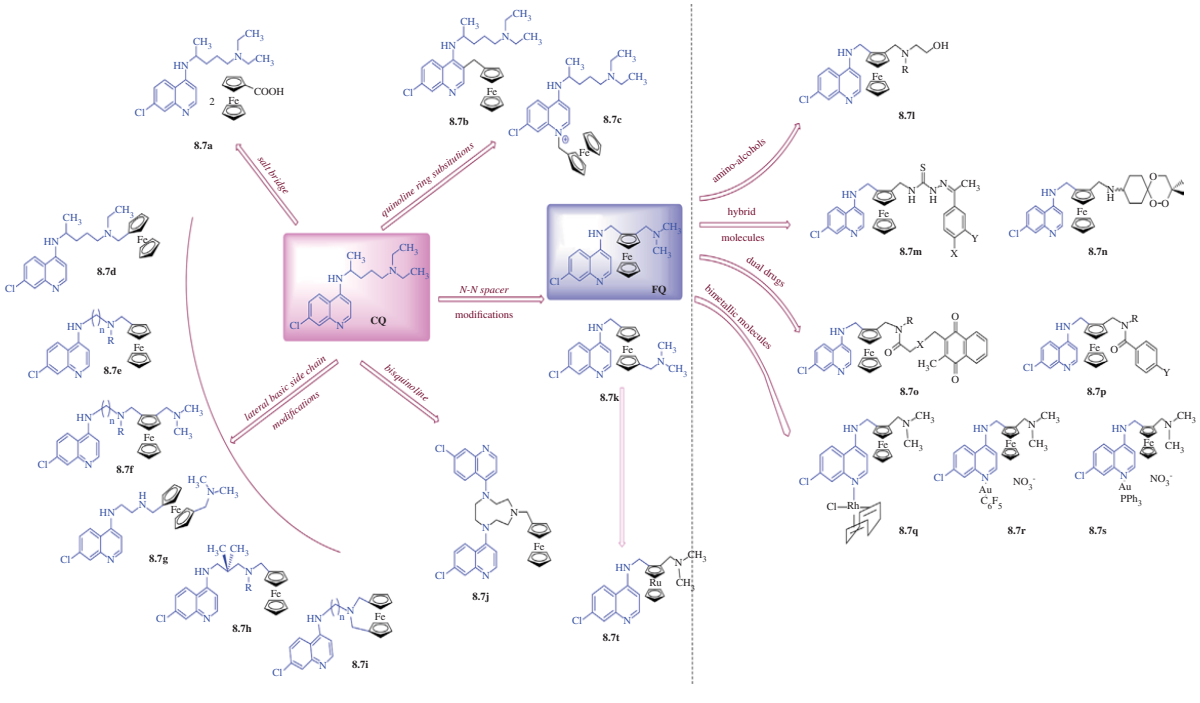

Figure 8.7 *Proposed structures of selected ferrocene analogues*

measured for FQ that ranged from 1.96 to 3.89 mg kg^{-1} per day. The curative dose observed was 10 mg kg^{-1} per day for all strains tested, irrespective of the route of administration [61, 62].

Pharmacokinetics of FQ shows that it has an apparent terminal half life of roughly two weeks, whereas the same parameter for its equally active main metabolite is reported to be more than one month [63]. Owing to its pharmacokinetic profile, FQ seems to be apt to cover (together with an appropriate partner) both cure and post treatment of prophylaxis of malaria.

During the industrial development of FQ by the pharmaceutical industries (Pierre Fabre laboratories and now Sanofi), Biot *et al.* studied in detail the mechanism of action and the induction of resistance to FQ. Indeed, knowing how and where FQ works can aid the development of new medicines for other pathogens that have become resistant to the current treatments. Recently, FQ was patented as a novel interesting anti-Hepatitis C virus molecule that could be used in combination with other direct acting antiviral agents [64, 65]. FQ was also shown to exhibit a significant *in vitro* activity on *Trypanosoma brucei brucei* and *Trypanosoma brucei gambiense,* the agents of African trypanosomiasis. *In vivo,* FQ demonstrated a weak but significant trypanocidal activity [66]. Furthermore, clarifying the mechanisms of action can reveal how the organometallic-based analogues' strategy can guide the design of new treatments.

The synchrotron-based nano-imaging technique shed light on the localization of FQ within the DV of a CQ-susceptible *P. falciparum* strain [67]. Molecular modeling suggested that FQ, which forms an intramolecular H-bond when it comes into contact with the growing crystal face of haemozoin, opens up and seems to act through its stereospecific interaction with those faces and thus inhibits their growth [68]. FQ's inhibition of the haemozoin growth leads to the accumulation of toxic haem (free or complexed with FQ) and thus to the death of malaria parasite. In addition, possible interactions between the malaria pigment and FQ may destabilize haemozoin, thereby irreversibly damaging the membrane.

The intriguing difference between CQ and FQ for CQ-resistant *P. falciparum* strains was investigated [69]. Evidence was found that shows FQ accumulates within the DV along with sulfur-containing compound(s). As accumulation of sulfur most likely arises from the influx of glutathione and its accumulation, FQ, under the oxidizing conditions of the DV, should be capable of undergoing redox reactions and thus causes lipid oxidation. As a consequence, FQ unlike CQ might be capable of producing oxidative stress.

After the first reports of the biological activity of the FQ, an extensive investigation was carried out in searching for analogues (Figure 8.7) with better activities, improved properties as a drug and better understanding of structure–activity relationships. Changes in the tertiary amines (for example ethyl groups instead of methyl groups) showed strong antimalarial activity, especially against the CQ-resistant Dd2 and W2 strains. These compounds were two- to ten-fold more active than CQ and as active as FQ [59]. In the search of mimicking the antimalarial drug hydroxychloroquine (HCQ), three FQ derivatives were prepared (**8.6l**). Theses complexes differed from FQ in their side chains on the tertiary amines; additionally the OH group is introduced with the aim of reducing the cytotoxic effects compared with FQ. The results in strains 3D7 and W2 showed an increase in activity with respect to CQ, but a decrease with respect to FQ [70].

Changes in the secondary amines also resulted in antimalarial activity comparable to that of FQ. All these compounds exhibited better inhibitory activity against the Dd2 strain than CQ itself [71]. These studies showed that the remarkable activity of FQ depends on the position of the ferrocenic nucleus in the side chain and that the *in vitro* antimalarial activity was not disturbed by slight modifications in the lateral basic side chain.

A series of analogues was synthesized from the combination of FQ with thiosemicarbazones (**8.7m**), a covalent binding between both active fragments was envisaged by merging the amino groups. In order to compare the contribution of each fragment, analogues without the ferrocenic moiety and analogues without the 4-aminoquinoline moiety were also synthesized [72]. With this work, the authors concluded that the presence of the aminoquinoline structure, allowing transport of the compounds to the FV of the parasite, seems to

be the major contributor to antimalarial activity and that the presence of the ferrocene moiety within the lateral chain is the main condition required to retain a strong antimalarial activity on CQ-resistant *P. falciparum.*

Analogues of ferrocene complexes have also proven to be highly advantageous as drugs with medical applications [73]. A library of ~150 antimalarial complexes has been prepared based on ferrocene-conjugate (or metallocene-conjugate) analogues of known antimalarial drugs such as artemisinin [74], atovaquone [75], mefloquine, quinine [76], a ferrocenylpyrrolo[1,2-*a*]quinoxaline [77], ciprofloxacin [78–80], ferrocenyl carbohydrate conjugates [81] and mepacrine [29]. The *in vitro* antimalarial activity was systematically assessed in comparison with the organic parent drug. No enhancement of the antimalarial activity was noted except in the case of ciprofloxacin, where the complex exceeded the activity of organic compounds more than twenty times in CQ-resistant strains (IC_{50} ciprofloxacin 122.3 μM, IC_{50} ferrocenyl derivatives 4.82 μM after 48~hours).

These compounds showed only moderate antimalarial activities in eight parasite strains, which implies that the presence of the ferrocenyl moiety in these structures does not significantly change their biological activity in malaria [82].

Another interesting approach was the study of CQDP associated with ferrocene carboxylic acid via a salt bridge (**8.7a**). This salt showed a low antimalarial activity and suggested an antagonist effect between both parts [83]. Then, the condensation of ferrocene at C-3 (**8.7b**) or on the endocyclic nitrogen (**8.7c**) [84], or attachment of the ferrocenyl group to the terminal nitrogen (**8.7d**) associated with a modulation of the lateral chain length [59], led to a decreased activity compared with CQ. Moreover, these results indicated a risk of cross-resistance with CQ for these molecules. The bisquinolines (**8.7j**) appeared as promising compounds as they were active against CQ-resistant strains [85]. The ferrocenyl bisquinoline remained more efficient against the CQ-resistant strain (D2d), although this compound was less active on the CQ-susceptible strain (HB3) [86].

Mixed CQ and/or FQ metal complexes [RhCl(COD)L](**8.7q**), $[Au(L)(C_6F_5)NO_3]$ (**8.7r**) and $[Au(L)(PPh_3)NO_3]$ (**8.7s**) were also synthesized. The coordination complexes of metal-CQ show improved efficacy against CQ-resistant strains of *P. falciparum* with respect to CQ. However, there is a three-fold drop in efficacy in moving from the CQ-susceptible to the CQ-resistant strain. The ferrocenyl 4-aminoquinolines improved the efficacy with respect to CQ in both sensitive and resistant strains, FQ being the most efficacious. However, complexation of the second metal to these compounds at best has little effect on the overall efficacy of the compounds and at worst there appears to be a significant antagonistic effect: the presence of the second metal centre makes the ferrocenyl moiety far more difficult to oxidize. It should be noted that whilst the gold and rhodium heterobimetallic compounds do not show additive or synergistic behaviour, this does not preclude this possibility with other metal combinations [87].

In the same Figure 8.7, the ruthenocene (**8.7i** or RQ) analogue of FQ was also reported, exhibiting similar activity to CQ *in vitro* [88], much like FQ, but not *in vivo*. This observation is consistent with the hypothesis that the mechanism for drug resistance in the *Plasmodium* parasites is compound specific. It has been suggested that FQ has reduced affinity for the *P. falciparum* CQ resistance transporter (PfCRT). Additionally, these results are consistent with previous structure–activity relations performed on aminoquinolines where a hydrophobic group, for example an alkyl spacer, and an amino group for pH trapping are essential for high antimalarial activity. The subsequent substitution of tri-n-butylstannyl groups in bis(tri-n-butylstannyl)ferrocene was used to prepare several ferrocene–CQ analogues. Most of the compounds exhibited moderate to strong antimalarial activity when tested against both CQ-susceptible (D10) and CQ-resistant (K1) strains of *P. falciparum* [89, 90].

To investigate the role of the electron-donating ferrocenyl moiety, new organometallic analogues of CQ bearing a cyclopentadienyltricarbonylrhenium moiety with an electron-withdrawing effect were prepared and evaluated. The evaluation of antimalarial activity was measured *in vitro* against the CQ-resistant strain (W2) and the CQ-susceptible strain (3D7) of *P. falciparum.* This showed that these cyrhetrene conjugates are less active compared with their ferrocene and organic analogues, suggesting an original mode-of-action

of FQ and ferrocenyl analogues in relationship with the redox pharmacophore [91]. Following the idea of studying 'half sandwich' systems, two new (η^6-arene-quinoline)$Cr(CO)_3$ complexes, specifically the [η^6-*N*-(7-chloroquinolin-4-yl)-*N*′-[2-(dimethylaminomethyl)benzyl]ethane-1,2-diamine]tricarbonylchromium compounds were synthesized and evaluated, showing high *in vitro* activity against CQ-susceptible and CQ-resistant strains of *P. falciparum.* The activity of this complex against the CQ-resistant parasite strain was three times greater than that presented by CQDP (IC_{50} values of 33.9 nM versus 109.5 nM) [92].

Another strategy to produce new more active complexes at a more affordable cost for industrial production was the dual drug strategy using an association of FQ with glutathione reductase (GR) inhibitors [93] (**8.7o**). The biological results show two important aspects; first a slight modification of the basic side chain does not affect the activity if the substituents are not too large, and second a decrease in the antimalarial activity of the dual molecules was observed, compared with that of FQ analogues, which might be explained by the fact that both the amide bond and the side chain of the FQ derivative are cleaved following the oxidative metabolism in the DV.

8.3.3 Trioxaquines as a ligand in the design of metal-based antimalarial agents

Based on the concept of hybrid molecules with a dual mode of action, a new class of antimalarial agents named trioxaquines has been reported [94]. These molecules contain two covalently linked pharmacophores; 1,2,4-trioxane, as in artemisinin, and 4-aminoquinoline, as in CQ. Such hybrid molecules might be considered a possible response to the recently growing resistance of various parasites to artemisinin [95, 96] and the first generation of trioxaquines were already highly active against CQ-resistant strains of *P. falciparum* [97, 98]. From more than 100 trioxaquines, PA1103/SAR116242 was selected as a drug candidate [99]. Recently, the syntheses of complexes containing 4-aminoquinoline, ferrocene and trioxane were reported (**8.7n**), as well as their biological studies which showed that they are active *in vitro* against CQ-resistant *P. falciparum.* Also, the *in vivo* experiments in *P. vinckei petteri*-infected mice showed that they caused a reduction of the parasitemia below detectable level.

8.3.4 Other standard antimalarial drugs and diverse ligands used in the design of metal-based antimalarial agents

Primaquine and amodiaquine metal derivatives (**8.8a** and **8.8b**) were synthesized and evaluated as antimalarial drugs, [100], however these compounds did not increase the activities compared with the organic drugs. Mefloquine (MQ, **8.3e**, another antimalarial drug, was coordinated to cobalt(II) and nickel(II) of proposal formula $[MCl_2(MQ)_2]$. Only the cobalt complex was tested *in vivo* against *P. yoelli nigeriensis,* showing significant reduction of the parasitemia, but particular toxicity was also reported [101].

As shown in Figure 8.8, other antimalarial drugs were synthesized using a group of metal complexes with chelating ligands such as ethylenediamine-*N*,*N*′-bis[propyl(2-hydroxy-(*R*)-benzylimino)] (ENBPI) **8.8c** [102, 103], and [1,12-bis(2-hydroxy-3-ethylbenzyl)-1,5,8,12-tetraazadodecane] (Eadd) **8.8d** [104]. Both ligands are capable of forming stable compounds with Fe^{III}, Ga^{III} and In^{III}. These compounds can be easily modified by variation of the substituents on both the aromatic rings and the hydrocarbon backbone independently, while retaining the biologically desirable lipophilic monocationic characteristics, and thus they represent interesting amenable leads to metallopharmaceutical development. All the complexes except those of indium(III)

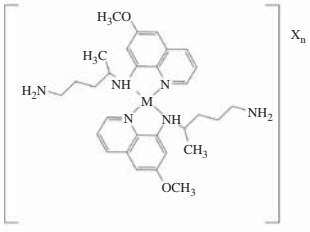

M: Cu(II), Co(II), Zn(II), Sn(II), Ag(I), Pd(II), Hg(II) and Cd(II); X: univalent anion; n: oxidation state of metal ion.

8.8a

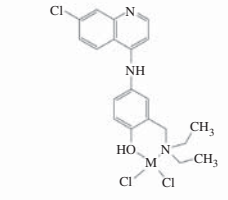

M: Cu(II), Co(II), Zn(II), Sn(II), Pt(II), Pd(II), Hg(II) and Cd(II).

8.8b

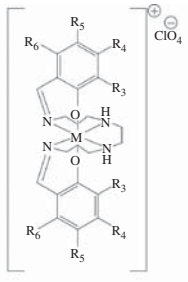

M: Fe(III), Ga(III), In(III).
(a) $R_3 = OCH_3$; $R_4 = R_5 = R_6 = H$
(b) $R_4 = R_6 = OCH_3$; $R_3 = R_5 = H$

8.8c

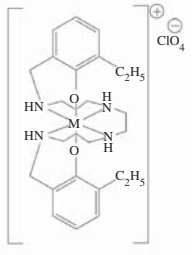

M: Fe(III), Ga(III).

8.8d

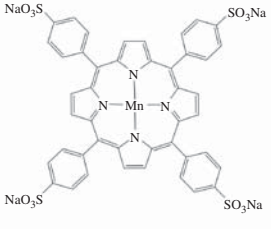

8.8e

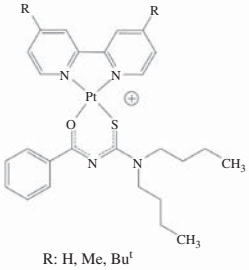

R: H, Me, Bu^t

8.8f

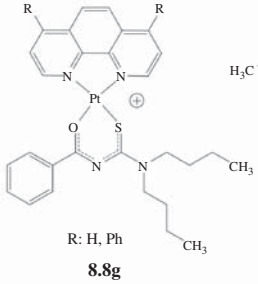

R: H, Ph

8.8g

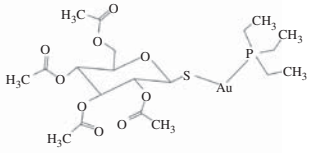

8.8h

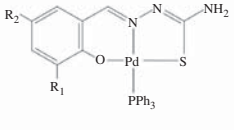

(a) $R_1 = R_2 = H$
(b) R_1 = *tert-butyl*, $R_2 = H$
(c) R_1 = methoxy, $R_2 = H$
(d) R_2 = chloro, $R_1 = H$

8.8i

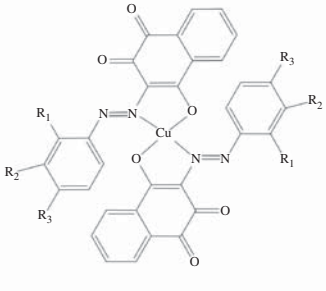

(a) $R_1 = R_2 = R_3 = H$
(b) $R_1 = CH_3$, $R_2 = R_3 = H$
(c) $R_2 = CH_3$, $R_1 = R_3 = H$
(d) $R_3 = CH_3$, $R_1 = R_2 = H$

8.8j

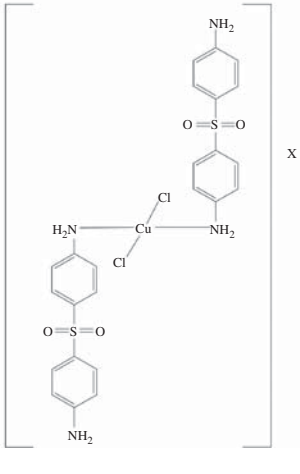

X: $(CH_3OH)_2$, $(CH_3CO)_2(H_2O)$

8.8k

Figure 8.8 *Different approach in the design of metal-based antimalarial drugs*

are active against CQ-susceptible (HB3) and CQ-resistant (FCR-3 and Indo-1) strains of *P. falciparum.* The 4,6-dimethoxy-ENBPI Fe^{III} complex proved to be the most potent among the series tested, inhibiting both CQ-susceptible and CQ-resistant parasites. The antimalarial potency of these compounds correlated well with their ability to inhibit formation of β-haematin *in vitro,* possibly via the formation of a specific drug/haem propionate salt.

Studies using metal-free porphyrins showed the inhibition of the formation of β haematin through an apparent π-π interaction with haematin. Ferrous-protoporphyrin IX [Fe^{II}PPIX] also inhibited haemozoin polymerization [105]. The activity of the endoperoxide drug artemisinin was increased 11-fold by the complex [meso-tetrakis(4-sulfonatophenylporphyrin)Mn] (Mn-TPPS, **8.8e**) [106]. Further *in vitro* and *in vivo* studies with Mn-TPPS show indeed synergistic effects of the complex with artemisinin and other endoperoxide analogues like artemether and arteflene *in vitro,* but experimental results *in vivo* using infected mice with *P. vinckei petteri* displayed good results only with artemisinin [107].

Mixed-ligand cationic diimine–*N*-acyl-*N*′,*N*′-dialkylthioureate complexes of platinum(II) showed a pronounced tendency to undergo marked, concentration-dependent self-association or aggregation presumably through π-cation-type interactions in acetonitrile solution [108]. The self-stacking tendency of these complexes is strikingly similar to that exhibited by porphyrins, suggesting that these mixed-ligand Platinum(II) complexes may associate with Fe^{III}PPIX. Accordingly, a series of novel 2,2′-bipyridyl (**8.8f**) and 1,10-phenanthroline benzoylthiourea complexes of platinum(II) (**8.8g**) with various substituents on the bipyridyl and phenanthroline ligands was synthesized and it was found that these complexes exhibit a strong interaction with haematin and had the ability to inhibit β-haematin formation. The activities of these complexes in CQ-susceptible (D10) and CQ-resistant (K1) strains of malaria parasite were lower than those obtained for CQ in the same conditions, so these results discarded these compounds as potential new antimalarial drugs [109].

Auranofin (**8.8h**), a clinically established gold-based antiarthritic drug, strongly inhibited *P. falciparum* growth *in vitro* [110].

Several gold(I), gold(III), palladium, copper and cobalt complexes have been synthesized using thiosemicarbazone derivatives (see **8.8i,** for example). The biological activities of the thiosemicarbazone ligands and metal complexes have been investigated against two strains of the malaria parasite *Plasmodium falciparum,* W2 (CQ-resistant), and D10 (CQ-sensitive). These metal complexes show enhanced *in vitro* antiplasmodial activity in comparison with their thiosemicarbazone ligand [111–113].

Similarly, hydroxynaphthoquinones (**8.8j**) and 4,4-diaminophenylsulfone (dapsone **8.5e**) (**8.8k**) have been coordinated to copper. Their antimalarial activities were evaluated, finding that **8.8j**(a) shows better activity than the uncoordinated ligand [114], while complexes **8.8k** exhibited lower antimalarial activities than the free ligand and CQ [115].

The present chapter was focused in the importance of the choice of ligand in the search for successful metalloantimalarial drugs; however, there are very interesting and recent reviews related to this matter, which are recommended for further reading [116–119].

8.4 Conclusion

In this chapter, we deal with malaria and antimalarial therapy, emphasizing the efforts made by chemists and biologists to develop metal-based compounds that could overcome the drug resistance problem. Metal-containing compounds clearly provide new opportunities for designing unique structures in complement to the purely organic templates. We hope that this new possibility will convince and attract new researchers.

Acknowledgements

C.B. gratefully acknowledges financial support from Ministère de l'Enseignement Supérieur and Université Lille1. M.N. wishes to thank Murdoch University and her graduate students Legna Colina, Wilmer Villarreal and Dr. William Castro.

References

1. WHO (2011) http://www.who.int/malaria/world_malaria_report_2011/worldmalariareport2011.pdf (accessed 6 November 2013).
2. Murray, C.J., Rosenfeld, L.C., Lim, S.S. *et al.* (2012) Global malaria mortality between 1980 and 2010: a systematic analysis. *The Lancet*, **379** (9814), 413.
3. Rosenthal, P.J. (ed) (2001) *Anti-Malarial Chemotherapy: Mechanisms of Action, Resistance, and New Directions in Drug Discovery*, Humana Press, New York.
4. Dronamraju, K.R. and Arese, P. (2010) *Malaria: Genetic and Evolutionary Aspects (Emerging Infectious Diseases of the 21st Century)*, Springer, New York.
5. Olliaro, P.L. and Taylor, W.R. (2003) Antimalarial compounds: from bench to bedside. *J. Exp. Biol.*, **206**, 3753.
6. Foley, M. and Tilley, L. (1998) Quinoline antimalarials: mechanisms of action and resistance and prospects for new agents. *Pharmacol. Ther.*, **79** (1), 55.
7. Tilley, L., Loria, P. and Foley, M. (2001) *Antimalarial Chemotherapy: Mechanisms of Action, Resistance and New Directions in Drugs Discovery*, 1st edn, Humana Press, Totowa, NJ, p. 87.
8. Ziegler, J., Linck, R. and Wright, D.W. (2001) Heme aggregation inhibitors: antimalarial drugs targeting an essential biomineralization process. *Curr. Med. Chem.*, **8** (2), 171.
9. Cohen, S.N., Kenneth, O.P. and Lemone, Y.K. (1964) Complex Formation between Chloroquine and Ferrihæmic Acid in vitro, and its effect on the Antimalarial Action of Chloroquine. *Nature*, **202** (4934), 805.
10. Vippagunta, S.R., Dorn, A., Matile, H. *et al.* (1999) Structural specificity of chloroquine-hematin binding related to inhibition of hematin polymerization and parasite growth. *J. Med. Chem.*, **42** (22), 4630.
11. Egan, T.J., Hunter, R., Kaschula, C.H. *et al.* (2000) Structure-function relationships in aminoquinolines: effect of amino and chloro groups on quinoline-hematin complex formation, inhibition of beta-hematin formation, and antiplasmodial activity. *J. Med. Chem.*, **43** (2), 283.
12. Sullivan, D.J., Gluzman, I.Y., Russell, D.G. and Goldberg, D.E. (1996) On the molecular mechanism of chloroquine's antimalarial action. *Proc. Natl. Acad. Sci. U.S.A.*, **93**, 11865.
13. Combrinck, J.M., Mabotha, T.E., Ncokazi, K.K. *et al.* (2013) Insights into the role of heme in the mechanism of action of antimalarials. *ACS Chem. Biol.*, **18** (8), 133.
14. Egan, T.J. (2004) Haemozoin formation as a target for the rational design of new antimalarials. *Drug Des. Rev.*, **1** (1), 93.
15. Gildenhuys, J., le Roex, T., Egan, T.J. and de Villiers, K.A. (2013) The single crystal X-ray structure of β-hematin DMSO solvate grown in the presence of chloroquine, a β-hematin growth-rate inhibitor. *J. Am. Chem. Soc.*, **135** (3), 1037.
16. Dzekunov, S.M., Ursos, L.M.B. and Roepe, P.D. (2000) Digestive vacuolar pH of intact intraerythrocytic P. falciparum either sensitive or resistant to chloroquine. *Mol. Biochem. Parasitol.*, **110** (1), 107.
17. Goldberg, D.E., Slater, A.F.G., Beavis, R. *et al.* (1991) Hemoglobin degradation in the human malaria pathogen Plasmodium falciparum: a catabolic pathway initiated by a specific aspartic protease. *J. Exp. Med.*, **173** (4), 961.
18. Gluzman, I.Y., Francis, S.E., Oksman, A. *et al.* (1994) Order and specificity of the Plasmodium falciparum hemoglobin degradation pathway. *J. Clin. Invest.*, **93** (4), 1602.
19. Francis, S.E., Gluzman, I.Y., Oksman, A. *et al.* (1996) Characterization of native falcipain, an enzyme involved in Plasmodium falciparum hemoglobin degradation. *Mol. Biochem. Parasitol.*, **83** (2), 189.
20. Becker, K., Tilley, L., Vennerstrom, J.L. *et al.* (2004) Oxidative stress in malaria parasite-infected erythrocytes: host-parasite interactions. *Int. J. Parasitol.*, **34** (2), 163.

21. Abdalla, S. and Pasvol, H.G. (2004) *Malaria: A Hematological Perspective: A Hematological Perspective*, Tropical Medicine: Science and Practice, vol. **4**, Imperial College Press, London.
22. Pisciotta, J.M. and Sullivan, D. (2008) Hemozoin: oil versus water. *Parasitol. Int.*, **57** (2), 89.
23. Sullivan, D.J., Gluzman, I.Y. and Goldberg, D.E. (1996) Plasmodium hemozoin formation mediated by histidine-rich proteins. *Science*, **271**, 219.
24. Egan, T.J. (2008) Recent advances in understanding the mechanism of hemozoin (malaria pigment) formation. *J. Inorg. Biochem.*, **102** (5-6), 1288.
25. Brown, W.H. (1911) Malarial pigment (so-called melanin): its nature and mode of production. *J. Exp. Med.*, **13** (2), 290.
26. Slater, A.F., Swiggard, W.J., Orton, B.R. and Flitter, W.D. (1991) An iron-carboxylate bond links the heme units of malaria pigment. *Proc. Natl. Acad. Sci. U.S.A.*, **88**, 325.
27. Pagola, S., Stephens, P.W., Bohle, D.S. *et al.* (2000) The structure of malaria pigment beta-haematin. *Nature*, **404**, 307.
28. Avery, M., Alvim-Gaston, M., Vroman, J. *et al.* (2002) Structure-activity relationships of the antimalarial agent artemisinin. 7. Direct modification of (+)-artemisinin and in vivo antimalarial screening of new, potential preclinical antimalarial candidates. *J. Med. Chem.*, **45** (19), 4321.
29. Posner, G.J. (1997) Antimalarial Endoperoxides that are Potent and Easily Synthesized. *J. Pharm. Pharmacol.*, **49** (Suppl. 2), 55.
30. Meunier, B. and Robert, A. (2010) Heme as trigger and target for trioxane-containing antimalarial drugs. *Acc. Chem. Res.*, **43** (11), 1444.
31. Posner, G., Oh, C., Wang, D. *et al.* (1994) Mechanism-based design, synthesis, and in vitro antimalarial testing of new 4-methylated trioxanes structurally related to artemisinin: the importance of a carbon-centered radical for antimalarial activity. *J. Med. Chem.*, **37** (9), 1256.
32. Posner, G., Cumming, J., Ploypradith, P. and Oh, C. (1995) Evidence for Fe(IV)=O in the Molecular Mechanism of Action of the Trioxane Antimalarial Artemisinin *J. Am. Chem. Soc.*, **117** (21), 5885.
33. Robert, A., Coppel, Y. and Meunier, B. (2002) Alkylation of heme by the antimalarial drug artemisinin. *Chem. Commun. (Camb.)*, **5**, 414.
34. Choi, S.R., Mukherjeea, P. and Avery, M.A. (2008) The fight against drug-resistant malaria: novel plasmodial targets and antimalarial drugs. *Curr. Med. Chem.*, **15**, 161.
35. Dieckmann, A. and Jung, A. (1986) The mechanism of pyrimethamine resistance in Plasmodium falciparum. *Parasitology*, **93** (2), 275.
36. Sibley, C.H., Hyde, J.E., Sims, P.F.G. *et al.* (2001) Pyrimethamine-sulfadoxine resistance in Plasmodium falciparum: what next? *Trends Parasitol.*, **17** (12), 582.
37. Rosenberg, B., Van Camp, L. and Krigas, T. (1965) Inhibition of cell division in escherichia coli by electrolysis products from a platinum electrode. *Nature*, **205**, 698.
38. Rosenberg, B., Van Camp, L., Trosko, J.E. and Mansour, V.H. (1969) Platinum compounds: a new class of potent antitumour agents. *Nature*, **222**, 385.
39. Alessio, E. (2011) *Bioinorganic Medicinal Chemistry*, Wiley-VCH Verlag & Co., Weinheim.
40. Sánchez-Delgado, R.A., Navarro, M., Pérez, H. and Urbina, J.A. (1996) Toward a novel metal-based chemotherapy against tropical diseases. 2. Synthesis and antimalarial activity in vitro and in vivo of new ruthenium- and rhodium-chloroquine complexes. *J. Med. Chem.*, **39** (5), 1095.
41. Navarro, M., Sánchez-Delgado, R.A. and Pérez, H. (1997) Toward a Novel Metal-Based Chemotherapy against Tropical Diseases. 3. Synthesis and Antimalarial Activity in Vitro and in Vivo of the New Gold-Chloroquine Complex [Au(PPh3)(CQ)]PF6. *J. Med. Chem.*, **40** (12), 1937.
42. Navarro, M., Vásquez, F., Sánchez-Delgado, R.A. *et al.* (2004) Toward a novel metal-based chemotherapy against tropical diseases. 7. Synthesis and in vitro antimalarial activity of new gold-chloroquine complexes. *J. Med. Chem.*, **47** (21), 5204.
43. Rajapakse, C.S.K., Martínez, A., Naoulou, B. *et al.* (2009) Synthesis, characterization, and in vitro antimalarial and antitumor activity of new ruthenium(II) complexes of chloroquine. *Inorg. Chem.*, **48** (3), 1122.
44. Navarro, M., Pekerar, S. and Pérez, H.A. (2007) Synthesis, characterization and antimalarial activity of new iridium-chloroquine complexes. *Polyhedron*, **26** (12), 2420.
45. Bellotti de Souza, N., Carmo, A.M.L., Lagatta, D.C. *et al.* (2011) 4-aminoquinoline analogues and its platinum (II) complexes as antimalarial agents. *Biomed. Pharmacother.*, **65** (4), 313.

46. Ajibade, P.A. and Kolawole, G.A. (2008) Synthesis, characterization and antiprotozoal studies of some metal complexes of antimalarial drugs. *Transition Met. Chem.*, **33** (4), 493.
47. Navarro, M., Castro, W., Higuera-Padilla, A.R. *et al.* (2011) Synthesis, characterization and biological activity of trans-platinum(II) complexes with chloroquine. *J. Inorg. Biochem.*, **105**, 1684.
48. Dorn, A.S., Vippagunta, R., Matile, H. *et al.* (1998) An assessment of drug-haematin binding as a mechanism for inhibition of haematin polymerisation by quinoline antimalarials. *Biochem. Pharmacol.*, **55** (6), 727.
49. Egan, T.J., Hempelmann, E. and Mavuso, W.W. (1999) Characterisation of synthetic beta-haematin and effects of the antimalarial drugs quinidine, halofantrine, desbutylhalofantrine and mefloquine on its formation. *J. Inorg. Biochem.*, **73** (1-2), 101.
50. Martínez, A., Rajapakse, C.S.K., Naoulou, B. *et al.* (2008) The mechanism of antimalarial action of the ruthenium(II)-chloroquine complex $[RuCl_2(CQ)]_2$. *J. Biol. Inorg. Chem.*, **13** (5), 703.
51. Martínez, A., Rajapakse, C.S.K., Jalloh, D. *et al.* (2009) The antimalarial activity of Ru-chloroquine complexes against resistant Plasmodium falciparum is related to lipophilicity, basicity, and heme aggregation inhibition ability near water/n-octanol interfaces. *J. Biol. Inorg. Chem.*, **14** (6), 863.
52. Navarro, M., Castro, W., Martínez, A. and Sánchez-Delgado, R.A. (2011) The mechanism of antimalarial action of $[Au(CQ)(PPh_3)]PF_6$: structural effects and increased drug lipophilicity enhance heme aggregation inhibition at lipid/water interfaces. *J. Inorg. Biochem.*, **105** (2), 276.
53. Baelmans, R., Deharo, E., Muñoz, V. *et al.* (2000) Experimental conditions for testing the inhibitory activity of chloroquine on the formation of beta-hematin. *Exp. Parasitol.*, **96** (4), 243.
54. Blauer, G. and Akkawi, M. (1997) Investigations of B- and beta-hematin. *J. Inorg. Biochem.*, **66** (2), 145.
55. Domínguez, J.N., León, C., Rodrigues, J. *et al.* (2005) Synthesis and antimalarial activity of sulfonamide chalcone derivatives. *II Fármaco*, **60** (4), 307.
56. Egan, T.J., Chen, J.Y.J., de Villiers, K.A. *et al.* (2006) Haemozoin (beta-haematin) biomineralization occurs by self-assembly near the lipid/water interface. *FEBS Lett.*, **580** (21), 5105.
57. Biot, C., Glorian, G., Maciejewski, L.A. and Brocard, J.S. (1997) Synthesis and antimalarial activity in vitro and in vivo of a new ferrocene-chloroquine analogue. *J. Med. Chem.*, **40** (23), 3715.
58. Biot, C., Nosten, F., Fraisse, L. *et al.* (2011) The antimalarial ferroquine: from bench to clinic. *Parasite*, **18** (3), 207.
59. Biot, C., Daher, W., Ndiaye, C.M. *et al.* (2006) Probing the role of the covalent linkage of ferrocene into a chloroquine template. *J. Med. Chem.*, **49** (15), 4707.
60. Fraisse, L. and Ter-Minassian, D. (2006) International Application PCT/FR2006/000842.
61. Delhaes, L., Abessolo, H., Biot, C. *et al.* (2001) In vitro and in vivo antimalarial activity of ferrochloroquine, a ferrocenyl analogue of chloroquine against chloroquine-resistant malaria parasites. *Parasitol. Res.*, **87** (3), 239.
62. Yayon, A., Cabantchik, Z.I. and Ginsburg, H. (1985) Susceptibility of human malaria parasites to chloroquine is pH dependent. *Proc. Natl. Acad. Sci. U.S.A.*, **82** (9), 2784.
63. Supan, C., Mombo-Ngoma, G., Dal-Bianco, M.P. *et al.* (2012) Pharmacokinetics of ferroquine, a novel 4-aminoquinoline, in asymptomatic carriers of Plasmodium falciparum infections. *Antimicrob. Agents Chemother.*, **56** (6), 3165.
64. French Patent LV/cc - F0644CAS341/FR. 0000.
65. Vausselin, T, Calland N, Belouzard S *et al*. (2013) The antimalarial ferroquine is an inhibitor of hepatitis C virus. *Hepatology*, **58** (1), 86.
66. Pomel, S., Biot, C., Bories, C. and Loiseau, P.M. (2013) Antiprotozoal activity of ferroquine. *Parasitology*, **112** (2), 665.
67. Dubar, F., Bohic, S., Slomianny, C. *et al.* (2012) In situ nanochemical imaging of label-free drugs: a case study of antimalarials in Plasmodium falciparum-infected erythrocytes. *Chem. Commun.*, **48**, 910.
68. Dubar, F., Egan, T.J., Pradines, B. *et al.* (2011) The antimalarial ferroquine: role of the metal and intramolecular hydrogen bond in activity and resistance. *ACS Chem. Biol.*, **6**, 275.
69. Dubar, F., Bohic, S., Dive, D. *et al.* (2012) Deciphering the resistance-counteracting functions of the antimalarial ferroquine in Plasmodium falciparum-infected erythrocytes. *ACS Med. Chem. Lett.*, **3**, 480.
70. Biot, C., Daher, W., Chavain, N. *et al.* (2006) Design and synthesis of hydroxyferroquine derivatives with antimalarial and antiviral activities. *J. Med. Chem.*, **49** (9), 2845.
71. Biot, C., Delhaes, L., N'Diaye, C.M. *et al.* (1999) Synthesis and antimalarial activity in vitro of potential metabolites of ferrochloroquine and related compounds. *Bioorg. Med. Chem.*, **7** (12), 2843.

72. Biot, C., Pradines, B., Sergeant, M.H. *et al.* (2007) Design, synthesis, and antimalarial activity of structural chimeras of thiosemicarbazone and ferroquine analogues. *Bioorg. Med. Chem. Lett.*, **17** (23), 6434.
73. Van Staveren, D.R. and Metzler-Nolte, N. (2004) Bioorganometallic chemistry of ferrocene. *Chem. Rev.*, **104** (12), 5931.
74. Delhaes, L., Biot, C., Berry, L. *et al.* (2000) Novel ferrocenic artemisinin derivatives: synthesis, in vitro antimalarial activity and affinity of binding with ferroprotoporphyrin IX. *Bioorg. Med. Chem.*, **8** (12), 2739.
75. Baramee, A., Coppin, A., Mortuaire, M. *et al.* (2006) Synthesis and in vitro activities of ferrocenic aminohydroxynaphthoquinones against Toxoplasma gondii and Plasmodium falciparum. *Bioorg. Med. Chem.*, **14** (5), 1294.
76. Biot, C., Delhaes, L., Maciejewski, L.A. *et al.* (2000) Synthetic ferrocenic mefloquine and quinine analogues as potential antimalarial agents. *Eur. J. Med. Chem.*, **35** (7-8), 707.
77. Guillon, J., Moreau, S., Mouray, S. *et al.* (2008) New ferrocenic pyrrolo[1,2-a]quinoxaline derivatives: synthesis, and in vitro antimalarial activity. *Bioorg. Med. Chem.*, **16** (20), 9133.
78. Saleh, A., Friesen, J., Baumesteir, S. *et al.* (2007) Growth inhibition of Toxoplasma gondii and Plasmodium falciparum by nanomolar concentrations of 1-hydroxy-2-dodecyl-4(1H)quinolone, a high-affinity inhibitor of alternative (type II) NADH dehydrogenases. *Antimicrob. Agents Chemother.*, **51** (4), 1217.
79. Winter, R., Kelly, W.J.X., Smilkstein, M.J. *et al.* (2008) Antimalarial quinolones: synthesis, potency, and mechanistic studies. *Exp. Parasitol.*, **118** (4), 487.
80. Dubar, F., Wintjens, R., Martins-Duarte, E.S. *et al.* (2011) Ester prodrugs of ciprofloxacin as DNA-gyrase inhibitors: synthesis, antiparasitic evaluation and docking studies. *Med. Chem. Commun.*, **2**, 430.
81. Ferreira, C.L., Ewart, C.B., Barta, C.A. *et al.* (2006) Synthesis, structure, and biological activity of ferrocenyl carbohydrate conjugates. *Inorg. Chem.*, **45** (20), 8414.
82. Quirante, J., Dubar, F., González, A. *et al.* (2011) Ferrocene-indole hybrids for cancer and malaria therapy. *J. Organomet. Chem.*, **696** (5), 1011.
83. Domarle, O., Blampain, G., Agnaniet, H. *et al.* (1998) In vitro antimalarial activity of a new organometallic analog, ferrocene-chloroquine. *Antimicrob. Agents Chemother.*, **42** (3), 540.
84. Biot, C., Delhaes, L., Abessolo, H. *et al.* (1999) Novel metallocenic compounds as antimalarial agents. Study of the position of ferrocene in chloroquine. *J. Organomet. Chem.*, **589** (1), 59.
85. Raynes, K. (1999) Bisquinoline antimalarials: their role in malaria chemotherapy. *Int. J. Parasitol.*, **29** (3), 367.
86. Biot, C., Dessolin, J., Ricard, I. and Dive, D. (2004) Easily synthesized antimalarial ferrocene triazacyclononane quinoline conjugates. *J. Organomet. Chem.*, **689** (25), 4678.
87. Blackie, M.A.L., Beagley, P., Chibale, K. *et al.* (2003) Synthesis and antimalarial activity in vitro of new heterobimetallic complexes: Rh and Au derivatives of chloroquine and a series of ferrocenyl-4-amino-7chloroquinolines. *J. Organomet. Chem.*, **688** (1-2), 144.
88. Beagley, P., Blackie, M.A.L., Chibale, K. *et al.* (2002) Synthesis and antimalarial activity *in vitro* of new ruthenocene–chloroquine analogues. *J. Chem. Soc., Dalton Trans.*, (10), 4426.
89. Beagley, P., Blackie, M.A.L., Chibale, K. *et al.* (2003) Synthesis and antiplasmodial activity *in vitro* of new ferrocene–chloroquine analogues. *Dalton Trans.*, (15), 3046.
90. Blackie, M.A.L., Beagley, P., Croft, S.L. *et al.* (2007) Metallocene-based antimalarials: an exploration into the influence of the ferrocenyl moiety on in vitro antimalarial activity in chloroquine-sensitive and chloroquine-resistant strains of Plasmodium falciparum. *Bioorg. Med. Chem.*, **15** (20), 6510.
91. Arancibia, R., Dubar, F., Pradines, B. *et al.* (2010) Synthesis and antimalarial activities of rhenium bioorganometallics based on the 4-aminoquinoline structure. *Bioorg. Med. Chem.*, **18** (22), 8085.
92. Glans, L., Taylor, D., de Kock, C. *et al.* (2011) Synthesis, characterization and antimalarial activity of new chromium arene-quinoline half sandwich complexes. *J. Inorg. Biochem.*, **105** (7), 985.
93. Chavain, N., Davioud-Charvet, E., Trivelli, X. *et al.* (2009) Antimalarial activities of ferroquine conjugates with either glutathione reductase inhibitors or glutathione depletors via a hydrolyzable amide linker. *Bioorg. Med. Chem.*, **17** (23), 8048.
94. Bellot, F., Coslédan, F., Vendier, L. *et al.* (2010) Trioxaferroquines as new hybrid antimalarial drugs. *J. Med. Chem.*, **53** (10), 4103.
95. Dondorp, A.M., Nosten, F., Yi, P. *et al.* (2009) Artemisinin resistance in Plasmodium falciparum malaria. *N. Engl. J. Med.*, **361** (5), 455.
96. Taylor, S.M., Juliano, J.J. and Meshnick, S.R. (2009) Artemisinin resistance in Plasmodium falciparum malaria. *N. Engl. J. Med.*, **361** (18), 1807.

97. Dechy-Cabaret, O., Benoit-Vical, F., Robert, A. and Meunier, B. (2000) Preparation and antimalarial activities of "Trioxaquines", new modular molecules with a trioxane skeleton linked to a 4-aminoquinoline. *ChemBioChem*, **1** (4), 281.
98. Robert, A., Dechy-Cabaret, O., Cazelles, J. and Meunier, B. (2002) From mechanistic studies on artemisinin derivatives to new modular antimalarial drugs. *Acc. Chem. Res.*, **35** (3), 167.
99. Cosledan, F., Fraisse, L., Pellet, A. *et al.* (2008) Selection of a trioxaquine as an antimalarial drug candidate. *Proc. Natl. Acad. Sci. U.S.A.*, **105** (45), 17579.
100. Wash, N., Singh, H.B., Gajanana, A. and Raichowdhary, A.N. (1987) Synthesis of metal complexes of antimalarial drugs and in-vitro evaluation of their activity against *Plasmodium falciparum*. *Inorg. Chim. Acta*, **135** (2), 133.
101. Fermi, A.J. and Ayoola, O.J. (2012) Co(II) Complex of mefloquine hydrochloride: Synthesis, antimicrobial potential, antimalaria and toxicological Activities. *E-J. Chem.*, **9**, 2245.
102. Goldberg, D.E., Sharma, V., Oksman, A. *et al.* (1997) Probing the chloroquine resistance locus of Plasmodium falciparum with a novel class of multidentate metal(III) coordination complexes. *J. Biol. Chem.*, **272** (10), 6567.
103. Ziegler, J., Schuerle, T., Pasierb, L. *et al.* (2000) The propionate of heme binds N4O2 Schiff base antimalarial drug complexes. *Inorg. Chem.*, **39**, 3731.
104. Harpstrite, S.E., Beatty, A.A., Collins, S.D. *et al.* (2003) Metalloantimalarials: targeting of P. falciparum strains with novel iron(III) and gallium(III) complexes of an amine phenol ligand. *Inorg. Chem.*, **42**, 2294.
105. Monti, D., Vodopivec, B., Basilico, N. *et al.* (1999) A novel endogenous antimalarial: Fe(II)-protoporphyrin IX alpha (heme) inhibits hematin polymerization to beta-hematin (malaria pigment) and kills malaria parasites. *Biochemistry*, **38** (28), 8858.
106. Benoit-Vical, F., Robert, A. and Meunier, B. (1999) Potentiation of artemisinin activity against chloroquine-resistant *Plasmodium falciparum* strains by using heme models. *Antimicrob. Agents Chemother.*, **43** (10), 2555.
107. Benoit-Vical, F., Robert, A. and Meunier, B. (2000) In vitro and in vivo potentiation of artemisinin and synthetic endoperoxide antimalarial drugs by metalloporphyrins. *Antimicrob. Agents Chemother.*, **44** (10), 2836.
108. Koch, K.R., Sacht, C. and Lawrence, C. (1998) Self-association of new mixed-ligand diimine–N-acyl-N′,N′-dialkyl thioureate complexes of platinum(II) in acetonitrile solution. *J. Chem. Soc., Dalton Trans.*, **4**, 689.
109. Egan, T.J., Koch, K.R., Swan, P.L. *et al.* (2004) In vitro antimalarial activity of a series of cationic 2,2′-bipyridyl- and 1,10-phenanthrolineplatinum(II) benzoylthiourea complexes. *J. Med. Chem.*, **47** (11), 2926.
110. Sannella, A.R., Casini, A., Gabbiani, C. *et al.* (2008) New uses for old drugs. Auranofin, a clinically established antiarthritic metallodrug, exhibits potent antimalarial effects in vitro: mechanistic and pharmacological implications. *FEBS Lett.*, **582** (6), 844.
111. Chellan, P., Shunmoogam-Gounden, N., Hendricks, D.T. *et al.* (2010) Synthesis, structure and in vitro biological screening of palladium(II) complexes of functionalised salicylaldimine thiosemicarbazones as antimalarial and anticancer agents. *Eur. J. Inorg. Chem.*, **2010** (22), 3520.
112. Khanye, S.D., Wan, B., Franzblau, S.G. *et al.* (2011) Synthesis and in vitro antimalarial and antitubercular activity of gold(III) complexes containing thiosemicarbazone ligands. *J. Organomet. Chem.*, **696** (21), 3392.
113. Meshnick, S.R., Scott, M.D., Lubin, B. *et al.* (1990) Antimalarial activity of diethyldithiocarbamate. Potentiation by copper. *Biochem. Pharmacol.*, **40** (2), 213.
114. Gokhale, N.H., Shirisha, K., Padhye, S.B. *et al.* (2006) Metalloantimalarials: synthesis, X-ray crystal structure of potent antimalarial copper (II) complex of arylazo-4-hydroxy-1,2-naphthoquinone. *Bioorg. Med. Chem. Lett.*, **16** (2), 430.
115. Tella, A.C. and Obaleye, J.A. (2009) Copper(II) complexes of 4, 4- diaminodiphenylsulphone: Synthesis, characterization and biological studies. *E-J. Chem.*, **6** (S1), S311.
116. Biot, C., Castro, W., Botté, C.Y. and Navarro, M. (2012) The therapeutic potential of metal-based antimalarial agents: Implications for the mechanism of action. *Dalton Trans.*, **41**, 6335.
117. Navarro, M., Castro, W. and Biot, C. (2012) Bioorganometallic compounds with antimalarial targets: inhibiting hemozoin formation. *Organometallics*, **31**, 5715.
118. Sekhon, B.S. and Bimal, N. (2012) Transition metal-based anti-malarial. *J. Pharm. Educ. Res.*, **3** (2), 52.
119. Salas, P.F., Herrmann, C. and Orvig, C. (2013) Metalloantimalarials. *Chem. Rev.*, **113** (5), 3450.

9

Therapeutic Gold Compounds

Susan J. Berners-Price[1] and Peter J. Barnard[2]

[1]*Institute for Glycomics, Griffith University, Gold Coast Campus, Gold Coast Queensland, 4222, Australia*
[2]*Department of Chemistry, La Trobe Institute for Molecular Science, La Trobe University, Melbourne Victoria, 3086, Australia*

9.1 Introduction

Whilst the use of gold drugs in medicine has a very long history, in both western cultures [1] and in Chinese medicine [2], the concept of ligand design in this field is relatively new [3]. Certainly the gold(I) thiolate drugs (e.g. **1** and **2**, Figure 9.1), which have been used for the treatment of rheumatoid arthritis (RA) since the 1920s, are typical of metal-based drugs that have reached clinical use *via* serendipity rather than any rational design process. Their use can be traced back to Robert Koch's discovery (in 1890) of the anti-tubercular activity of gold cyanide, which proved too toxic for clinical use, but led to the widespread adoption of water-soluble gold(I) thiolate salts for the treatment of tuberculosis during the so called 'gold decade' (1925–1935). Observations that gold therapy (chrysotherapy) brought about significant reductions in joint pain in a group of non-tubercular patients prompted a study of gold compounds for treatment of RA [4]. The fact that these gold(I) thiolate drugs are still in clinical use today (despite issues of toxicity) is because they are effective in retarding the progression of the disease and are included in the class of disease-modifying antirheumatic drugs (DMARDs) [5].

One of the first examples of the use of ligand design in medicinal inorganic chemistry is the work of Sutton and co-workers in the 1970s, in the development of an orally active gold drug for RA treatment, by incorporation of a lipophilic phosphine ligand. Auranofin (**3**, Figure 9.1, Trade name 'Ridaura') was approved for clinical use in 1985 [6, 7]. The observation in the 1980s that auranofin was cytotoxic to tumour cells *in vitro* [8], led to the search and identification of other Au^{I} phosphines with a broader spectrum of antitumour activity; notably $[Au(dppe)_2]Cl$ (where $dppe = Ph_2P(CH_2)_2PPh_2$), in which incorporation of the bis-chelated diphosphine ligands reduced non-productive reactions with protein thiols [9]. Around this time

Ligand Design in Medicinal Inorganic Chemistry, First Edition. Edited by Tim Storr.

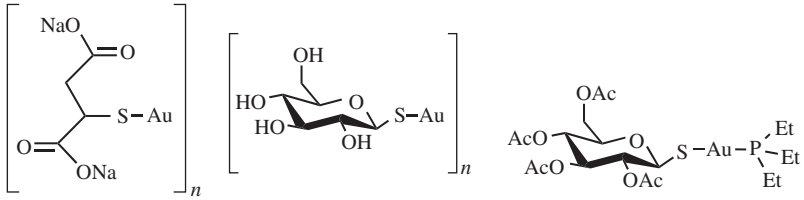

(**1**) (**2**) (**3**)

Figure 9.1 *The structures of Au^{I} drugs used for the treatment of rheumatoid arthritis: sodium aurothiomalate (Myocrisin) (**1**), aurothioglucose (Solganol) (**2**) and tetraacetyl-β-D-thioglucose gold(I) triethylphosphine (auranofin) (**3**)*

gold(III) complexes were first investigated as potential antitumour agents, based on the premise that being d^8 square planar complexes they may mimic the activity of cisplatin. However, only in the 1990s were promising results reported for several classes of Au^{III} antitumour compounds [10], with stabilisation of the Au^{III} oxidation state achieved through appropriate ligand design.

Over the past few years there has been unprecedented interest in the design of gold compounds (both Au^{I} and Au^{III}) to treat a wide range of different diseases [3, 11–17]. The stimulus for this research has been recognition of the unique chemistry of gold (high affinity for cysteine and selenocysteine residues) combined with the emergence of a variety of thiol and selenol protein drug targets, whose dysfunction in cells can cause or contribute to a variety of human diseases. These protein targets include thioredoxin reductase (TrxR) which has been implicated in several chronic diseases (e.g. cancer and RA) [18]; cysteine proteases [19] (implicated in inflammatory airway diseases, bone and joint disorders, parasitic diseases and cancer [20]), including the cathepsins B, K and S [20–25] and protein tyrosine phosphatases (PTPs) [26] which have been implicated in autoimmune diseases, obesity and cancer [27]. The potential application of gold drugs against major tropical diseases has also received recent attention [28] and is an area of growing importance due to the variety of unique thiol and selenol proteins that have been validated as drug targets (e.g. trypanothione reductase (TR) in *Leishmania* parasites [29]). Exploitable differences exist also in the redox metabolism of the host and parasite; for example structural differences have been identified in the *C*-terminal redox centre in the different TrxR enzymes in malaria parasite, human host and insect vector [30]. Gold-based drugs offer new avenues for antimicrobial development, with potential to overcome the increasing problem of multidrug resistance [31], for example by targeting selenium metabolism in selenium-dependent pathogens [32, 33].

While gold drugs offer enormous potential as potent inhibitors of novel thiol/selenol disease targets, the challenge in the drug design process is to understand and exploit the complex biotransformation reactions of gold that are known to occur *in vivo*. This topic has recently been reviewed in detail elsewhere [3]. In this chapter we focus on the *design* of gold-based drugs and the role of ligands in controlling the reactivity of the metal centre, or in influencing cellular uptake and modulation of biological activity. While we have arranged the chapter with a focus on treatment of specific diseases, the existence of common protein targets and overlapping signalling pathways, means that it is axiomatic that gold compounds often display therapeutic activity in multiple disease types. Auranofin is a case in point with activity reported for an extraordinarily large range of diseases such as RA [34], cancer [8], HIV [35–37], malaria [38] and a variety of other parasitic diseases including leishmaniasis [29], schistosomiasis [39] and human amoebiasis [40]. Much attention has been devoted to investigation of auranofin because it is already approved for clinical use in humans, and finding new uses for old drugs is a suggested strategy for cutting down the time and costs of bringing new

drugs to market [41]. There is now an opportunity to design improved (less toxic and more selective) gold drugs by bringing together the wealth of accumulated knowledge on the biological chemistry of gold, with the new ideas of ligand design and molecular targeting.

9.2 Antiarthritic gold drugs

RA is a chronic inflammatory disease characterised by the migration of activated phagocytes and leukocytes into synovial tissue, leading to joint swelling and progressive destruction of cartilage and bone. The mechanism of action of gold drugs is multi-factorial in this complex disease [42] with an overriding theme being the interaction with protein cysteine (or selenocysteine) residues. These different protein targets for gold compounds in RA have been reviewed recently elsewhere [3, 17, 43].

9.2.1 Gold (I) thiolates

The injectable Au^I thiolate complexes such as aurothiomalate (Myocrisin) and aurothioglucose (Solganol) (**1** and **2**, Figure 9.1) are polymers with thiolate S bridging linear Au^I ions. The crystal structure of aurothiomalate [44] shows linear S-Au-S units arranged into double-helical chains, in good agreement with the results of early EXAFS and WAXS studies which indicated chain and cyclic structures [45, 46]. After administration, these linear gold(I) complexes rapidly undergo ligand exchange reactions so that the administered drugs are unlikely to be the pharmacologically active species. For example, it is known that gold from these drugs is transported in blood by human serum albumin by binding to the cysteine 34 residue [47]. Early EXAFS and Mössbauer studies of gold thiomalate (STm) derivatives of serum albumin supported formation of albumin-S-Au-Stm and albumin-S-(Au-μStm)*n*-Au-STm [48]. As such, the different ligands in these Au^I thiolates (thiomalate, thioglucose, etc.) probably have no significant role, other than allowing formation of water-soluble Au^I complexes that have to be administered by intramuscular injection. On the other hand the ligands may subtly influence the interaction with protein targets. It is interesting to note that a crystal structure of a cathepsin K/aurothiomalate complex shows linear S-Au-S coordination with Au bound to the active site cysteine residue and a thiomalate ligand still coordinated [24].

9.2.2 Gold (I) phosphines

In the original development of orally-active gold drugs for treatment of RA by Sutton *et al*. a series of alkylphosphine Au^I complexes (R_3PAuX) were investigated [6]. The nature of the phosphine ligand (R_3P) influences the extent of oral absorption and complexes with ethyl substituents were more effective both in producing a therapeutic response and developing serum Au levels than were methyl, isopropyl or *n*-butyl complexes [6]. Et_3PAuCl was initially selected for clinical trial but the tetraacetylated thioglucose derivative (auranofin) was better tolerated. Based on initial clinical trial results auranofin appeared to offer significant advantages over the traditional injectable Au^I thiolates, having comparable efficacy and only mild side-effects [34, 49], whilst avoiding the need for monthly injections associated with long-term chrysotherapy. However, in the longer term, auranofin proved to be less effective than the injectable gold drugs [50] and now seems to be rarely used clinically [51].

From a ligand design perspective, the phosphine confers membrane solubility and affects the pharmacological profile of the Au^I complex, including uptake into cells. Arylphosphines were not investigated initially,

but subsequent studies [52] showed that triphenylphosphine Au^I complexes were more active in the rat model of arthritis and are no more toxic than auranofin. In most model reactions release of the phosphine (Et_3P) does not occur readily, but Et_3PO has been identified in the urine of auranofin-treated patients [34] and studies with ^{195}Au, ^{35}S and ^{32}P-radiolabelled auranofin in dogs showed that the ^{35}S and ^{32}P are excreted more rapidly than ^{195}Au [53]. On binding to albumin the acetylthioglucose ligand is substituted first and the phosphine ligand is liberated slowly (with formation of Et_3PO) driven by the liberated acetylthioglucose ligand and thiol ligands such as glutathione (GSH) [54]. Once the phosphine is released the products of auranofin metabolism are likely to be similar to those of the Au^I thiolate drugs.

In antiarthritic complexes of the type R_3PAuX, the leaving ligand (X) clearly also has an influence on the biological activity. Recent studies have investigated the seleno-auranofin (Se-AF) analogue and, whilst *in vivo* serum gold levels were comparable to auranofin, Se-AF was inactive in the orally administered carragenan-induced assay in rats [55]. The difference was attributed to more rapid metabolism of Se-AF, originating in a greater extent of ligand exchange reactions. Se-AF reacted with serum albumin to form $AlbSAuPEt_3$ with evidence for facile reduction of disulfide bonds at cysteine 34 and very rapid formation of Et_3PO [55]. Other investigations have incorporated a bioactive ligand as the leaving ligand (X), for example imido ligands such as riboflavin [56], thionucleobases which possess antiarthritic activity in their own right [52] and recently benzyl-substituted derivatives of 6-benzylaminopurine, which are growth regulators (cytokines) [57].

9.2.3 Design of specific enzyme inhibitors

The multiple possible targets for gold-based DMARDs, combined with their biotransformation reactions, present challenges in terms of drug design, but some recent studies by Barrios and co-workers have focused on optimising inhibition of specific enzyme targets.

Cathepsins are lysosomal cysteine proteases implicated in inflammation and joint destruction and play a role in antigen processing and presentation and have been implicated in autoimmune disorders [21]. Recent studies have focused on understanding the mechanism of inhibition of cathepsin B by auranofin and in tuning the potency by alteration of the phosphine ligand [21–23]. The Ph_3P analogue of auranofin was found to be over 700 times more potent than auranofin in inhibiting cathepsin B [21], and the potency follows the order $PPh_3 > PEtPh_2 > PEt_2Ph > PEt_3$ [22]. Changing the thiolate ligand had little effect on the inhibition. By use of molecular modelling of the binding of different Au^I phosphine fragments to the cysteine residue at the active site of cathepsin B, the observed structure-activity relationships could be attributed to favourable interactions of the more sterically bulky Au^I-PR_3 fragments with the enzyme active site [22]. To fine-tune the activity, the steric and electronic properties of the phosphine ligand were systematically modified in the evaluation of a series of 13 complexes of type $R'R''R'''PAuCl$, revealing a dramatic impact on the ability to potently inhibit cathepsin B across the series. The addition of one positively charged amino group at the *para*-position of the triphenylphosphine resulted in the most potent inhibitor identified, with over 1200-fold greater potency than auranofin [23].

Other studies [26, 58, 59] have focused on cysteine-dependent PTPs, which play a prominent role in many cellular signalling events and have been implicated in a number of human diseases including autoimmune diseases such as RA. Whilst PTPs are of interest as therapeutic targets, the high degree of homology in the active sites of these enzymes is a barrier to achieving selectivity in PTP inhibitor development. By synthesis of a library of 40 complexes of type R_3PAuCl, and screening against a number of PTP substrates, (2-pyridine)Ph_2PAuCl was identified as one of the most potent and selective inhibitors of lymphoid tyrosine phosphatase (LYP) identified to date, with 10-fold selectivity for LYP over PTP-PEST, HePTP and CD45 [59]. The mechanism for LYP selective inhibition is attributed to coordination of Au^I by both the active site cysteine residue, as well as two cysteine residues in close proximity to the active site cysteine [58].

A series of four Au^{I} *N*-heterocyclic carbene (NHC) complexes of type (R_2Im)AuCl were also investigated as PTP selective inhibitors [26]. As discussed further in Section 9.3.1.3.1, an attractive option in future drug design of gold-based therapeutics is the use of NHC ligands to fine-tune the Au^{I} reactivity by systematic modification of the substituents on the simple imidazolium salt precursor. Ultimately, replacing the phosphine ligand of auranofin with an NHC ligand may offer an attractive alternative in the redesign of this orally-active DMARD, given that phosphine oxidation is likely to contribute to toxic side effects [3].

9.3 Gold complexes as anticancer agents

Gold-based drugs (both Au^{I} and Au^{III}) offer great potential as anticancer drugs, and have been the subject of intense recent investigation, because they have been shown to act by DNA-independent molecular mechanisms and hence have activity in tumours that are resistant to cisplatin and other anticancer drugs.

9.3.1 Gold(I) compounds

Gold(I) antitumour compounds have previously been broadly divided into two distinct classes based on coordination chemistry, lipophilic-cationic properties and propensity to undergo ligand exchange reactions with biological thiols and selenols [11, 60]. The two classes are (i) neutral, linear, two-coordinate complexes (auranofin and related compounds) and (ii) lipophilic cationic complexes such as $[Au(dppe)_2]^+$ and cationic Au^{I} NHC complexes. For both classes tumour cell mitochondria are likely targets [17], and the mechanism may involve apoptosis induction due to alteration of the thiol redox balance in cells, as a result of TrxR inhibition [17, 61, 62]. The single SeCys residue of this enzyme, which lies near the protein's *C*-terminus, is a likely binding site for Au^{I} [63]. A recent report [64] suggests a new mechanism for anticancer Au^{I} phosphine complexes as potent autophagy-inducing agents, as several different complexes were shown to enhance the accumulation of autophagosomes, which has recently been reported to be associated with cell death. A number of recent articles have reviewed the topic of gold-based anticancer agents in detail [3, 15, 17] and we focus here on how ligand design has been used to influence activity for these different classes of Au^{I} compounds.

9.3.1.1 Auranofin and related compounds

Auranofin was first reported to be cytotoxic (against HeLa cancer cells) in 1979 [65] and was shown subsequently to increase the survival times of mice with P388 leukaemia [66]. A comprehensive study involving 15 tumour models in mice [8] showed, however, that it was active only in this one tumour model. It is likely that high reactivity towards protein thiols (a characteristic feature of linear two-coordinate Au^{I} complexes) limits the antitumour activity of auranofin *in vivo*, as the cytotoxicity to cultured tumour cells *in vitro* was significantly reduced when the culture medium contained serum proteins [8]. In an interesting recent approach to address this problem, Stenzel and coworkers designed a polymeric version of deacetylated auranofin (**4**, Figure 9.2), which in micellar form displayed higher activity against human ovarian cancer cells than its small molecule analogue [67]. The concept provides the dual advantage of protecting auranofin from interaction with serum proteins, whilst allowing preferential accumulation in tumour tissue *via* the enhanced permeability and retention (EPR) effect. A related approach to drug delivery based on the EPR effect proposes the use of dendrimers [68], and a series of first to fourth generation (triazolato)Au^{I} dendrimers have been prepared from alkyne-terminated precursors and (tricyclohexylphosphine)Au^{I} azide. The first generation dendrimer is cytotoxic toward 3T3 mouse fibroblast cells and induces apoptosis.

In the 1980s a comprehensive structure activity study [73] investigated the *in vitro* cytotoxic activity and *in vivo* antitumour activity (against P388 leukaemia) of a series of 63 Au^{I} complexes of type LAuX, where

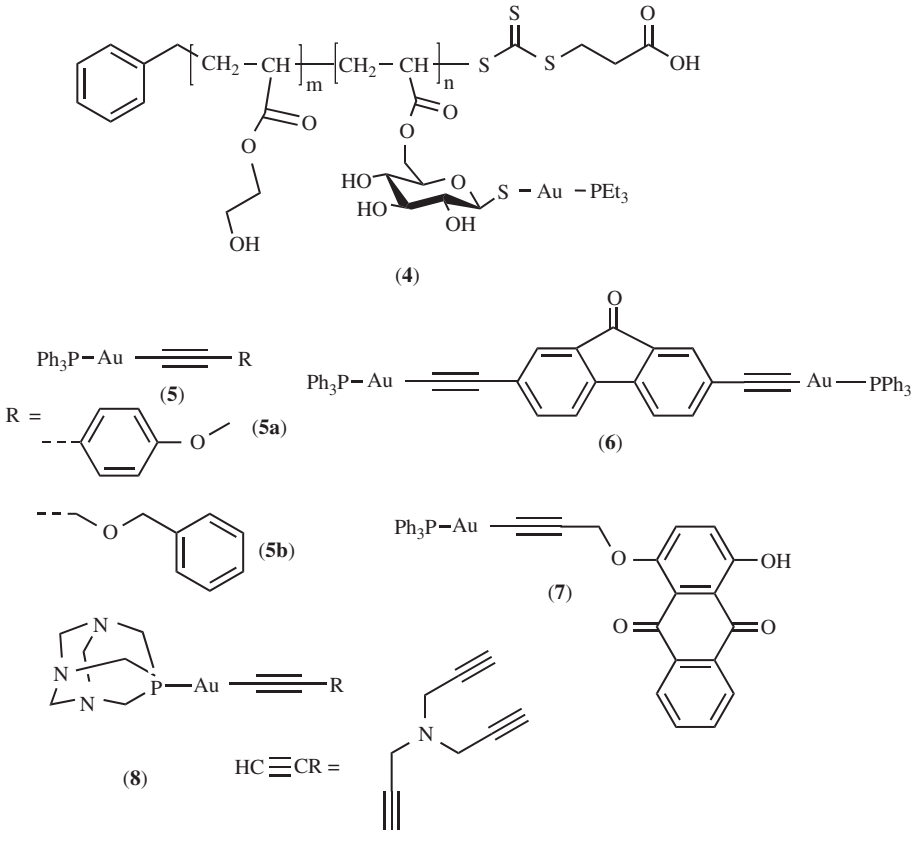

Figure 9.2 *Some recent examples of cytotoxic Au^{I} phosphine complexes incorporating ligand design: polymeric version of deacetylated auranofin (**4**) [67]; alkynyl phosphine Au^{I} complexes (**5a** and **b**) [69], (**6**) [70], (**7**) [71] and (**8**) [72]. The substituted anthroquinone ligand in complex **7** confers useful luminescent properties for application in cell imaging studies. Complex **8** is also luminescent and contains the water-soluble 1,3,5-triaza-7-phosphaadamantane (PTA) ligand*

L is generally, but not exclusively, a phosphine ligand. The highest *in vivo* antitumour activity was found for complexes with both phosphine and thiosugar ligands (i.e. auranofin analogues), and variation of the phosphine substituent modulated the antitumour activity. These early studies on Au^{I} compounds suggested that the phosphine ligands were a necessary requirement for activity [74], but antitumour activity has since been reported for linear Au^{I} complexes with NHC ([75] Section 9.3.1.3), cyclodiphosphazene [76], phosphole [77], pentafluorophenyl [78] and *N,N′*-disubstituted cyclic thiourea [79] ligands in place of phosphines. The role of the ligand is likely to be related to cellular uptake since polymeric Au^{I} thiolates (which do not readily enter cells) were found to exhibit very low cytotoxicity and were totally inactive against *i.p.* P388 leukaemia [73]. Aurothiomalate, in contrast to auranofin, is poorly effective in inhibiting TrxR and inducing apoptosis in Jurkat T cells [80]. Interestingly, however, both aurothiomalate and aurothioglucose exhibit potent antitumour effects *in vitro* and *in vivo* pre-clinical models of non-small cell lung cancer [81] and the mechanism has been attributed to selective targeting of Cys-69 within the PB1 domain of protein kinase Cι [82].

Despite the limited *in vivo* activity of auranofin, a large number of related complexes have been investigated in recent years and cytotoxic activity has been reported for a variety of other complexes of type

R_3PAuSR', with S-ligands such as thionucleobases and dithiocarbamates [14, 83], sulfanylpropenoates [84] and bioactive ligands such as vitamin K_3 [85], azacoumarin [86], naphthalimide [87, 88] and mercaptopteridine [89]. A number of studies [72, 90, 91] have used ligand design to increase water solubility through use of water-soluble phosphine ligands such as 1,3,5-triaza-7-phosphaadamantane (PTA), 3,7-diacetyl-1,3,7-triaza-5-phosphabicyclo[3.3.1]nonane (DAPTA) and triphenylphosphine trisulfonate (TPPTS). Improved water-solubility of triphenylphosphine Au^I complexes has also been addressed *via* the use of azolate (substituted pyrazolate and imidazolate) ligands [92]. Many of these studies report that the complexes inhibit isolated TrxR and exhibit cytotoxicity against human cell lines *in vitro*, but as for auranofin, facile reactions with protein thiols are likely to limit their application as anticancer agents.

A few recent studies have investigated alkynyl phosphine Au^I complexes [69, 70, 72, 93]. A series of six triphenylphosphine Au^I complexes with alkynyl ligands were cytotoxic to human cancer cells and showed strong inhibition of TrxR [69]. The Au–C bond is stronger than the Au–P bond, and hence such complexes offer the potential to be less reactive (more selective) in binding to protein targets. Mass spectrometry was used to investigate binding to a selenocysteine-containing model peptide for the most active TrxR inhibitors from this series (**5a** and **b**, Figure 9.2) and both Au(alkynyl) and $AuPPh_3$ fragments coordinated to selenocysteine were identified, showing that both phosphine and alkynyl ligands can be released. It is likely that a different mechanism of action is responsible for the antitumour activity of a dinuclear triphenylphosphine Au^I diethynylfluorene derivative (**6**, Figure 9.2), which has shown antitumour activity *in vivo* in the Hep3B xenograft model nude mice, with limited adverse effects on vital organs including liver and kidney [70]. The related compound which lacks the central carbonyl unit has low cytotoxicity, suggesting that the strong Au–C bond hinders binding of Au^I to protein targets. The generation of reactive oxygen species (ROS) from the carbonyl group of the central ligand spacer is believed to be essential for the cytotoxicity.

Ligand design has also been used to produce luminescent derivatives of cytotoxic Au^I phosphine complexes for application in cell imaging studies. A series of mono- and dimetallic Au^I triphenylphosphine complexes derived from 1,2-, 1,4- and 1,8-dialkynyloxyanthraquinones (e.g. **7**, Figure 9.2) have useful room-temperature anthraquinone-based visible luminescence, which allowed their successful application as fluorophores in cell imaging microscopy [71]. The luminescence of certain Au^Ialkyne complexes (e.g. **8**, Figure 9.2) has allowed their intracellular distribution to be probed by epifluorescence microscopy [72].

9.3.1.2 Tetrahedral Au^I diphosphines and related compounds

An early example of the use of ligand design in medicinal inorganic chemistry is the investigations of Au^I complexes with chelated diphosphines [74], and the development of $[Au(dppe)_2]Cl$ (**9**, Figure 9.3), shown to exhibit significant antitumour activity against a range of tumour models in mice [9]. Bis-chelated Au^I complexes undergo ligand exchange reactions *via* a ring-opening mechanism and, in contrast to auranofin, $[Au(dppe)_2]^+$ retains its structural integrity in the presence of thiols and in human plasma [9, 94]. Structure-activity relationships revealed that for complexes of the type $[Au(R_2P(CH_2)_nPR'_2)_2]Cl$, highest activity was found where $R = R' =$ phenyl and $n = 2,3$ or *cis*-CH=CH. In general, activity was reduced, or lost altogether, when the phenyl substituents on the phosphine were replaced by alkyl substituents, likely to be related to the ease of ligand oxidation [74, 95]. Structure-activity relationships for the series of linear digold complexes $ClAu(Ph_2P(CH_2)nPPh_2)AuCl$ ($n = 1–6$) and XAu(dppe)AuX (X = e.g. Cl, Br, OAc, SMan, SGlu, $SGlu(Ac)_4$ and $SMan(Ac)_4$) [96] showed that antitumour activity was related to whether they could undergo ring closure reactions to form bis-chelated $[Au(P\text{-}P)_2]^+$ species *in vivo*, by reaction with thiols [74, 94].

A recent study has investigated the influence of anion on the cytotoxicity of $[Au(dppey)_2]X$ (where dppey is *cis*-$Ph_2P(CH=CH)PPh_2$) and water-soluble halogen and triflate salts were approximately twice as potent towards MCF7 and MDA-MB-231 tumour cell lines compared with PF_6^- and BF_4^- derivatives [101].

An important aspect of the mechanism of action of $[Au(dppe)_2]^+$ and related antitumour compounds was identified [102] as stemming from their properties as 'delocalised lipophilic cations' (DLCs) [103], that accumulate in the mitochondria of tumour cells, driven by the elevated mitochondrial membrane potential that is a characteristic feature of these cells [104]. The high lipophilicity of $[Au(dppe)_2]^+$ results in its non-selective concentration into mitochondria, causing general membrane permeabilisation and accounting for the severe toxicities to heart, liver and lung that precluded clinical development [105–108]. The unfavourable toxicological profile was overcome through ligand design and replacement of the phenyl substituents with pyridyl groups, with the N atom in either the 2-, 3- or 4-position in the ring [97, 109]. The series of compounds of type $[Au(dnpype)_2]Cl$ (**10**, Figure 9.3) are structurally similar to $[Au(dppe)_2]Cl$ but the hydrophilic-lipophilic character spans a very large range. Antitumour activity in colon 38 tumours in mice was optimised for the 2-pyridyl analogue, with intermediate lipophilicity, and activity correlated with highest drug concentrations in plasma and tumour tissue [97]. This compound $[Au(d2pype)_2]Cl$, has been shown to accumulate preferentially in the mitochondrial fractions of cancer cells, driven by the mitochondrial membrane potential [109]. To further fine-tune the hydrophilic-lipophilic balance in the optimal range, the related compound $[Au(d2pypp)_2]^+$ (**11**,

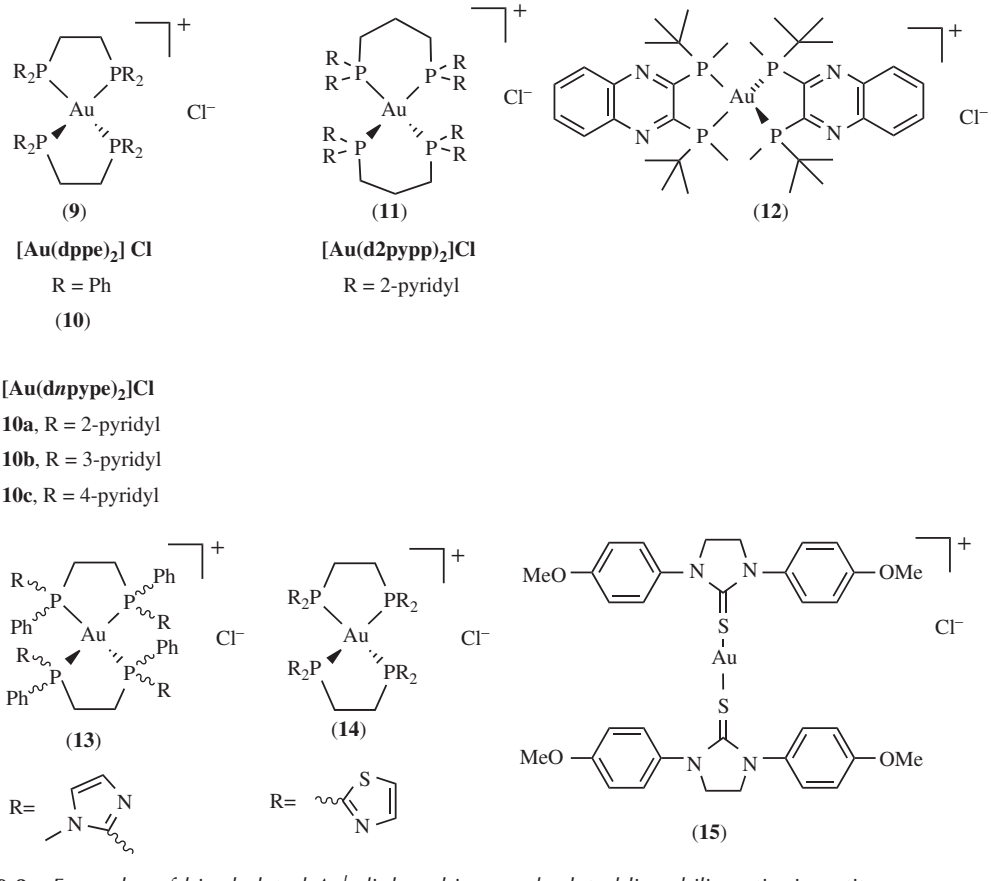

Figure 9.3 *Examples of bis-chelated Au^I diphosphines and related lipophilic cationic antitumour compounds: $[Au(dppe)_2]Cl$ (**9**) [9], $[Au(dnpype)_2]Cl$ (**10**) [97],$[Au(d2pypp)_2]Cl$ (**11**) [98], GC20 (**12**) [99], Au^I complexes of imidazole- (**13**) and thiazole-based (**14**) diphos-type ligands [100] and $[Au(TU)_2]Cl$ (**15**) [79]*

Figure 9.3), with the propyl-bridged 2-pyridylphosphine ligand (d2pypp), was designed with the idea of combining the features of the two distinct classes of Au^I phosphines, that is retaining the lipophilic cationic properties of the tetrahedral bis-chelated complexes that allow accumulation into mitochondria, but enhancing the reactivity towards protein thiols/selenols that underlies the inhibition of TrxR by auranofin [98, 110]. Ligand exchange reactions will be more facile, compared with $[Au(dppe)_2]^+$ and its pyridylphosphine analogues, due to the increased chelate ring size. $[Au(d2pypp)_2]^+$ is selectively toxic to breast cancer cells but not to normal breast cells and selectively induces apoptosis of breast cancer cells but not of normal breast cells [98]. The proposed mechanism (Figure 9.4) involves TrxR inhibition, *via* a chelate ring opening mechanism, following selective accumulation of the DLC in the mitochondria of cancer cells driven by the high membrane potential [98].

Other recent approaches have used ligand design to prepare other soluble bis-chelated Au^I disphosphine complexes. One approach incorporates a phosphinoquinoxaline ligand (**12**, Figure 9.3). This compound (GC20) has been shown to be strongly cytotoxic to a broad spectrum of human cancer cell lines and to significantly reduce tumour growth in several tumour xenograft mouse models. The mechanism is attributed to selective inhibition of TrxR [99]. Bis-chelated Au^I complexes of imidazole and thiazole-based diphos-type ligands have been investigated [100]. The complexes with intermediate lipophilicity (**13** and **14**, Figure 9.3) showed significant cytotoxic activity in different cell lines, induced apoptosis and inhibited TrxR and GSH reductase.

Also of interest in this series are hydrophilic four-coordinate Au^I complexes with monodentate phosphine ligands. $[Au(P(CH_2OH)_3)_4]Cl$ has been shown to be cytotoxic *in vitro* against several human tumour cell lines and a mouse tumour model *in vivo* [111], and to be well tolerated in pharmacokinetic studies in dogs [112]. Hydrophilic, monocationic $[Au(L)_4]PF_6$ complexes have been investigated where L is tris(hydroxymethyl)phosphine, PTA and tris(hydroxypropyl)phosphine, but these complexes have marginal cytotoxicity in human tumour cell lines and are less cytotoxic than Cu^I and/or Ag^I analogues [113].

Finally in the context of lipophilic cationic Au^I complexes is an Au^I complex of *N,N′*-disubstituted cyclic thiourea, $[Au(TU)_2]Cl$ (**15**, Figure 9.3), which has been shown recently to exhibit activity in NCI-H460 non-small cell lung model in mice, as well as inhibition of TrxR activity in cells and is one of the most potent TrxR inhibitors reported [79]. The complex is cationic and more similar in structure to the cationic Au^I NHC complexes described in the next section.

9.3.1.3 Au^I N-heterocyclic carbene compounds

NHCs are one of the most important and widely studied ligand classes in contemporary organometallic chemistry [114]. The main reason for this high level of interest is the outstanding activity of NHC-metal complexes in homogeneous chemical catalysis [115–118]. Many studies have shown that NHCs have similar properties to phosphines in the way they interact with metals and NHCs have been used in place of phosphines to prepare catalysts, perhaps most notably for the second generation Grubbs catalyst [116, 119]. In terms of ligand design, NHCs are attractive as they provide excellent framework flexibility and the synthesis of NHC-based ligands is often relatively straightforward. In addition, NHCs are chemically amendable for the conjugation to biomolecules (e.g. peptides and proteins). In comparison to phosphines, NHC-metal complexes, including those of gold, often show enhanced stability to air and moisture and this stability can be attributed to the robust metal-carbene bond and the strong σ-donating properties of NHCs.

Interest in the medicinal inorganic chemistry of NHC-metal complexes has grown considerably in recent years and developments in this field are described in several reviews [11, 120–124]. The biomedical applications of NHCs with the coinage metals Ag and Au have probably received the greatest attention, with Ag-NHC chemistry being directed towards the design of novel antimicrobial agents, while the main focus of Au-NHCs has been on the development of antitumour agents [125].

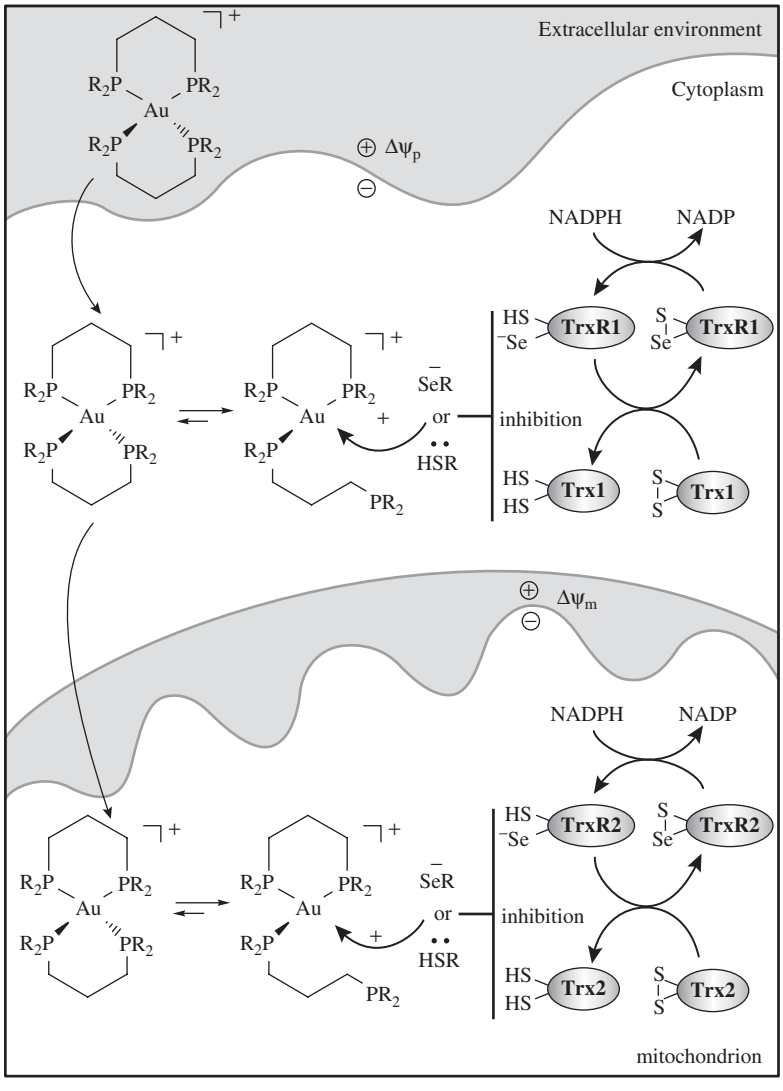

Figure 9.4 *Proposed mechanism of uptake and activity of [Au(d2pypp)$_2$]$^+$ in cells. Trx, thioredoxin and TrxR, thioredoxin reductase. Reprinted from Ref. [98] with permission from Elsevier*

Mononuclear complexes As discussed in Section 9.3.1, apoptotic cell death pathways mediated by the mitochondrion now represent an important target for the development of new anti-cancer agents. Utilising the framework flexibility of NHCs, a family of linear, cationic [Au(NHC)$_2$]$^+$ complexes (**16a–e**, Figure 9.5) were prepared. A range of different wingtip R groups (positions 1 and 3 on the imidazol-2-ylidene ring) were used to fine-tune the lipophilicity of the resultant complexes, with log *P* values varying across the series within a wide range from log *P* = −1.09 (R = Me) to 1.73 (R = cyclohexyl) [126]. An initial study showed that these cationic complexes induced cyclosporin A-sensitive swelling in isolated rat liver mitochondria, with the rate at which swelling occurred correlating with lipophilicity. These results suggest that compounds of this type could potentially target mitochondrial cell death pathways [126]. Subsequently it was shown that these

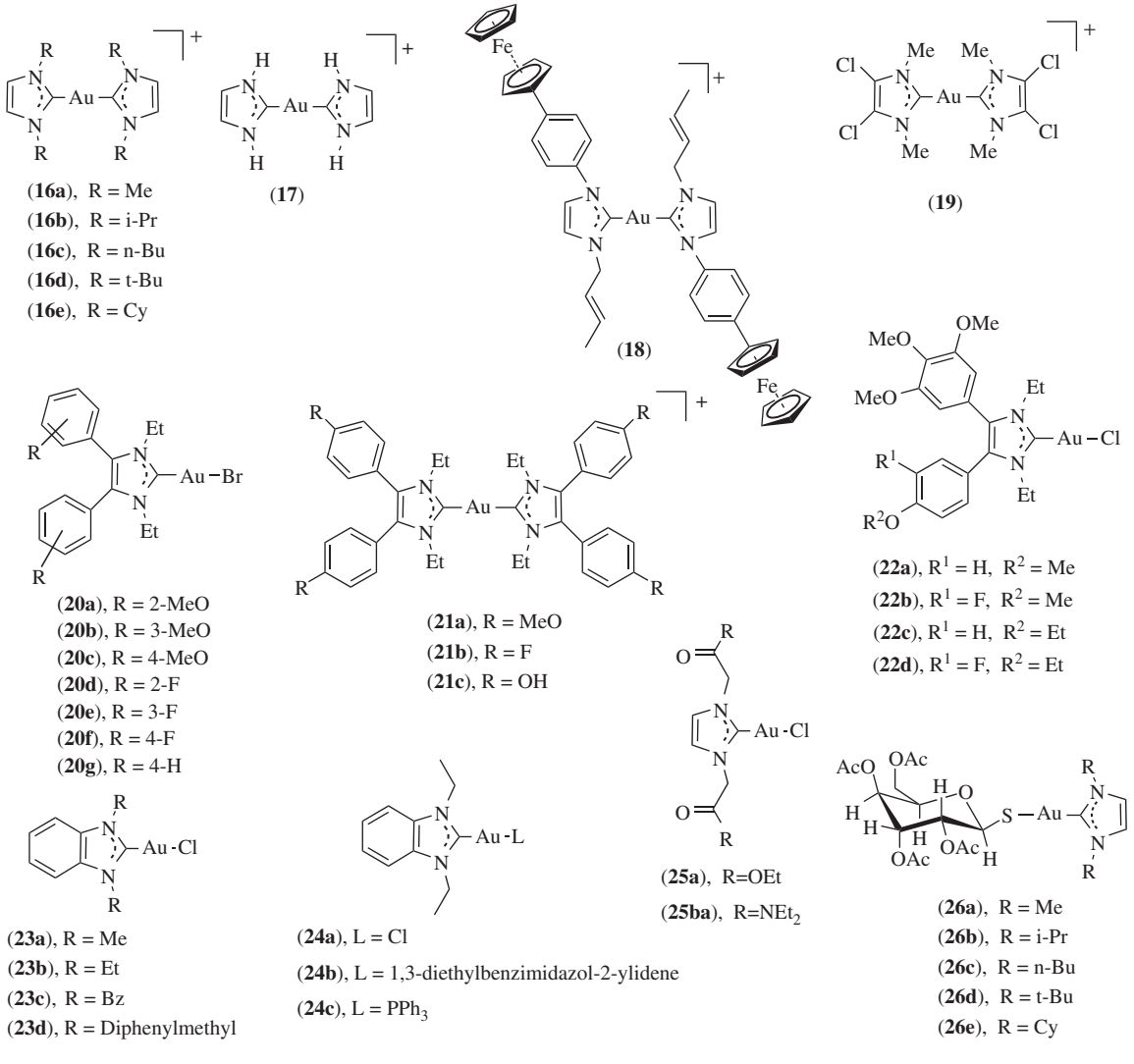

Figure 9.5 *Examples of mononuclear Au^{I} NHC complexes with antitumour activity*

complexes are selectively toxic in two highly tumourigenic breast cancer cell lines and not to normal breast cells, and the degree of selectivity and potency were optimised by modification of the R-group substituents and consequently the complex lipophilicity (Figure 9.6) [75]. Model studies with cysteine (Cys) and selenocysteine (Sec) showed that release of the NHC ligands occurs by two-step ligand exchange reactions and, at physiological pH, the rate constants for the reactions with Sec are 20- to 80-fold higher than those with Cys. Consistent with this result, the lead compound $[(i\mathrm{Pr}_2\mathrm{Im})_2\mathrm{Au}]^+$ (**16b**, Figure 9.5) was shown to accumulate in mitochondria of cancer cells and to cause cell death through a mitochondrial apoptotic pathway and (in treated cells) to inhibit the activity of (TrxR) but not the closely related and Se-free enzyme GSH reductase (Figure 9.6).

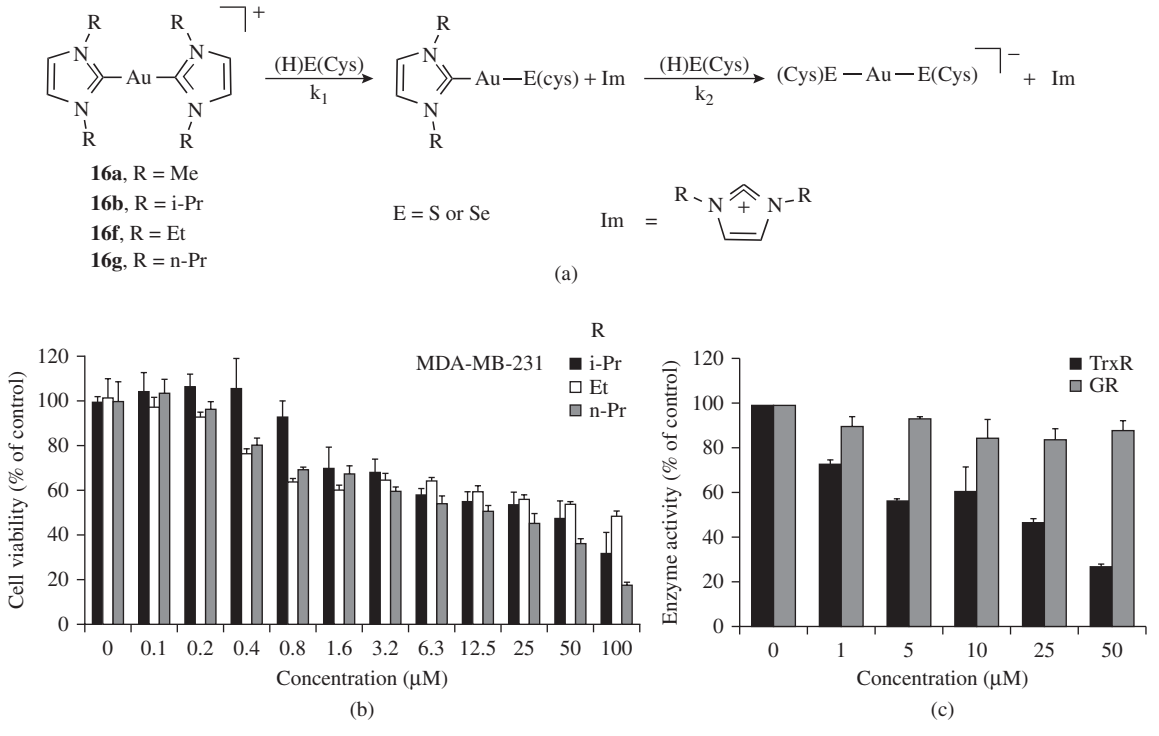

Figure 9.6 *(a) Mechanism for the reaction between the cationic Au^{I} N-heterocyclic complexes with Cys and Sec, which was shown (for **16a** and **b**) to occur by a two-step reaction involving displacement of the NHC ligands by the Cys/Sec. This provides a potential model of the reaction between the selenocysteine residues of TrxR reactions and the [(R$_2$Im)$_2$Au]$^+$ complexes. (b) Selective cytotoxicity of **16b**, **f** and **g** in MDA-MB-231 breast cancer cells. (c) Selective inhibition of intracellular thioredoxin reductase (TrxR) compared with glutathione reductase (GR) activity by [(i-Pr$_2$Im)$_2$Au]$^+$ (**16b**). Adapted with permission from Ref. [75]. Copyright © 2008 American Chemical Society*

The synthesis of a homoleptic bis-protic $[Au(NHC)_2]^+$ complex, (**17**, Figure 9.5) has recently been described [127]. This complex has excellent aqueous solubility and is stable under acidic conditions. Preliminary studies showed the complex had low cytotoxicity in two cancer cell lines, however increased toxicity was observed in cells which overexpressed the copper transporter CTR1 [127]. In an effort to further modulate the cytotoxic properties of cationic, $[Au(NHC)_2]^+$ complexes the NHC ligands were functionalised with ferrocene moieties, on the basis that Au^{I} complexes linked to ferrocene derivatives often exhibit strong cytotoxic effects. This compound (**18**, Figure 9.5) displayed significant cytotoxicity against a range of cancer cell lines [128].

In terms of ligand design, modification of the wingtip R-groups represents the most obvious approach to the modulation of the biological activity of Au-NHC complexes, as the appropriately substituted precursor imidazolium salts are often easily prepared. Positions 4 and 5 of the imidazol-2-ylidene ring represent alternative sites for the introduction of additional functionality. The cytotoxic properties of a cationic $[Au(NHC)_2]^+$ complex with chlorine atoms at positions 4 and 5 of the imidazol-2-ylidene ring (**19**, Figure 9.5) were evaluated in the NCI-H460 lung cancer cell line. However, this modification caused little difference in activity, with respect to the analogous compound with hydrogen atoms at positions 4 and 5 [129]. The antiproliferative

properties of neutral Au(NHC)L complexes of the same 4,5-dichloro-1,3-dimethylimidazol-2-ylidene NHC ligand (L = Cl^- or pyrimidine-2-thiolate) have also been evaluated in a series of human cancer cell lines [130].

A series of neutral complexes of the general form Au(NHC)X, where X = Br or Cl and the NHC is derived from 4,5-diarylimidazolium salts (**20a–g**, Figure 9.5), showed high growth inhibitory effects in MCF-7 and MDA-MB 231 breast cancer cells, as well as HT-29 colon cancer cells. It was found that the nature of the substituent on the aryl rings (OMe or F) influenced the growth inhibitory properties of the complex towards particular cell lines. Although relatively few substituents at positions 1 and 3 of the imidazol-2-ylidene ring were evaluated, these substituents and the oxidation state of the metal (Au^I and Au^{III}) were found to have a lesser effect on the biological properties of the complexes. The complexes inhibited TrxR in the micromolar range; however, results suggested the involvement of further biological targets [131]. Cationic $[Au(NHC)_2]^+$ complexes of the 4,5-diarylimidazol-2-ylidene ligands (**21a–c**, Figure 9.5) were also prepared and these compounds showed a marked increase in growth inhibition in the cancer cell lines investigated, with certain complexes being 10-times more active than cisplatin [132]. A closely related series of Au-NHC complexes have been prepared, which incorporate structural features of the drug Combretastatin A-4 (**22a–d**, Figure 9.5). These gold complexes displayed cytotoxicity in the micromolar range with significant variation amongst the cell lines investigated [133].

Based on the crystal structure of an Au-phosphole complex (GoPI), covalently bound in the active site of GSH reductase [134], a series of neutral Au(NHC)Cl complexes based on the benzimidazol-2-ylidene core (structurally related to the phosphole ligand) were prepared (**23a–d**, Figure 9.5) [135]. These complexes showed low reactivity with GSH under physiological conditions and selective inhibition of TrxR compared with GSH reductase was observed. The enzyme inhibition studies showed no relationship between the lipophilicity of the complex (*via* modification of the benzimidazol-2-ylidene nitrogen R-groups (alkyl or aryl)) and enzyme inhibition. Antiproliferative effects in cultured tumour cells occurred in the low micromolar range and results suggested that this was caused by the formation of ROS [135]. A series of complexes with the general formula Au(NHC)L, where NHC = 1,3-diethylbenzimidazol-2-ylidene and L = Cl, NHC or PPh_3, (**24a–c**, Figure 9.5) were evaluated in various biological assays. The cationic charge of **24b** and **24c** contributed to their cellular uptake (being approximately threefold higher than the neutral complex **24a**) and also increased levels of uptake in isolated mitochondria. Additionally the cationic complexes displayed increased cytotoxic properties [136].

The design and synthesis of water-soluble and biocompatible Au-NHC complexes has been the focus of several research groups. Probably the earliest examples of water-soluble Au-NHC complexes were prepared from a series of sulfonated imidazolium salts, for potential chemical catalytic applications, rather than biological studies [137]. Ester- and amide-functionalised imidazolium salts were used to prepare a series of neutral, water-soluble Au(NHC)Cl complexes (**25a** and **b**, Figure 9.5) [138]. The cytotoxic properties of these molecules were assessed in several human cancer cell lines and they were found to be potent inhibitors of TrxR in the nanomolar range [138].

In an early study, a series of neutral Au(NHC)X complexes were prepared, where X is the biologically relevant tetraacetylthioglucose ligand (**26a–e**, Figure 9.5), as NHC-based analogues of auranofin [139]. An extensive series of biofunctionalised, neutral Au(NHC)X complexes (X = 2′,3′,4′,6′-tetra-*O*-acetyl-β-D-glucopyranosyl-1-thiolato, proline, cysteine, alanine and L-DOPA, estradiol and saccharin) were synthesised and screened against LNCaP and MDA-MB 231 cancer cell lines. All but the NHC-auranofin analogue showed little or no activity in the evaluated cell lines [140].

Given the high level of interest in the antitumour properties of Au-NHC complexes, it is also pertinent to consider the potential cytotoxic properties of azolium salt, NHC ligand precursors. As discussed above [75], reaction of Au-NHC complexes with thiol- and selenol-containing biomolecules can cause loss of the NHC ligand and re-formation of the azolium salt. Despite this, there are few studies investigating the biological properties of the azolium precursors. One study has demonstrated that bis(benzimidazolium) salts do

possess anti-proliferative activity in a human colorectal cancer cell line (HCT 116). This study showed that the compounds evaluated exhibited dose dependent cytotoxicity, with IC_{50} values in the range between 0.1 and 17.6 μM [141].

Dinuclear complexes A variety of dinuclear Au^I-NHC complexes (e.g. **27, 28**, Figure 9.7), prepared from cyclophane-based bidentate imidazolium salts, were designed as DLCs with the potential to accumulate in the mitochondria of tumour cells [142]. The rates and levels of Au uptake into mitochondria for these compounds were measured; however, Au uptake did not correlate strongly with the rate at which the complexes induced mitochondrial swelling [143]. Structural analysis for a number of the synthesised complexes showed that, through relatively simple modifications to the cyclophane ligand framework, the intra-molecular distance between the gold atoms could be controlled. For example, compound (**27**), with an *ortho*-substitution pattern on the phenyl linker group, supports a short Au···Au interaction of 3.0485(3) Å, while a *meta*-substitution pattern on the aryl-linker (compound **28**) gave rise to a significantly longer Au···Au distance of 3.7917(4) Å [142]. Short Au···Au distances of less than 3.6 Å are generally considered to indicate the presence of an attractive (aurophilic) interaction and compounds displaying these short Au···Au are often luminescent. This relationship is clearly demonstrated by these molecules with (**27**) (Au···Au = 3.0485 Å) being luminescent (both in the solid state and in solution), whilst the *meta*-substituted compound (**28**) supporting the longer Au···Au distance (3.7917 Å) was not [142]. The luminescence profile of (**27**) (λ_{ex} 260 nm and λ_{em} 400 nm) was unsuitable for confocal fluorescence live cell imaging studies, as the high-energy excitation wavelength required would lead to non-specific absorption and auto-fluorescence from other cellular components. Ligand design was used to overcome this problem [144], based on observations that the excitation and emission energies associated with short Au···Au interactions are, in some cases, red-shifted as a result of a contraction of the Au···Au distance [145–148]. Guided by this qualitative relationship, a new dinuclear Au^I complex (**29**, Figure 9.7) was prepared. The unsymmetrical ligand yields the dinuclear complex in two isomeric forms, these being the *cis* (syn) and *trans* (anti) isomers. The *cis* isomer was selected for cellular localisation studies based on its higher aqueous solubility. The emission profile for (**29**) is highly sensitive to the nature of the anion and in the case of Br^-, excitation at 355 nm, gave rise to emission at 496 nm [144, 149]. This excitation and emission profile was suitable to allow study of the cellular distribution of (**29**) in a mouse macrophage (RAW264.7) cancer cell line using confocal fluorescence microscopy (Figure 9.7) [144]. Colocalisation studies using LysoTracker red (lysosome stain) and MitoTracker green (mitochondrial stain) suggested lysosomal rather than mitochondrial uptake for (**29**). Interestingly, it exhibits only modest cytotoxicity in this cell line and was shown to be remarkably unreactive with GSH after prolonged incubation under physiological conditions (pH 7, 37 °C).

This series of dinuclear Au^I NHC complexes was expanded by further modification of the supporting cyclophane ligand structure to include either benzimidazolylidene units in place of the imidazolylide units in **29**, or increasing the size of the cyclophane ring, by the incorporation of a butane-1,4-diyl (rather than propane-1,3-diyl) linker group [150]. The incorporation of the benzimidazolylidene units resulted in increased lipophilicity ($\log P = -1.15$) in comparison with **29** ($\log P = -2.36$), but a very similar intramolecular Au···Au distance (2.9329(1) Å). Whilst the increased cyclophane ring size resulted in non-luminescent complexes (presumably as a result of the longer intramolecular Au···Au distances), the uptake of the benzimidazolium derivative of **29** (25 μM) into live MDA MB 231 breast cancer cells has been tracked using the intense fluorescence originating from the Au^I complex. Significant uptake was observed in as little as 30 minutes, demonstrating that dinuclear Au^I-NHC complexes of this type may have application as luminescent cellular probes, where the luminescence and cellular uptake characteristics can be controlled by ligand design [151].

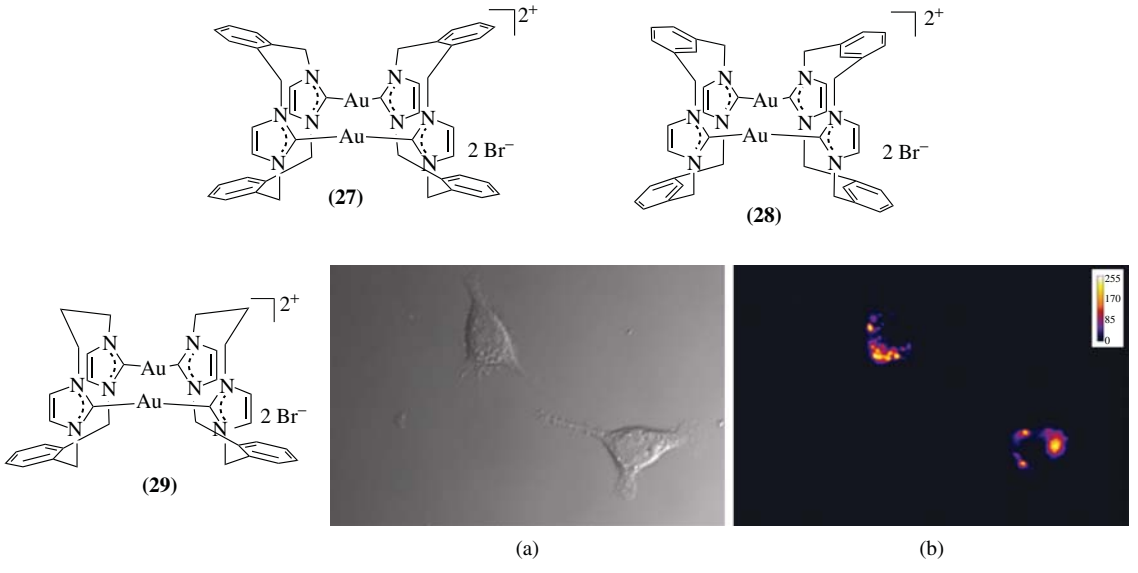

Figure 9.7 *Examples of dinuclear Au^{I} NHC complexes. Both (**27**) and (**29**) are luminescent as a result of a short Au···Au interaction. Ligand design was used to fine-tune the Au···Au distance in **29**, to obtain an ideal excitation wavelength for live cell imaging studies. The brightfield image (a) and luminescence image (λ_{ex} 351 nm) (b) of RAW264.7 cells after incubation with **29** for 15 hours at 37 °C. Adapted from [144]. (See plate section for the colour version of this figure)*

9.3.2 Gold (III) compounds

Considerable research interest has been directed towards the development of novel anti-cancer agents based on Au^{III}, in part this is due to similarities in the chemistry of Au^{III} and Pt^{II}, the latter metal being well known for its anti-cancer properties. Despite this, until relatively recently there were few known Au^{III} complexes with antitumour activity, including some dimethylgold(III) compounds with modest activity in *i.p.* P388 leukaemia in mice [152]. This early lack of success resulted mainly from the general low stability displayed by Au^{III} compounds under physiological conditions. Gold(III) compounds are prone to reduction to gold(I), due to the often high reduction potentials and fast rates of hydrolysis. However, in recent times a range of strategies have been used to stabilise the Au^{III} oxidation state and a variety of different classes of Au^{III} compounds have been shown to have significant antitumour properties. Some examples are shown in Figure 9.8 (see [10, 12, 15] for recent reviews).

A particularly important development in this area is the utilisation of organometallic compounds (incorporating C-donor ligands), which stabilise the Au^{III} oxidation state. Compound (**30**), which incorporates an anionic phenyl donor in the five-membered chelate ring, has been evaluated as a cisplatin analogue [153]. Differential toxicity in a panel of human tumour cell lines was observed and acetate and malonate derivatives were found to be moderately active *in vivo* against human carcinoma xenografts [154]. Based on the assumption that the carbon–gold(III) bond is important for the stabilisation of the Au^{III} centre, a series of cyclometallated complexes (e.g. **31** and **32**) [155, 156] were tested against a panel of human tumour cell lines, and significant activity was observed, with cytotoxicity values falling in the low μM range. Gold(III) complexes

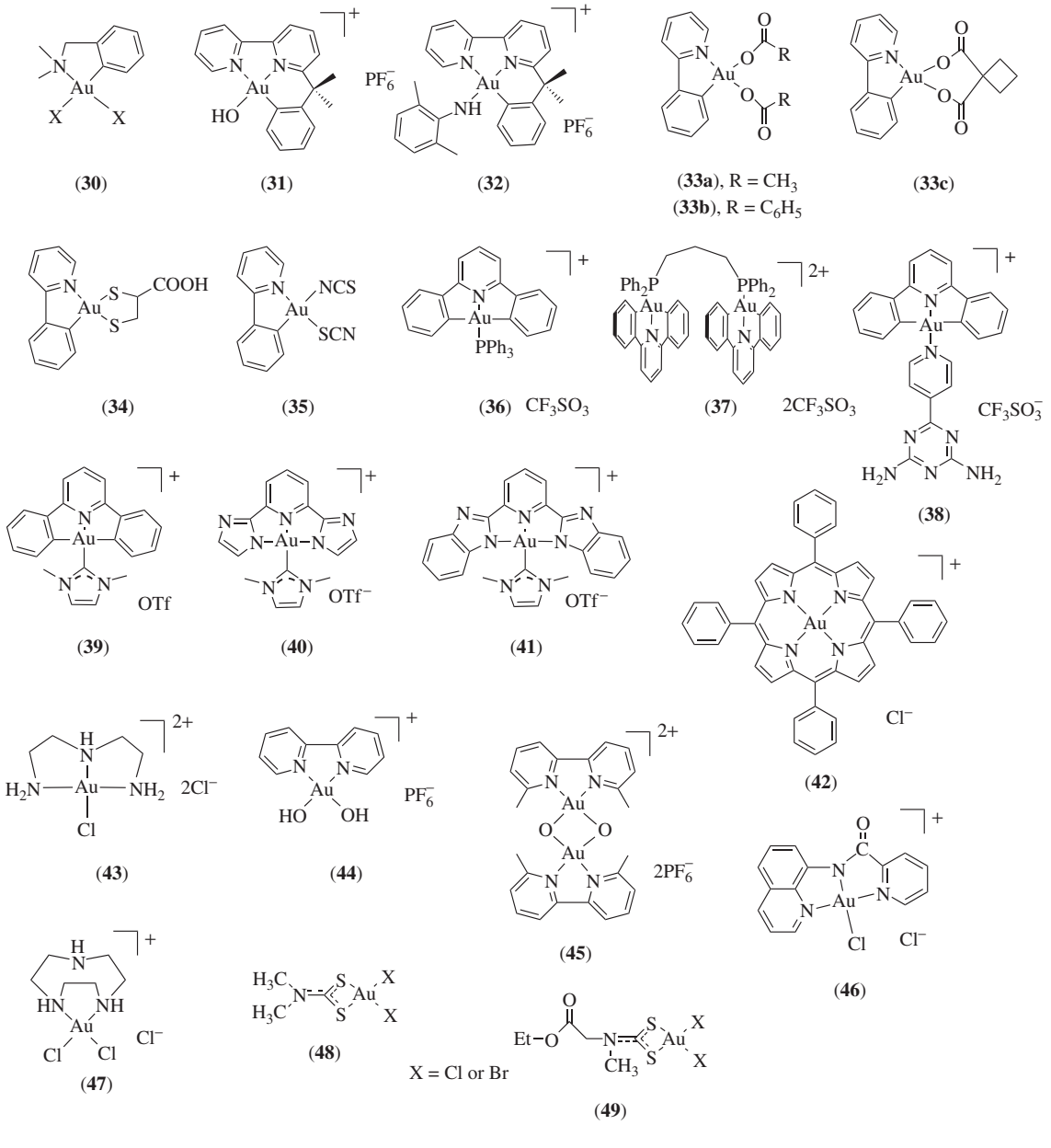

Figure 9.8 *Examples of Au^{III} complexes compounds with antitumour activity*

of cyclometallated 2-phenylpyridine with a variety of carboxylate (**33a–c**) [157] and thiolate (e.g. **34** and **35**) [158] ancillary ligands have been reported. Both groups of complexes were tested for cytotoxic properties against human (MOLT-4) and mouse (C2C12) cancer cell lines. Differential cytotoxicity was observed and the complexes displayed similar activity to cisplatin against the MOLT-4 cell line [157, 158].

A library of cyclometallated Au^{III} compounds of the form $[Au_m(C\hat{}N\hat{}C)_mL]^{n+}$ ($m = 1-3$; $n = 0-3$; HC^N^CH = 2,6-diphenylpyridine), which contain a variety of N-donor or phosphine ligands (L) have been prepared and their biological properties evaluated [159]. The choice of ligand L gave either mononuclear complexes (e.g. $L = PPh_3$, pyridine and 1-methylimidazole) or binuclear and trinuclear complexes (e.g. L = μ-bis(diphenylphosphino)C_n, where C_n is a saturated hydrocarbon linker with $n = 1-6$) (e.g. **36** and **37**). The compounds were stable under physiological conditions and in the presence of GSH and this stability was attributed to the dianionic cyclometallated [C^N^C] ligand. The prepared complexes were evaluated against a panel of cancer cell lines including a cisplatin-resistant variant, and the mononuclear complexes exerted anticancer potency comparable to that of cisplatin. The cytotoxic properties of these compounds appear to result from a variety of different mechanisms dependent on the nature of the auxiliary ligand, which influences the DNA-binding affinity. The dinuclear complex with the bridging bidentate ligand, dppp (1,3-bis(diphenylphosphino)propane) $[Au_2(C\hat{}N\hat{}C)_2(\mu\text{-dppp})]^{2+}$ (**37**) was the most cytotoxic of the complexes evaluated ($IC_{50} = \sim 50$ nM) and was found to interact only weakly with DNA. In a highly significant recent *in vivo* study, (**37**) was evaluated for the inhibition of tumour growth in nude mice bearing PLC cells and hepatocellular carcinoma (HCC)-bearing rats [160]. In the nude mice bearing PLC cells, 77% inhibition of tumour growth was observed compared with vehicle controls, whereas 28% inhibition was found for cisplatin. In the HCC-bearing rats the median survival time was increased from 30 days (control group) to 43 days [160]. Additionally, (**37**) is a potent inhibitor of TrxR and the obtained results suggested that cell death was induced by endoplasmic reticulum stress associated with TrxR inhibition [160]. Recently the $[Au^{III}(C\hat{}N\hat{}C)]^+$ core has been combined with the monodentate ligand 2,4-diamino-6-(4-pyridyl)-1,3,5-triazine (**38**). In acetonitrile solution this complex self-assembles into a supramolecular polymer. This novel polymeric material has been investigated as an agent for the sustained released of cytotoxic Au species (i.e. $[Au^{III}(C\hat{}N\hat{}C)]$-GSH adducts) and a higher level of cytotoxicity was observed in cancer cell lines than normal cells [161].

Given the success obtained for the $[Au(C\hat{}N\hat{}C)]^+$ core in conjunction with phosphine ligands, this work has recently been extended by the conjugation of NHC ligands, yielding a new series of lipophilic cationic anti-cancer agents [162]. As was the case for the previously described series of compounds, monodentate NHCs yielded mononuclear complexes (e.g. **39**) and bridging bidentate NHC ligands gave dinuclear complexes. In Tris-buffered solution (**39**) binds to calf-thymus DNA *via* an intercalative mechanism, and in addition it was found to inhibit the relaxation of super-coiled DNA by the enzyme topoisomerase I (TopoI) at concentrations lower than the established TopoI poison, camptothecin [162]. The $[Au(C\hat{}N\hat{}C)NHC]^+$ complexes were cytotoxic towards a panel of cancer cell lines in the low micromolar range and when evaluated *in vivo* in nude mice bearing PLC tumour cells, significant inhibition of tumour growth (47%) was observed [162].

A related series of Au^{III} complexes, which incorporate N^N^N and NHC ligands, have been recently reported (e.g. **40** and **41**) [163]. These complexes are stable in aqueous solution, however they are rapidly reduced by GSH accompanied by the loss of the tridentate ligand and the formation of $[Au^{I}(NHC)(GSH)]$ and GSSG. The precursor Au^{III} complexes are non-emissive but upon reduction with GSH the highly fluorescent tridentate ligand is released, serving as a fluorescent probe for GSH. The complexes inhibited the growth of a panel of different cancer cell lines, with IC_{50} values ranging from 1.4–55 μM [163].

Che and co-workers [164–175] have studied extensively a series of Au^{III} complexes of porphyrin ligands, which show potent *in vitro* anticancer properties towards a range of human cancer cell lines with some selectivity for cancer cells over normal cells. The dianionic porphyrinato ligands form square-planar monocationic Au^{III} complexes, which are stable in buffered aqueous solution and in the presence of GSH [164]. The prototypical compound $[Au^{III}(TPP)]Cl$ (**42**), which has been studied most extensively, exhibits promising *in vivo* activity against HCC [166], nasopharyngeal carcinoma [170] and colon cancer [173]. Additionally, when compared with the cytotoxicity in the cancer cell lines, this compound (**42**) is less cytotoxic towards normal

cells such as lung fibroblasts [172, 176]. It is proposed that the compound interacts with biomolecular targets through non-covalent interactions as no reduction in activity occurs in the presence of foetal calf serum [168].

The *in vivo* antitumour effects of $[Au^{III}(TPP)]^+$ was investigated in a rat HCC model [166]. In this study the gold drug was injected directly into the tumour at different doses and significantly prolonged survival was seen for the HCC-bearing rats compared with the vehicle control group. In a more recent study $[Au^{III}(TPP)]^+$ was found to prolong the survival of NPC metastasis-bearing mice and markedly reduced tumour microvessel formation [177]. It appears that the anticancer activity of $[Au^{III}(TPP)]^+$ occurs *via* an apoptotic pathway [164]. Rapid depletion of the mitochondrial membrane potential is found to occur shortly after cellular uptake and additionally Bcl-2 protein suppression is observed. These findings suggest that cell death occurs *via* caspase-dependent and caspase-independent mitochondrial cell death pathways [165–167].

The reduction potential of Au^{III} complexes may be lowered by the use of simple chelating polyamines (e.g. $[Au(en)_2]Cl_3$ and $[Au(dien)Cl]Cl_2$ (**43**) [178]) and 2,2′-bipyridyl-based ligands such as $[Au(bipy)(OH)_2]PF_6$ (**44**) [179]. More recently a series of structurally related oxo-bridged dinuclear Au^{III} compounds, with the general structure $[Au_2(\mu\text{-}O)_2(N\text{^}N)_2](PF_6)_2$, where *N*^*N* is 2,2′-bipyridine or a substituted 2,2′-bipyridine [180, 181] (e.g. **45**), were found to have good stability under physiological conditions. In a recent study the activity of 13 of these compounds (including the cyclometallated compounds **31** and **32**) were evaluated against a panel of human tumour cell lines. This study identified a variety of DNA-independent molecular mechanisms for the cytotoxic properties, based on analysis with the Compare algorithm [182]. The results showed a relationship between complex reactivity (redox properties and stability in aqueous solution) and cytotoxicity. For example, $[Au(cyclam)]^{3+}$ is very stable towards both reduction and ligand substitution reactions [178] and is not cytotoxic (IC_{50} values > 100 μM [178]). Increased complex reactivity led to increased cytotoxic properties, for example the dinuclear Au^{III} oxo complexes were reduced by GSH and ascorbic acid at physiologically relevant concentrations [181], and the compound $[Au_2(\mu\text{-}O)_2(6,6'\text{-}Me_2bipy)_2](PF_6)_2$, that is most easily reduced, was ranked highest in terms of tumour selectivity and cytotoxic potency [182]. Guo and co-workers have reported cytotoxic Au^{III} complexes with aminoquinoline (e.g. **46**) [183] and 1,4,7-triazacyclononane (TACN) (**47**) ligands [184], as well as several Au^{III} terpyridine derivatives [185] that extended earlier study on $[Au(terpy)Cl]Cl_2$ [178]. These complexes are not reduced by GSH and there is a correlation between DNA-binding affinity and cytotoxicity suggesting that, in contrast to most Au^{III} complexes, DNA is a possible target.

Gold(III) complexes of dithiocarbamate ligands [186–190] have received sustained attention as potential antitumour agents. The complexes $[Au(DMDT)X_2]$ (**48**) and $[Au(ESDT)X_2]$ (**49**) (where DMDT = *N*,*N*-dimethylthiocarbamate and ESDT = ethylsarcosinedithiocarbamate; X = Cl, Br) are more cytotoxic *in vitro* than cisplatin (including in human tumour cell lines intrinsically resistant to cisplatin) [186]. A representative compound of this series $[Au(DMDT)Br_2]$ was shown to significantly inhibit the growth of MDA-MB-231 breast cancer xenografts in nude mice [188]. More recently the effects of Au^{III}-dithiocarbamato compounds (**48** and **49**) on mitochondrial functions have been examined and results show that the compounds trigger cell death by activating both apoptotic and non-apoptotic pathways. The compounds induce mitochondrial membrane permeabilisation and stimulate ROS formation and strongly inhibit the activity of TrxR [191].

9.4 Gold complexes as antiparasitic agents

There is urgent need for affordable antiparasitic drugs to tackle tropical diseases, such as malaria (more information in Chapter 8), sleeping sickness, Chagas' disease and leishmaniasis, that are major health problems in poverty-stricken areas [28]. A recent review has highlighted that tropical diseases affect more than two

billion people worldwide and cause nearly 2 million deaths per year [192]. Medicinal inorganic chemistry has a long history in this field (for example antimony compounds are still used for treatment of some forms of leishmaniasis) and there has been a resurgence of interest over the past few years in the development of metal-based antiparasitic agents, with particular emphasis on gold compounds. We consider here two different approaches to ligand design: (i) gold compounds that incorporate known 'organic' antiparasitic drugs and (ii) the potential to design compounds that are specific for unique validated thiol/selenol protein drug targets.

9.4.1 Metal drug synergism

A recent review by Navarro [28] has discussed the concept of 'metal-drug synergism' in the design of gold compounds in the treatment of parasitic diseases, in which a conventional organic drug is complexed to a metal ion to achieve longer residence time of the drug in the organism and more efficient biological targeting. For example the emergence of chloroquine (CQ)-resistant malarial parasites has been a major setback in the control of malaria and the Au^{I} complex $[Au(PPh_3)(CQ)]PF_6$ (**50**, Figure 9.9) is very effective against two CQ resistant strains of *P. falciparum* [193]. In the case of Chagas' disease, 2-mercaptopyridine *N*-oxide (mpo) can block *T. cruzi* growth through inhibition of NADH–fumarate reductase, affecting all stages of a parasite's cycle without affecting mammalian cells. The Au^{I} complex $[Au_2(mpo\text{-}H)_2(PPh_3)_2]$ (**51**, Figure 9.9) showed significantly increased activity compared with mpo on epimastigotes of different *T. cruzi* strains and was more active than nifurtimox, one of the conventional drugs used for treatment of Chagas' disease. There was a clear correlation between parasite inhibition and enzyme inhibition, highlighting NADH–fumarate reductase as the probable main target of $[Au_2(mpo\text{-}H)_2(PPh_3)_2]$ [194].

9.4.2 Emerging parasite drug targets for gold compounds

Very recent research highlights that gold-based drugs offer enormous potential in this field due to the variety of thiol and selenol proteins that have been identified as drug targets in trypanosomes (African sleeping sickness, Chagas' disease and leishmaniasis), malaria-causing plasmodia and schistosomiasis [30, 39, 195]. Reports on the activity of gold compounds are starting to appear and there is much potential to explore the use of ligand design to optimise inhibition of these specific enzyme targets.

The cysteine proteases of the trypanosomatid parasitic protozoa have been validated as drug targets for the treatment of Chagas' disease and leishmaniasis [195]. In a recent study one Au^{III} cyclometallated compound was included amongst several metal compounds tested on the parasitic cysteine proteases, cruzain from *T. cruzi* and cpB from *L. major* [195].

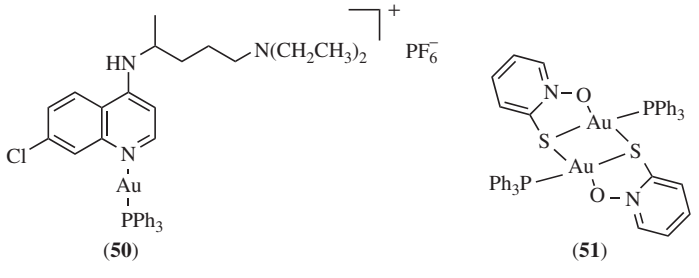

Figure 9.9 *Antiparasitic gold drugs based on the concept of metal-drug synergism: (**50**) $[Au(PPh_3)(CQ)]PF_6$ (CQ is chloroquine) [191] and (**51**) $[Au_2(mpo\text{-}H)_2(PPh_3)_2]$ (mpo is 2-mercaptopyridine N-oxide) [192]*

Important differences between the redox metabolism of the host and parasite can be exploited to develop new drugs [30]. For example, trypanosomatids have a unique redox metabolism based on the thiol-polyamine conjugate trypanothione and the flavoenzyme TR, which replaces glutathione reductase (GR) and probably also TrxR in these parasites. TR is a target in both trypanosomiasis and leishmaniasis. A recent study has shown that auranofin strongly inhibits TR, thereby killing the *Leishmania* parasite. The X-ray structure of TR from *Leishmania infantum* in complex with auranofin reveals a dual mechanism of enzyme inhibition with gold bound to the two active site cysteine residues, and the thiosugar moiety of auranofin bound to the trypanothione binding site [29].

Schistosomiasis is a tropical disease affecting more than 200 million people and in *S. mansoni* both TrxR and GR are absent and replaced by a unique selenium-containing enzyme, thioredoxin glutathione reductase (TGR) [196]. The enzyme is efficiently inhibited by the Au^{I} antiarthritic drugs auranofin, aurothioglucose and aurothiomalate, with auranofin being particularly potent ($K_i = 10$ nM) [39]. Auranofin was shown to kill parasites rapidly in culture at physiological concentrations and to partially cure mice infected by *S. mansoni* [39].

For malaria, both TrxR [197] and the cysteine protease falcipains [198] are possible drug targets for gold compounds. Auranofin and a few related gold complexes were shown to strongly inhibit *P. falciparum* growth *in vitro* [38], and whilst the effects were first attributed to the direct inhibition of *P. falciparum* TrxR, more recent studies investigating a variety of gold (and other metal) compounds have shown that multiple mechanisms are more likely [199–201]. A number of Au^{I} and Au^{III} compounds cause pronounced inhibition of falcipain 2 (Fp2) and effectively block *P. falciparum* growth *in vitro*, but no direct correlation was established between Fp2 inhibition and reduction of *P. falciparum* growth [199, 201]. Apart from direct inhibition of TrxR and falcipains, gold compounds could act by inducing severe oxidative stress to which *P. falciparum* is extremely sensitive [202].

In a recent example of ligand design, and metal drug synergism, several Au^{I} thiosemicarbazone (TSC) complexes were synthesised and evaluated for antimalarial activity [201]. (See Chapter 7 for more details of this ligand class). TSCs have been identified as antitrypanosomal inhibitors of cruzain – an important cysteine protease in the life cycle of *T. cruzi* (see above) and therefore complexes were designed as potential inhibitors of the malarial cysteine protease Fp2. The Au^{I} complexes of type $[Au(TSC)_2]Cl$ incorporated TSC ligands shown to exhibit significant activity against cruzain and trypanocidal activity in cell cultures. The Au^{I} complexes exhibited both enhanced efficacy against *P. falciparum* (CQ-sensitive and -resistant strains) and enhanced inhibition of Fp2 compared with the free TSC ligands. Once again there was no direct correlation between their antiplasmodial activity and the ability to inhibit Fp2, indicating that multiple mechanisms are likely [201].

9.5 Concluding remarks: Design of gold complexes that target specific proteins

The last decade has seen remarkable interest in the therapeutic potential of gold compounds and the field is no longer reliant on serendipity, but is now underpinned by ligand design, building on the experience of nearly a century of clinical use of antiarthritic gold compounds. This new era has been stimulated by identification of new thiol/selenol disease targets [17], and proteomic approaches continue to uncover new pathways and possible protein targets for therapeutic gold compounds [203, 204].

While there is much potential to use ligand design to fine-tune interactions within an enzyme active site, and hence to design gold compounds as specific enzyme inhibitors, the real challenge in the development of useful therapeutic gold agents is to consider also the complex biotransformation reactions of gold that are known to occur *in vivo*. For example, for Au^{III} compounds reduction to Au^{I} is likely to occur, as has been demonstrated recently for selected cytotoxic Au^{III} compounds (e.g. **31** and **45**, Figure 9.8), which were shown to produce stable Au^{I} adducts upon reaction with the copper chaperone Atox-1 [205].

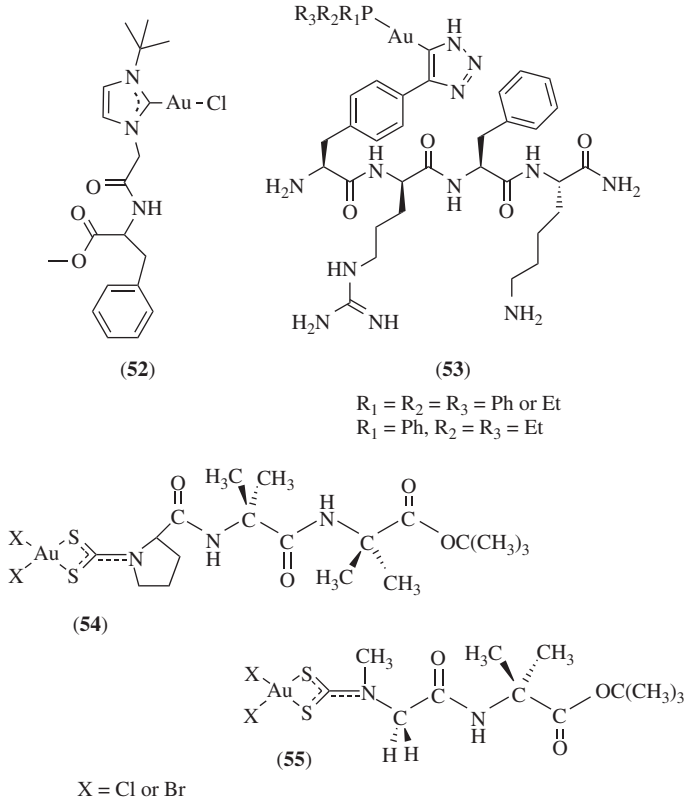

Figure 9.10 *Recent examples of gold compounds designed to target peptide transporters*

A particularly exciting recent development has been the design of gold-based anticancer peptidomimetics for targeted drug delivery [206–209]. NHCs are particularly well suited to conjugation to biomolecules and a phenylalanine-NHCAuCl conjugate (**52**, Figure 9.10) showed significant cytotoxic activity in HeLa, HepG2 and HT-29 cancer cell lines [206]. A non-catalysed [3+2] cycloaddition reaction was used to couple a precursor (phosphine)Au^{I}-azide complex with an alkynyl peptide. This approach provides both the coordinated NHC ligand (derived from 1,2,3-triazole) and the bioconjugate in one step (**53**, Figure 9.10). A tetrapeptide, mitochondrial-targeting sequence was used and the resultant complexes showed strong antiproliferative activity in a range of cancer cell lines including p53-mutant MDA-MB231 breast cancer cells. Additionally the bioconjugates were strong selective inhibitors of TrxR [207]. A related approach has seen the development of 'second generation' Au^{III} dithiocarbamate derivatives of oligopeptides, as improved drug delivery systems supported by peptide transport proteins [208, 209]. The Au^{III} dithiocarbamate-dipeptide bioconjugates (e.g. **54** and **55**, Figure 9.10) specifically target two peptide transporters (namely, PEPT1 and PEPT2), which are upregulated in several tumour cells. The α-aminoisobutyric acid-containing complexes displayed the highest cytotoxicity levels toward a series of human tumour cell lines, with IC_{50} values lower than that of cisplatin [208, 209]. These approaches pave the way for the design of gold-based peptide conjugates that can specifically target malignant cells, for example by overexpression of certain membrane receptors.

Acknowledgements

The Australian Research Council is acknowledged for financial support. We thank Dr Louise Wedlock for helpful comments on the manuscript.

References

1. Higby, G.J. (1982) Gold in medicine. *Gold Bull.*, **15**, 130–140.
2. Zhao, H. and Ning, Y. (2001) China's ancient gold drugs. *Gold Bull.*, **34**, 24–29.
3. Berners-Price, S.J. (2011) Gold-based therapeutic agents: a new perspective, in *Bioinorganic Medicinal Chemistry* (ed E. Alessio), Wiley-VCH Verlag GmbH, Weinheim, pp. 197–221.
4. Kean, W.F., Forestier, F., Kassam, Y. *et al*. (1985) The history of gold therapy in rheumatoid disease. *Semin. Arthritis Rheu.*, **14**, 180–186.
5. Eisler, R. (2003) Chrysotherapy: a synoptic review. *Inflamm. Res.*, **52**, 487–501.
6. Sutton, B.M., McGusty, E., Walz, D.T. and DiMartino, M.J. (1972) Oral gold. Antiarthritic properties of alkylphosphinegold coordination complexes. *J. Med. Chem.*, **15**, 1095–1098.
7. Sutton, B.M. (1986) Gold compounds for rheumatoid arthritis. *Gold Bull.*, **19**, 15–16.
8. Mirabelli, C.K., Johnson, R.K., Sung, C.M. *et al*. (1985) Evaluation of the *in vivo* antitumor activity and *in vitro* cytotoxic properties of auranofin, a coordinated gold compound, in murine tumor models. *Cancer Res.*, **45**, 32–39.
9. Berners-Price, S.J., Mirabelli, C.K., Johnson, R.K. *et al*. (1986) *In vivo* antitumor activity and *in vitro* cytotoxic properties of bis[1,2-bis(diphenylphosphino)ethane]gold(I) chloride. *Cancer Res.*, **46**, 5486–5493.
10. Messori, L. and Marcon, G. (2004) Gold complexes as antitumor agents. *Met. Ions Biol. Syst.*, **42**, 385–424.
11. Barnard, P.J. and Berners-Price, S.J. (2007) Targeting the mitochondrial cell death pathway with gold compounds. *Coord. Chem. Rev.*, **251**, 1889–1902.
12. Gabbiani, C., Casini, A. and Messori, L. (2007) Gold(III) compounds as anticancer drugs. *Gold Bull.*, **40**, 73–81.
13. Casini, A., Hartinger, C., Gabbiani, C. *et al*. (2008) Gold(III) compounds as anticancer agents: relevance of gold-protein interactions for their mechanism of action. *J. Inorg. Biochem.*, **102**, 564–575.
14. Tiekink, E.R.T. (2008) Anti-cancer potential of gold complexes. *Inflammopharmacology*, **16**, 138–142.
15. Ott, I. (2009) On the medicinal chemistry of gold complexes as anticancer drugs. *Coord. Chem. Rev.*, **253**, 1670–1681.
16. Nobili, S., Mini, E., Landini, I. *et al*. (2010) Gold compounds as anticancer agents: chemistry, cellular pharmacology, and preclinical studies. *Med. Res. Rev.*, **30**, 550–580.
17. Berners-Price, S.J. and Filipovska, A. (2011) Gold compounds as therapeutic agents for human diseases. *Metallomics*, **3**, 863–873.
18. Gromer, S., Urig, S. and Becker, K. (2004) The thioredoxin system – from science to clinic. *Med. Res. Rev.*, **24**, 40–89.
19. Fricker, S.P. (2010) Cysteine proteases as targets for metal-based drugs. *Metallomics*, **2**, 366–377.
20. Fricker, S.P. (2007) Metal based drugs: from serendipity to design. *Dalton Trans.*, 4903–4917.
21. Gunatilleke, S.S. and Barrios, A.M. (2006) Inhibition of lysosomal cysteine proteases by a series of Au(I) complexes: a detailed mechanistic investigation. *J. Med. Chem.*, **49**, 3933–3937.
22. Gunatilleke, S.S., de Oliveira, C.A.F., McCammon, J.A. and Barrios, A.M. (2008) Inhibition of cathepsin B by Au(I) complexes: a kinetic and computational study. *J. Biol. Inorg. Chem.*, **13**, 555–561.
23. Gunatilleke, S.S. and Barrios, A.M. (2008) Tuning the Au(I)-mediated inhibition of cathepsin B through ligand substitutions. *J. Inorg. Biochem.*, **102**, 555–563.
24. Weidauer, E., Yasuda, Y., Biswal, B.K. *et al*. (2007) Effects of disease-modifying anti-rheumatic drugs (DMARDs) on the activities of rheumatoid arthritis-associated cathepsins K and S. *Biol. Chem.*, **388**, 331–336.
25. Zhu, Y., Cameron, B.R., Mosi, R. *et al*. (2011) Inhibition of the cathepsin cysteine proteases B and K by square-planar cycloaurated gold(III) compounds and investigation of their anti-cancer activity. *J. Inorg. Biochem.*, **105**, 754–762.

26. Krishnamurthy, D., Karver, M.R., Fiorillo, E. *et al*. (2008) Gold(I)-mediated inhibition of protein tyrosine phosphatases: a detailed *in vitro* and cellular study. *J. Med. Chem.*, **51**, 4790–4795.
27. Zhang, Z.-Y. (2002) Protein tyrosine phosphatases: structure and function, substrate specificity, and inhibitor development. *Annu. Rev. Pharmacol. Toxicol.*, **42**, 209–234.
28. Navarro, M. (2009) Gold complexes as potential anti-parasitic agents. *Coord. Chem. Rev.*, **253**, 1619–1626.
29. Ilari, A., Baiocco, P., Messori, L. *et al*. (2012) A gold-containing drug against parasitic polyamine metabolism: the X-ray structure of trypanothione reductase from *Leishmania infantum* in complex with auranofin reveals a dual mechanism of enzyme inhibition. *Amino Acids*, **42**, 803–811.
30. Krauth-Siegel, R.L., Bauer, H. and Schirmer, H. (2005) Dithiol proteins as guardians of the intracellular redox milieu in parasites: old and new drug targets in trypanosomes and malaria-causing plasmodia. *Angew. Chem. Int. Ed.*, **44**, 690–715.
31. Fillat, M.F., Gimeno, M.C., Laguna, A. *et al*. (2011) Synthesis, structure and bactericide activity of (aminophosphane)gold(I) thiolate complexes. *Eur. J. Inorg. Chem.*, **2011**, 1487–1495.
32. Jackson-Rosario, S. and Self, W.T. (2009) Inhibition of selenium metabolism in the oral pathogen *Treponema denticola*. *J. Bacteriol.*, **191**, 4035–4040.
33. Jackson-Rosario, S., Cowart, D., Myers, A. *et al*. (2009) Auranofin disrupts selenium metabolism in *Clostridium difficile* by forming a stable Au-Se adduct. *J. Biol. Inorg. Chem.*, **14**, 507–519.
34. Blodgett, R.C.J., Heuer, M.A. and Pietrusko, R.G. (1984) Auranofin: a unique oral chrysotherapeutic agent *Semin. Arthritis Rheu.*, **13**, 255–273.
35. Shapiro, D.L. and Masci, J.R. (1996) Treatment of HIV associated psoriatic arthritis with oral gold. *J. Rheumatol.*, **23**, 1818–1820.
36. Fonteh, P.N., Keter, F.K. and Meyer, D. (2010) HIV therapeutic possibilities of gold compounds. *Biometals*, **23**, 185–196.
37. Lewis, M.G., Dafonseca, S., Chomont, N. *et al*. (2011) Gold drug auranofin restricts the viral reservoir in the monkey AIDS model and induces containment of viral load following ART suspension. *AIDS*, **25**, 1347–1356.
38. Sannella, A.R., Casini, A., Gabbiani, C. *et al*. (2008) New uses for old drugs. Auranofin, a clinically established antiarthritic metallodrug, exhibits potent antimalarial effects in vitro: mechanistic and pharmacological implications. *FEBS Lett.*, **582**, 844–847.
39. Kuntz, A.N., Davioud-Charvet, E., Sayed, A.A. *et al*. (2007) Thioredoxin glutathione reductase from *schistosoma mansoni*: an essential parasite enzyme and a key drug target. *PLoS Med.*, **4**, 1071–1086.
40. Debnath, A., Parsonage, D., Andrade, R.M. *et al*. (2012) A high-throughput drug screen for Entamoeba histolytica identifies a new lead and target. *Nat. Med.*, **18**, 956–960.
41. Chong, C.R. and Sullivan, D.J. (2007) New uses for old drugs. *Nature*, **448**, 645–646.
42. Shaw, C.F. III, (1999) Gold complexes with anti-arthritic, anti-tumour and anti-HIV activity, in *Uses of Inorganic Chemistry in Medicine* (ed N.P. Farrell), Royal Society of Chemistry, Cambridge, pp. 26–57.
43. Bhabak, K.P., Bhuyan, B.J. and Mugesh, G. (2011) Bioinorganic and medicinal chemistry: aspects of gold(I)-protein complexes. *Dalton Trans.*, **40**, 2099–2111.
44. Bau, R. (1998) Crystal structure of the antiarthritic drug gold thiomalate (myochrysine): a double-helical geometry in the solid state. *J. Am. Chem. Soc.*, **120**, 9380–9381.
45. Mazid, M.A., Razi, M.T., Sadler, P.J. *et al*. (1980) An EXAFS study of gold coordination in the anti-arthritic drugs myocrisin and solganol. *J. Chem. Soc., Chem. Commun.*, 1261–1263.
46. Elder, R.C., Ludwig, K., Cooper, J.N. and Eidsness, M.K. (1985) EXAFS AND WAXS structure determination for an antiarthritic drug, sodium gold(I) thiomalate. *J. Am. Chem. Soc.*, **107**, 5024–5025.
47. Shaw, C.F. III, (1999) Gold-based therapeutic agents. *Chem. Rev.*, **99**, 2589–2600.
48. Shaw, C.F. III,, Schaeffer, N.A., Elder, R.C. *et al*. (1984) Bovine serum albumin-gold thiomalate complex: 197Au Mossbauer, EXAFS and XANES, electrophoresis, 35S-radiotracer, and fluorescent probe competition studies. *J. Am. Chem. Soc.*, **106**, 3511–3521.
49. Chaffman, M., Brogden, R.N., Heel, R.C. *et al*. (1984) Auranofin – A preliminary review of its pharmacological properties and therapeutic use in rheumatoid arthritis. *Drugs*, **27**, 378–424.
50. Felson, D.T., Anderson, J.J. and Meenan, R.F. (1990) The comparative efficacy and toxicity of 2nd-line drugs in rheumatoid arthritis – results of 2 metaanalyses. *Arthritis Rheum.*, **33**, 1449–1461.

51. Pope, J.E., Hong, P. and Koehler, B.E. (2002) Prescribing trends in disease modifying, antirheumatic drugs for rheumatoid arthritis: a survey of practicing Canadian rheumatologists. *J. Rheumatol.*, **29**, 255–260.
52. Whitehouse, M.W., Cookson, P.D., Siasios, G. and Tiekink, E.R.T. (1998) Anti-arthritic activity in rats of some phosphinegold(I) thionucleobases and related thiolates. *Metal-Based Drugs*, **5**, 245–249.
53. Intoccia, A.P., Flanagan, T.L., Walz, D.T. *et al*. (1982) Pharmacokinetics of auranofin in animals. *J. Rheumatol.*, **9** (Suppl. 8), 90–98.
54. Coffer, M.T., Shaw, C.F.I., Hormann, A.L. *et al*. (1987) Thiol competition for Et_3PAuS-albumin. A non enzymatic mechanism for Et_3PO formation. *J. Inorg. Biochem.*, **30**, 177–187.
55. Hill, D.T., Isab, A.A., Griswold, D.E. *et al*. (2010) Seleno-auranofin (Et_3PAuSe-tagl): synthesis, spectroscopic (EXAFS, 197Au Mössbauer, 31P, 1H, 13C, and 77Se NMR, ESI-MS) characterization, biological activity, and rapid serum albumin-induced triethylphosphine oxide generation. *Inorg. Chem.*, **49**, 7663–7675.
56. Berners Price, S.J., Dimartino, M.J., Hill, D.T. *et al*. (1985) Tertiary phosphine complexes of gold(I) and gold(III) with imido ligands - H-1, P-31 and N-15 NMR-spectroscopy, antiinflammatory activity, and X-ray crystal-structure of (phthalimido)(triethylphosphine)gold(I). *Inorg. Chem.*, **24**, 3425–3434.
57. Trávníček, Z., Starha, P., Vančo, J. *et al*. (2012) Anti-inflammatory active gold(I) complexes involving 6-substituted-purine derivatives. *J. Med. Chem.*, **55** (10), 4568–4579.
58. Karver, M.R., Krishnamurthy, D., Bottini, N. and Barrios, A.M. (2010) Gold(I) phosphine mediated selective inhibition of lymphoid tyrosine phosphatase. *J. Inorg. Biochem.*, **104**, 268–273.
59. Karver, M.R., Krishnamurthy, D., Kulkarni, R.A. *et al*. (2009) Identifying potent, selective protein tyrosine phosphatase inhibitors from a library of Au(I) complexes. *J. Med. Chem.*, **52**, 6912–6918.
60. Berners-Price, S.J. and Filipovska, A. (2008) The design of gold-based, mitochondria-targeted chemotherapeutics. *Aust. J. Chem.*, **61**, 661–668.
61. Bindoli, A., Rigobello, M.P., Scutari, G. *et al*. (2009) Thioredoxin reductase: a target for gold compounds acting as potential anticancer drugs. *Coord. Chem. Rev.*, **253**, 1692–1707.
62. Gandin, V., Fernandes, A.P., Rigobello, M.P. *et al*. (2010) Cancer cell death induced by phosphine gold(I) compounds targeting thioredoxin reductase. *Biochem. Pharmacol.*, **79**, 90–101.
63. Pratesi, A., Gabbiani, C., Ginanneschi, M. and Messori, L. (2010) Reactions of medicinally relevant gold compounds with the *C*-terminal motif of thioredoxin reductase elucidated by MS analysis. *Chem. Commun.*, **46**, 7001–7003.
64. Tian, S., Siu, F.-M., Kui, S.C.F. *et al*. (2011) Anticancer gold(I)-phosphine complexes as potent autophagy-inducing agents. *Chem. Commun.*, **47**, 9318–9320.
65. Simon, T.M., Kunishima, D.H., Vibert, G.J. *et al*. (1979) Inhibitory effects of a new oral gold compound on HeLa cells. *Cancer*, **44**, 1965–1975.
66. Simon, T.M., Kunishima, D.H., Vibert, G.J. and Lorber, A. (1981) Screening trial with the coordinated gold compound auranofin using mouse lymphocytic leukemia P388. *Cancer Res.*, **41**, 94–97.
67. Pearson, S., Scarano, W. and Stenzel, M.H. (2012) Micelles based on gold-glycopolymer complexes as new chemotherapy drug delivery agents. *Chem. Commun.*, **48**, 4695–4697.
68. Robilotto, T.J., Alt, D.S., Von Recum, H.A. and Gray, T.G. (2011) Cytotoxic gold(I)-bearing dendrimers from alkyne precursors. *Dalton Trans.*, **40**, 8083–8085.
69. Meyer, A., Bagowski, C.P., Kokoschka, M. *et al*. (2012) On the biological properties of alkynyl phosphine gold(I) complexes. *Angew. Chem. Int. Ed.*, **51**, 8895–8899.
70. Chui, C.-H., Wong, R.S.-M., Gambari, R. *et al*. (2009) Antitumor activity of diethynylfluorene derivatives of gold(I). *Bioorg. Med. Chem.*, **17**, 7872–7877.
71. Balasingham, R.G., Williams, C.F., Mottram, H.J. *et al*. (2012) Gold(I) complexes derived from alkynyloxy-substituted anthraquinones: syntheses, luminescence, preliminary cytotoxicity, and cell imaging studies. *Organometallics*, **31**, 5835–5843.
72. Vergara, E., Cerrada, E., Casini, A. *et al*. (2010) Antiproliferative activity of gold(I) alkyne complexes containing water-soluble phosphane ligands. *Organometallics*, **29**, 2596–2603.
73. Mirabelli, C.K., Johnson, R.K., Hill, D.T. *et al*. (1986) Correlation of the *in vitro* cytotoxic and *in vivo* antitumor activities of gold(I) coordination complexes. *J. Med. Chem.*, **29**, 218–223.
74. Berners-Price, S.J. and Sadler, P.J. (1988) Phosphines and metal phosphine complexes: relationship of chemistry to anticancer and other biological activity. *Struct. Bond.*, **70**, 27–102.

75. Hickey, J.L., Ruhayel, R.A., Barnard, P.J. *et al*. (2008) Mitochondria-targeted chemotherapeutics: the rational design of gold(I) *N*-heterocyclic carbene complexes that are selectively toxic to cancer cells and target protein selenols in preference to thiols. *J. Am. Chem. Soc.*, **130**, 12570–12571.
76. Suresh, D., Balakrishna, M.S., Rathinasamy, K. *et al*. (2008) Water-soluble cyclodiphosphazanes: synthesis, gold(I) metal complexes and their *in vitro* antitumor studies. *Dalton Trans.*, 2812–2814.
77. Viry, E., Battaglia, E., Deborde, V. *et al*. (2008) A sugar-modified phosphole gold complex with antiproliferative properties acting as a thioredoxin reductase inhibitor in MCF-7 cells. *ChemMedChem*, **3**, 1667–1670.
78. Gabrielli, W.F., Nogai, S.D., Nell, M. *et al*. (2012) Neutral mononuclear and dinuclear complexes of gold(I) featuring azole ligands: synthesis, structure and cytotoxicity. *Polyhedron*, **34** (1), 188–197.
79. Yan, K., Lok, C.-N., Bierla, K. and Che, C.-M. (2010) Gold(I) complex of *N*,*N*′-disubstituted cyclic thiourea with *in vitro* and *in vivo* anticancer properties-potent tight-binding inhibition of thioredoxin reductase. *Chem. Commun.*, **46**, 7691–7693.
80. Rigobello, M.P., Folda, A., Dani, B. *et al*. (2008) Gold(I) complexes determine apoptosis with limited oxidative stress in Jurkat T cells. *Eur. J. Pharmacol.*, **582**, 26–34.
81. Stallings-Mann, M., Jamieson, L., Regala, R.P. *et al*. (2006) A novel small-molecule inhibitor of protein kinase C iota blocks transformed growth of non-small-cell lung cancer cells. *Cancer Res.*, **66**, 1767–1774.
82. Edrogan, E., Lamark, T., Stallings-Mann, M. *et al*. (2006) Aurothiomalate inhibits transformed growth by targeting the PB1 domain of protein kinase Cι. *J. Biol. Chem.*, **281**, 28450–28459.
83. Tiekink, E.R.T. (2002) Gold derivatives for the treatment of cancer. *Crit. Rev. Oncol. Hemat.*, **42**, 225–248.
84. Barreiro, E., Casas, J.S., Couce, M.D. *et al*. (2008) Synthesis, structure and cytotoxicity of triphenylphosphinegold(I) sulfanylpropenoates. *J. Inorg. Biochem.*, **102**, 184–192.
85. Casas, J.S., Castellano, E.E., Couce, M.D. *et al*. (2006) A gold(I) complex with a vitamin K3 derivative: characterization and antitumoral activity. *J. Inorg. Biochem.*, **100**, 1858–1860.
86. Casas, J.S., Castellano, E.E., Couce, M.D. *et al*. (2007) Novel gold(I) 7-azacoumarin complex: synthesis, structure, optical properties, and cytotoxic effects. *Inorg. Chem.*, **46**, 6236–6238.
87. Ott, I., Qian, X. and Xu, Y. (2009) A gold(I) phosphine complex containing a naphthalimide ligand functions as a TrxR inhibiting antiproliferative agent and angiogenesis inhibitor. *J. Med. Chem.*, **52**, 763–770.
88. Bagowski, C.P., You, Y., Scheffler, H. *et al*., (2009) Naphthalimide gold(I) phosphine complexes as anticancer metallodrugs. *Dalton Trans.*, 10799–10805.
89. Mullice, L.A., Mottram, H.J., Hallett, A.J. and Pope, S.J.A. (2012) Gold(I) complexes incorporating emissive mercapto-pteridine ligands: syntheses, X-ray structure, luminescence and preliminary cytotoxic evaluation. *Eur. J. Inorg. Chem.*, **2012**, 3054–3060.
90. Vergara, E., Casini, A., Sorrentino, F. *et al*. (2010) Anticancer therapeutics that target selenoenzymes: synthesis, characterization, *in vitro* cytotoxicity, and thioredoxin reductase inhibition of a series of gold(I) complexes containing hydrophilic phosphine ligands. *ChemMedChem*, **5**, 96–102.
91. Vergara, E., Cerrada, E., Clavel, C. *et al*. (2011) Thiolato gold(I) complexes containing water-soluble phosphane ligands: a characterization of their chemical and biological properties. *Dalton Trans.*, **40**, 10927–10935.
92. Galassi, R., Burini, A., Ricci, S. *et al*. (2012) Synthesis and characterization of azolate gold(I) phosphane complexes as thioredoxin reductase inhibiting antitumor agents. *Dalton Trans.*, **41**, 5307–5318.
93. Schuh, E., Valiahdi, S.M., Jakupec, M.A. *et al*. (2009) Synthesis and biological studies of some gold(I) complexes containing functionalised alkynes. *Dalton Trans.*, 10841–10845.
94. Berners-Price, S.J., Jarrett, P.S. and Sadler, P.J. (1987) ^{31}P NMR studies of $[Au_2(\mu\text{-dppe})]^{2+}$ antitumor complexes. Conversion into $[Au(dppe)_2]^{+}$ induced by thiols and blood plasma. *Inorg. Chem.*, **26**, 3074–3077.
95. Berners-Price, S.J., Girard, G.R., Hill, D.T. *et al*. (1990) Cytotoxicity and antitumour activity of some tetrahedral bis(diphosphino)gold(I) chelates. *J. Med. Chem.*, **33**, 1386–1392.
96. Mirabelli, C.K., Hill, D.T., Faucette, L.F. *et al*., (1987) Antitumor activity of bis(diphenylphosphino)alkanes, their gold(I) coordination complexes, and related compounds. *J. Med. Chem.*, **30**, 2181–2190.
97. McKeage, M.J., Berners-Price, S.J., Galettis, P. *et al*., (2000) Role of lipophilicity in determining cellular uptake and antitumour activity of gold phosphine complexes. *Cancer Chemother. Pharmacol.*, **46**, 343–350.

98. Rackham, O., Nichols, S.J., Leedman, P.J. *et al*. (2007) A gold(I) phosphine complex selectively induces apoptosis in breast cancer cells: implications for anticancer therapeutics targeted to mitochondria. *Biochem. Pharmacol.*, **74**, 992–1002.
99. Wang, Y., Liu, M., Cao, R. *et al*. (2013) A soluble bis-chelated gold(I) diphosphine compound with strong anticancer activity and low toxicity. *J. Med. Chem.*, **56**, 1455–1466.
100. Wetzel, C., Kunz, P.C., Kassack, M.U. *et al*. (2011) Gold(I) complexes of water-soluble diphos-type ligands: synthesis, anticancer activity, apoptosis and thioredoxin reductase inhibition. *Dalton Trans.*, **40** (36), 9212–9220.
101. Healy, P.C., Loughrey, B.T., Williams, M.L. and Parsons, P.G. (2010) Synthesis, structure and cytotoxicity studies of four-coordinate bis(*cis*-bis(diphenylphosphino)ethene) gold(I) complexes, $[Au(dppey)_2]X$. *J. Inorg. Biochem.*, **104**, 625–631.
102. McKeage, M.J., Maharaj, L. and Berners-Price, S.J. (2002) Mechanisms of cytotoxicity and antitumor activity of gold(I) phosphine complexes: the possible role of mitochondria. *Coord. Chem. Rev.*, **232**, 127–135.
103. Modica-Napolitano, J.S. and Aprille, J.R. (2001) Delocalised lipophilic cations selectively target the mitochondria of carcinoma cells. *Adv. Drug Delivery Rev.*, **49**, 63–70.
104. Chen, L.B. (1988) Mitochondrial membrane potential in living cells. *Annu. Rev. Cell Biol.*, **4**, 155–181.
105. Rush, G.F., Alberts, D.W., Meunier, P. *et al*. (1987) *In vivo* and *in vitro* hepatotoxicity of a novel antineoplastic agent, SK&F 101772, in male beagle dogs. *Toxicologist*, **7**, 59.
106. Hoke, G.D., Rush, G.F., Bossard, G.E. *et al*. (1988) Mechanism of alterations in isolated rat liver mitochondrial function induced by gold complexes of bidentate phosphines. *J. Biol. Chem.*, **263**, 11203–11210.
107. Smith, P.F., Hoke, G.D., Alberts, D.W. *et al*. (1989) Mechanism of toxicity of an experimental bidentate phosphine gold complexed antineoplastic agent in isolated rat hepatocytes. *J. Pharmacol. Exp. Ther.*, **249**, 944–950.
108. Hoke, G.D., Macia, R.A., Meunier, P.C. *et al*. (1989) *In vivo* and *in vitro* cardiotoxicity of a gold-containing antineoplastic drug candidate in the rabbit. *Toxicol. Appl. Pharmacol.*, **100**, 293–306.
109. Liu, J.J., Galettis, P., Farr, A. *et al*. (2008) *In vitro* antitumour and hepatotoxicity profiles of Au(I) and Ag(I) bidentate pyridyl phosphine complexes and relationships to cellular uptake. *J. Inorg. Biochem.*, **102**, 303–310.
110. Humphreys, A.S., Filipovska, A., Berners-Price, S.J. *et al*. (2007) Gold(I) chloride adducts of 1,3-bis(di-2-pyridylphosphino)propane: synthesis, structural studies and antitumour activity. *Dalton Trans.*, 4943–4950.
111. Pillarsetty, N., Katti, K.K., Hoffman, T.J. *et al*. (2003) *In vitro* and *in vivo* antitumor properties of Tetrakis((trishydroxymethyl)phosphine)gold(I) Chloride. *J. Med. Chem.*, **46**, 1130–1132.
112. Higginbotham, M.L., Henry, C.J., Katti, K.V. *et al*. (2003) Preclinical tolerance and pharmacokinetic assessment of MU-Gold, a novel chemotherapeutic agent, in laboratory dogs. *Vet. Ther.*, **4**, 76–82.
113. Santini, C., Pellei, M., Papini, G. *et al*. (2011) *In vitro* antitumour activity of water soluble Cu(I), Ag(I) and Au(I) complexes supported by hydrophilic alkyl phosphine ligands. *J. Inorg. Biochem.*, **105**, 232–240.
114. Bourissou, D., Guerret, O., Gabbai, F. and Bertrand, G. (2000) Stable carbenes. *Chem. Rev.*, **100**, 39–92.
115. Herrmann, W.A. and Köcher, C. (1997) *N*-heterocyclic carbenes. *Angew. Chem., Int. Ed. Engl.*, **36**, 2162–2187.
116. Herrmann, W.A. (2002) *N*-heterocyclic carbenes: a new concept in organometallic catalysis. *Angew. Chem. Int. Ed.*, **41**, 1290–1309.
117. Nolan, S.P. (ed) (2006) *N-heterocyclic Carbenes in Synthesis*, Wiley-VCH Verlag GmbH, Weinheim.
118. Díez-González, S., Marion, N. and Nolan, S.P. (2009) *N*-heterocyclic carbenes in late transition metal catalysis. *Chem. Rev.*, **109**, 3612–3676.
119. Scholl, M., Ding, S., Lee, C.W. and Grubbs, R.H. (1999) Synthesis and activity of a new generation of ruthenium-based olefin metathesis catalysts coordinated with 1,3-dimesityl-4,5-dihydroimidazol-2-ylidene ligands. *Org. Lett.*, **1**, 953–956.
120. Hindi, K.M., Panzner, M.J., Tessier, C.A. *et al*. (2009) The medicinal applications of imidazolium carbene – metal complexes. *Chem. Rev.*, **109**, 3859–3884.
121. Gasser, G., Ott, I. and Metzler-Nolte, N. (2011) Organometallic anticancer compounds. *J. Med. Chem.*, **54**, 3–25.
122. Gautier, A. and Cisnetti, F. (2012) Advances in metal-carbene complexes as potent anti-cancer agents. *Metallomics*, **4**, 23–32.
123. Oehninger, L., Rubbiani, R. and Ott, I. (2013) *N*-heterocyclic carbene metal complexes in medicinal chemistry. *Dalton Trans.*, **42**, 3269–3284.

124. Liu, W. and Gust, R. (2013) Metal *N*-heterocyclic carbene complexes as potential antitumor metallodrugs. *Chem. Soc. Rev.*, **42**, 755–773.
125. Lin, J.C.Y., Huang, R.T.W., Lee, C.S. *et al*. (2009) Coinage metal – *N*-heterocyclic carbene complexes. *Chem. Rev.*, **109**, 3561–3598.
126. Baker, M.V., Barnard, P.J., Berners-Price, S.J. *et al*. (2006) Cationic, linear Au(I) *N*-heterocyclic carbene complexes: synthesis, structure and anti-mitochondrial activity. *Dalton Trans.*, 3708–3715.
127. Kunz, P.C., Wetzel, C., Kogel, S. *et al*. (2011) $[(C_3H_4N_2)_2Au]Cl$-a bis protic gold(I)-NHC. *Dalton Trans.*, **40**, 35–37.
128. Horvath, U.E.I., Bentivoglio, G., Hummel, M. *et al*., (2008) A cytotoxic bis(carbene)gold(I) complex of ferrocenyl complexes: synthesis and structural characterisation. *New J. Chem.*, **32**, 533–539.
129. Siciliano, T.J., Deblock, M.C., Hindi, K.M. *et al*. (2011) Synthesis and anticancer properties of gold(I) and silver(I) *N*-heterocyclic carbene complexes. *J. Organomet. Chem.*, **696**, 1066–1071.
130. Schuh, E., Pflüger, C., Citta, A. *et al*. (2012) Gold(I) carbene complexes causing thioredoxin 1 and thioredoxin 2 oxidation as potential anticancer agents. *J. Med. Chem.*, **55**, 5518–5528.
131. Liu, W., Bensdorf, K., Proetto, M. *et al*. (2011) NHC gold halide complexes derived from 4,5-diarylimidazoles: synthesis, structural analysis, and pharmacological investigations as potential antitumor agents. *J. Med. Chem.*, **54**, 8605–8615.
132. Liu, W., Bensdorf, K., Proetto, M. *et al*. (2012) Synthesis, characterization, and *in vitro* studies of bis[1,3-diethyl-4,5-diarylimidazol-2-ylidene]gold(I/III) complexes. *J. Med. Chem.*, **55**, 3713–3724.
133. Kaps, L., Biersack, B., Müller-Bunz, H. *et al*. (2012) Gold(I)–NHC complexes of antitumoral diarylimidazoles: structures, cellular uptake routes and anticancer activities. *J. Inorg. Biochem.*, **106**, 52–58.
134. Urig, S., Fritz-Wolf, K., Réau, R. *et al*. (2006) Undressing of phospine gold(I) complexes as irreversible inhibitors of human disulfide reductases. *Angew. Chem. Int. Ed.*, **45**, 1881–1886.
135. Rubbiani, R., Kitanovic, I., Alborzinia, H. *et al*. (2010) Benzimidazol-2-ylidene gold(I) complexes are thioredoxin reductase inhibitors with multiple antitumor properties. *J. Med. Chem.*, **53**, 8608–8618.
136. Rubbiani, R., Can, S., Kitanovic, I. *et al*. (2011) Comparative *in vitro* evaluation of *N*-heterocyclic carbene gold(I) complexes of the benzimidazolylidene type. *J. Med. Chem.*, **54**, 8646–8657.
137. Almássy, A., Nagy, C.E., Bényei, A.C. and Joó, F. (2010) Novel sulfonated *N*-heterocyclic carbene gold(I) complexes: homogeneous gold catalysis for the hydration of terminal alkynes in aqueous media. *Organometallics*, **29**, 2484–2490.
138. Pellei, M., Gandin, V., Marinelli, M. *et al*. (2012) Synthesis and biological activity of ester- and amide-functionalized imidazolium salts and related water-soluble coinage metal *N*-heterocyclic carbene complexes. *Inorg. Chem.*, **51**, 9873–9882.
139. Baker, M.V., Barnard, P.J., Berners-Price, S.J. *et al*. (2005) Synthesis and structural characterization of linear Au(I) *N*-heterocyclic carbene complexes: new analogues of the Au(I) phosphine drug Auranofin. *J. Organomet. Chem.*, **690**, 5625–5635.
140. Weaver, J., Gaillard, S., Toye, C. *et al*. (2011) Cytotoxicity of gold(I) *N*-heterocyclic carbene complexes assessed by using human tumor cell lines. *Chem. Eur. J.*, **17**, 6620–6624.
141. Haque, R.A., Iqbal, M.A., Ahamed, M.B.K. *et al*. (2012) Design, synthesis and structural studies of meta-xylyl linked bis-benzimidazolium salts: potential anticancer agents against 'human colon cancer'. *Chem. Cent. J.*, **6**, 68.
142. Barnard, P.J., Baker, M.V., Berners-Price, S.J. *et al*. (2004) Dinuclear gold(I) complexes of bridging bidentate carbene ligands: synthesis, structure and spectroscopic characterisation. *Dalton Trans.*, 1038–1047.
143. Barnard, P.J., Baker, M.V., Berners-Price, S.J. and Day, D.A. (2004) Mitochondrial permeability transition induced by dinuclear gold(I)-carbene complexes: potential new antimitochondrial antitumour agents. *J. Inorg. Biochem.*, **98**, 1642–1647.
144. Barnard, P.J., Wedlock, L.E., Baker, M.V. *et al*. (2006) Luminescence studies of the intracellular distribution of a dinuclear gold(I) *N*-heterocyclic carbene complex. *Angew. Chem. Int. Ed.*, **45**, 5966–5970.
145. Bowmaker, G.A. (1999) Spectroscopic methods in gold chemistry, in *Gold: Progress in Chemistry Biochemistry and Technology* (ed H. Schmidbaur), John Wiley & Sons, Ltd, Chichester, pp. 841–881.
146. Assefa, Z., McBurnett, B.G., Staples, R.J. *et al*. (1995) Syntheses, structures, and spectroscopic properties of gold(I) complexes of 1,3,5-triaza-7-phosphaadamantane (TPA). Correlation of the supramolecular Au· · ·Au interaction and photoluminescence for the species (TPA)AuCl and [(TPA-HCl)AuCl]. *Inorg. Chem.*, **34**, 75–83.

147. van Zyl, W.E., López-de-Luzuriaga, J.M., Mohamed, A.A. *et al*. (2002) Dinuclear gold(I) dithiophosphonate complexes: synthesis, luminescent properties, and X-ray crystal sructures of $[AuS_2PR(OR')]_2$ (R = Ph, R′ = C_5H_9; R = 4-C_6H_4OMe, R′ = (1*S*,5*R*,2*S*)-(-)-Menthyl; R = Fc, R′ = $(CH_2)_2O(CH_2)_2$OMe). *Inorg. Chem.*, **41**, 4579–4589.
148. Coker, N.L., Krause Bauer, J.A. and Elder, R.C. (2004) Emission energy correlates with inverse of gold-gold distance for various $[Au(SCN)_2]^-$ salts. *J. Am. Chem. Soc.*, **126**, 12–13.
149. Wedlock, L.E., Aitken, J.B., Berners-Price, S.J. and Barnard, P.J. (2013) Bromide ion binding by a dinuclear gold(I) *N*-heterocyclic carbene complex: a spectrofluorescence and X-ray absorption spectroscopic study. *Dalton Trans.*, **42**, 1259–1266.
150. Wedlock, L.E., Barnard, P.J., Baker, M.V. *et al*. (2007) Probing the intracellular distribution of dinuclear luminescent Au(I) *N*-heterocyclic carbene complexes: potential antitumour agents that target mitochondria. *J. Biol. Inorg. Chem.*, **12** (Suppl 1), S50.
151. Wedlock, L.E. (2011) A study into the chemistry, spectroscopic properties, and subcellular distribution of some gold(I) complexes of pharmacological interest. PhD Thesis. University of Western Australia.
152. Sadler, P.J., Nasr, M. and Narayanan, V.L. (1984) The design of metal complexes as anticancer agents, in *Platinum Coordination Complexes in Cancer Chemotherapy* (eds M.P. Hacker, E.B. Douple and I.H. Krakoff), Martinus Nijhoff Publishing, Boston, MA, pp. 290–304.
153. Parish, R.V., Howe, B.P., Wright, J.P. *et al*. (1996) Chemical and biological studies of dichloro(2-((dimethylamino)-methyl)phenyl)gold(III). *Inorg. Chem.*, **35**, 1659–1666.
154. Buckley, R.G., Elsome, A.M., Fricker, S.P. *et al*. (1996) Antitumor properties of some 2-[(dimethylamino)methyl]-phenylgold(III) complexes. *J. Med. Chem.*, **39**, 5208–5214.
155. Messori, L., Marcon, G., Cinellu, M.A. *et al*. (2004) Solution chemistry and cytotoxic properties of novel organogold(III) compounds. *Bioorg. Med. Chem.*, **12**, 6039–6043.
156. Coronnello, M., Mino, E., Caciagli, B. *et al*. (2005) Mechanism of cytototoxicity of selected organogold(III) compounds. *J. Med. Chem.*, **48**, 6761–6765.
157. Fan, M., Yang, C.T., Ranford, J.D. *et al*. (2003) Chemical and biological studies of the dichloro(2-phenylpyridine) gold(III) complex and its derivatives. *Dalton Trans.*, 2680–2685.
158. Fan, D.M., Yang, C.T., Ranford, J.D. *et al*. (2003) Synthesis, characterization, and biological activities of 2-phenylpyridine gold(III) complexes with thiolate ligands. *Dalton Trans.*, 3376–3381.
159. Li, C.K.-L., Sun, R.W.-Y., Kui, S.C.-F. *et al*. (2006) Anticancer cyclometalated $[Au^{III}{}_m(C\text{^}N\text{^}C)_mL]^{n+}$ compounds: synthesis and cytotoxic properties. *Chem. Eur. J.*, **12**, 5253–5266.
160. Sun, R.W.-Y., Lok, C.-N., Fong, T.T.-H. *et al*. (2013) A dinuclear cyclometalated gold(III)-phosphine complex targeting thioredoxin reductase inhibits hepatocellular carcinoma in vivo. *Chem. Sci.*, **4**, 1979–1988.
161. Zhang, J.-J., Lu, W., Sun, R.W.-Y. and Che, C.-M. (2012) Organogold(III) supramolecular polymers for anticancer treatment. *Angew. Chem. Int. Ed.*, **51**, 4882–4886.
162. Yan, J.J., Chow, A.L.-F., Leung, C.-H. *et al*. (2010) Cyclometalated gold(III) complexes with *N*-heterocyclic carbene ligands as topoisomerase I poisons. *Chem. Commun.*, **46**, 3893–3895.
163. Zou, T., Lum, C.T., Chui, S.S.-Y. and Che, C.-M. (2013) Gold(III) complexes containing *N*-heterocyclic carbene ligands: thiol "switch-on" fluorescent probes and anti-cancer agents. *Angew. Chem. Int. Ed.*, **52**, 2930–2933.
164. Che, C.-M., Sun, R.W.-Y., Yu, W.-Y. *et al*. (2003) Gold(III) porphyrins as a new class of anticancer drugs: cytotoxicity, DNA binding and induction of apoptosis in human cervix epitheloid cancer cells. *Chem. Commun.*, 1718–1719.
165. Wang, Y., He, Q.-H., Sun, R.W.-Y. *et al*. (2005) Gold(III)porphyrin 1a induced apoptosis by mitochondrial death pathways related to reactive oxygen species. *Cancer Res.*, **65**, 11553–11564.
166. Lum, C.T., Yang, Z.F., Li, H.Y. *et al*. (2006) Gold(III) compound in a novel chemocytotoxic agent for hepatocellular carcinoma. *Int. J. Cancer*, **118**, 1527–1538.
167. Wang, Y., He, Q.-Y., Che, C.-M. and Chiu, J.-F. (2006) Proteomic characterization of the cytotoxic mechanism of gold(III) porphyrin 1a, a potential anticancer drug. *Proteomics*, **6**, 131–142.
168. Wang, Y., He, Q.-Y., Sun, R.W.-Y. *et al*. (2007) Cellular pharmacological properties of gold(III) porphyrin 1a, a potential anticancer drug lead. *Eur. J. Pharmacol.*, **554**, 113–122.
169. Wang, Y., He, Q.-Y., Che, C.-M. *et al*. (2008) Modulation of gold(III) porphyrin 1a-induced apoptosis by mitogen-activated protein kinase signaling pathways. *Biochem. Pharmacol.*, **75**, 1282–1291.

170. To, Y.F., Sun, R.W.-Y., Chen, Y. *et al*. (2009) Gold(III) porphyrin complex is more potent than cisplatin in inhibiting growth of nasopharyngeal carcinoma *in vitro* and *in vivo*. *Int. J. Cancer*, **124**, 1971–1979.
171. Li, W., Xie, Y., Sun, R.W.Y. *et al*. (2009) Inhibition of Akt sensitises neuroblastoma cells to gold(III) porphyrin 1a, a novel antitumour drug induced apoptosis and growth inhibition. *Br. J. Cancer*, **101**, 342–349.
172. Sun, R.W.-Y. and Che, C.-M. (2009) The anti-cancer properties of gold(III) compounds with dianionic porphyrin and tetradentate ligands. *Coord.Chem. Rev.*, **253**, 1682–1691.
173. Tu, S., Wai-Yin Sun, R., Lin, M.C.M. *et al*. (2009) Gold (III) porphyrin complexes induce apoptosis and cell cycle arrest and inhibit tumor growth in colon cancer. *Cancer*, **115**, 4459–4469.
174. Lum, C.T., Huo, L., Sun, R.W.-Y. *et al*. (2011) Gold(III) porphyrin 1a prolongs the survival of melanoma-bearing mice and inhibits angiogenesis. *Acta Oncol.*, **50**, 719–726.
175. Lum, C.T., Wong, A.S.-T., Lin, M.C.M. *et al*., (2013) A gold(III) porphyrin complex as an anti-cancer candidate to inhibit growth of cancer-stem cells. *Chem. Commun.*, **49**, 4364–4366.
176. Che, C.-M. and Sun, R.W.-Y. (2011) Therapeutic applications of gold complexes: lipophilic gold(III) cations and gold(I) complexes for anti-cancer treatment. *Chem. Commun.*, **47**, 9554–9560.
177. Lum, C.T., Liu, X., Sun, R.W.-Y. *et al*. (2010) Gold(III) porphyrin 1a inhibited nasopharyngeal carcinoma metastasis *in vivo* and inhibited cell migration and invasion *in vitro*. *Cancer Lett.*, **294**, 159–166.
178. Messori, L., Abbate, F., Marcon, G. *et al*. (2000) Gold(III) complexes as potential antitumor agents: solution chemistry and cytotoxic properties of some selected gold(III) compounds. *J. Med. Chem.*, **43**, 3541–3548.
179. Marcon, G., Carotti, S., Coronnello, M. *et al*. (2002) Gold(III) complexes with bipyridyl ligands: solution chemistry, cytotoxicity, and DNA binding properties. *J. Med. Chem.*, **45**, 1672–1677.
180. Casini, A., Cinellu, M.A., Minghetti, G. *et al*. (2006) Structural and solution chemistry, antiproliferative effects, and DNA and protein binding properties of a series of dinuclear gold(III) compounds with bipyridyl ligands. *J. Med. Chem.*, **49**, 5524–5531.
181. Gabbiani, C., Casini, A., Messori, L. *et al*. (2008) Structural characterization, solution studies, and DFT calculations on a series of binuclear gold(III) oxo complexes: relationships to biological properties. *Inorg. Chem.*, **47**, 2368–2379.
182. Casini, A., Kelter, G., Gabbiani, C. *et al*. (2009) Chemistry, antiproliferative properties, tumor selectivity, and molecular mechanisms of novel gold(III) compounds for cancer treatment: a systematic study. *J. Biol. Inorg. Chem.*, **14**, 1139–1149.
183. Yang, T., Tu, C., Zhang, J. *et al*. (2003) Novel Au(III) complexes of aminoquinoline derivatives: crystal structure, DNA binding and cytotoxicity against melanoma and lung tumour cells. *Dalton Trans.*, 3419–3424.
184. Shi, P., Jiang, Q., Lin, J. *et al*. (2006) Gold(III) compounds of 1,4,7-triazacyclononane showing high cytotoxicity against A-549 and HCT-116 tumor cell lines. *J. Inorg. Biochem.*, **100**, 939–945.
185. Shi, P., Jiang, Q., Zhao, Y. *et al*. (2006) DNA binding properties of novel cytotoxic gold(III) complexes of terpyridine ligands: the impact of steric and electrostatic effects. *J. Biol. Inorg. Chem.*, **11**, 745–752.
186. Ronconi, L., Giovagnini, L., Marzano, C. *et al*. (2005) Gold dithiocarbamate derivatives as potential antineoplastic agents: design, spectroscopic properties, and in vitro antitumor activity. *Inorg. Chem.*, **44**, 1867–1881.
187. Ronconi, L., Marzano, C., Zanello, P. *et al*. (2006) Gold(III) dithiocarbamate derivatives for the treatment of cancer: solution chemistry, DNA binding and hemolytic properties. *J. Med. Chem.*, **49**, 1648–1657.
188. Milacic, V., Chen, D., Ronconi, L. *et al*. (2006) A novel anticancer gold(III) dithiocarbamate compound inhibits the activity of a purified 20S proteasome and 26S proteasome in human breast cancer cell cultures and xenografts. *Cancer Res.*, **66**, 10478–10486.
189. Milacic, V. and Dou, Q.P. (2009) The tumor proteasome as a novel target for gold(III) complexes: Implications for breast cancer therapy. *Coord. Chem. Rev.*, **253**, 1649–1660.
190. Cattaruzza, L., Fregona, D., Mongiat, M. *et al*. (2011) Antitumor activity of gold(III)-dithiocarbamato derivatives on prostate cancer cells and xenografts. *Int. J. Cancer*, **128**, 206–215.
191. Saggioro, D., Rigobello, M.P., Paloschi, L. *et al*. (2007) Gold(III) - dithiocarbamato complexes induce cancer cell death triggered by thioredoxin redox system inhibition and activation of ERK pathway. *Chem. Biol.*, **14**, 1128–1139.
192. Navarro, M., Gabbiani, C., Messori, L. and Gambino, D. (2010) Metal-based drugs for malaria, trypanosomiasis and leishmaniasis: recent achievements and perspectives. *Drug Discov. Today*, **15**, 1070–1078.

193. Navarro, M., Vasquez, F., Sanchez-Delgado, R.A. *et al*. (2004) Toward a novel metal-based chemotherapy against tropical diseases. 7. Synthesis and *in vitro* antimalarial activity of new gold-chloroquine complexes. *J. Med. Chem.*, **47**, 5204–5209.
194. Vieites, M., Smircich, P., Guggeri, L. *et al*. (2009) Synthesis and characterization of a pyridine-2-thiol N-oxide gold(I) complex with potent antiproliferative effect against *Trypanosoma cruzi* and *Leishmania sp*. insight into its mechanism of action. *J. Inorg. Biochem.*, **103**, 1300–1306.
195. Fricker, S.P., Mosi, R.M., Cameron, B.R. *et al*. (2008) Metal compounds for the treatment of parasitic diseases. *J. Inorg. Biochem.*, **102**, 1839–1845.
196. Alger, H.M. and Williams, D.L. (2002) The disulfide redox system of *Schistosoma mansoni* and the importance of a multifunctional enzyme, thioredoxin glutathione reductase. *Mol. Biochem. Parasitol.*, **121**, 129–139.
197. Andricopulo, A.D., Akoachere, M.B., Krogh, R. *et al*., (2006) Specific inhibitors of *Plasmodium falciparum* thioredoxin reductase as potential antimalarial agents. *Bioorg. Med. Chem. Lett.*, **16**, 2283–2292.
198. Rosenthal, P.J. (2004) Cysteine proteases of malaria parasites. *Int. J. Parasitol.*, **34**, 1489–1499.
199. Micale, N., Cinellu, M.A., Maiore, L. *et al*. (2011) Selected gold compounds cause pronounced inhibition of Falcipain 2 and effectively block *P. falciparum* growth *in vitro*. *J. Inorg. Biochem.*, **105**, 1576–1579.
200. Gabbiani, C., Messori, L., Cinellu, M.A. *et al*. (2009) Outstanding plasmodicidal properties within a small panel of metallic compounds: hints for the development of new metal-based antimalarials. *J. Inorg. Biochem.*, **103**, 310–312.
201. Khanye, S.D., Smith, G.S., Lategan, C. *et al*. (2010) Synthesis and *in vitro* evaluation of gold(I) thiosemicarbazone complexes for antimalarial activity. *J. Inorg. Biochem.*, **104**, 1079–1083.
202. Becker, K., Tilley, L., Vennerstrom, J.L. *et al*. (2004) Oxidative stress in malaria parasite-infected erythrocytes: host-parasite interactions. *Int. J. Parasitol.*, **34**, 163–189.
203. Magherini, F., Modesti, A., Bini, L. *et al*. (2010) Exploring the biochemical mechanisms of cytotoxic gold compounds: a proteomic study. *J. Biol. Inorg. Chem.*, **15**, 573–582.
204. Guidi, F., Landini, I., Puglia, M. *et al*. (2012) Proteomic analysis of ovarian cancer cell responses to cytotoxic gold compounds. *Metallomics*, **4**, 307–314.
205. Gabbiani, C., Scaletti, F., Massai, L. *et al*. (2012) Medicinal gold compounds form tight adducts with the copper chaperone Atox-1: biological and pharmacological implications. *Chem. Commun.*, **48**, 11623–11625.
206. Lemke, J., Pinto, A., Niehoff, P. *et al*. (2009) Synthesis, structural characterisation and anti-proliferative activity of NHC gold amino acid and peptide conjugates. *Dalton Trans.*, 7063–7070.
207. Köster, S.D., Alborzinia, H., Can, S. *et al*. (2012) A spontaneous gold(I)-azide alkyne cycloaddition reaction yields gold-peptide bioconjugates which overcome cisplatin resistance in a p53-mutant cancer cell line. *Chem. Sci.*, **3** (6), 2062–2072.
208. Kouodom, M.N., Boscutti, G., Celegato, M. *et al*. (2012) Rational design of gold(III)-dithiocarbamato peptidomimetics for the targeted anticancer chemotherapy. *J. Inorg. Biochem.*, **117**, 248–260.
209. Kouodom, M.N., Ronconi, L., Celegato, M. *et al*. (2012) Toward the selective delivery of chemotherapeutics into tumor cells by targeting peptide transporters: tailored gold-based anticancer peptidomimetics. *J. Med. Chem.*, **55**, 2212–2226.

10

Ligand Design to Target and Modulate Metal–Protein Interactions in Neurodegenerative Diseases

Michael W. Beck[1], Amit S. Pithadia[1], Alaina S. DeToma[1], Kyle J. Korshavn[1], and Mi Hee Lim[1,2,3]

[1]*Department of Chemistry, University of Michigan, 930 North University Avenue, Ann Arbor, Michigan, 48109, USA*
[2]*Life Sciences Institute, University of Michigan, 210 Washtenaw Avenue, Ann Arbor, Michigan, 48109, USA*
[3]*Department of Chemistry, Ulsan National Institute of Science and Technology (UNIST), 50 UNIST-gil, Eonyan-eup, Ulju-gun, Ulsan, 698-798, Korea*

10.1 Introduction

10.1.1 Metals in the brain

Understanding the function of metals in different biological environments and organs especially the brain (metalloneurochemistry) has been an area of particular interest in the past 30 years [1, 2]. The complex functions of the brain require suitable levels of metal ions for a variety of processes including neurotransmission, dioxygen (O_2) transport, electron transfer mechanisms, and reactive oxygen species (ROS) detoxification [1, 3–13] (Table 10.1). Owing to the broad spectrum of metal ions' action within the brain, precise control of their uptake, distribution, and clearance is essential for proper function. The misregulation and miscompartmentalization of metals, particularly transition metals, have been implicated as a possible source of toxicity associated with neurodegenerative diseases ("metal ion hypothesis," *vide infra*). The recent development of both chemical tools to study the potential involvement of metals in neurodegenerative diseases and therapeutics based on this hypothesis is presented in this chapter. First, the roles of metals in neurodegenerative diseases are briefly discussed in the context of their normal functions.

Ligand Design in Medicinal Inorganic Chemistry, First Edition. Edited by Tim Storr.

Table 10.1 *Metal ions in the brain*

Metal ion	Function in the brain	Localization[a]
Na^+	Action potential: depolarization of transmembrane voltage along the axon [12]	Axon
K^+	Action potential: repolarization of transmembrane voltage along the axon [12]	Axon
Mg^{2+}	Synaptic plasticity: voltage dependent block of *N*-methyl-D-aspartate receptors [14]	Hippocampus
Ca^{2+}	Neurotransmission: neurotransmitter release and excitability [15]	Synapse
$Mn^{2+/4+}$	Enzymatic cofactor for neuronal and glial cell function, as well as neurotransmitter synthesis [16]	Globus pallidus
$Fe^{2+/3+}$	Enzymatic cofactor for energy metabolism, O_2 transport, electron transfer, and neurotransmitter synthesis [11]	Basal ganglia
$Cu^{+/2+}$	Enzymatic cofactor for energy metabolism, cellular respiration, ROS detoxification, and neurotransmitter synthesis [11]	Locus coeruleus
Zn^{2+}	Neurotransmitter and enzymatic cofactor for protein structure and conformation [11]	Hippocampus

[a]Indicates the area with highest concentration in the brain.

Transition metal ions, such as $Cu^{+/2+}$, Zn^{2+}, and $Fe^{2+/3+}$, have various functions in the brain despite occurring in trace amounts [11, 17]. Copper is a redox active metal commonly found in the +1 and +2 oxidation states. Owing to its redox properties, copper is involved in the function of a number of enzymes, including those for the respiratory activity of cytochrome *c* oxidase (C*c*O) and ROS detoxification by copper and zinc superoxide dismutase (Cu,Zn-SOD1) [11], as well as the oxidation of Fe^{2+} to Fe^{3+} in ceruloplasmin [18]. Additionally, copper serves as a cofactor for enzymes and proteins that maintain neurotransmitter and neuropeptide homeostasis. Copper is distributed to various parts of the brain with average concentrations of up to 400 μM in the substantia nigra, 2.5 μM in the cerebral spinal fluid (CSF), and 30 μM in the synaptic cleft [1, 11].

Zinc is distributed in gray matter (about 500 μM), specifically the neocortex, amygdala, and hippocampus (where zinc concentrations can reach up to 300 μM) [11, 19]. It has been suggested that Zn^{2+} is released from the presynapse into the synaptic cleft during neurotransmission, and postsynaptic uptake occurs through calcium-permeable 2-amino-3-(3-hydroxy-5-methylisoxazol-4-yl)propanoic acid (AMPA)-kainate channels [11, 20]. The uptake and distribution of Zn^{2+} throughout neuronal cells are performed by zinc transporter proteins (ZnTs) [11, 21]. The role of Zn^{2+} in neurotransmission has not been completely elucidated; however, it has been reported that Zn^{2+} could inhibit *N*-methyl-D-aspartate receptors (NMDARs) as well as AMPA gated channels [11, 22–25].

Iron is the most abundant metal in the body; within the brain it is primarily concentrated in the basal ganglia, oligodendrocytes, microglia, and neurons [26, 27]. Iron, when bound to transferrin, can be transported across the blood brain barrier (BBB) *via* transferrin receptors (TfRs) resulting in neuronal iron concentrations ranging between 0.5–1.0 mM [28, 29]. Iron is typically found in the +2 and +3 oxidation states, depending on the environment and role in biological systems. Higher oxidation states can also be observed in catalytic

cycles of metalloproteins (e.g., cytochrome P450). The oxidation state of iron is controlled by electron transfer facilitated by ferricreductases and ferroxidases [12, 13, 30]. A number of functions require iron including cell respiration (C*c*O), ROS detoxification (catalase), and neurotransmitter biosynthesis (tyrosine hydroxylase) [11–13]. Iron ion homeostasis is regulated through the iron storage protein, ferritin, and the iron transport protein, transferrin [11, 12, 31, 32].

10.1.2 Aberrant metal–protein interactions

Metals are not always beneficial in biology as metal ion misregulation can cause dysfunction. Research into neurodegenerative diseases has investigated the roles of aberrant metal–protein interactions upon various diseases (Figure 10.1); it is believed that many diseases are exacerbated by metal ion dyshomeostasis. Abnormal metal binding could promote the formation and stabilization of misfolded protein conformations, accelerate protein aggregation, and/or lead to the overproduction of ROS [1, 33–40]. The non-native interaction of metal ions with proteins could interfere with the normal functioning of each component, along with the uptake, transport, and release of proteins and metal ions. For example, in Alzheimer's disease (AD), the misfolded protein, amyloid-β (Aβ) (Figure 10.1), which can bind metals, has been suggested to aggregate in the synapse

Figure 10.1 *Selected metals and proteins involved in the pathogenesis of neurodegenerative diseases. Alzheimer's disease (AD; Cu, Zn, and Fe; amyloid-β (Aβ) (PDB 2LFM) [46]), amyotrophic lateral sclerosis (ALS; Cu and Zn; superoxide dismutase (SOD) (PDB 1SPD) [47]), Parkinson's disease (PD; Fe and Zn; α-synuclein (α-syn) (PDB 2KKW) [48]), Huntington's disease (HD; Cu and Fe; huntingtin (htt) (PDB 4FED) [49]), and prion disease (Mn, Cu, and Zn; prion protein (PrP) (PDB 1QLX) [50])*

where high concentrations of metal ions are found during neurotransmission (up to about 200–300 μM for Zn^{2+}; about 30 μM for $Cu^{+/2+}$), potentially disrupting normal metal ion homeostasis [15, 18, 19, 33, 35, 38, 39, 41, 42]. Furthermore, loosely bound redox active metal ions (e.g., $Cu^{+/2+}$ and $Fe^{2+/3+}$) can exert toxic effects *via* the production of ROS [33, 43–45].

10.1.3 Oxidative stress

Oxidative stress can be defined as an imbalance between the generation and clearance of ROS that may ultimately cause the direct oxidation and dysfunction of biomolecules (e.g., DNA, proteins, and lipids) [51]. The high O_2 consumption in the brain makes it especially prone to damage by ROS, and oxidative stress can occur easily if the mechanisms to detoxify ROS are dysfunctional. This can lead to more rapid aging, excitotoxicity of neurons, and neuronal death [52, 53]. ROS can be produced through the Fenton reaction and Haber-Weiss cycle (Figure 10.2) when redox active metal ions, such as $Fe^{2+/3+}$ and $Cu^{+/2+}$, are misregulated and/or miscompartmentalized [40, 54–56]. Mitochondrial dysfunction could be an additional source of ROS due to its role in cellular respiration and O_2 reduction. During these processes, premature e^- transfer to O_2 in the electron transport chain (ETC) could result in the generation of superoxide ($O_2^{\bullet -}$), a potent ROS [53].

Defense mechanisms against ROS utilize metalloenzymes, such as Cu,Zn-SOD1 and catalase, as well as small molecule antioxidants, such as glutathione (GSH) [57, 58]. Cu,Zn-SOD1 is responsible for the disproportionation of $O_2^{\bullet -}$ to O_2 and hydrogen peroxide (H_2O_2), which is broken down to either water or O_2 and water by GSH and catalase, respectively [57–59]. In the presence of an abnormal level of redox active metal ions, however, H_2O_2 can be cycled into the Fenton and Haber-Weiss reactions instead of being broken down by catalase and GSH. Through these cycles H_2O_2 can be converted to less stable ROS (Figure 10.2) [40, 55, 56].

Prolonged and elevated oxidative stress has been implicated in the pathogenesis of several neurodegenerative diseases, including AD, Parkinson's disease (PD), and amyotrophic lateral sclerosis (ALS) (*vide infra*). Metal ion dyshomeostasis and mitochondrial dysfunction could be the sources of oxidative stress in these neurodegenerative diseases. In AD, for example, the interaction of Aβ and redox active $Cu^{+/2+}$ or $Fe^{2+/3+}$ (Figure 10.1) may facilitate ROS production, resulting in oxidative damage [33, 35, 45]. It has also been reported that heme–Aβ complexes can have peroxidase activity in AD [45, 60]. In PD, a pathological feature is the accumulation of Fe^{3+} in the substantia nigra of diseased neurons, which could increase the likelihood for an overabundance of ROS [61, 62]. H_2O_2 has also been shown to interact with Cu,Zn-SOD1, through the oxidation of residues near the copper metal binding site, which can cause copper release and subsequently deactivate the enzyme, a concern in ALS [63]. Despite their similarities, however, each neurodegenerative disease has specific hallmarks (Figure 10.1).

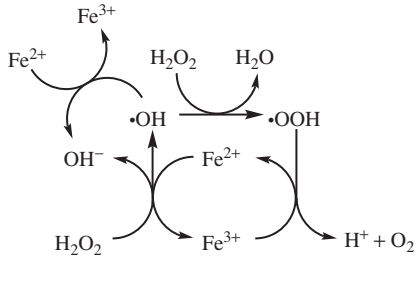

Figure 10.2 *Fenton reaction and Haber-Weiss cycle for the catalytic production of ROS by $Fe^{2+/3+}$ (similar redox chemistry occurs for $Cu^{+/2+}$)*

10.2 Neurodegenerative diseases

10.2.1 Alzheimer's disease (AD)

AD is hallmarked by the accumulation of senile plaques and neurofibrillary tangles (NFTs), composed primarily of Aβ, and hyperphosphorylated tau protein (ptau), respectively, in the brain [18, 33, 35, 42–45, 64–72]. Along with these histopathological characteristics, concentrations of Cu, Zn, and Fe are found to be elevated in *ex vivo* tissue samples collected from AD brains (about 400, 1000, and 900 μM, respectively, in the plaques) [10, 33, 34, 42–45]. It remains unclear, however, whether the total concentration of metals in the brain is altered or their local pools are miscompartmentalized upon initiation and progression of AD [18, 39, 73]. Still, the current consensus is that metal ion dyshomeostasis occurs in AD [33, 44, 64].

Additionally, *in vitro* studies confirm that these metals can generate complexes with Aβ and tau. The coordination chemistry of Aβ with metals has been extensively studied *in vitro* as summarized in Table 10.2 [33–35, 43, 45, 64, 74–80]. The interactions between metal ions and Aβ are shown to accelerate Aβ aggregation and be associated with ROS production *via* Fenton chemistry [54]. It is suggested that these interactions also stabilize toxic, oligomeric Aβ species [33, 34, 81]. Thus, modulation and/or disruption of these interactions could be a potential target for the future design of chemical tools, diagnostics, or therapeutics in order to understand or combat AD [33, 64, 68, 77, 82].

Unlike Aβ, information on metal binding to tau has been relatively limited. As shown in Table 10.2, some binding studies of Cu^{2+}, Al^{3+}, and $Fe^{2+/3+}$ with both full length and fragments of tau and ptau *in vitro* have been reported [35, 83, 102, 103]. Upon binding to ptau, Cu^{2+} has been shown to slightly promote its aggregation [35, 83]. Al^{3+} and Fe^{3+}, but not Fe^{2+}, could also be involved in enhancement of ptau aggregation [35, 83, 102, 103]. Despite these initial studies, the interaction of metals and tau/ptau and the role of metal–tau/ptau species in AD pathogenesis have not been uncovered.

10.2.2 Parkinson's disease (PD)

PD is characterized by the loss of dopaminergic neurons in the substantia nigra region of the brain [61, 84, 104–108]. An increased degradation of the neurotransmitter dopamine by monoamine oxidase (MAO) is also indicative of PD [62, 105]. Along with altered dopamine concentrations, PD can be identified by the accumulation of misfolded α-synuclein (α-syn, Figure 10.1), which aggregates to generate inclusions known as Lewy bodies [84, 85, 107, 109–114]. In PD, distribution of metal ions in the brain has been found to be altered [11, 61, 75, 85, 108–110, 115, 116]. Evidence from atomic absorption spectroscopy, inductively coupled plasma spectroscopy, and biochemical assays has suggested an enhanced concentration of Cu, Zn, Fe, and Al in the substantia nigra of the PD-afflicted brain [85, 109, 110, 115, 117–123]. α-Syn is known to interact with Fe^{2+}, $Cu^{+/2+}$, and Zn^{2+} as presented in Table 10.2 [84–91, 124, 125]. The interaction of metal ions with α-syn has been shown to directly influence structural changes in the peptide, and certain metal ions (e.g., Al^{3+}, $Fe^{2+/3+}$, Co^{3+}, $Cu^{+/2+}$, and Zn^{2+}) could also modify the propensity of α-syn to aggregate [1, 84, 90, 109, 126–128]. Additionally, redox active metal ions bound to α-syn could contribute to the overproduction of ROS [61, 62, 85, 86, 127, 129–134]. While the details of metal interactions with α-syn have not been fully elucidated, it is clear that metals could be linked to the neuropathogenesis of PD; thus, modulation of the interaction between metals and α-syn is a possible drug target for this disease.

10.2.3 Prion disease

Prion diseases, also known as transmittable spongiform encephalopathies (TSE), are a class of neurodegenerative diseases, which include scrapie in sheep, bovine spongiform encephalopathy (BSE) in cattle, and kuru,

Table 10.2 *Amino acid residues involved in metal coordination in proteins and binding affinities*[a]

Metal ions	AD (amyloid-β) [35, 75, 78]	AD (tau) [35, 83]	PD (α-synuclein) [38, 75, 84–91]	Prion (PrP) [75, 92–95]	HD (huntingtin) [96]	ALS (Cu,Zn-superoxide dismutase) [63, 97–101]
Cu^{2+}	CN[b] = 4	**R2 and R3 units** His299, His329, and His330	CN = 4	CN = 4	His82, His98	CN = 5
	Component I (3N1O) (His6, His13, His14, and either Asp1-Ala2 (backbone carbonyl) or Asp1) or (N-terminal amine, two His residues, and Asp1-Ala2 (backbone carbonyl) or Asp1)	**R2 and R3 units** Cys291 and Cys322	**Site 1** (2N2O) (Met1 (N-terminal amine), Asp2 (deprotonated backbone amide, and carboxylate side chain), and a water molecule) ($K_d = 10^{-9}$ M)	**Inter-repeat mode** His61, His69, His77, and either His85 or a water molecule ($K_d = 10^{-6}$ M)		His46, His48, His63, His120, a water molecule
	Component II (3N1O or 4N) (His6, His13, His14, and Ala2 (backbone carbonyl)) or (N-terminal amine, Ala1-Asp2 (deprotonated backbone amide), Ala2-Glu3 (back carbonyl), one His residue) (His6, His13, His14, and either N-terminal amine or Ala1-Asp2 (deprotonated backbone amide)) (K_d[c] = 10^{-11}–10^{-7} M)	($K_d = 10^{-6}$ M)	**Site 2** (3N1O) (Val49 (deprotonated backbone amide), His50 (deprotonated backbone amide and side chain), and a water molecule) ($K_d = 10^{-6}$ M) **Site 1 and 2 macrochelate** (3N1O) (Met1 (N-terminal amine), Asp2 (deprotonated backbone amide and carboxylate side chain), and His50) ($K_d = 10^{-10}$ M) **Site 3** (4O) (Asp119, Asp121, Glu123 (carboxylates), and Asn122 (backbone carbonyl)) ($K_d = 10^{-3}$ M)	**Intra-repeat mode** One His residue, two backbone amides, and one backbone carbonyl of two neighboring, Gly residues ($K_d = 10^{-6}$ M) **Fifth binding site** Involving His96 and His111		($K_d = 10^{-18}$ M)

Cu^{+}	CN = 2 Two His residues ($K_d = 10^{-14}$ or 10^{-7} M)	–	CN = 2 **Site 1** Met1 and Met5 **Site 2** Met116 and Met127 ($K_d = 10^{-6}$–10^{-5} M)	–	–	CN = 3 His46, His48, His120 ($K_d = 10^{-15}$ M)
Zn^{2+}	CN = 4–6 His6, His13, His14, and a combination of Asp1 (N-terminal amine or carboxylate), Arg5 (backbone amide), Tyr10, Glu11, a water molecule ($K_d = 10^{-9}$–10^{-6} M)		**Site 3** Asp119, Asp121, Glu123 (carboxylates), and Asn122 (backbone carbonyl) ($K_d = 10^{-3}$ M)	One His residue, two backbone amides, and one backbone carbonyl of two neighboring, Gly residues ($K_d = 10^{-4}$ M) **Fifth binding site** Involving His96 and His111		CN = 4 His63, His71, His80, Asp83 ($K_d = 10^{-14}$ M)
Fe^{2+}	CN = 6 Asp1, Glu3, His6, His13 or His14, Ala2 (backbone carbonyl), *N*-terminal amine ($K_d = 10^{-4}$ M)	–	**Site 3** Asp119, Asp121, Glu123 (carboxylates), and Asn122 (backbone carbonyl) ($K_d = 10^{-3}$ M)	–	–	–
Mn^{2+}	–	–	–	**Fifth binding site** Involving His96 and His111 ($K_d = 10^{-4}$ M)	–	–

[a]Residues listed are those known to have specific interaction.
[b]CN, coordination number
[c]K_d, dissociation constant.

along with various forms of Creutzfeldt-Jakob disease (CJD) in humans. Prion diseases can be sporadic, genetic, or acquired through exposure to misfolded, aggregation-prone prion proteins (PrP^{Sc}; variant form) [135–138]. Pathologically, it is characterized by the loss of GABAergic neurons (neurons primarily responsible for the production of gamma-aminobutyric acid), the formation of vacuoles (spongiosis) in gray matter, and the production of plaques containing misfolded, aggregation-prone PrP^{Sc} [92, 135–140]. Prion protein (PrP, Figure 10.1) and its fragments can interact with several divalent metals, including Mn^{2+}, Cu^{2+}, and Zn^{2+}, *in vitro* (Table 10.2) [92, 136, 140–143]. Cu^{2+} is suggested to be necessary for some of the neuroprotective properties of normally folded prion protein (PrP^{C}); however, high Cu^{2+} concentrations can lead to the conversion of PrP^{C} to the neurotoxic protein conformation (PrP^{Sc}) [140]. The coordination of Mn^{2+} to PrP^{C} also destabilizes the structure, which can cause the transformation of PrP^{C} to PrP^{Sc} and subsequent aggregation [140, 141]. These observed effects upon PrP^{C} binding to metal ions have motivated the exploration of the link between metal-PrP interactions and pathogenesis in prion diseases [75, 144].

10.2.4 Huntington's disease (HD)

The suggested causative agent in Huntington's disease (HD) is the expansion of the polyglutamine (polyQ) repeat region near the *N*-terminus in huntingtin (htt, Figure 10.1) from normal levels (about 11–34 glutamine residues) to abnormally high levels (>37 glutamine residues) [96, 145–150]. The expanded polyQ region of htt results in a large "sticky" region which facilitates contacts with proteins involved in a variety of cellular processes (e.g., transcription, signaling, and metabolism) and alters their function [149, 151]. This expanded region also decreases the stability of the folded state of polyQ htt compared with normal htt and allows for the aggregation of polyQ htt, possibly leading to neurotoxicity [149, 151–154]. A twofold increase of Cu and Fe has been found in areas of the brain that are most affected by HD [96, 118, 154]. Relatively little has been reported about metal binding to polyQ htt. The only report of metal binding to polyQ htt by Fox *et al*. demonstrated that Cu^{2+} interaction was observed with amino acids within the first 171 residues of both normal and polyQ htt [96]. Additionally, Cu^{2+} binding was found to be dependent on the presence of both His82 and His98, and upon binding to htt, reduction to Cu^{+} was found to occur. Experiments with Fe^{3+} also indicated reduction to Fe^{2+} upon incubation with htt, but no evidence of its coordination to polyQ htt was found [96]. Interaction between htt and $Fe^{2+/3+}$ suggests that polyQ htt could facilitate the production of ROS through Fenton chemistry leading to oxidative stress. Furthermore, both Cu^{2+} and Fe^{3+} have been observed to enhance the aggregation rate of polyQ htt *in vitro* [96, 151]. Additional studies are needed to conclusively decipher the potential role of metal–htt/polyQ htt interactions in HD development.

10.2.5 Amyotrophic lateral sclerosis (ALS)

ALS is categorized as a motor neuron disease and most cases are sporadic with some consideration of familial risk factors [63, 155]. Imbalanced levels of metal ions, specifically $Fe^{2+/3+}$ and Zn^{2+}, have been found in sporadic ALS cases while a portion of familial ALS cases is associated with a mutation in the *SOD1* gene that codes for the antioxidant metalloenzyme, Cu,Zn-SOD1 [47, 63, 107, 156–159]. Over 105 major mutations of the *SOD1* gene have been identified and linked to familial ALS. Interestingly, these mutations occur at a variety of sites, but produce similar outcomes. Normal Cu,Zn-SOD1 is a homodimer that contains two subunits, each consisting of 153 amino acids [63, 97, 160]. Each subunit has two adjacent metal binding sites, one for Cu and one for Zn, acting together to allow Cu,Zn-SOD1 to serve as a superoxide scavenger [63]. Metal binding to Cu,Zn-SOD1 has been extensively studied as outlined in Table 10.2 [63, 97, 98]. Common mutations that affect metal binding are substitutions of the histidine residues or amino acid residues surrounding the metal binding site [63, 98, 99]. These mutations could cause the enzyme to produce ROS rather than

scavenge it, thus elevating oxidative stress in the brain and/or destabilize the folded state of Cu,Zn-SOD1 causing it to misfold and form toxic aggregates [63, 160–162].

Along with the aggregation of Cu,Zn-SOD1, studies have identified inclusions, composed of transactivation response-DNA binding protein (TDP-43) aggregates, localized in hippocampal and frontal cortical neurons of ALS patients [163, 164]. Overexpression of TDP-43 in animal models resulted in toxicity upon aggregation [164]. Recently, it has also been shown that TDP-43 can form aggregates in the presence of Zn^{2+}, but not in the presence of Cu^{2+} or Fe^{2+}, which has been linked to neuronal death in ALS [165]. Overall, the involvement of metal ions with proteins in ALS is multifactorial and remains to be fully elucidated.

10.3 Ligand design to target and modulate metal–protein interactions

The previous sections demonstrated that neurodegenerative diseases are associated with various factors. Developing adequate therapeutics is difficult due to a lack of understanding of both disease etiology and the interconnection of multiple elements with neuropathogenesis. Current treatments for these diseases have focused on attenuating one specific pathogenic factor and consequently only offer symptomatic relief instead of disease-modifying effects [104, 166–172]. Given the influence of metals on multiple neurodegenerative diseases, as stated throughout this chapter, metal chelation therapy has been suggested as a method to disrupt disease-related metal–protein interactions as well as restore metal ion homeostasis and proper protein cellular functions in the body [166]. In order to control the interactions between metal ions and misfolded proteins shown in Figure 10.1, metal chelating agents with traditional applications in metal overload diseases, along with other common chelating compounds (Figure 10.3), were employed and shown to modulate this interaction to varying extents *in vitro* [107, 166, 173–184]. For example, 2,2′,2″,2‴-(ethane-1,2-diylbis(azanetriyl))tetraacetic acid (EDTA) was shown to resolubilize insoluble Cu^{2+}– and Zn^{2+}–Aβ aggregates and affect the morphology of Cu^{2+}–Aβ species generated upon co-incubation with EDTA [178, 179]. Additionally, EDTA has been shown to disaggregate insoluble Al^{3+}-treated tau and ptau species [185] as well as Cu^{2+}-treated htt [96]. DFO (Figure 10.3) has also been studied as a treatment for AD. Administration to AD patients over two years appeared to slow the clinical progression of AD-associated symptoms [186]. Phen (Figure 10.3), together with two of its derivatives, bathocuproine and bathophenanthroline, has been demonstrated to disaggregate metal-associated Aβ aggregates into soluble species [187, 188]. These ligands also mitigated H_2O_2 production by Cu–Aβ species, suggesting a possible use for ROS scavenging or ROS production control [189]. Furthermore, D-penicillamine has shown a minor ability to disaggregate Cu^{2+}-induced Aβ aggregates *in vitro* [190]. D-Penicillamine (Figure 10.3) has also been applied to control the aggregation of co-incubated α-syn and Cu,Zn-SOD1 in addition to decreasing copper levels associated with PrP, diminishing the conversion of PrP^{C} into pathogenic PrP^{Sc} in prion diseases [191, 192].

The application of these traditional chelators for both the study and treatment of neurodegenerative diseases, however, has been limited due to poor brain uptake, inadequate specificity for targeting aberrant metal–protein interactions, and disruption of essential metal–protein cellular functions due to their high metal binding affinities [166, 173, 174, 180, 193–197]. Despite these issues, the results suggest that regulating metal–protein interactions may be a productive method in ligand design for chemical tools to uncover pathogenesis of neurodegenerative diseases and effective diagnostics or therapeutics (*vide infra*).

Recent advancements in the design of tools and treatments have sought to specifically and simultaneously target and modulate multiple disease-related factors caused by deleterious metal–protein interactions by applying a “one molecule-multiple targets” approach. In this chapter we will focus on small molecules which specifically target and modulate metal–protein interactions and regulate ROS production. Such molecules have mainly been fashioned through three design strategies: functionalization, attachment/linkage,

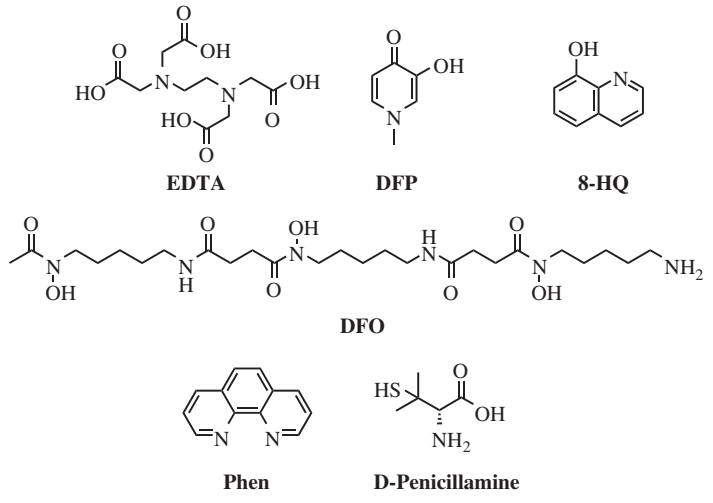

Figure 10.3 *Structures of selected metal chelators. EDTA, 2,2′,2″,2‴-(ethane-1,2-diylbis(azanetriyl))tetraacetic acid; DFP, 3-hydroxy-1-methylpyridin-4(1H)-one; 8-HQ, 8-hydroxyquinoline; DFO, N′-{5-[acetyl(hydroxy)-amino]pentyl}-N-[5-({4-[(5-aminopentyl)(hydroxy)amino]-4-oxobutanoyl}amino)pentyl]-N-hydroxysuccinamide); phen, 1,10-phenanthroline; and* D*-penicillamine, (S)-2-amino-3-mercapto-3-methylbutanoic acid*

and incorporation [106, 166, 198]. Using these approaches, metal binding moieties are combined with frameworks that target and regulate disease-related metal–protein interactions. To prevent the introduction of additional dyshomeostasis and misregulation of metals, the binding affinities of these designed molecules for metals must be balanced in the appropriate range. The affinity for metal ions ought to be strong enough to modulate aberrant metal–protein interactions but weak enough to avoid interference with essential metal–protein interactions for biological functions (generally $K_d \geq 10^{-10}$ M) [33, 199, 200]. These molecules should also demonstrate selectivity for metal ions associated with the diseases (e.g., $Fe^{2+/3+}$ for PD) to hinder exacerbation of metal ion dyshomeostasis. Tuning these properties can often be achieved by consideration of basic inorganic chemistry concepts such as hard-soft acid base principle, the Irving-Williams series, denticity, and the chelate effect [106, 180, 193, 195]. Simple theories cannot always completely describe metal binding properties of small molecules in the heterogeneous *in vivo* environment, however, due to multiple parameters affecting the ability of a ligand to bind to a specific metal ion (e.g., charge at local pH, oxidation state, stability, rate of complexation, and competition with biomolecules) [106, 173, 201–203]. In addition to tuning the metal binding properties of these molecules, the design of the moiety that targets disease-related proteins is important. Unfortunately, there is no set of rules governing the interaction of small molecules with proteins, and most of the molecules known to interact are natural products, discovered through experimental observations, with little structure-interaction relationship exploration [204, 205]. For example, in one of the few structure-interaction relationship studies, the presence of a methyl amino moiety, with the combined hydrogen bond donor (HBD)/hydrogen bond acceptor (HBA) properties of the amine and the hydrophobicity of the methyl group(s), in derivatives of thioflavin-T (ThT), a fluorescent dye that is specific for amyloid fibrils, has been suggested to be important for targeting Aβ fibrils [206–208]. Other structural moieties utilized to target disease-related proteins to identify and regulate potentially pathological metal–protein interactions are discussed later in this chapter.

Along with targeting and modulating aberrant metal–protein complexes, it is critical for designed compounds to be able to penetrate the BBB. Adherence to Lipinski's rules for drug likeness and the use of

calculated brain-blood partitioning values (logBB) are particularly useful in predicting passive diffusion of a ligand across the BBB. The restricted terms of Lipinski's rules dictate that molecules for brain applications should generally have a molecular weight (MW) ≤ 450 g/mol, a calculated logarithm of the octanol-water partition coefficient (*c*logP) ≤ 5, HBD ≤ 5, HBA ≤ 10, and polar surface area (PSA) ≤ 90 Å^2 [209, 210]. The logBB calculation estimates the expected permeability based on an equation (typically defined as logBB = $-0.0148 \times \text{PSA} + 0.152 \times c\text{logP} + 0.139$) [211]. Molecules with logBB values ≤−1.00 are expected to have poor diffusion across the BBB [211]. Alternatively, structural groups that are known to be actively transported through the BBB (e.g., glucose) can be added to the parent framework to improve uptake into the brain [181, 212]. Lastly, these ligands and their corresponding complexes should display low cytotoxicity. Overall, chemical structures capable of targeting and modulating abnormal metal–protein interactions, while also being nontoxic, bioavailable, and BBB permeable, could be employed to construct chemical tools to investigate the molecular basis for or as therapeutics for the treatment of neurodegenerative diseases. Design considerations for molecules and their effects on metal–protein interactions are discussed in detail in the following sections.

10.3.1 Metal chelating compounds

As discussed in the previous section, there are several issues limiting the use of metal chelators *in vivo*. This next section discusses some of the modifications made to frameworks of these compounds in order to improve their properties. A good example of several types of possible modifications comes from the work with deferiprone (DFP) (Figure 10.3). Glycosylated derivatives have been developed in order to both improve DFP's BBB permeability and limit the interaction of this strong chelator (K_d, about 10^{-21} and 10^{-13} in a 1 : 2 M^{2+}:DFP stoichiometry for Cu^{2+} and Zn^{2+}, respectively; 10^{-12} M in a 1 : 3 M^{2+}:DFP fashion for Fe^{3+}) with metals outside the brain [213]. A DFP prochelator employed a glucose moiety that unmasks the metal binding site upon cleavage by β-glycosidase [181]. Additionally, Orvig and co-workers have capitalized on the active uptake of glucose to prepare a family of DFP derivatives to target and modulate metal-associated Aβ [213]. The core DFP framework was *O*-glycosylated, and an Aβ-interacting methylamino phenyl and benzothiazolyl moieties were appended to the *N*-position. Cu^{2+}- and Zn^{2+}-induced Aβ aggregation was attenuated using these new compounds. When benzothiazolyl derivatives were appended onto the framework at the *N*-position, selective resolubilization of Cu^{2+}-induced Aβ aggregates was visualized, suggesting specificity for Cu^{2+}–Aβ over Zn^{2+}–Aβ species [213]. Deferiprone, combined with polystyrene nanoparticles (DFP-NPs), retains the metal binding properties of the ligand while improving its viability in cells and efficacy to reach the brain [214]. The DFP-NP conjugates inhibited Aβ fibril formation; however, their influence on metal–protein interactions observed in neurodegenerative diseases has yet to be studied.

The most well-studied metal chelator based framework for controlling metal–protein interactions in neurodegenerative diseases is 8-hydroxyquinoline (8-HQ; Figure 10.3), which can act as a bidentate chelator [215, 216]. Derivatives of 8-HQ have been found to modulate aberrant metal–protein interactions in neurodegenerative diseases, including AD, with sufficient success to have reached clinical trials [215–217]. The 8-HQ derivative clioquinol (CQ; Table 10.3) is an approved topical antiseptic and was once administered as an oral intestinal amebicide before being pulled from the market in 1970s due to a possible side effect, subacute myelo-optic neuropathy (SMON) [217–219]. The ability of CQ to chelate transition metals (K_d, about 10^{-10} M for Cu^{2+}; about 10^{-9} M for Zn^{2+}) and to passively cross the BBB suggests that this compound could be a viable treatment for neurological conditions, serving as a modulator for disease-associated metal–protein interactions [33, 217, 219–223]. The proposed mechanism of action for CQ is twofold: (i) it can chelate metal ions from disease-related proteins, which influences aggregation [218, 224, 225] and (ii) it can act as an ionophore, possibly mitigating changes in metal ion homeostasis by redistributing metal ions across membranes into cells and areas with lower metal ion concentrations [175, 224, 226]. Molecules possessing both of these properties are termed metal–protein attenuating compounds (MPACs) [224]. CQ has

Table 10.3 *8-Hydroxyquinoline (8-HQ) derivatives and their metal-interacting protein targets in neurodegenerative diseases*

	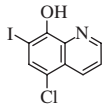	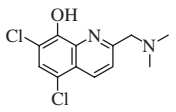	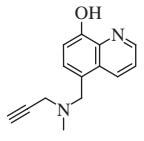	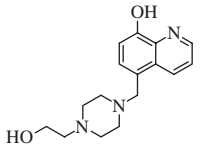	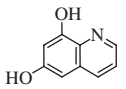	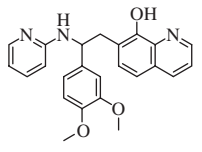
Protein	CQ	PBT-2	M30	VK-28	HQ-161	HQ-415
Amyloid-β	✓	✓	–	–	–	–
Tau	–	✓	–	–	–	–
α-Synuclein	✓	–	–	–	×[a]	✓
Prion protein	✓	–	–	–	–	–
Huntingtin	✓	✓	–	–	×	✓
TDP-43[b]	×	–	✓	✓	✓	✓

[a]HQ-161 was only found to improve α-syn-induced toxicity in *C. elegans* [226].

[b]TDP-43, transactivation response-DNA binding protein.

✓Denotes that modulation of the metal–protein interaction by the compound was observed; × represents that control of the metal–protein interaction by the compound was not observed – interaction was not determined. CQ, 5-chloro-7-iodoquinolin-8-ol; PBT-2, 5,7-dichloro-2-[(dimethylamino)methyl]quinolin-8-ol; M30, 5-[(*N*-methyl-*N*-propargylamino)methyl]quinolin-8-ol; VK-28, 5-[[4-(2-hydroxyethyl)-1-piperazinyl]methyl]quinolin-8-ol; HQ-161, quinoline-6,8-diol; and HQ-415, 7-[2-(3,4-dimethoxyphenyl)-2-(pyridin-2-ylamino)ethyl] quinolin-8-ol.

been shown to chelate metal ions from Aβ aggregates, cause at least partial disaggregation, and change the morphology of aggregated species [218, 224, 225].

In AD transgenic mice, the amount of amyloid plaques was lessened upon CQ administration with improved symptoms and no observable adverse side effects [217, 222, 227]. Several human trials followed, the first of which was an uncontrolled study with 20 patients treated daily with an 80 mg dose of CQ for 21 days; resulting in patients displaying signs of improved cognitive function [227, 228]. Subsequent phase II clinical trials had similar outcomes for AD patients with moderate dementia, but patients with more severe AD symptoms showed less significant improvement [199, 227, 228]. In PD, CQ demonstrated the ability to curtail the α-syn-induced toxicity in yeast cultures, and to lower the toxicity of 1-methyl-4-phenyl-1,2,3,6-tetrahydropyridine (MPTP), a neurotoxin that causes PD-like symptoms, in mice [226, 229]. It is important to point out in the latter case that genetically reducing the amount of iron in the mice had similar effects, suggesting reduced bioavailability of iron caused the observed decrease in toxicity rather than the modulation of a specific metal–protein interaction [229]. CQ was found to inhibit aggregation of polyQ htt in HD, affording diminished polyQ htt aggregates, and improved HD-like symptoms in transgenic mice [96, 230]. CQ has also been tested in prion disease and was able to diminish the amount of PrP^{Sc} in PrP^{Sc}-infected Neuro-2a (N2a) neuroblastoma cells; however, in PrP^{Sc}-infected hamsters no change in the amount of PrP^{Sc} was observed upon CQ treatment [231, 232].

While CQ has some properties that made it suitable to modulate aberrant metal–protein interactions in the brain (e.g., BBB permeability, metal binding affinity in optimal range), it still lacks specificity to localize within the brain and selectively target potentially pathological metal–protein interactions [233–236]. In addition, scale-up reactions for clinical trials produced toxic di-iodinated byproducts of CQ, which prevented larger scale testing of CQ in humans [236]. As a result, clinical trials with CQ ceased and attention has shifted to another 8-HQ derivative, PBT-2 (Table 10.3), which was carefully designed to avoid scale-up production

problems and to maximize oral bioavailability [234, 235]. Furthermore, the structure of PBT-2 contains a dimethylamino moiety which has been proposed to help target Aβ plaques in AD [75, 208, 237].

Initial *in vitro* studies of PBT-2 demonstrated that this compound has similar metal binding affinities for Cu^{2+} and Zn^{2+} (K_d, about 10^{-10} M for Cu^{2+} and Zn^{2+}) as CQ but is a superior ionophore [238]. Studies with metal–Aβ have shown PBT-2 is able to regulate Cu–Aβ-induced H_2O_2 production to a greater extent than CQ [238]. PBT-2 was, however, unable to match CQ's ability to disaggregate metal–Aβ aggregates. *In vivo*, PBT-2 was shown to improve the cognitive abilities of AD and PD mouse models as well as limit paralysis in a *Caenorhabditis elegans* model of HD caused by polyQ proteins [239]. Furthermore, PBT-2, but not CQ, could decrease abnormal tau phosphorylation in AD mice [238]. Clinical trials of PBT-2 on AD patients, like those of CQ, indicated that cognitive improvement between placebo and PBT-2-treated patients were only significant at earlier stages of the disease [228, 240, 241]. Although PBT-2 was well tolerated in early clinical trials, more rigorous clinical trials will be beneficial to fully assess this compound's utility improving cognition in AD [228, 241].

There have also been some reports of other 8-HQ derivatives in other neurodegenerative diseases (Table 10.3). The effects of VK-28 and M30 in an ALS mouse model mice (Cu,Zn-SOD1 G93A) were examined by Wang *et al*. [156]. Both of these chelators could modulate iron levels, oxidative stress, and decrease the aggregation of TDP-43. In a study by Tardiff *et al*. [226], the properties and performance in several neurodegenerative disease models of two 8-HQ derivatives, HQ-161 and HQ-415, were compared with CQ. Both compounds were found able to lower toxicity caused by TDP-43 in an ALS yeast model in comparison with CQ, which was unable to regulate toxicity of TDP-43 in the same system [226]. Additionally, HQ-415 was shown to act similarly to CQ in PD and HD yeast models, reducing toxicity of α-syn and polyQ-htt, respectively, while HQ-161 had little effect [226]. All of these compounds, however, were capable of reducing toxicity of α-syn in a *C. elegans* model of PD. Furthermore, toxicity studies suggested that HQ-415 (but not HQ-161) induced metal ion starvation in cells [226]. The differences in reactivity were suggested to result from their hydrophilicity and ability to interact with intracellular pools of metal ions. More systematic and comprehensive investigations are required to further evaluate the relationship between structural variations and their influence on reactivity toward metal–protein complexes.

10.3.2 Small molecules designed for metal–protein complexes

As an alternative to utilizing traditional chelators and their analogs, new small molecules containing structural moieties to target and modulate specific metal–protein interactions have been developed (*vide infra*). Some of these molecules were constructed by connecting structural moieties for metal chelation and protein interaction (i.e., linkage approach), or installing a metal chelation site into a protein-targeting structure (i.e., incorporation approach) [166, 198, 242].

ThT (Figure 10.4) has a high affinity for Aβ fibrils (nanomolar K_d) [206–208]. Thus, several compounds have been based on its framework to target metal – Aβ species and modulate the interaction between metal and Aβ. The first reported example is XH1 (Figure 10.4) which is composed of two ThT-like molecules linked with diethylenetriaminepentaacetic acid (DTPA), a strong metal chelator for Fe^{2+}, Fe^{3+}, Cu^{2+}, and Zn^{2+} (K_d, about 10^{-16}, 10^{-28}, 10^{-21}, and 10^{-18} M, respectively) [243]. XH1 influenced Zn^{2+}-induced Aβ aggregation *in vitro* and reduced plaque load in an AD mouse model [243]. Moreover, when compared with DTPA's effects on Zn^{2+}-triggered Aβ aggregation *in vitro*, XH1 was able to decrease aggregation by about 50% more, which demonstrates the value of having moieties targeting both metal ions and proteins simultaneously to disrupt aberrant metal–protein interactions.

FC1 (Figure 10.4) is another multifunctional molecule derived from the ThT framework. The molecule is based on a neutral ThT backbone in which the dimethylamino group is replaced with the moderate metal binding moiety di-(2-picolyl)amine (DPA) (K_d, about 10^{-9} M for Cu^{2+} and 10^{-7} M for Zn^{2+}) [156]. FC1 was

found to partially transform Cu^{2+} – and Zn^{2+} – Aβ aggregates into small, amorphous aggregates. When HeLa cells exposed to metal – Aβ were treated with FC1, however, increased toxicity was observed, implying that FC1 may stabilize the generation of toxic Aβ oligomers [156].

Mirica and co-workers took a similar approach to the design of L1 and L2 (Figure 10.4) where a dipyridylmethyl (L1) or a pyridylmethyl (L2) group was installed onto a ThT derivative with the dimethylaminophenyl group replaced with one derived from *o*-vanillin, previously shown to interact with Aβ [244]. As expected, tetradentate L1 could bind Cu^{2+} and Zn^{2+} more strongly than tridentate L2 (K_d, about 10^{-10} M *versus* 10^{-8} M for Cu^{2+}; about 10^{-8} M *versus* 10^{-7} M for Zn^{2+}). Moreover, for Aβ interaction, L2 (K_i about 30 nM) was able to bind more strongly to Aβ fibrils than L1 (K_i about 200 nM). Despite these differences both L1 and L2 were capable of inhibiting the formation of metal – Aβ aggregates as well as disaggregate preformed aggregates. Similar to FC1, however, treatment of N2a cells with Aβ, Cu^{2+} or Zn^{2+}, and L1 or L2 resulted in increased toxicity over L1- or L2-untreated cells [244].

HBX, HBT, and BM (iodinated forms; Figure 10.4) were discovered by *in silico* screening commercially available ThT derivatives for BBB permeability, antioxidant properties, and synthetic ease of iodination for possible use as imaging agents [245]. The properties of Aβ interaction (ThT) and metal chelation (a portion of ThT and a phenol or aniline ring) were introduced into one framework. The iodinated forms of these

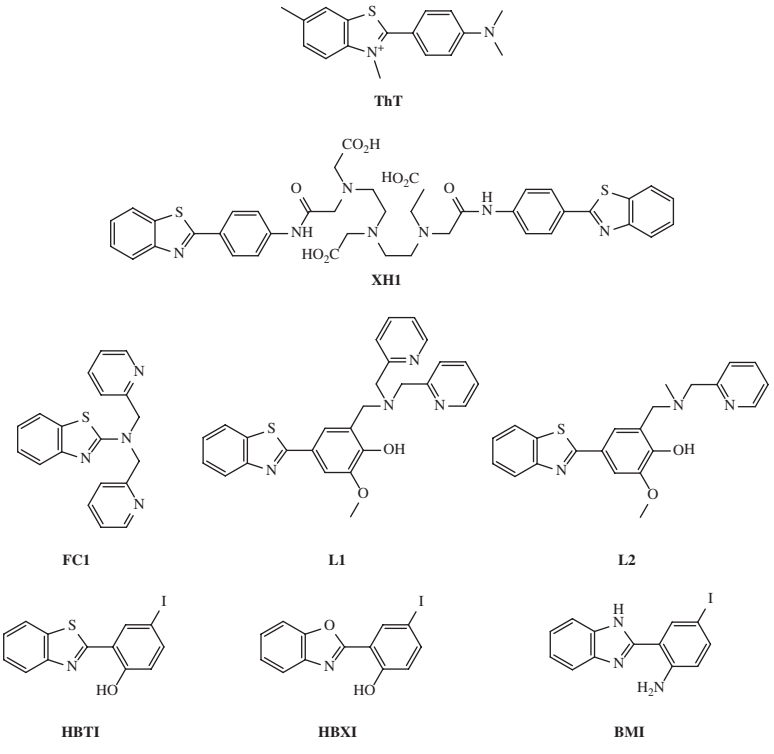

Figure 10.4 *Structures of thioflavin-T (ThT) derivatives. ThT, 4-(3,6-dimethylbenzothiazol-3-ium-2-yl)-N,N-dimethylaniline; XH1, ([(4-(benzothiazol-2-yl)phenylcarbamoyl)methyl]-{2-[(2-{[(4-(benzothiazol-2-yl)phenylcarbamoyl)methyl](carboxymethyl)amino}ethyl)(carboxymethyl)amino] ethyl}amino)acetic acid; FC1, N,N-bis(pyridin-2-ylmethyl)-3a,7a-dihydrobenzothiazol-2-amine; L1, 4-(3a,7a-dihydrobenzothiazol-2-yl)-2-methoxy-6-((methyl(pyridin-2-ylmethyl)amino)methyl)phenol; L2, 2-((bis(pyridin-2-ylmethyl)amino)methyl)-4-(3a,7a--dihydrobenzothiazol-2-yl)-6-methoxyphenol; HBTI, 2-(benzothiazol-2-yl)-4-iodophenol; HBXI, 2-(benzoxazol-2-yl)-4-iodophenol; and BMI, 2-(1H-benzimidazol-2-yl)-4-iodoaniline*

compounds, HBXI, HBTI, and BMI (Figure 10.4), were found to be mostly neutral at physiological pH, suggesting that they may passively cross the BBB. Furthermore, all of the derivatives were able to coordinate Cu^{2+} and Zn^{2+} with K_d values similar to CQ as well as inhibit metal-induced Aβ aggregation [245].

Stilbene derivatives, previously used as imaging agents for Aβ aggregates, have demonstrated an ability to target Aβ fibrils with nanomolar binding affinities (Figure 10.5a) [246–248]. L1-b (Figure 10.5a) was designed by incorporating two nitrogen donor atoms into the structure of the stilbene derivative (for Aβ interaction) to impart metal chelation [188]. This compound was able to modulate metal-induced Aβ aggregation and diminish metal – Aβ-induced cytotoxicity [249]. Owing to limited solubility of L1-b in aqueous media, the reduced amine form, L2-b (Figure 10.5a), was designed to combat this problem [250]. L2-b was capable of binding metal ions with affinities for Cu^{2+} and Zn^{2+} (K_d, about 10^{-10} and 10^{-6} M,

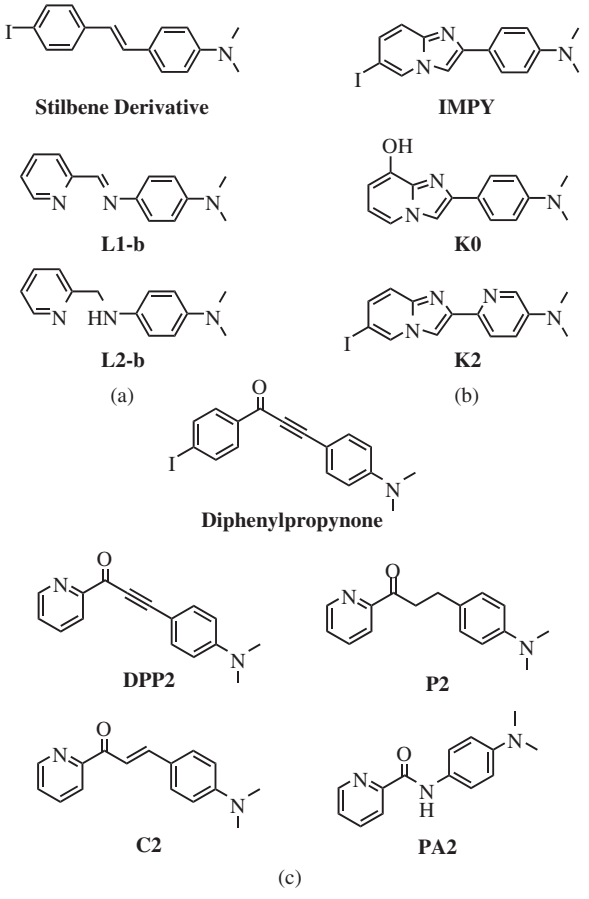

Figure 10.5 *Structures of small molecules designed based on the frameworks of (a) the stilbene derivative (4-(dimethylamino)-4′-iodostilbene), (b) IMPY ((2-(4′-dimethylaminophenyl)-6-iodoimidazo[1,2-a]pyridine)), and (c) diphenylpropynone (3-(4-(dimethylamino)phenyl)-1-(4-iodophenyl)-2-propyn-1-one. L1-b, N^1,N^1-dimethyl-N^4-(pyridin-2-ylmethylene)benzene-1,4-diamine; L2-b, N^1,N^1-dimethyl-N^4-(pyridin-2-ylmethyl)-benzene-1,4-diamine; K0, 2-[4-(dimethylamino)phenyl]imidazo[1,2-a]pyridin-8-ol; K2, 6-(6-iodoimidazo[1,2-a]pyridin-2-yl)-N,N-dimethylpyridin-3-amine; DPP2, 3-(4-(dimethylamino)phenyl)-1-(pyridin-2-yl)prop-2-yn-1-one; C2, (E)-3-(4-(dimethylamino)phenyl)-1-(pyridin-2-yl)prop-2-en-1-one; P2, 3-(4-(dimethylamino)phenyl)-1-(pyridin-2-yl)propan-1-one; and PA2, N-(4-(dimethylamino)phenyl)picolinamide*

respectively) in the appropriate range needed to target metal-associated Aβ. Two dimensional ^{1}H-^{15}N Transverse relaxation-optimized-heteronuclear single quantum coherence nuclear magnetic resonance spectroscopy (TROSY HSQC) NMR demonstrated L2-b could interact directly with Aβ near the metal binding region. As a result, L2-b could control metal-mediated Aβ aggregation pathways *in vitro* and reduce the toxicity induced by metal – Aβ species in human neuroblastoma M17 cells. Additionally, it was shown to disaggregate *ex vivo* Aβ plaques in brain homogenates obtained from human AD patients [250].

Another compound, IMPY (2-(4′-dimethylaminophenyl)-6-iodoimidazo[1,2-*a*]pyridine) (Figure 10.5b), was developed as an imaging agent for Aβ plaques [247]. IMPY binds to Aβ fibrils, and this property was exploited by using this framework as a template to design new molecules for targeting and controlling metal–Aβ interactions. A hydroxy group was incorporated into the IMPY framework to produce K0 (Figure 10.5b) which could bind Cu^{2+} and modulate Cu^{2+}-triggered Aβ aggregation *in vitro* [188]. For the second generation of compounds, the metal chelation site was modified from an N,O donor atom site to an N,N donor atom site by incorporating a single N donor atom into the IMPY structure, generating K2 [251]. These compounds were able to moderately regulate Cu^{2+}- and Zn^{2+}-mediated Aβ aggregate formation and disassembly [251].

The compound DPP2 (Figure 10.5c) was generated by the installation of an N donor atom into a proposed Aβ imaging agent based on a diphenylpropynone framework [252]. The N,O donor atom metal binding site of DPP2 could bind Cu^{2+} with high nanomolar K_d, control both metal-free and metal-induced Aβ aggregation, and disaggregate preformed aggregates. Moreover, DPP2 has the potential to cross the BBB passively, as confirmed by an *in vitro* assay [252]. The application of DPP2, however, was limited by its low micromolar cytotoxicity, possibly due to the carbonyl-triple bond moiety acting as a Michael acceptor which could react with biomolecules forming covalent adducts [252, 253]. Thus, DPP2 was recently structurally modified to ameliorate its cytotoxicity while maintaining BBB permeability [253]. The triple bond of DPP2 was reduced to a double or single bond, to generate new compounds, C2 and P2 (Figure 10.5c), respectively. In addition, PA2 (Figure 10.5c) was designed by replacing the 2-methylpyridine in L2-b (Figure 10.5a) with the 2-pyridyl ketone from DPP2 (Figure 10.5c). All of these derivatives maintained DPP2's BBB permeability; noticeably, their reactivity with metal-free Aβ and metal – Aβ species was altered [253]. The diminished reactivity of P2 and C2, compared with DPP2, is believed to stem from increased flexibility of the overall structure. In contrast to DPP2 and C2 which could modulate metal-free as well as metal – Aβ aggregation, PA2 was only able to modulate the aggregation of metal – Aβ species. Structural modification of DPP2 was shown to reduce cytotoxicity [253]. C2 with a double bond was slightly less cytotoxic than DPP2; complete removal of an unsaturated bond in P2 and PA2 demonstrated the greatest reduction in cytotoxicity [253]. In all of the above Aβ imaging agent-based molecules, maintaining the dimethylamino group in the frameworks proved important for activity. This highlights the value of selecting and retaining key structural groups and backbones from molecules known to interact with Aβ for the design of new compounds to target and modulate metal – Aβ species [159, 188, 250, 251, 253].

10.3.3 Other relevant compounds

Pyridine-based compounds have been developed to interrogate metal – Aβ interactions in AD (*vide infra*). Specifically, ENDIP (N^1,N^2-bis(pyridin-2-ylmethyl)ethane-1,2-diamine) (Figure 10.6), a tetradentate ligand, has demonstrated its ability to modulate Cu^{2+}- and Zn^{2+}-induced Aβ aggregation by chelating the metal from Aβ [254]. The binding affinities of this ligand (K_d, about 10^{-12} M for Cu^{2+}; about 10^{-7} M for Zn^{2+}) are also appropriate for interaction with metal – Aβ species rather than other metalloproteins present in the brain [76, 254]. Compound L1′ (Figure 10.6) also contains a pyridyl group, along with a triazole moiety, to manipulate metal–Aβ interactions [255]. L1′ was shown to influence Cu^{2+}- and Zn^{2+}-mediated Aβ aggregation *in vitro* [255]. These data suggest that pyridine moieties could be utilized for the development of small molecules for the regulation of metal–protein interactions, if optimized for specific protein targets (*vide infra*).

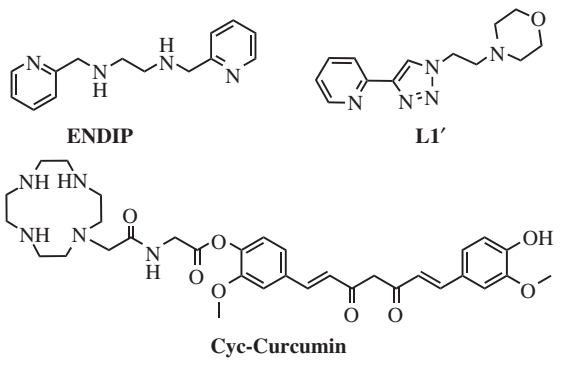

Figure 10.6 *Structures of pyridine- and cyclen-based ligands. ENDIP, N^1,N^2-bis(pyridin-2-ylmethyl)ethane-1,2-diamine; L1′, 4-(2-(4-(pyridin-2-yl)-1H-1,2,3-triazol-1-yl)ethyl)morpholine; and cyc-curcumin, 4-((1E,6E)-7-(4-hydroxy-3-methoxyphenyl)-3,5-dioxohepta-1,6-dienyl)-2-methoxyphenyl (2-(1,4,7,10-tetraazacyclododecan-1-yl)acetyl)glycinate*

Derivatives of cyclam and cyclen (K_d, about 10^{-28} and 10^{-23} M for Cu^{2+}, respectively) [256, 257] are also of interest in the design of agents to target metal–Aβ species and modulate their interaction and reactivity in AD. Initial studies suggested that Co^{3+}-cyclen (Co^{3+}-cyc) complexes were able to proteolytically cleave Aβ by hydrolysis of amide bonds [258]. This finding has led to the construction of cyc-KLVFF and cyc-curcumin (Figure 10.6), two synthetic analogs of Aβ targeting molecules produced through the linkage approach [256]. KLVFF is the self-recognition motif in Aβ [256]. This compound could coordinate Cu^{2+} and disrupt Cu – Aβ aggregates *in vitro* as well as cleave Aβ oligomers [256]. Cyc-curcumin has shown a similar ability to modulate Cu-induced aggregation and proteolytically cleave Aβ; however, it has been neither as potent nor as stable under aqueous conditions as cyc-KLVFF. One drawback to the use of cyclen and cyclam are their high binding affinities for Cu^{2+} and Zn^{2+}, which may allow them to perturb metalloproteins nonspecifically and further disrupt metal ion homeostasis. These results, however, lend support to the potential of covalently linked small molecules and peptides to target and mediate metal–protein interactions in neurodegenerative diseases [256].

10.3.4 Naturally occurring molecules

Naturally occurring compounds (in particular, polyphenolic compounds) have also been investigated for their ability to probe and influence metal–protein interactions in neurodegenerative diseases [43, 166]. A polyphenolic flavonoid, myricetin (Figure 10.7), was studied by Lim and co-workers [259]. Myricetin was observed to influence metal-induced Aβ aggregation to a greater extent than metal-free Aβ aggregation *in vitro*, as well as diminish toxicity related to metal – Aβ species, proposing a possible use in AD research and treatment [259]. The polyphenolic compound from green tea, epigallocatechin-3-gallate (EGCG; Figure 10.7), has been studied to understand and treat numerous diseases, including AD and PD (*vide infra*). EGCG could lower Aβ-related neurotoxicity and generate non-toxic Aβ oligomers under both metal-free and metal-present conditions [260–262], and it was capable of disaggregating preformed α-syn fibrils [261, 263]. The molecular mechanisms of these effects toward Aβ and metal – Aβ were recently investigated using biochemical and biophysical methods [264]. EGCG could form complexes with metal-free Aβ as well as metal-associated Aβ, showing compaction of Aβ conformations [264, 265].

Another polyphenol, resveratrol (Figure 10.7), a plant-derived antioxidant, is of particular interest in the study of metal – Aβ species. Conflicting reports on the effects of resveratrol on Aβ aggregation have been made, and these discrepancies arise from the different methodologies employed in sample preparation [266–268]. Based on these studies, no significant alteration in Cu^{2+}-associated Aβ aggregation by resveratrol

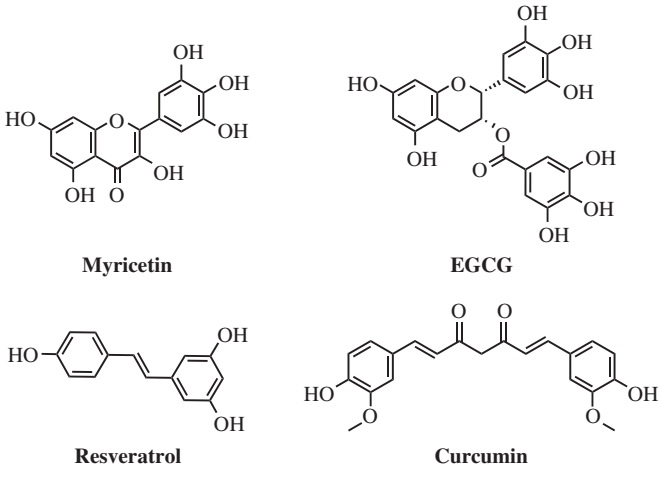

Figure 10.7 *Structures of selected, naturally occurring compounds. Myricetin, 3,5,7-trihydroxy-2-(3,4,5-trihydroxyphenyl)-4-chromenone; EGCG, [(2R,3R)-5,7-dihydroxy-2-(3,4,5-trihydroxyphenyl)chroman-3-yl] 3,4,5-trihydroxybenzoate; resveratrol, 3,4′,5-trihydroxy-trans-stilbene; and curcumin, (1E,6E)-1,7-bis-(4-hydroxy-3-methoxyphenyl)-1,6-heptadiene-3,5-dione*

has been shown [266]. Studies have indicated, however, that resveratrol could be as a potent antioxidant against ROS generated by $Cu^{+/2+}$ – Aβ and $Fe^{2+/3+}$ – Aβ, suggesting that further investigations on this framework are warranted [266].

Additionally, curcumin (Figure 10.7), a naturally occurring curcuminoid found in turmeric, has been studied for its ability to interact with metal–protein complexes found in neurodegenerative diseases [269–271]. Curcumin has antioxidative, anti-inflammatory, and anti-microbial properties similar to other natural products used as possible therapeutic agents for multiple neurodegenerative diseases [270]. Curcumin is also shown to interact with metal – Aβ species [270, 271]. It has an approximately micromolar and nanomolar K_d values for Cu^{2+} and Aβ, respectively [271, 272]. These properties allow it to alter the aggregation pathway of Aβ in the presence of metal ions and, at low concentrations, scavenge ROS generated by metal ions [273]. Owing to its poor solubility and bioavailability as well as its instability in aqueous media, structural modifications are needed to improve the viability of this framework prior to further use as a chemical tool or in therapeutic applications [269].

10.4 Conclusions

Neurodegenerative diseases have been the focus of intense research recently, especially given their broad impact on public health. The complex and relatively unknown etiology of many of these illnesses and the relative lack of diagnostic and treatment methodologies make progress of paramount importance. It has been well established that metal ion dyshomeostasis and subsequent interaction between metal ions and proteins are two of a number of common factors in a variety of neurological diseases, including AD, PD, HD, prion, and ALS. Research efforts have striven to develop selective ligands and probes to target and mediate or interrupt the metal–protein interactions which are suggested to promote toxic protein aggregation in each of these diseases. The current understanding of the specific interactions between metal ions and proteins that can contribute to the onset and/or progression of neurodegenerative diseases has resulted in the design of molecules that target these potentially pathological metal–protein interactions. Several of these frameworks

have shown initial promise as chemical tools to provide insights into the relationship between metal–protein interactions and pathogenesis in neurodegenerative diseases. Clarification of the link between metal ions, misfolded proteins, and neurodegeneration could lead to the design of compounds with more promising therapeutic qualities in the future.

Abbreviations

α-Syn	α-Synuclein
Aβ	Amyloid-β
AD	Alzheimer's disease
ALS	Amyotrophic lateral sclerosis
AMPA	2-Amino-3-(3-hydroxy-5-methylisoxazol-4-yl)propanoic acid
BBB	Blood-brain barrier
BSE	Bovine spongiform encephalopathy
CJD	Creutzfeldt-Jakob disease
*c*logP	Calculated logarithm of the octanol-water partition coefficient
C*c*O	Cytochrome *c* oxidase
CQ	Clioquinol; 5-chloro-7-iodoquinolin-8-ol
CSF	Cerebral spinal fluid
Cu,Zn-SOD1	Copper and zinc superoxide dismutase
DβM	Dopamine β monooxygenase
DFO	Deferoxamine; *N*-{5-[acetyl(hydroxy)amino]pentyl}-*N*-[5-({4-[(5-aminopentyl)(hydroxy)amino]-4-oxobutanoyl}amino)pentyl]-*N*-hydroxysuccinamide)
DFP	Deferiprone; 3-hydroxy-1-methylpyridin-4(1*H*)-one
DFP-NP	Deferiprone functionalized with polystyrene nanoparticles
DPA	Di-(2-picolyl)amine
DTPA	Diethylenetriaminepentaacetic acid
EDTA	2,2′,2″,2‴-(Ethane-1,2-diylbis(azanetriyl))tetraacetic acid
EGCG	Epigallocatechin-3-gallate
ENDIP	N_1,N_2-Bis(pyridin-2-ylmethyl)ethane-1,2-diamine
ETC	Electron transport chain
GSH	Glutathione
H_2O_2	Hydrogen peroxide
HBA	Hydrogen bond acceptor
HBD	Hydrogen bond donor
HD	Huntington's disease
HQ	Hydroxyquinoline
htt	Huntingtin
IMPY	2-(4′-Dimethylaminophenyl)-6-iodoimidazo[1,2-*a*]pyridine
MAO	Monoamine oxidase
MPACs	Metal–protein attenuating compounds
MPTP	1-Methyl-4-phenyl-1,2,3,6-tetrahydropyridine
MW	Molecular weight
N2a	Neuro-2a
NFTs	Neurofibrillary tangles
NMDAR	*N*-methyl-D-aspartate receptor
O_2	Dioxygen

$O_2^{\bullet-}$	Superoxide
PD	Parkinson's disease
PolyQ	Polyglutamine
PrP	Prion protein
PrP^C	Normally folded prion protein
PrP^{Sc}	Misfolded, aggregation-prone prion protein
PSA	Polar surface area
pTau	Hyperphosphorylated tau protein
ROS	Reactive oxygen species
SMON	Subacute myelo-optic neuropathy
TDP-43	Transactivation response-DNA binding protein
ThT	Thioflavin T; 4-(3,6-dimethylbenzothiazol-3-ium-2-yl)-*N*,*N*-dimethylaniline
TfR	Transferrin receptor
TSE	Transmittable spongiform encephalopathy
ZnTs	Zinc transporter proteins

References

1. Bush, A.I. (2000) Metals and neuroscience. *Curr. Opin. Chem. Biol*, **4** (2), 184–191.
2. Burdette, S.C. and Lippard, S.J. (2003) Meeting of the minds: metalloneurochemistry. *Proc. Natl. Acad. Sci. U.S.A.*, **100** (7), 3605–3610.
3. Kandel, E.R., Schwartz, J.H., Jessell, T.M. *et al*. (2012) *Principles of Neural Science*, McGraw-Hill Professional, New York.
4. Gerhardsson, L., Lundh, T., Minthon, L. and Londos, E. (2008) Metal concentrations in plasma and cerebrospinal fluid in patients with Alzheimer's disease. *Dement. Geriatr. Cogn. Disord.*, **25** (6), 508–515.
5. Frederickson, C.J., Koh, J.Y. and Bush, A.I. (2005) The neurobiology of zinc in health and disease. *Nat. Rev. Neurosci.*, **6** (6), 449–462.
6. Frederickson, C.J. and Bush, A.I. (2001) Synaptically released zinc: physiological functions and pathological effects. *BioMetals*, **14** (3–4), 353–366.
7. Li, Y.V., Hough, C.J. and Sarvey, J.M. (2003) Do we need zinc to think? *Sci. STKE*, **2003** (182), pe19.
8. Frederickson, C. (2003) Imaging zinc: old and new tools. *Sci. STKE*, **2003** (182), pe18.
9. Kay, A.R. (2006) Imaging synaptic zinc: promises and perils. *Trends Neurosci.*, **29** (4), 200–206.
10. Lovell, M.A., Robertson, J.D., Teesdale, W.J. *et al*. (1998) Copper, iron and zinc in Alzheimer's disease senile plaques. *J. Neurol. Sci.*, **158** (1), 47–52.
11. Que, E.L., Domaille, D.W. and Chang, C.J. (2008) Metals in neurobiology: probing their chemistry and biology with molecular imaging. *Chem. Rev.*, **108** (5), 1517–1549.
12. Lippard, S.J. and Berg, J.M. (1994) *Principles of Bioinorganic Chemistry*, University Science Books, Mill Valley, CA.
13. Gray, H.B., Stiefel, E.I., Valentine, J.S. and Bertini, I. (2007) *Biological Inorganic Chemistry: Structure and Reactivity*, University Science Books, Sausalito, CA.
14. Slutsky, I., Abumaria, N., Wu, L.-J. *et al*. (2010) Enhancement of learning and memory by elevating brain magnesium. *Neuron*, **65** (2), 165–177.
15. Leal, S.S., Botelho, H.M. and Gomes, C.M. (2012) Metal ions as modulators of protein conformation and misfolding in neurodegeneration. *Coord. Chem. Rev.*, **256** (19-20), 2253–2270.
16. Bowman, A.B., Kwakye, G.F., Herrero Hernández, E. and Aschner, M. (2011) Role of manganese in neurodegenerative diseases. *J. Trace Elem. Med. Biol.*, **25** (4), 191–203.
17. Zheng, W. and Monnot, A.D. (2012) Regulation of brain iron and copper homeostasis by brain barrier systems: implication in neurodegenerative diseases. *Pharmacol. Ther.*, **133** (2), 177–188.
18. Ayton, S., Lei, P. and Bush, A.I. (2013) Metallostasis in Alzheimer's disease. *Free Radical Biol. Med.*, **65**, 76–89.

19. Frederickson, C.J. (1989) Neurobiology of zinc and zinc-containing neurons. *Int. Rev. Neurobiol.*, **31**, 145–238.
20. Levenson, C.W. and Tassabehji, N.M. (2007) Role and regulation of copper and zinc transport proteins in the central nervous system, in *Handbook of Neurochemistry and Molecular Neurobiology* (ed M.E. Reith), Springer, New York, pp. 257–284.
21. Kambe, T., Yamaguchi-Iwai, Y., Sasaki, R. and Nagao, M. (2004) Overview of mammalian zinc transporters. *Cell. Mol. Life Sci.*, **61** (1), 49–68.
22. Assaf, S.Y. and Chung, S.H. (1984) Release of endogenous Zn^{2+} from brain tissue during activity. *Nature*, **308** (5961), 734–736.
23. Howell, G.A., Welch, M.G. and Frederickson, C.J. (1984) Stimulation-induced uptake and release of zinc in hippocampal slices. *Nature*, **308** (5961), 736–738.
24. Li, Y., Hough, C.J., Suh, S.W. *et al*. (2001) Rapid translocation of Zn^{2+} from presynaptic terminals into postsynaptic hippocampal neurons after physiological stimulation. *J. Neurophysiol.*, **86** (5), 2597–2604.
25. Sensi, S.L., Canzoniero, L.M.T., Yu, S.P. *et al*. (1997) Measurement of intracellular free zinc in living cortical neurons: routes of entry. *J. Neurosci.*, **17** (24), 9554–9564.
26. Connor, J.R. and Menzies, S.L. (1995) Cellular management of iron in the brain. *J. Neurol. Sci.*, **134** (Suppl.), 33–44.
27. Hill, J.M. and Switzer, R.C. III, (1984) The regional distribution and cellular localization of iron in the rat brain. *Neuroscience*, **11** (3), 595–603.
28. Jefferies, W.A., Brandon, M.R., Hunt, S.V. *et al*. (1984) Transferrin receptor on endothelium of brain capillaries. *Nature*, **312** (5990), 162–163.
29. Fiedler, A., Reinert, T., Morawski, M. *et al*. (2007) Intracellular iron concentration of neurons with and without perineuronal nets. *Nucl. Instrum. Methods Phys. Res., Sect. B*, **260** (1), 153–158.
30. Kosman, D.J. (2010) Redox cycling in iron uptake, efflux, and trafficking. *J. Biol. Chem.*, **285** (35), 26729–26735.
31. Schade, A.L. and Caroline, L. (1946) An iron-binding component in human blood plasma. *Science*, **104** (2702), 340–341.
32. Connor, J.R., Boeshore, K.L., Benkovic, S.A. and Menzies, S.L. (1994) Isoforms of ferritin have a specific cellular distribution in the brain. *J. Neurosci. Res.*, **37** (4), 461–465.
33. Kepp, K.P. (2012) Bioinorganic chemistry of Alzheimer's disease. *Chem. Rev.*, **112** (10), 5193–5239.
34. Viles, J.H. (2012) Metal ions and amyloid fiber formation in neurodegenerative diseases. Copper, zinc and iron in Alzheimer's, Parkinson's and prion diseases. *Coord. Chem. Rev.*, **256** (19–20), 2271–2284.
35. Savelieff, M.G., Lee, S., Liu, Y. and Lim, M.H. (2013) Untangling amyloid-β, tau, and metals in Alzheimer's disease. *ACS Chem. Biol.*, **8** (5), 856–865.
36. Outten, F.W. and Twining, B.S. (2008) Metal homeostasis, in *Wiley Encyclopedia of Chemical Biology* (ed T.P. Begley), John Wiley & Sons, Inc., Hoboken, NJ.
37. Bleackley, M.R. and Macgillivray, R.T. (2011) Transition metal homeostasis: from yeast to human disease. *BioMetals*, **24** (5), 785–809.
38. Barnham, K.J. and Bush, A.I. (2008) Metals in Alzheimer's and Parkinson's diseases. *Curr. Opin. Chem. Biol.*, **12** (2), 222–228.
39. Greenough, M.A., Camakaris, J. and Bush, A.I. (2013) Metal dyshomeostasis and oxidative stress in Alzheimer's disease. *Neurochem. Int.*, **62** (5), 540–555.
40. Rivera-Mancía, S., Pérez-Neri, I., Ríos, C. *et al*. (2010) The transition metals copper and iron in neurodegenerative diseases. *Chem. Biol. Interact.*, **186** (2), 184–199.
41. Tamano, H. and Takeda, A. (2011) Dynamic action of neurometals at the synapse. *Metallomics*, **3** (7), 656–661.
42. Faller, P., Hureau, C. and Berthoumieu, O. (2013) Role of metal ions in the self-assembly of the Alzheimer's amyloid-β peptide. *Inorg. Chem.*, **52** (21), 12193–12206.
43. DeToma, A.S., Salamekh, S., Ramamoorthy, A. and Lim, M.H. (2012) Misfolded proteins in Alzheimer's disease and type II diabetes. *Chem. Soc. Rev.*, **41** (2), 608–621.
44. Rauk, A. (2009) The chemistry of Alzheimer's disease. *Chem. Soc. Rev.*, **38** (9), 2698–2715.
45. Pithadia, A.S. and Lim, M.H. (2012) Metal-associated amyloid-β species in Alzheimer's disease. *Curr. Opin. Chem. Biol.*, **16** (1–2), 67–73.
46. Vivekanandan, S., Brender, J.R., Lee, S.Y. and Ramamoorthy, A. (2011) A partially folded structure of amyloid-beta(1-40) in an aqueous environment. *Biochem. Biophys. Res. Commun.*, **411** (2), 312–316.

47. Deng, H.X., Hentati, A., Tainer, J.A. *et al*. Amyotrophic lateral sclerosis and structural defects in Cu,Zn superoxide dismutase, *Science*, **261** (5124), 1047–1051 (1993).
48. Rao, J.N., Jao, C.C., Hegde, B.G. *et al*. (2010) A combinatorial NMR and EPR approach for evaluating the structural ensemble of partially folded proteins. *J. Am. Chem. Soc.*, **132** (25), 8657–8668.
49. Kim, M. (2013) Beta conformation of polyglutamine track revealed by a crystal structure of Huntingtin *N*-terminal region with insertion of three histidine residues. *Prion*, **7** (3), 221–228.
50. Zahn, R., Liu, A., Lührs, T. *et al*. (2000) NMR solution structure of the human prion protein. *Proc. Natl. Acad. Sci. U.S.A.*, **97** (1), 145–150.
51. Molina-Holgado, F., Hider, R.C., Gaeta, A. *et al*. (2007) Metals ions and neurodegeneration. *BioMetals*, **20** (3–4), 639–654.
52. Reddy, P.H. (2006) Mitochondrial oxidative damage in aging and Alzheimer's disease: implications for mitochondrially targeted antioxidant therapeutics. *J. Biomed. Biotechnol*, **2006** (3), 31372.
53. Adam-Vizi, V. (2005) Production of reactive oxygen species in brain mitochondria: contribution by electron transport chain and non-electron transport chain sources. *Antioxid. Redox Sign.*, **7** (9–10), 1140–1149.
54. Huang, X., Atwood, C.S., Hartshorn, M.A. *et al*. (1999) The Aβ peptide of Alzheimer's disease directly produces hydrogen peroxide through metal ion reduction. *Biochemistry*, **38** (24), 7609–7616.
55. Koppenol, W.H. (2001) The haber-weiss cycle-70 years later. *Redox Rep.*, **6** (4), 229–234.
56. Wardman, P. and Candeias, L.P. (1996) Fenton chemistry: an introduction. *Radiat. Res.*, **145** (5), 523–531.
57. Briner, W. (2012) The role of metal regulatory proteins in brain oxidative stress: a tutorial. *Oxid. Med. Cell. Longev.*, **2012**, 981561.
58. Nicholls, P. (2012) Classical catalase: ancient and modern. *Arch. Biochem. Biophys.*, **525** (2), 95–101.
59. V.I. Lushchak, Glutathione homeostasis and functions: potential targets for medical interventions, *J. Amino Acids*, 2012, 736837 (2012).
60. Atamna, H. and Boyle, K. (2006) Amyloid-beta peptide binds with heme to form a peroxidase: relationship to the cytopathologies of Alzheimer's disease. *Proc. Natl. Acad. Sci. U.S.A.*, **103** (9), 3381–3386.
61. Mounsey, R.B. and Teismann, P. (2012) Chelators in the treatment of iron accumulation in Parkinson's disease, *Int. J. Cell Biol*., **2012** 983245.
62. Bisaglia, M., Tessari, I., Mammi, S. and Bubacco, L. (2009) Interaction between alpha-synuclein and metal ions, still looking for a role in the pathogenesis of Parkinson's disease. *Neuromol. Med.*, **11** (4), 239–251.
63. Valentine, J.S., Doucette, P.A. and Zittin Potter, S. (2005) Copper-zinc superoxide dismutase and amyotrophic lateral sclerosis. *Annu. Rev. Biochem.*, **74**, 563–593.
64. Jakob-Roetne, R. and Jacobsen, H. (2009) Alzheimer's disease: from pathology to therapeutic approaches. *Angew. Chem. Int. Ed.*, **48** (17), 3030–3059.
65. Rauk, A. (2008) Why is the amyloid beta peptide of Alzheimer's disease neurotoxic? *Dalton Trans.*, **2008** (10), 1273–1282.
66. Alzheimer's Association, (2012) 2012 Alzheimer's disease facts and figures. *Alzheimers Dement.*, **8** (2), 131–168.
67. Mayeux, R. (2010) Early Alzheimer's disease. *N. Engl. J. Med.*, **362** (23), 2194–2201.
68. Biran, Y., Masters, C.L., Barnham, K.J. *et al*. (2009) Pharmacotherapeutic targets in Alzheimer's disease. *J. Cell. Mol. Med.*, **13** (1), 61–86.
69. Alonso, A.C., Grundke-Iqbal, I. and Iqbal, K. (1996) Alzheimer's disease hyperphosphorylated tau sequesters normal tau into tangles of filaments and disassembles microtubules. *Nat. Med.*, **2** (7), 783–787.
70. Wang, J.-Z., Xia, Y.-Y., Grundke-Iqbal, I. and Iqbal, K. (2013) Abnormal hyperphosphorylation of tau: sites, regulation, and molecular mechanism of neurofibrillary degeneration. *J. Alzheimers Dis.*, **33**, S123–S139.
71. Morris, M., Maeda, S., Vossel, K. and Mucke, L. (2011) The many faces of tau. *Neuron*, **70** (3), 410–426.
72. Köpke, E., Tung, Y.C., Shaikh, S. *et al*. (1993) Microtubule-associated protein tau. Abnormal phosphorylation of a non-paired helical filament pool in Alzheimer disease. *J. Biol. Chem.*, **268** (32), 24374–24384.
73. Schrag, M., Mueller, C., Oyoyo, U. *et al*. (2011) Iron, zinc and copper in the Alzheimer's disease brain: a quantitative meta-analysis. Some insight on the influence of citation bias on scientific opinion. *Prog. Neurobiol.*, **94** (3), 296–306.
74. Alies, B., Hureau, C. and Faller, P. (2013) The role of metal ions in amyloid formation: general principles from model peptides. *Metallomics*, **5** (3), 183–192.
75. Telpoukhovskaia, M.A. and Orvig, C. (2013) Werner coordination chemistry and neurodegeneration. *Chem. Soc. Rev.*, **42** (4), 1836–1846.

76. Faller, P. and Hureau, C. (2009) Bioinorganic chemistry of copper and zinc ions coordinated to amyloid-β peptide. *Dalton Trans.*, 1080–1094.
77. Hureau, C. (2012) Coordination of redox active metal ions to the amyloid precursor protein and to amyloid-β peptides involved in Alzheimer disease. Part 1: an overview. *Coord. Chem. Rev.*, **256** (19–20), 2164–2174.
78. Feaga, H.A., Maduka, R.C., Foster, M.N. and Szalai, V.A. (2011) Affinity of Cu^{+} for the copper-binding domain of the amyloid-β peptide of Alzheimer's disease. *Inorg. Chem.*, **50** (5), 1614–1618.
79. Alies, B., Badei, B., Faller, P. and Hureau, C. (2012) Reevaluation of copper(I) affinity for amyloid-β peptides by competition with ferrozine–an unusual copper(I) indicator. *Chem. Eur. J.*, **18** (4), 1161–1167.
80. Bousejra-ElGarah, F., Bijani, C., Coppel, Y. *et al*. (2011) Iron(II) binding to amyloid-β, the Alzheimer's peptide. *Inorg. Chem.*, **50** (18), 9024–9030.
81. Solomonov, I., Korkotian, E., Born, B. *et al*. (2012) Zn^{2+}-$A\beta_{40}$ complexes form metastable quasi-spherical oligomers that are cytotoxic to cultured hippocampal neurons. *J. Biol. Chem.*, **287** (24), 20555–20564.
82. Crouch, P.J. and Barnham, K.J. (2012) Therapeutic redistribution of metal ions to treat Alzheimer's disease. *Acc. Chem. Res.*, **45** (9), 1604–1611.
83. Soragni, A., Zambelli, B., Mukrasch, M.D. *et al*. (2008) Structural characterization of binding of Cu(II) to tau protein. *Biochemistry*, **47** (41), 10841–10851.
84. Binolfi, A., Rasia, R.M., Bertoncini, C.W. *et al*. (2006) Interaction of α-synuclein with divalent metal ions reveals key differences: a link between structure, binding specificity and fibrillation enhancement. *J. Am. Chem. Soc.*, **128** (30), 9893–9901.
85. Valiente-Gabioud, A.A., Torres-Monserrat, V., Molina-Rubino, L. *et al*. (2012) Structural basis behind the interaction of Zn^{2+} with the protein α-synuclein and the Aβ peptide: a comparative analysis. *J. Inorg. Biochem.*, **117**, 334–341.
86. Binolfi, A., Valiente-Gabioud, A.A., Duran, R. *et al*. (2011) Exploring the structural details of Cu(I) binding to α-synuclein by NMR spectroscopy. *J. Am. Chem. Soc.*, **133** (2), 194–196.
87. Binolfi, A., Quintanar, L., Bertoncini, C.W. *et al*. (2012) Bioinorganic chemistry of copper coordination to alpha-synuclein: relevance to Parkinson's disease. *Coord. Chem. Rev.*, **256** (19–20), 2188–2201.
88. Lee, J.-H., Bhak, G., Lee, S.-G. and Paik, S.R. (2008) Instantaneous amyloid fibril formation of α-synuclein from the oligomeric granular structures in the presence of hexane. *Biophys. J.*, **95** (2), L16–L18.
89. Jackson, M.S. and Lee, J.C. (2009) Identification of the minimal copper(II)-binding α-synuclein sequence. *Inorg. Chem.*, **48** (19), 9303–9307.
90. Rasia, R.M., Bertoncini, C.W., Marsh, D. *et al*. (2005) Structural characterization of copper(II) binding to α-synuclein: insights into the bioinorganic chemistry of Parkinson's disease. *Proc. Natl. Acad. Sci. U.S.A.*, **102** (12), 4294–4299.
91. Binolfi, A., Lamberto, G.R., Duran, R. *et al*. (2008) Site-specific interactions of Cu(II) with α and β-synuclein: bridging the molecular gap between metal binding and aggregation. *J. Am. Chem. Soc.*, **130** (35), 11801–11812.
92. Kozlowski, H., Luczkowski, M., Remelli, M. and Valensin, D. (2012) Copper, zinc and iron in neurodegenerative diseases (Alzheimer's, Parkinson's and prion diseases). *Coord. Chem. Rev.*, **256** (19–20), 2129–2141.
93. Arena, G., La Mendola, D., Pappalardo, G. *et al*. (2012) Interactions of Cu^{2+} with prion family peptide fragments: considerations on affinity, speciation and coordination. *Coord. Chem. Rev.*, **256** (19–20), 2202–2218.
94. Walter, E.D., Stevens, D.J., Visconte, M.P. and Millhauser, G.L. (2007) The prion protein is a combined zinc and copper binding protein: Zn^{2+} alters the distribution of Cu^{2+} coordination modes. *J. Am. Chem. Soc.*, **129** (50), 15440–15441.
95. Migliorini, C., Porciatti, E., Luczkowski, M. and Valensin, D. (2012) Structural characterization of Cu^{2+}, Ni^{2+} and Zn^{2+} binding sites of model peptides associated with neurodegenerative diseases. *Coord. Chem. Rev.*, **256** (1–2), 352–368.
96. J.H. Fox, J A. Kama, G. Lieberman, *et al*. (2007) Mechanisms of copper ion mediated Huntington's disease progression, *PLoS One*, **2**(3), e334.
97. Hart, P.J., Balbirnie, M.M., Ogihara, N.L. *et al*. (1999) A structure-based mechanism for copper-zinc superoxide dismutase. *Biochemistry*, **38** (7), 2167–2178.
98. Hough, M.A. and Hasnain, S.S. (1999) Crystallographic structures of bovine copper-zinc superoxide dismutase reveal asymmetry in two subunits: functionally important three and five coordinate copper sites captured in the same crystal. *J. Mol. Biol.*, **287** (3), 579–592.

99. Hough, M.A. and Hasnain, S.S. (2003) Structure of fully reduced bovine copper zinc superoxide dismutase at 1.15 Å. *Structure*, **11** (8), 937–946.
100. Crow, J.P., Sampson, J.B., Zhuang, Y. *et al*. (1997) Decreased zinc affinity of amyotrophic lateral sclerosis-associated superoxide dismutase mutants leads to enhanced catalysis of tyrosine nitration by peroxynitrite. *J. Neurochem.*, **69** (5), 1936–1944.
101. Banci, L., Bertini, I., Ciofi-Baffoni, S. *et al*. (2010) Affinity gradients drive copper to cellular destinations. *Nature*, **465** (7298), 645–648.
102. Shin, R.-W., Lee, V.M.-Y. and Trojanowski, J.Q. (1994) Aluminum modifies the properties of Alzheimer's disease PHF τ proteins *in vivo* and *in vitro*. *J. Neurosci.*, **14** (11), 7221–7233.
103. Yamamoto, A., Shin, R.W., Hasegawa, K. *et al*. (2002) Iron (III) induces aggregation of hyperphosphorylated τ and its reduction to iron (II) reverses the aggregation: implications in the formation of neurofibrillary tangles of Alzheimer's disease. *J. Neurochem.*, **82** (5), 1137–1147.
104. Jankovic, J. and Aguilar, L.G. (2008) Current approaches to the treatment of Parkinson's disease. *Neuropsychiatr. Dis. Treat.*, **4** (4), 743–757.
105. Leong, S.L., Cappai, R., Barnham, K.J. and Pham, C.L.L. (2009) Modulation of α-synuclein aggregation by dopamine: a review. *Neurochem. Res.*, **34** (10), 1838–1846.
106. Scott, L.E. and Orvig, C. (2009) Medicinal inorganic chemistry approaches to passivation and removal of aberrant metal ions in disease. *Chem. Rev.*, **109** (10), 4885–4910.
107. Bourassa, M.W. and Miller, L.M. (2012) Metal imaging in neurodegenerative diseases. *Metallomics*, **4** (8), 721–738.
108. Hare, D.J., Adlard, P.A., Doble, P.A. and Finkelstein, D.I. (2013) Metallobiology of 1-methyl-4-phenyl-1,2,3,6-tetrahydropyridine neurotoxicity. *Metallomics*, **5** (2), 91–109.
109. Breydo, L. and Uversky, V.N. (2011) Role of metal ions in aggregation of intrinsically disordered proteins in neurodegenerative diseases. *Metallomics*, **3** (11), 1163–1180.
110. Camponeschi, F., Valensin, D., Tessari, I. *et al*. (2013) Copper(I)-α-synuclein interaction: structural description of two independent and competing metal binding sites. *Inorg. Chem.*, **52** (3), 1358–1367.
111. Dev, K.K., Hofele, K., Barbieri, S. *et al*. (2003) Part II: α-synuclein and its molecular pathophysiological role in neurodegenerative disease. *Neuropharmacology*, **45** (1), 14–44.
112. Goedert, M. (2001) Alpha-synuclein and neurodegenerative diseases. *Nat. Rev. Neurosci.*, **2** (7), 492–501.
113. Fink, A.L. (2006) The aggregation and fibrillation of α-synuclein. *Acc. Chem. Res.*, **39** (9), 628–634.
114. Ross, C.A. and Poirier, M.A. (2004) Protein aggregation and neurodegenerative disease. *Nat. Med.*, **10** (Suppl), S10–S17.
115. Dudzik, C.G., Walter, E.D., Abrams, B.S. *et al*. (2013) Coordination of copper to the membrane-bound form of α-synuclein. *Biochemistry*, **52** (1), 53–60.
116. Wright, J.A. and Brown, D.R. (2008) Alpha-synuclein and its role in metal binding: relevance to Parkinson's disease. *J. Neurosci. Res.*, **86** (3), 496–503.
117. Connor, J.R., Snyder, B.S., Arosio, P. *et al*. (1995) A quantitative analysis of isoferritins in select regions of aged, Parkinsonian, and Alzheimer's diseased brains. *J. Neurochem.*, **65** (2), 717–724.
118. Dexter, D.T., Carayon, A., Javoy-Agid, F. *et al*. (1991) Alterations in the levels of iron, ferritin and other trace metals in Parkinson's disease and other neurodegenerative diseases affecting the basal ganglia. *Brain*, **114** (4), 1953–1975.
119. Dexter, D.T., Wells, F.R., Lees, A.J. *et al*. (1989) Increased nigral iron content and alterations in other metal ions occurring in brain in Parkinson's disease. *J. Neurochem.*, **52** (6), 1830–1836.
120. Riederer, P., Sofic, E., Rausch, W.D. *et al*. (1989) Transition metals, ferritin, glutathione, and ascorbic acid in Parkinsonian brains. *J. Neurochem.*, **52** (2), 515–520.
121. Turnbull, S., Tabner, B.J., El-Agnaf, O.M.A. *et al*. (2001) α-Synuclein implicated in Parkinson's disease catalyses the formation of hydrogen peroxide in vitro. *Free Radic. Biol. Med.*, **30** (10), 1163–1170.
122. Popescu, B.F.G., George, M.J., Bergmann, U. *et al*. (2009) Mapping metals in Parkinson's and normal brain using rapid-scanning x-ray fluorescence. *Phys. Med. Biol.*, **54** (3), 651–663.
123. Jellinger, K.A. (1999) The role of iron in neurodegeneration: prospects for pharmacotherapy of Parkinson's disease. *Drugs Aging*, **14** (2), 115–140.
124. Drew, S.C., Leong, S.L., Pham, C.L.L. *et al*. (2008) Cu^{2+} binding modes of recombinant α-synuclein-insights from EPR spectroscopy. *J. Am. Chem. Soc.*, **130** (24), 7766–7773.
125. Sung, Y.-H., Rospigliosi, C. and Eliezer, D. (2006) NMR mapping of copper binding sites in alpha-synuclein. *Biochim. Biophys. Acta*, **1764** (1), 5–12.

126. Uversky, V.N., Li, J. and Fink, A.L. (2001) Metal-triggered structural transformations, aggregation, and fibrillation of human α-synuclein. A possible molecular link between Parkinson's disease and heavy metal exposure. *J. Biol. Chem.*, **276** (47), 44284–44296.
127. Bolognin, S., Messori, L. and Zatta, P. (2009) Metal ion physiopathology in neurodegenerative disorders. *Neuromol. Med.*, **11** (4), 223–238.
128. Alimonti, A., Bocca, B., Pino, A. *et al*. (2007) Elemental profile of cerebrospinal fluid in patients with Parkinson's disease. *J. Trace Elem. Med. Biol.*, **21** (4), 234–241.
129. Zheng, H., Gal, S., Weiner, L.M. *et al*. (2005) Novel multifunctional neuroprotective iron chelator-monoamine oxidase inhibitor drugs for neurodegenerative diseases: *In vitro* studies on antioxidant activity, prevention of lipid peroxide formation and monoamine oxidase inhibition. *J. Neurochem.*, **95** (1), 68–78.
130. Arreguin, S., Nelson, P., Padway, S. *et al*. (2009) Dopamine complexes of iron in the etiology and pathogenesis of Parkinson's disease. *J. Inorg. Biochem.*, **103** (1), 87–93.
131. Santner, A. and Uversky, V.N. (2010) Metalloproteomics and metal toxicology of α-synuclein. *Metallomics*, **2** (6), 378–392.
132. Wang, C., Liu, L., Zhang, L. *et al*. (2010) Redox reactions of the α-synuclein-Cu^{2+} complex and their effects on neuronal cell viability. *Biochemistry*, **49** (37), 8134–8142.
133. Lucas, H.R., Debeer, S., Hong, M.-S. and Lee, J.C. (2010) Evidence for copper-dioxygen reactivity during α-synuclein fibril formation. *J. Am. Chem. Soc.*, **132** (19), 6636–6637.
134. Lucas, H.R. and Lee, J.C. (2010) Effect of dioxygen on copper(II) binding to α-synuclein. *J. Inorg. Biochem.*, **104** (3), 245–249.
135. Yusa, S.-I., Oliveira-Martins, J.B., Sugita-Konishi, Y. and Kikuchi, Y. (2012) Cellular prion protein: from physiology to pathology. *Viruses*, **4** (11), 3109–3131.
136. Singh, N., Das, D., Singh, A. and Mohan, M.L. (2010) Prion protein and metal interaction: physiological and pathological implications. *Curr. Issues Mol. Biol.*, **12** (2), 99–108.
137. Sikorska, B., Knight, R., Ironside, J.W. and Liberski, P.P. (2012) Creutzfeldt-Jakob disease. *Adv. Exp. Med. Biol.*, **724**, 76–90.
138. Aguzzi, A., Sigurdson, C. and Heikenwaelder, M. (2008) Molecular mechanisms of prion pathogenesis. *Annu. Rev. Pathol. Mech. Dis.*, **3**, 11–40.
139. Pan, K.-M., Baldwin, M., Nguyen, J. *et al*. (1993) Conversion of α-helices into β-sheets features in the formation of the scrapie prion proteins. *Proc. Natl. Acad. Sci. U.S.A.*, **90** (23), 10962–10966.
140. Brown, D.R. (2011) Prions and manganese: a maddening beast. *Metallomics*, **3** (3), 229–238.
141. Brazier, M.W., Davies, P., Player, E. *et al*. (2008) Manganese binding to the prion protein. *J. Biol. Chem.*, **283** (19), 12831–12839.
142. Leach, S.P., Salman, M.D. and Hamar, D. (2006) Trace elements and prion diseases: a review of the interactions of copper, manganese and zinc with the prion protein. *Anim. Health Res. Rev.*, **7** (1–2), 97–105.
143. Brown, D.R., Hafiz, F., Glasssmith, L.L. *et al*. (2000) Consequences of manganese replacement of copper for prion protein function and proteinase resistance. *EMBO J.*, **19** (6), 1180–1186.
144. Brazier, M.W., Volitakis, I., Kvasnicka, M. *et al*. (2010) Manganese chelation therapy extends survival in a mouse model of M1000 prion disease. *J. Neurochem.*, **114** (2), 440–451.
145. Li, S.-H. and Li, X.-J. (2004) Huntingtin-protein interactions and the pathogenesis of Huntington's disease. *Trends Genet.*, **20** (3), 146–154.
146. Ross, C.A. and Shoulson, I. (2009) Huntington disease: pathogenesis, biomarkers, and approaches to experimental therapeutics. *Parkinsonism Relat. Disord.*, **15** (S3), S135–S138.
147. Vonsattel, J.-P., Myers, R.H., Stevens, T.J. *et al*. (1985) Neuropathological classification of Huntington's disease. *J. Neuropathol. Exp. Neurol.*, **44** (6), 559–577.
148. Crichton, R.R. and Ward, R.J. (2006) Huntington's disease and polyglutamine expansion neurodegenerative diseases, in *Metal-Based Neurodegeneration: from molecular mechanisms to therapeutic strategies*, John Wiley & Sons, Ltd, Chichester, pp. 95–111.
149. Dragatsis, I., Levine, M.S. and Zeitlin, S. (2000) Inactivation of *Hdh* in the brain and testis results in progressive neurodegeneration and sterility in mice. *Nat. Genet.*, **26** (3), 300–306.
150. Zheng, Q. and Joinnides, M. (2009) Hunting for the function of Huntingtin. *Dis. Models Mech.*, **2** (5–6), 199–200.

151. Hands, S.L. and Wyttenbach, A. (2010) Neurotoxic protein oligomerisation associated with polyglutamine diseases. *Acta Neuropathol.*, **120** (4), 419–437.
152. Sánchez, I., Mahlke, C. and Yuan, J. (2003) Pivotal role of oligomerization in expanded polyglutamine neurodegenerative disorders. *Nature*, **421** (6921), 373–379.
153. Thakur, A.K., Jayaraman, M., Mishra, R. *et al*. (2009) Polyglutamine disruption of the huntingtin exon 1 N terminus triggers a complex aggregation mechanism. *Nat. Struct. Mol. Biol.*, **16** (4), 380–389.
154. Bartzokis, G., Lu, P.H., Tishler, T.A. and Perlman, S. (2006) *In vivo* assessment of iron in Huntington's disease and other age-related neurodegenerative brain diseases, in *Neurodegenerative Diseases and Metal Ions* (eds A. Sigel, H. Sigel and R.K.O. Sigel), John Wiley & Sons, Ltd, Chichester, pp. 151–177.
155. Rowland, L.P. and Shneider, N.A. (2001) Amyotrophic lateral sclerosis. *N. Engl. J. Med.*, **344** (22), 1688–1700.
156. Wang, Q., Zhang, X., Chen, S. *et al*. (2011) Prevention of motor neuron degeneration by novel iron chelators in $SOD1^{G93A}$ transgenic mice of amyotrophic lateral sclerosis. *Neurodegener. Dis.*, **8** (5), 310–321.
157. Rhoads, T.W., Lopez, N.I., Zollinger, D.R. *et al*. (2011) Measuring copper and zinc superoxide dismutase from spinal cord tissue using electrospray mass spectrometry. *Anal. Biochem.*, **415** (1), 52–58.
158. Tomik, B., Chwiej, J., Szczerbowska-Boruchowska, M. *et al*. (2006) Implementation of X-ray fluorescence microscopy for investigation of elemental abnormalities in amyotrophic lateral sclerosis. *Neurochem. Res.*, **31** (3), 321–331.
159. Li, X., Jankovic, J. and Le, W. (2011) Iron chelation and neuroprotection in neurodegenerative diseases. *J. Neural Transm.*, **118** (3), 473–477.
160. Valentine, J.S. and Hart, P.J. (2003) Misfolded CuZnSOD and amyotrophic lateral sclerosis. *Proc. Natl. Acad. Sci. U.S.A.*, **100** (7), 3617–3622.
161. Wang, J., Xu, G. and Borchelt, D.R. (2002) High molecular weight complexes of mutant superoxide dismutase 1: age-dependent and tissue-specific accumulation. *Neurobiol. Dis.*, **9** (2), 139–148.
162. Arai, T., Hasegawa, M., Akiyama, H. *et al*. (2006) TDP-43 is a component of ubiquitin-positive tau-negative inclusions in frontotemporal lobar degeneration and amyotrophic lateral sclerosis. *Biochem. Biophys. Res. Commun.*, **351** (3), 602–611.
163. Blokhuis, A.M., Groen, E.J., Koppers, M. *et al*. (2013) Protein aggregation in amyotrophic lateral sclerosis. *Acta Neuropathol.*, **125** (6), 777–794.
164. Caragounis, A., Price, K.A., Soon, C.P.W. *et al*. (2010) Zinc induces depletion and aggregation of endogenous TDP-43. *Free Radical Biol. Med.*, **48** (9), 1152–1161.
165. Rodríguez-Rodríguez, C., Telpoukhovskaia, M. and Orvig, C. (2012) The art of building multifunctional metal-binding agents from basic molecular scaffolds for the potential application in neurodegenerative diseases. *Coord. Chem. Rev.*, **256** (19–20), 2308–2332.
166. Faller, P., Hureau, C., and Berthoumieu, O. (2013) Role of metal ions in the self-assembly of the Alzheimer's amyloid-β peptide. *Inorg. Chem.*, **52** (21), 12193–12206.
167. Zhang, H.-Y. (2005) One-compound-multiple-targets strategy to combat Alzheimer's disease. *FEBS Lett.*, **579** (24), 5260–5264.
168. Massoud, F. and Léger, G.C. (2011) Pharmacological treatment of Alzheimer's disease. *Can. J. Psychiatry*, **56** (10), 579–588.
169. Lleó, A. (2007) Current therapeutic options for Alzheimer's disease. *Curr. Genomics*, **8** (8), 550–558.
170. Ross, C.A. and Tabrizi, S.J. (2011) Huntington's disease: from molecular pathogenesis to clinical treatment. *Lancet Neurol.*, **10** (1), 83–98.
171. Zoccolella, S., Santamato, A. and Lamberti, P. (2009) Current and emerging treatments for amyotrophic lateral sclerosis. *Neuropsychiatr. Dis. Treat.*, **5**, 577–595.
172. Karapetyan, Y.E., Sferrazza, G.F., Zhou, M. *et al*. (2013) Unique drug screening approach for prion diseases identifies tacrolimus and astemizole as antiprion agents. *Proc. Natl. Acad. Sci. U.S.A.*, **110** (17), 7044–7049.
173. Andersen, O. (1999) Principles and recent developments in chelation treatment of metal intoxication. *Chem. Rev.*, **99** (9), 2683–2710.
174. Blanusa, M., Varnai, V.M., Piasek, M. and Kostial, K. (2005) Chelators as antidotes of metal toxicity: therapeutic and experimental aspects. *Curr. Med. Chem.*, **12** (23), 2771–2794.

175. Bolognin, S., Drago, D., Messori, L. and Zatta, P. (2009) Chelation therapy for neurodegenerative diseases. *Med. Res. Rev.*, **29** (4), 547–570.
176. Olzscha, H., Schermann, S.M., Woerner, A.C. *et al*. (2011) Amyloid-like aggregates sequester numerous metastable proteins with essential cellular functions. *Cell*, **144** (1), 67–78.
177. Born, T., Kontoghiorghe, C.N., Spyrou, A. *et al*. (2013) EDTA chelation reappraisal following new clinical trials and regular use in millions of patients: review of preliminary findings and risk/benefit assessment. *Toxicol. Mech. Methods*, **23** (1), 11–17.
178. Huang, X., Atwood, C.S., Moir, R.D. *et al*. (1997) Zinc-induced Alzheimer's Aβ1-40 aggregation is mediated by conformational factors. *J. Biol. Chem.*, **272** (42), 26464–26470.
179. Atwood, C.S., Moir, R.D., Huang, X. *et al*. (1998) Dramatic aggregation of Alzheimer Aβ by Cu(II) is induced by conditions representing physiological acidosis. *J. Biol. Chem.*, **273** (21), 12817–12826.
180. Liu, Z.D. and Hider, R.C. (2002) Design of iron chelators with therapeutic application. *Coord. Chem. Rev.*, **232** (1–2), 151–171.
181. Schugar, H., Green, D.E., Bowen, M.L. *et al*. (2007) Combating Alzheimer's disease with multifunctional molecules designed for metal passivation. *Angew. Chem. Int. Ed.*, **46** (10), 1716–1718.
182. Bebbington, D., Monck, N.J.T., Gaur, S. *et al*. (2000) 3,5-Disubstituted-4-hydroxyphenyls linked to 3-hydroxy-2-methyl-4(1H)-pyridinone: potent inhibitors of lipid peroxidation and cell toxicity. *J. Med. Chem.*, **43** (15), 2779–2782.
183. Bebbington, D., Dawson, C.E., Gaur, S. and Spencer, J. (2002) Prodrug and covalent linker strategies for the solubilization of dual-action antioxidants/iron chelators. *Bioorg. Med. Chem. Lett.*, **12** (22), 3297–3300.
184. Ferenci, P. (2004) Diagnosis and current therapy of Wilson's disease. *Aliment. Pharmacol. Ther.*, **19** (2), 157–165.
185. Li, W., Ma, K.K.Y., Sun, W. and Paudel, H.K. (1998) Phosphorylation sensitizes microtubule-associated protein τ to Al^{3+}-induced aggregation. *Neurochem. Res.*, **23** (12), 1467–1476.
186. Crapper McLachlan, D.R., Dalton, A.J., Kruck, T.P.A. *et al*. (1991) Intramuscular desferrioxamine in patients with Alzheimer's disease. *Lancet*, **337** (8753), 1304–1308.
187. Cherny, R.A., Barnham, K.J., Lynch, T. *et al*. (2000) Chelation and intercalation: complementary properties in a compound for the treatment of Alzheimer's disease. *J. Struct. Biol.*, **130** (2–3), 209–216.
188. Hindo, S.S., Mancino, A.M., Braymer, J.J. *et al*. (2009) Small molecule modulators of copper-induced Aβ aggregation. *J. Am. Chem. Soc.*, **131** (46), 16663–16665.
189. Bush, A.I., Huang, X. and Fairlie, D.P. (1999) The possible origin of free radicals from amyloid β peptides in Alzheimer's disease. *Neurobiol. Aging*, **20** (3), 335–337.
190. Cui, Z., Lockman, P.R., Atwood, C.S. *et al*. (2005) Novel D-penicillamine carrying nanoparticles for metal chelation therapy in Alzheimer's and other CNS diseases. *Eur. J. Pharm. Biopharm.*, **59** (2), 263–272.
191. Kim, K.S., Choi, S.Y., Kwon, H.Y. *et al*. (2002) Aggregation of α-synuclein induced by the Cu,Zn-superoxide dismutase and hydrogen peroxide system. *Free Radical Biol. Med.*, **32** (6), 544–550.
192. Sigurdsson, E.M., Brown, D.R., Alim, M.A. *et al*. (2003) Copper chelation delays the onset of prion disease. *J. Biol. Chem.*, **278** (47), 46199–46202.
193. Gaeta, A. and Hider, R.C. (2005) The crucial role of metal ions in neurodegeneration: the basis for a promising therapeutic strategy. *Br. J. Pharmacol.*, **146** (8), 1041–1059.
194. Harris, D.C. (2007) *Quantitative Chemical Analysis*, W.H. Freeman and Co., New York.
195. Liu, Z.D. and Hider, R.C. (2002) Design of clinically useful iron(III)-selective chelators. *Med. Res. Rev.*, **22** (1), 26–64.
196. Budimir, A. (2011) Metal ions, Alzheimer's disease and chelation therapy. *Acta Pharm.*, **61** (1), 1–14.
197. Barnham, K.J., Kenche, V.B., Ciccotosto, G.D. *et al*. (2008) Platinum-based inhibitors of amyloid-β as therapeutic agents for Alzheimer's disease. *Proc. Natl. Acad. Sci. U.S.A.*, **105** (19), 6813–6818.
198. Braymer, J.J., DeToma, A.S., Choi, J.S. *et al*. (2011) Recent development of bifunctional small molecules to study metal-amyloid-β species in Alzheimer's disease. *Int. J. Alzheimers Dis.*, **2011**, Article ID 623051.
199. Ritchie, C.W., Bush, A.I., Mackinnon, A. *et al*. (2003) Metal-protein attenuation with iodochlorhydroxyquin (clioquinol) targeting Aβ amyloid deposition and toxicity in Alzheimer disease: a pilot phase 2 clinical trial. *Arch. Neurol.*, **60** (12), 1685–1691.

200. Rimola, A., Alí-Torres, J., Rodríguez-Rodríguez, C. *et al*. (2011) Ab initio design of chelating ligands relevant to Alzheimer's disease: influence of metalloaromaticity. *J. Phys. Chem. A*, **115** (45), 12659–12666.
201. Martell, A.E. (1952) The behavior of metal complexes in aqueous solutions. *J. Chem. Educ.*, **29** (6), 270–280.
202. Jones, C.J. and Thornback, J.R. (2007) Metallopharmaceuticals design, in *Medicinal Applications of Coordination Chemistry*, Royal Society of Chemistry, Cambridge, pp. 324–339.
203. Andersen, O. and Aaseth, J. (2002) Molecular mechanisms of *in vivo* metal chelation: implications for clinical treatment of metal intoxications. *Environ. Health Perspect.*, **110** (S5), 887–890.
204. Ono, K., Hirohada, M. and Yamada, M. (2008) α-Synuclein assembly as a therapeutic target of Parkinsons disease and related disorders. *Curr. Pharm. Des.*, **14** (30), 3247–3266.
205. Stains, C.I., Mondal, K. and Ghosh, I. (2007) Molecules that target β-amyloid. *ChemMedChem*, **2** (12), 1674–1692.
206. LeVine, H. III, (1999) Quantification of β-sheet amyloid fibril structures with thioflavin T. *Methods Enzymol.*, **309**, 274–284.
207. LeVine, H. III, (1993) Thioflavin T interaction with synthetic Alzheimer's disease beta-amyloid peptides: detection of amyloid aggregation in solution. *Protein Sci.*, **2** (3), 404–410.
208. Yona, R.L., Mazeres, S., Faller, P. and Gras, E. (2008) Thioflavin derivatives as markers for amyloid-β fibrils: insights into structural features important for high-affinity binding. *ChemMedChem*, **3** (1), 63–66.
209. Clark, D.E. (2005) Computational prediction of blood-brain barrier permeation. *Annu. Rep. Med. Chem.*, **40**, 403–415.
210. Rodríguez-Rodríguez, C., Rimola, A., Alí-Torres, J. *et al*. (2011) In silico strategies for the selection of chelating compounds with potential application in metal-promoted neurodegenerative diseases. *J. Comput. Aided Mol. Des.*, **25** (1), 21–30.
211. Clark, D.E. and Pickett, S.D. (2000) Computational methods for the prediction of 'drug-likeness'. *Drug Discov. Today*, **5** (2), 49–58.
212. Gabathuler, R. (2010) Approaches to transport therapeutic drugs across the blood-brain barrier to treat brain diseases. *Neurobiol. Dis.*, **37** (1), 48–57.
213. Scott, L.E., Telpoukhovskaia, M., Rodríguez-Rodríguez, C. *et al*. (2011) *N*-aryl-substituted 3-(β-D-glucopyranosyloxy)-2-methyl-4(1*H*)-pyridinones as agents for Alzheimer's therapy. *Chem. Sci.*, **2** (4), 642–648.
214. Liu, G., Men, P., Kudo, W. *et al*. (2009) Nanoparticle-chelator conjugates as inhibitors of amyloid-β aggregation and neurotoxicity: a novel therapeutic approach for Alzheimer disease. *Neurosci. Lett.*, **455** (3), 187–190.
215. Collin, G. and Höke, H. (2000) Quinoline and isoquinoline, in *Ullman's Encyclopedia of Industrial Chemistry*, Wiley-VCH Verlag GmbH, Weinheim pp. 1–5.
216. Pierre, J.-L., Baret, P. and Serratrice, G. (2003) Hydroxyquinolines as iron chelators. *Curr. Med. Chem.*, **10** (12), 1077–1084.
217. Bareggi, S.R. and Cornelli, U. (2012) Clioquinol: review of its mechanisms of action and clinical uses in neurodegenerative disorders. *CNS Neurosci. Ther.*, **18** (1), 41–46.
218. Mancino, A.M., Hindo, S.S., Kochi, A. and Lim, M.H. (2009) Effects of clioquinol on metal-triggered amyloid-β aggregation revisited. *Inorg. Chem.*, **48** (20), 9596–9598.
219. Mao, X. and Schimmer, A.D. (2008) The toxicology of clioquinol. *Toxicol. Lett.*, **182** (1–3), 1–6.
220. Di Vaira, M., Bazzicalupi, C., Orioli, P. *et al*. (2004) Clioquinol, a drug for Alzheimer's disease specifically interfering with brain metal metabolism: structural characterization of its zinc(II) and copper(II) complexes. *Inorg. Chem.*, **43** (13), 3795–3797.
221. Jenagaratnam, L. and McShane, R. (2006) Clioquinol for the treatment of Alzheimer's disease. *Cochrane Database Syst. Rev.*, CD005380 (1).
222. Cherny, R.A., Atwood, C.S., Xilinas, M.E. *et al*. (2001) Treatment with a copper-zinc chelator markedly and rapidly inhibits β-amyloid accumulation in Alzheimer's disease transgenic mice. *Neuron*, **30** (3), 665–676.
223. Ferrada, E., Arancibia, V., Loeb, B. *et al*. (2007) Stoichiometry and conditional stability constants of Cu(II) or Zn(II) clioquinol complexes; implications for Alzheimer's and Huntington's disease therapy. *Neurotoxicology*, **28** (3), 445–449.
224. Bush, A.I. and Tanzi, R.E. (2008) Therapeutics for Alzheimer's disease based on the metal hypothesis. *Neurotherapeutics*, **5** (3), 421–432.

225. Raman, B., Ban, T., Yamaguchi, K. *et al*. (2005) Metal ion-dependent effects of clioquinol on the fibril growth of an amyloid β peptide. *J. Biol. Chem.*, **280** (16), 16157–16162.
226. Tardiff, D.F., Tucci, M.L., Caldwell, K.A. *et al*. (2012) Different 8-hydroxyquinolines protect models of TDP-43 protein, α-synuclein, and polyglutamine proteotoxicity through distinct mechanisms. *J. Biol. Chem.*, **287** (6), 4107–4120.
227. Doraiswamy, P.M. and Finefrock, A.E. (2004) Metals in our minds: therapeutic implications for neurodegenerative disorders. *Lancet Neurol.*, **3** (7), 431–434.
228. Sampson, E.L., Jenagaratnam, L. and McShane, R. (2012) Metal protein attenuating compounds for the treatment of Alzheimer's dementia. *Cochrane Database Syst. Rev.*, (5), CD005380.
229. Kaur, D., Yantiri, F., Rajagopalan, S. *et al*. (2003) Genetic or pharmacological iron chelation prevents MPTP-induced neurotoxicity *in vivo*: a novel therapy for Parkinson's disease. *Neuron*, **37** (6), 899–909.
230. Nguyen, T., Hamby, A. and Massa, S.M. (2005) Clioquinol down-regulates mutant huntingtin expression *in vitro* and mitigates pathology in a Huntington's disease mouse model. *Proc. Natl. Acad. Sci. U.S.A.*, **102** (33), 11840–11845.
231. Bareggi, S.R., Braida, D., Pollera, C. *et al*. (2009) Effects of clioquinol on memory impairment and the neurochemical modifications induced by scrapie infection in golden hamsters. *Brain Res.*, **1280**, 195–200.
232. Formentin, E.A.M., Puricelli, M., Pollera, C. and Ponti, W. (2006) Evaluation of clioquinol activity towards transmissible spongiform encephalopathies (TSE) in cellular models and cell-free systems. *Vet. Res. Commun.*, **30** (S1), 253–255.
233. Dickens, M.G. and Franz, K.J. (2010) A prochelator activated by hydrogen peroxide prevents metal-induced amyloid β aggregation. *ChemBioChem*, **11** (1), 59–62.
234. Filiz, G., Caragounis, A., Bica, L. *et al*. (2008) Clioquinol inhibits peroxide-mediated toxicity through up-regulation of phosphoinositol-3-kinase and inhibition of p53 activity. *Int. J. Biochem. Cell Biol.*, **40** (5), 1030–1042.
235. Relkin, N.R. (2008) Testing the mettle of PBT2 for Alzheimer's disease. *Lancet Neurol.*, **7** (9), 762–763.
236. National Institute of Neurological Disorders and Stroke (2009) CINAPS Compound Dossier: 'Clioquinol'.
237. Zhuang, Z.-P., Kung, M.-P., Wilson, A. *et al*. (2003) Structure-activity relationship of imidazo[1,2-α]pyridines as ligands for detecting β-amyloid plaques in the brain. *J. Med. Chem.*, **46** (2), 237–243.
238. Adlard, P.A., Cherny, R.A., Finkelstein, D.I. *et al*. (2008) Rapid restoration of cognition in Alzheimer's transgenic mice with 8-hydroxy quinoline analogs is associated with decreased interstitial Aβ. *Neuron*, **59** (1), 43–55.
239. Cherny, R.A., Ayton, S., Finkelstein, D.I. *et al*. (2012) PBT2 reduces toxicity in a C. Elegans model of polyQ aggregation and extends lifespan, reduces striatal atrophy and improves motor performance in the R6/2 mouse model of Huntington's disease. *J. Huntington's Dis.*, **1** (2), 211–219.
240. Faux, N.G., Ritchie, C.W., Gunn, A. *et al*. (2010) PBT2 rapidly improves cognition in Alzheimer's disease: additional phase II analyses. *J. Alzheimers Dis.*, **20** (2), 509–516.
241. Lannfelt, L., Blennow, K., Zetterberg, H. *et al*. (2008) Safety, efficacy, and biomarker findings of PBT2 in targeting Aβ as a modifying therapy for Alzheimer's disease: a phase IIa, double-blind, randomised, placebo-controlled trial. *Lancet Neurol.*, **7** (9), 779–786.
242. Hureau, C., Sasaki, I., Gras, E. and Faller, P. (2010) Two functions, one molecule: a metal-binding and a targeting moiety to combat Alzheimer's disease. *ChemBioChem*, **11** (7), 950–953.
243. Dedeoglu, A., Cormier, K., Payton, S. *et al*. (2004) Preliminary studies of a novel bifunctional metal chelator targeting Alzheimer's amyloidogenesis. *Exp. Gerontol.*, **39** (11–12), 1641–1649.
244. Sharma, A.K., Pavlova, S.T., Kim, J. *et al*. (2012) Bifunctional compounds for controlling metal-mediated aggregation of the $A\beta_{42}$ peptide. *J. Am. Chem. Soc.*, **134** (15), 6625–6636.
245. Rodríguez-Rodríguez, C., Sánchez de Groot, N., Rimola, A. *et al*. (2009) Design, selection, and characterization of thioflavin-based intercalation compounds with metal chelating properties for application in Alzheimer's disease. *J. Am. Chem. Soc.*, **131** (4), 1436–1451.
246. Kung, H.F., Lee, C.-W., Zhuang, Z.-P. *et al*. (2001) Novel stilbenes as probes for amyloid plaques. *J. Am. Chem. Soc.*, **123** (50), 12740–12741.
247. Ono, M., Wilson, A., Nobrega, J. *et al*. (2003) ^{11}C-labeled stilbene derivatives as Aβ-aggregate-specific PET imaging agents for Alzheimer's disease. *Nucl. Med. Biol.*, **30** (6), 565–571.
248. Zhang, W., Oya, S., Kung, M.-P. *et al*. (2005) F-18 polyethyleneglycol stilbenes as PET imaging agents targeting Aβ aggregates in the brain. *Nucl. Med. Biol.*, **32** (8), 799–809.
249. Braymer, J.J., Choi, J.-S., DeToma, A.S. *et al*. (2011) Development of bifunctional stilbene derivatives for targeting and modulating metal-amyloid-β species. *Inorg. Chem.*, **50** (21), 10724–10734.

250. Choi, J.-S., Braymer, J.J., Nanga, R.P. *et al*. (2010) Design of small molecules that target metal–Aβ species and regulate metal-induced Aβ aggregation and neurotoxicity. *Proc. Natl. Acad. Sci. U.S.A.*, **107** (51), 21990–21995.
251. Choi, J.-S., Braymer, J.J., Park, S.K. *et al*. (2011) Synthesis and characterization of IMPY derivatives that regulate metal-induced amyloid-β aggregation. *Metallomics*, **3** (3), 284–291.
252. Pithadia, A.S., Kochi, A., Soper, M.T. *et al*. (2012) Reactivity of diphenylpropynone derivatives toward metal-associated amyloid-β species. *Inorg. Chem.*, **51** (23), 12959–12967.
253. Liu, Y., Kochi, A., Pithadia, A.S. *et al*. (2013) Tuning reactivity of diphenylpropynone derivatives with metal-associated amyloid-β species via structural modifications. *Inorg. Chem.*, **52** (14), 8121–8130.
254. Lakatos, A., Zsigó, É., Hollender, D. *et al*. (2010) Two pyridine derivatives as potential Cu(II) and Zn(II) chelators in therapy for Alzheimer's disease. *Dalton Trans.*, 1302–1315.
255. Jones, M.R., Service, E.L., Thompson, J.R. *et al*. (2012) Dual-function triazole-pyridine derivatives as inhibitors of metal-induced amyloid-β aggregation. *Metallomics*, **4** (9), 910–920.
256. Wu, W.-H., Lei, P., Liu, Q. *et al*. (2008) Sequestration of copper from β-amyloid promotes selective lysis by cyclen-hybrid cleavage agents. *J. Biol. Chem.*, **283** (46), 31657–31664.
257. Lima, L.M.P., Esteban-Gómez, D., Delgado, R. *et al*. (2012) Monopicolinate cyclen and cyclam derivatives for stable copper(II) complexation. *Inorg. Chem.*, **51** (12), 6916–6927.
258. Suh, J., Yoo, S.H., Kim, M.G. *et al*. (2007) Cleavage agents for soluble oligomers of amyloid β peptides. *Angew. Chem. Int. Ed.*, **46** (37), 7064–7067.
259. DeToma, A.S., Choi, J.-S., Braymer, J.J. and Lim, M.H. (2011) Myricetin: a naturally occurring regulator of metal-induced amyloid-β aggregation and neurotoxicity. *ChemBioChem*, **12** (8), 1198–1201.
260. Lopez del Amo, J.M., Fink, U., Dasari, M. *et al*. (2012) Structural properties of EGCG-induced, nontoxic Alzheimer's disease Aβ oligomers. *J. Mol. Biol.*, **421** (4–5), 517–524.
261. Bieschke, J., Russ, J., Friedrich, R.P. *et al*. (2010) EGCG remodels mature α-synuclein and amyloid-β fibrils and reduces cellular toxicity. *Proc. Natl. Acad. Sci. U.S.A.*, **107** (17), 7710–7715.
262. Ehrnhoefer, D.E., Bieschke, J., Boeddrich, A. *et al*. (2008) EGCG redirects amyloidogenic polypeptides into unstructured, off-pathway oligomers. *Nat. Struct. Mol. Biol.*, **15** (6), 558–566.
263. Bae, S.Y., Kim, S., Hwang, H. *et al*. (2010) Amyloid formation and disaggregation of α-synuclein and its tandem repeat (α-TR). *Biochem. Biophys. Res. Commun.*, **400** (4), 531–536.
264. Hyung, S.-J., DeToma, A.S., Brender, J.R. *et al*. (2013) Insights into antiamyloidogenic properties of the green tea extract (-)-epigallocatechin-3-gallate toward metal-associated amyloid-β species. *Proc. Natl. Acad. Sci. U.S.A.*, **110** (10), 3743–3748.
265. Zhang, B., Cheng, X.R., da Silva, I.S. *et al*. (2013) Electroanalysis of the interaction between (−)-epigallocatechin-3-gallate (EGCG) and amyloid-β in the presence of copper. *Metallomics*, **5** (3), 259–264.
266. Granzotto, A. and Zatta, P. (2011) Resveratrol acts not through anti-aggregative pathways but mainly via its scavenging properties against Aβ and Aβ-metal complexes toxicity. *PLoS One*, **6** (6), e21565.
267. Ono, K., Yoshiike, Y., Takashima, A. *et al*. (2003) Potent anti-amyloidogenic and fibril-destabilizing effects of polyphenols *in vitro*: implications for the prevention and therapeutics of Alzheimer's disease. *J. Neurochem.*, **87** (1), 172–181.
268. Rivière, C., Richard, T., Quentin, L. *et al*. (2007) Inhibitory activity of stilbenes on Alzheimer's β-amyloid fibrils *in vitro*. *Bioorg. Med. Chem.*, **15** (2), 1160–1167.
269. Anand, P., Kunnumakkara, A.B., Newman, R.A. and Aggarwal, B.B. (2007) Bioavailability of curcumin: problems and promises. *Mol. Pharm.*, **4** (6), 807–818.
270. Hatcher, H., Planalp, R., Cho, J. *et al*. (2008) Curcumin: from ancient medicine to current clinical trials. *Cell. Mol. Life Sci.*, **65** (11), 1631–1652.
271. Ryu, E.K., Choe, Y.S., Lee, K.-H. *et al*. (2006) Curcumin and dehydrozingerone derivatives: synthesis, radiolabeling, and evaluation for β-amyloid plaque imaging. *J. Med. Chem.*, **49** (20), 6111–6119.
272. Baum, L. and Ng, A. (2004) Curcumin interaction with copper and iron suggests one possible mechanism of action in Alzheimer's disease animal models. *J. Alzheimers Dis.*, **6** (4), 367–377.
273. Huang, H.-C., Lin, C.-J., Liu, W.-J. *et al*. (2011) Dual effects of curcumin on neuronal oxidative stress in the presence of Cu(II). *Food Chem. Toxicol.*, **49** (7), 1578–1583.

11

Rational Design of Copper and Iron Chelators to Treat Wilson's Disease and Hemochromatosis

Christelle Gateau[1], Elisabeth Mintz[2], and Pascale Delangle[1]

[1] *UMR-E3, Laboratoire Reconnaissance Ionique et Chimie de Coordination, Université Joseph Fourier – Grenoble 1/CEA/Institut Nanoscience et Cryogénie/SCIB, 17 rue des martyrs, 38054, Grenoble, France*

[2] *UMR 5249, Laboratoire Chimie et Biologie des Métaux, Université Joseph Fourier – Grenoble 1/CNRS/CEA/Institut de Recherches en Sciences et Technologies pour le Vivant/LCBM, 17 rue des martyrs, 38054, Grenoble, France*

11.1 Introduction

Metals are abundantly present in the body, where they play major biological roles. Indicative quantities for a 70 kg person vary from 1 kg for calcium to only a few micrograms for the less abundant metals [1].

Essential metals such as Fe, Cu, or Zn are necessary for a variety of vital functions, such as oxygen transport (Fe), respiration (Cu), or DNA transcription (Zn in zinc fingers) but may become toxic in case of misregulation of their concentration. Therefore, their concentrations are tightly regulated in all cells to confine these metals to their vital functions. Other metals like Hg, Cd, and Pb, have no physiological function at all and are purely toxic.

Mechanisms leading to metal toxicity are numerous: production of reactive oxygen species (ROS), substitution of essential metal ions in key binding sites of enzymes or modification of the structure of proteins. Redox active metal ions have an ambiguous role *in vivo* because, on the one hand, the oscillation between their oxidation states is necessary for many enzymes' functions but, on the other hand, it is also responsible for their potential toxicity. Therefore, they may induce oxidative stress, if they are weakly bound, in the intracellular medium [2]. At its reduced state, the metal may react with hydrogen peroxide (H_2O_2),

Ligand Design in Medicinal Inorganic Chemistry, First Edition. Edited by Tim Storr.

a by-product of oxygen metabolism [3], to produce ROS such as the hydroxyl radical in a Fenton type reaction (see Equations 11.1 or 11.2). The return to the reduced state is then performed by reductants that are available in cells, such as O_2^- or glutathione (GSH), a cysteine-containing tripeptide. So, redox active metals such as Cu or Fe catalyze hydroxyl radical formation. The final product $OH^\bullet$ is very reactive and damages all kinds of molecules in the cell: sugars, amino acids, phospholipids, purine, and pyrimidine bases and organic acids [4].

$$Cu^+ + H_2O_2 = Cu^{2+} + OH^\bullet + OH^- \tag{11.1}$$

$$Fe^{2+} + H_2O_2 = Fe^{3+} + OH^\bullet + OH^- \tag{11.2}$$

Metal ion toxicity may also be associated with binding to inappropriate sites. For instance, native metals such as Zn^{2+} may be replaced in important protein binding sites by other elements like the toxic metal ions Cd^{2+} or Hg^{2+} and this may alter major biological functions [5]. There is also accumulating evidence that metal ion binding may be responsible for aggregation of intrinsically disordered proteins and therefore that altered metal homeostasis may be related to the progression of neurodegenerative diseases [6–9].

Therefore, metal overload is involved in several diseases; some are due to toxic metal poisoning like saturnism or hydrargyria, which are related to exposures to lead or mercury, respectively [10, 11], others are neurological disorders like Alzheimer's or Parkinson's disease in which metals are implicated although their mechanisms of action are not yet fully understood [7, 9, 12, 13]. Finally, metal overload can be the result of disrupted homeostasis due to a genetic disorder. For instance, this is the case for copper in Wilson's disease and for iron in hemochromatosis. In the following, we will focus on these two genetic disorders and the strategies that the medicinal inorganic chemist may apply to design novel chelation therapies to treat these iron or copper overload diseases. In particular, the emphasis will be put on the requirement of having a good understanding of the biology of metals to design more effective and more specific chelating drugs.

We will first briefly present the basic principles of coordination chemistry, which are used for designing appropriate chelating agents, and then we will describe recent and specific developments in the field.

11.2 Chelating agents

11.2.1 Thermodynamic parameters

Chelation therapy aims at removing the metal overload from the body with molecules that efficiently and selectively complex the metal and promote its excretion. Therefore, key parameters are the thermodynamic equilibrium constants, which define the affinity and selectivity of the chelating agent for the targeted metal in its major form. The equilibrium constants are given by Equations 11.3 and 11.4 and also predict potential competing metal ions in the organism [14].

$$M + L = ML \quad K = [ML]/[M][L] \tag{11.3}$$

$$mM + lL + hH = M_mL_lH_h \quad K_{mlh} = [M_mL_lH_h]/[M]^m[L]^l[H]^h \tag{11.4}$$

Redox potentials are other important thermodynamic parameters since they are related to the ability of metal ions to be reduced or oxidized. For instance, a metal complex can catalyze the formation of hydroxyl radicals if: (i) the reduced complex has a redox potential allowing the Fenton reaction, that is, the transfer of one electron to H_2O_2 (see Equations 11.1 and 11.2), which is possible if the standard potential is lower than +460 mV/NHE (E° ($H_2O_2/OH^\bullet,OH^-$)) (where NHE stands for Normal Hydrogen Electrode) and (ii) the oxidized complex is reducible by cellular reducing agents usually present in cells, such as superoxide

O_2^-, GSH, or NADH (nicotinamide adenine dinucleotide). This is thermodynamically allowed for complexes whose redox potentials are in the $-324\,\text{mV} < E^\circ < +460\,\text{mV}$ range under standard conditions of equilibrium [15]. The redox potentials are, therefore, parameters that have been taken into account to avoid oxidative stress, in particular in the design of Fe^{3+} chelators. Obviously, the standard conditions of equilibrium are not always fulfilled within cells and *in vivo* redox properties of metal complexes are difficult to predict [15].

The stability of a complex is governed by the properties of both the metal ion and the chelating agent.

11.2.2 Principles of coordination chemistry applied to chelation therapy

11.2.2.1 HSAB theory

Metal ions are Lewis acids that are classified in three categories depending on their affinities for selected donor atoms according to the Hard Soft Acid Base (HSAB) theory proposed by Ralph G. Pearson in the 1960s [16, 17]. Cu is classified either as soft (Cu^+) or borderline (Cu^{2+}), whereas Fe is classified as borderline (Fe^{2+}) or hard (Fe^{3+}). Since hard acids bind preferentially to hard bases, forming ionic or electrostatic bonds, whereas soft acids bind preferentially to soft bases forming bonds with a covalent character, it appears essential to know which oxidation state to consider in designing efficient chelating molecules.

Indeed, *in vivo*, the abundant hard alkali and alkaline earth metal ions, like Ca^{2+}, are usually bound by the hard oxygen donors of carboxylates in aspartates or glutamates or phenolates in tyrosinates. The same behavior is expected for Fe^{3+}. On the other hand, the borderline cations Fe^{2+} and Cu^{2+} are commonly coordinated by histidine nitrogen atoms. One of the most striking illustrations of the HSAB theory is the very efficient coordination of soft metal ions, such as Cu^+, Hg^{2+}, and Cd^{2+}, by the soft cysteine sulfur donors of metallothioneins (MTs), which are sulfur-rich proteins dedicated to cell protection against toxic metals [18, 19].

11.2.2.2 Chelation

Chelation refers to coordination of several donor atoms from a single ligand to a central metal atom and generally enhances the thermodynamic stability of metal complexes with respect to monodentate or lower denticity ligands [20]. Five- and six-membered chelate rings, obtained when two donor atoms of the same molecule interact with one metal ion, are particularly favorable and the stabilization is optimal if the number and size of the chelate rings minimize steric strain upon metal binding [21]. Therefore, polydentate ligands with multiple donor atoms as metal binding sites are commonly used to design high stability metal complexes for various applications. One of the most famous examples of such ligands is the hexadentate ethylenediaminetetraacetic acid (EDTA, Figure 11.1), which efficiently binds a large range of metal ions by forming multiple five-membered chelate rings with its oxygen and nitrogen donors; Table 11.1 illustrates the binding ability of EDTA for several biologically-relevant cations. Fe^{3+}, a hard cation, forms a stable complex with EDTA and is preferred to Ca^{2+}, a divalent hard cation, or to Fe^{2+}, Cu^{2+}, and Zn^{2+}, borderline cations. Interestingly, $CaNa_2$-EDTA was tested for removal of hard ions such as actinides in the 1950s but its efficacy as an actinide chelator was limited due to the competition with Ca^{2+} cations [22].

11.2.2.3 Geometric preferences due to the electronic configuration of the metal ion

The electronic configuration of the metal ion influences significantly its preferred geometry. Iron is a transition metal with either an $[Ar]3d^5$ (Fe^{3+}) or $[Ar]3d^6$ (Fe^{2+}) electronic configuration and preferred octahedral coordination. Copper in the +I oxidation state, Cu^+, exhibits an $[Ar]3d^{10}$ configuration; the most common geometries are linear, trigonal planar, or tetrahedral. In contrast, Cu^{2+} has an $[Ar]3d^9$ electronic configuration

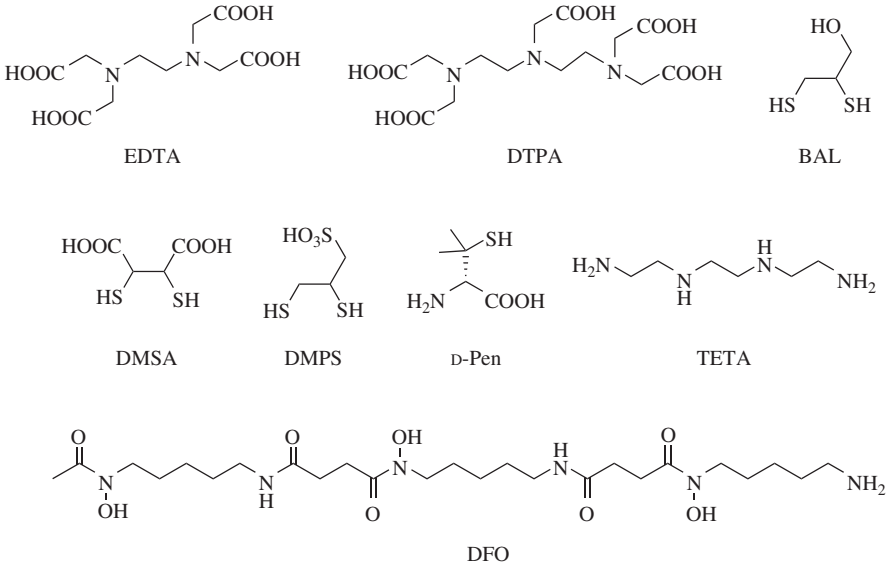

Figure 11.1 *Selected ligands developed for metal removal by chelation therapy*

and is subject to Jahn-Teller distortion if placed in a cubic environment. Therefore, Cu^{2+} commonly exhibits distorted tetrahedral or octahedral coordination spheres.

11.2.3 Examples of classical chelating agents

Coordination chemistry principles have been applied to the design of metal chelators used for the treatment of metal overloads since the industrial revolution, which promoted the use of metals in many applications [10, 24]. The first treatments were aiming at removing toxic metals such as lead, mercury, antimony, and arsenic from the human body. These targeted metals are either borderline or soft in the HSAB theory and consequently the first molecules used as chelating agents included soft sulfur donors such as thiolates.

British Anti-Lewisite (BAL, Figure 11.1), was developed during World War II as an antidote against an arsenic derivative, dichlorovinylarsine or Lewisite [25]. Since the latter was never used, the first application of BAL as a medical treatment was in intoxications due to arsenic drugs against syphilis [26]. In 1951, BAL was also used to treat copper overload in Wilson's disease with striking success [27]. However, BAL is a lipophilic derivative given by painful intramuscular injections, and the need for novel and more convenient detoxification agents has led to the development of other sulfur compounds. Two derivatives of BAL, *meso*-2,3-dimercaptosuccinic acid (DMSA, Figure 11.1) [28] and D,L-2,3-dimercapto-1-propanesulfonic acid (DMPS, Figure 11.1) were proposed a few years later as less toxic and more hydrophilic compounds that are now registered for mercury detoxification in some countries [24]. BAL and derivatives such as DMSA and DMPS are still used in cases of acute poisoning by these toxic ions. D-Penicillamine (D-Pen, Figure 11.1) is an orally active copper chelator used since 1956 to treat copper overload in Wilson's disease, whereas triethylenetetramine (TETA, Figure 11.1) was proposed in the 1980s for Wilson's disease patients intolerant to D-Pen.

Other chelators were developed at the same period to treat metal overload with ions belonging to the "hard" or "borderline" families. In the 1950s, the EDTA polyaminocarboxylate ligand, already discussed in

Table 11.1 *Equilibrium constants ($\log K_{110}$) of some metal-EDTA complexes at 298 K and 0.1 M ionic strength [23]*

Na^{+}	1.86	Ca^{2+}	10.65	Fe^{3+}	25.1
Fe^{2+}	14.3	Cu^{2+}	18.8	Zn^{2+}	16.5

Section 11.2.2.2, was in clinical use to fight lead and radionuclide intoxication. However, EDTA treatments could not be used over long periods because of the lack of selectivity with respect to essential metals such as calcium and zinc (Table 11.1). Finally, desferrioxamine B (DFO) was the first drug approved for iron overload in the 1970s.

11.3 Modern medicinal inorganic chemistry and chelation therapy

To apply the principles of coordination chemistry to the design of efficient chelating agents, it is of course necessary to know the place in the body where the metal overload may be the most toxic and which oxidation state of the metal should be targeted.

Modern medicinal chemistry has contributed to the development of chelators having a higher affinity for the targeted metal ion associated to larger selectivities with respect to essential metal ions that are naturally present in the body, and thus should not be depleted by chelation therapy. For instance, the lack of selectivity of EDTA (Figure 11.1 and Table 11.1) is mainly due to its hexadentate character, which accommodates similarly metal ions of both d- and f-blocks. Indeed, actinides such as Pu^{4+} are f elements, which are hard and form complexes with no specific geometries since their valence 5f-orbitals are core orbitals. Therefore, they accommodate larger coordination numbers than metal ions of the d-block. Diethylenetriaminepentaacetic acid (DTPA, Figure 11.1), which is an octadentate analog of EDTA, displays a larger affinity for Pu^{4+} as well as significantly higher selectivities with respect to calcium and zinc [22]. Therefore, DTPA has rapidly replaced EDTA for chelation therapy of radionuclides. Similar strategies are used for other *in vivo* applications, such as the design of lanthanide (4f) complexes for imaging. The lanthanide complex should be very stable *in vivo* in the presence of endogeneous cations, such as Ca^{2+} and Zn^{2+}, to avoid the release of the toxic free lanthanide ion in the body [29]. Large affinities and selectivities for the targeted metal ion are not sufficient to design efficient chelators to treat metal overload. Indeed, toxicity and biodistribution are also key parameters.

Today, the development of novel and more efficient chelating agents is also aiming at combining several functions in the same therapeutic molecule, such as selective metal chelation, targeting of specific organs and demonstrating pro-drug properties. Indeed, the chelating agents presented in Section 11.2.3 have the common drawbacks of systemic drugs, that is, even biodistribution throughout the body and poor specificity toward a pathological site. This is the reason why large doses of these chelators are used to achieve high local concentrations at the desired place in the body and to increase toxic metal excretion. This lack of specificity, of course, induces unwanted side-effects. Drug targeting has been proposed to solve the problems due to systemic drug therapy by achieving specific drug accumulation in a target zone. Paul Ehrlich proposed the concept of the "magic bullet" about a century ago to selectively target a bacterium without affecting other organisms to treat syphilis. This concept is used nowadays for the development of highly-selective drugs without significant side-effects [30].

This approach has been applied to the delivery of metallodrugs specifically to tumors. Indeed, cisplatin and its derivatives are highly efficient anti-cancer drugs that induce severe toxic side-effects [31]; therefore, the design of platinum complexes having an exclusive selectivity for the tumor would afford drugs exhibiting less systemic toxicity [32]. Hence, various vectors, like liposomes, nanoparticles, or macrocyclic carriers

have been used to deliver metallodrugs to tumors. Another strategy is to covalently functionalize the drug with biomolecular units, which target either the "enhanced permeability and retention" (EPR) effect or an organ-specific feature [33]. In addition to targeting, the pro-drug concept is also very attractive to develop efficient drugs with a minimum of side-effects. Indeed, a pro-drug is an inert compound that provides the delivery of the active component only at the desired target.

Thus, current medicinal inorganic chemistry involves the rational design of specific chelators associated to targeting and/or pro-drugs properties. To develop such polyfunctional molecules, the chemist needs to understand the biology of the targeted metal *in vivo* and the nature of the overload. This is why medicinal inorganic chemistry has become a multidisciplinary area gathering chemists, biologists, and physicians. Here are some important parameters that have to be taken into account in the design:

- The oxidation state of the excess metal ion
- Its localization in the body (organs or fluids, intracellular or extracellular)
- Its main available forms (binding to biological ligands)
- If possible the mechanism of excretion

The next three sections are dedicated to the design of chelators to treat two genetic diseases associated with metal overload, Wilson's disease (Cu overload) and hemochromatosis (Fe overload). The purpose of this chapter is not to present an exhaustive review about chelation therapy. We will rather try to emphasize the relation between the biology of the metal in overload and the chemical design of effective and specific chelating drugs from examples selected in the literature.

Fe and Cu are essential elements for all living cells, since their redox properties make them major sources and acceptors of electrons in many enzymes' activities. However, the redox properties of the two couples Fe^{3+}/Fe^{2+} and Cu^{2+}/Cu^{+} have paradoxical effects on cell physiology since they are also responsible for oxidative stress and toxicity. This is the reason why Cu or Fe overload have to be treated by chelation therapy.

11.4 Iron overload

11.4.1 Iron distribution and homeostasis

A healthy adult body contains about 4 g of iron, 70% of which is dedicated to oxygen transport by hemoglobin in red blood cells and to heme formation in immature red blood cells. The remaining iron is found mainly in the liver and the spleen, where senescent red blood cells are degraded, and also in the muscles where myoglobin, another heme protein, stores oxygen. Circulating iron in the plasma represents less than 0.1% of total iron; however, it is this low amount of iron that plays a role in many essential functions in each cell, either in heme-containing proteins, or in iron-sulfur cluster-containing proteins or as a simple cofactor in oxidases or reductases [34]. Since the focus of this chapter is metal overload, we will concentrate on the mechanisms responsible for these overloads when some of these processes are ill-functioning.

Dietary iron is absorbed by the small intestine, crossing the enterocytes to reach the circulatory system (Figure 11.2).

At the apical membrane of enterocytes, dietary Fe^{3+} is reduced by DCytB, a membrane bound reductase. Fe^{2+} is then transported through the apical membrane by DMT1, the divalent cation transporter. Once inside the cell, Fe^{2+} is either inactivated as $Fe(OH)_3$ and bound to **ferritin**, the protein dedicated to iron storage, or transported out of the cell through the basolateral membrane by FPN, the protein named ferroportin. When outside the cell, Fe^{2+} is oxidized by HPN, a ferroxidase named hephaestin (HP) at the basolateral membrane. The resulting Fe^{3+} can bind Tf, the plasmatic **transferrin**. The circulating Fe_2Tf complex can enter almost

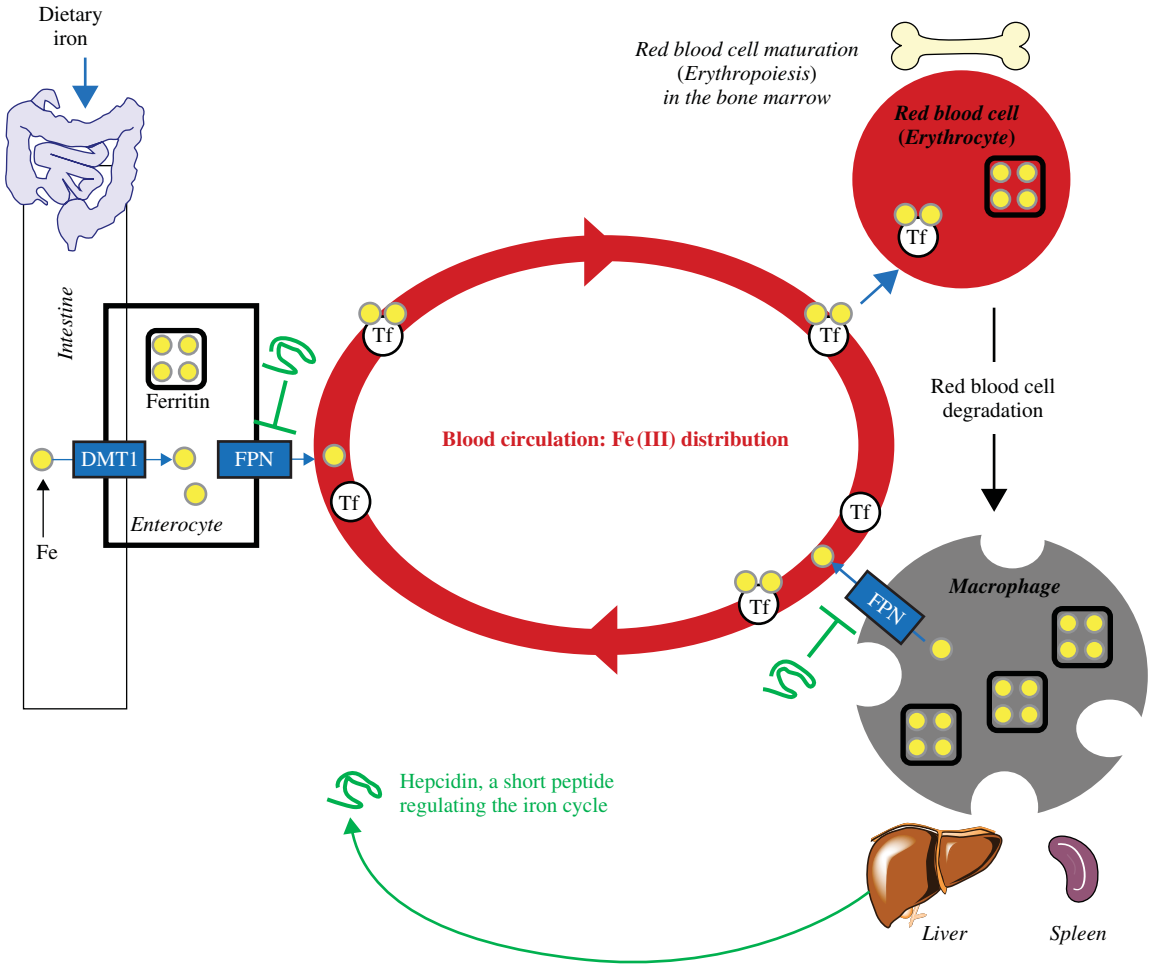

Figure 11.2 *Fe distribution and regulation – a simplified view*

any cell as the transferrin receptor is widely expressed in the body. Dietary absorption represents 1–2 mg iron per day as does the daily loss in urine and faeces.

The main target for circulating iron is in the bone marrow, where immature red blood cells need iron to renew the senescent red blood cells at a high rate (200 billion red blood cells per day). After 120 days of life, red blood cells are degraded by macrophages in the spleen and in the liver. Macrophages incorporate senescent red blood cells in big vesicles where, the heme oxygenase (HO) metabolizes the heme. Once in the cytosol, Fe is either stored in ferritin or transferred to the circulation by FPN. Fe^{2+} is then oxidized by a circulating ferroxidase called ceruloplasmin (CP) so that the Fe_2Tf complex is formed again in the plasma, ready to be incorporated by any cell. Tf is able to bind two Fe^{3+} ions in similar distorted octahedral binding sites consisting of two Tyr, one His, one Asp, and one bidentate carbonate anion [35]. A structure of diferric human transferrin is shown in Figure 11.3b.

Iron incorporation in cells starts with the binding of the Fe_2Tf complex to the transferrin receptor that is followed by endocytosis. In the endosome, acidification of the medium by a proton pump results in Fe^{3+}

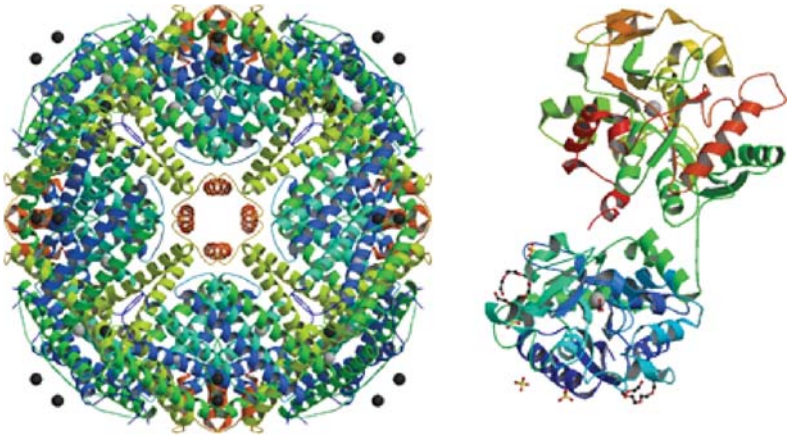

Figure 11.3 *Ferritin and transferrin, two important proteins involved in iron distribution. (a) (Left-hand structure) Human H Ferritin biological assembly showing the iron storage cavity. Image from the RSC PDB (www.pdb.org) of PDB ID 1FHA [36]. (b) (Right-hand structure) Crystal structure of diferric human transferrin. Image from the RSC PDB (www.pdb.org) of PDB ID 3V83 [37]*

dissociation from Tf; then a reductase allows Fe^{2+} to be transported into the cytoplasm by DMT1. Fe is then sent to the mitochondria to be incorporated into heme and into iron-sulfur clusters [38]. When there is excess of iron, hepatocytes store iron in ferritin, a protein able to bind 4500 Fe atoms in a cavity shown in the structure of human apo-ferritin in Figure 11.3a.

The intracellular mechanisms described above and the proteins responsible for them are tightly regulated so that each cell protects itself against the toxicity coming from excessive iron. However, the overall regulation of the iron cycle occurs from **hepcidin**, a 25-amino acid peptide produced by hepatocytes in the liver and secreted into the circulation. In case of excessive iron, hepcidin impairs iron input into the circulation from enterocytes (dietary iron), macrophages (recycled iron from senescent red blood cells) and hepatocytes (iron-stores). The key step is, therefore, the iron-dependent synthesis of hepcidin by hepatocytes, which is initiated by an increase in the Tf saturation above 20–30%, which is the normal status and results in endocytosis and degradation of ferroportin. However, as there is no mechanism devoted to excretion of Fe out of the body, any perturbation of this regulation can induce an overload.

11.4.2 Iron overload diseases

Iron overload diseases, both acquired and inherited, are characterized by an accumulation of iron in tissues such as the liver. The accumulation first overwhelms the defence capacities of the cells, secondly, those of the organ, leading to liver damage and eventually failure. In the plasma, a so-called "labile iron pool" appears that has toxic effects (Fe bound to citrate, acetate among other small molecules or albumin). Hereditary hemochromatosis refers to primary Fe overload diseases caused by mutations found in at least five different genes that involve the hepcidin-ferroportin interaction. The genes involved are those of hepcidin, ferroportin, and proteins involved in inducing hepcidin synthesis [39].

Beta-thalassemia is a secondary Fe overload disease in which one hemoglobin subunit is defective, inducing abnormal red blood cell maturation and anemia. In response to anemia, hepcidin production is inhibited and Fe absorption is increased, resulting in Fe overload. Transfusions meant to fight anemia bring even more Fe

to the body. For these diseases, bloodletting or phlebotomy is the standard treatment. When iron overload is associated with anemia, then chelation therapy can be considered.

Genetic hemochromatosis and transfusion-induced iron overload are the main forms of human iron overload. Despite a sophisticated homeostatic regulation (uptake, storage, and distribution), no mechanism for excreting excessive iron is present in the human organism and iron accumulates mainly in the liver and the spleen, more precisely in two types of cells, hepatocytes and macrophages. Both cell types store overloading Fe in ferritin, as Fe^{3+}.

11.4.3 Fe^{3+} chelators

Fe^{3+}, the major iron oxidation state present in humans, is a spherical symmetric tripositive cation of radius 0.65 Å having an [Ar]3d^5 electronic configuration. As such, Fe^{3+} is classified as a hard Lewis acid according to Pearson's theory. It binds preferentially six hard oxygen atoms in an octahedral arrangement. The most efficient chemical motifs to achieve this coordination mode are bidentate oxygen donors, such as catecholates, hydroxamates, and hydroxypyridinones [40].

An "ideal" iron chelating agent for the treatment of iron overload should efficiently and selectively trap Fe^{3+} within the iron-loaded cells and excrete it without being toxic. To achieve this, the chelator should possess:

- High affinity for Fe^{3+} ($pFe^{3+} > 20$, pFe^{3+} being the negative logarithm of the free metal concentration in standard conditions) to effectively compete with iron-loaded proteins such as transferrin ($pFe^{3+} = 20.3$) [41] and minimize the redistribution of iron within the body
- High selectivity to minimize depletion of other metals ions
- A redox potential value of the Fe^{3+}/Fe^{2+} couple at pH 7.4 below −300 mV (vs NHE) to effectively prevent the production of ROS [15]
- Suitable lipophilicity to reach the desired target sites where iron-loading has occurred

Microorganisms produce low molecular weight chelating agents with high Fe^{3+} affinity and selectivity to mediate iron acquisition and transport. These "iron carriers" called siderophores, designed by Nature are an unlimited source of inspiration to design Fe^{3+} scavenging molecules for iron chelation therapy. Naturally, the first drug approved for iron overload has been the fungal siderophore isolated from *Streptomyces pilosus*, **desferrioxamine B** (Figure 11.1) [42, 43] also known as deferoxamine, desferal™ (marketed by Novartis) or DFO. Since the 1970s, this compound is the most routinely used therapeutic agent for iron chelation therapy. DFO B is an hydroxamate-based hexadentate chelator that binds Fe^{3+} with a high affinity (pFe^{3+} 26.3) [41] and exhibits a great selectivity for trivalent over divalent essential metal ions. DFO also prevents the formation of damaging ROS (Fe^{3+}/Fe^{2+} redox potential at pH 7 = −480 mV/NHE) [44]. However, this hydrophilic compound has major drawbacks since it is orally inactive and rapidly removed by kidneys. Thus, it requires prolonged subcutaneous infusions (for 8–12 hours a day, 5–7 days a week) to achieve enough iron excretion. Furthermore, numerous side-effects have been reported in long-term treated patients [45].

This is the reason why many studies have been devoted to the design of synthetic iron chelating drugs for the treatment of iron overload. Over the past 40 years, several hundred compounds have been synthesized as iron chelating agents. Amongst them, two compounds have emerged as orally active iron chelating drugs.

In 1987, **deferiprone**, **DFP** or 1,2-dimethyl-3-hydroxypyridin-4-one [46] also known as Ferriprox™ (marketed by Apotex) or CP20 was the first compound to emerge (Figure 11.4). It was approved in Europe in 1999 and by the FDA in 2011. This optimized member of the extensively studied hydroxypyridinone family is a bidentate chelator leading to a neutral 3 : 1 Fe^{3+} complex, identified as the major species present under biological conditions [47]. DFP shows a high affinity (pFe^{3+} 20.5), selectivity for Fe^{3+} over divalent metal ions and redox inertness (Fe^{3+}/Fe^{2+} redox potential at pH 7 = −380 mV/NHE) [48] under biological conditions.

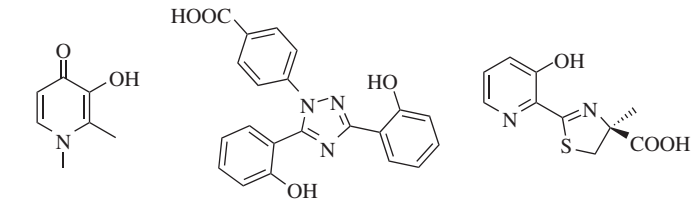

Deferiprone (DFP) Deferasirox Desferrrithiocin (DFT)

Figure 11.4 *Iron chelators*

Thanks to its low molecular weight and lipophilicity, DFP is orally active and efficiently removes iron from iron-loaded hepatocytes, macrophages, and cardiac cells [49]. Despite these promising features and due to extensive metabolic activity (namely the formation of a glucuronide conjugate at the hydroxy group in the 3-position) [50], the dose required to ensure enough iron excretion is high. Furthermore, DFP side-effects are still debated.

Deferasirox [51, 52], also known as ICL670 or Exjade™ (marketed by Novartis), which was approved by the FDA in 2005 as the first orally active iron chelating drug taken once per day, is now available worldwide. Thanks to the presence of one triazole nitrogen and two phenolate oxygen atoms, this tridentate chelator forms exclusively a trianionic 2 : 1 Fe^{3+} complex with high and specific affinity for Fe^{3+} (pFe^{3+} 22.5) under physiological conditions [53]. Furthermore, deferasirox prevents the formation of damaging ROS (Fe^{3+}/Fe^{2+} redox potential at pH 7 = −390 mV/NHE) [48]. Its lipophilicity, counterbalanced by its ability to bind albumin [54], allows deferasirox to be relatively non-toxic. It promotes the excretion of iron stores from hepatocytes but it is less effective at removing iron stores from cardiac cells [49]. Furthermore, deferasirox presents several side-effects such as nephrotoxicity.

Desferrithiocin [55] or DFT, isolated from *Streptomyces antibioticus*, is the first natural siderophore found to be orally active and it has been the subject of extensive studies. This tridentate chelator binds Fe^{3+} with one phenolate oxygen, one carboxylate oxygen and one thiazole nitrogen atom leading to a stable 2 : 1 Fe^{3+} complex. DFT shows a high affinity for Fe^{3+} but, unfortunately, it also binds Zn^{2+} tightly [56, 57]. Furthermore, it caused severe nephrotoxic effects and was therefore banned from the clinic [58].

11.4.4 Current developments

Over the past few years, a large volume of literature has been devoted to the design of new iron chelating agents, boosted by more and more indications that iron plays a role in a broad range of diseases, from cancers [59] to neurodegenerative [60] diseases. However, we focus here only on selected recent developments dedicated to the treatment of iron overload diseases based on the existing drugs described in Figures 11.1 and 11.4 to emphasize the relation between the chemical design and the physicochemical and pharmacological properties.

The strategy to optimize these drugs is mainly based on two approaches:

- Chemical modifications mainly to improve the oral activity and/or the bioavailability at the iron-loaded sites and reduce the toxicity
- Incorporation of bidentate or tridentate moieties in polydentate scaffolds to enhance chelating capability

Some examples of chemical modifications of DFO, DFP, and DFT are presented in Figure 11.5.

To overcome the major flaw of DFO, that is, its short residence time in plasma, high molecular weight and more lipophilic analogs have been prepared. In such an approach, conjugation of parent DFO with

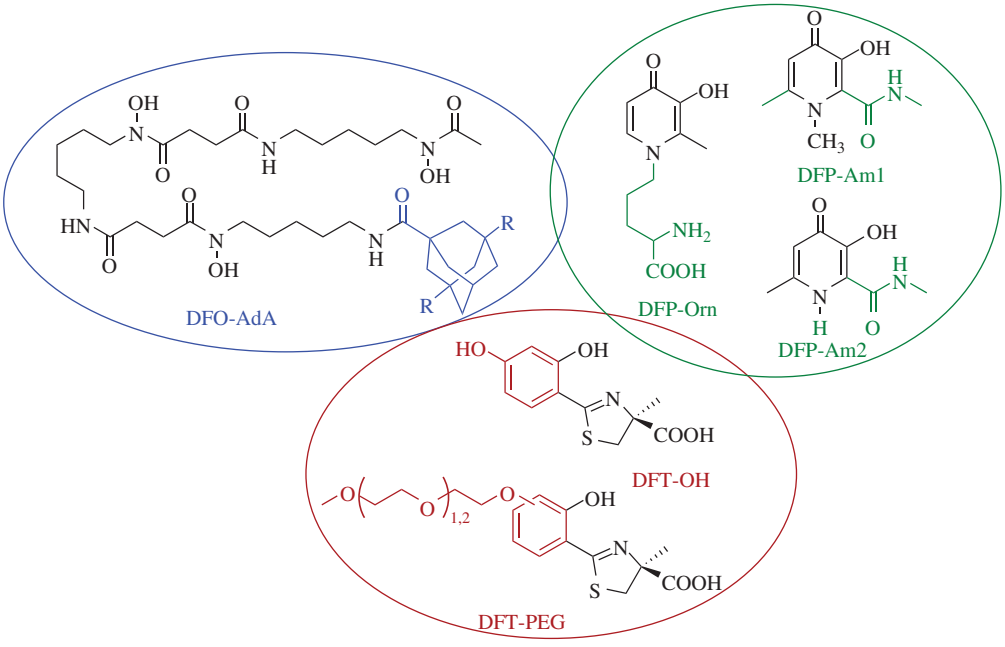

Figure 11.5 *Illustrative examples of chemical modifications on desferrioxamine (DFO), deferiprone (DFP), and desferrithiocin (DFT)*

hydroxyethyl starch-desferrioxamine (HES-DFO) allows a significant increase of the drug residence time from few minutes for DFO to several hours for the high molecular weight analog [61]. More recently, lipophilic adamantate derivatives (DFO-AdA), known for their favorable pharmacological properties, have been appended at the terminal amine of DFO. This alteration of the lipophilic character of the parent DFO, without changing the coordination properties, was supposed to improve the capacity of these molecules to cross cell membranes and trap intracellular iron. Actually, these compounds are more than twice as effective in comparison with the parent DFO in terms of iron chelation in cells and are significantly less toxic [62].

A large range of 3-hydroxypyridin-4-ones with varying substituents at the 1 and 2 positions have been proposed as DFP successors [63]. One main objective of these chemical modifications was to reduce the metabolism of DFP, by hindering the 3′-hydroxyl function, which is the target of the glucuronidation. Numerous studies have illustrated the role of the substitution of 3-hydroxypyridin-4-one on iron binding affinity and biodistribution. Among the most promising candidates are the ornithine based 3-hydroxypyridin-4-one (DFP-Orn) [64] and 2-*N*-methylcarbamoyl-3-hydroxypyridin-4-one (DFP-Am1) [65] derivatives. These DFP analogs bind Fe^{3+} more strongly than the parent DFP. In addition to the enhanced pFe value, the 1-H substituted compound (DFP-Am2) shows an increased lipophilicity due to a highly stable intramolecular hydrogen bond between the amido and the adjacent hydroxy group. Despite these interesting properties, its ability to remove iron is slightly lower than that of the compound bearing a methyl group at the 1 position, but it is still higher than that of DFP [65].

As presented in Section 11.4.3, DFT is a very promising compound to treat iron overload, which needs further chemical optimization to reduce the induced nephrotoxicity. A first attempt consisted in replacing the pyridinyl ring by a phenyl one and to introduce a hydroxy group at the 4′ position of the aromatic ring [66]. Even though the new compound DFT-OH is less nephrotoxic than the parent DFT, it is still banned from clinical use. The nephrotoxicity problem was solved by introducing a polyether chain on the

deazadesferrithiocin moiety. Extended studies were conducted to select the appropriate length and position of the polyether chain. The chelator needs to be rigorously designed to tune its lipophilic character and to improve the iron clearing efficiency without being toxic. The introduction of a poly(ethylene glycol) (PEG) chain, namely a (2-(2-methoxyethoxy)ethoxy) fragment in 3′ position or a (2-(2-(2-methoxyethoxy) ethoxy)ethoxy) fragment in 3′ or 4′ position of the aromatic ring, eventually solved the nephrotoxicity issue and, as a bonus, improved the iron clearance efficiency. The compounds DFT-PEG are under clinical evaluation [67, 68].

The toxicity associated with the low denticity drugs prompted chemists to design ligands with increased denticity. Hexadentate ligands bearing three bidentate 2,3- or 3,4-hydroxypyridone units attached to suitable backbones are used to better satisfy the coordination sphere of the metal and thus lead to optimized kinetic and thermodynamic stability [69, 70]. For instance, three 3-hydroxypyridin-4-one units were appended to either tricarboxylic acid scaffolds (nitrilotriacetic acid, nitrilotripropionic acid (NTP), 1,3,5-trimethylcyclohexane-1,3,5-tricarboxylic acid [71], and 4-acrylamido-4-(2-carboxyethyl)heptanedioic acid [72] or triamino scaffolds (namely tris(2-aminoethyl)amine) [73]. All these hexadentate 3-hydroxypyridin-4-one based chelators share a strong iron chelating affinity with pFe^{3+} from 26.8 to 30.5, higher than that of DFO. One example of this strategy is illustrated in Figure 11.6, which shows the enhancement of the Fe^{3+} affinity with the hexadentate ligand $NTP(DFP)_3$ [71]. Despite its high molecular weight, this NTP derivative exhibits higher efficacy than deferriprone in terms of clearance and biodistribution in metal overloaded mice [71].

Among the numerous synthetic iron chelators reported in the literature, two hexadentate ligands composed of three terephthalamide units linked to a tris(2-aminoethyl)amine scaffold [74] or with 2-(2-aminoethoxy)ethylamine spacers [75] are to our knowledge the strongest Fe^{3+} chelators. These ligands exhibit an impressive affinity for Fe^{3+}, with pFe^{3+} values of 34.2 and 34.4 respectively. Furthermore, they have been shown to efficiently remove iron from transferrin and are therefore very promising agents for iron chelation therapy [76]. Similarly, two tridentate deazadesferrithiocin moieties were appended to a 1,3-dipropoxypropane backbone to obtain a potential hexadentate ligand [77]. Despite the expected gain in affinity, this compound is less efficient in iron overloaded monkeys than DFO and the tridentate parent alone.

Hundreds of iron chelators with various chemical functions involved in Fe^{3+} coordination are described in the literature. Even though impressive affinities for Fe^{3+} are obtained *in vitro*, the design of efficient therapeutic iron chelators having optimal pharmacological activities still remains a challenge.

Cu and Fe are tightly connected *in vivo* since their metabolism profiles are highly dependent. For instance, the ferroxidases described in Section 11.4.1 use copper as cofactor to oxidize iron. Copper is therefore essential for the absorption of iron. The next two sections will focus on Cu overload and associated treatments.

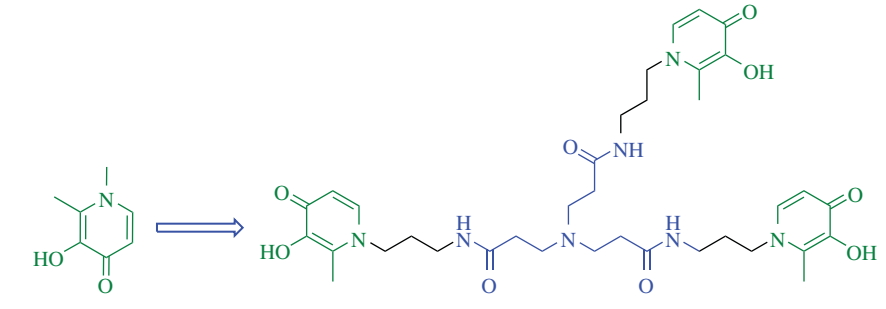

Figure 11.6 *Illustrative example of incorporation of bidentate 3,4-hydroxypyridone moieties into a polydentate scaffold*

11.5 Copper overload in Wilson's disease

11.5.1 Copper metabolism

Intracellular Cu is primarily found as cofactor in enzymes' active sites, where it oscillates between its Cu^{+} and Cu^{2+} redox states. Very important examples of the variety of enzymatic functions that use Cu as a cofactor are dioxygen reduction into water by cytochrome c oxidase (CcO) or antioxidant reactions by superoxide dismutase (SOD1). Besides, Cu is involved in Fe^{3+} loading onto transferrin by CP in the serum or HP in the intestine, which illustrates that both Cu and Fe metabolism are tightly connected and that copper is essential for the absorption of iron.

In humans, Cu is needed in all organs. Dietary copper enters the body at the level of the small intestine and crosses enterocytes to enter the portal circulation and to reach the liver (see Figure 11.7.). At this point, Cu enters the hepatic cells (named hepatocytes) and is further secreted into the whole body circulation either as a cofactor at the active site of CP (a Cu-dependent ferroxidase required for iron uptake by transferrin), or bound to various small proteins or ligands, such as albumin or histidine. In the latter, Cu is labile and exchangeable with other ligands. These Cu complexes are distributed to the other organs or tissues, as needed. In contrast to Fe, Cu is naturally excreted from the body in case of overload: the excess of Cu is excreted from the hepatocytes into the bile and finally out of the body with the faeces. The liver is therefore the organ responsible for Cu distribution into the whole body as well as for Cu excretion out of the body, a function that can be seen as detoxifying. An adult body contains about 72 mg copper, although the dietary intake is around 0.8 mg per day [78]. Chocolate, nuts, and seafoods such as oysters, calamari, and lobsters, are particularly copper-rich nutrients.

Dietary copper is in the common +II oxidation state, Cu^{2+}; in blood circulation, the Cu redox state is not clearly established and is probably a mixture of Cu^{2+} and Cu^{+} depending on the ligands interacting with

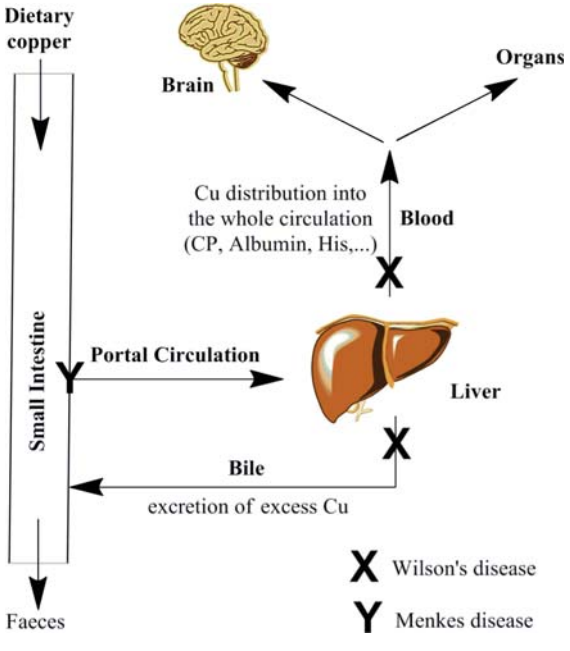

Figure 11.7 *Cu absorption and distribution in the body. X represents major steps impaired in Wilson's and Y Menkes diseases. Reproduced from [79] with permission of The Royal Society of Chemistry*

the metal ion. However, the millimolar concentration of GSH [80] found in the intracellular medium makes it very unlikely that free copper, if there is any, is in the Cu^{2+} state. Indeed, Cu^{2+} is expected to be readily reduced to Cu^{+} by the thiol GSH according to Equation 11.5.

$$2Cu^{2+} + 2GSH = 2Cu^{+} + GSSG + 2H^{+} \quad (11.5)$$

Actually, the balance between reduced (GSH) and oxidized glutathione (GSSG) is one means to evaluate the intracellular oxidative stress. Such measurement in blood plasma shows that blood is oxidized with respect to intracellular medium [81].

Owing to the fact that the Cu ion can be both essential and toxic, its amount, its redox state and its speciation are tightly regulated to maintain the physiological state of the cell. Cu homeostasis therefore requires regulation of Cu uptake, delivery to the Cu-enzymes, sequestration, and excretion. The fine tuning of the intracellular Cu concentration requires Cu-dependent expression of genes, Cu-dependent synthesis, localization, and degradation of proteins. All these genes and proteins work together and achieve Cu homeostasis [82].

11.5.2 Copper homeostasis

For the purpose of understanding copper homeostasis related to Wilson's disease, we will focus on the major proteins that transport Cu into and out of cells, and in addition, proteins that store Cu inside cells. Cu trafficking in a hepatic cell is described in Figure 11.8.

11.5.2.1 Cu entry into the cells

Cu enters the cell by crossing the plasma membrane taking advantage of a favorable concentration gradient via the Cu^{+}-specific transporter CTR1. Extracellular Cu is reduced by a Cu-reductase also inserted in the membrane [83]. Extracellular Met-XX-Met motifs (X can be any amino acid) and a membrane Met-XXX-Met motif participate in Cu^{+} transfer across CTR1. Short peptides containing a "Mets motif" were demonstrated to bind Cu^{+} with several Met in a thioether-only binding site that is selective for Cu^{+} [84, 85]. X-ray absorption spectroscopy studies proved that the "Mets motifs" found in CTR1 bind Cu^{+} optimally with the thioether sulfur atoms of 3 Met even though some of the binding sequences incorporate more than

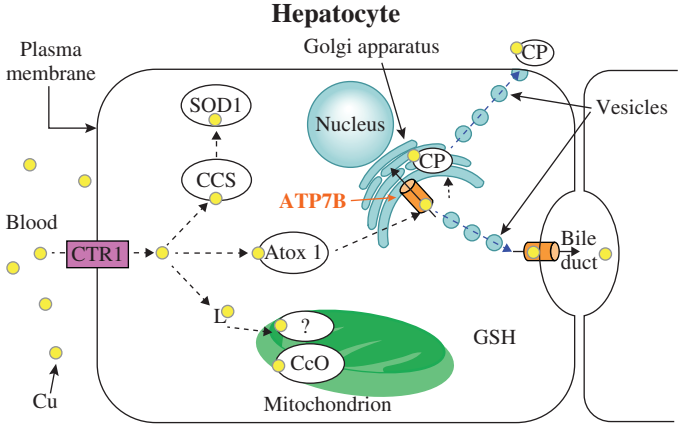

Figure 11.8 *Cu trafficking in a hepatic cell. Reproduced from [79] with permission of The Royal Society of Chemistry*

3 Met [84]. The dissociation constants found for a series of "Mets motifs" are in the micromolar range and independent of the pH. This suggests that the extracellular "Mets motifs" bind Cu^+ with a relatively low affinity, which easily promotes transfer to other Cu^+ binding sites.

At variance with the extracellular medium, the intracellular environment is reducing, in particular because of millimolar GSH, which limits the formation of disulfide bridges. Once in the intracellular medium, Cu^+ binds to GSH and to micromolar metallochaperones [82, 86]. Thus Cu homeostasis deals with Cu in the +I oxidation state and, since Cu^+ is a soft metal ion, it is mainly bound to soft sulfur donors of GSH or Met and Cys amino acids.

11.5.2.2 Intracellular copper transport

In all cells, Cu is required for superoxide dismutation and for reduction of dioxygen into water at the end of the respiration chain. The former reaction is achieved by the cytoplasmic SOD1 and the latter, by the mitochondrial CcO. At variance with these two ubiquitous enzymes, the other enzymes are found in various tissues and organs. Once synthesized in the cell that produces them, these enzymes are found in vesicles that move from the Golgi apparatus to the plasma membrane of the cell. A protein like CP is enclosed inside these vesicles; therefore, vesicle fusion with the plasma membrane allows excretion of CP from hepatocytes into the circulation. Another protein like HP is embedded in the vesicle membrane of enterocytes; in this case, vesicle fusion with the plasma membrane results in HP insertion into the enterocytes plasma membrane. Interestingly, both CP and HP are multicopper ferroxidases responsible for iron oxidation into Fe^{3+} in the blood circulation so as to ensure its transport by transferrin.

Hence, the cells express several types of Cu-dependent enzymes, which can be seen as three targets for copper delivery (Figure 11.8 for hepatocytes). SOD1 is in the cytoplasm, CcO is embedded in the inner membrane of the mitochondrion and the proteins such as HP or CP are found in vesicles from the secretory pathway, also made of phospholipid membranes. For each of these Cu-dependent enzymes, the insertion of the cofactor is a tightly regulated process that requires one or more specific protein(s) whose function is to bring Cu at the right protein to the right place, avoiding the toxic effects of free Cu. These proteins named metallochaperones are shown in Figure 11.8; most of them have been discovered first in yeast [87].

Metallochaperones deliver Cu^+ to their specific target proteins SOD1, CcO, or ATP7B The Copper Chaperone for Superoxide dismutase (CCS) delivers copper to SOD1 [88, 89], whereas many proteins have been identified (Cox17, Sco1, Cox11, among others) as necessary to bring Cu to CcO, but the detailed mechanism still needs to be unraveled [90]. These proteins have Cys-rich sequences involved in potential disulfide bridges and Cu^+ binding [91].

As for the secreted proteins, Cu delivery to the secretory vesicles is achieved by the metallochaperone **Atox1**. This protein binds Cu^+ at a Met-X-Cys-XX-Cys site that is exposed to the intracellular medium and delivers it to a similar Cu^+-binding site that belongs to another protein embedded in the Golgi membrane (ATP7A or ATP7B) [92]. The latter is a Cu-ATPase that pumps Cu^+ from the cytoplasm into the Golgi using the energy provided by the break of the adenosine triphosphate (ATP) γ-phosphate bond [93]. The Cu-ATPase comprises six Cu^+-binding units that are able to receive Cu^+ from Atox1. Cu^+ is then transferred to the Cys-Pro-Cys site of the Cu-ATPase, which belongs to the domain embedded in the Golgi membrane. From there, Cu^+ is transported into the Golgi using the energy from ATP. How Cu is further incorporated into the secreted protein such as CP or HP is still unknown [94].

Cu chaperones like Atox1 and the soluble binding domains of copper ATPases like ATP7A or ATP7B contain a conserved N-terminal Met-X-Cys-XX-Cys sequence motif that binds metal ions with two Cys [92, 95]. This motif is even conserved in the binding loop of many soft metal transporters such as MerP, a soluble Hg-transport protein [96], or P-type ATPases for Cd or Zn [97, 98]. The solution structure of the Cu^+ complex

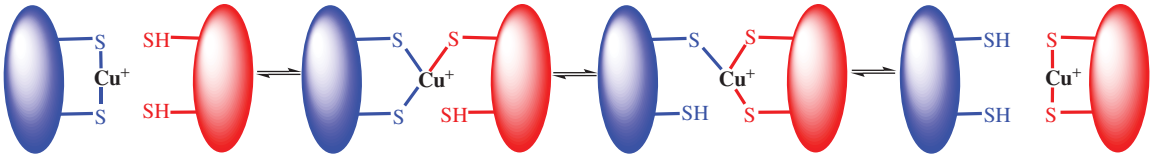

Figure 11.9 *Proposed mechanism for the transfer of Cu from the chaperone Atox1 to the ATPase ATP7B [87]*

of Atox1 [99] shows that Atox1 binds Cu^+ with two cysteines in a CuS_2 linear coordination. Interestingly the solid-state X-ray structure of the same complex [92] demonstrates a dimer with Cu^+ coordinated by cysteine residues from two separate Atox1 proteins in an environment which may be either described as a distorted tetrahedral coordination (CuS_4) or a trigonal coordination (CuS_3) with a proximal sulfur of the fourth weakly bound cysteine. This structure suggests that Cu^+ exchange between the Met-X-Cys-XX-Cys binding sites of the two partner proteins may proceed through a trigonal coordination of Cu^+ with three thiolates of cysteines assisted by docking of Atox1 with its target protein as described in Figure 11.9 [100].

11.5.2.3 Cellular copper detoxification

When a cell suffers from an excess of intracellular Cu, different events take place. The first kind is a cellular response that changes the localization of some proteins involved in Cu homeostasis. The obvious one is to stop Cu uptake by suppressing CTR1 at the plasma membrane. This phenomenon is observed as soon as extracellular Cu reaches 1 μM. Plasma membrane vesicles embedding CTR1 are internalized so that CTR1 has no more contact with the extracellular Cu [101–103]. Although not entirely deciphered, the mechanism for Cu concentration sensing relies on Met-rich sequences of CTR1 N-terminus that are in the extracellular medium.

Cu-ATPases also respond to excessive copper by changing their localization. As stated above, ATP7A's and ATP7B's housekeeping function is to transfer Cu into the Golgi. When there is an excess of Cu in the cell, vesicles are formed from the Golgi membrane that migrate toward the plasma membrane. These vesicles embedding the pumping Cu-ATPase are filled with Cu. They reach eventually the plasma membrane and Cu is expelled from the cell. Interestingly, the change in ATP7B localization as a function of Cu concentration has been evidenced in WIF-B9 hepatic cells [104]. Indeed, these particular hepatic cells are able to reconstitute stable and polarized epithelia with functional bile canaliculi within a few days (Figure 11.10) [105–107], which is not the case with HepG2, the most commonly used human hepatic cells. ATP7B localization is related to the intracellular Cu concentration. Indeed, at low Cu concentration, ATP7B plays its housekeeping role and is therefore located between the nucleus and the apical membrane (Figure 11.10a). At high Cu concentration, ATP7B is mainly localized in a continuous crown around the canaliculus to excrete the excess of Cu into the bile (Figure 11.10b) [104].

Another kind of cellular response is to chelate the excess of Cu so as to avoid high free Cu. Metallothioneins, **MTs** are small proteins comprising up to 20 Cys organized so as to bind metals in clusters formed with Zn^{2+} and/or Cu^+ under normal conditions [108]. *In vitro*, a yeast MT can bind up to eight Cu^+ ions as shown in the crystal structure of a truncated form of yeast copper thionein [109]. These complexes are very stable and represent an efficient chelation mechanism since, in these clusters, Cu^+ is not exchangeable [19]. As their affinity for Cu^+ is higher than for Zn^{2+}, excess of Cu^+ displaces Zn^{2+} and the resulting free Zn^{2+} induces more MT synthesis to chelate more metal ions. However, this mechanism, because it requires new protein synthesis, is rather slow when compared with the fast localization change of the Cu-ATPases (hour versus minute time scale).

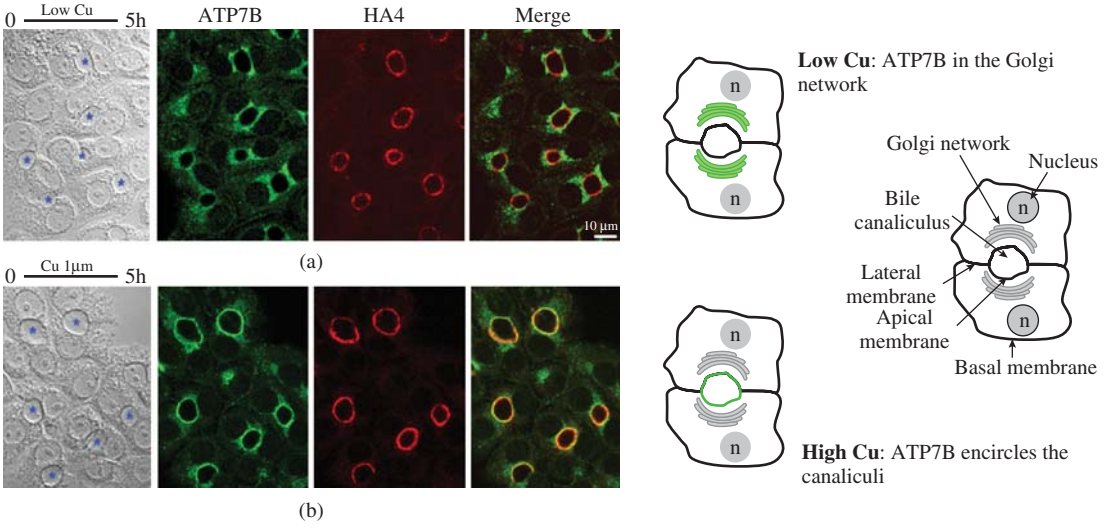

Figure 11.10 *Effect of Cu on ATP7B localization in WIF-B9 cells. ATP7B and HA4 (a canalicular membrane marker) were detected by indirect immunofluorescence and imaged by confocal microscopy. In each panel are presented from left to right, the Nomarski image, the two images of the sum of two confocal sections taken in the middle of the cell layer and the merged image. On the Nomarski images, bile canaliculi are indicated by asterisks. (a) Cells kept in the basal culture medium for 5 hours and (b) cells kept in the basal culture medium plus 1 µM Cu for 5 hours. Reproduced with permission from [158] . Copyright © 2012 WILEY-VCH Verlag GmbH & Co. KGaA, Weinheim. (See plate section for the colour version of this figure)*

11.5.3 Wilson's disease

Wilson's disease is an autosomal recessive disease due to a variety of mutations (over 300 are known) on the ATP7B gene found on the 13th chromosome. Since ATP7B is malfunctioning in the hepatocytes (Figure 11.7), there is a defect in Cu distribution and detoxification, leading to Cu overload. Wilson's disease is a rare disease (1/30 000 to 1/100 000 births). The age of onset varies from 3 to 50 years of age. The disease can be silent for years, especially because there is no clear clinical symptom related to the disease, except for the Kayser-Fleischer ring in the cornea that is due to Cu deposition. The disease induces two types of syndromes, one is neurological, the other one is hepatic. Otherwise, the patients can suffer chronic liver disease, heart seizures, neurological manifestations like movement disorders, personality changes, depression, and psychoses, all due to an excess of Cu in their body. The diagnosis is confirmed by a high Cu concentration in the urine when the patient is treated with chelators. In the absence of diagnosis, people can develop fulminant hepatitis, which requires liver transplantation [110, 111].

Menkes disease is a related orphan disease due to mutations on the ATP7A gene (X chromosome) which induces a malfunctioning of the ATP7A protein in the enterocytes (Figure 11.7). This induces a defect in dietary Cu absorption and therefore in Cu distribution in most tissues. This recessive genetic disease is rare (from 1/360 000 to 1/100 000 depending on the continent) and tends to decrease since it is more and more often detected during pregnancy. The origin of the disease is Cu malabsorption at the level of the intestine, the treatment is Cu supplementation by subcutaneous injections of Cu-His. This improves the condition of mild Menkes disease patients [112].

Wilson's disease is known since the early 1900s, when two doctors described rings in corneal pigmentation (the Kayser-Fleischer ring) that are still the only clear-cut sign to diagnose the disease. The link with Cu

Table 11.2 *Mechanism of action of current treatments [79]*

	Mechanism of action	Pro and con
D-Pen	Reductive chelator	Highly effective
	Stimulates Cu excretion in urine	Side-effects (including severe)
TETA	Cu^{2+} chelator	Effective, fewer side-effects
	Limits Cu absorption	Poorly available in Europe
	Stimulates Cu excretion in urine	
Zinc salts	MT induction in enterocytes	No toxic side-effects
	Limits Cu absorption	Slow response

overload was found in the 1940s and the gene responsible for the disease in 1993. Since then, genetic analysis allowed the finding of many disease-causing mutations and there has been a big hope that such knowledge would improve the ability to predict the disease development, and therefore to improve the patient's condition as early as possible in their life. Unfortunately, it is still very difficult to link the mutations to the symptoms and there has been no innovating treatment for Wilson's disease in the recent years. All treatments are systemic treatments that tend to limit the Cu-load in the body [113]. Since there is no curative treatment, the drugs must be taken life-long. In some cases that resist all the known treatments, liver transplantation may be required.

The first treatment appeared in 1951 with the use of the BAL molecule that relieved Wilson's disease patients from neurological symptoms [27]. BAL acts by chelating toxic metal ions such as arsenic, gold, antimony, lead, or mercury (Figure 11.1).

Since BAL has many adventitious side-effects, other chelators were searched for. D-Pen was introduced first in 1956, then TETA in 1982 [110]. D-Pen is currently the most used treatment around the globe, TETA is used in the USA but hardly accessible in Europe.

In the meantime, another treatment has been adopted to limit Cu-absorption in the intestine. It consists in taking zinc salts to stimulate MT synthesis in the enterocytes which have then a higher capacity to chelate dietary Cu and therefore limit Cu-transfer into the portal circulation [114]. This medication is mainly used to treat pre-symptomatic patients, such as siblings known to have the genetic disease without any visible symptoms yet [115]. The mechanisms and effects of the current treatments are summarized in Table 11.2.

11.6 Current developments in copper overload treatments

Since Wilson's disease is an orphan disease, very few drugs have been developed to treat copper overload. Recently, tetrathiomolybdate (TTM) was used in the USA as a copper chelator for patients who were intolerant to D-Pen and TETA, but TTM has not obtained the FDA approval [114].

In this context, we proposed a few years ago the design of specific copper chelators to treat localized copper overload in the liver.

11.6.1 From Cu homeostasis understanding to the rational design of drugs

Novel medicinal chemistry approaches may offer solutions to develop treatments for Wilson's disease with a higher specificity than the systemic drug therapy used until now. We have seen in Section 11.5 that copper concentration is highly regulated in the body to avoid deleterious effects due to copper redox properties. The main organ of copper regulation is the liver with the major protein ATP7B in charge of excreting excess

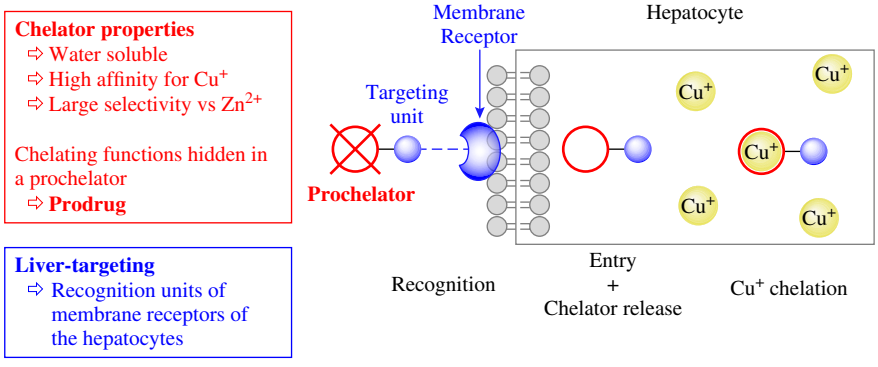

Figure 11.11 *Cu^+ prochelators targeted at the liver. (See plate section for the colour version of this figure)*

copper into the bile. In Wilson's disease this protein is malfunctioning, which leads to copper accumulation in the liver. Therefore, we propose to target specifically intracellular copper in this organ. Since the pool of intracellular Cu is in the +I oxidation state, we figured that a chelator that would enter the hepatic cells and be specific for Cu^+ could potentially represent an improved alternative. Moreover, to benefit from a pro-drug effect, the chelating functions are hidden in a prochelating unit, which releases the Cu^+ chelator only once inside the reducing medium of the targeted cells. This strategy is outlined in Figure 11.11.

Intracellular Cu chelation should decrease the toxicity due to excess of labile Cu. Yet, the best scenario would be excretion of the complex into the bile, which would promote Cu excretion from the body via the faeces, whether Cu is bound to the chelator in the bile or not and whatever its oxidation state. Important characteristics of the molecule include high water solubility and selectivity with respect to potential metal competitors in the cells, such as Zn^{2+}, another abundant metal ion in the intracellular medium.

The next two subsections describe the design of the subunit for chelation and the subunit for liver targeting, respectively.

11.6.2 Cu^+ chelating units inspired from proteins involved in Cu homeostasis

As the intracellular medium is a reducing environment, especially due to the high concentration of GSH, the pool of copper that can be mobilized is Cu^+. Therefore, the design of molecules that efficiently chelate excess of Cu in the liver should target Cu^+. As Cu^+ is a soft metal ion, it shares some similarities with divalent mercury and cadmium, and shows in particular a high affinity for sulfur donors like thioethers or thiols. Besides, this property has been extensively utilized by Nature to obtain copper-trafficking proteins, which complex Cu^+ with sulfur atoms of Cys and/or Met as described in Section 11.5. Sulfur donors have also been widely used to design synthetic Cu^+ complexing agents, either to help to elucidate the mechanisms of copper transport and sequestration and to explore Cu cell biology or for detoxification. A series of polythioethers, either opened or macrocyclic, have in particular been developed to probe intracellular copper with picomolar affinities for Cu^+ [116–126].

To design efficient Cu^+ chelating agents, we choose to take advantage of the amazing complexation properties of proteins involved in copper homeostasis. The Cu-binding sites in these proteins involve mainly sulfur donors like Met and Cys to provide high affinity and selectivity for Cu^+ together with lability to facilitate ligand-exchange reactions for metal transfer as described in Figure 11.9. Moreover the design of chelating agents based on amino acids or peptides provides water-soluble agents, suitable for *in vivo* applications.

Recently, the role of three amino acids in the coordination of Cu^+, namely Met, His and Cys, which are found in CTR1 motifs from different organisms has been investigated with small peptides of sequences Met-Gly_2-X-Gly_2-Met-Lys, where X is either Met, His, or Cys [127]. The relative affinities of these peptides for Cu^+ showed different trends depending on the pH: Cys > His > Met at pH 7.4 and Cys > Met > His at pH 4.5. The inversion between His and Met at low pH is assigned to the protonation of His with a p*K*a value of 6. Although the thiol function of Cys is a very weak acid with a p*K*a value of 8, Cys binds Cu^+ more efficiently than any other amino acid even at low pH, due to the strong interaction of the negatively charged thiolate group with Cu^+. Another major difference between the sulfur donors, Cys and Met, is the susceptibility of Cys to oxidation, which promotes the formation of disulfide bridges in an oxidative environment. In contrast, the thioether function of Met is less prone to oxidation and therefore Met appears to be an optimal amino acid to bind Cu^+ in the extracellular environment, which is more oxidizing. At variance with the extracellular medium, the intracellular environment is reducing in particular because of millimolar GSH, which limits the formation of disulfide bridges. Therefore, intracellular transport proteins mainly bind Cu^+ with high affinity thiolate functions of Cys and may be used as models to develop efficient Cu^+-chelating agents.

11.6.3 Cu^+ chelators inspired from metallochaperones

We first took our inspiration from copper chaperones to design Cu^+ intracellular chelating agents. The metal binding loops of copper chaperones like Atox1 are exposed to solvent, therefore they are satisfactorily mimicked by small peptides. The cyclic peptide $\mathbf{P^C}$ was proposed a few years ago to model these binding loops (Figure 11.12): this model compound provides the binding sequence Met-Thr-Cys-Ser-Gly-Cys-Ser of the yeast copper chaperone Atx1, which is equivalent to Atox1 in humans, and an X-Pro-Gly-X motif forming a turn, which rigidifies the cyclopeptide and acts as an anchor for the metal binding site. Solution NMR structures of the apo peptide and its Hg-loaded form revealed that the simple cyclic peptide P^C was an excellent structural model of Atx1 binding loop [128]. Moreover, this short peptide sequence mimics the coordination of Cu^+ by the whole chaperone with the formation of an S-Cu^+-S adduct and a dissociation constant value similar to Atx1 ($10^{-17.4}$ at physiological pH) [129]. The Met-X-Cys-XX-Cys consensus sequence was revealed to be highly selective for Cu^+ and Hg^{2+}, compared with the essential ion Zn^{2+} that could compete *in vivo* or compared with the toxic ions Pb^{2+} and Cd^{2+} [130].

The high affinity of this short peptide sequence for Cu^+ together with its extremely high selectivity versus Zn^{2+}, that is, 10 orders of magnitude, led us to propose that simple peptide sequences incorporating two Cys could be efficient intracellular Cu-chelating agents. More constrained peptide scaffolds with two β-turns, such as $\mathbf{P^1}$ in Figure 11.12, were also evaluated for Cu^+ chelation. The advantage of such scaffolds is to define

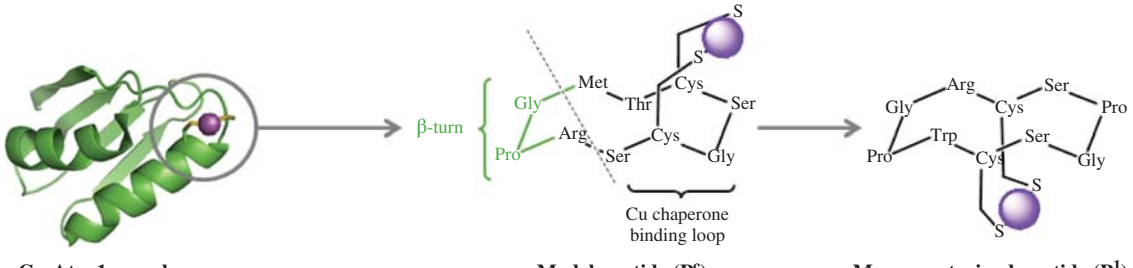

Figure 11.12 *Cyclodecapeptides mimicking the metal binding loop of copper chaperones as efficient Cu^+ chelating agents. Structure of the Cu^+-Atox1 complex (Solution NMR, PDB 1TL4) [99]*

two independent faces, one for metal chelation with two Cys and the second for targeting specific cells, like hepatocytes [131]. These two peptides form mononuclear complexes with a CuS_2 coordination. The slightly lower affinity of $\mathbf{P^1}$ for Cu^+ suggests that unfavorable constraints are induced upon metal binding by these more rigid peptide scaffolds in comparison with the flexible binding loop of $\mathbf{P^C}$, which adapts easily to diverse coordination geometries. These peptides are therefore good candidates for the selective coordination of Cu^+ in presence of Zn^{2+} as found in the intracellular medium.

11.6.4 Cysteine-rich compounds inspired from metallothioneins

Cu^+ binding sites found in MTs are also good sources of inspiration to design high affinity Cu^+ chelators. Indeed these small Cys-rich proteins that sequester metals, in particular Cu and Zn, demonstrate a very high affinity for Cu^+ ($K_d \sim 10^{-19}$) [18, 132, 133]. Metal ligands in these proteins are again thiolates, arranged in Cys-X-Cys and Cys-XX-Cys sequences, to form Cu^+-thiolate clusters with bridging thiolates. Examples of such clusters found in Cu-MTs are Cu_4S_9, Cu_6S_9 or Cu_6S_{11}. Extended X-ray absorption fine structure (EXAFS) studies of metal bound MT demonstrated that there are different coordination geometries for the binding of monovalent and divalent metal ions to MT and that Cu^+ ions are digonally and/or trigonally coordinated by two or three Cys in contrast to tetrahedrally coordinated Zn^{2+} ions [19, 134]. Moreover, the crystal structure of the yeast copper thionein bound to Cu^+ shows that two Cu^+ are digonally coordinated to Cys, whereas the six other ions are trigonally bound, in a Cu_8-thiolate cluster [109]. All these data suggest that the trithiolato coordination environment affords very stable complexes of Cu^+ and therefore ligands with three Cys promoting an MS_3 coordination geometry are very attractive. This led us to design pseudopeptide [135] ligands with three Cys attached with peptide bonds to nonbiological scaffolds, which act as platforms to orient all the thiolate binding arms in the same direction to coordinate metal ions [136, 137]. Nitrilotriacetic acid (NTA) was chosen as a tripodal anchor and was functionalized by Cys with different carbonyl groups, namely ester in $\mathbf{L^1}$ and amide in $\mathbf{L^2}$ (Figure 11.13) [136]. These two tripodal ligands were revealed to be very efficient Cu^+ chelators as they form mononuclear Cu^+ complexes with a CuS_3 coordination geometry which are stabilized by a hydrogen-bond network in the upper-cavity of the podates. The dissociation constants ($K_d \sim 10^{-19}$) are similar to those of MT (Figure 11.13). Furthermore, these mononuclear complexes

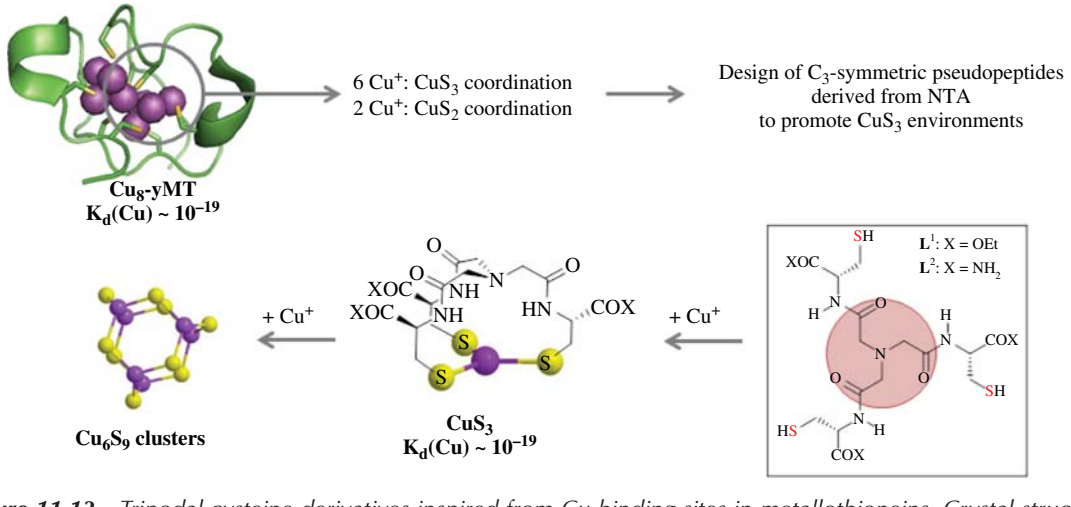

Figure 11.13 *Tripodal cysteine derivatives inspired from Cu binding sites in metallothioneins. Crystal structure of a truncated form of yeast copper thionein (PDB 1RJU) [109]*

transform into polymetallic Cu^+ complexes of Cu_6L_3 stoichiometry in agreement with a Cu_6S_9 core described in some MT, where each Cu^+ adopts a nearly trigonal planar coordination with exclusively bridging thiolates [138, 139]. Therefore, **L[1]** and **L[2]** may be considered as good mimics of the thiol-rich MT and are particularly efficient Cu^+ binding agents. Their selectivity for Cu^+ versus Zn^{2+} remains especially large, 8–9 orders of magnitude. Therefore, they could be used for the selective detoxification of Cu in cells.

Other peptide or chemical scaffolds providing three thiolate binding arms are being tested at the moment. This ongoing work suggests that the preorganization of the NTA scaffold due to H-bond stabilizing interactions in the upper cavity of the chemical scaffold is a crucial factor for the formation of the mononuclear CuS_3 adduct and for the large stability of the Cu^+ complexes.

Sulfur derivatives inspired from Cu^+ binding sites in proteins involved in Cu homeostasis, like **P[1]**, a peptide with two cysteines, and **L[1,2]**, tripods with three cysteines, display high affinity for Cu^+ with dissociation constants ranging from 10^{-19} to 10^{-16}. Excess of intracellular Cu is expected to be bound to MTs (high stability and inertness of the Cu complexes) or weakly bound to GSH, a thiol-containing tripeptide present in the cytosol in the millimolar concentration range, which displays an affinity for Cu^+ in the picomolar range [79]. Thus, the Cu^+ chelators **P[1]** and **L[1,2]** are expected to be able to chelate excess of intracellular weakly bound Cu. The question is how to promote the entry of these promising Cu^+ chelators into the targeted cells. One answer may be to functionalize with specific recognition elements of hepatic cells to target the liver.

11.6.5 Liver-targeting: the ASGP-R

An efficient strategy to target hepatocytes is to use ligands of the asialoglycoprotein receptor (ASGP-R), a hepatic lectin expressed mostly at the surface of these cells [140–142]. The receptor consists of two homologous subunits, designated H1 and H2 in the human system, which are membrane proteins and form a non-covalent heterooligomeric complex with an estimated ratio of 2–5 : 1, respectively. The ASGP-R, randomly distributed over the plasma membrane facing blood (Figure 11.8), is responsible for the clearance of desialylated, galactose-terminal glycoproteins from the circulation by receptor-mediated endocytosis. Both subunits display carbohydrate-recognition domains belonging to the superfamily of C-type, (i.e., Ca^{2+}-dependent) lectins and bind terminal galactose and *N*-acetylgalactosamine (GalNAc) residues. The affinity of ligands for this receptor is strongly dependent on the valency and the display of the sugar residues. While the affinity between lectins and simple monosaccharides is quite weak ($K_d \approx 0.1–1$ mM), it can be greatly enhanced by multivalent interactions commonly known as the "cluster glycoside effect." This leads to a 100–1000-fold increase in the affinity for ASGP-R with each additional carbohydrate from mono to triantennary structures [143, 144]. Since the fourth sugar moiety present in tetraantennary ligands does not markedly enhance the affinity for the receptor, the binding model presented in Figure 11.14 was proposed, with a cell-surface receptor bearing three sugar-binding sites [145].

Interestingly, the efficiency of such targeting units has been demonstrated for gene or drug delivery to cultured cells or to animals [146–149]. Therefore, this strategy has been applied for the targeting of the sulfur-based Cu^+ chelating agent presented in Sections 11.6.3 and 11.6.4 to hepatocytes.

11.6.6 Two glycoconjugates that release high affinity Cu chelators in hepatocytes

The sulfur-based compounds **P[1]** and **L[2]** were chemically modified to obtain glycoconjugates, able to target hepatic cells and to release the high affinity Cu^+ chelators in the intracellular medium. Since the ASGP-R has been shown to recognize GalNAc with a higher affinity than galactose, several GalNAc units were introduced

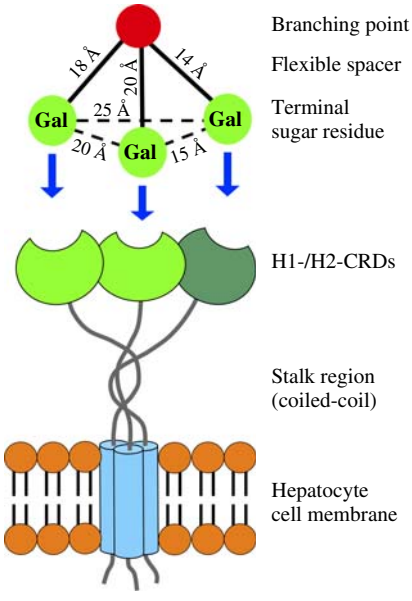

Figure 11.14 *Binding model for ASGP-R ligands in an optimal conformation to the heterooligomeric receptor consisting of H1 and H2 subunits. Dashed line indicates the distance between the C-4 of each Gal moietys; filled line represents approximate distance between branching point and C-6 of Gal (14–20 Å). Reprinted from [145] with permission from Elsevier*

in the chelator's chemical architectures [150]. Moreover, to obtain prochelating species, unable to chelate metal ions in the extracellular medium, the thiol chelating functions have been oxidized in disulfide bridges, which are expected to be cleaved in the reducing intracellular medium. The two glycoconjugates Chel1 and Chel2 are presented in Figure 11.15.

A thiol-containing glycopeptide (Chel1) [131]. Constrained cyclopeptide scaffolds, with their two independent faces, are good candidates to target active compounds to specific cell types [151]. Indeed, incorporation of two Pro-Gly sequences as β-turn inducers constrains the cyclodecapeptide backbone conformation into an antiparallel β sheet [152–154], with two faces, which can be used either for targeting or for another function like metal chelation. This controlled conformation has been exploited successfully for diverse applications such as the design of nanovectors, synthetic vaccines, and protein mimics [151]. Furthermore, clusters of carbohydrates grafted at the surface of the scaffold ensure the specific recognition for lectins with a significantly enhanced affinity through multivalent interactions [155–157]. Therefore, we designed the glycopeptide Chel1, which associates a prochelating unit made of two cysteines oxidized into a disulfide bridge on the "lower face" and four GalNAc units grafted on its "upper face" that are devoted to ASGP-R recognition and hepatocyte targeting [131].

A sulfur tripod glycoconjugate (Chel2) [158]. The glycoconjugate Chel2 was designed to release the high affinity chelator $\mathbf{L^2}$ into the hepatocytes. Indeed, our synthetic strategy consists in tethering to each chelating thiolate of $\mathbf{L^2}$ one carbohydrate via a disulfide bond which will be cleaved in the reducing intracellular medium. Therefore, Chel2 will acquire its specificity for Cu^+ chelation by entering the cells. Interestingly, among the structures proposed for optimal ASGP-R recognition are tripods bearing on each arm a β-linked

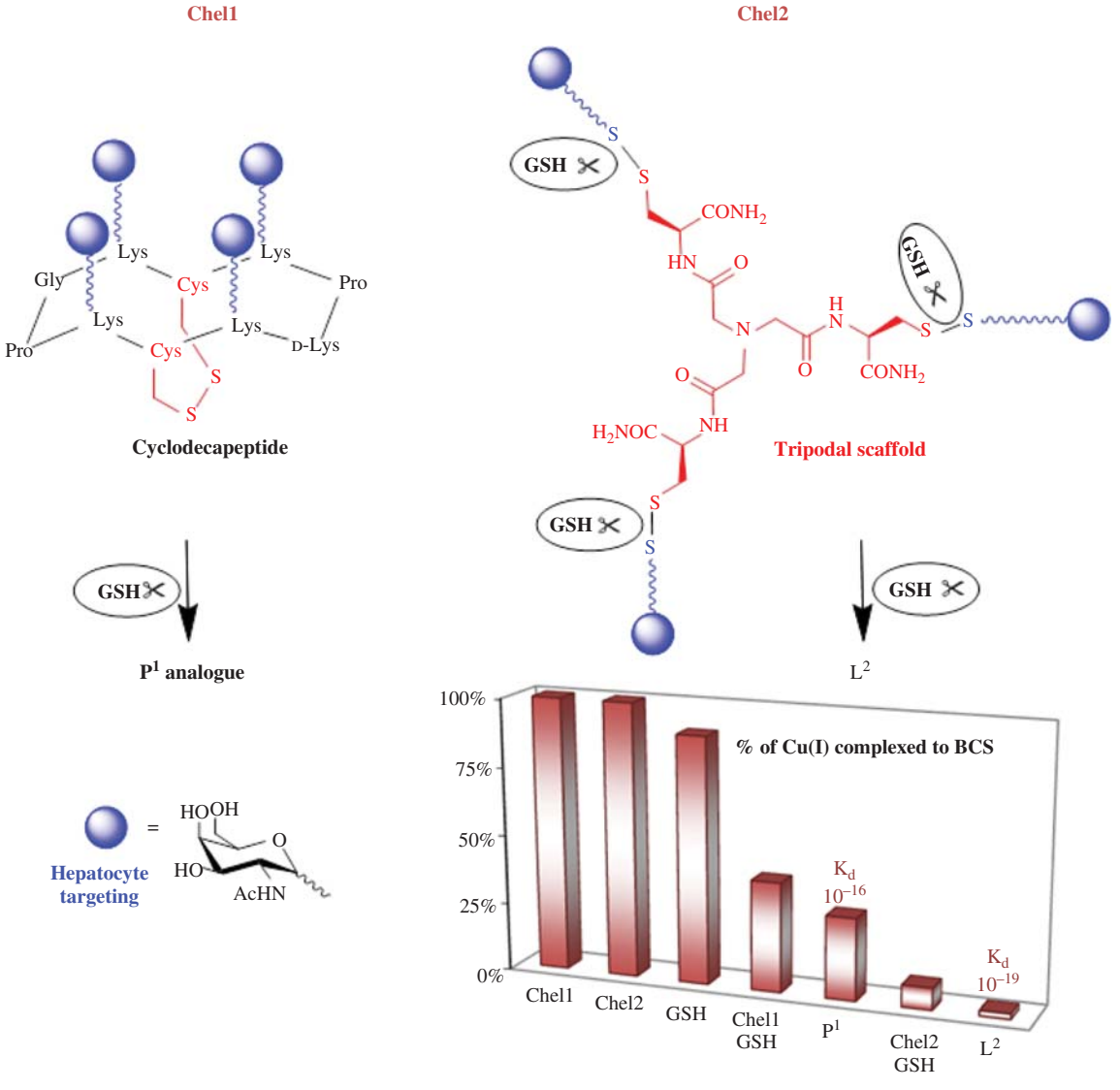

Figure 11.15 *The two glycoconjugates Chel1 and Chel2, combining a prochelating unit (disulfide bridges) and a targeting system to the hepatocytes (N-acetylgalactosamine). The bar diagram represents the percentage of Cu^+ complexed by BCS in competition experiments with 50 μM of the potential Cu ligand (Chel1, Chel2, P^1, or L^2), 45 μM Cu^+ and 90 μM BCS. 1 mM GSH was added to the medium to mimic the reducing intracellular medium, when GSH is indicated. (See plate section for the colour version of this figure)*

GalNAc moiety kept 20 Å away from the branching point of the tripod by an ethylene glycol spacer (See Figure 11.14) [145, 159, 160]. The tripodal architecture of **L^2** is thus perfectly suitable for the design of the triantennary glycoside cluster Chel2. To ensure an optimal orientation of the three terminal β-linked GalNAc for recognition by ASGP-R, a nine-atom ethylene glycol spacer has been chosen to establish the 20-Å connections between the GalNAc and the branching point.

11.6.6.1 Cu^+ chelation by Chel1 and Chel2

In vitro, the prochelators Chel1 and Chel2 were demonstrated to become efficient Cu^+ chelators only in the presence of GSH that mimics the intracellular reducing environment. Indeed, GSH reduces the disulfide bridges into thiolate functions generating the chelating agents (Figure 11.15). The Cu^+ chelating properties of Chel1 and Chel2 were evaluated in the test tube, by competition with bathocuproine disulfonate (BCS). The $Cu^I(BCS)_2$ complex is easily detected by its visible absorption band (483 nm, 13 300 M^{-1} cm^{-1}) [161]. Thus, when BCS is added to any Cu^IL complex, as shown in Equation 11.6 , the more intense is the band at 483 nm, the lower is the stability of Cu^IL.

$$Cu^IL + 2\ BCS \rightarrow L + Cu^I(BCS)_2 \tag{11.6}$$

As expected, the two glycoconjugates do not bind Cu^+ as they contain disulfide bridges and no free thiolate functions: 100% Cu is bound to BCS (Figure 11.15). GSH (1 mM) was used to mimic the reducing intracellular medium and it induced a 10%-decrease of $Cu^I(BCS)_2$, in agreement with the low affinity of GSH for Cu^I. However, when GSH was added together with Chel1 or Chel2, $Cu^I(BCS)_2$ decreased dramatically to 40 and 8% of the total copper, respectively. This evidences the release of high affinity Cu^+ chelators after reduction of the disulfide bridges of the glycoconjugates into free thiolates in the presence of GSH. For comparison, $Cu^I(BCS)_2$ in the presence of $Cu^I\mathbf{P^1}$ and $Cu^I\mathbf{L^2}$ represents 30 and 2% of the total copper, respectively. These experiments demonstrate that the glycoconjugates Chel1 and Chel2 are not Cu^+ chelators. However, their reduction by GSH converts them into efficient Cu^+ chelators, confirming their potential ability to bind Cu^+ once entered in the hepatic cells.

Therefore, cellular uptake and ability to lower intracellular Cu were studied in hepatic cell lines. They showed that the two compounds Chel1 and Chel2 are good candidates to fight Cu overload in the liver [131, 158]. First, analogs bearing a carboxytetramethylrhodamine fluorescent unit were demonstrated to enter hepatic cells. Moreover, the ability of Chel1 and Chel2 to decrease the pool of available Cu was confirmed using ATP7B localization as an intracellular Cu sensor in WIF-B9 cells, in experiments similar to what is presented in Figure 11.10. Chel1 and Chel2 are able to cancel the detoxification process that is induced by the excess of intracellular Cu. Therefore, the prochelators, once in the reducing environment of hepatocytes, become intracellular Cu^+ chelators.

In conclusion, the two glycoconjugates Chel1 and Chel2 are promising agents to treat copper overload in Wilson's disease, since they have been demonstrated to release efficient Cu^+ chelating agents in hepatocytes. We have highlighted that the design of bioinspired intracellular copper chelating agents benefits from the very high affinity of thiolates for Cu^+ in CuS_2 or CuS_3 coordination environments. Another asset of these sulfur compounds is their great selectivity for Cu^+ versus Zn^{2+}, another abundant and essential metal ion in cells. Finally, the chelating ability can be hidden in disulfide bridges to provide prochelating molecules that release the Cu^+ chelator only once in the reducing medium of the targeted cells. All these properties make sulfur chelators targeted to hepatocytes excellent candidates to treat Cu overload in Wilson's disease. This strategy is of course at an early stage of development as the efficiency of the targeted Cu^+ chelators has been demonstrated only in cell lines. The next step will be to test the ability of these molecules to promote Cu excretion in animal models of Wilson's disease, that is, Long-Evans Cinnamon (LEC) rats [162] or $ATP7B^{-/-}$ mice [163].

11.7 Conclusion

Wilson's disease and hemochromatosis are genetic disorders due to metal homeostasis disruption of copper and iron, respectively. In both diseases, the metal overload has to be treated by chelation therapy to promote

metal excretion from the body. Systemic chelators have been used for decades to treat these genetic disorders. Nowadays, inorganic medicinal chemistry principles may help in the rational design of more efficient and more specific chelating agents, with fewer unwanted side-effects. To develop such molecules chemists need to understand the homeostasis of the targeted metal and the nature of the overload *in vivo*, that is, the oxidation state of the excess of metal ion, its localization in the body and its main form or speciation. This is why medicinal inorganic chemistry is a multidisciplinary field, which must gather chemists, biologists, and physicians.

The comparison between the development of iron and copper chelators is very illustrative of the principles of inorganic chemistry. Indeed, the targeted form of iron is Fe^{3+}, which is strongly bound to proteins such as transferrin or ferritin. Therefore iron chelators are mainly hard oxygen donors which promote an octahedral coordination of Fe^{3+} with very high affinities to be able to compete with endogenous ligands. The targeted form of copper is less clear; in the circulation it is probably mainly Cu^{2+}, whereas in the cells it is Cu^{+} strongly bound to sulfur proteins or weakly bound to GSH or cysteine. Indeed, sulfur or nitrogen ligands have been demonstrated to efficiently treat copper overload, even though their mechanism of action is not totally clear, in particular the targeted metal oxidation state and its location in the body.

Current developments in the field generally aim at obtaining higher affinity chelators able to treat local metal accumulation, thanks to better cellular penetration either by passive diffusion with lipophilic compounds (see examples in Section 11.4.4 for iron chelation) or by targeting the chelating agent to specific organs. Of course, there is a long way from the rational design of efficient metal ligands by the medicinal inorganic chemist in his/her laboratory to the development of a novel drug successfully treating patients.

Acknowledgments

This research is supported by the "Agence Nationale pour la Recherche" (COPDETOX, ANR-11-EMMA-025), the "Fondation pour la Recherche Médicale" (grant DCM20111223043) and the Labex ARCANE (ANR-11-LABX-0003-01). We thank all the people who have contributed to the design and studies of the intracellular Cu(I) chelators developed in our two laboratories.

References

1. Emsley, J. (1998) *The Elements*, Clarendon Press, Oxford, .
2. Rae, T.D., Schmidt, P.J., Pufahl, R.A. *et al*. (1999) Undetectable intracellular free copper: the requirement of a copper chaperone for superoxide dismutase. *Science*, **284**, 805–808.
3. Valko, M., Morris, H. and Cronin, M.T. (2005) Metals, toxicity and oxidative stress. *Curr. Med. Chem.*, **12** (10), 1161–1208.
4. Halliwell, B. and Gutteridge, J.M. (1990) Role of free radicals and catalytic metal ions in human disease: an overview. *Methods Enzymol.*, **186**, 1–85.
5. Heinz, U., Hemmingsen, L., Kiefer, M. and Adolph, H.W. (2009) Structural adaptability of zinc binding sites: different structures in partially, fully, and heavy-metal loaded states. *Chem. Eur. J.*, **15** (30), 7350–7358.
6. Breydo, L. and Uversky, V.N. (2011) Role of metal ions in aggregation of intrinsically disordered proteins in neurodegenerative diseases. *Metallomics*, **3** (11), 1163–1180.
7. Gaggelli, E., Kozlowski, H., Valensin, D. and Valensin, G. (2006) Copper homeostasis and neurodegenerative disorders (Alzheimer's, prion, and Parkinson's diseases and amyotrophic lateral sclerosis). *Chem. Rev.*, **106** (6), 1995–2044.
8. Kozlowski, H., Janicka-Klos, A., Brasun, J. *et al*. (2009) Copper, iron, and zinc ions homeostasis and their role in neurodegenerative disorders (metal uptake, transport, distribution and regulation). *Coord. Chem. Rev.*, **253** (21-22), 2665–2685.

9. Molina-Holgado, F., Hider, R.C., Gaeta, A. *et al*. (2007) Metals ions and neurodegeneration. *Biometals*, **20** (3-4), 639–654.
10. Andersen, O. (1999) Principles and recent developments in chelation treatment of metal intoxication. *Chem. Rev.*, **99** (9), 2683–2710.
11. Andersen, O. (2004) Chemical and biological considerations in the treatment of metal intoxications by chelating agents. *Mini Rev. Med. Chem.*, **4** (1), 11–21.
12. Faller, P. (2012) Copper in Alzheimer disease: too much, too little, or misplaced? *Free Radical Biol. Med.*, **52** (4), 747–748.
13. Faller, P. and Hureau, C. (2009) Bioinorganic chemistry of copper and zinc ions coordinated to amyloid-beta peptide. *Dalton Trans.*, (7), 1080–1094.
14. Martell, A.E. and Motekaitis, R.J. (1992) *Determination and Use of Stability Constants*, John Wiley & Sons, Inc., New York.
15. Pierre, J.L. and Fontecave, M. (1999) Iron and activated oxygen species in biology: the basic chemistry. *Biometals*, **12** (3), 195–199.
16. Pearson, R.G. (1963) Hard and soft acids and bases. *J. Am. Chem. Soc.*, **85** (22), 3533–3539.
17. Pearson, R.G. and Songstad, J. (1967) Application of principle of hard and soft acids and bases to organic chemistry. *J. Am. Chem. Soc.*, **89** (8), 1827–1836.
18. Stillman, M.J. (1995) Metallothioneins. *Coord. Chem. Rev.*, **144**, 461–511.
19. Vasak, M. and Meloni, G. (2011) Chemistry and biology of mammalian metallothioneins. *J. Biol. Inorg. Chem.*, **16** (7), 1067–1078.
20. Lippard, S.J. and Berg, J.M. (1994) *Principles of Bioinorganic Chemistry*, University Science Book, Mill Valley, CA.
21. Martell, A.E., Hancock, R.D. and Motekaitis, R.J. (1994) Factors affecting stabilities of chelate, macrocyclic and macrobicyclic complexes in solution. *Coord. Chem. Rev.*, **133**, 39–65.
22. Gorden, A.E., Xu, J., Raymond, K.N. and Durbin, P. (2003) Rational design of sequestering agents for plutonium and other actinides. *Chem. Rev.*, **103** (11), 4207–4282.
23. R.M. Smith, A.E. Martell, and R.J. Motekaitis (2001) NIST Standard Reference Database 46. NIST Critically Selected Stability Constants of Metal Complexes Database, http://www.nist.gov/srd/upload/46_8.htm.
24. Aposhian, H.V., Maiorino, R.M., Gonzalezramirez, D. *et al*. (1995) Mobilization of heavy-metals by newer, therapeutically useful chelating-agents. *Toxicology*, **97** (1-3), 23–38.
25. Peters, R.A., Stocken, L.A. and Thompson, R.H. (1945) British anti-lewisite (BAL). *Nature*, **156**, 616–619.
26. Carleton, A.B., Peters, R.A., Stocken, L.A. *et al*. (1946) Clinical uses of 2,3-dimercaptopropanol (Bal). Vi. The treatment of complications of arseno-therapy with Bal (British Anti-Lewisite). *J. Clin. Invest.*, **25** (4), 497–527.
27. Vilensky, J.A. and Redman, K. (2003) British anti-Lewisite (dimercaprol): an amazing history. *Ann. Emergency Med.*, **41** (3), 378–383.
28. Aposhian, H.V. and Aposhian, M.M. (1990) Meso-2,3-dimercaptosuccinic acid – chemical, pharmacological and toxicological properties of an orally effective metal chelating agent. *Annu. Rev. Pharmacol. Toxicol.*, **30**, 279–306.
29. Caravan, P., Ellison, J.J., McMurry, T.J. and Lauffer, R.B. (1999) Gadolinium(III) chelates as MRI contrast agents: structure, dynamics, and applications. *Chem. Rev.*, **99**, 2293–2352.
30. Torchilin, V.P. (2000) Drug targeting. *Eur. J. Pharm. Sci.*, **11** (Suppl. 2), S81–S91.
31. Lippert, B. (1999) *Cisplatin, Chemistry and Biochemistry of a Leading Anticancer Drug*, Wiley-VCH Verlag GmbH, Weinheim.
32. Galanski, M. and Keppler, B.K. (2007) Searching for the magic bullet: anticancer platinum drugs which can be accumulated or activated in the tumor tissue. *Anti-Cancer Agents Med. Chem*, **7** (1), 55–73.
33. Sanchez-Cano, C. and Hannon, M.J. (2009) Novel and emerging approaches for the delivery of metallo-drugs. *Dalton Trans.*, 10702–10711.
34. Lawen, A. and Lane, D.J. (2013) Mammalian iron homeostasis in health and disease: uptake, storage, transport, and molecular mechanisms of action. *Antioxid. Redox Signaling*, **18** (18), 2473–2507.
35. Sun, H., Li, H. and Sadler, P.J. (1999) Transferrin as a metal ion mediator. *Chem. Rev.*, **99** (9), 2817–2842.
36. Lawson, D.M., Artymiuk, P.J., Yewdall, S.J. *et al*. (1991) Solving the structure of human H-Ferritin by genetically engineering intermolecular crystal contacts. *Nature*, **349** (6309), 541–544.

37. Noinaj, N., Easley, N.C., Oke, M. *et al*. (2012) Structural basis for iron piracy by pathogenic Neisseria. *Nature*, **483** (7387), U53–U92.
38. Chen, C. and Paw, B.H. (2012) Cellular and mitochondrial iron homeostasis in vertebrates. *Biochim. Biophys. Acta*, **1823** (9), 1459–1467.
39. Pietrangelo, A. (2010) Hereditary hemochromatosis: pathogenesis, diagnosis, and treatment. *Gastroenterology*, **139** (2), 393–408, 408 e1-2.
40. Zhou, T., Ma, Y.M., Kong, X.L. and Hider, R.C. (2012) Design of iron chelators with therapeutic application. *Dalton Trans.*, **41** (21), 6371–6389.
41. Motekaitis, R.J. and Martell, A.E. (1991) Stabilities of the iron(III) chelates of 1,2-dimethyl-3-hydroxy-4-pyridinone and related ligands. *Inorg. Chim. Acta*, **183** (1), 71–80.
42. Albahary, C., Labarbe, P., Renault, J. and Giraud, J. (1962) Le traitement des sideroses Par La desferrioxamine B – comparaison avec l'action de deux autres chelateurs. *Presse Med.*, **70** (57), 2823.
43. Bannerman, R.M., Williams, D.L. and Callender, S.T. (1962) Effect of desferrioxamine and DTPA in iron overload. *Br. Med. J.*, **2** (5319), 1573–1577.
44. Spasojevic, I., Armstrong, S.K., Brickman, T.J. and Crumbliss, A.L. (1999) Electrochemical behavior of the Fe(III) complexes of the cyclic hydroxamate siderophores alcaligin and desferrioxamine E. *Inorg. Chem.*, **38** (3), 449–454.
45. Kontoghiorghes, G.J. (1995) Comparative efficacy and toxicity of desferrioxamine, deferiprone and other iron and aluminum chelating drugs. *Toxicol. Lett.*, **80** (1-3), 1–18.
46. Kontoghiorghes, G.J., Aldouri, M.A., Hoffbrand, A.V. *et al*. (1987) Effective chelation of iron in beta-thalassemia with the oral chelator 1,2-dimethyl-3-hydroxypyrid-4-one. *Br. Med. J.*, **295** (6612), 1509–1512.
47. Dobbin, P.S., Hider, R.C., Hall, A.D. *et al*. (1993) Synthesis, physicochemical properties, and biological evaluation of N-substituted 2-alkyl-3-hydroxy-4(1H)-pyridinones – orally-active iron chelators with clinical potential. *J. Med. Chem.*, **36** (17), 2448–2458.
48. Merkofer, M., Kissner, R., Hider, R.C. and Koppenol, W.H. (2004) Redox properties of the iron complexes of orally active iron chelators CP20, CP502, CP509, and ICL670. *Helv. Chim. Acta*, **87** (12), 3021–3034.
49. Kontoghiorghes, G.J., Eracleous, E., Economides, C. and Kolnagou, A. (2005) Advances in iron overload therapies. Prospects for effective use of deferiprone (L1), deferoxamine, the new experimental chelators ICL670, GT56-252, L1NAll and their combinations. *Curr. Med. Chem.*, **12** (23), 2663–2681.
50. Singh, S., Epemolu, R.O., Dobbin, P.S. *et al*. (1992) Urinary metabolic profiles in human and rat of 1,2-dimethyl-substituted and 1,2-diethyl-substituted 3-hydroxypyridin-4-ones. *Drug Metab. Dispos.*, **20** (2), 256–261.
51. Heinz, U., Hegetschweiler, K., Acklin, P. *et al*. (1999) 4-[3,5-bis(2-hydroxyphenyl)-1,2,4-triazol-1-yl]benzoic acid: a novel efficient and selective iron(III) complexing agent. *Angew. Chem. Int. Ed.*, **38** (17), 2568–2570.
52. Nisbet-Brown, E., Olivieri, N.F., Giardina, P.J. *et al*. (2003) Effectiveness and safety of ICL670 in iron-loaded patients with thalassaemia: a randomised, double-blind, placebo-controlled, dose-escalation trial. *Lancet*, **361** (9369), 1597–1602.
53. Steinhauser, S., Heinz, U., Bartholoma, M. *et al*. (2004) Complex formation of ICL670 and related ligands with Fe-III and Fe-II. *Eur. J. Inorg. Chem.*, **2004** (21), 4177–4192.
54. Weiss, H.M., Fresneau, M., Camenisch, G.P. *et al*., (2006) In vitro blood distribution and plasma protein binding of the iron chelator deferasirox (ICL670) and its iron complex Fe-[ICL670](2) for rat, marmoset, rabbit, mouse, dog, and human. *Drug Metab. Dispos.*, **34** (6), 971–975.
55. Naegeli, H.U. and Zahner, H. (1980) Metabolites of microorganisms.193. Ferrithiocin. *Helv. Chim. Acta*, **63** (6), 1400–1406.
56. Anderegg, G. and Raber, M. (1990) Metal-complex formation of a new siderophore desferrithiocin and of 3 related ligands. *J. Chem. Soc., Chem. Commun.*, **17**, 1194–1196.
57. Bergeron, R.J., Wiegand, J., Dionis, J.B. *et al*. (1991) Evaluation of desferrithiocin and its synthetic analogs as orally effective iron chelators. *J. Med. Chem.*, **34** (7), 2072–2078.
58. Baker, E., Wong, A., Peter, H. and Jacobs, A. (1992) Desferrithiocin is an effective iron chelator in vivo and in vitro but ferrithiocin is toxic. *Br. J. Haematol.*, **81** (3), 424–431.
59. Yu, Y., Gutierrez, E., Kovacevic, Z. *et al*. (2012) Iron chelators for the treatment of cancer. *Curr. Med. Chem.*, **19** (17), 2689–2702.

60. Hider, R.C., Roy, S., Ma, Y.M. *et al*. (2011) The potential application of iron chelators for the treatment of neurodegenerative diseases. *Metallomics*, **3** (3), 239–249.
61. Dragsten, P.R., Hallaway, P.E., Hanson, G.J. *et al*. (2000) First human studies with a high-molecular-weight iron chelator. *J. Lab. Clin. Med.*, **135** (1), 57–65.
62. Liu, J., Obando, D., Schipanski, L.G. *et al*. (2010) Conjugates of Desferrioxamine B (DFOB) with derivatives of adamantane or with orally available chelators as potential agents for treating iron overload. *J. Med. Chem.*, **53** (3), 1370–1382.
63. Santos, M.A., Marques, S.M. and Chaves, S. (2012) Hydroxypyridinones as "privileged" chelating structures for the design of medicinal drugs. *Coord. Chem. Rev.*, **256** (1-2), 240–259.
64. Santos, M.A., Gil, M., Gano, L. and Chaves, S. (2005) Bifunctional 3-hydroxy-4-pyridinone derivatives as potential pharmaceuticals: synthesis, complexation with Fe(III), Al(III) and Ga(III) and in vivo evaluation with Ga-67. *J. Biol. Inorg. Chem.*, **10** (5), 564–580.
65. Piyamongkol, S., Ma, Y.M., Kong, X.L. *et al*. (2010) Amido-3-hydroxypyridin-4-ones as Iron(III) Ligands. *Chem. Eur. J.*, **16** (21), 6374–6381.
66. Bergeron, R.J., Wiegand, J., McManis, J.S. *et al*. (1999) Effects of C-4 stereochemistry and C-4' hydroxylation on the iron clearing efficiency and toxicity of desferrithiocin analogues. *J. Med. Chem.*, **42** (13), 2432–2440.
67. Bergeron, R.J., Bharti, N., Wiegand, J. *et al*. (2010) The impact of polyether chain length on the iron clearing efficiency and physiochemical properties of desferrithiocin analogues. *J. Med. Chem.*, **53** (7), 2843–2853.
68. Bergeron, R.J., Wiegand, J., Bharti, N. *et al*. (2011) Desferrithiocin analogue iron chelators: iron clearing efficiency, tissue distribution, and renal toxicity. *Biometals*, **24** (2), 239–258.
69. Turcot, I., Stintzi, A., Xu, J.D. and Raymond, K.N. (2000) Fast biological iron chelators: kinetics of iron removal from human diferric transferrin by multidentate hydroxypyridonates. *J. Biol. Inorg. Chem.*, **5** (5), 634–641.
70. Harrington, J.M., Chittamuru, S., Dhungana, S. *et al*. (2010) Synthesis and iron sequestration equilibria of novel exocyclic 3-hydroxy-2-pyridinone donor group siderophore mimics. *Inorg. Chem.*, **49** (18), 8208–8221.
71. Chaves, S., Marques, S.M., Matos, A.M.F. *et al*. (2010) New Tris(hydroxypyridinones) as iron and aluminium sequestering agents: synthesis, complexation and in vivo studies. *Chem. Eur. J.*, **16** (34), 10535–10545.
72. Zhou, T., Le Kong, X., Liu, Z.D. *et al*. (2008) Synthesis and iron(III)-chelating properties of novel 3-hydroxypyridin-4-one hexadentate ligand-containing copolymers. *Biomacromolecules*, **9** (5), 1372–1380.
73. Piyamongkol, S., Zhou, T., Liu, Z.D. *et al*. (2005) Design and characterisation of novel hexadentate 3-hydroxypyridin-4-one ligands. *Tetrahedron Lett.*, **46** (8), 1333–1336.
74. Jurchen, K.M.C. and Raymond, K.N. (2006) Terephthalamide-containing analogues of TREN-Me-3,2-HOPO. *Inorg. Chem.*, **45** (3), 1078–1090.
75. Abergel, R.J. and Raymond, K.N. (2006) Synthesis and thermodynamic evaluation of mixed hexadentate linear iron chelators containing hydroxypyridinone and terephthalamide units. *Inorg. Chem.*, **45** (9), 3622–3631.
76. Abergel, R.J. and Raymond, K.N. (2008) Terephthalamide-containing ligands: fast removal of iron from transferrin. *J. Biol. Inorg. Chem.*, **13** (2), 229–240.
77. Bergeron, R.J., Huang, G.F., Weimar, W.R. *et al*. (2003) Desferrithiocin analogue based hexacoordinate iron(III) chelators. *J. Med. Chem.*, **46** (1), 16–24.
78. van den Berghe, P.V. and Klomp, L.W. (2009) New developments in the regulation of intestinal copper absorption. *Nutr. Rev.*, **67** (11), 658–672.
79. Delangle, P. and Mintz, E. (2012) Chelation therapy in Wilson's disease: from D-Penicillamine to the design of selective bioinspired intracellular Cu(I) chelators. *Dalton Trans.*, **41**, 6359–6370.
80. Meister, A. and Anderson, M.E. (1983) Glutathione. *Annu. Rev. Biochem.*, **52**, 711–760.
81. Jones, D.P. (2002) Redox potential of GSH/GSSG couple: assay and biological significance. *Methods Enzymol.*, **348**, 93–112.
82. Kim, B.E., Nevitt, T. and Thiele, D.J. (2008) Mechanisms for copper acquisition, distribution and regulation. *Nat. Chem. Biol.*, **4** (3), 176–185.
83. Ohgami, R.S., Campagna, D.R., McDonald, A. and Fleming, M.D. (2006) The steap proteins are metalloreductases. *Blood*, **108** (4), 1388–1394.
84. Rubino, J.T., Riggs-Gelasco, P. and Franz, K.J. (2010) Methionine motifs of copper transport proteins provide general and flexible thioether-only binding sites for Cu(I) and Ag(I). *J. Biol. Inorg. Chem.*, **15** (7), 1033–1049.

85. Jiang, J.F., Nadas, I.A., Kim, M.A. and Franz, K.J. (2005) Mets motif peptide found in copper transport proteins selectively binds Cu(I) with methionine-only coordination. *Inorg. Chem.*, **44** (26), 9787–9794.
86. Freedman, J.H., Ciriolo, M.R. and Peisach, J. (1989) The role of glutathione in copper metabolism and toxicity. *J. Biol. Chem.*, **264** (10), 5598–5605.
87. Rosenzweig, A.C. (2001) Copper delivery by metallochaperone proteins. *Acc. Chem. Res.*, **34**, 119–128.
88. Lamb, A.L., Torres, A.S., O'Halloran, T.V. and Rosenzweig, A.C. (2001) Heterodimeric structure of superoxide dismutase in complex with its metallochaperone. *Nat. Struct. Biol.*, **8** (9), 751–755.
89. Furukawa, Y., Torres, A.S. and O'Halloran, T.V. (2004) Oxygen-induced maturation of SOD1: a key role for disulfide formation by the copper chaperone CCS. *EMBO J.*, **23** (14), 2872–2881.
90. Cobine, P.A., Pierrel, F. and Winge, D.R. (2006) Copper trafficking to the mitochondrion and assembly of copper metalloenzymes. *Biochim. Biophys. Acta*, **1763** (7), 759–772.
91. Leary, S.C. (2010) Redox regulation of SCO protein function: controlling copper at a mitochondrial crossroad. *Antioxid. Redox Signaling*, **13** (9), 1403–1416.
92. Wernimont, A.K., Huffman, D.L., Lamb, A.L. *et al*. (2000) Structural basis for copper transfer by the metallochaperone for the Menkes/Wilson disease proteins. *Nat. Struct. Biol.*, **7** (9), 766–771.
93. Gourdon, P., Liu, X.Y., Skjorringe, T. *et al*. (2011) Crystal structure of a copper-transporting PIB-type ATPase. *Nature*, **475** (7354), 59–64.
94. Lutsenko, S., LeShane, E.S. and Shinde, U. (2007) Biochemical basis of regulation of human copper-transporting ATPases. *Arch. Biochem. Biophys.*, **463** (2), 134–148.
95. Arnesano, F., Banci, L., Bertini, I. *et al*. (2002) Metallochaperones and metal-transporting ATPases: a comparative analysis of sequences and structures. *Genome Res.*, **12**, 255–271.
96. Steele, R.A. and Opella, S.J. (1997) Structures of the reduced and mercury-bound forms of MerP, the periplasmic protein from the bacterial mercury detoxification system. *Biochemistry*, **36**, 6885–6895.
97. Banci, L., Bertini, I., Ciofi-Baffoni, S. *et al*. (2002) A new zinc-protein coordination site in intracellular metal trafficking: solution structure of the Apo and Zn(II) forms of ZntA(46-118). *J. Mol. Biol.*, **323**, 883–897.
98. Banci, L., Bertini, I., Ciofi-Baffoni, S. *et al*. (2006) Structural basis for metal binding specificity: the N-terminal cadmium binding domain of the P1-type ATPase CadA. *J. Mol. Biol.*, **356** (3), 638–650.
99. Anastassopoulou, I., Banci, L., Bertini, I. *et al*. (2004) Solution structure of the Apo and copper(I)-loaded human metallochaperone HAH1. *Biochemistry*, **43** (41), 13046–13053.
100. Pufahl, R.A., Singer, C.P., Peariso, K.L. *et al*. (1997) Metal ion chaperone function of the soluble Cu(I) receptor Atx1. *Science*, **278**, 853–856.
101. Guo, Y., Smith, K., Lee, J. *et al*. (2004) Identification of methionine-rich clusters that regulate copper-stimulated endocytosis of the human Ctr1 copper transporter. *J. Biol. Chem.*, **279** (17), 17428–17433.
102. Gupta, A. and Lutsenko, S. (2009) Human copper transporters: mechanism, role in human diseases and therapeutic potential. *Future Med. Chem.*, **1** (6), 1125–1142.
103. Nose, Y., Wood, L.K., Kim, B.E. *et al*. (2010) Ctr1 is an apical copper transporter in mammalian intestinal epithelial cells in vivo that is controlled at the level of protein stability. *J. Biol. Chem.*, **285** (42), 32385–32392.
104. Guo, Y., Nyasae, L., Braiterman, L.T. and Hubbard, A.L. (2005) NH2-terminal signals in ATP7B Cu-ATPase mediate its Cu-dependent anterograde traffic in polarized hepatic cells. *Am. J. Physiol. - Gastrointestinal Liver Physiol.*, **289**, G904–G916.
105. Decaens, C., Durand, M., Grosse, B. and Cassio, D. (2008) Which in vitro models could be best used to study hepatocyte polarity? *Biol. Cell*, **100** (7), 387–398.
106. Shanks, M.R., Cassio, D., Lecoq, O. and Hubbard, A.L. (1994) An improved polarized rat hepatoma hybrid cell line. Generation and comparison with its hepatoma relatives and hepatocytes in vivo. *J. Cell Sci.*, **107**, 813–825.
107. Ihrke, G., Neufeld, E.B., Meads, T. *et al*. (1993) WIF-B cells: an in vitro model for studies of hepatocyte polarity. *J. Cell Biol.*, **123** (6Pt. 2), 1761–1775.
108. Palacios, O., Atrian, S. and Capdevila, M. (2011) Zn- and Cu-thioneins: a functional classification for metallothioneins? *J. Biol. Inorg. Chem.*, **16**, 991–1009.
109. Calderone, V., Dolderer, B., Hartmann, H.J. *et al*. (2005) The crystal structure of yeast copper thionein: the solution of a long-lasting enigma. *Proc. Natl. Acad. Sci. U.S.A.*, **102** (1), 51–56.
110. Walshe, J.M. (2006) History of Wilson's disease: 1912 to 2000. *Mov. Disorders*, **21** (2), 142–147.

111. Gitlin, J.D. (2003) Wilson disease. *Gastroenterology*, **125** (6), 1868–1877.
112. Sarkar, B., Lingertat-Walsh, K. and Clarke, J.T. (1993) Copper-histidine therapy for Menkes disease. *J. Pediatr.*, **123** (5), 828–830.
113. Sarkar, B. (1999) Treatment of Wilson and Menkes diseases. *Chem. Rev.*, **99** (9), 2535–2544.
114. Brewer, G.J. (2009) Drug development for orphan diseases in the context of personalized medicine. *Transl. Res.*, **154** (6), 314–322.
115. Huster, D. (2010) Wilson disease. *Best Pract. Res. Clin. Gastroenterol.*, **24** (5), 531–539.
116. Yang, L.C., McRae, R., Henary, M.M. *et al*. (2005) Imaging of the intracellular topography of copper with a fluorescent sensor and by synchrotron x-ray fluorescence microscopy. *Proc. Natl. Acad. Sci. U.S.A.*, **102** (32), 11179–11184.
117. Zeng, L., Miller, E.W., Pralle, A. *et al*. (2006) A selective turn-on fluorescent sensor for imaging copper in living cells. *J. Am. Chem. Soc.*, **128** (1), 10–11.
118. Miller, E.W., Zeng, L., Domaille, D.W. and Chang, C.J. (2006) Preparation and use of coppersensor-1, a synthetic fluorophore for live-cell copper imaging. *Nat. Protoc.*, **1** (2), 824–827.
119. Verma, M., Chaudhry, A.F., Morgan, M.T. and Fahrni, C.J. (2010) Electronically tuned 1,3,5-triarylpyrazolines as Cu(I)-selective fluorescent probes. *Org. Biomol. Chem.*, **8** (2), 363–370.
120. Chaudhry, A.F., Mandal, S., Hardcastle, K.I. and Fahrni, C.J. (2011) High-contrast Cu(I)-selective fluorescent probes based on synergistic electronic and conformational switching. *Chem. Sci.*, **2** (6), 1016–1024.
121. Dodani, S.C., Domaille, D.W., Nam, C.I. *et al*. (2011) Calcium-dependent copper redistributions in neuronal cells revealed by a fluorescent copper sensor and X-ray fluorescence microscopy. *Proc. Natl. Acad. Sci. U.S.A.*, **108** (15), 5980–5985.
122. Domaille, D.W., Zeng, L. and Chang, C.J. (2010) Visualizing ascorbate-triggered release of labile copper within living cells using a ratiometric fluorescent sensor. *J. Am. Chem. Soc.*, **132** (4), 1194–1195.
123. Dodani, S.C., Leary, S.C., Cobine, P.A. *et al*. (2011) A targetable fluorescent sensor reveals that copper-deficient SCO1 and SCO2 patient cells prioritize mitochondrial copper homeostasis. *J. Am. Chem. Soc.*, **133** (22), 8606–8616.
124. Que, E.L. and Chang, C.J. (2010) Responsive magnetic resonance imaging contrast agents as chemical sensors for metals in biology and medicine. *Chem. Soc. Rev.*, **39** (1), 51–60.
125. Que, E.L., Gianolio, E., Baker, S.L. *et al*. (2010) A copper-activated magnetic resonance imaging contrast agent with improved turn-on relaxivity response and anion compatibility. *Dalton Trans.*, **39** (2), 469–476.
126. Que, E.L., Gianolio, E., Baker, S.L. *et al*. (2009) Copper-responsive magnetic resonance imaging contrast agents. *J. Am. Chem. Soc.*, **131** (24), 8527–8536.
127. Rubino, J.T., Chenkin, M.P., Keller, M. *et al*. (2011) A comparison of methionine, histidine and cysteine in copper(I)-binding peptides reveals differences relevant to copper uptake by organisms in diverse environments. *Metallomics*, **3** (1), 61–73.
128. Seneque, O., Crouzy, S., Boturyn, D. *et al*. (2004) Novel model peptide for Atx1-like metallochaperones. *Chem. Commun.*, **7**, 770–771.
129. Xiao, Z.G., Brose, J., Schimo, S. *et al*. (2011) Unification of the copper(I) binding affinities of the metallo-chaperones atx1, atox1, and related proteins detection probes and affinity standards. *J. Biol. Chem.*, **286** (13), 11047–11055.
130. Rousselot-Pailley, P., Seneque, O., Lebrun, C. *et al*. (2006) Model peptides based on the binding loop of the copper metallochaperone Atx1: selectivity of the consensus sequence MxCxxC for metal ions Hg(II), Cu(I), Cd(II), Pb(II), and Zn(II). *Inorg. Chem.*, **45** (14), 5510–5520.
131. Pujol, A.M., Cuillel, M., Renaudet, O. *et al*. (2011) Hepatocyte targeting and intracellular copper chelation by a thiol-containing glycocyclopeptide. *J. Am. Chem. Soc.*, **133** (2), 286–296.
132. Koch, K.A., Pena, M.M.O. and Thiele, D.J. (1997) Copper-binding motifs in catalysis, transport, detoxification and signaling. *Chem. Biol.*, **4** (8), 549–560.
133. Faller, P. (2010) Neuronal growth-inhibitory factor (metallothionein-3): reactivity and structure of metal-thiolate clusters. *FEBS J.*, **277** (14), 2921–2930.
134. Bogumil, R., Faller, P., Binz, P.A. *et al*. (1998) Structural characterization of Cu(I) and Zn(II) sites in neuronal-growth-inhibitory factor by extended X-ray absorption fine structure (EXAFS). *Eur. J. Biochem.*, **255** (1), 172–177.

135. Gelinsky, M., Vogler, R. and Vahrenkamp, H. (2002) Tripodal pseudopeptides with three histidine or cysteine donors: synthesis and zinc complexation. *Inorg. Chem.*, **41** (9), 2560–2564.
136. Pujol, A.M., Gateau, C., Lebrun, C. and Delangle, P. (2011) A series of tripodal cysteine derivatives as water-soluble chelators highly selective for copper (I). *Chem. Eur. J.*, **17**, 4418–4428.
137. Pujol, A.M., Gateau, C., Lebrun, C. and Delangle, P. (2009) A cysteine-based tripodal chelator with a high affinity and selectivity for copper(I). *J. Am. Chem. Soc.*, **131** (20), 6928–6929.
138. Nielson, K.B., Atkin, C.L. and Winge, D.R. (1985) Distinct metal-binding configurations in metallothionein. *J. Biol. Chem.*, **260**, 5342–5350.
139. Presta, A., Green, A.R., Zelazowski, A. and Stillman, M.J. (1995) Copper-binding to rabbit liver metallothionein – formation of a continuum of copper(I)-thiolate stoichiometric species. *Eur. J. Biochem.*, **227** (1-2), 226–240.
140. Spiess, M. (1990) The asialoglycoprotein receptor: a model for endocytic transport receptors. *Biochemistry*, **29** (43), 10009–10018.
141. Meier, M., Bider, M.D., Malashkevich, V.N. *et al*. (2000) Crystal structure of the carbohydrate recognition domain of the H1 subunit of the asialoglycoprotein receptor. *J. Mol. Biol.*, **300** (4), 857–865.
142. Ashwell, G. and Harford, J. (1982) Carbohydrate-specific receptors of the liver. *Annu. Rev. Biochem.*, **51**, 531–554.
143. Lee, Y.C. and Lee, R.T. (1995) Carbohydrate-protein interactions: basis of glycobiology. *Acc. Chem. Res.*, **28**, 321–327.
144. Lee, Y.C., Townsend, R.R., Hardy, M.R. *et al*. (1983) Binding of synthetic oligosaccharides to the hepatic Gal Galnac lectin – dependence on fine-structural features. *J. Biol. Chem.*, **258** (1), 199–202.
145. Khorev, O., Stokmaier, D., Schwardt, O. *et al*. (2008) Trivalent, Gal/GalNAc-containing ligands designed for the asialoglycoprotein receptor. *Bioorg. Med. Chem.*, **16** (9), 5216–5231.
146. Yang, W., Mou, T., Peng, C. *et al*. (2009) Fluorine-18 labeled galactosyl-neoglycoalbumin for imaging the hepatic asialoglycoprotein receptor. *Bioorg. Med. Chem.*, **17** (21), 7510–7516.
147. Cai, G., Jiang, M., Zhang, B. *et al*. (2009) Preparation and biological evaluation of a glycosylated fusion interferon directed to hepatic receptors. *Biol. Pharm. Bull.*, **32** (3), 440–443.
148. Kim, E.M., Jeong, H.J., Park, I.K. *et al*. (2005) Asialoglycoprotein receptor targeted gene delivery using galactosylated polyethylenimine-graft-poly(ethylene glycol): in vitro and in vivo studies. *J. Controlled Release*, **108** (2-3), 557–567.
149. Wu, J., Nantz, M.H. and Zern, M.A. (2002) Targeting hepatocytes for drug and gene delivery: emerging novel approaches and applications. *Front. Biosci.*, **7**, d717–d725.
150. Baenziger, J.U. and Maynard, Y. (1980) Human hepatic lectin – physiochemical properties and specificity. *J. Biol. Chem.*, **255** (10), 4607–4613.
151. Boturyn, D., Defrancq, E., Dolphin, G.T. *et al*. (2008) RAFT nano-constructs: surfing to biological applications. *J. Pept. Sci.*, **14** (2), 224–240.
152. Bonnet, C.S., Fries, P.H., Crouzy, S. *et al*. (2009) A gadolinium-binding cyclodecapeptide with a large high-field relaxivity involving second-sphere water. *Chem. Eur. J.*, **15**, 7083–7093.
153. Peluso, S., Rückle, T., Lehmann, C. *et al*. (2001) Crystal structure of a synthetic cyclodecapeptide for template-assembled synthetic protein design. *ChemBioChem*, **2**, 432–437.
154. Dumy, P., Eggleston, I.M., Esposito, G. *et al*. (1996) Solution structure of regioselectively addressable functionalized templates: an NMR and restrained molecular dynamics investigation. *Biopolymers*, **39**, 297–308.
155. Renaudet, O. and Dumy, P. (2003) Chemoselectively template-assembled glycoconjugates as mimics for multivalent presentation of carbohydrates. *Org. Lett.*, **5** (3), 243–246.
156. Singh, Y., Renaudet, O., Defrancq, E. and Dumy, P. (2005) Preparation of a multitopic glycopeptide-oligonucleotide conjugate. *Org. Lett.*, **7** (7), 1359–1362.
157. Renaudet, O. and Dumy, P. (2006) On-bead synthesis and binding assay of chemoselectively template-assembled multivalent neoglycopeptides. *Org. Biomol. Chem.*, **4**, 2628–2636.
158. Pujol, A.M., Cuillel, M., Jullien, A.-S. *et al*. (2012) A sulfur tripod glycoconjugate releases a high affinity copper chelator in hepatocytes. *Angew. Chem. Int. Ed.*, **51** (30), 7445–7448.
159. Westerlind, U., Westman, J., Tornquist, E. *et al*. (2004) Ligands of the asialoglycoprotein receptor for targeted gene delivery, part 1: synthesis of and binding studies with biotinylated cluster glycosides containing N-acetylgalactosamine. *Glycoconjugate J.*, **21** (5), 227–241.

160. Rensen, P.C.N., van Leeuwen, S.H., Sliedregt, L.A.J.M. *et al*. (2004) Design and synthesis of novel N-acetylgalactosamine-terminated glycolipids for targeting of lipoproteins to the hepatic asialoglycoprotein receptor. *J. Med. Chem.*, **47** (23), 5798–5808.
161. Xiao, Z., Loughlin, F., George, G.N. *et al*. (2004) C-terminal domain of the membrane copper transporter Ctr1. *J. Am. Chem. Soc.*, **126**, 3081–3090.
162. Sasaki, N., Hayashizaki, Y., Muramatsu, M. *et al*. (1994) The gene responsible for LEC hepatitis, located on rat chromosome 16, is the homolog to the human Wilson disease gene. *Biochem. Biophys. Res. Commun.*, **202** (1), 512–518.
163. Buiakova, O.I., Xu, J., Lutsenko, S. *et al*. (1999) Null mutation of the murine ATP7B (Wilson disease) gene results in intracellular copper accumulation and late-onset hepatic nodular transformation. *Hum. Mol. Genet.*, **8** (9), 1665–1671.

12

MRI Contrast Agents

Célia S. Bonnet and Éva Tóth

Centre de Biophysique Moléculaire, UPR 4301 CNRS, Rue Charles Sadron, Université d'Orléans, Orléans, 45071, France

12.1 Introduction to MRI contrast agents

Thanks to its exceptional resolution and unlimited tissue penetration, magnetic resonance imaging (MRI) is one of the most efficient diagnostic modalities in clinical radiology and biomedical research today. MR images are based on water proton density and water proton relaxation dynamics which vary according to the tissue under examination. Around 30–40% of clinical MR applications use paramagnetic, superparamagnetic, or ferromagnetic substances as a contrast medium. These agents shorten the relaxation times of water protons, yielding improved contrast of the images [1, 2]. Given its high electron spin ($S = 7/2$) and slow electron spin relaxation, the trivalent Gd^{3+} is the most efficient relaxation agent among all paramagnetic cations. To avoid the toxicity of the free Gd^{3+} ion, it is chelated with appropriate multidentate ligands, preferentially poly(aminocarboxylates), which ensure a high thermodynamic stability and kinetic inertness. The majority of clinical Gd^{3+}-based agents, which represent around 90% of all clinical contrast agent injections, are of low molecular weight, localized in the extracellular space and non-specific. They are mainly derivatives of DTPA (diethylenetriaminepentaacetic acid) or DOTA (1,4,7,10-tetraazacyclododecane-1,4,7,10-tetraacetic acid) (Scheme 12.1). Other paramagnetic metal ions, in particular manganese(II) with five unpaired electrons, have been also considered as MRI contrast agents [3].

In the last decade, a new family of MRI contrast agents, based on Chemical Exchange Saturation Transfer (CEST), appeared which now make their way to human applications [4, 5]. The CEST MR image is based on the decrease of the water proton signal intensity following saturation of slowly exchanging protons of the CEST agents. Paramagnetic, mostly lanthanide complexes are commonly used as CEST probes (PARACEST) since they ensure large chemical shifts, which is particularly interesting for CEST applications.

Ligand Design in Medicinal Inorganic Chemistry, First Edition. Edited by Tim Storr.

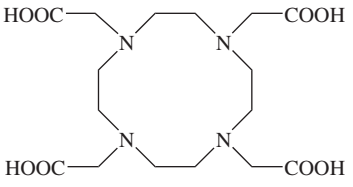

H_4DOTA
Dotarem, Guerbet

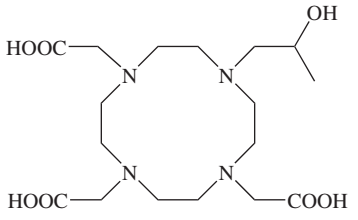

H_3HP-DO3A
ProHance, Bracco

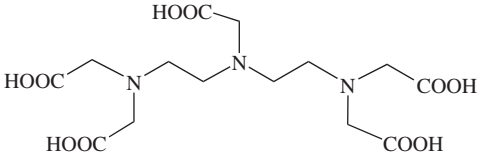

H_5DTPA
Magnevist, Bayer Schering

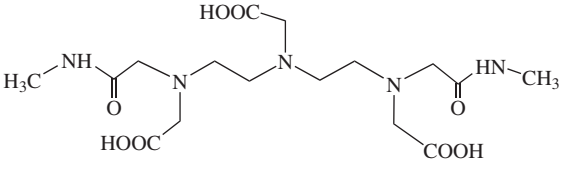

H_3DTPA-BMA
Omniscan, Nycomed-Amersham-GE

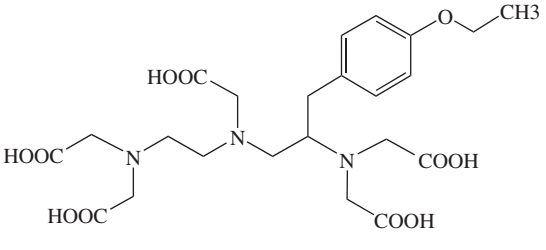

H_5EOB-DTPA
Eovist,
Bayer Schering

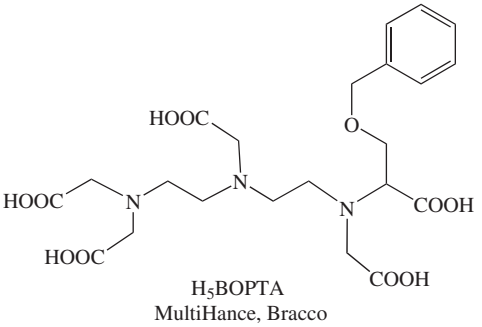

H_5BOPTA
MultiHance, Bracco

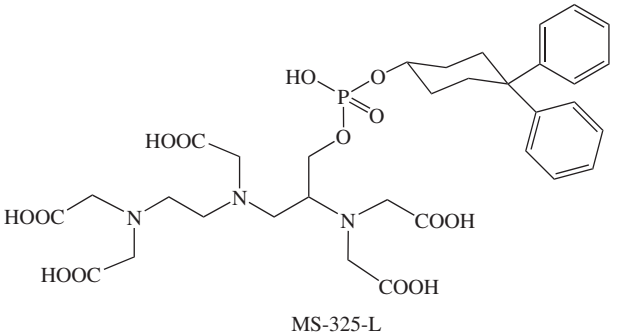

MS-325-L
AngioMARK, EPIX-Bayer Schering

Scheme 12.1 *Ligands in commercially available Gd^{3+} complexes*

Traditionally, MRI produces anatomical (morphological) images. In the last few years, molecular imaging has emerged as a new area aiming at non-invasive visualization of expression and function of bioactive molecules at the molecular, sub-cellular, or cellular level [6]. By detecting specific molecular signatures in disease processes, molecular imaging is aimed at the detection of biochemical or physiological abnormalities of the disease, rather than its structural consequences as detected by classical MR imaging. Although the potential of molecular imaging in clinical settings has been recognized early on, the limited sensitivity and specificity of current approaches remains a major problem and often prevents real applications.

In this chapter, we will discuss ligand design for the two major families of MRI agents based on lanthanide complexes: (i) Gd^{3+} complexes as T_1 relaxation agents and (ii) PARACEST probes. We will shortly survey the different relaxation mechanisms and how ligand design can contribute to increase the efficacy of Gd^{3+}-based contrast agents and to exploit the CEST effect for Ln^{3+} chelates. The second part of the chapter will be dedicated to design principles of molecular imaging probes that are capable of providing an MRI response to various biochemical variables, such as pH, metal ions, or enzymes. The development of such responsive or smart probes requires an understanding of the relaxation phenomena involved and it is most often based on coordination chemistry approaches via appropriate design of the metal chelating ligands.

12.2 Ligand optimization to increase relaxivity

The efficacy of a paramagnetic chelate as a contrast enhancing agent is given by its proton relaxivity, r_1 or r_2, which refers to the paramagnetic enhancement of the longitudinal or transverse water proton relaxation rate, $1/T_1$ and $1/T_2$, respectively, by a unity concentration of the agent (1 mM) [equation (12.1)]:

$$\frac{1}{T_{i,obs}} = \frac{1}{T_{i,d}} + \frac{1}{T_{i,p}} = \frac{1}{T_{i,d}} + r_i[Gd] \quad i = 1, 2 \tag{12.1}$$

The observed proton relaxation rate, $1/T_{i,obs}$ is the sum of a diamagnetic contribution, $1/T_{i,d}$, and the paramagnetic relaxation rate enhancement, $1/T_{i,p}$, which is linearly proportional to the concentration of the paramagnetic species, [Gd]. Given the preponderance of T_1-agents in practice, "proton relaxivity" most often refers to longitudinal relaxation (r_1).

The relaxation of water protons originates from the dipole-dipole interactions between the proton nuclear spins and the fluctuating local magnetic field caused by the Gd^{3+} unpaired electron spins and is described by the Solomon-Bloembergen-Morgan theory of paramagnetic relaxation [2]. We distinguish two major contributions: (i) Inner sphere relaxivity originates from the interaction with water protons in the inner coordination sphere of the complex which then exchange with bulk water. (ii) Bulk solvent molecules experience also a paramagnetic effect by diffusing near the complex, defined as outer sphere relaxation (Figure 12.1). Water molecules hydrogen-bound to the ligand can give rise to a second sphere relaxivity term, which, in certain cases, might represent an important contribution. For low molecular weight Gd^{3+}-based contrast agents, the inner and outer sphere relaxation mechanisms contribute equally to the overall relaxivity. While the outer sphere effect is practically impossible to modulate, the inner sphere term can be substantially increased by rational design of the ligand complexing the Gd^{3+}. Thus the optimization of the efficacy of Gd^{3+}-based contrast agents primarily involves modification of the structural and dynamic parameters of the complexes which influence the inner sphere contribution to relaxivity. We will shortly survey these parameters and discuss ligand design for their optimization.

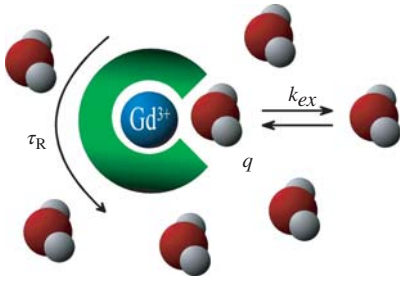

Figure 12.1 *Schematic representation of a Gd^{3+} complex with one inner-sphere water molecule ($q = 1$), surrounded by the bulk. k_{ex} refers to the water/proton exchange rate of this molecule and τ_R to the rotational correlation time of the system*

According to the Solomon-Bloembergen-Morgan theory, the main factors that influence proton relaxivity are:

1. hydration number of the complex (q)
2. water exchange rate between the inner sphere and the bulk (k_{ex})
3. rotational correlation time (τ_R)
4. electron spin relaxation rates ($1/T_{1,2e}$)
5. gadolinium–water proton distance (r_{GdH}).

Parameters (1)–(3) can be modulated by the choice of the ligand, while electronic relaxation and the Gd–water proton distance are difficult to change on a rational basis. The relaxivity of current clinical contrast agents is much lower than the theoretically attainable values, since neither their rotational correlation time (~100 ps), nor their proton exchange rate (~10^6 s^{-1}) is optimal (Figure 12.2). In order to attain maximum relaxivities, these two parameters should be optimized simultaneously, that is, the rotational motion should be slowed down, and the exchange should be accelerated.

12.2.1 Hydration number

The inner sphere relaxivity is linearly proportional to the hydration number. Gd^{3+} is typically eight- or nine-coordinated in aqueous solution. The hydration state of the Gd^{3+} complex is therefore determined by the number of donor atoms of the ligand available for lanthanide coordination as water coordination will complete the coordination sphere. While all clinical agents are monohydrated complexes, it is evident that one could gain in efficacy by increasing the hydration number to two (or more). Although the thermodynamic stability and kinetic inertness of bishydrated Gd^{3+} complexes is often considered to be insufficient for application in human medicine, there is intensive research to design stable chelates with two inner sphere water molecules [7–10].

Bishydrated Gd^{3+} chelates based on TREN-HOPO (hydroxypyridinonate, Scheme 12.2) derivatives possess high thermodynamic stability, with stability constants, $\log K_{ML} = 19–21$, though likely low kinetic inertness [11–13]. Aime *et al*. reported the heptadentate ligand, the 6-amino-6-methylperhydro-1,4-diazepine-1,4,N^6,N^6-tetraacetate (AAZTA, Scheme 12.2) which also forms stable bishydrated lanthanide complexes [9]. Near physiological conditions, $[Gd(AAZTA)]^-$ is significantly more inert than $[Gd(DTPA)]^{2-}$, allowing its potentially safe use as contrast agent in MRI [14]. Among bishydrated Gd^{3+} complexes, those formed with the pyridine-containing twelve-membered macrocycle are likely kinetically the most inert [15].

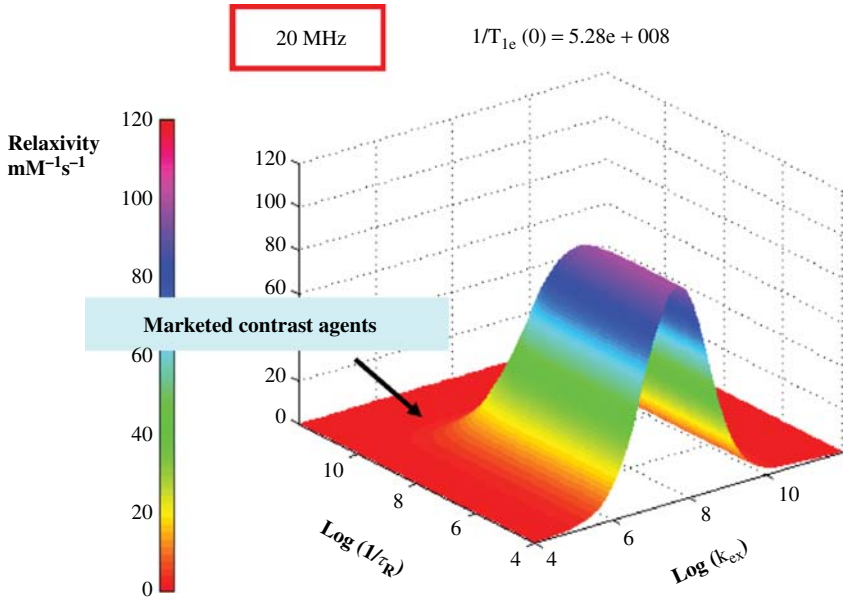

Figure 12.2 *Calculated proton relaxivity at 20 MHz, for a monohydrated complex, as a function of the rotational correlation time τ_R, and the water exchange rate k_{ex}, for an electronic relaxation rate fixed at $1/T_{1e} = 5.28 \times 10^8\ s^{-1}$. (See plate section for the colour version of this figure)*

Bishydrated complexes formed with diethylenetriamine-tetraacetate (DTTA, Scheme 12.2) ligands [16, 17] or with the pyridine-containing analog (Py^{4-}) [18] attached to various scaffolds have been also investigated. Some DTTA-chelates have been injected into mice to perform *in vivo* imaging experiments and showed no apparent toxicity [19, 20]. Cellular and *in vivo* toxicity studies in mice evidenced the non-toxicity of the bishydrated pyridinic complexes in animal experiments [18].

An important issue to consider for bishydrated chelates is their potential tendency to form ternary complexes in biological media via the replacement of the two inner sphere water molecules by small endogenous ligands such as carbonate, phosphate, citrate, and so on. This leads to a decrease of the relaxivity and therefore it is not desirable. In general, DO3A-type Ln^{3+} chelates which have the two water molecules in geminal positions tend to form ternary complexes with a variety of endogenous carboxylate donors. With GdDO3A, both monodentate (with acetate, propionate, and alanine) [21], and bidentate binding was observed (with hydrogencarbonate, lactate, malonate, citrate, and with carboxylate functions of proteins) [22]. DO3A-type chelates can interact with carboxylate groups in proteins such as serum albumin as well. Several of the non-macrocyclic bishydrated chelates show resistance to anion binding, such as complexes of HOPO- [23], AAZTA- [9], DTTA- [19, 20], or Py-derivatives [10].

12.2.2 Optimization of water exchange kinetics via rational ligand design

The water exchange rate has a dual effect on proton relaxivity: (i) it modulates the efficiency of chemical exchange from the inner sphere of the metal to the bulk and (ii) it contributes to the overall correlation time that governs the dipole-dipole interaction between the electron and nuclear spin. The rate and the mechanism of the water exchange can be directly assessed by variable temperature ^{17}O transverse relaxation rate measurements. The activation volume, obtained from variable pressure ^{17}O NMR data, is a further, unambiguous

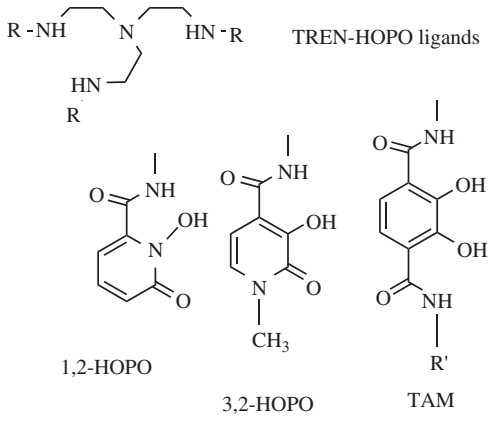

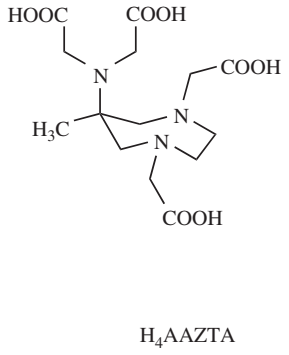

H_4AAZTA

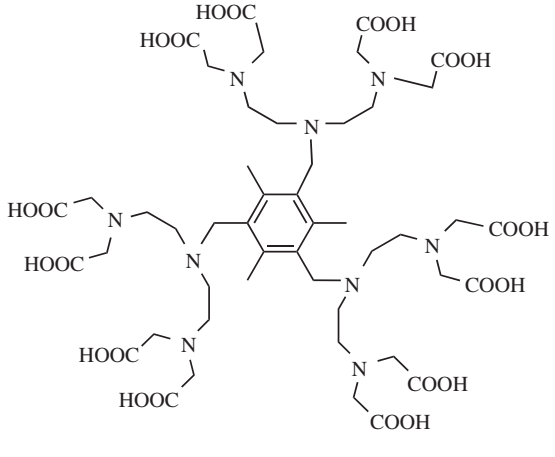

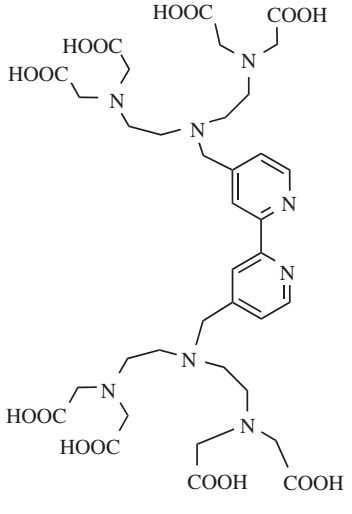

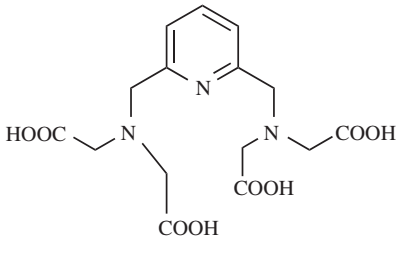

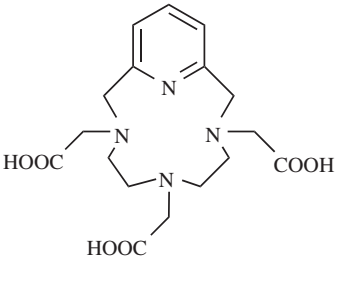

Scheme 12.2 *Ligands forming bishydrated Gd^{3+} complexes*

tool to determine the mechanism of the exchange process. At the traditionally used MRI field strengths (20–60 MHz), the optimal value of the water exchange rate to attain maximum proton relaxivities is around $5-10\times10^7\ s^{-1}$. The optimal water exchange rate varies significantly with magnetic field, but it also depends on the rotational correlation time.

The structure of the ligand has a primordial role to determine the rate and the mechanism of the water exchange on the Gd^{3+} complex. Water exchange rates vary over 4 orders of magnitude from DOTA-tetraamide complexes ($k_{ex}^{298}=4.5\times10^4\ s^{-1}$ for $[Gd(DOTMA)(H_2O)]^{3+}$) (where DOTMA stands for (1R,4R,7R,10R)-α, α′, α′′, α′′′-tetramethyl-1,4,7,10-tetraazacyclododecane-1,4,7,10-tetraacetic acid) [24] to the highest $k_{ex}^{298}=8\times10^8\ s^{-1}$ for the aqua ion) [25]. Since the late 1990s, considerable work has been performed to understand the relationship between ligand structure and water exchange rate and to optimize ligand design to obtain Gd^{3+} complexes with fast water exchange [2, 26].

Based on this huge body of data, we can identify the most important structural factors that determine water exchange rate. The majority of the Gd^{3+} poly(aminocarboxylate) complexes with an interest to MRI undergo dissociatively activated water exchange, implying that the rate determining step is the leaving of the coordinated water molecule [26]. In these processes, the negative charge of the complex and an increased steric crowding around the water binding site are the two main factors to contribute to the acceleration of the water exchange. As an empirical rule, it was generally observed for all DTPA- and DOTA-derivatives that the replacement of one negatively charged carboxylate in the complex with a neutral amide decreases the exchange rate to about one third. Increasing the negative charge on the complex is not a viable route to optimize water exchange. On the other hand, the design of ligands ensuring steric compression has proved to be a successful strategy. Steric compression has been induced in the acyclic DTPA- or the macrocyclic DOTA-type complexes by the intercalation of an additional CH_2 group either in the amine backbone of the ligand (EPTPA and TRITA), or in the carboxylate arm (DTTA-N′prop and DTTA-Nprop; Scheme 12.3).

While the elongation of the amine backbone results in an almost 2 orders of magnitude increase in the water exchange rate of the Gd^{3+} complex in comparison with the parent $[Gd(DOTA)(H_2O)]^-$ or $[Gd(DTPA)(H_2O)]^{2-}$, with the propionate derivative ligands DTTA-Nprop, DO3A-Nprop we observe a moderate increase of the water exchange rate [27, 28]. The bifunctional DO3A-α-aminopropionate chelator seems particularly interesting since it ensures versatile conjugation possibilities to develop high efficiency Gd^{3+}-based agents [29]. This demonstrates that by minor, appropriate changes in the ligand structure one can fine-tune the steric compression around the water binding site, which translates to the fine-tuning of the rate of water exchange. The introduction of one six-membered chelate ring in the complex always gives rise to an increased steric crowding. The steric crowding and the consequent acceleration of the water exchange are more important on the elongation of the amine backbone (EPTPA and TRITA) than on the elongation of the carboxylate pendant arm (DTTA-Nprop and DO3A-Nprop). The water exchange is also accelerated when an acetate function is replaced by a sterically more demanding phosphorus containing pendant arm, both in macrocylic and linear ligands [30].

Bishydrated complexes also provide faster water exchange. This is related to the flexibility of the inner coordination sphere which allows easier passage from the starting complex to the transition state in the water exchange process, implying lower activation energy. The water exchange rate of bishydrated DTTA-derived Gd^{III} complexes is about double ($k_{ex}^{298}=8-9\times10^6\ s^{-1}$) [16, 31] of that for the monohydrated $[Gd(DTPA)(H_2O)]^{2-}$ ($k_{ex}^{298}=3.3\times10^6\ s^{-1}$). The Gd^{3+} complex formed with the hexadentate heterotripodal HOPO-type ligand, $[Gd(TREN\text{-}bis(6\text{-}Me\text{-}HOPO)\text{-}TAMTRI)(H_2O)_2]$, has an even faster water exchange ($k_{ex}^{298}=5.3\times10^7\ s^{-1}$), which is related to the octadentate nature of the complex resulting in an associative exchange mechanism [32].

On DOTA-type complexes, the water exchange rate is strongly dependent on the relative abundance of the TSA/SA isomers, the TSA isomers having a much faster exchange (SA = square-antiprismatic; TSA = twisted square-antiprismatic) [33–37]. k_{ex}^{298} is 40 times higher on the TSA isomer of the Eu^{III} complex of DOTAM

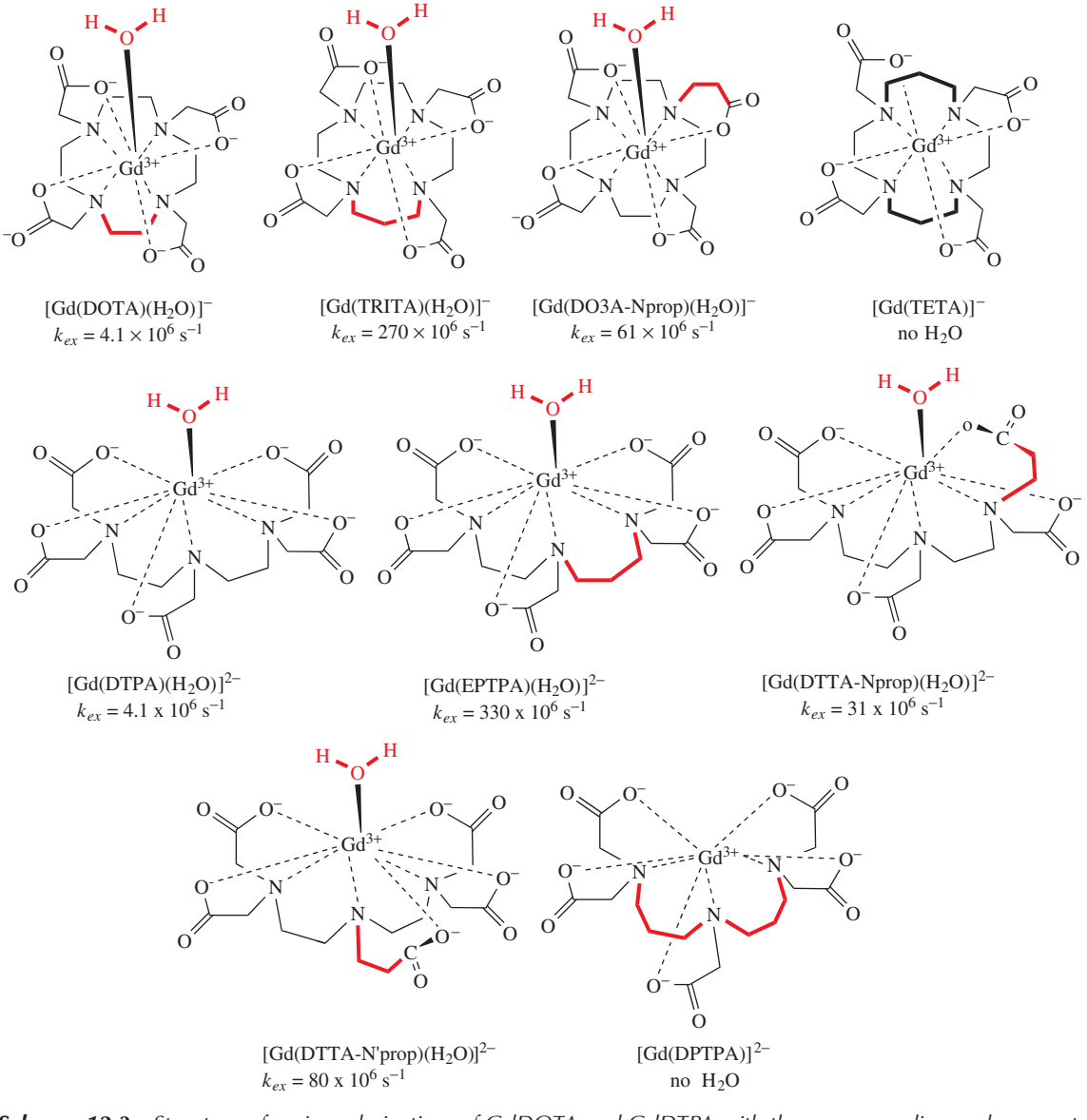

Scheme 12.3 *Structure of various derivatives of GdDOTA and GdDTPA with the corresponding exchange rate of the inner-sphere water molecule*

(DOTA tetrAMide) than on the SA analog [38]. The water exchange kinetics of the mono-capped TSA being much closer to optimal than those of the mono-capped square antiprism render the TSA isomer more desirable for high relaxivity applications. Several systems have been developed that allow for selection of the TSA coordination geometry in DOTA-type chelates [37].

The water exchange is little affected when a Gd^{3+} chelate is attached to a macromolecular scaffold as has been evidenced for dendrimeric systems bearing surface-conjugated Gd^{3+} complexes [39, 40] or micelles [41, 42]. In contrast, protein-binding of the chelate can lead to a diminution or suppression of the water exchange when the binding occurs via electrostatic forces between the protein and negatively charged groups of the Gd^{3+} chelate in a way that the inner sphere water molecule becomes blocked between the protein and the metal ion [43, 44].

12.2.3 Optimization of the rotational dynamics via rational ligand design: Size and flexibility

In the last two decades, most of the work on the optimization of the relaxivity of MRI contrast agents was dedicated to modulation of the rotational dynamics [1, 2, 45, 46]. The Solomon-Bloembergen-Morgan relaxation theory predicts that a long rotational correlation time leads to higher relaxivities at magnetic fields of current clinical MRI (0.15–3 T). Slower rotation can be achieved by covalent or non-covalent binding of the Gd^{3+} complex to natural or synthetic macromolecules. To increase the molecular weight and thus slow down tumbling, different strategies based on proteins [47], dendrimers [48], linear polymers [49], micelles [50], or liposomes [51], various inorganic nanoparticles, and so on, have been developed. Most of these approaches allow not only optimization of the relaxivity by unit of Gd^{3+}, but also assembling hundreds or thousands of paramagnetic centers in one molecular entity.

The effect of the rotation on the relaxivity is highly field-dependent. At Larmor frequencies between 10 and 130 MHz (0.2 and 3 T), long rotational correlation times lead to a characteristic hump on the relaxivity profile; however, at very high fields (above 9.4 T), the dependence on τ_R is inverted as r_1 becomes proportional to ${\tau_R}^{-1}$ (Figure 12.3) [52].

The internal flexibility of macromolecular systems is also an important issue and should be reduced as much as possible to attain high relaxivities. The most widely applied dynamic model to describe the relaxation, and

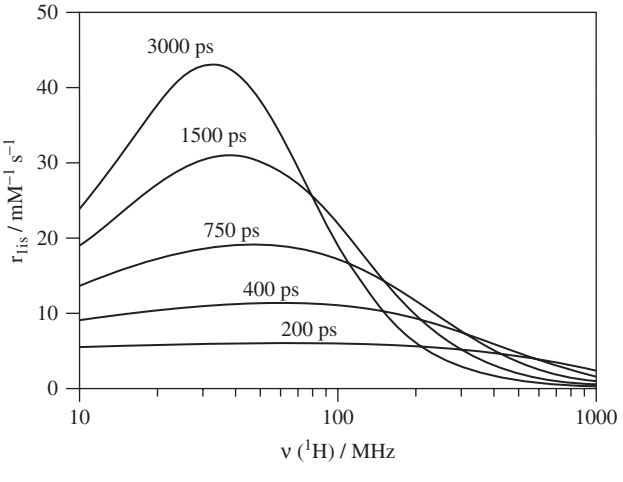

Figure 12.3 *Inner-sphere relaxivities calculated (Solomon-Bloembergen-Morgan theory) for ^{1}H Larmor frequencies from 10–1000 MHz for various rotational correlation times τ_R. The water exchange rate k_{ex} was fixed at $10 \times 10^6\ s^{-1}$, and the parameters for the electronic relaxation were the following: $\tau_V = 20$ ps and $\Delta^2 = 0.1 \times 10^{20}\ s^{-2}$*

the underlying rotational motion of flexible macromolecular Gd^{3+} complexes, is based on the model-free Lipari and Szabo approach which has been adapted for the longitudinal ^{1}H and ^{17}O relaxation [46, 49]. The isotropic overall reorientation of the large particle (global rotational correlation time, τ_g) is supposed to be uncorrelated with the faster internal motions (local rotational correlation time, τ_l); the degree of restriction of the internal motion being expressed by an order parameter S ($S = 1$ for a completely restricted, and $S = 0$ for a free internal motion).

The importance of the flexibility has been demonstrated for micellar or liposomic Gd^{3+} complexes. For micelles, the relaxivities remain typically below 25 $mM^{-1}\,s^{-1}$ for monohydrated complexes in the frequency range 20–60 MHz, due to limitation by relatively fast rotational motions [41, 42]. These data evidenced an important internal flexibility of the micelles, shown by the largely different values reported for the local and global rotational correlation times as well as by the low values of the $S^2 = 0.2–0.4$ representing small restriction of the internal motion.

In contrast, the attachment of two hydrophobic chains, instead of one, on adjacent donor groups of DOTA-type ligands considerably reduced the flexibility of the Gd^{3+} chelate both in a micellar form and when it is incorporated into liposomes [53]. As a consequence, much higher relaxivities are measured for the amphiphilic complexes bearing two hydrophobic chains (101% increase at 20 MHz and 298 K), which is mainly the result of a higher order parameter S^2 (characterizing the coupling between local and global motions) and a higher local rotational correlation time, both indicative of a reduced rotational flexibility (Figure 12.4). The r_1 value of $GdDOTA(GAC_{12})_2$ (34.8 $mM^{-1}\,s^{-1}$ at 298 K and 20 MHz) is the highest reported to date for monohydrated Gd-based paramagnetic micelles. Analogously, the incorporation of the two-chain complex into liposomal structures also brings an important relaxivity gain with respect to the mono-chain derivative (+135% at 0.47 T and +99% at 1.41 T).

In MRI, higher field strength offers higher signal-to-noise ratio, thus increased spatial and temporal resolution. Nowadays, 3 T scanners are becoming widely available in the clinics, and for experimental studies, much higher fields (≥9.4 T; 400 MHz) are commonly used [54, 55].

While slowing down rotation results in a remarkable relaxivity improvement at intermediate frequencies (20–60 MHz), above 60 MHz r_1 drops sharply with increasing magnetic field and, at high frequencies (above 100 MHz), macromolecular systems are hardly superior to small chelates. As the Solomon-Bloembergen-Morgan theory predicts, at proton Larmor frequencies above 200 MHz r_1 increases with the inverse rotational correlation time $1/\tau_R$, in contrast to lower frequencies, where it is proportional to τ_R (Figure 12.3). Thus at high frequencies, intermediate-size, rigid molecules are favored over large ones, with an optimal τ_R of ∼400 ps at 400 MHz. Some systems specifically developed for high field applications are based on self-assembly. Fe^{2+} is well-known to form stable complexes with phenanthroline (Phen), bipyridine (bpy), and terpyridine (tpy) ligands in 1 : 3 and 1 : 2 metal: ligand ratios. When attached to Gd^{3+} chelates, such ligands can promote the formation of supramolecular assemblies in the presence of Fe^{2+}. These assemblies formed around the Fe^{2+} core are rigid and have a considerably larger size than the monomer Gd^{3+} complex alone, which results in a reduced rotational mobility leading to a relaxivity enhancement [56–59]. One of the first examples is the metallostar system (Figure 12.5), with a remarkable relaxivity at high magnetic fields (16.4 $mM^{-1}\,s^{-1}$/15.9 $mM^{-1}\,s^{-1}$ at 200 MHz and 25 °C/37 °C, respectively, in comparison with 4.02 $mM^{-1}\,s^{-1}$ and 3.86 $mM^{-1}\,s^{-1}$ for GdDOTA under the same conditions) [16, 60]. MRI studies at 200 MHz in mice have confirmed that the approximately four times higher relaxivity of the metallostar with respect to the commercial GdDOTA is retained under *in vivo* conditions [19]. The high relaxivity of the metallostar is related to the rigidity of the self-assembly and to the bishydrated nature of the Gd^{3+}-chelate. The replacement of the iron core by Ru^{2+} endows the self-assembled structure with an increased thermodynamic and kinetic stability, while it has essentially no influence on the relaxometric properties of the metallostar [61].

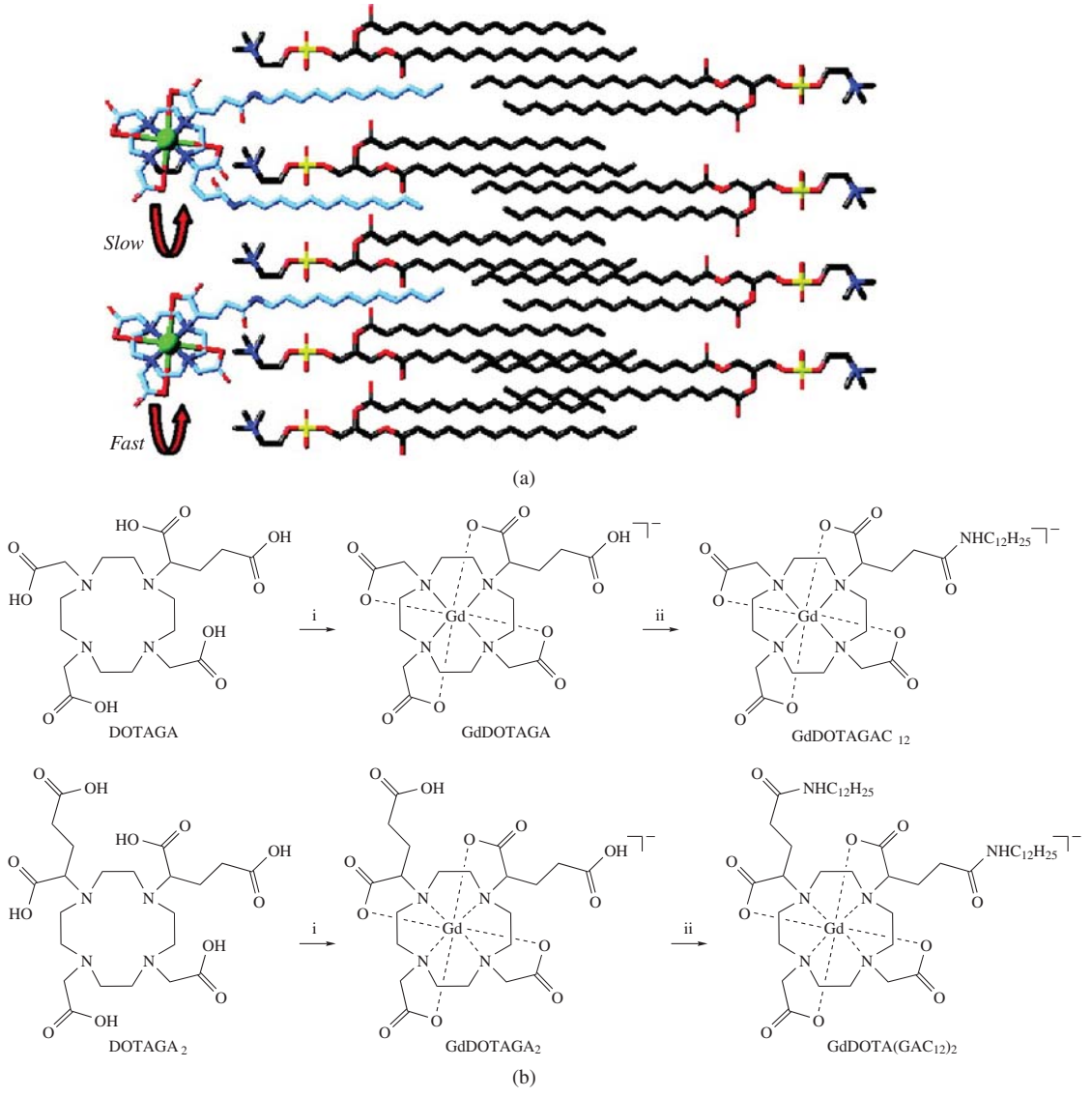

Figure 12.4 *(a) Schematic representation of the complexes GdDOTA(GAC$_{12}$)$_2$ (top) and GdDOTAGAC$_{12}$ (bottom) in the lipid bilayer. (b) Synthesis of the complexes; reaction conditions: (i) GdCl$_3$, H$_2$O, and pH 6. (ii) C$_{12}$H$_{25}$NH$_2$, DMF (dimethylformamide),TNTU [2-(endo-5-norbornene-2.3-dicarboxylimide)-1,1,3,3-tetramethyluronium tetrafluoroborate], and DIPEA (N,N-diisopropylethylamine) [53] Reprinted (adapted) with permission from ([53]). Copyright (2010) American Chemical Society. (See plate section for the colour version of this figure)*

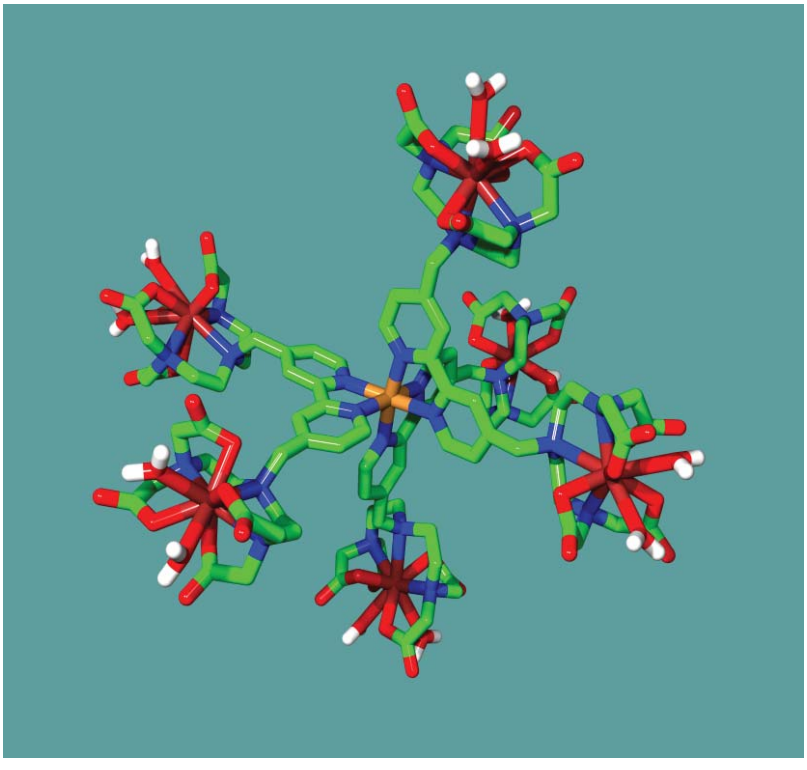

Figure 12.5 *Metallostar compound formed by self-assembly around an Fe^{2+} ion. (See plate section for the colour version of this figure)*

12.3 Ligand design for CEST agents

A CEST effect can be observed for compounds containing protons in chemical exchange with the bulk water protons [62]. Upon saturating the NMR signal of these exchangeable protons, their NMR signal is reduced or disappears. In parallel, the chemical exchange will also transfer the saturation to the bulk water protons leading to the intensity decrease of its NMR signal as well. This water proton intensity decrease can be then translated to an MR image. Slowly exchanging protons giving rise to a CEST effect are typically situated either on functional groups of the molecule (such as amides, amines, and hydroxy groups) or on a very slowly exchanging water molecule of a lanthanide chelate.

To observe a high CEST effect, one needs slow relaxation, high concentration of the CEST agent and fast exchange. On the other hand, for selective saturation of one pool, the chemical exchange must be slow on the NMR time scale, which brings a higher limit for the exchange rate (k_{ex}). The exchange rate must be no greater than the frequency difference ($\Delta\omega$) between the two proton pools [equation (12.2)]:

$$\Delta\omega \geq 1/\tau_b = k_{ex} \tag{12.2}$$

Since $\Delta\omega$ is proportional to the magnetic field, higher fields allow for exploiting faster exchanges which consequently leads to a more important CEST effect. More detailed explanation of the CEST theory [4, 63, 64] can be found in literature.

12.3.1 Application of paramagnetic ions – PARACEST

In order to increase the value of the chemical shift difference between bulk water protons and protons of the CEST agent, and thus to exploit faster proton exchange rates and increase the CEST effect, paramagnetic complexes are applied as CEST agents (PARACEST) [65]. A paramagnetic ion results in dramatic changes in the proton chemical shifts of the ligand, up to hundreds of parts per million. As the irradiation frequency is far from the bulk water resonance, saturation spillover will be minimized and shorter irradiation times are needed. The disadvantage of paramagnetic complexes inducing large $\Delta\omega$ is in shortening of the T_1 relaxation time of bulk water which might limit the sensitivity gain. The production of CEST contrast is unique for several reasons. The application of a selective radio frequency (RF) irradiation acts as a switch to turn contrast on; therefore no pre-contrast image is needed. The contrast will be generated by comparing two post-contrast experiments, one upon irradiation at the saturation frequency and another upon irradiation at the opposite frequency, which is the saturation frequency compared with the frequency of water (defined as 0). Most importantly, several CEST agents can be simultaneously visualized, provided their saturation frequencies do not overlap. CEST effects may be made independent of the agent concentration, which opens new possibilities to develop ratiometric approaches by using two proton pools in exchange with bulk water. The two pools can be found within a single molecule [66].

The first PARACEST effect was referred for DOTA tetraamide complexes of various lanthanide ions, including Nd^{3+}, Eu^{3+}, Tb^{3+}, Dy^{3+}, Tm^{3+}, and Yb^{3+}. The CEST effect was observed for both the coordinated water and for amide protons. PARACEST agents can also be targeted to specific biological structures. Bifunctional PARACEST agents allowing for attachment of targeting functionalities were studied [67] and, later, used for attachment of fibrin-targeting nanoparticles [68]. Another bifunctional DOTA amide was used for labeling of adenovirus particles [69]. Several DOTA amides containing albumin-binding groups were studied in order to extend the blood retention of the PARACEST agent [70].

Similarly to relaxation agents, the detection limits for on-resonance saturation fall in low millimolar concentration of the PARACEST agents. An innovative approach to decrease the detection limit of CEST agents was introduced by Aime *et al*. [71]. The CEST effect is proportional to the number of exchangeable protons or water molecules. When a lanthanide ion is entrapped in a liposome, the signal of the water protons inside the liposome is shifted and two separate water signals can be found in the ^{1}H NMR spectra. As the inner water molecules are in slow exchange with the bulk, such a structure could be used as a PARACEST (LIPOCEST) agent. The high number of water molecules entrapped in the liposome increases efficiency of the LIPOCEST agent and the detection limit is several orders of magnitude lower than for other PARACEST agents. The properties of LIPOCEST agents were improved by application of non-spherical liposomes [72, 73]. Beside liposomes, other macromolecular PARACEST agents, such as dendrimers or supramolecular adducts, have been also investigated to increase sensitivity [74].

12.4 Ligand design for responsive probes

Responsive probe should display relaxivity *selectively* influenced by the physiological parameter to be detected. The relaxivity is related to the microscopic properties of the contrast agent. As already stated, the most important parameters that can be easily tailored by the chemist are the hydration number, the exchange rate of the water molecules with the surrounding water (bulk) and the motional dynamics of the molecules. Consequently, most of the responsive probes will be based on a change of the number of inner-sphere water molecules q, or on a change of the rotational correlation time of the complex, τ_R (change of size). The literature on responsive probes is quite extensive [75–79], and here we will focus on a few examples to highlight the importance of ligand design for such probes.

12.4.1 Probes responsive to pH

The determination of pH *in vivo* is an important goal to achieve because pH changes have been associated with numerous diseases such as infections, strokes, kidney disease and cancers. Indeed, the extracellular pH in solid tumors can be 0.5–0.6 pH units lower than that of healthy tissue due to a disturbance of the balance between the uptake of glucose and oxygen, and the removal of H^+ and lactate [80]. pH-sensitive probes could also indicate neuronal activity, which induces a slight acidification of the extracellular medium (pH 7.2–7.4) [81].

12.4.1.1 Small paramagnetic Gd-based complexes

In order to design ligands that upon complexation to Gd^{3+} will give rise to pH-sensitive contrast agents, people have mainly used the chelating DOTA-unit that has been modified in order to append a pH reporting group. Upon pH changes, this pH reporter will be affected and will in turn affect the microscopic properties of the whole of the complex, influencing the relaxivity. The changes on the complex will mainly occur through three mechanisms: a change in the hydration number, a change in the rotational correlation time of the complex or a change of the water exchange rate of the molecule directly coordinated to Gd^{3+}.

The most straightforward approach relies on the design of chelating moieties that are involved in a protonation/deprotonation step that yields changes in the denticity of the ligand. In turn, this results in changes in the number of water molecules coordinated to the paramagnetic metal ion.

The first example of such a ligand contains a sulfonamide group (DO3A-SA, Scheme 12.4), which is deprotonated in basic media, giving rise to a complex with no water molecule on the Ln^{3+} center, whereas in acidic media the nitrogen is protonated leading to the presence of water molecules on the Ln^{3+} center. This behavior is reversible and the pH dependence can be finely tuned by the presence of different *p*-substituents on the arylsulfonamide moiety. Indeed the protonation constants are determined by the substituent and are, for example, 5.7, 6.4, and 6.7 for the CF_3, Me, and OMe substituent respectively [82].

In order to be applicable *in vivo*, it is necessary to determine the local concentration of every responsive probe. Without this information, the detected changes in T_1 could be ascribed either to changes in the relaxivity, or to changes in the local concentration of the paramagnetic metal complexes. This problem has been tackled in three different ways in the case of the GdDO3A-SA complex (Scheme 12.4). In a first approach, the Gd-complex has been functionalized with an adamantane moiety, known to form strong host-guest interactions with the β-cyclodextrin cavity (β-CD) (Figure 12.6) [83]. Upon formation of a supramolecular adduct with a poly-β-CD substrate, the relaxivity of the probe shows a pronounced increase, particularly at pH < 6 where the complex is bishydrated. The information on the concentration is provided by a different reporting molecule bearing a highly sensitive NMR heteronucleus (e.g., ^{19}F and ^{31}P). In this case a CF_3 group has been attached to a functionalized adamantane. By using appropriate molar ratios of the substrate, ^{19}F-reporter and Gd-complex (20 : 5 : 1), it was possible to assess the pH by MRI using the ^{19}F NMR signal to evaluate the probe concentration and normalize the relaxation rates measured *in vitro* on samples of different pH and concentrations.

The second approach is based on the use of a dual MRI/SPECT system [SPECT (Single Photon Emission Computed Tomography)] in which the probes are represented by two Ln^{3+} DO3A-arylsulfonamide complexes only differing in the metal ion: Gd^{3+} as MRI reporter and Ho^{3+} as SPECT tracer [84]. The GdDO3A-SA and HoDO3A-SA complexes have identical biodistribution and an appropriate mixture of the two complexes can be employed. ^{166}Ho will provide quantitative information necessary to transform the relaxivity changes into a pH map.

Finally, the complex has been included in liposomes, and it does experience a different intraliposomal distribution depending on the pH conditions [85]. The ratiometric method consists of measuring the pH dependence

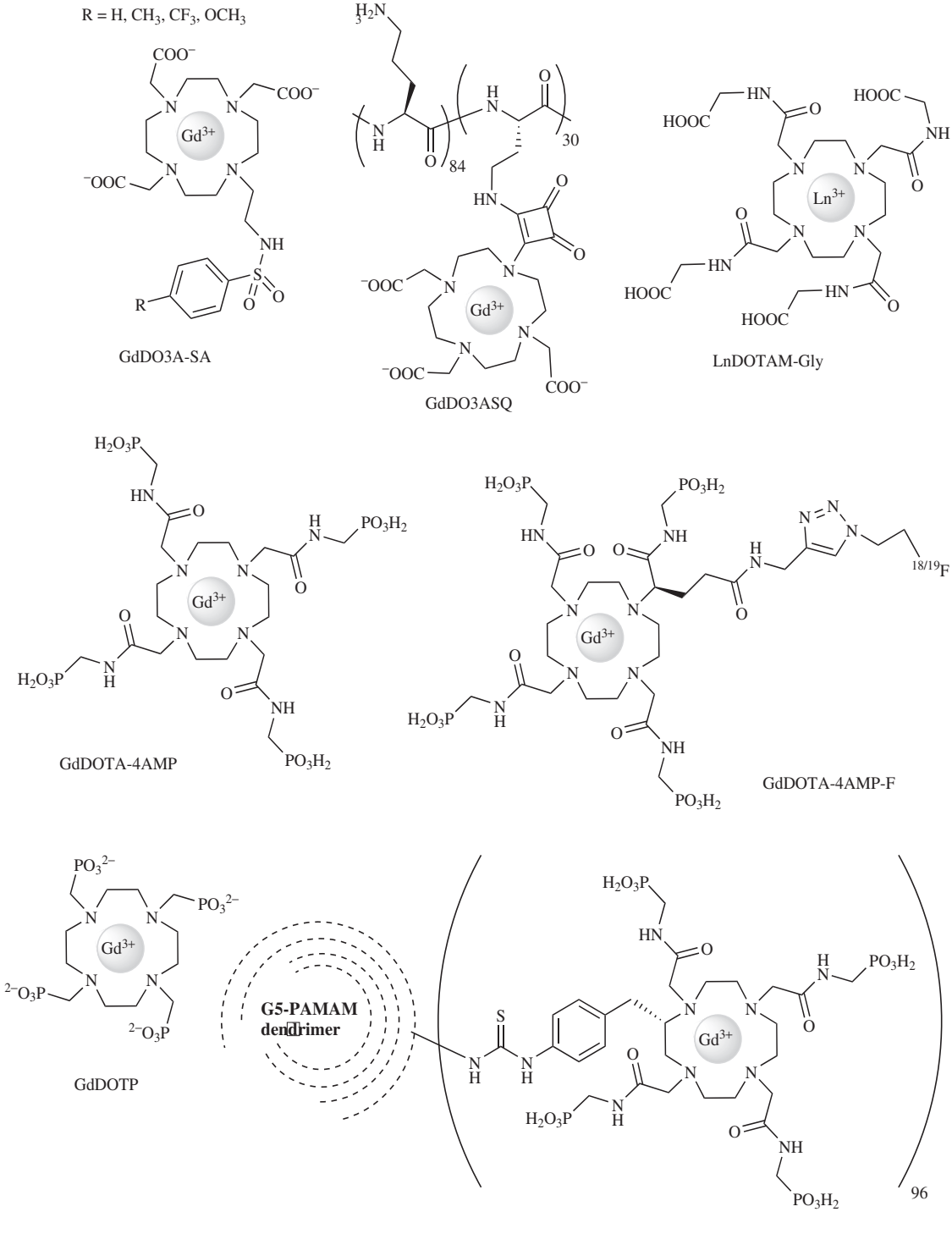

Scheme 12.4 *Ln^{3+} complexes for pH sensing*

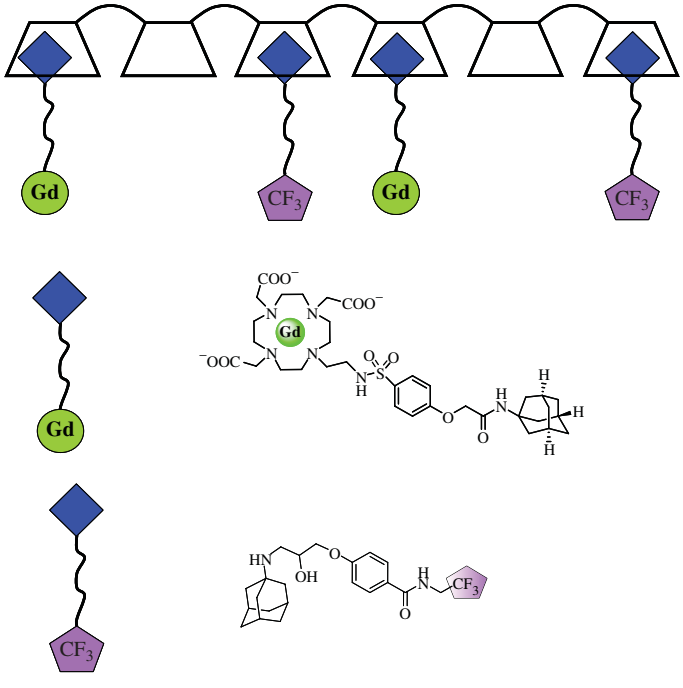

Figure 12.6 *Schematic representation of the pH-responsive supramolecular adducts between poly-β-CD, the Gd^{3+} complex and the ^{19}F reporter. (See plate section for the colour version of this figure)*

of the ratio between the longitudinal paramagnetic contribution to the water proton relaxation rates ($1/T_{i,p}$) at two different magnetic fields, thus removing the concentration dependence.

Another approach to design pH-dependent contrast agents consists in designing complexes that will undergo structural changes as a function of pH, which will in turn affect the overall rotational correlation time of the complex. Very often they are made of polymeric or peptidic chains. For example, a squaric acid moiety was attached to a DO3A (GdDO3ASQ, Scheme 12.4), and exploiting the easy reaction of squaric esters with amines, thirty GdDO3ASQ chelates were bound to a polyaminoacid chain consisting of 114 ornithine residues [86]. At acidic pH the amino groups of the side chain of ornithine are protonated and highly hydrated, thus they tend to stay as far apart as possible, leading to a complex with a relatively high degree of mobility. At higher pH the deprotonation of the $-NH_3^+$ groups induces a rigidification due to the formation of intramolecular hydrogen bonds between adjacent peptidic linkages. This results in a lengthening of τ_R, and an increase in the relaxivity. An interesting method has also been proposed in order to make the pH-responsive properties of the system concentration-independent: the ratio of the paramagnetic contribution to the longitudinal (R_{1p}) and transverse (R_{2p}) relaxation rates of the water protons, $R_{2p}/R_{1p,}$ has been considered. This ratio is independent of the concentration of the paramagnetic probe but it has a dependence on the molecular mobility of the system for $\tau_R \geq 1$ ns. If the rotational mobility changes with pH then this ratiometric procedure may be exploited to obtain accurate pH values [87].

An unusual pH dependence of relaxivity has also been reported for a complex of a tetraamide derivative of cyclen with extended phosphonate non-coordinating side chains, GdDOTA-4AMP (Scheme 12.4). The relaxivity increases between pH 4 and 6, reaches a maximum near pH 6, gradually decreases to a minimum near pH 8.5, then remains relatively insensitive until pH 10.5 before increasing again at higher pH values [88]. The mechanism to explain this pH dependence is complicated. The phosphonate groups are able to

catalyze the exchange of the protons of the water molecule directly coordinated to the Gd^{3+} center with bulk solvent protons through an H-bonding network. The effectiveness of the phosphonate at catalyzing this proton exchange is then dependent upon their protonation state and as the phosphonate groups become protonated, the rate of the proton exchange increases, increasing the relaxivity as a result. Second-sphere water molecules, retained at the vicinity of the Gd^{3+} by H-bonding, also contribute to the overall relaxivity of the complex in a pH-dependent manner. GdDOTA-4AMP was successfully used to map pH values *in vivo* in renal acidosis [89] and brain-tumor models [90]. In a first attempt to estimate the concentration of the agent *in vivo*, the corresponding pH-insensitive complex GdDOTP (Scheme 12.4) was injected. Given their structure and charge similarity, identical renal pharmacokinetics was assumed for the two complexes. However, this approach can be misleading as small changes in the structure of the complexes can result in dramatic effects on the biodistribution. Recently, a different approach was envisaged by using a bimodal MRI-PET agent [PET (Positron Emission Tomography)] for quantitative pH mapping. GdDOTA-4AMP was modified to incorporate a fluorine atom (either ^{19}F or ^{18}F) and give GdDOTA-4AMP-F (Scheme 12.4) which did not change the pH dependence of the relaxivity [91]. By mixing appropriate amounts of the ^{18}F- and ^{19}F-compound to account for the very different sensitivity of the two techniques, the concentration of the radiochemical agent, proportional to the PET signal, could be determined which enabled quantitative *in vitro* mapping of the pH.

Another important factor to take into account to determine the effectiveness of an agent is the difference between the relaxivity of the "on" state compared with that of the "off" state. It has been demonstrated that the amplitude of the relaxivity response to pH variation of the previous probe was largely improved (more than doubled) by conjugating it to a macromolecular dendrimeric scaffold. The GdDOTA-AMP complex was therefore modified by incorporating a functionalized benzyl group onto the macrocylic backbone of the complex in order to retain the pH dependence provided by the phosphonate group [92]. This nitrobenzyl moiety was further coupled to a G5-PAMAM dendrimer [PAMAM (Poly(AMidoAMine))] (Scheme 12.4). However, improving the relaxivity response to pH through increased molecular weight may also negatively impact the effectiveness of such agents. Large molecules, such as dendrimers, remain in vasculature longer than discrete agents, which are better able to diffuse into all extracellular space. Furthermore, large molecules also tend to clear more slowly from the body as a result of increased liver uptake. This extends the retention time of Gd^{3+} in the body. Further studies into the *in vivo* behavior of dendrimer-based MRI contrast media will be required to establish if this approach, which is successful for increasing the relaxivity response, will yield agents that can actually be applied *in vivo*.

12.4.1.2 CEST agents

PARACEST agents have a great potential to report on pH. The PARACEST effect originates from proton exchange between the paramagnetic probe and bulk water and the magnitude of the observed effect is intrinsically dependent on the exchange rate, itself related to pH.

Unlike traditional Gd^{3+}-based agents, it is possible to administer and independently visualize two PARACEST agents in the same experiment and thus develop a concentration independent, ratiometric method for pH determination. For instance, one can acquire the PARACEST pH profiles for a cocktail of two isostructural probes including an identical ligand but two different paramagnetic metal ions. The individual PARACEST response of the two probes to pH will be different, while their distribution in tissue should be identical. Consequently, the ratio of the two PARACEST profiles is concentration independent and can be used to determine pH directly without knowing the analytical concentration of either agent. For example, the complexes YbDOTAM-Gly and EuDOTAM-Gly (Scheme 12.4) possess two pools of exchangeable protons represented by the coordinated water and the amide protons [93]. YbDOTAM-Gly displays the most interesting CEST properties when its amide N-H resonance is irradiated. As the exchange rate of amide is base-catalyzed, YbDOTAM-Gly is an efficient pH-responsive probe in the 5.5–8.1 pH range.

EuDOTAM-Gly has more interesting CEST properties when irradiated on its coordinated water protons, and this effect is not dependent upon pH on the range 5.5–8.5. So the use of a concentration mixture of YbDOTAM-Gly and EuDOTAM-Gly produces a pH dependent CEST effect which is the function of the concentration ratio of the two complexes. More recently a mixture of two isomers of Yb-HPDO3A (Scheme 12.1) has been used to detect pH independently of the concentration of the probe. The same complex is also used to detect temperature, exploiting the large temperature dependence of the paramagnetic shift, unaffected by pH [94].

12.4.2 Probes responsive to physiological cations

Sensing of biological cations has been an important and growing area of research for the past several years. Indeed, they play a major role in living systems, but they can also promote cytotoxic reactions, so their concentrations are tightly regulated by the cells in terms of accumulation, transport, distribution, storage, recycling, and export. Misregulation of these ions has been connected to different pathologies including strokes, cancers, and neurodegenerative diseases. Consequently there has been a growing interest in imaging and quantifying these ions in living systems both for a better understanding of biological processes, and for early clinical diagnosis. In this chapter, we will focus on the MRI detection of the most abundant and relevant cations, such as calcium, zinc, copper, and manganese.

As for pH sensing, the smart probes responsive to metal ions will mainly function on the basis of changes in the hydration number of Gd^{3+}, or in the rotational correlation time of the complex, and sometimes of both of them. The strategy for modulating the hydration number of a Gd^{3+} complex in the presence of a cation is illustrated Figure 12.7. For metal ion sensing however a few more points must be taken into account: (i) the probe must be responsive to the desired cation in the physiologically relevant concentration range and (ii) it must show a good selectivity for the metal ion to sense.

In recent years significant progress has been made in the development of such probes, but very few of them have been applied *in vivo*. For practical applications, one must keep in mind that the flux of ion can be very rapid, and thus accurate quantification of the metal ion concentration changes by MRI might require rapid measurement and consequently further development of new imaging techniques.

12.4.2.1 Changes in the hydration number

Most of the cation responsive probes function on the basis of changes of the hydration number, and are designed following the same scheme: a DOTA or DTPA derivative and a unit selective to the metal to sense are covalently attached through an appropriate linker. In the absence of the analyte, one (or more) donor groups from a metal specific binding site are coordinated to Gd^{3+}. In the presence of the analyte, these donor groups

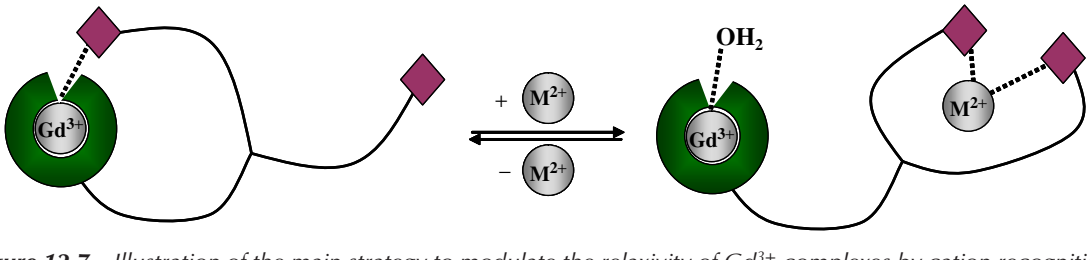

Figure 12.7 *Illustration of the main strategy to modulate the relaxivity of Gd^{3+} complexes by cation recognition, using a change in the number of inner-sphere water molecules, q*

will dissociate from Gd^{3+} and coordinate to the ion to sense, leaving space for one (or more) water molecule to enter the inner sphere coordination of Gd^{3+}, leading to an increase in relaxivity (flipping mechanism) as illustrated Figure 12.7.

In the case of Ca^{2+} sensing, a Ca^{2+} selective unit has been appended to a GdDOTA complex, or more often, linked between two GdDOTA complexes. The first Ca^{2+} complexing unit to be proposed was the well-known BAPTA (1,2-bis(o-aminophenoxy)ethane-*N*,*N*,*N*′,*N*′-tetraacetic acid), which bridges two GdDO3A units to give GdDOPTA (Scheme 12.5) [95, 96]. The BAPTA ligand was earlier developed by Tsien and shows a good selectivity for Ca^{2+} over endogenous cations, and pH insensitivity for Ca^{2+} complexation thanks to the low protonation constants (6.36 and 5.47, below physiological pH) [97]. Upon Ca^{2+} complexation, a change of relaxivity of nearly 80% is observed, with an affinity constant of about 6. The system is therefore adapted for Ca^{2+} detection in the micromolar range, which corresponds to intracellular Ca^{2+} concentration. This could be problematic as intracellular delivery of MRI probes in a sufficient concentration (1 to 0.1 mM due to the sensitivity of the technique) is not highly probable. Targeting extracellular Ca^{2+} concentrations, which lie in the millimolar range, seems more realistic. A series of responsive probes with a reduced affinity for Ca^{2+} has been developed, and the most interesting in terms of relaxivity changes (80% change upon binding) is composed of an EGTA (ethylene glycol tetraacetic acid) derivative for Ca^{2+} complexation bridging two GdDO3A complexes (Scheme 12.5) [98]. The relaxivity increase has been ascribed to the increase in the hydration number, and in a slight rigidification of the complex induced by Ca^{2+} binding (τ_R increase). The complex has also been studied in artificial cerebrospinal fluid and showed also an encouraging relaxivity response to Ca^{2+}.

As mentioned earlier, a key factor for developing responsive probes is the selectivity toward the desired cation, so the metal-ion binding site needs to be designed with a coordination number, donor preference adapted to the cation. Therefore small changes on the binding site can lead to dramatic changes in the selectivity. Indeed, a six-, and an eight-coordinated pyro-EGTA-based binding moieties have been linked to a GdDOTA unit, and used to detect Zn^{2+}, and Ca^{2+} respectively (Schemes 12.5 and 12.6) [99]. These systems have been shown to be sensitive to the presence of bicarbonate, a physiological anion known to quench relaxivity, but still show relaxivity enhancements in the presence of Ca^{2+} and this anion.

Concerning Zn^{2+} detection, as the bis-(2-pyridylmethyl)amine (DPA) is known to be a Zn^{2+} specific chelator, most of the complexes studied are based on this unit or derivatives of this unit. First, two DPA units were appended on both sides of a Gd-DTPA complex to give Gd-DTPA-1 (Scheme 12.6) [100]. When complexing Zn^{2+}, the relaxivity decreases up to one equivalent of Zn^{2+} added and it was hypothetized that the resulting complex has fewer water molecules directly bound to Gd^{3+}. In this case the DPA units are not directly coordinating the Gd^{3+} center and the complex does not operate through the "flipping mechanism." Zn^{2+} is coordinated by the two DPA units and is presumably situated above the water binding site of the Gd^{3+} complex, leading to the elimination of the inner-sphere water, or at least a blockage of the water exchange. The main problem of this system is the formation of a 2 : 1 adduct in the presence of an excess of Zn^{2+}, which causes the relaxivity to increase and to reach nearly its initial value (without Zn^{2+}) when two equivalents of Zn^{2+} are added. To circumvent this problem, the system has been modified by replacing one pyridine unit of each DPA by a carboxylate function to give Gd-DTPA-2 (Scheme 12.6) [101]. A relaxivity decrease of about 30% upon Zn^{2+} binding is observed with no further increase. It was hypothetized that in this case the 1/1 complex formed is more stable and does not dissociate to form a bimetallic species. Interestingly, a similar complex with just a longer linker Gd-DTPA-3 (Scheme 12.6) does not show any relaxivity response to Zn^{2+}, highlighting the importance of the choice of the linker, and of optimizing each part of the complex.

Similarly some Gd-DOTA-based complexes have been studied. First, a diaminoacetate for Zn^{2+} complexation linked to a GdDO3A derivative through a linker comprising three methylenes has been studied (Gd-daa3, Scheme 12.6) [102]. This compound shows 73% relaxivity increase in aqueous buffer and 33% in male blood serum. Surprisingly, the complex Gd-daa2 which differs only by the presence of a shorter

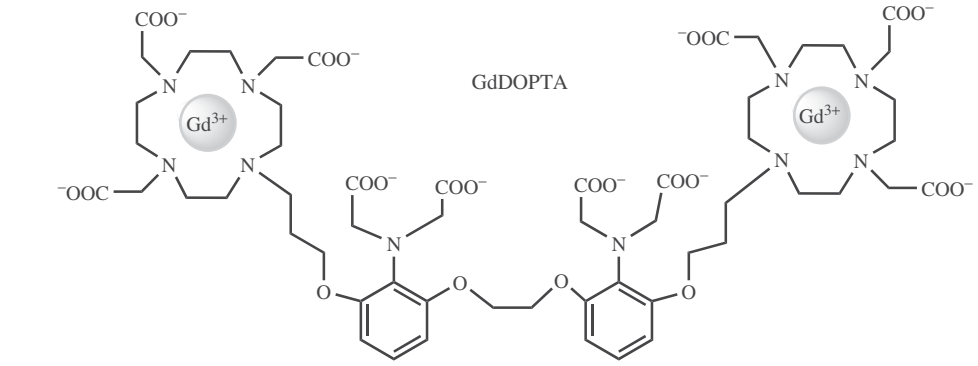

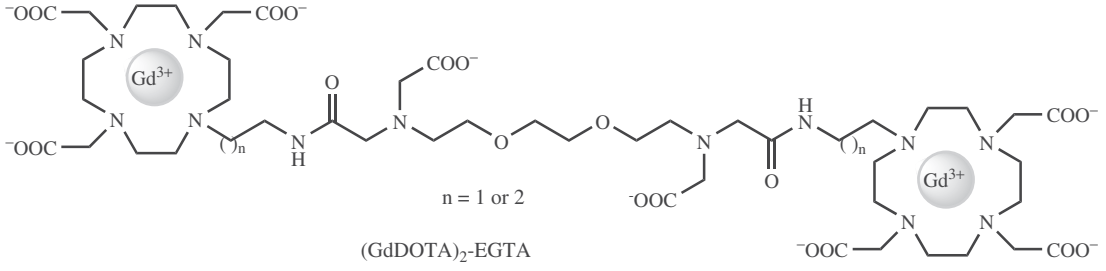

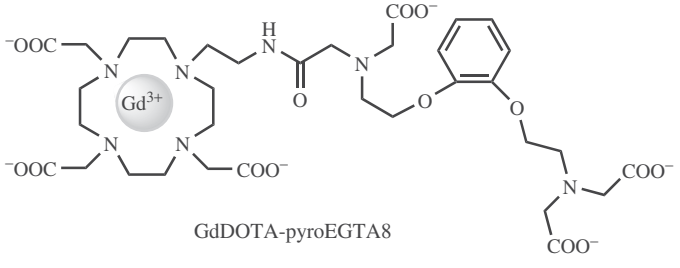

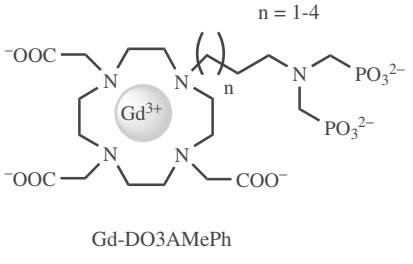

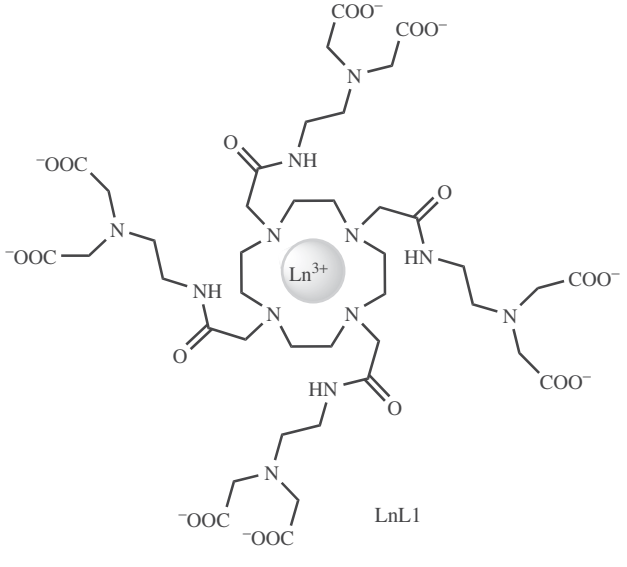

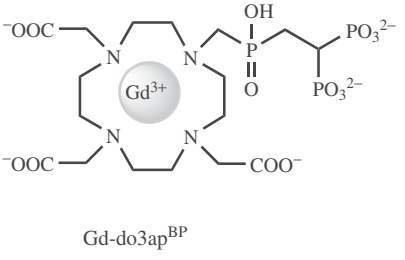

Scheme 12.5 *Ln^{3+} complexes for Ca^{2+} sensing*

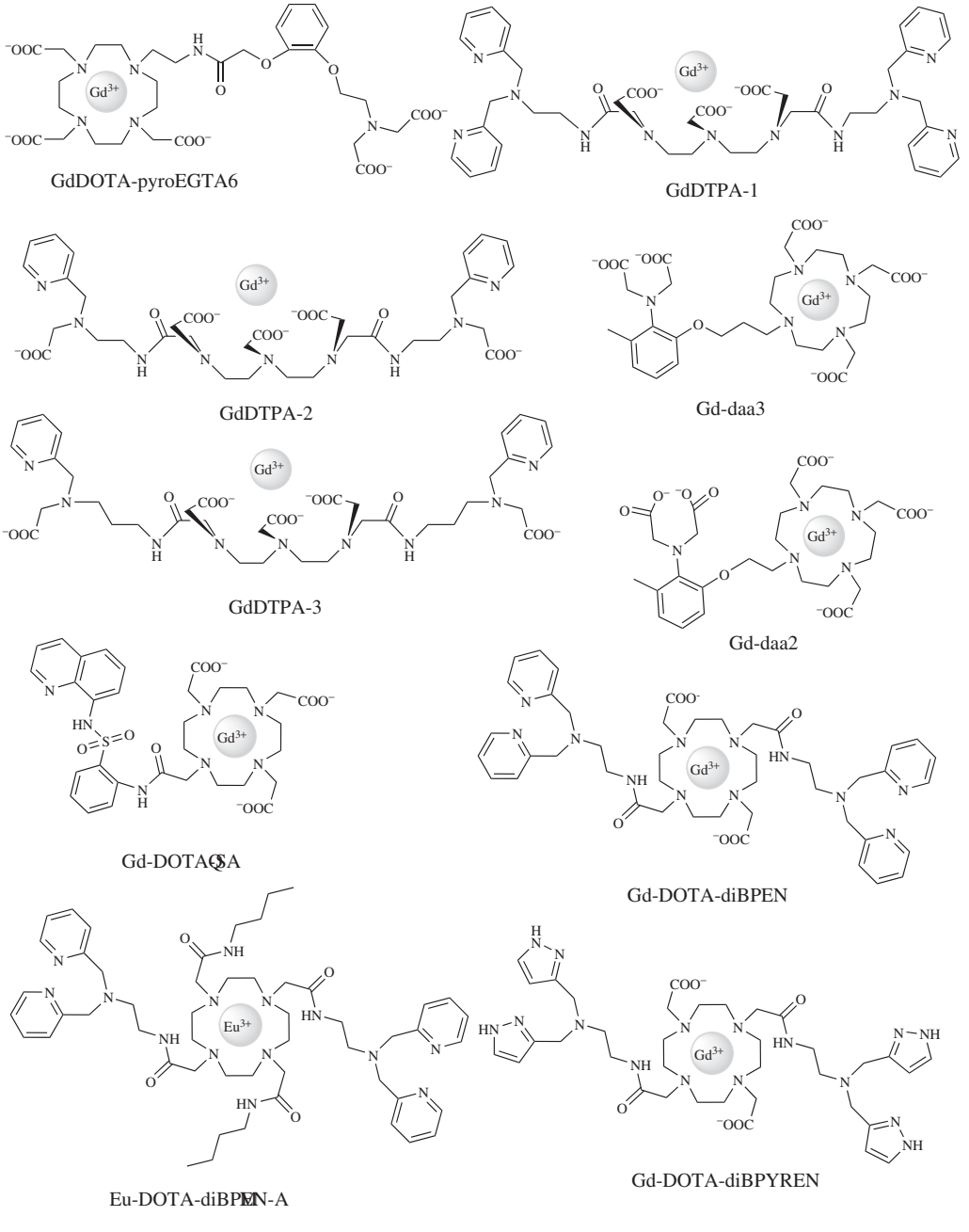

Scheme 12.6 *Ln^{3+} complexes for Zn^{2+} sensing*

linker (two methylenes instead of three) shows no relaxivity changes upon Zn^{2+} binding. This highlights the difficulty in designing responsive probes, and choosing the correct linker: in the previous example, for which the mechanism was different, the responsive complex was the one with the longest linker.

Concerning copper, the first compound to be studied Gd-CG1 (Scheme 12.7) was very similar to Gd-daa3, lacking only a methyl group on the benzene ring [103]. Despite a good affinity for Cu^{2+}, and a relaxivity turn on response, as expected, this compound lacks selectivity for Cu^{2+} over Zn^{2+}. Given the more important Zn^{2+} concentration compared with that of Cu^{2+} (around 10 times higher) what was not a big issue for Zn^{2+} detection becomes highly problematic for Cu^{2+} detection. So different chelating units have been designed, taking into account the specificity of copper. An additional difficulty with copper compared with zinc and calcium must be taken into account, as copper can exist in two different oxidation states. Ideally, the chelating unit should be specific for one oxidation state.

The idea to target $Cu^{+/2+}$ selectively over Zn^{2+} was to introduce softer functions such as thioether-based receptors, which are also believed to improve copper binding affinities. A series of such complexes was developed and Gd-CG2 responds to Cu^{+} but not to Cu^{2+}, whereas Gd-CG6 respond equally to Cu^{+} and Cu^{2+} (Scheme 12.7) [104]. The binding affinity of Gd-CG2 is improved by about 9 orders of magnitude compared with Gd-CG1 and it shows a turn-on response in the presence of copper of 360%. This compound is specific of copper over other biologically relevant metal ions such as Na^{+}, K^{+}, Ca^{2+}, Mg^{2+}, Zn^{2+}, Fe^{2+}, and Fe^{3+} but the relaxivity response is affected by the presence of physiological anions such as lactate, carbonate, and citrate, to a lesser extent. Two improvements were made on this compound. First, the acetate arms were replaced by hexanedioate arms in Gd-CG7 (Scheme 12.7) in order to reduce the response to anions [105]. Surprisingly, in this case, the increase in relaxivity is not related to a change in the number of coordinated water molecule on the Gd^{3+} center, but to a change in the overall correlation time of the complex (4 times longer in the presence of Cu^{+}). Secondly, an octaarginine tail was conjugated to one carboxylate function of CG2 to give Gd-Arg_8CG2 with a marked increase in cellular uptake (ninefold greater concentration in cells than Gd-CG2) [106].

Finally another mechanism aiming at changing the number of water molecules directly coordinated to Gd^{3+} has been explored, and it consists of an agglomeration of Gd^{3+} complexes in the presence of the metal to sense, which leads to a reduction of the hydration number. It has been observed on bisphosphonate derivatives of DO3A, Gd-DO3AMePh for Ca^{2+} sensing (Scheme 12.5) [107]. In the presence of Ca^{2+}, the bisphophonate arms will coordinate Ca^{2+} resulting in the formation of aggregated complexes. This phenomenon is dependent upon complex concentration, and also on the size of the linker: for the smaller linker, no aggregation is observed. Contrary to the previous mechanism, this phenomenon leads to a decrease in relaxivity in the presence of the ion to sense, and the design of such complexes is difficult to predict and rationalize.

12.4.2.2 Changes in the rotational correlation time

The second main parameter to be modulated through cation sensing is the rotational correlation time of the complex by changing the overall size of the complex. This very often results in smaller relaxivity changes than a change in the hydration number, and this also means that the agent will not respond equally over the whole range of fields, and will be more efficient at approximately 40 MHz.

Complexes with bisphosphonate arms have been studied as they are known to form polynuclear clusters. Gd-do3ap^{BP} combines a GdDOTA-like complex with a bisphosphonate group (Scheme 12.5). In the presence of metal ions (Ca^{2+}, Mg^{2+}, and to a lesser extent Zn^{2+}), Gd-do3ap^{BP} appears to show the formation of coordination oligomers leading to an increase in relaxivity up to 200–500% [108]. Unfortunately the selectivity on such system is very poor.

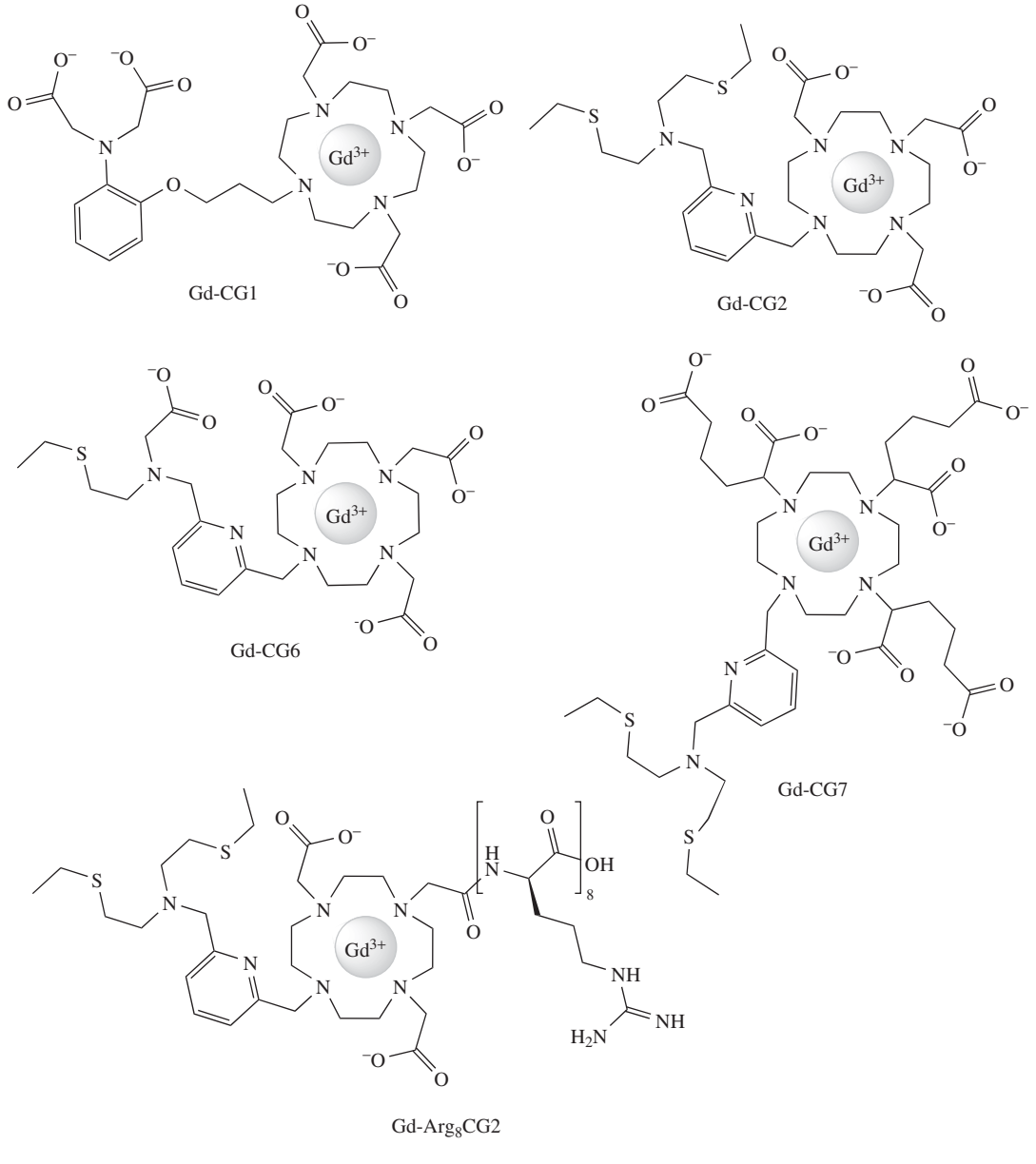

Scheme 12.7 *Gd^{3+} complexes for $Cu^{+/2+}$ sensing*

A sulfonamidoquinoline group has been appended to a Gd-DOTA-like complex in order to design a Zn^{2+} bimodal responsive contrast agent in MRI and optical imaging, Gd-DOTA-SAQ (Scheme 12.6) [109]. Both the fluorescence of the sulfonamidoquinoline group and the relaxivity of the complex are enhanced upon Zn^{2+} binding. The relaxivity reaches a maximum for 0.5 equivalent of Zn^{2+} bound, when a sandwich complex is formed between Zn^{2+} and two Gd^{3+} complexes. This species has a slower rotational correlation time leading to a higher relaxivity.

Concerning Zn^{2+} detection, a Gd-DOTA complex with two DPA units has also been developed (GdDOTA-diBPEN, Scheme 12.6) [110]. This complex shows a small increase in relaxivity when two equivalents of Zn^{2+} are added. Given that the complex has two aromatic rings per DPA unit, it could possibly interact with human serum albumin (HSA) through hydrophobic interactions. Indeed, the complex interacts only weakly with HSA in the absence of Zn^{2+}, but the interaction is very strong in the presence of Zn^{2+}. This results in an increase of the rotational correlation time of the complex, and therefore of the relaxivity. This agent has been used *in vivo* for the detection of Zn^{2+} released into the extracellular space of pancreatic islet β-cells of mice during glucose-stimulated insulin secretion [111]. This is the first example of a cation responsive contrast agent used *in vivo*. With the aim of reducing Zn^{2+} affinity, GdDOTA-diBPYREN (Scheme 12.6) with pyrazole groups instead of the pyridine groups was developed [112]. The affinity for Zn^{2+} is indeed four orders of magnitude lower, and the complex shows an improved binding interaction with HSA which results in the highest reported relaxivity change in human serum upon Zn^{2+} recognition.

12.4.2.3 CEST agents

Contrary to pH detection, the design of PARACEST agents for cation sensing is not straightforward. The Yb^{3+} and Eu^{3+} complexes of a tetramide derivative of DOTA with imino(diacetate) moieties for Ca^{2+} binding have been studied (Scheme 12.5) [113]. The CEST effect originating from the slow exchange of the amide protons, and of the coordinated water protons for the Yb^{3+} and Eu^{3+} complexes respectively, decreases considerably in the presence of Ca^{2+}. Given the low affinity constant for Ca^{2+}, the ion coordinates only to one of the iminodiacetate arms. The complexes respond also to the presence of Mg^{2+}.

Eu-DOTA-diBPEN-AM (Scheme 12.6), which is very similar to Gd-DOTA-diBPEN, has been studied for Zn^{2+} detection. In the design of the ligand, the acetate arms have been replaced by butylacetamide arms to slow down the water exchange rate of the molecule directly coordinated to the Eu^{3+} center [114]. The CEST changes observed upon Zn^{2+} binding were explained by an acceleration of the proton exchange, or by the possible presence of a H_2O molecule coordinated to Zn^{2+} which could be partially deprotonated at neutral pH. Owing to its proximity to the Eu^{3+} center, it could catalyze a prototropic exchange between the Eu^{3+} water molecule and the bulk solvent. Although the underlying mechanism has not been clearly identified, the system has been estimated to be able to detect changes in the concentration of Zn^{2+} ranging from 5 nM to 0.12 μM.

12.4.3 Probes responsive to enzymes

The detection of enzymatic activity by MRI is a particularly active field of research since the presence of enzymatic reactions in tissues can provide the signature of a given disease. Indeed, the importance of mis-regulated enzymatic activity has been established in the process of tumor formation, growth, and metastasis. Furthermore enzyme targeting offers the advantage of an improved sensitivity and selectivity compared with other biomarkers. Indeed, the poor sensitivity of MRI can be overcome because a relatively low concentration of the enzyme can catalytically convert a high concentration of MRI contrast agent into its activated form. Secondly, the specificity of enzymatic reactions is usually very high, which means that the observed changes

in the contrast can be unambiguously attributed to the targeted enzyme. The purpose here is not to give an exhaustive overview of enzyme-activated MRI contrast agents, but to select a few examples of complexes to highlight the specificity of ligand design when targeting enzymes.

12.4.3.1 Small Gd^{3+} chelates

First, a change in the hydration number of Gd^{3+} has been exploited in the example of a GdDO3A derivative, GdDO3A-GAD (GAD = glutamic acid decarboxylase) (Scheme 12.8) which contains two glutamate moieties [115]. These two units are responsible for a marked reduction of Gd^{3+} hydration state with respect to the parent GdDO3A complex. Through the action of GAD the complex exhibits an enhanced relaxivity. The evidence that the observed relaxation enhancement is the result of the specific GAD enzymatic activity relies on the observation of a "quenching" effect associated with the presence of chelidamic acid, a well-known inhibitor of GAD activity. The release of CO_2 from the complex after the action of GAD leads to a complex with an increased hydration number, and also with a residual positive charge. It is hypothesized that this new complex can interact with macromolecular structures present in the GAD protein preparation.

Historically, the first enzymatically responsive contrast agent was based on steric hindrance preventing water access to the Gd^{3+} ion. It was used to detect β-glucosidase [116, 117]. It is composed of a GdDO3A, GdEgadMe, bearing a galactopyranose residue (hindering Gd^{3+} from water) (Scheme 12.8). In the presence of the enzyme, the sugar moiety is cleaved from the complex, opening the access of water molecules to Gd^{3+}. This enzymatic reaction results in an increase of relaxivity, and an irreversible activation of the agent. This agent has been successfully used to detect β-galactosidase messenger ribonucleic acid expression in living *Xenopus laevis* embryos.

Changes in the rotational correlation times have also been used to detect enzymes, exploiting the differences in protein binding affinity following enzymatic cleavage. For example, GdEnz1 (Scheme 12.8) can be cleaved by a human carboxypeptidase B, thrombin-activatable fibrinolysis inhibitor [118], an enzyme implicated in thrombotic disease. The agent is composed of four moieties: a masking group (three lysine residues), an HSA binding group, a glycine linker, and the paramagnetic complex GdDTPA. Before enzymatic reaction, the complex has very poor affinity for HSA, while after enzymatic reaction the HSA affinity, thus the relaxivity, is improved. The origin of the relaxivity increase is the slower rotation for the protein-bound supramolecular adduct. Contrast agents sensitive to enzymatic polymerization and/or oxidation have been studied with the idea that the contrast agent can be activated on-site through enzyme-mediated oxidation, resulting in the formation of highly reactive species and subsequent oligomerization of the probe. GdDTPA-diTyr bearing tyramide and hydroxytryptamide moieties were used for peroxidase and tyrosinase imaging (Scheme 12.8). Following the enzymatic reaction, a net increase in longitudinal relaxivity explained by the slower rotational correlation time of the oligomer compared with the monomer was observed [119, 120]. The replacement of the hydroxytyramide moiety by a 5-hydroxytryptamide-(serotonin) moiety enables imaging of myeloperoxidase (MPO), an enzyme secreted by leukocytes during inflammation. The covalent GdDOTA-serotonin conjugate was efficiently polymerized in the presence of MPO resulting in a 70–100% increase in relaxivity, and the MPO activity could be demonstrated in a model tissue-like system [121]. MPO in living animals has also been tracked non-invasively during stroke [122].

Finally, solubility changes have been exploited to design enzyme-responsive contrast agents. The idea is to change the solubility of the contrast agent upon the action of the enzyme. For example, a GdDOTA complex bearing an alkyl chain is linked to a solubility switch (peptide sequence) and to a poly(ethylene glycol) (PEG) chain. The switch is efficiently cleavable by the proinvasive enzyme matrix metalloproteinase-2, decreasing the solubility and the relaxivity of the resulting complex. The complex was successfully tested in an animal model bearing two tumors with different levels of enzyme activity [123, 124].

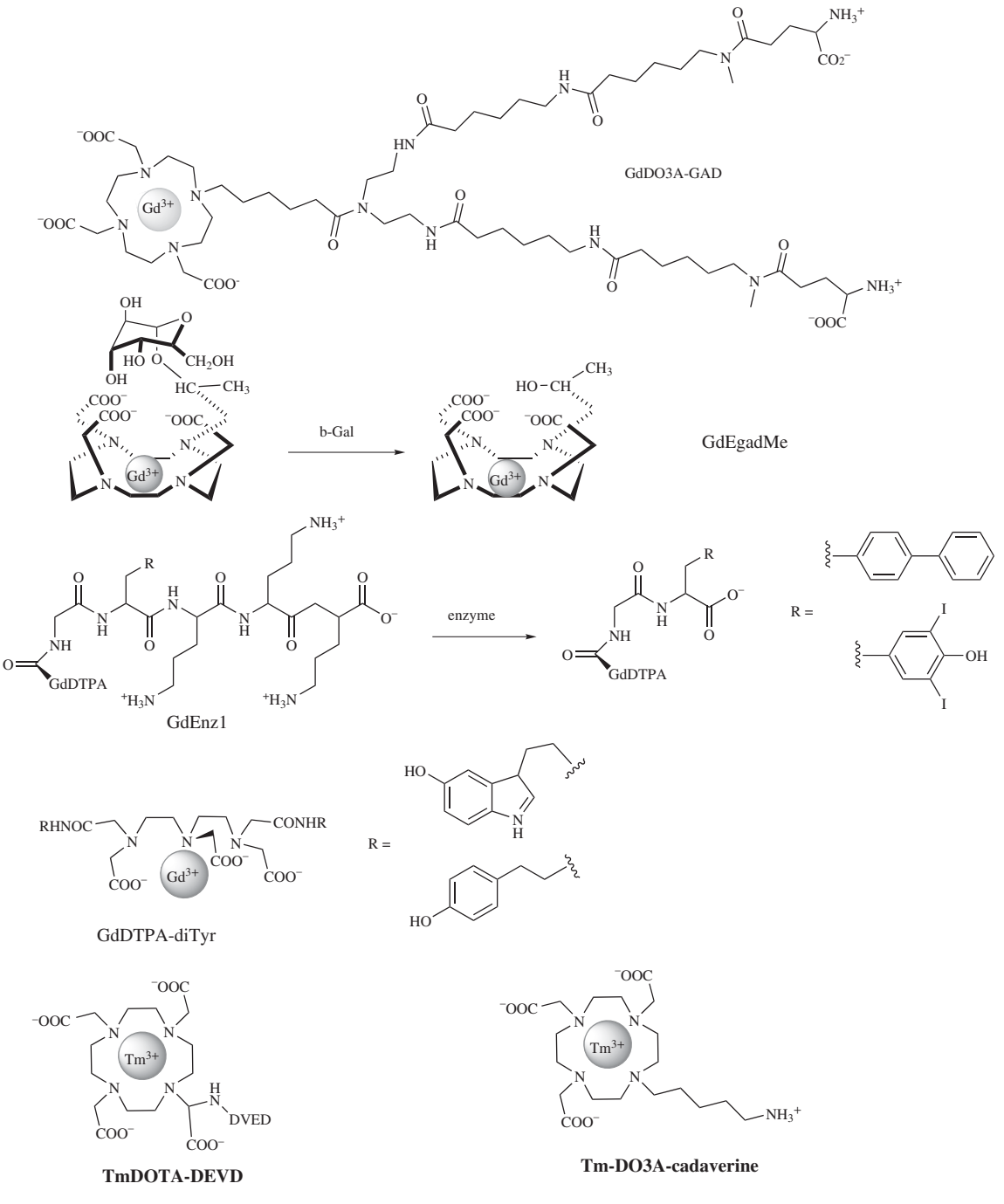

Scheme 12.8 *Ln^{3+} complexes responsive to enzymatic activity*

12.4.3.2 CEST agents

Proteases are particularly interesting targets for PARACEST agents as the conversion of an amide into an amine will affect the CEST properties of the agent by changing the chemical exchange rate of the amide/amine group and water. A probe based on a Tm-DOTA unit with a peptide substrate of Caspase-3, DEDV (Asp-Glu-Val-Asp), TmDOTA-DEVD (Scheme 12.8) was designed [125, 126]. Following the enzymatic cleavage, the CEST effect originating from the amide proton disappears due to the hydrolysis of the amide bond. The agent shows a good selectivity for Caspase-3 over Caspase-8, with a good sensitivity (up to nanomolar detection of the enzyme) at physiological pH and temperature, and the enzyme can be detected within the 15 minutes time frame of typical MRI studies. Recently, a CEST agent that detects the catalytic activity of transglutaminase (TGase), which creates a covalent bond between the agent and the side chain of a glutamine amino acid residue, has been designed [127]. The conjugation of the CEST agent (Tm-DO3A-cadaverine, Scheme 12.8) to a protein's glutamine side chain by TGase converts an amine into an amide that generates the CEST effect. The MR frequencies and amplitude of the CEST effect were found to be dependent upon the protein sequence, which demonstrated the sensitivity of CEST agents to ligand conformation.

In a different design, an Ln^{3+} complex has been linked to the enzyme-specific substrate via a self-immolative unit (Figure 12.8). This offers the advantage that the substrate can be modified at will without changing the CEST properties of the agent [128, 129]. With a benzyl carbamate moiety as the self-immolative unit, the substrate can be any enzyme-recognized moiety capable of transitionally reducing the electron donor capabilities of the phenyl substituent. The enzymatic cleavage of the substrate initiates an electron cascade and leads to the spontaneous elimination of the spacer. This results in the appearance of a

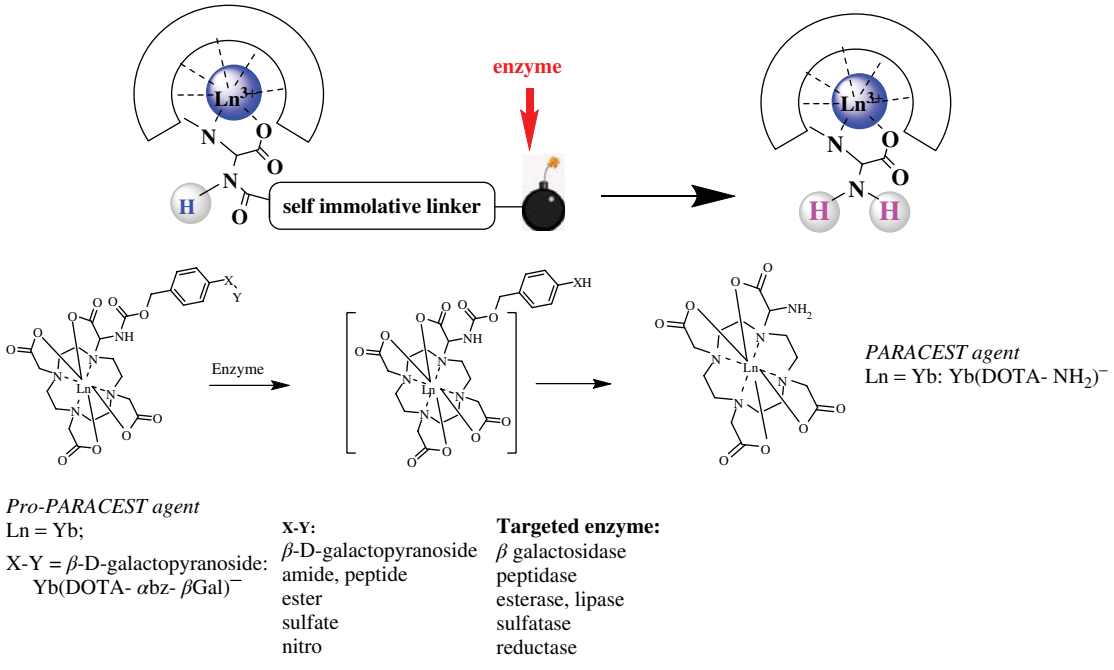

Figure 12.8 *A PARACEST self-immolative contrast agent: the enzyme specifically reacts with the substrate leading to the spontaneous elimination of the self-immolative linker*

PARACEST effect attributed to the exchange of the amine protons. So, the system works as a switch *off–on* probe which can be a further advantage in practical *in vivo* or *in vitro* applications.

12.5 Conclusions

Ligand design is primordial for creating non-toxic and high efficiency MRI agents based on lanthanide complexes. To ensure non-toxicity, the ligand has to form complexes of high thermodynamic stability and kinetic inertness. For Gd^{3+} complexes as relaxation agents, the most obvious approach to increase proton relaxivity is to slow down rotation by increasing molecular size and simultaneously avoiding internal flexibility. In an effort parallel to the increase of the rotational correlation time, one has to increase the water exchange rate as well.

Doubling the inner sphere contribution to the proton relaxivity can be achieved with bishydrated Gd^{3+} chelates. PARACEST agents have to possess protons in slow to intermediate exchange with bulk water. Their unique features, in particular the frequency encoding, make them very promising for molecular imaging.

A large number of responsive Gd^{3+}-based or PARACEST MRI probes with potential utility for molecular imaging applications have been reported. So far only a few of them have progressed to *in vivo* tests. Work is in progress to extend applications of these agents to living animals, as well as on exploring new ways of creating molecular MRI probes in order to meet requirements such as higher specificity, lower detection limits, and quantitative imaging.

Abbreviations

DTPA	Diethylenetriaminepentaacetic acid
DOTA	1,4,7,10-tetraazacyclododecane-1,4,7,10-tetraacetic acid
DOTMA	(1R,4R,7R,10R)-α, α′, α″, α‴-tetramethyl-1,4,7,10-tetraazacyclododecane-1,4,7,10-tetraacetic acid
DOTAM	DOTA tetrAMide
SPECT	Single Photon Emission Computed Tomography
PET	Positron Emission Tomography
PAMAM	Poly (AMido AMine)
PEG	PolyEthylene Glycol
DMF	DiMethyl Formamide
TNTU	2-(endo-5-norbornene-2.3-dicarboxylimide)-1,1,3,3-tetramethyluronium tetrafluoroborate
DIPEA	*N*,*N*-Diisopropylethylamine

References

1. Caravan, P., Ellison, J.J., McMurry, T.J. and Lauffer, R.B. (1999) Gadolinium(III) chelates as MRI contrast agents: structure, dynamics, and applications. *Chem. Rev.*, **99** (9), 2293–2352.
2. Merbach, A.E., Helm, L. and Toth, E. (2013) *The Chemistry of Contrast Agents in Medical Magnetic Resonance Imaging*, 2nd edn, John Wiley & Sons, Ltd, Chichester.
3. Drahos, B., Lukes, I. and Toth, E. (2012) Manganese(II) complexes as potential contrast agents for MRI. *Eur. J. Inorg. Chem.*, **2012** (12), 1975–1986.
4. Woods, M., Woessner, D.E. and Sherry, A.D. (2006) Paramagnetic lanthanide complexes as PARACEST agents for medical imaging. *Chem. Soc. Rev.*, **35**, 500–511.

5. E. Terreno, W. Dastru, D. Delli Castelli, et al. Advances in metal-based probes for MR molecular imaging applications, *Curr. Med. Chem.*, **17**(31), 3684-3700 (2010).
6. Sosnovik, D.E. and Weissleder, R. (2007) Emerging concepts in molecular MRI. *Curr. Opin. Biotechnol.*, **18**, 4–10.
7. Kubicek, V. and Toth, E. (2009) Design and function of metal complexes as contrast agents in MRI, in *Advances in Inorganic Chemistry*, Metal Ion Controlled Reactivity, vol. **61** (eds R. Eldik van, and C.D. Hubbard), Elsevier, pp. 63–129.
8. J.C. Jocher, E.G. Moore, S. Avedano, et al. 1,2-Hydroxypyridonates as contrast agents for magnetic resonance imaging: TREN-1,2-HOPO, *Inorg. Chem.*, **46**, 9182-9191 (2007).
9. S. Aime, L. Calabi, C. Cavallotti, et al. [Gd-AAZTA] -: a new structural entry for an improved generation of MRI contrast agents, *Inorg. Chem.*, **43** 7588- 7590 (2004).
10. L. Pellegatti, J. Zhang, B. Drahos, et al. Pyridine-based lanthanide complexes: towards bimodal agents operating as near infrared luminescent and MRI reporters, *Chem. Commun.*, (48), 6591-6593 (2008).
11. S. Hajela, M. Botta, S. Giraudo, et al. A tris-hydroxymethyl-substituted derivative of Gd-TREN-Me-3,2-HOPO: an MRI relaxation agent improved efficiency, *J. Am. Chem. Soc.*, **122**, 11228-11229 (2000).
12. Pierre, V.C., Botta, M., Aime, S. and Raymond, K.N. (2006) Tuning the coordination number of hydroxypyridonate-based gadolinium complexes: implications for MRI contrast agents. *J. Am. Chem. Soc.*, **128**, 5344–5345.
13. J.C. Jocher, M. Botta, S. Avedano, et al. Optimized relaxivity and stability of [Gd(H(2,2)-1,2-HOPO)(H2O)] for use as an MRI contrast agent, *Inorg. Chem.*, **46**, 4796-4798 (2007).
14. Z. Baranyai, F. Uggeri, G.B. Giovenzana, et al. Equilibrium and kinetic properties of the lanthanoids(III) and various divalent metal complexes of the heptadentate ligand AAZTA, *Chem. Eur. J.*, **15**(7), 1696-1705 (2009).
15. Tircso, G., Kovacs, Z. and Sherry, A.D. (2006) Equilibrium and formation/dissociation kinetics of some LnIIIPCTA complexes. *Inorg. Chem.*, **45**, 9269–9280.
16. J.B. Livramento, A. Sour, A. Borel, et al. A starburst-shaped heterometallic compound incorporating six densely packed Gd3+ ions, *Chem. Eur. J.*, **12**(4), 989-1003 (2006).
17. Costa, J., Toth, E., Helm, L. and Merbach, A.E. (2005) Dinuclear, bishydrated Gd-III polyaminocarboxylates with a rigid xylene core display remarkable proton relaxivities. *Inorg. Chem.*, **44** (13), 4747–4755.
18. C.S. Bonnet, F. Buron, F. Caillé, et al. Pyridine-based lanthanide complexes combining MRI and NIR luminescence activities, *Chem. Eur. J.*, **18**(5), 1419-1431 (2012).
19. J.B. Livramento, C. Weidensteiner, M.I. Prata, et al. First in vivo MRI assessment of a self-assembled metallostar compound endowed with a remarkable high field relaxivity, *Contrast Media Mol. Imaging*, **1**(1), 30-39 (2006).
20. P.L. de Sousa, J.B. Livramento, L. Helm , et al. In vivo MRI assessment of a novel Gd-III-based contrast agent designed for high magnetic field applications, *Contrast Media Mol. Imaging*, **3**(2), 78-85 (2008).
21. S. Aime, M. Botta, J.I. Bruce, et al. Modulation of the water exchange rates in [Gd-DO3A] complex by formation of ternary complexes with carboxylate ligands, *Chem. Commun.*, 115-116 (2001).
22. S. Aime, E. Gianolio, Terreno, et al. Ternary Gd(III)L-HSA adducts: evidence for the replacement of inner-sphere water molecules by coordinating groups of the protein. Implications for the design of contrast agents for MRI, *J. Biol. Inorg. Chem.*, **5**, 488-497 (2000).
23. Raymond, K.N. and Pierre, V.C. (2005) Next generation, high relaxivity gadolinium MR1 agents. *Bioconjugate Chem.*, **16** (1), 3–8.
24. Aime, S. and Barge, A. (1999) NMR, relaxometric, and structural studies of the hydration and exchange dynamics of cationic lanthanide complexes of macrocyclic tetraamide ligands. *J. Am. Chem. Soc.*, **121** (24), 5762–5771.
25. Micskei, K., Helm, L., Powell, D.H. *et al*. (1993) Water exchange on [Gd(H2O)8]3+ and [Gd(PDTA)(H2O)2]- in aqueous solution: a variable-pressure, -temperature, and -magnetic field 17O NMR study. *Magn. Reson. Chem.*, **31**, 1011–1020.
26. Helm, L. and Merbach, A.E. (2005) Inorganic and bioinorganic solvent exchange mechanisms. *Chem. Rev.*, **105**, 1923–1959.
27. Laus, S., Ruloff, R., Toth, E. and Merbach, A.E. (2003) Gd-III complexes with fast water exchange and high thermodynamic stability: potential building blocks for high-relaxivity MRI contrast agents. *Chem. Eur. J.*, **9** (15), 3555–3566.
28. R. Ruloff, E. Toth, R. Scopelliti, et al. Accelerating water exchange for Gd-III chelates by steric compression around the water binding site, *Chem. Commun.*, (22), 2630-2631 (2002).

29. M.F. Ferreira, A.F. Martins, J.A. Martins, et al. Gd(DO3A-N-alpha-aminopropionate): a versatile and easily available synthon with optimized water exchange for the synthesis of high relaxivity, targeted MRI contrast agents, *Chem. Commun.*, 42, 6475-6477 (2009).
30. Hermann, P., Kotek, J., Kubicek, V. and Lukes, I. (2008) Gadolinium(III) complexes as MRI contrast agents: ligand design and properties of the complexes. *Dalton Trans.*, (23), 3027–3047.
31. J.B. Livramento, L. Helm, A. Sour, et al. A benzene-core trinuclear Gd-III complex: towards the optimization of relaxivity for MRI contrast agent applications at high magnetic field, *Dalton Trans.*, (9), 1195-1202 (2008).
32. M.K. Thompson, M. Botta, S. Aime, et al. A highly stable Gd complex with a fast, associative mechanism of water exchange, *J. Am. Chem. Soc.*, **125**, 14274-14275 (2003).
33. Dunand, F.A., Dickins, R.S., Parker, D. and Merbach, A.E. (2001) Towards rational design of fast water-exchanging Gd(dota-like) contrast agents? Importance of the M/m ratio. *Chem. Eur. J.*, **7** (23), 5160–5167.
34. Rudovsky, J. and Cigler, P. (2005) Lanthanide(III) complexes of a mono (methylphosphonate) analogue of H(4)dota: the influence of protonation of the phosphonate moiety on the TSAP/SAP isomer ratio and the water exchange rate. *Chem. Eur. J.*, **11** (8), 2373–2384.
35. Woods, M., Botta, M., Avedano, S. *et al*. (2005) Towards the rational design of MRI contrast agents: a practical approach to the synthesis of gadolinium complexes that exhibit optimal water exchange. *Dalton Trans.*, (24), 3829–3837.
36. K.J. Miller, A.A. Saherwala, B.C. Webber, et al. The population of SAP and TSAP isomers in cyclen-based lanthanide(III) chelates is substantially affected by solvent, *Inorg. Chem.*, **49**(19), 8662-8664 (2010).
37. G. Tircso, B.C. Webber, B.E. Kucera, et al. Analysis of the conformational behavior and stability of the SAP and TSAP isomers of lanthanide(III) NB-DOTA-type chelates, *Inorg. Chem.*, **50**(17), 7966-7979 (2011).
38. Dunand, F.A., Aime, S. and Merbach, A.E. (2000) First 17O NMR observation of coordinated water on both isomers of [Eu(DOTAM)(H2O)]3+: a direct access to water exchange and its role in the isomerization. *J. Am. Chem. Soc.*, **122**, 1506–1512.
39. E. Toth, D. Pubanz, S. Vauthey, et al. The role of water exchange in attaining maximum relaxivities for dendrimeric MRI contrast agents, *Chem. Eur. J.*, **2**(12), 1607-1615 (1996).
40. G.M. Nicolle, E. Toth, H. Schmitt-Willich, et al. The impact of rigidity and water exchange on the relaxivity of a dendritic MRI contrast agent, *Chem. Eur. J.*, **8**(5), 1040-1048 (2002).
41. G.M. Nicolle, E. Toth, K.-P. Eisenwiener, et al. From monomers to micelles: investigation of the parameters influencing proton relaxivity, *J. Biol. Inorg. Chem.*, **7**(7-8), 757-769 (2002).
42. S. Torres, J.A. Martins, J.P. Andre, et al. Supramolecular assembly of an amphiphilic Gd-III chelate: tuning the reorientational correlation time and the water exchange rate, *Chem. Eur. J.*, **12**(3), 940-948 (2006).
43. P. Caravan, J.C. Amedio, Jr,, S.U. Dunham, et al. When are two waters worse than one? Doubling the hydration number of a Gd-DTPA derivative decreases relaxivity, *Chem. Eur. J.*, **11**, 5866-5874 (2005).
44. S. Aime, M. Botta,S. Geninatti Crich, et al. Towards MRI contrast agents of improved efficacy. NMR relaxometric investigations of the binding interaction to HSA of a novel heptadentate macrocyclic triphosphonate Gd(III) complex, *J. Biol. Inorg. Chem.*, **2**, 470-479 (1997).
45. Caravan, P., Farrar, C.T., Frullano, L. and Uppal, R. (2009) Influence of molecular parameters and increasing magnetic field strength on relaxivity of gadolinium- and manganese-based T1 contrast agents. *Contrast Media Mol. Imaging*, **4** (2), 89–100.
46. Caravan, P. (2006) Strategies for increasing the sensitivity of gadolinium based MRI contrast agents. *Chem. Soc. Rev.*, **35**, 512–523.
47. Caravan, P. (2009) Protein-targeted gadolinium-based Magnetic Resonance Imaging (MRI) contrast agents: design and mechanism of action. *Acc. Chem. Res.*, **42** (7), 851–862.
48. Villaraza, A.J.L., Bumb, A. and Brechbiel, M.W. (2010) Macromolecules, dendrimers, and nanomaterials in magnetic resonance imaging: the interplay between size, function, and pharmacokinetics. *Chem. Rev.*, **110** (5), 2921–2959.
49. Toth, E., Helm, L., Kellar, K. and Merbach, A.E. (1999) Gd(DTPA-bisamide)alkyl copolymers: a hint for the formation of MRI contrast agents with very high relaxivity. *Chem. Eur. J.*, **5** (4), 1202–1211.
50. Accardo, A., Tesauro, D., Aloj, L. *et al*. (2009) Supramolecular aggregates containing lipophilic Gd(III) complexes as contrast agents in MRI. *Coord. Chem. Rev.*, **253** (17-18), 2193–2213.

51. W.J. Mulder, G.J. Strijkers, G.A. van Tilborg, et al. Nanoparticulate assemblies of amphiphiles and diagnostically active materials for multimodality imaging, *Acc. Chem. Res.*, **42**(7), 904-914 (2009).
52. Helm, L. (2006) Relaxivity in paramagnetic systems: theory and mechanisms. *Prog. NMR Spectrosc.*, **49**, 45–64.
53. Kielar, F., Tei, L., Terreno, E. and Botta, M. (2010) Large relaxivity enhancement of paramagnetic lipid nanoparticles by restricting the local motions of the Gd(III) chelates. *J. Am. Chem. Soc.*, **132** (23), 7836–7837.
54. Pautler, R.G. and Fraser, S.E. (2003) The year(s) of the contrast agent – micro-MRI in the new millennium. *Curr. Opin. Immunol.*, **15**, 385–392.
55. A.G. van der Kolk, J. Hendrikse, J.J. Zwanenburg , et al. Clinical applications of 7 T MRI in the brain, *Eur. J. Radiol.*, **82**(5), 708-718 (2013).
56. Ruloff, R., van , G., Koten, A.E. and Merbach (2004) Novel heteroditopic chelate for self-assembled gadolinium(III) complex with high relaxivity. *Chem. Commun.*, 842–843.
57. Costa, J., Ruloff, R., Burai, L. *et al*. (2005) Rigid MIIL2Gd2III (M = Fe, Ru) complexes of a terpyridine-based heteroditopic chelate: a class of candidates for MRI contrast agents. *J. Am. Chem. Soc.*, **127**, 5147–5157.
58. T.N. Parac-Vogt, L.V. Elst, K. Kimpe, et al. Pharmacokinetic and in vivo evaluation of a self-assembled gadolinium(III)-iron(II) contrast agent with high relaxivity, *Contrast Media Mol. Imaging*, **1**(6), 267-278 (2006).
59. J. Paris, C. Gameiro, V. Humblet, et al. Auto-assembling of ditopic macrocyclic lanthanide chelates with transition-metal ions. Rigid multimetallic high relaxivity contrast agents for magnetic resonance imaging, *Inorg. Chem.*, **45**(13), 5092-5102 (2006).
60. J.B. Livramento, E. Toth, A. Sour, et al. High relaxivity confined to a small molecular space: a metallostar-based, potential MRI contrast agent, *Angew. Chem. Int. Ed.*, **44**(10), 1480-1484 (2005).
61. L. Moriggi, A. Aebischer,C. Cannizzo, et al. A ruthenium-based metallostar: synthesis, sensitized luminescence and H-1 relaxivity, *Dalton Trans.*, (12), 2088-2095 (2009).
62. Wolff, S.D. and Balaban, R.S. (1989) Magnetization Transfer Contrast (MTC) and tissue water proton relaxation in vivo. *Magn. Reson. Med.*, **10** (1), 135–144.
63. S.R. Zhang, M. Merritt, D.E. Woessner, et al. PARACEST agents: modulating MRI contrast via water proton exchange, *Acc. Chem. Res.*, **36**(10), 783-790 (2003).
64. Woessner, D.E., Zhang, S.R., Merritt, M.E. and Sherry, A.D. (2005) Numerical solution of the Bloch equations provides insights into the optimum design of PARACEST agents for MRI. *Magn. Reson. Med.*, **53** (4), 790–799.
65. Soesbe, T.C., Wu, Y.K. and Sherry, A. (2013) Advantages of paramagnetic Chemical Exchange Saturation Transfer (CEST) complexes having slow to intermediate water exchange properties as responsive MRI agents. *NMR Biomed.*, **26** (7), 829–838.
66. Aime, S., Delli Castelli, D. and Terreno, E. (2002) Novel pH-reporter MRI contrast agents. *Angew. Chem. Int. Ed.*, **41** (22), 4334–4336.
67. C. Adair, M. Woods, P. Zhao, et al. Spectral properties of a bifunctional PARACEST europium chelate: an intermediate for targeted imaging applications, *Contrast Media Mol. Imaging*, **2**(1), 55-58 (2007).
68. P.M. Winter, K.J. Cai, J. Chen, et al. Targeted PARACEST nanoparticle contrast agent for the detection of fibrin, *Magn. Reson. Med.*, **56**(6), 1384-1388 (2006).
69. O. Vasalatiy, R.D. Gerard, P. Zhao, et al. Labeling of adenovirus particles with PARACEST agents, *Bioconjugate Chem.*, **19**(3), 598-606 (2008).
70. M.M. Ali, M. Woods, E.H. Suh, et al. Albumin-binding PARACEST agents, *J. Biol. Inorg. Chem.*, **12**(6), 855-865 (2007).
71. S. Aime, D. Delli Castelli, E. Terreno. Highly sensitive MRI chemical exchange saturation transfer agents using liposomes,. *Angew. Chem. Int. Ed.*, **44**(34), 5513-5515 (2005).
72. J.M. Zhao, Y.E. Har-El, M.T. McMahon, et al. Size-induced enhancement of chemical exchange saturation transfer (CEST) contrast in liposomes, *J. Am. Chem. Soc.*, **130**(15), 5178-5184 (2008).
73. E. Terreno, C. Cabella, C. Carrera, et al. From spherical to osmotically shrunken paramagnetic liposomes: an improved generation of LIPOCEST MRI agents with highly shifted water protons, *Angew. Chem. Int. Ed.*, **46**(6), 966-968 (2007).
74. Castelli, D.D., Terreno, E., Longo, D. and Aime, S. (2013) Nanoparticle-based chemical exchange saturation transfer (CEST) agents. *NMR Biomed.*, **26** (7), 839–849.

75. Shen, C. and New, E.J. (2013) Promising strategies for Gd-based responsive magnetic resonance imaging contrast agents. *Curr. Opin. Chem. Biol.*, **17** (2), 158–166.
76. Bonnet, C.S. and Toth, E. (2010) Smart MR imaging agents relevant to potential neurologic applications. *Am. J. Neuroradiol.*, **31** (3), 401–409.
77. Bonnet, C.S., Tei, L., Botta, M. and Toth, E. (2013) Responsive probes, in *The Chemistry of Contrast Agents in Medical Magnetic Resonance Imaging* (eds A.E. Merbach, L. Helm and E. Toth), John Wiley & Sons, Ltd, Chichester, pp. 343–385.
78. L.M. De Leon-Rodriguez, A.J.M. Lubag, C.R. Malloy, et al. Responsive MRI agents for sensing metabolism in vivo, *Acc. Chem. Res.*, **42**(7), 948-957 (2009).
79. Geraldes, C. and Laurent, S. (2009) Classification and basic properties of contrast agents for magnetic resonance imaging. *Contrast Media Mol. Imaging*, **4** (1), 1–23.
80. Gillies, R.J., Raghunand, N., Karczmar, G.S. and Bhujwalla, Z.M. (2002) MRI of the tumor microenvironment. *J. Magn. Reson. Imaging*, **16** (4), 430–450.
81. Chesler, M. (2003) Regulation and modulation of pH in the brain. *Physiol. Rev.*, **83** (4), 1183–1221.
82. M.P. Lowe, D. Parker, O. Reany, et al. pH-dependent modulation of relaxivity and luminescence in macrocyclic gadolinium and europium complexes based on reversible intramolecular sulfonamide ligation, *J. Am. Chem. Soc.*, **123**(31), 7601-7609 (2001).
83. E. Gianolio, R. Napolitano, F. Fedeli, et al. Poly-[small beta]-cyclodextrin based platform for pH mapping via a ratiometric 19F/1H MRI method, *Chem. Commun.*, (40), 6044-6046 (2009).
84. E. Gianolio, L. Maciocco, D. Imperio, et al. Dual MRI-SPECT agent for pH-mapping, *Chem. Commun.*, **47**(5), 1539-1541 (2011).
85. E. Gianolio, S. Porto, R. Napolitano, et al. Relaxometric investigations and MRI evaluation of a liposome-loaded pH-responsive gadolinium(III) complex, *Inorg. Chem.*, **51**(13), 7210-7217 (2012).
86. Okada, S., Mizukami, S. and Kikuchi, K. (2012) Switchable MRI contrast agents based on morphological changes of pH-responsive polymers. *Bioorg. Med. Chem.*, **20** (2), 769–774.
87. Aime, S., Fedeli, F., Sanino, A. and Terreno, E. (2006) A R2/R1 ratiometric procedure for a concentration-independent, pH-responsive, Gd(III)-based MRI agent. *J. Am. Chem. Soc.*, **128** (35), 11326–11327.
88. F.K. Kalman, M. Woods, P. Caravan, et al. Potentiometric and relaxometric properties of a gadolinium-based MRI contrast agent for sensing tissue pH, *Inorg. Chem.*, **46**(13), 5260-5270 (2007).
89. N. Raghunand, C. Howison, A.D. Sherry, et al. Renal and systemic pH imaging by contrast-enhanced MRI, *Magn. Reson. Med.*, **49**(2), 249-257 (2003).
90. M.L. Garcia-Martin, G.V. Martinez, N. Raghunand, et al. High resolution pHe imaging of rat glioma using pH-dependent relaxivity, *Magn. Reson. Med.*, **55**(2), 309-315 (2006).
91. L. Frullano, C. Catana, T. Benner, et al. Bimodal MR-PET agent for quantitative pH imaging, *Angew. Chem. Int. Ed.*, **49**(13), 2382-2384 (2010).
92. M. Meser Ali, M. Woods, P. Caravan, et al. Synthesis and relaxometric studies of a dendrimer-based pH-responsive MRI contrast agent, *Chem. Eur. J.*, **14**(24), 7250-7258 (2008).
93. S. Aime, A. Barge, D. Delli Castelli, et al. Paramagnetic Lanthanide(III) complexes as pH-sensitive chemical exchange saturation transfer (CEST) contrast agents for MRI applications, *Magn. Reson. Med.*, **47**(4), 639-648 (2002).
94. Delli Castelli, D., Terreno, E. and Aime, S. (2011) YbIII-HPDO3A: a dual pH- and temperature-responsive CEST agent. *Angew. Chem. Int. Ed.*, **50** (8), 1798–1800.
95. Li, W.H., Fraser, S.E. and Meade, T.J. (1999) A calcium-sensitive magnetic resonance imaging contrast agent. *J. Am. Chem. Soc.*, **121** (6), 1413–1414.
96. W.H. Li, G. Parigi, M. Fragai, et al. Mechanistic studies of a calcium-dependent MRI contrast agent, *Inorg. Chem.*, **41**(15), 4018-4024 (2002).
97. Tsien, R.Y. (1980) New calcium indicators and buffers with high selectivity against magnesium and protons: design, synthesis and properties of prototype structures. *Biochemistry*, **19**, 2396–2404.
98. G. Angelovski, P. Fouskova, I. Mamedov, et al. Smart magnetic resonance imaging agents that sense extracellular calcium fluctuations, *ChemBioChem*, **9**(11), 1729-1734 (2008).

99. Mishra, A., Logothetis, N.K. and Parker, D. (2011) Critical in vitro evaluation of responsive MRI contrast agents for calcium and zinc. *Chem. Eur. J.*, **17** (5), 1529–1537.
100. Hanaoka, K., Kikuchi, K., Urano, Y. and Nagano, T. (2001) Selective sensing of zinc ions with a novel magnetic resonance imaging contrast agent. *J. Chem. Soc., Perkin Trans. 2*, (9), 1840–1843.
101. K. Hanaoka, K. Kikuchi, Y. Urano, et al. Design and synthesis of a novel magnetic resonance imaging contrast agent for selective sensing of zinc ion, *Chem. Biol.*, **9**(9), 1027-1032 (2002).
102. Major, J.L., Parigi, G., Luchinat, C. and Meade, T.J. (2007) The synthesis and in vitro testing of a zinc-activated MRI contrast agent. *Proc. Natl. Acad. Sci. U.S.A.*, **104** (35), 13881–13886.
103. Que, E.L. and Chang, C.J. (2006) A smart magnetic resonance contrast agent for selective copper sensing. *J. Am. Chem. Soc.*, **128** (50), 15942–15943.
104. E.L. Que, E. Gianolio, S.L. Baker, et al. Copper-responsive magnetic resonance imaging contrast agents, *J. Am. Chem. Soc.*, **131**(24), 8527-8536 (2009).
105. E.L. Que, E. Gianolio, S.L. Baker, et al. A copper-activated magnetic resonance imaging contrast agent with improved turn-on relaxivity response and anion compatibility, *Dalton Trans.*, **39**(2), 469-476 (2010).
106. Que, E.L., New, E.J. and Chang, C.J. (2012) A cell-permeable gadolinium contrast agent for magnetic resonance imaging of copper in a Menkes disease model. *Chem. Sci.*, **3** (6), 1829–1834.
107. J. Henig, I. Mamedov, P. Fouskova, et al. Influence of calcium-induced aggregation on the sensitivity of aminobis(methylenephosphonate)-containing potential MRI contrast agents, *Inorg. Chem.*, **50**(14), 6472-6481 (2011).
108. V. Kubíček, T. Vitha, J. Kotek, et al. Towards MRI contrast agents responsive to Ca(II) and Mg(II) ions: metal-induced oligomerization of dota–bisphosphonate conjugates, *Contrast Media Mol. Imaging*, **5**(5), 294-296 (2010).
109. J. Luo, W.S. Li, P. Xu, et al. Zn2+ responsive bimodal magnetic resonance imaging and fluorescent imaging probe based on a gadolinium(III) complex, *Inorg. Chem.*, **51**(17), 9508-9516 (2012).
110. A.C. Esqueda, J.A. Lopez, G. Andreu-de-Riquer, et al. A new gadolinium-based MRI zinc sensor, *J. Am. Chem. Soc.*, **131**(32), 11387-11391 (2009).
111. Lubag, A.J.M., De Leon-Rodriguez, L.M., Burgess, S.C. and Sherry, A.D. (2011) Noninvasive MRI of beta-cell function using a Zn2+-responsive contrast agent. *Proc. Natl. Acad. Sci. U.S.A.*, **108** (45), 18400–18405.
112. L.M. De Leon-Rodriguez, A.J.M. Lubag, J.A. Lopez, et al. A second generation MRI contrast agent for imaging zinc ions in vivo, *Med. Chem. Commun.*, **3**(4), 480-483 (2012).
113. G. Angelovski, T. Chauvin, R. Pohmann, et al. Calcium-responsive paramagnetic CEST agents, *Bioorg. Med. Chem.*, **19**(3), 1097-1105 (2011).
114. Trokowski, R., Ren, J.M., Kalman, F.K. and Sherry, A.D. (2005) Selective sensing of zinc ions with a PARACEST contrast agent. *Angew. Chem. Int. Ed.*, **44** (42), 6920–6923.
115. R. Napolitano, G. Pariani, F. Fedeli, et al. Synthesis and relaxometric characterization of a MRI Gd-based probe responsive to glutamic acid decarboxylase enzymatic activity, *J. Med. Chem.*, **56**(6), 2466-2477 (2013).
116. A.Y. Louie, M.M. Huber, E.T. Ahrens, et al. In vivo visualization of gene expression using magnetic resonance imaging, *Nat. Biotechnol.*, **18**(3), 321-325 (2000).
117. Moats, R.A., Fraser, S.E. and Meade, T.J. (1997) A "Smart" magnetic resonance imaging agent that reports on specific enzymatic activity. *Angew. Chem., Int. Ed. Engl.*, **36** (7), 726–728.
118. A.L. Nivorozhkin, A.F. Kolodziej, P. Caravan, et al. Enzyme-activated Gd3+ magnetic resonance imaging contrast agents with a prominent receptor-induced magnetization enhancement, *Angew. Chem. Int. Ed.*, **40**(15), 2903-2906 (2001).
119. M. Querol, D.G. Bennett, C. Sotak, et al. A paramagnetic contrast agent for detecting tyrosinase activity, *ChemBioChem*, **8**(14), 1637-1641 (2007).
120. Querol, M., Chen, J.W., Weissleder, R. and Bogdanov, A. (2005) DTPA-bisamide-based MR sensor agents for peroxidase imaging. *Org. Lett.*, **7** (9), 1719–1722.
121. Chen, J.W., Pham, W., Weissleder, R. and Bogdanov, A. (2004) Human myeloperoxidase: a potential target for molecular MR imaging in atherosclerosis. *Magn. Reson. Med.*, **52** (5), 1021–1028.
122. M.O. Breckwoldt, J. W. Chen, L. Stangenberg, et al. Tracking the inflammatory response in stroke in vivo by sensing the enzyme myeloperoxidase, *Proc. Natl. Acad. Sci. U.S.A.*, **105**(47), 18584-18589 (2008).

123. B. Jastrzebska, R. Lebel, H. Therriault, et al. New enzyme-activated solubility-switchable contrast agent for magnetic resonance imaging: from synthesis to in vivo imaging, *J. Med. Chem.*, **52**(6), 1576-1581 (2009).
124. R. Lebel, B. Jastrzębska, H. Therriault, et al. Novel solubility-switchable MRI agent allows the noninvasive detection of matrix metalloproteinase-2 activity in vivo in a mouse model, *Magn. Reson. Med.*, **60**(5), 1056-1065 (2008).
125. Yoo, B. and Pagel, M.D. (2006) A PARACEST MRI contrast agent to detect enzyme activity. *J. Am. Chem. Soc.*, **128** (43), 14032–14033.
126. Yoo, B., Raam, M.S., Rosenblum, R.M. and Pagel, M.D. (2007) Enzyme-responsive PARACEST MRI contrast agents: a new biomedical imaging approach for studies of the proteasome. *Contrast Media Mol. Imaging*, **2** (4), 189–198.
127. Hingorani, D.V., Randtke, E.A. and Pagel, M.D. (2013) A catalyCEST MRI contrast agent that detects the enzyme-catalyzed creation of a covalent bond. *J. Am. Chem. Soc.*, **135** (17), 6396–6398.
128. T. Chauvin, P. Durand, M. Bernier , et al. Detection of enzymatic activity by PARACEST MRI: a general approach to target a large variety of enzymes, *Angew. Chem. Int. Ed.*, **47**(23), 4370-4372 (2008).
129. T. Chauvin, S. Torres, M. Bernier, et al. Lanthanide(III) complexes that contain a self-immolative arm: potential enzyme responsive contrast agents for magnetic resonance imaging, *Chem. Eur. J.*, **18**(5), 1408-1418 (2012).

13

Photoactivatable Metal Complexes and Their Use in Biology and Medicine

Tara R. deBoer-Maggard and Pradip K. Mascharak

Department of Chemistry and Biochemistry, University of California, 1156, High Street, Santa Cruz, CA, 95064, USA

13.1 Introduction

The structural and electronic features of the coordinating ligand(s) play critical roles in dictating the overall properties and function of a coordination complex. As a consequence, rational design of ligands is an absolute requirement for conferring selective properties to metal complexes intended for specific purposes. Initial inspiration for the rational design of coordination complexes was drawn from nature, with the general goal of elucidating biological processes through the use of model systems. A textbook example is the "picket fence" phorphyrin (Figure 13.1) designed by Collman and coworkers to model the reversible binding of molecular oxygen to ferrous iron center in myoglobin [1]. The ortho-substituted meso-tetraphenylporphyrin ligand in this complex provides a hydrophobic cavity that encourages the coordination of molecular oxygen, while protecting the active site from irreversible oxidation and dimerization. The spatial orientation of the auxiliary pivalamide groups (the pickets) around the porphyrin ring imposes the right structural environment essential for promoting and maintaining reversible oxygen binding at the iron(II) center.

The design of the ligand becomes even more important when one considers the use of a metal complex in a photochemical process because electronic transitions are strongly dependent on the energies of the molecular orbitals (MOs) comprised largely of ligand character. Absorption of light (photons) excites an electron from the ground state of a metal complex to an excited state. Photochemical reactions can occur through multiple pathways in the decay of excited state back to the ground state. For example, two of the fundamental electronic pathways that have been exploited in light-controlled generation of singlet oxygen ($^1O_2$) and triggered photodissociation of ligand(s) are represented in the energy diagrams shown in Figures 13.2 and 13.3 respectively. Generation of $^1O_2$ with a chemical source (photosensitizer) for photodynamic therapy

Ligand Design in Medicinal Inorganic Chemistry, First Edition. Edited by Tim Storr.

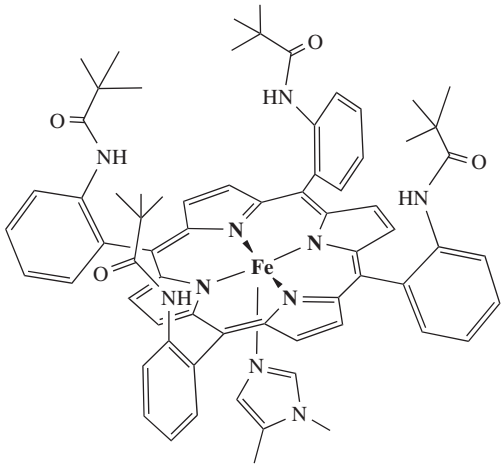

Figure 13.1 *Structure of the picket fence porphyrin designed to model reversible coordination of molecular oxygen to the Fe^{II} center of myoglogbin*

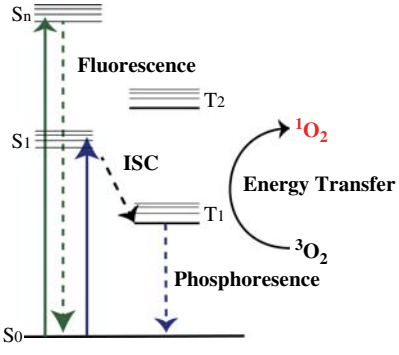

Figure 13.2 *Jablonksi diagram showing generation of $^1O_2$ from a photosensitizer*

(PDT) is based on a multiple-stage process [2–4]. Upon irradiation, an electron from a ground singlet state (S_0) of the photosensitizer is excited to a higher energy singlet state (S_n, n = 1, 2, …), and then undergoes a spin-forbidden intersystem crossing (ISC) to an excited triplet (T) state. This excited state finally interacts with the triplet ground state of molecular oxygen to generate $^1O_2$ (spin-allowed Type II photochemical reaction). Design of a coordination complex capable of generating $^1O_2$ therefore is heavily dependent on the electronic states of the ligand frame. Tetrapyrrolic macrocycles (much like the porphyrin ligand of Figure 13.1) are relatively efficient at undergoing ISC. Incorporation of a heavy metal center in such ligands also promotes ISC [5].

Photodissociation of ligands typically occurs through a metal-to-ligand charge transfer (MLCT) transition in which an electron from a metal-centered d-orbital is excited to an unoccupied anti-bonding orbital with significant ligand character (Figure 13.3) [6]. This electronic transition is most commonly observed in low-valent metal complexes derived from electron-accepting ligands such as polypyridine and α,α′-diimines. One such example is the octahedral ruthenium(II) polypyridine complex $[Ru(bpy)_3]^{2+}$ (**1**, bpy = 2,2′-bipyridine, Figure 13.4) which is often employed as a light-harvesting unit [7]. This parent unit

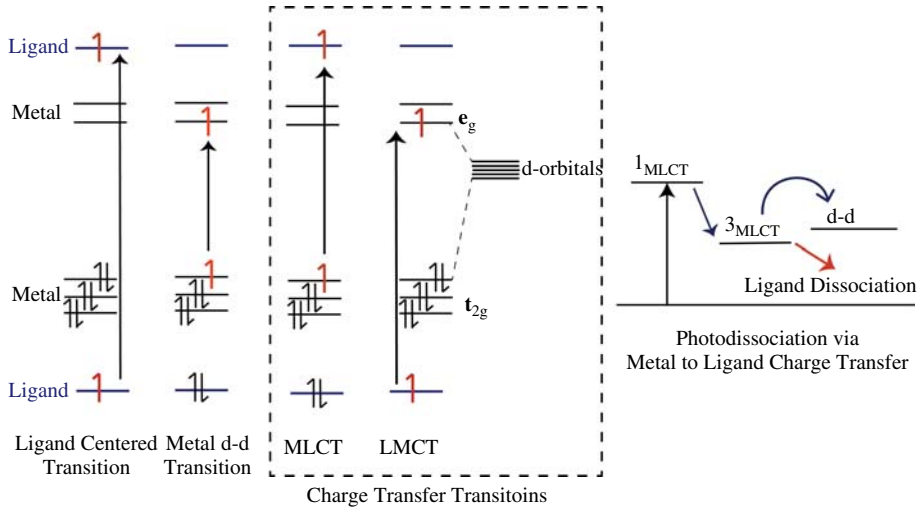

Figure 13.3 *Generalized energy diagram depicting the electronic transitions associated with photoactivation of metal complexes*

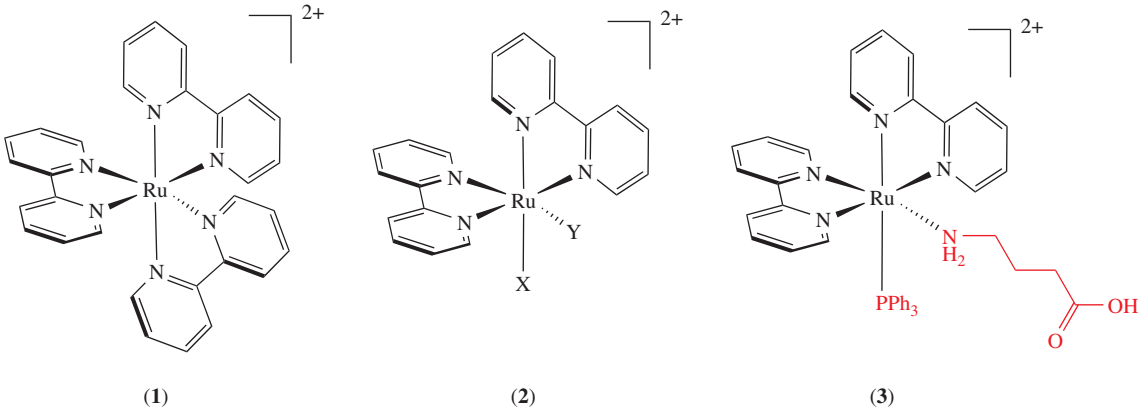

Figure 13.4 *Structures of $[Ru(bpy)_2(X)(Y)]^{2+}$ derivatives*

exhibits photodissociative properties when one of the bpy ligands is replaced with two monodentate ligands (X and Y), providing the general structure $[Ru(bpy)_2XY]^{n+}$ (**2**, Figure 13.4). The monodentate ligands in such "caged" complexes are released readily upon illumination. For example, $[Ru(bpy)_2(GABA)_2]^{2+}$ delivers the neurotransmitter γ-aminobutyric acid (GABA) to biological targets under the control of light [8]. When the sixth site of the $[Ru(bpy)_2(GABA)_2]^{2+}$ is substituted by triphenylphosphine, the π-accepting character of this ligand in $[Ru(bpy)_2(GABA)(PPh_3)]^{2+}$ (**3**, Figure 13.4) causes reduction of electron density at the metal center and results in a hypsochromic shift of the MLCT band and increased quantum efficiency (ϕ) of GABA release, from 0.03 to 0.21. This simple set of metal complexes exemplifies the ease with which a desired outcome (photo delivery of a neurotransmitter) can be readily achieved through the right choice of ligands and design of the coordination sphere.

During the past three decades, ligands of more intricate designs have been employed to synthesize photoactivatable metal complexes for their applications as photopharmaceuticals and as probes in biochemical investigations. Excellent accounts on these complexes can be found in several reviews published in recent years [9–13]. Instead of another catalog of research results in this area, this chapter emphasizes the power of a smart design approach that researchers have utilized to isolate photoactivatable metal complexes. In the following sections, selected examples have been highlighted to demonstrate how the choice of the ligands and alterations of their organic frameworks lead to the desired properties needed for specific uses. Sections of the coordination spheres of the complexes that emphasize special role(s) of ligand(s) are indicated in different hue throughout the chapter.

13.2 Cisplatin-inspired photoactivatable chemotherapeutics

The discovery of the chemotherapeutic effects of *cis*-$[PtCl_2(NH_3)_2]$ (cisplatin, **4**, Figure 13.5) provided the much-needed stimulus to metal-based chemotherapy agents as effective alternatives to standard chemotherapeutics. This simple coordination complex disrupts the DNA structure by forming intrastrand and interstrand cross-links, ultimately leading to cell death [14, 15]. Unfortunately, cisplatin also suffers from undesirable toxicity effects due to its systemic administration. Such effects could be circumvented with the use of light-activated non-toxic prodrugs that strictly deliver the actual cytotoxic agents under the control of light. This control provides site-specific activation of the therapeutic agent only at the malignant site. Design of such photoactivatable therapeutics requires the prodrug to be sensitive to low-energy light, ideal for optimal tissue penetrations (600–900 nm) [16]. It is also desirable that they remain completely non-active and non-toxic in the absence of light.

With the proven efficacy of cisplatin as an anticancer agent in mind, second- generation platinum-based complexes with built-in light control have been designed. These complexes are non-toxic and non-active prodrugs that undergo photochemical reduction and activation to induce Pt-nucleotide crosslinking of guanine residues within DNA. One such example is the octahedral platinum(IV) all-*trans* complex $[Pt(N_3)_2(OH)_2(NH_3)(py)]$ (py = pyridine) (**5**) designed by Sadler and coworkers (Figure 13.5) [17]. Although platinum(IV) diazido complexes are not sensitive to light, the incorporation of π-acceptor pyridine ligand sensitizes the coordination complex to UVA light via an azide-to-Pt ligand-to-metal charge transfer

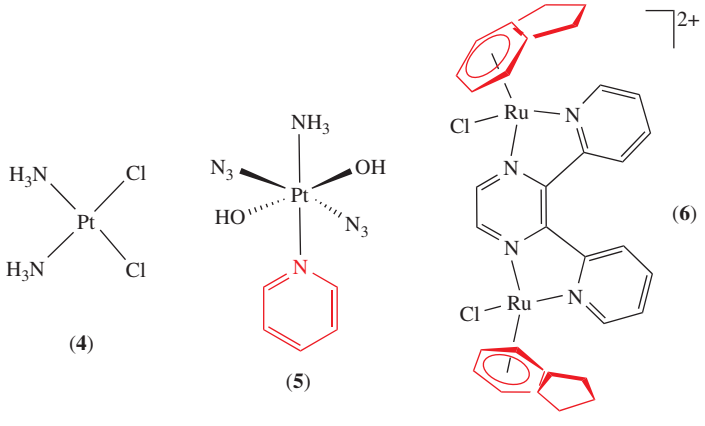

Figure 13.5 *Structures of cisplatin and the photoactivatable Pt^{IV} and Ru^{II} prodrugs*

(LMCT) band. While inactive in the absence of light, this prodrug generates a highly reactive Pt^{II} species that exhibits more potency than cisplatin upon illumination.

Organometallic complexes have also shown potential as photoactivated chemotherapy (PACT) agents [11]. For example, the dinuclear ruthenium(II) complex $[((\eta^6\text{-indan})_2Ru_2Cl_2)(\mu\text{-2,3-dpp})](PF_6)_2$ (**6**, 2,3-dpp = 2,3-dipyridylpyrazine, Figure 13.5) can also be activated through exposure to UVA light. Loss of the arene moieties (through LMCT) from this prodrug generates a dinuclear Ru^{II} species that induces DNA crosslinking upon exposure to light [18]. The need for UVA light for the activation of these photocontrollable prodrugs, an unfavorable feature for biomedical applications, has prompted further exploration of biocompatible prodrugs that exhibit sensitivity to visible light. The piano-stool Ru^{II} complex $[(p\text{-cymene})Ru(bpm)(py)](PF_6)_2$ (bpm = 2, 2′-bipyrimidine) (**7**, Figure 13.6) is one such prodrug that metallates the DNA base guanine upon exposure to visible light [19]. Metallation of guanine occurs upon photodissociation of the pyridine ligand and subsequent aquation to yield the reactive $[(p\text{-cymene})Ru(bpm)(H_2O)](PF_6)_2$ complex.

It is important to note here that the analogs of the Ru^{II} arene complex such as $[(p\text{-cymene})RuCl(en)]PF_6$ (en = ethylenediamine) and $[(p\text{-cymene})RuCl_2(\text{isonicotinamide})]$ are not photoactive. Not until incorporation of py and bpm ligands into the coordination sphere, complexes of this type exhibit sensitivity to light. Photoactivation of (**7**) has been attributed to excitation of an electron from a Ru-N(bpm) orbital to Ru-N(py) σ*-antibonding orbital (strong absorption band with λ_{max} at 383 nm) that contributes to the photodissociation of pyridine. In the absence of light, (**7**) is very stable and non-reactive towards guanine. Comparison of the Ru^{II} arene complexes of the general type $[(\eta^6\text{-arene})Ru(N,N')(L)]^{2+}$ (N,N′ = bidentate chelating ligand, L = π-accepting ligands such as pyridine, 1,2,4-triazole) with those of type $[(\eta^6\text{-arene})Ru(L)_3]^{2+}$ ($L = NH_3$, H_2O) highlights the significance of ancillary ligand choice in the synthesis of photoactivatable prodrugs. Complexes of the former type release L upon exposure to light while irradiation of complexes of the latter

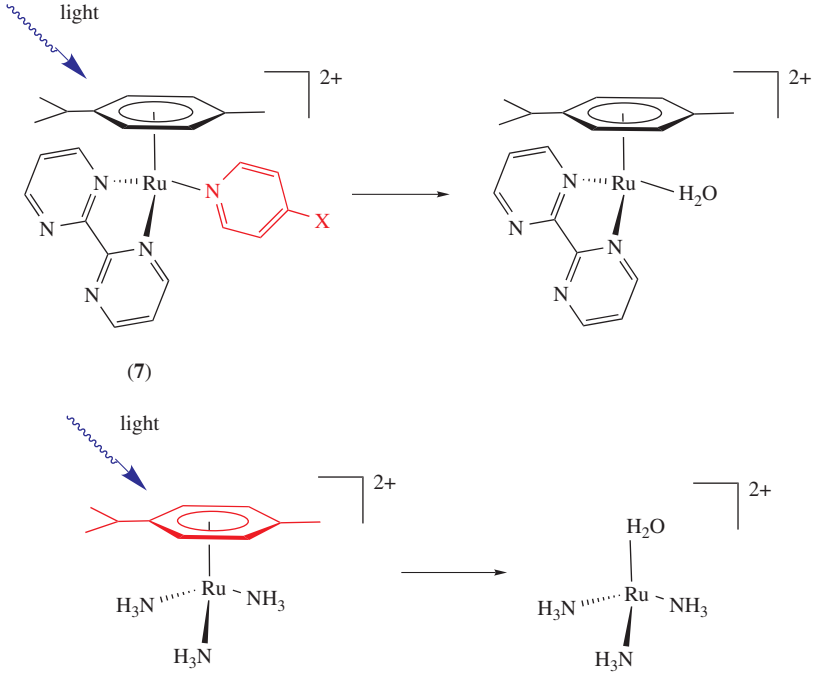

Figure 13.6 *Differential photorelease of ligands from Ru^{II} arene complexes*

type results in the photodissociation of the η^6-arene ligand (Figure 13.6) [20]. Furthermore, the efficacy of photochemical aquation of the photoactivatable ruthenium(II) arene complex [(*p*-cymene)Ru(bpm)(py)]$^{2+}$ (**7**) can be tuned through derivatization of the pyridine ring. Incorporation of electron-donating substituents at the *para* position of the pyridine ligand enhances the extent of photoinduced aquation and DNA binding.

13.3 Metal-based photosensitizers in photodynamic therapy

As mentioned above, the success of PDT relies on eradication of malignant cells with singlet oxygen ($^1O_2$) through the use of photosensitizers [2–4]. The FDA-approved procedures utilize macrocyclic molecules such as porphyrins, phthalocyanine, and naphthalocyanine because they are relatively efficient at undergoing spin forbidden ISC to yield long-lived triplet states. Incorporation of metals into such scaffolds can further enhance the therapeutic capacity by promoting triplet state formation and sensitizing the therapy agent toward light of longer wavelengths. The palladium(II) porphyrin complex tetrakis-2,3-[5,6-di(2-pyridyl)pyrazino]porphyrazin (**8**, Figure 13.7) is an example of a potent PDT agent that generates $^1O_2$ with high quantum efficiency ($\phi = 0.89$) [21]. Enhancement of photosensitization of this Pd^{II} complex can be attributed to the electron deficiency of the designed ligand frame compared with those of alternative macrocycles, such as phthalocyanine analogs, which effectively lowers the energies of the excited singlet and triplet states. Such lowering optimizes the proximity of the excited triplet state of the PDT agent to the triplet state of molecular oxygen, an event that encourages efficient energy transfer between the photosensitizer and oxygen with minimal to no energy loss as fluorescence or phosphorescence (Figure 13.2).

Macrocycles with extended conjugation like porphyrins can be altered readily to shift their low-energy absorption band (the so-called Q-band, employed for PDT) to any region of the therapeutic window (600–900 nm). Simple 2-electron reduction of the porphyrin ring redshifts the Q-band from 532 nm (for porphyrin) to 544 nm (for chlorin), to 590 nm (for bacteriochlorin) (Figure 13.8). Addition of substituents

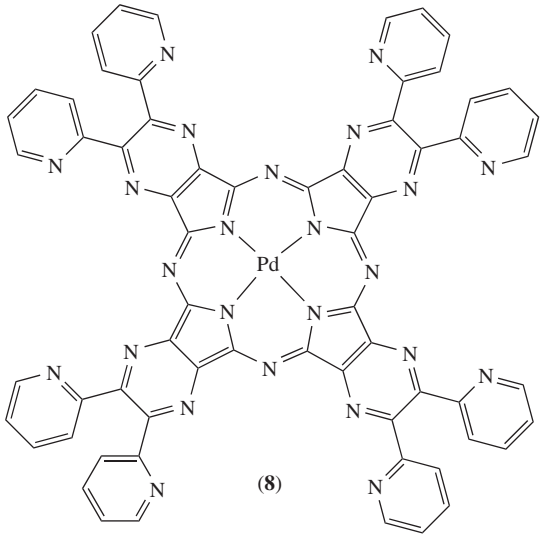

(**8**)

Figure 13.7 *Structure of Pd^{II} complex of tetrakis-2,3-[5,6-di(2-pyridyl)pyrazino]porphyrazin*

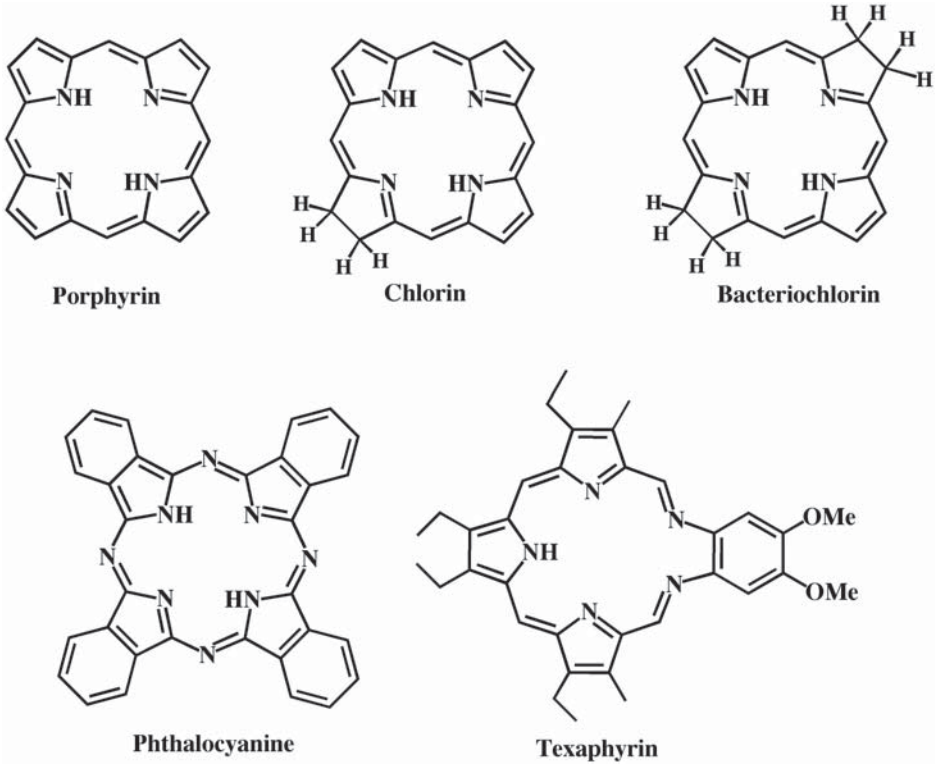

Figure 13.8 *Examples of macrocyclic ligand frames suitable for use as photosensitizers*

at the periphery of the macrocyles also shifts their absorption maxima in a significant way [22]. Major redshifts are noted when heteroatoms are introduced in the main frame. For instance, phthalocyanine (Figure 13.8) exhibits its strong absorption band at 698 nm. Incorporation of metals into the macrocyclic scaffolds of Figure 13.8, in most cases, stabilizes the ground state and moderately increases the values of $\Delta E_{S\text{-}T}$ (the energy difference between the ground state and the first excited triplet state). For example, LUTRIN™ (the lutetium complex of texaphyrin, Figure 13.8) exhibits its Q-band at 732 nm (free texaphyrin value = 650 nm). Theoretical studies in recent years have provided insight into how changes in ligand scaffolds could affect the $\Delta E_{S\text{-}T}$ values that ultimately dictate the efficacy of $^1O_2$ production by metal-based photosensitizers [23].

In PDT, photosensitizers are generally administered intravenously prior to their activation by light. As a consequence, the solubility of a photosensitizer is a critical component of its therapeutic index. A close look at the composition of metal-based photosensitizers such as (**8**) (soluble in dimethylformamide) however indicates that use of conjugated organic frameworks often results in their insolubility in aqueous media. This problem is generally addressed in the ligand design through the incorporation of charged peripheral appendages to increase the net charge of the metal-based photosensitizing agents. Two examples of such alterations are shown in Figure 13.9. The phenyl-decorated porphyrin complex (**9**) is functionalized with anionic sulfonate groups while alkyl groups have been added to the pyridyl-decorated porphyrin complex (**10**) to induce a net cationic charge. Further improvement in solubility of **10** can be achieved by addition of hydrophilic functional groups where R can be NH_2 or OH. Clearly, designed ligands not only impart

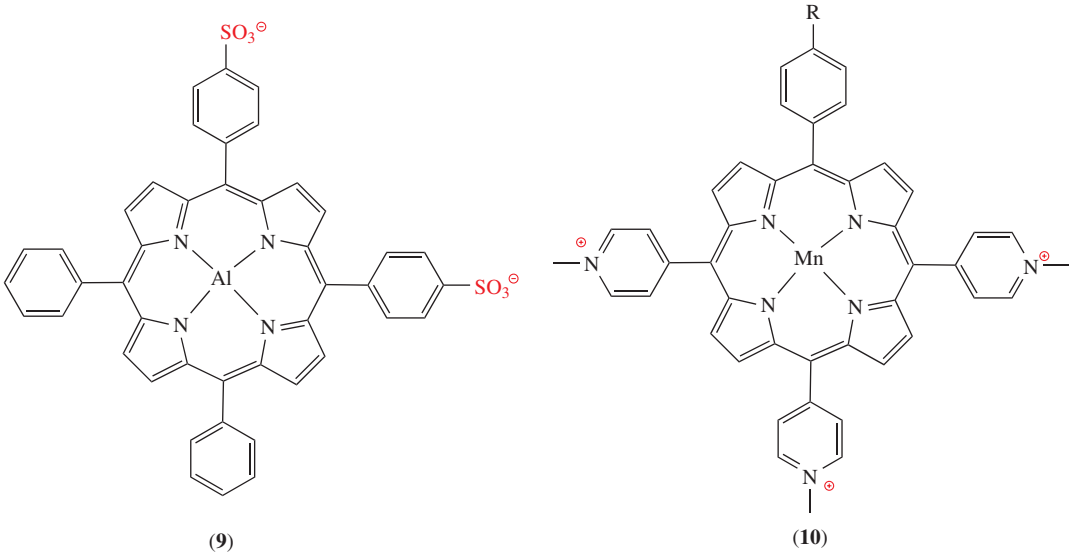

Figure 13.9 *Structures of water-soluble metal-based photosensitizers*

desirable electronic and photochemical properties to metal-based photosensitizers but also can alter their physical properties (such as solubility) for optimal therapeutic utility. Quite expectedly several metal-based (M = Mn, Zn, Al, Sn, and Lu) photosensitizers are currently in use and a few more are in various stages of clinical trial.

13.4 Photoinduced interactions of coordination complexes with DNA

13.4.1 Photocleavage of DNA with coordination complexes

Metal complexes bind to DNA through (i) direct ligation to nucleotide bases (as in cisplatin binding), (ii) intercalation of planar portion of ligands in DNA, and (iii) docking of chiral isomers into the right- or left-handed spiral structure of the host. Such binding could lead to various events including chemical or photochemical strand cleavage, differed recognition of DNA sequences by other biomolecules, and interruption in crucial signaling processes. Classical coordination complexes employed in DNA footprinting (method of investigating the sequence specificity of DNA-binding proteins) include $[Cu(phen)_2]^+$ (**11**, phen = 1,10-phenanthroline) and the methidiumpropyl-conjugated iron(II) EDTA complex (**12**, EDTA = ethylenediaminetetraacetic acid, Figure 13.10) developed by the research groups of Sigman and Dervan respectively [24, 25]. These footprinting agents paved the way for the use of metal complexes in DNA-based sensing, signaling, and therapeutics. The planar phen ligand of (**11**) and the methidiumpropyl (MPE) appendage of the MPE-Fe[EDTA] complex (**12**) intercalates into the staircase structure of DNA through π-π stacking. In the presence of oxygen and a reducing agent, both (**11**) and (**12**) promote oxidative damage at the surface of DNA and ultimately non-specific DNA cleavage through $OH^\bullet$ radical-mediated chemistry. The possibility of introducing selectivity in such DNA cleavage reactions by metal complexes was evident when Barton and coworkers demonstrated selective DNA binding by chiral metal complexes such as the Λ and Δ enantiomers of $[Ru(phen)_3]^{2+}$ (**13**, Figure 13.11) [26–28]. The importance of helical symmetry has since been an integral part of designing

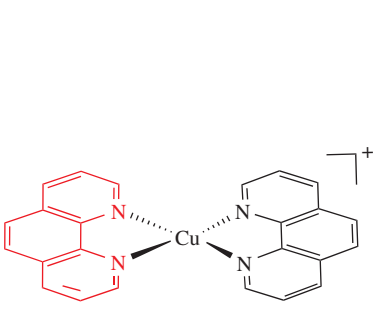

[Cu(phen)$_2$]$^+$ (11)

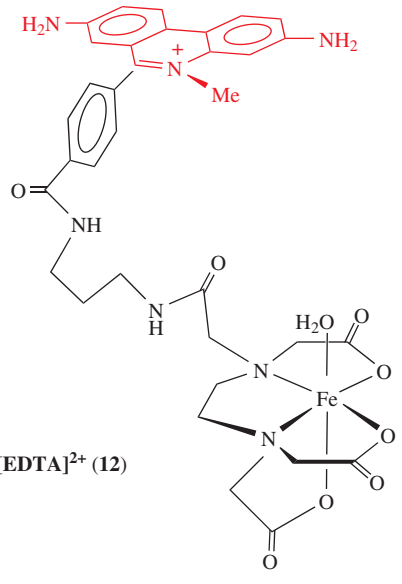

MPE-Fe[EDTA]$^{2+}$ (12)

Figure 13.10 *Metal-based DNA footprinting agents*

coordination complexes as DNA probes and drugs that inflict sequence-specific DNA damage. The discovery of photooxidation of DNA bases by ruthenium and rhodium complexes of phen-type ligands (Figure 13.11) finally allowed development of photoactivatable DNA-cleaving agents [29].

Planar polyazaaromatic ligand frames such as dipyrido[3,2-*a*:2′,3′-*c*]phenazine (dppz), 1,4,5,8-tetraazaphenanthrene (TAP), and 1,4,5,8,9,12-hexaazatriphenylene (HAT) (Figure 13.11) are employed to isolate photoactivatable DNA-cleaving complexes because they (i) afford helical complexes with excellent intercalative properties [27, 30] and (ii) the resultant complexes promote oxidation of guanine(G) bases through proton-coupled electron transfer from the high energy triplet MLCT (^{3}MLCT) state following photoactivation with visible light. The oxidized G radical cations abstract H atoms from the nearby ribose residues, which after several reactions give rise to the strand breaks and photoadducts with G-appended ligands [29]. One such example is the $[Ru(TAP)_3]^{2+}$ (**14**) which is isosteric with the phen complex (**13**), but comprises two additional N atoms within the ligand frame. Incorporation of TAP ligands in (**14**) increases the hydrophilicity of the complex, and raises the reduction potential of the photoexcited ^{3}MLCT state (E^*_{red}, +1.30 V). As a consequence, (**14**) induces DNA cleavage upon illumination with visible light [31]. Substitution of one of the TAP ligands of (**14**) with phen, dip (4,7-diphenyl-1,10-phenanthroline), and bpy attenuates the reduction potential of the photoexcited ^{3}MLCT state to +1.15 , +1.14 , and +1.10 V, respectively. Such reduction lowers the extent of oxidative DNA damage by the photoactivatable ruthenium(II) complexes. In contrast, $[Ru(HAT)_3]^{2+}$ exhibits an E^*_{red} value of +1.49 V and promotes rapid DNA strand cleavage upon illumination. These results demonstrate the role of ligands in modulation of redox potentials of the excited electronic states of metal complexes and provide insight into design of photoactivatable metal complexes that promote *oxygen-independent* DNA strand scission.

Metal complexes derived from polyazaaromatic ligands such as $[Co(dpq)_3]^{3+}$ (**15**, dpq = dipyrido[3,2-*f*:2′,3′-*h*]quinoxaline, Figure 13.12) can also act as photonucleases through *oxygen-dependent* mechanisms, much like (**11**) and (**12**). The larger extension of dpq increases the binding affinity of (**15**) to DNA by virtue of intercalation, a feature absent in chiral recognition of (**13**) by DNA. Irradiation of (**15**) induces the formation of $^1O_2$ that propagates cleavage along the DNA strands [32]. Chakravarty and coworkers have also

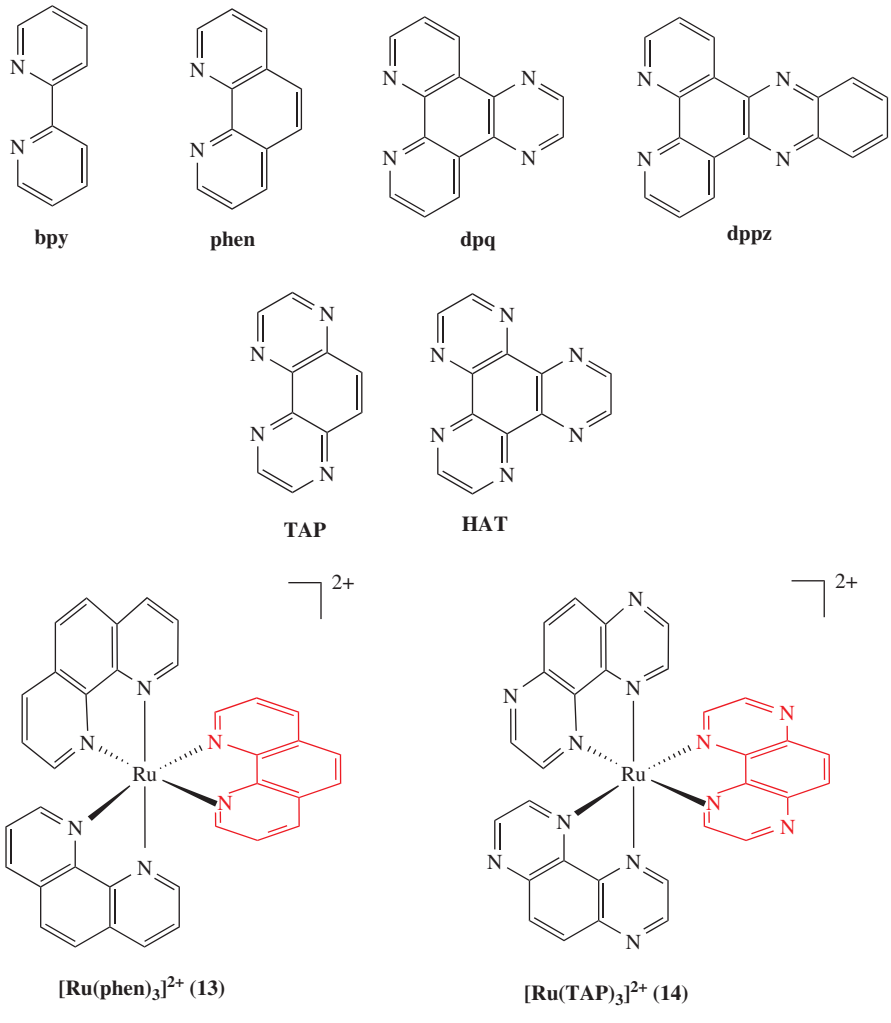

Figure 13.11 *Planar polyazaaromatic ligand frames and chiral Ru^{II} complexes of phen and TAP*

reported DNA cleavage by $[Cu(L\text{-}arg)_2]^{2+}$ (**16**, L-arg = L-arginine, Figure 13.12) through generation of $^1O_2$ upon illumination with 650 nm light [33]. This netropsin-mimic employs the guanidinium functional group of L-arg to selectively bind the minor groove of DNA at the AT-rich sequence of double-stranded DNA. Interestingly, substitution of an L-arg ligand with the DNA-intercalating ligand dppz (Figure 13.12) results in diminished DNA-binding affinity but shows enhanced DNA photocleavage at 650 nm due to the increased photosensitizing character of dppz. Collectively, these results demonstrate how the choice of the ligands alters the mode of DNA binding in such designed photonucleases [34].

13.4.2 Photoactivatable complexes as antisense agents

Photoactivatable complexes attached to small complementary oligonucleotide sequences can photocrosslink mRNA strands and interfere with gene expression through mRNA inactivation. Such antisense strategy can

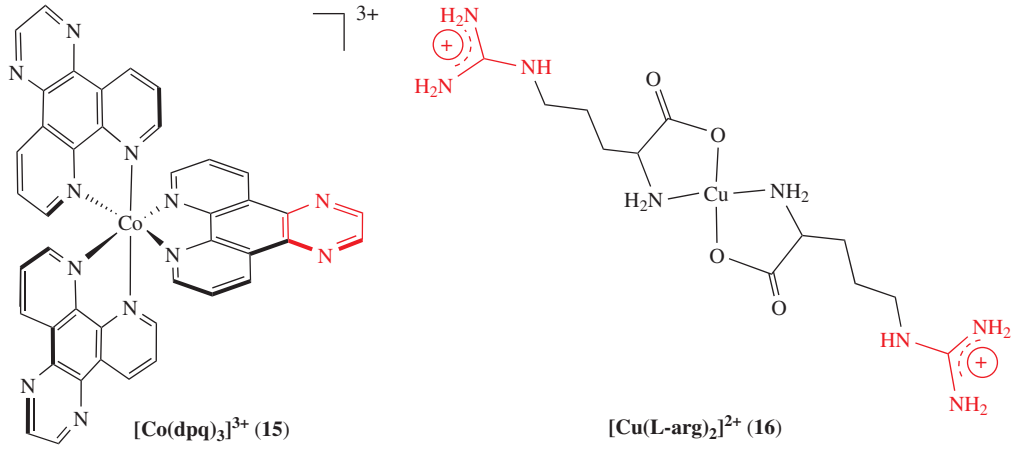

Figure 13.12 *Structures of $[Co(dpq)_3]^{3+}$ (binds DNA through intercalation) and $[Cu(L\text{-}arg)_2]^{2+}$ (binds DNA through electrostatic interaction)*

be used as anticancer therapy for metastatic malignancies originating from oncogenes [35, 36]. Antisense agents currently under clinical investigation work by either disrupting ribosomal assembly to prevent protein transcription or by initiating the activation of RNase that would cleave the mRNA-oligonucleotide duplex from the remaining single-strand of mRNA, rendering it inactive. Antisense agents with photoactive metal complexes comprise a complement oligomer of a targeted mRNA sequence tethered to metal complexes of the type $[Ru(N,N)_2(N',N')]^{2+}$ (where N,N = pyrazine ligands such as TAP or HAT and N′,N′ = bipyridine derivatives such as phen and dip). These modified oligomers can selectively bind to targeted sequence of mRNA and, once illuminated, link the two strands through covalent binding to G bases (Figure 13.13). The extent of crosslinking is strongly dependent on the photoelectronic properties derived from the N,N-ligand, specifically the oxidizing power of the ^{3}MLCT state (as described above). Such conjugates have been proposed as potential antisense candidates for cancer therapy [37].

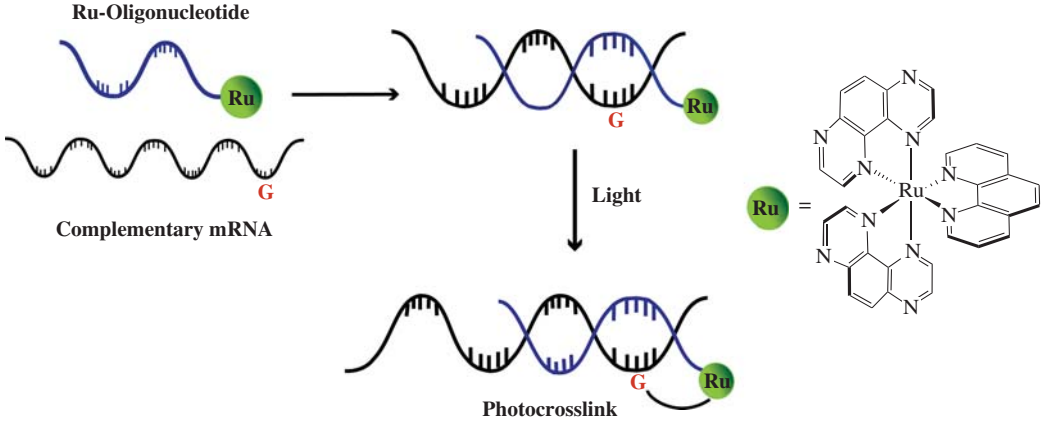

Figure 13.13 *Crosslinking of antisense agents with photoactive metal complexes to m-RNA*

Incorporation of photoactive metal-complexes into oligonucleotides also imparts an added feature to *silence targeted DNA sequence* because unlike traditional antisense agents that anneal to their complement mRNA sequence through standard Watson-Crick base pairing, the metal-containing oligonucleotides also covalently bind to their complementary sequence (photocrosslinking) following illumination. Metal-complexes known to induce photocleavage of DNA through oxygen-independent pathways are good candidates for such applications because they covalently coordinate to G bases upon visible light irradiation. The clinical significance of such designed complexes for use as antisense agents has recently been illustrated through the incorporation of $[Ru(TAP)_2(phen)]^{2+}$ (**17**, Figure 13.14) to the 3′ end of gene E6 antisense oligodeoxynucleotide (Ru-ASO). The 21-base-pair gene E6 sequence is proposed to be an oncogene, which contributes to the onset of human papilloma virus positive (HPV^+) cervical cancer. This gene codes for protein E6 that has been hypothesized to suppress the apoptotic regulation by p53 through complexation [38]. Treatment of HPV^+ SiHa cancer cells with the Ru-ASO followed by exposure to visible light induced >60% attenuation of E6 protein expression and 50–60% growth inhibition. Further, this reduction in E6 results in reciprocal enhancement of p53 expression [39]. The capacity of gene silencing by antisense agents such as Ru-ASO is generally enhanced by the fact that their DNA conjugates are quite resistant to DNA polymerases [40]. Further, the selectivity of these oligonucleotide derivatives toward targeted sequences of DNA provides a convenient tool to silence a specific gene associated with a disease.

The oligonucleotide part of the metal complex-based antisense agents such as Ru-ASO is the key for its selective binding to specific sequences on the DNA target. As a consequence, these conjugates can be used as probes to expose DNA mismatches. Mismatch base pairs within DNA can ultimately lead to diseases when left uncorrected. While mismatches are frequently formed during DNA replication, the cell is equipped with mismatch repair (MMR) machinery that efficiently identifies and corrects those mismatched bases (examples include CC, CA, and AG) introduced as point mutations. The genes that code for the proteins of this curative system are also susceptible to mutations, and alterations to this gene set also have a high probability of leading to tumorogenesis. Design of metal complexes that selectively recognize thermodynamically destabilized DNA mismatches require sterically bulky ancillary ligands [34]. One such example is the expansive aromatic ligand 5,6-chrysene quinonediimine (chrysi), which is too bulky to intercalate between stacking base pairs like parent ligand 9,10-phenanthrenequinone diimine (phi). The rhodium(III) complex $[Rh(bpy)_2(phi)]^{3+}$ (**18**, Figure 13.14) induces non-selective photocleavage of DNA upon illumination. The substitution of phi with chrysi does not alter the photochemical properties of the complex but instead imparts recognition properties

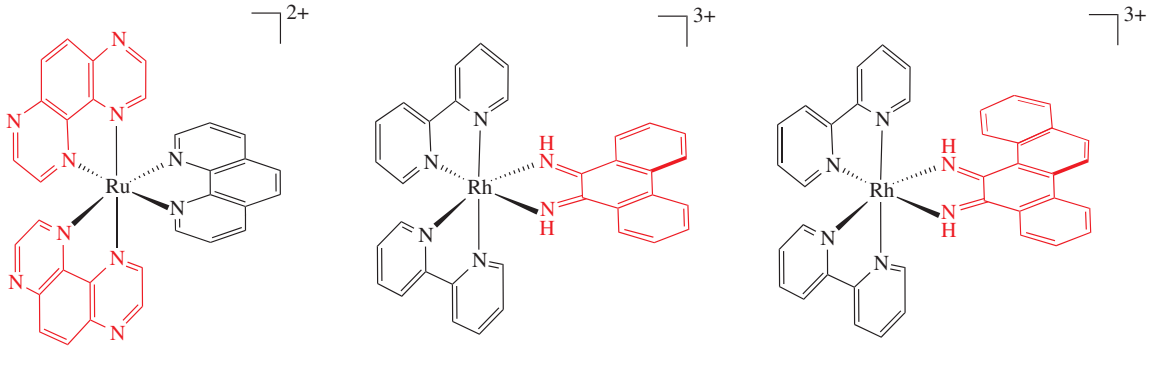

$[Ru(TAP)_2(phen)]^{2+}$ (17) **$[Rh(bpy)_2(phi)]^{3+}$ (18)** **$[Rh(bpy)_2(chrysi)]^{3+}$ (19)**

Figure 13.14 *Photoactivatable metal complexes employed in antisense gene silencing (**17**) and mismatch recognition (**18** and **19**)*

that allow the resulting complex $[Rh(bpy)_2(chrysi)]^{3+}$ (**19**, Figure 13.14) to selectively bind to mismatched pairs within DNA.

13.5 Photoactivatable metal complexes that release small bioactive molecules

Despite the long-held belief that NO and CO are two extremely harmful gases (the toxic twins), it has now been established that both molecules are produced endogenously in mammals and they function as signaling molecules in numerous physiological and pathological pathways [41–43]. NO is synthesized from arginine by the enzyme nitric oxide synthase (NOS). In endothelial cells, eNOS generates nanomolar concentrations of NO that maintains vascular tone and blood pressure through activation of soluble guanylate cyclase (sGC)/cGMP pathway. The inducible iNOS can generate low millimolar concentrations of NO as part of our innate immune system. In addition to its antimicrobial effects, NO can also induce programmed cell death (apoptosis), making it a natural therapeutic agent. CO is generated as a byproduct of the heme breakdown pathway, a process mediated by the enzyme heme-oxygenase (HO) [44]. Surprisingly, low doses of CO have been shown to impart cytoprotective effects under oxidative damage and inhibit pro-inflammatory mediators such as mitogen-activated protein kinase (MAPK) [45]. The beneficial effects of NO and CO have therefore prompted design of NO- and CO-releasing molecules as potential therapeutic agents in recent years.

The affinity of both NO and CO for transition metal centers has inspired the use of coordination complexes as vehicles for their delivery. Indeed, sodium nitroprusside ($Na_2[Fe(CN)_5(NO)]$) was one of the first documented metal nitrosyls shown to release NO. In order to avoid the inexorability of NO release by systemic NO drugs like nitroglycerin, attention has now been placed on designed metal nitrosyls and carbonyl complexes that release NO and CO *at selected sites under the total control of light*. The roles of ligand design in such complexes have been crucial because the efficacy of NO and CO delivery critically depends on the nature of electronic transitions that assist photorelease of these ligands upon illumination.

The feasibility of photoactive metal nitrosyls in NO delivery has been firmly established by Mascharak and coworkers [46]. The first designed ligand that this group synthesized for such purpose was *N*-[2-(bis(2-pyridylmethyl)amino)ethyl]-2-pyridinecarboxamide ($PaPy_3H$). This pentadentate polypyridine ligand was inspired by the coordination sphere of the iron center of the microbial non-heme enzyme nitrile hydratase (Fe-NHase) [47]. This photosensitive enzyme catalyzes the hydration of nitriles to their corresponding amides. In its inactive "dark" form, the iron(III) center is coordinated to NO. Upon illumination, NO is replaced by a molecule of water and the "active" form promotes hydration of nitriles. The unique coordination of deprotonated carboxamido-N donors around the iron center in this enzyme is believed to be responsible for its photoregulation through NO dissociation. This hypothesis prompted Mascharak and coworkers to include a carboxamide moiety in the ligand frame of $PaPy_3H$. Indeed, the placement of the deprotonated carboxamido-N donor (a strong σ-donor) *trans* to the bound NO in the Fe^{III} complex of this ligand, namely $[Fe(PaPy_3)(NO)](ClO_4)_2$ (**20**, Figure 13.15), does promote rapid loss of NO upon exposure to low-power visible light (500 nm) [48]. While (**20**) efficiently releases NO under the control of light, its instability in biological media presents complications for its use as a potential NO donor. Although the corresponding ruthenium(III) nitrosyl $[Ru(PaPy_3)(NO)](ClO_4)_2$ (**21**) displays superior stability compared with (**20**), it requires higher energy UV light (410 nm) for NO release. In contrast, the manganese(II) nitrosyl, namely $[Mn(PaPy_3)(NO)]ClO_4$ (**22**) exhibits facile NO photodissociation (quantum yield at 550 nm $\phi_{550} = 0.38$) upon illumination with visible light and still maintains adequate stability in aqueous media. This robust metal nitrosyl has been established as an efficient NO donor and it exhibits vast therapeutic potential as an effective antimicrobial agent [49].

The electronic transition that promotes NO photolability in (**20–22**) (photobands) has been identified by the use of density functional theory (DFT) and time-dependent DFT calculations (TD-DEF) [50]. Results

from these calculations reveal that there are two types of electronic pathways, *direct* and *indirect*, that lead to the photodissociation of NO from their respective metal centers. The *direct* pathway is observed in all three complexes (**20–22**) with an MLCT from a predominately metal NO/carboxamido bonding HOMO (dπ(M)-π*(NO)) to a dπ(M)-π*(NO) antibonding orbital, giving rise to NO photorelease. This MLCT band is present at 500, 450, and 400 nm in (**20**), (**21**), and (**22**) respectively. The electronic spectrum of (**22**) also shows a lower energy absorbance band at 635 nm. This band has been identified to promote NO release through an *indirect* pathway where an electron is transferred from a predominately metal-character HOMO to an excited state LUMO with pyridine character. This excited singlet state ultimately interconverts to a triplet state with significant antibonding Mn-NO character, leading to NO dissociation (Figure 13.3). Similar indirect pathways have also been suggested in photodissociation of ligands from $[Ru(bpy)_2(L)_2]^{2+}$-type complexes, where L = py, 4-aminopyridine, and butylamine [8].

The *indirect* photodissociation mechanism of (**22**) introduces a level of design where the ligand frame can be modified to tune the photoband to longer wavelengths. When the charged carboxamido-N of $PaPy_3H$ is replaced with a neutral imine-N donor atom to afford the Schiff base ligand *N*,*N*-bis(2-pyridylmethyl)amine-*N*-ethyl-2-pyridine-2-aldimine ($SBPy_3$), TD-DFT studies reveal that the energy gap between the excited singlet and triplet state is reduced compared with that of (**22**) due to decreased ligand field strength of the N_{imine} donor. Experimental spectrophotometry verifies the theoretical data as the photoband of the Mn-Schiff base complex $[Mn(SBPy_3)(NO)]^{2+}$ (**23**, Figure 13.15) is red-shifted (720 nm) compared with the photoband of (**22**) (635 nm). Further, substitution of a pyridine ligand within the equatorial plane with a quinoline group results in a bathochromic shift of the photoband to 785 nm [50].

While the designed pentadentate ligand frames (i) impart facile photorelease of NO from the corresponding metal nitrosyls and (ii) tightly chelate and stabilize the potentially reactive metal center, tetradentate ligand frames open up the possibility of attaching additional ligands *trans* to NO to further tune the photoactivity of these metal nitrosyls. Mascharak and coworkers have also designed a series of tetradentate dicarboxamide ligands of the type R_2bpb^{2-} where bpb = 1,2-bis(pyridine-2-carboxamido)benzene and R = H, Me, and OMe, in order of increasing electron-donating character (Figure 13.16). The photobands of the corresponding Ru^{III} metal nitrosyls, namely $[Ru(H_2bpb)(NO)(Cl)]$ (**24**), $[Ru(Me_2bpb)(NO)(Cl)]$ (**25**), and $[Ru((OMe)_2bpb)(NO)(Cl)]$ (**26**) are red-shifted from 380 nm (for **24**) to 395 nm (for **25**) to 420 nm (for **26**).

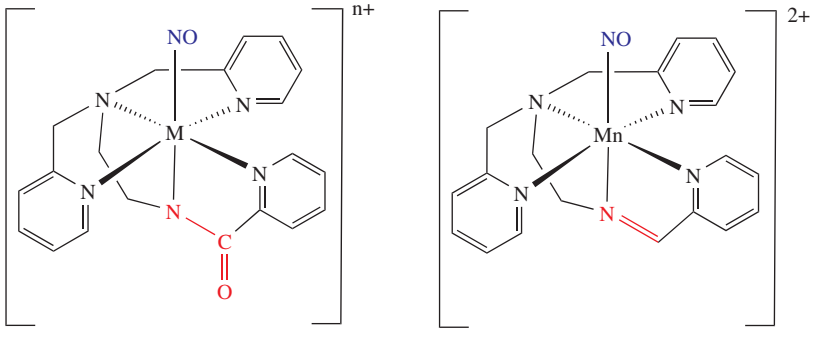

$[M(PaPy_3)(NO)]^{n+}$

M = Fe, n = 2 (20)
M= Ru, n = 2 (21)
M = Mn, n =1 (22)

$[Mn(SBPy_3)(NO)]^{2+}$ (23)

Figure 13.15 *Designed metal nitrosyls that release NO upon illumination*

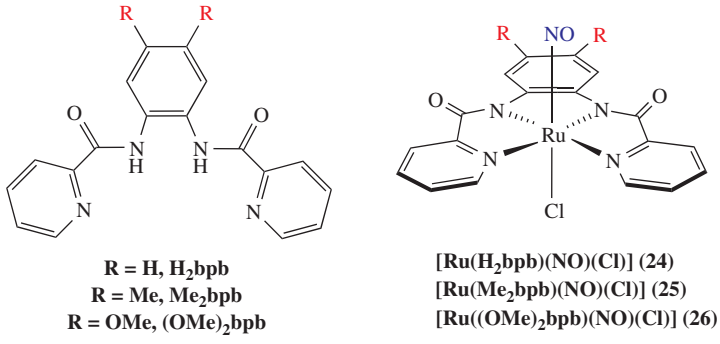

Figure 13.16 *Tetradentate dicarboxamide ligands and their Ru nitrosyls*

TD-DFT studies corroborate these experimental observations and reveal that the characteristic photoband of these Ru nitrosyls corresponds to a π(PDA)-π(RuNO) to π*(RuNO)-π(py) transition (PDA = phenylenediamine moiety) [50]. The incorporation of electron-donating groups destabilizes the ground state of this transition thus decreasing the energy gap between the two energy states. Substitution of the pyridine moieties of the bipyridine frame with quinoline moieties also red-shifts the photobands of these Ru nitrosyls.

While alterations to the equatorial ligand frame can effectively tune the position of the photoband, NO photorelease from the Ru nitrosyls (**24–26**) remains modest. In attempts to photosensitize these nitrosyls towards visible light, Mascharak and coworkers have directly attached dye chromophores (as light-harvesting units) to the metal center, *trans* to the NO. While alternative dye-attachment techniques that employ *indirect* coordination of a chromophore to the periphery ligand (as a pendant) do result in a moderate improvement of NO photorelease [51], *direct* linkage of dyes to the metal-NO unit leads to superior photorelease. Such improvements are evident when one compares the quantum efficiency of NO photorelease of parent Ru nitrosyl (**25**) ($\phi_{500} = 0.0008$) with that of the dye conjugate [Ru(Me_2bpb)(NO)(**Resf**)] (**25-Resf**, $\phi_{500} = 0.052$), where **Resf** is the phenoxazine dye resorufin (Figure 13.17). In addition to the increased quantum yield, the photoband of (**25**) (395 nm) is red-shifted to 500 nm in case of **25-Resf**. Results of theoretical studies indicate that strong π-π* transitions of the dye moiety interact with the π(PDA)-π(RuNO) → π*(RuNO)-π(Py) transition, leading to enhanced NO photodissociation from **25-Resf** [52]. In addition to increased sensitization to visible light, direct tethering of a light-harvesting unit to metal nitrosyls affords *trackable* NO delivery agents [53]. For example, the direct linkage of **Resf** to (**25**) results in a fluorescent nitrosyl **25-Resf**. Because the release of NO from the metal complex quenches the dye fluorescence, due to the formation of a paramagnetic Ru photoproduct, one can track **25-Resf** in cellular matrices and follow the loss of NO from **25-Resf**. The utility of such dye-nitrosyl conjugates has been demonstrated by induction of apoptosis in human breast cancer cells (MDA-MB-231) by **25-Resf** through light-controlled NO delivery [54].

At present, research in the area of designed photoactivatable CO-releasing molecules (photoCORMs) is at its early stage compared with that of photoactive metal nitrosyls [55]. While CO exhibits poor Lewis basicity, coordination of this neutral ligand to low-valent metal centers is strengthened by π-back donation of electron density from the d-orbitals of the metal center to the π* orbitals of CO. In 2002, Motterlini and coworkers explored the possibility of light-induced CO delivery with simple metal carbonyls such as dimanganese decacarbonyl ([$Mn_2(CO)_{10}$], **27**) and iron pentacarbonyl ([$Fe(CO)_5$], **28**). Both carbonyls released CO upon illumination and (**27**) induced vasoconstriction in precontracted rat aortic rings [56]. Unfortunately, these homoleptic carbonyls are toxic, sparingly soluble in biological media, and lack ligand-derived options to tune the photochemical parameters of the CO donors. Later research therefore focused more on the development of metal carbonyls derived from designed ligands that release CO under the control of light.

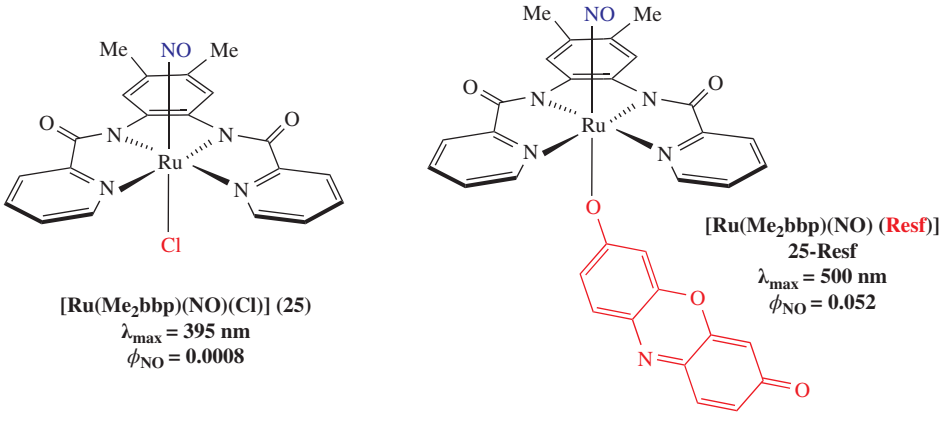

Figure 13.17 *Sensitization of Ru nitrosyls to visible light through dye attachment*

Schatzschneider and coworkers have utilized the *fac*-{$Mn^{I}(CO)_3$} moiety along with a series of designed tridentate ligands to isolate photoCORMs for biological applications. The first compound in this series, namely $[Mn(CO)_3(tpm)]^+$ (**29**, tpm = tris(pyrazolyl)methane, Figure 13.18), releases at least two equivalents of CO upon exposure to 365 nm light. This CORM has demonstrated potential as a PDT agent as it exhibits cytotoxic effects in colon cancer cells [57]. The CO release parameter(s) of the *fac*-{$Mn^{I}(CO)_3L$} complexes can be readily altered by systematically varying the steric bulk and the frame composition of the tridentate ligand L. For example, when L is changed from the tris(imidazol-2-yl)phosphine (2-TIP, Figure 13.18) to the tris(imidazol-4(5)-yl)-λ^5-phosphane oxide (4-TIPO, Figure 13.18), the resulting complex releases half the equivalent of CO upon illumination with UV light [58].

Mascharak and coworkers have also employed a series of tridentate polypyridine ligands with varying degrees of conjugation to explore the design parameters that dictate CO photorelease from *fac*-{$Mn^{I}(CO)_3$}, especially under the control of visible light. This group hypothesized that electronic transition from the low-valent metal center to an auxiliary ligand could potentially diminish the extent of π-backbonding between the metal and CO thus promoting CO loss. Accordingly, ligands with extended conjugation in their frameworks were utilized to promote such transitions in the visible region. For example, coordination of 2-pyridyl-*N*-(2′-methylthiophenyl)methyleneimine (pmtpm) and the quinoline-substituted analog

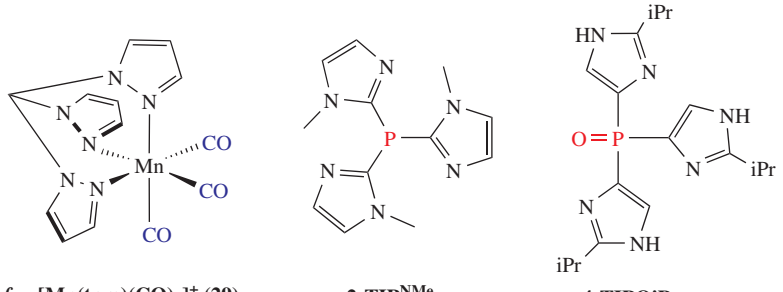

***fac*-[Mn(tpm)(CO)$_3$]$^+$ (29)** **2-TIP^{NMe}** **4-TIPOiPr**

Figure 13.18 *Tripodal ligands employed in different fac-Mn^{I}tricarbonyl complexes*

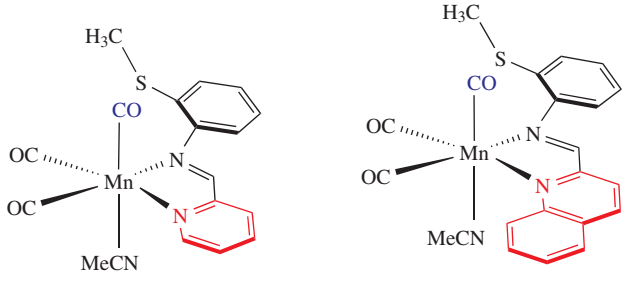

***fac*-[Mn(MeCN)(pmtpm)(CO)$_3$] (30)** ***fac*-[Mn(MeCN)(qmtpm)(CO)$_3$] (31)**

Figure 13.19 *Designed manganese carbonyls sensitive to visible light*

2-quinolyl-*N*-(2′-methylthiophenyl)methyleneimine (qmtmp) to the *fac*-{$Mn^I(CO)_3$} moiety afforded *fac*-[Mn(pmtpm)$(CO)_3$(MeCN)]ClO_4 (**30**, Figure 13.19) and *fac*-[Mn(qmtpm)$(CO)_3$(MeCN)]ClO_4 (**31**, Figure 13.19), respectively [59]. The electronic absorption spectra of **30** and **31** show a red-shift in the absorption band from 390 to 435 nm with simple substitution of the pyridine ligand of pmtpm with a quinoline group in qmtpm. As a consequence, **31** exhibits efficient CO photorelease upon illumination with *visible light*. When the MeCN ligand is replaced by Br^- (a better σ-donor) in both **30** and **31**, the absorption band shifts farther in the visible region, to 500 and 535 nm respectively. In addition to such bathochromic shifts, enhanced quantum efficiency is also observed.

Results of theoretical calculations on **30** and **31**, and their bromo-analogs, reveal that in all cases the absorption band in the visible region arises from promotion of electron density from the predominantly Mn-CO bonding HOMO-2 to LUMO, consisting of pyridine/quinoline and imine character [59]. This transition reduces the affinity of the Mn center toward CO through attenuation of Mn-CO(π*) backbonding and leads to CO photorelease. Substitution of pyridine by the more conjugated quinoline unit in **31** stabilizes the LUMO and shifts the photoband of **31** to lower energy (435 nm) compared with **30** (390 nm). Addition of the σ-donating Br^- in place of MeCN (a moderate π-acceptor) raises the energy of the HOMO-2 level and shifts the photobands of the bromo analogs farther in the visible region (500 and 535 nm respectively). Collectively, these results strongly suggest that a combination of smart design of auxiliary ligands with support from computational studies will afford potentially therapeutic photoCORMs that deliver CO under the total control of visible to near-IR light.

13.6 Conclusion

During the past few decades, use of designed ligands has been extended to impart a wide range of desirable properties to metal complexes in relation to their application in biology and medicine [60]. In this chapter the utility of the designed ligands in controlling the photoactivity of the metal complexes has been highlighted. In most cases, light facilitates the delivery of small molecules from the first coordination sphere of the metal centers. In selected cases the metal complexes are designed to generate reactive species at the target sites (as in PDT) while in some cases the metal complexes bind to their biological targets and disrupt their functions. Because of such diverse utility, photoactivatable metal complexes have become an integral part of medicinal chemistry. The unique capacity of a designed ligand to impart a specific light-driven property

to a metal complex has opened up a broad area of research that will afford many safe and highly effective phototherapeutics to combat various maladies.

References

1. Collman, J.P., Cange, R.R., Halbert, T.R. *et al*. (1973) Reversible oxygen adduct formation in ferrous complexes derived from a "Picket Fence" porphyrin: a model for oxymyoglobin. *J. Am. Chem. Soc.*, **95**, 7868–7870.
2. Josefsen, L.B. and Boyle, R.W. (2008) Photodynamic therapy and the development of metal-based photosensitisers, in *Metal-Based Drugs* (ed M.J. Cook), Hindwai Publishing Corporation, New York, pp. 1–24.
3. Ethirajan, M., Chen, Y., Joshi, P. and Pandey, R.K. (2011) The role of porphyrin chemistry in tumor imaging and photodynamic therapy. *Chem. Soc. Rev.*, **40**, 340–362.
4. Plaetzer, K., Krammer, B., Berlanda, J. *et al*. (2009) Photophysics and photochemistry of photodynamic therapy: fundamental aspects. *Lasers Med. Sci.*, **24**, 259–268.
5. Koziar, J.C. and Cowan, D.O. (1978) Photochemical heavy-atom effects. *Acc. Chem. Res.*, **11**, 334–341.
6. Vlcek, A. (1998) Mechanistic roles of metal-to-ligand charge-transfer excited states in organometallic photochemistry. *Coord. Chem. Rev.*, **177**, 219–256.
7. Herman, L., Ghosh, S., Defrancq, E. and Kirsch-De Mesmaeker, A. (2008) Ru (II) complexes and light: molecular tools for biomolecules. *J. Phys. Org. Chem.*, **21**, 670–681.
8. Lopes-dos-Santos, V., Campi, J., Filevich, O. *et al*. (2011) In vivo photorelease of GABA in the mouse cortex. *Braz. J. Med. Biol. Res.*, **44**, 688–693.
9. Crespy, D., Landfester, K., Schubert, U.S. and Schiller, A. (2010) Potential photoactivated metallopharmaceuticals: from active molecules to supported drugs. *Chem. Commun.*, **46**, 6651–6662.
10. Schatzschneider, U. (2010) Photoactivated biological activity of transition-metal complexes. *Eur. J. Inorg. Chem.*, **2010**, 1451–1467.
11. Farrer, N.J., Salassa, L. and Sadler, P.J. (2009) Photoactivated chemotherapy (PACT): the potential of excited-state d-block metals in medicine. *Dalton Trans.*, 10690–10701.
12. Haas, K.L. and Franz, K.J. (2009) Application of metal coordination chemistry to explore and manipulate cell biology. *Chem. Rev.*, **109** (10), 4921–4960.
13. Chakravarty, A.R. and Roy, M. (2012) Photoactivated DNA cleavage and anticancer activity of 3d metal complexes, in *Progress in Inorganic Chemistry* (ed K.D. Karlin), John Wiley & Sons, Inc., Hoboken, NJ, pp. 119–202.
14. Wang, D. and Lippard, S.J. (2005) Cellular processing of platinum anticancer drugs. *Nat. Rev. Drug Discovery*, **4**, 307–320.
15. Jamieson, E.R. and Lippard, S.J. (1998) Structure, recognition, and processing of cisplatin-DNA adducts. *Chem. Rev.*, **99**, 2467–2498.
16. Celli, J.P., Sprin, B.Q., Rizvi, I. *et al*. (2010) Imaging and photodynamic therapy: mechanism, monitoring, and optimization. *Chem. Rev.*, **110** (5), 2795–2838.
17. Mackay, F.S., Woods, J.A., Heringova, P. *et al*. (2007) A potent cytotoxic photoactived platinum complex. *Proc. Natl. Acad. Sci. U.S.A.*, **104** (52), 20743–20748.
18. Magennis, S.W., Habtemariam, A., Novakova, O. *et al*. (2007) Dual triggering of DNA binding and fluorescence via photoactivation of a dinuclear ruthenium arene complex. *Inorg. Chem.*, **46**, 5059–5068.
19. Betanos-Lara, S., Salassa, L., Habtemariam, A. and Sadler, P.J. (2009) Photocontrolled nucleobase binding to an organometallic Ru^{II} arene complex. *Chem. Commun.*, **43**, 6622–6624.
20. Betanzos-Lara, S., Salassa, L., Habtemariam, A. *et al*. (2012) Photoactivatable organometallic pyridyl ruthenium (II) arene complexes. *Organometallics*, **31**, 3466–3479.
21. Donzello, M.P., Viola, E., Bergami, C. *et al*. (2008) Tetra-2,3-pyrazinoporphyrazines with externally appended pyridine rings. 6. Chemical and redox properties and highly effective photosensitizing activity for singlet oxygen production of penta- and mono-palladated complexes in dimethylformamide solution. *Inorg. Chem.*, **47**, 8575–8766.
22. F. Nifiatis, J.C. Athas, D.D. Gunaratne, Y. Gurung, K.M. Monette, and P.J. Shivokevich, Substituent effects of porphyrin on singlet oxygen generation quantum yields, *Open Spectrosc. J*., **5**, 1–12 (2011).

23. Quartarolo, A.D., Russo, N., Sicilia, E. and Adamo, C. (2012) The contribution of theoretical chemistry to the drug design in photophysical therapy, in *Photosensitizers in Medicine, Environment, and Security* (eds T. Nyokong and V. Ahsen), Springer, pp. 121–134.
24. Sigman, D.S. (1986) Nuclease activity of 1,10-phenanthroline-copper ion. *Acc. Chem. Res.*, **19**, 180–186.
25. Hertzberg, R.P. and Dervan, P.B. (1984) Cleavage of DNA with methidiumpropyl-EDTA-Iron(II): reaction conditions and product analysis. *Biochemistry*, **23**, 3934–3945.
26. Barton, J.K., Danishefsky, A.T. and Goldberg, J.M. (1984) Tris(phenanthroline)ruthenium(II): stereoselectivity in binding DNA. *J. Am. Chem. Soc.*, **106**, 2127–2176.
27. Pyle, A.M., Rehmann, J.P., Meshoyrer, R. *et al*. (1989) Mixed-ligand complexes of ruthenium(II): factors governing binding to DNA. *J. Am. Chem. Soc.*, **111**, 3051–3058.
28. Erkkila, K.E., Odom, D.T. and Barton, J.K. (1999) Recognition and reaction of metallointercalators with DNA. *Chem. Rev.*, **99**, 2777–2795.
29. Elias, C.B. and Kirsch-De Mesmaeker, A. (2006) Photoreduction of polyazaaromatic Ru(II) complexes by biomolecules and possible applications. *Coord. Chem. Rev.*, **250**, 1627–1641.
30. Turro, C. (2011) To intercalate or semiintercalate, or both? *Proc. Natl. Acad. Sci. U.S.A.*, **108** (43), 17573–17574.
31. Uji-i, H., Foubert, P., De Schryver, F.C. *et al*. (2006) $[Ru(TAP)_3]^{2+}$-photosensitized DNA cleavage studied by atomic force microscopy and gel electrophoresis: a comprehensive study. *Chem. Eur. J.*, **12**, 758–762.
32. Sun, Y., Zhour, Q.-X., Chen, J.-R. *et al*. (2009) DNA photocleavage activity of cobalt(III) polypyridyl complexes containing dpq ligand. *J. Inorg. Biochem.*, **103**, 1658–1665.
33. Patra, A.K., Bhowmick, T., Roy, S. *et al*. (2009) Copper(II) complexes of L-arginine as netropsin mimics showing DNA cleavage activity in red light. *Inorg. Chem.*, **28**, 1024–1033.
34. Zeglis, B.M., Pierre, V.C. and Barton, J.K. (2007) Metallo-intercalators and metallo-insertors. *Chem. Commun.*, 4565–4579.
35. Kurreck, J. (2003) Antisense technologies: improvement through novel chemical modifications. *Eur. J. Biochem.*, **270**, 1628–1644.
36. Tamm, I., Dorken, B. and Hartmann, G. (2001) Antisense therapy in oncology: new hope for an old idea? *Lancet*, **358** (9280), 489–497.
37. Moucheron, C. (2009) From cisplatin to photoreactive Ru complexes: targeting DNA for biomedical applications. *New J. Chem.*, **33**, 235–245.
38. Lechner, M.M.S., Mack, D.H., Finicle, A.B. *et al*. (1992) Human papillomavirus E6 proteins bind p53 *in vivo* and abrogate p53-mediated repression of transcription. *EMBO J.*, **11** (8), 3045–3052.
39. Marcélis, L., Moucheron, C. and Kirsch-De Mesmaeker, A. (2013) Ru-TAP complexes and DNA: from photo-induced electron transfer to gene photo-silencing in living cells. *Philos. Trans. R. Soc. London, Ser. A*, **371**, 20120131.
40. Lentzen, O., Defrancq, E., Constant, J.-F. *et al*. (2004) Determination of DNA guanine sites forming photo-adducts with Ru(II)-labeled oligonucleotides; DNA polymerase inhibition by the resulting photo-crosslinking. *J. Biol. Inorg. Chem.*, **9**, 100–108.
41. Ignarro, L.J. (ed) (2000) *Nitric Oxide: Biology and Pathobiology*, Academic Press, San Diego, CA.
42. Fang, F.C. (ed) (1999) *Nitric Oxide and Infection*, Kluwer Academic/Plenum Publishers, New York.
43. Wang, R. (ed) (2004) *Signal Transduction and the Gasotransmitters: NO, CO and H_2S in Biology and Medicine*, Humana Press, Totowa, NJ.
44. Kikuchi, G., Yoshida, T. and Noguchi, M. (2005) Heme oxygenase and heme degradation. *Biochem. Biophys. Res. Commun.*, **338** (1), 558–567.
45. Kim, H.P., Ryter, S.W. and Choi, A.M.K. (2006) CO as a cellular signaling molecule. *Annu. Rev. Pharmacol. Toxicol.*, **46**, 411–449.
46. Rose, M.J. and Mascharak, P.K. (2008) Fiat Lux: selective delivery of high flux of nitric oxide (NO) to biological targets using photoactive metal nitrosyls. *Curr. Opin. Chem. Biol.*, **12**, 238–244.
47. Nagashima, S., Nakasako, M., Dohmae, N. *et al*. (1998) Novel non-heme iron center of nitrile hydratase with a claw setting of oxygen atoms. *Nat. Struct. Biol.*, **5**, 347–351.
48. Patra, A.K., Afshar, R.K., Olmstead, M.M. and Mascharak, P.K. (2002) The first non-heme iron(III) complex with ligated carboxamido group that exhibits photolability of bound NO ligand. *Angew. Chem. Int. Ed.*, **41**, 2512–2515.

49. Heilman, B. and Mascharak, P.K. (2013) Light-triggered nitric oxide delivery to malignant sites and infection. *Philos. Trans. R. Soc. London, Ser. A*, **371**, 20120368.
50. Fry, N.L. and Mascharak, P.K. (2012) Photolability of NO in designed metal nitrosyls with carboxamido-N donors: a theoretical attempt to unravel the mechanism. *Dalton Trans.*, **41**, 4726–4735.
51. Wecklser, S.R., Hutchison, J. and Ford, P.C. (2006) Toward development of water soluble dye derivatized nitrosyl compounds for photochemical delivery of NO. *Inorg. Chem.*, **45**, 1192–1200.
52. Fry, N.L. and Mascharak, P.K. (2011) Photoactive ruthenium nitrosyls as NO donors: how to sensitize them toward visible light. *Acc. Chem. Res.*, **44** (4), 289–298.
53. Rose, M.J. and Mascharak, P.K. (2008) A photosensitive $\{Ru\text{-}NO\}^6$ nitrosyl bearing dansyl chromophore: novel NO donor with a fluorometric on/off switch. *Chem. Commun.*, 3933–3935.
54. Rose, M.J., Fry, N.L., Marlow, R. *et al*. (2008) Sensitization of ruthenium nitrosyls to visible light via direct coordination of the dye resorufin; trackable NO donors for light-triggered NO delivery to cellular targets. *J. Am. Chem. Soc.*, **130**, 8834–8846.
55. Schatzschneider, U. (2011) PhotoCORMs: light-triggered release of carbon monoxide from the coordination sphere of transition metal complexes for biological applications. *Inorg. Chim. Acta*, **374**, 19–23.
56. Motterlini, R., Clark, J.E., Foresti, R. *et al*. (2002) Carbon monoxide-releasing molecules: characterization of biochemical and vascular activities. *Circ. Res.*, **90**, e17–e24.
57. Niesel, J., Pinto, A., Peindy N'Dongo, H.W. *et al*. (2008) PhotoCORMs: photoinduced CO release, cellular uptake and cytotoxicity of a tris(pyrazolyl)methane (tpm) manganese tricarbonyl complex. *Chem. Commun.*, 1798–1800.
58. Kunz, P.C., Huber, W., Rojas, A. *et al*. (2009) Tricarbonylmanganese(I) and rhenium(I) complexes of imidazol-based phosphane ligands: influence of the substitution pattern on the CO releasing properties. *Eur. J. Inorg. Chem.*, **2009**, 5358–5366.
59. Gonzales, M.A., Carrington, S.J., Fry, N.L. *et al*. (2012) Syntheses, structures, and properties of new manganese carbonyls as photoactive CO-releasing molecules: design strategies that lead to CO photolability in the visible region. *Inorg. Chem.*, **51**, 11930–11940.
60. Ronconi, L. and Sadler, P.J. (2007) Using coordination chemistry to design new medicines. *Coord. Chem. Rev.*, **251**, 1633–1648.

14

Metalloprotein Inhibitors

David P. Martin, David T. Puerta, and Seth M. Cohen

Department of Chemistry and Biochemistry, 9500 Gilman Drive, University of California, San Diego, CA, 92093, USA

14.1 Metal binding groups in metalloprotein inhibitor design

Metal ions are essential to life and are involved in a wide variety of biological processes including photosynthesis, oxygen transport and activation, cell signaling, and transcriptional regulation. These ions can be used to stabilize protein structure [1], facilitate electron transport [2], and catalyze chemical transformations [3]. Transition metals have many characteristics that make them suitable for these functions including flexible coordination environments, tunable redox potentials, and Lewis acidity. Although most transition metal ions have multiple accessible oxidation states, the majority of metalloproteins do not rely on redox chemistry at the catalytic metal center for biological functions [3]. Rather, the two primary roles of metal ions in enzymatic catalysis are to activate substrates or to stabilize anionic intermediates and transition states [3].

The misregulation of metalloenzymes has been implicated in several diseases including tumor growth and metastasis, hypertension, and inflammation [4]. There are also many examples of pathogenic metalloproteins that are crucial for the survival and virulence of bacteria and viruses. As such, a number of metalloproteins have attracted interest for the treatment of diseases such as cancer, hypertension, and infection (both bacterial and viral) among others, as summarized in Table 14.1. The majority of metalloprotein therapeutics are designed to bind to the catalytic metal ion in the active site.

The activation of substrates by transition metal ions relies on the Lewis acidity of metals, which can be utilized in several ways. When a substrate is bound to a Lewis acidic metal ion, electron density is withdrawn from the metal-bound atom, polarizing its bonds. This mechanism is demonstrated in hydrolases, a large subset of metalloproteins in which polarization of the O-H bond of a metal-bound water molecule leads to facile deprotonation, generating a hydroxide ion that can be used for nucleophilic attack on a wide variety of substrates (Figure 14.1a). Similarly, in the case of farnesyltransferase, the metal-bound species is a cysteine

Ligand Design in Medicinal Inorganic Chemistry, First Edition. Edited by Tim Storr.

Table 14.1 *Examples of metalloproteins that have garnered attention as therapeutic targets*

Human enzyme	Cofactor	Disease
Adamalysin	Zn(II)	Cancer
Angiotensin converting enzyme[a]	Zn(II)	Hypertension
Carbonic anhydrase[a]	Zn(II)	Glaucoma
Farnesyltransferase	Zn(II)	Cancer
Histone deacetylase[a]	Zn(II)	Cancer
Matrix metalloprotease	Zn(II)	Cancer
Neprilysin	Zn(II)	Hypertension
TNF-α converting enzyme	Zn(II)	Cancer
Lipoxygenase[a]	Fe(II)	Asthma
Histone demethylase	Fe(II)	Cancer
Tyrosinase	Cu(II)	Cancer
Methionine aminopeptidase	Mn(II)	Cancer
Pathogenic enzyme	**Cofactor**	**Organism**
Anthrax lethal factor	Zn(II)	*B. anthracis*
Botulinum neurotoxin	Zn(II)	*C. botulinum*, *C. butyricum*, and *C. baratii*
LpxC	Zn(II)	Gram-negative bacteria
Metallo-β-lactamases	Zn(II)	Gram-negative and positive bacteria
Methionine aminopeptidase	Fe(II)	Gram-negative and positive bacteria
Peptide deformylase	Fe(II)	Gram-negative and positive bacteria
Influenza polymerase (subunit)	Mn(II)	Influenza virus
HIV integrase[a]	Mg(II)	Human immunodeficiency virus

[a] FDA-approved inhibitors available against these metalloproteins

residue that, upon polarization and subsequent deprotonation, attacks the C-1 atom of a farnesyldiphosphate substrate [5]. Deprotonation of a metal-bound species can also facilitate electronic rearrangement of the substrate, as is the case in alcohol dehydrogenase (Figure 14.1b). Alternatively, bond polarization without deprotonation leads to increased electrophilicity of neighboring atoms. In glutamine cyclase, the binding of a ketone functionality allows for electrophilic attack on the carbonyl carbon by the terminal amine of the substrate (Figure 14.1c) [6]. There are also cases of metalloproteins that combine these mechanisms, such as dinuclear metallo-β-lactamases. By employing two metal centers in close proximity, a nucleophile bound to the dinuclear metal center can be positioned ideally for attack on an activated electrophile also bound to the metal centers (Figure 14.1d).

The common aspect of all Lewis acid-mediated catalytic metal sites is that substrate turnover requires a metal-bound species. Preventing this metal–substrate interaction abolishes enzyme activity, and hence the majority of metalloprotein inhibitors against these enzymes act by direct coordination to the catalytic metal ion. Inhibitors of metalloproteins can be viewed as consisting of two general components: a metal-binding group (MBG) that serves to coordinate the metal ion, and a backbone designed to interact with the surrounding active site utilizing more traditional ligand–protein interactions such as hydrogen bonding and hydrophobic contacts. While the latter interactions have been extensively studied and are relatively well understood, MBG–metal interactions have not received the same amount of attention in medicinal chemistry. There are

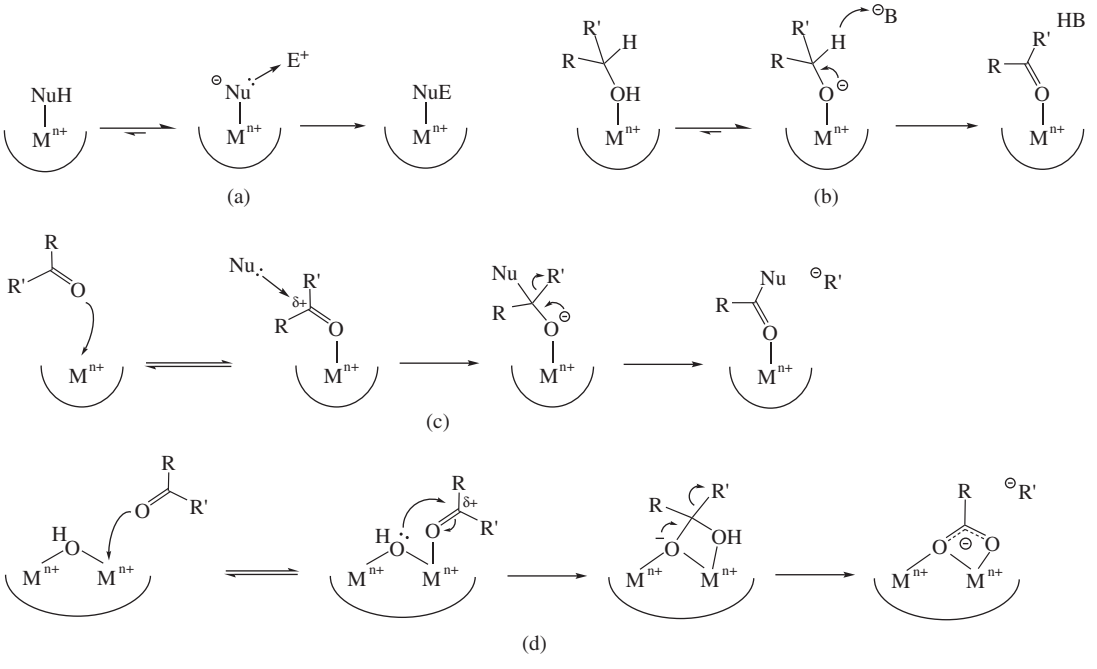

Figure 14.1 *Examples of metal-catalyzed enzymatic reactions that do not involve redox chemistry at the metal center. (a) The metal center can activate a bound atom for nucleophilic attack on an electrophilic substrate. This can lead directly to product formation, as in carbonic anhydrases or farnesyltransferase, or to bond cleavage in the substrate, as is the case in histone deacetylases. (b) Deprotonation of the substrate can lead to a rearrangement, such as in alcohol dehydrogenase. (c) Binding to a metal ion results in bond polarization, increasing the electrophilicity of neighboring atoms, as in glutamine cyclase. (d) Utilizing two metal ions, a protein can activate a nucleophile for attack on an adjacent electrophile, for example in dinuclear metallo-β-lactamases*

many variables about an MBG that can be optimized for specific targets including size, acidity, and the number, composition, and relative geometry of donor atoms provided by the MBG. Despite the large number of MBGs available for inhibitor design, which is evidenced by the extensive number and diversity of ligands in the field of inorganic chemistry, a survey of metalloprotein inhibitors reveals that only four classes of MBGs in metalloprotein inhibitors have been widely used in modern medicinal chemistry: carboxylates, thiols, phosphonates/phosphinates, and hydroxamic acids (Figure 14.2).

With ever more metalloproteins being discovered as potential therapeutic targets, the importance of designing target-specific metalloprotein inhibitors is apparent [4]. Because many of these enzymes act on structurally similar peptide substrates, backbone design alone may not be enough to accomplish this task. In addition to the numerous factors that contribute to the efficacy of an MBG, the local protein environment can play a significant role in the coordination and thus the overall binding of the inhibitor to the metalloprotein. Many metalloprotein inhibitors, particularly those based on hydroxamic acids, have poor pharmacokinetic properties such as low oral bioavailability and inadequate metabolic stability; the other three classes of MBG have had prodrug strategies developed to overcome these pharmacokinetic issues [7]. It has been suggested that a holistic approach to metalloprotein drug design, considering both the MBG and backbone as equally

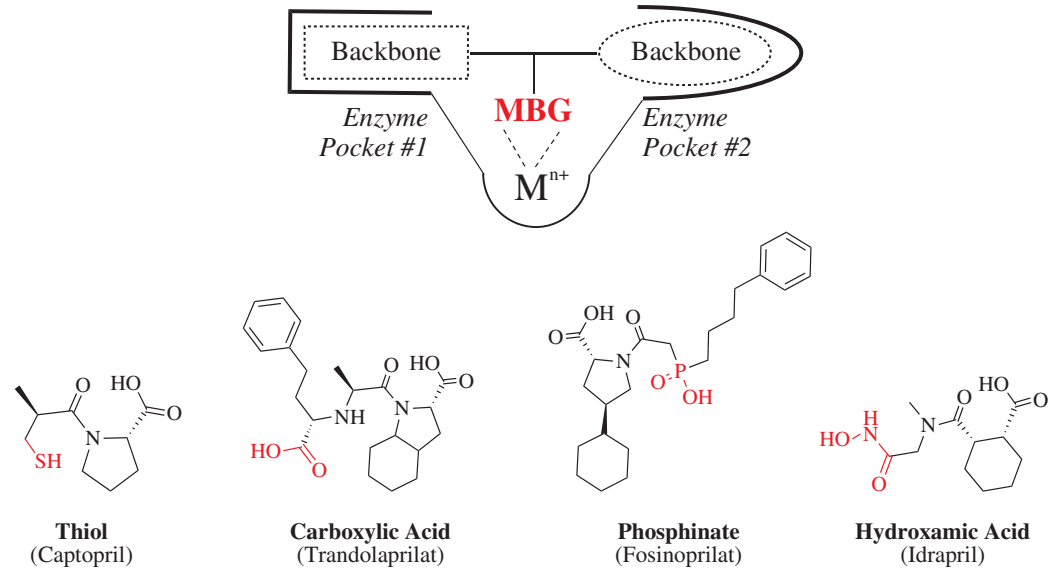

Figure 14.2 *Metalloprotein inhibitors. Top: A schematic of the general structure of metalloprotein inhibitors. Bottom: A representative series of angiotensin converting enzyme (ACE) inhibitors that utilize the four most common MBGs (shown in boxes). All but idrapril are approved by the U.S. Food and Drug Administration (FDA). Presently, only one inhibitor based on a primary hydroxamic acid MBG (vorinostat, a histone deacetylase inhibitor) has been approved as a therapeutic by the FDA*

important components, is required to discover the next generation of metalloprotein inhibitors. Balancing the interactions of the MBG and the backbone with the protein can be used to obtain more tailored compounds. To that end, utilizing a wider collection of MBGs to parallel the diversity found in traditional pharmacophores in the drug design process may help overcome some of the hurdles that have hampered the development of metalloprotein inhibitor-based therapeutics. This chapter explores the spectrum of MBGs that have been crystallographically characterized bound to active-site metal ions in order to highlight common features of current MBGs and to identify potentially underexplored chemical space in metalloprotein inhibitor design.

For this study, the Protein Data Bank (PDB) was searched for crystallographic structures that contained first-row transition metals (Mn, Fe, Co, Ni, Cu, and Zn) and further filtered to only those containing the keyword "inhibitor" (www.pdb.org). Structural metal sites, as well as artifacts of crystallization (salts, surface-bound metal ions, etc.) were discarded. Structures with inhibitors not coordinated to active-site metal ions were also discarded. The resulting structures were then inspected and representative examples of several enzymes and MBGs were selected for further discussion. This is not meant to be an exhaustive review of all inhibitor-bound structures, but instead an analysis of representative examples of several classes of MBG. Heme iron centers were not included in this analysis. Bond-length data analyzed in Figures 14.3 and 14.5 were obtained from Kawai and Nagata, who recently published a review on exogenous ligands bound to Zn^{II} ions in crystal structures of metalloproteins from the PDB [8] by searching the PDB for structures containing a Zn^{II} ion and compiling a list of ligands that bind the metal; suitable ligands were defined as being closer to the metal than the sum of the van der Waals radii. The first part of this chapter focuses on the four "conventional" MBGs mentioned above. The second part explores MBGs that either mimic conventional MBGs or augment them with additional donor atoms. The third section highlights some of the more recent developments in MBGs for metalloprotein inhibitor design.

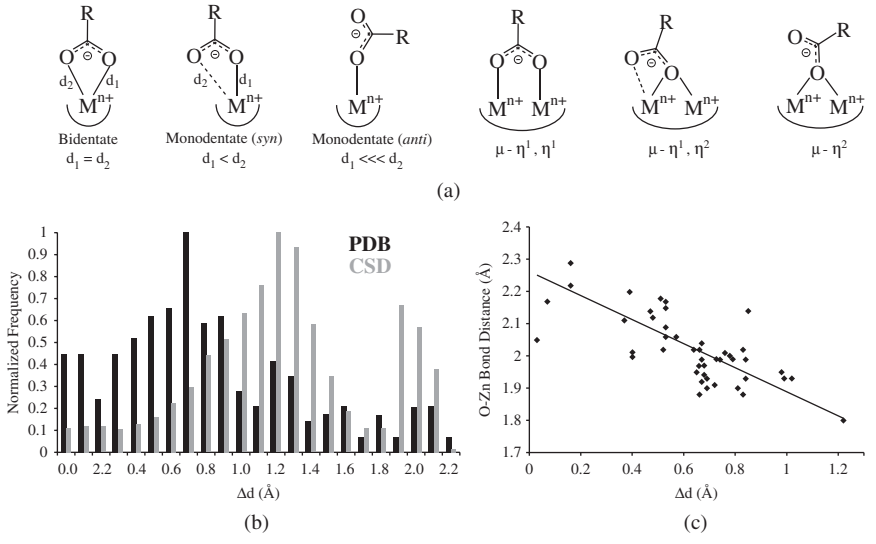

Figure 14.3 *Analysis of carboxylate MBG binding modes. (a) Diagrams of the coordination modes available for carboxylates binding to mono- and dinuclear active sites. (b) Frequency of Δd values for both protein (from the Protein Data Bank, PDB) and small-molecule (from the Cambridge Structural Database, CSD) crystal structures containing zinc(II)-bound carboxylate groups. The values are normalized to the maximum frequency for comparison. (c) The effect of binding symmetry on O–Zn bond lengths in protein crystal structures. The shorter O–Zn bond length, d_1 (shown on the y axis), generally increases as the carboxylate becomes more bidentate ($\Delta d \rightarrow 0$)*

14.2 Thiols, carboxylates, phosphates, and hydroxamates

Nature primarily utilizes four amino acid residues to bind metal ions in proteins: the carboxylate of Asp or Glu, the thiol of Cys, and the imidazole of His residues. The dominance of these three groups in protein-derived metal binding would seem to suggest that they could serve as MBGs in inhibitors. Although this is true for thiols and carboxylates, significantly fewer imidazole-based inhibitors have been reported. This may be due in part to the fact that imidazole-based compounds are known to inhibit human cytochrome P450 metalloenzymes via heme iron coordination, posing significant potential for drug–drug interactions [9]. The imidazole MBG has, however, been used in the development of inhibitors of some zinc(II)-dependent enzymes, including glutamine cyclase and farnesyltransferase [10].

Thiol ligands are widely found in both synthetic and biological coordination chemistry and have been observed bound to a wide variety of metal ions and active sites (PDB IDs 4AL3, 1UZW, 2PHO, 1JAO, 3RQD, and 2FU8 are representative examples). The C–S–Zn bond angle is generally between 90° and 115° with the ideal value predicted to be around 105° [11]. The combination of ionic and covalent coordinate bonding makes thiols a well-suited ligand for binding many physiologically-relevant transition metal ions. However, free thiols have pharmacokinetic liabilities that can arise from off-target protein binding and can produce adverse side effects associated with therapeutics based on this MBG [12]. Captopril, the first inhibitor of angiotensin converting enzyme (ACE, a zinc(II)-dependent hydrolase) to gain FDA approval, is the only metalloprotein-targeted drug that contains a free thiol. Only one other metalloprotein inhibitor utilizing a thiol MBG has been approved by the FDA, the histone deacetylase (HDAC) inhibitor romidepsin, which is administered as a disulfide prodrug that likely helps reduce the possible side effects associated with free thiols.

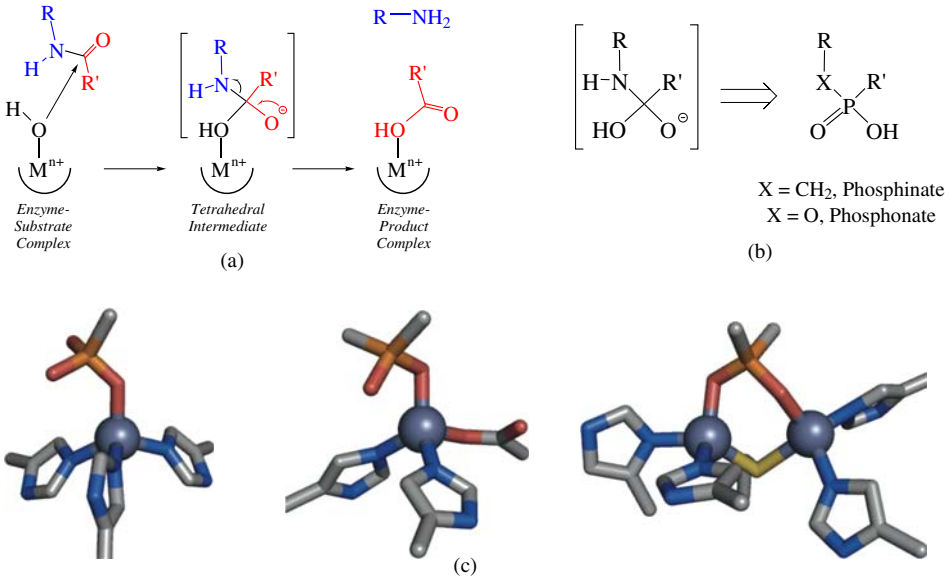

Figure 14.4 *Biological inspiration for phosphate-based MBGs. (a) The mechanism of hydrolases proceeds through a tetrahedral intermediate. Although only one transition state is shown for simplicity, the proton can migrate to the other oxygen atom, transferring the negative charge on the metal-bound atom. Both resonance forms can lead to product formation. (b) The tetrahedral intermediate can be mimicked by phosphate-based MBGs. (c) Crystal structures of phosphonate- (left, PDB 1ZVX) and phosphinate-based (middle, PDB 2X96) inhibitors bound to mononuclear zinc(II) ion centers of MMP-8 and ACE, respectively. Phosphorus-based MBGs can also be used to bind dinuclear active sites such as the zinc(II)-dependent enzyme N-acyl-D-glutamate amidohydrolase (right, PDB 3GIQ). (See plate section for the colour version of this figure)*

While the binding affinity of carboxylates to metal ions is generally weaker than that of thiols [11], carboxylic acid MBGs do not undergo reactions with Cys residues, and hence do not result in the same off-target immunotoxic side effects associated with thiol-based drugs [12]. Carboxylates can adopt a variety of conformations bound to metal ions (Figure 14.3a) and carboxylates account for the largest fraction of inhibitor–metalloprotein structures in the PDB (found bound to Mn^{II}, Fe^{II}, and Zn^{II} active sites). Kawai and Nagata found that nearly 30% of all molecules bound to zinc(II) ions in the PDB do so through a carboxylate MBG [8]. The following discussion on coordination modes of carboxylates will include only Zn^{II}-bound complexes, because these complexes make up the majority of carboxylate-bound structures in the PDB. The observed trends also apply to the other metalloenzyme complexes that have been structurally characterized.

The difference between the two oxygen–metal bond distances ($\Delta d = d_2 - d_1$, Figure 14.3a) will be used here to describe how symmetric the binding of a carboxylate is to the active site metal ion. A Δd of zero indicates a perfectly symmetric bidentate coordination mode, and Δd values as large as 0.3 Å are considered bidentate, as these values are within the error of many lower-resolution protein crystal structures. To elucidate trends in binding mode, the occurrence of respective Δd values for zinc(II)-bound carboxylates were tabulated (Figure 14.3b, black). *Syn*-monodentate ($0.3\ Å < \Delta d < 1.5\ Å$) binding is by far the most common mode of binding, corresponding to the maximum observed frequency at a Δd of 0.7 Å. The O–Zn distance for the oxygen atom further from the Zn^{II} ion is highly variable, causing a relatively flat distribution between Δd values of 0.3 and 1 Å. Both bidentate ($\Delta d < 0.3\ Å$) and *anti*-monodentate ($\Delta d > 1.5\ Å$) binding modes are significantly less common, comprising 14 and 12% of structures in the PDB, respectively.

In an effort to understand the influence of the protein environment on the binding mode of carboxylates, an analysis of Zn^{II}-bound carboxylates in the Cambridge Structural Database (CSD), a database of small-molecule structures, was performed and compared with those found in the PDB (Figure 14.3b, gray). The CSD was searched for carboxylic acids that were bound by at least one oxygen atom to a zinc(II) ion. The *syn*-monodentate coordination mode is also the most common in the CSD, but the maximum frequency is at a Δd of 1.2 , 0.5 Å longer than in the protein structures. The distribution is much sharper, although this is at least partially due to the larger sample size (~17 000 CSD vs. ~250 PDB structures) and higher resolution of the small-molecule structures. Relative to protein-bound carboxylates, bidentate binding is less common in small-molecule crystal structures, while the frequency of Δd values corresponding to *anti*-monodentate coordination is much larger. The infrequency of the bidentate binding mode is understandable considering the unfavorably small bite angle of this ligand. In fact, as the carboxylate moves from *syn*-monodentate to bidentate, the closer metal-bound oxygen atom must move away from the metal ion to accommodate the second donor (Figure 14.3c). The frequency of *anti*-monodentate structures from the CSD is also influenced by structures of carboxylates bound to multiple metal centers, but these cases could not be easily excluded from the full data set. The decreased frequency of *anti*-monodentate and increase in bidentate binding in protein structures could be partly due to hydrogen bonding, as many metalloenzymes often have hydrophilic residues optimally positioned to stabilize metal-bound substrates and intermediates, which would be able to interact with the second carboxylate oxygen and hold it closer to the metal ion.

In addition to thiol and carboxylate MBGs, phosphates were among the early MBGs investigated for metalloprotein-inhibitor design. In the early 1970s, the phosphate-containing natural product phosphoramidon was isolated and shown to inhibit zinc(II)-dependent proteases such as thermolysin and carboxypeptidase A [13], a discovery that eventually led to the development and FDA approval of the ACE inhibitor fosinopril. The tetrahedral geometry of the phosphorus atom makes it a stable analog of the intermediate formed by hydrolases after nucleophilic attack by the metal-bound hydroxide (Figure 14.4). Phosphonates and phosphinates, which differ only in whether the phosphorus atom has one or two alkyl substituents, are by far the most commonly used phosphorous-containing MBG with phosphinates being slightly more common. The biological inspiration for inhibitor design based on the phosphate MBG is relatively easily defined; the carbonyl of the scissile peptide bond in the substrate can be replaced by a phosphate functionality, yielding a competitive inhibitor. Similar to carboxylates, the geometry of phosphates is such that bidentate binding is not favorable. Owing to the larger phosphorous atom, the two oxygen atoms in the phosphate group are ~0.2 Å further from each other than in carboxylates. This results in far more asymmetric binding; in the case of mononuclear zinc(II) structures, the O–Zn distance for the coordinated atom is on average ~0.1 Å shorter for phosphates than carboxylates, while the second oxygen is roughly 0.3 Å further from the metal center. The changes in MBG geometry also alter how the molecules coordinate to dinuclear centers. The wider O–O separation seems to encourage the μ-η^1,η^1 coordination mode (Figure 14.3a), as a survey of phosphate-bound dinuclear metal sites in the PDB shows far more equal distribution of μ-η^1,η^1 and μ-η^1,η^2 binding than found for carboxylates which display almost exclusively μ-η^1,η^2 coordination.

Hydroxamic acids are perhaps the most well known MBGs and their role as ligands in natural products such as bacterial siderophores has been well described [14]. Hydroxamates have good affinity for most first-row transition metals, are relatively easy to prepare, and were highly popularized by their use in matrix metalloproteinase (MMP)-inhibitor design. Unlike the MBGs discussed above, hydroxamic acids are almost always bidentate ligands, coordinating through both oxygen atoms and forming a stable five-member chelate ring (Figure 14.5a). Monodentate binding has been observed only in the active site of carbonic anhydrase (CA), where acetohydroxamic acid binds through a deprotonated nitrogen atom and the oxygen atoms of the ligand make hydrogen bonding contacts to protein residues (Figure 14.5a). Similar hydrogen bonding patterns are a primary reason why sulfonamide MBGs, which are weak inhibitors of most metalloproteins, are very effective MBGs for CA inhibitors [15]. Several reviews on sulfonamide inhibitors of CA are available and

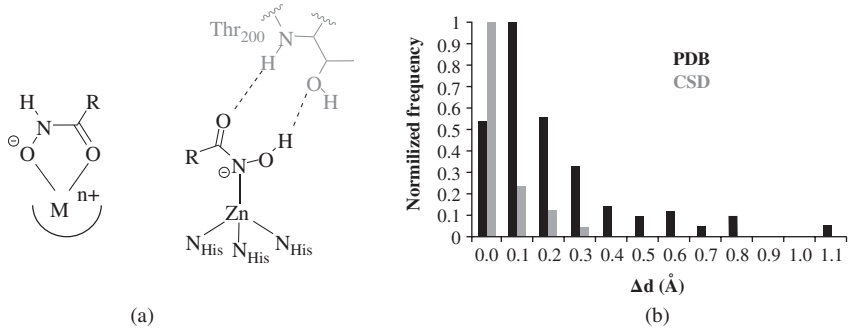

Figure 14.5 *Analysis of hydroxamic acid binding modes. (a) The coordination mode of hydroxamic acids to metal ions is almost always bidentate (left), except in the case of carbonic anhydrase (right, PDB 1AM6). (b) Frequency of Δd values, as described earlier, for both protein (PDB, zinc(II) only) and small-molecule (CSD, any transition metal, gray) structures. For comparison, the values are normalized to the maximum frequency*

hence a more extensive discussion is not provided here [15, 16]. Monodentate binding of a hydroxamate-based inhibitor also has been reported for HDAC-4 (PDB 2VQM), but this appears to be an improper interpretation of electron density. When the structure was re-refined from the structure factor file provided in the PDB, the ligand electron density unambiguously corresponds to the product of ligand hydrolysis, a carboxylic acid (D.P. Martin, D.T. Puerta, S.M. Cohen, unpublished results).

The binding of hydroxamic acids in metalloprotein active sites is similar to that seen in small-molecule metal complexes in the CSD (Figure 14.5b). The distribution of Δd values is flatter for protein structures, but over 70% of the complexes in the CSD show a Δd of less than 0.3 Å. As is the case with the carboxylate-bound structures, this trend is likely both a result of the interactions between the MBG and the local protein active site as well as an artifact of the lower resolution of these structures. Despite the extensive characterization of the hydroxamic acid as an MBG and the development of many inhibitors that have very high potency *in vitro* and *in vivo*, hydroxamic acid-based inhibitors have had very modest success in the clinic. In fact, only one inhibitor based on this MBG has obtained FDA approval [17]. One drawback of hydroxamates is their relatively short half-lives. The hydroxamic acid MBG is very susceptible to hydrolysis yielding hydroxylamine and the corresponding carboxylic acid in solution. Hydroxamic acids have also been shown to be prone to metabolic transformations such as glucuronidation [18]. The resulting metabolites are often inactive or much less active against the intended target [19].

14.3 MBGs related to hydroxamic acids

In order to improve on the MBGs described above, many derivatives of these molecules have been developed. Second-generation MBGs have been developed to improve on a wide variety of characteristics including potency, selectivity, and pharmacokinetics. Given the pre-clinical success of inhibitors based on the hydroxamic acid MBG, derivatives of hydroxamic acids have been widely explored. These molecules have been designed with the intent of yielding both greater hydrolytic stability and improved target specificity. *N*-Formylhydroxylamines (i.e., reverse hydroxamic acids, Figure 14.6) are isomers of hydroxamic acids with the inhibitor extending from the nitrogen atom instead of the carbonyl and terminating in an aldehyde functionality. Molecules of this type have been shown to have significantly longer half-lives than hydroxamic acids both *in vitro* and *in vivo* [20]. One reason for this is that replacing the hydrogen atom on the nitrogen atom with an alkyl substituent may stabilize the resonance form containing an iminium cation (see Figure 14.6a),

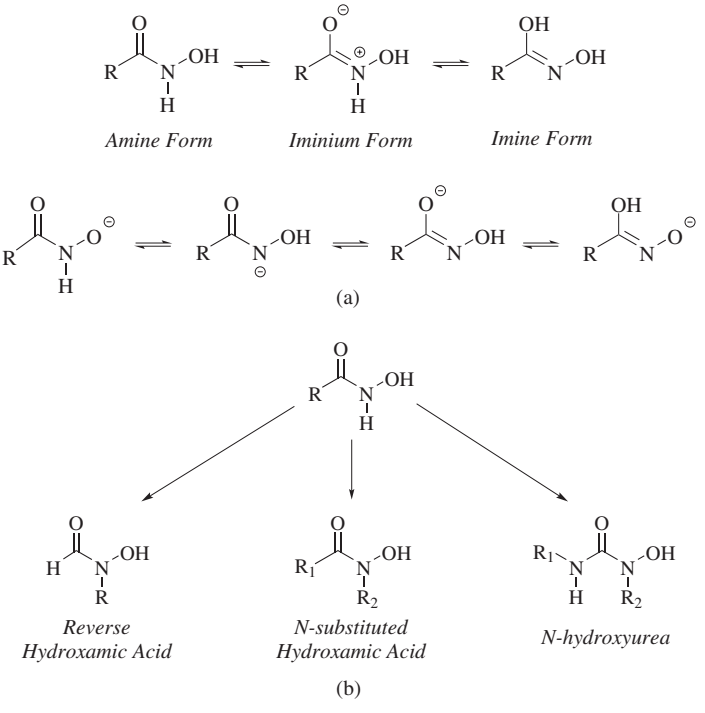

Figure 14.6 *Derivatives of the terminal hydroxamic acid MBG. (a) Resonance forms of protonated (top) and deprotonated (bottom) terminal hydroxamic acids. (b) Structures of MBGs related to terminal hydroxamic acids*

which is less susceptible to hydrolysis than the ketone/amine form [21]. It is also possible that, although there are enzymes that metabolize hydroxamic acids, these pathways may not be as competent in the metabolism of these so-called "reverse" hydroxamates.

One drawback of utilizing either terminal hydroxamic acids or reverse hydroxamic acids is that inhibitors can only be functionalized in one direction relative to the MBG. Although these MBGs are generally limited to interactions on one side of the metal ion due to the inherent geometry of the ligand, selected inhibitors based on terminal hydroxamic acids have been developed to interact with multiple active-site pockets [22]. Many metalloproteins act on non-terminal substrate bonds and thus generally have substrate-binding sites on both sides of the catalytic metal ion that can be targeted to gain specificity. *N*-Substituted hydroxamic acids (Figure 14.6b), which contain substituents on both the carbonyl and nitrogen atoms, yield inhibitors that can be extended in two directions in the active site, potentially improving both potency and target specificity. A related class of molecules, *N*-hydroxyureas, are similar to hydroxamic acids but include an additional nitrogen atom adjacent to the carbonyl. Using this scaffold, MBGs analogous to hydroxamic acids ($R_1 \neq H$, $R_2 = H$), reverse hydroxamic acids ($R_1 = H$, $R_2 \neq H$), and *N*-substituted hydroxamic acids ($R_1, R_2 \neq H$) can be obtained.

While many studies describe inhibitors based on reverse and *N*-substituted hydroxamic acids, there are far less structural data. Based on an analysis of the available structures, the coordination chemistry of *N*-substituted hydroxamic acids is generally similar to that of the terminal hydroxamates, showing that bidentate binding is preferred. As opposed to terminal hydroxamates, which favor symmetric binding, the *N*-hydroxy group of reverse hydroxamic acids binds, on average, 0.3 Å closer to the metal ion than does the aldehyde oxygen. Another significant difference between reverse and terminal hydroxamic acids is the absence of hydrogen bond-donating ability from the terminal N-H. As discussed above, a number of

metalloproteins contain residues capable of hydrogen bonding in close proximity to the catalytic metal ion in order to stabilize metal-bound substrates and intermediates, and these residues can have an impact on MBG coordination. Although crystallographic data on inhibitors based on the reverse hydroxamic acid MBG are limited, there are several examples of structurally similar inhibitors containing both terminal and reverse hydroxamic acid MBGs crystallized with the same protein. The coordination modes of these inhibitors have been compared in three zinc(II)-dependent hydrolase families: MMP, adamalysin (ADAM), and peptide deformylase (PDF) (Figure 14.7). In MMPs and several related enzymes including the ADAM family of peptidases, the hydroxamic acid MBG acts as a hydrogen bond donor through the N-H to the backbone carbonyl of a nearby protein residue (Gly119 in ADAM-TS1, Ala189 in MMP-9, Figure 14.7a). The reverse hydroxamic acid does not have this capability, which has been shown to lead to a roughly 10-fold decrease in potency when the rest of the inhibitor is unchanged [23]. In the active site of PDF, the carbonyl on the analogous residue (Gly61) is ~0.3 Å further from the metal center, decreasing the potential strength of this interaction. While this analysis is based on static structural data with limited resolution, it is interesting to note that for PDF, which does not appear to utilize this hydrogen bonding interaction, there is no drop-off in potency when switching to a reverse hydroxamic acid [24]. In all three cases, a Glu residue has a strong (2.6–2.7 Å) interaction with the metal-bound terminal oxygen. In PDF, the N-H of terminal hydroxamic acid inhibitors interacts with the second oxygen atom of the Glu residue. Additionally, there are residues in PDF (Leu112 and Gln65) that interact with the second bound oxygen of the inhibitors as well (Figure 14.7b) that do not have analogous interactions in MMPs and ADAMs. To compare the differences in binding between standard and reverse hydroxamate MBGs in the three enzymes, the MBGs from inhibitors with similar backbones were overlaid (backbones and non-coordinating residues were removed for this alignment). Consistent with the similar potency of hydroxamate- and reverse hydroxamate-based PDF inhibitors, the two MBGs overlay well with each other in the active site of PDF (Figure 14.7c). This is likely a result of the more extensive interactions between the protein and MBG; in the other two enzymes (MMPs and ADAMs), where there are fewer interactions, there is a large difference in coordination mode between the hydroxamic acid and reverse hydroxamic acid MBG.

N-Substituted hydroxamic acids, which can support inhibitor backbones on both sides of the MBG, have been utilized in inhibitors targeting several metalloproteins including leukotriene A4 hydrolase (LAH) and fructose bisphosphate aldolase [25]. Similar to phosphate mimics of the tetrahedral intermediates of hydrolases, *N*-substituted hydroxamic acids mimic metal-bound species in the catalytic cycle of these enzymes. Reported structures with *N*-substituted hydroxamic acid based inhibitors of aldolase show the expected bidentate coordination mode to the catalytic Zn^{II} ion (Figure 14.8a). As with the reverse hydroxamic acid MBG, the *N*-substituted hydroxamic acid seems to favor asymmetric binding with the *N*-hydroxy group ~0.3 Å closer to the metal ion than the carbonyl oxygen atom. This is in contrast to small-molecule structures of *N*-substituted hydroxamic acids from the CSD, which show a preference for symmetric binding much like terminal hydroxamic acids. Surprisingly, in the case of LAH, an inhibitor based on the *N*-substituted hydroxamic acid MBG has been shown to adopt a monodentate coordination mode through the *N*-hydroxy group (Figure 14.8b). This binding mode still results in a potent inhibitor, with an IC_{50} value against the target (2 nM) that is lower than that of an analogous inhibitor based on the terminal hydroxamic acid MBG (15 nM), the latter of which adopts the expected bidentate coordination mode (Figure 14.8b, *left*). This observation validates an advantage of *N*-substituted hydroxamates, whereby extending in two directions from the MBG compensates for any loss in potency arising from decreases in metal–ligand binding. In fact, the unexpected coordination mode is likely a result of these additional interactions (Figure 14.8b, *right*). The *N*-substituted hydroxamate adopts an *E* conformation (oxygen atoms are positioned on opposite sides of the C–N bond), allowing the carbonyl group to have a close interaction (2.52 Å) with a nearby Glu residue. The inhibitor also has an amine group near the MBG that makes two strong hydrogen bonds with the protein (Figure 14.8b, *right*). If the MBG were to adopt bidentate coordination, these interactions would most likely be lost. Although it might be surprising

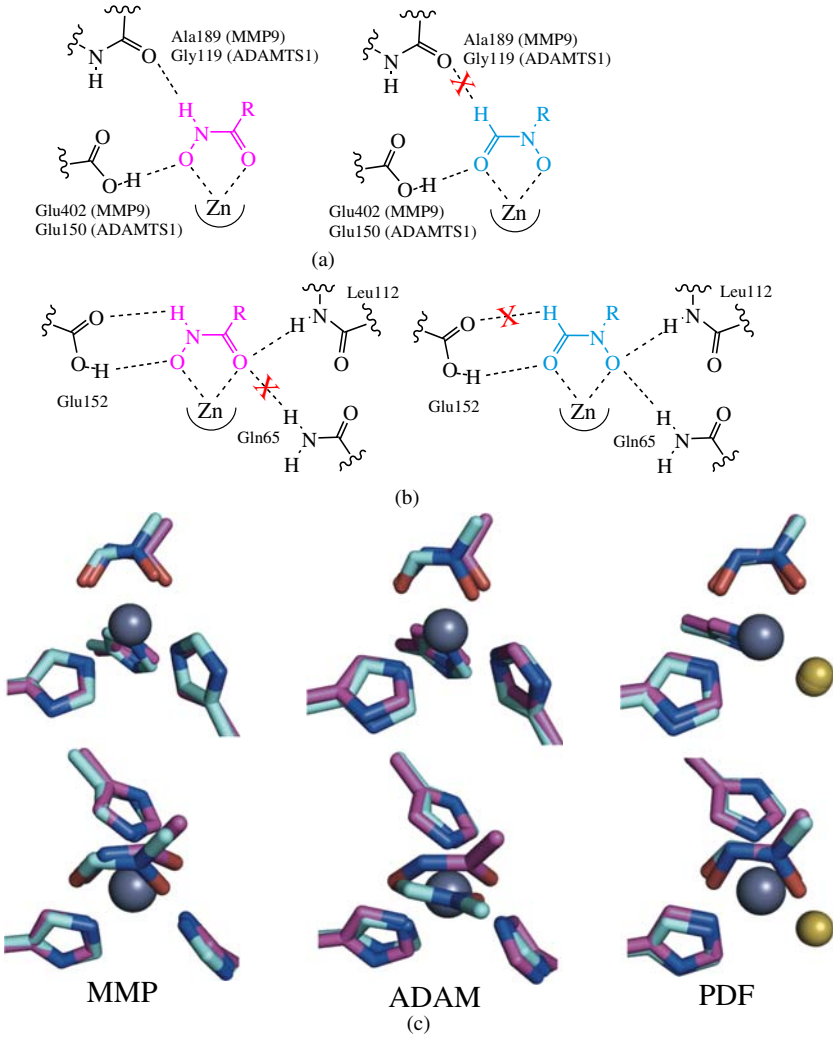

Figure 14.7 *Comparison of the coordination of terminal and reverse hydroxamates. (a) Schematic of the hydrogen bonds formed between the hydroxamic acid MBG and active-site residues of MMPs and ADAMs. Reverse hydroxamic acids cannot make some of these interactions, marked by a red "X." (b) Hydrogen bonding interactions between the MBGs and the active site of PDF, some of which (Leu112 and Gln65) do not occur for the other enzymes discussed. (c) Differences in binding modes of hydroxamic acids (shown in magenta, PDBs 1MMQ, 2RJQ, and 4DR9 from left to right) and reverse hydroxamic acids (shown in blue, PDBs 1GKC, 3Q2G, and 3U7N from left to right) for three different zinc(II)-dependent enzymes. Ligand–metal bonds have been omitted and inhibitors have been truncated for clarity. The cysteine donor of PDF is shown as a yellow sphere, as only the sulfur atom was used for alignment. (See plate section for the colour version of this figure)*

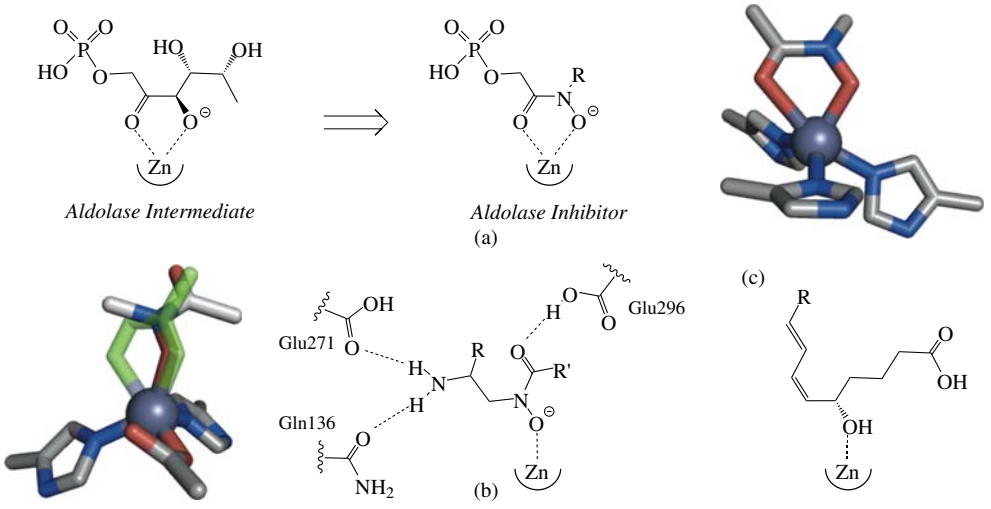

Figure 14.8 *Binding modes of N-substituted hydroxamate MBGs. (a) N-Substituted hydroxamic acids mimic intermediates in the catalytic cycles of enzymes such as aldolase, where the ligand binds in the expected bidentate fashion. (b) Unlike a terminal hydroxamate-based inhibitor (PDB 3B7U, shown in green), the N-substituted hydroxamate MBG displays monodentate coordination to the zinc(II) ion of leukotriene A4 hydrolase (LAH, PDB 2VJ8). This unexpected binding mode is stabilized by other interactions with the protein, shown on the right. (c) The product of LAH is a monodentate ligand. Inhibitors have been truncated for clarity. (See plate section for the colour version of this figure)*

that hydrogen bonding interactions would be preferred over optimal metal binding, it is worth noting that the product of LAH is an alcohol and as such is a monodentate ligand (Figure 14.8c) [26].

N-Hydroxyureas, which are isosteric with hydroxamates, have also attracted attention as alternative MBGs for inhibitor design. This was validated by the FDA approval of zileuton, an inhibitor of the Fe-dependent enzyme 5-lipoxygenase (5-LO), for the treatment of asthma (Figure 14.9a). Although it is proposed that zileuton binds the catalytic metal ion, there is no crystal structure of zileuton or any other *N*-hydroxyurea-based inhibitor bound in the active site of 5-LO. However, there are structures of this class of inhibitor bound to the zinc(II)-dependent enzymes MMP-8 and carboxypeptidase A. In all cases, the MBG adopts the '*E*' conformation with respect to the two oxygen atoms, precluding bidentate coordination. Unlike hydroxamates, which are most stable in a '*Z*' conformation, *N*-hydroxyureas have been shown to be more stable in the '*E*' conformation (Figure 14.9b). Computational studies have verified that the '*E*' conformation is ~2 kcal/mol more favorable than the '*Z*' conformation in the gas phase [27]. Bound to MMP-8, the hydroxyurea functionality adopts a conformation in which the metal-bound *N*-hydroxy group is out of the plane of the rest of the MBG (Figure 14.9c). The MBG does not make any other direct contacts with the surrounding protein environment that would drive monodentate coordination, unlike the case with the previously discussed LAH inhibitor. While inhibitors of LAH based on *N*-substituted hydroxamic acids do not lose activity relative to corresponding hydroxamic acids, the change in coordination mode with the *N*-hydroxyurea MBG results in a loss in affinity compared with analogous hydroxamic acids [28].

In another case, the crystal structures of two enantiomers of an inhibitor based on the *N*-hydroxyurea MBG bound to carboxypeptidase A have been reported and show interesting differences [29]. While the D-isomer is monodentate through the *N*-hydroxy group, the L-isomer binds through the carbonyl oxygen (Figure 14.9d). The phenyl groups of both isomers occupy the hydrophobic S1′ pocket of the enzyme and hydrogen bond

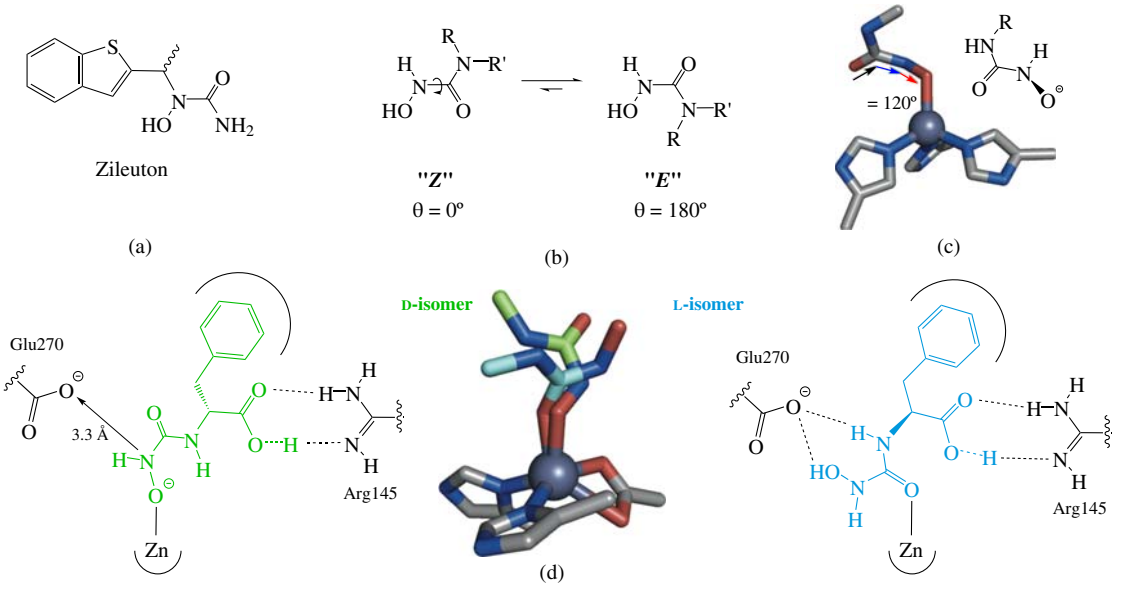

Figure 14.9 *The N-hydroxyurea MBG shows several distinct coordination modes. (a) The structure of zileuton, a clinically-approved 5-LO inhibitor based on the hydroxyurea MBG. (b) The 'Z' conformer of hydroxyurea, required for bidentate binding, is less favorable than the 'E' conformer. (c) Bound to the zinc(II) ion of MMP-8 (PDB 1ZP5), the MBG is nonplanar, displaying a torsion angle of 120°, between that of the 'E' and 'Z' conformers. (d) Bound to the zinc(II) ion of carboxypeptidase A, two enantiomers of the same inhibitor based on the N-hydroxyurea MBG adopt different binding modes (PDB 1HDQ and 1HEE). Inhibitors have been truncated for clarity. (See plate section for the colour version of this figure)*

through carboxylic acid functionalities to an active-site Arg residue. Owing to stereochemical considerations, the L-isomer cannot maintain these interactions if coordinated to the Zn^{II} ion through the *N*-hydroxy oxygen atom. Although binding to the Zn^{II} ion by the carbonyl oxygen atom is likely weaker than binding by the *N*-hydroxy oxygen atom, the two inhibitors have a similar affinity for the enzyme (4.6 and 1.5 μM for the L- and D-isomer, respectively) [29]. The unbound *N*-hydroxy group in the L-isomer makes a short hydrogen bond (2.74 Å) with an active-site Glu residue, which likely compensates for any loss in metal binding affinity. The wide variety of coordination modes of the *N*-hydroxyurea functionality suggests that, in the absence of structural data, this MBG may be a challenging starting point for metalloprotein inhibitor design.

14.4 MBGs related to carboxylic acids

As discussed previously, carboxylic acids most often bind in a monodentate fashion due to the small bite angle of the carboxylic acid functional group and the small four-member chelate ring formed upon bidentate coordination. By adding a donor atom α- to the carboxylic acid, a much more favorable five-member chelate ring can be formed. MBGs related to carboxylic acids include: α-keto acids, α-hydroxy acids, and picolinic acids (Figure 14.10). α-Ketoglutaric acid (α-KG, Figure 14.10) is required by many iron(II)-dependent oxygenases as a cofactor in order to activate dioxygen for substrate hydroxylation [30]. Molecules based on the α-keto acid MBG can therefore be competitive inhibitors by mimicking substrate binding. α-Hydroxy acids, which

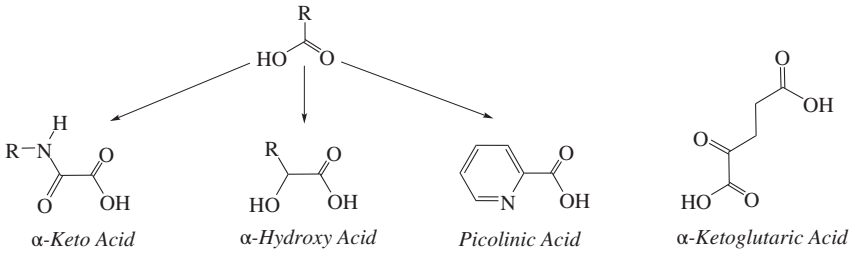

Figure 14.10 *MBGs related to carboxylic acids via addition of donor atoms*

have the same donor atoms but slightly different geometry due to the sp^3 hybridized carbon, have also been explored as MBGs [31]. These molecules have been well-studied as metal chelators, with over 300 crystal structures in the CSD of the α-hydroxy acid MBG bound to transition metal ions, compared with ∼20 with α-keto acids. Picolinic acids, which have a 2-pyridyl functionality appended to a carboxylic acid, have been even more extensively studied as metal chelators, with over 600 crystal structures in the CSD of the ligand bound to transition metals.

Iron(II)-dependent oxygenases are involved in a wide variety of physiological processes including oxygen sensing, nucleic acid repair, and chromatin remodeling [31]. The mechanism of hydroxylation via Fe^{II}-dependent oxygenases requires a metal-bound α-KG cofactor. Binding of dioxygen is followed by decarboxylation of the cofactor to yield an activated iron species that can be used to hydroxylate a wide variety of substrates (Figure 14.11a). Crystal structures of α-KG bound to Fe^{II}-dependent enzymes such as HIF-1α inhibitor (FIH), a prolyl hydroxylase, and ceKDM7A, a lysine demethylase, show the ligand coordinates the metal ion in a bidentate fashion through one carboxylic acid oxygen (presumably deprotonated) and the α-ketone (Figure 14.11b). The octahedral coordination sphere of the Fe^{II} ion is completed by two His imidazole donors, a monodentate Asp donor, and a water molecule, which occupies the O_2 binding site. The iron–oxygen bond to the carboxylic acid of α-KG is generally 0.1–0.3 Å shorter than to the ketone, presumably due to stronger electrostatic binding from the anionic carboxylic acid. Full-length inhibitors of this class of enzymes utilizing the α-keto acid MBG have not been developed, likely because the inhibitor could be metabolized like α-KG.

The most commonly explored inhibitor of α-KG-dependent iron(II) enzymes is *N*-oxalylglycine (NOG), which is isostructural with α-KG but differs in that the α-ketone is part of an amide bond (Figure 14.12a). The presence of an amide bond contributes to a stable resonance form, thereby eliminating the molecule as a cofactor and producing an effective inhibitor. NOG appears to adopt a more symmetric binding mode than α-KG, which may be a manifestation of the resonance structure that is responsible for its inactivity as a cofactor; a partial negative charge resides on the α-keto-oxygen atom, which may draw it closer to the metal center. It should be emphasized that due to the relatively low resolution of many of the crystal structures (∼2 Å), subtle changes in bond lengths may be within the uncertainty of the data. Given the large number of α-KG-dependent iron(II) oxygenases (estimated to be over 60), target specificity of NOG-based inhibitors is challenging; there is only one carbon atom in the molecule that can be functionalized (Figure 14.12a) [31]. A crystal structure of AlkB, a DNA demethylase, and an inhibitor based on NOG, shows that the α-keto acid group adopts the expected bidentate coordination mode (Figure 14.12b). In addition, NOG has been crystallographically characterized bound to a Ni^{II}-substituted version of JMJD2A, an Fe^{II}-dependent lysine demethylase, and shows the same metal binding mode. The α-keto acid MBG is not exclusive to inhibitors of iron(II)-dependent oxidases as it has also been used for inhibitors of LeuA, a zinc(II)-dependent isopropylmalate synthase, and an inhibitor in this class has been crystallographically observed bound bidentate to the

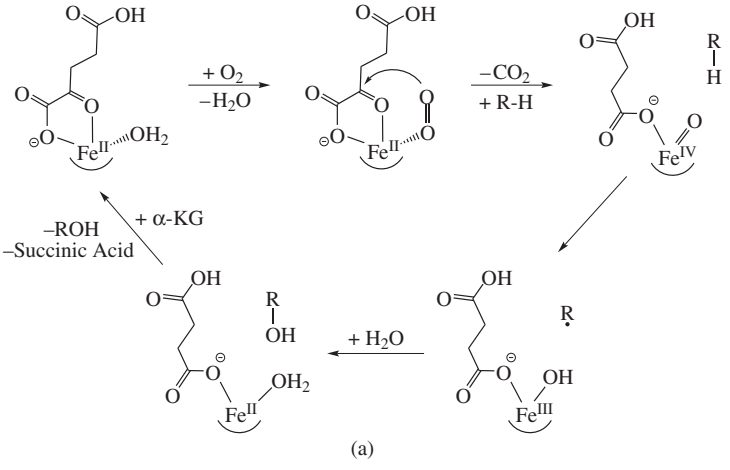

Figure 14.11 *Iron(II) oxygenases require a metal-bound cofactor, α-KG. (a) The mechanism of oxygen activation by α-KG-dependent iron(II) oxygenases. (b) α-KG bound bidentate to the iron(II) ion (PDB 2Y0I, α-KG is truncated for clarity). (See plate section for the colour version of this figure)*

catalytic Zn^{II} ion (PDB 3HPZ). Unlike iron(II)-dependent oxygenases, LeuA does not use α-KG as a cofactor. However, LeuA utilizes an α-keto acid as its substrate [32].

Another cofactor mimic of α-KG-dependent enzymes that has been used as an inhibitor is 2-hydroxyglutaric acid (2HG, Figure 14.12a). By changing the α-ketone to an alcohol, metal binding is maintained but catalytic activity is lost. Similar to NOG, substitution of the ketone for an alcohol makes the α-carbon less electropositive, decreasing its susceptibility to nucleophilic attack by O_2. The change in hybridization around the α-carbon also disrupts the planarity of the MBG, which could affect enzymatic turnover. Although the ligand itself has a different geometry, with respect to metal coordination, the ketone and alcohol bind similarly; superposition of α-KG- and 2HG-bound structures show that the oxygen atoms essentially overlay with each other (PDBs 2Y0I and 2YC0 respectively). A wide variety of 2-hydroxy acids, including glycolic, malic, and tartaric acid, are currently used in many food and cosmetic applications [33]. Despite widespread use with

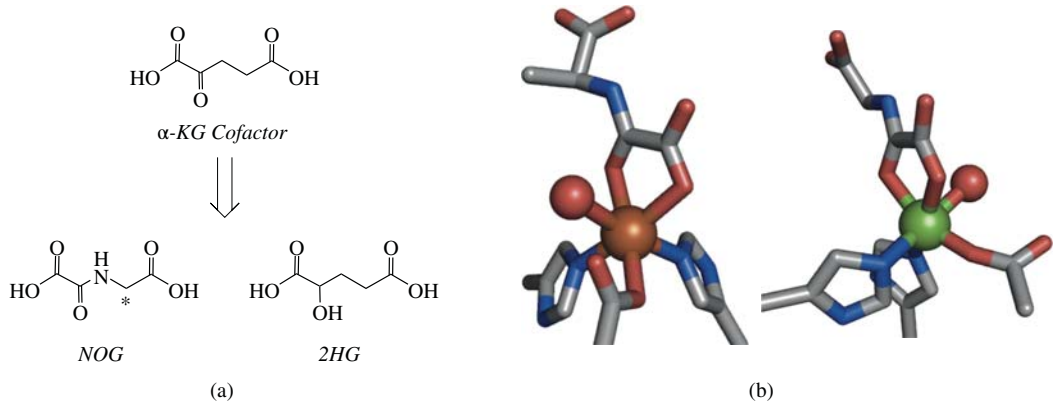

Figure 14.12 *Binding mode of α-keto acid-based MBGs. (a) The inhibitor N-oxalylglycine (NOG) is structurally similar to the α-KG cofactor of iron(II) oxygenases but cannot be turned over by the enzyme due to the addition of an amide bond. This molecule contains only one carbon atom that can be functionalized (marked with a star). 2-Hydroxyglutaric acid (2HG), which has an alcohol in place of the α-ketone, is also a cofactor mimic. (B) The structures of NOG bound to the iron(II) ion of AlkB (left, PDB 3T4H, inhibitor is truncated for clarity) and nickel(II)-substituted JMJD2A (right, PDB 4EYU) show the expected bidentate coordination. (See plate section for the colour version of this figure)*

significant human exposure, these MBGs have not attracted significant attention as therapeutics. The ability of these and other α-substituted carboxylic acids to bind a wide variety of metal ions would seem to make them ideal MBGs, but they have not been widely utilized in inhibitor design outside of those enzymes that utilize α-keto acids. One possible drawback to these MBGs is that, due to the involvement of this functional group in many metabolic cycles including the citric acid cycle [34], inhibitors containing α-keto or α-hydroxy acids would be metabolized too quickly to be practical for therapeutic use.

Picolinic acids have many features that make them appealing MBGs for inhibitor design including well-characterized metal binding (as evidenced by the large number of crystal structures in the CSD) and physiological compatibility [35]. They have primarily been applied to inhibitors of iron(II) α-KG-dependent oxygenases, but picolinic acids have also been used for inhibitors of the zinc(II)-dependent metallo-β-lactamase CphA [36]. The MBG pyridine-2,4-dicarboxylic acid, which has a carboxylate *para*- to the pyridyl nitrogen, structurally mimics the α-KG cofactor (Figure 14.13a). The crystal structure of pyridine-2,4-dicarboxylic acid in the active site of HIF-1α prolyl hydroxylase (FIH) shows the ligand adopting a binding mode similar to that of α-KG, maintaining all of the ligand–protein interactions. The carboxylate moieties of the inhibitor and cofactor overlay, while the pyridyl nitrogen atom occupies the coordination site of the α-KG ketone oxygen. The coordination mode of pyridine-2,4-dicarboxylic acid in the active site of JMJD2A, although still bidentate, is different to that of α-KG (Figure 14.13b). The pyridine nitrogen still occupies the same coordination site as the α-ketone oxygen, but the ligand is rotated such that the carboxylic acid occupies the same coordination site of a bound water molecule in the α-KG-bound structure. This rotation does not interfere with the hydrogen bonding of the carboxylic acid *para*- to the pyridine nitrogen as the carboxylate moieties of the inhibitor and cofactor still overlay. The sixth coordination site is filled by a water molecule which overlays with the cofactor's carboxylic acid in the α-KG-bound structure. The inhibitor-bound structure contains a Ni^{II} ion substituted as the active site metal, but this is not likely to be the cause of the shift in coordination geometry; α-KG binds in the same position to both the Fe^{II} and Ni^{II} JMJD2A active sites. This is not an anomaly, as the crystal structure of pyridine-2,4-dicarboxylic

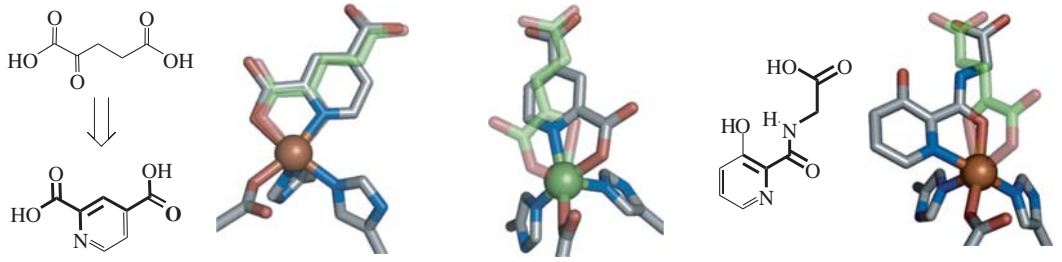

Figure 14.13 *Pyridine-derived MBGs based on α-KG isosteres. (a) Pyridine-2,4-dicarboxylic acid is structurally similar to α-KG, shown in green, and binds to the iron(II) ion of FIH in a similar fashion (PDB 2W0X). (b) Pyridine-2,4-dicarboxylic acid binds to nickel(II)-substituted JMJD2A in a similar mode but different orientation to that in α-KG (PDB 2VD7). (c) A picolinamide-based inhibitor shows a third, unique binding mode in the active site of AlkB (PDB 3T3Y). Bonds shown in bold highlight similarities between the inhibitors and α-KG. (See plate section for the colour version of this figure)*

acid bound to a different isoform, Ni-substituted JMJD2E, shows the same "rotated" coordination (PDB 2W2I).

The crystal structure of a picolinamide-based inhibitor (2-(3-hydroxypicolinamido)acetic acid, Figure 14.13c) bound in the active site of the iron(II)-dependent enzyme AlkB shows yet another accessible coordination mode of picolinic acid-based MBGs. As there is no carboxylate *para*- to the pyridine nitrogen of this inhibitor, it is positioned such that the amide substituent, which terminates in a carboxylic acid, can maintain the hydrogen bonding interactions similar to that of α-KG. This rotation positions the pyridine nitrogen in the O_2 binding site, while the amide carbonyl oxygen occupies the coordination site of the ketone of α-KG. This positions the hydroxy group on the pyridine ring for a strong hydrogen bond with a nearby Ser residue (Ser145). This is likely to be the interaction that is driving the change in coordination mode, as molecules lacking this hydroxy group lose inhibitory activity [37]. It is worth noting that, because of the amide functionality, both donor atoms bind the metal as neutral species (although there is a partial negative charge on the ketone oxygen from the amide resonance), likely weakening the metal–ligand interaction relative to that of unsubstituted picolinic acid. This change in the metal–ligand bond may contribute to the change in conformation.

It is important to mention that the widely used hydroxamic acid MBG has been explored as an alternative in the development of inhibitors of several α-KG-dependent oxygenases. Only one crystal structure of a hydroxamate-based oxygenase inhibitor bound to the active-site Fe^{II} ion has been reported. In that structure (PDB 2WA4), two inhibitor molecules bind the metal ion. One inhibitor binds in the expected position, occupying the coordination sites of α-KG, while the other displaces an Asp and water ligand from the iron center.

14.5 MBGs related to thiols

Given the popularity of thiols as MBGs, it is not unexpected that a number of MBGs related to thiols have been explored in an effort to exploit the favorable metal binding properties while addressing some of the clinical issues associated with these MBGs. Replacing the oxygen atoms of carboxylic acids with sulfur atoms can generate MBGs that capitalize on the strength of sulfur–metal binding while possibly avoiding some of the

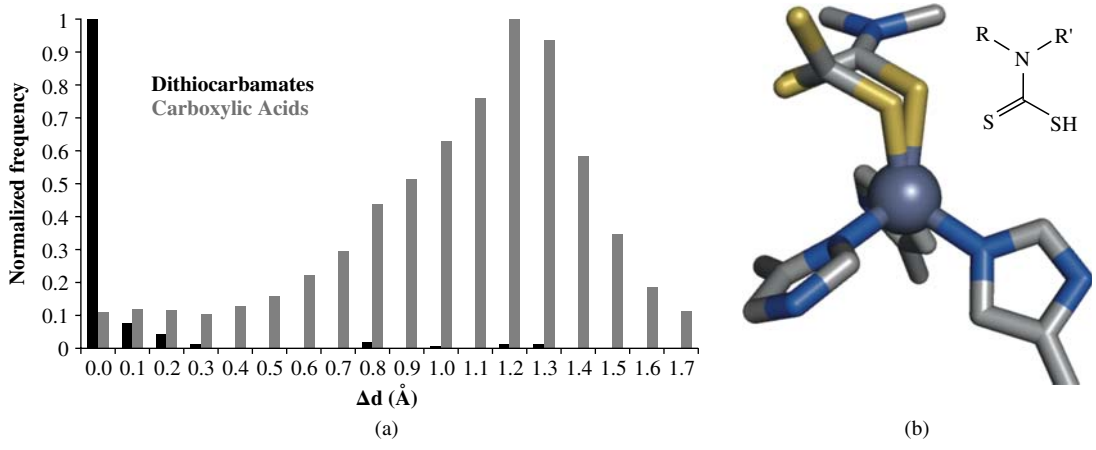

Figure 14.14 *Binding modes of the dithiocarbamate MBG. (a) Analysis of dithiocarbamates (black) compared with carboxylic acids (gray) bound to transition metals in the CSD. (b) The CS_3^{2-} anion (PDB 3K7K) and a dithiocarbamate-based inhibitor (PDB 3P58, truncated for clarity) both show monodentate coordination to the zinc(II) ion of human carbonic anhydrase II. (See plate section for the colour version of this figure)*

clinical issues seen with inhibitors based on the sulfhydryl MBG. The side effects associated with this MBG are thought to originate from an immune response triggered by off-target binding of the sulfhydryl group [38]. Dithiocarbamates have a slightly lower reduction potential than alkyl thiols, thus are more likely to circulate in their less reactive disulfide form [39]. Also, dithiocarbamates have been investigated as immunosuppressants, and this activity could mitigate the effects of adduct formation [40]. One FDA-approved drug contains the dithiocarbamate moiety (administered as the disulfide disulfiram, an inhibitor of acetaldehyde dehydrogenase, a non-metalloprotein), and others have proceeded to Phase III clinical trials [41]. The clinical success of these compounds suggests that the dithiocarbamate functionality may have favorable biocompatibility as an MBG. Although they are structurally similar to carboxylic acids, analysis of small-molecule crystal structures of dithiocarbamates bound to transition metals reveals that an overwhelming majority (~85%) bind in a symmetric bidentate coordination mode ($\Delta d < 0.1$, Figure 14.14a). This is in contrast to carboxylic acids, which prefer *syn*-monodentate binding. The larger atomic radii of sulfur atoms compared with oxygen atoms result in longer carbon–sulfur bonds in dithiocarbamates compared with the carbon–oxygen bonds in carboxylic acids, leading to a wider spacing (~3.0 Å vs. ~2.3 Å) between the donor atoms. This increases the bite angle of the ligand by ~10°, making bidentate binding more favorable. Recently, dithiocarbamates have been investigated as inhibitors of CAs. Given the preference for bidentate binding in small-molecule structures, it is surprising that these inhibitors coordinate the Zn^{II} ion of CA in a monodentate fashion (Figure 14.14b). This is not caused by the presence of an inhibitor backbone, as the CS_3^{2-} anion has been crystallized in the active site of CA and also shows monodentate coordination (PDB 3K7K). In both cases, the sulfur atom not coordinated to the metal center is directed toward a hydrophobic pocket in the active site, suggesting that this interaction may be playing a role in favoring the monodentate binding mode.

Inhibitors based on a β-mercapto ketone MBG take advantage of both the strength of sulfur–metal binding and formation of a five-member chelate ring with metal coordination through the ketone and thiol donors. While this class of MBG will likely have the same pharmacokinetic drawbacks as the thiol MBG in the clinic, they may benefit from increased potency and/or selectivity arising from the second donor atom. Similar to α-hydroxy acids, the α-mercapto ketone MBG is not a planar molecule, with observed torsion angles between 45° and 80°. The configuration of the sulfur-bound carbon atom, if chiral, allows for directionality

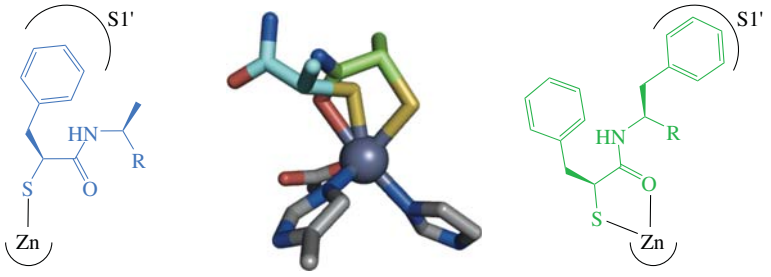

Figure 14.15 *Two binding modes of an α-mercapto ketone MBG-based inhibitor. Coordination of the zinc(II) ion of thermolysin by monodentate (blue, PDB 1QF2) and bidentate (green, PDB 1QF2) inhibitors based on the α-mercaptoketone MBG. Inhibitors are truncated for clarity. The change in coordination is driven by the hydrophobic interaction of the inhibitor backbone in the S1′ pocket. (See plate section for the colour version of this figure)*

to be introduced into the inhibitor. Crystal structures of several mercapto ketone-based inhibitors bound to the zinc(II)-dependent hydrolase thermolysin have been obtained, and some show bidentate coordination to the metal ion (Figure 14.15). The C–S–Zn bond angles are ~106° with a bond length of 2.3 Å, consistent with S–Zn binding. The O–Zn bond length is long (2.4 Å), but the geometry around the Zn^{II} ion is close to ideal trigonal bipyramidal, suggesting that the O–Zn interaction is significant. However, a related inhibitor containing the same MBG but a different backbone shows monodentate coordination through the thiol. In order to satisfy a favorable hydrophobic interaction in the S1′ pocket of the enzyme, the inhibitor is shifted in the active site, moving the keto-oxygen atom nearly 5 Å from the Zn^{II} ion. While this change in coordination leads to a 30-fold decrease in potency against thermolysin relative to the two bidentate inhibitors studied, all three inhibitors have roughly the same potency against neprilysin and ACE, two related zinc(II) hydrolases [42]. The two bidentate ligands have also been crystallized in the active site of neprilysin and show the same bidentate coordination mode. The metal–ligand bond lengths are significantly shorter than those in the thermolysin adducts (1.84 and 2.10 Å for the oxygen and sulfur, respectively), and the C–S–Zn angles for the thiol (<90°) are far from ideal [11]. This apparent distorted binding may be an artifact of the low resolutions of the two structures (2.35 and 2.6 Å), so conclusions about metal coordination, other than the bidentate binding mode, cannot be made.

14.6 Amine, alcohol, and carbonyl MBGs

Although the metal binding of amines, alcohols, and carbonyls is significantly weaker than that of sulfur-based ligands, these functional groups can avert thiol-related clinical issues. Primary amines have not been commonly utilized in metalloprotein inhibitors as MBGs, with the exception of the 2-aminoimidazole MBG used to target the dinuclear Mn^{II}-dependent enzyme arginase [43]. Examination of the crystal structure of an 2-aminoimidazole-based inhibitor bound to arginase reveals a mode of binding in which the amine group displaces a bridging hydroxide from the dinuclear Mn^{II} active site (Figure 14.16a). While the nitrogen appears to be coordinated to one Mn^{II} ion, the long distance (~2.9 Å) to the second Mn^{II} ion and an unfavorable C–N–Mn angle of ~90° indicate that the amine is not acting in a bridging fashion between the two metal ions. In mononuclear active sites, it is more common for the terminal amine of peptide-based inhibitors of metalloproteins, both natural and synthetic, to be involved in metal binding. Structures of two such inhibitors bound to HDAC-8 show monodentate coordination through the terminal amine group of the inhibitor, resulting in distorted tetrahedral geometry around the Zn^{II} ion (Figure 14.16b). Along with the apparent geometry, the

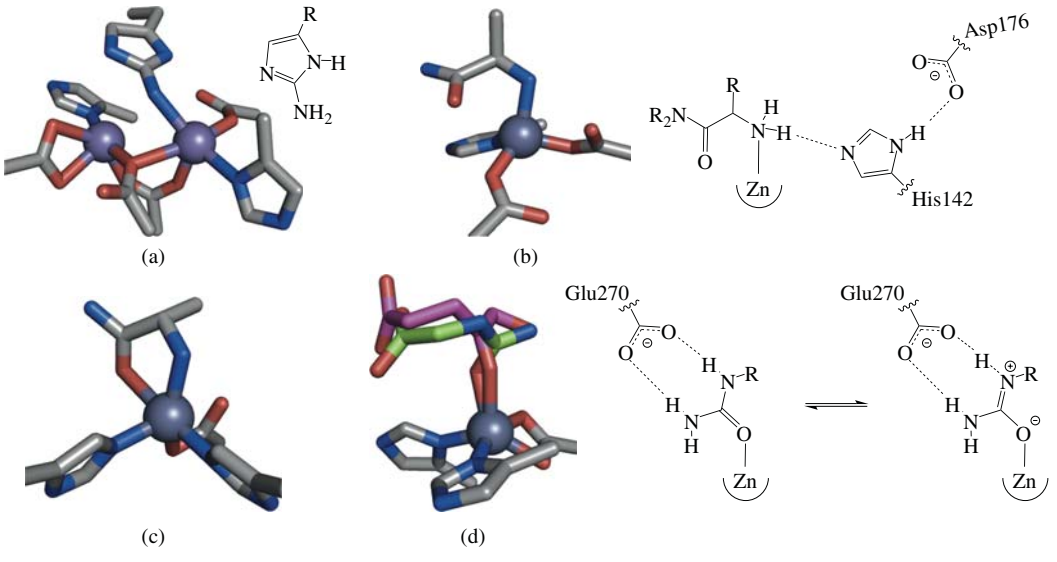

Figure 14.16 *Binding modes of selected amine and carbonyl-based MBGs. (a) Binding of the 2-aminoimidazole MBG to the dinuclear manganese(II) active site of arginase I (PDB 3MFV). (b) The monodentate binding mode of the terminal amine of a peptide-based inhibitor of HDAC8 (PDB 3SFH) may be stabilized by a hydrogen bonding network, diagrammed on the right. (c) The amino termini of peptidic inhibitors of C. botulinum neurotoxin A act as bidentate ligands (PDB 3QW6). (d) Bound to the zinc(II) ion of carboxypeptidase A, inhibitors based on α-hydroxy ketone and urea MBGs act as monodentate ligands (PDBs 3FVI and 1HDU, respectively). The urea has a shorter O–Zn bond length, possibly due to stabilization of an anionic resonance structure by an active-site Glu residue, diagrammed on the right. Inhibitors have been truncated for clarity. (See plate section for the colour version of this figure)*

O–Zn distance (> 2.7 Å) and unfavorable C–O–Zn angle (~90°) suggest that there is no significant interaction with the amide oxygen. The coordination of the amine is likely enhanced by its participation in a hydrogen bonding network with His142 and Asp176 (Figure 14.16b). In the case of a series of peptide inhibitors of botulinum neurotoxin A, a zinc(II)-dependent hydrolase, the amide oxygen also coordinates to the metal ion (~2.3 Å) to form a five-member chelate ring, resulting in trigonal bipyramidal geometry around the metal ion (Figure 14.16c). As with HDAC-8, there is a hydrogen bond acceptor ideally positioned near the coordinated amine group (Glu224, 2.73 Å). The ketone also makes a close interaction (~2.7 Å) with Tyr366, which may play a role in positioning the oxygen atom closer to the metal ion.

The ketone functionality alone has been utilized as a monodentate MBG as demonstrated in the development of inhibitors of carboxypeptidase A, a zinc(II)-dependent hydrolase. An inhibitor based on the α-hydroxy ketone MBG acts as a monodentate ligand, with the hydroxy group not making any significant (< 3 Å) interactions with the protein (Figure 14.16c). The Zn^{II}-binding Glu residue of the enzyme acts as a bidentate ligand, leading to a trigonal bipyramidal geometry upon monodentate MBG coordination. A urea-based inhibitor shows similar coordination though a monodentate ketone, but at 2.0 Å, the ketone oxygen is closer to the Zn^{II} ion by ~0.2 Å compared with the previous example. An examination of the hydrogen bonding environment around the MBG shows that a nearby carboxylate (Glu270) is positioned to stabilize the imine form of the urea functionality, increasing the anionic character of the coordinating oxygen atom and thus increasing the electrostatic attraction to the metal center (Figure 14.16d). In the case of an inhibitor based on a ketone that is not part of amide bond, this resonance form is not accessible so the partial negative charge on the oxygen

atom would be diminished, likely weakening the ligand–metal bond. Despite the likely weaker interaction with the metal ion of carboxypeptidase A, the α-hydroxy ketone-based inhibitor is 20-fold more potent than its urea analog; positioning the urea MBG for metal coordination disrupts other key hydrogen bonding and hydrophobic interactions of the inhibitor, which may negate any benefit stemming from stronger metal binding. The influence of the hydrogen bonding interactions on the coordination of the urea MBG is demonstrated by the binding of a urea-based inhibitor to another zinc(II)-dependent enzyme, glutamate carboxypeptidase II (GCPII). In the case of GCPII, there are not any analogous carboxylate residues positioned to interact with the nitrogen atoms of the urea MBG, resulting in a significantly longer O–Zn bond length (2.7 Å).

Bestatin, a compound known to inhibit several zinc(II)-dependent enzymes, contains an α-hydroxy ketone MBG (Figure 14.17a). As an inhibitor of LAH, in contrast to the previously described inhibitor based on the *N*-substituted hydroxamic acid MBG, which acts as a monodentate ligand, bestatin adopts bidentate coordination to the Zn^{II} ion (Figure 14.17b). The carboxylic acid of Glu296, positioned 2.5 Å from the metal-bound hydroxy group, can act as a proton acceptor, favoring deprotonation of the α-hydroxy group. The coordinating ketone occupies the axial position (2.6 Å) in the distorted trigonal bipyramidal geometry. The ketone oxygen also has a close interaction (2.8 Å) with Tyr383, which may contribute to a lengthening of the O–Zn bond. Bidentate coordination by bestatin is also observed in the crystal structure of the inhibitor bound to an M1 family zinc(II)-dependent aminopeptidase (human aminopeptidase N, Figure 14.17c, in green). A similar inhibitor, which differs in that an amide functionality replaces the carboxylic acid and the Leu side chain is replaced by Ala (Figure 14.17a, *right*), binds as a monodentate ligand through its hydroxy group (Figure 14.17c, *right*). The change in coordination is most likely an effect of the hydrophobic groups; another amide-functionalized derivative of bestatin with a Val side chain substitution shows bidentate coordination (Figure 14.17c, *left*). In addition to mononuclear aminopeptidases, bestatin is also an inhibitor of dinuclear metallopeptidases. The molecule mimics the intermediate of peptide cleavage by coordinating to one metal ion with its ketone group, the other through its primary amine, with its hydroxy group acting as a bridging ligand (Figure 14.17d).

14.7 Other MBGs

Several other moieties have been utilized in metalloprotein inhibitor design to directly mimic the intermediates of metal-mediated hydrolysis. Substrate analogs that contain silanediols, which are similar in shape and size to phosphates but are less acidic (pK_a values of ~3 and ~10 for the phosphate and silanediol MBGs, respectively [44]) have been investigated as inhibitors of a wide variety of zinc(II)-dependent hydrolases including MMPs and ACE [45]. Comparison of silanediol- and phosphate-based inhibitors bound to thermolysin show that the MBGs essentially overlay; the O–Zn bond length does not change significantly (Figure 14.18). One would expect this bond length to be longer for a neutral hydroxy species, but the presence of His231 close to the coordinated oxygen may diminish this effect. This residue can act either as a hydrogen bond acceptor with a protonated species or as a proton/hydrogen bond acceptor for a deprotonated species. Additionally, the unbound oxygen atom of the MBG makes an interaction with the carboxylate group of Glu270 (Figure 14.18). While the hydroxy group of the silanediol MBG would not require protonation of the carboxylic acid to make an interaction, the phosphate can only act as a hydrogen bond acceptor and thus requires protonation of the carboxylic acid. Although the coordination of the neutral silicon-based MBG is likely weaker than that of the anionic phosphate, inhibitors maintain potency upon substitution by the silanediol MBG (10 and 40 nM for phosphate- and silanediol-based inhibitors, respectively) [44]. It is likely that the flexibility of the hydrogen bonding environment around the Zn^{II} ion contributes to the similar potency of inhibitors based on the phosphate and silanediol MBGs.

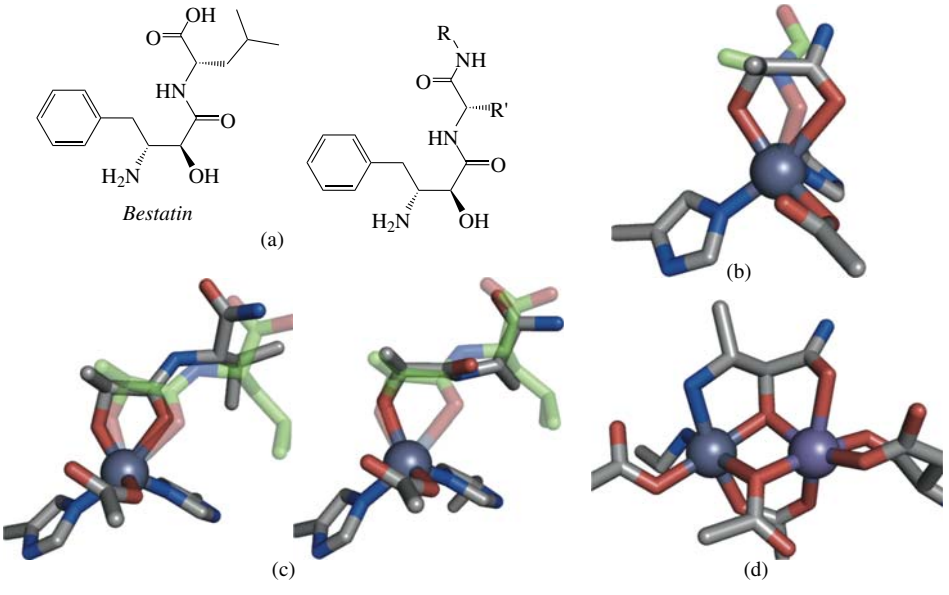

Figure 14.17 *Coordination modes of bestatin. (a) Structures bestatin (left) and the amide derivatives of bestatin (right). (b) Bound to the zinc(II) ion of leukotriene A4 hydrolase, the α-hydroxy ketone of bestatin acts as a bidentate ligand (PDB 3FTX). An inhibitor based on the N-substituted hydroxamic acid MBG is shown in green. (c) Bound to an M1 family aminopeptidase, amide derivatives of bestatin show both bidentate (left, PDB 4FYT) and monodentate (right, PDB 3T8V) coordination modes. Bestatin bound to the same enzyme is shown in green for comparison (PDB 3EBH). (d) Bestatin can also bind dinuclear metal centers, such as leucine aminopeptidase (PDB 3H8G). Ligands are truncated for clarity. (See plate section for the colour version of this figure)*

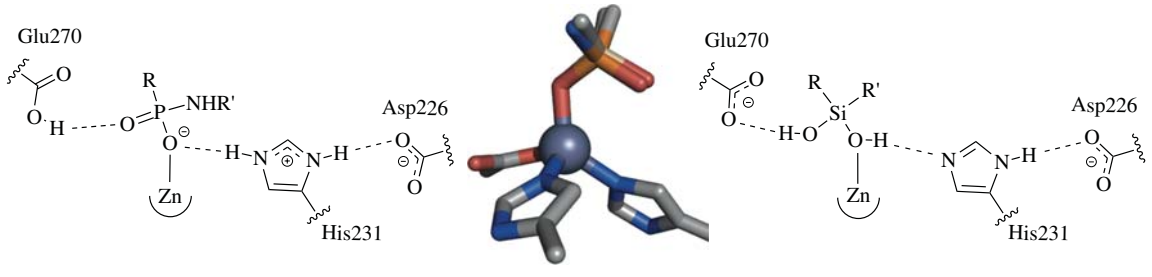

Figure 14.18 *Binding mode comparison of silanediol and phosphate MBGs. The binding modes of inhibitors based on the silanediol MBG (PDB 1Y3G) and phosphate MBG (PDB 4D9W) nearly overlay. Inhibitors are truncated for clarity. The rich hydrogen bonding environment around the metal ion is suitable for both charged (phosphate) and neutral (silanediol) donors. The unbound hydroxy group of the silanediol MBG can either donate or accept a hydrogen bond from Glu270 depending on the protonation state of that residue. (See plate section for the colour version of this figure)*

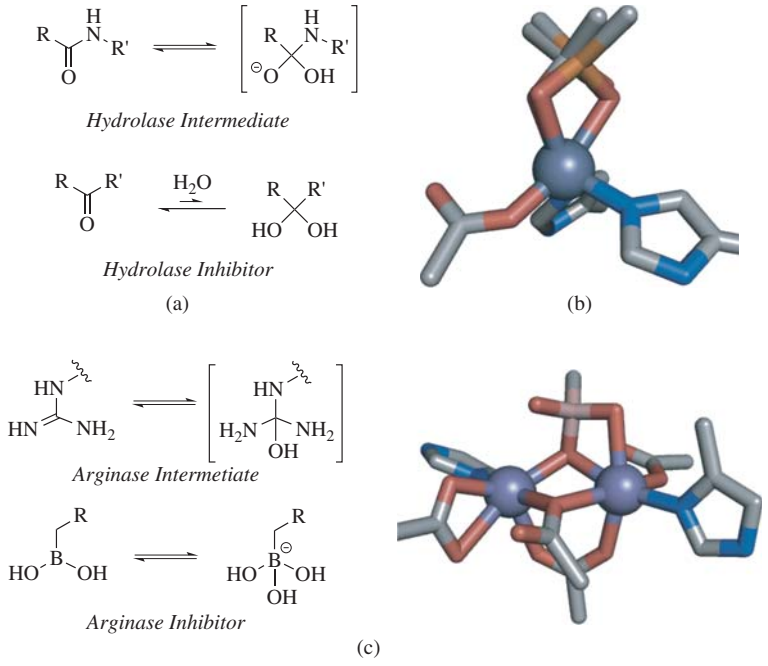

Figure 14.19 *Binding modes of inhibitors that are modified in solution. (a) Ketones can be hydrated, either in solution or potentially by target enzymes, to yield geminal diol mimics of the peptide hydrolase intermediate. (b) Comparison of the binding modes of an inhibitor based on this diol metal-binding motif (PDB 3BKK) to that of a phosphate-based inhibitor (PDB 2OC2) reveals that the coordination modes are very similar. (c) Boronic acids can be hydrated by the dinuclear manganese(II) active site of arginase to yield metal-bound boronate anions (PDB 1D3V). Inhibitors are truncated for clarity. (See plate section for the colour version of this figure)*

In addition to the ability to serve as a monodentate MBG, the ketone functionality can be hydrated to form a geminal diol, a direct mimic of the tetrahedral intermediate of hydrolases (Figure 14.19a) [46]. However, the MBG is not cleaved due to the lack of an amine leaving group. Although these hydrated ketones are generally not present in significant amounts in solution (less than 0.2% for peptide mimics), crystal structures of several ketone-based inhibitors bound to target enzymes show that the hydrated diols are selectively bound by the targets [46]. There is no direct evidence that the enzymes are involved in the hydration of the ketone moiety, but it is a possibility given the function of these enzymes. Other inhibitors have been designed with electron-withdrawing groups α- to the ketone such as CF_3 or NO_2, which promote hydration to the point that the geminal diol is the predominant species in solution [47]. Geminal diol inhibitors generally bind similarly to the analogous inhibitors based on the phosphate MBG (Figure 14.19b). Crystal structures of the diol MBG bound to the Zn^{II} ions of ACE, HDAC-4, and carboxypeptidase A have been obtained and all show asymmetric binding modes with one O–Zn bond length of 2.0–2.1 Å and the other between 2.3 and 2.5 Å.

Similarly, boronic acids have emerged as promising MBGs for inhibition of arginase [48]. Although synthesized as neutral species, the MBG is most often bound as its tetrahedral boronate anion, structurally similar to the transition state of arginase (Figure 14.19b). The enzyme is most likely responsible for the hydration; boronic acids have also been used for inhibition of serine proteases, where the boron atom is covalently bound to the active serine residue [49]. Bound in the active site of arginase, one hydroxy group of the boronate anion replaces the active hydroxy group of the inhibitor-free enzyme, bridging the two Mn^{II} ions symmetrically at

2.2 Å. Another hydroxy group from the inhibitor binds to one Mn^{II} ion at a slightly longer distance (2.36 Å), while the last hydroxy group does not appear to make any significant interactions with the protein.

Another class of MBGs that have attracted attention is that of nitrogen-containing heterocycles. Although the imidazole functional group has not been a widely used MBG, the hydantoin and barbiturate heterocycles have been used in the development of TNF-alpha converting enzyme (TACE) and MMP inhibitors (Figure 14.20). Despite the two enzymes being closely related, these heterocycles have been used to yield class- and isoform-specific inhibitors [50]. Both MBGs bind the catalytic Zn^{II} ions in a monodentate fashion through an endocyclic nitrogen atom. The Zn^{II} ions are coplanar with the heterocycle, consistent with the nitrogen atoms binding as imines. The imine resonance form is also stabilized by the ability of the resulting hydroxy group of the MBG to donate a hydrogen bond to an active-site Glu residue (~2.7 Å to either Glu223 of MMP13 or Glu406 of TACE). In addition, the unbound endocyclic nitrogen atoms have hydrogen bonding interactions with a backbone carbonyl from the protein in both cases. This interaction requires that the nitrogen atom is protonated, so it is likely that the second endocyclic nitrogen of the barbiturate MBG is in the amine form. Furthermore, the second carbonyl of the barbiturate MBG appears to accept a hydrogen bond from the amine of a backbone amide (Leu185, 2.8 Å). The hydantoin heterocycle lacks the carbonyl *para*- to the coordinated nitrogen to make this interaction. Given the similarity of the interactions of the two MBGs with their respective targets, the MBG itself is likely not responsible for the selectivity. The directionality of the inhibitors is likely the cause. Owing to the difference in ring sizes, the 5-position of the two heterocycles, from which the inhibitor backbones are extended, are oriented ~30° differently from each other with respect to the N–Zn bond, positioning the backbone substituents in different active-site pockets [51].

Although it is not a common metal chelator in the inorganic community (only one crystal structure in the CSD), the benzamide moiety was found to be an effective MBG for inhibitors of histone deacetylases (HDACi). Entinostat, an HDACi based on this MBG, is in Phase II clinical trials for a variety of cancers (Figure 14.21a) [52]. The crystal structure of a representative inhibitor bound to HDAC-2 reveals that the primary coordination to the Zn^{II} ion is through the 2-amino group (~2.1 Å). Although aromatic amines are not very nucleophilic, the metal-binding interaction is likely enhanced, both through positioning and increasing the anionic character on the nitrogen atom, as well as by the donation of hydrogen bonds through both amine hydrogen atoms to His residues in the active site. The MBG makes a second interaction with the Zn^{II} ion through the amide oxygen (~2.5 Å) in the axial position of a distorted trigonal bipyramidal geometry, forming a seven-member chelate ring. Much like the previously described heterocyclic MBGs, the 2-aminobenzamide functionality maximizes hydrogen bonding interactions with the surrounding active site in addition to binding the metal ion. Although the ligand could potentially coordinate through both nitrogen atoms to form a favorable five-member chelate ring, hydrogen bonding is maximized with the seven-member chelate. Additionally, the coordinated amide oxygen accepts a hydrogen bond from Tyr308 and the amide nitrogen donates a hydrogen bond to the backbone amide oxygen of Glu154. Comparison of the binding mode with that of a hydroxamic acid-based inhibitor to HDAC-8 shows that the donor atoms bind the Zn^{II} ion in similar positions (Figure 14.21b). The active site of HDACs sits at the bottom of a hydrophobic tunnel, through which both inhibitors extend. The unique aspect of the 2-aminobenzamide MBG is that the benzamide ring also occupies the second hydrophobic pocket or "foot region" [53]. The size of this group, which can be modulated by functionalization of the benzene ring, is used to tailor HDAC isoform specificity of the inhibitors [54]. Examination of the binding orientation of the hydroxamic acid MBG reveals that the nitrogen N–H is pointed away from the foot region, suggesting that even with substitution on the amine, inhibitors based on the *N*-substituted hydroxamic acid MBG would not be able to make this hydrophobic contact while maintaining the same coordination mode.

Recently, other metal chelators, such as bipyridines, pyrazolylpyridines, and hydroxyquinolines (Figure 14.22) have attracted attention as MBGs in the design of inhibitors of iron(II)-dependent oxygenases [31]. Although the size of these molecules may hamper their use as MBGs for some metalloproteins, the active

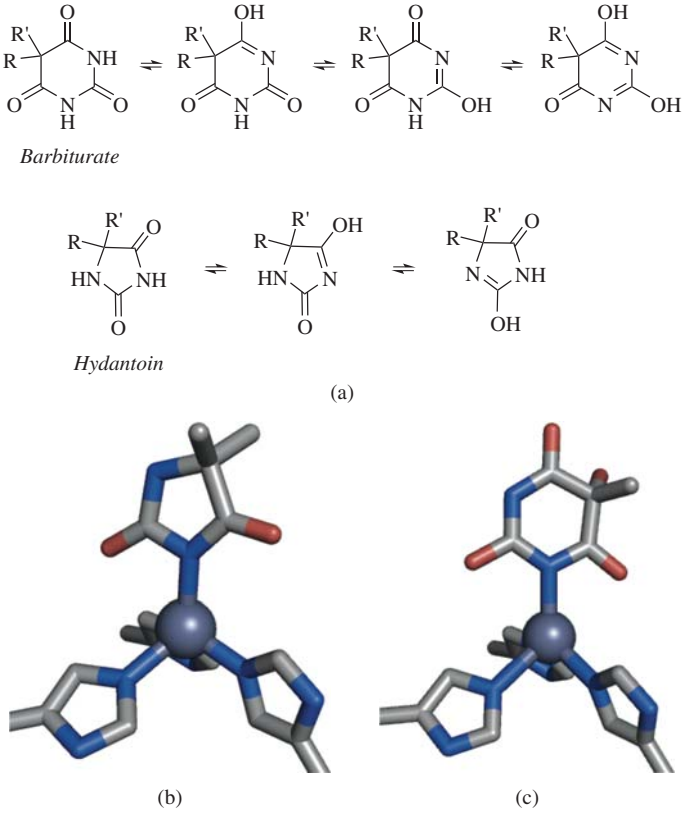

Figure 14.20 *Selected nitrogen-containing heterocycles that have been utilized as MBGs. (a) The resonance forms of barbiturates and hydantoins allow for metal binding and hydrogen bonding interaction to be maximized in protein-active sites. (b) The hydantoin MBG has been used in the development of TACE inhibitors, and binds as a monodentate ligand (PDB 3LEA). (c) The barbiturate MBG binds to the zinc(II) ion of MMPs in a similar monodentate fashion (PDB 1YOU). Inhibitors are truncated for clarity. (See plate section for the colour version of this figure)*

sites of Fe^{II}-dependent oxygenases are generally more open, since they must accommodate both the substrate and α-KG. The emergence of these ligands in the field of medicinal chemistry is a promising sign that an inorganic chemistry approach is beginning to be applied to metalloprotein inhibitor design. Although these molecules have for the most part been applied as α-KG mimics, their potential has only begun to be realized.

14.8 Conclusion

The diversity of metalloproteins and the diseases in which they are implicated provides numerous opportunities for the design and development of new therapeutics. In other fields of traditional medicinal chemistry, the diversity of enzymatic targets is reflected in the variety of pharmacophores developed to drug such targets. In contrast, the number of MBGs that have been developed into inhibitors of metalloproteins is surprisingly small; aside from the four most popular MBGs (thiols, carboxylic acids, phosphates, and hydroxamic acids)

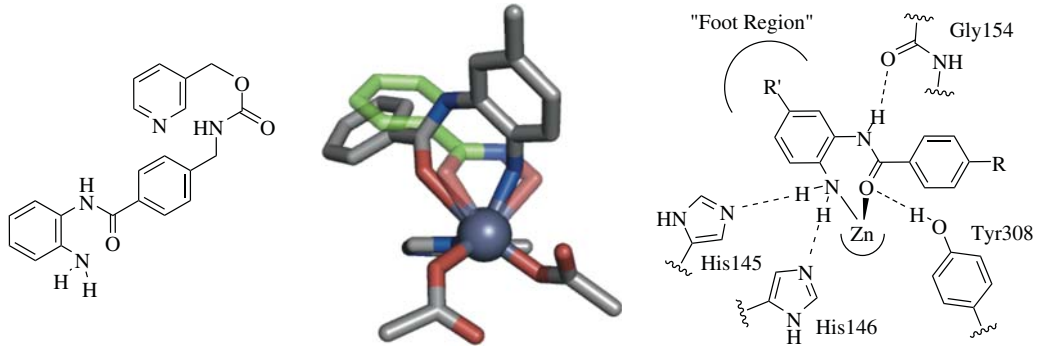

Figure 14.21 *Benzamide-based inhibitors of HDACs bind in a unique fashion. (a) The chemical structure of entinostat, an inhibitor of HDACs that is in Phase II clinical trials for the treatment of several cancers. (b) The crystal structure of an inhibitor based on the 2-aminobenzamide MBG bound in the active site of HDAC-2 (PDB 3MAX). For comparison, an inhibitor based on the terminal hydroxamate MBG bound to HDAC-8 (PDB 1W22) is shown in green. (c) Schematic of the hydrogen bonding interaction between the 2-aminobenzamide MBG and the active site of HDAC-2. (See plate section for the colour version of this figure)*

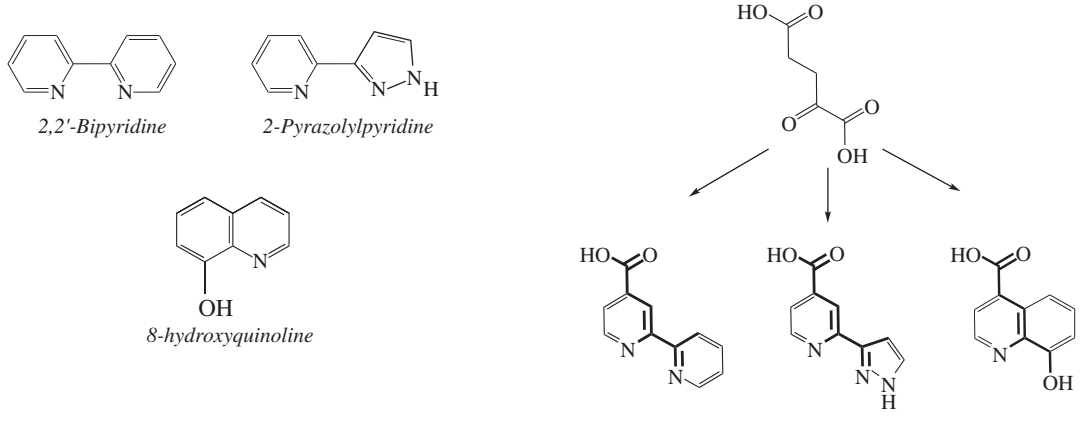

Figure 14.22 *Bipyridines, pyrazolylpyridines, and hydroxyquinolines, common ligands used in the inorganic chemistry community, have begun to be utilized in the design of metalloprotein inhibitors, mostly as mimics of α-KG. (See plate section for the colour version of this figure)*

and related molecules, there has been little exploration into novel scaffolds. This review presents several examples of inhibitor–protein interactions, including hydrogen bonding and hydrophobic contacts, which can have a substantial influence on the mode of metal coordination by inhibitors. These findings are in stark contrast to the view of metal binding provided by traditional coordination chemistry, or even bioinorganic model compounds, which lack the subtleties of a protein active site. It is clear from the observations in this review that metal–ligand interactions involved in metalloprotein inhibition are greatly influenced by the structure and chemical features of the protein active site. Hence, it is possible that even inhibitors with weak metal-binding affinities can be highly active by maximizing other interactions with the protein. Given the influence of these interactions, it would seem that metalloprotein inhibitor design would best be served by an approach to inhibitor design that balances both metal–ligand and protein–ligand interactions. This cooperative approach may yield inhibitors conferring additional benefits such as selectivity and biocompatibility. As such, a more thorough synthetic and structural exploration of the chemical space of MBGs is necessary to both understand and capitalize on the influence of the surrounding protein environment on metal coordination. In addition, more structural information on the binding of MBGs and inhibitors bound to metalloprotein active sites will be of great benefit in advancing this important subfield of drug development. The insight from such studies is likely to enlighten and surprise both inorganic and medicinal chemists alike.

References

1. Berg, J.M. and Shi, Y.G. (1996) The galvanization of biology: a growing appreciation for the roles of zinc. *Science*, **271** (5252), 1081–1085.
2. Lill, R. (2009) Function and biogenesis of iron-sulphur proteins. *Nature*, **460** (7257), 831–838.
3. Andreini, C., Bertini, I., Cavallaro, G. *et al*. (2008) Metal ions in biological catalysis: from enzyme databases to general principles. *J. Biol. Inorg. Chem.*, **13** (8), 1205–1218.
4. (a) Rouffet, M. and Cohen, S.M. (2011) Emerging trends in metalloprotein inhibition. *Dalton Trans.*, **40**, 3445–3454. (b) Jacobsen, F.E., Lewis, J.A. and Cohen, S.M. (2007) The design of inhibitors for medicinally relevant metalloproteins. *ChemMedChem*, **2** (2), 152–171.
5. Sousa, S.F., Fernandes, P.A. and Ramos, M.J. (2005) Unraveling the mechanism of the farnesyltransferase enzyme. *J. Biol. Inorg. Chem.*, **10** (1), 3–10.
6. Calvaresi, M., Garavelli, M. and Bottoni, A. (2008) Computational evidence for the catalytic mechanism of glutaminyl cyclase. A DFT investigation. *Proteins*, **73** (3), 527–538.
7. (a) Maag, H. (2007) Prodrugs of carboxylic acids. *Biotechnol. Pharm. Asp.*, **V**, 703–729. (b) Krise, J.P. and Stella, V.J. (1996) Prodrugs of phosphates, phosphonates, and phosphinates. *Adv. Drug Deliv. Rev.*, **19** (2), 287–310.
8. Kawai, K. and Nagata, N. (2012) Metal-ligand interactions: an analysis of zinc binding groups using the Protein Data Bank. *Eur. J. Med. Chem.*, **51**, 271–276.
9. Zhang, W., Ramamoorthy, Y., Kilicarslan, T. *et al*. (2002) Inhibition of cytochromes p450 by antifungal imidazole derivatives. *Drug Metab. Dispos.*, **30** (3), 314–318.
10. (a) Sousa, S.F., Fernandes, P.A. and Ramos, M.J. (2008) Farnesyltransferase inhibitors: a detailed chemical view on an elusive biological problem. *Curr. Med. Chem.*, **15** (15), 1478–1492. (b) Buchholz, M., Hamann, A., Aust, S. *et al*. (2009) Inhibitors for human glutaminyl cyclase by structure based design and bioisosteric replacement. *J. Med. Chem*, **52** (22), 7069–7080.
11. Gresh, N. (1995) Energetics of Zn2+ binding to a series of biologically relevant ligands: a molecular mechanics investigation grounded on ab initio self-consistent field supermolecular computations. *J. Comput. Chem.*, **16** (7), 856–882.
12. Lin, J.H. and Lu, A.Y.H. (1997) Role of pharmacokinetics and metabolism in drug discovery and development. *Pharmacol. Rev.*, **49** (4), 403–449.

13. (a) Suda, H., Aoyagi, T., Takeuchi, T. and Umezawa, H. (1973) Thermolysin inhibitor produced by actinomycetes – phosphoramidon. *J. Antibiot.*, **26** (10), 621–623. (b) Kam, C.-M., Nishino, N. and Powers, J.C. (1979) Inhibition of thermolysin and carboxypeptidase A by phosphoramidates. *Biochemistry*, **18** (14), 3032–3038.
14. Sandy, M. and Butler, A. (2009) Microbial iron acquisition: marine and terrestrial siderophores. *Chem. Rev.*, **109** (10), 4580–4595.
15. Krishnamurthy, V.M., Kaufman, G.K., Urbach, A.R. *et al*. (2008) Carbonic anhydrase as a model for biophysical and physical-organic studies of proteins and protein-ligand binding. *Chem. Rev.*, **108** (3), 946–1051.
16. Martin, D.P., Hann, Z.S. and Cohen, S.M. (2013) Metalloprotein-inhibitor binding: human carbonic anhydrase II as a model for probing metal-ligand interactions in a metalloprotein active site. *Inorg. Chem.*, 12207–12215.
17. Marks, P.A. and Breslow, R. (2007) Dimethyl sulfoxide to vorinostat: development of this histone deacetylase inhibitor as an anticancer drug. *Nat. Biotechnol.*, **25** (1), 84–90.
18. Kantharaj, E. and Jayaraman, R. (2011) Histone deacetylase inhibitors as therapeutic agents for cancer therapy: drug metabolism and pharmacokinetic properties, in *Drug Development – A Case Study Based Insight into Modern Strategies* (ed C. Rundfeldt), InTech.
19. Fingleton, B. (2008) MMPs as therapeutic targets – still a viable option? *Semin. Cell Dev. Biol.*, **19** (1), 61–68.
20. Crul, M., Beerepoot, L.V., Stokvis, E. *et al*. (2002) Clinical pharmacokinetics, pharmacodynamics and metabolism of the novel matrix metalloproteinase inhibitor ABT-518. *Cancer Chemother. Pharmacol.*, **50**, 473–478.
21. Fife, T.H. (1993) Kinetic and mechanistic effects of ease of C-N bond breaking in amide hydrolysis. The mechanisms of hydrolysis of N-acylimidazoles and N-acylbenzimidazoles. *Acc. Chem. Res.*, **26**, 325–331.
22. Georgiadis, D. and Yiotakis, A. (2008) Specific targeting of metzincin family members with small-molecule inhibitors: progress toward a multifarious challenge. *Bioorg. Med. Chem.*, **16**, 8781–8794.
23. Michaelides, M.R., Dellaria, J.F., Gong, J. *et al*. (2001) Biaryl ether retrohydroxamates as potent, long-lived, orally bioavailable MMP inhibitors. *Bioorg. Med. Chem. Lett.*, **11** (12), 1553–1556.
24. (a) Clements, J.M., Beckett, R.P., Brown, A. *et al*. (2001) Antibiotic activity and characterization of BB-3497, a novel peptide deformylase inhibitor. *Antimicrob. Agents Chemother.*, **45** (2), 563–570. (b) Boularot, A., Giglione, C., Petit, S. *et al*. (2007) Discovery and refinement of a new structural class of potent peptide deformylase inhibitors. *J. Med. Chem.*, **50** (1), 10–20.
25. (a) Fonvielle, M., Coinçon, M., Daher, R. *et al*. (2008) Synthesis and biochemical evaluation of selective inhibitors of class II fructose bisphosphate aldolases: toward new synthetic antibiotics. *Chem. Eur. J.*, **14** (28), 8521–8529. (b) Hogg, J.H., Ollmann, I.R., Haeggström, J.Z. *et al*. (1995) Amino hydroxamic acids as potent inhibitors of leukotriene A4 hydrolase. *Bioorg. Med. Chem.*, **3** (10), 1405–1415.
26. Thunnissen, M.M., Nordlund, P. and Haeggström, J.Z. (2001) Crystal structure of human leukotriene A(4) hydrolase, a bifunctional enzyme in inflammation. *Nat. Struct. Biol.*, **8** (2), 131–135.
27. Gregorio, G.D., Manna, F.L., Paniagua, J.C. and Vilaseca, E. (2004) Conformational analysis of N-hydroxyurea in the gas phase. *J. Mol. Struct. THEOCHEM*, **673**, 87–92.
28. Campestre, C., Agamennone, M., Tortorella, P. *et al*. (2006) Hydroxyurea as zinc binding in matrix metalloproteinase inhibition: mode of binding in a complex with MMP-8. *Bioorg. Med. Chem. Lett.*, **16**, 20–24.
29. Cho, J.H., Kim, D.H., Chung, S.J. *et al*. (2002) Insight into the stereochemistry in the inhibition of carboxypeptidase A with N-(hydroxyaminocarbonyl)phenylalanine: binding modes of an enantiomeric pair of the inhibitor to carboxypeptidase A. *Bioorg. Med. Chem.*, **10**, 2015–2022.
30. Kovaleva, E.G. and Lipscomb, J.D. (2008) Versatility of biological non-heme Fe(II) centers in oxygen activation reactions. *Nat. Chem. Biol.*, **4** (3), 186–193.
31. Rose, N.R., McDonough, M.A., King, O.N.F. *et al*. (2011) Inhibition of 2-oxoglutarate dependent oxygenases. *Chem. Soc. Rev.*, **40**, 4364–4397.
32. Carvalho, L.P.S. and Blanchard, J.S. (2006) Kinetic and chemical mechanism of alpha-isopropylmalate synthase from mycobacterium tuberculosis. *Biochemistry*, **45**, 8988–8999.
33. (a) Berry, S.K. (2001) Role of acidulents in food industry. *J. Food Sci. Technol.*, **38** (2), 93–104. (b) Babilas, P. and Knie, U. (2012) Cosmetic and dermatologic use of alpha hydroxy acids. *J. Dtsch. Dermatol. Ges.*, **10** (7), 488–491.
34. Yu, R.J. and Van Scott, E.J. (2004) Alpha-hydroxy acids and carboxylic acids. *J. Cosmet. Dermatol.*, **3** (2), 76–87.
35. Grant, R.S., Coggan, S.E. and Smythe, G.A. (2009) The physiological action of picolinic acid in the human brain. *Int. J. Tryptophan Res.*, **2**, 71–79.

36. Horsfall, L.E., Garau, G., Liénard, B.M.R. *et al*. (2007) Competitive inhibitors of the CphA metallo-β-lactamase from aeromonas hydrophila. *Antimicrob. Agents Chemother.*, **51** (6), 2136–2142.
37. Woon, E.C.Y., Demetriades, M., Bagg, E.A.L. *et al*. (2012) Dynamic combinatorial mass spectrometry leads to inhibitors of a 2-oxoglutarate-dependent nucleic acid demethylase. *J. Med. Chem.*, **55**, 2173–2184.
38. Edmonds, S., Gibb, A. and Sim, E. (1993) Effect of thiol compounds on human complement component C4. *Biochem. J.*, **289**, 801–805.
39. Nichols, P.J. and Grant, M.W. (1982) Reduction potentials of thiuram disulfide/dithiocarbamate couples in acetone/water. *Aust. J. Chem.*, **35**, 2455–2463.
40. Martínez-Martínez, S., Gomez delArco, P., Armesilla, A.L. *et al*. (1997) Blockade of T-cell activation by dithiocarbamates involves novel mechanisms of inhibition of nuclear factor of activated T cells. *Mol. Cell Biol.*, **17** (11), 6437–6447.
41. Suh, J.J., Pettinati, H.M., Kampman, K.M. and O'Brien, C.P. (2006) The status of disulfiram: a half of a century later. *J. Clin. Psychopharmacol.*, **26** (3), 290–302.
42. Gaucher, J.F., Selkti, M., Tiraboschi, G. *et al*. (1999) Crystal structures of α-mercaptoacyldipeptides in the thermolysin active site: structural parameters for a zn monodentation or bidentation in metalloendopeptidases. *Biochemistry*, **38** (39), 12569–12576.
43. Ilies, M., Costanzo, L.D., North, M.L. *et al*. (2010) 2-Aminoimidazole amino acids as inhibitors of the binuclear manganese metalloenzyme human arginase I. *J. Med. Chem.*, **53** (10), 4266–4276.
44. Kim, J. and Sieburth, S.M. (2004) A silanediol inhibitor of the metalloprotease thermolysin: synthesis and comparison with a phosphinic acid inhibitor. *J. Org. Chem.*, **69** (9), 3008–3014.
45. (a) Mutahi, M.W., Nittoli, T., Guo, L. and Sieburth, S.M. (2002) Silicon-based metalloprotease inhibitors: synthesis and evaluation of silanol and silanediol peptide analogues as inhibitors of angiotensin-converting enzyme. *J. Am. Chem. Soc.*, **124** (25), 7363–7375. (b) Sieburth, S.M., Nittoli, T., Mutahi, A.M. and Guo, L. (1998) Silanediols: a new class of potent protease inhibitors. *Angew. Chem., Int. Ed. Engl.*, **37** (6), 812–814.
46. Shoham, G., Christianson, D.W. and Oren, D.A. (1988) Complex between carboxypeptidase A and a hydrated ketomethylene substrate analog. *Proc. Natl. Acad. Sci. U.S.A.*, **85**, 684–688.
47. Jones, P., Bottomley, M.J., Carfí, A. *et al*. (2008) 2-Trifluoroacetylthiophenes, a novel series of potent and selective class II histone deacetylase inhibitors. *Bioorg. Med. Chem. Lett.*, **18** (11), 3456–3461.
48. Cox, J.D., Kim, N.N., Traish, A.M. and Christianson, D.W. (1999) Arginase-boronic acid complex highlights a physiological role in erectile function. *Nat. Struct. Mol. Biol.*, **6**, 1043–1047.
49. Fuhrmann, C.N., Daugherty, M.D. and Agard, D.A. (2006) Subangstrom crystallography reveals that short ionic hydrogen bonds, and not a His-Asp low-barrier hydrogen bond, stabilize the transition state in serine protease catalysis. *J. Am. Chem. Soc.*, **128** (28), 9086–9102.
50. Fisher, J.F. and Mobashery, S. (2006) Recent advances in MMP inhibitor design. *Cancer Metastasis Rev.*, **25**, 115–136.
51. (a) Sheppeck, J.E., Gilmore, J.L., Yang, A. *et al*. (2007) Discovery of novel hydantoins as selective non-hydroxamate inhibitors of tumor necrosis factor-α converting enzyme. *Bioorg. Med. Chem. Lett.*, **17** (5), 1413–1417. (b) Kim, S.-H., Pudzianowski, A.T., Leavitt, K.J. *et al*. (2005) Structure-based design of potent and selective inhibitors of collagenase-3 (MMP-13). *Bioorg. Med. Chem. Lett.*, **15** (4), 1101–1106.
52. Syndax (2013) http://www.syndax.com/dev-clinical.aspx (accessed 30 August 2013).
53. Wang, D.-F., Wiest, O., Helquist, P. *et al*. (2004) On the function of the 14 Å long internal cavity of histone deacetylase-like protein: implications for the design of histone deacetylase inhibitors. *J. Med. Chem.*, **47** (13), 3409–3417.
54. Methot, J.L., Chakravarty, P.K., Chenard, M. *et al*. (2008) Exploration of the internal cavity of histone deacetylase (HDAC) with selective HDAC1/HDAC2 inhibitors. *Bioorg. Med. Chem. Lett.*, **18** (3), 973–978.

15

Ruthenium Anticancer Compounds with Biologically-derived Ligands

Changhua Mu and Charles J. Walsby

Department of Chemistry, Simon Fraser University, 8888 University Drive, Burnaby, British Columbia, V5A 1S6, Canada

15.1 Introduction

In recent years, ruthenium-based anticancer compounds have become a leading area of development in medicinal chemistry. Numerous promising *in vitro* and *in vivo* studies, along with clinical successes, continue to stimulate interest in these compounds. Furthermore, a diverse range of complexes have been reported with a variety of differing targets and activities. This has led to a rapidly increasing number of studies on both the development of new compounds and the mechanisms of their activities. Ruthenium complexes have fundamental characteristics that make them particularly amenable to development as anticancer drugs including: (i) well-established coordination chemistry, (ii) slow ligand exchange rates that are often in the range of the rate of cell-division, (iii) oxidation states of 2+, 3+, and 4+ that are accessible under physiological conditions, and (iv) octahedral geometry, which provides for structural diversity and potentially for distinct activity from square-planar Pt^{II} compounds [1, 2]. Ligand design has increasingly become a key aspect in the development of new ruthenium anticancer compounds, and in this review we have focused on the application of ligands that are derived from biological molecules. As described in this review, such ligands potentially can provide a variety of ways to influence the activity of ruthenium chemotherapeutics including: (i) unique coordination modes, (ii) specific interactions with biological species, (iii) increased cellular uptake, and (iv) synergistic activity enhancement between the ligand and the metal center. While numerous studies have reported adducts of ruthenium compounds with a variety of biological species, in this review we have focused on studies where bio-relevant ligands were installed as key components of the original complex design.

In reports of ruthenium anticancer compounds with biological functionalities, the fundamental molecular scaffold is typically derived from one of the well-known families of active complexes. With this in mind,

Ligand Design in Medicinal Inorganic Chemistry, First Edition. Edited by Tim Storr.

we first present a description of the main types of ruthenium chemotherapeutic candidates, each of which have served as scaffolds for biologically derived ligands. Numerous review articles [1, 3–14] have done an excellent job of describing the state of the field in general [10, 15–21] and have also provided more detailed analysis of different types of compounds [22–29], and we will not try to replicate their efforts here. However, the following section will hopefully help to put the remainder of the chapter into context.

15.1.1 Simple coordination complexes

Although reports of the biological testing of ruthenium compounds go back as far as 1952 [30], the development of modern Ru anticancer compounds is generally considered to have started with the reports of Clarke and co-workers of chloride–ammine complexes in the 1980s [5, 8, 9, 31]. Examples of these compounds include the Ru^{III} complexes *fac*-[$RuCl_3(NH_3)_3$] (**1**) and *cis*-[$RuCl_2(NH_3)_4$]Cl (**2**), both of which exhibited activity against primary tumors, with the former showing promising activity against a variety of cell lines [32] (Figure 15.1). Ultimately, (**1**) was found to have insufficient aqueous solubility to be suitable as a drug [6, 33], and has not undergone further development. Subsequently, Alessio, Sava and co-workers reported highly water-soluble Ru^{II} chloride-dimethyl sulfoxide (DMSO) complexes [19, 25]. Notable examples include the Ru^{II} complexes *cis*-[$RuCl_2$(DMSO-*S*)$_3$(DMSO-*O*)] (**3**) and *trans*-[$RuCl_2$(DMSO-*S*)$_4$] (**4**) (Figure 15.1). Compound (**3**) was found to be non-cytotoxic *in vitro*, but showed activity against primary tumors and metastases in mice [25, 34]. The *trans* isomer (**4**) was found to be significantly more active against primary tumors and metastases in murine models [35, 36]. Particularly notable was the comparison in activity between (**4**) and cisplatin; although cisplatin was more active against primary tumors, (**4**) demonstrated superior selective activity against metastases [25]. Subsequently, this type of behavior, with relatively low cytotoxicity but good antimetastatic activity, has been reported in many studies of Ru–DMSO complexes [19, 28, 37, 38].

15.1.2 Ruthenium(III) complexes with heterocyclic N-donor and/or DMSO ligands

The next major phase of development for ruthenium anticancer compounds came with reports of Ru^{III} complexes containing heterocyclic nitrogen donor ligands. The first of these reports were from Keppler and co-workers who described a new family of anionic bis-azole complexes [39–41]. These compounds have nitrogen-coordinated heterocyclic ligands in the *trans* configuration, four equatorial chlorides, and charge compensation provided by the protonated azole ligands or sodium ions. Two compounds, imidazolium [*trans*-$RuCl_4$(1*H*-imidazole)$_2$] (**KP418**, ICR) (**5**) and indazolium [*trans*-$RuCl_4$(1*H*-indazole)$_2$] (**KP1019**)

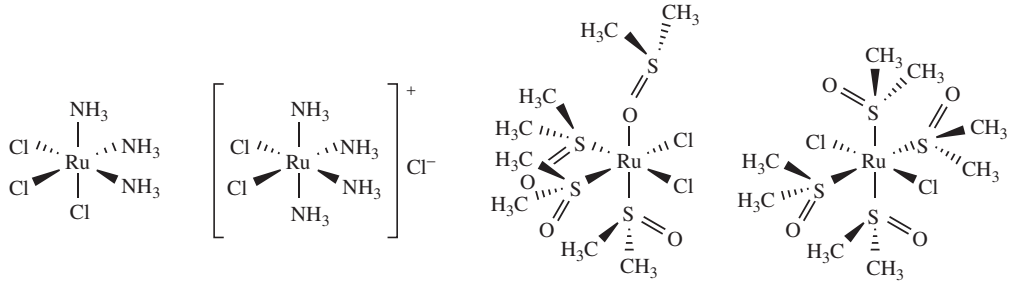

Figure 15.1 *Ruthenium coordination compounds exhibiting anticancer activity in early studies*

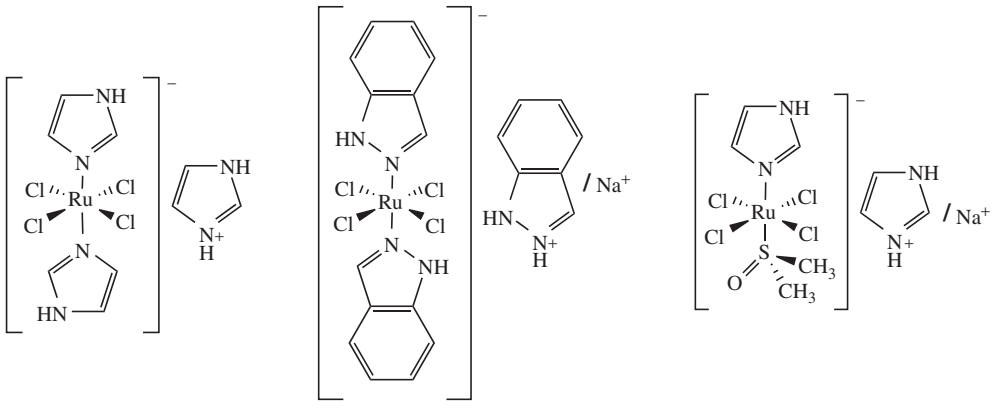

Figure 15.2 *Ruthenium(III) anticancer candidates with heterocyclic nitrogen donor ligands*

(**6**), were the primary focus of early studies (Figure 15.2). Both **KP418** and **KP1019** exhibit conventional antineoplastic properties and demonstrated very promising activity against colorectal cancer cell lines and platinum-resistant colorectal autochthonous tumors [42, 43]. **KP1019** demonstrated promising activity in several *in vitro* and *in vivo* studies [42, 44–47] with particularly significant results against human colon carcinoma cells [48]. *In vitro* studies of **KP418** also demonstrated strong antiproliferative activity against human colon cancer cell lines [46, 49], indicating similar modes of activity. However, **KP418** exhibited significantly higher nephrotoxicity in murine models than **KP1019**, making it unsuitable for human trials [49, 50]. This is an interesting consequence of the differences between the axial ligands and may be related to different interactions with serum proteins *in vivo*, particularly human serum albumin [51]. **KP1019** successfully completed phase-I clinical trials [52, 53] but ultimately failed in phase-II trials due in large part to insufficient aqueous solubility [54]. Recently, clinical development has resumed with the more soluble sodium-compensated analog of the complex, **KP1339** (**7**) [55, 56] (Figure 15.2).

In the early 1990s a second type of structurally similar complex was reported by Alessio and co-workers. These compounds are similar to **KP418** and **KP1019** but with one azole ligand replaced by DMSO. The first of these compounds, sodium [*trans*-$RuCl_4$(1*H*-imidazole)(DMSO-*S*)] **NAMI** (**9**) (Figure 15.2) was found to selectively inhibit the formation of solid tumor metastasis in mice [57–59]. Ultimately, the imidazolium-compensated analog of this compound, imidazolium [*trans*-$RuCl_4$(1*H*-imidazole)(DMSO-*S*)] **NAMI-A** (**8**) (Figure 15.2), was found to be more suitable to formulation for clinical use, while exhibiting the same antimetastatic properties. **NAMI-A** was the first ruthenium compound to enter phase I clinical trials, in 1999 [60], and has subsequently undergone further clinical development [54]. Although a detailed understanding of the antimetastatic activity of **NAMI-A** is still lacking, significant progress toward this goal has been made in recent years. It is notable that while **NAMI-A** is structurally similar to the bis-imidazole complex **KP418**, it shows essentially no cytotoxicity in common cancer cell lines [61, 62]. *In vitro* studies have indicated that the antimetastatic properties of **NAMI-A** may originate from interactions with components of the extracellular matrix [63, 64] or cell-surface interactions with actin-type proteins [65, 66], which result in reduced cellular motility [21].

Although these two families of compounds clearly have quite different modes of activity, they do share a number of similarities in terms of fundamental chemistry and biological interactions that are directly relevant to their *in vivo* behaviors. First, they undergo aqueous ligand exchange to yield a variety of aquated species

in solution through the loss of chloride ligands, and DMSO in the case of **NAMI-A**, so that they are best described as prodrugs [67–69]. Secondly, they readily form interactions with serum proteins, primarily with albumin but also with transferrin and other proteins [51, 70–74]. Third, their Ru^{III} centers can be reduced to Ru^{II} to give species that are activated toward interactions with various biomolecules via ligand exchange, a process that could potentially occur selectively in hypoxic tumor environments [75, 76]. However, although significant effort has been expended to uncover the origin of the anticancer activity of both **NAMI-A**- and **KP1019**-type complexes, key details remain elusive. This represents a barrier to the further development of these types of compounds and possibly explains the dearth of reports of derivatives with improved activity.

15.1.3 Ruthenium(II) arene complexes

Recently, the focus of ruthenium anticancer research has increasingly been on organometallic ruthenium(II) arene complexes, such as shown in Figure 15.3. Indeed, a survey of the literature in the past few years reveals that reports on these compounds are now appearing much more frequently than those for other ruthenium anticancer candidates, and overall these complexes have the greatest number of derivatives [21]. However, none of these compounds have yet entered clinical trials. Development in this area has centered primarily around two families of closely related compounds containing η^6-arene ligands and exchangeable chlorides.

Sadler and co-workers have developed a series of Ru^{II} complexes with the general formula $[(\eta^6\text{-arene})Ru(L)Cl]^+$, where L is typically a bidentate nitrogen- and/or oxygen-donor ligand, and the chloride ligand can be replaced by other halides or exchangeable ligands [23, 29, 77, 78]. Initial studies focused on complexes with chelating nitrogen ligands such as ethylenediamine (en) and *N*-ethylethylenediamine, producing compounds such as $[(\eta^6\text{-}p\text{-cymene})Ru(en)Cl]^+$ **(10)** and $[(\eta^6\text{-}p\text{-tetrahydroanthracene})Ru(en)Cl]^+$

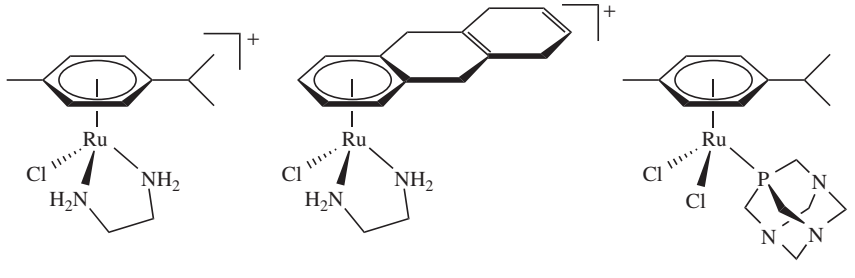

(10) **(11)** **RAPTA-C (12)**

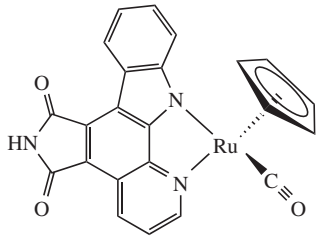

(13)

Figure 15.3 *Anticancer ruthenium(II)-arene complexes*

(11) [23, 79] (Figure 15.3). These compounds show very good activity *in vitro*, with IC_{50} values below 10 μM for growth inhibition of A2780 human ovarian cancer cells, which is similar to carboplatin [79]. Evaluation of structure–activity relationships have demonstrated that there are three major factors in maximizing the activity of these compounds: (i) hydrophobic arene ligands, (ii) stable bidentate chelating ligands, and (iii) a single exchangeable halide [23, 44, 78].

A wide variety of Ru^{II} arene compounds have been reported and an early conclusion of this work was that increasing the hydrophobicity of the arene ligand can increase their anticancer activity significantly [23, 78]. This was initially reported in comparison of the activity of (**10**) and (**11**) against the A2780 human ovarian cancer cell line, with the tetrahydroanthracene complex showing 10-fold greater activity than the *p*-cymene compound [44]. Many different modifications have been made to the arene ligands of Ru^{II} arene complexes to enhance cytotoxicity and selectivity. DNA-intercalating arenes have been the focus of a number of reports, with studies of the interactions of (**11**) with DNA duplexes being an example of such work [80]. In this case (**11**) induces distortion of the DNA duplexes and inhibits polymerization. The arene ligands can also be functionalized by tethering of targeting molecular functionalities. This is particularly relevant to this review since it enables the inclusion of biologically relevant moieties as part of rational drug designs, and several examples are described in the following text.

Hydrolysis of Ru^{II} arene complexes via exchange of chloride ligands is considered to be a key component of their cytotoxicity. The resulting species, such as $[(\eta^6\text{-arene})Ru(L)H_2O]^{2+}$, where L is a bidentate donor ligand, are then active in binding to DNA nucleobases [78, 81]. Such binding of (**10**) to DNA has been shown to occur to guanine bases specifically [79]. Furthermore, studies of interactions with DNA duplexes show that (**10**) forms guanine adducts that lead to conformational changes and reduced stability. However, the adducts of (**10**) are removed from DNA by different mechanisms than observed for platinum-based drugs, possibly indicating a different mode of activity [78, 80]. Interestingly, chloride ligand exchange from these types of complexes provides a pathway for selective activation. In blood plasma, hydrolysis is suppressed by the relatively high concentration of chloride ($[Cl^-] = 104$ mM) leading to a predominance of the less activated chloro complex [82]. However, aqueous exchange becomes favored after the complexes enter cells due to the lower chloride concentrations in the cytoplasm ($[Cl^-] = 23$ mM), and the nucleus ($[Cl^-] = 4$ mM), enhancing the potential for biomolecule interactions [21, 23, 78, 82].

The chelating ligands of these types of compounds also provide scope for enhanced targeting and activity. In the simplest case the rate of halide ligand exchange can be increased by electron-donating chelating ligands [78, 83]. However, more targeted strategies have included, for example, chelation of kinase inhibitors [84–86] and DNA-intercalating ligands [87]. This has found application in the inclusion of bio-relevant molecules, as described in the following text.

Dyson and co-workers have developed complexes of the type $[(\eta^6\text{-arene})RuCl_2(pta)]$, where pta = 1,3,5-triaza-7-phosphatricyclo[3.3.1.$1^{3,7}$]decane [4, 15, 88]. In contrast to the complexes described above, these so-called "RAPTA" complexes, such as **RAPTA-C (12)** [89] (Figure 15.3) show activity reminiscent of NAMI-A with only modest cytotoxicity apparent *in vitro* but promising antimetastatic properties [88, 90, 91]. The pta ligand in RAPTA complexes enhances aqueous solubility and may also play a role in selectivity observed in tumorigenic cell lines [4]. However, modification of the pta ligand has not shown improved activity [92]. Furthermore, replacement of the chlorides with non-labile bidentate ligands, such as oxalate, was found to have little effect on the inhibition of cancer cell growth proliferation nor on binding with oligonucleotides [93]. These results suggest that aquation may not be a major factor in the activity of some RAPTA complexes. However, the hydrophobicity of RAPTA complexes has been increased by replacing one of the chlorides with neutral donor ligands such as phosphine, which increases uptake of the compounds but reduces selectivity [4, 94]. Thus, modification of the η^6-arene ligand continues to be a major focus in the development of these complexes, and is of relevance to this review as a potential site for the appending of biologically important species.

RAPTA compounds have also shown promise as enzyme inhibitors [4]. For example, **RAPTA-C** (**12**) was found to be a good inhibitor of cysteine protease cathepsin B (cat B) [95], an enzyme that plays a significant role in tumor progression [96]. Further development of arene complexes in this area has included inert half-sandwich complexes such as (**13**) [97] (Figure 15.3). The metal center serves as a three-dimensional scaffold which in the case of (**13**) enables the Ru-arene moiety to mimic the carbohydrate fragment of the protein kinase inhibitor staurosporine, resulting in a potent inhibitor [98]. This is just one example of the great variety of anticancer compounds accessible through the derivatization of Ru^{II} arene complexes.

15.1.4 Polypyridyl complexes

Another important group of ruthenium anticancer compounds are those containing any of a wide variety of polypyridyl ligands [99]. These can be divided into two groups: (i) complexes containing exchangeable monodentate ligands in addition to multidentate polypyridyl ligands, such as (**14**) and (ii) those containing three polypyridyl-based ligands and thus not exhibiting ligand exchange under physiological conditions, such as (**15**) (Figure 15.4). The cytotoxicity of the first type of compound has been investigated for complexes containing 2,2′-bipyridine (bpy) and/or 2,2′;6′,2″-terpyridine (terpy) along with different numbers of chlorine ligands. Amongst the most promising chloro-polypyridyl complexes is *mer*-$[Ru^{II}Cl_3(terpy)]$ (**14**), which has shown good activity against both L1210 murine leukemia and human cervical carcinoma HeLa cell lines [100, 101]. Complex (**14**) and the related compounds $[Ru^{II}(terpy)(bpy)Cl]Cl$ and *cis*-$[Ru^{II}(bpy)_2Cl_2]$ were all found to coordinate to DNA specifically via guanine bases and *in vitro* studies demonstrated that this process can terminate DNA synthesis [100]. However, the formation of these types of adducts was not found to correlate with the biological activity of the compounds. Compound (**14**) also showed the ability to form interstrand cross-links following covalent DNA binding, suggesting this could be related to its mode of action [101].

Tris-ligand ruthenium(II) polypyridyl complexes have been studied extensively in a variety of biological applications including cancer therapy [102]. Although these types of compounds do not have exchangeable ligands, they can potentially act as DNA intercalators due to their aromatic polycyclic ligands. Changes in DNA secondary structure by intercalators can inhibit DNA replication, consequently preventing further growth of cancers or leading to cell death [102]. $[Ru(phen)_3]^{2+}$ (phen = 1,10-phenanthroline) was an early focus of ruthenium intercalator studies, with the Δ isomer of the complex shown to bind to DNA by intercalation and the Λ isomer exhibiting surface interactions [103]. A wide array of related compounds have subsequently been reported, many containing large aromatic polycyclic ligands for DNA intercalation [8, 102, 104].

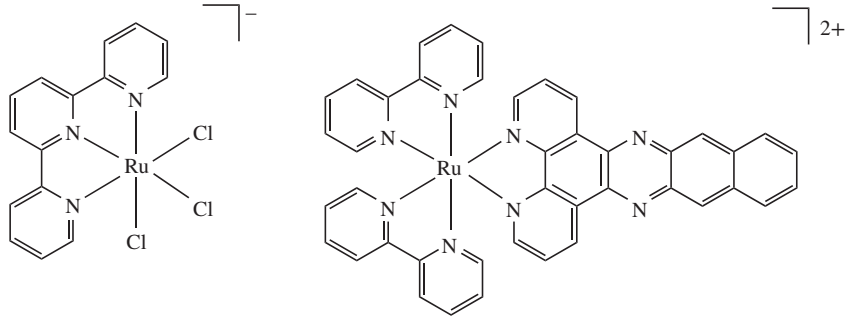

(14) **(15)**

Figure 15.4 *Ruthenium(II)-polypyridyl complexes*

A notable example is $[Ru(bpy)_2(dppn)]^{2+}$ (**15**) (dppn = benzo[*i*]-dipyrido[3,2-*a*:2′,3′-*c*]phenazine), which showed cytotoxicity against HT-29 and MCF-7 cell lines that was comparable to that of cisplatin [105].

Ruthenium(II) polypyridyl complexes have also been studied as potential sensitizers for the photodynamic therapy of cancer [8]. Compound (**15**) is a candidate for this application since it efficiently cleaves DNA following irradiation with visible light [106]. This compound readily intercalates and is thought to photocleave DNA by oxidation of guanine and the production of reactive oxygen species derived from singlet oxygen ($^1O_2$) [106]. Numerous similar reports of DNA photocleavage by ruthenium polypyridyl complexes [26, 104] indicate that these compounds should have certain characteristics to be effective for photodynamic therapy: (i) preferential accumulation in cancer cells, (ii) absorb strongly at longer wavelengths, which are not absorbed significantly by biological tissues, and (iii) produce singlet oxygen or radical intermediates with high quantum yield [8, 21].

As shown in several examples below, functionalization of the pyridyl ligands of these types of complexes can significantly modify their behavior *in vitro* and potentially *in vivo*. In particular, by tethering of biological species to the ligands, the transport, and targeting, of the compounds can be significantly enhanced.

15.1.5 Other ruthenium anticancer compounds

In addition to the four prominent families of compounds described above, a wide variety of other ruthenium species have also been studied as potential chemotherapeutic agents. These include: (i) ruthenium arylazopyridine complexes [101, 107, 108], (ii) ruthenium nitrosyls [109, 110], (iii) ruthenium chelates, particularly those with polyaminocarboxylate ligands [22], (iv) multinuclear ruthenium compounds and clusters [3, 111, 112], (v) complexes with macrocyclic ligands, notably porphyrin conjugates [113, 114], and (vi) heteronuclear complexes, particularly those containing platinum moieties [115, 116]. The diversity in the structures and properties of these complexes highlights the scope for future development of novel ruthenium anticancer compounds. Furthermore, studies of any of these types of compounds with biologically relevant ligands are relatively rare, suggesting untapped potential for compounds with new modes of action.

15.2 Amino acids and amino acid-containing ligands

The coordination chemistry of amino acids and their derivatives with metal ions has been studied extensively [117, 118] and this field has been a target in the development of anticancer drugs for several decades [119]. To date, consideration of amino acids as ligands for ruthenium anticancer candidates has been more focused toward understanding coordination to proteins under physiological conditions, rather than as an intrinsic part of complex design. Generally speaking, amino acids can be coordinated to ruthenium to generate new therapeutics via one of three modes: (i) direct monodentate coordination to give a pendent amino acid ligand; (ii) through coupling of amino acids to a coordinating intermediary group; and (iii) chelation via the amino, carboxyl, and even side chains of the amino acid.

The application of a monodentate, directly coordinated amino acid has been reported by Goldbach *et al*. with the synthesis of a Ru^{II} polypyridyl complex with an *N*-acetylmethionine ligand coordinated via the sulfur of the thioether (**16**) [120] (Figure 15.5). In this case, the amino acid-derived ligand was used as a photocleavable protecting group to prevent the non-specific exchange of chloride ligands, potentially enhancing the specificity of the complex. Irradiation with visible light generated the biologically active monoaqua species while releasing the biologically harmless *N*-acetylmethionine ligand. Thus, complex (**16**) acts as a potential photodynamic therapy prodrug that can be photoactivated selectively *in situ*.

Tethering of amino acids to ruthenium anticancer complexes via intermediary groups has the potential not only to control the coordination to the Ru center, but also to install additional chemical reactivity. This has been

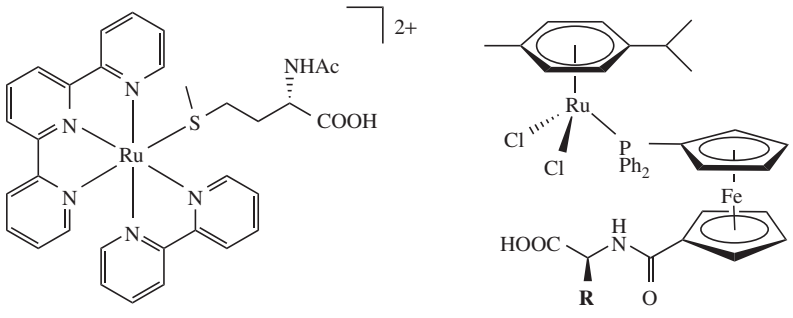

(16) (17)

Figure 15.5 *Ruthenium complexes with pendant amino-acid moieties*

demonstrated in reports of Ru^{II} arene complexes containing phosphinoferrocene ligands functionalized with carboxamide substituents derived from amino acids, such as (**17**) [121, 122] (Figure 15.5). These compounds are chemically related to RAPTA-type compounds such as (**12**), and the primary role of the amino acid-based ligands in this design was as a biological directing group. Inclusion of the ferrocenyl group is a strategy that has been employed in other studies to enhance anticancer activity [123, 124], including in derivatives of Ru^{II} arene complexes [125] and is thought to promote activity through Fenton-like chemistry at the Fe center [126]. An array of phosphinoferrocene Ru^{II} arene complexes functionalized with different amino acid-based carboxamides were tested against the human ovarian cancer cell line A2780, and its cisplatin-resistant derivative A2780cisR, and showed moderate to good cytotoxic activity [121]. It was observed that modification of the pendant amino acid-based ligands at functional group **R** (Figure 15.5, compound (**17**)) affected the activity of the compounds, as did modification at the O-terminus of the amino acid. This demonstrated the relevance of these groups to the *in vitro* mechanism of action of the complexes.

Although chelation of amino acids to prospective ruthenium anticancer compounds potentially inhibits their ability to participate in biological recognition, it nonetheless provides for the generation of novel complexes. Several simple octahedral ruthenium(III) complexes with *N*-methyl derivatives of glycine have been reported [127, 128]. These compounds, such as (**18**) (Figure 15.6), were synthesized by treating either *N*-methylglycine (sarcosine) or *N*,*N*-dimethylglycine (dmgly) with $RuCl_3$ to give either the mono or bis complexes of the ligands coordinated in a bidentate fashion, with the remaining coordination sites occupied by chloride ligands. The resulting complexes were tested against several cell lines and generally found to have mild antiproliferative activity. Of the complexes reported, the most active had a single bidentate dmgly ligand and showed activity against rat astrocytoma C6 cells *in vitro*. Interestingly, this compound had minimal cytotoxicity against primary astrocytes or macrophages, indicating good specificity [127].

Amino acid ligands with higher coordination number have also been investigated as anticancer agents. A ruthenium(III) complex of the glycine-derived 1,3-trimethylenediamine-*N*,*N*′-diacetato ligand, which undergoes tetradentate coordination following reaction with $RuCl_3$ to give the octahedral dichloro complex (**19**), has been reported [128] (Figure 15.6). This compound exhibited moderate antiproliferative activity toward myelogenous leukemia K562 cells. In a related study, a hexadentate ligand formed from the condensation of L-glutamic acid with formaldehyde and ethylenediamine (en) was used to produce a coordinatively saturated Ru^{III} complex [129]. Although the structure of this compound was not characterized in detail, the absence of exchangeable chloride ligands possibly suggests a different mode of activity from the other Ru^{II} amino acid chelates, since coordination to DNA or other biomolecules is precluded. However, this compound was shown to bind with calf thymus DNA via intercalation. Furthermore, the complex showed activity against colorectal (HT-29), liver (HepG-2), and cervical (HeLa) cancer cell lines.

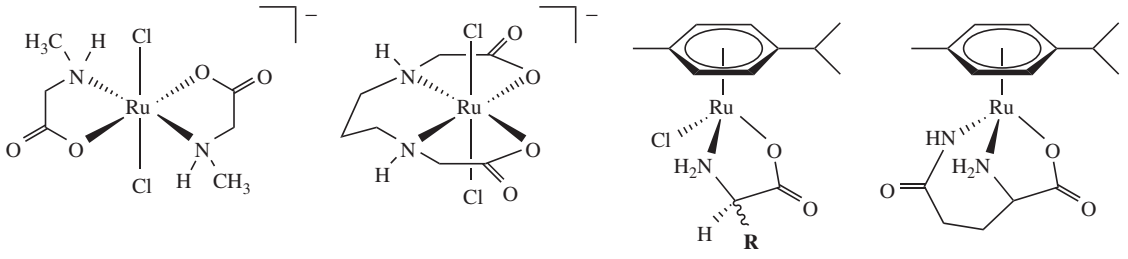

(18) **(19)** **(20)** **(21)**

Figure 15.6 *Ruthenium complexes with chelating amino acid-based ligands*

Amino acids have also been chelated to Ru^{II} arene complexes. As discussed in the introductory section of this chapter, bidentate ligands such as en are a common feature of many Ru^{II} arene anticancer compounds [23, 83]. As part of an extensive study on structure-activity relationships in Ru^{II} arene complexes, Habtemariam *et al*. [130] synthesized *p*-cymene complexes with glycine, L/D-alanine, β-alanine, and L/D-phenylalanine with general structures as shown in Figure 15.6, (**20**), as well as a biphenyl complex with L-proline. However, in each case the complexes were found to be relatively inactive toward the A2780 human ovarian cancer cell line, with $IC_{50} > 100\,\mu M$. The low activity of these compounds, as compared with many other Ru^{II} arene complexes, was correlated to unusually favorable hydrolysis of the chloride ligand, even in the presence of significant free chloride in solution. This suggests that the reactive aqua derivatives of these complexes will interact with various biomolecules before reaching target sites. Interestingly, although these compounds showed minimal activity, they were able to form stable adducts with 9-ethylguanine, demonstrating their potential to form DNA lesions. In a related study, the amino acid complex [(η^6-benzene)Ru(L-proline)Cl] has been reported to have activity toward P388 leukemia cells, although experimental data are not presented [131].

The potential for generation of further Ru^{II} arene complexes with chelating amino acids has also been illustrated in reactions of amino acids with the hexanuclear ruthenium arene assemblies such as $[(p\text{-cymene})_6Ru_6(oxalate)_3(tpt)_2]^{6+}$ (tpt = 2,4,6-tri(pyridin-4-yl)-1,3,5-triazine), which themselves exhibit anticancer activity [132–134]. ESI-mass spectra have shown that these reactions lead to production of mononuclear Ru^{II}–cymene complexes of the general formula $[(p\text{-cymene})Ru(\text{amino acid})]^+$ by replacement of the bridging ligands of the metalla-prisms. Several different amino acids have been shown to promote these reactions resulting in either bidentate or tridentate coordination to the resulting $(p\text{-cymene})Ru^{II}$ complexes, such as the glycine derivative (**21**) (Figure 15.6). Generation of bidentate amino acid adducts to arene complexes can also be achieved by direct replacement of suitable chelating ligands. This has been demonstrated in reactions of $[(\eta^6\text{-}p\text{-cymene})Ru(L)Cl]^+$ complexes where L = chelating pyronato, thiopyronato, or pyridonato [135]. In these cases the chelating ligands were replaced by methionine in aqueous solution. Although the goal of this work was to model protein interactions, it nonetheless demonstrates that amino acids are good nucleophiles for coordination to ruthenium arene centers.

15.3 Peptides and peptide-functionalized ligands

The pharmaceutical potential of peptides has been realized through the development of several widely used peptide-based drugs [136, 137]. While the peptide drugs produced to date have been limited to extracellular targets, cell-penetrating peptides also provide promise as pharmaceuticals since they can target intracellular

proteins [137, 138] and cell compartments [139]. Consequently, the application of such peptides as ligands has the potential to promote intracellular transport while providing enhanced targeting and specificity for metal-based drugs. Indeed, peptide coordinated metallodrugs in particular are increasingly finding applications in both diagnostic and therapeutic applications, and compounds with a variety of different peptides and metal centers have been reported [140–150]. However, as pointed out recently by Meier *et al*. [151], this approach has not yet been fully exploited for ruthenium anticancer compounds.

As described below, Ru^{II} arene complexes have shown particular potential as scaffolds for peptide conjugates. In a recent example of these types of compounds, the neuropeptide [Leu^5]-enkephalin was tethered to the metal center of a Ru^{II} arene complex via coordination of a hydroxypyrone derivative of the peptide to give compound (**22**) (Figure 15.7) [151]. The peptide-based ligand was synthesized from the N-terminal alkyne-functionalized peptide, which was linked to the hydroxypyrone metal-coordinating moiety via "click" chemistry using a Cu^I-promoted alkyne-azide cycloaddition reaction. *In vitro* testing of the antiproliferative activity of the Ru^{II} arene peptide complex (**22**) showed promising activity against the ovarian (CH1) cell line, with an IC_{50} of 13 μM. However, similar activity was observed in the absence of the peptide, suggesting that the triazolyl-pyronato linker is a key component in the specific activity of the compound. In previous studies, Ru^{II} arene pyronato complexes have been shown to form adducts with biomolecules following chloride ligand exchange [135], suggesting that this is the dominant factor in the activity of the peptide adduct as well. Nevertheless, the activity of the peptide conjugate is significant given that other reports, described below, have found that addition of peptide ligands often reduces the antiproliferative activity of Ru anticancer agents.

The potential of peptide ligands to target cell-surface receptors has been explored in a study of Ru^{II} arene complexes tethered to the dicarba analog of the octreotide peptide, using the complexes (**23**) and (**24**) [152] (Figure 15.7). Octreotide is a cyclic-octapeptide analog of the neuroendocrine hormone somatostatin [153]. Somatostatin receptors are overexpressed in several tumor types [154] and octreotide shows particularly high affinity for the type-2 receptor (sst_2) [155], which is the subtype found most commonly in tumor cells [152]. The potential to take advantage of this receptor transport pathway has been demonstrated through conjugation of octreotide to a number of cytotoxic organic compounds, which was shown in some cases to enhance their selectivity and reduce toxicity [156, 157]. The ruthenium arene complexes used in this study were synthesized using a solid-phase approach and linked to the Ru center either by an imidazole-benzoic acid (**23**) or a chelating diaminopropionic acid moiety (**24**). The octreotide ligand itself was modified by replacing the disulfide bond of the original peptide with a CH_2-CH_2 linkage to give the dicarba analog [152, 158]. This modification increases the stability of the peptide in reducing cellular environments and does not significantly impact on sst_2 receptor affinity [159]. Interestingly, compounds (**23**) and (**24**) show distinct solution behavior. Compound (**24**) undergoes chloride hydrolysis to generate the activated aqua species which then coordinates to guanines in DNA oligonucleotides. By contrast, (**23**) does not undergo ligand exchange and consequently does not coordinate to DNA. Surprisingly, screening against MCF-7 human breast adenocarcinoma cells revealed that (**23**) shows activity ($IC_{50} = 63$ μM) while (**24**) is inactive, demonstrating a non-DNA-related origin of the observed cytotoxicity. Comparison of the activity of conjugate (**24**) with that of its parent Ru^{II} arene compound, which has a coordinated imidazole-benzoic acid methyl ester, demonstrates that inclusion of dicarba-octreotide significantly reduces the cytotoxicity of the complex. However, the benefit of including the peptide in (**23**) was demonstrated by: (i) observation of higher levels of intracellular ruthenium in MCF-7 cells following exposure to the dicarba-octreotide conjugate as compared with the parent compound and (ii) increased activity in DU-145 human prostate tumor cells, which exhibit higher sst_2 receptor expression. Together, these results show the ability of the peptide to promote selectivity.

As described above, the ability of peptide carriers to enhance the transport and selectivity of ruthenium(II) arene complexes can result in concomitant loss of antiproliferative activity. An elegant solution to this problem has been reported by Barragán *et al*. by employing photocleavage of coordinated peptide moieties [160]. In this work, dicarba-octreotide (**25**) or the tripeptide Arg-Gly-Asp (**26**) were modified with 4-pyridylacetic

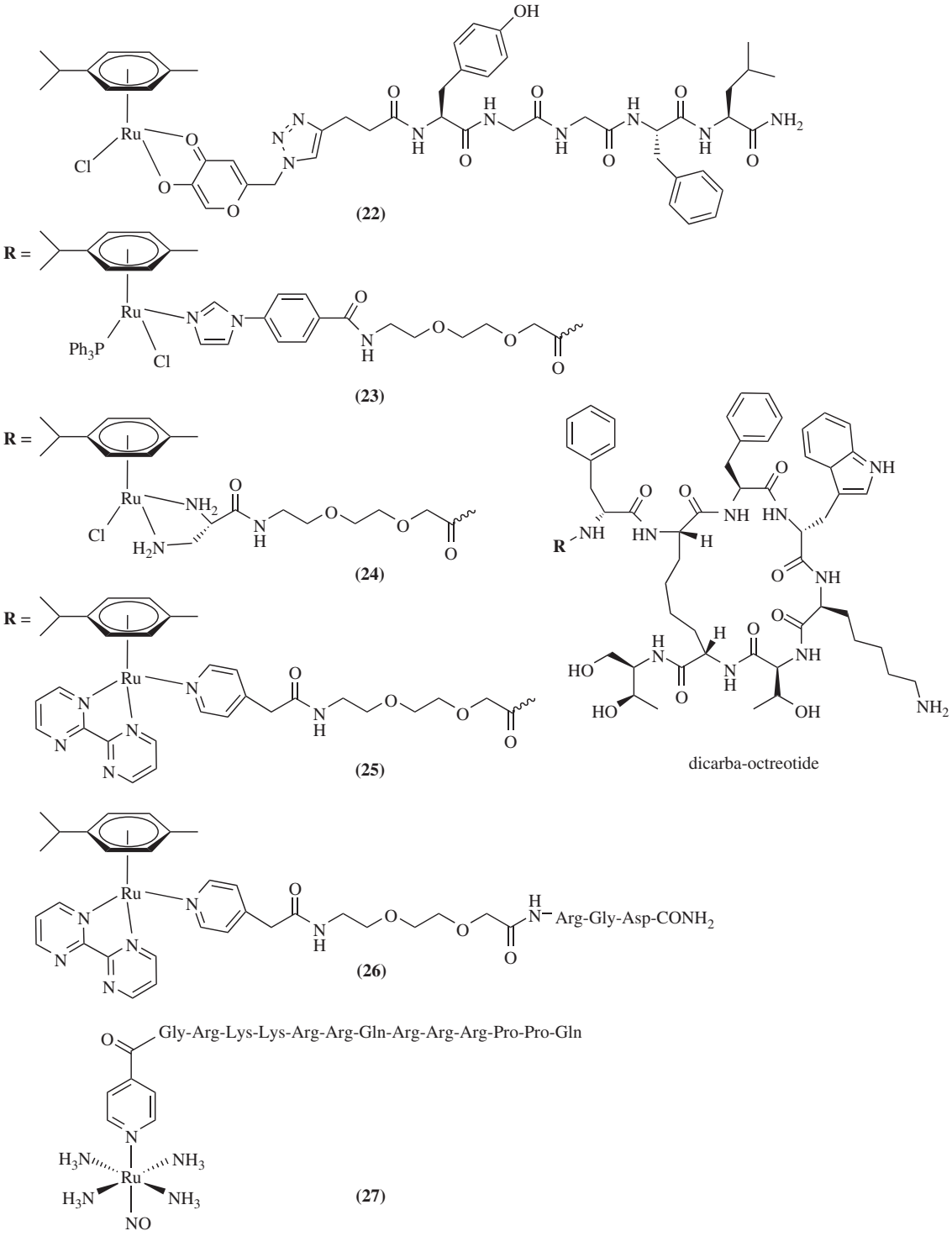

Figure 15.7 *Ruthenium complexes with peptide-based ligands*

acid at their *N*-termini, which enabled coordination to ruthenium. As shown in Figure 15.7, the resulting Ru^{II} arene complexes also contain chelating bipyrimidine ligands, which promote photolysis to initiate dissociation of the peptide ligands. Analogs with poly(ethylene glycol) spacers were also synthesized to reduce interference of the Ru-arene moiety with protein reception, and to improve solubility. Irradiation of each of these complexes with visible light releases the peptide ligands, resulting in the formation of the aqua complex $[(\eta^6\text{-}p\text{-cymene})Ru(bipyrimidine)H_2O]^{2+}$ in each case. This species forms adducts with oligonucleotides by coordinating to guanine nucleobases, as expected for these types of Ru^{II} arene species, indicating a pathway for activity via DNA interactions. Interestingly, irradiation of the dicarba-octreotide conjugate (**25**) also results in loss of the *p*-cymene ligand which enables coordination to DNA via two guanines. Overall, this strategy provides two pathways for increased selectivity: (i) peptide ligands targeting receptors that are overexpressed in tumor membranes act as a "tumor-targeting device" and (ii) direct photoactivation of the complexes within tumors promotes site-specific activation.

Ruthenium nitrosyls have been intensively studied as NO donors [109, 110, 161] and are relevant to this review since NO concentrations can impact on tumor growth [162]. Indeed, a number of ruthenium nitrosyls have been shown to exhibit anticancer activity [109, 110]. A recent report has probed the ability of a cell-penetrating peptide to increase the cytotoxicity of a ruthenium nitrosyl compound [163]. The compound used in this study was *trans*-$[Ru(NH_3)_4(L)(NO)]^{3+}$ where L was either isonicotinic acid (ina) or a cell-penetrating peptide modified at the N-terminus via a peptide bond with the carboxylic acid group of ina. The peptide used in this case was Tat48-60, which is a 13-residue fragment (Gly-Arg-Lys-Lys-Arg-Arg-Gln-Arg-Arg-Arg-Pro-Pro-Gln) of the Tat protein, a regulatory protein of the HIV virus. It has been shown that the Tat48-60 peptide is capable of penetrating the membrane of HeLa cells and can accumulate in nuclei [164]. The resulting complex (**27**) (Figure 15.7) with the ina-Tat48-60 ligand was tested against the B16-F10 melanoma cell line and showed good activity ($IC_{50} = 21\ \mu M$) that was similar to that of the parent compound ($IC_{50} = 23\ \mu M$). In each case the observed activity was attributed to NO release from the complexes. The similarity in the activity of the complexes suggests that, in the case of ruthenium nitrosyls, coordination of targeting peptides need not reduce activity, and could be very useful for increasing the specificity of the compounds.

Direct evidence for cell targeting using peptide conjugation to ruthenium complexes has been provided by several studies of peptide-functionalized Ru^{II} polypyridyl complexes [165–167]. Notable studies include those by Barton and coworkers who have used luminescence imaging of Ru^{II} dipyridophenazine (dppz) complexes conjugated to positively charged peptides to study cellular uptake in human cervical carcinoma HeLa cells [165, 166]. In one example of this work the tetrapeptide Arg-D-Arg-Arg-Lys, which is known to target the nucleus of HeLa cells, was tethered to a Ru^{II} dppz molecule to give complex (**28**) [166] (Figure 15.8). The peptide was found to strongly enhance uptake in HeLa cells compared with the unconjugated complex. Interestingly, subcellular localization was found to be concentration dependent (Figure 15.8). At lower concentrations the peptide-conjugated complex is only observed in the cytoplasm of the cells with a granular distribution, consistent with endocytosis leading to entrapment of the compounds in endosomes. However, at higher concentrations, diffusion throughout the cytoplasm and nuclear fractions was observed, indicating transport via passive diffusion. As shown by this and other studies [165, 167] the charge introduced by the peptides to the complexes enables them to use the membrane potential as a driving force for cellular entry.

15.4 Coordinated proteins as ligands

Interactions of ruthenium anticancer compounds with proteins have been studied extensively [168, 169]. Although the serum proteins albumin and transferrin have been a particular focus of this work because of their importance to the transport of pharmaceuticals *in vivo* [31, 51, 70–74, 170–180], interactions with a

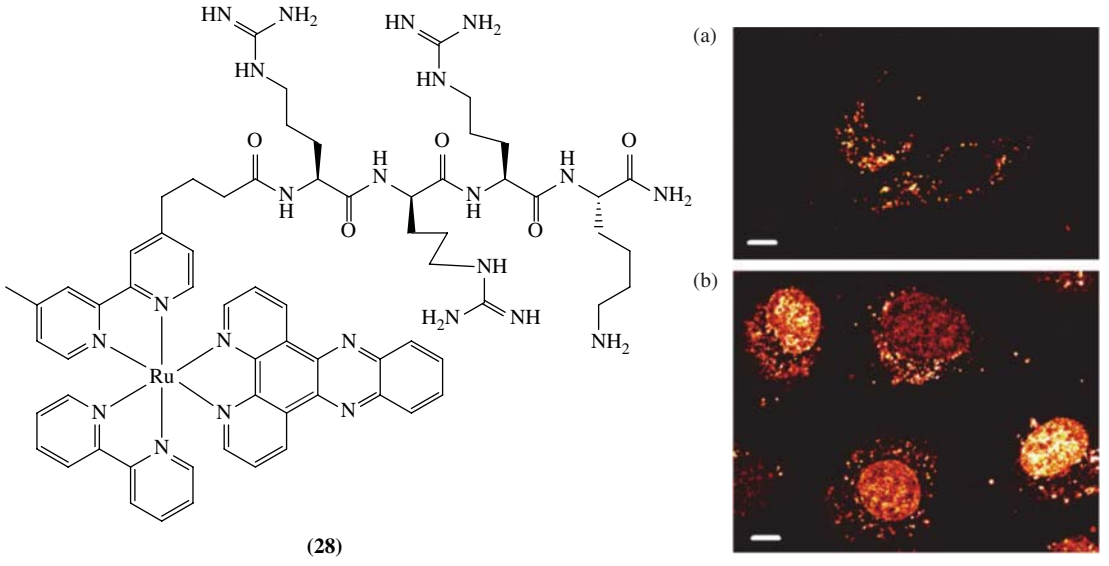

(28)

Figure 15.8 *Ruthenium(II) dipyridophenazine complex with appended Arg-D-Arg-Arg-Lys peptide. Subcellular distribution of* ***(28)*** *in HeLa cells in serum-free media, with concentration of (A) 20 μM or (B) 40 μM. Scale bars are 10 μm. Reprinted from [167], with permission from Elsevier. (See plate section for the colour version of this figure)*

number of other proteins have also been reported [181–186]. Protein conjugates have been exploited as carriers of a variety of organic anticancer drugs, and have shown the potential to reduce *in vivo* toxicity and improve activity compared with the free compounds [169, 187]. A number of reports have demonstrated coordination of ruthenium anticancer compounds to proteins. Ligand exchange with histidine imidazoles has been implicated as the origin of the majority of these interactions, although direct evidence for this has not yet been reported [70, 188–192]. Following coordination, proteins such as albumin can be considered as ligands of the ruthenium complexes, with the potential to effect speciation and transport *in vivo*. However, the use of protein ligands as an intrinsic part of the design of ruthenium compounds has been comparatively rare.

Human serum transferrin has received considerable attention as a potential targeting vector for ruthenium(III) complexes. In many cancers, expression of transferrin receptors is upregulated [193], providing a pathway for targeted delivery of transferrin-bound drugs to cancer cells [194, 195]. Kratz *et al*. have studied adducts of the Ru^{III} bis-azole complexes **KP418** (**5**) and **KP1019** (**6**) with both the apo form (apo-hsTF) and the fully iron-loaded form of the protein ($Fe^{III}{}_2$-hsTF) [49]. Under the conditions described in these experiments the complexes are likely coordinated to the protein, as determined in a number of other reports [49, 70, 181, 190]. Although the concentration of ruthenium species was not probed directly in this study, the relative activity of the transferrin adducts was compared with that of the free complexes against the SW707 human colon cancer cell line. For both **KP418** (**5**) and **KP1019** (**6**), adducts with $Fe^{III}{}_2$-hsTF exhibited high antiproliferative activity, exceeding that of the free complexes. This result is particularly significant given that $Fe^{III}{}_2$-hsTF on its own has a stimulatory effect on cell growth. These observations are consistent with enhancement of activity due to increased intracellular transport via transferrin receptors. However, the results of similar studies with the apo protein are somewhat less clear since an enhanced inhibitory effect was observed for the **KP418** (**5**) adduct with apo-hsTF, as compared with the free complex, but reduced activity was found for **KP1019** (**6**) bound to apo-hsTF [49]. The unexpected activity of the apo-hsTF – **KP418** (**5**) adduct was

suggested to be due to a change in the protein conformation with binding of the complex that was similar to that induced by binding of Fe^{III}. This could then enhance the affinity of the protein-complex conjugate for the transferrin receptor. It was also proposed that this process is more favorable for **KP418** (**5**) due to its smaller imidazole ligands, as compared with the indazole ligands of **KP1019**.

The antimetastatic Ru^{III} compound **NAMI-A** (**8**) is known to interact with hsA both by coordination following ligand exchange and by the formation of non-coordinate interactions with the protein [71, 72, 74, 196]. Human serum albumin is known to accumulate preferentially in tumor cells, as compared with normal cells, and has been employed as a carrier of a variety of anticancer drugs [187, 197–199]. However, it has been shown that coordination of **NAMI-A** to hsA lowers the activity of the complex, likely due to reduced bioavailability, indicating that this is a mechanism for drug inactivation *in vivo* [72]. Nevertheless, Liu *et al*. have reported a study of the antimetastatic activity of an adduct of **NAMI-A** with bovine serum albumin (BSA) [200]. In this report **NAMI-A** was incubated with BSA under conditions expected to give protein coordination [71, 72, 74, 185, 196]. Direct evidence for coordination of **NAMI-A** to BSA was given by spectroscopic studies, particularly X-ray absorption spectroscopy, indicating that the protein is effectively acting as a biological ligand [200]. The potential effect of BSA coordination on the antimetastatic activity of **NAMI-A** was investigated using the invasive human lung adenocarcinoma cell line A549. A series of assays to study substrate adhesion, motility (Figure 15.9), and invasion were performed to evaluate the effect of BSA coordination. In each assay a 1 : 1 adduct of **NAMI-A** with BSA showed similar activity to the free complex, demonstrating that under these conditions protein binding did not lead to inactivation, as observed previously with hsA [72].

The studies of protein adducts described above have relied on adventitious coordination of ruthenium species to proteins, likely via amino acid side chains. This approach gives limited control over the protein coordination sites and leaves some uncertainty about the species involved. By contrast, Ang *et al*. have described a more specific strategy for tethering Ru^{II} arene complexes to proteins, specifically recombinant

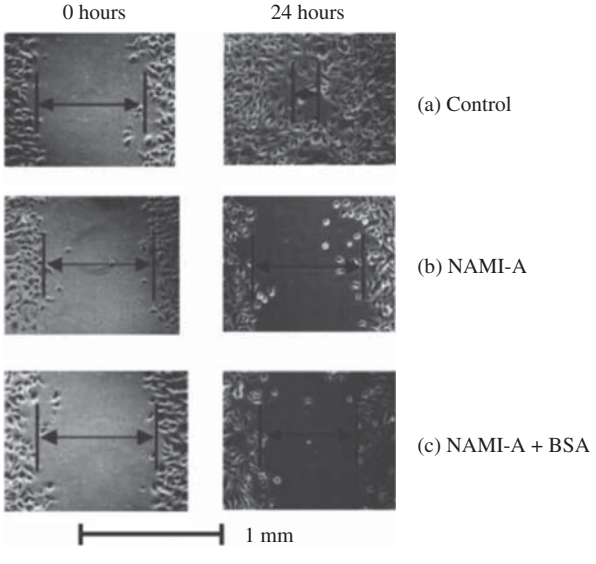

Figure 15.9 *Cell motility assays for A549 human lung adenocarcinoma cells: (a) in the absence of either NAMI-A or BSA, (b) with 10 μM NAMI-A, and (c) with 1 : 1 adduct of NAMI-A and BSA. Adapted with permission from [177], Copyright 2010, Wiley-VCH Verlag GmbH & Co*

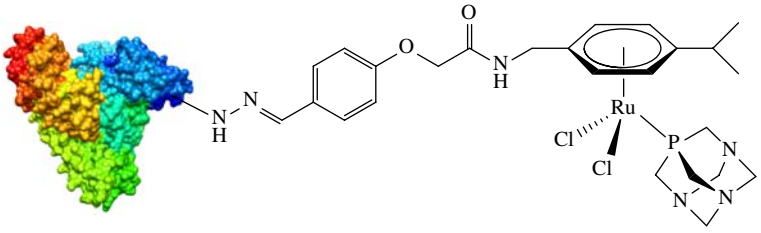

(29)

Figure 15.10 *Adduct of ruthenium(II)-arene, RAPTA-type complex with recombinant human serum albumin*

hsA [201]. As pointed out by the authors, since the ruthenium center is susceptible to nucleophilic attack and redox processes, conjugation of the ruthenium complex to the protein needs to occur under mild conditions [201]. The complex used in this case was a derivative of **RAPTA-C** (**12**) with the arene ring modified with an aldehyde-terminated linker. To enable conjugation of the complex to hsA, the protein was functionalized with hydrazine groups on the side chains of lysine residues. The complex and the functionalized protein were then allowed to react in phosphate-buffered saline and condensation of the aldehyde and the hydrazine moieties led to formation of a protein conjugate joined through a hydrazone linker (**29**) (Figure 15.10). Hydrazone bonds are acid labile and this type of protein conjugation enables targeted release of drugs within the acidic environments found in the lysosomes of tumor cells [202, 203]. The effect of hsA conjugation on cancer cell growth inhibition was tested against the A2780 ovarian carcinoma cell line and the protein conjugate showed good activity ($IC_{50} = 11\ \mu M$). By contrast, the non-conjugated complex was essentially inactive ($IC_{50} = 288\ \mu M$), demonstrating that hsA has a significant effect, possibly by facilitating cellular uptake of the RAPTA complex via endocytosis and subsequent controlled release via hydrolysis of the hydrazone linkage. The success of this approach is further highlighted by the observation that the known cytotoxin **RAPTA-C** (**12**) is essentially inactive against the A2780 cell line [201].

15.5 Carbohydrate-based ligands

Carbohydrate compounds have been reported with diverse medicinal properties including antibiotic, antiviral, and anticancer activities [204]. As ligands for metallodrugs, carbohydrates are particularly promising since they can enhance biocompatibility and solubility while targeting specific binding domains, transport systems, and enzyme activities [205, 206].

A number of studies of the synthesis and biological properties of ruthenium(II) arene complexes modified with carbohydrate-derived phosphite ligands have been reported. In one such study, Berger *et al*. have described analogs of **RAPTA-C** (**12**) where the pta ligand was replaced with carbohydrate-phosphite ligands [207]. These ligands included 1,2-*O*-isopropylidene-α-D-glucofuranose 3,5,6-bicyclophosphite to give compound (**30**) (Figure 15.11) and three other derivatives with different modifications of the furanose ring. In buffer solution the complexes were observed to undergo chloride ligand exchange and hydrolysis of a P–O bond of the phosphite ligands, a process that ultimately led to the formation of dinuclear species. Studies with 9-ethylguanine indicated coordination to (**30**) and its derivatives, both by exchange of chloride ligands and by adduct formation with hydrolyzed phosphite ligands, suggesting that DNA interactions may be relevant to the observed *in vitro* activity of the compounds. The compounds were screened against several cancer cell lines and found to have moderate activity. Comparison of four different carbohydrate phosphite ligands

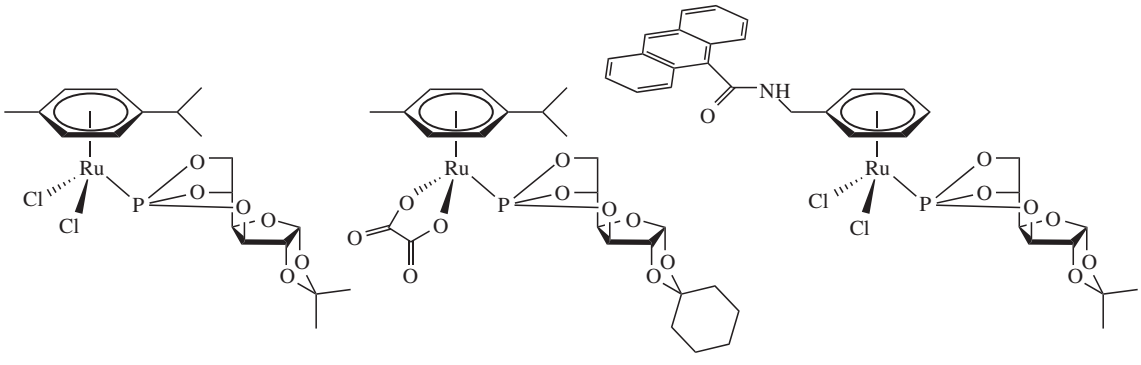

Figure 15.11 *Ruthenium(II)-arene complexes with carbohydrate-phosphite ligands*

suggested that modification of the furanose ring with more lipophilic groups may promote activity, possibly due to increased cellular uptake [206].

A related report by Hanif *et al*. [208] provides insight into the origin of the activity of these types of complexes. In this study, analogs of the Ru^{II} arene compounds with carbohydrate-phosphite ligands as described above, but with the chloride ligands replaced with chelating biscarboxylato ligands, were synthesized giving compounds such as (**31**) (Figure 15.11). The resulting complexes were inert toward aquation as compared with their dichloro counterparts, and did not show significant interactions with the DNA model 5′-guanosine monophosphate, or with cysteine, methionine, or the ubiquitin protein. The biscarboxylato complexes also showed significantly lower *in vitro* anticancer activity than their dichloro analogs. Taken together, these observations indicate that coordination to biological targets is a key component of the anticancer activity of these types of compounds.

Two analogs of (**30**) with anthracene tethered to the arene ring have also been reported [209]. Incorporation of anthracene gave fluorescent molecules such as (**32**) (Figure 15.11) whose intracellular speciation could then be probed by fluorescence microscopy. These studies revealed that the compounds were transported into A549 lung carcinoma cells but did not accumulate in the nucleus. Compound (**32**) showed only mild activity against a panel of cancer cell lines, but nonetheless represents an interesting example of a ruthenium anticancer compound as a potential "theranostic".

The 1,2-*O*-isopropylidene-α-D-glucofuranoside 3,5,6-bicyclophosphite ligand used in compounds (**30**) and (**32**) has also found application in novel triruthenium-carbonyl clusters with cytotoxic and cytostatic activity [210]. In these studies, compound (**33**) (Figure 15.12) and analogs with 2, 3, or 4 carbohydrate-phosphite ligands were synthesized. Biological testing against four human cancer cell lines revealed that the compounds with one or two carbohydrate ligands were cytotoxic, but that the compound with three carbohydrate-phosphites was inactive. The lower activity of the complex with three carbohydrate substituents was correlated with lower lipophilicity and intracellular uptake. Interestingly, in cell invasion assays, the compound with three carbohydrate-phosphite ligands showed the greatest activity. Furthermore, this compound inhibited angiogenesis in chicken embryo chorioallantoic membrane assays, where it outperformed clinically used small-molecule angiogenesis inhibitors [210].

The potential for carbohydrate ligands to enhance transport of ruthenium complexes into cancer cells has also been demonstrated using substituted Ru^{II} bipyridyl complexes. Gottschaldt *et al*. have reported functionalization of the $Ru(bpy)_3^{2+}$ complex with thiolated β-D-gluco, β-D-galacto, or α-D-manno ligands,

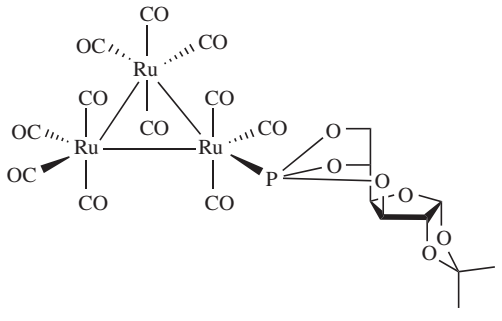

(33)

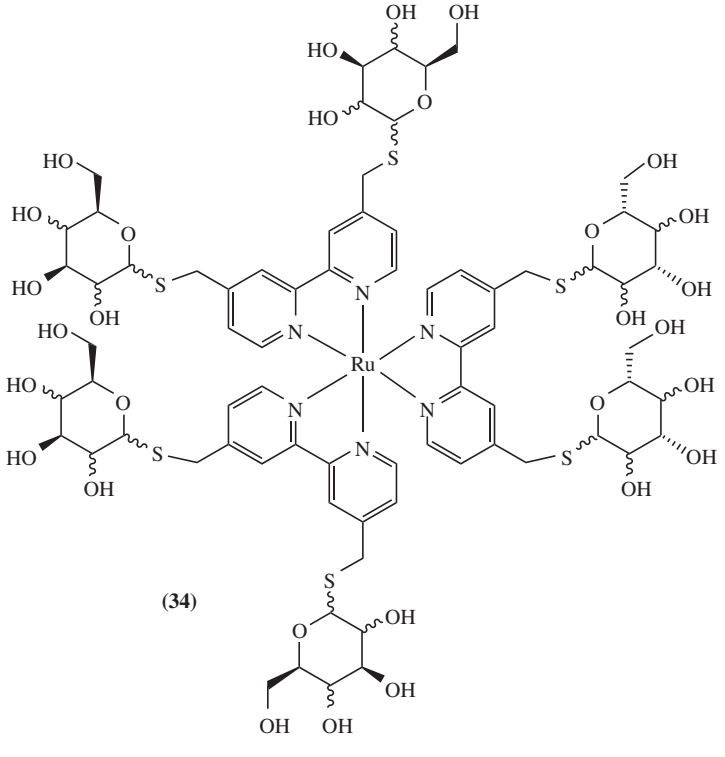

(34)

Figure 15.12 *Triruthenium-carbonyl cluster with carbohydrate-phosphite ligand (**33**) and carbohydrate-functionalized ruthenium tris-bipyridyl complex (**34**)*

to give compounds (**34**) [211] (Figure 15.12). Fluorescence imaging revealed that the D-glucose complex was internalized most effectively by HepG2 human hepatocarcinoma cells, and a granular distribution of the complex within the cytoplasm of the cells suggesting uptake by an endocytotic mechanism. By contrast, the D-galactose and D-mannose complexes were found to have significantly lower intracellular concentrations and relatively homogeneous distributions in the cytoplasm. Since the three different carbohydrate ligands used are diastereomers, the corresponding complexes have the same size, lipophilicity, and charge. As a result, the greater cellular uptake of the D-glucose-functionalized complex is a carbohydrate-specific effect. This

is a particularly notable result given that, as described above, the lipophilicity of ruthenium carbohydrate complexes is generally considered to be the dominant factor in their cellular transport and activity [206, 207, 210].

15.6 Purine, nucleoside, and oligonucleotide ligands

The earliest report of the biological activity of ruthenium purine and nucleoside complexes [212] significantly predates even the first studies of chloride-ammine complexes [5, 8, 9, 31]. Kelman *et al*. reported several complexes of the general formula $Ru^{III}(NH_3)_5$ L, where L was one of: (i) the purine bases guanine (compound (**35**) (Figure 15.13)) xanthine, hypoxanthine, adenine, or their methylated derivatives, or (ii) the nucleosides inosine, adenosine, or (iii) the phosphorylated nucleosides inosine diphosphate or guanine monophosphate [212]. Several of these complexes demonstrated the ability to inhibit DNA synthesis, and to a lesser extent, protein synthesis in human nasopharyngeal carcinoma cells. Different coordination modes were observed between some of the ligands L, which coordinated either via N1, N3, N7, or N9 of their purine cores, and this was implicated as a component of the differences in the activity of the compounds. For example, the greater activity of the adenine complex (coordinated at N1), over the inosine complex (coordinated at N7) was related to the greater stability of the former compound. Overall, the wide range of activities observed in the compounds studied in this report demonstrated the potential for purine bases and nucleosides as interesting ligands in the design of new ruthenium anticancer compounds.

Two **NAMI-A (8)** type compounds with guanine-based ligands have been reported by Turel *et al*. [213]. One of these compounds [*trans*-$RuCl_4$(guaH)(DMSO-S)]•$2H_2O$ (guaH = protonated guanine) is a direct analog of **NAMI-A** with a protonated guanine coordinated at the N9 position. *In vitro* testing of this compound revealed biological activity very similar to that of **NAMI-A**. Only very weak antiproliferative activity was observed against TS/A adenocarcinoma cells but promising proadhesive properties were found with the same cell line, suggesting potential antimetastatic activity. Two related compounds with the guanine derivative acyclovir (acv) [*mer*-$RuCl_3$(acv)(DMSO-*S*)(C_2H_5OH)]•C_2H_5OH **(36)** (Figure 15.13) and [*mer*-$RuCl_3$(acv)(DMSO-*S*)(CH_3OH)]•CH_3OH have also been studied [213, 214]. Acyclovir (9-{(2-hydroxyethoxy)methyl}guanine) is a widely used antiviral drug, primarily in the treatment of infections by the herpes simplex virus [215] and has been reported as a ligand to a variety of metal centers [214, 216–218]. In compound (**36**) and its methanol derivative, acyclovir coordinates at the N7 position and forms hydrogen bonding interactions with the alcohol ligands. Both compounds show **NAMI-A** like activity *in vitro* with low antiproliferative activity but promising effects on cell adhesion, suggesting potential use against malignancy [213].

Another **NAMI-A** (**8**) derivative has been reported with an axial 5,7-dimethyl[1, 2, 4]triazolo[1,5-*a*]-pyrimidine (dmtp) ligand [219]. This complex, (Hdmtp)[*trans*-$RuCl_4$(DMSO-*S*)(dmtp)] (**37**) (Figure 15.13) and its sodium analog (Na)[*trans*-$RuCl_4$(DMSO-*S*)(dmtp)], were found to form the relatively stable first hydrolysis product [*mer*-$RuCl_3(H_2O)$(DMSO-*S*)(dmtp)]•H_2O. The dmtp ligand plays a direct role in the solution behavior of the complexes by stabilizing this aquation product through intramolecular hydrogen bonding of the pyrimidinic nitrogen (N(6), using the numbering scheme in Figure 15.13) with the water ligand. As with the purine derivatives of **NAMI-A** described above, (**37**) was found to have low cytotoxicity against murine and human tumor cell lines, nor did it have any effect on cell distribution among cell cycle phases [219]. However, the complex did show a marked effect *in vitro* on tumor cell invasion, indicating antimetastatic activity. This was confirmed by *in vivo* studies in which (**37**) inhibited the growth of metastases in mice with MCa mammary carcinoma tumors, suggesting that this compound could be a legitimate alternative to **NAMI-A** [219].

A more bulky derivative of dmtp has been used to produce compounds that are structurally related to **KP1019** (**6**). The ligand used in these studies, 5,7-di-*tert*-butyl[1, 2, 4]triazolo[1,5-*a*]pyrimidine (dbtp), was

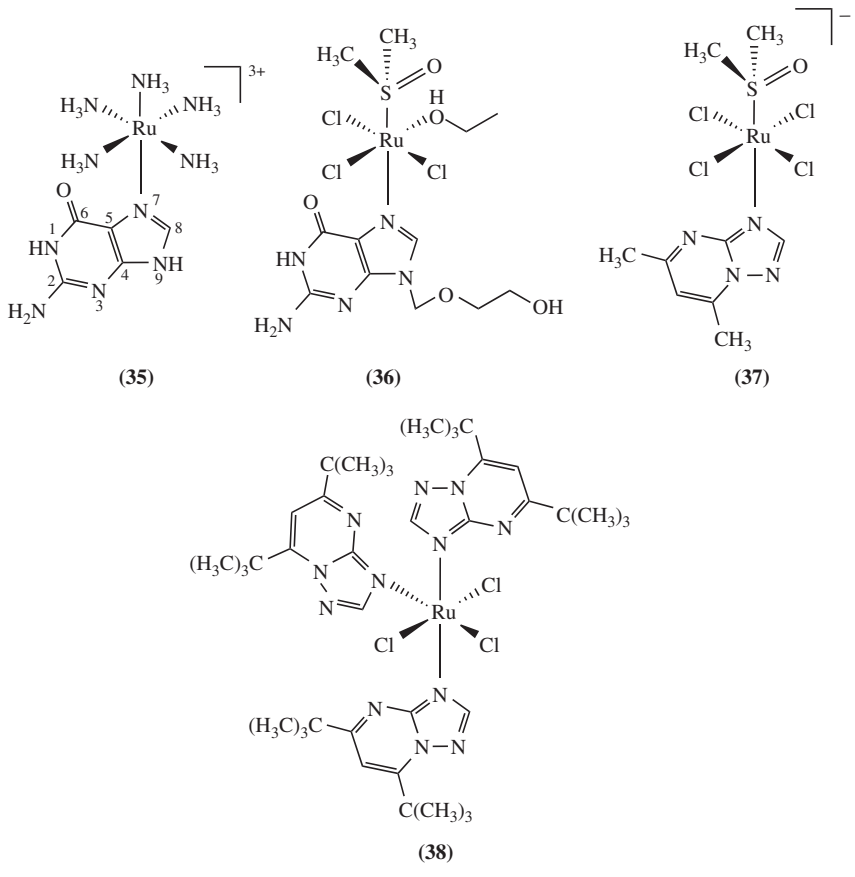

Figure 15.13 *Biologically active ruthenium complexes with purine ligands*

used to generate two complexes: *trans*-$RuCl_3(H_2O)(dbtp)_2$ and *mer*-$RuCl_3(dbtp)_3$ (**38**) [220] (Figure 15.13). The bis-dbtp compound is a direct analog of the first aquation product of **KP1019** [221], while the tris-dbtp compound replaces the coordinated water with an additional dbtp ligand. Both compounds show excellent cytotoxicity with IC_{50} values ranging between 0.06 and 2.4 μM against both A549 non-small cell lung carcinoma and T47D breast cancer cell lines, being in each case much more active than cisplatin. The dbtp ligands are thought to play several roles related to the activity of the compounds. First, as with the dmtp compounds described above, the dbtp ligand can influence the stability of hydrolysis products through hydrogen bonding interactions. Secondly, the additional bulk provided by the *tert*-butyl groups may help to prevent deactivation of the compounds by biological nucleophiles. Lastly, the bis-dbtp and the tris-dbtp (**38**) complexes are relatively lipophilic, suggesting that they can cross cell membranes by passive diffusion [220].

A recent report by Reschner *et al*. [222] describes the use of polyazaaromatic ruthenium(II) complexes tethered to oligonucleotides for gene-specific therapy of human papillomavirus (HPV)-related cancers. The central ruthenium-based moiety in these studies was the $[Ru(TAP)_2(phen)]^{2+}$ complex (TAP = 1,4,5,8-tetraazaphenanthrene) as shown in Figure 15.14. This was tethered to oligonucleotides via a

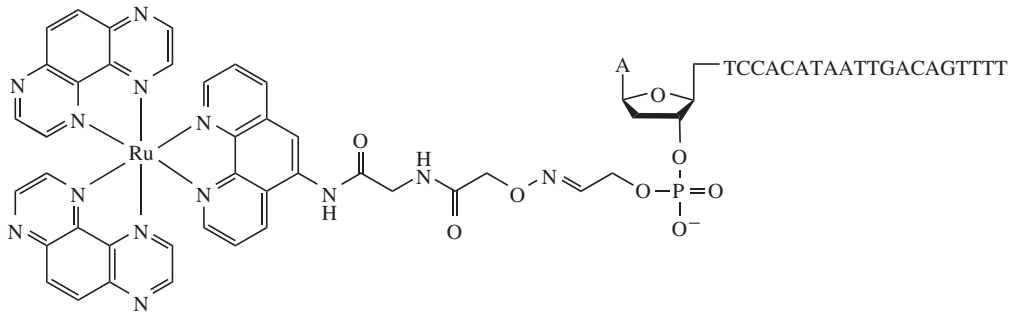

(39)

Figure 15.14 *$[Ru(TAP)_2(phen)]^{2+}$ complex tethered to E6 antisense oligonucleotide*

condensation reaction between the aminooxy-functionalized phen ligand and oligonucleotides functionalized with the complementary reactive aldehyde group to give an oxime linkage [223]. Polyazaaromatic Ru^{II} complexes such as $[Ru(TAP)_2(phen)]^{2+}$ can form photoadducts with DNA or oligonucleotides by formation of a covalent bond between guanine bases and one of the TAP ligands [224]. The tumorigenic effect of HPVs has been linked to the expression of the E6 oncogene, and HPVs are thus an excellent target for gene silencing therapy [225]. By tethering the $[Ru(TAP)_2(phen)]^{2+}$ complex to the antisense oligonucleotides of the E6 oncogene of HPV16 a highly selective photodynamic therapeutic was generated. Two $[Ru(TAP)_2(phen)]^{2+}$-tethered E6 antisense oligonucleotides were studied and were shown to form cross-links with their complimentary sequences after irradiation. One of the oligonucleotide adducts (**39**) (Figure 15.14) also strongly inhibited the proliferation of cervical cancer SiHa cells *in vitro* following illumination by visible light. This approach thus couples the spatial selectivity of photodynamic therapy with gene silencing to provide high efficiency in terms of specificity and growth inhibition.

15.7 Other selected ruthenium complexes with biological ligands

15.7.1 steroids

The development and growth of many breast and prostate cancers is controlled by steroid hormones [226, 227]. Consequently treatment with competitive binders to hormone receptors can be effective in the treatment of these types of cancers [228, 229]. However, the effectiveness of such treatments can be inhibited by the emergence of resistance following prolonged treatment [230]. This problem can potentially be addressed by coupling to cytotoxins, where the role of the steroid in the adduct can be to promote accumulation of the drug at the site of disease [231, 232].

Ruthenium(II) arene complexes coupled to androgens and estrogens have been reported using *N*-coordinated isonicotinate linkers to give compounds such as (**40**) [233] (Figure 15.15). A variety of complexes were prepared with the androgens androstenedione and androsterone, or derivatives of the estrogens estrone or estradiol. The compounds were studied for their affinity for the estrogen receptor (ERα) and for the sex hormone-binding globulin (SHBG) protein. SHBG transports steroids in the blood and has also been implicated in their cellular uptake suggesting it is a promising drug target [234]. Surprisingly, none of the Ru^{II} arene–steroid complexes reported showed affinity for the estrogen receptor ERα. However, several of the estrogen complexes such as (**40**) with **R** = methoxy or methylthio groups showed high affinities for SHBG. This was a particularly promising result since a number of 2-alkoxy estrogens have been shown

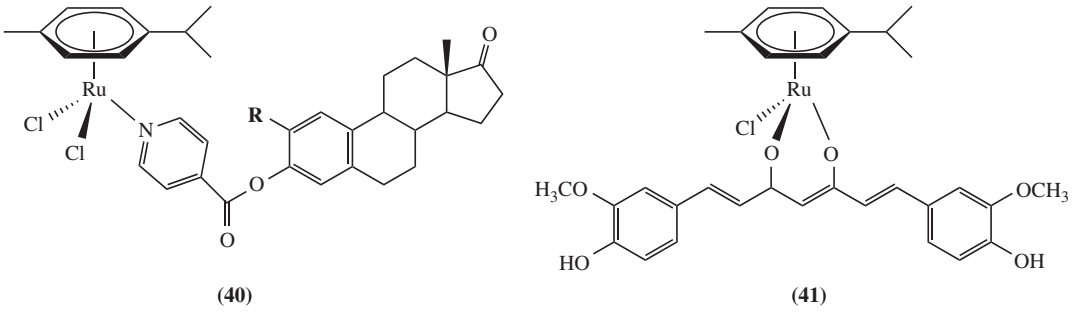

Figure 15.15 *Ruthenium(II)-arene complex conjugated to estrogens (**40**) and ruthenium(II)-arene complex with coordination to curcumin*

to be highly cytotoxic [235] suggesting that addition of the cytotoxic Ru^{II} arene functionality could give a synergistic increase in activity. *In vitro* screening of the Ru^{II}-arene–steroid complexes against several cancer cell lines showed good activity in most cases [233]. Generally, linking of the Ru^{II}-arene core did not reduce the intrinsic cytotoxicity of the steroids. Indeed, for the complexes coordinated to 2-substituted estrones, (**40**), greater activity was observed in hormone-independent 518A2 melanoma cells than with the parent steroids alone, suggesting a synergistic effect of both fragments. Several of the Ru^{II}-arene–steroid compounds with higher affinities for SHBG were also tested against hormone-dependent KB-V1/Vb1 cervical carcinoma cells in the presence of the SHBG protein, which led to a two- to eightfold decrease in activity. This observation suggests that SHBG sequesters the complexes, rather than promoting cellular uptake. The estrogen complexes were also tested for potential anti-invasive activity and one of the complexes, (**40**) with **R** = OEt, showed a distinct retardation of cell motility.

15.7.2 Curcumin – an example of a natural product ligand

Approximately half of cancer chemotherapeutics in clinical use are natural products or related compounds [236], and they continue to be a major focus of anticancer drug development [237]. Many of these compounds contain functional groups that allow them to act as ligands, potentially generating new metal-based anticancer compounds with unique properties. One such compound is curcumin [diferuloylmethane or 1,7-bis(4-hydroxy-3-methoxyphenyl)-1,6-heptadiene-3,5-dione], which is extracted from the rhizomes of *Curcuma longa* (turmeric). Curcumin has been shown to exhibit a variety of medicinal properties including antiviral, anti-inflammatory, and neuroprotective activities [238–241]. Furthermore, this compound has demonstrated anticancer activity [242, 243] and is being evaluated in clinical trials [244]. However, curcumin has limitations as a drug candidate since it has low aqueous solubility, low bioavailability, poor absorption, and is metabolized and cleared rapidly from the body [245, 246]. This has motivated the development of derivatives of curcumin, including metal complexes [247–249]. Two studies have reported curcumin as a bidentate ligand to Ru^{II}-arene complexes, to give compounds such as (**41**) [250, 251] (Figure 15.15). These compounds show very good activity against several cancer cell lines *in vitro*, with (**41**) having $IC_{50} = 14\ \mu M$ against the HCT116 human colon carcinoma cell line. The binding of the complexes with DNA was studied and compound (**41**) showed a significantly higher binding affinity than free curcumin, indicating the importance of the Ru^{II}-arene moiety to these interactions [250]. It has been reported in several studies that curcumin is an antioxidant and can prevent the peroxidation of DNA by free radicals and oxidative damage to proteins. The ruthenium-curcumin complexes were shown to reduce levels of cytoplasmic reactive oxygen species and oxidized proteins, with similar efficacy to free curcumin [250]. Together, these results show how

the individual Ru^{II} arene and curcumin components contribute to the *in vitro* behavior of the compounds, and potentially how this synergy contributes to their very good observed activity.

15.8 Conclusion

The well-established coordination chemistry of ruthenium provides an array of potential routes for the coordination of biological species with useful pharmacological properties. As described above, this has allowed a wide variety of compounds with biologically-derived ligands to be synthesized and tested for anticancer activity. While some of these compounds involve relatively simple use of such ligands, such as in the case of chelating amino acids, recent reports have shown that much more sophisticated approaches are beginning to be developed. The use of receptor-targeting peptides and antisense oligonucleotides are examples of modern approaches that herald a new direction in the development of ruthenium chemotherapeutics. While a great number of studies have focused on the derivatization of well-established ruthenium anticancer compounds, these developments have been hampered by a lack of knowledge regarding the origin of their activity. Addition of biological ligands allows for rational design of new complexes based on the known *in vivo* behavior and molecular biology of the biological species. This research area is still relatively undeveloped, but the variety of ruthenium complexes and biologically-derived ligands of interest provide an almost limitless potential for new complexes with novel modes of targeting and activity.

References

1. Jakupec, M.A., Galanski, M., Arion, V.B. *et al*. (2008) Antitumor metal compounds: more than theme and variations. *Dalton Trans.*, (2), 183–194.
2. Reedijk, J. (2008) Metal-ligand exchange kinetics in platinum and ruthenium complexes. Significance for effectiveness as anticancer drugs. *Platinum Met. Rev.*, **52** (1), 2–11.
3. Alessio, E., Mestroni, G., Bergamo, A. and Sava, G. (2004) Ruthenium antimetastatic agents. *Curr. Top. Med. Chem.*, **4** (15), 1525–1535.
4. Ang, W.-H., Casini, A., Sava, G. and Dyson, P.J. (2011) Organometallic ruthenium-based antitumor compounds with novel modes of action. *J. Organomet. Chem.*, **696** (5), 989–998.
5. Clarke, M.J. (1980) Oncological implication of the chemistry of ruthenium. *Met. Ions Biol. Syst.*, **11**, 231–283.
6. Clarke, M.J. (1989) Ruthenium chemistry pertaining to the design of anticancer agents. *Prog. Clin. Biochem. Med.*, **10**, 25–39(Ruthenium and other Non-Platinum Metal Complexes in Cancer Chemotherapy).
7. Clarke, M.J. (2002) Ruthenium metallopharmaceuticals. *Coord. Chem. Rev.*, **232** (1–2), 69–93.
8. Clarke, M.J. (2003) Ruthenium metallopharmaceuticals. *Coord. Chem. Rev.*, **236** (1–2), 209–233.
9. Clarke, M.J., Zhu, F. and Frasca, D.R. (1999) Non-platinum chemotherapeutic metallopharmaceuticals. *Chem. Rev.*, **99** (9), 2511–2533.
10. Galanski, M., Arion, V.B., Jakupec, M.A. and Keppler, B.K. (2003) Recent developments in the field of tumor-inhibiting metal complexes. *Curr. Pharm. Des.*, **9** (25), 2078–2089.
11. Kostova, I. (2006) Ruthenium complexes as anticancer agents. *Curr. Med. Chem.*, **13** (9), 1085–1107.
12. Ott, I. and Gust, R. (2007) Non platinum metal complexes as anti-cancer drugs. *Arch. Pharm.*, **340** (3), 117–126.
13. Sava, G. and Bergamo, A. (2000) Ruthenium-based compounds and tumor growth control (review). *Int. J. Oncol.*, **17** (2), 353–365.
14. Zhang, C.X. and Lippard, S.J. (2003) New metal complexes as potential therapeutics. *Curr. Opin. Chem. Biol.*, **7** (4), 481–489.
15. Ang, W.H. and Dyson, P.J. (2006) Classical and non-classical ruthenium-based anticancer drugs: towards targeted chemotherapy. *Eur. J. Inorg. Chem.*, **2006** (20), 4003–4018.
16. Allardyce, C.S. and Dyson, P.J. (2001) Ruthenium in medicine: current clinical uses and future prospects. *Platinum Met. Rev.*, **45** (2), 62–69.

17. Antonarakis, E.S. and Emadi, A. (2010) Ruthenium-based chemotherapeutics: are they ready for prime time? *Cancer Chemother. Pharmacol.*, **66** (1), 1–9.
18. Bergamo, A. and Sava, G. (2011) Ruthenium anticancer compounds: myths and realities of the emerging metal-based drugs. *Dalton Trans.*, **40** (31), 7817–7823.
19. Bratsos, I., Jedner, S., Gianferrara, T. and Alessio, E. (2007) Ruthenium anticancer compounds: challenges and expectations. *Chimia*, **61** (11), 692–697.
20. Bruijnincx, P.C.A. and Sadler, P.J. (2008) New trends for metal complexes with anticancer activity. *Curr. Opin. Chem. Biol.*, **12** (2), 197–206.
21. Levina, A., Mitra, A. and Lay, P.A. (2009) Recent developments in ruthenium anticancer drugs. *Metallomics*, **1** (6), 458–470.
22. Chatterjee, D., Mitra, A. and De, G.S. (2006) Ruthenium polyaminocarboxylate complexes. Prospects for their use as metallopharmaceuticals. *Platinum Met. Rev.*, **50** (1), 2–12.
23. Dougan, S.J. and Sadler, P.J. (2007) The design of organometallic ruthenium arene anticancer agents. *Chimia*, **61** (11), 704–715.
24. Hartinger, C.G., Phillips, A.D. and Nazarov, A.A. (2011) Polynuclear ruthenium, osmium and gold complexes. The quest for innovative anticancer chemotherapeutics. *Curr. Top. Med. Chem.*, **11** (21), 2688–2702.
25. Mestroni, G., Alessio, E., Sava, G. *et al*. (1994) Water-soluble ruthenium(III)-dimethylsulfoxide complexes: chemical behavior and pharmaceutical properties. *Met.-Based Drugs*, **1** (1), 41–63.
26. Moucheron, C., Kirsch-De Mesmaeker, A. and Kelly, J.M. (1997) Photoreactions of ruthenium(II) and osmium(II) complexes with deoxyribonucleic acid (DNA). *J. Photochem. Photobiol. B*, **40** (2), 91–106.
27. Peacock, A.F.A. and Sadler, P.J. (2008) Medicinal organometallic chemistry: designing metal arene complexes as anticancer agents. *Chem. Asian J.*, **3** (11), 1890–1899.
28. Sava, G., Alessio, E., Bergamo, A. and Mestroni, G. (1999) Sulfoxide ruthenium complexes: non-toxic tools for the selective treatment of solid tumor metastases. *Top. Biol. Inorg. Chem.*, **1**, 143–169 (Metallopharmaceuticals I).
29. Suess-Fink, G. (2010) Arene ruthenium complexes as anticancer agents. *Dalton Trans.*, **39** (7), 1673–1688.
30. Dwyer, F.P., Gyarfas, E.C., Rogers, W.P. and Koch, J.H. (1952) Biological activity of complex ions. *Nature*, **170**, 190–191.
31. Frasca, D., Ciampa, J., Emerson, J. *et al*. (1996) Effects of hypoxia and transferrin on toxicity and DNA binding of ruthenium antitumor agents in HeLa cells. *Met.-Based Drugs*, **3** (4), 197–209.
32. Clarke, M.J. (1980) The potential of ruthenium in anticancer pharmaceuticals, in *Inorganic Chemistry in Biology and Medicine*, vol. **190** (ed A.E. Martell), American Chemical Society, Washington, DC, pp. 157–180.
33. Clarke, M.J. (1993) Ruthenium complexes: potential role in anti-cancer pharmaceuticals, in *Metal Complexes in Cancer Chemotherapy* (ed B.K. Keppler), Wiley-VCH Verlag GmbH, Weinheim, pp. 129–156.
34. Mestroni, G., Alessio, E., Sava, G. *et al*. (1993) The development of tumor-inhibiting ruthenium dimethylsulfoxide complexes, in *Metal Complexes in Cancer Chemotherapy* (ed B.K. Keppler), Wiley-VCH Verlag GmbH, Weinheim, pp. 157–185.
35. Alessio, E., Mestroni, G., Nardin, G. *et al*. (1988) *cis*- and *trans*-dihalotetrakis(dimethyl sulfoxide)ruthenium(II) complexes ($RuX_2(DMSO)_4$; X = Cl, Br): synthesis, structure, and antitumor activity. *Inorg. Chem.*, **27** (23), 4099–4106.
36. Coluccia, M., Sava, G., Loseto, F. *et al*. (1993) Anti-leukemic action of $RuCl_2(DMSO)_4$ isomers and prevention of brain involvement in P388 leukemia and in P388/DDP subline. *Eur. J. Cancer*, **29A** (13), 1873–1879.
37. Alessio, E., Mestroni, G., Sava, G. *et al*. (1997) Ruthenium-sulfoxide complexes with a specific antimetastatic activity. *NATO ASI Ser., Ser. 2: Environ.*, **26**, 457–466(Cytotoxic, Mutagenic and Carcinogenic Potential of Heavy Metals Related to Human Environment).
38. Bergamo, A. and Sava, G. (2007) Ruthenium complexes can target determinants of tumor malignancy. *Dalton Trans.*, (13), 1267–1272.
39. Keppler, B.K. and Rupp, W. (1986) Antitumor activity of imidazolium-bisimidazole-tetrachlororuthenate(III). A representative of a new class of inorganic antitumor agents. *J. Cancer Res. Clin. Oncol.*, **111** (2), 166–168.
40. Keppler, B.K., Rupp, W., Juhl, U.M. *et al*. (1987) Synthesis, molecular structure, and tumor-inhibiting properties of imidazolium *trans*-bis(imidazole)tetrachlororuthenate(III) and its methyl-substituted derivatives. *Inorg. Chem.*, **26** (26), 4366–4370.

41. Keppler, B.K., Henn, M., Juhl, U.M. *et al*. (1989) New ruthenium complexes for the treatment of cancer. *Prog. Clin. Biochem. Med.*, **10**, 41–69 (Ruthenium and Other Non-Platinum Metal Complexes in Cancer Chemotherapy).
42. Kapitza, S., Pongratz, M., Jakupec, M.A. *et al*. (2005) Heterocyclic complexes of ruthenium(III) induce apoptosis in colorectal carcinoma cells. *J. Cancer Res. Clin. Oncol.*, **131** (2), 101–110.
43. Keppler, B.K., Lipponer, K.G., Stenzel, B. and Kratzin, F. (1993) New tumor-inhibiting ruthenium complexes, in *Metal Complexes in Cancer Chemotherapy* (ed B.K. Keppler), Wiley-VCH Verlag GmbH, Weinheim, pp. 187–220.
44. Aird, R.E., Cummings, J., Ritchie, A.A. *et al*. (2002) *In vitro* and *in vivo* activity and cross resistance profiles of novel ruthenium (II) organometallic arene complexes in human ovarian cancer. *Br. J. Cancer*, **86** (10), 1652–1657.
45. Depenbrock, H., Schmelcher, S., Peter, R. *et al*. (1997) Preclinical activity of *trans*-indazolium [tetrachlorobisindazoleruthenate (III)] (NSC 666158; IndCR; KP1019) against tumor colony-forming units and hematopoietic progenitor cells. *Eur. J. Cancer*, **33** (14), 2404–2410.
46. Galeano, A., Berger, M.R. and Keppler, B.K. (1992) Antitumor activity of some ruthenium derivatives in human colon cancer cell lines in vitro. *Arzneim.-Forsch.*, **42** (6), 821–824.
47. Kapitza, S., Jakupec Michael, A., Uhl, M. *et al*. (2005) The heterocyclic ruthenium(III) complex KP1019 (FFC14A) causes DNA damage and oxidative stress in colorectal tumor cells. *Cancer Lett.*, **226** (2), 115–121.
48. Kreuser, E.D., Keppler, B.K., Berdel, W.E. *et al*. (1992) Synergistic antitumor interactions between newly synthesized ruthenium complexes and cytokines in human colon carcinoma cell lines. *Semin. Oncol.*, **19** (2, Suppl. 3), 73–81.
49. Kratz, F., Keppler, B.K., Hartmann, M. *et al*. (1996) Comparison of the antiproliferative activity of two antitumor ruthenium(III) complexes with their apotransferrin and transferrin-bound forms in a human colon cancer cell line. *Met.-Based Drugs*, **3** (1), 15–23.
50. Kersten, L., Braunlich, H., Keppler, B.K. *et al*. (1998) Comparative nephrotoxicity of some antitumor-active platinum and ruthenium complexes in rats. *J. Appl. Toxicol.*, **18** (2), 93–101.
51. Cetinbas, N., Webb, M.I., Dubland, J.A. and Walsby, C.J. (2010) Serum-protein interactions with anticancer Ru(III) complexes KP1019 and KP418 characterized by EPR. *J. Biol. Inorg. Chem.*, **15** (2), 131–145.
52. Hartinger, C.G., Jakupec, M.A., Zorbas-Seifried, S. *et al*. (2008) KP1019, a new redox-active anticancer agent – preclinical development and results of a clinical phase I study in tumor patients. *Chem. Biodivers.*, **5** (10), 2140–2155.
53. Hartinger, C.G., Zorbas-Seifried, S., Jakupec, M.A. *et al*. (2006) From bench to bedside - preclinical and early clinical development of the anticancer agent indazolium *trans*-[tetrachlorobis(1*H*-indazole)ruthenate(III)] (KP1019 or FFC14A). *J. Inorg. Biochem.*, **100** (5–6), 891–904.
54. Bergamo, A., Gaiddon, C., Schellens, J.H.M. *et al*. (2012) Approaching tumour therapy beyond platinum drugs: status of the art and perspectives of ruthenium drug candidates. *J. Inorg. Biochem.*, **106** (1), 90–99.
55. Henke, M.M., Richly, H., Drescher, A. *et al*. (2009) Pharmacokinetic study of sodium trans-[tetrachlorobis(1H-indazole)-ruthenate (III)]/-indazole hydrochloride (1:1:1) (FFC14A) in patients with solid tumors. *Int. J. Clin. Pharmacol. Ther.*, **47** (1), 58–60.
56. Trondl, R., Heffeter, P., Jakupec, M.A. *et al*. (2012) NKP-1339, a first-in-class anticancer drug showing mild side effects and activity in patients suffering from advanced refractory cancer. *BMC Pharmacol. Toxicol.*, **13**, A82.
57. Sava, G., Pacor, S., Mestroni, G. and Alessio, E. (1992) Na[*trans*-$RuCl_4$(DMSO)Im], a metal complex of ruthenium with antimetastatic properties. *Clin. Exp. Metastasis*, **10** (4), 273–280.
58. Gagliardi, R., Sava, G., Pacor, S. *et al*. (1994) Antimetastatic action and toxicity on healthy tissues of Na[*trans*-$RuCl_4$(DMSO)Im] in the mouse. *Clin. Exp. Metastasis*, **12** (2), 93–100.
59. Sava, G., Pacor, S., Coluccia, M. *et al*. (1994) Response of Mca mammary carcinoma to cisplatin and to Na[*trans*-$RuCl_4$(DMSO)Im]: selective inhibition of spontaneous lung metastases by the ruthenium complex. *Drug Invest.*, **8** (3), 150–161.
60. Rademaker-Lakhai, J.M., van den Bongard, D., Pluim, D. *et al*. (2004) A phase I and pharmacological study with imidazolium-*trans*-DMSO-imidazole-tetrachlororuthenate, a novel ruthenium anticancer agent. *Clin. Cancer Res.*, **10** (11), 3717–3727.

61. Bergamo, A., Gagliardi, R., Scarcia, V. *et al*. (1999) In vitro cell cycle arrest, in vivo action on solid metastasizing tumors, and host toxicity of the antimetastatic drug NAMI-A and cisplatin. *J. Pharmacol. Exp. Ther.*, **289** (1), 559–564.
62. Bergamo, A., Gava, B., Alessio, E. *et al*. (2002) Ruthenium-based NAMI-A type complexes with in vivo selective metastasis reduction and in vitro invasion inhibition unrelated to cell cytotoxicity. *Int. J. Oncol.*, **21** (6), 1331–1338.
63. Casarsa, C., Mischis, M.T. and Sava, G. (2004) TGFβ1 regulation and collagen-release-independent connective tissue re-modelling by the ruthenium complex NAMI-A in solid tumours. *J. Inorg. Biochem.*, **98** (10), 1648–1654.
64. Sava, G., Zorzet, S., Turrin, C. *et al*. (2003) Dual action of NAMI-A in inhibition of solid tumor metastasis: selective targeting of metastatic cells and binding to collagen. *Clin. Cancer Res.*, **9** (5), 1898–1905.
65. Gava, B., Zorzet, S., Spessotto, P. *et al*. (2006) Inhibition of B16 melanoma metastases with the ruthenium complex imidazolium *trans*-imidazoledimethylsulfoxide-tetrachlororuthenate and down-regulation of tumor cell invasion. *J. Pharmacol. Exp. Ther.*, **317** (1), 284–291.
66. Sava, G., Frausin, F., Cocchietto, M. *et al*. (2004) Actin-dependent tumour cell adhesion after short-term exposure to the antimetastasis ruthenium complex NAMI-A. *Eur. J. Cancer*, **40** (9), 1383–1396.
67. Pieper, T., Peti, W. and Keppler, B.K. (2000) Solvolysis of the tumor-inhibiting Ru(III)-complex trans-tetrachlorobis(indazole)ruthenate(III). *Met.-Based Drugs*, **7** (4), 225–232.
68. Bacac, M., Hotze, A.C.G., van der Schilden, K. *et al*. (2004) The hydrolysis of the anti-cancer ruthenium complex NAMI-A affects its DNA binding and antimetastatic activity: an NMR evaluation. *J. Inorg. Biochem.*, **98** (2), 402–412.
69. Sava, G., Bergamo, A., Zorzet, S. *et al*. (2002) Influence of chemical stability on the activity of the antimetastasis ruthenium compound NAMI-A. *Eur. J. Cancer*, **38** (3), 427–435.
70. Kratz, F., Hartmann, M., Keppler, B. and Messori, L. (1994) The binding properties of two antitumor ruthenium(III) complexes to apotransferrin. *J. Biol. Chem.*, **269** (4), 2581–2588.
71. Messori, L., Vilchez, F.G., Vilaplana, R. *et al*. (2000) Binding of antitumor ruthenium(III) complexes to plasma proteins. *Met.-Based Drugs*, **7** (6), 335–342.
72. Bergamo, A., Messori, L., Piccioli, F. *et al*. (2003) Biological role of adduct formation of the ruthenium(III) complex NAMI-A with serum albumin and serum transferrin. *Invest. New Drugs*, **21** (4), 401–411.
73. Piccioli, F., Sabatini, S., Messori, L. *et al*. (2004) A comparative study of adduct formation between the anticancer ruthenium(III) compound HInd *trans*-[$RuCl_4(Ind)_2$] and serum proteins. *J. Inorg. Biochem.*, **98** (6), 1135–1142.
74. Webb, M.I. and Walsby, C.J. (2011) Control of ligand-exchange processes and the oxidation state of the antimetastatic Ru(III) complex NAMI-A by interactions with human serum albumin. *Dalton Trans.*, **40** (6), 1322–1331.
75. Reisner, E., Arion, V.B., Keppler, B.K. and Pombeiro, A.J.L. (2008) Electron-transfer activated metal-based anticancer drugs. *Inorg. Chim. Acta*, **361** (6), 1569–1583.
76. Graf, N. and Lippard, S.J. (2012) Redox activation of metal-based prodrugs as a strategy for drug delivery. *Adv. Drug Delivery Rev.*, **64** (11), 993–1004.
77. Smith, G.S. and Therrien, B. (2011) Targeted and multifunctional arene ruthenium chemotherapeutics. *Dalton Trans.*, **40** (41), 10793–10800.
78. Yan, Y.K., Melchart, M., Habtemariam, A. and Sadler, P.J. (2005) Organometallic chemistry, biology and medicine: ruthenium arene anticancer complexes. *Chem. Commun.*, (38), 4764–4776.
79. Morris, R.E., Aird, R.E., Murdoch, P.D.S. *et al*. (2001) Inhibition of cancer cell growth by ruthenium(II) arene complexes. *J. Med. Chem.*, **44** (22), 3616–3621.
80. Novakova, O., Kasparkova, J., Bursova, V. *et al*. (2005) Conformation of DNA modified by monofunctional Ru(II) arene complexes: recognition by DNA binding proteins and repair. Relationship to cytotoxicity. *Chem. Biol.*, **12** (1), 121–129.
81. Chen, H., Parkinson, J.A., Morris, R.E. and Sadler, P.J. (2003) Highly selective binding of organometallic ruthenium ethylenediamine complexes to nucleic acids: novel recognition mechanisms. *J. Am. Chem. Soc.*, **125** (1), 173–186.
82. Wang, F., Chen, H., Parsons, S. *et al*. (2003) Kinetics of aquation and anation of ruthenium(II) arene anticancer complexes, acidity and X-ray structures of aqua adducts. *Chem. Eur. J.*, **9** (23), 5810–5820.

83. Fernandez, R., Melchart, M., Habtemariam, A. *et al*. (2004) Use of chelating ligands to tune the reactive site of half-sandwich ruthenium(II)-arene anticancer complexes. *Chem. Eur. J.*, **10** (20), 5173–5179.
84. Schmid, W.F., John, R.O., Arion, V.B. *et al*. (2007) Highly antiproliferative ruthenium(II) and osmium(II) arene complexes with paullone-derived ligands. *Organometallics*, **26** (26), 6643–6652.
85. Williams, D.S., Atilla, G.E., Bregman, H. *et al*. (2005) Switching on a signaling pathway with an organoruthenium complex. *Angew. Chem. Int. Ed.*, **44** (13), 1984–1987.
86. Meggers, E., Atilla-Gokcumen, G.E., Gruendler, K. *et al*. (2009) Inert ruthenium half-sandwich complexes with anticancer activity. *Dalton Trans.*, (48), 10882–10888.
87. Ruiz, J., Vicente, C., de Haro, C. and Bautista, D. (2009) A novel ruthenium(II) arene based intercalator with potent anticancer activity. *Dalton Trans.*, (26), 5071–5073.
88. Dyson, P.J. (2007) Systematic design of a targeted organometallic antitumor drug in pre-clinical development. *Chimia*, **61** (11), 698–703.
89. Allardyce, C.S., Dyson, P.J., Ellis, D.J. and Heath, S.L. (2001) [Ru(η^6-*p*-cymene)Cl_2(pta)] (pta = 1,3,5-triaza-7-phosphatricyclo[3.3.1.$1^{3,7}$]decane): a water soluble compound that exhibits pH dependent DNA binding providing selectivity for diseased cells. *Chem. Commun.*, (15), 1396–1397.
90. Scolaro, C., Bergamo, A., Brescacin, L. *et al*. (2005) In vitro and in vivo evaluation of ruthenium(II)-arene PTA complexes. *J. Med. Chem.*, **48** (12), 4161–4171.
91. Bergamo, A., Masi, A., Dyson, P.J. and Sava, G. (2008) Modulation of the metastatic progression of breast cancer with an organometallic ruthenium compound. *Int. J. Oncol.*, **33** (6), 1281–1289.
92. Renfrew, A.K., Phillips, A.D., Egger, A.E. *et al*. (2009) Influence of structural variation on the anticancer activity of RAPTA-type complexes: ptn versus pta. *Organometallics*, **28** (4), 1165–1172.
93. Ang, W.H., Daldini, E., Scolaro, C. *et al*. (2006) Development of organometallic ruthenium-arene anticancer drugs that resist hydrolysis. *Inorg. Chem.*, **45** (22), 9006–9013.
94. Scolaro, C., Chaplin, A.B., Hartinger, C.G. *et al*. (2007) Tuning the hydrophobicity of ruthenium(II)-arene (RAPTA) drugs to modify uptake, biomolecular interactions and efficacy. *Dalton Trans.*, (43), 5065–5072.
95. Casini, A., Gabbiani, C., Sorrentino, F. *et al*. (2008) Emerging protein targets for anticancer metallodrugs: inhibition of thioredoxin reductase and cathepsin B by antitumor ruthenium(II)-arene compounds. *J. Med. Chem.*, **51** (21), 6773–6781.
96. Elliott, E. and Sloane, B.F. (1996) The cysteine protease cathepsin B in cancer. *Perspect. Drug Discovery Des.*, **6**, 12–32 (Cysteine Proteases).
97. Hartinger, C.G., Metzler-Nolte, N. and Dyson, P.J. (2012) Challenges and opportunities in the development of organometallic anticancer drugs. *Organometallics*, **31** (16), 5677–5685.
98. Meggers, E., Atilla-Gokcumen, G.E., Bregman, H. *et al*. (2007) Exploring chemical space with organometallics: ruthenium complexes as protein kinase inhibitors. *Synlett*, (8), 1177–1189.
99. Brabec, V. and Novakova, O. (2006) DNA binding mode of ruthenium complexes and relationship to tumor cell toxicity. *Drug Resist. Updat.*, **9** (3), 111–122.
100. Novakova, O., Kasparkova, J., Vrana, O. *et al*. (1995) Correlation between cytotoxicity and DNA binding of polypyridyl ruthenium complexes. *Biochemistry*, **34** (38), 12369–12378.
101. van Vliet, P.M., Toekimin, S.M.S., Haasnoot, J.G. *et al*. (1995) *mer*-[Ru(terpy)Cl_3] (terpy = 2,2′:6′,2″-terpyridine) shows biological activity, forms interstrand cross-links in DNA and binds two guanine derivatives in a *trans* configuration. *Inorg. Chim. Acta*, **231** (1–2), 57–64.
102. Wheate, N.J., Brodie, C.R., Collins, J.G. *et al*. (2007) DNA intercalators in cancer therapy: organic and inorganic drugs and their spectroscopic tools of analysis. *Mini Rev. Med. Chem.*, **7** (6), 627–648.
103. Rehmann, J.P. and Barton, J.K. (1990) Proton NMR studies of tris(phenanthroline) metal complexes bound to oligonucleotides: characterization of binding modes. *Biochemistry*, **29** (7), 1701–1709.
104. Moucheron, C. (2009) From cisplatin to photoreactive Ru complexes: targeting DNA for biomedical applications. *New J. Chem.*, **33** (2), 235–245.
105. Schatzschneider, U., Niesel, J., Ott, I. *et al*. (2008) Cellular uptake, cytotoxicity, and metabolic profiling of human cancer cells treated with ruthenium(II) polypyridyl complexes [Ru(bpy)$_2$(N-N)]Cl_2 with N-N = bpy, phen, dpq, dppz, and dppn. *ChemMedChem*, **3** (7), 1104–1109.

106. Sun, Y., Joyce, L.E., Dickson, N.M. and Turro, C. (2010) Efficient DNA photocleavage by $[Ru(bpy)_2(dppn)]^{2+}$ with visible light. *Chem. Commun.*, **46** (14), 2426–2428.
107. Velders, A.H., Kooijman, H., Spek, A.L. *et al*. (2000) Strong differences in the in vitro cytotoxicity of three isomeric dichlorobis(2-phenylazopyridine)ruthenium(II) complexes. *Inorg. Chem.*, **39** (14), 2966–2967.
108. Hotze, A.C.G., van der Geer, E.P.L., Kooijman, H. *et al*. (2005) Characterization by NMR spectroscopy, X-ray analysis and cytotoxic activity of the ruthenium(II) compounds $[RuL_3](PF_6)_2$ (L = 2-phenylazopyridine or *o*-tolylazopyridine) and $[RuL'_2L'](PF_6)_2$ (L′,L′′ = 2-phenylazopyridine, 2,2′-bipyridine). *Eur. J. Inorg. Chem.*, (13), 2648–2657.
109. Tfouni, E., Doro, F.G., Figueiredo, L.E. *et al*. (2010) Tailoring NO donors metallopharmaceuticals: ruthenium nitrosyl ammines and aliphatic tetraazamacrocycles. *Curr. Med. Chem.*, **17** (31), 3643–3657.
110. Tfouni, E., Truzzi, D.R., Tavares, A. *et al*. (2012) Biological activity of ruthenium nitrosyl complexes. *Nitric Oxide*, **26** (1), 38–53.
111. Therrien, B., Ang, W.H., Cherioux, F. *et al*. (2007) Remarkable anticancer activity of triruthenium-arene clusters compared to tetraruthenium-arene clusters. *J. Cluster Sci.*, **18** (3), 741–752.
112. Iengo, E., Mestroni, G., Geremia, S. *et al*. (1999) Novel ruthenium(III) dimers $Na_2[\{trans\text{-}RuCl_4(Me_2SO\text{-}S)\}_2(\mu\text{-L})]$ and $[\{mer,cis\text{-}RuCl_3(Me_2SO\text{-}S)(Me_2SO\text{-}O)\}2(\mu\text{-L})]$ (L = bridging heterocyclic N-donor ligand) closely related to the antimetastatic complex $Na[trans\text{-}RuCl_4(Me_2SO\text{-}S)(Him)]$. *J. Chem. Soc., Dalton Trans.*, (19), 3361–3371.
113. Rani-Beeram, S., Meyer, K., McCrate, A. *et al*. (2008) A fluorinated ruthenium porphyrin as a potential photodynamic therapy agent: synthesis, characterization, DNA binding, and melanoma cell studies. *Inorg. Chem.*, **47** (23), 11278–11283.
114. Gianferrara, T., Bergamo, A., Bratsos, I. *et al*. (2010) Ruthenium-porphyrin conjugates with cytotoxic and phototoxic antitumor activity. *J. Med. Chem.*, **53** (12), 4678–4690.
115. Anderson, C.M., Taylor, I.R., Tibbetts, M.F. *et al*. (2012) Hetero-multinuclear ruthenium(III)/platinum(II) complexes that potentially exhibit both antimetastatic and antineoplastic properties. *Inorg. Chem.*, **51** (23), 12917–12924.
116. Herman, A., Tanski, J.M., Tibbetts, M.F. and Anderson, C.M. (2008) Synthesis, characterization, and in vitro evaluation of a potentially selective anticancer, mixed-metal [ruthenium(III)-platinum(II)] trinuclear complex. *Inorg. Chem.*, **47** (1), 274–280.
117. Hay, R.W. and Nolan, K.B. (1990) Metal complexes of amino acids and peptides. *Amino Acids Pept.*, **21**, 301–328.
118. Severin, K., Bergs, R. and Beck, W. (1998) Metal complexes with biologically important ligands, part 100. Bioorganometallic chemistry-transition metal complexes with α-amino acids and peptides. *Angew. Chem., Int. Ed. Engl.*, **37** (12), 1635–1654.
119. Williams, D.R. (1972) Anticancer drug design involving complexes of amino-acids and metal ions. *Inorg. Chim. Acta, Rev.*, **6**, 123–133.
120. Goldbach, R.E., Rodriguez-Garcia, I., van Lenthe, J.H. *et al*. (2011) *N*-cetylmethionine and biotin as photocleavable protective groups for ruthenium polypyridyl complexes. *Chem. Eur. J.*, **17** (36), 9924–9929.
121. Tauchman, J., Suss-Fink, G., Stepnicka, P. *et al*. (2013) Arene ruthenium complexes with phosphinoferrocene amino acid conjugates: synthesis, characterization and cytotoxicity. *J. Organomet. Chem.*, **723**, 233–238.
122. Tauchman, J., Therrien, B., Suss-Fink, G. and Stepnicka, P. (2012) Heterodinuclear arene ruthenium complexes containing a glycine-derived phosphinoferrocene carboxamide: synthesis, molecular structure, electrochemistry, and catalytic oxidation activity in aqueous media. *Organometallics*, **31** (10), 3985–3994.
123. Fouda, M.F.R., Abd-Elzaher, M.M., Abdelsamaia, R.A. and Labib, A.A. (2007) On the medicinal chemistry of ferrocene. *Appl. Organomet. Chem.*, **21** (8), 613–625.
124. Hillard, E.A., Vessieres, A. and Jaouen, G. (2010) Ferrocene functionalized endocrine modulators as anticancer agents. *Top. Organomet. Chem.*, **32**, 81–117 (Medicinal Organometallic Chemistry).
125. Auzias, M., Therrien, B., Suess-Fink, G. *et al*. (2008) Ferrocenoyl pyridine arene ruthenium complexes with anticancer properties: synthesis, structure, electrochemistry, and cytotoxicity. *Inorg. Chem.*, **47** (2), 578–583.
126. E. Hillard, A. Vessieres, B.F. Le, *et al*., A series of unconjugated ferrocenyl phenols: prospects as anticancer agents, *ChemMedChem*, **1**(5), 551–559 (2006).
127. Djinovic, V., Momcilovic, M., Grguric-Sipka, S. *et al*. (2004) Novel ruthenium complex $K_2[Ru(dmgly)Cl_4]\cdot 2H_2O$ is toxic to C6 astrocytoma cell line, but not to primary rat astrocytes. *J. Inorg. Biochem.*, **98** (12), 2168–2173.

128. Djinovic, V.M., Todorovic, T., Zizak, Z. *et al*. (2009) Ru(III) complexes derived from *N*-methyl derivatives of glycine and 1,3-propylenediamine-*N*,*N*′-diacetato ligands and their activities against HeLa, K562 cell lines and human PBMC. *J. Coord. Chem.*, **62** (2), 328–336.
129. Ali, I., Wani, W.A., Saleem, K. and Wesselinova, D. (2013) Syntheses, DNA binding and anticancer profiles of L-glutamic acid ligand and its copper(II) and ruthenium(III) complexes. *Med. Chem.*, **9** (1), 11–21.
130. Habtemariam, A., Melchart, M., Fernandez, R. *et al*. (2006) Structure-activity relationships for cytotoxic ruthenium(II) arene complexes containing N,N-, N,O-, and O,O-chelating ligands. *J. Med. Chem.*, **49** (23), 6858–6868.
131. Sheldrick, W.S. and Heeb, S. (1990) Synthesis and structural characterization of η^6-arene-ruthenium(II) complexes of alanine and guanine derivatives. *Inorg. Chim. Acta*, **168** (1), 93–100.
132. Paul, L.E.H., Furrer, J. and Therrien, B. (2013) Reactions of a cytotoxic hexanuclear arene ruthenium assembly with biological ligands. *J. Organomet. Chem.*, **734**, 45–52.
133. Paul, L.E.H., Therrien, B. and Furrer, J. (2012) Investigation of the reactivity between a ruthenium hexacationic prism and biological ligands. *Inorg. Chem.*, **51** (2), 1057–1067.
134. Paul, L.E.H., Therrien, B. and Furrer, J. (2012) Interaction of a ruthenium hexacationic prism with amino acids and biological ligands: ESI mass spectrometry and NMR characterization of the reaction products. *J. Biol. Inorg. Chem.*, **17** (7), 1053–1062.
135. Meier, S.M., Hanif, M., Kandioller, W. *et al*. (2012) Biomolecule binding vs. anticancer activity: reactions of Ru(arene)[(thio)pyr-(id)one] compounds with amino acids and proteins. *J. Inorg. Biochem.*, **108** (1), 91–95.
136. Albericio, F. and Kruger, H.G. (2012) Therapeutic peptides. *Future Med. Chem.*, **4** (12), 1527–1531.
137. Milletti, F. (2012) Cell-penetrating peptides: classes, origin, and current landscape. *Drug Discovery Today*, **17** (15–16), 850–860.
138. Heitz, F., Morris, M.C. and Divita, G. (2009) Twenty years of cell-penetrating peptides: from molecular mechanisms to therapeutics. *Br. J. Pharmacol.*, **157** (2), 195–206.
139. Horton, K.L., Stewart, K.M., Fonseca, S.B. *et al*. (2008) Mitochondria-penetrating peptides. *Chem. Biol.*, **15** (4), 375–382.
140. Abramkin, S., Valiahdi, S.M., Jakupec, M.A. *et al*. (2012) Solid-phase synthesis of oxaliplatin-TAT peptide bioconjugates. *Dalton Trans.*, **41** (10), 3001–3005.
141. Albada, H.B., Wieberneit, F., Dijkgraaf, I. *et al*. (2012) The chemoselective reactions of tyrosine-containing G-protein-coupled receptor peptides with $[Cp^*Rh(H_2O)_3](OTf)_2$, including 2D NMR structures and the biological consequences. *J. Am. Chem. Soc.*, **134** (25), 10321–10324.
142. Garcia-Garayoa, E., Schibli, R. and Schubiger, P.A. (2007) Peptides radiolabeled with Re-186/188 and Tc-99m as potential diagnostic and therapeutic agents. *Nucl. Sci. Tech.*, **18** (2), 88–100.
143. Gross, A., Neukamm, M. and Metzler-Nolte, N. (2011) Synthesis and cytotoxicity of a bimetallic ruthenocene dicobalt-hexacarbonyl alkyne peptide bioconjugate. *Dalton Trans.*, **40** (6), 1382–1386.
144. Metzler-Nolte, N. (2010) Biomedical applications of organometal–peptide conjugates, in *Topics in Organometallic Chemistry*, vol. **32** (eds N. Metzler-Nolte and G. Jaouen), Springer-Verlag, Berlin, Heidelberg, pp. 195–217.
145. Neukamm, M.A., Pinto, A. and Metzler-Nolte, N. (2008) Synthesis and cytotoxicity of a cobaltcarbonyl-alkyne enkephalin bioconjugate. *Chem. Commun.*, (2), 232–234.
146. Neundorf, I., Hoyer, J., Splith, K. *et al*. (2008) Cymantrene conjugation modulates the intracellular distribution and induces high cytotoxicity of a cell-penetrating peptide. *Chem. Commun.*, (43), 5604–5606.
147. Pinto, A., Hoffmanns, U., Ott, M. *et al*. (2009) Modification with organometallic compounds improves crossing of the blood–brain barrier of [Leu5]-enkephalin derivatives in an in vitro model system. *ChemBioChem*, **10** (11), 1852–1860.
148. Splith, K., Hu, W., Schatzschneider, U. *et al*. (2010) Protease-activatable organometal-peptide bioconjugates with enhanced cytotoxicity on cancer cells. *Bioconjugate Chem.*, **21** (7), 1288–1296.
149. Struthers, H., Mindt, T.L. and Schibli, R. (2010) Metal chelating systems synthesized using the copper(I) catalyzed azide-alkyne cycloaddition. *Dalton Trans.*, **39** (3), 675–696.
150. van Rijt, S.H., Kostrhunova, H., Brabec, V. and Sadler, P.J. (2011) Functionalization of osmium arene anticancer complexes with (Poly)arginine: effect on cellular uptake, internalization, and cytotoxicity. *Bioconjugate Chem.*, **22** (2), 218–226.

151. Meier, S.M., Novak, M., Kandioller, W. *et al*. (2013) Identification of the structural determinants for anticancer activity of a ruthenium arene peptide conjugate. *Chem. Eur. J.*, **19** (28), 9297–9307.
152. Barragán, F., Carrion-Salip, D., Gomez-Pinto, I. *et al*. (2012) Somatostatin subtype-2 receptor-targeted metal-based anticancer complexes. *Bioconjugate Chem.*, **23** (9), 1838–1855.
153. Bauer, W., Briner, U., Doepfner, W. *et al*. (1982) SMS 201–995: a very potent and selective octapeptide analog of somatostatin with prolonged action. *Life Sci.*, **31** (11), 1133–1140.
154. Schaer, J.C., Waser, B., Mengod, G. and Reubi, J.C. (1997) Somatostatin receptor subtypes sst1, sst2, sst3 and sst5 expression in human pituitary, gastroentero-pancreatic and mammary tumors: comparison of mRNA analysis with receptor autoradiography. *Int. J. Cancer*, **70** (5), 530–537.
155. Janecka, A., Zubrzycka, M. and Janecki, T. (2001) Somatostatin analogs. *J. Pept. Res.*, **58** (2), 91–107.
156. Mezo, G. and Manea, M. (2010) Receptor-mediated tumor targeting based on peptide hormones. *Expert Opin. Drug Delivery*, **7** (1), 79–96.
157. Sun, L.-C. and Coy, D.H. (2008) Cytotoxic conjugates of peptide hormones for cancer chemotherapy. *Drugs Future*, **33** (3), 217–223.
158. Barragán, F., Moreno, V. and Marchan, V. (2009) Solid-phase synthesis and DNA binding studies of dichloroplatinum(II) conjugates of dicarba analogues of octreotide as new anticancer drugs. *Chem. Commun.*, (31), 4705–4707.
159. D'Addona, D., Carotenuto, A., Novellino, E. *et al*. (2008) Novel sst5-selective somatostatin dicarba-analogs: synthesis and conformation-affinity relationships. *J. Med. Chem.*, **51** (3), 512–520.
160. Barragán, F., Lopez-Senin, P., Salassa, L. *et al*. (2011) Photocontrolled DNA binding of a receptor-targeted organometallic ruthenium(II) complex. *J. Am. Chem. Soc.*, **133** (35), 14098–14108.
161. Tfouni, E., Krieger, M., McGarvey, B.R. and Franco, D.W. (2003) Structure, chemical and photochemical reactivity and biological activity of some ruthenium amine nitrosyl complexes. *Coord. Chem. Rev.*, **236** (1–2), 57–69.
162. Xu, W., Liu, L.Z., Loizidou, M. *et al*. (2002) The role of nitric oxide in cancer. *Cell Res.*, **12** (5–6), 311–320.
163. Figueiredo, L.E., Cilli, E.M., Molina, R.A.S. *et al*. (2013) Synthesis and cytotoxicity of a ruthenium nitrosyl nitric oxide donor with isonicotinic acid and a cell penetrating peptide. *Inorg. Chem. Commun.*, **28**, 60–63.
164. Vives, E., Brodin, P. and Lebleu, B. (1997) A truncated HIV-1 Tat protein basic domain rapidly translocates through the plasma membrane and accumulates in the cell nucleus. *J. Biol. Chem.*, **272** (25), 16010–16017.
165. Puckett, C.A. and Barton, J.K. (2009) Fluorescein redirects a ruthenium-octaarginine conjugate to the nucleus. *J. Am. Chem. Soc.*, **131** (25), 8738–8739.
166. Puckett, C.A. and Barton, J.K. (2010) Targeting a ruthenium complex to the nucleus with short peptides. *Bioorg. Med. Chem.*, **18** (10), 3564–3569.
167. Cosgrave, L., Devocelle, M., Forster, R.J. and Keyes, T.E. (2010) Multimodal cell imaging by ruthenium polypyridyl labelled cell penetrating peptides. *Chem. Commun.*, **46** (1), 103–105.
168. Casini, A., Guerri, A., Gabbiani, C. and Messori, L. (2008) Biophysical characterisation of adducts formed between anticancer metallodrugs and selected proteins: new insights from X-ray diffraction and mass spectrometry studies. *J. Inorg. Biochem.*, **102** (5–6), 995–1006.
169. Kratz, F. and Beyer, U. (1998) Serum proteins as drug carriers of anticancer agents: a review. *Drug Delivery*, **5** (4), 281–299.
170. Arsene, A.L., Uivarosi, V., Mitrea, N. *et al*. (2011) The binding properties of some novel ruthenium (III) complexes with human serum transferrin. *Biopolym. Cell*, **27** (2), 141–146.
171. B. Demoro, R.F. de Almeida, F. Marques, *et al*., Screening organometallic binuclear thiosemicarbazone ruthenium complexes as potential anti-tumour agents: cytotoxic activity and human serum albumin binding mechanism, *Dalton Trans.*, **42**(19), 7131–7146 (2013).
172. Matos, C.P., Valente, A., Marques, F. *et al*. (2013) New polydentate Ru(III)-Salan complexes: synthesis, characterization, anti-tumour activity and interaction with human serum proteins. *Inorg. Chim. Acta*, **394**, 616–626.
173. Vilchez, F.G., Vilaplana, R., Blasco, G. and Messori, L. (1998) Solution studies of the antitumor complex dichloro-1,2-propylendiaminetetraacetate ruthenium (III) and of its interactions with proteins. *J. Inorg. Biochem.*, **71** (1-2), 45–51.
174. Ravera, M., Baracco, S., Cassino, C. *et al*. (2004) Electrochemical measurements confirm the preferential bonding of the antimetastatic complex [ImH][$RuCl_4$(DMSO)(Im)] (NAMI-A) with proteins and the weak interaction with nucleobases. *J. Inorg. Biochem.*, **98** (6), 984–990.

175. Beckford, F.A. (2010) Reaction of the anticancer organometallic ruthenium compound, [(η^6-*p*-cymene)Ru(ATSC)-Cl]PF_6 with human serum albumin. *Int. J. Inorg. Chem.*, **2010**, 1–7.
176. Sulyok, M., Hann, S., Hartinger, C.G. *et al*. (2005) Two dimensional separation schemes for investigation of the interaction of an anticancer ruthenium(III) compound with plasma proteins. *J. Anal. Atom. Spectrom.*, **20** (9), 856–863.
177. Liu, Y., Yu, Q., Wang, C. *et al*. (2012) Ruthenium (II) complexes binding to human serum albumin and inducing apoptosis of tumor cells. *Inorg. Chem. Commun.*, **24**, 104–109.
178. Rajendiran, V., Palaniandavar, M., Periasamy, V.S. and Akbarsha, M.A. (2012) New [Ru(5,6-dmp/3,4,7,8-tmp)$_2$-(diimine)]$^{2+}$ complexes: non-covalent DNA and protein binding, anticancer activity and fluorescent probes for nuclear and protein components. *J. Inorg. Biochem.*, **116**, 151–162.
179. Groessl, M., Hartinger, C.G., Polec-Pawlak, K. *et al*. (2008) Elucidation of the interactions of an anticancer ruthenium complex in clinical trials with biomolecules utilizing capillary electrophoresis hyphenated to inductively coupled plasma-mass spectrometry. *Chem. Biodivers.*, **5** (8), 1609–1614.
180. Timerbaev, A.R., Foteeva, L.S., Rudnev, A.V. *et al*. (2007) Probing the stability of serum protein-ruthenium(III) drug adducts in the presence of extracellular reductants using CE. *Electrophoresis*, **28** (13), 2235–2240.
181. Smith, C.A., Sutherland-Smith, A.J., Keppler, B.K. *et al*. (1996) Binding of ruthenium(III) anti-tumor drugs to human lactoferrin probed by high resolution X-ray crystallographic structure analyses. *J. Biol. Inorg. Chem.*, **1** (5), 424–431.
182. Casini, A., Mastrobuoni, G., Terenghi, M. *et al*. (2007) Ruthenium anticancer drugs and proteins: a study of the interactions of the ruthenium(III) complex imidazolium *trans*-[tetrachloro(dimethyl sulfoxide)(imidazole)ruthenate(III)] with hen egg white lysozyme and horse heart cytochrome *c*. *J. Biol. Inorg. Chem.*, **12** (8), 1107–1117.
183. Trynda-Lemiesz, L. (2004) Interaction of an anticancer ruthenium complex HInd[$RuInd_2Cl_4$] with cytochrome c. *Acta Biochim. Pol.*, **51** (1), 199–205.
184. Vergara, A., D'Errico, G., Montesarchio, D. *et al*. (2013) Interaction of anticancer ruthenium compounds with proteins: high-resolution X-ray structures and Raman microscopy studies of the adduct between hen egg white lysozyme and AziRu. *Inorg. Chem.*, **52** (8), 4157–4159.
185. Ascone, I., Messori, L., Casini, A. *et al*. (2008) Exploiting soft and hard X-ray absorption spectroscopy to characterize metallodrug/protein interactions: the binding of [*trans*-$RuCl_4$(Im)(dimethylsulfoxide)][ImH] (Im = imidazole) to bovine serum albumin. *Inorg. Chem.*, **47** (19), 8629–8634.
186. Hartinger, C.G., Casini, A., Duhot, C. *et al*. (2008) Stability of an organometallic ruthenium-ubiquitin adduct in the presence of glutathione: relevance to antitumor activity. *J. Inorg. Biochem.*, **102** (12), 2136–2141.
187. Tuan, G.C.V., Kragh-Hansen, U. and Otagiri, M. (2002) Pharmaceutical strategies utilizing recombinant human serum albumin. *Pharm. Res.*, **19** (5), 569–577.
188. Zitka, O., Ryvolova, M., Hubalek, J. *et al*. (2012) From amino acids to proteins as targets for metal-based drugs. *Curr. Drug Metab.*, **13** (3), 306–320.
189. Groessl, M., Hartinger, C.G., Egger, A. and Keppler, B.K. (2006) The binding of ruthenium(III) anticancer complexes to serum proteins: an ESI-MS study. *Met. Ions Biol. Med.*, **9**, 111–116.
190. Kratz, F., Keppler, B.K., Messori, L. *et al*. (1994) Protein-binding properties of two antitumor Ru(III) complexes to human apotransferrin and apolactoferrin. *Met.-Based Drugs*, **1** (2–3), 169–173.
191. Smith, C.A., Sutherland-Smith, A.J., Keppler, B.K. *et al*. (1996) Binding of ruthenium(III) anti-tumor drugs to human lactoferrin probed by high resolution X-ray crystallographic structure analyses. *J. Biol. Inorg. Chem.*, **1** (5), 424–431.
192. Timerbaev, A.R., Hartinger, C.G., Aleksenko, S.S. and Keppler, B.K. (2006) Interactions of antitumor metallodrugs with serum proteins: advances in characterization using modern analytical methodology. *Chem. Rev.*, **106** (6), 2224–2248.
193. Richardson, D.R. and Ponka, P. (1997) The molecular mechanisms of the metabolism and transport of iron in normal and neoplastic cells. *Biochim. Biophys. Acta, Rev. Biomembr.*, **1331** (1), 1–40.
194. Qian, Z.M., Li, H., Sun, H. and Ho, K. (2002) Targeted drug delivery via the transferrin receptor-mediated endocytosis pathway. *Pharmacol. Rev.*, **54** (4), 561–587.
195. Wagner, E., Curiel, D. and Cotten, M. (1994) Delivery of drugs, proteins and genes into cells using transferrin as a ligand for receptor-mediated endocytosis. *Adv. Drug Delivery Rev.*, **14** (1), 113–135.

196. Webb, M.I., Chard, R.A., Al-Jobory, Y.M. *et al*. (2012) Pyridine analogues of the antimetastatic Ru(III) complex NAMI-A targeting non-covalent interactions with albumin. *Inorg. Chem.*, **51** (2), 954–966.
197. Elsadek, B. and Kratz, F. (2012) Impact of albumin on drug delivery – new applications on the horizon. *J. Controlled Release*, **157** (1), 4–28.
198. Kratz, F. (2008) Albumin as a drug carrier: design of prodrugs, drug conjugates and nanoparticles. *J. Controlled Release*, **132** (3), 171–183.
199. Kratz, F. and Elsadek, B. (2012) Clinical impact of serum proteins on drug delivery. *J. Controlled Release*, **161** (2), 429–445.
200. Liu, M., Lim, Z.J., Gwee, Y.Y. *et al*. (2010) Characterization of a ruthenium(III)/NAMI-A adduct with bovine serum albumin that exhibits a high anti-metastatic activity. *Angew. Chem. Int. Ed.*, **49** (9), 1661–1664.
201. Ang, W.H., Daldini, E., Juillerat-Jeanneret, L. and Dyson, P.J. (2007) Strategy to tether organometallic ruthenium-arene anticancer compounds to recombinant human serum albumin. *Inorg. Chem.*, **46** (22), 9048–9050.
202. Beyer, U., Roth, T., Schumacher, P. *et al*. (1998) Synthesis and in vitro efficacy of transferrin conjugates of the anticancer drug chlorambucil. *J. Med. Chem.*, **41** (15), 2701–2708.
203. Kratz, F., Beyer, U., Roth, T. *et al*. (1998) Albumin conjugates of the anticancer drug chlorambucil. Synthesis, characterization, and in vitro efficacy. *Arch. Pharm.*, **331** (2), 47–53.
204. Witczak, Z.J. (1995) Carbohydrates as drugs and potential therapeutics. *Curr. Med. Chem.*, **1** (5), 392–405.
205. Gottschaldt, M. and Schubert, U.S. (2009) Prospects of metal complexes peripherally substituted with sugars in biomedicinal applications. *Chem. Eur. J.*, **15** (7), 1548–1557.
206. Hartinger, C.G., Nazarov, A.A., Ashraf, S.M. *et al*. (2008) Carbohydrate-metal complexes and their potential as anticancer agents. *Curr. Med. Chem.*, **15** (25), 2574–2591.
207. Berger, I., Hanif, M., Nazarov, A.A. *et al*. (2008) In vitro anticancer activity and biologically relevant metabolization of organometallic ruthenium complexes with carbohydrate-based ligands. *Chem. Eur. J.*, **14** (29), 9046–9057.
208. Hanif, M., Meier, S.M., Kandioller, W. *et al*. (2011) From hydrolytically labile to hydrolytically stable Ru^{II}-arene anticancer complexes with carbohydrate-derived co-ligands. *J. Inorg. Biochem.*, **105** (2), 224–231.
209. Nazarov, A.A., Risse, J., Ang, W.H. *et al*. (2012) Anthracene-tethered ruthenium(II) arene complexes as tools to visualize the cellular localization of putative organometallic anticancer compounds. *Inorg. Chem.*, **51** (6), 3633–3639.
210. Nazarov, A.A., Baquie, M., Nowak-Sliwinska, P. *et al*. (2013) Synthesis and characterization of a new class of anti-angiogenic agents based on ruthenium clusters. *Sci. Rep.*, **3**, 1485.
211. Gottschaldt, M., Schubert, U.S., Rau, S. *et al*. (2010) Sugar-selective enrichment of a D-glucose-substituted ruthenium bipyridyl complex inside HepG2 cancer cells. *ChemBioChem*, **11** (5), 649–652.
212. Kelman, A.D., Clarke, M.J., Edmonds, S.D. and Peresie, H.J. (1977) Biological activity of ruthenium purine complexes. *J. Clin. Hematol. Oncol.*, **7** (1), 274–288.
213. Turel, I., Pecanac, M., Golobic, A. *et al*. (2004) Solution, solid state and biological characterization of ruthenium(III)-DMSO complexes with purine base derivatives. *J. Inorg. Biochem.*, **98** (2), 393–401.
214. Turel, I., Pecanac, M., Golobic, A. *et al*. (2002) Novel Ru^{III}-DMSO complexes of the antiherpes drug acyclovir. *Eur. J. Inorg. Chem.*, **2002** (8), 1928–1931.
215. De Clercq, E. (2004) Antiviral drugs in current clinical use. *J. Clin. Virol.*, **30** (2), 115–133.
216. A. Garcia-Raso, J.J. Fiol, F. Badenas, R. Cons, A. Terron and M. Quiros, Synthesis and structural characteristics of metal-acyclovir (ACV) complexes: $[Ni(or\ Co)(ACV)_2(H_2O)_4]Cl_2{\cdot}2ACV$, $[Zn(ACV)Cl_2(H_2O)]$, $[Cd(ACV)Cl_2]{\cdot}H_2O$ and $[\{Hg(ACV)Cl_2\}_x]$. Recognition of acyclovir by Ni-ACV, *J. Chem. Soc., Dalton Trans.*, (2), 167–174 (1999).
217. Turel, I., Bukovec, N., Goodgame, M. and Williams, D.J. (1997) Synthesis and characterization of copper(II) coordination compounds with acyclovir: crystal structure of triaquabis[9-{(2-hydroxyethoxy)methyl}guanine]copper(II) nitrate hydrate. *Polyhedron*, **16** (10), 1701–1706.
218. Grabner, S., Plavec, J., Bukovec, N. *et al*. (1998) Synthesis and structural characterization of platinum(II)-acyclovir complexes. *J. Chem. Soc., Dalton Trans.*, (9), 1447–1451.
219. Velders, A.H., Bergamo, A., Alessio, E. *et al*. (2004) Synthesis and chemical-pharmacological characterization of the antimetastatic NAMI-A-type Ru(III) complexes (Hdmtp)[*trans*-$RuCl_4$(dmso-*S*)(dmtp)],

(Na)[*trans*-$RuCl_4$(dmso-*S*)(dmtp)], and [*mer*-$RuCl_3(H_2O)$(dmso-*S*)(dmtp)] (dmtp = 5,7-Dimethyl[1,2,4]triazolo-[1,5-a]pyrimidine). *J. Med. Chem.*, **47** (5), 1110–1121.
220. Lakomska, I., Fandzloch, M., Muziol, T. *et al*. (2013) Synthesis, characterization and antitumor properties of two highly cytotoxic ruthenium(III) complexes with bulky triazolopyrimidine ligands. *Dalton Trans.*, **42** (17), 6219–6226.
221. Cebrian-Losantos, B., Reisner, E., Kowol, C.R. *et al*. (2008) Synthesis and reactivity of the aquation product of the antitumor complex *trans*-$[Ru^{III}Cl_4(indazole)_2]^-$. *Inorg. Chem.*, **47** (14), 6513–6523.
222. Reschner, A., Bontems, S., Le, G.S. *et al*. (2013) Ruthenium oligonucleotides, targeting HPV16 E6 oncogene, inhibit the growth of cervical cancer cells under illumination by a mechanism involving p53. *Gene Ther.*, **20** (4), 435–443.
223. Villien, M., Deroo, S., Gicquel, E. *et al*. (2007) The oxime bond formation as an efficient tool for the conjugation of ruthenium complexes to oligonucleotides and peptides. *Tetrahedron*, **63** (46), 11299–11306.
224. Elias, B. and Kirsch-De, M.A. (2006) Photo-reduction of polyazaaromatic Ru(II) complexes by biomolecules and possible applications. *Coord. Chem. Rev.*, **250** (13-14), 1627–1641.
225. DeFilippis, R.A., Goodwin, E.C., Wu, L. and DiMaio, D. (2003) Endogenous human papillomavirus E6 and E7 proteins differentially regulate proliferation, senescence, and apoptosis in HeLa cervical carcinoma cells. *J. Virol.*, **77** (2), 1551–1563.
226. Henderson, B.E. and Feigelson, H.S. (2000) Hormonal carcinogenesis. *Carcinogenesis*, **21** (3), 427–433.
227. Clemons, M. and Goss, P. (2001) Estrogen and the risk of breast cancer. *N. Engl. J. Med.*, **344** (4), 276–285.
228. Hong, W.K. and Sporn, M.B. (1997) Recent advances in chemoprevention of cancer. *Science*, **278** (5340), 1073–1077.
229. Smith, C.L. and O'Malley, B.W. (2004) Coregulator function: a key to understanding tissue specificity of selective receptor modulators. *Endocr. Rev.*, **25** (1), 45–71.
230. Rau, K.M., Kang, H.Y., Cha, T.L. *et al*. (2005) The mechanisms and managements of hormone-therapy resistance in breast and prostate cancers. *Endocr.-Relat. Cancer*, **12** (3), 511–532.
231. Descoteaux, C., Provencher-Mandeville, J., Mathieu, I. *et al*. (2003) Synthesis of 17β-estradiol platinum(II) complexes: biological evaluation on breast cancer cell lines. *Bioorg. Med. Chem. Lett.*, **13** (22), 3927–3931.
232. Barnes, K.R., Kutikov, A. and Lippard, S.J. (2004) Synthesis, characterization, and cytotoxicity of a series of estrogen-tethered platinum(IV) complexes. *Chem. Biol.*, **11** (4), 557–564.
233. Schobert, R., Seibt, S., Effenberger-Neidnicht, K. *et al*. (2011) (Arene)Cl_2Ru(II) complexes with N-coordinated estrogen and androgen isonicotinates: interaction with sex hormone binding globulin and anticancer activity. *Steroids*, **76** (4), 393–399.
234. Hammond, G.L. and Bocchinfuso, W.P. (1995) Sex hormone-binding globulin/androgen-binding protein: steroid-binding and dimerization domains. *J. Steroid Biochem. Mol. Biol.*, **53** (1–6), 543–552.
235. Edsall, A.B., Mohanakrishnan, A.K., Yang, D. *et al*. (2004) Effects of altering the electronics of 2-methoxyestradiol on cell proliferation, on cytotoxicity in human cancer cell cultures, and on tubulin polymerization. *J. Med. Chem.*, **47** (21), 5126–5139.
236. Mann, J. (2002) Natural products in cancer chemotherapy: past, present and future. *Nat. Rev. Cancer*, **2** (2), 143–148.
237. Newman, D.J. and Cragg, G.M. (2007) Natural products as sources of new drugs over the last 25 years. *J. Nat. Prod.*, **70** (3), 461–477.
238. Aggarwal, B.B. and Harikumar, K.B. (2009) Potential therapeutic effects of curcumin, the anti-inflammatory agent, against neurodegenerative, cardiovascular, pulmonary, metabolic, autoimmune, and neoplastic diseases. *Int. J. Biochem. Cell Biol.*, **41** (1), 40–59.
239. Kim, K.J., Kim, K.H., Kim, H.Y. *et al*. (2010) Curcumin inhibits hepatitis C virus replication via suppressing the Akt-SREBP-1 pathway. *FEBS Lett.*, **584** (4), 707–712.
240. Rechtman, M.M., Har-Noy, O., Bar-Yishay, I. *et al*. (2010) Curcumin inhibits hepatitis B virus via down-regulation of the metabolic coactivator PGC-1α. *FEBS Lett.*, **584** (11), 2485–2490.
241. Kelsey, N.A., Wilkins, H.M. and Linseman, D.A. (2010) Nutraceutical antioxidants as novel neuroprotective agents. *Molecules*, **15**, 7792–7814.
242. Duvoix, A., Blasius, R., Delhalle, S. *et al*. (2005) Chemopreventive and therapeutic effects of curcumin. *Cancer Lett.*, **223** (2), 181–190.

243. Lin, L. and Lee, K.-H. (2006) Structure-activity relationships of curcumin and its analogs with different biological activities. *Stud. Nat. Prod. Chem.*, **33**, 785–812 (Bioactive Natural Products (Part M)).
244. Yang, C., Su, X., Liu, A. *et al*. (2013) Advances in clinical study of curcumin. *Curr. Pharm. Des.*, **19** (11), 1966–1973.
245. Anand, P., Kunnumakkara, A.B., Newman, R.A. and Aggarwal, B.B. (2007) Bioavailability of curcumin: problems and promises. *Mol. Pharmaceutics*, **4** (6), 807–818.
246. Anand, P., Thomas, S.G., Kunnumakkara, A.B. *et al*. (2008) Biological activities of curcumin and its analogues (Congeners) made by man and mother nature. *Biochem. Pharmacol.*, **76** (11), 1590–1611.
247. Dutta, S., Murugkar, A., Gandhe, N. and Padhye, S. (2001) Enhanced antioxidant activities of metal conjugates of curcumin derivatives. *Met.-Based Drugs*, **8** (4), 183–188.
248. Valentini, A., Conforti, F., Crispini, A. *et al*. (2009) Synthesis, oxidant properties, and antitumoral effects of a heteroleptic palladium(II) complex of curcumin on human prostate cancer cells. *J. Med. Chem.*, **52** (2), 484–491.
249. Zebib, B., Mouloungui, Z. and Noirot, V. (2010) Stabilization of curcumin by complexation with divalent cations in glycerol/water system. *Bioinorg. Chem. Appl.*, **2010**, 292760.
250. Bonfili, L., Pettinari, R., Cuccioloni, M. *et al*. (2012) Arene-RuII complexes of curcumin exert antitumor activity via proteasome inhibition and apoptosis induction. *ChemMedChem*, **7** (11), 2010–2020.
251. Caruso, F., Rossi, M., Benson, A. *et al*. (2012) Ruthenium-Arene Complexes of Curcumin: X-ray and Density Functional Theory Structure, Synthesis, and Spectroscopic Characterization, in Vitro Antitumor Activity, and DNA Docking Studies of (*p*-Cymene)Ru(curcuminato)chloro. *J. Med. Chem.*, **55** (3), 1072–1081.

Index

Ligand Design in Medicinal Inorganic Chemistry, First Edition. Edited by Tim Storr.

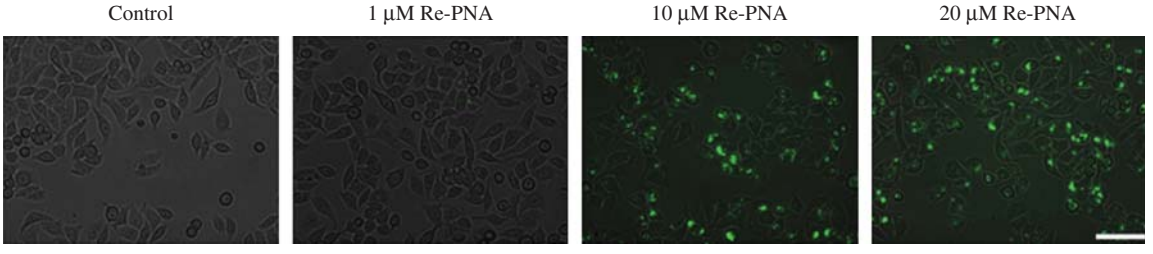

Figure 4.5 *Imaging with Re-PNA SAAQ conjugate. Reproduced from Ref. [45] with permission of The Royal Society of Chemistry.*

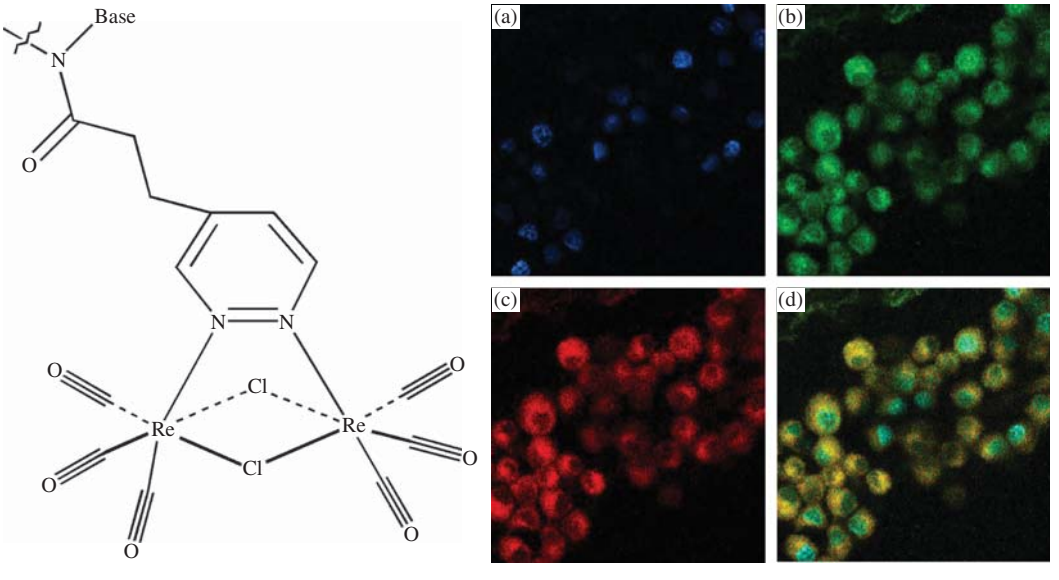

Figure 4.6 *Molecular structure of [Re_2(μ-Cl)$_2$(CO)$_6$(μ-1,2-diazine)] PNA conjugates and luminescence images in macrophages through 485/30 (a), 535/50 (b) and 600/40 (c) bandpass filters and their superposition (d) to show the differential emission. Reprinted with permission from Ref. [46]. Copyright © (2012) American Chemical Society.*

Ligand Design in Medicinal Inorganic Chemistry, First Edition. Edited by Tim Storr.

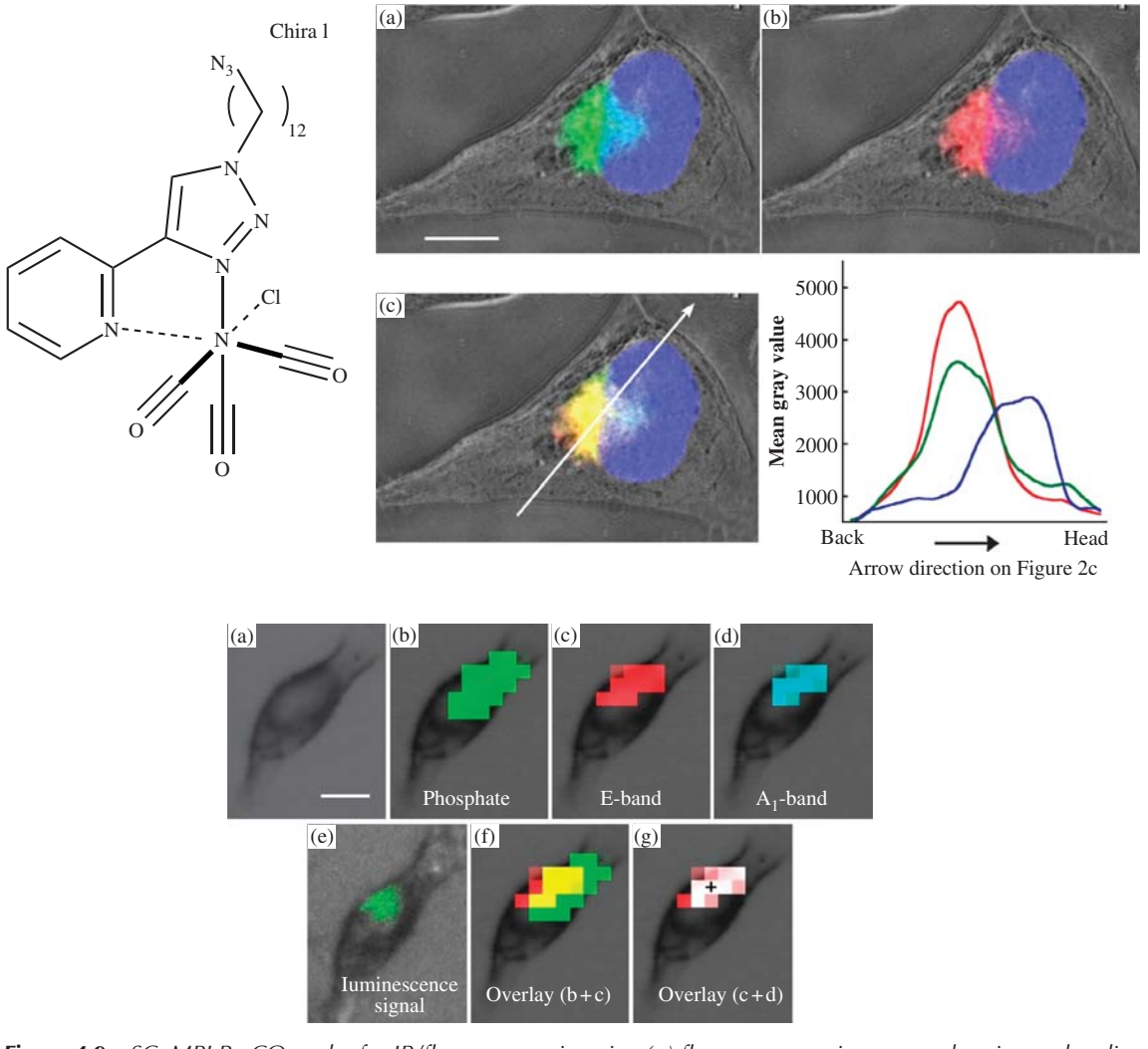

Figure 4.9 *SCoMPI Re-CO probe for IR/fluorescence imaging (a) fluorescence microscopy showing co-localisation with Golgi stain (b) and IR microscopy (c). Reproduced from Ref. [78] with permission of The Royal Society of Chemistry.*

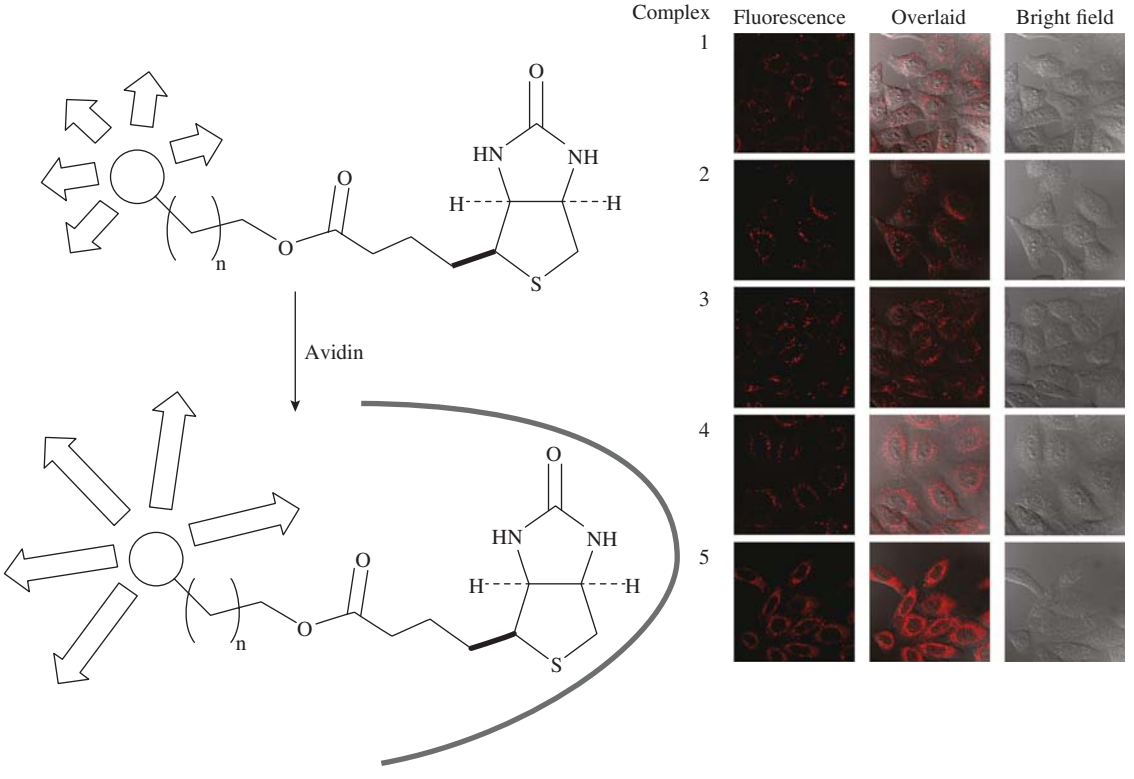

Scheme 4.5 *Luminescence enhancement on avidin binding of biotin-appended lumophores, and cell imaging with biotinylated iridium complexes. Reprinted with permission from Ref. [36]. Copyright © (2009) American Chemical Society.*

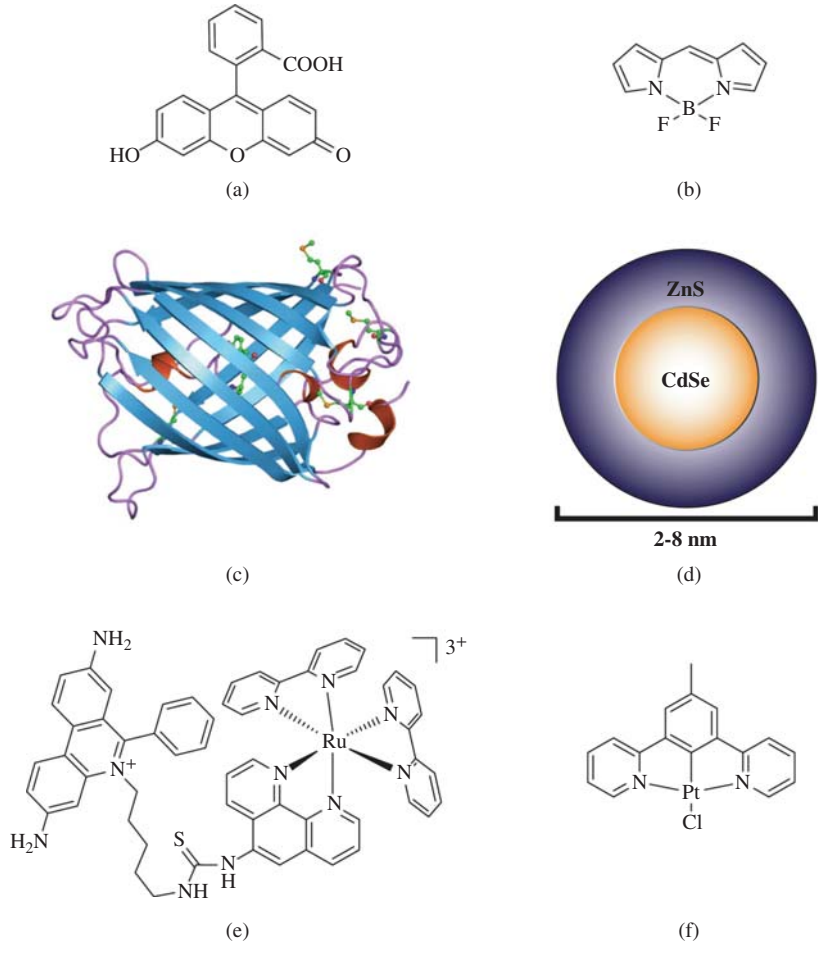

Figure 5.2 *Examples of luminescent probes: organic dyes (a) fluorescein and (b) BODIPY, (c) fluorescent protein GFP [11] (d) quantum dot, and transition metal complexes based on (e) ruthenium and (f) platinum.*

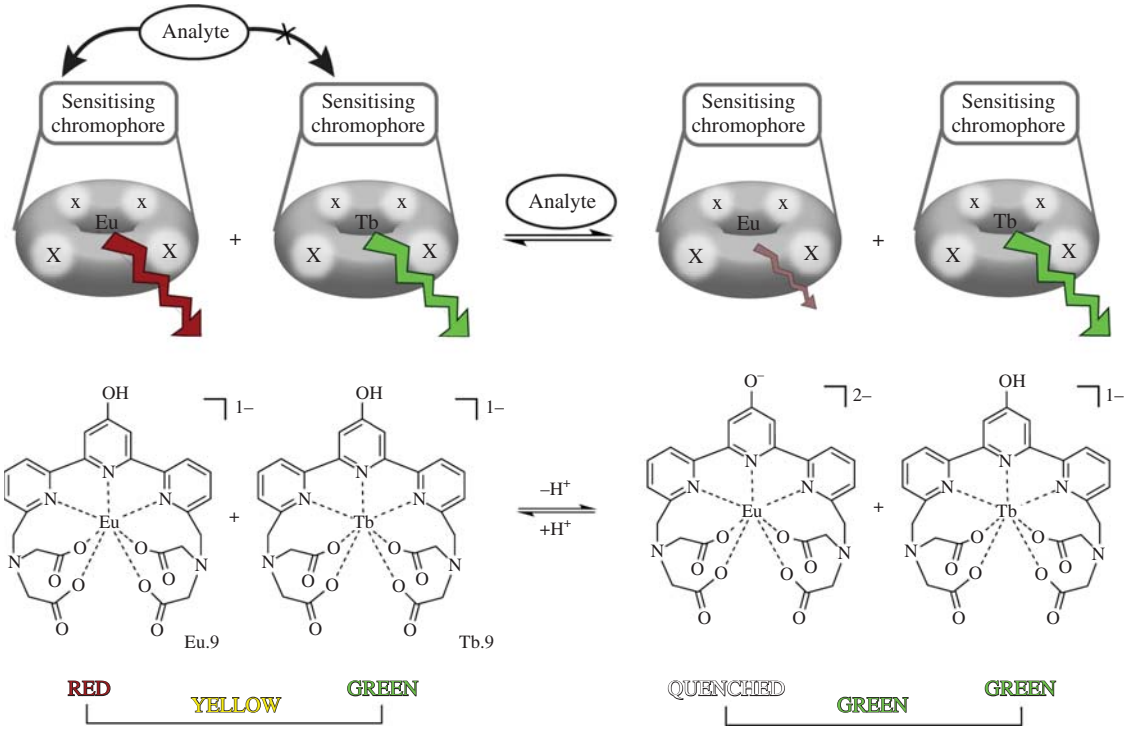

Figure 5.13 *Mixtures of Eu and Tb complexes of the same ligand can be used to give information about analytes.*

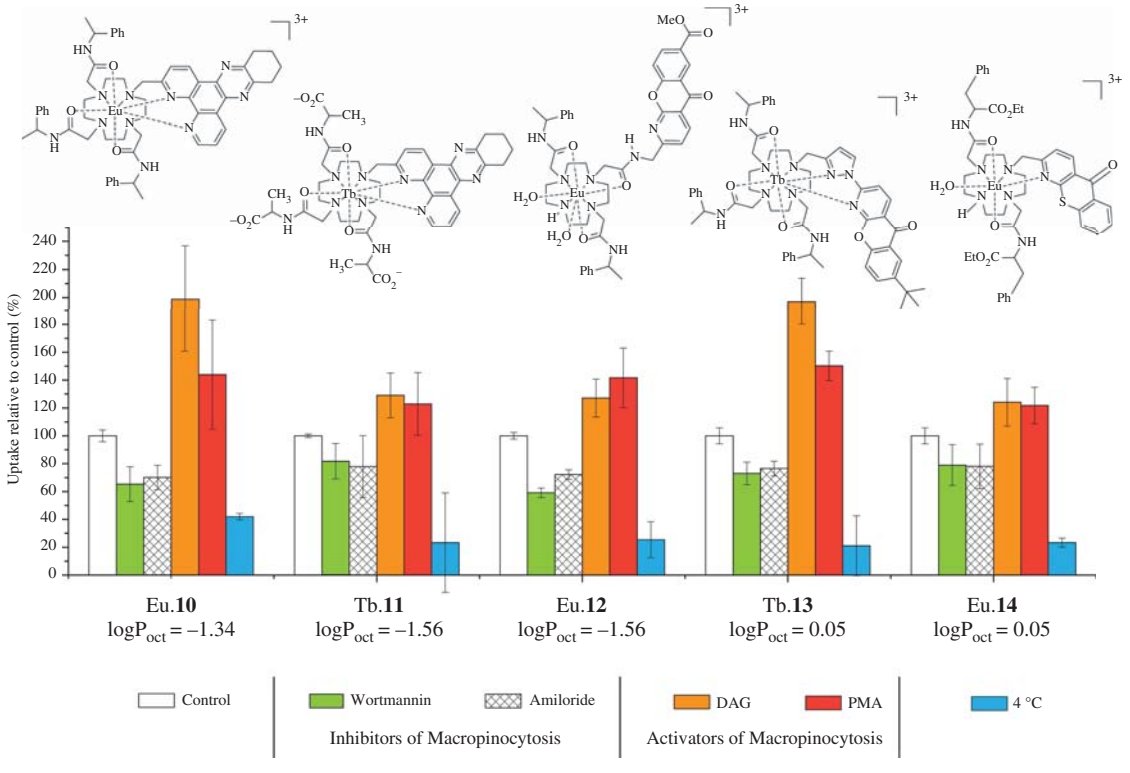

Figure 5.14 *A series of lanthanoid complexes with widely-diverging structures and lipophilicities all show comparable levels of cellular uptake. This uptake was decreased at low temperatures and in the presence of inhibitors of macropinocytosis, and was increased in the presence of activators of macropinocytosis.*

Figure 5.15 *Fluorescence microscopy images of Chinese Hamster Ovary (CHO) cells treated with [Eu.12]Cl$_3$ (100 μM) and FITC-dextran (70 kDa, 2.5 mg/ml) for 15 minute. (a) Eu luminescence, (b) fluorescein fluorescence and (c) overlay of Eu and fluorescein channels showing that the Eu complex is in the macropinosomes after 15 minute. Scale bar represents 20 μm [94]. Reproduced from [94] with permission of The Royal Society of Chemistry.*

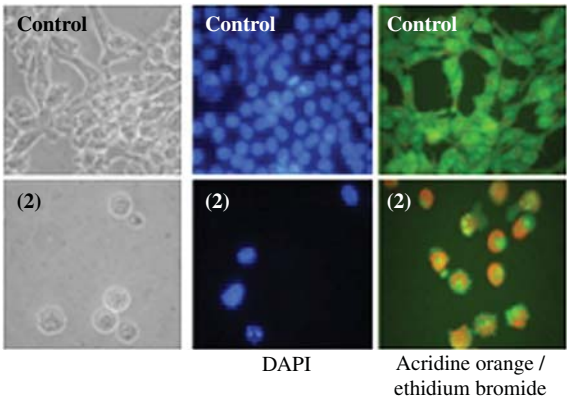

Figure 7.6 *Apoptosis (DAPI staining) and autophagy (AO/EB staining) in T98 cells induced by N^4-o-fluorophenyl-2-acetylpyridine thiosemicarbazone (compound 2).*

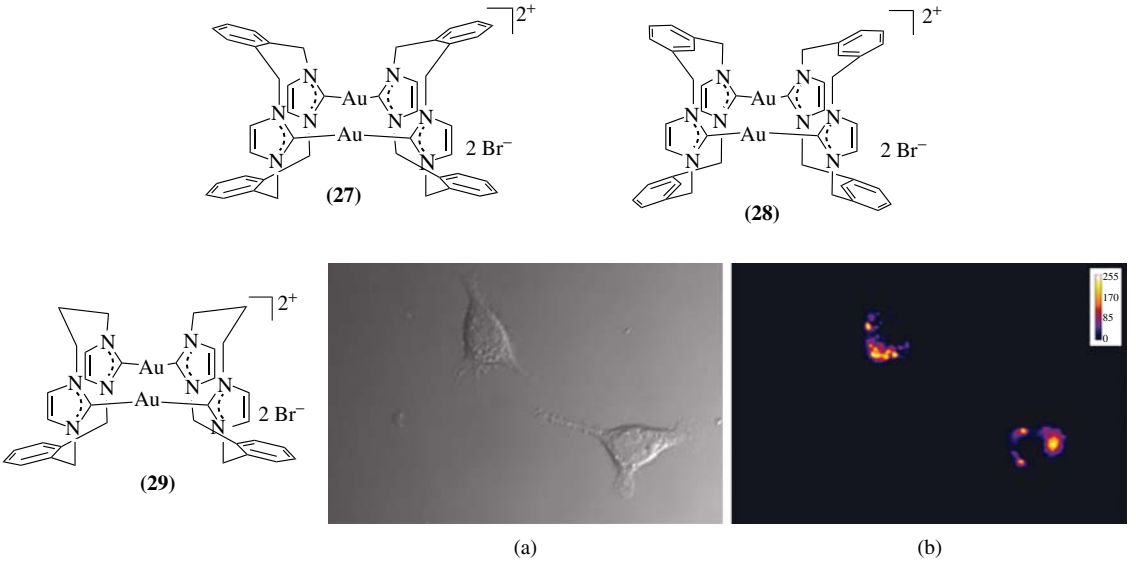

Figure 9.7 *Examples of dinuclear Au^I NHC complexes. Both (**27**) and (**29**) are luminescent as a result of a short Au···Au interaction. Ligand design was used to fine-tune the Au···Au distance in **29**, to obtain an ideal excitation wavelength for live cell imaging studies. The brightfield image (a) and luminescence image (λ_{ex} 351 nm) (b) of RAW264.7 cells after incubation with **29** for 15 hours at 37 °C. Adapted from [144].*

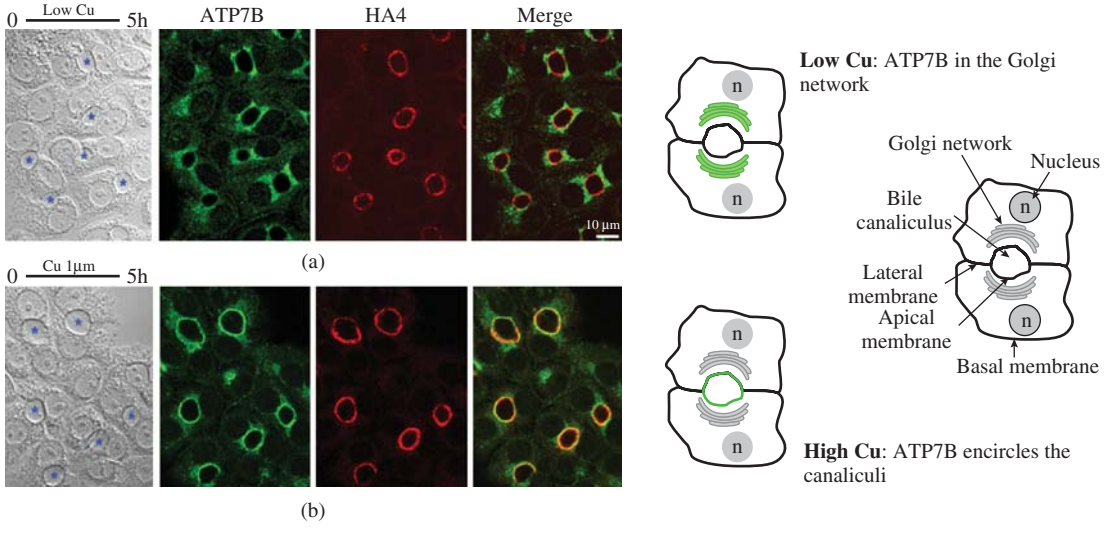

Figure 11.10 *Effect of Cu on ATP7B localization in WIF-B9 cells. ATP7B and HA4 (a canalicular membrane marker) were detected by indirect immunofluorescence and imaged by confocal microscopy. In each panel are presented from left to right, the Nomarski image, the two images of the sum of two confocal sections taken in the middle of the cell layer and the merged image. On the Nomarski images, bile canaliculi are indicated by asterisks. (a) Cells kept in the basal culture medium for 5 hours and (b) cells kept in the basal culture medium plus 1 µM Cu for 5 hours. Reproduced with permission from [158] . Copyright © 2012 WILEY-VCH Verlag GmbH & Co. KGaA, Weinheim.*

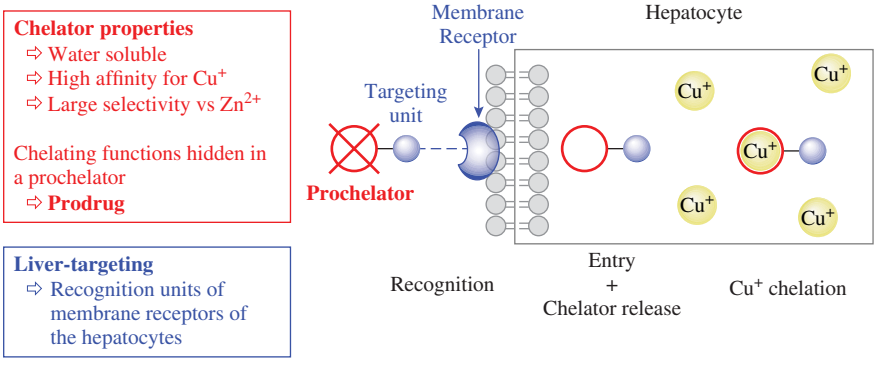

Figure 11.11 *Cu^{+} prochelators targeted at the liver.*

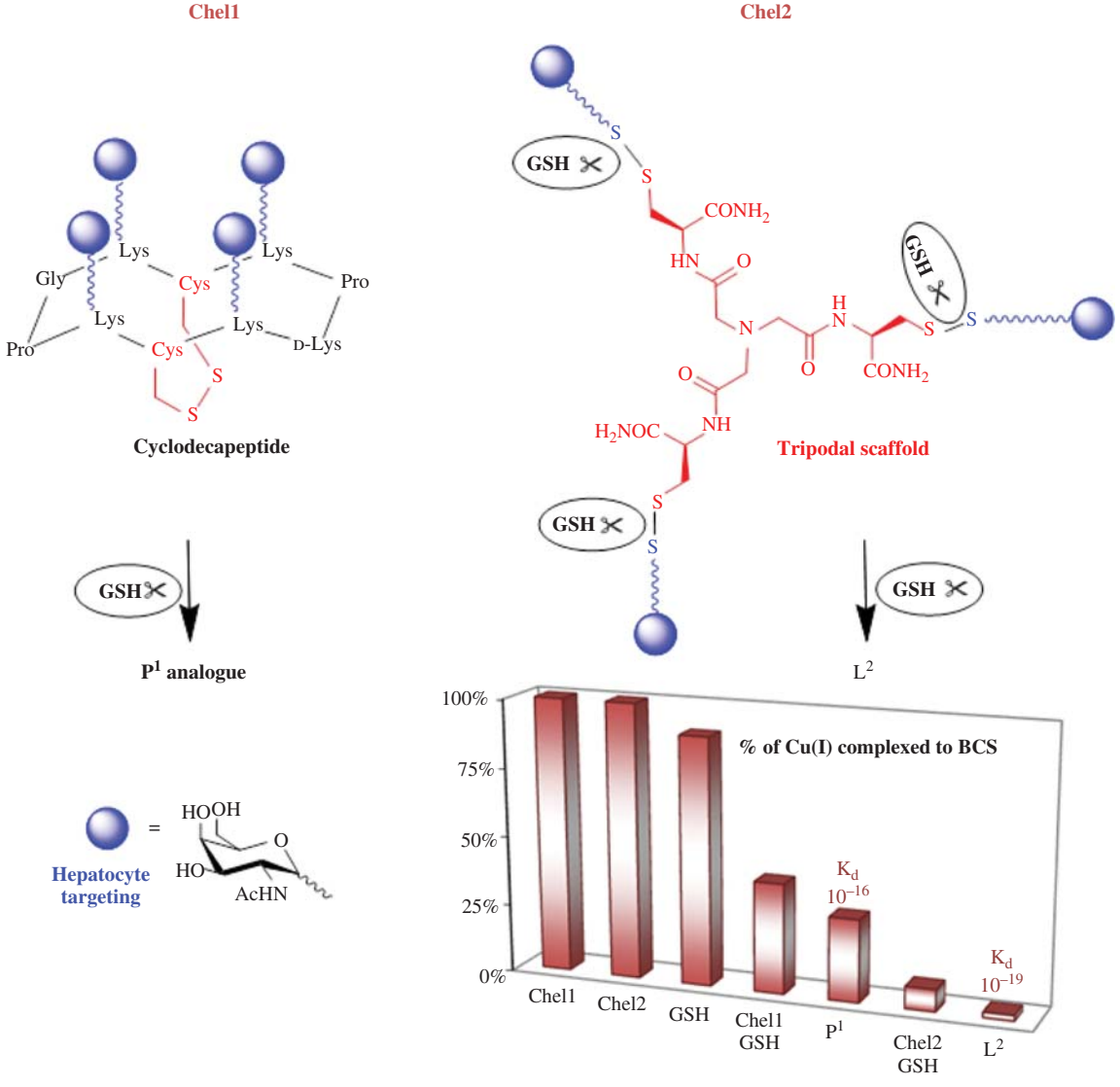

Figure 11.15 *The two glycoconjugates Chel1 and Chel2, combining a prochelating unit (disulfide bridges) and a targeting system to the hepatocytes (N-acetylgalactosamine). The bar diagram represents the percentage of Cu^+ complexed by BCS in competition experiments with 50 µM of the potential Cu ligand (Chel1, Chel2, P^1, or L^2), 45 µM Cu^+ and 90 µM BCS. 1 mM GSH was added to the medium to mimic the reducing intracellular medium, when GSH is indicated.*

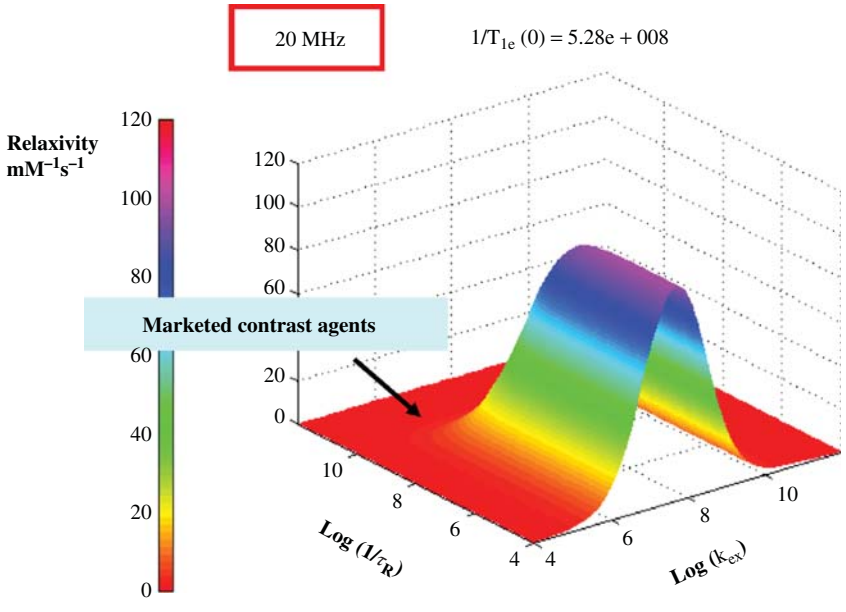

Figure 12.2 *Calculated proton relaxivity at 20 MHz, for a monohydrated complex, as a function of the rotational correlation time* τ_R*, and the water exchange rate* k_{ex}*, for an electronic relaxation rate fixed at* $1/T_{1e} = 5.28 \times 10^8\ s^{-1}$.

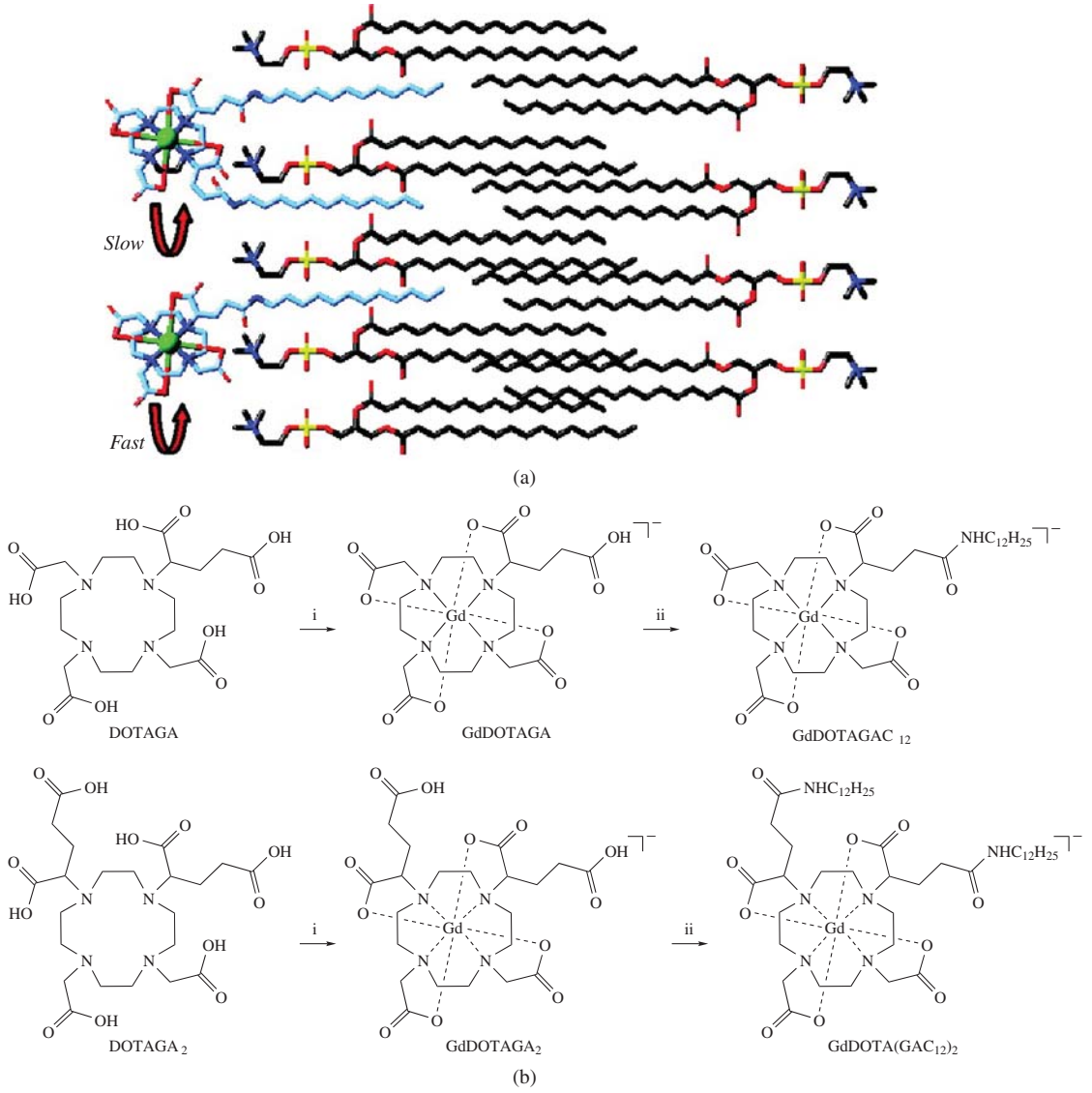

Figure 12.4 *(a) Schematic representation of the complexes GdDOTA(GAC$_{12}$)$_2$ (top) and GdDOTAGAC$_{12}$ (bottom) in the lipid bilayer. (b) Synthesis of the complexes; reaction conditions: (i) GdCl$_3$, H$_2$O, and pH 6. (ii) C$_{12}$H$_{25}$NH$_2$, DMF (dimethylformamide),TNTU [2-(endo-5-norbornene-2.3-dicarboxylimide)-1,1,3,3-tetramethyluronium tetrafluoroborate], and DIPEA (N,N-diisopropylethylamine) [53] Reprinted (adapted) with permission from (53). Copyright (2010) American Chemical Society.*

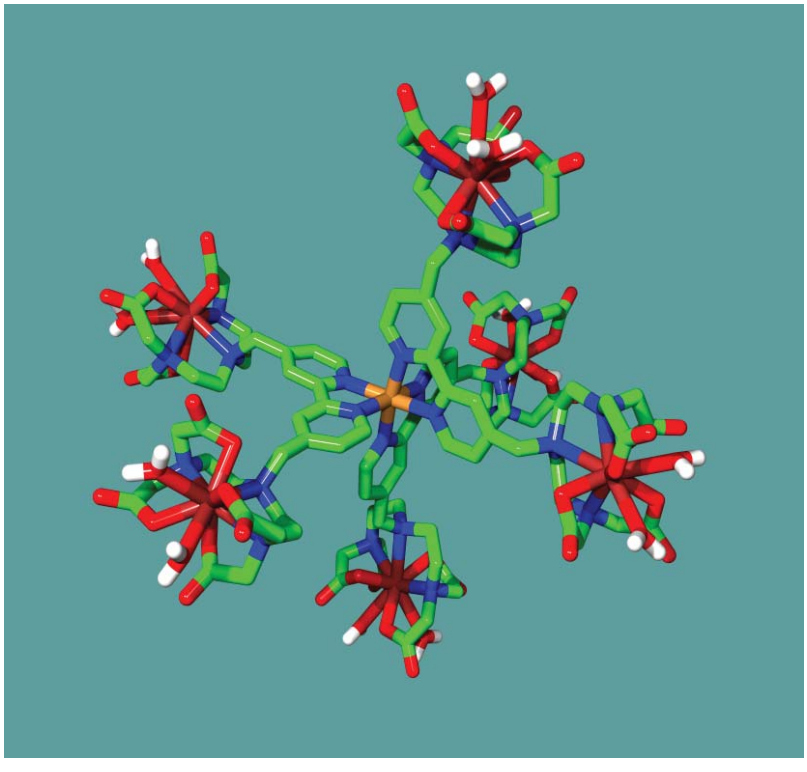

Figure 12.5 *Metallostar compound formed by self-assembly around an* Fe^{2+} *ion.*

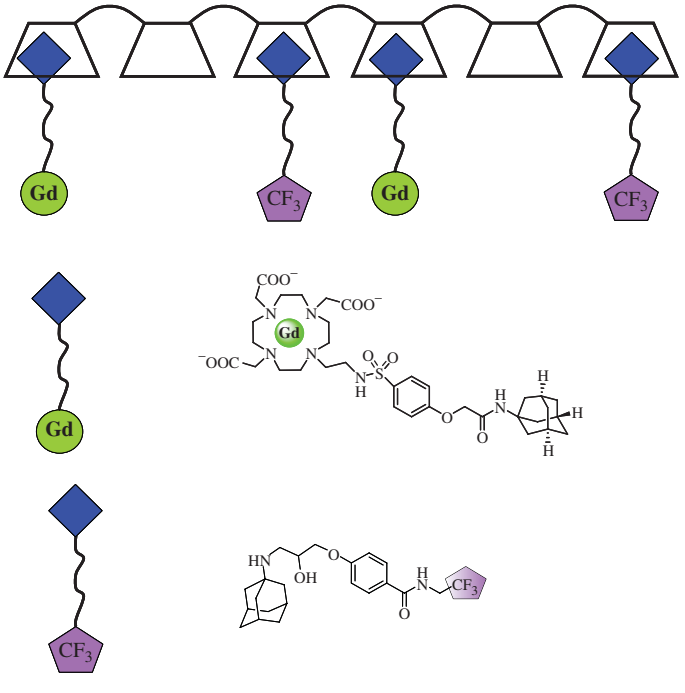

Figure 12.6 *Schematic representation of the pH-responsive supramolecular adducts between poly-β-CD, the Gd^{3+} complex and the ^{19}F reporter.*

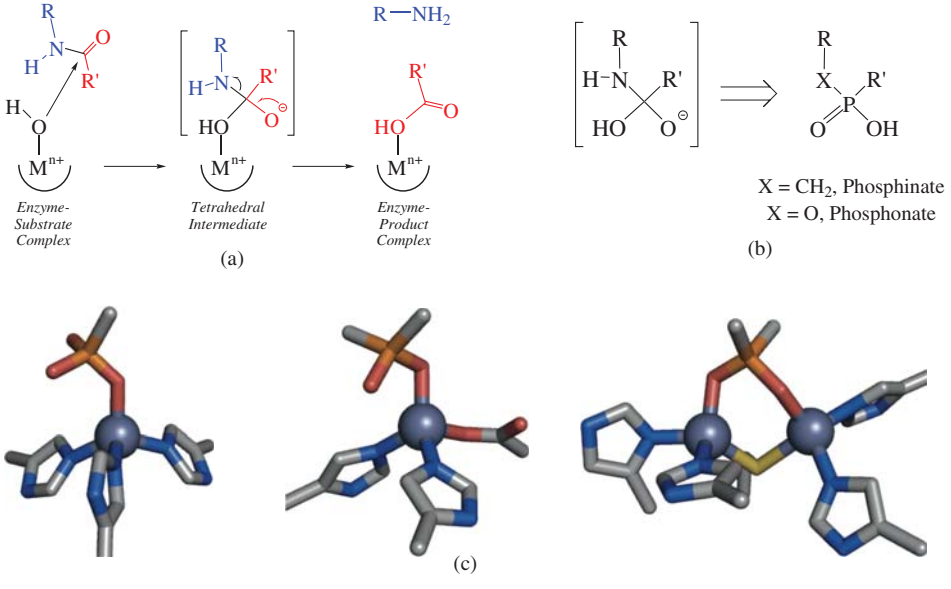

Figure 14.4 *Biological inspiration for phosphate-based MBGs. (a) The mechanism of hydrolases proceeds through a tetrahedral intermediate. Although only one transition state is shown for simplicity, the proton can migrate to the other oxygen atom, transferring the negative charge on the metal-bound atom. Both resonance forms can lead to product formation. (b) The tetrahedral intermediate can be mimicked by phosphate-based MBGs. (c) Crystal structures of phosphonate- (left, PDB 1ZVX) and phosphinate-based (middle, PDB 2X96) inhibitors bound to mononuclear zinc(II) ion centers of MMP-8 and ACE, respectively. Phosphorus-based MBGs can also be used to bind dinuclear active sites such as the zinc(II)-dependent enzyme N-acyl-D-glutamate amidohydrolase (right, PDB 3GIQ).*

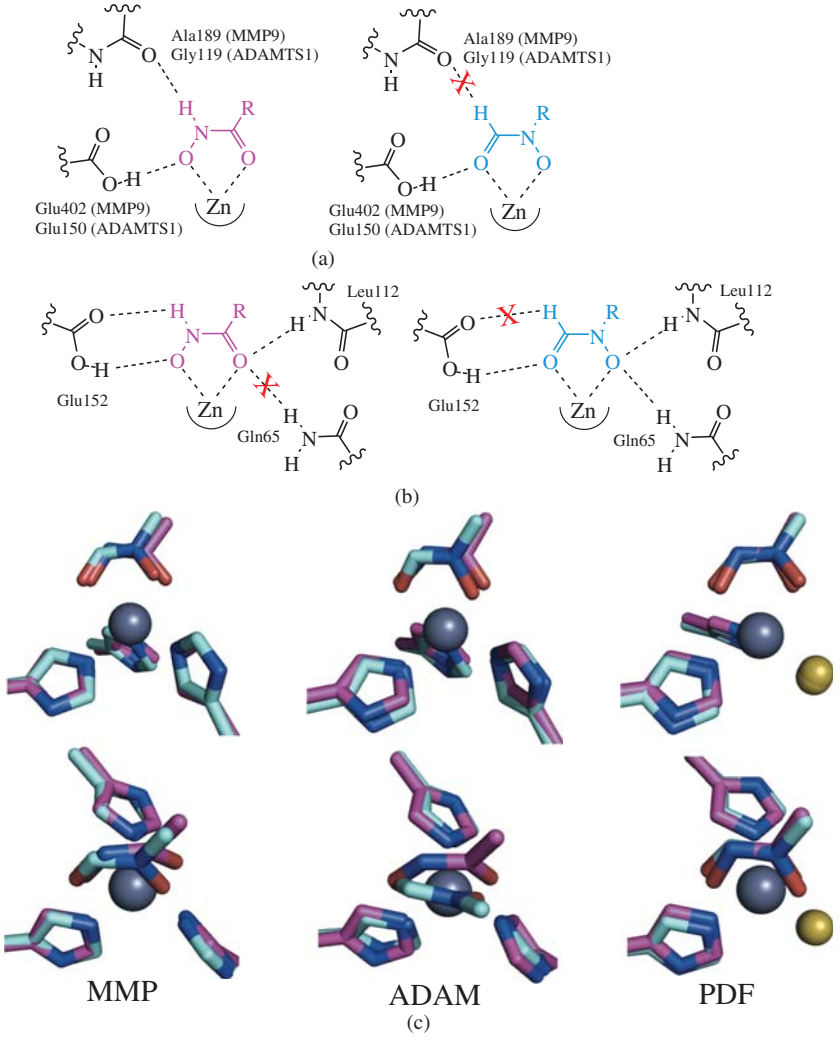

Figure 14.7 *Comparison of the coordination of terminal and reverse hydroxamates. (a) Schematic of the hydrogen bonds formed between the hydroxamic acid MBG and active-site residues of MMPs and ADAMs. Reverse hydroxamic acids cannot make some of these interactions, marked by a red "X." (b) Hydrogen bonding interactions between the MBGs and the active site of PDF, some of which (Leu112 and Gln65) do not occur for the other enzymes discussed. (c) Differences in binding modes of hydroxamic acids (shown in magenta, PDBs 1MMQ, 2RJQ, and 4DR9 from left to right) and reverse hydroxamic acids (shown in blue, PDBs 1GKC, 3Q2G, and 3U7N from left to right) for three different zinc(II)-dependent enzymes. Ligand–metal bonds have been omitted and inhibitors have been truncated for clarity. The cysteine donor of PDF is shown as a yellow sphere, as only the sulfur atom was used for alignment.*

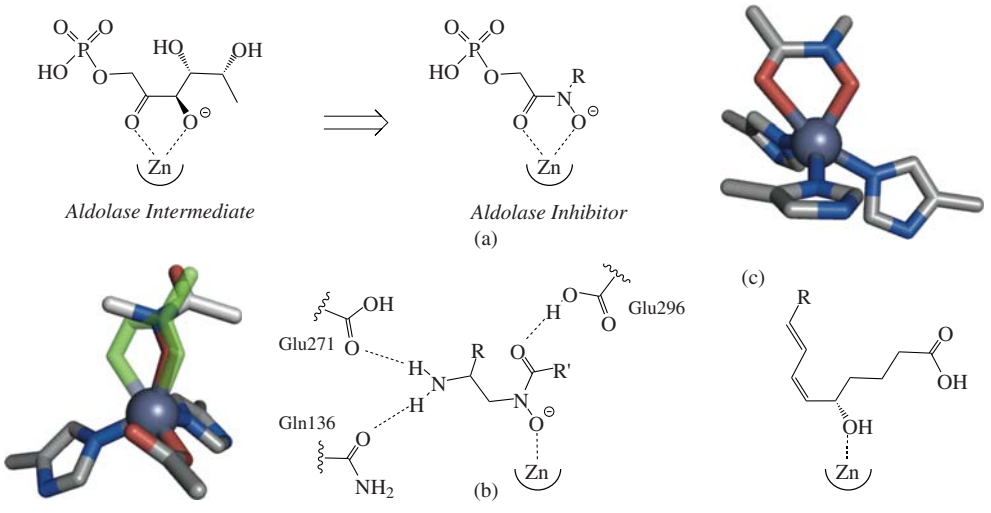

Figure 14.8 *Binding modes of N-substituted hydroxamate MBGs. (a) N-Substituted hydroxamic acids mimic intermediates in the catalytic cycles of enzymes such as aldolase, where the ligand binds in the expected bidentate fashion. (b) Unlike a terminal hydroxamate-based inhibitor (PDB 3B7U, shown in green), the N-substituted hydroxamate MBG displays monodentate coordination to the zinc(II) ion of leukotriene A4 hydrolase (LAH, PDB 2VJ8). This unexpected binding mode is stabilized by other interactions with the protein, shown on the right. (c) The product of LAH is a monodentate ligand. Inhibitors have been truncated for clarity.*

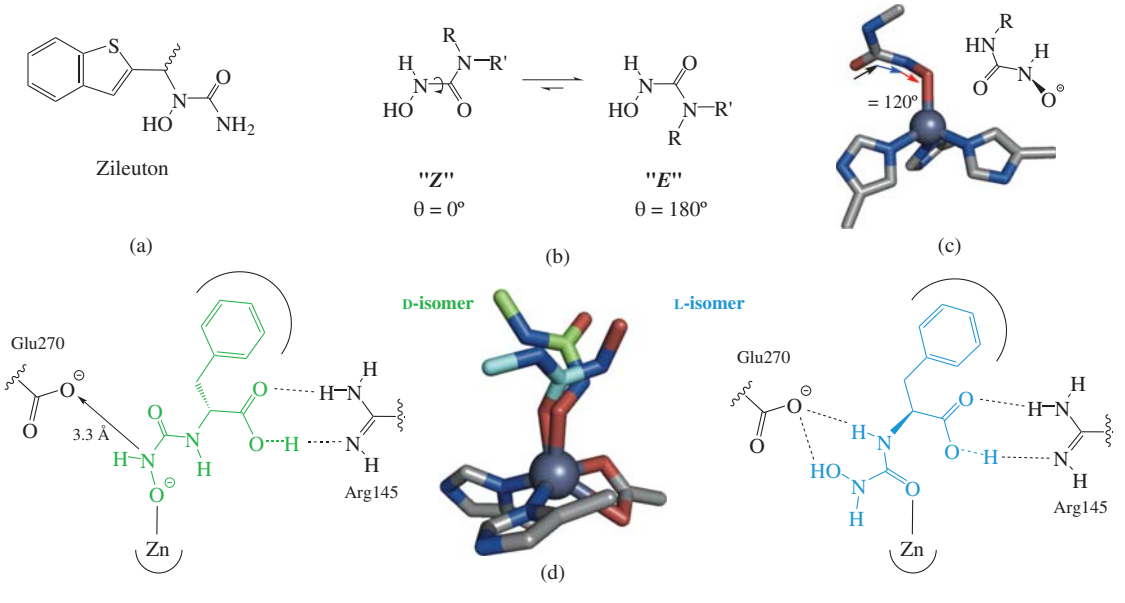

Figure 14.9 *The N-hydroxyurea MBG shows several distinct coordination modes. (a) The structure of zileuton, a clinically-approved 5-LO inhibitor based on the hydroxyurea MBG. (b) The 'Z' conformer of hydroxyurea, required for bidentate binding, is less favorable than the 'E' conformer. (c) Bound to the zinc(II) ion of MMP-8 (PDB 1ZP5), the MBG is nonplanar, displaying a torsion angle of 120°, between that of the 'E' and 'Z' conformers. (d) Bound to the zinc(II) ion of carboxypeptidase A, two enantiomers of the same inhibitor based on the N-hydroxyurea MBG adopt different binding modes (PDB 1HDQ and 1HEE). Inhibitors have been truncated for clarity.*

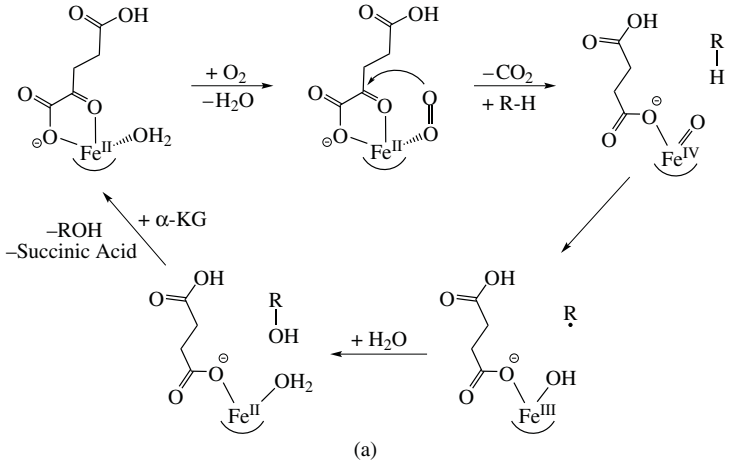

(a)

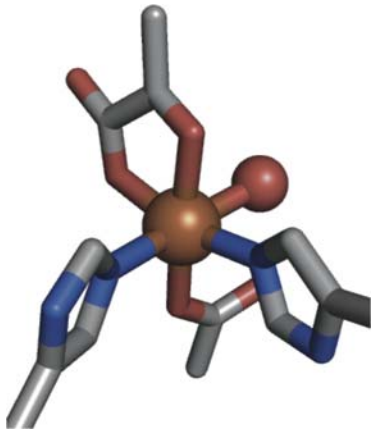

(b)

Figure 14.11 *Iron(II) oxygenases require a metal-bound cofactor, α-KG. (a) The mechanism of oxygen activation by α-KG-dependent iron(II) oxygenases. (b) α-KG bound bidentate to the iron(II) ion (PDB 2Y0I, α-KG is truncated for clarity).*

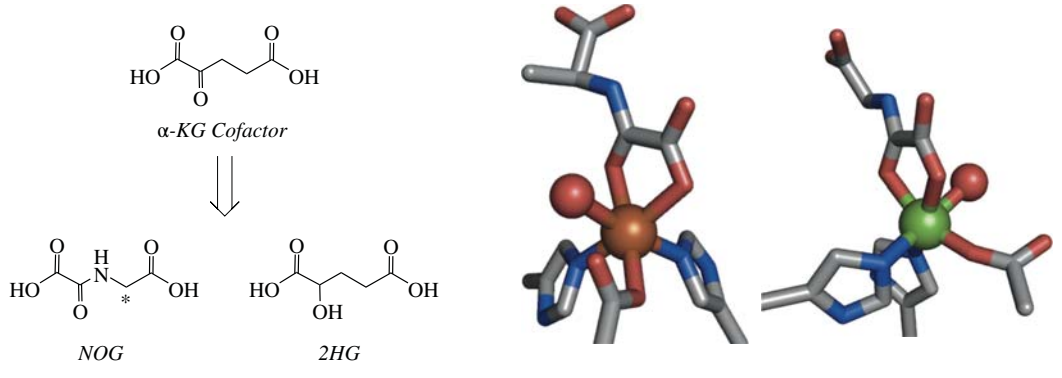

Figure 14.12 *Binding mode of α-keto acid-based MBGs. (a) The inhibitor N-oxalylglycine (NOG) is structurally similar to the α-KG cofactor of iron(II) oxygenases but cannot be turned over by the enzyme due to the addition of an amide bond. This molecule contains only one carbon atom that can be functionalized (marked with a star). 2-Hydroxyglutaric acid (2HG), which has an alcohol in place of the α-ketone, is also a cofactor mimic. (B) The structures of NOG bound to the iron(II) ion of AlkB (left, PDB 3T4H, inhibitor is truncated for clarity) and nickel(II)-substituted JMJD2A (right, PDB 4EYU) show the expected bidentate coordination.*

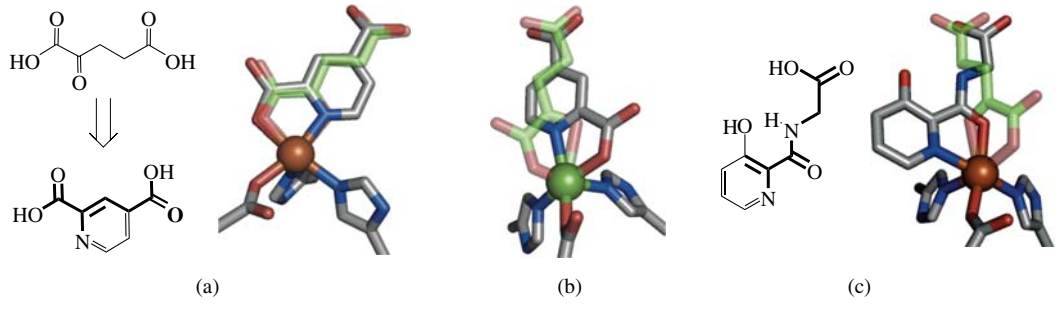

Figure 14.13 *Pyridine-derived MBGs based on α-KG isosteres. (a) Pyridine-2,4-dicarboxylic acid is structurally similar to α-KG, shown in green, and binds to the iron(II) ion of FIH in a similar fashion (PDB 2W0X). (b) Pyridine-2,4-dicarboxylic acid binds to nickel(II)-substituted JMJD2A in a similar mode but different orientation to that in α-KG (PDB 2VD7). (c) A picolinamide-based inhibitor shows a third, unique binding mode in the active site of AlkB (PDB 3T3Y). Bonds shown in bold highlight similarities between the inhibitors and α-KG.*

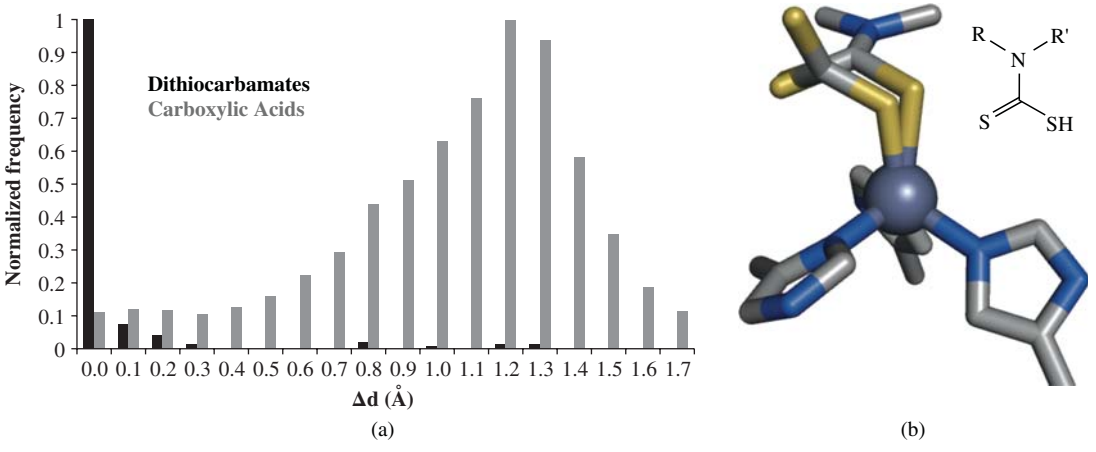

Figure 14.14 *Binding modes of the dithiocarbamate MBG. (a) Analysis of dithiocarbamates (black) compared with carboxylic acids (gray) bound to transition metals in the CSD. (b) The CS_3^{2-} anion (PDB 3K7K) and a dithiocarbamate-based inhibitor (PDB 3P58, truncated for clarity) both show monodentate coordination to the zinc(II) ion of human carbonic anhydrase II.*

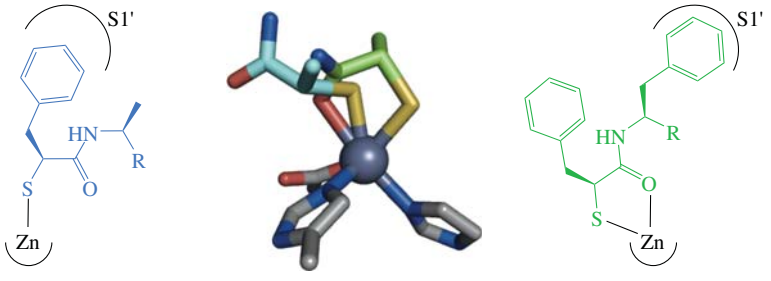

Figure 14.15 *Two binding modes of an α-mercapto ketone MBG-based inhibitor. Coordination of the zinc(II) ion of thermolysin by monodentate (blue, PDB 1QF2) and bidentate (green, PDB 1QF2) inhibitors based on the α-mercaptoketone MBG. Inhibitors are truncated for clarity. The change in coordination is driven by the hydrophobic interaction of the inhibitor backbone in the S1′ pocket.*

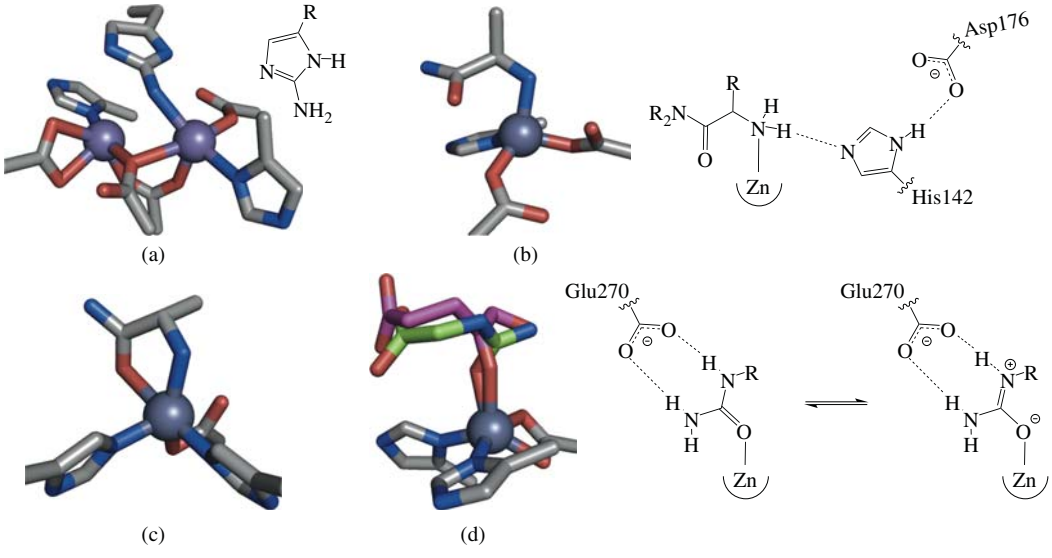

Figure 14.16 *Binding modes of selected amine and carbonyl-based MBGs. (a) Binding of the 2-aminoimidazole MBG to the dinuclear manganese(II) active site of arginase I (PDB 3MFV). (b) The monodentate binding mode of the terminal amine of a peptide-based inhibitor of HDAC8 (PDB 3SFH) may be stabilized by a hydrogen bonding network, diagrammed on the right. (c) The amino termini of peptidic inhibitors of C. botulinum neurotoxin A act as bidentate ligands (PDB 3QW6). (d) Bound to the zinc(II) ion of carboxypeptidase A, inhibitors based on α-hydroxy ketone and urea MBGs act as monodentate ligands (PDBs 3FVI and 1HDU, respectively). The urea has a shorter O–Zn bond length, possibly due to stabilization of an anionic resonance structure by an active-site Glu residue, diagrammed on the right. Inhibitors have been truncated for clarity.*

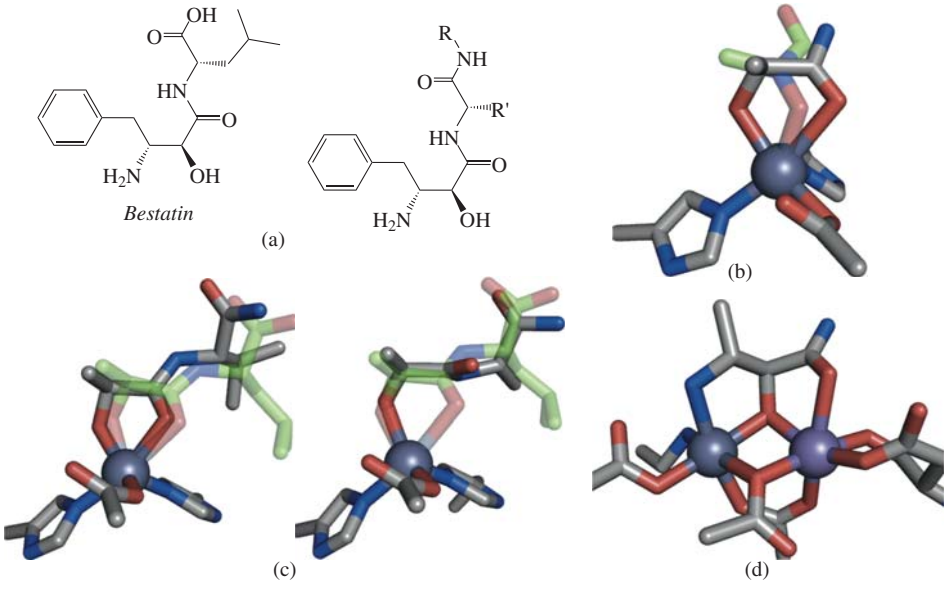

Figure 14.17 *Coordination modes of bestatin. (a) Structures bestatin (left) and the amide derivatives of bestatin (right). (b) Bound to the zinc(II) ion of leukotriene A4 hydrolase, the α-hydroxy ketone of bestatin acts as a bidentate ligand (PDB 3FTX). An inhibitor based on the N-substituted hydroxamic acid MBG is shown in green. (c) Bound to an M1 family aminopeptidase, amide derivatives of bestatin show both bidentate (left, PDB 4FYT) and monodentate (right, PDB 3T8V) coordination modes. Bestatin bound to the same enzyme is shown in green for comparison (PDB 3EBH). (d) Bestatin can also bind dinuclear metal centers, such as leucine aminopeptidase (PDB 3H8G). Ligands are truncated for clarity.*

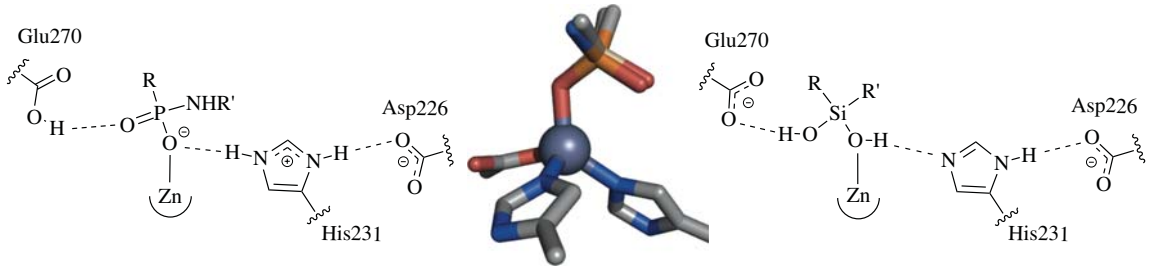

Figure 14.18 *Binding mode comparison of silanediol and phosphate MBGs. The binding modes of inhibitors based on the silanediol MBG (PDB 1Y3G) and phosphate MBG (PDB 4D9W) nearly overlay. Inhibitors are truncated for clarity. The rich hydrogen bonding environment around the metal ion is suitable for both charged (phosphate) and neutral (silanediol) donors. The unbound hydroxy group of the silanediol MBG can either donate or accept a hydrogen bond from Glu270 depending on the protonation state of that residue.*

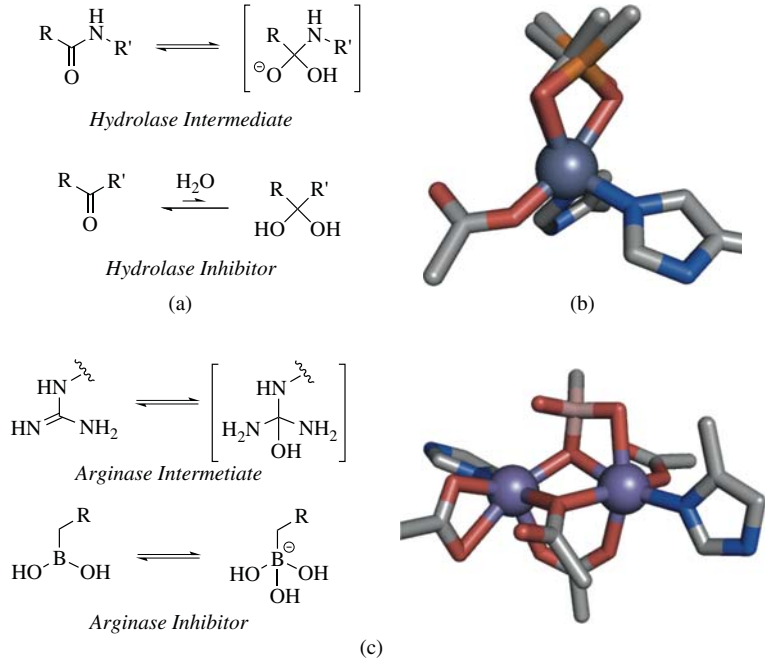

Figure 14.19 *Binding modes of inhibitors that are modified in solution. (a) Ketones can be hydrated, either in solution or potentially by target enzymes, to yield geminal diol mimics of the peptide hydrolase intermediate. (b) Comparison of the binding modes of an inhibitor based on this diol metal-binding motif (PDB 3BKK) to that of a phosphate-based inhibitor (PDB 2OC2) reveals that the coordination modes are very similar. (c) Boronic acids can be hydrated by the dinuclear manganese(II) active site of arginase to yield metal-bound boronate anions (PDB 1D3V). Inhibitors are truncated for clarity.*

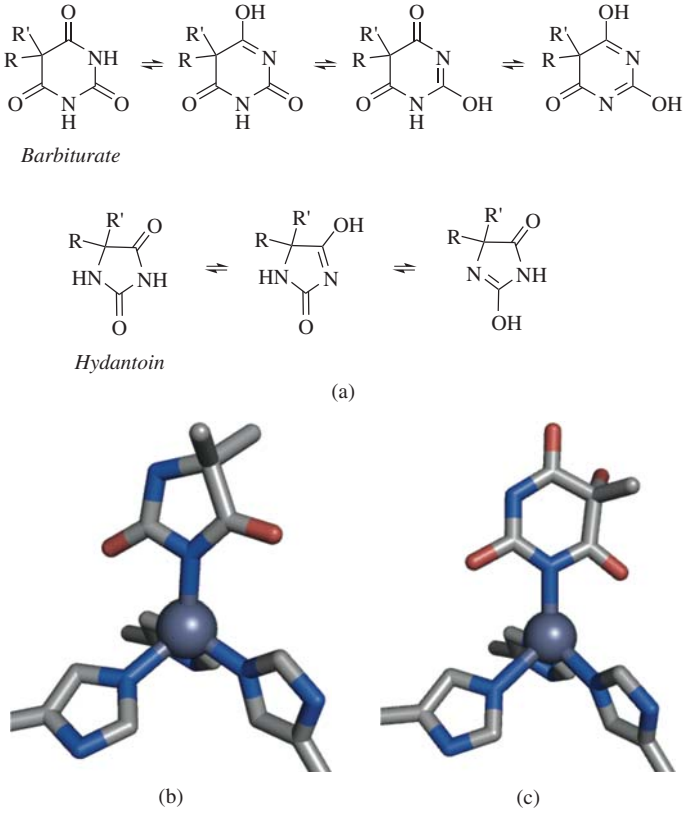

Figure 14.20 *Selected nitrogen-containing heterocycles that have been utilized as MBGs. (a) The resonance forms of barbiturates and hydantoins allow for metal binding and hydrogen bonding interaction to be maximized in protein-active sites. (b) The hydantoin MBG has been used in the development of TACE inhibitors, and binds as a monodentate ligand (PDB 3LEA). (c) The barbiturate MBG binds to the zinc(II) ion of MMPs in a similar monodentate fashion (PDB 1YOU). Inhibitors are truncated for clarity.*

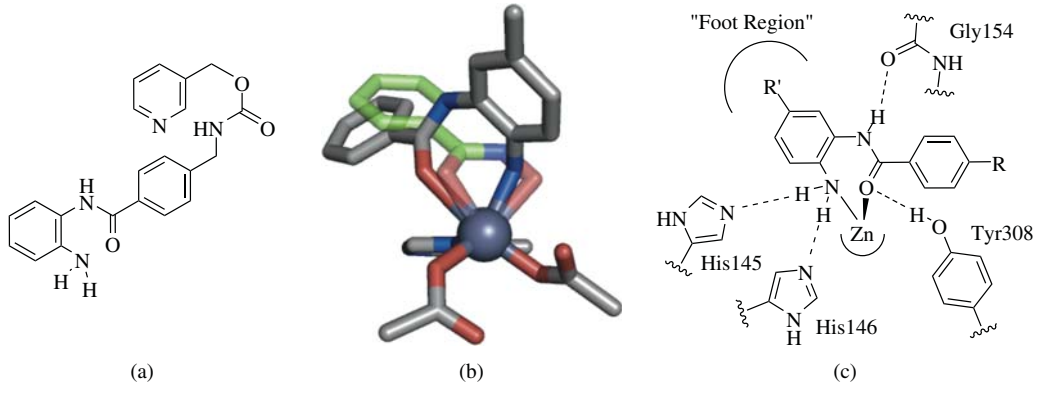

Figure 14.21 *Benzamide-based inhibitors of HDACs bind in a unique fashion. (a) The chemical structure of entinostat, an inhibitor of HDACs that is in Phase II clinical trials for the treatment of several cancers. (b) The crystal structure of an inhibitor based on the 2-aminobenzamide MBG bound in the active site of HDAC-2 (PDB 3MAX). For comparison, an inhibitor based on the terminal hydroxamate MBG bound to HDAC-8 (PDB 1W22) is shown in green. (c) Schematic of the hydrogen bonding interaction between the 2-aminobenzamide MBG and the active site of HDAC-2.*

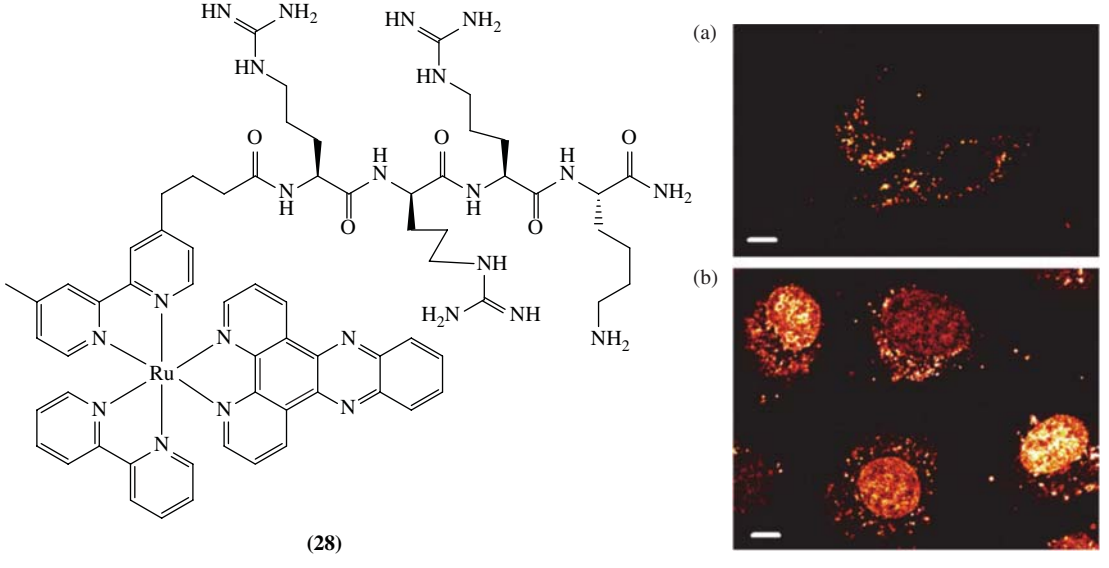

(28)

Figure 15.8 *Ruthenium(II) dipyridophenazine complex with appended Arg-D-Arg-Arg-Lys peptide. Subcellular distribution of* ***(28)*** *in HeLa cells in serum-free media, with concentration of (A) 20 μM or (B) 40 μM. Scale bars are 10 μm. Reprinted from [167], with permission from Elsevier.*